

INJECTION AND COMBUSTION OF LIQUID FUELS

A. A. PUTNAM, F. BENINGTON, H. EINBINDER, H. R. HAZARD,
J. D. KETTELE, JR., A. LEVY, C. C. MIESSE, J. M. PILCHER,
R. E. THOMAS, A. E. WELLER, AND B. A. LANDRY

BATTELLE MEMORIAL INSTITUTE

MARCH 1957

AERONAUTICAL RESEARCH LABORATORY
CONTRACT No. AF 33(038)-13501
WADC TASK 70148
WADC PROJECT 3012

WRIGHT AIR DEVELOPMENT CENTER
AIR RESEARCH AND DEVELOPMENT COMMAND
UNITED STATES AIR FORCE
WRIGHT-PATTERSON AIR FORCE BASE, OHIO



FOREWORD

This report was prepared by the staff of Battelle Memorial Institute for the Aeronautical Research Laboratory, Wright-Patterson Air Force Base, under Contract AF 33(038)-13501, Task 70148, Project 3012, "Monograph on Injection of Liquids Into a Gas Stream".

Work on this report was performed by A. A. Putnam, F. Benington, H. Einbinder, H. R. Hazard, J. D. Kettelle, Jr., A. Levy, C. C. Miesse, J. M. Pilcher, R. E. Thomas, and A. E. Weller under the administrative direction of B. A. Landry. Editing was carried out by R. E. Thomas and A. A. Putnam of Battelle Memorial Institute.

The project was initiated by Dr. D. G. Samaras in 1950, and was supervised by Joseph Loch until May, 1954. Since that time, Dr. D. G. Samaras acted as the Task Scientist for the Aeronautical Research Laboratory, Wright Air Development Center, Wright-Patterson Air Force Base, Ohio.

This Monograph contains a review of material in the unclassified literature relating directly to the fundamental physical phenomena involved in steady flow processes in high-intensity combustors. To systematize the presentation, the report has been divided into six parts, as follows: I. Atomization of Liquid Fuels, II. Ballistics of Droplets, III. Evaporation of Droplets, IV. Fluid Dynamics, V. Homogeneous Combustion, and VI. Heterogeneous Combustion. The sections have been further subdivided into a total of 19 chapters. The information in each of these chapters may be summarized briefly as follows:

Part I. Atomization of Liquid Fuels

Chapter 1. "The Mechanism of Atomization" - It is shown that atomization generally takes place in three steps: (a) the initial disturbance of the surface of the liquid jet, (b) the formation of ligaments which then break up into fragments, and (c) the further breakup of the fragments into smaller droplets. The most important factors that influence drop size in the atomization process are: (a) nozzle design, (b) operating conditions, especially pressure, (c) the properties of the liquid and of the air into which it is injected, and (d) the relative velocity between the liquid and the air.

Chapter 2. "Methods of Atomization" - Five basically different methods of atomization are (1) solid injection, using pressure nozzles, (2) two-fluid atomization, whereby the liquid is disintegrated when it encounters a high-velocity stream of gas, (3) atomization by rotating discs or cups, (4) atomization by vibrating devices employing sonic or mechanical vibrations, and (5) atomization by impinging jets, whereby the collision of two or more liquid jets results in atomization.

Chapter 3. "Design of Atomizers" - The requirements of a good fuel-spray nozzle are summarized, and the fundamental principles of nozzle design are discussed.

Chapter 4. "Spray Analysis" - Six classes of experimental methods for determining drop-size distribution are: (1) microscopic examination of drops collected on slides or in cells, (2) freezing of drops in spray followed by sieving, (3) direct photographic methods, (4) optical methods based on the scattering or absorption of light, (5) electronic and radioautographic techniques, and (6) selective impaction. Each method has its advantages, but none is entirely satisfactory. Mathematical representations of drop-size distribution are discussed. Other important factors in spray analysis are the angles formed by the conical spray and the distribution of droplets about the axis.

Part II. Ballistics of Droplets

Chapter 5. "Ballistics of a Single Droplet" - The methods of classical hydrodynamics are employed to obtain those fundamental results which pertain to the translation and rotation of solid spheres in an ideal fluid; these results are then extended to the motion of solid or liquid spheres in real fluids. Recent modifications to these treatments are covered, the various theories regarding the wake formation behind a moving sphere are compared, a mathematical analysis of droplet deformations is given, and the equations for the motion of a droplet injected into a uniform and curved flow field are developed.

Chapter 6. "Dynamics of Dispersions" - This treatment is based on the assumption that the injection process may be analyzed by applications of basic results which have been established in the related fields of fixed beds, fluidized beds, and pneumatic transport. The problems of sedimentation, flocculation, diffusion, coalescence, and sonic agglomeration are treated briefly.

Part III. Evaporation of Droplets

Chapter 7. "The Thermodynamics and Kinetics of Evaporation" - A fundamental discussion is given of the principal factors that enter into both the thermodynamics and kinetics of evaporation. Both of these aspects of the evaporation process are interrelated through transition energies. Kinetics, however, determine the rate of material transport during the phase change by specifying the energy necessary for the activation of phase transitions having thermodynamic feasibility. Experimentally determined evaporation rates of a wide variety of liquids are found to be in good agreement with theoretical rates.

Chapter 8. "Single-Droplet Evaporation" - The Maxwell theory of droplet evaporation is presented, then modified by introducing the Fuchs' concept of a stagnant boundary layer surrounding the evaporating droplet, and finally the theory is extended to include the evaporation of drops in a finite enclosure. It is shown that while diffusion transport of small molecules from the boundary layer can be completely described by theory, the opposing thermal-transport process is less completely understood.

Chapter 9. "Evaporation of a Moving Droplet" - The evaporation of a rigid liquid sphere under conditions of ambient-gas motion is described in terms of a set of simultaneous differential equations which relate heat and mass transfer to the hydrodynamic variables of gas flow in the region of the liquid surface.

Chapter 10. "Spray Evaporation" - An analysis of dynamic-spray evaporation is given that is based upon the aerodynamic and transport aspects of single-droplet evaporation. The evaporation rates for individual drops are integrated to obtain a total evaporation rate; droplet-interaction effects are neglected.

Part IV. Fluid Dynamics

Chapter 11. "The Equations of Fluid Dynamics" - The basic equations of fluid flow are derived in Cartesian tensor notation. Included are the continuity equation, the equation for the dissipation of energy by viscosity, the energy equation for a viscous fluid, and the Navier-Stokes' equation.

Chapter 12. "Turbulence" - This review is divided into two main sections, the phenomenological theories of turbulence, and the statistical theory of turbulence. In both sections, experimental data from the literature are compared with the various theories.

Chapter 13. "Hydrodynamic Recirculation" - Most of the work recorded in the literature has been carried out on isothermal-flow systems, such as the stable flow pattern around a bluff body at low Reynolds numbers, (2) the unstable flow pattern around a bluff body at high Reynolds numbers, and (3) the unstable flow pattern typical of a closed system with one or more entries and exits. The changes made in these flow patterns by the presence of a flame are discussed. The types of recirculation encountered in practice are illustrated by the use of typical combustion units.

Part V. Homogeneous Combustion

Chapter 14. "Laminar Flame Propagation" - The various theories of flame propagation are outlined, methods of measuring burning velocity are covered, and their limitations and advantages noted. The physical effect on burning velocity of temperature, pressure, mixed fuels, and non-hydrocarbon fuels are considered.

Chapter 15. "Turbulent Flames of Premixed Gases" - The theories of turbulent flame propagation fall naturally into three groups - those in which the scale of turbulence is considerably

smaller than the flame thickness, those in which the scale of turbulence is considerably larger than the flame thickness, and those in which the scale of turbulence and the flame thickness are about the same. The various treatments of flame instability which might lead to flame-generated turbulence are covered. Following the evaluation of the mathematical aspects of the turbulent flame phenomena, the experimental data reported in the literature are discussed.

Chapter 16. "The Stability Limits of Premixed Flames" - The flammability limits of a static mixture are considered first. These limits are affected by composition, pressure, and chamber size in a manner that seems related to certain phenomena observed in studies of flame stability. The stability of flames in low-velocity streams is next examined, both from an experimental and theoretical point of view. Finally, flame stability in a high-velocity stream is covered; stability in this latter case appears to depend on a different mechanism than stability in a low-velocity stream.

Chapter 17. "Ignition of Combustible Mixtures" - Weaknesses in early research techniques used in studies of spark ignition resulted in conclusions at variance with present knowledge. Recent workers have been more successful in correlating ignition test data with significant variables and with theories. Important variables are: (a) properties of the gas mixture, including fuel properties, and proportions of fuel, oxygen, and diluents, (b) imposed conditions of pressure and temperature, and (c) spark conditions, including energy and duration of the discharge, and shape and spacing of the electrodes.

Part VI. Heterogeneous Combustion

Chapter 18. "Droplet Combustion" - The various theories of droplet combustion, which are closely related to theories of evaporation, are considered. The experimental results of studies of flammability limits and propagation rates in fuel mists, and the effect of the physical properties of sprays on flame stability limits in high-velocity stream are discussed.

Chapter 19. "Diffusion Flames" - Diffusion flames may be classified into four types: the confined laminar flame, the unconfined laminar flame, and the confined and unconfined turbulent flames. In the confined flame, both fuel and oxidant are in limited supply, while in the unconfined flame, only the fuel is limited. Also, in the unconfined flame, buoyancy effects may play a large part in the observed phenomena. The mixing process is usually the rate-controlling factor in the diffusion flame; thus, the conditions of mixing are often of more importance than chemical kinetic considerations.

PUBLICATION REVIEW

The publication of this report does not constitute approval by the Air Force of the findings or conclusions contained herein. It is published only for the exchange and stimulation of ideas.

FOR THE COMMANDER:

Nathan L. Kriseberg
NATHAN L. KRISBERG, Colonel, USAF
Chief, Aeronautical Research Laboratory
Directorate of Research, WADC

TABLE OF CONTENTS

	<u>Page</u>
FOREWORD	ii
ABSTRACT	iii
INTRODUCTION	1
 CHAPTER 1 THE MECHANISM OF ATOMIZATION	
PHYSICAL PROCESSES	1-2
Summary of the Physical Processes of Atomization	1-25
THEORETICAL ANALYSIS OF JET INSTABILITY AND OF SECONDARY ATOMIZATION	1-26
Rayleigh's Analysis	1-31
Capillary Force, Nonviscous Liquids	1-31
Capillary Force, Viscous Liquids	1-32
The Dynamic Effect	1-33
Summary of Rayleigh's Analysis	1-35
Weber's Analysis	1-35
Effect of Surface Tension	1-35
Exact Solution	1-36
Influence of Jet Velocity	1-38
Atmospheric Effects	1-38
Elasticity Analogy	1-39
Summary of Weber's Analysis	1-40
Siestrunck's Analysis	1-41
Littaye's Analysis	1-42
Baron's Analysis	1-43
Borodin and Dityakin's Analysis	1-45
Balje' and Larson's Analysis	1-46
Summary	1-48
THE VARIOUS FACTORS THAT INFLUENCE ATOMIZATION	1-48
Mechanical Factors	1-49
Operational Factors	1-50
Fuel Factors	1-51
Ambient-Gas Factors	1-53
Summary of Various Factors Influencing Atomization	1-54
REFERENCES	1-54
 CHAPTER 2 METHODS OF ATOMIZATION	
SOLID INJECTION	2-1
Swirl-Type Atomization	2-1
Modified Plain-Orifice Nozzles	2-2

CHAPTER 5

BALLISTICS OF A SINGLE DROPLET

METHODS OF CLASSICAL HYDRODYNAMICS	5-2
Fundamental Concepts of Potential Flow	5-2
Axially Symmetric Flow	5-2
Irrotational Flow	5-4
Vorticity	5-4
Velocity Potential	5-5
General Properties of the Velocity Potential	5-5
The Velocity Potential in Terms of Surface Zonal Harmonics	5-6
Relation Between the Stream Function and the Velocity Potential	5-7
Basic-Flow Configurations	5-8
Sources and Sinks	5-8
Flow Due to a Simple Source	5-8
Uniform Flow Parallel to an Axis of Symmetry	5-8
Flow Due to a Doublet	5-9
A Solid Sphere in an Ideal Fluid	5-10
The Sphere Theorem	5-10
Sphere at Rest in a Uniform Stream	5-10
Sphere Moving Uniformly in a Fluid at Rest	5-11
Navier-Stokes Equations of Motion	5-12
Pressure Equation for Irrotational Flow	5-13
Bernoulli's Equation	5-13
Pressure Distribution on the Surface of a Sphere	5-13
Motions Derivable From Kinetic Energy	5-14
Kinetic Energy of a Fluid in Irrotational Motion	5-14
Kinetic Energy of a Fluid Due to the Uniform Motion of a Sphere	5-14
Virtual Mass of a Moving Sphere	5-15
The Approach of Two Spheres	5-15
Two Spheres in Uniform Parallel Motion	5-16
Hamilton's Principle and the Euler-Lagrange Equation	5-16
Moving Sphere in the Vicinity of a Wall	5-17
Flow Past Spheroids	5-18
The Motion of Spheroids in a Fluid	5-18
Linear Motion of a Prolate Spheroid	5-19
Linear Motion of an Oblate Spheroid	5-20
Rotation of an Ellipsoid	5-21
A Solid Sphere in a Real Fluid	5-22
Some Properties of Real Fluids	5-22
Steady Flow of a Real Fluid Past a Solid Sphere	5-24
Stokes Law of Drag	5-24
Terminal Velocity of Fall for Small Reynolds Numbers	5-25
Translation and Rotation of a Solid Sphere in a Real Fluid	5-25
A Liquid Sphere in a Real Fluid	5-26
Linear Motion of a Liquid Sphere in a Real Fluid	5-26
Terminal Velocity of a Liquid Sphere in a Real Fluid	5-27
Internal Circulation Due to Slow Translation	5-27
Oscillations of a Viscous Sphere	5-27
Circulation Due to Oscillations of a Viscous Sphere	5-28

TABLE OF CONTENTS
(Continued)

	<u>Page</u>
TWO-FLUID ATOMIZATION	2-3
Special Methods Employing Two-Fluid Atomization	2-3
ROTATING DISKS AND CUPS	2-5
Power Required	2-8
Mechanism of Disk Atomization	2-9
Dimensional Analysis of Ligament Formation and Transition	2-11
Applications of Disk Atomization	2-15
METHODS BASED ON VIBRATIONS	2-16
IMPINGING LIQUID JETS	2-20
SUMMARY OF METHODS OF ATOMIZATION	2-21
REFERENCES	2-23

CHAPTER 3

DESIGN OF ATOMIZERS

REQUIREMENTS OF A GOOD NOZZLE	3-1
FUNDAMENTAL PRINCIPLES OF NOZZLE DESIGN	3-3
Experimental Studies of Swirl Atomizers	3-3
S. M. Doble's Investigations	3-3
E. A. Watson's Investigations	3-6
Comparison of Doble and Watson Methods	3-7
Bowen's and Joyce's Investigations	3-7
P. H. Schweitzer's Investigations	3-8
J. P. Longwell's Investigations	3-8
E. Söhngen's Study of Spray Angle	3-10
Theoretical Analyses of Swirl Atomizers	3-10
G. I. Taylor's Analysis	3-10
I. I. Novikov's Analysis	3-13
Harvey and Hermandorfer's Analysis	3-16
SPRAY NOZZLES FOR AIRCRAFT GAS TURBINES	3-18
The Simplex Nozzle	3-18
The Duplex Nozzle	3-20
Variable Area Nozzles	3-21
The Spill-Return Nozzle	3-22
FUEL VAPORIZING SCHEMES	3-23
Advantages of Fuel Vaporizers	3-23
Description of Fuel Vaporizers	3-24

TABLE OF CONTENTS
(Continued)

	<u>Page</u>
INJECTORS FOR ROCKET PROPELLANTS	3-25
Types of Injectors	3-25
Flow and Stability of Injected Liquids	3-30
Flow Discontinuity or Hydraulic "Flip"	3-31
Equations for Hydraulic Flip	3-32
Flip Transition Time	3-32
Effect of Cross-Velocity on Flow Discontinuity	3-33
Types of Instability in Liquid Jets	3-33
Relation Between Flow Stability and Injector Design	3-33
Liquid Phase Mixing of Impinging Jets	3-33
SUMMARY	3-34
REFERENCES	3-37

CHAPTER 4

SPRAY ANALYSIS

SECTION I — EXPERIMENTAL METHODS FOR DETERMINING DROP-SIZE
DISTRIBUTION

.	4-1
Methods Based on Collection of Drops on Slides or in Cells	4-2
Frozen-Drop and Wax Methods	4-6
Frozen-Drop Method	4-6
Wax Method	4-9
Photographic Methods	4-12
Stubbs and York Method	4-13
NACA Flight Camera	4-15
Optical Methods	4-16
Four Types of Light-Scattering Methods	4-16
Methods Based on Light Transmission	4-16
Methods Based on the Intensity of the Scattered Light	4-16
Method Based on the Color of the Scattered Light	4-17
Method Based on the Polarization of the Scattered Light	4-17
NACA Optical Methods	4-17
JPL Optical Methods	4-19
Diffraction-Ring Method	4-19
Photometer Method	4-21
Electronic and Radioautograph Methods	4-22
Cascade-Impactor Method	4-24
May's Cascade Impactor	4-25
Isokinetic Sampling With the Cascade Impactor	4-27
Determination of Size Distribution Among Stages by Mass Methods	4-27
Sampling of Volatile Sprays	4-27
Sonkin's Modified Cascade Impactor	4-28
Laskin's Modified Cascade Impactor	4-28
Battelle Cascade Impactor	4-29
Cascade Impactor Used for Flight Measurement of Droplet Size	4-29
Ranz's Cascade Impactor	4-30
Theory of Jet Impactors	4-31
Problems Related to the Experimental Determination of	
Drop-Size Distribution	4-33
Fraction of Slide Area That Should be Covered With Droplets	4-33

Continued
TABLE OF CONTENTS
 (Continued)

	<u>Page</u>
Automatic Scanning Devices for Measuring Drop-Size Distribution	4-33
Rupe's Differentiating Droplet Counter	4-33
Marshall's Scanning Device	4-34
Pigford's Automatic Drop-Size Counter	4-35
British Methods for Automatic Counting	4-35
Battelle Semiautomatic Counter	4-36
Collection Efficiency	4-36
Flattening Coefficient and Impression Coefficient	4-40
Flattening Coefficient	4-40
Impression Coefficient	4-43
Microscopic Techniques	4-45
Critical Impact Velocity	4-45
Summary	4-47
SECTION II - MATHEMATICAL EXPRESSIONS FOR DROP-SIZE DISTRIBUTIONS	4-50
The Concept of Mean Diameters	4-52
The Nukiyama-Tanasawa Equation	4-53
The Rosin-Rammler Equation	4-56
Semiempirical Derivation	4-56
The Bennett Diagram and Inner Percentages	4-58
The Effect of the Parameters b and n	4-60
The Graphico-Analytical Criterion	4-63
Iteration Method for Determining b and n for Equivalent Infinite Consist	4-64
Mean Diameters for Rosin-Rammler Equation	4-66
The Weibull Equation	4-66
The Logarithmico-Normal Equation	4-68
Statistical Approach	4-68
Exponential Law of Decay	4-69
Log-Probability Coordinates and Goodness of Fit	4-70
Inner Percentage and the Logarithmico-Normal Equation	4-75
Limited Logarithmico-Normal Equations	4-76
Mean Diameters for Logarithmico-Normal Equation	4-78
The Griffith Comminution Function	4-80
Roller's Size-Distribution Function	4-83
Multimodal Size Distribution	4-84
Persistence of Form	4-86
Summary	4-88
SECTION III - SPRAY PATTERN AND DISTRIBUTION	4-93
Factors Influencing Weight-Flow Distribution	4-93
Methods for Determining Spray Distribution	4-94
Rapid Spray Analyzer	4-97
Applications of the Rapid Spray Analyzer	4-99
Deposition and Dispersion of Sprays	4-99
Summary	4-101
REFERENCES	4-102
BIBLIOGRAPHY - PART I	
ATOMIZATION OF LIQUID FUELS	I

TABLE OF CONTENTS

(Continued)

	<u>Page</u>
RECENT MODIFICATIONS OF HYDRODYNAMICS	5-29
Modern Approach to Fluid Flow	5-29
Oseen's Equation of Motion	5-30
Prandtl's Theory of the Boundary Layer	5-30
The Wake Formation Behind a Sphere	5-31
Drag on a Solid Sphere Moving in a Real Fluid	5-32
Skin Friction, Pressure Drag, and Hydrodynamic Drag	5-33
Corrections to the Drag Laws	5-33
Corrections for a Finite Field of Flow	5-34
Corrections Due to the Molecular Structure of the Fluid	5-34
Corrections for Nonviscous Flow	5-35
Corrections for Accelerated Motion	5-37
Droplet Deformations and Drag Coefficients	5-38
Deformation of a Liquid Drop Moving in a Real Fluid	5-38
Disintegration of Liquid Drops	5-38
The Effects of Surface Tension on Internal Circulation	5-39
Mathematical Analysis of Droplet Deformations	5-39
The Drag Coefficient for Liquid Droplets	5-42
Oscillations of a Liquid Droplet	5-43
Equations of Motion	5-43
Equations of Motion of a Droplet in a Gas Stream	5-43
Equations of Motion for Small Reynolds Numbers	5-44
Motion of a Droplet Injected Into a Uniform Gas Stream	5-44
Motion of a Droplet in a Field of Curved Streamlines	5-45
Time Required to Attain Stream Velocity	5-45
Motion of a Droplet Injected at Right Angles to a Uniform Gas Stream	5-46
The Motion of a Droplet During Preheating	5-47
SUMMARY	5-51
REFERENCES	5-52

CHAPTER 6

DYNAMICS OF DISPERSIONS

NOMENCLATURE TABLE	6-3
FIXED BEDS	6-6
Discussion	6-9
SEDIMENTATION	6-10
Flocculation	6-12
Diffusion	6-13
Sedimentation in Horizontal Flow	6-14
Discussion	6-14
FLUIDIZED BEDS	6-15
Flocculation	6-18
Density of a Fluidized Bed	6-19

Contrails
TABLE OF CONTENTS
 (Continued)

	<u>Page</u>
Mixing in a Fluidized Bed	6-19
Heat and Mass Transfer	6-19
Discussion	6-19
PNEUMATIC TRANSPORT	6-19
Discussion	6-20
COALESCENCE	6-21
Discussion	6-23
SONIC AGGLOMERATION	6-24
Covibration	6-24
Hydrodynamic Forces	6-24
Radiation Pressures	6-24
Discussion	6-25
CONCLUDING REMARKS	6-25
REFERENCES	6-26

CHAPTER 7

THE THERMODYNAMICS AND KINETICS OF EVAPORATION

THERMODYNAMIC THEORY OF THE EQUILIBRIUM BETWEEN SUPERSATURATED VAPOR AND A DROP OF LIQUID	7-1
Surface Energy, Vapor Pressure, and Drop Size	7-2
Heterophase Fluctuations in Phase Change	7-6
THE KINETICS OF PHASE TRANSITION	7-9
Treatment by Classical Statistics	7-9
Treatment by Quantum Statistics	7-16
MULTICOMPONENT EVAPORATION	7-21
REFERENCES	7-22

CHAPTER 8

SINGLE-DROPLET EVAPORATION

MAXWELL'S EQUATION FOR THE EVAPORATION OF A SINGLE DROP	8-1
Correction for Temperature- and Pressure-Dependent Parameters	8-4
The Corrections for Both Finite Vapor Pressure and Limited Space of Evaporation	8-6
The Nonstationary Evaporation Process	8-8
THE VAPOR-CONCENTRATION DISCONTINUITY AT A DROP SURFACE	8-10

TABLE OF CONTENTS
(Continued)

	<u>Page</u>
The Case of Evaporation in an Infinite Atmosphere	8-10
The Case of Evaporation into a Finite Vessel With Absorbing Walls	8-12
DIFFUSION OF DROP EVAPORATION	8-17
Simple Diffusion Theory and Hydrocarbon Molecules	8-18
The Calculation of Diffusion Coefficients From Critical Data	8-20
HEAT TRANSFER AND DROP EVAPORATION	8-21
Conduction of Heat	8-22
Absorption of Radiant Energy	8-24
CONCLUDING REMARKS	8-25
REFERENCES	8-26

CHAPTER 9

EVAPORATION OF A "MOVING" DROPLET

THEORETICAL RESULTS	9-1
Evaporation From a Plane Surface	9-2
Evaporation From a Spherical Drop in a Moving Gas Stream	9-7
Evaporation of Drops in a High-Temperature Gas Stream	9-16
The Lifetime of Small Droplets at High Temperatures	9-24
Evaporation of Droplets Under Special Cases of Motion	9-26
Free Fall	9-26
Rapid Droplet Deceleration	9-29
The Contribution of Radiant Heat Transfer to Droplet Evaporation	9-32
Droplet Deformation and Evaporation	9-35
Evaporation From Multicomponent Drops	9-36
EXPERIMENTAL RESULTS	9-43
Sources of Error in Experimental Measurements of Drop Evaporation	9-43
Deviations From Spherical Shape	9-43
The Compressibility of the Surrounding Gas	9-44
Effect of Turbulence	9-44
Transient Conditions	9-44
Vapor Pressure at the Drop Surface	9-44
Effect of Drop Curvature on Vapor Pressure	9-45
Deviations From the Ideal-Gas Law	9-45
Self-Cooling of the Drop	9-46
Correlations of Experimental Measurements	9-46
REFERENCES	9-55

CHAPTER 10

SPRAY EVAPORATION

SIZE DISTRIBUTION OF DROPLETS IN A SPRAY	10-1
THE EFFECT OF DROP SIZE AND STREAM VELOCITY UPON THE MASS RATE OF SPRAY EVAPORATION	10-2

Contrails
TABLE OF CONTENTS
 (Continued)

	<u>Page</u>
THE MEAN SPRAY-VELOCITY APPROXIMATION	10-6
TURBULENCE AND SPRAY EVAPORATION	10-9
MASS AND HEAT BALANCE IN DYNAMIC-SPRAY EVAPORATION	10-11
THE EFFECT OF A CYLINDRICAL DUCT UPON SPRAY EVAPORATION	10-13
EXPERIMENTAL MEASUREMENTS OF SPRAY-EVAPORATION RATES	10-17
EVAPORATION OF A SPRAY IN A MOVING GAS STREAM	10-19
Streamline Flow	10-19
Turbulent Flow	10-20
CONCLUDING REMARKS	10-23
REFERENCES	10-24

CHAPTER 11

THE EQUATIONS OF FLUID DYNAMICS

CARTESIAN TENSOR NOTATION	11-1
THE EQUATION OF CONTINUITY	11-4
THE NAVIER-STOKES EQUATION	11-5
THE DISSIPATION OF ENERGY BY VISCOSITY	11-11

CHAPTER 12

TURBULENCE

REYNOLDS NOTATION	12-1
PHENOMENOLOGICAL THEORIES OF TURBULENCE	12-4
Prandtl's Mixing Length Theory	12-4
Taylor's Vorticity Transport Theory	12-6
Reichardt's Hypotheses	12-9
THE STATISTICAL THEORY OF TURBULENCE	12-14
Isotropic Turbulence	12-16
The Correlation Tensor	12-16
The Microscale of Turbulence	12-19
Correlations Between Derivatives of Velocities	12-19
Triple Correlations	12-20
Correlations Between Scalars and Velocities	12-21
The Correlation Between Fluctuating Density and Fluctuating Velocity	12-23
The Propagation of the Correlation	12-23
The Decay of Isotropic Turbulence	12-24

Continued
TABLE OF CONTENTS
 (Continued)

	<u>Page</u>
Some Properties of the Microscale	12-25
The Decay of the Scale and Intensity of Turbulence	12-25
The Loitsianskii Invariant	12-33
Partially Self-Preserving Turbulence	12-34
Turbulent Diffusion	12-35
Kolmogoroff's Theory of Local Isotropy	12-37
Correlation in Locally Isotropic Turbulence	12-38
Similarity Hypotheses in Locally Isotropic Turbulence	12-39
The Navier-Stokes Equation for Locally Isotropic Turbulence	12-40
Comparison of Kolmogoroff's Theory With Experiment	12-41
The Spectrum of Turbulence	12-44
Applications to the Dynamics of Turbulence	12-47
The Generation of Turbulence	12-47
 CONCLUDING REMARKS	 12-48
 REFERENCES	 12-49
CHAPTER 13	
HYDRODYNAMIC RECIRCULATION	
 RECIRCULATION IN ADIABATIC FLOW	 13-1
The Stationary Regime	13-3
The Shedding of Vortices	13-8
The Vortex Street	13-9
Flow Within Closed Chambers	13-14
 RECIRCULATION IN DIABATIC FLOW	 13-15
Flow Behind Bluff Bodies	13-16
Vortex Shedding Behind Flame Holders	13-18
Modeling of Combustion	13-22
 RECIRCULATION IN PRACTICAL COMBUSTION SYSTEMS	 13-22
Spin-Stabilized Burner	13-22
Baffle Flame Holder	13-23
Asymmetric Flame Holder	13-23
Can-Type Combustor	13-24
Controlled Recirculation Burner	13-24
 CONCLUDING REMARKS	 13-25
Adiabatic Flow	13-25
Diabatic Flow	13-26
 REFERENCES	 13-26

Continued
TABLE OF CONTENTS
(Continued)

Page

CHAPTER 14

LAMINAR FLAME PROPAGATION

THEORIES OF FLAME PROPAGATION	14-1
Thermal Theories	14-2
Species Diffusion Theories	14-5
Wave-Propagation Theory	14-10
Theories Combining Thermal and Diffusion Mechanisms	14-10
The Hirschfelder-Curtiss Analysis	14-11
The Von Karman-Penner Theory	14-11
The Boys and Corner Theory	14-12
The Friedman and Burke Development	14-12
Empirical Equations for Burning Velocity	14-13
THE MEASUREMENT OF BURNING VELOCITY	14-13
Bunsen Burner Methods	14-14
Propagation in Tubes	14-17
The Bubble Method	14-17
Flat Flame Method	14-18
Remarks on the Measurement of Burning Velocity	14-19
PHYSICAL EFFECTS ON BURNING VELOCITY	14-20
The Effect of Temperature	14-20
The Effect of Pressure	14-21
Effect of Mixed Fuels	14-24
Non-Hydrocarbon Systems	14-24
COMPARISON OF THERMAL AND DIFFUSION THEORIES	14-26
REFERENCES	14-28

CHAPTER 15

TURBULENT FLAMES OF PREMIXED GASES

THEORY OF TURBULENT FLAMES	15-1
Small-Scale Turbulence	15-1
Large-Scale Turbulence	15-3
Moderate Intensity	15-3
High-Intensity Turbulence	15-8
Summary of High Intensity Turbulence Equations	15-12
Transition Region of Turbulence	15-12
FLAME INSTABILITY	15-13
EXPERIMENTS ON TURBULENT FLAMES	15-21
CONCLUDING REMARKS	15-30
REFERENCES	15-33

CHAPTER 16

THE STABILITY LIMITS OF THE PREMIXED FLAME

FLAMMABILITY LIMITS OF STATIC MIXTURE	16-1
Absolute Limits	16-1
Limiting Effect of Chamber Size	16-5
LOW VELOCITY LIMITS OF STABILITY	16-8
Theories of Flame Stability	16-8
Experimental Results	16-11
Quenching Distance	16-14
HIGH VELOCITY FLAME STABILIZATION	16-16
Experimental Studies	16-16
Related Experimental Studies	16-21
Theories of Flame Holding	16-24
CONCLUDING REMARKS	16-27
REFERENCES	16-28

CHAPTER 17

IGNITION OF COMBUSTIBLE MIXTURES

HISTORY OF RESEARCH ON SPARK IGNITION	17-1
H. F. Coward, 1912-1927	17-2
W. M. Thornton, 1912-1924	17-2
R. V. Wheeler, 1914-1924	17-2
J. D. Morgan, 1916-1934	17-2
C. C. Patterson and N. Campbell, 1918 Bone, Frazier, and Witt, 1927	17-3
G. I. Finch and Associates, 1931-1937	17-3
H. W. Thompson, 1932	17-4
G. Mole, 1936	17-4
H. G. Landau, 1937	17-4
H. Herzing, 1937	17-4
R. Viillard, 1938-1948	17-5
A. Hayakawa and R. Goto, 1941	17-5
Y. Toryama, S. Saito, and R. Saito, 1942-1943	17-5
J. W. Linnett and Associates, 1945-1949	17-5
A. R. Boyle and F. J. Llewellyn, 1942-1947	17-6
B. Lewis, G. von Elbe, P. G. Guest, M. V. Blanc, and W. Roth, 1944-1952	17-6
H. Morris, 1949	17-12
R. Friedman and E. Burke, 1949	17-12
C. C. Swett, Jr., 1948-1951	17-12
H. F. Calcote and Associates, 1949-1952	17-14
Y. B. Zeldovich and N. N. Simonov, 1949	17-16
H. L. Olsen and E. L. Gayhart, 1951	17-17

TABLE OF CONTENTS

(Continued)

	<u>Page</u>
A. J. Metzler, 1952	17-17
H. R. Hazard, 1952	17-18
A. E. Weller, 1953-1955	17-18
IGNITION THEORIES	17-18
The Thermal Theory of Taylor-Jones, Morgan, and Wheeler	17-19
Mole's Activation Theory of Spark Ignition, 1936	17-20
Landau's Theory of Ignition by Chain Branching, 1937	17-20
Correlations of Ignition Data by Linnett, Raynor, Frost, and Nutbourne, 1945	17-21
The Lewis and von Elbe Theory of Minimum Ignition Theory: The 1947 Theory	17-22
The 1951 Lewis and von Elbe Theory of Minimum Ignition Energy	17-24
Fenn's Reaction Rate Theory	17-24
The Zeldovich and Simonov Theory	17-25
CONCLUDING REMARKS	17-25
Ignition of Gas Mixtures	17-25
Ignition of Liquid-Fuel Mists	17-26
REFERENCES	17-26

CHAPTER 18

DROPLET COMBUSTION

THE EFFECT OF SIZE DISTRIBUTION	18-1
THEORY OF DROPLET COMBUSTION	18-3
THE STABILIZATION OF FLAMES IN MISTS AND SPRAYS	18-14
FLAME STABILITY IN HIGH-VELOCITY SYSTEMS	18-18
CONCLUDING REMARKS	18-20
REFERENCES	18-21

CHAPTER 19

DIFFUSION FLAMES

LAMINAR DIFFUSION FLAMES	19-1
Confined Flames	19-1
Unconfined Flames	19-7
TURBULENT DIFFUSION FLAMES	19-11
Unconfined Flames	19-13
Enclosed Flames	19-16
CONCLUDING REMARKS	19-19
REFERENCES	19-19

LIST OF ILLUSTRATIONS

	<u>Page</u>
Table 1-1. Characteristics of Holfelder's Test Nozzles	1-50
Table 3-1. Significance of Longwell's Dimensionless Ratios	3-9
Table 3-2. Flow Range for Typical Poppet Nozzles	3-21
Table 4-1. Jet Dimensions and Range of Droplet Sizes for May's Cascade Impactor	4-26
Table 4-2. Houghton's Incremental Numerical Drop-Size Data and Drop-Size Distribution Derived Therefrom	4-51
Table 4-3. Mean Diameters	4-52
Table 5-1. Values of a_m for Various Values of λ/d	5-35
Table 5-2. Comparison of Brownian and Gravitational Displacements for Spherical Particles Suspended in Air and Water	5-35
Table 5-3. The Drag Coefficient of Spheres as a Function of Reynolds Number	5-37
Table 5-4. Change in Surface Tension With Radius	5-39
Table 5-5. Critical Velocities for the Breakup of Water Drops	5-41
Table 5-6. The Critical Weber Number for the Breakup of Water Drops	5-42
Table 6-1. Typical Values of the Discrepancy Between the Theoretical and Actual Sizes of Floccs as Indicated by Their Fall Velocities	6-13
Table 7-1. The Effect of Boundary-Layer Thickness on Surface Tension for Small Drops	7-4
Table 7-2. Maximum Possible Rate of Decrease of Droplet Radius With Time for Various Liquids	7-17
Table 7-3. Comparison of the Predicted Evaporation Rates for Several Liquids by the Knudsen and Absolute-Rate Equations.	7-19
Table 7-4. Comparison of Evaporation Coefficients With Free-Angle Ratio for Several Liquids	7-20
Table 8-1. Comparison of Langmuir and Fuchs Theories of Evaporation	8-12
Table 8-2. Experimental Collision Radii for Hydrocarbons	8-19
Table 8-3. Radii of Hydrocarbon Molecules Calculated From Collision Equation	8-19
Table 9-1. Comparison of Calculated and Observed Evaporation Rates	9-6
Table 9-2. Rates of Evaporation of Various Liquids Relative to Water	9-6
Table 9-3. Numerical Values of Temperature Ratio as a Function of (k_1^t/n_0) and (k_a/k_ℓ)	9-21
Table 9-4. Values of \underline{G} as a Function of (k_a/k_1) and (k_1^t/n_0^2)	9-23
Table 9-5. Comparison of Predicted Droplet Life for n-Hexane	9-25

LIST OF ILLUSTRATIONS
(Continued)

	<u>Page</u>
Table 9-6. Measured and Calculated Self-Cooling Effects in Droplets Under Static and Dynamic Conditions of Evaporation	9-46
Table 9-7. Numerical Data Used in the Determination of the Evaporation Constant $k' = 0.276$	9-48
Table 10-1.	10-13
Table 10-2.	10-22
Table 13-1. Critical Reynolds Numbers for the Shedding of Vortices From Circular Cylinders as a Function of the Ratio of the Channel Width, D, to Its Diameter, d	13-9
Table 14-1. Comparison of Calculated Burning Velocities With Experimental Results for the Ozone Reaction	14-8
Table 14-2. Coefficients for Calculating Maximum Burning Velocity	14-13
Table 14-3. A Comparison of Burning Velocity Measurements	14-18
Table 14-4. Effect of Temperature on Burning Velocity of Stoichiometric Mixtures of Natural Gas and Air	14-20
Table 14-5. The Variation of Burning Velocity Pressure as Predicted by Different Theories	14-22
Table 14-6. The Variation of Burning Velocity With Pressure as Determined Experimentally	14-22
Table 14-7. Burning Velocity of Various Hydrogen-Bromine Mixtures and Comparison With Thermal Theory	14-25
Table 16-1. Flammability Limits of Various Fuels	16-2
Table 16-2. Flammability Limits for Methane-Air Mixtures With Additives	16-3
Table 16-3. Ignition and Flame Temperatures for Several Paraffin Hydrocarbons at the Lower Limit	16-5
Table 16-4. Comparison of Experimental and Theoretical Values of Flash-Back and Quenching Distance for Propane-Air Mixtures	16-10
Table 16-5. Application of Quenching Theory to Minimum Pressure for Ignition	16-15
Table 16-6. The Variation of Stability Parameter, V/D^n , With Different Fuels	16-17
Table 17-1. Minimum Ignition Energies for Explosive Dust Cloths and Vapor-Air Mixtures	17-6
Table 18-1. Comparison of Calculated and Observed Combustion Radii	18-10
Table 18-2. Comparison of Propagation Rates in Mists and in Completely Vaporized Mixtures	18-17

LIST OF ILLUSTRATIONS

(Continued)

	<u>Page</u>
Table 18-3. The Effect of CO ₂ in Suppressing the Inflammability of Oil Mists	18-17
Table 19-1. Flame Height Proportional to Gas Flow	19-5
Table 19-2. Effect of Increase in i	19-5
Table 19-3. Effect of Gas Diffusivity	19-5
Table 19-4. Effect of Temperature on Methane Flame	19-5
Figure 1-1. Surface Disturbances	1-3
Figure 1-2. Disintegration Phenomena	1-4
Figure 1-3. Continuous Sprays at Various Injection Pressures. NACA Spark Photographs	1-6
Figure 1-4. Forms of Jet Disintegration Described by Haenlein	1-7
Figure 1-5. Photomicrographs of a Low-Velocity Fuel Jet at Different Distances From the Nozzle	1-8
Figure 1-6. Effect of Air Density on Fuel Jets	1-10
Figure 1-7. Effect of Injection Pressure on Jet Disintegration	1-11
Figure 1-8. Jets of Various Liquids Injected at 1500 PSI	1-12
Figure 1-9. Simple Scheme of a Swirl Chamber	1-13
Figure 1-10. Three Stages of Atomization	1-15
Figure 1-11. Opposing Forces Causing Initial Deformation of a Droplet Placed in an Air Stream	1-19
Figure 1-12. Effect of Centrifugal Forces on a Moving Liquid Droplet	1-19
Figure 1-13. Formation of Strings From the Partition Surface for Three Successive Instants of Time	1-20
Figure 1-14. Breakup of Water Drops in Steady Stream of Air	1-22
Figure 1-15. Shatter of Drops in Transient Air Stream	1-22
Figure 1-16. Spark Photographs of Shatter of Drops in Supersonic Air Stream	1-23
Figure 1-17. Formation of Hole in a Thin Sheet of Liquid	1-24
Figure 1-18. Variation of $\mu' = \mu/\sqrt{\sigma/\rho a^3}$ With Ka for Inviscid Fluid Where Surface Tension Predominates	1-32
Figure 1-19. Diagram of Coordinate System and Variables Along Surface of Separation	1-34
Figure 1-20. Coordinate System for Weber's Analysis	1-35

LIST OF ILLUSTRATIONS
(Continued)

	<u>Page</u>
Figure 1-21. Variation of $u' = u/\sqrt{\sigma/2\rho a^3}$ With Ka as Predicted by Various Equations	1-40
Figure 1-22. Influence of Liquid Viscosity on Drop Size	1-52
Figure 1-23. Effect of Viscosity on Mean Droplet Size (Swirl-Type Atomizers)	1-53
Figure 2-1. Principle of Simple Swirl-Type Atomizer	2-2
Figure 2-2. Two-Fluid Atomizing Nozzles	2-4
Figure 2-3. Rotating-Disk Atomizer	2-5
Figure 2-4. Liquid Flow on a Vaned Disk	2-7
Figure 2-5. Effect of Feed Rate, Disk Speed, and Disk Size on Power Consumption of Disk Atomizers	2-8
Figure 2-6. Supply and Flow of Liquid Within Rotating Cup	2-9
Figure 2-7. Disintegration by Direct Drop Formation	2-10
Figure 2-8. Disintegration by Ligament Formation	2-10
Figure 2-9. Disintegration by Film Formation.	2-10
Figure 2-10. Flow Conditions in Torus Around Edge of Cup	2-12
Figure 2-11. Experimental Data on Number of Ligaments Grouped Around a Semiempirical Curve	2-14
Figure 2-12. Correlation of Experimental Data on Transition From the Ligament State to Film Formation	2-15
Figure 2-13. Continuous Fuel-Injection System With Rotating Fuel Chamber	2-16
Figure 2-14. Rotating Fuel Injection System Used by Turboméca	2-17
Figure 2-15. AN-F-32 Atomized by a Rotating Disk	2-18
Figure 2-16. Vibrating-Type Nozzle	2-19
Figure 2-17. Microflash Photographs of Formation of Spray by Two Impinging Jets of Water. Views Perpendicular and Parallel to Plane of Jets are Shown	2-22
Figure 3-1. Components of Swirl Nozzle	3-4
Figure 3-2. Relation of Discharge Coefficient to Nozzle Design	3-6
Figure 3-3. Longwell's Experimental Nozzle	3-8
Figure 3-4. Schematic Diagram of Swirl Atomizer With Variables Used in Taylor's Analysis	3-10
Figure 3-5. Variation of K, z, and α With y for Maximum Flow (Q)	3-12

LIST OF ILLUSTRATIONS
(Continued)

	<u>Page</u>
Figure 3-6. Schematic Diagram of Nozzle and Liquid Sheath for Novikov's Analysis . . .	3-14
Figure 3-7. Comparison of Experimental Data for the Mean Drop Sizes of Sprays With Novikov's Theoretical Curve	3-15
Figure 3-8. Graphical Construction of Spray Angle Profile for Simple Swirl Atomizer . .	3-16
Figure 3-9. Comparison of Theoretical and Experimental Variation in Spray Angle With Supply Pressure for a Typical Swirl Atomizer	3-17
Figure 3-10. Simplex Nozzle Designs	3-19
Figure 3-11. Faults in Orifices	3-19
Figure 3-12. Duplex Nozzle	3-20
Figure 3-13. Variable Area Nozzle, Poppet Type	3-21
Figure 3-14. Spill-Type Nozzle	3-22
Figure 3-15. Fuel-Vaporizing Tube and Combustion Chamber	3-24
Figure 3-16. BAC Type 008 Injector	3-26
Figure 3-17. BAC Type 243 Injector	3-27
Figure 3-18. BAC Type 201 Injector	3-27
Figure 3-19. BAC Type 017 Injector	3-28
Figure 3-20. Random Showerhead Injection	3-29
Figure 3-21. Splash Injection	3-29
Figure 3-22. Impinging (Liquid-Liquid) Injection	3-30
Figure 3-23. Schematic Diagrams of Flow Through an Orifice	3-31
Figure 4-1. Drop Sampler for Frozen-Drop Method	4-7
Figure 4-2. Apparatus for Sieving Frozen Droplets	4-8
Figure 4-2A. Cross Section of Drop-Measuring Instrument	4-8
Figure 4-3. Collecting Funnel for Wax Spray	4-10
Figure 4-4. Filter Unit Components	4-11
Figure 4-5. System for Taking Shadowgraphs of Spray	4-13
Figure 4-6. Arrangement of Elements for Photographing Sprays	4-14
Figure 4-7. Limits of Known Volume Photographed	4-14
Figure 4-8. Arrangement for Double Exposure	4-15

Cascade
LIST OF ILLUSTRATIONS
(Continued)

	<u>Page</u>
Figure 4-9. Number of Reds Observed Plotted Against Droplet Diameter	4-17
Figure 4-10. Experimental Arrangement for Measuring Particle Sizes by Light-Scattering Methods	4-18
Figure 4-11. Experimental Arrangement for Measuring Particle Size and Concentration by Light-Transmission Method	4-19
Figure 4-12. Laboratory Setup for Study of Droplet Sizes in Sprays by Diffraction Ring Method	4-21
Figure 4-13. Photoelectric Photometer	4-22
Figure 4-14. Block Diagram of Electronic Spray Analyzer	4-23
Figure 4-15. Schematic Diagram Showing Principle of the Cascade Impactor	4-25
Figure 4-16. May's Four-Stage British Cascade Impactor	4-26
Figure 4-17. Laskin's Modified Cascade Impactor	4-28
Figure 4-18. Battelle No. 4 Cascade Impactor	4-29
Figure 4-19. Cascade Impactor for Flight Measurement of Droplet Size	4-30
Figure 4-20. Ranz's Cascade Impactors	4-31
Figure 4-21. Theory of Jet Impactors	4-32
Figure 4-22. Electronic Drop Size Distribution Analyzer	4-34
Figure 4-23. Comparison of Collection Effectiveness Calculated by Several Investigators	4-37
Figure 4-24. Collection Effectiveness of One-Inch Microscope Slide	4-37
Figure 4-25. Collection Effectiveness of 16-Gage Wire (1295 Microns)	4-38
Figure 4-26. Collection Effectiveness of 24-Gage Wire (511 Microns)	4-38
Figure 4-27. Curve for Estimating Impaction Efficiency of Jets	4-39
Figure 4-28. Curves for Computing Original Drop Diameter from Lens Diameter	4-41
Figure 4-29. Relation Between Flattening Coefficient and Contact Angle	4-42
Figure 4-30. Contact Angle, θ , for a Flattened Oil Drop	4-42
Figure 4-31. Actual Spherical Diameter Against Measured Flattened Diameter for Dibutyl Phthalate Droplets	4-43
Figure 4-32. Experimental Relationship Between Weber's Number and the Ratio of Track Diameter to Droplet Diameter	4-44

LIST OF ILLUSTRATIONS

(Continued)

	<u>Page</u>
Figure 4-33. Critical Impact Velocities of Water Droplets Penetrating Kerosine-Air Interface	4-46
Figure 4-34. Typical Droplet Breakup for Impact Velocities Slightly Higher Than Critical Velocity	4-47
Figure 4-35. Graph of Normalized Incremental Numerical Distribution From Houghton's Data Against $4\sqrt{x}$	4-54
Figure 4-36. Comparison of Nukiyama and Tanasawa's Theoretical Curve with Normalized Incremental Numerical Distribution From Houghton's Data	4-55
Figure 4-37. Variation of the Residue \underline{R} With the Rate of Output \underline{M} for Various Screens	4-57
Figure 4-38. Bennett Diagram for Houghton's Cumulative Volume Distribution; (A) From Raw Data; (B) From Data Adjusted to Account for Upper and Lower Size Limits	4-59
Figure 4-39. Variation of dV/dx with \underline{x} for Various Values of \underline{n}	4-61
Figure 4-40. Variation of dN/dx with \underline{x} for Various Values of \underline{n}	4-62
Figure 4-41. Incremental Volume Distribution From Houghton's Data	4-64
Figure 4-42. Bennett Diagram for Houghton's Cumulative Volume Distribution, Using $x_0 = 7.5$ for Weibull's Equation	4-68
Figure 4-43. Log-Probability Graph of Houghton's Raw Data for Cumulative Volume Distribution	4-71
Figure 4-44. Standard Error Band for Log-Probability Graph of Houghton's Raw Data for Cumulative Volume Distribution	4-72
Figure 4-45. Best-Fit Straight Line Approximation to Houghton's Raw Data for Cumulative Volume Distribution as Determined by Brunt's Method	4-75
Figure 4-46. Log-Probability Graph of Houghton's Cumulative Volume Data, After Making Allowance for Size Limits, Using the Concept of Inner Percentages	4-76
Figure 4-47. Log-Probability Graph of Houghton's Cumulative Volume Distribution Data Using Special Upper Limit Function	4-79
Figure 4-48. Log-Probability Graph of Houghton's Cumulative Volume Data Using Limited Logarithmic-Normal Function	4-79
Figure 4-49. Comparison of Griffith's Theoretical Curve With Normalized Incremental Numerical Distribution From Houghton's Data	4-82
Figure 4-50. Correlation of Houghton's Cumulative Volume Distribution by Means of Roller's Function	4-84

LIST OF ILLUSTRATIONS

(Continued)

	<u>Page</u>
Figure 4-51. Comparison of Theoretical Curve Obtained, Using O'Toole's Method for a Bimodal Distribution, With Normalized Incremental Volume Distribution From Houghton's Data	4-85
Figure 4-52. Comparison of Theoretical Curve Obtained, Using O'Toole's Method for a Trimodal Distribution, With Normalized Incremental Volume Distribution From Houghton's Data	4-86
Figure 4-53. Comparison of Nukiyama-Tanasawa's and Griffith's Empirical Curves With Normalized Incremental Numerical Distribution From Houghton's Data	4-89
Figure 4-54a. Comparison of Empirical Curves With Houghton's Data on Cumulative Per Cent Undersize	4-90
Figure 4-54b. Comparison of Empirical Curves With Houghton's Data on Cumulative Per Cent Undersize	4-91
Figure 4-54c. Comparison of Empirical Curves With Houghton's Data on Cumulative Per Cent Undersize	4-92
Figure 4-55. Three Stages of Atomization	4-94
Figure 4-56. Spray Distribution Sampler	4-95
Figure 4-57. Geometrical Relations Used in Representing Spray Distribution	4-96
Figure 4-58. Pickup Element of the Rapid Spray Analyzer	4-98
Figure 4-59. Cylindrical Fuel Injector for Study of Spray Dispersion	4-100
Figure 5-1. Coordinate Systems for Axially Symmetric Flow	5-3
Figure 5-2. Uniform Flow Through a Disk	5-9
Figure 5-3. Formation of a Doublet From a Source and a Sink	5-9
Figure 5-4. Geometrical Relations of Two Approaching Spheres	5-16
Figure 5-5. Rotation of an Ellipsoid	5-21
Figure 5-6. Stream Lines and Their Orthogonal Trajectories in a Vertical Plane Through the Axis of a Falling Droplet	5-28
Figure 5-7. Streamlines Due to Oscillations of a Liquid Droplet	5-29
Figure 5-8. Wake Formation Behind a Sphere	5-32
Figure 5-9. The Drag Coefficient of Spheres as a Function of Reynolds Number	5-36
Figure 5-10. Drag Coefficient of Spheres and Drops	5-42
Figure 5-11. Terminal Velocities of Spheres and Drops	5-43

LIST OF ILLUSTRATIONS

(Continued)

	<u>Page</u>
Figure 5-12. Dimensionless Plot of the Preheating Time and the Velocity and Coordinates at the End of the Preheating Period	5-50
Figure 6-1. Various Types of Dispersion Systems Arising From an Injection of Liquid Droplets in a Gas Stream	6-2
Figure 6-2. Friction Factor as a Function of Reynolds Number for Fluid Flow Through Porous Carbon	6-7
Figure 6-3. Fixed-Bed Data of Wilhelm and Kwauk as Compared With Carman-Kozeny Curve and Leva Curve	6-8
Figure 6-4. Comparison of Burgers' and Steinour's Correction for the Settling Velocity of Dispersions	6-12
Figure 6-5. Concentration Decay Curves of a Settling Dispersion in a Horizontal Tube	6-14
Figure 6-6. Apparatus for Fluidization Studies	6-16
Figure 6-7. Characteristic Behavior of Fluidized Beds	6-17
Figure 6-8. Graph of Friction Factor Against Modified Reynolds Number for Fluidized Beds	6-18
Figure 6-9. Comparison of the Air Fluidization Data of Wilhelm and Kwauk With the Carman-Kozeny Curve	6-18
Figure 6-10. Collision Efficiency as a Function of the Falling Drop Radius and the Dispersed Droplet Based on Langmuir's Analysis	6-22
Figure 6-11. Comparison of Langmuir's Collision Efficiency Curve, $E(r)$, With Experimental Collection Efficiency Curve, $\bar{E}(r)$, Obtained by Gunn and Hitschfeld	6-23
Figure 6-12. Calculated Change in Concentration of Smoke Particles due to Radiation Pressure in a Standing Wave Field	6-25
Figure 7-1. The Range in Entropy of a Water Drop as a Function of its Radius	7-6
Figure 7-2. Relation of f and N to g	7-14
Figure 8-1. Rates of Evaporation of Dibutyl Phthalate Drops as a Function of Pressure	8-14
Figure 9-1. Geometric Representation of Droplet Evaporation Variables	9-9
Figure 9-2. Comparative Behavior of the Kronig and Kramers Correlations	9-16
Figure 9-3. Incremental Representation of Conduction and Evaporation in Second Period	9-21
Figure 9-4. Droplet Radius as a Function of Time for Five Liquids	9-23

Continued
LIST OF ILLUSTRATIONS
(Continued)

	<u>Page</u>
Figure 9-5. Comparison of Evaporation Dates of Several Liquids Under Isothermal and Conductive Behavior	9-24
Figure 9-6. Experimental Value of the Drag Coefficient as a Function of the Reynolds Number	9-28
Figure 9-7. Graphical Values of the Reduced Time as a Function of the Reynolds Number	9-31
Figure 9-8. Graphical Values of the Reduced Distance as a Function of the Reynolds Number	9-31
Figure 9-9. Graphical Solution to $\int \frac{d Re}{c_d Re^{1.5}}$	9-32
Figure 9-10. Quadrant of a Cylindrical Combustion Chamber With a Volume Element DV Moving Along its Axis	9-33
Figure 9-11. Correlation of Corrected Evaporation Rate of Aniline Against $Re^{1/2}$	9-47
Figure 9-12. Correlation of Corrected Evaporation Rate for Nitrobenzene Against $Re^{1/2}$	9-47
Figure 9-13. Mass Transfer for Evaporating Water Drops	9-49
Figure 9-14. Mass-Transfer Correlation for Evaporating Benzene Drops	9-50
Figure 9-15. Free Connection of Heat From Spheres. Correlation Line $Nu = 2.0 + 0.60 Pr^{1/3} Gr^{1/4}$	9-51
Figure 9-16. Composite Heat and Mass Transfer Correlations for Spheres	9-52
Figure 9-17. Schematic Diagram of Vaporization Apparatus	9-53
Figure 9-18. Correlation of Evaporation Rates for Nine Liquids	9-54
Figure 10-1. Per Cent of Spray Unevaporated as a Function of Evaporation Index	10-8
Figure 10-2. Deposition of Spray on the Walls of a Straight Duct at High Levels of Turbulence	10-15
Figure 10-3. Photographic Trace of Pressure-Time Relation for Successive Injections of Oil Sprays Into a Heated Bomb	10-18
Figure 10-4. Evaporation Fraction as a Function of Downstream Distance at Various Stream Velocities	10-21
Figure 10-5. Mean Spray Velocity as a Function of Downstream Distance	10-22
Figure 10-6. Spray Evaporation as a Function of Distance From Nozzle Under Turbulent Flow Conditions	10-23

LIST OF ILLUSTRATIONS
(Continued)

	<u>Page</u>
Figure 12-1. A Comparison of the Mixing Length Theories With Experimental Data of the Temperature Distribution in the Wake of a Heated Body of Revolution	12-8
Figure 12-2. Velocity and Concentration Profiles in a Jet of Nitrogen	12-13
Figure 12-3. Momentum Flux Density Profiles in a Jet of Air	12-13
Figure 12-4. Measured Values of the Correlation Coefficient, R_y , Behind a Grid	12-15
Figure 12-5. Measured Values of the Triple Correlation Coefficient, h , Behind a Grid	12-23
Figure 12-6. The Decay of Turbulent Intensity Behind a Grid	12-29
Figure 12-7. The Decay of the Turbulent Scale	12-30
Figure 12-8. Decay of the Microscale, λ	12-31
Figure 12-9. Decay of Turbulence Behind Grids of Differing Shapes	12-32
Figure 12-10. Stewart's Measurements of $S(r)$	12-42
Figure 12-11. The Shear Correlation, R_{12} , as a Function of Frequency	12-42
Figure 12-12. Comparison of Kolmogoroff's Theory With Experiment	12-44
Figure 12-13. Comparison of $f(r)$ Calculated From the Spectrum With Experimental Data	12-46
Figure 13-1. Flow Behind a Flat Plate at a Low Reynolds Number	13-2
Figure 13-2. The Formation and Discharge of Vortices From a Cylinder	13-2
Figure 13-3. Flow of a Nonviscous Fluid Around a Cylinder	13-3
Figure 13-4. Formation of Vortices Behind a Cylinder Moving From Rest With Constant Acceleration	13-4
Figure 13-5. Calculated Streamlines About a Sphere for $Re = 1$	13-6
Figure 13-6. Calculated Streamlines About a Cylinder for $Re = 4$	13-7
Figure 13-7. Recirculating Region Behind a Cylinder for Varying Reynolds Numbers	13-8
Figure 13-8. The Vortex Street	13-10
Figure 13-9. The Karman Vortex Street	13-10
Figure 13-10. Variation of Strouhal Number With Reynolds Number for a Circular Cylinder	13-11

LIST OF ILLUSTRATIONS
(Continued)

	<u>Page</u>
Figure 13-11. Vorticity Transport Parameter Plotted Against Strouhal Number . . .	13-13
Figure 13-12. Flow Patterns in an Ellipse, Single Entry With a Double Exit. Four Positions of the Unstable "Swinging" Jet	13-15
Figure 13-13. Streamlines Above a Wire With a Flat End, Wire Diameter 0.21 Cm . . .	13-16
Figure 13-14. Flow About a Rod	13-17
Figure 13-15. Vortex Shedding From a Flat Plate With an Attached Lean-Propane Flame ($Re \approx 9,000$)	13-19
Figure 13-16. Schematic Diagram of the Flow Pattern Behind a Flame Holder, Showing the High-Velocity Gradients Near the Flame	13-20
Figure 13-17. Shadowgraphs of the Vortex Formation Behind Rod Flame Holders. V is the Main Stream Velocity in Ft Per Sec; d , the Diameter of the Rod, and $1/f$ is the Mass Air-Fuel Ratio	13-21
Figure 13-18. Shadowgraph of V-Flame in Combustion Chamber. $d = 0.125$ In., $V = 15$ Ft Per Sec	13-21
Figure 13-19. Spin-Stabilized Oil Burner	13-23
Figure 13-20. Asymmetric Flame Holder	13-23
Figure 13-21. Combustor for General Electric 4800-Hp Locomotive Gas Turbine, for Residual Fuel Oil	13-24
Figure 13-22. Schematic Diagram of High-Velocity Burner	13-24
Figure 13-23. The Combustion Chamber of the Curtiss-Wright J-65	13-25
Figure 14-1. A Generalized Temperature Distribution Across the Flame Front . . .	14-2
Figure 14-2. Correlation Between Burning Velocity and Free-Radical Concentration .	14-9
Figure 14-3. Heat Release and Species-Formation Patterns	14-12
Figure 14-4. Burning Velocities of Propane-Air Mixtures as Obtained by Several Workers	14-14
Figure 14-5. Variation of Burning Velocity With the Distance r From Axis of Burner Tube	14-15
Figure 14-6. Variation in Burning Velocity With the Method and Position of Measurement	14-15
Figure 14-7. Change of Burning Velocity With Pressure	14-23
Figure 14-8. Variation of the Burning Velocity of an 8 Per Cent Ethylene-Air Mixture With the Fraction of Active Radicals	14-24
Figure 15-1. Photographs of a Turbulent Natural Gas - Air Flame	15-3

LIST OF ILLUSTRATIONS
(Continued)

	<u>Page</u>
Figure 15-2. Schematic Diagram of Distorted Flame Front	15-4
Figure 15-3. Advance of Flame in Distorted Front.	15-7
Figure 15-4. Combined Effect of Eddy Diffusion and Flame Propagation	15-8
Figure 15-5. Distortion of Stabilized Flames During Passage of Single Eddies	15-9
Figure 15-6. Schematic Diagram of Highly Turbulent Flame	15-9
Figure 15-7. Burning Velocity of Stretched Flame as a Function of Velocity Gradient	15-11
Figure 15-8. Schematic Diagram of Laminar Unstable Flame Front	15-16
Figure 15-9. Schematic Diagram of Turbulent Flame Front	15-20
Figure 15-10. Plot of K_{Tm} as a Function of f	15-21
Figure 15-11. Damköhler's Turbulent Burning Velocity Data	15-22
Figure 15-12. Turbulent Flame Velocities Calculated From Measured Flame Width	15-28
Figure 16-1. Effect of Tube Diameter on Pressure Flammability Limit (Low Concentration Part of Total Curves)	16-6
Figure 16-2. Limit Curve for Propane-Air as a Function of Pressure	16-7
Figure 16-3. Flammability Region of Propane ($O_2 + \alpha N_2$) Mixtures	16-7
Figure 16-4. Stabilization of a Combustion Wave in Laminar Flow	16-8
Figure 16-5. Temperature Profiles Between Cooling Surfaces	16-9
Figure 16-6. Critical Velocity Gradients for Methane, Propane, and Butane	16-13
Figure 16-7. Correlation of Blowout Data for Propane and Air	16-17
Figure 16-8. Correlation of Blow-Off Data for Various Fuels Using the Dezubay Factor, $V/d \cdot 85p^{.95}$	16-19
Figure 16-9. Correlation Curves for Flames Stabilized by a Bluff Body in a Premixed Gas Stream	16-26
Figure 17-1. Relation of Minimum Ignition Energy to Spark-Gap Spacing and Shape for Mixture Containing 8.5 Per Cent Methane in Air, at 250 mm Hg Absolute	17-8
Figure 17-2. Minimum Spark Ignition Energies in Millijoules of Propane, Oxygen, and Nitrogen at One Atmosphere Pressure and Lower, and Quenching Distances Between Flanged Electrodes for the Same Mixtures. Curves Correspond to Constant Ratios of Oxygen and Nitrogen	17-8

LIST OF ILLUSTRATIONS
(Continued)

	<u>Page</u>
Figure 17-3. Relation of Quenching Distance to Static Pressure for Methane, Propane, Butane, Hexane, Heptane, and Ethane With Air	17-9
Figure 17-4. Relation of Minimum Ignition Energy to Static Pressure for Hydrocarbon Fuels in Air	17-10
Figure 17-5. Relation of Minimum Ignition Energy to Quenching Distance for Hydrocarbon-Oxygen-Nitrogen Mixtures	17-11
Figure 17-6. Relation of Minimum Ignition Energy to Static Pressure for a Number of Compounds in Air	17-15
Figure 18-1. The Influence of the Distribution Factor on the Evaporative Process	18-3
Figure 18-2. The Distribution of Vapor Surrounding a Drop	18-4
Figure 18-3. The Temperature and Concentration Gradients in the Double Layer Film	18-11
Figure 18-4. The Combustion Rate of Kerosene Sprays	18-13
Figure 18-5. Comparison of the Spalding and the Wolfhard and Parker Analyses for the Burning Rates of Kerosene Droplets	18-15
Figure 18-6. Effect of Atomizing Velocity on Stability Limits	18-19
Figure 19-1. Laminar Diffusion Flames (Schematic)	19-2
Figure 19-2. Flame Shapes Calculated by Equation 19-3	19-2
Figure 19-3. Distribution of Gases in a Diffusion Flame	19-8
Figure 19-4. Temperature and Concentration Gradients at the Reaction Surface	19-8
Figure 19-5. Change in Flame Appearance With Varying Nozzle Velocity	19-10
Figure 19-6. Stability Ranges of Diffusion Flames for Carburetor-Type Jets	19-14

INTRODUCTION

Less than twenty years ago, workers in the field of combustion were divided into several groups, each functioning more or less independently of the others. There were those interested in the burning of solid fuels in beds, and those interested in the burning of these same fuels in pulverized form or in suspension. Some were interested in the burning of light fuel oils, principally for residential heating, while others were developing or improving burners and auxiliary equipment for the burning of the heavy fuel oils in boiler furnaces. Gas burners, both small and large, had been studied, burning velocities had been measured and the data used to design against flashback. The advantage of turbulent flames had been recognized and empirical burner designs were developed that permitted the use of such flames. Piston engines of the internal combustion type had been studied and the influence of fuel properties, defined by octane and cetane numbers, were well recognized. Some liquid-propelled rockets had been successfully fired. Finally, small groups, here and there, were tackling the intricate questions of combustion kinetics by ingenious if not always completely rewarding experiments. Then, reaction propulsion became a practical reality in the field of aeronautics.

Combustion engineers were immediately faced with the problem of supporting a flame in air streams moving at hurricane velocities, of releasing huge quantities of heat in small enclosures, and of ensuring that combustion would be completed before the hot gases passed to a turbine or nozzle. By dint of ingenuity, satisfactory solutions of a temporary nature were found to the problems of burner design for aircraft reaction power plants. However, the growing requirements for more speed and power in aircraft constantly place greater stress on the combustion art, so that a strong scientific basis for what may be called the unit processes of high duty combustion is needed. The processes of high duty combustion are now under intensive study, and the various segments of the previously separated fields of combustion research are becoming united. To the fields of science previously associated with combustion have been added those of aerodynamics and thermodynamics.

It was originally planned that this monograph would comprise an integration of the information in the various fields of science associated with combustion, and that the monograph would be a joint effort of several people working in the separate fields. However, it was soon discovered that even the uniting of the information in each of the separate fields from the viewpoint of combustion was a great task. Many of the contributions to the literature, especially from workers not directly concerned with combustion, were felt to be of great importance. On the other hand, the understanding of the total combustion problem is not yet at a state where relative importance can always be weighed. Thus, the evaluation of the literature by the authors of this monograph could not be as critical as was desired. In the light of the above discussed experience, the aim of the monograph was therefore altered from one of critically surveying and correlating this literature to one of bringing together descriptions of some of the more important findings relating directly or indirectly to understanding the fundamental physical phenomena involved in steady flow processes in high duty combustors.

Because the entire combustion process, from atomization to completion of combustion, takes place rapidly, and in a compact region, it is not usually possible in production-type combustion equipment to separate, time- and space-wise, all the various effects that follow one another and cooperate in the establishment of a stable flame. Thus knowledge of these effects must be obtained from separate studies sometimes far removed from combustion conditions. This monograph contains a review of the literature in a number of separate fields related in some degree to the combustion process. To systematize the presentation, the fields have been divided into six categories: I. Atomization of Liquid Fuels; II. Ballistics of Droplets; III. Evaporation of Droplets; IV. Fluid Dynamics; V. Homogeneous Combustion; VI. Heterogeneous Combustion. In each of these arbitrary classifications of the various unit processes in combustion, the subject matter has been further subdivided into chapters. The styles of the various chapters reflect the individuality and viewpoints of the different authors.

One of the challenges that faces workers in the field of combustion research is to provide the means for the extrapolation and the integration of data obtained with relatively slow transport or slow reaction processes, to represent conditions of high intensity combustion. It is hoped that this monograph will encourage further research to obtain data better suited for this difficult problem of extrapolation and integration, and that it will stimulate work on methods of using such data in design.

*This manuscript was released for publication by the authors May 1954.

"INJECTION AND COMBUSTION OF LIQUID FUELS"

CHAPTER 1. THE MECHANISM OF ATOMIZATION

ABSTRACT

The numerous theories postulated for the mechanism by which a jet of liquid is disintegrated into droplets are reviewed. Atomization generally takes place in three steps, (a) the initial disturbance of the surface of the jet of liquid, (b) the formation of ligaments which then break up into fragments, and (c) the further breakup of the fragments into smaller droplets. The problem of determining theoretically the form of disturbance that most rapidly leads to jet instability has been solved for several typical cases, based on a number of reasonable physical assumptions; but the ultimate problem of determining the drop-size distribution that finally results is far from solution. It has been established, however, that the most important factors that influence drop size are (a) nozzle design, (b) operating conditions, especially pressure, and (c) the properties of the liquid and of the air into which it is injected. The major consideration is the relative velocity between the liquid and the air.

Contracts

THE MECHANISM OF ATOMIZATION

by

J. M. Pilcher and C. C. Miesse

Atomization is the first and possibly the most important step involved in the combustion of liquid fuels in propulsion devices. The combustion of liquid fuel is a vapor-phase process, and to accelerate vaporization by breaking up the liquid into droplets of the proper size is the fundamental function of atomization. An additional and equally important function of atomization is to distribute the fuel particles throughout the combustion space. The distribution of droplets is the initial step in the mixing of the fuel with air. The three processes of atomization, vaporization, and mixing are, therefore, closely related. All three processes greatly affect the functioning of the fuel and combustion systems that Lucas⁽¹⁻¹⁾ calls the "heart and soul" of the aircraft turbine power unit.

The literature includes several hundred papers and reports on the atomization of liquids for many different uses, for example: agricultural and insecticidal sprays, therapeutic aerosols, internal-combustion engines, humidification and scrubbing operations, and sprays for drying solids suspended in liquids. In this monograph, however, the references on atomization will be restricted to literature related to the continuous injection of liquids into gases, as for jet engines and rockets; this is considered to include all fundamental studies of atomization, such as its mechanism, and the resulting drop-size distribution, regardless of application. The available literature is extensive, and care was exercised to select the most pertinent and useful references. Intermittent processes, such as diesel-fuel injection, and the injection of liquid into liquid, or of gas into either liquid or gas, will not be considered here.

The extent to which atomization increases the surface area of the liquid exposed to air is effectively illustrated by Joyce⁽¹⁻²⁾, who points out that the surface area of 1 cu cm of liquid in the form of a single sphere is only 4.83 sq cm; whereas the same volume of liquid in a normal spray containing 10 million particles, ranging from 5 microns up to 500 microns in diameter, has a surface area that may range up to 1200 sq cm. The surface area of a given weight of liquid is inversely proportional to the diameter of the droplets.

The energy of the surface of the droplets, as determined by multiplying the surface of the droplets by the surface tension of the liquid, is small; however, because the efficiency of atomization is usually less than one per cent, considerable energy is required to accomplish a high degree of atomization.

The influence of spray particle size and distribution in the combustion of oil droplets is emphasized by Probert⁽¹⁻³⁾, who showed that by far the most important characteristic of a spray is the size constant of the Rosin-Rammler relation, whereas the distribution constant has a marked effect on the time required for complete evaporation of the spray. These considerations will be enlarged upon later.

Before going into a discussion of the mechanisms of atomization, the meaning of a few terms peculiar to the art will be discussed. The term "atomization", according to Romp⁽¹⁻⁴⁾, was probably introduced in 1875 by Commander Isherwood, of the American Navy, who made a study of oil burning for naval purposes. The etymology of the word, as explained by Castleman⁽¹⁻⁵⁾, implies the formation of drops so fine as to be indivisible. Such a concept has a definite physical significance for liquid jets, Castleman claims, because of a limit in drop fineness that is reached. However, the existence of a lower size limit of about seven microns is a controversial matter that is discussed later in the following section on Physical Processes that describes various mechanisms of atomization. Since "atomization" means the formation of very fine droplets, Castleman recommends that the term "disintegration" be used when the drop sizes are larger than the limiting value that he claims does exist. Although "atomization", in the connotation of "reducing liquid to

atoms", is a very exaggerated term for the formation of sprays of liquids, it is, nevertheless, a term now generally used in all English-speaking countries and will be used here.

The recent literature tends to make a distinction between "atomizing nozzles" and "spray nozzles". The former are two-fluid or pneumatic-type atomizers that use air or steam to accomplish atomization, and the latter are pressure-type nozzles in which the pressure on the liquid supplies the energy for "breakup". The use of the adjective "atomizing" for two-fluid nozzles probably results from the fact that smaller droplets usually are formed with them than with the pressure-type "spray nozzles".

To summarize the terminology: "breakup" refers to the initial breaking up of a liquid jet; "disintegration" implies the formation of more or less coarse drops; and "atomization" means the formation of very fine droplets.

From the practical point of view, Mock and Ganger⁽¹⁻⁶⁾ claim that the achievement of a high degree of atomization and evenness of distribution, particularly at low fuel rates, are major needs in the field of fuel-spray nozzles for gas-turbine power plants. Similarly, Lawrence⁽¹⁻⁷⁾ states that a highly atomized fuel is required under idling conditions at altitude when the fuel flow rate is least.

PHYSICAL PROCESSES

Numerous theories have been postulated concerning the mechanism by which a liquid jet breaks up, disintegrates, and is atomized; in many instances the various writers do not agree. Much of the disagreement is attributed to two facts: (a) the mechanism by which atomization is accomplished is quite different for different conditions; and (b) atomization may, and usually does, take place in successive stages involving more than one single mechanism. There is general agreement, however, on one point: the atomization of a liquid is an extremely complicated process.

The actual physical steps involved in the transformation of a liquid into droplets have been studied principally with the aid of high-speed photography. The purely theoretical analyses that have been made will be reviewed more thoroughly in the succeeding section entitled, "Theoretical Analysis of Jet Instability and of Secondary Atomization".

The most logical order for the discussion of physical mechanisms is a chronological one that shows how the thinking has progressed from the time of the early work of Lord Rayleigh, in 1878, to the present.

Rayleigh⁽¹⁻⁸⁾. The classical work of Lord Rayleigh was the first theoretical investigation concerning the breakup of liquid jets. Rayleigh very properly treated the problem as one of instability resulting from two causes. The first is operative in the case of jets of heavy liquids, as for water projected into air, and is due to capillary force, or surface tension, which renders the cylinder unstable and favors its breakup into detached masses of larger diameter, the aggregate surface of which is less than that of the cylinder. The principal problem here was to determine the wavelength of the disturbance from which may be determined the number of masses into which a given length of jet may be expected to distribute itself. Rayleigh showed that the growth rate of the disturbance caused by surface tension was at maximum when the wavelength was 4.508 times the diameter of the jet. The size of drops formed would then be slightly less than twice the size of the nozzle opening.

The second cause of instability, which operates even when the jet and its environment are of the same material, is dynamical in character and has its origin in the general translatory motion of the jet. Lord Rayleigh's mathematical treatment of this dynamic effect, illustrated by the influence of wind on waves in water, will be reserved for the theoretical analyses of atomization in the next section. A point to be kept in mind, when considering Rayleigh's excellent contribution to

a better understanding of the mechanism of disintegration, is that his theoretical work provides a basis for computing the initial size of the droplets into which a low-velocity jet will disintegrate, but it in no way explains the complicated mechanism of the limiting form of disintegration, namely atomization, which is of much greater practical significance in combustion systems.

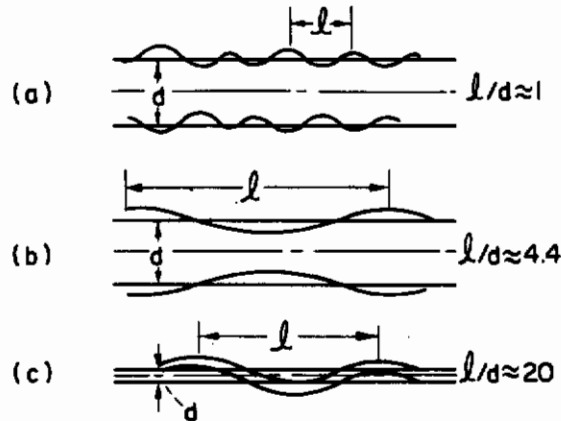


FIGURE 1-1. SURFACE DISTURBANCES
 (a) and (b) Rotationally symmetric
 (c) One-sided wavelike
 (Haenlein)¹⁻⁹

Haenlein⁽¹⁻⁹⁾ and Weber⁽¹⁻¹⁰⁾. Haenlein made an experimental investigation of the process of disintegration and atomization in its simplest form, and his results were then treated analytically by Weber. Haenlein's shadow pictures showed five characteristic forms of disintegration as follows:

(1) Surface disturbances resulting from imperfections in the jet, from vibrations of the nozzle, or from particles of dust or from air bubbles.

Figures 1-1(a) and 1-1(b) show the most important rotationally symmetric disturbances and Figure 1-1(c) shows the one-sided wave-like disturbances that occur in different places. The ratio of the wavelength to the jet diameter l/d is characteristic of its effect on the jet. The initial disturbances occur simultaneously and overlap one another. These disturbances increase or decrease according to the forces acting on them, and thus lead to the disintegration of the jet.

(2) Drop formation without the influence of the surrounding air occurs at low velocities, when the air does not appreciably affect the shape of the jet. The only disturbing force then acting on the jet is the surface tension, which causes the jet to become unstable because of rotationally symmetric disturbances, and to break up into drops as described by Lord Rayleigh⁽¹⁻⁸⁾. Rayleigh, it will be remembered, found that the drops were formed most easily when the disturbance gave a ratio of l/d equal to about 4.5. Haenlein, however, found that, for viscous liquids, this ratio was somewhat greater, and that ratios were as high as 30 to 40 for castor oil. If it is assumed that the initial disturbances are of uniform magnitude, a constant disintegration time elapses from the beginning of the disturbance to the formation of a drop. Consequently, a definite disintegration length, L , is developed until a drop is cut off, which length increases in proportion to the velocity.

Figure 1-2(a) represents the disintegration of a jet without air influence for an initial disturbance of $l/d = 4.42$. Since the initial disturbances actually fluctuate, the disintegration length of constant velocity is not perfectly constant, but oscillates about a mean value, and the differences in the disturbances may be so great that the jet will be simultaneously broken up into drops at several points.

(3) Drop formation with the influence of air is shown in Figure 1-2(b). The aerodynamic forces act similarly to wind blowing over water and produce a definite initial disturbance. The air velocity increases over the wave crests and decreases over the troughs. At the same time, the pressure decreases over the crests and increases over the troughs so that the wave motion is intensified and drops are formed.

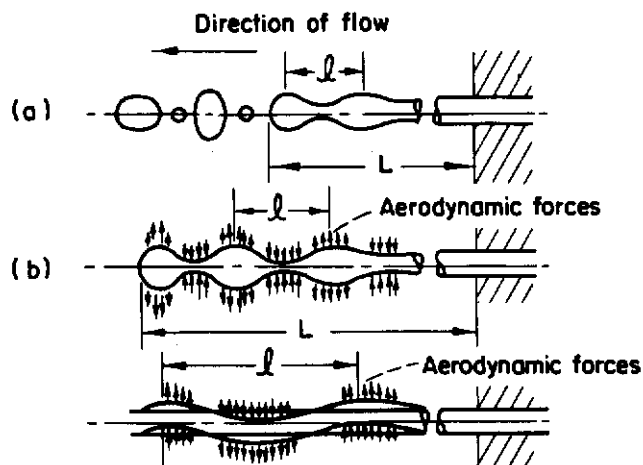


FIGURE 1-2. DISINTEGRATION PHENOMENA
 (a) Drop Formation Without Air Influence
 (b) Drop Formation With Air Influence
 (c) Wave Formation Through Air Influence

(Haenlein)¹⁻⁹

(4) Wave formation due to the action of air occurs when the velocity is further increased, and the initial disturbances become one-sided under the augmented influence of the air, as shown in Figure 1-2(c). The one-sided disturbances seem to be trying to bend the jet, and develop more rapidly than the rotationally symmetric disturbances, as shown in Figure 1-2(b). Surface tension has a retarding effect on wave formation by tending to return the jet to its original form with the minimum surface tension.

(5) Complete disintegration of the jet occurs when the velocity is further increased, and the jet loses all regularity of form. The liquid flowing from the nozzle is broken up in a chaotic and entirely irregular manner under the influence of the air; however, Haenlein offers no explanation concerning the mechanism of this last and most important form of disruption of the jet.

The transitions between the different jet forms take place gradually, so that the formation of drops and of waves, or of waves and complete disintegration of the jet, may take place simultaneously.

Weber made a theoretical investigation, which is discussed in the next section, in which he derived mathematical relations that in character agree with the experimental results of Haenlein.

Castleman⁽¹⁻⁵⁾⁽¹⁻¹¹⁾. The actual process of atomization, according to Castleman, is rather simple and is explained by his "ligament theory". A portion of the large mass of liquid is caught up by the air and, being anchored at the other end, is drawn out into a fine ligament. This ligament is quickly cut off by the rapid growth of a dent in its surface, and the detached mass, being quite small, is quickly drawn up into a spherical drop. Atomization occurs at the surface under

the influence of the relative motion of gas and liquid, and the physical mechanism is identical whether atomization takes place in an air stream or accompanies solid injection. According to Castleman, a minimum drop size is reached at an air speed of about 330 to 400 ft per sec. The minimum diameter that he reported for water droplets was about 10 microns when atomized in a high-speed air stream. Diameters of 7 to 8 microns were found for the smallest droplets of gas oil atomized by solid injection into air of atmospheric density. This compares favorably with the mean diameter of about 7 microns found by Sauter⁽¹⁻¹²⁾ in the high-speed air-stream atomization of kerosene, which has a surface tension about the same as that of gas oil. The size of the smallest drops was observed to be practically independent of the injection pressure, and, since a spray becomes more homogeneous the higher the relative air speed, the mean drop size approaches the minimum. In other words, a higher degree of atomization means that a greater percentage of the droplets are of the smallest size, not that the smallest droplets are any smaller.

Figure 1-3 shows spark photographs of continuous sprays at injection pressures varying from 30 psi to 1500 psi. These photographs, obtained by Lee and Spencer⁽¹⁻¹³⁾, tend to support Castleman's theory in that they indicate ligament formation as an intermediate step in the detachment of a small drop from a large mass of liquid, the ligaments extending from the unatomized mass in the direction of relative motion, and appearing to decrease in size and length as the relative air speed is increased.

Castleman considers that Haenlein's explanation of atomization as a result of increase in waviness is insufficient, and that the small drops are formed only by means of ligaments torn from the main mass. A difference in the methods for producing the sprays used by Haenlein and by Castleman may account for this difference of opinion concerning the physical mechanism of atomization.

Lee and Spencer⁽¹⁻¹⁴⁾. A large number of excellent photomicrographs of fuel sprays were taken by Lee and Spencer, who studied the structure of sprays and the process of spray formation. These investigators supported the theory advanced by Castleman, and observed that with injected sprays, the fuel leaves the nozzle as an unbroken column, becomes ruffled, and then is torn into small irregular ligaments by the action of air. The ligaments are then quickly drawn up into drops by the surface tension of the fuel. They learned further that turbulence accelerates the disintegration of the fuel jet by ruffling its surface close to the orifice, but turbulence has relatively small disintegrating power in itself. They found that the degree of disintegration of the jet increases with the distance from the nozzle, the air density, the fuel velocity, or the fuel turbulence, but decreases with an increase of fuel viscosity, surface tension, or nozzle-orifice diameter.

Figure 1-4 is an excellent illustration of three of the forms of jet disintegration described by Haenlein, caused by rotationally symmetric and wave-like disturbances. In Figure 1-4(a) the jet velocity is so low that the air plays no part, and the fuel column is separated into drops solely by the forces of surface tension.

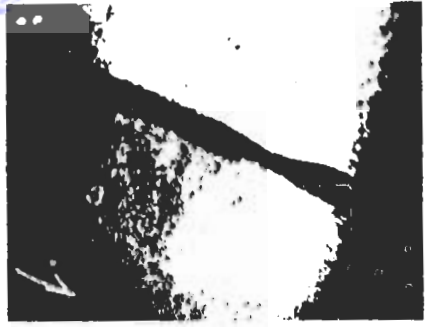
In Figure 1-4(b), taken at higher magnification than (a), the jet velocity has been increased until the aerodynamic forces also play a part in the disintegration of the jet.

In Figure 1-4(c) the jet velocity is still greater, and waves have been formed in addition to the rotationally symmetric disturbances. These waves are also the result of aerodynamic forces, and at the higher velocities they develop more rapidly than do the rotationally symmetric disturbances, causing the jet to be broken into many irregular parts.

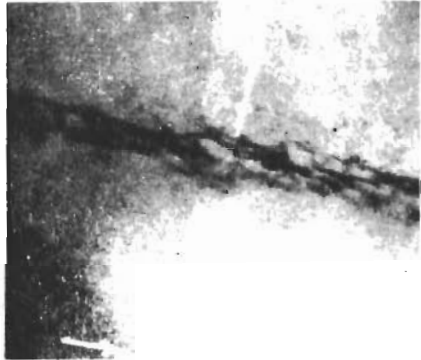
Figure 1-5 shows the progressive effect of the various forces acting on the fuel jet at increasing distances from the nozzle. The jet issuing from the orifice contains slight irregularities that may be caused by fuel turbulence, imperfections in the nozzle, or by vibrations of the nozzle. These irregularities are accentuated by the action of air until the jet consists of many irregular parts; these parts are then drawn out into ligaments by further action of the air, and the ligaments subsequently collapse to form drops.



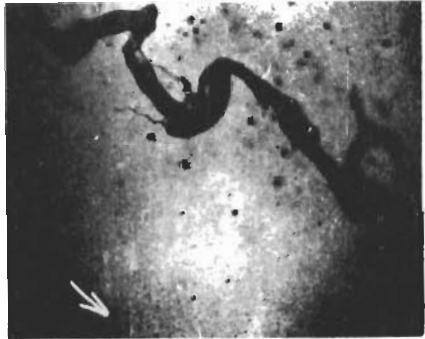
Injection pressure 100 psi



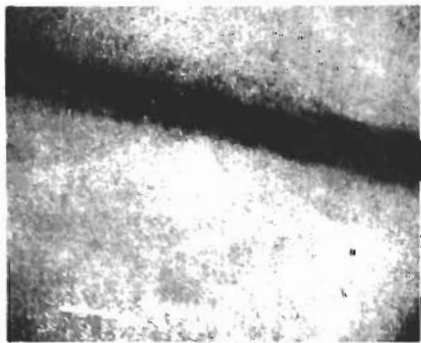
Injection pressure < 30 psi



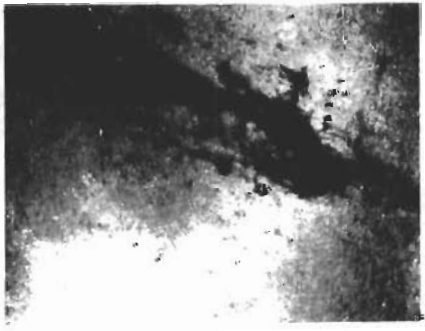
Injection pressure 750 psi



Injection pressure 200 psi



Injection pressure 1,500 psi
0.008-in. orifice diameter
15/16 in. from orifice



Injection pressure 700 psi
0.020-in. orifice diameter
4-3/4 in. from orifice

FIGURE 1-3. CONTINUOUS SPRAYS AT VARIOUS INJECTION PRESSURES.
NACA SPARK PHOTOGRAPHS (Lee and Spencer) ¹⁻¹³

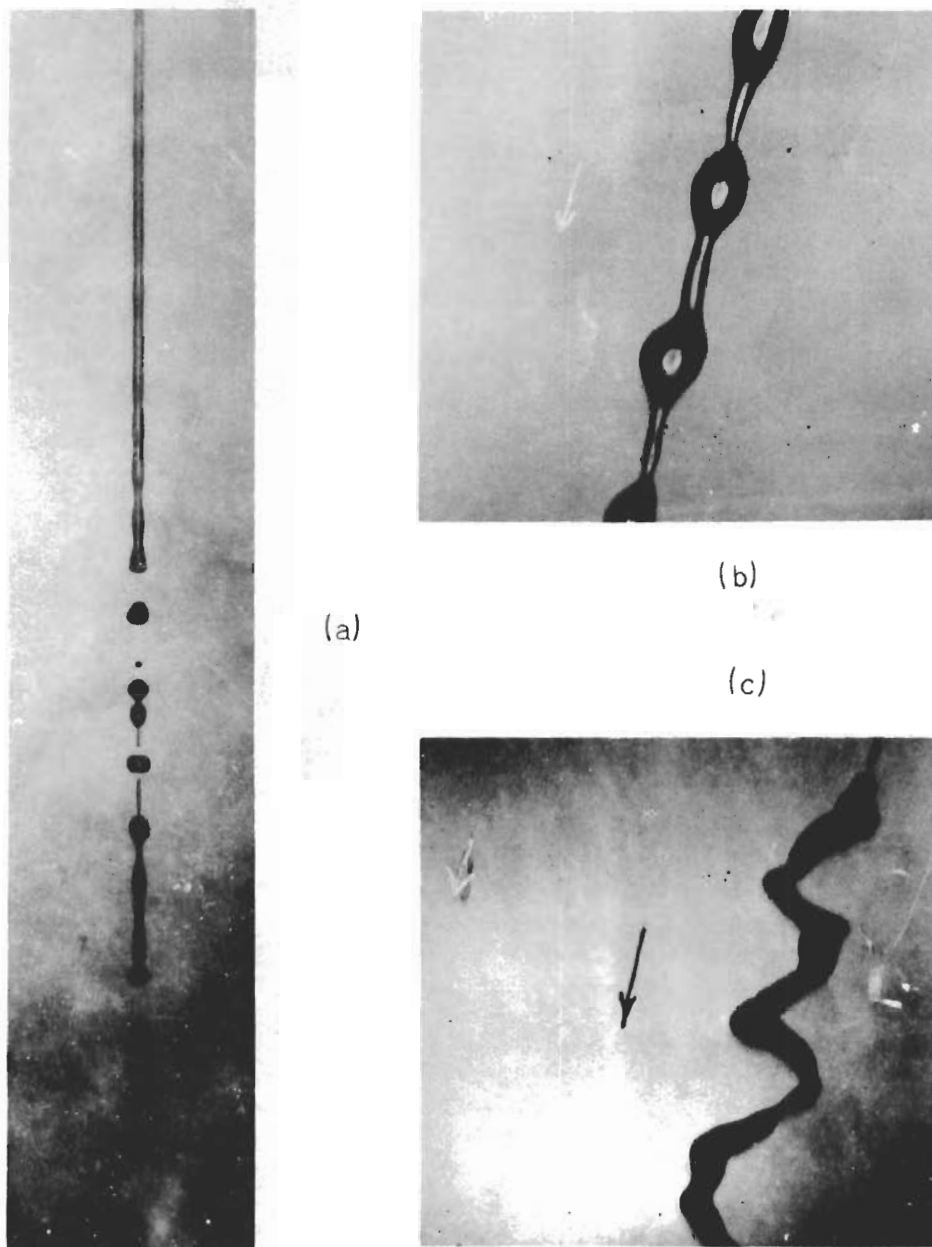
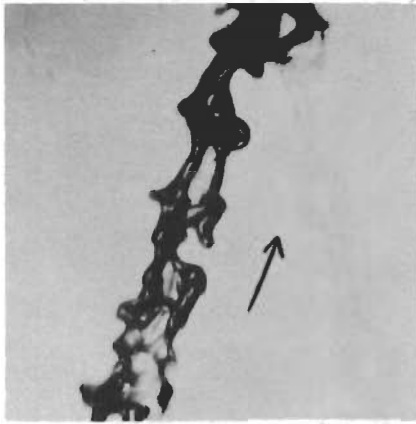


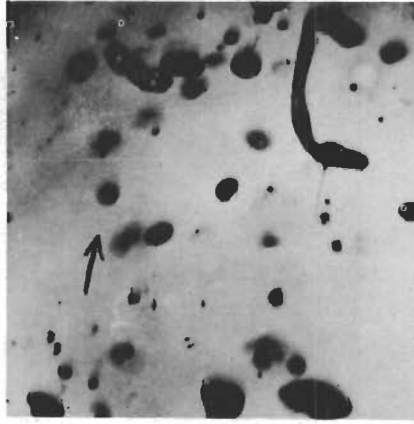
FIGURE 1-4. FORMS OF JET DISINTEGRATION DESCRIBED BY HAENLEIN 1-9

- (a) Rotationally Symmetric Disturbances Without Air Influence, x3.25. Injection Pressure Less Than 10 Pounds per Square Inch
- (b) Rotationally Symmetric Disturbances With Air Influence, x10. Injection Pressure, 50 Pounds per Square Inch
- (c) Wave Formation, x10. Injection Pressure, 100 Pounds per Square Inch (Lee and Spencer) 1-14

Contrails



3 inches from nozzle



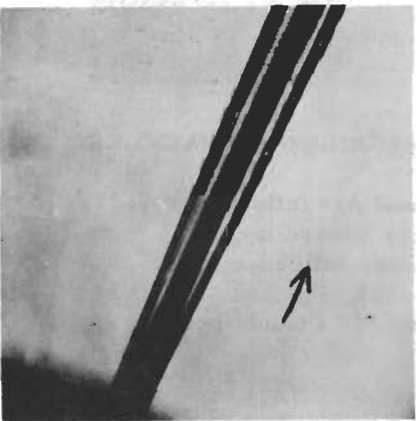
10 inches from nozzle



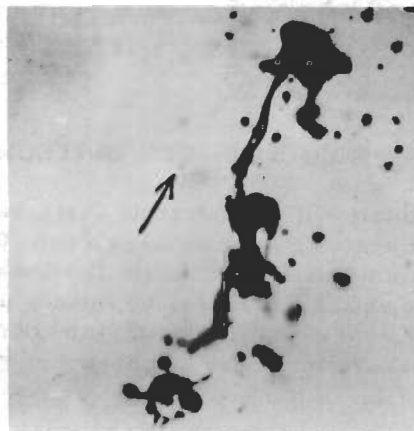
1 inch from nozzle



7.5 inches from nozzle



At the nozzle



5 inches from nozzle

FIGURE 1-5. PHOTOMICROGRAPHS OF A LOW-VELOCITY FUEL JET AT DIFFERENT DISTANCES FROM THE NOZZLE

Injection Pressure, 100 psi; Orifice Diameter, 0.020 inch; Air Density, 1 atmosphere (Lee and Spencer) 1-14

Figure 1-6 shows that, as the air density is increased, the degree of disintegration of the jet at a given distance from the nozzle becomes greater, and the sizes of the fuel particles are apparently reduced. Substantially the same results may be obtained, however, by keeping the air density constant and increasing the distance from the nozzle. Thus, the disintegration process is not completed immediately, but continues as long as the fuel retains enough velocity to be acted upon by the air. In dense air, the process is more quickly carried to the limits obtainable with the jet velocity being used, but in air of low density, the jet loses velocity more slowly and travels farther; in both cases the final effect is the same.

Figure 1-7 shows the effect of injection velocity on the disintegration of fuel jets. As the injection velocity is increased, the disintegrating forces which result from air action and from jet turbulence increase. At 20 psi, when these forces are slight, the entire jet is seen in the initial form of jet disintegration. At higher injection velocities the irregular surface is accentuated by air action and the fuel is divided into smaller and smaller parts until the air forces can no longer overcome the resistance forces due to the surface tension and viscosity of the fuel. These smallest parts then collapse to form drops.

Figure 1-8 shows the qualitative effects of viscosity and surface tension on spray formation at an injection pressure of 1500 psi. The degree of disintegration of the jet is seen to decrease as the viscosity is increased. With water, the increased surface tension (68 dynes per cm, compared with 21 for gasoline and 24 for ethyl alcohol) causes a noticeable reduction in the degree of jet disintegration. However, for the minor differences in surface tension among the various fuels (21 to 31 dynes per cm), the effect is negligible.

This photographic study by Lee and Spencer has been a valuable contribution to a better understanding of the physical mechanism of atomization.

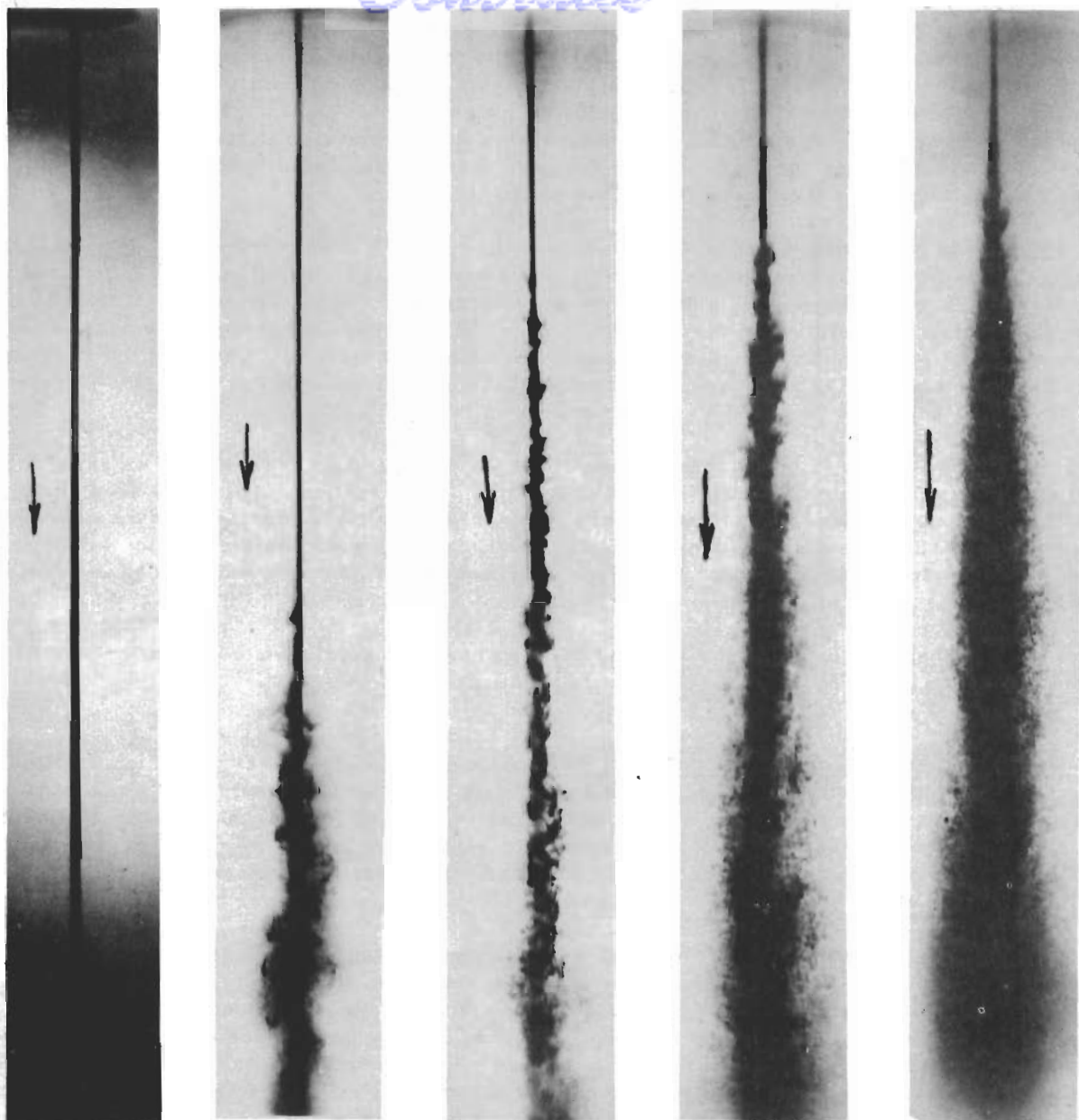
DeJuhasz, Zahn, and Schweitzer⁽¹⁻¹⁵⁾⁽¹⁻¹⁶⁾. According to Schweitzer, turbulence is the dominant factor influencing atomization and, for high-velocity jets, surface tension plays a subordinate role. He points out that air friction cannot atomize a laminar jet so long as the velocity distribution adjacent to the skin remains parabolic, dropping to zero at the periphery. However, the combined effects of air friction and surface tension eventually give rise to surface irregularities that lead to disintegration of the jet.

Schweitzer describes three types of flow of liquid through the nozzle orifice, namely, turbulent, semiturbulent, and laminar. If the flow is turbulent in its entirety, the orifice wall is bombarded by liquid particles having radial velocity components and, as soon as the restraint of the orifice wall ceases, the particles are kept in bounds only by the surface film which may soon break, resulting in a general disruption of the jet. A laminar layer may retard this disintegration only for a short period. When a jet is turbulent throughout, no air friction is necessary for dispersion, but high air pressure does improve dispersion.

If the jet is semiturbulent, consisting of a turbulent core and a laminar envelope, the laminar envelope will prevent turbulent liquid particles from passing the surface and prevent any action on the part of air friction, so that no disintegration will take place adjacent to the orifice exit. However, the more rapidly moving turbulent core will soon forge ahead of the laminar envelope, and breakup will occur after the jet has traveled the required breakup distance. For a purely laminar jet, a greater breakup distance will precede disintegration.

Schweitzer admits that, in all three conditions, high air friction acts in favor of disintegration, but that an ever-so-small surface disturbance is always present, even in laminar jets, to give the air stream an opportunity to tear off small masses of liquid which quickly form drops. Surface tension tends to heal up minor surface disturbances, whereas air friction tends to tear the jet further apart.

To summarize Schweitzer's concept of the mechanism of disintegration, an actual jet will ordinarily disintegrate under the combined influence of liquid turbulence and air friction. If the inherent liquid turbulence is sufficiently high, it will disperse the jet, unaided, close to the orifice.



(a) 0.0013 atm

(b) 1 atm

(c) 4.4 atm

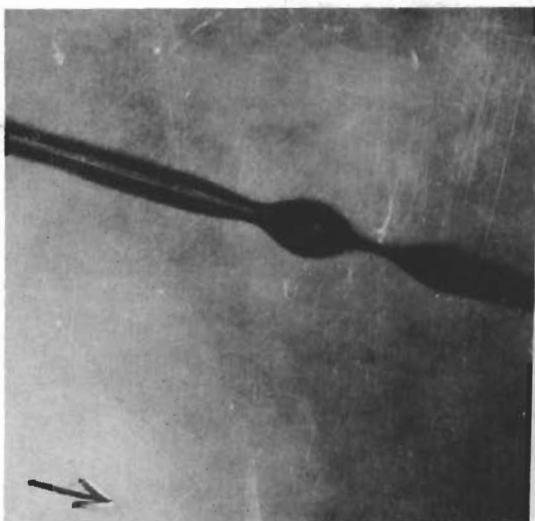
(d) 7.8 atm

(e) 14.5 atm

FIGURE 1-6. EFFECT OF AIR DENSITY ON FUEL JETS

Effective Injection Pressure, 250 psi; Orifice Diameter, 0.020 inch; Fuel Viscosity, 0.130 poise at 22 C (Lee and Spencer) ¹⁻¹⁴

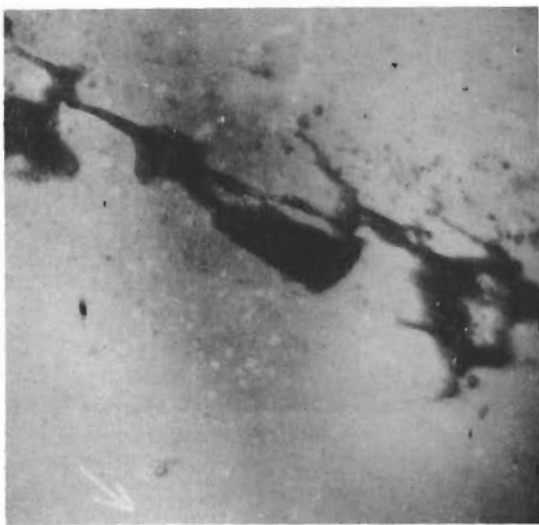
Contrails



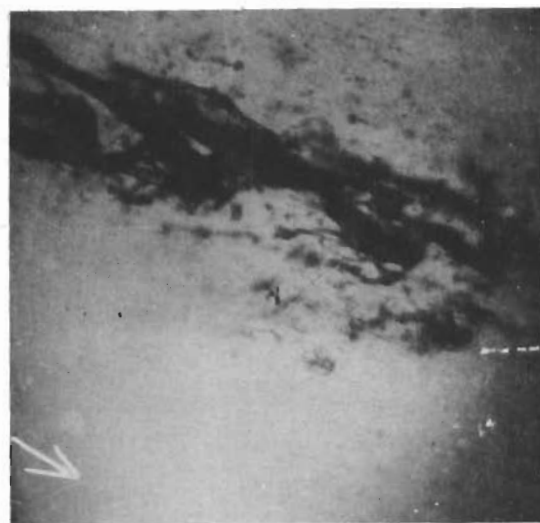
20 pounds per square inch



200 pounds per square inch



300 pounds per square inch



900 pounds per square inch

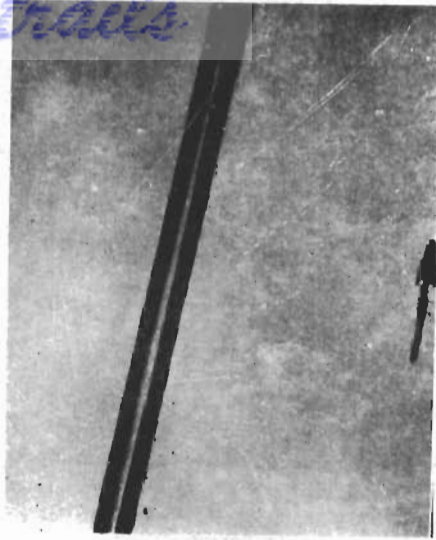
FIGURE 1-7. EFFECT OF INJECTION PRESSURE ON JET DISINTEGRATION

Orifice Diameter, 0.020 inch; Air Density, 1 atmosphere;
Distance From Nozzle, 4.75 inches (Lee and Spencer) 1-14

Contracts



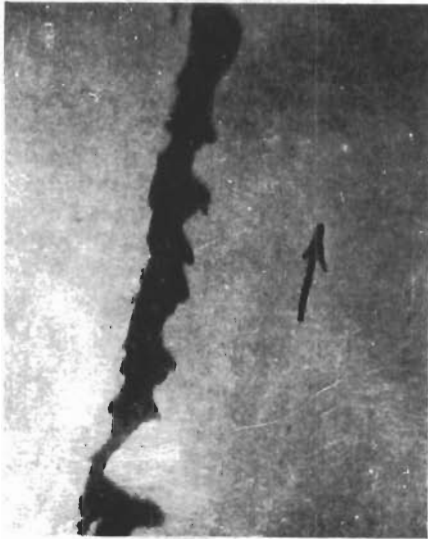
Ethyl alcohol



Lubricating oil



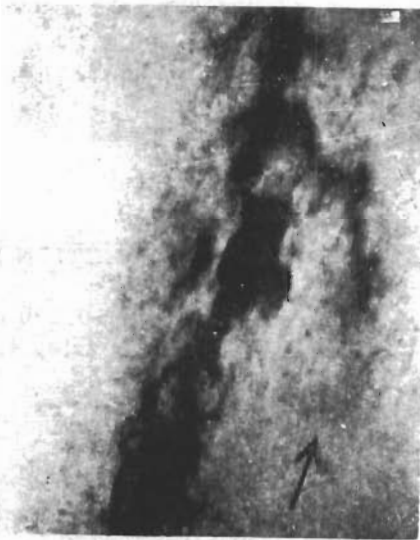
Water



Diesel fuel No. 2



Gasoline



Diesel fuel No. 1

FIGURE 1-8. JETS OF VARIOUS LIQUIDS INJECTED AT 1500 PSI

Orifice Diameter, 0.020 inch; Air Density, 1 atmosphere;
Distance From Nozzle, 5 inches (Lee and Spencer) 1-14

Laminar or semiturbulent jets also disintegrate quite rapidly while moving in dense air with high velocity, but not before traversing a definite breakup distance.

The chief concept introduced by Schweitzer is the extremely important role played by turbulence, from which he concludes that viscosity is the most important liquid property that influences jet disintegration.

Tyler⁽¹⁻¹⁷⁾. Using spark photographs, Tyler measured the wavelengths and sizes of drops formed when a cylindrical column of liquid moving at low velocity breaks up. His measurements of wavelength agree well with the theoretical value of 4.5 times the jet diameter, as developed by Rayleigh. In addition to verifying Rayleigh's theory, Tyler observed that these slowly moving drops do not at once assume and retain the spherical form, but execute a series of vibrations, being alternately compressed and elongated in the direction of the axis of symmetry.

Romp⁽¹⁻⁴⁾. A kinematic analysis of the movement of liquid fuel in the swirl chamber of a simple pressure atomizer is given by Romp. In view of the fact that this method of atomization is of the greatest practical importance, it will be worth while to consider in some detail the mechanism by which atomization is achieved.

Figure 1-9 shows the simple scheme of a cylindrical orifice and a cylindrical swirl chamber into which the fuel enters through a tangential slot. Assuming the liquid to be frictionless, the particles are subjected to two simultaneous movements: (1) a spiral motion from the outer wall of the swirl chamber to its center, which takes place in planes at right angles to the axis; and (2) a translatory motion parallel to the nozzle axis, which forces the liquid to travel through the orifice. In addition, the particles may possess individual rotations, thus spinning around their own centers.

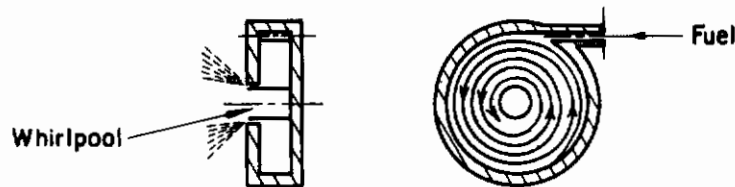


FIGURE 1-9. SIMPLE SCHEME OF A SWIRL CHAMBER (Romp)¹⁻⁴

Comparing the flow of the liquid through the swirl to the winding up of a ribbon, the rotational velocity increases rapidly towards the center, and, for a frictionless liquid, the product of rotation velocity and radius is constant through the swirl chamber, as inferred by Bernoulli's theorem. Thus, if the tangential velocity of an oil particle somewhere in the swirl chamber at a diameter of 1 inch is equal to 1 ft per sec, its velocity must be increased to 10 ft per sec if it is moved to a diameter of 0.1 inch in order for the momentum to remain constant. Although this simple relation, as applied to frictionless liquids, becomes more complicated for real liquids, the general conclusion still holds good in principle.

In order to picture the important function of the swirl chamber without becoming involved in mathematics, Romp proposed four successive stages of development by which the spiral motion of the oil may be established. (1) Disregarding gravity and assuming laminar flow of liquid between straight parallel walls, the velocity will be uniform and the pressure drop will be simply determined according to Poiseuille's law. (2) In the second stage, this ribbon-like flow of liquid is wound up into a spiral form that results in no appreciable change in flow conditions, as the centrifugal action causes only a slight increase in pressure at the outer wall and slight decrease in pressure at the inner wall of the ribbon. (3) In the third stage, the walls may be considered as being perfectly flexible, so that the small pressure differences caused by centrifugal action are allowed to build up a larger total pressure difference between the center and the outermost wall of the spirally-wound ribbon. This pressure tends to reduce the quantity of liquid flowing, and a higher initial pressure will be required than in the second stage. This increased pressure

includes an increase in energy which, not being required to make up for friction losses, must be converted into kinetic energy according to the Bernouilli theorem. (4) In the last stage, the imaginary flexible walls may be considered removed, in which case the only change in the conditions of flow will be that the external friction losses caused by the contact of liquid with the walls of the ribbon will be replaced by the internal friction losses of the liquid caused by the velocity differences of neighboring layers; the only consequence will be that the "Poiseuille pressure" will be replaced by the "internal friction pressure".

The liquid particles move towards the center against the artificial field of gravitation created by centrifugal action, and obtain a higher potential energy, by storage of kinetic energy that may be used for atomization as soon as the liquid has been set free. Thus, the swirl chamber serves to convert as much as possible of the initial pressure into velocity.

This analysis shows the great importance of the viscosity factor, especially since the internal friction of the layers of fuel moving in the swirl chamber determines how much of the initial pressure will be available for conversion into velocity.

It should be pointed out here that the droplets do not move in spiral orbits through the combustion chamber, as sometimes claimed, but follow straight lines, provided the air is motionless. Of course, a spiral movement of the combustion air will take the droplets with it, but the idea of giving the air a rotary motion opposite to the rotary motion of the liquid in the spray nozzle, in order to improve mixing, is not based on clear theoretical views.

Nukiyama and Tanasawa⁽¹⁻¹⁸⁾. Three successive stages in the atomization of a liquid jet by an air stream are delineated by Nukiyama and Tanasawa.

Figure 1-10 shows sketches prepared from photographs representing the three stages as follows: (1) Dropwise atomization. At very low air velocities, the relative motion between the air and the liquid streams produces bead-like swellings and contractions with continuously increasing amplitude, until the liquid jet finally breaks up into several separated drops, as shown in (1) and (2) of Figure 1-10. (2) Twisted ribbon-like atomization. If the velocity of the air is somewhat increased, the fluttering action of the jet begins, forming the shape of a twisted ribbon of liquid. A portion of the ribbon is caught up and drawn out into a fine ligament as shown in (3) and (4), and as described by Castleman. (3) Filmwise atomization. A still further increase in the air velocity causes the flattening action of the horizontal part of the twisted ribbon, and thus forms a cobweb-like film, which is so thin that it tears itself apart and diffuses into microdroplets as shown in (5) and (6). Increase of the air velocity gradually increases the number of films, at the same time making them smaller, and filmwise atomization occurs as shown by (7) and (8).

Fogler and Kleinschmidt⁽¹⁻¹⁹⁾. In a study of spray drying, Fogler and Kleinschmidt describe the mechanism of spray formation as the dragging out of the liquid into thin flat sheets or filaments which, under the combined action of surface tension, internal viscous forces, and turbulence in the surrounding medium, break up into particles. This is quite similar to Castleman's theory; however, they point out that the characteristics of particles formed from the breaking up of films or sheets of liquid are essentially different from those of particles formed by the breaking up of filaments or threads.

The mechanism by which a film breaks up into drops is compared to that of a flag flying in the breeze. The waves in the film build up very rapidly and cause an actual whipping of the surface so that it curls back on itself until the surface may actually join in a hollow tube. Such a tube immediately breaks off and, since it is statically unstable, necks down in places and breaks into a series of hollow spheres. Fogler and Kleinschmidt demonstrated experimentally this tendency of film-forming nozzles to form hollow particles.

Siestrunck⁽¹⁻²⁰⁾ and Littaye⁽¹⁻²¹⁾⁽¹⁻²²⁾⁽¹⁻²³⁾. Siestrunck made a study of the way in which a liquid jet breaks up when it is introduced into an air current of high velocity. He concluded that breakup was principally determined by the agitation of the air.

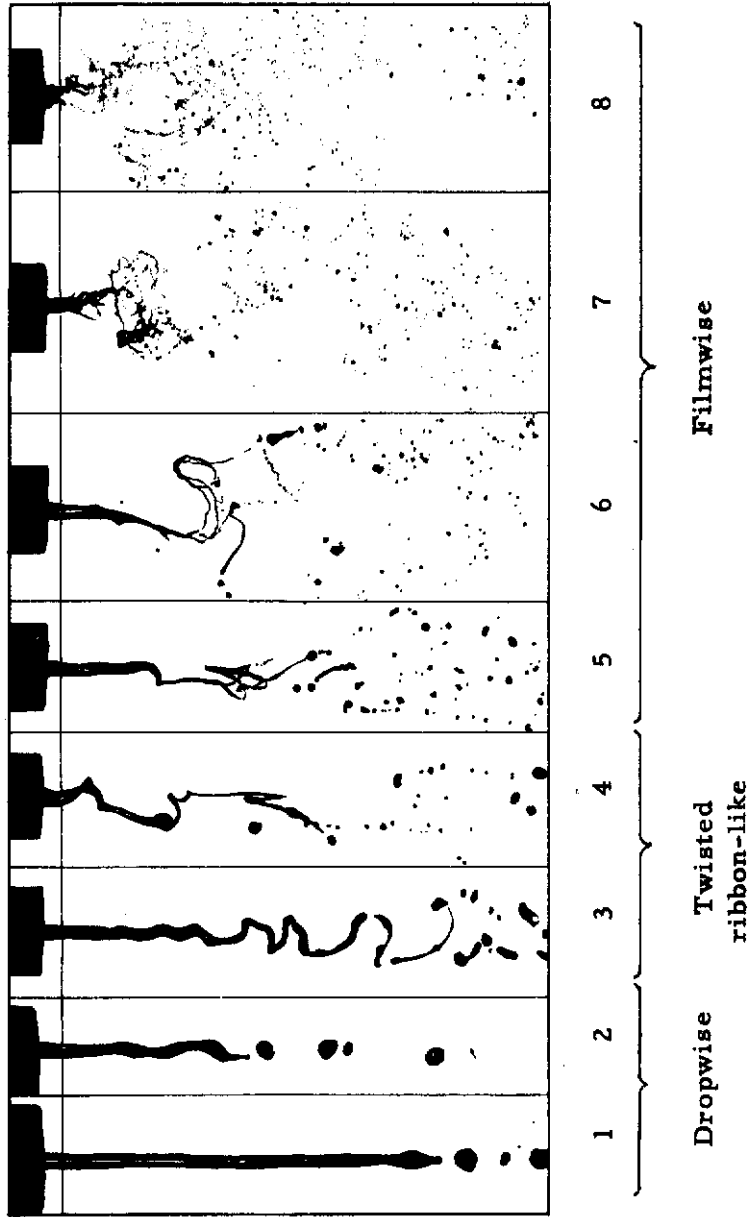


FIGURE 1-10. THREE STAGES OF ATOMIZATION
(Nukiyama and Tanasawa) 1-18

For low air velocities, disintegration was observed similar to that for nonblast-propelled jets, producing drops having a diameter of the same order as that of the jet. When the velocity exceeds a well-determined value, the drops continue to subdivide and become considerably finer.

Two factors cause the drops to burst into smaller droplets: (1) a reduced pressure owing to the difference in the velocities of the drop and the surrounding air, and (2) a centrifugal force (or pressure) resulting from rotations of the drop.

Siestrunck developed equations for evaluating these two pressure differences and shows that bursting of the drop occurs when the sum of these two pressures is about 50 per cent greater than the surface tension for his experimental conditions.

When the velocity of the air is increased still further, the continuous part of the jet shows, at its extremity, some liquid swellings which are probably due to an amplification of the natural oscillations of the jet by the drag. The constrictions which separate any two consecutive swellings disappear and the jet bursts into fine drops.

For air velocities above 500 ft per sec, the agitation of the air current is high enough, and friction on the liquid jet is strong enough that the jet bursts into microscopic drops, corresponding to the condition of atomization. However, Siestruck fails to offer any explanation of the exact mechanism by which this final stage of atomization occurs.

Littaye⁽¹⁻²¹⁾ employed Siestruck's proposed explanation for disintegration and extended it to atomization. He used the experimental apparatus devised by Siestruck and verified the latter's theory.

Littaye distinguishes three principal and successive stages by which a liquid jet is converted into drops when introduced into a current of air. The first stage is called drop formation and occurs at low air velocities, giving drops having diameters greater than the diameter of the jet. The second stage is called disintegration; it occurs at a well-determined value of air velocity, and results in a great number of much more minute drops. The third stage, called pneumatic atomization, occurs after a certain higher value of air velocity is reached, at which time the jet is transformed into a fog of microscopic drops. This last stage is assumed to be reached when the largest drops have a diameter less than some fixed value. When the jet diameter is small, it is possible to pass directly from the drop-formation stage (Stage No. 1) to that of atomization (Stage No. 3).

In contrast to the conclusions of Castleman⁽¹⁻⁵⁾, Littaye⁽¹⁻²¹⁾ makes a very sharp distinction between pneumatic atomization (called air-stream atomization by Castleman) and solid injection. This may be due to a difference in the atomization mechanism itself in the two cases.

In Littaye's second paper⁽¹⁻²²⁾, he uses Siestruck's theory again to show that the diameter of the largest drops, after disintegration, depends solely on (1) the density of the gas, (2) the surface tension of the liquid, and (3) the relative velocity of the two fluids. Actually, the droplet is quickly entrained by the air stream and attains a velocity practically equal to that of the air, so that the relative velocity approaches zero and disintegration ceases.

Here, again, Littaye disagrees with Castleman⁽¹⁻¹¹⁾ and claims that there are no "atomized drops", or no limiting value of the order of several microns, below which the diameter of the drops may not go, however great the relative velocity of the liquid and the air is.

An interesting conclusion made by Littaye is that the drop breaks up at the end of a very short path, about six-tenths of one drop diameter. On this basis he disagrees with Siestruck's argument that centrifugal action plays a significant part in breakup, because there is not sufficient time for the drop to receive a rapid rotary movement.

In the third paper, Littaye⁽¹⁻²³⁾, from experiments in which he atomized alcohol and water by a high-velocity air current, showed that the diameter of the smallest drops does not stop decreasing regularly when the velocity increases, at least down to a diameter of 1μ . More precisely, he claims that the drop diameter is inversely proportional to the velocity of the air,

except for the largest drops, in which case the diameter is inversely proportional to the square of this velocity. This shows that the greater the velocity, the more regular, or more uniform, is the mist obtained. Moreover, the minimum diameter of the drops is proportional to the surface tension of the liquid, so that a better disintegration will be obtained with a liquid having low surface tension.

Finally, Littaye's experiments show that, for liquids of low surface tension, drops of a diameter less than 1μ are ordinarily obtained whenever the air velocity is greater than 330 ft per sec. For solid injection, the diameter of the drops does not go below 3 to 4μ . This demonstrates the superiority of pneumatic atomization over solid injection, and seems to prove that the effect of air on the jet is not the sole cause of production of fine drops by solid injection.

One important point, completely ignored by Littaye, is the possible extent to which vaporization of the droplets may have reduced the diameter between the time they were formed and the time they were collected and measured microscopically. It is possible for a droplet of 10μ to reduce in size to 1μ after evaporation for a short time, especially when in contact with a turbulent blast of air.

Hinze(1-24). The mechanism by which a solid jet disintegrates when issuing at high speeds, in excess of 300 ft per sec, was studied by Hinze, who places considerable emphasis on the turbulence of the liquid jet. He claims that, when the flow of the liquid in the orifice is turbulent, radial movements of liquid particles cause surface disturbances in the form of local protuberances, the height and number of which increase with increasing turbulence. By air action these protuberances are torn off into fine, irregular ligaments; surface tension and liquid viscosity counteract this process, whereas air speed, air density, and air viscosity increase the rate of tearing off. These ligaments can be considered as small and approximately cylindrical columns of liquid which will break up into droplets according to the theory of Rayleigh⁽¹⁻⁸⁾. These droplets continue to be split up into smaller ones as long as the speed of the droplets relative to the air is still above a certain limiting velocity.

Accordingly, Hinze considers that disintegration takes place in three stages, as follows: (1) formation of initial surface disturbances; (2) formation, by air action, of ligaments which break up into drops; and (3) further splitting up of these drops.

Hinze claims that turbulence within the jet is the main source of initial disturbances. A protuberance-like disturbance may be described in terms of the mean diameter and the maximum height of the disturbance; for wave-like disturbances, the corresponding dimensions would be wavelength and amplitude, respectively. The scale of turbulence determines the upper limit of the value of the mean diameter of the protuberance, or the wavelength of the wave-like disturbance. The intensity of turbulence must be sufficiently high to counteract the effect of the surface tension of the liquid.

The ligaments, once having been formed by the action of air on the initial disturbances, may be bodily severed from the jet and may break up into small drops; or they may break up into small drops before being severed. For sufficiently long ligaments this breaking up may take place according to the theories of Rayleigh and Weber, and the detached liquid particles will turn quickly into globules by surface tension.

Merrington and Richardson(1-25). Three types of breakup are described by Merrington and Richardson. The first type results from axial-symmetric oscillations causing the jet to become varicose, as described by Rayleigh. The second type of disturbance causes the jet to become sinuous or wavy, as described by Haenlein, and the resistance of the air to the passage of the humps becomes more important than surface tension. For low-speed jets the varicose form of disturbance will cause breakup, while at higher speeds the sinuous disturbance controls. The third type of breakup, by which the jet is disrupted or atomized, occurs at still higher velocities, above a critical velocity, and is controlled by viscous and inertia forces.

Merrington and Richardson conclude that any expression deduced for this third, and most important, type of breakup should involve the characteristic factors that enter into viscous flow; that is, velocity, drop diameter, and the kinematic viscosity of the liquid.

Larcombe⁽¹⁻²⁶⁾. The mechanism of spray formation from pressure-type nozzles consists, according to Larcombe, in first drawing out the fluid into thin sheets, threads, or filaments. All these forms are very unstable and break up into droplets under the combined action of surface tension, internal viscous forces, and turbulence of the surrounding air. If the liquid has any rotary motion as it passes through the jet, as might be imparted by a swirl chamber, the predroplet characteristic is a thin, cone-shaped sheet; if no rotary motion is present, the predroplet characteristic is a thread form.

Larcombe agrees with Fogler and Kleinschmidt⁽¹⁻¹⁹⁾ that, since the fluid sheet is not rigid, the action of turbulence on the surface creates a series of waves similar to those in a flag flying in a breeze. The waves build up quickly and cause a whipping effect on the surface, so that the sheet curls back on itself to form a hollow tube of fluid which, because it is unstable, breaks down into hollow spheres. It has been proved, by spraying hot fluids into relatively cold atmospheres, that the hollow particles are not formed by expansion of vapor within the particle, but by "flag waving".

The important matter of recombination of droplets is discussed by Larcombe, who concludes that recombination will take place if good dispersion of droplets of a similar size is not achieved.

With pressure nozzles, especially, recombination is a serious problem. Assuming that droplets are to be projected from the nozzle into still air and that they are of a size to obey Stokes' law, they will travel into the air for distances approximately proportional to their respective diameters before air friction brings them to the stage where gravity is the only force acting on them. The smaller particles will, therefore, tend to collect in considerable numbers nearer the nozzle than the larger particles which, because of their greater travel, will collide with the smaller particles, which will combine with them on impact.

In view of this, it will be seen that a narrow droplet-size range is desirable if recombination is to be reduced to the minimum. If the droplet-size distribution were accurately known, it would be possible to calculate the probable amount of recombination, but this is seldom possible.

Joyce⁽¹⁻²⁾. The process of atomization of a liquid film is considered by Joyce to involve some form of enforced attenuation, or thinning, followed by ligament or filament formation and disruption into droplets of a wide range of sizes.

Joyce states that it must not be assumed that there is a clear line of demarcation between the two phases of attenuation and filament disruption. The formation of the filaments is due in part to the applied force causing attenuation and partly to surface tension, and there is an interplay of these forces during the atomization process, perhaps also with the intervention of outside influences, as of combustion air directed into the spray.

Joyce claims that the process of atomization will continue in this way as long as liquid is fed to the atomizer and is subjected to the attenuation process.

Baron⁽¹⁻²⁷⁾. It will be remembered that Littaye⁽¹⁻²²⁾ concluded that drops in an air stream break up at the end of a very short path, about six-tenths of one drop diameter, and, for this reason, rotational effects were negligible in the breaking up of droplets. Baron disagrees with Littaye, and claims that breakup may occur only after quite a large number of vibrations of the drop, during which time its length of travel might be 15 drop diameters, which is ample distance for the drop to acquire a significant amount of rotation.

The actual mechanism of drop atomization, as postulated by Baron, is analyzed with the aid of Figure 1-11.

Two equal and opposing forces, the force of drag and the force of acceleration, cause the initially spherical droplet to be deformed. Such deformation is accompanied by an increase in the

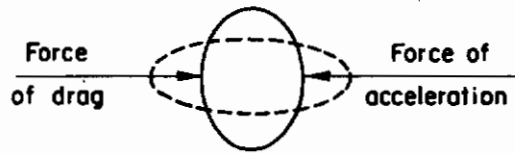


FIGURE 1-11. OPPOSING FORCES CAUSING INITIAL DEFORMATION OF A DROPLET PLACED IN AN AIR STREAM

(Baron)¹⁻²⁸

surface. As a result, the surface tension will tend to restore the drop to its initial spherical shape just as the spring forces tend to restore a spring-mass system to its equilibrium position. Also, corresponding to the spring-mass system, there will be a tendency toward oscillations about the equilibrium configuration, which in this case is spherical. Thus, the drop, when in the position indicated by the full line in Figure 1-11, has a natural tendency to assume the shape indicated by the dotted line. Such oscillations, however, cannot occur exactly this way, since the change in shape, from the full line to the dotted line, is opposed by the forces which caused the deformation in the first place.

Baron concludes that, in order to be able to oscillate and still not oppose the drag and inertia forces, the drop must execute a quarter turn for every half period of oscillation. This motion will result in a combination of rotation and oscillation that is so synchronized that for a stationary (nonrotating) observer the drop will always be in the position shown in Figure 1-11.

On the basis of this mechanism, Baron makes a quantitative estimate for the speed of rotation and of the effects of the centrifugal forces. He shows that centrifugal effects play an important role in the atomization of the drop, in contradiction to Littaye, and that one-third of the resistance of surface tension to explosion is overcome by centrifugal forces, irrespective of the size or material of the droplet. In the above considerations, Baron did not take into account the effects of viscosity, but he points out that as long as the damping due to viscosity is not excessive, the period of vibration will not be materially affected.

Baron then considers what happens to the drop when the deformation results in an increase in radius that exceeds a critical value.

Figure 1-12(a) shows how the centrifugal forces will drive the liquid toward the periphery of the drop, resulting in a gradual thinning of the liquid near the center. Figure 1-12(b) shows how most of the liquid concentrates at the periphery and the thin center membrane is blown out into a cup shape.



FIGURE 1-12. EFFECT OF CENTRIFUGAL FORCES ON A MOVING LIQUID DROPLET

(Baron)¹⁻²⁸

The drop then splits up into two or more parts. As will be shown later in this section, W. R. Lane⁽¹⁻³¹⁾ has recently succeeded in taking flash photographs of droplets that indicate that this type of breakup actually occurs.

Borodin and Dityakin⁽¹⁻²⁸⁾. By a consideration of unstable capillary waves on the surface of separation of two viscous liquids, Borodin and Dityakin attempt to explain the appearance of droplets of different diameters as a result of the breakup of a liquid jet.

Figure 1-13 shows three successive instants of time in the formation of strings of different dimensions which finally break away from the surface of separation to produce a spectrum of droplets.

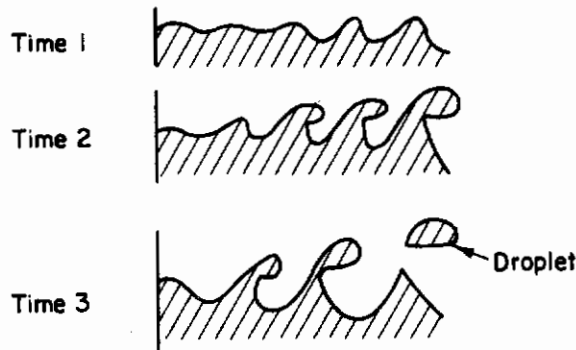


FIGURE 1-13. FORMATION OF STRINGS FROM THE PARTITION SURFACE FOR THREE SUCCESSIVE INSTANTS OF TIME

(Borodin and Dityakin)¹⁻¹³

The mathematical basis for the possibility of the appearance of droplets of different diameters resulting from this type of breakup, as provided by Borodin and Dityakin, will be discussed in a succeeding section on the theoretical analyses of atomization.

Balje' and Larson⁽¹⁻²⁹⁾. In an investigation of the mechanism of jet disintegration, in order to derive mathematical relations for computing droplet sizes produced by insecticide spray equipment, Balje' and Larson point out that the maximum drop size for a spray is readily determined by the original disintegration resulting from instability of the jet as first described by Lord Rayleigh⁽¹⁻⁸⁾. If the surface tension of this droplet is sufficient to withstand the ram pressure as it moves through the air, this droplet will maintain its original shape, assuming that there is no evaporation. A spray of uniform size will result.

However, if the surface tension of the droplet is so small that it cannot maintain its stability under the ram pressure (which is the case in most practical considerations of fuel atomization) the droplet will change its shape and disintegrate. A spectrum of drop sizes results. The maximum drop size will be that of the original droplet, and the minimum size approaches molecular dimensions. Balje' and Larson point out, as do most of the investigators of atomization, that the relative velocity between the liquid and the gas is the major factor that determines the degree of atomization.

A practical conclusion made by Balje' and Larson is that by imprinting a definite wavelength on the jet by outer forces (for example, by mechanical vibration of the nozzle), the liquid will probably disintegrate into a certain droplet size if the outer forces are strong enough to overcome the other forces acting on the jet. Thus, it may be possible to produce uniform droplet sizes where normally a droplet spectrum would result, provided that this droplet size is small enough to be stable.

Donnelly and Wohl⁽¹⁻³⁰⁾. Experiments were conducted by Donnelly and Wohl to determine the effect of effervescence upon the atomization process. They saturated water with carbon dioxide, at various pressures, before spraying into air. On the basis of instantaneous shadow and schlieren pictures, they observed that, at low pressures of 5 to 10 psig, the absorbed gas generates irregularities in the spray sheet. These irregularities cause sufficient disturbances in the flow pattern within the sheet to augment the shearing action at the interface to such an extent that early collapse of the sheet occurs.

At higher pressures the effect of carbon dioxide saturation is negligible. This is attributed to the greater shearing force at the interface, owing to increased velocity difference, plus perhaps increased internal turbulence, nullifying the effect of irregularities generated by effervescence of the carbon dioxide.

Practical advantage may be taken of this tendency of effervescence to play a part in the mechanism of atomization.

Lane⁽¹⁻³¹⁾. A clearer understanding of the action of aerodynamic forces in effecting the atomization of liquids was achieved by Lane, who obtained excellent flash and spark photographs of the shatter of drops in streams of air. He distinguishes three stages in the shatter process, irrespective of whether the shatter of the liquid is brought about by the emergence of liquid at high speed into still air (solid injection), or by the interaction of a slow-moving stream of liquid and a fast-flowing gas stream (air-stream atomization). The three stages are as follows: (1) initiation of small disturbances at the surface of the liquid, in the form of local ripples or protuberances; (2) action of air pressure and tangential forces on these disturbances, forming ligaments which may break up into drops; and (3) further breaking up of these drops in movement through the air.

Figure 1-14 shows the mechanism of the breakup of water drops of comparatively large size in a steady stream of air as observed by Hochschwender⁽¹⁻³²⁾ as early as 1919. The drop becomes increasingly flattened, under the influence of the air stream, and at a critical velocity of the air it is blown out into the form of a hollow bag attached to a roughly circular rim. Bursting of this bag produces a shower of very fine droplets, and the rim, which contains at least 70 per cent of the mass of the original spherical drop, breaks up later into much larger drops.

This phenomenon is of interest because it demonstrates, in a striking way, the characteristic of most sprays that only a comparatively small fraction of the liquid mass is distributed among the finest droplets. It also shows that the fine droplets resulting from the breaking up of the hollow bag are generated from a thin stretched film of liquid.

Lane points out that some of the features of the bursting drop may be explained on the basis of well-established results of fluid mechanics. Measurements of the distribution of pressure over the surface of a rigid sphere placed in a wind tunnel show that a positive pressure exists over the front of the sphere, and a reduced pressure exists at its sides and rear. It is understandable, therefore, that a liquid drop introduced into a stream of air should become flattened on the side subjected to the positive pressure and extended at the sides and rear; this deformation will be opposed by the force of surface tension tending to keep the drop spherical, so that a depression might be expected to form at the center of the upper surface of the drop.

Figure 1-15 shows the breakup of drops subjected to fast air blasts. This mode of breakup is strikingly different from that observed at the critical velocity in a steady stream of air. Instead of the drops being blown out into a thin hollow bag anchored to a rim, as in Figure 1-14, it is deformed in the opposite direction and presents a convex surface to the flow of air. The edges of the saucer shape are drawn out into a thin sheet and then into fine filaments which, in turn, break up into droplets.

Figure 1-16 shows the type of shatter that results when drops are subjected to more powerful air blasts at supersonic speeds. In the early stages of shatter, the sequence of events is similar to that revealed in the less powerful blasts, the original spherical drop being distorted into a saucer-shaped disk while a thin layer of liquid is stripped off the drop and rapidly breaks up into droplets. The partially atomized drop is soon obscured in the opaque cloud of droplets. In the last photograph of the series, shatter of the drop appears to be almost complete.

Contrails

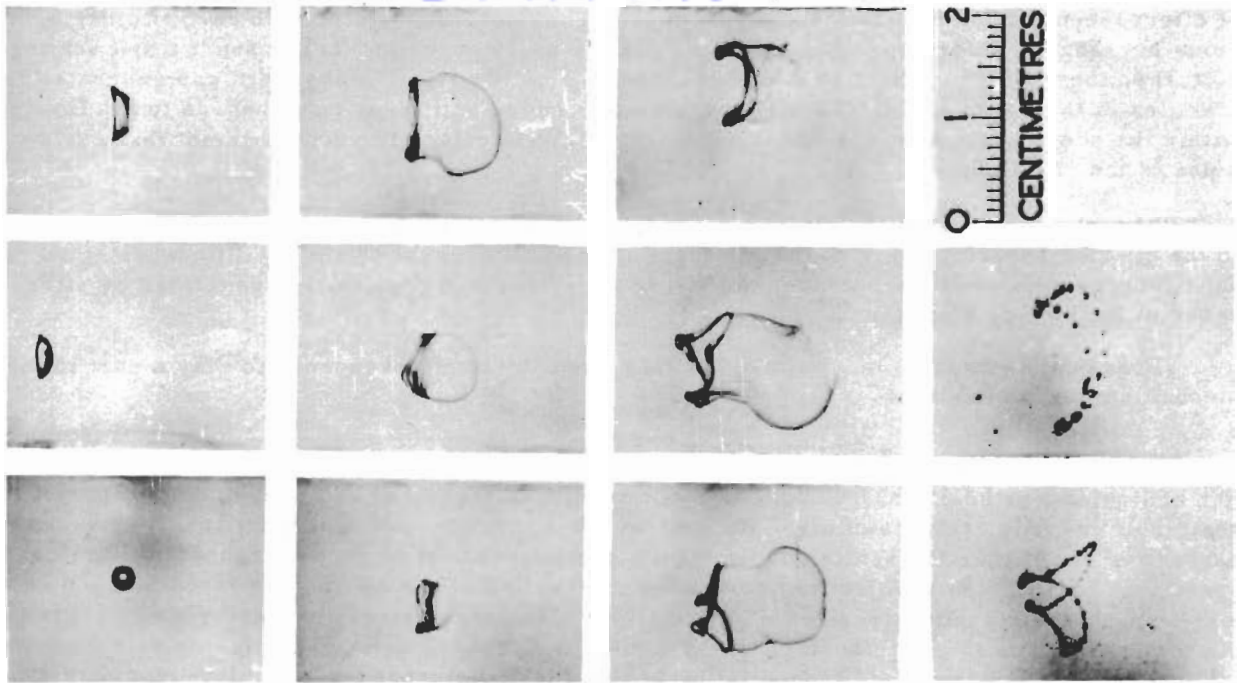


FIGURE 1-14. BREAKUP OF WATER DROPS IN STEADY STREAM OF AIR
(W. R. Lane and J. Edwards) 1-32

(Photographs Reproduced by Permission of the Controller
H. M. Stationary Office)

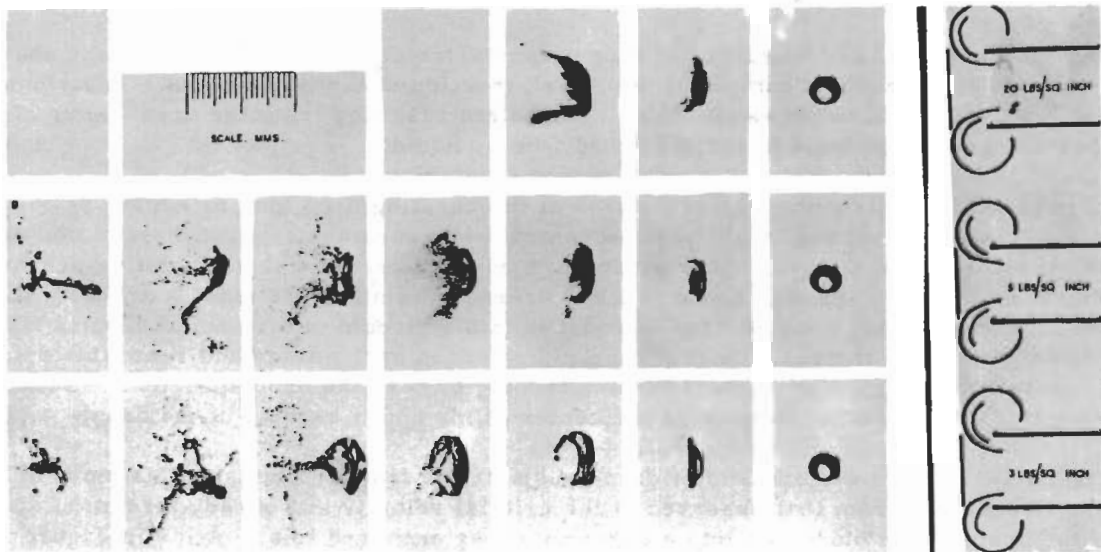


FIGURE 1-15. SHATTER OF DROPS IN TRANSIENT AIR STREAM

(W. R. Lane and J. Edwards) 1-32

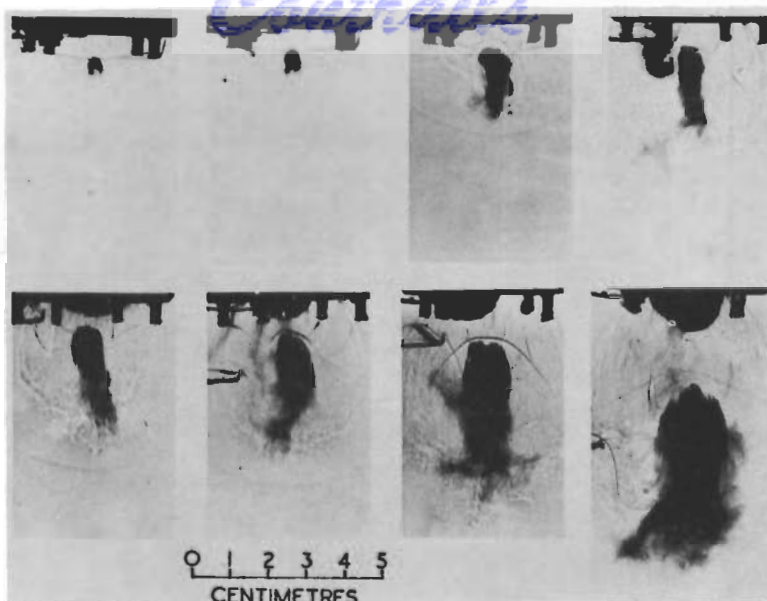


FIGURE 1-16. SPARK PHOTOGRAPHS OF SHATTER OF DROPS IN SUPERSONIC AIR STREAM
(W. R. Lane and J. Edwards)¹⁻³²

(Photographs Reproduced by Permission of the Controller H. M. Stationary Office)

The shattering process, as demonstrated by Lane, is extremely rapid, but not instantaneous, and, because of the acceleration of the deformed drop in the air blast, the relative velocity diminishes rapidly. The thickness of the layer stripped off the drop will therefore increase with time as the difference in velocity between air and drop decreases. Thus, the shatter of the drop into a cloud of droplets of a wide range of sizes can be accounted for, the largest droplets being formed at the latest stages of the shatter.

York⁽¹⁻³³⁾. York has observed another mechanism in atomization that, under certain conditions, may play a significant role in the process of atomization. This is associated with the occurrence of holes in otherwise continuous sheaths.

Figure 1-17 is a photograph of the spray sheath issuing from a Monarch Simplex nozzle. The hole in the sheath, shown above and to the left of center, is about six hundred microns in diameter and is located about one-quarter inch from the tip of the nozzle on the right. York estimates that the rim of fluid around the hole has an average diameter of about one hundred microns, and that the thickness of the sheath is between thirty and fifty microns at this distance of one-quarter inch from the nozzle orifice.

Pictures taken at a location one-half inch from the tip show a much larger number of holes, each of which is generally larger than the hole shown in Figure 1-17.

York points out that it seems quite logical that these holes should develop, considering the instability of thin fluid films, and that it is a natural manifestation of the transformation of energy. A thin sheath has a higher surface energy than the drops formed in the final spray if the diameters of the drops are at least three times the thickness of the sheath at the time of formation.

York, Stubbs, and Tek^(1-34A). York and associates made a mathematical and experimental analysis of the disintegration of a plane sheet of liquid of finite thickness. They showed that instability and wave formation at the interface are the major factors in the breakup of the sheet of liquid into drops.

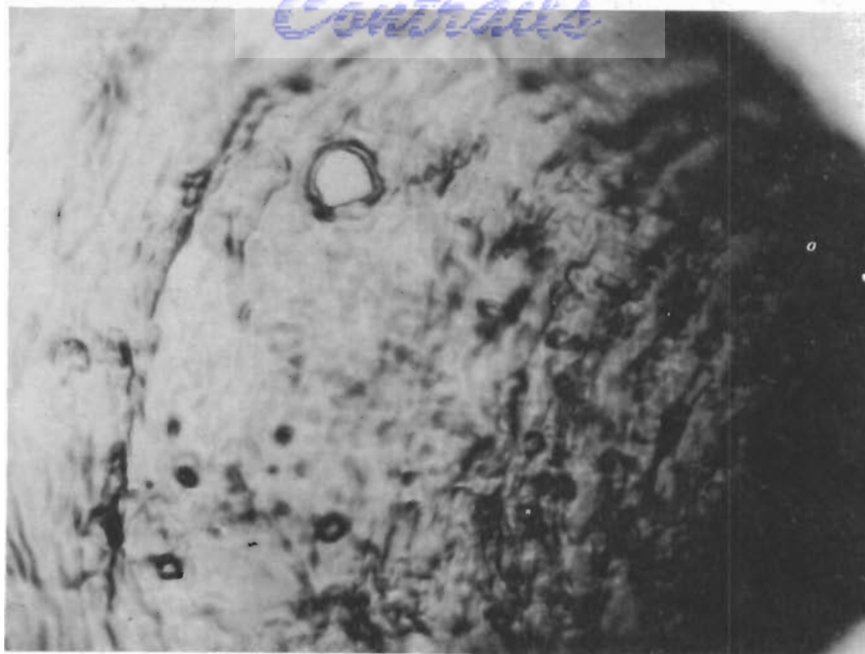


FIGURE 1-17. FORMATION OF HOLE IN A THIN SHEET OF LIQUID (York)¹⁻³⁴

The most useful result of this study was the development of an equation for predicting roughly the size of the drops in the spray from swirl nozzles. From plots of the maximum rate of growth of the waves on the surface of the sheet of liquid, the wavelength of the predominant disturbance can be determined. This disturbance will grow until the sheet disintegrates into rings, after which the rings break into drops by the action of surface tension. Rayleigh⁽¹⁻⁸⁾ showed that the wavelength of cylindrical instability is about 4.5 times the diameter, which is the length of cylindrical section separating to form a drop. The drop size of the spray may be approximated by calculating the diameter of the drop resulting from the typical successive disintegration, recognizing that a range of drop sizes is actually produced.

The resulting equation for drop radius is:

$$r \approx 1.06 \left(\frac{b W^* \sigma}{\rho_A V^2} \right)^{1/2}$$

where b is the thickness of the undisturbed sheet, σ is the interfacial tension, ρ_A is the mass density of the gas phase, V is the velocity of the bulk of the gas phase relative to the liquid phase and W^* is the Weber number based on the wavelength of disturbance for maximum growth rate. W^* can be determined from the density ratio of the gas to the liquid and the Weber number equal to

$$V^2 b \rho_A / 2\sigma.$$

The major problem is estimation of the sheet thickness at the breakup distance. In spite of many assumptions in the analysis, the results are reasonable and have been verified qualitatively by short-exposure photographs and high-speed motion pictures.

Fraser, Dombrowski, and Eisenklam^(1-34B). Another mechanism that may be a cause of disintegration in liquid sheets involves vibrations resulting from turbulent, unsteady flow behind the nozzle. However, no experimental confirmation of periodic vibrations in liquid jets is available.

Fraser, et al., observed that random centers of disturbance eventually break the film of liquid as it travels away from the nozzle mouth, and holes result as reported by York⁽¹⁻³⁴⁾. A mathematical analysis of these random disturbances shows that their origin is inside the nozzle just behind the mouth, and that the frequency of the observed ripples in the sheet is of the order of 10 kc per sec. Fraser points out that systematic work may reveal the cause of these disturbances and link them to possible vibrational phenomena inside the nozzle.

Summary of the Physical Processes of Atomization

The mechanisms of atomization are complex and varied and depend upon numerous factors including, principally, the properties of the liquid being atomized, the atomizing device, and the conditions of atomization, such as pressures employed and density of the air or other gas into which the liquid is to be injected. However, the process of atomization may be considered, in general, to take place in three steps.

The first step is the development of a disturbance of the surface of the jet that is due to instability. This initial disturbance may result from one or more of the following factors: (1) surface tension, (2) inertia forces, (3) imperfections of the nozzle orifice, (4) vibrations of the nozzle, (5) turbulence of the liquid, and (6) effervescence of a dissolved gas. Disturbances may occur simultaneously and overlap one another.

The second step is the formation of ligaments, threads, or films by the action of air on these initial disturbances. These ligaments then break up into fragments, possibly according to the Rayleigh theory, and the fragments become spherical drops under the influence of surface tension.

The third step is the further breakup of these drops into smaller droplets. This last step in breakup will continue as long as there is sufficient velocity of the drop with respect to the air. The mechanisms by which drops break up as they pass through the air may be one or more of the following: (1) at low velocities the drop may be formed into a hollow bag and then break into fragments, (2) at higher velocities shatter of the drop may occur following deformation in a direction opposite to that in (1), (3) centrifugal forces, resulting from rotation of the drops, may cause them to disrupt, and (4) at extremely high velocities a thin layer of liquid may be stripped off the drop, resulting in almost instantaneous atomization.

The transition between steps is usually gradual; however, at high velocities, the first step may be overshadowed by the second or third steps following in rapid succession.

Other mechanisms that may be involved are: (1) the formation of a hollow tube as a result of the flag-waving effect of a fluid sheet, (2) recombination of drops owing to eddy diffusivity as well as different axial velocities, and (3) formation of holes in thin sheets of liquid.

It may be stated with reasonable assurance that the major factor that determines the degree of atomization is the relative velocity between the liquid and the air or other gas into which it is injected. This is true for both solid injection and two-fluid, or pneumatic, atomization. For solid injection the difference in velocities is attained by injecting a high-velocity jet of liquid into relatively still air; whereas, in pneumatic atomization, the differential velocity is accomplished by passing a high-velocity stream of air over a relatively stationary liquid. In both instances the disruptive effect is essentially the same.

In a recent analysis of atomization, Dodge, Hagerty, and York⁽¹⁻³⁶⁾ point out that the most serious drawback to present theory is that three of the most important spray characteristics, drop size, drop-size distribution, and cone angle, cannot be predicted accurately, and that spray theory will be unsatisfactory until the above-mentioned characteristics can be predicted with some degree of certainty from purely theoretical considerations.

Although something is known about the mechanism of atomization in a general qualitative way, much remains to be learned in particular concerning the details of this complicated process.

The mechanism of atomization, when the rotating disk is used, will be considered later in the section on methods of atomization, because the physical process is quite different from that for pressure nozzles or for pneumatic atomizers.

THEORETICAL ANALYSIS OF JET INSTABILITY AND OF SECONDARY ATOMIZATION

The stability of certain fluid-motion configurations has been the topic of extensive and diverse research efforts. The method by which this problem can be analyzed theoretically is, first, to consider a stable configuration that is a given function of velocity, pressure, and density, and of the space coordinates, but which is usually independent of the time. A disturbance, which is usually assumed to be an exponential function of the time and a periodic function of the space coordinates, is then introduced. The expression for this disturbance is usually written as

$$F(x_j, t) = e^{\mu t} G(x_j), \quad \text{for } j = 1, 2, 3, \quad (1-1)$$

where the coefficient μ may be real or complex, and is added to the equation of the stable configuration. It should be noted that instability will result only if the amplitude of the disturbance grows with time, that is, if the real part of μ is positive.

The effect of the disturbance is then investigated by considering the physical conservation of mass, momentum, or energy. The equation for the physical configuration (original stable system plus assumed disturbance) is then substituted into the appropriate conservation equation, with the additional assumption that, at least initially, all variable quantities associated with the disturbance are small with respect to the corresponding quantities in the stable system. This last assumption permits linearization of the otherwise nonlinear equations of conservation; these can then be solved for the time rate of change of the disturbance, in terms of the other physical variables.

By assuming that the disturbances, of the assumed form, occur randomly, in which case all possible disturbances begin with the same amplitude, it is concluded that the disturbance which grows most rapidly, corresponding to the largest positive value of $\text{Re}(\mu)^*$, will be the most probable cause of the resultant instability. Accordingly, the equation for μ is maximized with respect to one of the variables, usually the spatial wavelength K of the assumed disturbance, and the value of the variable that leads to the maximum positive value of $\text{Re}(\mu)$ is thus determined. However, in some instances, such as for an imperfect machining of the nozzle, the original disturbance may be introduced in such a nonrandom manner that the initial amplitude corresponding to a particular wavelength μ_p is much larger than the amplitudes corresponding to the other wavelengths. Because of the large initial amplitude corresponding to μ_p , this disturbance may govern the breakup of the system, despite the fact that there are other solutions with larger positive values of $\text{Re}(\mu)$.

As noted above, these methods of theoretical analysis are valid only so long as the variable quantities initially associated with the disturbance are small with respect to the corresponding quantities associated with the original stable configuration. This means that, as soon as the ratio

* Real part of μ .

of these quantities becomes greater than, say, 0.15, the linear theories are no longer valid, and other methods must be employed for solving the problem. The methods used to solve the subsequent problems, such as are used for explaining secondary atomization or in the theory of ligament formation, have been chiefly conjectural in nature, since no method of linearizing the nonlinear equations of conservation has been advanced for this case. Although the conjectures regarding the subsequent processes in the formation of droplets have led to some interesting results, the physical validity of these conjectures has yet to be confirmed, in most instances.

The theoretical analyses of instability and of secondary atomization, as presented by various authors, are summarized in the following sections. Following these summaries, a critical comparison of the various methods of analysis will be made, as well as recommendations for fields in which further theoretical research is needed.

Nomenclature for Following Section

- A surface area
- B coefficient
- C velocity of droplets
- C_D coefficient of drag
- D (total) differential operator
- F general function
- G arbitrary function of spatial coordinates
- H amplitude of displacement
- H_j Haenkel function
- J Bessel function
- K spatial frequency coefficient
- L breakdown distance for jet
- L' breakdown distance for droplet
- M ratio of dynamic viscosities
- N dimensionless group
- P applied force
- R radius of droplet
- R_j radius of curvature
- S cross-sectional area of jet
- T kinetic energy per unit length
- U uniform velocity in x-direction
- V potential energy per unit length
- W Weber number
- Z length of jet
- a original radius of jet
- b linear dimension
- c velocity of sound
- d coefficient of damping

Contraails

e Napierian base

f general function

f_r frequency of rotation

g deceleration

h displacement of jet from equilibrium position

i imaginary unit

j numerical subscript

k coefficient of dimension, (1/L)

n time coefficient = $-i\mu$

p variable pressure

q deviation in surface pressure from equilibrium surface pressure

r variable radius of jet surface

s surface per unit length

t time

u velocity in x-direction

v velocity in y-direction

w velocity in z-direction

x longitudinal axis of jet

y horizontal axis of jet cross section

z vertical axis of jet cross section

Δ differential operator

Γ volume per unit length of axis

Φ time integral of velocity potential

X resonant amplitude of forced vibration

Ψ stream function

Ω ratio of jet surface to droplet surface

α fractional multiplier

ζ dimensionless spatial frequency = aK

η dynamic viscosity

θ breakdown time

Continued
 λ wavelength of disturbance

μ time coefficient

ν kinematic viscosity

ρ density of fluid

ρ_A density of air

σ surface tension

τ stress

ϕ velocity potential

ω angular frequency

α varies as

The classical treatment of the problem of the stability of jets was given by Lord Rayleigh in his paper, "On the Stability of Jets"⁽¹⁻⁸⁾. The instability is attributed to one of two causes, namely, the capillary force that is predominant in jets of liquids in gases, and the dynamic effect that prevails when the jet and its environment are both of essentially the same material.

Capillary Force, Nonviscous Liquids

Capillary force, the first cause of instability, was studied by introducing a disturbance of wavelength λ and variable amplitude H into the jet, such that the surface of the originally cylindrical jet of fluid was represented by

$$r = a + H \cos Kx, \tag{1-2}$$

where a is the radius of the original cylindrical jet, $K = 2\pi/\lambda$, and x is measured along the axis of the cylindrical jet. The mode of falling away from equilibrium was studied by Lagrange's method, which necessitated the determination of the potential and kinetic energies of the disturbed jet. To this end, the following "average" expressions (in which periodic terms drop out) for the surface s and volume Γ per unit of length along the axis were determined:

$$s = 2\pi \int_0^1 r \sqrt{1 + \left(\frac{dr}{dx}\right)^2} d(x/\lambda) \approx 2\pi a + \pi a K^2 H^2 / 2, \tag{1-3}$$

and

$$\Gamma = \pi \int_0^1 r^2 d(x/\lambda) = \pi a^2 + \pi H^2 / 2. \tag{1-4}$$

Equating the volumes [from Equation (1-4)] for the disturbed and undisturbed jets gives a relation between a and H for the disturbed jet and a_0 for the undisturbed jet. Eliminating a_0 from the relation for the difference between the surface areas of the disturbed and undisturbed jets [from Equation (1-3)] yields:

$$s - s_0 = \frac{\pi H^2}{2a} (K^2 a^2 - 1), \tag{1-5}$$

where s_0 was the surface area per unit length of the undisturbed jet. A value of $s - s_0 > 0$ indicates a stable configuration, since, under these conditions, the surface tension forces will tend to bring the configuration back to its equilibrium condition. Since the configuration of interest is the unstable one, the remainder of this section is devoted only to consideration of the case for $K^2 a^2 < 1$. The potential energy associated with the unstable configuration is:

$$V = -\sigma \left(\frac{\pi H^2}{2a} \right) (1 - K^2 a^2), \tag{1-6}$$

where σ is the cohesive tension. The corresponding velocity potential is⁽¹⁻⁸⁾

$$\phi = \frac{H J_0(iKr) \cos Kx}{iKa J'_0(iKa)}, \tag{1-7}$$

where $\dot{H} = dH/dt$, J_0 is the Bessel function of zero order, and J'_0 is its derivative with respect to iKr . Hence, the kinetic energy per unit length of the unstable configuration is found to be:

$$\begin{aligned} T &= 1/2 \rho \int_0^1 2\pi a \phi \left(\frac{d\phi}{dr} \right)_{r=a} \# a dx \\ &= 1/2 \rho \pi a^2 \frac{J_0(iKa) \dot{H}^2}{iKa J'_0(iKa)}, \end{aligned} \tag{1-8}$$

where ρ is the density of the liquid.

If it is now assumed that the disturbance amplitude H varies as $e^{\mu t}$, application of Lagrange's method results in

$$\mu^2 = \frac{\sigma}{\rho a^3} \frac{(1 - K^2 a^2) iKa J_0'(iKa)}{J_0(iKa)} \quad (1-9)$$

The ratio of wavelength to jet diameter for the kind of disturbance that leads most rapidly to the disintegration of a cylindrical jet is then found by expressing Equation (1-9) in a single power series in (Ka) , and by finding the value of (Ka) for which μ^2 is a maximum. This results in:

$$\lambda = 4.508 (2a) \quad (1-10)$$

Figure 1-18 shows the variation of the rate of growth μ with Ka for an inviscid (nonviscous) jet under the influence of surface tension. From this figure it becomes immediately obvious that μ has a definite maximum for $Ka \approx 0.7$. This, in turn, corresponds to a value of

$$\mu = 0.118 \sqrt{\frac{\sigma}{\rho a^3}}$$

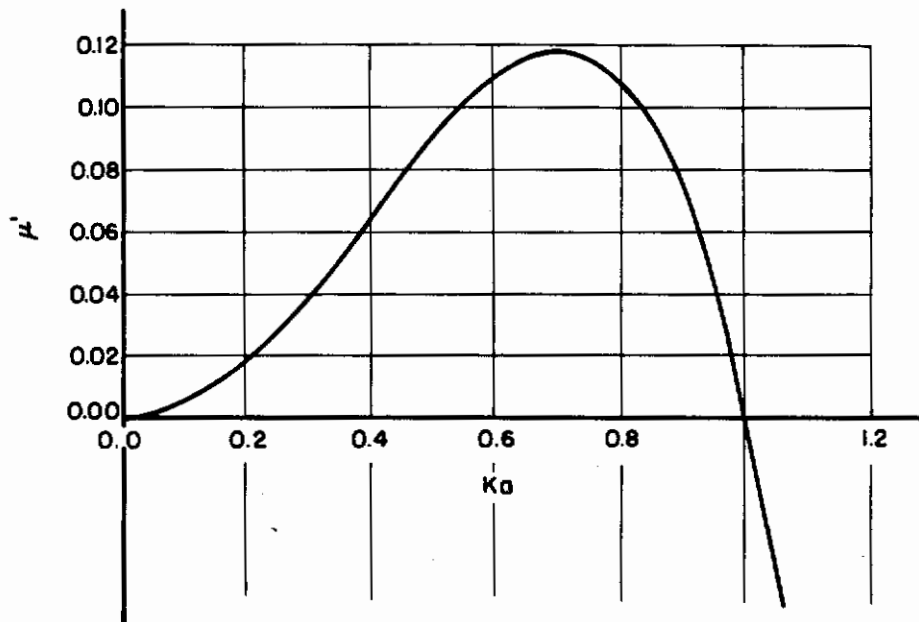


FIGURE 1-18. VARIATION OF $\mu' = \mu/\sqrt{\sigma/\rho a^3}$ WITH Ka FOR INVISCID FLUID WHERE SURFACE TENSION PREDOMINATES

(Equation 1-9)

Capillary Force, Viscous Liquids

In a subsequent paper⁽¹⁻³⁶⁾, Lord Rayleigh considered the same problem for very viscous liquids, such as heavy oil, and concluded that the wavelength of the disturbance which produces greatest instability, ν , will be very large in comparison with the diameter of the jet. Since viscous flow cannot be represented by a potential function, the flow in this case is represented by the stream function Ψ , which, for small motions, satisfies the equation:

$$\left(\frac{d^2}{dr^2} - \frac{1}{r} \frac{d}{dr} + \frac{d^2}{dx^2} - \frac{1}{\nu} \frac{d}{dt} \right) \left(\frac{d^2}{dr^2} - \frac{1}{r} \frac{d}{dr} + \frac{d^2}{dx^2} \right) \Psi = 0 \quad (1-11)$$

$$\Psi = \left[\Psi_1(r) + \Psi_2(r) \right] e^{i(nt + K_1 x)}, \quad (1-12)$$

where \underline{n} is the usual time coefficient, which may be real or complex, it is seen that Ψ_1 and Ψ_2 must satisfy the equations

$$\frac{d^2 \Psi_j}{dr^2} - \frac{1}{r} \frac{d \Psi_j}{dr} - K_j^2 \Psi_j = r \frac{d}{dr} \left(\frac{1}{r} \frac{d \Psi_j}{dr} \right) - K_j^2 \Psi_j = 0, \quad (1-13)$$

for

$$j = 1, 2,$$

and where

$$K_2^2 = K_1^2 + in/\nu. \quad (1-14)$$

The boundary conditions were then imposed, and it was noted that the functions Ψ_j ($j = 1, 2$) satisfied the conditions appropriate to a stream function when there are velocity potentials of the form:

$$\phi_j = e^{iK_j x} J_0(iK_j r), \quad j = 1, 2, \quad (1-15)$$

so that

$$\begin{aligned} \Psi_j &= \int r \frac{\partial \phi_j}{\partial r} dx = \frac{r}{iK_j} \frac{\partial \phi_j}{\partial r} \\ &= r e^{iK_j x} J_0'(iK_j r) = A_{jr} J_0'(iK_j r). \end{aligned} \quad (1-16)$$

By imposing the appropriate boundary condition on $\Psi = e^{i(nt + K_1 x)} (\Psi_1 + \Psi_2)$, a complicated relation for \underline{n} , in terms of $(iK_j a)$ and K_j ($j = 1, 2$), is obtained. This was simplified by assuming a large viscosity, which results in

$$K_2 \approx K_1. \quad (1-17)$$

The resultant equation for the rate of growth of the disturbance \underline{n} can then be written approximately as

$$in = T(1 - K^2 a^2) / \left(6\eta a + O \left[K^4 a^4 \right] \right), \quad (1-18)$$

where O means "terms of the order of". This obviously requires its maximum value for $Ka = 0$, which, by Equation (1-2), corresponds to an infinite wavelength λ .

The Dynamic Effect

Dynamic effect, the second cause of instability, was studied by introducing a surface of separation between the jet and the surrounding medium. This surface of separation was subjected to a disturbance such that its displacement \underline{h} from the equilibrium position was represented by the real part of the following equation:

$$h = H e^{i(nt + Kx)}. \quad (1-19)$$

Figure 1-19 shows the coordinate system, velocities, and assumed displacement of the surface of separation introduced by Rayleigh. The x-axis was taken along the originally undisturbed surface of discontinuity; the z-axis is normal to x. The displacement of the surface, because of the disturbance, is designated by \underline{h} , and the velocities U_j are the initial velocities on either side of the surface. The velocity potentials ϕ_j for the flows on either side of the surface of separation were written as

$$\phi_j = B_j e^{i(nt + Kx) + (-1)^j Kz} + U_j x, \quad j = 1, 2, \quad (1-20)$$

where the coefficients B_j are to be determined by the condition that the normal velocities at the surface of separation equal those determined from Equation (1-19). Hence,

$$\begin{aligned} (-1)^j \frac{d\phi_j}{dz} (z=0) &= KB_j e^{i(nt + Kx)} = \frac{Dh}{Dt} = \frac{\partial h}{\partial t} + U_j \frac{\partial h}{\partial x} \\ &= (iD + iKU_j) H e^{i(nt + Kx)}, \quad j = 1, 2; \end{aligned} \quad (1-21)$$

so that

$$B_j = iK^{-1} (n + KU_j) H,$$

and

$$\phi_j = (-1)^{j+1} iK^{-1} (n + KU_j) H e^{i(nt + Kx) + (-1)^j Kz} + U_j x, \quad j = 1, 2 \quad (1-22)$$

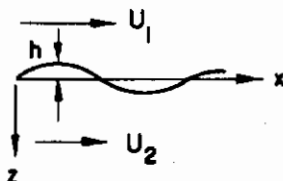


FIGURE 1-19. DIAGRAM OF COORDINATE SYSTEM AND VARIABLES ALONG SURFACE OF SEPARATION

By equating the pressures on either side of the surface of separation, the following relation among the densities ρ_j , the velocities U_j , and the coefficient \underline{K} is obtained:

$$\rho_1 (n + KU_1)^2 + \rho_2 (n + KU_2)^2 = 0, \quad (1-23)$$

which indicates that the disturbance grows most rapidly when its wavelength is small, and when the densities of the two media are the same. If it is assumed that the two portions of fluid are limited by rigid walls, the equations of which are: $z = \underline{b}$ and $z = \underline{-b'}$, respectively, then Equation (1-23) becomes

$$\rho_1 (n + KU_1)^2 \coth Kb + \rho_2 (n + KU_2)^2 \coth Kb' = 0. \quad (1-24)$$

By letting $b' \rightarrow \infty$, and $\coth Kb' = 1$, Equation (1-23) may be applied to a jet of width $2b$, symmetrical and symmetrically placed with respect to the line $z = b$, and moving with velocity U_1 in an infinite mass having a velocity of U_2 . Various other jet phenomena can be described by varying the equation for the displacement \underline{h} of the surface of discontinuity, and by varying the relation between ρ_j and U_j . The resultant expressions for \underline{n} then give an indication of the manner in which the jets fall away from equilibrium.

Rayleigh's analysis has thus shown that, when surface-tension forces are predominant in an essentially nonviscous liquid, the wavelength of the most probable disturbance will be roughly four-and-a-half times the diameter of the jet. As the liquid becomes more viscous, this wavelength increases to the limiting case of essentially infinite viscosity when the wavelength of the disturbance becomes infinite, which is quite reasonable from the physical point of view.

In the case of the instability of a plane surface of separation between a liquid and air caused by dynamic atmospheric effects, it was found that the most rapid rate of growth of the disturbance corresponds to a wavelength that approaches zero. This last analysis was then modified to account for the dynamic instability of a jet of liquid, and it was ascertained that the most rapid rate of growth of the disturbance again corresponds to a wavelength that approaches zero.

Weber's Analysis

A more detailed analysis of the breakdown of a liquid jet was given by C. Weber⁽¹⁻¹⁰⁾, in which he attributed the basic cause entirely to the forces arising from surface tension, and he proceeded to determine the wavelength that brings about the greatest amount of instability both for inviscid and for viscous liquids.

Effect of Surface Tension

The effect of surface tension was determined by investigating an infinitely long steady jet with circular cylindrical cross section of radius a . The surface tension associated with this cylindrical jet was designated by σ , so that the corresponding surface pressure was σ/a . Since only rotationally symmetric disturbances affect the breakdown of a cylindrical jet, Weber then considered the deviation from the cylindrical cross section to be $h(x)$.

Figure 1-20 is a schematic diagram for the coordinate system and assumptions used by Weber. Here it can be seen that the x -axis is taken as the longitudinal axis and the y - and z -axes are the horizontal and vertical axes, respectively, of the cross section; h is the amount of the deviation.

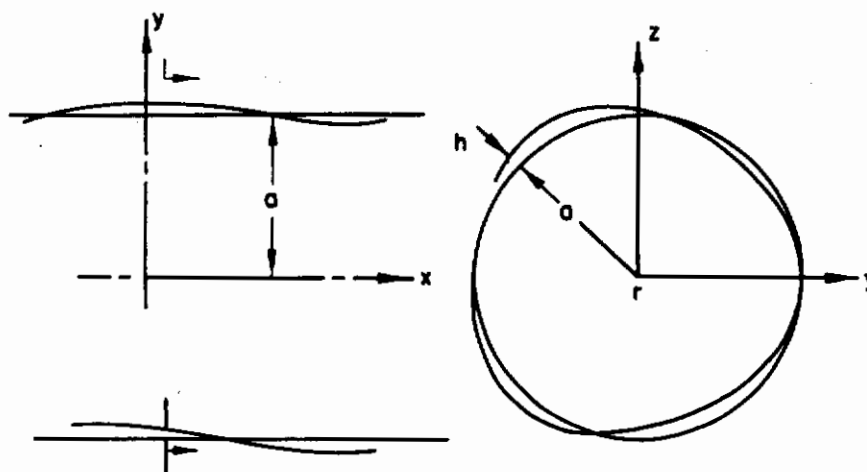


FIGURE 1-20. COORDINATE SYSTEM FOR WEBER'S ANALYSIS
(Weber)¹⁻¹⁰

According to this arbitrary deviation from cylindrical cross section, the local surface pressure can be expressed as

$$\frac{\sigma}{a} + q_{\sigma} = \sigma \left(\frac{1}{R_1} + \frac{1}{R_2} \right), \quad (1-25)$$

where q_{σ} is the deviation in surface pressure from that of the cylindrical jet, and R_1 and R_2 are the radii of curvature in the cross-sectional and longitudinal planes, respectively. Since the (variable) radius of the disturbed jet is $(a + \delta)$, the deviation in surface pressure can thus be determined as

$$q_{\sigma} = -\sigma \left(\frac{1}{a^2} + \frac{\partial^2}{\partial x^2} \right) h, \quad (1-26)$$

by dropping all terms involving products of \underline{h} or its derivatives, which are considered as negligible.

This dropping of product terms renders the equations of motion linear, so that the individual solutions for the deviations can be superimposed. Expanding the deviation \underline{h} in a cosine series and investigating the term with the wavelength

$$\lambda = \frac{2\pi}{K}, \quad (1-27)$$

where \underline{K} is the spatial frequency of the disturbance, yields

$$h = H \cos \frac{2\pi x}{\lambda} = H \cos Kx, \quad (1-28)$$

where H is the maximum amplitude of the disturbance. Hence,

$$q_{\sigma} = -\frac{\sigma H}{a^2} (1 - K^2 a^2), \quad (1-29)$$

which indicates that, with respect to surface tension alone, the system will be unstable for $Ka < 1$, that is, for $\lambda > 2\pi a \approx 6.28 a$.

Exact Solution

An exact solution of the linearized equations of motion is then obtained by noting first that

$$\Delta p = 0, \quad (1-30)$$

where the operator Δ is defined as

$$\Delta = \frac{\partial^2}{\partial r^2} + \frac{1}{r} \frac{\partial}{\partial r} + \frac{\partial^2}{\partial x^2}. \quad (1-31)$$

By setting $(\partial h / \partial t) \approx V_r$, the radial-deviation velocity, Equation (1-30), and the radial equation of motion lead to the following equation for \underline{h} :

$$\frac{\partial}{\partial t} \Delta_1 \left(\Delta_1 - \frac{\rho}{\eta} \frac{\partial}{\partial t} \right) h = 0, \quad (1-32)$$

where ρ is the density of the fluid, η is the viscosity, and

$$\Delta_1 f = \frac{\partial^2 f}{\partial x^2} + \frac{\partial}{\partial r} \left[\frac{1}{r} \frac{\partial}{\partial r} (rf) \right] \quad (1-33)$$

Since only those disturbances that grow with respect to time are of interest, the solution of Equation (1-32) that is independent of time is of no interest, and the pertinent solution becomes:

$$h = h_1 + h_2, \quad (1-34)$$

where h_1 and h_2 are the solutions of the equations

$$\Delta_1 h_1 = 0, \quad (1-35)$$

and

$$\left(\Delta_1 - \frac{\rho}{\eta} \frac{\partial}{\partial t} \right) h_2 = 0, \quad (1-36)$$

respectively. The boundary conditions for these solutions are

$$\left. \begin{aligned} (h_1 + h_2)_{r=a} &= h \\ \tau = \eta \left(\frac{\partial u}{\partial r} + \frac{\partial v_r}{\partial x} \right)_{r=a} &= 0 \\ \left(p + 2\eta \frac{\partial v_r}{\partial r} \right)_{r=a} &= q_\sigma \end{aligned} \right\} \quad (1-37)$$

If h is assumed to be of the form

$$h = H e^{\mu t} \cos Kx,$$

and substituted into Equation (1-32), Bessel equations for h_1 , and h_2 are obtained. Simultaneous consideration of the boundary conditions of Equation (1-37) then leads to the following approximate equation for the rate of growth, μ :

$$\mu^2 + \mu \frac{3\eta K^2}{\rho} = \frac{\sigma}{3\rho a^3} (1 - K^2 a^2) K^2 a^2, \quad (1-38)$$

which has zero or negative solutions for μ if $Ka = 0$ or 1 , and which has one positive and one negative solution for $0 < Ka < 1$. The criterion of $Ka < 1$ for an unstable system bears out the prediction of Equation (1-29).

For an inviscid fluid, the exact equation for μ corresponding to Equation (1-38) becomes:

$$\mu^2 = \frac{\sigma}{2\rho a^3} (1 - K^2 a^2) K^2 a^2 \frac{2(Ka)^{-1} J_1(Ka)}{J_0(Ka)} \approx \frac{\sigma}{2\rho a^3} (1 - K^2 a^2) K^2 a^2, \quad (1-39)$$

where $J_0(Ka)$ and $J_1(Ka)$ are the zero- and first-order Bessel functions of the first kind, respectively. The maximum value of μ , corresponding to the mode of initial disturbance which brings about instability most rapidly, is obtained when $Ka = \bar{Ka} = 1/\sqrt{2}$, where \bar{K} is the value of K for $\mu = \mu_{\max}$. This results in

$$\mu_{\max} = \sqrt{\frac{\sigma}{8\rho a^3}}. \quad (1-40)$$

The wavelength of the predominant disturbance for this case is determined, by consideration of Equations (1-27) and (1-40), to be

$$\lambda = 2\pi/\bar{K} = 4.44 (2a) \quad (1-41)$$

Influence of Jet Velocity

For a jet leaving the nozzle with the velocity \underline{U} , the deviation from a cylindrical surface is assumed to be of the approximate form:

$$h = He^{\mu(t + x/U)} \cos Kx \quad (1-42)$$

Consideration of the equations of motion reveals that Equation (1-42) is a valid approximation to the rigorous solution if the jet velocity

$$U > \sqrt{\frac{\sigma}{\rho a}} .$$

An approximation for the breakdown time $\underline{\theta}$ can be obtained from Equation (1-42) by assuming that the jet velocity \underline{U} is large, and that $x = \lambda$. Under these assumptions,

$$\theta = \frac{U}{\mu_{\max}} \ln \frac{a}{H} \quad (1-43)$$

and the breakdown distance \underline{L} becomes

$$L = \theta U = \frac{U}{\mu_{\max}} \ln \frac{a}{H} \quad (1-44)$$

By differentiating Equation (1-38) with respect to Ka , the predominant wavelength of disturbance for a viscous liquid becomes

$$\mu_{\max} = 1 \left/ \left(\sqrt{\frac{8\rho}{\sigma}} a^{3/2} + \frac{6\eta}{\sigma} a \right) \right. \quad (1-45)$$

and the corresponding breakdown time, $\underline{\theta}$ is

$$\theta = \left(\sqrt{\frac{8\rho}{\sigma}} a^{3/2} + \frac{6\eta}{\sigma} a \right) \ln \frac{a}{H} \quad (1-46)$$

Hence, for essentially inviscid liquids, the breakdown time varies as $a^{3/2}$, and for very viscous fluids, as a .

Atmospheric Effects

The atmospheric effects on the jet are considered by expressing the components of velocity of the air in the r , x , y , and z directions, respectively, by

$$v_r = \frac{\partial h}{\partial t} = \frac{\partial \phi}{\partial r} \quad ,$$

$$U = \frac{\partial \phi}{\partial x} \quad , \quad v = \frac{\partial \phi}{\partial y} \quad , \quad w = \frac{\partial \phi}{\partial z} \quad (1-47)$$

and by letting

$$h = \frac{\partial \Phi}{\partial r} = \frac{\partial}{\partial r} \left(\int \phi dt \right) \quad (1-48)$$

which will permit satisfaction of the linearized equation of motion. By assuming the initial expression for ϕ to be

$$\phi = H \cos K(x - Ut) , \quad (1-49)$$

substitution into the equation of continuity results in the following expression for the deviation \underline{h} :

$$h = H \cos K(x - Ut) \cdot H_1^{(1)}(iK_1 r) / H_1^{(1)}(K_1 a) , \quad (1-50)$$

where

$$K_1^2 = K^2 \left(1 - \frac{U^2}{c^2} \right) ;$$

\underline{c} is the local velocity of sound, and $H_1^{(1)}$ is the Haenkel function of the first order. The corresponding equation for μ is:

$$\begin{aligned} \mu^2 + \mu \frac{3\eta K^2}{\rho} = \frac{\sigma}{2\rho a^3} (1 - K^2 a^2) K^2 a^2 \\ - \frac{\rho_A U^2}{2\rho a^2} K^3 a^3 \frac{iH_0^{(1)}(iK_1 a)}{H_1^{(1)}(iK_1 a)} , \end{aligned} \quad (1-51)$$

where ρ_a is the density of the air, and $H_0^{(1)}$ is the Haenkel function of the zero order. By taking assumed values for \underline{a} , σ , ρ , ρ_A , and various values for \underline{U} , it is seen that μ_{\max} and θ increase with \underline{U} .

Elasticity Analogy

Finally, by considering the jet as an elastic beam and by modifying the elasticity equations, μ_{\max} for wave formation by air effects can be determined from the equation

$$\begin{aligned} \mu^2 + \mu \frac{\eta K^2 a^2}{1 - 2\rho a^2} \cdot \left(\frac{3\eta K^2}{\rho} + \mu \right) / \left(\frac{10}{3} \frac{\eta}{\rho a^2} + 3 \frac{\eta K^3 a^3}{\rho a^2} + \mu \right) \\ = - \frac{\rho_A}{\rho} \frac{U^2}{a^2} Ka \frac{H_1^{(1)}(iKa)}{H_1^{(1)'}(iKa)} - \frac{2\sigma}{a^3 \rho} K^2 a^2 ; \end{aligned} \quad (1-52)$$

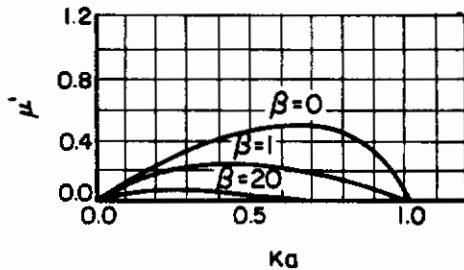
and the minimum velocity for breakdown to occur can be determined by setting the right side of Equation (1-52) equal to zero. Hence,

$$U(Ka)_{\min} = \sqrt{\frac{2\sigma Ka H_1^{(1)'}(iKa)}{a\rho H_1^{(1)}(iKa)}} . \quad (1-53)$$

It should be noted that Ka (μ_{\max}) increases with increasing \underline{U} ; hence, λ decreases as \underline{U} increases.

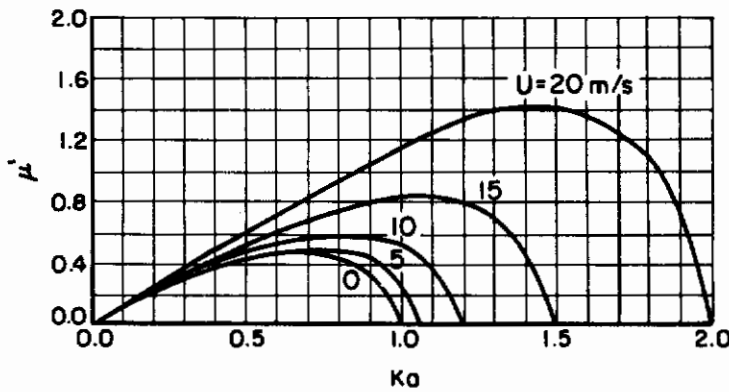
In summary, Weber's derivations indicate that the breakdown time for low velocities is invariant for a given fluid and jet strength, while the breakdown length increases with jet velocity. Under the influence of air forces, the breakdown time theoretically diminishes, so that with increasing velocity the breakdown length also decreases; experimentally, there is a sharp decrease. The effect of viscosity is to increase the breakdown time, while the effect of an increase in jet velocity is to decrease the breakdown time. The theoretical predictions have been confirmed by experimental data in each case.

Figure 1-21 presents a graphical summary of the variation of the dimensionless rate of growth $\mu' = \mu/\sqrt{\sigma/2\rho a^3}$ with the dimensionless spatial frequency Ka , for each of the cases considered by Weber. Figure 1-21a shows that the value of K for which μ is the maximum decreases with increasing viscosity and, hence, that the wavelength λ of the critical disturbance increases with viscosity. Figures 1-21b and 1-21c show that this critical value of K increases with increasing jet velocity U , and hence that the critical wavelength decreases with increasing velocity. Both of the above predicted trends are to be expected from physical considerations.

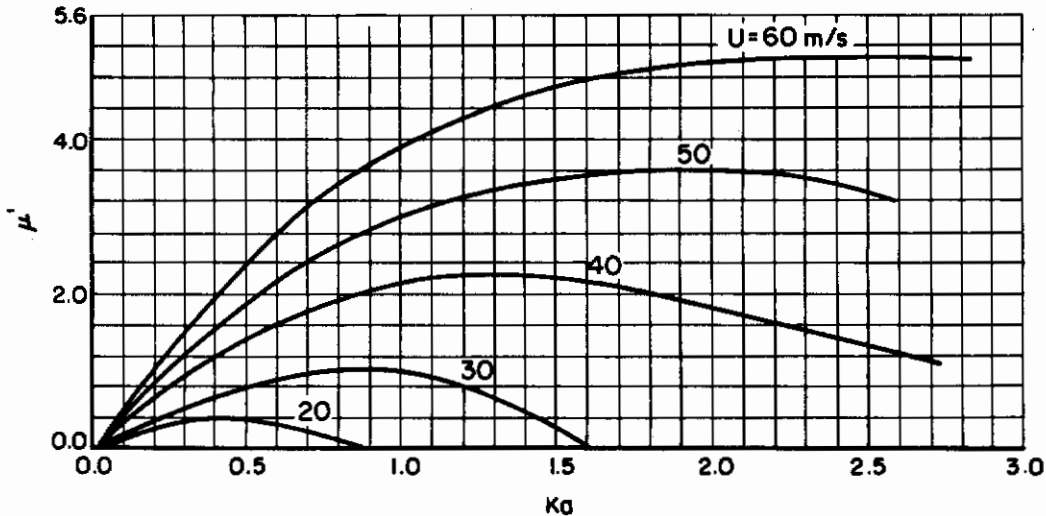


a) Viscous and nonviscous fluids at low jet velocity. Equation (1-38)

$$\beta = \frac{3}{2} \frac{\eta}{\rho a^3} / \sqrt{\frac{\sigma}{2\rho a^3}}$$



b) Atmospheric effects for various velocities of a nonviscous jet. Equation (1-51)



c) Wave formation by air effects, using elasticity analogy, for various velocities of a viscous liquid jet. Equation (1-52)

FIGURE 1-21. VARIATION OF $\mu' = \mu/\sqrt{\sigma/2\rho a^3}$ WITH Ka AS PREDICTED BY VARIOUS EQUATIONS (Weber)¹⁻¹⁰

A relatively simple derivation of the criterion for secondary atomization was given by R. Siestrunk⁽¹⁻²⁰⁾, who postulated that the subdivision of droplets formed by the primary disintegration of a liquid jet is due to the forces of suction and of centrifugal motion which occur when the air velocity \underline{U} exceeds a critical value U_0 . The physical system considered was that of a drop of velocity C_0 within an air jet moving with velocity \underline{U} . The moderate suction Δp_1 from the drag forces, which tends to burst the drop, is of the form:

$$\Delta p_1 = C_D (U - C_0)^2 \rho_A / 2 \quad , \quad (1-54)$$

where C_D is the drag coefficient and ρ_A is the air density. A second excess pressure is caused by the centrifugal force that is due to the angular frequency ω of the agitated drops of radius \underline{R} . The maximum value of this force, on the equator of the rotating drop can be expressed by:

$$\Delta p_2 = \rho \omega^2 R^2 / 3 \quad , \quad (1-55)$$

where ρ is the density of the liquid. The angular frequency ω can be expressed in terms of the air velocity \underline{U} by:

$$\omega = KU \quad , \quad (1-56)$$

where K is a function of the average mean agitation of the jet and of the frequency spectrum of the disturbances causing the agitation.

Siestrunck then conjectured that the droplets could burst when the sum of the above pressures would exceed a certain multiple α of the pressure associated with the surface tension σ of the liquid droplets (considered to be essentially spherical). Hence, the criterion becomes

$$\Delta p_1 + \Delta p_2 = C_D (U - C_0)^2 \rho_A / 2 + \rho K^2 U^2 R^2 / 3 = \frac{2 \alpha \sigma}{R} \quad . \quad (1-57)$$

From Equation (1-55) it can be seen that the relation between \underline{U} and C_0 becomes:

$$C_0 = U - \sqrt{\lambda + \lambda' U^2} \quad , \quad (1-58)$$

where

$$\lambda = \frac{4 \sigma \alpha}{\rho_A R C_D} \quad ,$$

and

$$\lambda' = \frac{2 \rho}{3 \rho_A} \frac{K^2 R^2}{C_D} \quad .$$

By setting the velocity of the liquid jet approximately equal to zero, it can be seen that an air blast of

$$U_0 = \sqrt{\lambda / (1 + \lambda')} \quad (1-59)$$

is necessary for initiation of secondary disintegration. For Siestrunk's experimental investigations, the value of α was found to be about 0.5.

The distance L' that a droplet normally traveled before it burst was investigated by assuming that this disintegration occurred at a time θ when the cross section \underline{S} of the jet was small enough to be broken by agitation of the flow. If the amount of flow "sucked up" by a swelling irregular mass of fluid is defined by

Conrails

$$Q = \int_0^\theta \frac{\Delta p}{\rho b} S(t) dt \quad , \quad (1-60)$$

where b is the distance between two swellings of the jet, and if it is assumed that Δp is essentially constant during the disintegration and that Q varies but little with U , Equations (1-54) and (1-60) yield:

$$L' = C_o \theta = \frac{\beta C_o}{\sqrt{\Delta p}} \frac{\lambda C_o}{U - C_o} \quad , \quad (1-61)$$

where

$$\beta = \sqrt{2 \rho b Q / S(t)} \quad ,$$

and

$$\lambda = \beta \sqrt{2 / \rho C_D} \quad .$$

Hence, the interval in which a jet disintegrates can be represented by a single constant parameter, along with the velocities of the liquid and air jets.

Littaye's Analysis

The analysis by Siestrunk was investigated experimentally by G. Littaye⁽¹⁻²²⁾, who found that the criterion for secondary atomization could be expressed by the equation:

$$\frac{\rho_A (U - C_o)^2 R}{\sigma} = \text{const.} \quad (1-62)$$

where the symbols are as defined previously, and where the second term of Equation (1-57), representing the centrifugal forces, is neglected.

Realizing that the velocity of the liquid C is not constant, but increases rapidly because of the entrainment by the air stream flowing at a velocity of U , Littaye then wrote the equation of motion for the droplets as,

$$m (dC/dt) = C_D (\rho_A / 2) (U - C)^2 S \quad , \quad (1-63)$$

where m is the mass of the droplet, and S is the great-circle area of the droplet. Integration of Equation (1-63) yields:

$$U - C = \frac{U - C_o}{1 + kt (U - C_o)} \quad , \quad (1-64)$$

where C_o is the initial velocity of the droplet, and

$$k = \frac{C_D \rho_A S}{m}$$

By assuming that the relative velocity $(U - C_o)$ has a limiting value, as prescribed by Equation (1-62), and that the breakup time can be represented approximately by the oscillation period θ of the droplet, as given by

$$\theta = \sqrt{3\pi m / (8\sigma)} \quad , \quad (1-65)$$

the author computed the relative velocity at breakup to be

$$\frac{(U - C)}{U - C_0} = 1 - \frac{C - C_0}{U - C_0} = \frac{1}{(1 + 0.013)} \quad (1-66)$$

for the case of water droplets in an air stream. Equation (1-66) demonstrates that breakup will occur when the change in droplet velocity ($C - C_0$) is less than two per cent of the initial relative velocity ($U - C_0$), regardless of the diameter of the droplet. This indicates that the criterion of Equation (1-62) is valid for any size of droplet, and hence that there is no limit value of the order of several microns below which the diameter of the drops may not go. For highly viscous liquids it is known that the period of oscillation θ increases. Hence Equation (1-66) indicates that, for more viscous liquids, the velocity difference ($C - C_0$) will increase with increasing viscosity.

Since

$$C = \frac{dx}{dt} \quad , \quad (1-67)$$

integration of Equation (1-64) yields:

$$x = (U - C_0)t + \frac{1}{k} \ln \left[1 + kt(U - C_0) \right] \approx \frac{1}{2k} \left[kt(U - C_0) \right]^2 \quad , \quad (1-68)$$

from which the distance L' traversed by a drop during its breakup can be determined as

$$L' = \frac{1}{2k} \left[k(U - C_0)\theta \right]^2 \quad . \quad (1-69)$$

For water droplets in air, $L'/R \approx 1.2$, which is independent of the nature of the liquid. This shows that the drop breaks up at the end of a very short path, so that there is insufficient time for rotation to bring about the centrifugal forces described by Siestrunk.

Baron's Analysis

Two significant contributions to the analysis of jet disintegration were made by T. Baron⁽¹⁻²⁷⁾. In the first place, he combined theory and dimensional analysis to derive a formula for breakup distance \underline{L} which was confirmed, qualitatively at least, by experiments. By assuming that surface tension σ is the main cause for the instability of a jet, and that the other important factors are the viscosity η that causes the initiation of the disturbance, the velocity of the jet \underline{U} , the density of the liquid ρ , and the radius of the tube \underline{a} , Baron concluded that the breakup distance \underline{L} , should be determinable by a relation of the type:

$$F(L, a, \sigma, \rho, U, \eta) = 0 \quad . \quad (1-70)$$

This can be expressed in dimensionless form as

$$F' \left[(L/a), \left(\frac{\rho a U^2}{\sigma} \right), \left(\frac{a U \rho}{\eta} \right) \right] = 0 \quad , \quad (1-71)$$

or

$$\frac{L}{a} = F'' \left\{ \left(\frac{\rho a U^2}{\sigma} \right), \left(\frac{a U \rho}{\eta} \right) \right\} = F'' \left\{ W_L, Re \right\} \quad , \quad (1-72)$$

where Re is the Reynolds number of the flow and W_L is the Weber capillarity number. Since the initial deformation is proportional to the size of the turbulent eddies in the surrounding gas, and since the size of these eddies is, in turn, proportional to the velocity \underline{U} , it was deduced that the breakup length \underline{L} should vary as the velocity \underline{U} . Hence, Equation (1-72) can be written

$$L = \frac{a^{3/2} \rho^{1/2} U}{\sigma^{1/2}} F'''(Re) \quad (1-73)$$

After consideration of Littaye's (1-22) analysis, Baron questioned the validity of setting the breakup time equal to the oscillation time of the droplet, and sought to modify Littaye's analysis by proposing a model for the oscillation of the droplet. He conjectured that the force of drag tends to flatten the originally spherical droplet into an ellipsoid, the force of surface tension then tending to restore the droplet to its spherical shape. This surface-tension effect is then assumed to overshoot its mark, creating an ellipsoid with a major axis perpendicular to the drag-created ellipsoid. The drag forces are now assumed to act in such a way that the droplet will execute a quarter turn for every half period of oscillation θ . This model leads to the following equations involving the frequency of rotation f_r :

$$f_r = \frac{1}{2\theta} = \frac{1}{2\sqrt{\pi^2 \rho R^3}} \frac{2\sigma}{\rho R^3} \quad (1-74)$$

Hence the pressure due to centrifugal forces is

$$\Delta p_2 = \frac{\rho \omega^2 R^2}{3} = \frac{2\sigma}{3R} \quad (1-75)$$

where ω is defined by Equation (1-56). Under the assumption that Δp_1 accounts for the entire surface-tension effect ($2\sigma/R$), Equation (1-75) thus indicates that

$$\Delta p_2 = 0.33 \Delta p_1 \quad (1-76)$$

and is not negligible, as assumed by Littaye. For very viscous liquids the period of oscillation would decrease, thus decreasing the relative effect of the centrifugal forces.

Under the assumption of the rotation-oscillation model described above, the drag and inertia forces are always in phase with the surface forces. Hence, the situation is one of forced vibration with viscous damping. By assuming harmonic vibrations, the resonant amplitude χ_o can be represented in terms of the amplitude of the applied force P_o , the coefficient of viscous damping \underline{d} , and the frequency of rotation ω as

$$\chi_o = \frac{P_o}{d\omega} \frac{P_o}{2d} \sqrt{\frac{\rho R^3}{2\sigma}} \quad (1-77)$$

Since the applied force P_o is, in fact, the drag force,

$$P_o \propto C_D \frac{\rho A}{2} (U - C)^2 S_o \quad (1-78)$$

Baron then hypothesized that atomization would result when the fractional increase in the radius (χ_o/R) exceeded a certain critical value $(\chi_o/R)_{crit}$. By assuming that the viscosity coefficient \underline{d} obeys Poiseuille's law for disk-shaped obstacles

$$d = \eta R \quad (1-79)$$

and by combining Equations (1-77), (1-78), and (1-79), the following criterion for atomization is obtained:

$$\frac{C_D \rho_A (U - C)^2 R^{1.5} (\rho)^{0.5}}{\eta \sigma^{0.5}} = 2 \left(\frac{\chi_0}{R} \right)_{\text{crit.}} = \text{const.} \quad (1-80)$$

It is noted that if $(\chi_0/R)_{\text{crit.}}$ is greater than about 0.15, the assumption of harmonic motion is not valid, and Equation (1-80) no longer gives an accurate criterion.

Inasmuch as Baron's Equation (1-80) takes into account the densities both of liquid and of gas, and the viscosity, it therefore appears to be a better criterion than Littaye's Equation (1-62); still, the approaches to both equations are based on conjectural models that may, or may not, be correct.

Borodin and Dityakin's Analysis

A very elegant, though complicated, mathematical solution to the problem of determining the unstable capillary waves on the surface of separation of two viscous liquids has been published by V. A. Borodin and Y. F. Dityakin⁽¹⁻²⁸⁾. The authors begin by considering that the velocities \underline{u} , and \underline{v} , associated with the disturbance, are derivable from a stream function Ψ . Substitution of this stream function into the Navier-Stokes equations for an incompressible fluid, and subsequent elimination of the pressure-variation term p from the two equations leads to the Helmholtz equation:

$$\nu \Delta \Delta \Psi - U \frac{\partial \Delta \Psi}{\partial x} - \frac{\partial \Delta \Psi}{\partial t} = 0 \quad , \quad (1-81)$$

where Δ is the operator,

$$\Delta = \frac{\partial^2}{\partial x^2} + \frac{\partial^2}{\partial y^2} \quad , \quad (1-82)$$

ν is the kinematic viscosity, and \underline{U} is the uniform velocity of the jet. The stream function Ψ is assumed to be of the form:

$$\Psi = f(y) e^{i(nt + Kx)} \quad , \quad (K = \frac{2\pi}{\lambda}) \quad , \quad (1-83)$$

where K is the propagated circular frequency of the vibrations, and $n = n_r + in_i$ is a complex quantity representing the time, frequency, and growth of the disturbance. Substitution of Equation (1-83) into Equation (1-81) yields

$$\nu f^{IV} - (2K^2\nu + in)f''' + (inK^2 + \nu K^4)f - iUK(f'' - K^2f) = 0 \quad , \quad (1-84)$$

where the derivatives are taken with respect to y . By setting

$$f'' - K^2f = F \quad , \quad (1-85)$$

Equation (1-84) is transformed into

$$F'' - \left(i \frac{n + UK}{\nu} + K^2 \right) F = 0 \quad . \quad (1-86)$$

The solution of Equation (1-86) then becomes:

$$F = C_1 e^{im_j y} + C_2 e^{-im_j y} \quad (1-87)$$

where $j = 1, 2$, corresponding to the liquid on either side of the surface of discontinuity, and

$$m_j = \sqrt{-i \frac{n + U_j K}{\nu_j} - K^2}, \quad j = 1, 2 \quad (1-88)$$

Substitution of Equation (1-87) into Equation (1-85) yields:

$$f = -\frac{e^{im_j y}}{m_j^2 + K^2} C_{1j} - \frac{e^{-im_j y}}{m_j^2 + K^2} C_{2j} + e^{Ky} C_{3j} + e^{-Ky} C_{4j} \quad (1-89)$$

and the stream functions corresponding to the liquids on either side of the surface of separation are determined, by substitution of Equation (1-89) into Equation (1-83), as

$$\psi_j = e^{i(Kx + nt)} \left(-\frac{e^{im_j y}}{m_j^2 + K^2} C_{1j} - \frac{e^{-im_j y}}{m_j^2 + K^2} C_{2j} + e^{Ky} C_{3j} + e^{-Ky} C_{4j} \right) \quad (1-90)$$

The boundary conditions imposed upon this solution are:

1. Finite solutions at infinity.
2. No slip on the surface of separation.
3. Continuous tangential stresses on the surface of separation.
4. Equality of the resultant of the normal stresses, at the surface of separation, with the internal pressure.

Application of these boundary conditions to the solution of Equation (1-90) leads to a series of four simultaneous homogeneous equations in the four coefficients (remaining after application of the first boundary condition), C_{21} , C_{41} , C_{12} , and C_{32} . Solution of these simultaneous equations is then indicated as the solution of an eighteenth-degree equation with complex coefficients in the dimensionless variable $z = n/(\nu_1 K^2)$. The corresponding solutions are then determined as roots of the characteristic equation in the M - N plane, where $M = n_1/n_2$, $N = \sigma \rho_1/n^2 K$. Each root of this characteristic equation for which $n_i < 0$ corresponds to the unstable configuration, the critical disturbance corresponding to maximum n_i .

Balje' and Larson's Analysis

In order to derive mathematical expressions for computing droplet sizes obtained by jet disintegration, O. E. Balje' and L. V. Larson⁽¹⁻²⁹⁾ considered the various analyses presented above. A criterion for droplet stability was obtained by consideration of Littaye's Equation⁽¹⁻⁶²⁾, in which the constant was set equal to 8, as a result of equating the ram pressure to the surface tension. Hence, the maximum stable droplet radius R_s is determined as

$$R_s = \frac{4\sigma}{\rho(U - C)^2} \quad (1-91)$$

A second criterion for stability was derived by comparing the surface areas of the liquid jet and of the droplet, and by noting that instability as a consequence of surface tension will result if the surface area of a given volume of the jet is greater than the surface area of a droplet containing the same volume. Under these considerations,

$$\Omega = \frac{A_j}{A_d} = \frac{R_d}{1.5R_j} \left(1 + \frac{R_j}{Z} \right), \quad (1-92)$$

where A and R are the surface area and radius, respectively, the subscripts j and d refer to the jet and droplet, respectively, and Z is the length of the jet. Equation (1-92) gives three criteria, depending on the value of Z :

1. For $Z \rightarrow \infty$, instability results if $R_d > 1.5 R_j$ (which is certainly true for the case investigated by Rayleigh).
2. For $R_j = Z/2$, instability results if $R_d > R_j$.
3. For $R_j > Z/2$, instability results for any relation between R_d and R_j .

After consideration of Weber's analysis, Balje' and Larson derived the following relation for determining the diameter of the droplets formed by the disintegration of a cylindrical jet:

$$R_d = R_j \sqrt[3]{\frac{3\pi}{2aK_{\max}}}, \quad (1-93)$$

where K_{\max} is the value of K for which the rate of growth of the disturbance μ is a maximum, and K is defined by Equation (1-27).

By assuming that unstable droplets (owing to the ram pressure) will not subdivide into droplets smaller than the maximum stable droplet, the authors then outline a probability theory by which drop-size spectra can be determined. Although the assumption upon which this theory is based is questionable, the idea appears to be worthy of further investigation.

The final analysis which Balje' and Larson make is that of the deceleration experienced by the droplets in a solid-impingement jet. By writing the air resistance R' of a globule as

$$R' = \frac{C_D S \rho_A C_o^2}{2}, \quad (1-94)$$

and by expressing the deceleration g as

$$g = \frac{R'}{m} = \frac{0.75 C_D C_o^2 \rho_A}{2\rho R_d}, \quad (1-95)$$

where m is the mass of the droplet, the authors determine the correction factor ξ , which is the ratio of the original jet velocity C_o to the instantaneous velocity C of the droplet at time of disintegration, to be

$$\xi = \frac{C_o}{C} = \sqrt{1 + \frac{0.75 C_D \rho_A L}{\rho R_d}} \approx 1 + \frac{0.75 C_D \rho_A L}{2\rho R_d}, \quad (1-96)$$

where L is the breakup length, as given by Weber. It should be noted that Equation (1-96) can also be obtained by integration of Littaye's Equation (1-63), if the air velocity U is set equal to zero.

Summary

The problem of determining the wavelength of the disturbance that will most rapidly lead to the instability of a liquid jet has been explored theoretically by several investigators, and solutions have been found for all cases where a linearization of the equations of conservation is possible. Lord Rayleigh's solution for the inviscid fluid has been fairly well confirmed by experimental observation, and the modifications of this solution for the cases where viscosity, jet velocity, or density ratios are important predict variations in the wavelengths which are physically reasonable. The analysis by Borodin and Dityakin, although elegant, appears to be too complicated to be practicable.

However, the problem of predicting either the cause or the effect of secondary atomization is by no means solved. Of the three theories derived for the determination of the droplet velocity C , Siestrunk's hypothesis of constant velocity is the only one that can definitely be discarded. Littaye and Baron have each made a conjecture regarding the criterion for droplet stability, but further analysis is necessary to determine the validity of these conjectures.

The breakup distance for liquid droplets, which is based upon the droplet velocity, is likewise subject to the validity of the conjectural mechanism.

Theoretical determinations of the breakup length of a jet were made both by Weber and by Baron. Of these two, Baron's analysis by dimensional considerations appears to be the better for the reason that allowance is made for the effect of the Reynolds number.

The ultimate problem of jet disintegration, which is actually the most important problem of practical interest, is the one on which the least theoretical work has been done. This is the problem of determining the drop-size distribution that will result upon disintegration of a jet. One step in the solution of this problem has been taken by Baron by using an elementary probability approach. This method, however, is highly conjectural in nature, and requires thorough investigation before its validity becomes established.

Thus it appears that few, if any, of the problems of secondary atomization can be considered to be solved by rigorous theoretical analysis. Any such analysis, of course, is extremely difficult to make, because the conservation equations, upon which the analyses of jet instability are based, cannot be linearized. Nevertheless, it is felt that the problem of secondary atomization is far from being impossible of solution.

THE VARIOUS FACTORS THAT INFLUENCE ATOMIZATION

It has been noted in the preceding sections on the mechanism of atomization that many factors affect this complicated process and determine the size of the droplets in the resultant spray. Some investigators claim that one factor is dominant, and others claim that another or several other factors predominantly control the process. An attempt is made here to summarize these various influences insofar as they are known.

Joyce⁽¹⁻²⁾ has divided the controlling factors into three groups; mechanical, operational, and fuel. Mechanical factors include the type and physical dimensions of the atomizer, dimensions being of great significance. Operational factors comprise the conditions of operation, primarily the pressure employed, which determines velocity. The fuel factors involved are the viscosity, surface tension, and density of the fuel. To these three groups may be added a fourth group that

influences atomization, the ambient-gas factors that normally would comprise the density and viscosity of the gas into which the fuel is to be injected.

Mechanical Factors

The type and size of spray nozzle used are, obviously, major factors that influence atomization. At present, however, little is known of the specific influence, in a quantitative way, except that the mean droplet size obtained from gas-atomizing nozzles is appreciably smaller than that obtained from pressure jets. Considerable data are available on the effect on atomization of nozzle dimensions, especially the influence of the diameter, and the length/diameter ratio, for a simple orifice.

Lee⁽¹⁻¹⁴⁾, ⁽¹⁻³⁹⁾, ⁽¹⁻⁴⁰⁾ has made an extensive study of the effect of dimensions of plain nozzles by injecting the fuel against plasticine targets and on smoked-glass plates. He found, as one might expect, that the drop size decreases as the orifice diameter decreases. He concluded that the optimum length/diameter ratio for the nozzle orifice is in the range of 2 to 3. In the course of his work he observed that the condition as to surface roughness or other irregularity of the inner walls of the conical approach to the cylindrical bore of the nozzle is an important factor in determining the coefficient of discharge, which, depending on these conditions, ranges from 0.65 to 0.95. Furthermore, Lee found that the size distribution of droplets from a plain nozzle was very uneven, in the sense that there was a wide difference between the sizes of the largest and smallest drops; whereas the distribution from centrifugal or swirl-type atomizers, and from sprays formed by a jet striking a metal lip, were more evenly distributed, in the sense that the size range was narrower. However, the efficiency of atomization, in terms of mean drop size, was the same for these various devices.

Holfelder⁽¹⁻⁴¹⁾ made a study of eleven different nozzle shapes, the results of which are summarized in Table 1-1. The discharge coefficients varied between 0.87 and 0.61 for a nominal diameter of 0.5 mm. Shape No. 2 has the largest coefficient, and Shape No. 6, with a tapered bore of approximately 12 degrees, has the next largest coefficient. Shape No. 7, with the short rounded inlet, also has a very favorable coefficient.

Longwell⁽¹⁻⁴²⁾ emphasizes the fact that for pressure nozzles, the variable that has the greatest effect on drop size is the radius of the orifice and that, to obtain fine atomization, small nozzles should be used.

Joyce⁽¹⁻²⁾ also studied simple pressure-jet atomizers and found that the mean size of droplets in the spray varies approximately as the square root of the diameter of the discharge orifice. Little has been done to establish the corresponding approximate quantitative relation for other types of atomizers, principally because so many more variables are involved.

Szlackin⁽¹⁻⁴³⁾ claims that, next to jet velocity, the most important factor in liquid atomization is orifice diameter. The atomization becomes finer and more uniform when small orifices are used, indicating that drop formation takes place at the surface of the jet. The chief effect of decrease in orifice size is to increase the ratio of the surface to volume of the jet as it emerges.

In a study of the effect of the shape of orifice, Szlackin found that, because of friction losses and eddies, the shape of the orifice affects the discharge coefficient and consequently the discharge velocity. Since atomization is very dependent upon liquid velocity, everything possible should be done to minimize friction losses and eddies. Szlackin recommends that the inner surface be smooth and free of burrs, but not polished. The shape of the orifice entrance is most important; it should be rounded, with the radius of curvature not less than the orifice diameter. Rounding the discharge end of the orifice has little effect.

The effect of orifice length/diameter ratio on atomization is insignificant, according to Szlackin. On the basis of work by Gelalles⁽¹⁻⁴⁴⁾, ⁽¹⁻⁴⁵⁾, ⁽¹⁻⁴⁶⁾, the coefficient of discharge is the same for length/diameter ratios between 1 and 4. To maintain the best depth of penetration

and discharge coefficient, the length/diameter ratio should be kept between 4 and 6. For ratios greater than 4-6 the coefficient of discharge gradually decreases, since friction losses become appreciable.

TABLE I-1. CHARACTERISTICS OF HOLFELDER'S TEST NOZZLES

Nozzle shape No.	1	2(a)	2(b)	3	4	5	6	7	8	9
Shape										
Bore length/ diameter ratio	10 5 3	2.5 (β 20°)	2.5 (β 60°)	5	10	10	5	5	5	5
----- Nominal diameter, 0.5 mm -----										
Smallest diameter, mm	0.540 0.549 0.541	0.549	0.569	0.632	0.560	0.530	0.628	0.550	0.752	0.574
Discharge coef- ficient	0.615 0.620 0.630	0.870	0.755	0.620	0.635	0.618	0.866	0.850	0.655	0.793
----- Nominal diameter, 1.0 mm -----										
Smallest diameter, mm	1.066 1.058 1.080	1.060	1.070	1.108	1.050	1.129	1.041	1.080	1.032	1.060
Discharge coef- ficient	0.585 0.600 0.610	0.900	0.785	0.595	0.610	0.590	0.895	0.885	0.660	0.845
----- Nominal diameter, 0.5 mm -----										
Disintegration time, T(a)	4.12 6.27 8.63	4.04	4.05	10.38	9.33	8.13	4.45	3.67	10.55	3.39

(a) $T = \frac{L}{v} (s \cdot 10^{-3})$, where L is disintegration distance for water jets, cm; and v is jet velocity at nozzle, m/s.

Watson(1-47) points out that, in aircraft gas-turbine work, in England, it is customary to express the dimensions of the atomizer by the "flow number", in place of the equivalent diameter of the nozzle orifice. However, this term is not generally used by American manufacturers. Flow number is defined as the ratio F/\sqrt{P} , where F is the flow in conventional units and P is the pressure. In England F is taken in gallons per hour, and P in lb per sq in. The chief advantage of the flow number is that it enables flows and pressures to be readily convertible for Simplex nozzles, the flow being equal to the flow number multiplied by the square root of the pressure. For high accuracy, a calibration at each pressure would, of course, be required.

Operational Factors

Pressure, as the principal operational factor for both gas atomizers and pressure nozzles, is important, not so much in itself, but because, by virtue of the pressure drop through the nozzle, velocity is imparted to the liquid or gas.

Joyce(1-2) made a quantitative study of the effect of pressure on simple swirl-type atomizers. Based on data obtained from over a hundred tests, he concluded that the surface mean-droplet size varies inversely as the applied fuel pressure to the 0.35 power.

According to Larcombe⁽¹⁻²⁶⁾, drop size is approximately inversely proportional to the square root of the pressure, which is in fair agreement with Joyce.

It should be pointed out here that varying the pressure does not greatly change the size of the smallest drops, but as the pressure is increased the number of the smaller drops is increased, so that the mean size is decreased.

Watson⁽¹⁻⁴⁷⁾ points out that the spray characteristics of a simple spray nozzle, having a fixed cone angle and flow number, depend upon the pressure employed. He presents, in the form of three-dimensional graphs, a large number of data showing drop size plotted against pressure and flow number.

Fuel Factors

The fuel factors include surface tension, density, and viscosity. Viscosity is probably the most important factor, one reason being that it may vary over such a wide range, while it also plays a major part in determining the intensity of turbulence of the issuing jet. Some investigators believe that the turbulence of the jet is the most important factor that influences breakup.

Schweitzer⁽¹⁻¹⁶⁾ states that, of the liquid properties, viscosity is recognized as having the decisive influence on jet disintegration, and that the effect of surface tension was found to be minor, at least with high-pressure sprays.

Lee and Spencer⁽¹⁻¹⁴⁾ deduced from their photomicrographic studies of fuel sprays that turbulent flow accelerates the disintegration of the fuel jet by ruffling its surface close to the orifice, but that it has relatively little disintegrating power in itself. Lee reports a decrease in disintegration with an increase in fuel viscosity, or surface tension, as one might expect.

Scheubel⁽¹⁻⁴⁸⁾ claims that the outstanding quantity of the whole atomization problem is the characteristic $K = \rho v^2 / \sigma$, where ρ and σ are the density and surface tension of the fuel, and v is the speed of the air relative to the fuel. Scheubel disagrees with Schweitzer and Lee; he considers viscosity least important, since it acts merely as a damping force.

Nukiyama and Tanasawa⁽¹⁻⁴⁹⁾ agree with Scheubel, and report that viscosity is of minor importance in determining drop size of liquids atomized by means of an air stream. They developed empirical equations for the mean diameter of drops from which it may be concluded that the magnitude of the drops is governed by the value of $\sqrt{\sigma} / (v\sqrt{\rho})$, when the ratio of air to liquid is large, and that viscosity is of little importance. But when the ratio of air to liquid becomes less, mean-drop size is mainly governed by the value of $(\mu/\sqrt{\sigma\rho})^{0.45} (1000 Q_1/Q_a)^{1.5}$, where Q_a and Q_1 are the quantities of air and liquid, respectively. In the latter equation, viscosity has become a significant factor, and the surface tension exerts only a slight influence.

Hinze⁽¹⁻²⁴⁾ states that the first effect of increase in viscosity of the liquid is a decrease of the rate of disintegration. Thicker ligaments may be formed, resulting in larger initial and also larger final drops, so that there is an increase of mean drop size. Based on photomicrographic studies of sprays made by Lee⁽¹⁻¹⁴⁾, Hinze points out that the influence of viscosity is more pronounced at low jet velocity and low air density.

Hinze describes the action of surface tension as being twofold: (1) at initial stages of disintegration (formation of ligaments and deformation of drops), surface tension counteracts disintegration; (2) at final stages (breaking up of ligaments and final stage of disruption or splitting up), surface tension favors disintegration. However, as the rate of disintegration is primarily determined by the rate of ligament formation and deformation of drops, the total result of the effect of increased surface tension is a decreased rate of disintegration.

Merrington and Richardson⁽¹⁻²⁵⁾ made extensive experiments with fixed nozzles and with moving nozzles (attached to an aircraft) discharging backwards. They found that the mean drop size depended on only two factors: (1) the relative speed, V , of the jet to the air; and (2) the viscosity of the liquid.

Figure 1-22 shows their results by a log-log plot of Vd/ν against ν , where V is the relative velocity between the jet and the surrounding air, d is the mean drop size, and ν is the kinematic viscosity of the liquid. The results, for both stationary and moving nozzles, satisfy the empirical formula $Vd/\nu^{0.2} = 500$. Since static and moving nozzles gave identical expressions for drop size, these authors concluded that breakup in the atomization region is initiated by turbulence within the jet, but is finally controlled by air friction on the jet surface. This is in agreement with the conclusions arrived at by Schweitzer⁽¹⁻¹⁶⁾, who found that atomization could not be obtained without air friction, but turbulence was essential to make air friction effective.

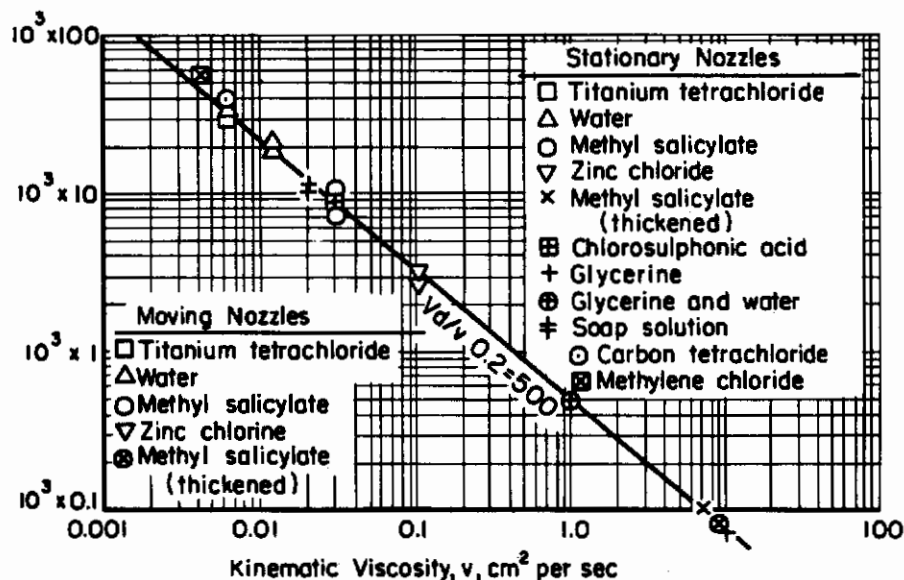


FIGURE 1-22. INFLUENCE OF LIQUID VISCOSITY ON DROP SIZE

(Merrington and Richardson)¹⁻²⁵

At very low velocities, this relation ceases to apply and the drop size reaches a limiting value. For example, with small nozzles (1-mm diameter), the constant drop size reached is roughly twice the nozzle diameter, with all but the highly viscous liquids.

The surface tensions of most of the liquids used by Merrington and Richardson are in the neighborhood of 30 dynes per cm, except for water and glycerine, which have values of 73 and 64 dynes per cm, respectively. These two liquids produced mean drop sizes expected from their respective viscosities, and showed no effects that could be ascribed to surface tension.

Joyce⁽¹⁻²⁾ is among those investigators who consider that viscosity is the significant fuel factor. He points out that surface tension in hydrocarbon-liquid fuels varies only slightly, and has little effect on the quality of atomization.

Figure 1-23 shows the quantitative effect of fuel viscosity as a factor affecting the atomization process. The dotted line drawn to intersect the curves at a common-surface mean diameter of 97 microns shows that, whereas at a viscosity level of 2 centistokes this mean droplet size is obtained with a supply pressure of 100 psi, the corresponding pressures at 8 and 18.5 centistokes are 185 and 300 psi, respectively.

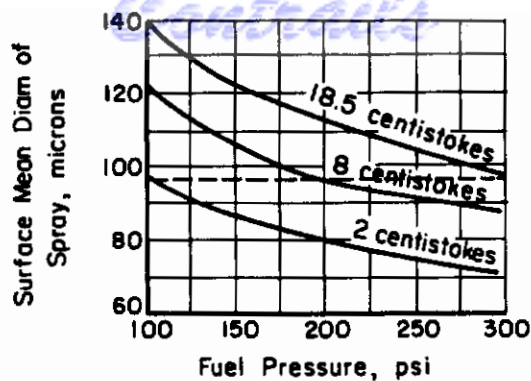


FIGURE 1-23. EFFECT OF VISCOSITY ON MEAN DROPLET SIZE (SWIRL-TYPE ATOMIZERS) (Joyce)¹⁻²

Lawrence⁽¹⁻⁷⁾, in discussing the practical performance of gas-turbine spray nozzles, states that the atomization obtained is basically a function of the Reynolds number; that is, the lower the viscosity of the fuel the better the atomization. Lawrence points out further that the viscosity of the fuel may be intrinsically low, as in the case of gasoline, or it may be artificially lowered by preheating, as adopted in industrial use of heavy oils. The effect of a low viscosity is to give adequate atomization at low pressures.

Watson⁽¹⁻⁴⁷⁾, in a practical paper on aircraft gas turbines, states that, of the physical properties of the fuel, viscosity is of major importance. Tests tend to suggest that an upper limit of viscosity for efficient atomization in the normal type of burner may be of the order of 7 to 10 centistokes. If the viscosity lies above this range, then a special burner, or preheating, may be necessary. The variation of the viscosity of fuels with temperature is therefore of prime practical importance.

Mock and Ganger⁽¹⁻⁵⁰⁾ believe that, from the practical standpoint, surface tension may be a major cause of spray-nozzle problems. They claim that, for swirl-type nozzles at low flows, the force of surface tension is strong enough, relative to the energy of the fuel, to interfere with atomization. The fuel adheres to the face of the orifice and forms glassy "olives" and "umbrellas" instead of continuing cones. They state further that achievement of a high degree of atomization, particularly at low fuel-flow rates, is the major need in the field of gas-turbine power-plant fuel-spray nozzles.

Ambient-Gas Factors

The properties of the gas into which liquid fuel is to be injected have an effect on atomization, principally by influencing the time interval and distance of travel before disintegration progresses to a given extent.

Figure 1-6 of this chapter shows the effect of air density on fuel jets. A decrease in air density results in the jets' disintegrating at a greater distance from the spray nozzle, but the final effect is about the same.

Holfelder⁽¹⁻⁴¹⁾ studied the effect of air density by injecting water into a chamber evacuated to 0.11 atmosphere absolute pressure. He reports that the disintegration distance does not increase excessively, despite the much retarded occurrence of disintegration by wave formation.

Szlackin⁽¹⁻⁴³⁾ injected liquid into an air chamber at 1, 5, and 10 atmospheres pressure, respectively, and obtained data which show that increase in the density of air has little effect on the ultimate fineness of atomization, but that it does cause atomization to take place closer to the nozzle.

Hinze⁽¹⁻²⁴⁾ claims that mean drop size decreases with increase in density or pressure of the ambient atmosphere; the decrease is appreciable at low densities, but very slight at high densities. Hinze also states that, without the harmful mutual interaction of liquid particles resulting in coalescence, an increased air density would result not only in an increased rate of disintegration but also in an increased fineness of atomization, at least at densities encountered in combustion-engine practice. Because of the mutual interaction of droplets, however, mean drop size remains essentially unchanged.

Schmidt⁽¹⁻⁵⁰⁾ made an experimental study of the behavior of liquids injected into a chamber having a pressure below the vapor pressure of the liquids, and observed that the jet fans out because of rapid evaporation of the liquid as it enters the low-pressure region.

Summary of Various Factors Influencing Atomization

Probably the most important information needed to advance the knowledge of atomization is a more complete understanding of how drop-size distribution is affected by nozzle design, by operating conditions, and by the properties of the liquid and of the air into which it is to be injected.

In solid injection, the nozzle diameter, pressure and viscosity of the liquid appear to be the most important factors. The status of present knowledge may be briefly and approximately summarized by the relation:

$$\text{Mean drop size} = f \left[\frac{(\text{orifice diam})^{0.5} (\text{kinematic vis.})^{0.2}}{(\text{liquid pressure})^{0.4}} \right]$$

The surface tension of the liquid and the density of the air, or other gas into which the liquid is injected, are of secondary importance.

In gas atomizers, the influence of the various factors is well shown by the following empirical equation derived by Nukiyama and Tanasawa⁽¹⁻⁴⁸⁾:

$$d_o = \frac{585\sqrt{\sigma}}{v\sqrt{\rho}} + 597\left(\frac{\mu}{\sqrt{\sigma\rho}}\right)^{0.45} \left(1000\frac{Q_l}{Q_a}\right)^{1.5}$$

where d_o (measured in microns) = the diameter of a single drop having the same volume/surface ratio as the total sum of the drops; v = relative velocity between the air stream and the liquid stream, meters per sec; Q_l/Q_a = ratio of volume flow rate of liquid to volume flow rate of air at vena contracta; ρ = liquid density, grams per cc; μ = liquid viscosity, poises; and σ = liquid surface tension in dynes per cm. This formula holds true for $0.8 < \rho < 1.2$; $30 < \sigma < 73$; and $0.01 < \mu < 0.3$.

Lewis, et al. ⁽¹⁻⁵¹⁾, corroborated and extended this work of Nukiyama and Tanasawa.

REFERENCES

- 1-1. Lucas, J., The Jet-Engine Fuel System; Flight, Vol. 49, January 10, 1946, p. 41.
- 1-2. Joyce, J. R., The Atomization of Liquid Fuels for Combustion; Jour. of Inst. of Fuel, Vol. 22, No. 124, February, 1949, p. 150.
- 1-3. Probert, R. P., The Influence of Spray Particle Size and Distribution in the Combustion of Oil Droplets; Phil. Mag., Vol. 37, February, 1946, p. 94.
- 1-4. Romp, H. A., Oil Burning; Martinus Nijhoff (The Hague), 1937.

- 1-5. Castleman, R. A., Jr., The Mechanism of the Atomization Accompanying Solid Injection; NACA Report No. 440, 1932, 12 pp.
- 1-6. Mock, F. C., and Ganger, D. R., Practical Conclusions on Gas Turbine Spray Nozzles; SAE Quarterly Trans., Vol. 4, No. 3, July, 1950, p. 357.
- 1-7. Lawrence, O. N., Gas Turbine Accessory Systems; J. Roy. Aeron. Soc. (England), 1948, p. 151.
- 1-8. Rayleigh, Lord, On the Instability of Jets; Proc. of London Math. Soc., Vol. 10, 1878, p. 4.
- 1-9. Haenlein, A., Ueber den Zerfall eines Flüssigkeitsstrahles; Forschung auf dem Gebiete des Ingenieurwesens, Vol. 2, No. 4, April, 1931, p. 139. (English Translation: Disintegration of a Liquid Jet; NACA Tech. Memo. No. 659, February, 1932).
- 1-10. Weber, C., Zum Zerfall eines Flüssigkeitsstrahles; Zeitschrift fuer angewandte Mathematik und Mechanik, Vol. 11, 1931, p. 136. (English Translation: On the Breakdown of a Fluid Jet; Ninth Progress Report, Project MX-833, Sect. II, University of Colorado, Boulder, Colorado.)
- 1-11. Castleman, R. A., Jr., The Mechanism of the Atomization of Liquids; Bur. Std. Jour. of Research, Vol. 6, No. 3, 1931, p. 369.
- 1-12. Sauter, J., Investigation of Atomization in Carburetors; NACA Tech. Memo. No. 518, 1929, 10 pp.
- 1-13. Lee, Dana W., and Spencer, R. C., Preliminary Photomicrographic Studies of Fuel Sprays; NACA Tech. Note No. 424, 1932.
- 1-14. Lee, Dana W., and Spencer, Robert C., Photomicrographic Studies of Fuel Sprays, NACA Report No. 454, 1933, 27 pp.
- 1-15. DeJuhasz, Kalman J., Zahn, O. F., and Schweitzer, P. H., On the Formation and Dispersion of Oil Sprays; Pennsylvania State College, Engr. Expt. Sta. Bulletin No. 40, 1932, 94 pp.
- 1-16. Schweitzer, P. H., Mechanism of Disintegration of Liquid Jets; Jour. of Applied Physics, Vol. 8, August, 1937, p. 513.
- 1-17. Tyler, E., Instability of Liquid Jets; Phil. Magazine (London), Vol. 16, 1933, p. 504.
- 1-18. Nukiyama, S., and Tanasawa, Y., An Experiment on the Atomization of Liquid (5th Report, The Atomization Pattern of Liquid by Means of Air Stream); Summary Section, Trans. SME, Japan, February, 1940, Vol. 6, No. 22, p. S-7.
- 1-19. Fogler, B. B., and Kleinschmidt, R. V., Spray Drying; Ind. Eng. Chem., Vol. 30, 1938, p. 1372.
- 1-20. Siestrunk, Raymond, Sur les Régimes de Résolution des Jets Liquides sous L'Influence d'un Soufflage Axial; Comptes Rendus, Vol. 215, 1942, p. 404.
- 1-21. Littaye, Guy, Sur une Théorie de la Pulvérisation des Jets Liquides; Comptes Rendus, Vol. 217, 1943, p. 99.
- 1-22. Littaye, Guy, Sur L'Atomisation d'un Jet Liquide; Comptes Rendus, Vol. 217, 1943, p. 340.
- 1-23. Littaye, Guy, Influence de la Vitesse de l'air sur le Diamètre des plus Petites Gouttes Obtenues par Atomisation Pneumatique; Comptes Rendus, Vol. 218, 1944, p. 440.

- 1-24. Hinze, J. O., On the Mechanism of Disintegration of High Speed Liquid Jets; Contribution to: 6me Congr. Intern. de la Mécanique Appliquée, Paris, September, 1946, Section 2, 8 pp. (Also corrections as of June, 1950).
- 1-25. Merrington, A. C., and Richardson, E. G., The Break-Up of Liquid Jets; Proc. of the Physical Soc., Vol. 59, Part I, No. 331, January, 1947, p. 1.
- 1-26. Larcombe, H. L. M., Principles of Pressure Spray Nozzles; Chemical Age (London), Vol. 57, 1947, Part I, pp. 563-566; Part II, pp. 597-598; Part III, pp. 621-623.
- 1-27. Baron, Thomas, Atomization of Liquid Jets and Droplets; Univ. of Illinois Technical Report No. 4, February 15, 1949, 24 pp. (Prepared under Contract N 6-ori-71, Task Order No. XI, Office of Naval Research, Navy Department.)
- 1-28. Borodin, V. A., and Dityakin, Y. F., Neustoichivye Kapilliarnye Volny na Poverkhnosti Razdela Dvukh Vyazkikh Zhidkostei; Prikladnaya Matematika i Mekhanika, Vol. XIII, No. 3, 1949, 19 pp. (Translation: Unstable Capillary Waves on Surface of Separation of Two Viscous Fluids; NACA Tech. Memo. No. 1281, April, 1951.)
- 1-29. Balje, O. E., and Larson, L. V., The Mechanism of Jet Disintegration; AAF Air Materiel Command, Engineering Division Memorandum Report No. MCREXE-664-531B, GS-USAF - Wright Patterson No. 179, August 29, 1949, 48 pp.
- 1-30. Donnelly, J. J., and Wohl, K., Progress on Spray Research; Chemical Engineering Project No. 62, University of Delaware Report No. 106, August 23, 1950, 18 pp and 25 fig.
- 1-31. Lane, W. R., Shatter of Drops in Streams of Air; Ind. Eng. Chem., Vol. 43, June, 1951, p. 1312.
- 1-32. Hochschwender, E., Dissertation, Heidelberg, 1919.
- 1-33. York, J. Louis, Associate Professor of Chemical Engineering, Univ. of Michigan, Ann Arbor, Mich., Private Communications, Sept. 14, 1951 and Sept. 28, 1951.
- 1-34. York, J. Louis, Stubbs, H. E., and Tek, M. R., The Mechanism of Disintegration of Liquid Sheets; ASME Paper No. 53-S-40 presented Apr. 30, 1953, at Cols., Ohio.
- 1-35. Fraser, R. P., Dombrowski, N., Eisenklam, P., Vibrations as a Cause of Disintegration in Liquid Sheets; NATURE, No. 4402, March 13, 1954, p. 495.
- 1-36. Dodge, R. A., Hagerty, W. W., and York, J. Louis, Continuous Fuel Sprays; AF Technical Report No. 6067, July, 1950, 71 pp., Power Plant Laboratory, Engineering Division, Air Materiel Command, Wright-Patterson Air Force Base, Dayton, Ohio.
- 1-37. Rayleigh, Lord, On the Instability of a Cylinder of Viscous Liquid Under Capillary Force; Phil. Mag., Vol. 34, 1892, p. 153.
- 1-38. Taylor, G. I., The Mechanics of Swirl Atomizers; Proc. of 7th Inter. Congress for Applied Mechanics, 1948, Vol. 2, Part I, p. 280.
- 1-39. Lee, Dana W., The Effect of Nozzle Design and Operating Conditions on the Atomization and Distribution of Fuel Sprays; NACA Report No. 425, 1932.
- 1-40. Lee, Dana W., A Comparison of Fuel Sprays From Several Types of Injection Nozzles; NACA Report No. 520, 1935, 38 pp.
- 1-41. Holfelder, Otto, Zur Strahlzerstaubung bei Dieselmotoren; Forsh. Ing. Wes., Sept./Oct., 1932, p. 229.

- 1-42. Longwell, J. P., Fuel Oil Atomization; D. Sc. Thesis, MIT, 1943, 167 pp., 38 figs.
- 1-43. Szlackin, J. A., Notes on Atomization of a Liquid at Low Injection Pressures; Bell Aircraft Corp., METEOR Report No. BAC-5, June 20, 1947, 11 pp.
- 1-44. Gelalles, A. G., and Marsh, E. T., Effect of Orifice Length/Diameter Ratio on the Coefficient of Discharge of Fuel Injection Nozzles; NACA Technical Note 369, 1931, 14 pp.
- 1-45. Gelalles, A. G., Effect of Orifice Length/Diameter Ratio on Fuel Sprays for Compression Ignition Engines; NACA Report No. 402, 1932, 13 pp.
- 1-46. Gelalles, A. G., Coefficient of Discharge of Fuel Injection Nozzles for Compression Ignition Engines; NACA Report No. 373, 1931, 19 pp.
- 1-47. Watson, E. A., and Clarke, J. S., Combustion and Combustion Equipment for Aero. Gas Turbines; Jour. of Inst. of Fuel, Vol. 21, No. 116, Oct., 1947, p. 1.
- 1-48. Scheubel, F. N., On Atomization in Carburetors; NACA Technical Memorandum No. 644, 1931, 10 pp. (Translated from "Jahrbuch der Wissenschaftlichen Gesellschaft fur Luft fahrt", pp. 140-6, 1927.)
- 1-49. Nukiyama, S., and Tanasawa, Y., An Experiment on the Atomization of Liquid (4th Report. The Effect of the Properties of Liquid on the Size of Drops); Summary Section, Trans. SME Japan, February, 1939, Vol. 5, No. 18, p. S-15.
- 1-50. Mock, Frank C., and Ganger, Dean R., Surface Tension Diagnosed as Cause of Spray Nozzle Problems; SAE Journal, Feb., 1950, p. 22.
- 1-51. Schmidt, Jacob M., An Experimental Study of the Behavior of Liquid Streams Injected Into a Low-Pressure Chamber; Progress Report No. 4-94, Jet Propulsion Lab., Cal. Inst. Tech., April 22, 1949.
- 1-52. Lewis, H. C., Edwards, D. G., Goglia, M. J., Rice, R. I., and Smith, L. W., Atomization of Liquids in High Velocity Gas Streams; Ind. Eng. Chem., Vol. 40, Jan., 1948, p. 67.

Contrails

CHAPTER 2. METHODS OF ATOMIZATION

ABSTRACT

Five basically different methods of atomization are briefly described and illustrated. They are: (1) solid injection, using pressure nozzles, (2) two-fluid atomization, whereby the liquid is disintegrated when it encounters a high-velocity stream of gas, (3) atomization by rotating disks or cups, (4) atomization by vibrating devices employing sonic or mechanical vibrations, and (5) atomization by impinging jets, whereby the collision of two or more liquid jets results in atomization. The solid injection and the two-fluid methods of atomization are the most frequently used. The efficiency of all methods is extremely low.

Contrails

METHODS OF ATOMIZATION

by

J. M. Pilcher and C. C. Miesse

A liquid may be disintegrated into droplets by five basically different methods of atomization as follows: (1) by solid injection, using pressure nozzles; (2) by two-fluid atomization, whereby the liquid is disintegrated when it encounters a high-velocity stream of gas - this is commonly called air-stream atomization; (3) by the use of rotating disks or cups, from the periphery of which the liquid is discharged at high velocity; (4) by vibrating devices employing sonic or mechanical vibrations; and (5) by impinging jets, whereby collision of the two liquid jets results in atomization.

The first two methods, one employing pressure nozzles and the other using two-fluid atomizers, are the most generally applied at present. During the past few years, however, much attention has been given to the rotating disk as a device for atomization. Little work has been reported on methods based on the use of vibrations; whereas, recent interest in rockets has stimulated work on the last-mentioned method involving impinging liquid jets.

A brief description and an illustration of each of the five methods follows, including a discussion of their respective advantages and disadvantages.

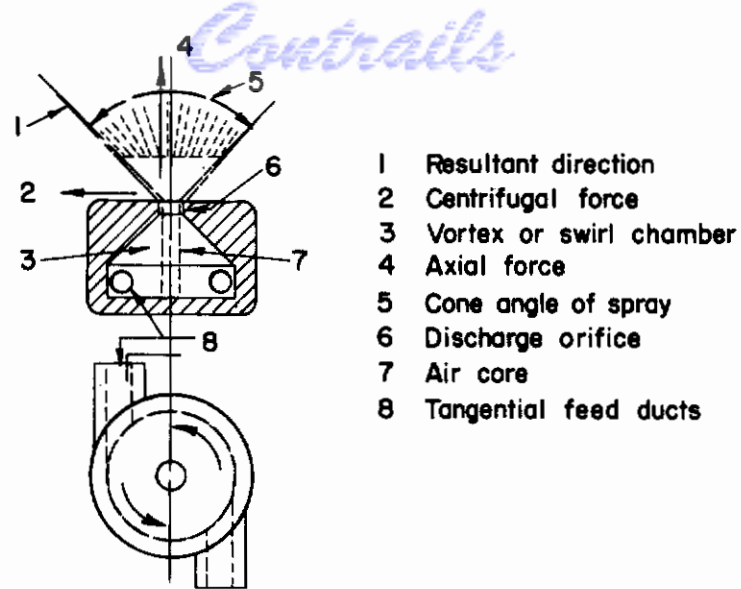
SOLID INJECTION

The most widely used method for atomizing liquid fuels is solid injection by pressure nozzles. This method depends primarily on the flow of liquid through an orifice under pressure to form an unstable jet of high velocity which disintegrates after leaving the nozzle orifice and coming in contact with the air or gases in the combustion chamber. This manner of preparing liquid fuel for combustion first enjoyed general application in 1902, when Körting succeeded in breaking up the liquid fuel by applying pressure and using a helical screw to impart rotary motion to the liquid before its escape through the orifice⁽²⁻¹⁾. Some 20 years elapsed, however, before the fundamental principles involved were studied, mainly in connection with research done on solid injection for diesel engines.

Joyce⁽²⁻²⁾ points out that there are two types of pressure-jet atomizers: (1) plain-orifice types, as used in diesel and other internal-combustion engines, employing pressures as high as 5,000 psi; and (2) centrifugal swirl types, as used almost universally in marine and stationary boilers and in the modern aircraft gas turbines. Fuel pressures required are much lower for swirl-type nozzles than for plain nozzles. Swirl-type nozzles will be discussed first.

Swirl-Type Atomization

Figure 2-1 shows the design principles of a simple swirl-type atomizer⁽²⁻²⁾. The liquid under pressure is fed through tangentially disposed ducts, slots, or channels leading to a circular space called the vortex chamber or swirl chamber. As the liquid spins or swirls around, its angular velocity increases inversely as the radius of swirl. This implies infinite velocity at the axis of the swirl chamber; this is unattainable. A core of air is formed, as shown in Figure 2-1. The rotating mass of liquid is forced forward, around this core of air, towards the discharge orifice, which has a small diameter as compared with that of the swirl chamber. The liquid is



- 1 Resultant direction
- 2 Centrifugal force
- 3 Vortex or swirl chamber
- 4 Axial force
- 5 Cone angle of spray
- 6 Discharge orifice
- 7 Air core
- 8 Tangential feed ducts

FIGURE 2-1. PRINCIPLE OF SIMPLE SWIRL-TYPE ATOMIZER

(Joyce)²⁻²

under the influence of two main forces: (1) the translational force moving the liquid axially forward, and (2) the centrifugal or spinning component which makes the liquid fly outwards, tangentially, immediately after it emerges from the restricting boundary wall of the orifice. As a result, the liquid emerges from the orifice as a divergent cone and forms a rapidly thinning conical film⁽²⁻²⁾.

Joyce⁽²⁻²⁾ points out that the formation of the air core is a characteristic feature of swirl-type atomization, which accounts for the low coefficients of discharge obtained with nozzles using this method of atomization. The air core increases in diameter as the supply pressure increases; a limit to its growth with increase in pressure results from the fact that, ultimately, the viscous losses impose an upper limit to the angular velocity, thus preventing further growth; thereafter, there is a slight diminution in the solid angle of the spray cone as more fuel is forced through the orifice owing to the increasing pressure.

Practically all of the various designs of spray nozzles used on aircraft gas turbines utilize this method of atomization; these designs are described in Chapter 3.

McEntee⁽²⁻³⁾ lists four general rules that apply to this method of atomization: (1) Capacity is nearly proportional to the square root of the pressure except at extremely high pressures, where friction limits the discharge. (2) For a given design of nozzle, the discharge at constant pressure is approximately proportional to the area of the orifice, although the orifice does not run full. (3) The rate of discharge does not decrease appreciably with increase in the viscosity of the liquid, until the viscosity is more than ten times that of water. (4) The included angle of the spray cone increases with increase in pressure (until a critical pressure is reached).

Modified Plain-Orifice Nozzles

The method of atomization by solid injection with the plain orifice may be modified by the addition of a metal lip or other surface against which the jet of fluid is allowed to impinge. The size distribution of fuel from plain nozzles, which usually is quite uneven or of a wide range, may be made more even or narrower in range by this means.

In two-fluid atomization, the liquid is broken up by impingement with a high-velocity stream of gas, usually air but sometimes steam. This method of atomization is also called air-stream atomization, air-blast atomization, pneumatic atomization, gas-atomization, or air injection, by various writers.

Joyce⁽²⁻²⁾ has proposed three classifications for this method of atomization based upon the air pressures used: (1) low-pressure air atomizers employ pressures ranging from about 10 to 25 inches of water; (2) medium-pressure atomizers use air at 1.5 to 10 psi; and (3) high-pressure atomizers use air at pressures up to 100 psi or more. Only about three per cent of the air necessary for combustion is required for atomization at medium or at high pressures; whereas, at least 25 per cent of the total air required is used for atomization at low pressures. In fact, it is common practice to pass all the combustion air through a low-pressure air atomizer.

Two-fluid atomization may be accomplished by causing the air and liquid streams to come together inside the nozzle, or just outside as the two streams leave the nozzle.

Figures 2-2(a) and 2-2(b) show illustrations of these two classes of two-fluid atomizers. For the specific external mixing atomizer that is shown in Figure 2-2(b), the liquid may be supplied by suction or under a slight gravity head.

The chief advantage of two-fluid atomization is that a greater fineness of atomization can be accomplished, resulting in a spray having a smaller mean drop size. In this regard, Green⁽²⁻⁴⁾ states that the main hope for achieving fine atomization lies in the application of aerodynamic forces. The main disadvantage, in certain applications, according to Lawrence⁽²⁻⁵⁾, lies in the difficulty in supplying compressed air. Even in the higher pressure units about two to three pounds of air is required per gallon of fuel burned.

Fogler and Kleinschmidt⁽²⁻⁶⁾ point out that an important difference and advantage of two-fluid atomization, as compared with methods involving the formation of a film of liquid as in solid injection, is that the energy that can be imparted to a pound of liquid in the form of pressure is very small in comparison with the energy available in a pound of air or steam.

Houghton⁽²⁻⁷⁾ states that an additional advantage of two-fluid atomization over pressure atomizers is that liquids of higher viscosity can be atomized satisfactorily, but that more power is required to spray at a given rate than with a pressure nozzle because the fluid is more finely divided.

Special Methods Employing
Two-Fluid Atomization

Limper⁽²⁻⁸⁾ made a study of a venturi atomizer in which the liquid is injected into a high-speed gas stream in the throat of a convergent-divergent diffuser. Axial injection in the center of the throat (which should be not more than one throat diameter in length) was found to be the most efficient arrangement. When the exit velocity was greater than 400 fps, there was no evidence of unatomized liquid leaving the discharge end. Limper concluded that, when using this method of atomization, the velocity of the liquid stream should be as low as possible to insure complete atomization in the throat section. Furthermore, the degree of atomization is improved by adding a straight length of throat section.

Ennis and James⁽²⁻⁹⁾ have developed a method for producing individual droplets of uniform size using a simple glass apparatus, termed a "droplet sizer", which is adaptable for delivering very small volumes of atomized liquid for experimental purposes.

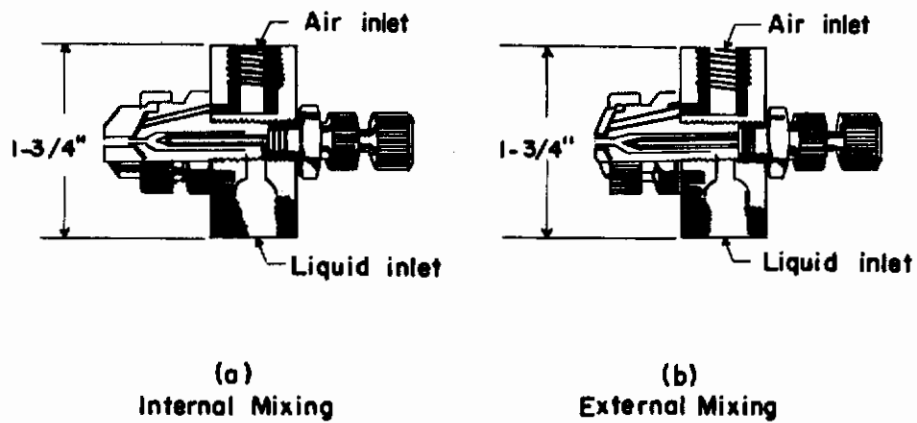


FIGURE 2-2. TWO-FLUID ATOMIZING NOZZLES
(Courtesy Spraying Systems Company)

Cadle and Magill⁽²⁻¹⁰⁾ have developed aerosol generators that disperse liquids by an aspirating action employing the method of two-fluid atomization using compressed air at about 5 psi.

Strehlow⁽²⁻¹¹⁾ has prepared an extensive bibliography on aerosols, listing many methods using the principle of two-fluid atomization. However, the size of droplets involved in aerosols is too small to justify further discussion in this monograph.

ROTATING DISKS AND CUPS

During the past few years much attention has been given to the method of atomization utilizing a rotating disk or a rotating cup. Devices based on this method of atomization are frequently referred to as "centrifugal atomizers"; however, this term leads to a likelihood of confusing "centrifugal disk atomizers" with "centrifugal nozzles", the latter meaning the swirl-type atomizing nozzle, shown in Figure 2-1. The two methods are entirely different although both employ centrifugal forces to accomplish atomization. To avoid confusion, the term "rotating" will be used in referring to the method of atomization employing disks, cones, bowls, cups or other shapes rotated at high speed by electric motors, or by air or steam turbines.

Walton and Prewett⁽²⁻¹²⁾ made a detailed study of the production of sprays by means of rotating disks, which, they point out, is a method contrasting strikingly with other methods of liquid disruption in that a spray of almost uniform drop size can be produced. Other methods, with the exceptions of the "droplet sizer", and of very low-velocity injection from narrow jets which are of no practical significance, give widely heterogeneous dispersions.

Figure 2-3 shows, diagrammatically, the section of a rotating-disk atomizer. The liquid is fed from a small-bore tube onto the center of the rotating surface and spreads over it to the periphery in a thin film. Care should be taken to see that the feed is central and continuous and that the rotor surface is completely wetted by the liquid; otherwise, an uneven film and nonuniform dispersion may result.

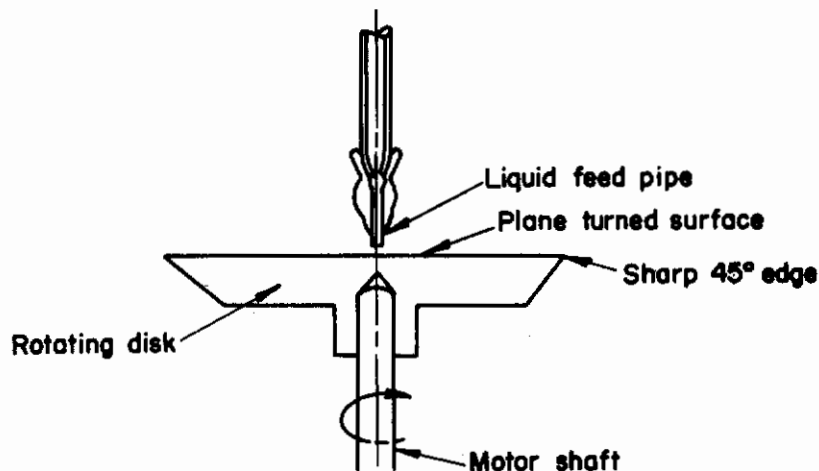


FIGURE 2-3. ROTATING-DISK ATOMIZER

(Walton and Prewett)²⁻¹²

Walton and Prewett's study covered a drop-size range from diameters of several millimeters down to about 15 microns. They found that the spray projected from the rotor always contains a number of fine satellite drops, in addition to the main spray which is homogeneous in drop size provided that the flow rate is sufficiently low. However, the percentage of the sprayed liquid

comprised in the satellite drops is extremely small. As the rate of liquid feed is increased, the size and distance of projection of the main drops remains unchanged, but the satellite drops increase in size, size-range, and number until at high flow rates a continuous spectrum of drop sizes is produced and there is no separation of the satellites from the main drops.

Walton and Prewett point out that in this method of atomization, liquid flows to the edge of the disk and accumulates until the centrifugal force on the collected mass is greater than the retaining forces due to surface tension. A drop is then thrown off. For a given type of disk-edge profile, it is therefore reasonable to expect a proportionality between the product of the mass of the drop by the accelerating force, and the product of the surface tension by the linear dimension of the drops. Using this reasoning, Walton and Prewett conducted a large number of experiments from which they developed the following empirical equation for the size of the drops in the main spray:

$$d = 3.8 / \omega (\sigma / D\rho)^{1/2} , \quad (2-1)$$

where d is the diameter of drop, cm; D is the diameter of the disk, cm; ω is the angular velocity of the disk, radians/sec; σ is the surface tension of the liquid, dyne/cm; and ρ is the density of the liquid, g/cu cm. It will be noted that viscosity does not appear as a variable in this equation. Within limits, viscosity appears to have little effect on this method of atomization, except that high viscosity does tend to increase the proportion of satellites in the spray and to reduce the maximum flow rate at which homogeneous drops are formed.

The Walton-Prewett formula has been modified using their data to give the following relation that applies more accurately for the formation of water sprays:*

$$d = \frac{3.59}{\omega D^{0.6237}} \left(\frac{\sigma}{\rho} \right)^{1/2} . \quad (2-2)$$

A re-examination of the data of Walton and Prewett, employing dimensional analysis, has led to the following equation that takes into consideration the effect of liquid viscosity:**

$$\frac{d}{D} = 6.855 \left(\frac{\eta^2}{\rho\sigma D} \right)^{0.041} \left(\frac{\omega^2 D^3 \rho}{\sigma} \right)^{-0.522} , \quad (2-3)$$

where η is the viscosity of the liquid.

Gumz also developed a semiempirical formula for predicting the distance of projection of droplets from a rotating disk, again using the data of Walton and Prewett:

$$\delta = \epsilon \times V_{\text{periph.}} \times V_{\text{term.}} / g , \quad (2-4)$$

where δ is the distance of projection, meters; $V_{\text{periph.}}$ is peripheral speed of the disk, meters/sec; $V_{\text{term.}}$ is the terminal velocity of the droplet, meters/sec; g is the gravitational constant, 9.81 meters/sq sec; and ϵ is a factor to include the effects of slippage, release of the droplets from the surface or edge, and acceleration of the droplets. For water droplets in the range of $d \leq 1000$ microns,

$$\epsilon = 0.30 + 1.59 \times 10^{-3} d - 1.66 \times 10^{-6} d^2 + 0.46 \times 10^{-9} d^3 . \quad (2-5)$$

For water drops in the range of $d \geq 1000$ microns,

$$\epsilon = 0.527 - 0.054 \times 10^{-3} d + 0.222 \times 10^3 d^{-1} . \quad (2-6)$$

* By W. Gumz, Battelle Consultant.

** By A. A. Putnam and C. C. Miesse, Battelle Memorial Institute.

Gumz states that the equation can be used safely for drops up to 2500 microns diameter.

May⁽²⁻¹³⁾ employed the rotating-disk method of atomization using a high-speed spinning top operated by compressed air. He found that water, because of its high surface tension, is more difficult to spray than oils. All grease must be removed from the rotor surface, and "parkerizing" of the rotor is recommended. The use of wetting agents is also helpful.

By applying a suction field around the rotor, May was able to withdraw the satellite drops while a crossflow of air carried off the main droplets. In this way, homogeneous oil mists having uniform droplet diameters as small as 6 microns were produced.

When spraying fine liquids such as oils or organic solvents that readily wet the rotor, May reports that 90 per cent of all droplets fall within a band of five per cent of the mean size in width, and the minimum observed drop is only six per cent smaller than the mean.

Marshall and Seltzer⁽²⁻¹⁴⁾ point out that several types of rotating disks may be used to atomize liquids. Although the simplest method is a flat, smooth disk, a second method may be visualized that involves a disk having a number of equally spaced radial vanes to prevent slippage of the liquid over the surface of the disk.

Figure 2-4 shows how, with such a disk, the liquid may be pictured as riding against the vanes. Marshall and Seltzer, in collaboration with R. L. Pigford of the University of Delaware, have developed equations expressing the time required for the liquid to reach the periphery of the disk for both the smooth and the vaned disks.

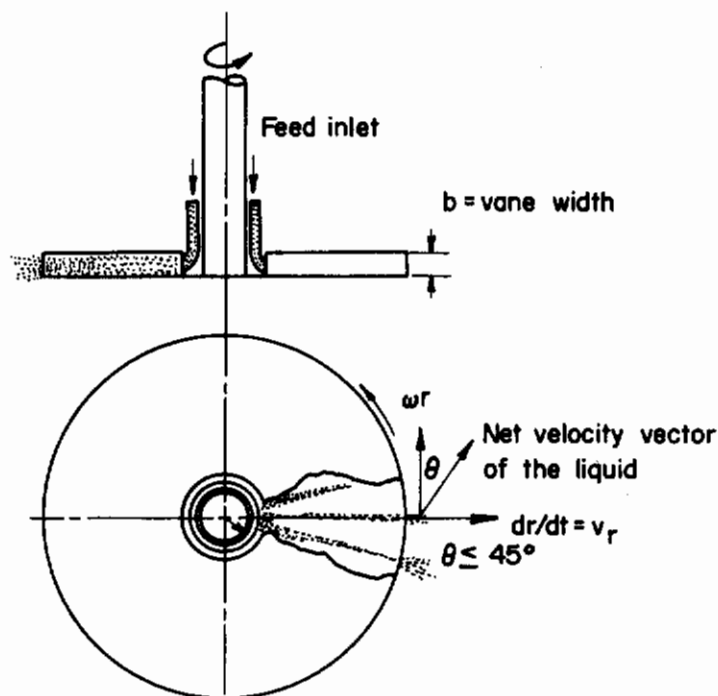


FIGURE 2-4. LIQUID FLOW ON A VANED DISK

(Marshall and Seltzer)²⁻¹⁴

Advantages of this method of atomization are: (1) Disks are more flexible than nozzles from the standpoint of variations in operating conditions. For example, the feed rate can be reduced essentially to zero and yet the fine atomization will be obtained. (2) Disks can handle liquids of high viscosity and liquids containing foreign matter that would plug the orifices of nozzles. (3) The trajectory of the drops of liquid leaving the rotating disk is not disturbed appreciably until high air velocities have been reached.

The theoretical net power for disk atomizers, based on the kinetic energy required to give the liquid a certain resultant velocity, as it leaves the disk, has been calculated by Adler and Marshall(2-15) from the relation,

$$P = \frac{wv^2}{2g_c} , \tag{2-7}$$

where P is the net power; w/g_c is the liquid feed rate; v is the resultant liquid velocity as it leaves the disk.

If the liquid is deposited at the center of the disk and friction is negligible, Adler and Marshall have shown that the power is given by:

$$P_k = 7.70 (10^{-9})w (Nr)^2 , \tag{2-8}$$

where P_k is net power required, kw; w is the liquid rate, lb/min; N is rpm; and r is the radius of disk, ft.

If the liquid is deposited not at the center of the disk, but at r_o from the center, Equation (2-8) becomes

$$P_k = 7.70 (10^{-9}) w N^2 \left[r^2 - (1/2)r_o^2 \right] . \tag{2-9}$$

For all types of disks studied by Marshall, the measured net power agreed well with this theoretical equation.

Figure 2-5 shows the effect of feed rate, disk speed, and disk size on power consumption. For disks on which liquid slippage is likely to occur, the net power will be below the curve. If a disk moves large quantities of air, in addition to accelerating the liquid, the net power may be greater than that predicted by the equation.

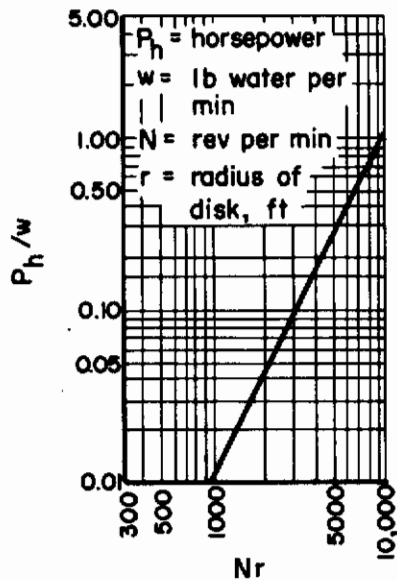


FIGURE 2-5. EFFECT OF FEED RATE, DISK SPEED, AND DISK SIZE ON POWER CONSUMPTION OF DISK ATOMIZERS

(Marshall and Seltzer) 2-14

Marshall calls attention to the fact that the power required to create new surface, based on thermodynamic considerations of the new surface created, is only a small fraction of that actually expended in a conventional atomizer. He cites a typical example in which the theoretical power for atomization is only 0.02 per cent of that which might actually be expended by a disk atomizer. A similar estimate for two-fluid atomization gives a correspondingly low percentage. Marshall states that this large difference between actual and theoretical power suggests the need of research to develop new methods of atomization which will consume much less energy per unit of surface created. It is to be recognized, however, that much of the energy consumed in atomization must go into dispersing the drops and mixing them with the surroundings.

Mechanism of Disk Atomization

Because the physical process of atomization by means of a rotating disk is so different from that involved in solid injection or in two-fluid atomization, this process was not considered in Chapter 1. Consequently, a brief review of the three essentially different types of disintegration that may take place around and beyond the edge of a rotating disk or cup are described below.

Hinze and Milborn⁽²⁻¹⁶⁾ conducted experiments in which liquid was supplied through a stationary tube to the inner part of a rotating cup widening toward a brim.

Figure 2-6 illustrates, schematically, the viscous flow of liquid toward the sharp edge of the cup. Three essentially different types of phenomena may take place around and beyond the edge of the cup. The type actually involved depends on working conditions, that is, on liquid feed rate, angular speed, and dimensions of the cup, and on the density, viscosity, and surface tension of the liquid.

Hinze and Milborn postulated three types of mechanisms: (1) disintegration by direct drop formation, (2) disintegration by ligament formation, and (3) disintegration by film formation.

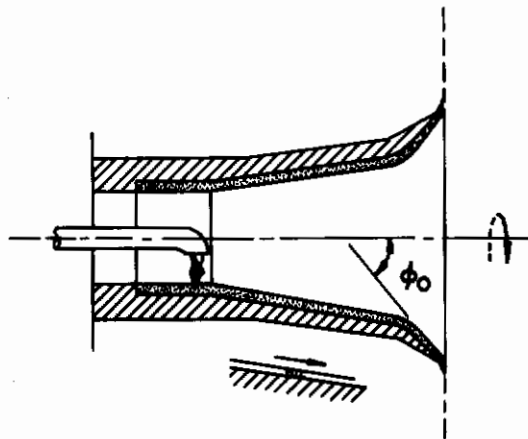


FIGURE 2-6. SUPPLY AND FLOW OF LIQUID WITHIN ROTATING CUP

(Hinze and Milborn)²⁻¹⁶

Figure 2-7 shows disintegration by direct drop formation, which occurs at a very low liquid-feed rate. The diameter of the liquid torus, formed around the edge, is determined mainly by equilibrium conditions between centrifugal and surface-tension forces. Because of disturbances the torus will be varicosely deformed, and drops will be formed singly at one or more bulges of the torus by the action of centrifugal forces. These drops are thrown off the edge as shown in the figure.

FIGURE 2-7.
DISINTEGRATION BY
DIRECT DROP FORMATION

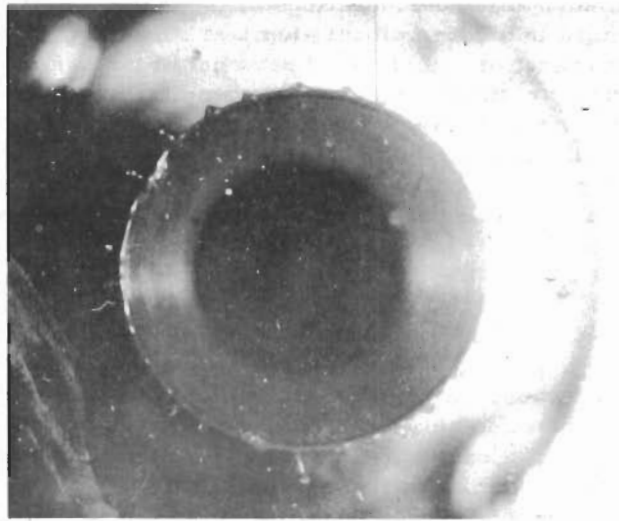


FIGURE 2-8.
DISINTEGRATION BY
LIGAMENT FORMATION

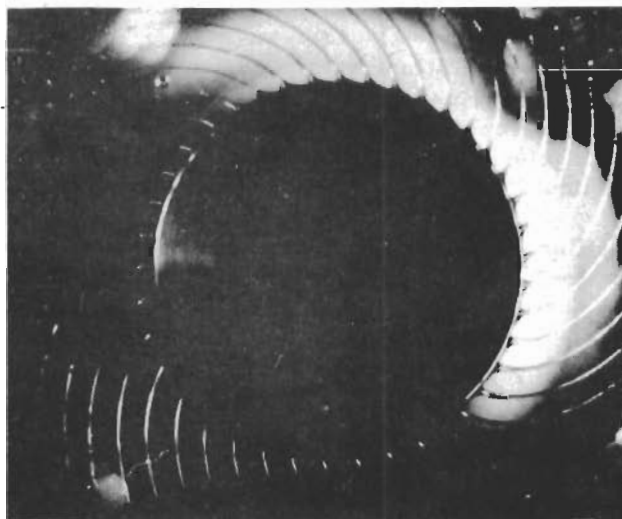


FIGURE 2-9.
DISINTEGRATION BY
FILM FORMATION

(Hinze and Milborn) 2-16



Figure 2-8 shows disintegration by ligament formation, which occurs when the liquid-feed rate is increased so that, instead of single drops forming at the bulges of the torus, complete thin jets or ligaments form. The number of these ligaments increases with increasing rate of supply up to a maximum value, after which the number remains constant, irrespective of the rate of supply. Apparently, in this state the ligaments grow in thickness with increasing rate of supply. The ligaments themselves are unstable, in view of imposed disturbances, and break up into drops at some distance from the edge of the cup.

Figure 2-9 shows the third type of disintegration which occurs when the liquid-supply rate is still further increased. A condition is reached where the number of ligaments can increase no more, nor can they grow in thickness. Consequently, a continuous film is formed, extending to a certain distance away from the edge, whereupon irregular breakup occurs resulting in ligaments and clots of liquid. The thickness of the film just beyond the edge is practically equal to that of the liquid layer within the cup at the edge. Hinze and Milborn call this process "disintegration by film formation".

It is plausible that the atomization of the liquid will be different for the three different stages of disintegration. In the stage of direct drop formation, the droplets are formed singly from protuberances originating from the bulges of the varicosely deformed liquid torus around the edge of the cup. The shapes of the protuberances at the instant when the droplets are split off generally will vary slightly, which means that the droplets will not be of exactly the same size. However, it is likely that they will have a diameter roughly equal to the thickness of the liquid torus.

In the stage of ligament formation, the ligaments break up into droplets by disturbances of rotational symmetry. This process of breaking up, identical with that of a straight liquid column and agreeing with Rayleigh's instability theory, is clearly shown in Figure 2-8.

Hinze and Milborn state that, if all the ligaments have the same diameter, if they all break up at the same distance from the edge of the cup, if this occurs by disturbances with the optimum value of wavelength, and if there is no effect of the stretching process of the ligaments on their breakup, then all droplets formed will have the same diameter. Actually, the drops are not all of equal size, but the atomization is more uniform than that obtained with other methods.

In the stage of film formation, air forces and other disturbing forces deform the film, tears arise, and surface tension action causes disruption into many irregular ligaments and clots of liquid, the latter mostly interconnected by thin threads of liquid that break up into fine droplets. It is reasonable to expect, generally, a less uniform atomization than that occurring during the stage of ligament formation.

Dimensional Analysis of Ligament Formation and Transition

Hinze and Milborn⁽²⁻¹⁶⁾ consider the problem of determining the number of ligaments formed under a given set of conditions by using the method of dimensional analysis. They assume that the number of ligaments Z will be affected by the diameter of the brim of the cup, D ; the cone angle of the cup, ϕ_0 ; the angular speed of the cup, ω ; the flow rate into the cup, Q ; the density of the liquid, ρ ; the surface tension of the liquid, σ ; and the dynamic viscosity of the liquid, μ . Using the Buckingham π -Theorem, it follows that the number of ligaments Z can be expressed as

$$Z = f\left(\frac{Q^2\rho}{D^3\sigma}, \frac{D^3\omega^2\rho}{\sigma}, \frac{\mu^2}{D\rho\sigma}, \phi_0\right). \quad (2-10)$$

The authors then proceed to determine the exact form of the function f by a semitheoretical method. The radial component of velocity for the liquid at the outside edge of the liquid torus is to be determined in terms of the physical properties of the system.

Figure 2-10 shows the vector diagram of the components of velocity in the torus, along with the dimensions of the torus. If the normal velocity on the inside edge of the torus is represented by V_D , and the corresponding tangential velocity by $1/2 \omega D$, then the resultant velocity V_R is determined by

$$V_R^2 = V_D^2 + \frac{1}{4} \omega^2 D^2 \quad (2-11)$$

Because of the conservation of angular momentum, the tangential velocity u on the outside rim of the torus becomes

$$u = \frac{1}{2} \frac{\omega D^2}{D+2h} \quad (2-12)$$

where h is the width of the torus. By neglecting the effects of viscosity, the normal component of velocity V_r on the outside rim of the torus can be determined by consideration of Figure 2-10 and Equation (2-12):

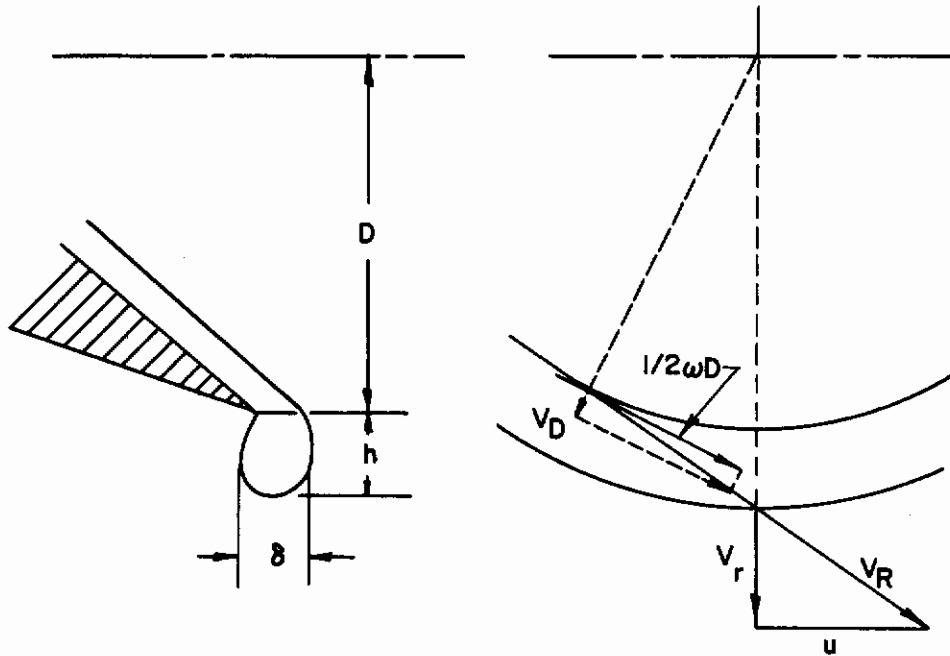


FIGURE 2-10. FLOW CONDITIONS IN TORUS AROUND EDGE OF CUP

(Hinze and Milbourn) 2-16

$$V_r^2 = V_R^2 - u^2 = \frac{\omega^2 D^2}{4} \left(1 - \frac{D^2}{(D+2h)^2} \right) + V_D^2$$

$$\approx \omega^2 D h + V_D^2 \approx \omega^2 D h \quad (2-13)$$

since $h \ll D$, and $V_D < \omega \sqrt{Dh}$, as indicated by numerous experiments. By assuming that the width of the torus, h , varies as its thickness, δ , Equation (2-13) can be written as

$$V_r^2 \propto \omega^2 D \delta \quad (2-14)$$

In order to account for viscosity effects, the Reynolds number, Re_t , of the liquid in the torus is introduced, so that

$$V_r^2 \propto \omega^2 D \delta (Re_t)^n = \omega^2 D \delta \left(\frac{\rho V_r \delta}{\mu} \right)^n, \quad (2-15)$$

where the exponent n is to be determined by test. The condition of equilibrium between the impact forces and surface tension at the outside rim of the torus prescribes that

$$\rho V_r^2 \propto \frac{\sigma}{\delta}. \quad (2-16)$$

Substitution of Equation (2-16) into Equation (2-15) and rearrangement of terms yields:

$$\frac{\delta}{D} \propto \left(\frac{\sigma}{\rho \omega^2 D^3} \right)^{\frac{2}{4+n}} \left(\frac{\mu^2}{\rho \sigma D} \right)^{\frac{n}{4+n}}. \quad (2-17)$$

If it is then assumed that the spacing of ligaments formed along the torus varies as the thickness of the torus δ , then the number of ligaments Z varies as D/δ , and

$$Z = k \left(\frac{\rho \omega^2 D^3}{\sigma} \right)^{\frac{2}{4+n}} \left(\frac{\rho \sigma D}{\mu^2} \right)^{\frac{n}{4+n}}, \quad (2-18)$$

where k is a constant of proportionality. It is noted that, given the values of the physical variables and the number of ligaments Z for a given experiment, the values of k and of n can be determined readily by the method of least squares.

Figure 2-11 shows the graphical correlation of experimental data, as determined by Hinze and Milbourn, using Equation (2-18) with $n = 4/5$.

The authors then extend the result of the above analysis to the determination of the conditions necessary for transition from the ligament state to the state of film formation. It is assumed that this transition will occur when the supply flow rate Q equals or exceeds the maximum flow capacity of the ligaments:

$$Q \propto Z \delta_L^2 (\max) V_L \propto Z \delta^2 V_L, \quad (2-19)$$

where $\delta_{L(\max)}$ is the maximum diameter of the ligaments, and V_L is the velocity of the fluid in the ligaments. It is further assumed that the velocity V_L in the ligament can be expressed in terms of the radial velocity V_r at the edge of the torus and a power of the Reynolds number Re_L in the ligament. Hence,

$$V_L \propto V_r (Re_L)^m = V_r \left(\frac{\rho V_L \delta}{\mu} \right)^m. \quad (2-20)$$

Substitution of Equation (2-16) into Equation (2-20) yields:

$$V_L \propto \sqrt{\frac{\sigma}{\rho \delta}} \left(\frac{\rho V_L \delta}{\mu} \right)^m. \quad (2-21)$$

Recalling that $\delta \propto D/Z$, substitution of Equation (2-21) into Equation (2-19) yields:

$$\frac{\rho Q^2}{\sigma D^3} Z^{\frac{1}{1-m}} \left(\frac{\mu^2}{\rho \sigma D} \right)^{\frac{m}{1-m}} = k', \quad (2-22)$$

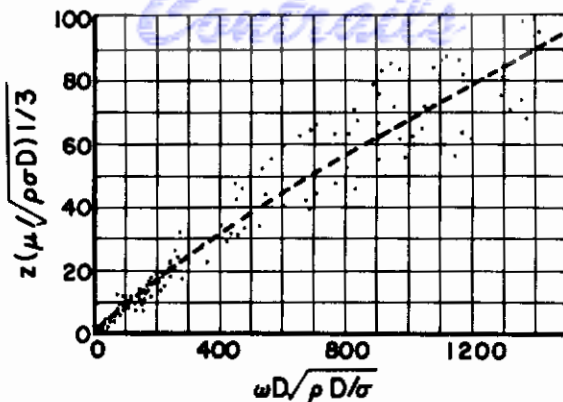


FIGURE 2-11. EXPERIMENTAL DATA ON NUMBER OF LIGAMENTS GROUPED AROUND A SEMIEMPIRICAL CURVE

(Hinze and Milbourn) 2-16

where k' is a constant of proportionality. Substitution of Equation (2-18) into Equation (2-22) then yields:

$$\begin{aligned} \frac{\rho Q^2}{\sigma D^3} \left(\frac{\rho \omega^2 D^3}{\sigma} \right)^{\frac{2}{(4+n)(1-m)}} \left(\frac{\mu^2}{\rho \sigma D} \right)^{\frac{1}{(1-m)} \left(m - \frac{n}{4+n} \right)} \\ = \frac{\rho Q^2}{\sigma D^3} \left(\frac{\rho \omega^2 D^3}{\sigma} \right)^x \left(\frac{\mu^2}{\rho \sigma D} \right)^{2x-1} = k'' \end{aligned} \quad (2-23)$$

where

$$x = \frac{2}{(4+n)(1-m)} \quad (2-24)$$

If the values of the physical variables are known, then the values of x and k'' can be obtained either by applying the method of least squares to Equation (2-23), or by plotting

$$\left(\frac{\rho Q^2}{\sigma D^3} \right) \left(\frac{\rho \sigma D}{\mu^2} \right)$$

against

$$\left(\frac{\rho \omega^2 D^3}{\sigma} \right) \left(\frac{\rho^2 \mu^4}{\sigma^2 D^2} \right)$$

on logarithmic paper. If the value of n in Equation (2-18) has already been determined, then the value of m can be obtained by application of the method of least squares to Equation (2-23).

Figure 2-12 shows a graphical correlation of transition data obtained by Hinze and Milbourn by using Equation (2-18) and (2-23) with $n = 4/5$ and $m \approx 0.25$.

Thus it has been shown that the theory of dimensional analysis, combined with elementary theoretical considerations, can be used effectively to correlate data obtained from atomization by a rotating cup.

McEntee⁽²⁻³⁾ points out that the widest application of this method of atomization is in the chemical industries, where it is particularly useful for spraying viscous liquids and thick slurries containing solid particles that would clog the small orifices of pressure nozzles. However, interest is increasing in the method as a means of atomizing liquid fuels.

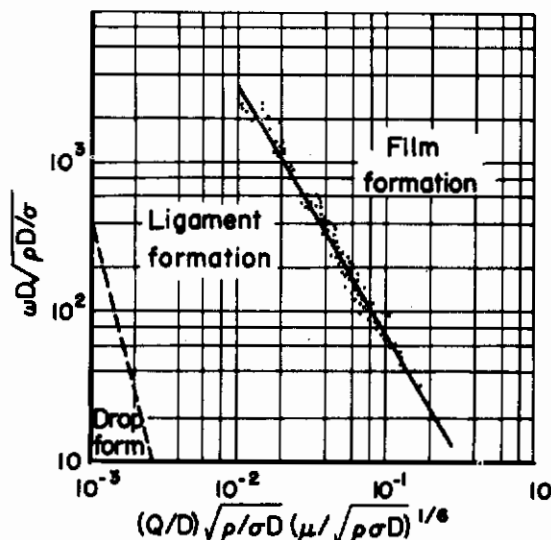


FIGURE 2-12. CORRELATION OF EXPERIMENTAL DATA ON TRANSITION FROM THE LIGAMENT STATE TO FILM FORMATION

(Hinze and Milbourn)²⁻¹⁶

Wilson, Page and Cartwright⁽²⁻¹⁷⁾, in a comprehensive investigation of spray drying of clay suspensions, describe rotors consisting of a disk, a simple cup, an inverted cup, a double bowl, or a cylinder, and rotors with vertical spray planes for accelerating the speed of fluid rotation. Many designs and shapes of rotating atomizers are, therefore, available.

Romp⁽²⁻¹⁾ describes various designs of "centrifugal atomizing burners" for atomizing fuel oil by means of rotating disks or cups. He makes the interesting statement that in this method of atomizing liquid fuel the effect depends entirely on the viscosity, but in just the opposite way to the effect of viscosity on pressure atomization by solid injection. Whereas viscosity opposes atomization by solid injection, so that finest atomization would be obtained with a liquid of zero viscosity, most rotating atomizing devices would not be able to atomize such an imaginary liquid at all, there being no way of imparting velocity to it. Reference is made to Chapter VI, "Mechanical Pulverization on the Kinetic Principle", of Romp's book⁽²⁻¹⁾ on "Oil Burning" for a more complete coverage of the application of rotating atomizers for liquid fuels.

Muraszew⁽²⁻¹⁸⁾ has devised a rotating fuel chamber which can conveniently be fitted onto the shaft of an aircraft gas turbine. It may form one end of an annular combustion chamber with the atomized fuel being discharged from the fuel chamber through a series of plain orifices, or from a circumferential slot.

Figure 2-13 shows this method of fuel injection for which Muraszew claims the following advantages: (1) Good atomization of the fuel is obtained over a wide range of load and speed, atomization improving with increasing speed. (2) The fuel pump is subjected only to low pressure, and high-pressure fuel pipes are eliminated. (3) Air-fuel mixing is improved, giving the possibility of a shorter flame or smaller combustion chamber.

The fuel sprays discharged from the orifices can be directed in relation to the air flow so that relative velocity is increased, thus improving both atomization and mixing.

Muraszew points out that the small "secondary" or "satellite" drops formed when this method of atomization is used, although only a trifling proportion of the total volume of fuel, may be helpful in the initiation of combustion.

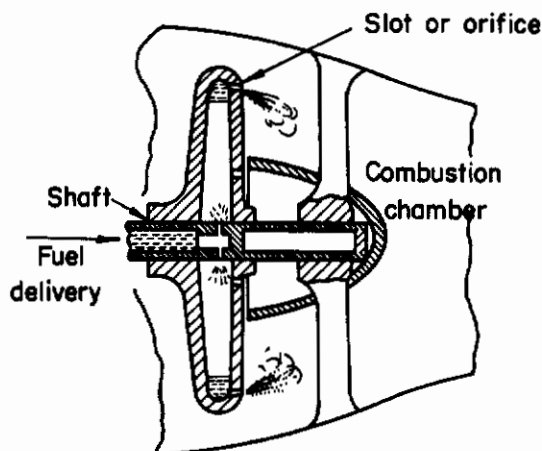


FIGURE 2-13. CONTINUOUS FUEL-INJECTION SYSTEM WITH ROTATING FUEL CHAMBER

(Muraszew) 2-18

The firm Turboméca⁽²⁻¹⁹⁾, in France, has recently conducted successful tests on the Aspin I which uses a rotating fuel-injection system.

Figure 2-14 shows details of the device by which the fuel, supplied along the main shaft, is atomized and projected into the annular combustion chamber through radial holes in a thrower flange. Speeds from 33,500 to 36,500 rpm were employed during test runs.

Pilcher and Terrill⁽²⁻²⁰⁾ atomized AN-F-32, JP-1 jet fuel by means of a rotating disk and produced droplets of uniform size that burned as a ring of flame around the disk.

Figure 2-15 is a photograph of a 3.40-inch disk rotating at 9800 rpm, and atomizing AN-F-32. The ring of flame is about ten inches in diameter.

Pilcher and Terrill found that the critical flow rate, above which a well-defined band of droplets of uniform size is no longer formed, increases with decrease in rpm or with increase in the diameter of the disk. Because the droplets are of uniform size the penetration distance is uniform and the band of flame is narrow.

METHODS BASED ON VIBRATIONS

Less common methods of atomization employing sonic or mechanical vibrations have been reported recently.

Joek⁽²⁻²¹⁾ has patented a method for atomizing liquids by ultrasonic vibrations. Atomization is accomplished by delivering a beam of ultrasonic energy into a chamber that is resonant to the frequency of the driver. A stream of liquid is subjected to the ultrasonic sound vibrations within the chamber to produce finely divided particles that may be vaporized and discharged from the other end of the chamber.



FIGURE 2-14. ROTATING FUEL INJECTION SYSTEM
USED BY TURBOMÉCA (2-19)

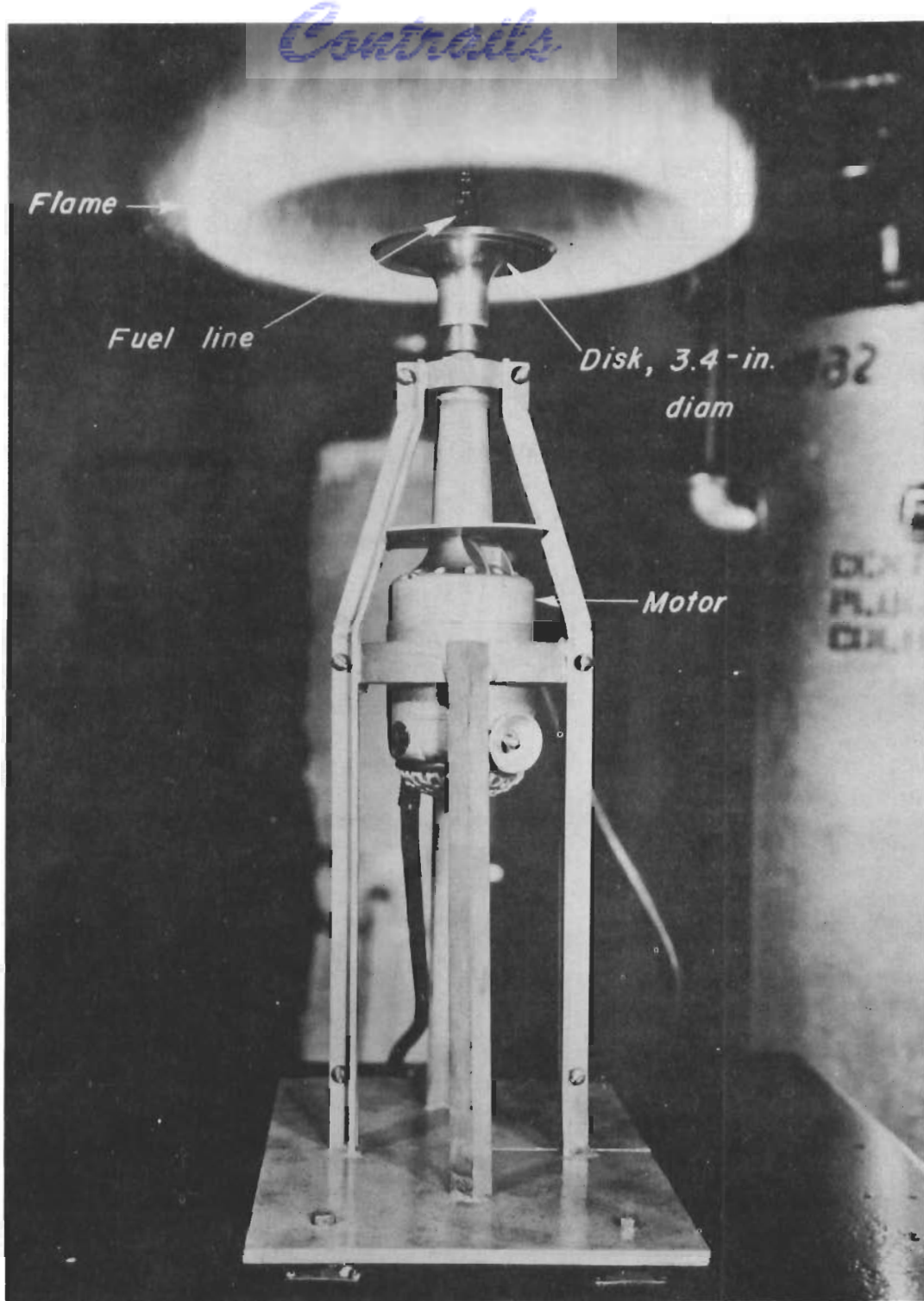


FIGURE 2-15. AN-F-32 ATOMIZED BY A ROTATING DISK
(Pilcher and Terrill)²⁻²⁰

Dimmock⁽²⁻²²⁾ describes a method of producing a stream of droplets of uniform size using a vibrating hollow reed actuated by a small electromagnet. Primary and subsidiary droplets are formed, and, by adjustment, uniform diameters of drops ranging from 10 to 300 microns may be obtained.

Dimmock suggests that the apparatus could be used to study single-droplet combustion. He believes that the uniformity of size in a single stream of drops from this apparatus is greater than that obtained with a rotating-disk-type sprayer, although it has the disadvantage of producing only a limited quantity.

Sliepcevich, Consiglio, and Kurata⁽²⁻²³⁾ describe a vibrating-type nozzle which is simple in construction and flexible in operation.

Figure 2-16 shows an assembly diagram of such a nozzle. A valve stem with a tapered head extends through the orifice into the chamber in the body of the nozzle. The force exerted by the valve head on the sharp-edged orifice is adjusted by means of the helical spring and nut. The pressure of the fluid forces the tapered head of the stem from its seat, during which time a pressure drop occurs as the fluid discharges from the orifice. The combined action of the helical spring and fluctuating fluid pressure produces a state of self-excited oscillations. Since the stem is always at least partly open, the discharge of fluid from the orifice is in the form of a continuous spray.

For each spring compression there exists a "critical" pressure below which audible vibration does not occur. This critical pressure usually occurs at pressures of 50 to 100 psi above the minimum spraying pressure. As the spraying pressure is increased above the critical pressure, both the intensity and frequency of vibration increase. At some still higher pressure the authors noted the appearance of two separate frequencies that seemed to fluctuate rapidly, producing what they describe as a "motorboat" effect which persisted over a pressure range of from 100 to 300 psi.

Sliepcevich, Consiglio, and Kurata believe that this vibrating type of nozzle can be advantageously adapted to fuel-injection systems.

Vonegut and Neubauer⁽²⁻²⁴⁾ report an electrical method for producing monodispersed liquid particles. Streams of highly electrified uniform droplets about 0.1 mm in diameter can be produced by applying potentials of 5-10 kv, a. c. or d. c., to liquids in small capillary tubes. Monodispersed aerosols having a particle radius of a micron or less can be formed if the capillary is positively charged and if liquids having low electrical conductivity are used.

Straubel⁽²⁻²⁵⁾ applied a direct current of 10 to 20 kv to a spray nozzle, with the other pole grounded or connected to a ring which was concentric with the nozzle, and achieved a high degree of atomization. He found that the higher the potential or field strength, the better the atomization.

In general the methods of atomization by vibration and by electrification are new and will require considerably more study and development.

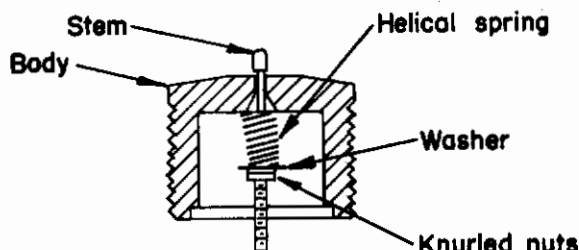


FIGURE 2-16. VIBRATING-TYPE NOZZLE

(Sliepcevich, Consiglio and Kurata)²⁻²³

IMPINGING LIQUID JETS

The study of impinging liquid jets as a method of atomization and of mixing of two liquid reactants has been considerably intensified during the past few years, owing to application of the process to liquid-fuel rockets. The method is used as a means of rapidly mixing the fuel and oxidant, as well as of increasing the surface by disintegration.

Spanogle and Hemmeter⁽²⁻²⁶⁾ conducted tests with two smooth jets impinging upon each other at an angle of 74 degrees. The point of impingement was kept as close as practicable to the nozzle exits so that more exact impingement might be obtained, and so that breakup of the solid jets before impingement would be minimized. They report that the resulting spray was so well dispersed that it could be carried along with an air stream of comparatively low velocity.

Falk⁽²⁻²⁷⁾ made a preliminary study of atomization of liquids upon impingement of opposed jets and observed that cones of spray are formed only if the pressure drops across the two jet orifices are the same.

Falk reports that it does not seem possible to form a cone if the area ratio of the impinging streams is too great. With the combination of a 1/32-inch and a 1/8-inch orifice, the wider stream seemed to overwhelm the narrower one.

Ryan⁽²⁻²⁸⁾ extended the above study, working with directly opposed jets, formed by sharp-edged orifices, meeting in an environment of atmospheric air. The orifices used had diameters ranging from 0.015 to 0.065 inch, and were employed in combinations such that the ratio of diameters (smaller to larger) ranged from 0.333 to 0.600. The orifice pressure drop was varied from 30 to 200 psi.

The jets were made to impinge in a closed chamber at known flow rates, and the spray was sampled. For the study of mixing as a function of location in the spray region, bulk samples of spray formed by one dyed and one clear jet were taken and analyzed colorimetrically. For the study of degree of mixing at the scale of individual drops, similar jets were used and drops were caught on a nonwetable microscope slide. The drops were then pressed between two microscopic slides, to form disks of uniform thickness, and were examined for difference in dye concentration.

Ryan concluded that: (1) the mixing of the two-jet liquids was complete in drops as small as 70 microns, the smallest drops observed; (2) the duration of time for mixing was about one millisecond; and (3) the volume-median drop diameter of the spray could be related to the variables studied by the empirical equation

$$\frac{D_m}{\sigma} = 3.16 + 38.7 \frac{1 - R_d}{p} , \quad (2-24)$$

where D_m is the volume median drop diameter, microns; σ is the surface tension of spray liquid, dynes/cm; R_d is the ratio of orifice diameters, smaller/larger; and p is the orifice pressure drop, psi.

Neither the viscosity of the liquids nor the scale of the apparatus was found to have any influence on the volume-median drop size. Ryan suggests that the absence of a scale factor may be a property of impinging-jet atomization; but, in view of the unusual character of this relation, he does not recommend its use for conditions other than those covered by his investigation.

Ryan made a preliminary study of the mechanism of jet impingement, which disclosed that: (1) the point of impingement could not be stabilized between the two orifices unless the momentum flux, per unit cross-sectional area, was the same for both jets; (2) the efficiency of impingement, defined as the ratio of the kinetic energy of the liquid leaving the point of impingement to that of the jets entering, was substantially unity.

Ryan states that continuation of studies of atomization is not recommended until more reliable methods of sampling and analyzing sprays have been developed.

Heidmann and Humphrey⁽²⁻²⁹⁾ made an extensive investigation of the flow characteristics and of the patterns of sprays formed by the impingement of two liquid jets. The study was made with the intent that it might be useful in determining the cause of the instability of combustion, in rocket engines, which appears to originate in the injection and mixing process.

The formation of a spray resulting from the impingement of two jets of water was studied by visual, photographic, and photoelectric techniques, and high-speed motion pictures and microflash photographs were taken of the spray pattern.

Figure 2-17 shows photographs of the formation of spray by two impinging jets of water. These photographs indicate that the formation of liquid drops is an intermittent, rather than a continuous, process. Upon impingement of two jets, a ruffled sheet of liquid is formed perpendicular to the plane of the two jets. This sheet of liquid disintegrates intermittently, forming groups of liquid drops and giving the appearance of waves propagating from an origin at the point of impingement. It should be noted that the groups of drops are of various sizes with irregular spacing between groups.

Heidmann and Humphrey made a quantitative evaluation of wave intensity, of the quantity of liquid per unit volume, and of the frequency from an oscilloscope trace obtained for a typical spray. The frequency of wave formation was observed to be constant over a finite time interval under constant operating conditions. The frequency varied between 1000 and 4000 cps for the range of test conditions used.

An increase in jet velocity resulted in an increase in wave frequency. An increase in impingement angle resulted in a decrease in wave frequency for impingement angles of from 50 to 100 degrees.

A diameter change from 0.025 to 0.057 inch had a negligible effect on wave frequency as compared with the effect of jet velocity and impingement angle. A change in jet length from 10 to 80 diameters before impingement had a negligible effect on wave frequency.

From the photographic and frequency data obtained, it appeared to Heidmann and Humphrey that the ruffling of the liquid sheet persists to the point of disintegration of the sheet and determines the frequency of the wave formation, and that irregularities in the jets before impingement may be as instrumental in controlling the ruffling of the liquid sheet as is the friction of the air.

Design problems relating to this method of atomization are discussed in the next chapter.

SUMMARY OF METHODS OF ATOMIZATION

The method of atomization most generally used for liquid fuels employs the principle of solid injection. This method has the definite advantages that simple nozzles with no moving parts may be used, and pressure on the liquid alone is required to accomplish atomization. Several devices employing this method are described in Chapter 3.

The two-fluid method of atomization is capable of producing a finer spray or mist, at lower pressures, but this process has the distinct disadvantage that a source of compressed gas or steam is required.

Atomization based on rotating devices offers considerable promise as a method of preparing liquid fuels for combustion. Atomization remains good at extremely low flow rates and only a low fuel pressure is needed.

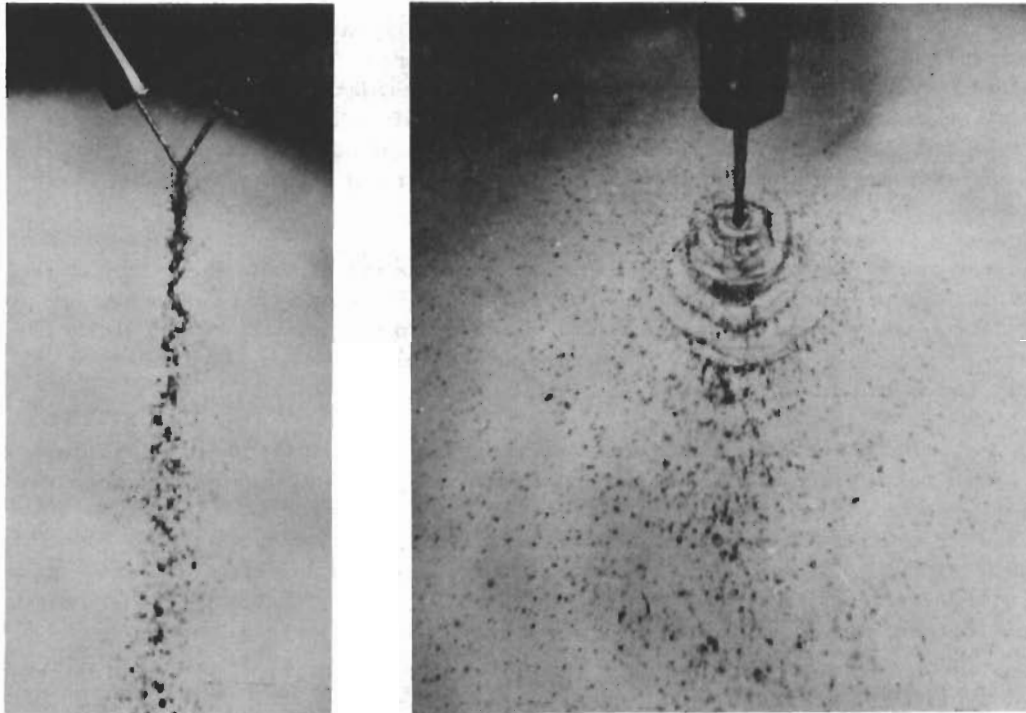


FIGURE 2-17. MICROFLASH PHOTOGRAPHS OF FORMATION OF SPRAY BY TWO IMPINGING JETS OF WATER. VIEWS PERPENDICULAR AND PARALLEL TO PLANE OF JETS ARE SHOWN
(Heidmann and Humphrey)²⁻²⁹

Methods of atomization by vibration show little promise for application to combustion systems.

Impinging liquid jets, in addition to accomplishing atomization, provide rapid mixing of two liquids, making this method well suited for rocket-fuel injection. Much remains to be learned, however, concerning this type of injection.

The efficiency of all methods of atomization is extremely low.

REFERENCES

- 2-1. Romp, H. A., Oil Burning; Martinus Nijhoff (The Hague) 1937, 336 pp.
- 2-2. Joyce, J. R., The Atomization of Liquid Fuels for Combustion; Jour. of Inst. of Fuel, Vol. 22, No. 124, February 1949, p. 150. Also, Methods of Atomizing Liquid Fuels; The Institute of Petroleum, Vol. 39, No. 350, (February 1953), p. 57.
- 2-3. McEntee, F. J., Jr., Methods of Atomization in Spray Drying; ASME Paper No. 50-PR1-5, Process Industries Conference, Pittsburgh, Pa., April 24-26, 1950. See Industrial Heating, Vol. 19, Mar. 1952, p. 504-510, 568. (A Condensation).
- 2-4. Green, H. L., Problems in the Atomization of Liquids; Chapt. 5 of Some Aspects of Fluid Flow by The Institute of Physics, Edward Arnold Company (London), 1951.
- 2-5. Lawrence, O. N., Gas Turbine Accessory Systems; Jour. Roy. Aeron. Soc. (England) 1948, p. 151.
- 2-6. Fogler, B. B., and Kleinschmidt, R. V., Spray Drying; Ind. Eng. Chem., Vol. 30, 1938, p. 1372.
- 2-7. Houghton, H. G., Section on Spray Nozzles; Perry's Chemical Engineers' Handbook, 3rd Edition, McGraw-Hill Pub. Co., Inc., pp. 1170-1175.
- 2-8. Limper, A. F., Atomization of Liquids by Injection Into High Velocity Gas Streams; M. S. Thesis, Dept. Chem. Engr., Univ. of Illinois, May 1947, 82 pages with tables, graphs, and drawings (ATI - 13087).
- 2-9. Ennis, W. B., Jr., and James, David T., A Simple Apparatus for Producing Droplets of Uniform Size from Small Volumes of Liquids; Science, Vol. 112, No. 2911, Oct. 13, 1950, p. 434.
- 2-10. Cadle, R. D., and Magill, P. L., Preparation of Solid- and Liquid-in-Air Suspensions; Ind. Eng. Chem., Vol. 43, No. 6, June 1951, p. 1331.
- 2-11. Strehlow, Richard A., Bibliography on Aerosols; Univ. of Illinois, Engr. Expt. Sta. SO-1003, Feb. 28, 1951, 1936 references and 7 symposia.
- 2-12. Walton, W. H., and Prewett, W. C., The Production of Sprays and Mists of Uniform Drop Size by Means of Spinning Disc-Type Sprayers; Proc. Phys. Soc. Vol. 62, Pt. 6-B, 1 June 1949, p. 341.
- 2-13. May, K. R., An Improved Spinning Top Homogeneous Spray Apparatus; Jour. Applied Phys., Vol. 20, October 1949, p. 932.
- 2-14. Marshall, W. R., Jr., and Seltzer, Edward, Principles of Spray Drying, Part I - Fundamentals of Spray-Dryer Operation. Part II - Elements of Spray-Dryer Design; Chem. Engr. Prog., Vol. 46, No. 10, Oct. 1950, p. 501, and No. 11, Nov. 1950, p. 575.

- 2-15. Adler, C. R., and Marshall, W. R., Jr., Performance of Spinning Disk Atomizers; Chem. Engr. Prog., Vol. 47, No. 10, October 1951, p. 515.
- 2-16. Hinze, J. O., and Milborn, H., Atomization of Liquids by Means of a Rotating Cup; Jour. of Applied Mechanics, Vol. 17, No. 2, June 1950, p. 145.
- 2-17. Wilson, Hewitt; Page, George A.; and Cartwright, Vance, S.; Dewatering Clay Suspensions by Spray Evaporation; U. S. Bureau of Mines, Report of Investigations 3248, January 1935, 42 pp.
- 2-18. Muraszew, A., Continuous Fuel-Injection System with Rotating Fuel Chamber; Engineering, Oct. 1, 1948, p. 316.
- 2-19. Anonymous, Aspin I, Turboméca Jet Unit with Variable Augmentation by Ducted Fan; Flight, 1 February 1951, p. 135.
- 2-20. Pilcher, J. M., and Terrill, F. B., Ignition and Combustion Research. Phase 2. Burning Characteristics of Fuel Mists; First Quarterly Progress Report to Hq. AMC, Wright-Patterson AF Base, Contract AF-33 (038)-12656, E. O. No. 460-35 S. R. -8, October 1950. (See also Figure 2 of Final Report on Contract AF-33 (038)-2038 E. O. No. 506-186 Add 2 S. R. -S Project MX-833, August 15, 1950.
- 2-21. Joeck, Thomas D., Method for Atomizing by Supersonic Sound Vibrations; U. S. Patent 2,532,554, Dec. 5, 1950.
- 2-22. Dimmock, N. A., Production of Uniform Droplets; Nature, Vol. 166, No. 4225, October 21, 1950, p. 686.
- 2-23. Slipevich, C. M.; Consiglio, J. A.; and Kurata, Fred; Operating Characteristics of a Vibrating-Type Atomizing Nozzle; Ind. Eng. Chem., Vol. 42, No. 11, November, 1950, p. 2353.
- 2-24. Vonegut B., and Neubauer, R. L., Production of Monodispersed Liquid Particles; J. Colloid Sci., Vol. 7, pp. 616-622, Dec., 1952.
- 2-25. Straubel, Harold, Electrostatic Atomization of Liquids; Die Naturwissenschaften, Vol. 40, p. 337, 1953.
- 2-26. Spanogle, J. A., and Hemmeter, G. T., Development of an Impinging Jet Fuel-Injection Valve Nozzle; NACA Technical Note No. 372, April 1931, 9 pp.
- 2-27. Falk, David M., Atomization of Liquids upon Impingement of Opposed Jets; M. S. Thesis, Dept. of Chem. Engr., MIT, September 12, 1947.
- 2-28. Ryan, Norman W., Mixing and Atomization by Impingement of Unconfined Liquid Jets, D. Sc. Thesis, Dept. of Chem. Engr., MIT, Dec. 30, 1948.
- 2-29. Heidmann, Marcus F., and Humphrey, Jack C., Fluctuations in a Spray Formed by Two Impinging Jets; NACA Technical Note 2349, April 1951, 35 pp. Also in J. of Amer. Rocket Soc., Vol 22, May-June 1952, pp. 127-131, 167.

CHAPTER 3. DESIGN OF ATOMIZERS

ABSTRACT

The requirements of a good fuel-spray nozzle are summarized, and the fundamental principles of nozzle design are discussed. The various designs of the vortex or swirl type of nozzle, now almost universally used on aircraft gas-turbine engines, are described. Attention is also given to two-fluid nozzles and to the design of reactant injectors for liquid-fueled rockets. Empirical formulas for evaluating spray angle and fineness of atomization are presented.

WADC TR 56-344

Contrails

DESIGN OF ATOMIZERS

by

J. M. Pilcher and C. C. Miesse

The design of fuel spray nozzles is one of the most important problems in high-duty combustion for aircraft. At first, it appeared that simple nozzles of the type already in use on stationary combustion equipment could be used to inject fuel into the combustion chamber of aircraft gas turbines; however, the wide range of power required in flight necessitates satisfactory atomization over a wide range of fuel flow rates. Therein lies one of the major problems.

A range of fuel flow rates of about 70 to 1 is needed, but designers have been forced to settle for a much lower range than this. Even with the recent designs of complex nozzles, which are troublesome and expensive, a ratio of maximum to minimum flow rates of from 10 or 20 to 1 is the best that can be expected.

In order to be able to start quickly, restart at altitude, and eliminate die-out during descent, the nozzle must produce a fine spray at the low range of flows. Unfortunately, atomization is usually coarse at low flows, when a fine spray is desired, and fine at high rates of flow when the degree of atomization is relatively unimportant.

In addition to producing a spray of sufficient fineness, a well-designed nozzle must distribute the fuel properly throughout the combustion chamber which means that the spray angle must be correct, and spray penetration must be of the proper magnitude and direction. In this respect, there must be close coordination between designers of nozzles and combustion chambers. Constancy of flow rate for a given load is important as is also the possibility of maintaining equal fuel flows to all nozzles of the engine.

The fundamental principles of nozzle design are discussed in this chapter, and the various designs of the vortex or swirl type of nozzle, now almost universally used on aircraft gas-turbine engines are described. Attention is also given to the design of two-fluid nozzles and to the design of reactant injectors for rockets, especially the impinging-jet type.

First, the requirements of a good nozzle will be discussed to serve as a basis for nozzle design.

REQUIREMENTS OF A GOOD NOZZLE

The requirements of an ideal spray nozzle for aircraft gas turbines have been summarized by Bolt and Saxton⁽³⁻¹⁾ as follows:

- (1) The nozzle should supply atomized fuel of such a spray pattern and degree of atomization that maximum combustion efficiency will be obtained.
- (2) The operation of the fuel nozzle should be such that ignition will be positive and a stable flame will be obtained under all operating conditions.
- (3) The nozzle should provide the necessary range of flow to meet all engine conditions with a minimum variation in pressure of the fuel supply.

- Continued*
- (4) It is especially important that a low probability exists of plugging with dirty fuels.
 - (5) The nozzle should not accumulate carbon around the orifice or otherwise be affected by service conditions.
 - (6) The minimum nozzle supply pressure should be not less than approximately 10 psi to avoid vapor formation in the liquid system.
 - (7) All nozzles in an engine should have flow rates as nearly equal as possible at each engine load.
 - (8) The nozzle should be small.

Ganger⁽³⁻²⁾ claims that more emphasis should be placed on design for easy removal, and that difficulty of removal has been a main reason why spray-nozzle development has lagged behind other engine developments.

Ganger stresses the importance of satisfactory atomization at the low range of fuel flows on the basis that it is most undesirable, while in the low power range, to have the flame go out in one segment of the circle of charge around the turbine guide vanes, and stay out for an appreciable duration of time.

Stark and Constantino⁽³⁻³⁾ believe that the major difficulty encountered in the development of spray nozzles is the matching of the nozzles to flow within ± 2 per cent of each other. Furthermore, these authors point out that durability of nozzles operating in combustion chambers is of utmost importance for two reasons: (1) to insure uniformity of flow among nozzles, and (2) to avoid damage to the blading from broken metal pieces in the gas stream, or from excessive temperatures resulting from increase in fuel flow following failure of a nozzle.

Park⁽³⁻⁴⁾ lists four basic requirements for a fuel-injection system. These are: (1) weight-flow distribution of fuel at the flame front should have the optimum configuration, (2) weight-flow distribution of fuel at the flame front should be stable throughout the range of operation, (3) the fuel/air ratio in the ignition zone should be near optimum, under all conditions, and (4) the quantity of fuel deposited on the walls or on other obstructions should be negligible.

Dodge, Hagerty, and York⁽³⁻⁵⁾ consider that the necessity for providing constant spray characteristics over a wide range of operation presents the most serious problem in the design of spray nozzles for aircraft gas turbines. They list five other major requirements as follows:

- (1) The spray pattern must be uniform and free of streaks around its periphery over the entire range of operation. Nonuniformity leads to formation of hot spots and consequent possible chamber burnouts.
- (2) At conditions of low rate of air flow and low injection pressure, the size of the droplets formed must be small enough to produce sufficient vapor for starting.
- (3) The cone angle of the spray must be wide enough at starting to bring vapor in contact with the ignition apparatus.
- (4) At cruising conditions, the size of droplet must be fine enough to give sufficient vaporization, yet be coarse enough for sufficient penetration to insure distributed combustion well down the length of the chamber.
- (5) The nozzle must have sufficient range, flexibility, and positiveness of operation in order that lean and rich blowouts will not occur upon rapid decelerations and accelerations.

These authors also stress the importance of matching nozzles for uniform metering characteristics so that unbalanced combustion and possible burnout will be avoided.

The many requirements described above for the ideal spray nozzles may never be completely filled. However, nozzle-design engineers have made much progress during the past few years.

Before describing the various designs of aircraft gas-turbine spray nozzles, some of the fundamental principles of nozzle design will be discussed.

FUNDAMENTAL PRINCIPLES OF NOZZLE DESIGN

A point that should be kept in mind when discussing nozzle design is that the actual breakup of liquid into droplets usually does not occur within the nozzle, but at some distance away from the nozzle after air or combustion gases have had the opportunity to act on the sheets or filaments of liquid. In the case of swirl nozzles, however, breakup usually occurs extremely close to the nozzle exit, even at low atmospheric pressures.

Most of the work on the design of spray nozzles has been empirical in nature and has been based on trial and error methods. Some fundamental experimental work has been done, however, to determine the possibility of designing nozzles to give sprays of predetermined characteristics. Other fundamental studies of a purely theoretical nature have been directed toward a better understanding of the various design parameters. In both instances, the major emphasis has been placed on swirl-type atomizers.

Experimental Studies of Swirl Atomizers

S. M. Doble's Investigations

Doble⁽³⁻⁶⁾ made a general study of swirl-type nozzles and formulated some general relations from which a nozzle could be designed to give a desired output at a stated pressure, a predetermined average particle size, and a desired apex angle of the cone of spray.

The elementary design of a plain nozzle in which the liquid is simply forced through a small orifice was promptly discarded by Doble as unsuitable because the cone angle was too small.

The first part of this investigation was concerned with the geometrical or mechanical features of the swirl-type nozzle in relation to the rate of flow and the supply pressure. The results were expressed in terms of the flow number, K, according to the relation

$$K = \frac{V}{\sqrt{P}} \quad (3-1)$$

where V is the discharge rate, gallons per hour, and P is the supply pressure, psi.

The value of K for a given nozzle is not absolutely constant over a wide range of pressures; however, for design purposes, the difference between the calculated and the actual discharge rates may be neglected, especially if extremely low pressures are not involved.

Figure 3-1 shows the components of the nozzle designed and used by Doble. The angle of the recessed cone behind the short parallel length of nozzle aperture, shown as 90 degrees in Figure 3-1, was varied to include the three angles of 60 deg, 90 deg, and 120 deg. Changes in this angle were found to have no influence on the output of the nozzle.

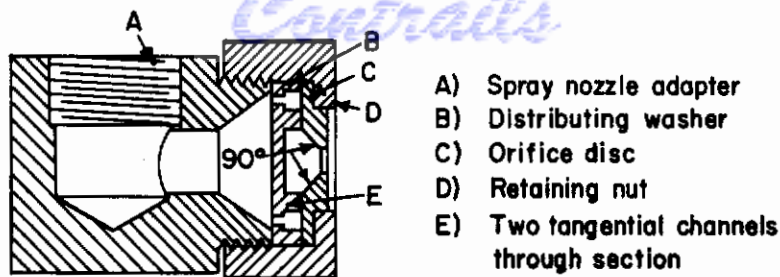


FIGURE 3-1. COMPONENTS OF SWIRL NOZZLE (Doble)³⁻⁶

Doble derived a general formula for relating the rate of flow of water for this swirl nozzle with the dimensions of the channels and of the orifice disks. The formula, given below, applies only for nozzles fitted with a distributing washer (B) having two channels leading into the swirl chamber. The spray cone produced with double channels was preferable to that obtained with a single channel in that distribution of liquid was more symmetrical around the axis.

For double rectangular channels:

$$K = \frac{7xy - 5x + 28}{35} = \frac{V}{\sqrt{P}} \quad (3-2)$$

where x is the total cross-sectional area of both channels, sq mm, and y is the orifice diameter, mm.

For nozzles fitted with double circular channels, up to 2.5 mm in diameter, the flow number is evaluated by the relation:

$$K = \frac{z(2y - 1.2) + 3(y + 1)}{9} \quad (3-3)$$

where z is the total cross-sectional area of both channels, sq mm, and y is the orifice diameter, mm, as for the previous equation.

If d is the diameter of each of the two equal channels, mm,

$$K = \frac{\pi d^2 (y - 0.6) + 3(y + 1)}{9} \quad (3-4)$$

And, from Equation (3-1),

$$V = K \sqrt{P} \quad (3-5)$$

Hence,

$$V = \frac{\sqrt{P}}{9} [\pi d^2 (y - 0.6) + 3(y + 1)] \quad (3-6)$$

Using the above equations, it is possible to design a nozzle for a desired output, within the range of 3 to 200 gph by various combinations of pressure, channel size, and orifice diameter.

Subsequently, Doble made a study of the relation of drop size to the above mentioned three design factors, in order that suitable components might be assembled in a nozzle to produce a spray with a known drop size distribution. Considering the difficulties involved in determining the sizes of the droplets comprising a spray, this was an ambitious undertaking.

The results of Doble's experimental investigation of the relation of spray characteristics to design features of the nozzle are summarized as follows:

(1) Increase of liquid pressure from 30 to 70 psi decreased average particle size slightly and had little effect on spray angle. It is unfortunate that Doble did not investigate a greater range of pressures.

(2) Increase of the orifice diameter, up to the limit of 5 mm covered by the investigation, decreased the particle size. From this Doble concluded that the size of the orifice should be as large as possible, depending upon the maximum angle of spray permissible for the specific application. This inverse relation between orifice diameter and drop size is contrary to reports of other investigators (see Chapter 1), and is difficult to accept. However, Doble reports that for two nozzles with disk apertures of 0.75 mm and 3.75 mm, but otherwise similar, the average particle size was 138 microns and 74 microns, respectively, both tested with water at 50 psi. A possible explanation, not offered by Doble, is that drop size may have been controlled primarily by the size of the double circular channels (1 mm diameter for both nozzles) leading into the swirl chamber, and that agglomeration or coalescence of droplets may have increased, as the orifice diameter was decreased, resulting in an increase of the average particle size for the final spray. The inverse relation between orifice diameter and drop size would surely never exist for a plain nozzle, that is a nozzle consisting of only a smooth round hole and no swirl chamber.

(3) Increase in the area of cross section of the channels in the distributing washers increased output with an associated decrease of velocity in the swirl chamber. Drop size was consequently increased to about 200 microns when the cross sectional area of the channels was a maximum, and the spray angle was decreased resulting in increased concentration of spray per unit area. Therefore, if a large spray angle is required and if small droplets are desired, the velocity of the liquid in the swirl chamber should be at a maximum, and to achieve this the cross sectional area of the channels should be a minimum.

(4) Double rectangular-section channels gave a slightly better distribution than channels of circular section.

(5) An increase of apex angle of the recessed cone behind the orifice disk led to a slight improvement in the volume distribution and presumably, also, to finer particle size; but the degree of either improvement was of little practical importance, while the total output and spray cone angle were unaffected. Doble regards a recessed cone angle of 90 degrees, as shown in Figure 3-1, as the most convenient for design.

To facilitate the application of the experimental results to spray-nozzle design, Doble has prepared a set of nomograms for establishing the design of a swirl nozzle to give a certain flow rate, at a specified pressure, and to produce a spray of given spray angle.

More recently Doble⁽³⁻⁷⁾ extended this work to include the design of nozzles with flow rates up to 1800 gph. As a result of the two investigations, it is possible to determine the dimensions necessary for a nozzle to deliver any quantity of water from 4 to 1800 gph in the pressure range of 20 to 100 psi. Furthermore, by the correct selection of the number, shape, and size of the channels in the distributing washers and of the size of the exit orifice diameter, a spray angle of any value up to 150 degrees can be obtained.

Doble⁽³⁻⁸⁾ also applied cyclone formulae to the problem of designing swirl-type spray nozzles and provided a theoretical explanation for the empirical relations obtained in the two previous references. He recommends that a nozzle should be designed so as to comply with the following ratios:

$$\phi = \frac{\text{spinning speed at inlet radius}}{\text{inlet velocity}} > 1.0$$

$$\frac{R_I}{R_E} = \frac{\text{mean inlet radius}}{\text{exit radius, i.e., half of the orifice diam}} > 1.0$$

$$\frac{t}{R_E} = \frac{\text{thickness of fluid film emerging}}{\text{exit radius, i.e., half of the orifice diam}} < 0.5$$

The work by Doble is a valuable contribution to the limited basic information available on the subject of nozzle design.

E. A. Watson's Investigations

Watson^(3-9, 3-10) considers that any theoretical treatment of the mechanics of a swirl atomizer, even for the simplest case where viscosity is neglected, is difficult. However, he does present a simplified treatment which enables the discharge coefficient and the cone angle to be evaluated in terms of three fundamental dimensions, namely, A_3 , the total area of the inlet slots or holes through which the fuel is supplied to the swirl chamber, D_2 , the diameter of the final orifice, and D_3 , the base diameter of the swirl chamber.

Watson points out that theory indicates, and experience confirms, that the discharge coefficient is a function only of A_3/D_2D_3 , and that it is independent of pressure as long as the pressure is sufficient to make the viscous losses in the atomizer negligible.

Figure 3-2 shows the relation of discharge coefficient to the ratio A_3/D_2D_3 . Knowing the value of the discharge coefficient, the flow number of the atomizer can be calculated from the area of the final orifice, $\pi D_2^2/4$.

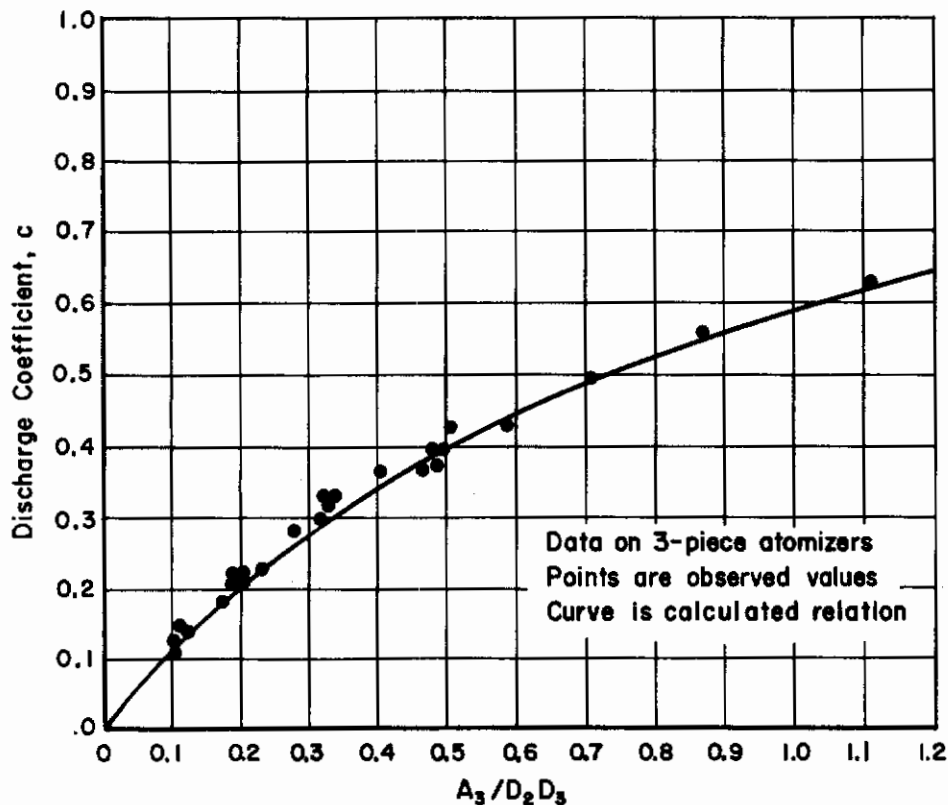


FIGURE 3-2. RELATION OF DISCHARGE COEFFICIENT TO NOZZLE DESIGN (Watson and Clarke)³⁻⁹

For a typical density of 0.805, the flow number, K , becomes:

$$K = 3.28 a c \quad (3-7)$$

where a is the area of the exit orifice, sq mm, and c is the discharge coefficient, $a c$ being the equivalent exit area. Knowing the flow number, K , the flow rate or discharge rate, V , can be determined from Equation (3-5).

Comparison of Doble and Watson Methods

In order to compare Doble's method for calculating flow number with Watson's method, the value of K has been computed for a hypothetical swirl-type nozzle with the following dimensions: orifice diameter, 3 mm; swirl chamber diam, 10 mm; size of rectangular inlet slots through which liquid is supplied to the chamber, 2 mm by 3.5 mm; total area of the two slots, 14 sq mm.

The flow number, K , according to Doble's Formula (3-2) is

$$K = \frac{7(14)(3) - 5(14) + 28}{35} = 7.2$$

where the liquid is assumed to be water.

For water, with unit density, Watson's Equation (3-7) becomes:

$$K = 2.96 a c \quad (3-7')$$

The discharge coefficient, c , determined as a function of Watson's ratio A_3/D_2D_3 , (0.467 for this example), has a value of 0.37. Then, from Equation (3-7'):

$$K = 2.96 [\pi(1.5)^2] 0.37 = 7.8.$$

The agreement between Doble's and Watson's methods is remarkably close. However, it should be mentioned that such good agreement can be expected only with conventional shapes, as Doble's formula completely ignores the diameter of the swirl chamber.

Bowen's and Joyce's Investigations

G. Bowen⁽³⁻¹¹⁾ and J. R. Joyce, in preparation for their experimental work, reviewed the existing theories regarding swirl atomizers. They point out that these theories lead to only two methods of correlation, (1) either cone angle and discharge coefficient are unique functions of A_3/D_2D_3 , or (2) they involve further variables in the proportions of the atomizers.

They were able to correlate satisfactorily with geometrical proportions their experimental data on the cone angle and discharge coefficient of Lucas atomizers. However, they recommend that more information be collected, and especially that the influence of the depth of the swirl chamber be studied.

Bowen and Joyce conclude that it is a mistake to attempt to embrace too wide a range of flow rates. Such an attempt reduces the possibility of proportioning the critical parts of the swirl nozzle in such a way that optimum performance may be ensured.

Schweitzer⁽³⁻¹²⁾ made a notable study of the design of spray nozzles for diesel engines; however, because his experiments were concerned with intermittent injection and have little application to the problem of continuous injection of aircraft fuels, his work will not be discussed here.

J. P. Longwell's Investigations

Longwell⁽³⁻¹³⁾ made an extensive experimental study of nozzle design with primary emphasis on the relation of drop size to various design factors. His work showed that the value of D_o , the weight-median drop diameter, at zero viscosity, was a satisfactory criterion of the performance of a nozzle. A justification for basing his nozzle design study on an oil of zero viscosity was that the viscosity of liquid fuels could, in general, be adjusted to such a value that Longwell's nozzles would operate satisfactorily.

Longwell points out that, at zero viscosity, the discharge coefficient and the cone angle remain the same for nozzles that are dimensionally similar. Consequently, the magnitude of $\sqrt{c_o} \sin(\alpha_o/2)$ does not depend on the size of the nozzle; in this expression, α_o is the cone angle of the spray for zero viscosity, and c_o is the discharge coefficient for a liquid of zero viscosity. Therefore, nozzles of different sizes can be judged as to design by the criterion, $\sqrt{c_o} \sin(\alpha_o/2)$, which Longwell calls the atomization criterion. It should be noted that no information as to the absolute value of D_o , the median drop size, is given by the atomization criterion, but for a given radius or discharge rate, the nozzle which has the largest value of $\sqrt{c_o} \sin(\alpha_o/2)$ will give the smallest drop size.

Figure 3-3 shows Longwell's experimental nozzle. The variables considered as affecting the performance of a nozzle were (1) the radius of the orifice, r_o , (2) the distance from the back of the swirl chamber to the orifice, L , (3) the average radius at the point where a particle of fluid enters the swirl chamber, and (4) the cross-sectional area of the tangential slots, A_s .

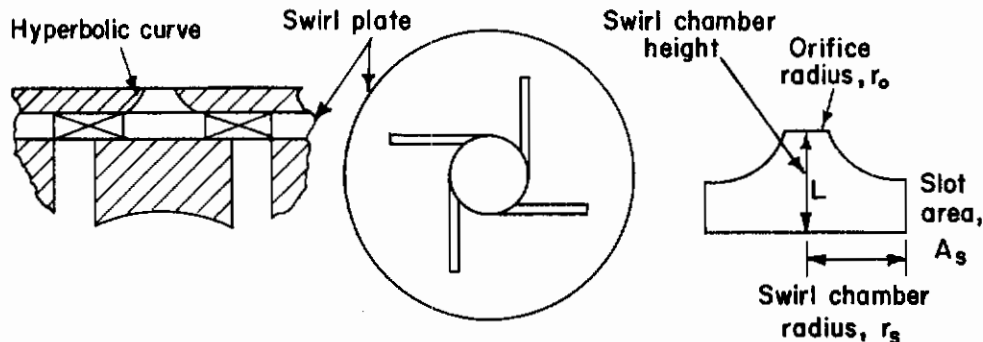


FIGURE 3-3. LONGWELL'S EXPERIMENTAL NOZZLE (Hawthorne)³⁻¹⁴

By control of these variables, he was able to determine the discharge coefficient, the cone angle, the conditions for the formation of a cone, and the conditions for the formation of a diverging cone. Only the formation of a diverging cone depends on the scale of the nozzles; therefore, Longwell used the dimensionless ratios L/r_o , r_s/r_o , and A_s/r_o^2 .

Longwell calls attention to the fact that the last ratio, A_s/r_o^2 , is directly related to the commonly used commercial term of nozzle ratio which is the ratio of ten times the area of the slots to the area of the orifice. For example, if the nozzle ratio is 40, then:

$$40 = 10 A_s / \pi r_o^2,$$

and

Contrails

$$A_g/r_o^2 = 12.6$$

The three dimensionless ratios may be used, with the aid of Longwell's experimental data, to determine the operating characteristics at zero viscosity for a nozzle of given design. A number of calculations of this type were made by Longwell, the results of which may be summarized as tabulated.

TABLE 3-1. SIGNIFICANCE OF LONGWELL'S DIMENSIONLESS RATIOS

Increase of	Discharge Coefficient	Cone Angle	Value of A_g/r_o^2 for Maximum $\sqrt{c_o} \sin(\alpha/2)$	Viscosity for Cone Formation	Viscosity for Formation of Diverging Cone*
A_g/r_o^2	Increases	Decreases over range of interest	--	Goes through maximum	Increases
L/r_o	Increases	Decreases	Decreases	Decreases	Increases slightly
r_g/r_o	Decreases	Increases	Increases	Small effect	Decreases

*Under certain conditions when a cone is formed the surface tension causes it to converge. Good atomization cannot be expected if the cone pulls together, so it is of interest to determine the conditions under which a diverging cone is obtained.

The effect of these three ratios on the value of the atomization criterion, $\sqrt{c_o} \sin(\alpha/2)$, is probably the factor of greatest interest. The atomization criterion goes through a maximum point which is of particular interest since the largest value of $\sqrt{c_o} \sin(\alpha_o/2)$ will give the smallest drop size. It is desirable, therefore, to have as large a value of the atomization criterion as is concordant with ease of construction and range of viscosity of the liquid which can be atomized. Longwell cautions that the advantage of going to a very large A_g/r_o^2 to obtain a high value of the atomization criterion is offset by a decreased viscosity for cone formation without a large increase in the atomization criterion. If range of atomization is of primary interest, for nozzles with r_o greater than 0.3 mm, a value of A_g/r_o^2 of 10 will give the best results with L/r_o and r_g/r_o set at 3.

The disadvantage of a large L/r_o is shown in the preceding tabulation which indicates that the smaller the value of L/r_o the better will be the performance of the nozzle.

Examination of Longwell's calculations indicates that a nozzle which would be a good compromise between range of atomization and fineness of atomization would have the following dimensions:

A_g/r_o^2	20
L/r_o	3
r_g/r_o	3

This nozzle would have a cone angle at zero viscosity of about 77 degrees and a discharge coefficient of about 0.53. If r_o was less than 0.3 mm, the viscosity at which a diverging cone would form would seriously limit the type of fluid which could be atomized by the nozzle. This limitation as well as the difficulty of maintenance of small nozzles will tend to set a lower limit on the diameter of nozzle orifice that is practical for use with an oil of a given viscosity.

With reference to the design of the tangential slots, Longwell considers that it is desirable to make them as short as possible in order to reduce the viscous losses through the slots. Only enough length to impart the proper direction to the flow of the fluid is necessary. It is also important that there be more than one slot and that the slots be symmetrically placed so that a symmetrical cone will be obtained. Longwell's experiments showed that if only one slot or an unsymmetrical arrangement of slots is used, the resulting cone is not axially symmetrical.

E. Söhngen's Study of Spray Angle

E. Söhngen⁽³⁻¹⁵⁾ conducted experiments with 18 different swirl-type nozzles and investigated the relations between the dimensions of the nozzles, the fuel flow rate and pressure, and the spray angle. He concluded that, because spray angle determines the rate at which fuel is supplied to a given space, the angle must be adapted to the combustion chamber. Söhngen emphasized that a nozzle can be evaluated conclusively only by ignition and combustion experiments with the nozzle installed in the combustion chamber. However, his experiments provide basic data that may be applied to nozzle design.

These experimental studies by Doble, Watson, Bowen, Joyce, Longwell, and Söhngen provide considerable information of practical value to the designers of swirl-type spray nozzles. The theoretical aspects of swirl atomizers will now be considered.

Theoretical Analyses of Swirl Atomizers

G. I. Taylor's Analysis

A rigorous mathematical analysis of the mechanics of swirl atomizers was given by G. I. Taylor⁽³⁻¹⁶⁾, who considered the conventional atomizers. Figure 3-4 is a schematic diagram of the nozzle considered by Taylor. Here, the radius of the atomizer is designated by r_c in the swirl chamber and by r_o in the orifice. The radius of the cone is designated by s_c in the swirl chamber and by s_o in the orifice. The fluid enters tangentially at r_c and is ejected at the orifice of radius r_o . Since the flow is assumed to be irrotational, the tangential velocity V_t is inversely proportional to the radius r :

$$V_t = \frac{\Omega}{r} , \tag{3-8}$$

where Ω depends on the tangential velocity and radius of swirl chamber at the point where the fluid is injected into the atomizer.

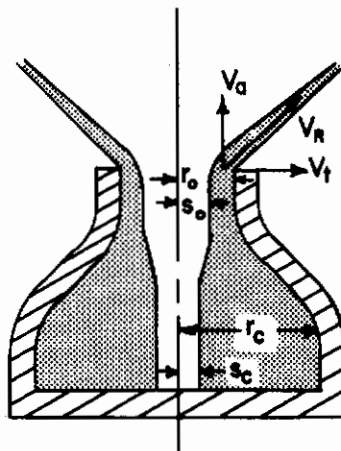


FIGURE 3-4. SCHEMATIC DIAGRAM OF SWIRL ATOMIZER WITH VARIABLES USED IN TAYLOR'S ANALYSIS (Taylor)³⁻¹⁶

If the axial velocity be represented by V_a and the velocity head by U , and if the radial velocity be considered as negligible, then Bernoulli's equation along the surface of the core can be written as

$$U^2 = V_a^2 + \frac{\Omega^2}{s^2} \quad (3-9)$$

which, at the orifice, becomes

$$1 = x^2 + y^2/z^2, \quad (3-10)$$

where

$$x = V_a/U, \quad (3-11a)$$

$$y = \Omega/r_o U, \quad (3-11b)$$

and

$$z = s_o/r_o \quad (3-11c)$$

The total flow rate \underline{Q} can be written as

$$\begin{aligned} Q &= \pi r_o^2 U (1-z^2)(1-y^2/z^2)^{1/2}, \\ &= \pi r_o^2 U K, \end{aligned} \quad (3-12)$$

where \underline{K} is the discharge coefficient. By assuming that \underline{y} is determined by the geometry of the chamber, the flow rate \underline{Q} is a maximum for

$$z^2 = \frac{y^2}{4} \sqrt{\frac{y^4}{16} + \frac{y^2}{2}}, \quad (3-13)$$

which hence gives the criterion for optimum performance.

Figure 3-5 is a graphical representation of the variation of \underline{z} and \underline{K} with respect to \underline{y} , along with the corresponding variation of the spray angle α , as determined below. This figure indicates that both the spray angle α and the relative thickness of the core \underline{z} decrease with respect to the radius r_o of the nozzle, but that the discharge coefficient \underline{K} increases, as is to be expected.

In order to determine the spray angle α , it is necessary to find an expression for the variable pressure p , and then to determine the axial velocity V_a of the liquid after emerging from the orifice. Bernoulli's equation for points within the fluid at the orifice can be written as

$$\begin{aligned} \frac{p}{\frac{1}{2} \rho U^2} &= 1 - \frac{y^2}{r^2/r_o^2} - x^2 \\ &= y^2 \left(\frac{1}{z^2} - \frac{r_o^2}{r^2} \right) \end{aligned} \quad (3-14)$$

Substitution of Equations (3-4), (3-6), and (3-7) into the equation of momentum

$$\rho Q (\bar{V}_a - V_a) = \int_{s_o}^{r_o} 2\pi r p dr, \quad (3-15)$$

yields

$$\cos \alpha = \frac{V_a}{U} = x + \frac{y\sqrt{z}}{(1-z^2)^{3/2}} \left[\frac{1}{2} \left(\frac{1}{z^2} - 1 \right) + \ln z \right] \quad (3-16)$$

since the total velocity of the particles leaving the orifice is U . The variation of α with y for Q_{\max} is also shown in Figure 3-5.

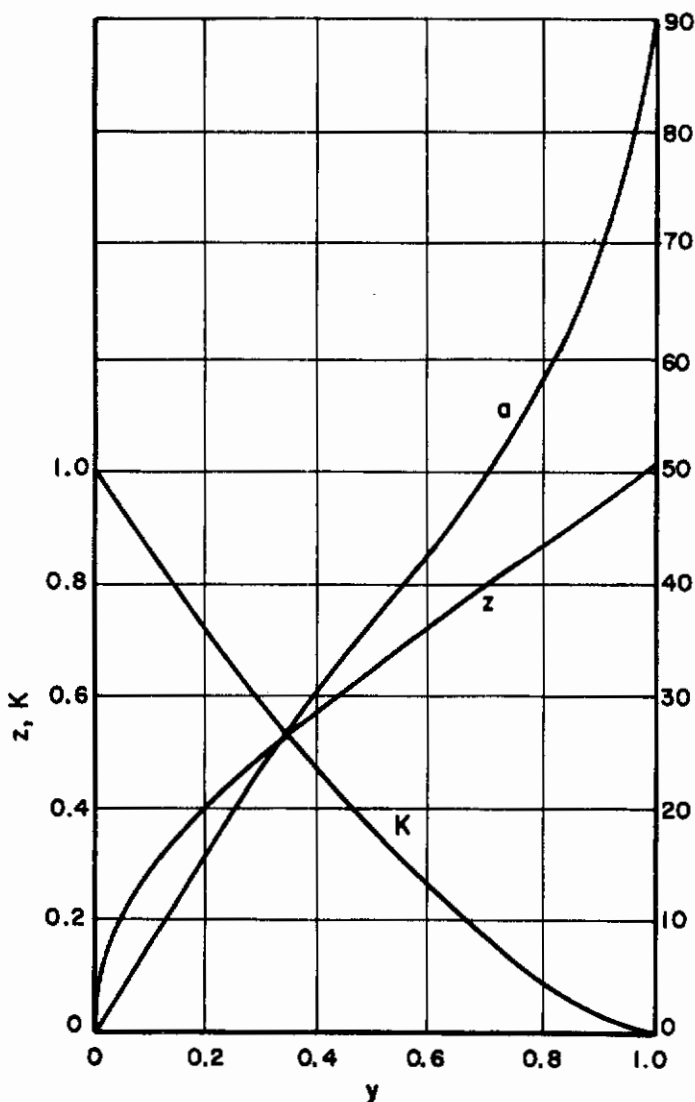


FIGURE 3-5. VARIATION OF K , z , AND α WITH y FOR MAXIMUM FLOW (Q) (Taylor)³⁻¹⁶

Since $V_a = 0$ at the outer surface of the liquid, far from the orifice, where the radius of the swirl chamber is r_c , Equation (3-9) reveals that

$$s_c = \frac{\Omega}{U} \quad (3-17)$$

Substitution of Equation (3-17) into Equation (3-11b) yields

$$s_c = y r_o \quad (3-18)$$

Now, since Equation (3-10) predicts that, for $V_a > 0$, z is always greater than y , it follows, from Equations (3-11c) and (3-18), that the radius s_o of the core at the orifice is greater than the radius s_c of the core in the swirl chamber. This, however, is contrary to experimental observations, which indicate that the radius of the core remains essentially constant. This discrepancy indicates that perfect fluid theory is not capable of describing the phenomenon adequately.

The discrepancy between experiment and theory is explained by assuming that a retarded boundary layer is formed close to the orifice, which then tends to make the radius of the core remain essentially constant. A detailed analysis of the effects of boundary layer and of surface tension, which is beyond the scope of this work, is given by G. I. Taylor in a subsequent paper⁽³⁻¹⁷⁾.

I. I. Novikov's Analysis

After beginning with an analysis which is identical with G. I. Taylor's Equations (3-8) to (3-14), I. I. Novikov⁽³⁻¹⁸⁾ proceeds to determine the spray angles α_1 and α_2 , which correspond to the outside and inside surfaces, respectively, of the spray sheath, as determined by consideration of the inertia forces alone. From Equations (3-10), (3-11), and (3-13), the outside angle α_1 can be determined by the equation

$$\tan \alpha_1 = \frac{V_{t1}}{V_{ao}} = \frac{U y}{U x} = \frac{z^2}{\sqrt{(1-z^2)/2}}, \quad (3-19)$$

and the inside angle α_2 can be determined by the equation

$$\tan \alpha_2 = \frac{V_{t2}}{V_{ao}} = \frac{U y/z}{U x} = \frac{z}{\sqrt{(1-z^2)/2}}, \quad (3-20)$$

where V_{t1} and V_{t2} are the tangential velocities at the surfaces of the nozzle and at the central core, respectively, and V_{ao} is the axial velocity at the nozzle.

Figure 3-6 shows a schematic diagram of the variables introduced by Novikov. Since experimental observation has indicated an abrupt swelling of the liquid sheath, immediately downstream of the nozzle, as indicated in the figure, an explanation of this effect is sought by considering the effect of the surface tension σ . If the pressure variation in the liquid is represented by the equation

$$\frac{dp}{dr} = \rho \frac{V_t^2}{r} = \rho \frac{\Omega^2}{r^3}, \quad (3-21)$$

where p is the pressure and ρ is the density, and if the pressure difference across the sheath is given by

$$\Delta p = \frac{2\sigma}{r}, \quad (3-22)$$

then substitution of Equation (3-15) into Equation (3-21) yields the following relation at the nozzle

$$\Delta r = \frac{2\sigma r_o^2}{\rho \Omega^2}. \quad (3-23)$$

Since experiments indicate that the thickness of the sheath approximately doubles upon emerging from the nozzle, the incremental thickness $\Delta'r$ added to the sheath thickness ($r_o - s_o$) is then

$$\Delta'r \approx (1/2) \Delta r = \frac{\sigma r_o^2}{\rho \Omega^2}. \quad (3-24)$$

It is readily seen that this incremental thickness $\Delta'r$ will cause the experimentally observed outside angle α_1' to be less than α_1 , as predicted by Equation (3-19). Also, a larger initial pressure, corresponding to a larger value of Ω , will cause a decrease in $\Delta'r$, as shown by Equation (3-24). Both of these tendencies are confirmed by experimental observation. Inspection of Figure 3-6 also indicates that the originally conical sheath is assumed to degenerate into a cylindrical sheath at some distance from the nozzle. This tendency, which is observed experimentally, can be explained theoretically by consideration of Equations (3-21) and (3-22), which show that the inertia effects

vary as $\frac{1}{r^3}$ and hence do not increase as rapidly with respect to r as the surface tension effects, which vary as $1/r$.

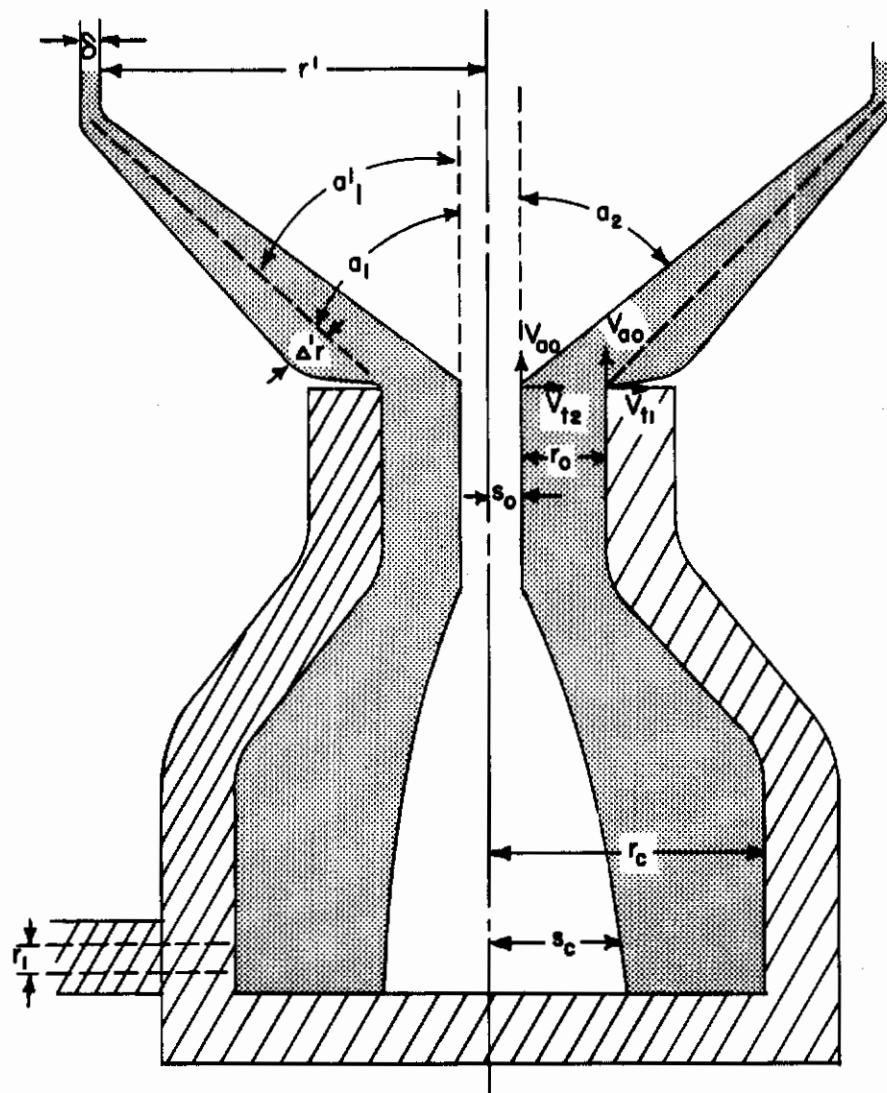


FIGURE 3-6. SCHEMATIC DIAGRAM OF NOZZLE AND LIQUID SHEATH FOR NOVIKOV'S ANALYSIS (Novikov)³⁻¹⁸

The thickness of the sheath δ is determined by considering Bernoulli's equation for the liquid sheath, where surface tension must be included:

$$2 \frac{p}{\rho} + v_t^2 + v_a^2 + \frac{4\sigma}{\rho\delta} = U^2 \quad (3-25)$$

From Equations (3-23) and (3-8), it is seen that

$$v_t^2 = \frac{2\sigma}{\rho\delta} \quad (3-26)$$

If the pressure on the inside surface of the sheath is then assumed to be

$$p = p_a - \frac{\sigma}{r'} \quad (3-27)$$

where p_a is the atmospheric pressure, and r' is the radius of the inside surface, then substitution

of Equation (3-26) and Equation (3-27) into Equation (3-25) yields the following Bernoulli equation for the inside surface of the sheath

$$v_a^2 = U^2 - \frac{2 p_a}{\rho} - \frac{2 \sigma}{\rho} \left(\frac{3}{\delta} - \frac{1}{r'} \right) \quad (3-28)$$

$$\approx U^2 - \frac{2}{\rho} \left(p_a + \frac{6 \sigma}{\delta} \right),$$

since $\delta \ll r'$. Consideration of the equation of continuity

$$\pi r_i^2 \frac{\Omega}{r_c} = 2 \pi r' \delta v_a, \quad (3-29)$$

where r_i is the radius of the tube which supplies the liquid to the nozzle, along with Equations (3-8), (3-26), and (3-28) yields the following equation for the sheath thickness, δ :

$$\delta = \sqrt[3]{\sigma r_i^4 / \left[2 \left(\rho U^2 - 2 p_a - \frac{6 \sigma}{\delta} \right) r_c^2 \right]}. \quad (3-30)$$

It is then assumed that the velocity head U can be expressed by

$$U = \frac{2}{\rho} (P + p_a), \quad (3-31)$$

where P is the over-pressure. Substitution of Equation (3-31) into Equation (3-30) yields

$$\delta = \sqrt[3]{\sigma r_i^4 / \left[4 \left(P - \frac{3 \sigma}{\delta} \right) r_c^2 \right]}$$

$$\approx \sqrt[3]{\sigma r_i^4 / \left[4 P r_c^2 \right]} \quad (3-32)$$

for $P > 1$ atmosphere, and $\delta > 10^{-3}$ cm.

Equation (3-32) is then applied to the problem of determining the average diameter a of droplets formed by the nozzle. On the assumption that the total surface area of the drops is equal to the surface area of the cylindrical sheath, the following relation is obtained

$$a = 3 \delta. \quad (3-33)$$

Consideration of Equations (3-32) and (3-33) indicates that the mean size of the droplets varies directly as the cube root of the surface tension σ and as the four-thirds power of the radius r_i of the supply tube, inversely as the cube root of the supply over-pressure, and inversely as the two-thirds power of the radius r_c of the chamber.

Figure 3-7 gives a comparison of experimental data with the theoretical curve, as predicted by Equations (3-32) and (3-33). The validity of Novikov's theoretical analysis is hence confirmed quite well by experimental observations.

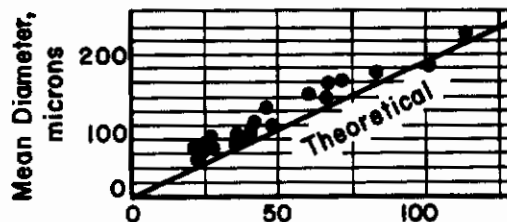


FIGURE 3-7. COMPARISON OF EXPERIMENTAL DATA FOR THE MEAN DROP SIZES OF SPRAYS WITH NOVIKOV'S THEORETICAL CURVE (Novikov)³⁻¹⁸

A less elegant derivation, but one which is more readily applicable to the problems of design, was given by J. F. Harvey and A. W. Hermandorfer⁽³⁻¹⁹⁾. They found that the experimental spray angle α lay between the angle determined by assuming a (mathematical) free vortex in the swirl chamber and the angle determined by assuming a forced vortex in the swirl chamber such that the whole mass of fluid moved as a rigid body. Figure 3-8 indicates the coordinates used and the geometrical configuration considered. From this figure, the equation for any point on the spray surface can be determined to be

$$\begin{aligned} \xi \tan \alpha &= \sqrt{(\eta + r_o)^2 - r_o^2} \\ &= \sqrt{\eta^2 + 2\eta r_o}, \end{aligned} \tag{3-34}$$

and the slope of the surface is given by

$$\frac{d\eta}{d\xi} = \frac{\xi \tan^2 \alpha}{\eta + r_o}, \tag{3-35}$$

where ξ and η are the axial and radial coordinates, respectively, of a droplet with respect to the rim of the nozzle orifice, r_o is the radius of the orifice, and

$$\tan \alpha = \frac{V_{to}}{V_{ao}}. \tag{3-36}$$

Inspection of Figure 3-8 and of Equation (3-35) reveals immediately that, although the spray surface is perpendicular to the nozzle in the immediate vicinity of the orifice, it becomes essentially

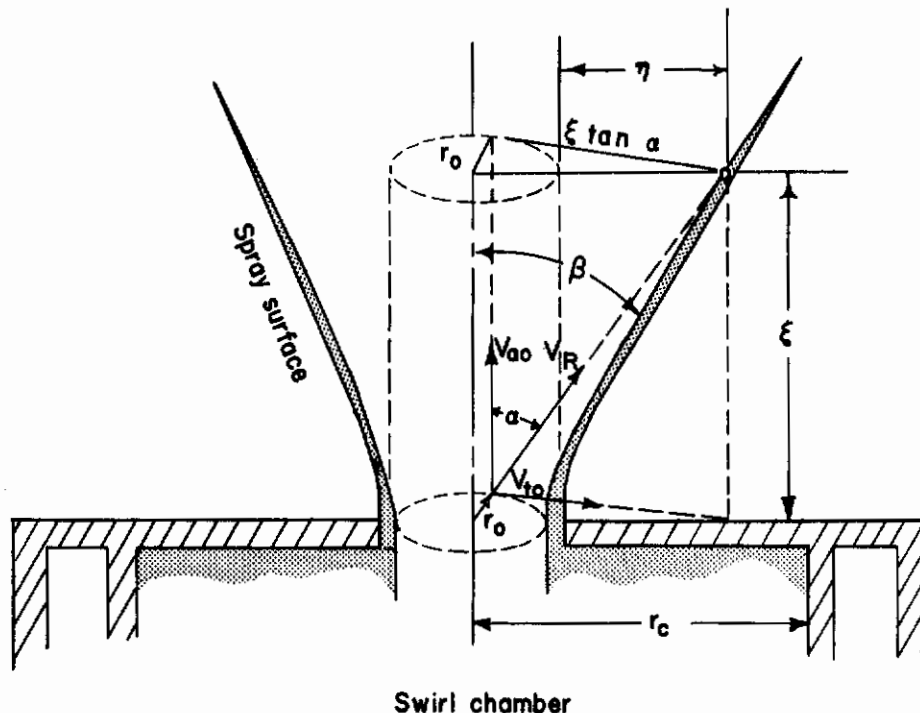


FIGURE 3-8. GRAPHICAL CONSTRUCTION OF SPRAY ANGLE PROFILE FOR SIMPLE SWIRL ATOMIZER (Harvey and Hermandorfer)³⁻¹⁹

a conical surface for $\eta \gg r_o$; and the angle β , which the surface makes with the axis, is essentially equal to the previously defined angle α . This identification of the spray angle β with the velocity angle α permits a ready determination of the spray angle from an assumed velocity variation in the chamber.

If the flow inside the swirl chamber is assumed to be that of a free vortex, where friction losses are neglected, the condition of constancy of angular momentum leads to

$$r V_t = r_c V_{tc} = \text{constant}, \quad (3-36)$$

where r is the radial distance from the center of the swirl chamber, r_c is the radius of the chamber wall, and V_{tc} is the tangential velocity at which the fluid is introduced into the chamber. From Equation (3-36), it can be seen that the tangential velocity at the orifice will be

$$V_{to} = \frac{r_c}{r_o} V_{tc} = \frac{r_c}{r_o} K_1 Q, \quad (3-37)$$

where Q is the volume flow rate and K_1 is a function of the configuration, and changes little with flow rate. Further considerations indicate that the axial velocity V_c in the swirl chamber is given by $K_2 Q$ where K_2 is also independent of flow rate. Thus, for the case of free vortex flow in the chamber, the spray angle β is given by

$$\tan \beta \approx \tan \alpha = \frac{r_c}{r_o} \left(\frac{K_1}{K_2} \right). \quad (3-38)$$

Equation (3-38) predicts no change in spray angle β with a variation in pressure.

Instead of assuming no friction effect, one might assume large friction effects as the other extreme. In this case, the central core will rotate as a solid body. By taking the extreme "forced vortex" case of this solid core, namely, by allowing the entire quantity of fluid inside the swirl chamber to rotate as a solid body, the tangential velocity can be expressed by

$$\frac{V_t}{r} = \frac{V_{tc}}{r_c} = \text{constant}. \quad (3-39)$$

The authors then assume that the axial velocity V_a is unaffected by friction and given by the same relation as before. Thus, the spray angle for a forced vortex flow is expressed by

$$\tan \beta \approx \tan \alpha = \frac{r_o}{r_c} \left(\frac{K_1}{K_2} \right). \quad (3-40)$$

This gives a lower bound for the spray angle, since $r_o < r_c$. Figure 3-9 shows a comparison of experimental spray-angle data with the angles as predicted by the theories of free forced vortices.

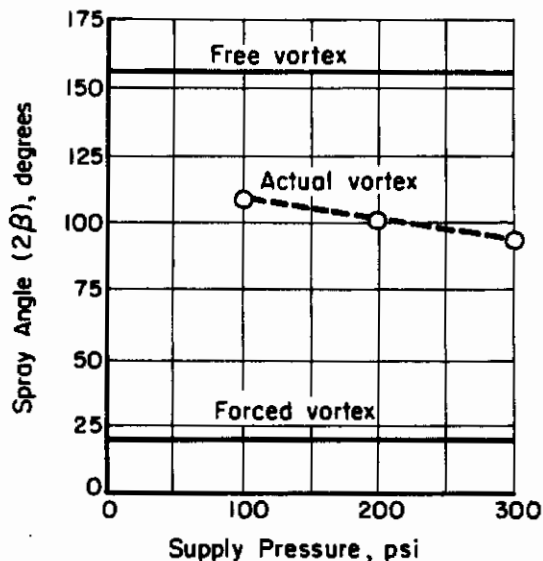


FIGURE 3-9. COMPARISON OF THEORETICAL AND EXPERIMENTAL VARIATION IN SPRAY ANGLE WITH SUPPLY PRESSURE FOR A TYPICAL SWIRL ATOMIZER (Harvey and Hermandorfer)³⁻¹⁹

Although neither the free vortex nor the "forced vortex" assumption is physically accurate, they give valid upper and lower bounds, respectively, for the experimental spray angle, as shown in this figure. Since the friction effect varies as the square of the velocity and since it was noted above that this effect will change the tangential velocity more than the axial velocity, it is physically reasonable to expect a decrease in the spray angle β with an increase in the supply pressure, as shown in Figure 3-7.

SPRAY NOZZLES FOR AIRCRAFT GAS TURBINES

All spray nozzles used on aircraft gas turbines employ the swirl principle discussed in the previous section. The simplest form of the swirl atomizer is the conventional fixed-orifice nozzle known as a simplex nozzle, or "simplex burner", the latter being the British term. The "Monarch" nozzle is a well-known example of this type of simplex swirl nozzle.

Because simplex nozzles obey the "square law", meaning that the liquid pressure is proportional to the square of the flow, they do not have as much flexibility as is required. For example, to accomplish a range of flow of 20 to 1, a pressure-drop variation of 400 to 1 would be necessary. Considering the fact that the minimum pressure drop that will give satisfactory atomization is about 15 psi, it is obvious that a simplex nozzle cannot meet the flow range requirements.

The solution to the problem lies in complex atomizers of various types that have a more favorable relation between flow rate and fuel pressure drop than the square law pressure relation. The simplex spray nozzle will be described first, and the various designs of complex atomizers, such as the duplex, variable-area, poppet, and spill-return, will then be discussed. The advantages and disadvantages of each will be pointed out.

The Simplex Nozzle

Figure 3-10 shows the construction of several common forms of the simplex nozzle as described by Joyce⁽³⁻²⁰⁾. Figure 3-10a shows the familiar Monarch type used in stationary oil burners. This is now considered as a sort of standard, or criterion, with which to compare other swirl-type atomizers. The construction is simple as it consists of only two parts: (1) a body containing the final orifice, and (2) a plug member with two or more tangential slots cut in the truncated conical tip. The conical inner surface of the body serves as the upper boundary for these slots so that liquid entering the body can find egress only after passing up the tangential slots and swirling in the swirl chamber before reaching the discharge orifice. This type of nozzle is available in capacities from 1 to 100 gph.

Parts (b), (c), and (d) of Figure 3-10 show the designs of disk- or plate-type atomizers which can be placed in a simple housing consisting of a body and cap, as shown in (e). In the case of (b) a single flat disk contains the three essential elements of the atomizer: (1) tangential slots, (2) swirl chamber, and (3) orifice. The flat top of the housing serves to provide the back wall of the vortex chamber, and to close the tangential slots along their length.

Part (c) is a slightly different design in which the slots are cut in one plate and the orifice and swirl chamber in the other. Part (d) is another form of two-disk assembly with the slotted member punched out or stamped. An advantage of the two-plate design is that different forms of slot plates can be used with one orifice plate, and conversely. Joyce cautions that it is vitally important that the two companion disks be assembled in exact coaxial alignment.

The final orifice of a simplex atomizer, and of the complex types also, is usually about one-fourth to one-half a diameter long. Joyce points out that the ideal orifice is probably of no length, that is a knife-edge, but that in practice it is not possible to use such an orifice, because (1) it is not practical to make a knife-edge hole of a precise size, and (2) such a hole would have no resistance to wear and would enlarge rapidly owing to erosion. It is appropriate, therefore, to consider some of the defects of manufacture that may result.

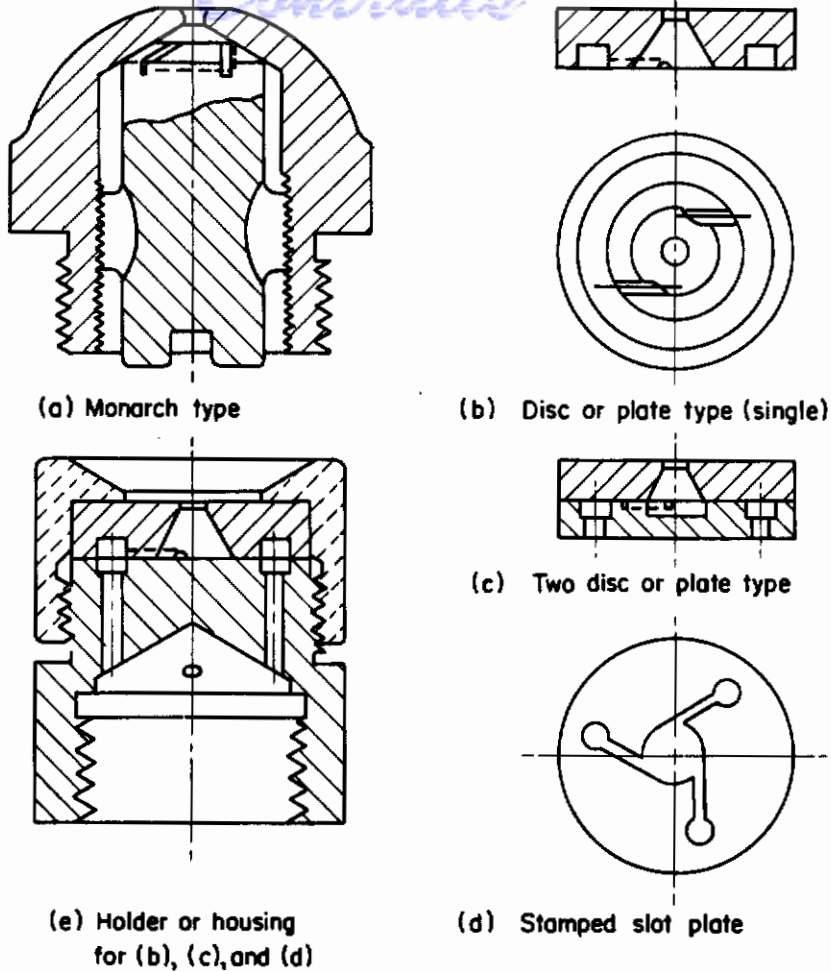


FIGURE 3-10. SIMPLEX NOZZLE DESIGNS (Joyce)³⁻²⁰

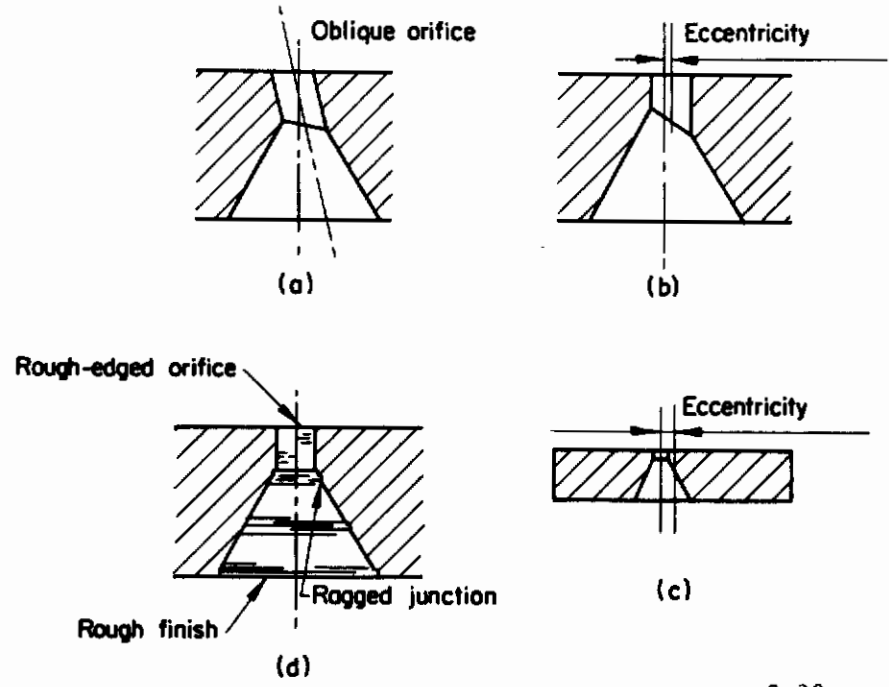


FIGURE 3-11. FAULTS IN ORIFICES (Joyce)³⁻²⁰

Figure 3-11 illustrates some common faults in orifices. Case (a) shows an orifice that is oblique to the axis of the swirl chamber, and case (b) shows the orifice eccentric to the swirl chamber. Case (c), where the orifice and swirl chamber are concentric to each other but eccentric to the center line of the disk, is probably less common. Case (d) shows a ragged finish at the apex of the swirl chamber where the orifice starts, and at the discharge end. Joyce's illustrations are purposely exaggerated to show more clearly the various types of faults; however, he emphasizes the fact that a minute eccentricity or obliquity will materially impair the performance of an atomizer. Also, fine finish and accuracy in these vital respects cannot be too strongly emphasized.

The Duplex Nozzle

Figure 3-12 shows the design of a duplex nozzle which is the most widely used for aircraft gas turbines today. Mock and Ganger⁽³⁻²¹⁾ point out that the duplex nozzle was developed because the flow range of the simplex nozzle was found to be inadequate. Pierce and Parker⁽³⁻²²⁾ substantiate this point by stating that the outstanding flow characteristic of the duplex nozzle is its ability to provide a good spray over a flow range of 20 to 1 or better with a pressure range as low as 16 to 1. A comparable flow range with a simplex nozzle would require a pressure range of 400 to 1 and would result in maximum fuel pressures well in excess of the values desired by most pump manufacturers.

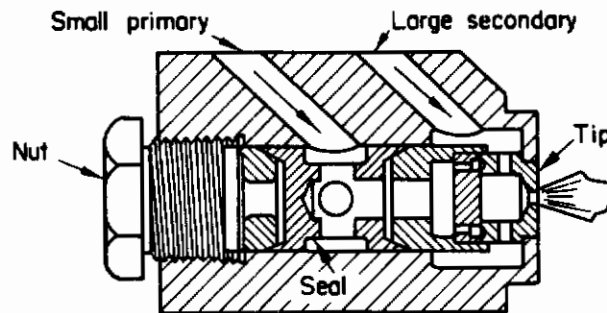


FIGURE 3-12. DUPLEX NOZZLE (Mock and Ganger)³⁻²¹

A special metering valve for duplex nozzles, termed a flow divider, is used to divide the fuel supply into two branches. One branch goes to the small primary manifold and the larger branch passes through the flow divider before reaching the large secondary manifold. At low pressures and low rates of flow, fuel is supplied to the small slots only and, as the pressure and flow rate increase, the flow divider diverts increasing proportions of fuel to the large slot through the larger secondary manifold. A typical duplex nozzle might consist of two small slots and four large slots all feeding a common swirl chamber along tangential paths.

Pierce and Parker⁽³⁻²²⁾ point out that two types of orifices are being used: (1) a plain cylindrical hole, and (2) a flared, bell-shaped exit which serves to control the spray angle at low flows. One-piece construction of the nozzle tip is recommended to insure a uniform pattern by minimizing the possibility of eccentricity of the swirl chamber with respect to the orifice.

Mock and Ganger⁽³⁻²¹⁾ point out that duplex nozzles with a single fuel manifold have been used and are attractive for engines requiring a large number of nozzles. However, since the valve areas, springs, and forces are so small it is difficult to avoid appreciable variation between different nozzles at the transfer or cut-in point when the large slots begin to supply fuel to the swirl chamber. The flow divider, with the two fuel manifolds, is preferred as it reduces the accuracy required at the initial setting of the nozzles, and compensates for variations encountered in service, and is also believed helpful in overcoming chatter. Even with the benefit of the flow divider the duplex nozzle is extremely sensitive to pressure change at the cut-in point so that it is difficult to maintain a flow tolerance of plus or minus 3 per cent without adjustment.

With reference to combustion performance, Alford⁽³⁻²³⁾ claims that the duplex nozzle, when compared to a simplex nozzle at a combustor pressure of one atmosphere, showed an improvement in efficiency of 12 per cent.

Variable Area Nozzles

Variable area nozzles may be designed to provide for variation of (1) the area of the exit orifice, (2) the area of the inlet slot, or (3) the areas of both the inlet slot and the exit orifice.

Figure 3-13 shows a poppet, or pintle, type nozzle with variable exit orifice. (3-1) Fuel is supplied through a manifold which is commonly made to house the nozzle spring and other nozzle components. The fuel from the supply manifold enters a series of axial transfer holes "A" and passes into the pre-orifice chamber, "B". As the fuel supply pressure is increased above the combustion chamber pressure an unbalance of forces causes the poppet to move outwardly against the calibrated spring. The movement of the poppet, which is directly related to the increase in fuel pressure, results in changes in the annular exit orifice around the tapered metering section of the poppet.

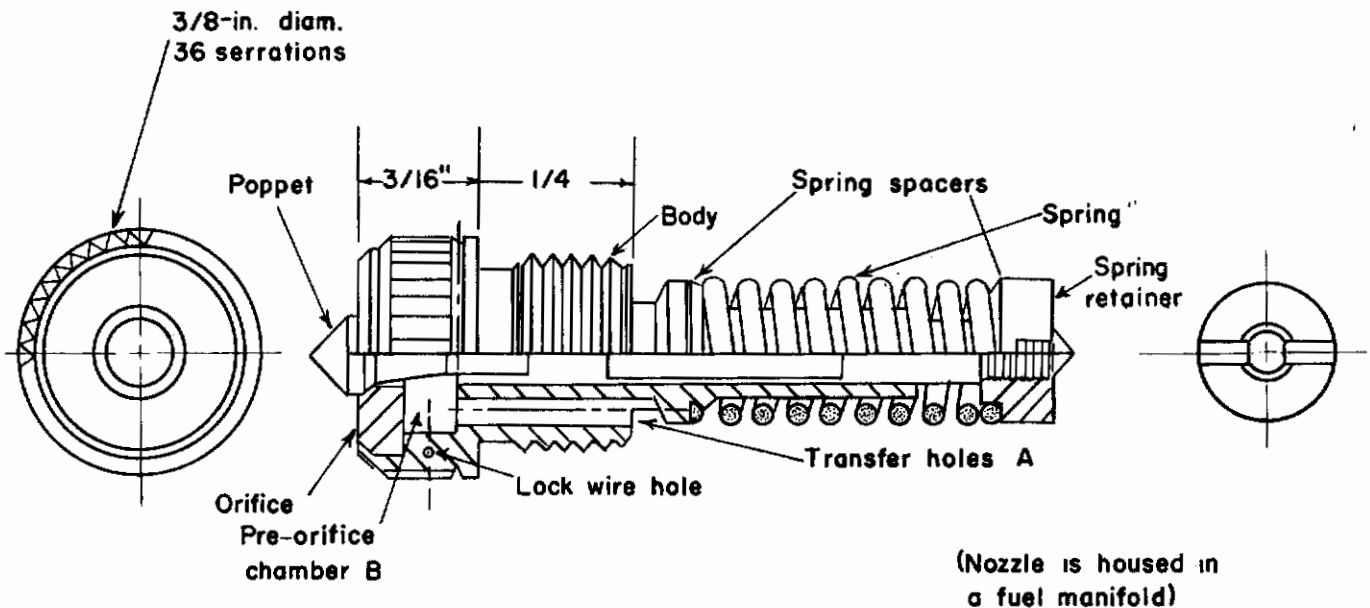


FIGURE 3-13. VARIABLE AREA NOZZLE, POPPET TYPE (Bolt, Lennox, and Saxton)³⁻¹

Therefore, fuel flow rate becomes a function of the variable orifice area as well as of the square root of the fuel pressure. The flow-versus-pressure relationship is practically linear. Flow data for several poppet nozzles used on ram-jet engines are shown below.

TABLE 3-2. FLOW RANGE FOR TYPICAL POPPET NOZZLES

Flow Range, lbs/hr	Pressure Range, psi	Flow Ratio	Pressure Ratio
17-170	50-200	10	4
30-500	50-200	17	4
50-860	75-300	17	4
20-400	50-200	20	4
30-1500	50-300	50	6
50-1080	15-150	20	10

Flow tolerances may be held to limits which are comparable to the flow tolerances of precision fixed-orifice nozzles. Limited flight experience has been favorable.

A basic fault of this type of nozzle is poor patterning; this is the main objection to its use in gas turbines and similar types of equipment.

Some of the significant advantages claimed for well-designed poppet nozzles are wide flow range, linear flow-pressure relationship, good atomization, good matching of a group of nozzles, sharp cut-off at a predetermined pressure, little difficulty from dirt so that micronic filtering is unnecessary, a simple fuel supply system, and low manufacturing costs.

It may be concluded that the poppet or pintle type of nozzle has been developed to the stage where it merits serious consideration as a simple, light weight, wide range atomizing device. Because of its basically poor patterning, efforts should be made to achieve good mixing of fuel and air, possibly by means of a baffle or similar device placed ahead of the region of combustion.

The second type of variable area nozzle, for which the area of the inlet slot may be varied, is also known as the Lubbock atomizer. Bolt and Saxton⁽³⁻²⁴⁾ describe this type of nozzle which embodies a stepped plunger, to uncover additional slot area as the fuel pressure is increased. As the inlet-slot area increases with increasing pressure, the ratio of inlet-slot area to exit-orifice area becomes larger, resulting in a larger spray angle at low flow rates.

The third type of variable area nozzle, designed so that an increase in flow results from an increase in the areas of both the inlet slot and exit orifice, is described by Stark and Constantino⁽³⁻³⁾. However, this design proved to be much too complicated to be practical, and difficulty was encountered in the matching of nozzles.

The Spill-Return Nozzle

Figure 3-14 shows the features of the spill-return type of swirl atomizer, sometimes called the Peabody-Fisher nozzle, as described by Joyce⁽³⁻²⁰⁾. The fuel flowing through the tangential swirl slots has two exit paths from the swirl chamber. These are (1) the normal exit orifice leading

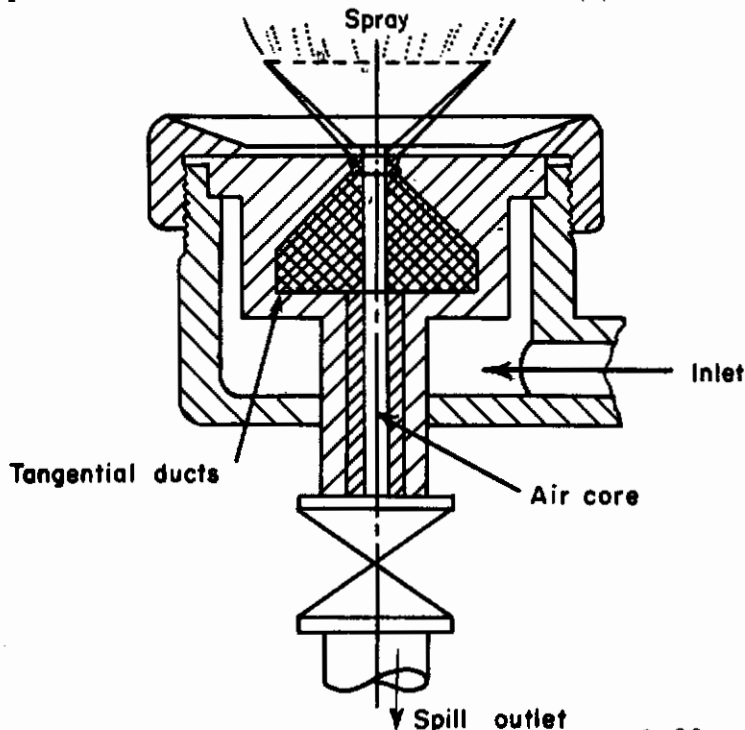


FIGURE 3-14. SPILL-TYPE NOZZLE (Joyce)³⁻²⁰

to the combustion space, and (2) another orifice concentric with the exit orifice but located in the rear wall of the swirl chamber, and generally of larger size. This is termed the spill orifice and is connected by a pipe, in which there is a control or throttle valve, to the fuel tank. If the valve in the spill line is fully open, the greater part of the fuel which flows through the tangential slots will be bled back to the fuel tank, and only a small proportion will pass out of the exit orifice. Joyce points out that it is even possible to adjust the relative sizes of the discharge and spill orifices so that all the fuel passes back to the tank and none emerges from the exit orifice. This simply requires that the exit orifice be of the same size or smaller in diameter than the air core.

Since zero flow rate is possible, it is easy to see that an extremely wide range of fuel flows can be attained even at one fixed supply pressure. Joyce states that a flow range of 20 to 1 can easily be obtained by spill control alone, using a constant supply pressure. If pressure is also varied over a range of 25 to 1, then a flow range of 100 to 1 would be obtained. However, the spray cone angle would vary greatly and would be very large at low flow rates when using this method to control flow.

Watson⁽³⁻¹⁰⁾ considers the spill-type atomizer in many ways the most attractive, particularly in its capacity to handle a wide range of fuel flows for a given range of pressure. A disadvantage pointed out by Watson is that a relatively large amount of fluid must pass through the swirl slots; this may cause difficulties at starting and at low speeds when the fluid is supplied by an engine-driven pump. Alternatively, the spilled fuel may be recirculated either by an auxiliary pump or by an ejector system, in which instance the engine pump has to supply only the fuel which the engine requires.

Bolt and Saxton⁽³⁻¹⁾ point out that the recirculated fluid in a spill-type nozzle provides energy for maintaining a strong vortex in the swirl chamber, which is particularly advantageous at low flows.

Lawrence⁽³⁻²⁵⁾ states that spill-type nozzles would appear to be the ideal choice, but for some drawbacks. First, it is necessary to pipe away the spilt fuel from the nozzles, and also to equalize the quantity spilled from each nozzle. Secondly, it is difficult to design a control to operate on the difference between the fuel supplied to the nozzle and the fuel taken away as representing the actual fuel sprayed into the engine.

The principal objection to the spill-type nozzle appears to be the complicated controls required to maintain properly balanced flow rates.

FUEL VAPORIZING SCHEMES

The vaporization of liquid fuel before it enters the burning space has been used in many types of combustion chambers and has been an attractive method of preparing fuel for combustion ever since the beginning of aircraft gas-turbine use. However, many difficulties were encountered with the result that liquid-fuel injection is the more common practice. Recent developments, however, have resulted in satisfactory vaporizers that have certain advantages over spray nozzles.

Advantages of Fuel Vaporizers

Pouchot and Hamm⁽³⁻²⁶⁾ found that the vaporization of fuel has four desirable features. (1) The combustor can be short and still maintain high efficiency and stability because the time interval required for vaporization is eliminated. (2) Burning is clean when using a wide range of fuels with the result that wall deposits are slight and the luminosity of the flame is low; the low luminosity reduces wall temperature. (3) Extremely low fuel pressures can be used without penalty in performance. (4) The chief virtue is a 40 per cent saving in burning length as compared with a comparable liquid-injection burner.

With respect to evenness of outlet-temperature distribution, fuel vaporizers are neither better nor worse than spray nozzles.

Description of Fuel Vaporizers

Figure 3-15 shows the principle of operation of fuel vaporizers and how fuel and air flow in the vaporizing tube and in the combustion chamber. This type of vaporizer was developed by Armstrong Siddeley and is used on the Sapphire and J65 engines.

No mechanical atomization by spray nozzles is involved. Instead fuel passes through 36 vaporizing tubes that are immersed in the flame; these serve to vaporize the liquid fuel and mix it with a portion of the combustion air referred to as primary air in Figure 3-15. The secondary-air ports supply the remainder of the air needed for combustion.

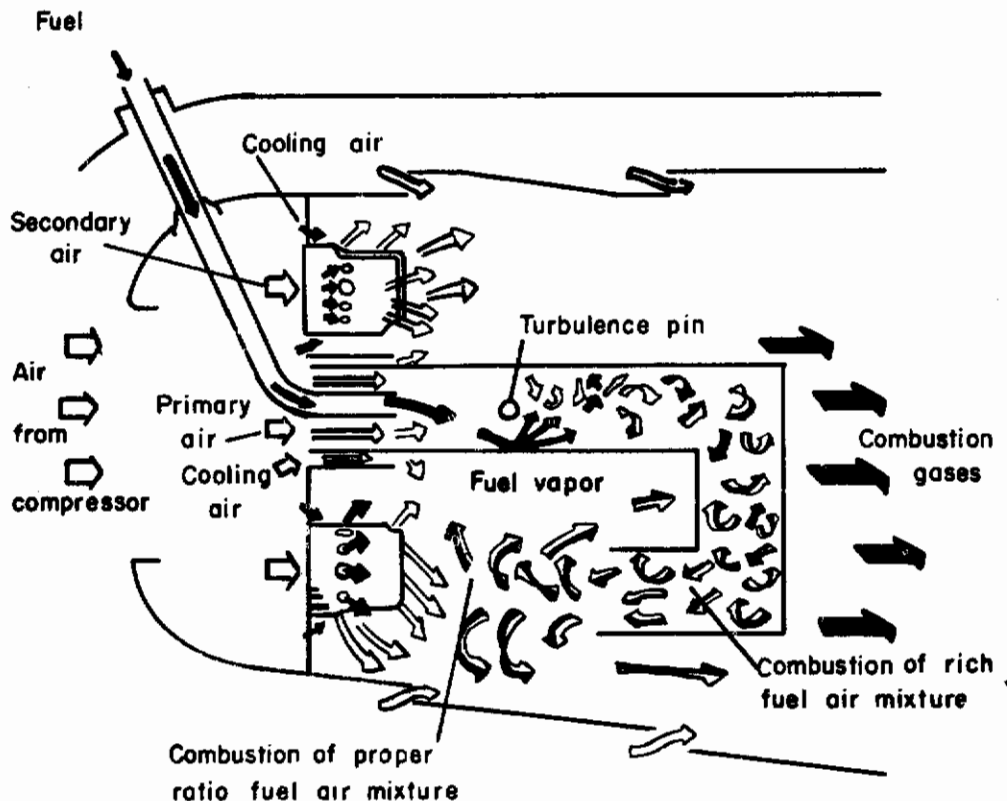


FIGURE 3-15. FUEL-VAPORIZING TUBE AND COMBUSTION CHAMBER (Stone)³⁻²⁷

Fuel pressure in the tubes feeding liquid fuel into the 36 vaporizing tubes is only sufficient to insure that the proper quantity of fuel will flow into the combustion chamber. Enough heat is transferred through the walls of the tubes to vaporize the liquid fuel. Cracking of the fuel on the inside walls of the tubes with consequent coke formation is prevented because the vaporization takes place in the presence of a large volume of air so that the temperature required to vaporize the fuel is relatively low, much below the distillation temperature. The rich fuel and air mixture is then mixed with secondary air to form a combustible mixture in the burning zone. Because mixing can be achieved in a short time interval, the vaporizing combustion chamber has a combustion zone about 40 per cent shorter than that for a corresponding atomizing-type combustor.

The main problem is to accomplish complete vaporization without overheating of the vaporizing tube material. If vaporization is incomplete, fuel may coke on the outside surface of the vaporizing tubes.

During the starting cycle, the vaporizing combustor requires auxiliary liquid fuel injection nozzles. After the vaporizer elements reach operating temperature, the auxiliary nozzles are no longer used, and the response to fuel-rate changes is excellent.

INJECTORS FOR ROCKET PROPELLANTS

The purpose of liquid-reactant injectors is to introduce the propellants so that they may be prepared for burning with maximum efficiency. Abramson⁽³⁻²⁸⁾ points out that the ideal theoretical conditions of complete combustion at the rocket-nozzle entrance can be approached only if the reactants are properly injected. The two fundamental requirements are (1) mixing of the fuel and oxidizer, and (2) atomization of the mixed particles.

Gunn⁽³⁻²⁹⁾ states that, for hypergolic propellants, degree of liquid-phase mixing is of great importance in determining ignition delay. When propellants are mixed by impingement of fuel and oxidizer jets, the efficiency of the mixing processes is dependent, in addition to such parameters as injection pressures, angle of impingement, etc., upon the compactness of the jets and the precision of their impingement. The production of well defined and accurately directed jets, over free stream lengths upwards of an inch and under injection pressures of 100 psi or more, is not easily achieved. The flow conditions upstream of the injection nozzles, the profile and smoothness of the nozzle flow channels and their exit sections, all affect markedly the cleanness of the jets produced.

Gunn⁽³⁻²⁹⁾ has studied the behavior of impinging liquid jets over free stream lengths up to 2 inches and under injection pressures up to 400 psi. He found that jets could be produced of sufficient continuity and compactness to establish and maintain a stable conducting path for electronic signals provided the following precautions were taken.

- (1) The passages immediately upstream of the nozzle entrance should be designed to insure that the local flow conditions are laminar and free of swirls and eddys.
- (2) The profile of the nozzle flow channel should consist of a trumpet-mouthed entrance section and a short straight section. The optimum length of the straight section is influenced by the degree to which "reservoir" flow conditions exist immediately upstream of the entrance section; in general, the L/D ratio should be between 1 and 5 and as close to 1 as the upstream flow conditions permit.
- (3) The surfaces of the nozzle flow channel should be lapped extremely smooth. This requirement becomes increasingly important as the diameter of the hole is reduced.

Abramson explains that mixing is essential because the fuel and oxidizer must be finely dispersed in the designed ratio for maximum performance. Decreasing the particle size and increasing the surface area by atomization assist in speeding up the reaction during the short time that the propellants are retained in the combustion chamber. Of these two essentials, Abramson considers mixing to be the more important, although both mixing and atomization take place to a varying degree in all injectors.

Abramson⁽³⁻³⁰⁾ states that the problem of injector design, as related to performance and heat transfer is recognized generally to be a critical one. For the most part two fundamental designs are used in present day rocket engines. They are the 1:1 impinging stream with a relatively short free stream length, and the so-called shower head, which consists of a very large number of holes, on the order of hundreds or thousands, which produces excellent atomization of each stream, and mixing by the proximity and the number of streams.

Types of Injectors

Figure 3-16 shows the design of an impinging-type injector, BAC (Bell Aircraft Corporation) Type 008, in which a central core of oxidizer impinges on an outer cylinder of fuel so that mixing

and atomization occur simultaneously. The cylinder is formed by broaching a drilled hole and inserting a core of diameter equal to the drilled-hole diameter, thus forming a family of orifices of approximately triangular cross section. The center core is drilled for the flow of oxidizer and a mechanical swirler is inserted so that the oxidizer that passes through the single orifice in the core will come out in the form of a hollow cone.

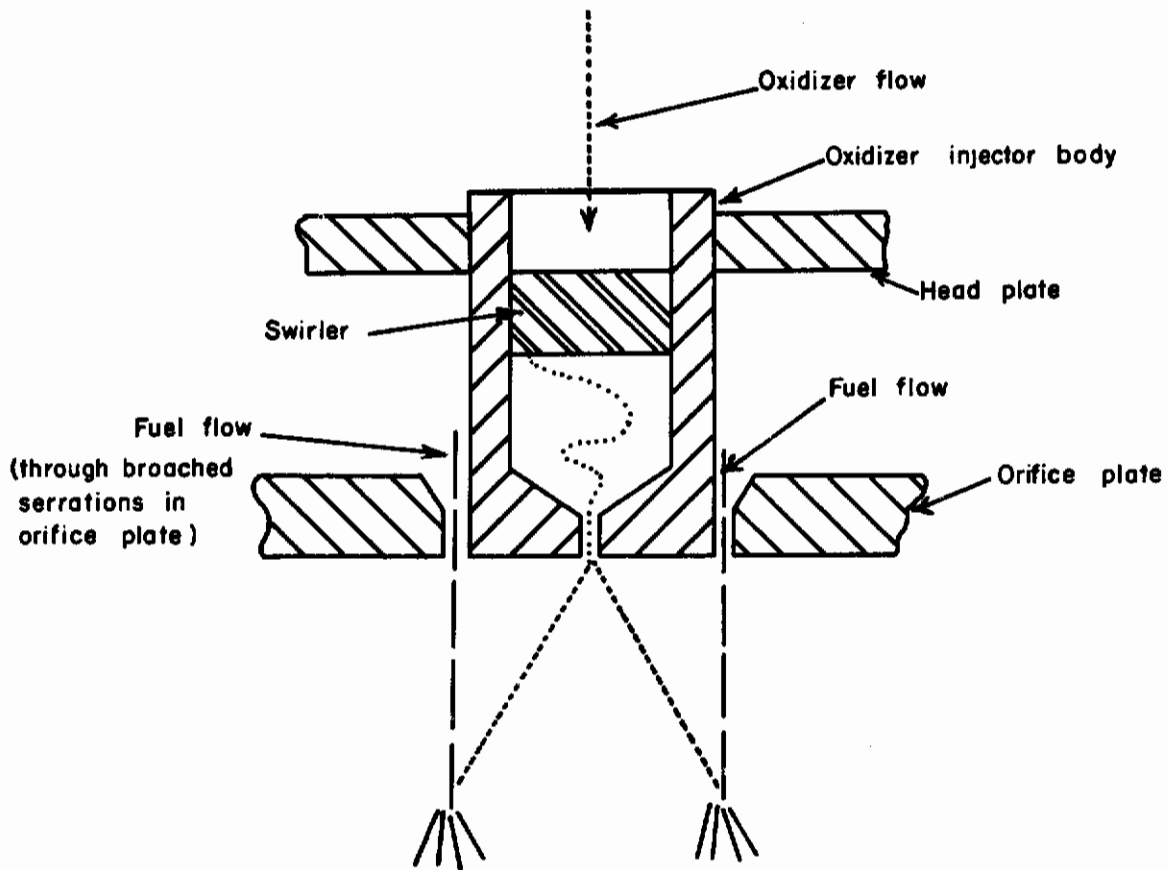


FIGURE 3-16. BAC TYPE 008 INJECTOR (Abramson)³⁻²⁸

Abramson reports that this type of injector gave good performance and may be produced in quantity by automatic machine work; however, the assembly procedure is delicate and a high percentage of scrap may result.

Figure 3-17 shows the BAC Type 243 impinging-jet-type injector, in which a family of pairs of fuel and oxidizer jets are made to impinge to accomplish atomization and mixing in one step. Each fuel jet in an outer ring of jets is made to impinge on its mating oxidizer jet in an inner ring. The configuration is such that in any pair the plane formed by the axes of the two jets is roughly in the position of a tooth of a hypoid gear. This allows maximum mixing of all sheets formed by the pairs of jets, and the sheets are then inclined in toward the center so that the heat transfer to the walls may be kept at a minimum. The angle of impingement was designed to be approximately 74 degrees in keeping with the best available information.

Figure 3-18 shows the BAC Type 201 injector which consists of a series of rings of serrated outside diameters which form a series of elements of concentric cylinders. The concentric cylinders are alternately fuel and oxidizer, with each pair of cylinders giving impingement at an angle of approximately 10 degrees. No attempt is made to impinge individual jets in pairs as in the Type 243 injector; instead, impingement takes place between pairs of cylindrical surfaces. Any deflection of one propellant inward or outward is met by intersection of the cylinder of the other propellant, thereby allowing no opportunity for a propellant to travel out of the chamber in an unmixed condition.

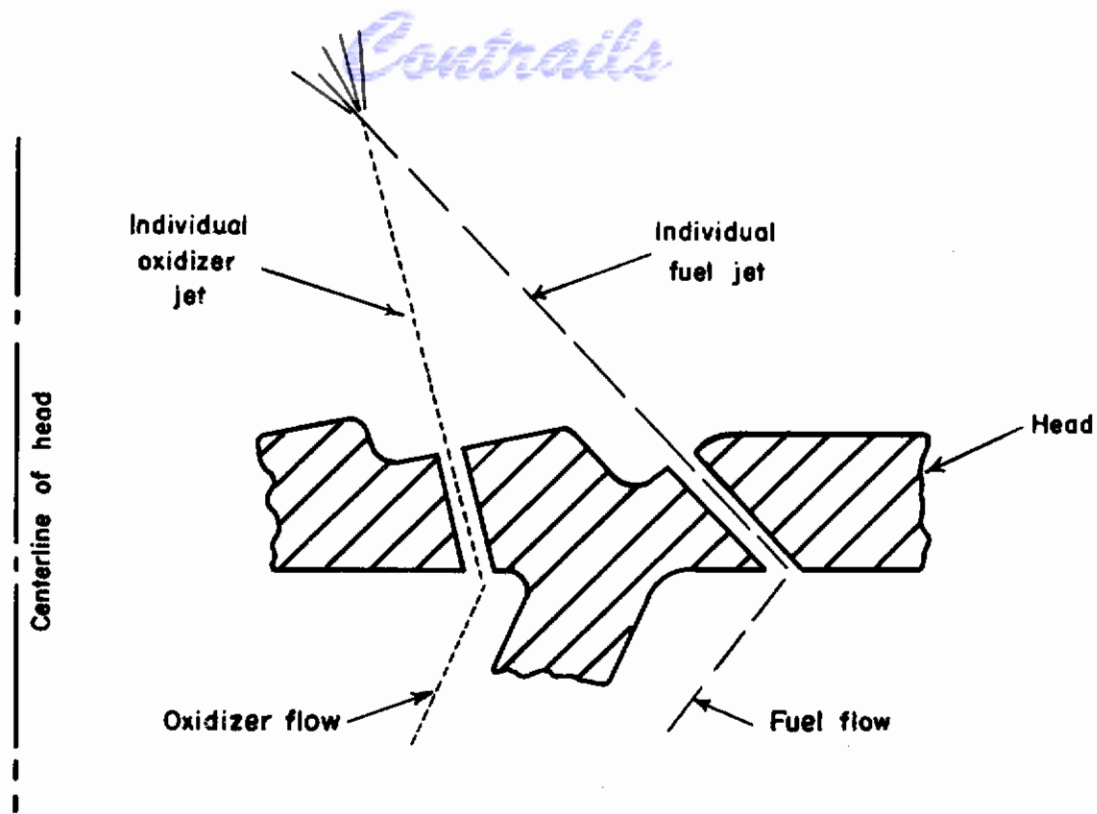


FIGURE 3-17. BAC TYPE 243 INJECTOR (Abramson)³⁻²⁸

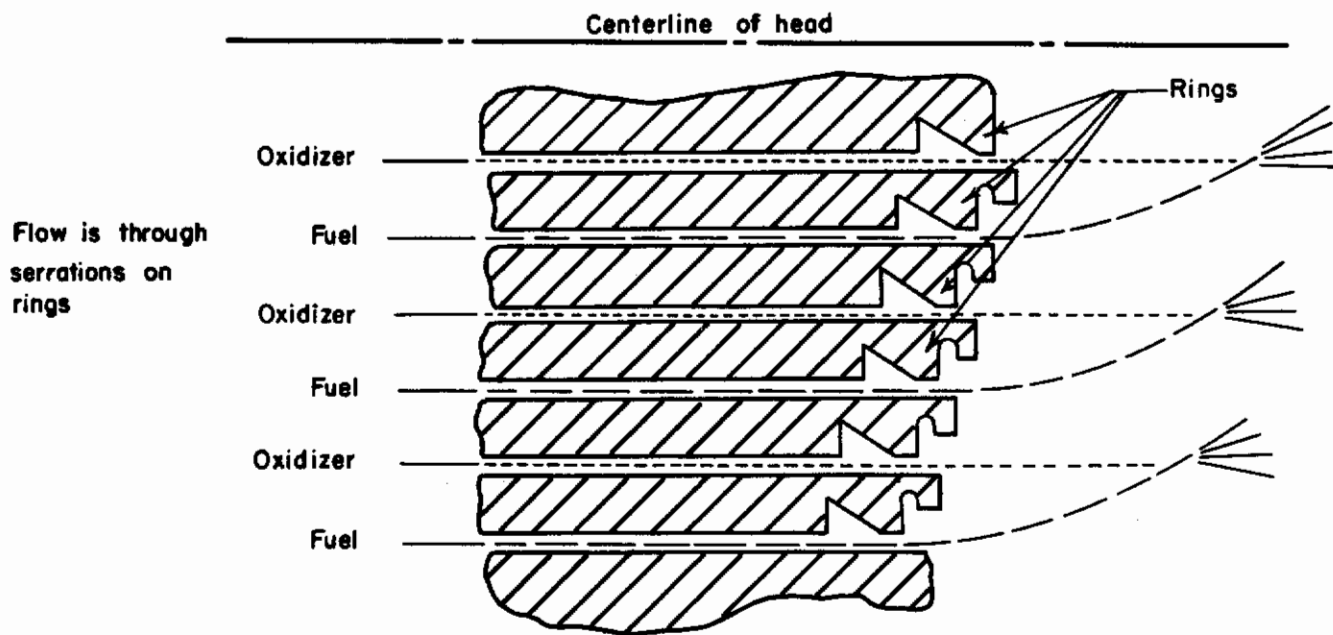


FIGURE 3-18. BAC TYPE 201 INJECTOR (Abramson)³⁻²⁸

The elements of the cylinders were formed by a finite number of single jets because of inability to hold a uniform annular orifice. The individual jets were formed by serrating the outside circumference of any ring with a triangular tool and pressing it into a ring equal to the outside diameter of the serrated ring, thereby forming a series of orifices of sector-shaped cross section.

Figure 3-19 shows the BAC Type 017 injector which is of the nonimpinging type. It was designed primarily from the standpoint of ease of fabrication.

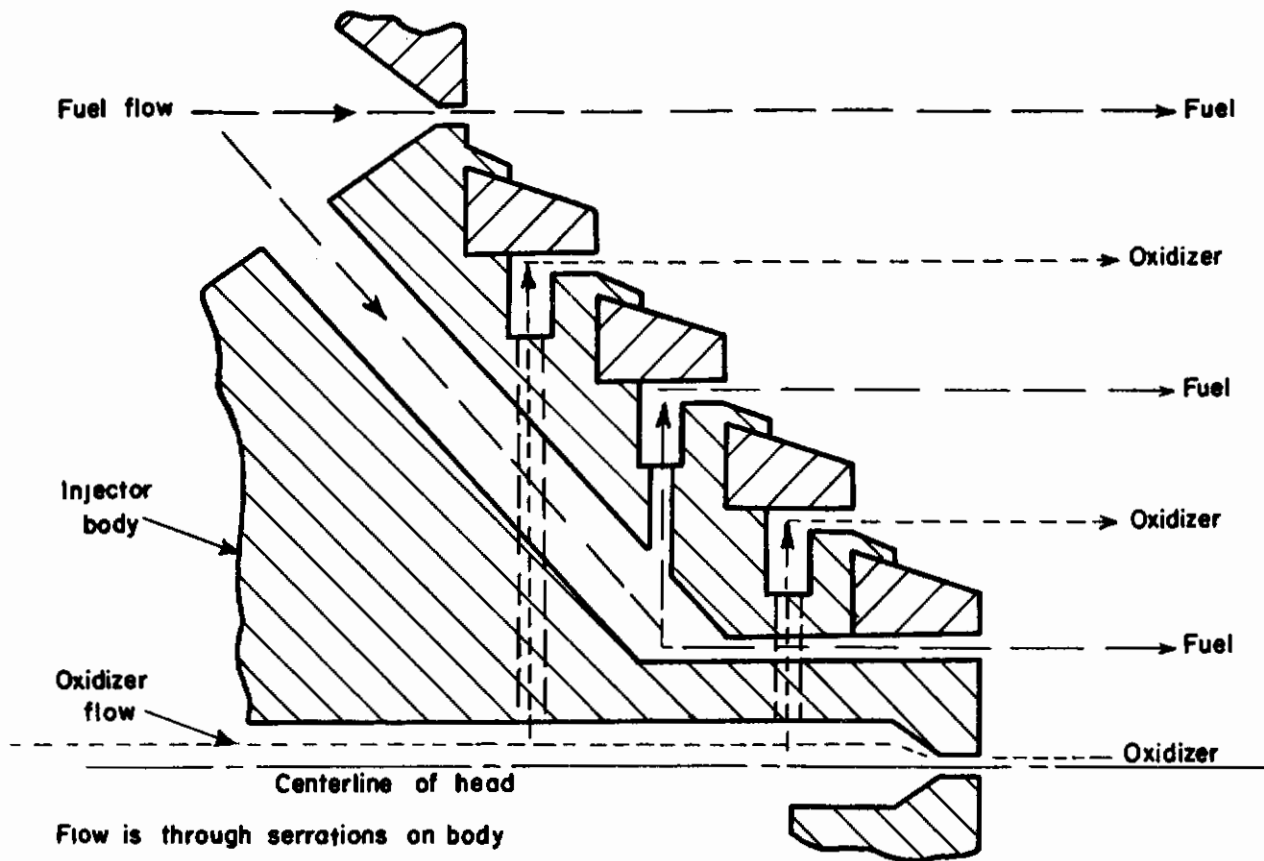


FIGURE 3-19. BAC TYPE 017 INJECTOR (Abramson)³⁻²⁸

The cylinders for the Type 017 are formed in a manner similar to those in the Type 201, but the concentric serrated rings are located at progressively different stations from the head, so that any ring may be accessible without removal of subsequent outer rings.

The last two types, shown in Figures 3-18 and 3-19 gave reasonably good performance, but only at the expense of excessive costs in manufacture, resulting from complex assembly and close tolerances.

A number of other designs, of less interest, are included in Abramson's report in which he concludes that injector manufacture is essentially a precision operation. If sufficient attention is not given to precision manufacturing, reproducible results will not be obtained.

According to most recent information⁽³⁻³¹⁾ among the various injectors described by Abramson, the impinging jet (oxidizer and fuel) type alone has survived as a production item for the rocket motor industry. However, interest has been shown in experimental configurations and devices such as splash plates and "flame-holding" cooled "grids".

Stehling⁽³⁻³²⁾ states that the basic function of the injector head is to introduce the propellants into the thrust chamber in the most efficient and auspicious manner so that the liquid propellant can be vaporized as quickly as possible. Stehling divides injection systems into three classes, "random", "splash", and "liquid-liquid", each of which will be described briefly with the aid of figures.

Figure 3-20 is a typical example of random injection using a "random showerhead". It usually consists of a matrix of holes drilled in the flat face of the injector. Oxidizer and fuel enter the chamber through adjacent orifices. Mixing depends upon the collision between droplets and upon the subsequent mingling, with the result that efficiency is generally low with nonhypergolic propellants. However, because combustion with this injector tends to be smooth with common propellants, further research is warranted to improve the combustion efficiency while retaining the stable combustion characteristics.

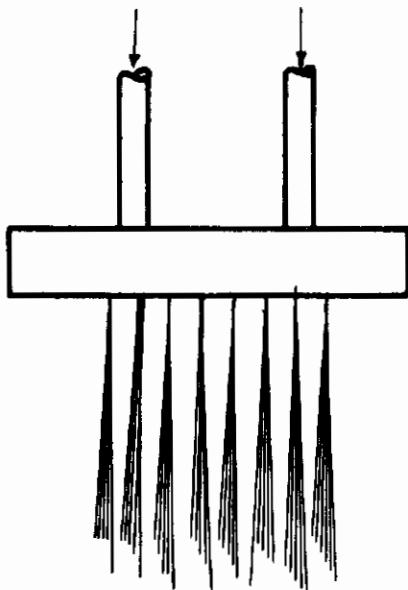


FIGURE 3-20. RANDOM SHOWERHEAD INJECTION (Stehling)³⁻³²

Figure 3-21 shows the principle of splash injection which involves impingement of the propellant stream upon the walls of the chamber or on some protuberance of the injector head, such

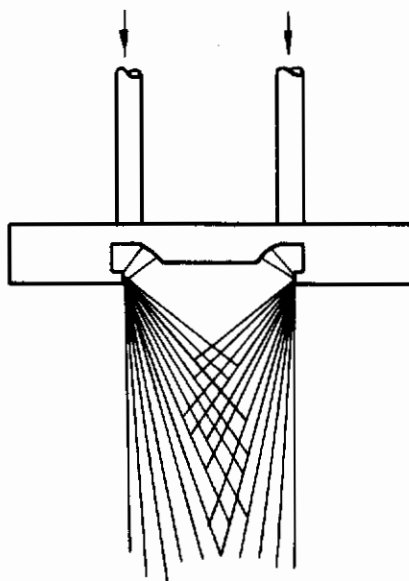


FIGURE 3-21. SPLASH INJECTION (Stehling)³⁻³²

as an annular ring or "splash plate". The plate serves to break up the streams for a more rapid rate of atomization. The German "Enzian" injector head is a classical example of splash injection. High specific impulses with relatively smooth combustion may be achieved; however, the combustion pattern tends to be uneven and the position and tolerance of the splash ring are critical.

Zucrow and Beighley⁽³⁻³³⁾, during an experimental study of the performance of WFNA-JP-3 rocket motors, observed that the main combustion occurs downstream of the turbulence ring (serves as splash ring also), and that the actions of the ring were essentially those of a mixing device and possibly a flameholder. The turbulence ring made combustion less sensitive to both injector hole alignments and the number of holes.

Figure 3-22 shows a typical example of the liquid-liquid principle of injection, sometimes known as "forced action injection". As previously stated this method comprises the largest segment

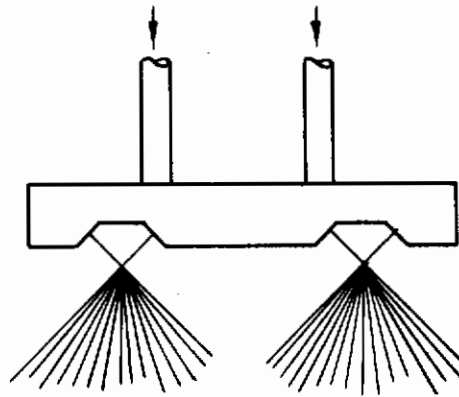


FIGURE 3-22. IMPINGING (LIQUID-LIQUID) INJECTION (Stehling)³⁻³²

of current injector practice. Its chief virtue lies in its ability to break up and mix the propellant streams, using some of the kinetic energy of the liquids.

The impinging shower head shown in Figure 3-22 is a favorite configuration employing liquid-liquid injection and is a close approach to a "standard" injector in the rocket motor industry. Generally, it consists of concentric rows of holes for fuel and oxidizer arranged so that the propellants impinge as close to the injector face as possible. Maximum utilization of the thrust chamber space is thereby achieved, and smooth combustion is more likely because the short path-lengths reduce perturbations of the individual streams by disturbing forces within the chamber or manifold. "Smooth" combustion here means an absence of high amplitude oscillations of frequencies less than 2 or 3 thousand cps.

Other types of liquid-liquid injectors, in addition to the impinging showerhead, are the hypoid showerhead, the concentric ring, and injection heads composed of common oil burner nozzles.

Premixing the propellants before introduction into the combustion chamber would appear to be a logical and obvious solution to the problems accompanying other methods of injection. However, as Stehling⁽³⁻³²⁾ explains, the flame front can progress upstream and, if the burning reaches a confined space, an explosion would occur.

Flow and Stability of Injected Liquids

In the design of injectors for rocket motors, small orifices are often used to introduce the reactants into the combustion chamber. Although many investigations have been made concerning relatively large orifices for measuring flow rate, little information is available on the flow characteristics of holes 1/16 inch in diameter and smaller.

Northup⁽³⁻³⁴⁾, therefore, made an extensive investigation of the flow and stability of liquids discharged through small orifices of 0.030 to 0.065-inch diameter. The variables that he studied included the pressure drop across the orifice, the cross-velocity to which the fluid was subjected before entering the orifice, the orifice configuration, and the type of liquid used and the atmosphere into which the liquid was injected.

Flow Discontinuity or Hydraulic "Flip"

Square-edged orifices of the sizes normally used for flow measurement and with length/diameter (L/D) ratios of about 2.5 will, when discharging into the atmosphere, show two distinct types of flow separated by a sharp break or discontinuity in the flow curve at the critical pressure drop. The discontinuity is referred to as hydraulic "flip" by Stehling⁽³⁻³²⁾. After the critical point has been passed the pressure drop may be decreased nearly to zero without the flow returning to the original state.

Figure 3-23 shows, schematically, the mechanism that results in discontinuity of flow. Sketch "A" shows how the stream jumps free from the sharp edge without touching the walls when L/D is less than 0.5. This occurs at all pressure drops and the typical curve for this thin orifice is smooth with no discontinuities.

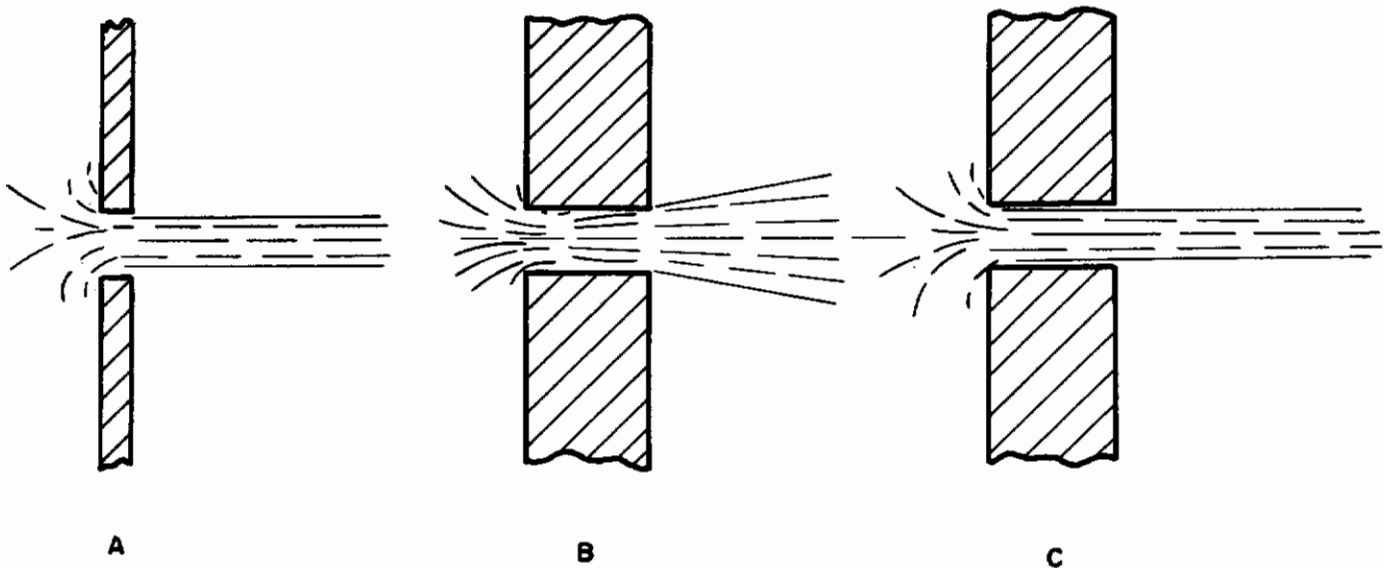


FIGURE 3-23. SCHEMATIC DIAGRAMS OF FLOW THROUGH AN ORIFICE (Northup)³⁻³⁴

Sketch "B" shows the type of flow when pressure drop is low and L/D ratio is large. The stream fails in its attempt to jump free from the wall at the upstream corner. The discharged liquid has a bushy or broomy appearance and the flow coefficient is much higher than for "A". The orifice walls are wetted by the liquid flowing through the orifice. However, if the walls of the orifice are treated with a substance such as oil, to prevent wetting, the stream will never develop the bushy appearance.

Sketch "C" shows how, as the pressure drop is increased, the stream suddenly jumps free of the wall for the entire length of the orifice. A point of discontinuity in the flow curve results because pressure drop rises suddenly and flow decreases. A comparison with sketch "A" shows that the flow characteristics are substantially the same as for a thin, sharp-edged orifice of the same diameter. With the aid of transparent orifices Northup and Stehling showed that this flow discontinuity, or hydraulic "flip", is a result of cavitation in the orifice. Cavitation begins at the upstream end of the hole and, as pressure drop increases, the cavitating area grows by moving downstream until the end of the hole is reached and the stream jumps completely free from the walls of the orifice. Good fluid flow measuring instruments avoid discontinuities by making the L/D ratio 1/8

or less. However, when the diameter of the hole is less than 1/16 inch, such a small L/D ratio is impractical. Northup found that discontinuities occurred for holes having L/D ratios a little greater than 1.0 and, in a few instances, discontinuities were observed when the L/D ratio was as low as 0.95. The flip point is not as distinct nor as readily observable when the liquid jet is discharged into a high-pressure atmosphere. In some instances two separate "jumps" or "flips" were noticed when injection took place in the region of 500 psi chamber pressure. Whether this is due to cavitation has not yet been determined. High frequency response flow meters are being developed to study this phenomenon.

Equations for Hydraulic Flip

Diamond⁽³⁻³⁵⁾ has developed equations for determining the differential pressure at which hydraulic flip occurs. The flip point was found to be a function of viscous and momentum forces, pressure and surface tension forces, and friction and boundary layer effects. An empirical equation for predicting flip, or cavitation point, within the experimental range covered is

$$\Delta P_f = 189.3 \left[P_a - P_v \right] \left[\frac{u^2 g}{(P_a - P_v) D^2 \rho} \right]^{0.19} \left[\frac{\sigma}{(P_a - P_v) D} \right]^{0.302} \left[\frac{L}{D} \right]^{0.69} \quad (3-41)$$

A modification of this equation for the discharge of water into a high pressure nitrogen atmosphere is:

$$\Delta P_{fi} = \Delta P_f \left[\frac{P_c}{1.66 P_a} \right] \text{ for } P_c > 2 P_a, \quad (3-42)$$

where P_f = differential pressure at which flip occurs with atmospheric chamber pressure.

P_{fi} = differential pressure at which flip occurs at a high chamber pressure.

P_a = atmospheric pressure, psi.

P_v = vapor pressure, psi.

u = dynamic viscosity, lb. sec/sq in.

D = orifice diameter, inches.

ρ = density, lb/cu in.

$g = 386.4 \text{ in./sec}^2$.

σ = surface tension, lb/in.

L = length of orifice, inches.

P_c = chamber pressure, psi.

Flip Transition Time

Stehling⁽³⁻³²⁾ reports that a reversible flip transition time of 1/320 sec has been measured with water. The main point of interest with respect to injector design is that if this transition time occurred with rocket motors and if a reversible flip action took place continuously, a combustion frequency of approximately 320 cycles per second might be expected. It is true that frequencies near this value have been detected with injectors that experienced hydraulic flip near the rated flow.

Effect of Cross-Velocity on Flow Discontinuity

Northup⁽³⁻³⁴⁾ investigated the effects of cross-velocity on the type of flow from the orifice. The term "cross-velocity" means the component of velocity, in the injector head, perpendicular to the axis of the holes through which the liquid issues.

The L/D ratio was found to be an important factor. When the L/D ratio was less than 0.95 no discontinuity in the flow-versus-pressure drop curve occurred for cross-velocities up to 20 ft per sec. For intermediate values of L/D (1.0 to 2.0) a discontinuity occurred at zero cross-velocity; but, as cross-velocity was increased the discontinuity was eliminated. However, for high values of L/D (2.0 to 4.0), as cross-velocity was increased, a higher pressure drop was required to reach the point of discontinuity.

Types of Instability in Liquid Jets

Based on visual observations and high-speed photographs, Northup concluded that there are two distinct and separate forms of instability present. The first type causes discontinuities in the flow curves with or without cross-velocity. The appearance of the stream is entirely different for the two flow regions. Without cross-velocity, as flow increases at the higher rates, the stream takes on an increasingly bushy appearance and becomes violently agitated just prior to the break point. As the stream jumps or breaks, it becomes smooth and clear as when issuing from an orifice of low L/D ratio. As a cross-velocity component is added to the flow, an additional bushiness is superimposed on the stream at all points on the flow curve.

The second type of instability is characterized by a constant flickering or jumping about of the stream at a constant pressure. As flow from the hole increases, this type of instability increases because of turbulence behind the orifice plate. Northup believes that this is probably the worst type of instability as far as rocket motor operation is concerned, especially where impingement of two streams is desired.

Relation Between Flow Stability and Injector Design

Rocket-motor stability is definitely affected by the manner in which the reactants are injected. When straight, sharp-edged orifices are used, certain ranges of pressure drops should be avoided. The undesirable range is easily defined for an orifice discharging to the atmosphere; however, the range is not readily defined when discharging a fluid into a combustion chamber during actual operation. In general, it seems that higher pressure drops tend to provide more stable flow, at least as far as the rocket motor is concerned.

Flow from an orifice with wetted walls is inherently unstable and may be affected by so many factors that it should be avoided if possible. If a low pressure drop is necessary, some form of orifice other than a sharp-edged orifice should be used.

The cross-velocity and turbulence level of the fluid before entering the orifice are important, especially when the resultant direction of flow must be controlled. For best results, cross-velocities should be held to a minimum. Also, turbulence should be minimized by making the reservoir behind the orifice as large as practical.

By giving proper consideration to the above mentioned factors, and by using suitable pressure drops, the sharp-edged orifice may successfully be used in many types of rocket motor injectors.

Liquid Phase Mixing of Impinging Jets

Rupe⁽³⁻³⁶⁾ has devised a technique for evaluating the liquid-phase mixing of a pair of impinging streams, and a number of controlling parameters were investigated.

In general, Rupe showed "that the mixing and distribution attained in the spray from a pair of impinging streams having good dynamic characteristics may be optimized in any configuration by controlling dynamic characteristics but that ideal mixing can be attained with only one particular arrangement. The optimum configuration is approached under the following conditions:

- (1) The total momentum ratio approaches unity.
- (2) The effective impingement area ratio approaches unity.
- (3) The impingement angle is approximately 45°. (The experiments indicated only that mixing improved as impingement angle decreased from 90 to 45°.)
- (4) The kinetic energy available for mixing approaches a maximum when referred to any predetermined fixed level.
- (5) The influence of absolute size of the effective impingement area is small but shows an increasing trend as scale increases.
- (6) The effect of impingement length as such is negligible.
- (7) Aside from an effect on the hydraulic characteristics of the orifices due to changes in Reynolds number, changes in fluid properties influence mixing only to the extent of the change in stream dynamics.
- (8) The variation of local mass rate across any great circle of the spherical surface about the impingement point for a pair of streams of optimum configuration may be defined by a near Gaussian distribution. The cross section of a dynamically balanced spray has an elliptical boundary in the plane perpendicular to the resultant momentum line. Within limits the length of the major axis of the ellipse which is aligned perpendicular to the plane of the stream center lines is a function of impingement angle.
- (9) The dynamic characteristics of the free streams have marked influence on stream stability, on spatial distribution, and, to some extent, on liquid-phase mixing. Stream dynamics are controlled by upstream conditions, orifice Reynolds number, and orifice design; the data available indicated that optimum stream pairs require symmetrical, similar (only in lieu of uniform), and stable free-stream velocity profiles.
- (10) From the limited data available it might be concluded that miscibility is an aid to mixing but does not alter the characteristic effect of varying momentum ratio."

SUMMARY

Nozzle design is probably as much an art as it is a science. The major problem in the design of atomizers for aircraft gas turbines is to obtain satisfactory atomization over a wide range of flow rates. A fine spray must be produced at the low rates of flow to eliminate die-out during descent, and to permit quick starts. Three other important requirements of good spray nozzles are: (1) flow rates of all nozzles in an engine should be as nearly equal as possible at each fuel pressure; (2) spray pattern should be uniform about the axis and fuel should be distributed properly, with reference to the combustion chamber configuration over the entire range of operation; and (3) nozzles should be designed for sturdiness, and for easy removal.

By the application of formulas developed by S. M. Doble and E. A. Watson, it is possible to design a swirl-type atomizer to give a desired output at a stated fuel pressure. Considerable information concerning the mean droplet size and the angle of the spray cone also can be predicted from the nozzle dimensions and from ratios of these dimensions. The methods of Doble and Watson, although different, are in good agreement, provided conventional shapes of swirl atomizers are used.

Continued

Swirl-type nozzles of different sizes can be judged as to design by Longwell's atomization criterion, $\sqrt{c_0} \sin(\alpha_0/2)$. The larger the value of the atomization criterion, the finer the spray. Longwell's experimental studies show that a nozzle which would be a good compromise between range of atomization and fineness of atomization would have the following dimensions:

$$\begin{array}{ll} A_s/r_o^2 & 20 \\ L/r_o & 3 \\ r_s/r_o & 3 \end{array}$$

This nozzle would have a cone angle at zero viscosity of about 77 degrees and a discharge coefficient of about 0.53.

Although Taylor gave the most valid theoretical analysis of flow and of optimum geometric relations inside the swirl-type nozzle, his rigorous determination of the spray angle is less applicable than either Harvey and Hermandorfer's or Novikov's analysis. Novikov's analysis of the spray angle, which is based on Taylor's analysis of flow inside the nozzle, appears to be the most valid, in that due consideration is given to the effects of surface tension, this consideration giving a physically reasonable explanation of the swelling of the liquid sheath immediately downstream of the nozzle. The analysis of Harvey and Hermandorfer, which like Taylor's disregards the effects of surface tension, gives upper and lower bounds on the spray angle which are justified by experimental observation.

The most applicable result of these analyses, however, appears to be Novikov's theoretical determination of the mean size of the droplets in the resultant spray, this theoretical determination being confirmed by experimental observation.

Little information has been published concerning the fundamental principles of design of two-fluid atomizers; however, work is in progress on this phase of nozzle design.

Swirl-type atomizers are used exclusively on aircraft gas turbines that employ spray nozzles. The conventional fixed-orifice, or simplex, nozzle that obeys the square law does not have sufficient range of flow for this application; consequently, complex nozzles, such as the duplex nozzle, which is essentially two nozzles in one, and variable-area and spill-return types of atomizers may be used. The duplex nozzle, which is capable of providing a satisfactory spray over a flow range of 20 to 1 with a pressure range of 16 to 1, is the most widely used today. Variable area nozzles in which a poppet or a plunger serves to provide additional exit-orifice area or additional inlet-slot area also make possible a more favorable relation between flow rate and pressure drop. The spill-return type of nozzle, in which a portion of the fuel that enters the swirl chamber is bled back to the fuel tank, shows special promise because of the extremely wide range of flow that is possible.

Matching nozzle flow rates, over the entire range, is a difficulty common to all types of complex swirl atomizers.

Fuel may be prepared for combustion by vaporizing in tubes as well as by atomization. The annular vaporizing combustor possesses, to a high degree, the operational and performance qualities needed for a good gas-turbine combustor. Compared with a typical annular liquid-injection combustor, its efficiency varies less with fuel-air ratio and it is appreciably shorter in length.

The two primary functions of liquid-reactant injectors for rockets are (1) to mix the fuel and oxidizer, and (2) to atomize the liquids so that surface area and rate of reaction will be increased. No single injector type or system is ideal or applicable to all circumstances. However, greater standardization inevitably will occur when more data on the significance of the injector are available, and when many of the empiricisms have been reduced to scientific foundations.

In order to hold pressure oscillations in the combustion chamber to a minimum, the injected streams must have considerable stability. There are at least two different forms of instability: (1) instability resulting from discontinuity in flow with or without cross-velocity behind the holes,

and (2) instability characterized by a constant flickering, or jumping about of the stream, at a constant pressure. The latter is probably the worse type of instability as far as rocket-motor operation is concerned, especially for impinging jets.

The mixing and distribution achieved in the spray from a pair of impinging streams may be optimized by controlling dynamic characteristics, but optimum mixing can be attained with only one particular arrangement.

REFERENCES

- 3-1. Bolt, J. A., Lennox, R. H., and Saxton, M. F., Poppet or Pintle Type Nozzles; The Engineered Products Company, Flint, Michigan, June 20, 1954 (Unpublished).
- 3-2. Ganger, Dean R., Practical Observations on Gas Turbine Spray Nozzles; presented at the Conference on Fuel Sprays, Univ. of Michigan, Ann Arbor, Michigan, March 30-31, 1949.
- 3-3. Stark, W. T., and Constantino, C. S., Considerations on Fuel Nozzle Problems on Gas Turbine Type Engines; presented at the Conference on Fuel Sprays, Univ. of Michigan, Ann Arbor, Mich., March 30-31, 1949, 5 pp and 5 fig.
- 3-4. Park, R. D., Combustion Heater Study Report No. 31, Douglas Aircraft Company, January, 1949.
- 3-5. Dodge, R. A., Hagerty, W. W., and York, J. Louis, Continuous Fuel Sprays; A. F. Technical Report No. 6067, Power Plant Laboratory, AMC, Wright-Patterson Air Force Base, Dayton, Ohio, July, 1950.
- 3-6. Doble, S. M., Design of Spray Nozzles; Engineering, Vol. 159, 1945, pp 21-23, 61-63, and 103-104.
- 3-7. Doble, S. M., Design of Centrifugal Spray Nozzles for Outputs up to 1800 Gallons per Hour; Proc. Inst. of Mech. Engrs., Vol. 157, 1947, p 103.
- 3-8. Doble, S. M., The Application of Cyclone Theories to Centrifugal Spray Nozzles; Proc. Inst. of Mech. Engrs. Vol. 157, 1947, p 111.
- 3-9. Watson, E. A., and Clarke, J. S., Combustion and Combustion Equipment for Aero Gas Turbines; paper presented to the Institute of Fuel, Burlington House, Piccadilly, W. 1, May 28, 1947, 34 pp.
- 3-10. Watson, E. A., Fuel Systems for the Aero Gas Turbine; The Engineer, London, December 19, 1947, pp 561-563 and 576-577. See also Proc. Inst. Mech. Engrs., Vol. 158, 1948, pp 187-201.
- 3-11. Bowen, G., and Joyce, J. R., Swirl Pressure Jet Atomizers; Tech. Report No. I. C. T. /16, The Shell Petroleum Company, Ltd., London, Dec. 30, 1947, 11 pp and 9 fig.
- 3-12. Schweitzer, P. H., Factors in Diesel Spray Nozzle Design in the Light of Recent Oil-Spray Research; ASME Trans., Vol. 52, 1930, p 121.
- 3-13. Longwell, J. P., Fuel Oil Atomization; D. Sc. Thesis, Mass. Inst. Tech., 1943, 167 pp.
- 3-14. Hawthorne, W. R., Notes on Atomiser Research done by Prof. Hottel, M. I. T., U. S. A.; R. A. E. Technical Note No. Eng. 167, June, 1943, 3 pp and 11 fig.

- 3-15. Söhngen, E., and Grigull, U., Der Strahlwinkel Von Brennstoff - Dralldüsen bei kontinuierlicher Einspritzung (The Spray Angle of Swirl Type Nozzles for Fuels with Continuous Injection), Forchung 17. Bd/Heft 3 (1951), pp 77-82.
- 3-16. Taylor, G. I., The Mechanics of Swirl Atomizers; Proceedings of the Seventh International Congress for Applied Mechanics; Vol. 2, pt. I, 1948, p 280.
- 3-17. Taylor, G. I., The Boundary Layer in the Converging Nozzle of a Swirl Atomizer; Quarterly Journal of Mechanics and Applied Mathematics, Vol. 3, pt. 1, 1950, p 129.
- 3-18. Novikov, I. I., Atomization of Liquids by Centrifugal Nozzles; Engineers' Digest, Vol. 10, No. 3, March, 1949, p 72.
- 3-19. Harvey, J. F., and Hermandorfer, A. W., The Design of Constant and Variable Capacity Mechanical Oil Atomizers; Trans. Soc. of Naval Architects and Marine Engineers; Vol. 51, 1943, p 61.
- 3-20. Joyce, J. R., Fuel Atomizers for Gas Turbines; Tech. Report No. I. C. T. /15 The Shell Petroleum Co., Ltd., London, 1947, 31 pp and 36 fig.
- 3-21. Mock, F. C., and Ganger, D. R., Practical Conclusions on Gas Turbine Spray Nozzles; SAE Quarterly Transactions, Vol. 4, No. 3, July, 1950, p 357.
- 3-22. Pierce, L. J., and Parker, Theo. B., The Design and Performance of the Duplex Nozzle System for Aircraft Gas Turbines; presented at Conference on Fuel Sprays, University of Michigan, March 30-31, 1949, 13 pp and 13 fig.
- 3-23. Alford, J. S., Aircraft Gas Turbines; Paper No. 7, Sect. G., presented at the Fourth World Power Conference, London, 1950.
- 3-24. Bolt, J. A., and Saxton, M. F., Fuel Spray Nozzles for Aircraft Gas Turbines; Automotive Industries, May 15, 1949, and June 1, 1949.
- 3-25. Lawrence, O. N., Gas Turbine Accessory Systems; J. Royal Aeron. Soc. (England), Vol. (1948), p 151.
- 3-26. Pouchot, W. D., and Hamm, J. R., Characteristics of a Vaporizing Combustor for Aviation Gas Turbines; Amer. Soc. Mech. Engr. Paper No. 53-A-182, presented at Annual Meeting in New York, N. Y., Nov. 29-Dec. 4, 1953.
- 3-27. Stone, Irving, Analysis Reveals Wright J-65 Details; Aviation Week, June 14, 1954, p 28.
- 3-28. Abramson, B. N., A Survey of Injector Designs for Use in Liquid Propellant Rocket Motors; Presented at the Third National Convention of American Rocket Society in conjunction with the ASME, Dec. 2, 1948, 10 pp.
- 3-29. Gunn, S. V., The Effects of Several Variables Upon the Ignition Lags of Hypergolic Fuels Oxidized by Nitric Acid; Ph D Thesis, Purdue University, 1953.
- 3-30. Abramson, B. N., U. S. Naval Air Rocket Test Station, Lake Denmark, Dover, N. J., Private Communication, 25 May 1954.
- 3-31. Stehling, Kurt R., Bell Aircraft Corporation, Buffalo 5, N. Y., Private Communication, June 12, 1954.
- 3-32. Stehling, Kurt R., Injector Spray and Hydraulic Factors in Rocket Motor Analysis; J. Amer. Rocket Society, May-June 1952, p 132.

Contrails

- 3-33. Zucrow, M. J., and Beighley, C. M., Experimental Performance of WFNA-JP-3 Rocket Motors at Different Combustion Pressures; J. of Amer. Rocket Soc., Nov.-Dec. 1952, pp 323-330.
- 3-34. Northup, R. P., Flow Stability in Small Orifices; Presented to American Rocket Society on 30 November, 1951, at Annual Meeting of the ASME in Atlantic City, N. J.
- 3-35. Diamond, P., Internal Report of Bell Aircraft Corp., See also Private communications from Kurt R. Stehling, Bell Aircraft Corp. dated June 12 and June 23, 1954.
- 3-36. Rupe, Jack H., The Liquid-Phase Mixing of a Pair of Impinging Jets; Jet Propulsion Lab., Calif. Inst. Tech. Progress Report No. 20-195, August 6, 1953.

Contrails

CHAPTER 4. SPRAY ANALYSIS

ABSTRACT

Six classes of experimental methods for determining drop-size distributions are described, including (1) microscopic examination of drops collected on slides or in cells, (2) freezing of drops in spray followed by sieving, (3) direct photographic methods, (4) optical methods based on the scattering or absorption of light, (5) electronic and radioautographic techniques, and (6) selective impaction. Each method has its advantages and disadvantages, but none is entirely satisfactory. Mathematical representations of drop-size distribution are discussed with special emphasis on the Rosin-Rammler expression, the Nukiyama-Tanasawa expression, and the logarithmic-normal distribution. The importance of taking both upper and lower cut-off sizes into consideration is stressed. Other important factors in spray analysis discussed in this chapter are the angles formed by the conical spray and the distribution of droplets about the axis, usually termed "patterning".

Contracts

SPRAY ANALYSIS

by

J. M. Pilcher, C. C. Miesse
and A. A. Putnam

The analysis of fuel sprays in terms of drop-size distribution, spray angle, and spray pattern is profoundly important for all studies of atomization of liquids. This is true whether the problem is an investigation of the mechanism of atomization, an examination of the influence of the various factors that affect atomization, research on methods of atomization, or a study of nozzle design. The importance of spray analysis in the field of atomization cannot be overemphasized. A formidable obstacle to research on atomization has been the lack of a simple, feasible, yet accurate method for determining the drop-size distribution of a spray. Numerous experimental methods have been used, such as: (1) microscopic examination of drops collected on slides or in cells, (2) freezing of drops in spray followed by sieving, (3) direct photographic methods, (4) other optical methods based on the scattering or absorption of light, (5) electronic and radioautographic techniques, and (6) the cascade-impactor method. Each method, which will be discussed later in more detail, has its advantages and disadvantages, but none is entirely satisfactory. The most common objection to any method is that it is too tedious and time consuming. Other disadvantages are that complicated equipment is involved, results are unreliable, drop-size range is inadequate, or calibration of the device is difficult or uncertain.

Sampling of a spray is one of the most difficult steps in the experimental methods that require collection of a sample. Unfortunately, the difficulty of obtaining a sample sufficiently representative has not been fully appreciated by some investigators.

Another major problem in spray analysis is the choice and use of a mathematical expression for drop-size distribution. It is desirable to be able to express the experimentally determined size-frequency data in a mathematical form involving only two parameters, one based on an average size and the other based on the dispersion of sizes. The three expressions most generally used are the Rosin-Rammler expression, the Nukiyama-Tanasawa expression, and the logarithmic-normal distribution. These methods of representation and others are discussed in detail in the section given later on "Mathematical Expressions for Drop-size Distributions".

Other important factors in spray analysis discussed in this chapter are the angle formed by the conical spray, and the distribution of droplets about the axis, usually termed "patterning".

SECTION I - EXPERIMENTAL METHODS FOR DETERMINING DROP-SIZE DISTRIBUTION

J. M. Pilcher

Much ingenious and painstaking work has been done, by approximately forty different investigators, on the determination of the drop-size distribution of atomized sprays. In many instances, the methods are similar; consequently, the various procedures used have been divided into six groups, or classes of methods, each of which will now be described.

The method for determining drop-size distribution that has been most generally employed consists of collecting a sample of the spray on a glass slide and making a microscopic size count of 200 to 1000 drops. This method requires the minimum of apparatus, consisting of only a microscope with a calibrated eyepiece; however, it is obvious that the method is time consuming. A more serious objection is that it is difficult, if not impossible, to obtain a sufficiently representative sample. This arises from the tendency for the smaller droplets to follow the air stream around the slide, rather than to be collected on the slide. Discrimination against the smaller sizes can be reduced by using narrow slides; however, the capture coefficient approaches unity only as the width of the slide approaches the dimensions of the drop.

Kuhn(4-1), as early as 1924, determined the sizes of particles of fuel oil in a spray by collecting the drops on a glass plate covered with a thin layer of soot in order to fix the oil drops. The glass plate was exposed to the atomized fuel for 0.0005 sec, with the aid of a shutter mechanism; the total weight of the drops collected was determined and the number of oil spots were counted. Knowing the density of the fuel oil, the average diameter of the drops could be computed. For example, for Kuhn's Experiment No. 342, 12,000 drops weighed 0.47 mg, which corresponded to an average diameter of 45 microns. The obvious objections to this method are: (1) the necessity for counting as many as several thousand drop impressions, (2) probable discrimination in the sampling procedure against the smallest drops, (3) with volatile liquids, the error in weighing introduced by evaporation, and (4) the number of determinations that must be made to insure reasonably accurate average measures.

Sauter(4-2), in 1926, employed a similar method by which the drops were caught on a screen. Mean size was computed from the total volume and number of drops.

Lee(4-3), of the NACA, modified and improved this general method in 1932. He injected the spray in a direction parallel to a plate coated with lampblack obtained from a kerosine flame. The drops descended slowly, after the forward velocity decreased nearly to zero and, when they touched the surface, made a hole in the lampblack. The most suitable thickness of lampblack, checked by means of a micrometer focusing screw, was found to be 0.006 to 0.012 inch (150 to 300 microns). A magnification of 50 diameters was found best. To illuminate the slide for taking photomicrographs, two diametrically opposite beams of light were directed slightly downward along the surface, so that the holes appeared as dark shadows.

Lee concluded that no great error was introduced if the diameters of the impressions were assumed to be equal to the diameters of the drops that made them. However, for higher accuracy, a correction should be applied as described later in the section on "Flattening Coefficients".

DeJuhasz, Zahn, and Schweitzer(4-4) used a method, similar to that of Woeltjen(4-5) and Sass(4-6), that consists in injecting the spray into a liquid. A sample of the liquid was then placed under the microscope and the number and diameter of droplets were determined. The choice of the receiving liquid is of greatest importance. An ideal receiving liquid must meet the following requirements: (1) the liquid must be immiscible with the spray being sampled, (2) droplets should not coalesce, and (3) the drop-liquid aggregate should remain stable during an interval of time sufficient for the microscopic size count. The receiving liquid must be less dense than the sprayed liquid because, if the drop rises to the surface, it loses its spherical shape and spreads to a thin layer on the liquid surface.

Glycerin and sodium silicate were found unsatisfactory, but a tanning product called Queol, originally used by Woeltjen for a similar purpose, was found satisfactory when diluted with about two parts of distilled water.

Photomicrographs of the drops in the receiving liquid were made at 200X and the number of drops in each of eight size ranges was counted.

Nukiyama and Tanasawa(4-7) used a similar method by which sprayed drops of water were collected in "specially prepared" oil spread over a glass placed in a small cylindrical shutter. The exposure time was 0.002 to 0.01 sec.

Houghton and Radford(4-8), in a comprehensive study of the drop-size distribution of water droplets in natural fogs and clouds, collected the sample on a glass slide coated with a thin film of petroleum grease (white vaseline). They developed an improved method of coating the slide which consisted of spreading a moderately heavy coating of vaseline on the surface of a perfectly clean slide and then placing the slide in a vertical position in an oven at a temperature of 300 F for three minutes. Houghton and Radford found that it was absolutely essential that the slide surface be clean before the grease was applied, as otherwise it might collect in spots instead of spreading uniformly. They found that the slides could be sufficiently well cleaned by first scouring them with concentrated chromic acid, then thoroughly rinsing them in distilled water, and finally allowing them to dry in a dust-free atmosphere.

Houghton and Radford fully appreciated the difficulty of obtaining an acceptably representative sample of fogs and clouds owing to the great difference in kinetic energy and drag between the large and the small drops. They were of the opinion that the small drops were being discriminated against.

The method of sampling used by Houghton and Radford was to expose the slides either horizontally, in a fog microscope-slide holder, or vertically facing the wind. Tests made in calm foggy air indicated that a sample obtained by moving a slide through the air at about 1 m per sec was substantially the same as one secured at a velocity of about 20 m per sec. The diameter of their fog particles ranged from about 1 to 100 microns, with a predominant size of about 40 microns. They definitely established that the sampling method discriminated against particles smaller than about 20 microns in diameter, and, because this effect became more pronounced as the drop size was reduced, an almost negligible proportion of the drops smaller than 5 microns was collected.

Application of correction factors to take care of the sampling difficulty was not entirely satisfactory. However, it was definitely demonstrated that 5-mm-square slides obtained a much truer sample of the fog than did the standard 25-mm-square slide. Consequently, they recommended the use of the small slide in all instances where drops smaller than 20 microns in diameter were of importance.

Burdette(4-9) determined the size distribution of air-float oil particles by collecting the droplets on a glass slide coated with liquid soap. As the particles fell on the soap solution they were immediately surrounded by a film of soap, creating a condition similar to that of oil globules in oil emulsions. The film of soap prevented the oil particles from coalescing and evaporating, and the particles remained spherical as long as the soap remained liquid.

Burdette added an oil-soluble red dye to the oil spray so that the particles could be more readily seen and measured by the use of transmitted light. He found that measuring 1000 particles gave nearly as good a cross section of the air-float oil spray as measuring 5000 particles. The size of droplets measured by Burdette varied from 1 to 100 microns.

Doble(4-10), in his study of spray-nozzle design, collected drops of water in castor oil in such a way that they were suspended from the free surface of the oil and remained almost perfectly spherical, and evaporation was prevented. If the drops of water were shaken from the surface, they fell to the bottom of the vessel, the specific gravity of the castor oil being 0.96, and a slight flattening occurred. However, if the bottom of the vessel was covered with a layer of vaseline, the drops continued to be spherical, whether they remained suspended from the upper surface of the castor oil or fell to the vaseline below.

Dimmock(4-11) also used this method for collecting water droplets in castor oil contained in shallow dishes. For small droplets, he found a mixture of paraffin oil (kerosine) and hydraulic fluid to be more suitable. If the droplets successfully penetrated and hung from the surface of the oil, their shape remained spherical, and they did not evaporate for an appreciable duration of time.

Pigford and Pyle⁽⁴⁻¹²⁾ sampled water sprays by collecting the drops on greased glass slides. They photographed the drops soon after exposure to the spray, but thought that evaporation of many of the smallest droplets was not prevented.

A shutter device was used to expose the greased slides at a point about 12 inches directly in front of the atomizing nozzle. Photographs were taken using a copying camera which gave a magnification of about ten times. Dark-field illumination was employed to get sharp edges. Pigford and Pyle counted 300 to 700 drops for each spray.

Merrington and Richardson⁽⁴⁻¹³⁾ measured drop size by allowing the droplets to fall on sheets of blotting paper. The stains, made more visible by mixing in a dye with the sprayed liquid, were measured and the relation between stain diameter and drop size was established by shooting single drops of the same liquid from a pipette directly onto the paper. The relation was linear except for extremely small drops. This method is simple, but it is not subject to a high degree of precision especially for the smallest sizes which may be important in many instances of spray analysis.

Pierce⁽⁴⁻¹⁴⁾ and Limper⁽⁴⁻¹⁵⁾ collected the spray on microscope slides, coated with magnesium oxide by passing them over a strip of burning magnesium ribbon. The thickness of the coating was made greater than the largest expected diameter of drop in order to eliminate spreading of the drop.

By placing the microscope light beam at an angle to the surface of the slide, the drops appeared as dark craters in the coating. Pierce found that drops of a size less than 20 microns were difficult to detect on the coating. He counted from 200 to 400 drops on each slide. Limper used this method for sampling both oil and water sprays. Exposure of the slide for a fraction of a second was accomplished by a special shutter driven by a clock spring. Drop size was measured by means of a microscope equipped with a special micrometer.

Maxwell⁽⁴⁻¹⁶⁾ also collected droplets on a glass slide coated with magnesium oxide. He used a special sampling device that acted like a focal-plane shutter and exposed a 1/16-inch x 7/8-inch piece of microscope cover glass for about 0.0002 sec. Maxwell stored his slides for at least one day in a water-saturated atmosphere to increase resistance to air blast. He photographed the drop impressions with a 35-mm Leica microscope camera at 210X.

It is probable that the smaller size drops were discriminated against by Pierce, by Limper, and by Maxwell. Also, errors probably resulted from differences between the diameter of the spherical droplet and the diameter of the impression made in the MgO coating.

Lewis, Edwards, Goglia, Rice, and Smith⁽⁴⁻¹⁷⁾ collected droplets from finely atomized oil sprays by simply waving a microscope slide through the spray cloud. The relation between drop diameters observed under the microscope and the diameter of spherical drops of equal volume was determined by measuring the focal lengths of the spherical lenses formed by the drops on the slides. Here, again, it appears probable that the small sizes of droplets were discriminated against.

Conroy and Johnstone⁽⁴⁻¹⁸⁾, in a study of atomization of molten sulfur preparatory to combustion, collected samples by waving microscope slides through the spray at a distance of 18 inches beyond the atomizer. Duplicate or triplicate samples were taken and from 400 to 500 drops from each slide, were counted and classified into ten or fifteen size ranges using a microscope equipped with a micrometer eyepiece. By measuring the heights and diameters of a large number of the supercooled and flattened sulfur drops, the ratio of height to diameter was found to be independent of drop size and equal to 0.65. By assuming the drops to approximate hemi-ellipsoids of revolution, the ratio of the diameter of the equivalent spherical drop to the diameter of a flattened drop was found to be equal to the cube root of 0.65. This assumption concerning the shape of the drops on the slides was supported qualitatively by their appearance under the microscope.

Rupe⁽⁴⁻¹⁹⁾, as part of an investigation of spray characteristics of constant-flow nozzles, made an extensive study of drop-size distribution of water sprays that deserves a detailed description. Basically, the procedure consisted of collecting a small sample of the spray in a suitable collecting cell, photographing this sample, then counting and measuring the droplets, and tabulating them into size groups.

Rupe recognized that it was extremely important that the apparatus and the method of sampling should not have a secondary influence on the size distribution. He concluded that the most convenient method of obtaining a spray sample in which the drops were spherical and did not evaporate or coalesce was to collect the drops in a cell filled with a suitable immersion medium, as done by Doble⁽⁴⁻¹⁰⁾. The drops fell to the bottom of the cell, where it was comparatively easy to photograph the horizontal profile of spherical drops using transmitted light. This procedure made it possible for Rupe to obtain high contrast and excellent definition.

The possibility that the horizontal profile might not be a true measure of the drop diameter was investigated by Rupe. He showed that the change in diameter owing to differences of specific gravities was negligible for his conditions, and that the increase in diameter was less than two per cent.

Rupe's collecting cells were constructed of 0.380-inch-I.D. tubing, 0.331 inch deep with the top edge beveled. An 0.068-inch-thick optical flat glass was cemented on the bottom and coated with G.E. Dri-Film No. 9987 to form a nonwetting surface. Sampling time could be controlled, to a minimum of 0.003 sec, by means of a variable-speed slit shutter rotating between the nozzle and the collecting cells. The cell holders were constructed with four arms 90 degrees apart and so held the collecting cells that 100 degrees of the great circle, having the nozzle orifice as its center, was included. Four different holders were used, making it possible to obtain data on spherical surfaces within the spray at distances of 2, 3, 4, and 6 inches from the orifice. For one position of each holder, samples could be obtained at 92 different points in the spray.

After investigating a number of immersion fluids, Rupe selected Stoddard Solvent (a petroleum fraction) as having a satisfactory surface tension, viscosity, density, vapor pressure, color, and chemical stability, as well as being immiscible with the sprayed fluid.

The photomicrographic setup used by Rupe was designed to attain a working magnification of 1000X. He used a magnification of 50X on the negative, which was a compromise to obtain the maximum field area which could be recorded on a negative of reasonable size, to retain definition of the 5-micron drops, to allow the use of a long-focal-length objective lens (which was necessary when using a comparatively deep collecting cell), and to limit the necessary magnification obtained by projection to 20X. Five photographs were taken of each cell, making it possible to count 43 per cent of the cell area.

The film used was contrast-process panchromatic on aerial base and was selected on the bases of definition, contrast, speed, and developing time. The object was illuminated with transmitted light from a 100-watt mercury-vapor arc operating on direct current and used in combination with a Wratten 61 N filter to produce a stable, high-intensity source of essentially monochromatic light to eliminate most of the chromatic aberration inherent in the optical system.

In order to eliminate distortion owing to the meniscus of the immersion fluid and to prevent fluid evaporation and dust collection, an optically flat glass cell cover was placed on the cell immediately after the sample was collected.

Using Rupe's apparatus, it was possible for an operator to obtain the spray samples and take as many as 800 photographs in one working day. To speed up the almost endless task of counting the drops of each size range, a semiautomatic differentiating droplet counter was devised. This equipment is described later in the section on "Automatic Scanning Devices".

Golitzine⁽⁴⁻²¹⁾ measured the size distribution of water droplets in clouds, fogs and sprays after collection on a slide covered with a special oil, Shell Spirax 250, to retard evaporation. The method of collecting the sample consisted of exposing a transparent plastic slide, 1/8 inch x 1/2 inch x 12 inches, covered along half its length with the special oil.

In taking samples of sprays, the slide was swung by hand across the spray, either edge on or face on, depending on the velocity of the droplets in the spray. In fog sampling, the slide was swung by hand, face on, several times through the fog, until a sufficient number of drops had been collected. In cloud sampling, the slide was exposed momentarily, face on to the air stream, out of a side window in the aircraft.

Confidential

Golitzine believes that the most important factor to consider in taking droplet samples is the time of exposure of the oil-treated slide in the spray, fog or cloud. If the slide is exposed for too short a time, the number of droplets collected is insufficient to represent well the variety of sizes. If the exposure is too long, too many droplets are collected, thereby increasing the probability of coalescence, and therefore of error in the observation. The best time of exposure must be determined by trial for each condition.

The droplets collected in the oil on the surface of the slide appear to be nearly spherical in shape. However, Golitzine recommends that the assumed spherical shape be verified by a comparison of measurements made by his method with data obtained from direct photographs using a spray composed of homogeneous droplets. Such a spray may be obtained using a spinning top, as described by May⁽⁴⁻²²⁾.

Frozen-Drop and Wax Methods

Holroyd⁽⁴⁻²³⁾ suggested that a better experimental method would be to use liquids that would solidify before coming into contact with any solid surface. The drops could then be studied at leisure. Holroyd tried atomizing melted beeswax with some success and suggested the use of alloys of low melting point. However, the frozen-drop method was really developed by J. P. Longwell⁽⁴⁻²⁴⁾, and the wax method was perfected by J. R. Joyce⁽⁴⁻²⁷⁾.

Frozen-Drop Method

Longwell⁽⁴⁻²⁴⁾ developed a technique that consisted of collecting the drops from a fuel spray in a stream of flowing fluid which was at room temperature. This stream of fluid, in which the drops were immiscible, removed the drops from under the opening of the sampler so that they would not fall on each other. The stream was allowed to flow far enough so that the drops would regain their spherical shape after being deformed by impact on the fluid surface. The fluid carrying the droplets was then fed into an alcohol bath kept at approximately the temperature of dry ice, which was cold enough to freeze the drops into solid spheres. The drops were then sieved while still cold, to separate them into different size groups. The relative amounts of the various fractions were determined by dissolving the oil in a known volume of benzene and comparing the color density with a colorimeter.

Figure 4-1 shows a cross section of the drop sampler used by Longwell. This sampler was so constructed that it could be opened and closed, by compressed air, at the proper points along a radius of a spray cone. The drops of oil fell in the opening of the sampler upon a glass plate over which a mixture of alcohol, water, and glycerin was flowing. The mixture of fluid and oil drops then fell into the cold alcohol bath and the oil drops froze. The sample was then transferred to a previously chilled beaker, which contained lumps of dry ice, where it was kept until sieved.

Figure 4-2 shows a cross section of Longwell's apparatus used for sieving the sample; this consisted of a series of sieves so mounted one above the other that the liquid carrying the frozen drops could flow through them. The smallest drops were filtered out by glass wool and the liquid was drawn out by an aspirator.

Usually four Tyler sieves, ranging in size from U.S. Standard No. 40 to No. 120, were used, which gave four points on a distribution curve. The drop sizes collected on these screens ranged from about 100 to 300 microns in diameter. After all of the liquid and oil-drop mixture had been poured through the sieves, the sieves were washed with cold alcohol to work the drops down to their proper sieve. The impact of the washing fluid, falling from a height of about one foot, helped to force the small drops through their holes. When the washing was completed, the sieves were removed and allowed to dry. The relative weights of the oil drops on each sieve were obtained by dissolving each size fraction of the oil in benzene, measuring the volumes of the solutions, and comparing their colors in a colorimeter.

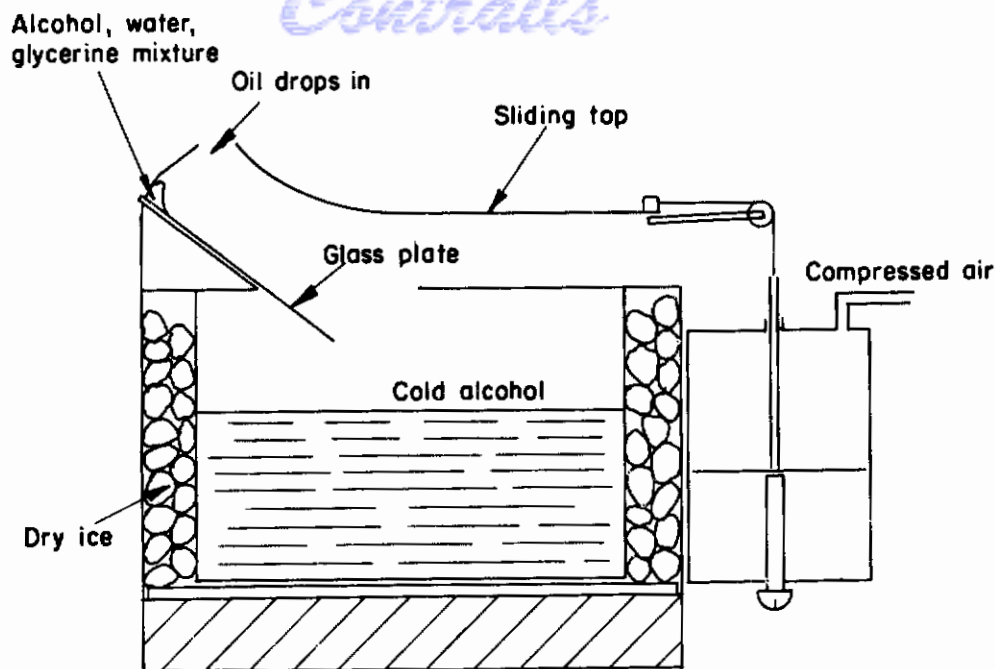


FIGURE 4-1. DROP SAMPLER FOR FROZEN-DROP METHOD
(Longwell)⁽⁴⁻²⁴⁾

Longwell⁽⁴⁻²⁵⁾ reports that the total frozen spray has been analyzed recently by conventional methods used for solid particles. For example, air elutriation with a Roller cascade analyzer has been used for determining the size distribution of frozen wax particles. The frozen-drop method involves considerable work, but the tedious and time-consuming operations of microscopic counting are eliminated.

Taylor and Harmon⁽⁴⁻²⁶⁾ designed an instrument for measuring drop-size distribution that combines the drop freezing technique and Stokes' law separation.

Figure 4-2A is a cross section of the final design. The water is spread over the edge of Box A. The water lands in the catching liquid, B, which is hexane cooled to about -20 C with dry ice which is kept in the space within the box and around the liquid pan. The drops freeze very quickly and fall to Shutter C. When all the drops are resting on the shutter, the shutter pull, D, is opened, which allows the drops to descend through the hexane to a scale pan, E. The drops fall approximately according to Stokes' law (neglecting interaction effects) and the largest drops arrive first at the scale pan. The weight on the scale pan is transferred to the cord, F, which passes around an aluminum cylinder, G, and then to a spring, H, which balances the force on the scale pan. The slight movement of the disk, G, is amplified by the pointer, I, which moves over a measuring scale, J, calibrated to indicate the differential weight on the scale pan. The weight on the pan versus time relationship is determined by use of a stop watch, though in a more complex instrument this could easily be done electrically with greater accuracy.

The weight falling on the pan can be transformed simply into equivalent drop diameters and total number of drops at each diameter by use of a drag coefficient which depends upon the velocity or Stokes' law for the smallest drops. It is then necessary to convert the measured sizes to true drop sizes by allowing for the density difference between the ice and the water which was sprayed.

The ratio of pointer tip movement to pan movement is 10 to 1. The pan moves approximately 1/4 inch. The total depth of fall of the drops is 12 inches, which gives a possible error of about 3 per cent from pan movement. The exact relationship may be calculated at any point if desired.

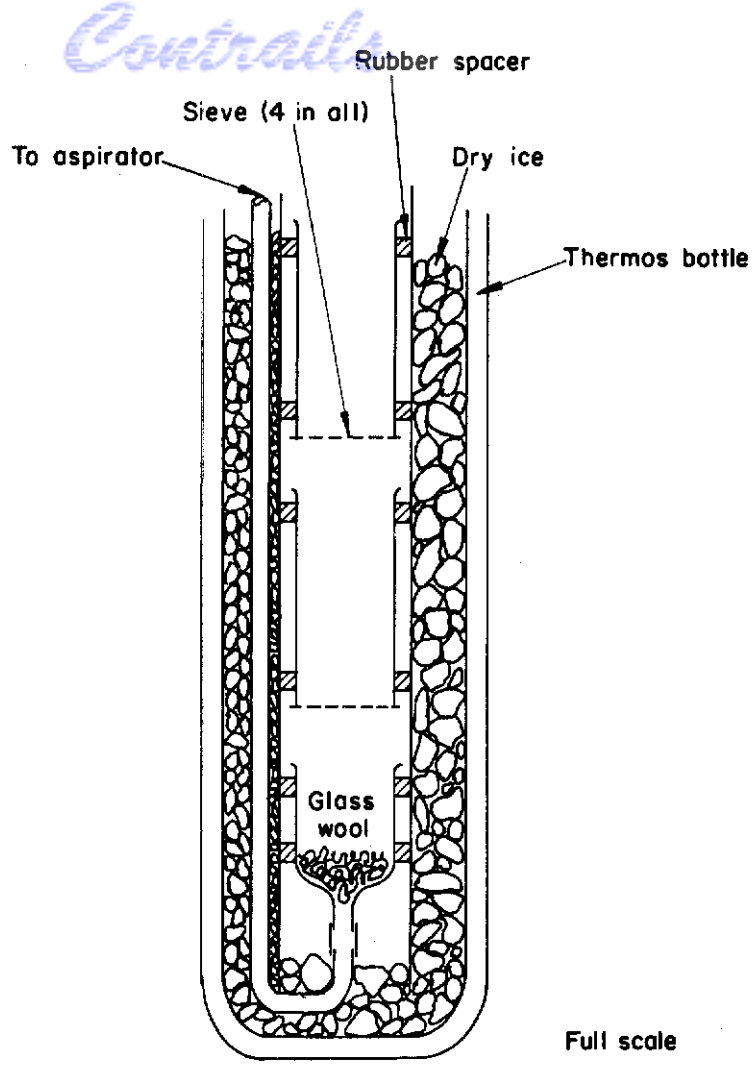


FIGURE 4-2. APPARATUS FOR SIEVING FROZEN DROPLETS
(Longwell)(4-24)

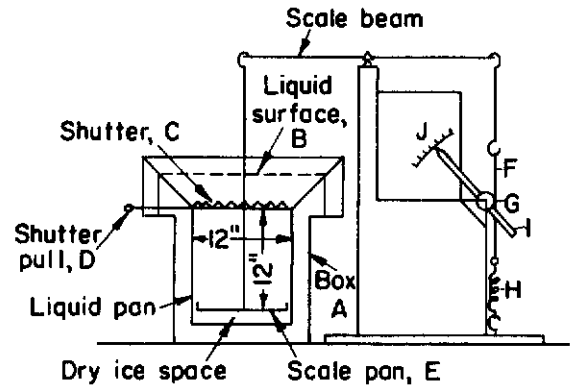


FIGURE 4-2A. CROSS SECTION OF DROP-MEASURING INSTRUMENT
(Taylor and Harmon)(4-26)

The method is rapid and requires no special sampling of spray.

Wax Method

Joyce^(4-27, 4-28) developed the wax method of spray-particle-size measurement to a high degree of perfection during the period 1942 to 1946. His technique is based upon the observation that paraffin wax, when heated to a suitable temperature level above its melting point, corresponds closely, in the significant characteristics of viscosity and surface tension, with jet fuel.

In making droplet-size tests, the spray nozzle was supplied with liquid paraffin wax and produced a spray to all appearances exactly like that produced with jet fuel. The small liquid-wax droplets solidified rapidly in the air, and the entire wax spray was directed into a funnel-like bath of flowing water, from which a sample of the water-borne spray was collected in a suitable vessel.

Figure 4-3 shows Joyce's collecting funnel for the wax spray. Usually, between five and ten grams of wax droplets were collected, and the sample was passed through a series of six or more graded gauze sieves. The smallest particles that passed through all the gauzes were trapped on the surface of a filter paper. The weight of wax droplets collected on each gauze and on the filter paper was then determined and was used to compute the spray distribution by weight in a set of known size groups.

Figure 4-4 shows the components of Joyce's filter unit. Wire gauzes of selected accuracy, complying with the standards of the Institute of Mining and Metallurgy, and known as I. M. M. gauzes, were used in his more recent apparatus. The gauze elements had an effective diameter of three inches and were carried in independent holder units, so that each mesh could be dealt with separately during the sieving process, without disturbing the assembly. The notches on the end of the gauze shown in Figure 4-4 were used to indicate the nominal mesh of the element. The meshes (per linear inch) of the various gauzes used were 50, 60, 70, 80, 100, 120, 140, and 200, corresponding to nominal sizes of 295, 245, 215, 180, 142, 122, 101, and 75 microns.

The sieving method described above has its limitations, as well as its distinct advantage of providing drop-size data without microscopic counts. The chief limitation is that the method does not provide information about the extremely fine particles; all particles that pass 200 mesh (75 microns nominal size) are in one size group. To obtain more complete information regarding the smallest, and also the largest, particles, it is necessary to examine the filter residues under the microscope, and to make some form of count and measurement. Also, it is difficult to determine reliably from a sieving test the number of droplets in the spray per unit volume of oil atomized. A count of the residue on each gauze screen can serve to make a determination of the mean diameter in each size group.

Joyce recognized these limitations and pointed out that, for certain detailed data, the use of the microscope was necessary to supplement the data derived directly from a sieving test.

Heath and Radcliff⁽⁴⁻²⁹⁾ used a molten-wax technique similar to that of Joyce in studying the performance of an air-blast atomizer. They moved a heating element directly on the burner nozzle and used an air heater to bring the air blast to the same temperature as the wax, so that the liquid characteristics were not altered at the moment of atomization.

After encountering difficulties in collecting and sampling the wax spray, Heath and Radcliff used five per cent Teepol in the water in the beaker into which the wax drops were transferred about 30 minutes after collection. The Teepol solution completely wetted the wax and enabled the sample to be broken into separate drops.

These investigators did not use the sieving technique devised by Joyce. Instead, they collected the drops on a microscope slide held vertically for just a moment in a beaker in which the wax particles were being agitated while dispersed in liquid. Photographs of the dry slides were taken and drop-size counts were made in steps of ten or twenty microns. They observed some lack of agreement for duplicate tests, especially for the small sizes, which they attributed to

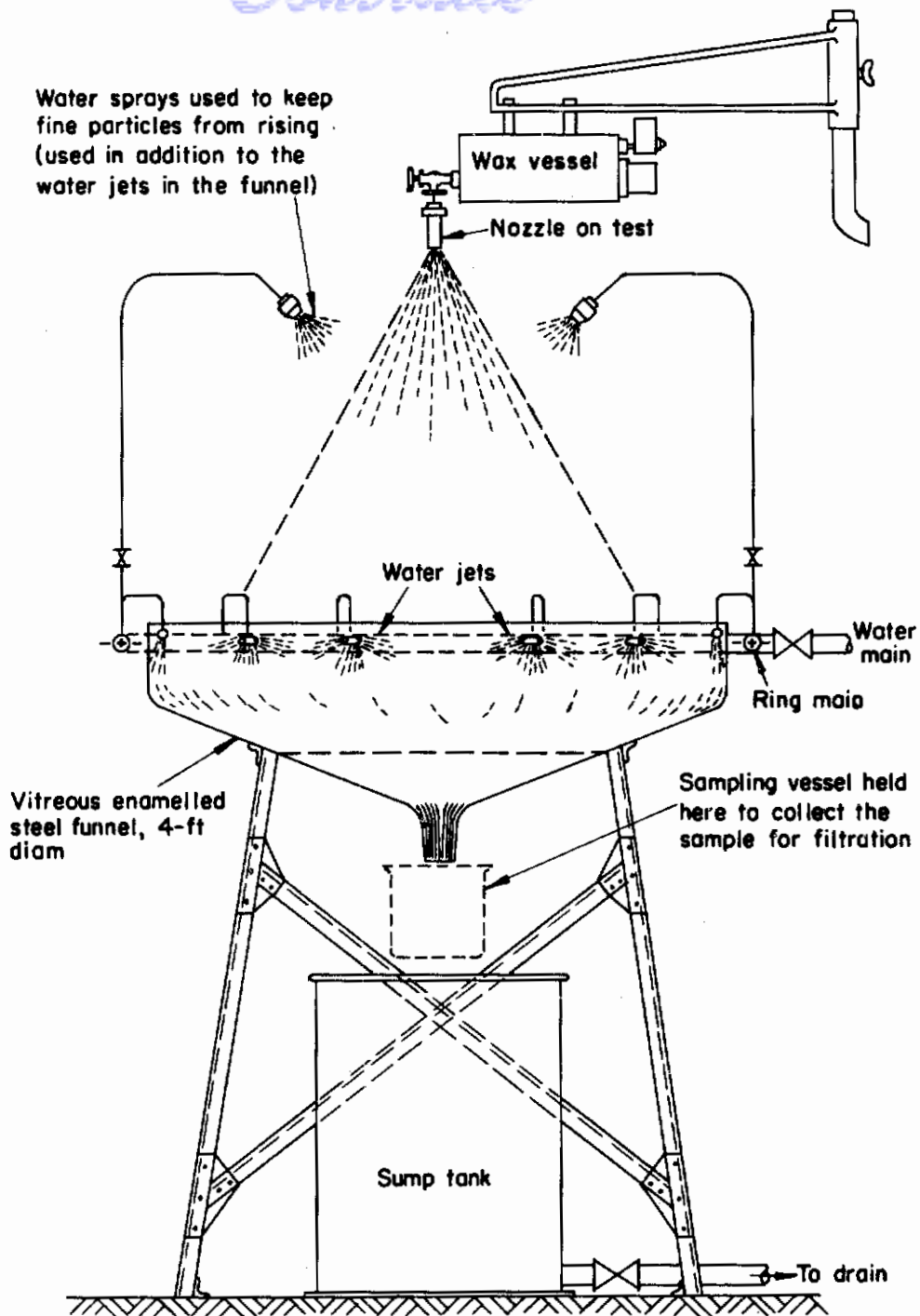


FIGURE 4-3. COLLECTING FUNNEL FOR WAX SPRAY
(Joyce)(4-27)

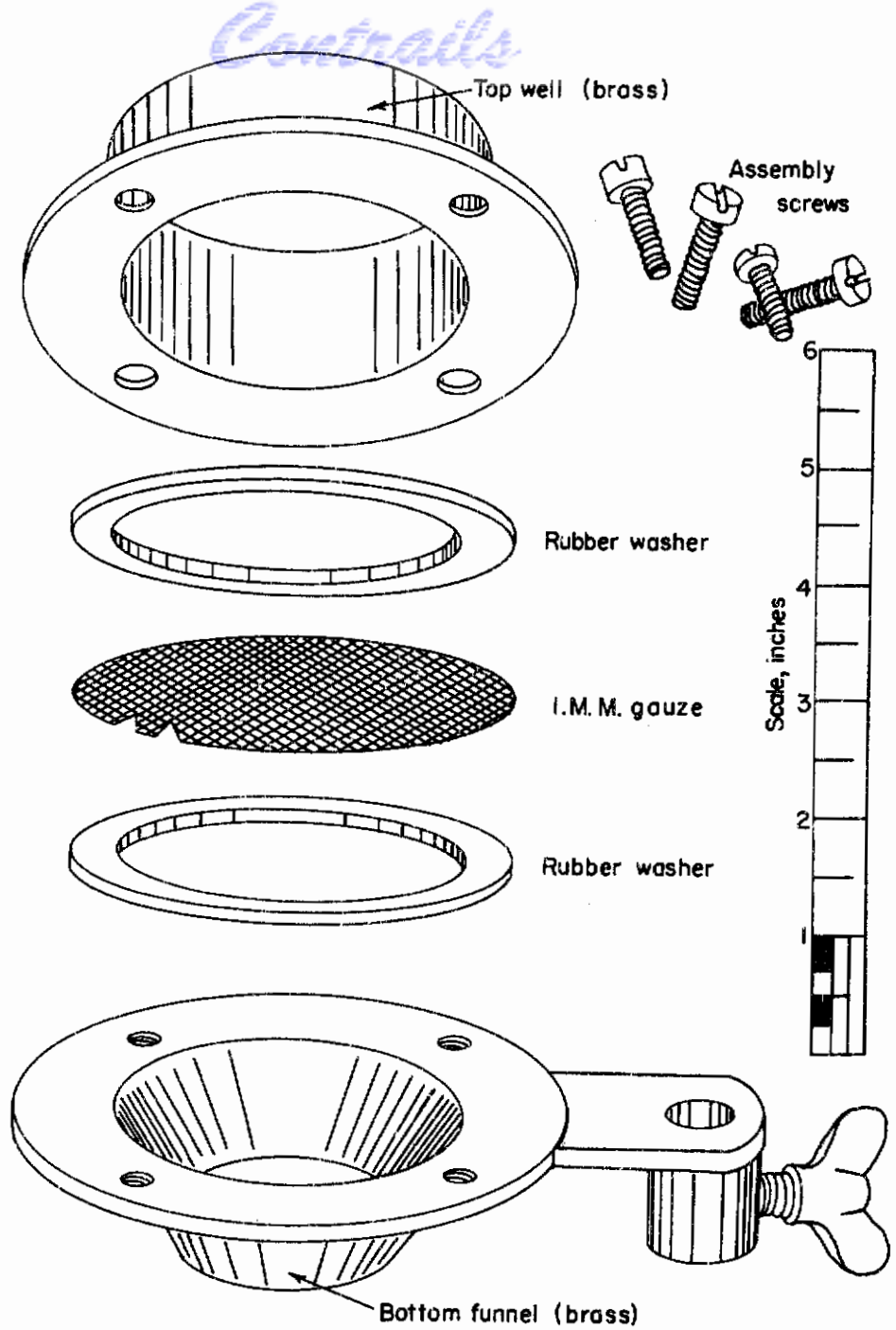


FIGURE 4-4. FILTER UNIT COMPONENTS
(Joyce)⁽⁴⁻²⁷⁾

the clusters of drops which occurred occasionally on the slides. It was difficult to measure small drops that were grouped around a larger neighbor.

By not using a sieving technique, Heath and Radcliff were not able to take advantage of the outstanding feature of Joyce's wax method, which is the elimination of microscopic counting for the larger sizes of drops.

Wetzel⁽⁴⁻³⁰⁾ atomized a molten wax and a molten alloy in the 2-inch throat of a venturi nozzle and studied the effects of air stream and liquid stream velocities on the particle-size distribution of the spray. Empirical equations were established for expressing the magnitudes of the effects of operating conditions as follows:

For the wax

$$(\rho = 0.83 \text{ gm/cc}; \mu = 9 \text{ cp}; \sigma = 29.5 \text{ dynes/cm})$$

$$\bar{d}_V = 4.2 \times 10^6 (u_A - u_L)^{-1.68} D_L^{0.35}$$

$$\sigma_g = 1.11 (\bar{d}_V)^{0.18}$$

For the low melting alloy

$$(\rho = 9.75 \text{ gm/cc}; \mu = 5.5 \text{ cp}; \sigma = 470 \text{ dynes/cm})$$

$$\bar{d}_V = 10^5 (u_A - u_L)^{-1.11}; \sigma_g = 0.0214 (\bar{d}_V)^{0.92}$$

where \bar{d}_V is the geometric mean drop diameter on a volume basis expressed in microns, u_A and u_L are the velocities of the air and liquid, respectively, expressed in ft/sec; D_L is the diameter of the liquid orifice expressed in inches; and σ_g is the dimensionless geometric standard deviation.

Wetzel concluded that the spray cooling of molten materials is a convenient method of studying the drop-size distribution of a spray. A permanent record of the spray is obtained so that large numbers of particles may be sized by physical sizing methods.

Photographic Methods

Methods of determining drop-size distribution based on photographing the undisturbed spray in space have the important advantage that no object is placed in the path of the droplets to cause discrimination. Another inherent advantage of photographic methods is that errors that might result from coalescence or evaporation of droplets, after sampling, are eliminated.

On the other hand, the photographic methods have two disadvantages: (1) the smallest droplets cannot be photographed satisfactorily in a fast-moving spray; and (2) the photograph records the spatial distribution of drops, that is, the size distribution in the volume included by the field of focus, whereas the temporal distribution, which is the size distribution of drops passing a cross-sectional area in a unit of time, is the information usually desired. However, if drop velocities are known, temporal distribution can be computed from spatial distribution, as will be discussed later.

Gilman⁽⁴⁻³¹⁾ employed the photographic method in 1942 to determine the size distribution of water droplets formed by spray nozzles. His procedure consisted essentially of photographing the moving particles in a thin focal plane. The time of exposure was short enough to limit the

distortion due to motion to a small fraction of the particle diameter. A shadowgraph of the particles was obtained, the negative was projected to a known magnification, and the images were measured and counted.

Some idea of the shortness of exposure required may be gained from a simple calculation. Assuming a 50-micron particle moving with a velocity of 10 cm per sec, and allowing 10 per cent distortion, the exposure time would be 5×10^{-5} second. Gilman provided this short exposure by means of a spark through an arc gap of 1.4 mm which required a voltage of 5.5 kv.

Figure 4-5 is a sketch of the system used by Gilman to take shadowgraphs of the droplets in a water spray. The light from the spark gap was focused on the lens of the camera by the condensing lens. The camera was focused on the plane of the drops, which was between the condensing lens and the camera. The condensing lens provided a defocused bright field upon which the shadow of the drop was sharply outlined by virtue of the refraction of the light that the drop intercepted. The drops of water in the focal plane of the camera had a sharp shadow, whereas all the others appeared indistinct.

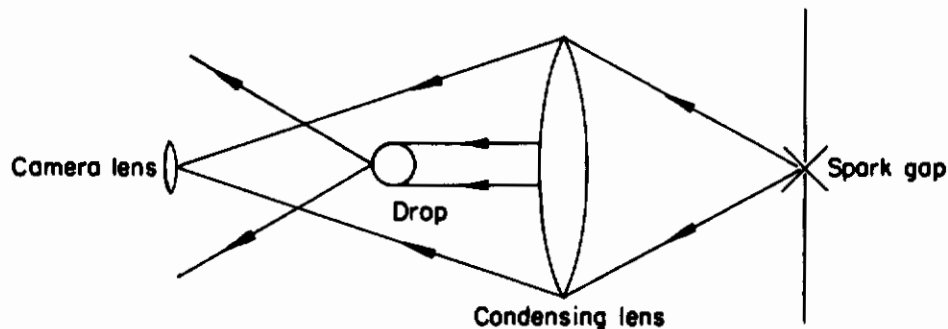


FIGURE 4-5. SYSTEM FOR TAKING SHADOWGRAPHS OF SPRAY
(Gilman)⁽⁴⁻³¹⁾

More recently, Stubbs and York⁽⁴⁻³²⁾, of the University of Michigan, have achieved marked success with the photographic method for determining drop-size distribution.

Stubbs and York Method

Stubbs and York⁽⁴⁻³²⁾ emphasize the fact that the photographic method does not require any collecting object in the spray and that the results are, therefore, free of bias from disturbances of the flow pattern.

These investigators overcame the objection that the photographic method gives spatial distribution, rather than the more desired temporal distribution, by determining the velocity of each droplet. Velocities were determined by taking double exposures of regions in the spray with a small known interval between exposures. The resulting photographs showed a pair of images for each drop, and the velocity was calculated from the distance between images and the interval between exposures.

Figure 4-6 shows the arrangement of elements used by Stubbs and York.

The camera used was a light-tight box with a receptacle for film holders and a viewing screen on the back, and a 5-mm-focal-length Argus Coated-Cintar lens in front. Although the front of the camera was wet by the spray, the optical properties of the lens were not seriously distorted by the water on the front surface. The distance from the lens to the film was about 20 inches, which resulted in a magnification of 10X and images of convenient size with maximum resolution.

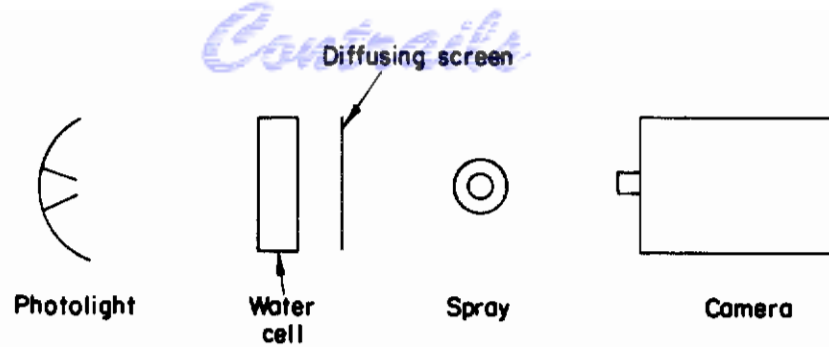


FIGURE 4-6. ARRANGEMENT OF ELEMENTS FOR PHOTOGRAPHING SPRAYS
(Stubbs and York)⁽⁴⁻³²⁾

Kodak Contrast Process Ortho film was used because of its high contrast and high resolution.

The open-shutter method was used and the light source was a General Electric Photolight* which has a duration of useful illumination of about 1 microsecond. The light from the Photolight passes through the water cell, shown in Figure 4-6, onto a ground-glass diffusing screen, then through the spray, and finally into the camera. The water cell was a Lucite vessel with flat sides containing a solution of nigrosin dye, of varying concentration, to control the intensity of illumination.** The diffusing screen made the illumination of the spray more uniform.

Drops ranging in size from 15- to 500-micron diameter could be measured and counted by placing the negatives in a Jones and Lamson comparator and projecting the images on a ground-glass screen. The projection produced a magnification of 10, so that the diameter of the image on the screen was 100 times the diameter of the drop.

Figure 4-7 shows that the volume of the spray that was photographed was bounded in two dimensions by the view of the camera and in the third dimension by the depth of field of the optical

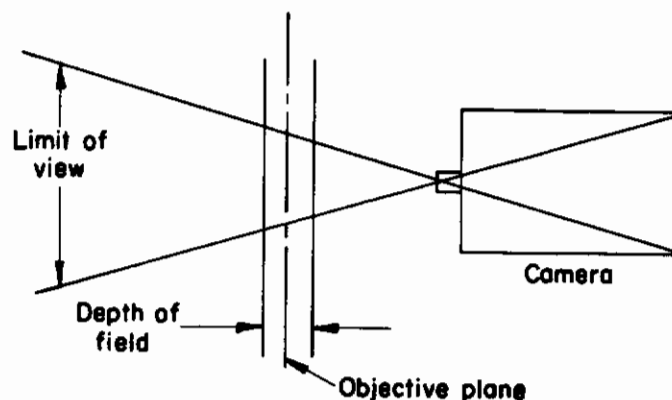


FIGURE 4-7. LIMITS OF KNOWN VOLUME PHOTOGRAPHED
(Stubbs and York)⁽⁴⁻³²⁾

*General Electric Photolight, Catalog 9364688G1.

**Stehling has found that crossed sheets of circular polarizer provide a convenient and continuously variable intensity control.

system. The extent of the depth of field was not as sharply defined as one would wish. The images of drops that were successively farther from the object plane were more and more blurred, so that the operator had to judge from the amount of blur whether a drop was within the arbitrary limits of the depth of field. Stubbs and York solved this problem of coordinating the judgements of various operators by means of "standard images". These were images of various sizes of drops, known to be at the limit of field depth, that were projected on the screen along with images of the drops to be sized and counted. Thus, the operator had to judge only whether a given image was more or less blurred than a standard image of the same size.

Because the depth of field for any fixed blur depends on the lens aperture, the aperture was held constant and exposure was controlled by varying the illumination by means of the water cell shown in Figure 4-6.

Figure 4-8 shows the arrangement used to measure the velocities of the drops. A double exposure was made using two Photolights fired one after the other by means of an electronic time-delay unit. A delay of 25 microseconds proved reasonable for the optical arrangement used by Stubbs and York for drops moving about 20 feet per second. The delay unit was calibrated mechanically by making a double exposure of a rotating saw blade. By measuring the angular velocity of the saw and calculating the distance a tooth moved between exposures, the interval between flashes was determined.

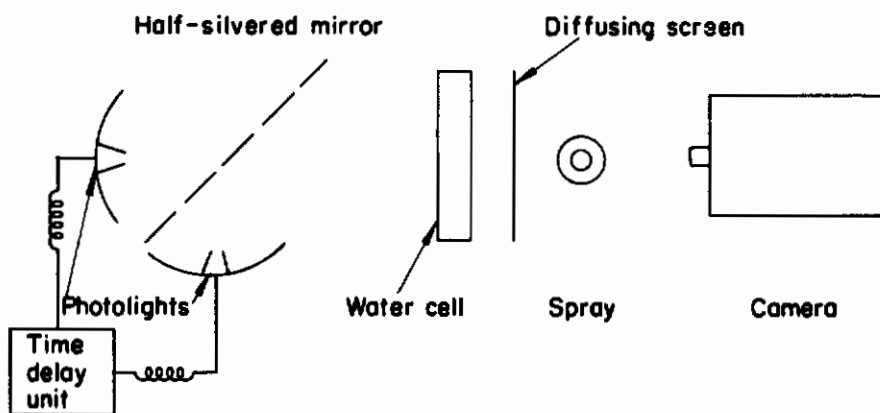


FIGURE 4-8. ARRANGEMENT FOR DOUBLE EXPOSURE
(Stubbs and York)⁽⁴⁻³²⁾

Stubbs and York point out that the photographic method is quite laborious, especially if data for a large number of points throughout a spray are desired. They suggest that, in many applications, it may not be worth while to obtain the detailed quantitative analysis of which the method is capable. Often the effort can be better spent getting semiquantitative information at a few points of a spray which would be sufficient to indicate the trends and general nature of the spray. Adaptations of this method might also be used to examine the mechanism of formation of a spray or its behavior as the spray impinged on an object or as it reached some other point of special interest.

It appears also that this photographic method might serve as a means of calibrating some other simple, indirect method which could be used for rapid spray analysis.

NACA Flight Camera

McCullough and Perkins⁽⁴⁻³⁴⁾ developed a camera at the National Advisory Committee for Aeronautics to photograph cloud droplets in their natural suspension in the atmosphere. A magnification of 32X was used to distinguish all sizes of droplets greater than 5 microns in diameter.

Flight tests conducted in cumulus clouds showed that droplet-size-distribution studies could be made with this camera, provided a large number of photographs were used.

Optical Methods

A great amount of time and effort is involved in the determination of drop-size distribution by methods involving the collection of drops on slides or in cells, by the frozen-drop or wax method, and by photographic methods. Therefore, indirect methods that require neither microscopic counts nor the separation and weighing of the various size fractions are desired and have been used.

Indirect optical methods based on the scattering of light are rapid and relatively simple, and do not disturb the spray pattern. However, the optical techniques are better suited to aerosols and to extremely fine mists or sprays than to typical fuel sprays. Also, the data obtained provide information concerning only the average drop size or predominant drop size, and drop-size distribution data cannot be obtained. The method is recommended, however, as a rapid means for studying the effects of certain variables on drop size and should play a significant role in spray analysis.

The measurement of small particle sizes by observation of the scattering of light is based primarily on the electromagnetic theory developed by Gustav Mie in 1908. The complete theory is given in compact form by Stratton⁽⁴⁻³⁵⁾ and the pertinent equations are outlined by Sinclair and LaMer⁽⁴⁻³⁶⁾, and will not be repeated here.

Four Types of Light-Scattering Methods

Sinclair and LaMer⁽⁴⁻³⁶⁾ have employed four types of light-scattering methods for size determination of particles below about 2 microns in diameter. These methods are briefly described below:

(1) Methods Based on Light Transmission. For transparent materials, the scattering cross section S_1 can be obtained by measuring the transmission of light as a function of wavelength. S is a complex function of the wavelength of the light used, the radius of the sphere, and the refractive index of the particle relative to the medium. Measurements at various concentrations showed that the transmission T could be expressed by the equation:

$$T = \frac{I}{I_0} = e^{-Snl} = e^{-Jc} ,$$

where I and I_0 are the intensities of the emergent and incident light, respectively, n is the particle-number concentration, c is the mass concentration, J is the scattering cross section per gram, and l is the length of the path in the aerosol or mist.

This method was applied in field measurements by means of a portable photoelectric meter developed by Seymore Hochberg called the "scope-o-meter". The relative transmissions at two wavelengths gave an average particle size, and the absolute transmission at one wavelength gave the concentration.

(2) Methods Based on the Intensity of the Scattered Light. The diameter of particles of a fog of uniform droplet size may be obtained by measuring the intensity of light scattered at directions varying from the forward to the backward direction and integrated over a sphere. The method is tedious, and the results are not as accurate as transmission measurements.

(3) Method Based on the Color of the Scattered Light. The third method used by Sinclair and LaMer was rapid and was based on visual observation of the color of the light scattered at different directions by a fog of uniform droplet size. When the fog was illuminated with a parallel beam of unpolarized white light, a series of bright colors was seen as the angle of observation was changed. The observation was made through a plane polarizer oriented with its vibration direction perpendicular to the plane of observation. As the angle of observation was varied from near zero toward 180 degrees, the sequence of colors resembled the spectrum in the order violet, blue, green, yellow, orange, and red. This spectral sequence was repeated several times, depending on the particle size. Near 90 degrees, the sequence of the colors was reversed. These spectral sequences have been designated as "higher order Tyndall spectra". The purity and brightness of the colors increased with uniformity of droplet size, and the number of times the spectral series was repeated increased with droplet radius. The droplet size could be measured with considerable accuracy by counting the number of times red, the most distinctive color, was seen.

Figure 4-9 shows the experimental curves obtained by Sinclair and LaMer with fogs of stearic acid ($m = 1.43$) and sulfur ($m = 2.00$), where m is the index of refraction. The ordinates are the number of reds seen when the angle of observation was varied from near zero to near 180 degrees. The abscissas are the diameters of the droplets in microns, obtained from measurements of the rate of settling in a convection-free chamber using Stokes' law. The calculated curve differed from the experimental curves by about 0.05 micron.

The chief limitation of this method, in addition to the fact that it is suitable for small sizes only, is that no colors can be seen in fogs having a wide distribution of sizes.

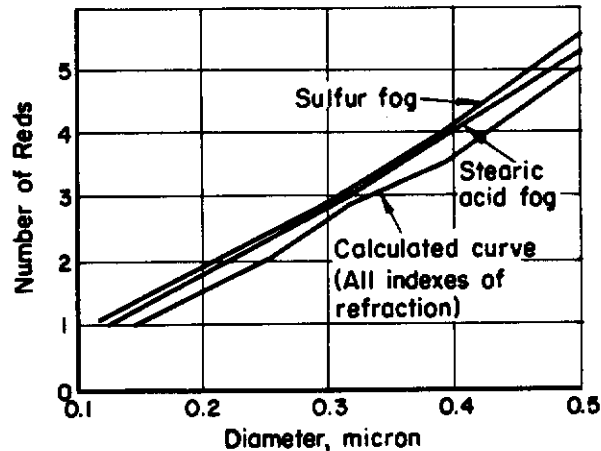


FIGURE 4-9. NUMBER OF REDS OBSERVED PLOTTED AGAINST DROPLET DIAMETER
(Sinclair and LaMer)⁽⁴⁻³⁶⁾

(4) Method Based on the Polarization of the Scattered Light. The polarization method can be used only for extremely small droplets, with diameters below about 0.4 micron; also, the fog must be sufficiently uniform in size. Because of these limitations, the polarization method is not described further, and reference should be made to Sinclair and LaMer⁽⁴⁻³⁶⁾ for more details.

Of the four light-scattering methods employed by these investigators, the methods based on transmission of light and on the color of scattered light appear more promising than the methods based on the intensity or on the polarization of scattered light.

NACA Optical Methods

Durbin⁽⁴⁻³⁷⁾ used two optical methods for measuring the size and concentration of condensation particles. One method was based on scattered-light measurements and the other method on

transmitted-light measurements. The methods are applicable provided that (1) steady-state conditions can be achieved during the time required for the measurement of light intensity, (2) the condensation particles are approximately spherical in shape and essentially uniform in size, and (3) the index of refraction of the condensation particles is known, approximately.

Durbin outlines the theory of light scattering for a single particle and points out that, for the results to be applicable to the measurement of fog particles, the light must be scattered only once in going from the incident beam to the observer. This type of scattering, he states, can be assumed to occur when the particles are separated by a distance of 100 times the particle radius. Scattering theory further assumes that the effects of individual particles can be added to determine the net effect of a group of particles.

Figure 4-10 shows the experimental arrangement used by Durbin. A monochromatic light consisting of the green line of the mercury spectrum was used to illuminate the fog. By measuring the intensity of the scattered light at two angles θ_1 and θ_2 , which were symmetrical about a line drawn normal to the direction of incidence, the particles in the fog could be classified according to size.

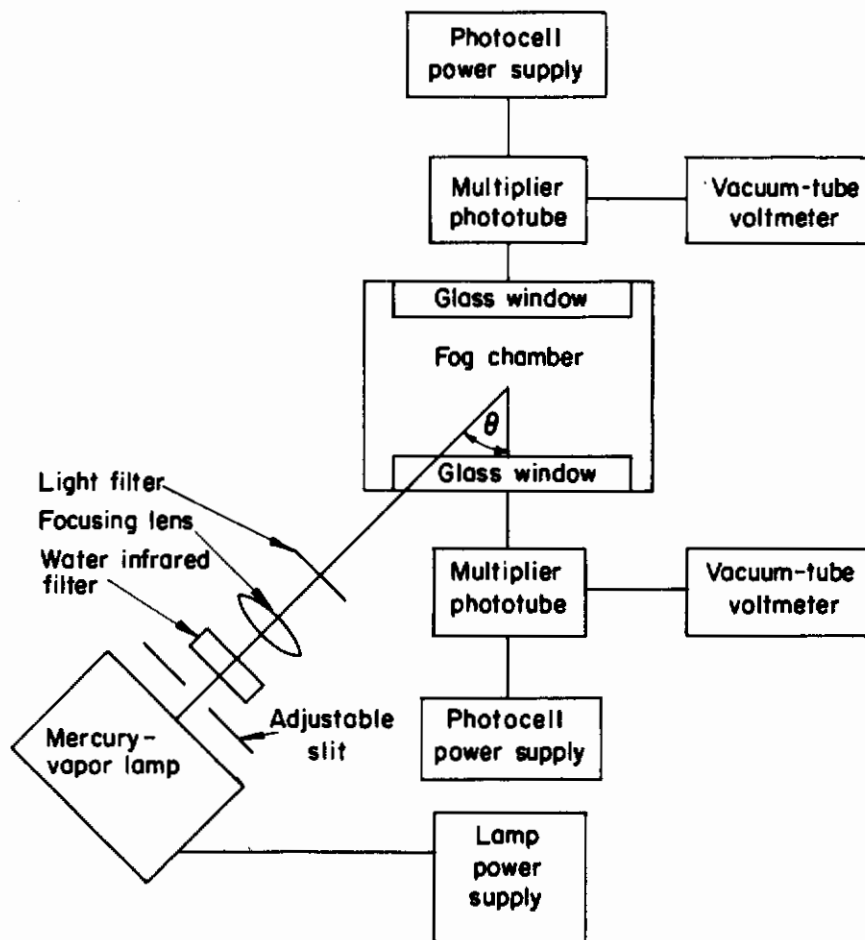


FIGURE 4-10. EXPERIMENTAL ARRANGEMENT FOR MEASURING PARTICLE SIZES BY LIGHT-SCATTERING METHODS (Durbin)⁽⁴⁻³⁷⁾

The National Bureau of Standards⁽⁴⁻³⁸⁾ has prepared tables of intensities based on the Mie theory which greatly reduce the labor involved in calculating particle size from light-scattering data.

Figure 4-11 shows the experimental arrangement used by Durbin in measuring fog-particle size by light-transmission methods. The fog was illuminated by the green line and the blue line of the mercury spectrum alternately. Both size and concentration of particles having diameters varying between 0.58 and 0.84 micron were measured. The results were in good agreement with the light-scattering measurements made with the arrangement shown in Figure 4-10.

JPL Optical Methods

Schmidt⁽⁴⁻³⁹⁾ (4-40) used two optical methods for measuring the mean drop size of atomized fuel. The methods, known as (1) the diffraction-ring method and (2) the photometer method, will be described in some detail.

Diffraction-Ring Method. The diffraction-ring method, also known as the corona method, was used by Schmidt to analyze sprays produced by hollow-cone injectors. The sizes of droplets varied so much when produced by other typical liquid atomizers that this method was not applicable.

The diffraction-ring method has the advantages that it is simple to use and does not disturb the spray pattern. On the other hand, this method has two definite limitations: (1) if the droplets are too large, the angle of diffraction will be so small that accurate measurements cannot be made, and if the droplet size approaches the wavelength of light, the diffraction rings disappear and the Tyndall effect appears; (2) if the size of droplets in the spray varies too much, the discrete rings will disappear and only a bright halo will surround the light source.

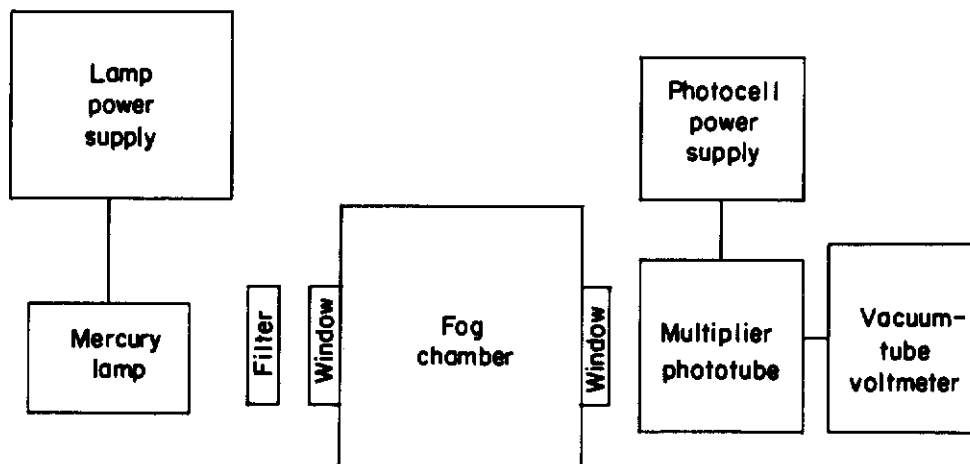
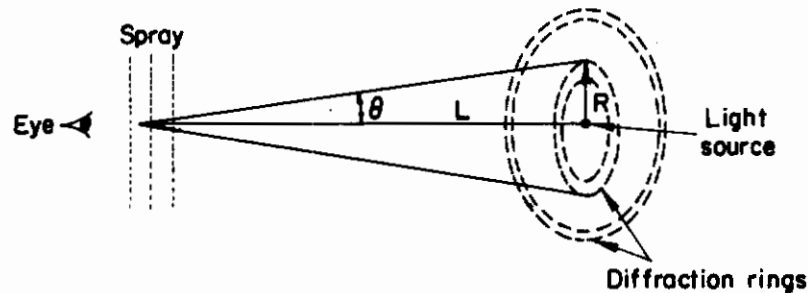


FIGURE 4-11. EXPERIMENTAL ARRANGEMENT FOR MEASURING PARTICLE SIZE AND CONCENTRATION BY LIGHT-TRANSMISSION METHOD (Durbin)⁽⁴⁻³⁷⁾

The principle of diffraction is shown in the accompanying sketch. If a point source of monochromatic light is observed through a spray consisting of small droplets of uniform size, diffraction rings will be seen around the light source, as shown in the sketch. The angle subtended at the eye is related to droplet diameter by the equation

$$\sin \theta_n = \frac{(n + 0.22) \lambda}{d}$$

where θ_n is the angle subtended at the eye by the radius of the n^{th} dark ring, d is the droplet diameter, and λ is the wavelength of the light.



Because the angle θ is small, $\sin \theta_n$ can be replaced by $\tan \theta_n$, which is equal to R_n/L where R_n is the radius of the n^{th} dark ring and L is the distance from the light source to the spray. The above equation can then be written

$$d = \frac{(n + 0.22) \lambda}{\sin \theta_n} = \frac{(n + 0.22) \lambda L}{R_n}$$

If white light is used instead of monochromatic light, various colored rings will appear and the analysis will become more complicated.

Figure 4-12 shows the laboratory setup used by Schmidt to determine the mean droplet diameter for sprays from small hollow-cone injectors. Visually, as many as four or five diffraction rings were observed, but the intensities of the outer rings were so low that they could not be photographed without overexposing the inner rings.

The radii of the diffraction rings were measured in two ways: (1) by the use of calipers, and (2) by a plot of density variations along a diameter of the rings using a Leeds and Northrup microdensitometer. The latter method was less subjective and more satisfactory.

The values obtained for droplet size, in the range of 50 to 100 microns, were consistent and reproducible. However, since the sprays were not homogeneous, the exact significance of the droplet diameter determined by the diffraction-ring method was not clear. That is, it is not definite whether the diameter was a linear mean diameter, a surface mean diameter, a volume mean diameter, or a median diameter.

Schmidt concluded that the diffraction-ring method is restricted in its use to applications where the droplets are of fairly uniform size. However, for heterogeneous types of sprays obtained by pressure injection of liquids through an orifice, the method may be of definite value in obtaining a qualitative comparison of the droplet sizes for various injection conditions.

It is of interest to note that Houghton and Radford⁽⁴⁻⁸⁾ applied this method, which they termed the corona method, to the analysis of natural fogs, but the results were uniformly unsatisfactory, presumably because of the rather wide range of drop sizes always present. They concluded that the corona method apparently was suitable only for fogs or clouds comprising particles of a very uniform size.

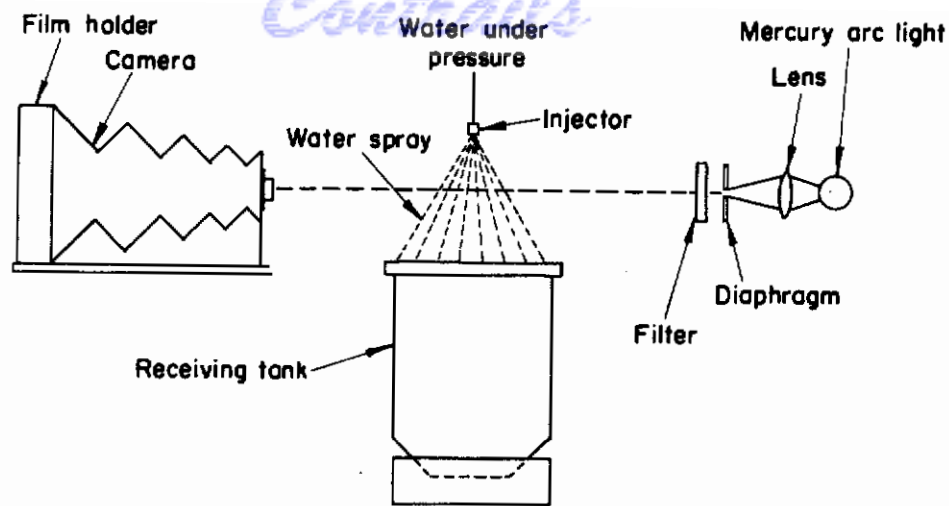


FIGURE 4-12. LABORATORY SETUP FOR STUDY OF DROPLET SIZES IN SPRAYS BY DIFFRACTION RING METHOD (Schmidt)⁽⁴⁻³⁹⁾

Photometer Method. Schmidt's⁽⁴⁻⁴⁰⁾ second method was based on the absorption of light by the spray and was suggested by the earlier work of Sauter^(4-2, 4-41).

Schmidt defined mean droplet radius, r_m , by the equation

$$r_m = 3 V/S \quad ,$$

where V is the total volume of the droplets and S is their total surface area. The value for r_m can then be determined experimentally by any method capable of measuring the ratio V/S .

The theory of the method and a description of the photometer used are given in an earlier reference⁽⁴⁻⁴²⁾.

Figure 4-13 is a sketch of the photoelectric photometer, which consisted essentially of a light source, two collimating lenses, and two Model 594 Type 3 Weston Photronic cells. The cells were connected as shown in Figure 4-13, so that the plus terminal of one cell was connected to the minus terminal of the other through a potentiometer forming a bridge circuit. The galvanometer could be made to read zero by a proper setting of the potentiometer. The use of polarized light in the photometer made the instrument more versatile and better adapted to the study of atomization of fuel injected into an air stream.

A beam of light was made to traverse a duct through which the spray was passed, and the percentage of light absorption due to the spray was measured by an absorption photometer. The mean drop size was then determined rapidly using the equation

$$r_m = \frac{\pi}{4} \frac{75 Q D}{Q' U}$$

where Q is the volume rate of flow of liquid, Q' is the volume rate of flow of air, D is the diameter of the duct, and U is the percentage of light absorption. This equation is based on the assumption that the droplets are completely opaque, and applies when the light beam traverses the complete cross section of the duct.

The photometer method is rapid and is recommended for applications involving the study of atomization when comparisons are to be made of sprays produced under various injection conditions and air velocities, or sprays formed from liquids having different physical properties. The

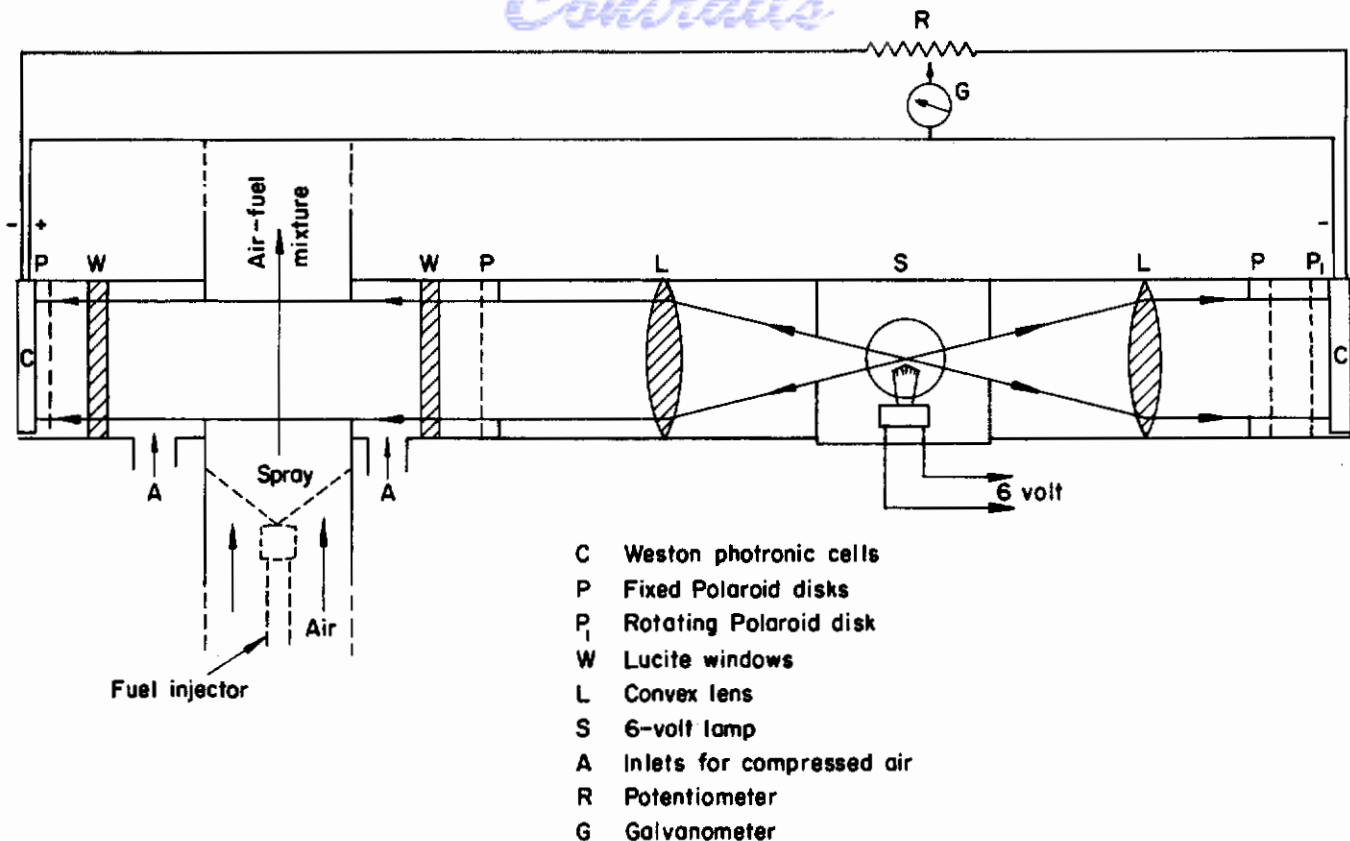


FIGURE 4-13. PHOTOELECTRIC PHOTOMETER (Schmidt)⁽⁴⁻⁴²⁾

photometer method, however, cannot be used to measure drop-size distribution. Schmidt recommends sampling the spray, using MgO-coated slides, when distribution data are required.

Mehlig⁽⁴⁻⁴³⁾ also applied a photometer method similar to Sauter's method to measure mean drop size of fuel sprays in diesel engines.

Electronic and Radioautograph Methods

Guyton⁽⁴⁻⁴⁴⁾ developed an electronic counter that depended upon the electrostatic charging of small particles forced at high velocities through a fine jet to impinge upon a metallic collector. Electrical pulses imparted to the collector by particles of 2.5 microns or larger were amplified to operate a mechanical counter. Guyton found that for solid particles that did not conduct electricity, the pulse amplitude was proportional to the square of the particle diameter.

Gucker and O'Konski⁽⁴⁻⁴⁵⁾ give a detailed description of Guyton's electrostatic particle counter. In addition to the electrostatic-charging method, Gucker and O'Konski used a combination light-scattering and electronic method. A fine stream of small particles, protected by a flowing sheath of pure air, was passed through a spot under intense dark-field illumination, and flashes of light were scattered forward upon a photocell. Each particle, about 0.6 micron or more in diameter, caused an electrical pulse that was sufficiently large, after suitable amplification, to operate a mechanical counter. The apparatus could count particles weighing 5×10^{-13} g at rates up to 1000 per minute and determine their size by means of an electronic discriminator.

Continued

Geist⁽⁴⁻⁴⁶⁾ developed an electronic spray analyzer somewhat similar in principle to Guyton's analyzer. Geist's apparatus consisted of a charged wire, inserted into a moving suspension or moving through the suspension of droplets, and connected to electronic circuits which amplified, classified, and counted the electrical pulses created upon interception of the particles by the probe.

Figure 4-14 shows the principal circuit components. The wire interceptor was maintained at a high positive electric potential.

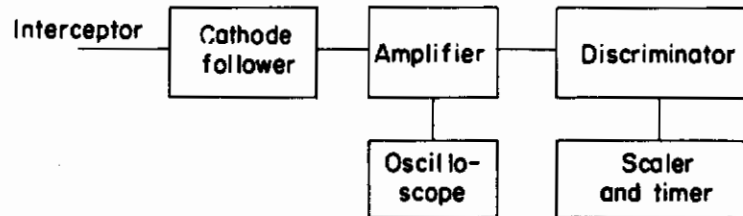


FIGURE 4-14. BLOCK DIAGRAM OF ELECTRONIC SPRAY ANALYZER
(Geist, York and Brown)⁽⁴⁻⁴⁷⁾

Impingement of solid or liquid particles which conduct electricity resulted in negative electrical pulses at the interceptor, the pulse varying with the particle size. These pulses were pre-amplified by a directly connected cathode follower to permit transmission by a shielded cable to a high-gain amplifier. The amplified pulses were sent to a discriminator that passed only pulses greater than a set voltage. The pulses that passed on were counted by a scaler.

After calibration, the data obtained by varying the set voltage at the discriminator, and counting the pulses to the scaler, provided cumulative size-distribution curves of the intercepted particles. The difference between successive counts was the number of intercepted particles in the size range corresponding to successive set voltages.

The relation between the particle size and the size of the pulse obtained at the input to the amplifier was apparently independent of the material of the drop, provided the material was a conductor of electricity. Metal spheres with diameters from 500 microns to 6340 microns, and water drops with diameters from 2590 microns to 4550 microns followed the same calibration curve. For drops of material having relatively high conductivity, the size of the pulse varied directly with the probe potential and approximately with the 1.6 power of the particle diameter, at least over a range from 1/2 to 6 times the diameter of the probe wire.

When inserted in a water spray, the probe functioned in a satisfactory manner, giving reproducible counts of particles over the size range covered by the calibration, although the greater portion of the spray was smaller than these sizes.

In order to make this device generally useful, it must be improved to apply to the smallest sizes of particles and to eliminate or control the effect of geometry of the probe.

Recently, the University of Mississippi has further developed Guyton's electrostatic particle counter as a means for sampling aerosols.

Dodd⁽⁴⁻⁴⁸⁾ used an apparatus built and described by Kunkel and Hansen⁽⁴⁻⁴⁹⁾ to determine the size and electrical charge of individual drops of liquid sprays after electrification. The method is based on Hopper and Laby's work on the determination of the electronic charge by horizontal deflection of particles settling under gravity. Drop diameters in a range of about 2 to 30 microns

and with charge-to-diameter ratios up to about 500 electrons per micron were measured. Measurements on over 6000 atomized drops indicated that the numbers of positively and negatively charged drops of poorly conducting liquids were roughly equal, as were their average charges, while drops of conducting liquids were predominantly positively charged. Dodd obtained data to illustrate the rather broad distribution in charge for a particular drop size and the variation of average charge per drop with drop size and with physical properties of the liquid.

Daniel and Brackett⁽⁴⁻⁵⁰⁾ made an analysis of the current-voltage (d-c) characteristics of a parallel-plate condenser through which small charged particles were passed. Because the electronic charge established a lower limit for particle charge, Daniel and Brackett were able to calculate size distributions on various assumptions concerning the relation between charge and particle radius.

In general, electronic methods are extremely rapid, but require calibration against some direct method for determining drop-size distribution. Also the electronic methods require considerably more development before they may be applied to the analysis of fuel sprays.

Leary^(4-51, 4-52) developed a new method employing a radioautograph technique to study particle-size distributions in aerosols of an alpha-emitting compound. The active material was collected on filter paper and placed in contact with nuclear track plates for various exposure times. By counting the number of tracks in the emulsion for a given exposure time, the size of each emitting particle was calculated from the derived equation

$$d = \left(\frac{KC}{t} \right)^{1/3},$$

where d is the particle size in microns, C is the number of tracks in the emulsion emitted from the particle, t is the exposure time, and K is a constant for a given radioactive material. The radioautograph method is particularly useful in the size range from 0.1 to 10 microns, but it is not limited to aerosols.

Leary points out the following limitations of this method: (1) the particles must be radioactive, as inert materials are not detected; (2) if there is a great abundance of large particles, the finer particles will be obscured in the radioautograph unless the large particles can be removed and studied separately; (3) the method is feasible as a research tool on only a few samples, as counting tracks in hundreds of clusters is a tedious and expensive procedure.

Leary verified the data obtained by his radioautograph method by means of the cascade impactor, a device for determining drop-size distribution that is described in the following section.

Cascade-Impactor Method

The determination of drop-size distribution by the cascade-impactor method is based upon the principle that a droplet moving at high velocity will, because of its momentum, impact upon a slide placed in the path.

Figure 4-15 shows, schematically, what happens when a fine spray approaches a glass slide in one of the early stages of a cascade impactor⁽⁴⁻⁵³⁾. The large droplets impact on the slide, whereas the small droplets follow the air stream into the next stage. As the velocity of the jet containing the droplets is increased by decreasing the area of the orifice through which the stream passes, smaller and smaller sizes of droplets can be made to impact. A distinct advantage of the cascade impactor, as compared with a single-stage impactor, is that the larger droplets are not subjected to extreme velocities of impaction, and the risk of shatter is minimized or eliminated.

Contrails

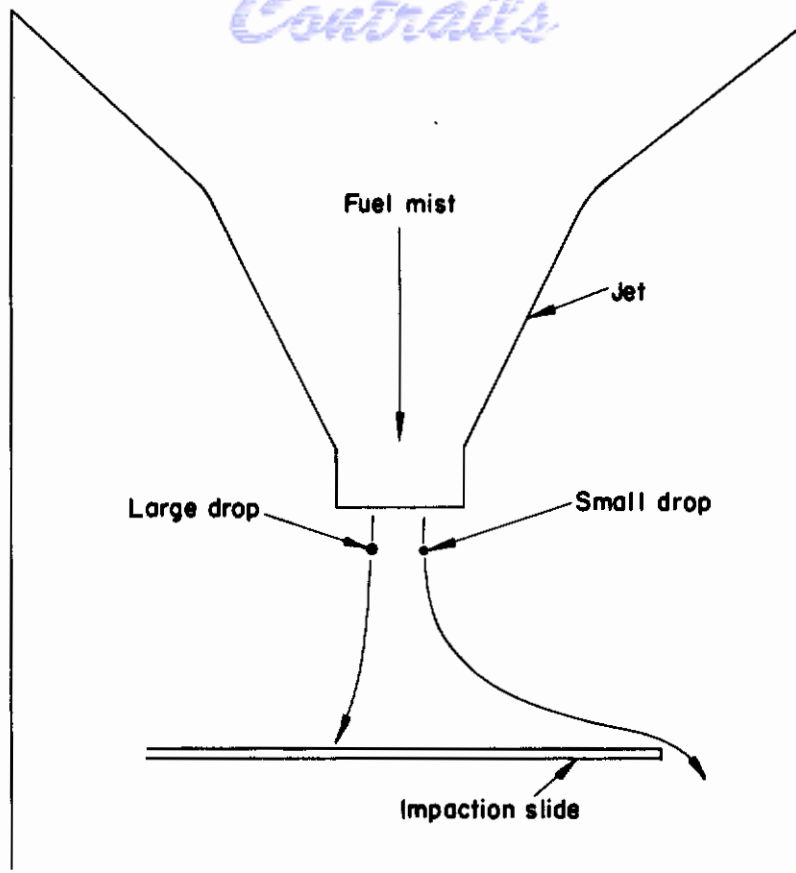


FIGURE 4-15. SCHEMATIC DIAGRAM SHOWING PRINCIPLE OF THE CASCADE IMPACTOR (Pilcher) (4-53)

May's Cascade Impactor

Figure 4-16 is a diagram of the British cascade impactor designed and calibrated by May⁽⁴⁻⁵⁴⁾.

The four jets are progressively smaller, so that the speed, and, therefore, the efficiency of impaction of particles increases from slide to slide when air is drawn through at a steady rate. A size grading results which greatly assists microscopic analysis.

Table 4-1 shows the jet dimensions, jet velocities, and range of sizes of droplets that impact for each stage of May's impactor.

Drops larger than 200 microns have a high chance of hitting the walls of the first orifice. Orifice-wall losses begin to be apparent at about 50 microns, so that the greatest efficiency of sampling is achieved in the size range of 50- to 1.5-micron diameter. May's experiments showed that when sampling a spray containing droplets ranging from 100 μ to less than 1 μ in a turbulent wind tunnel at 8 mph, the mass of sprayed drops washed off the inside of the orifice could be 20 per cent or more of the total sample on the four slides, depending upon the degree of turbulence. However, this loss was almost entirely due to droplets larger than 50 μ . To improve the sampling of coarse drops, the dimensions of the impactor should be enlarged.

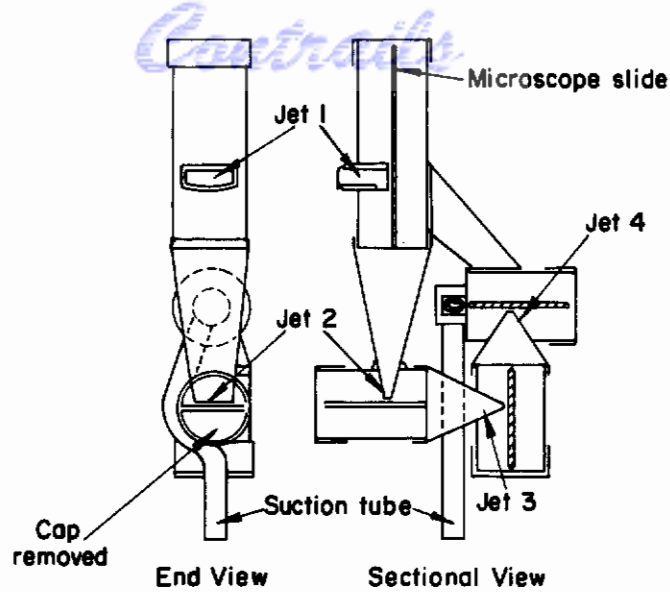


FIGURE 4-16. MAY'S FOUR-STAGE BRITISH CASCADE IMPACTOR
(May)⁽⁴⁻⁵⁴⁾

TABLE 4-1. JET DIMENSIONS AND RANGE OF DROPLET SIZES
FOR MAY'S CASCADE IMPACTOR

Jet Number	Dimensions of Jet, mm	Jet Vel, m/sec (at 17.5 l/min)	Approximate Drop Size, μ
1	19 x (6-7)	2.2	200* - 10
2	14 x 2	10.2	20 - 3
3	14 x 1	20.4	7 - 1
4	14 x 0.6	34.	3 - 0.7

*The upper limit of drop size effectively sampled is not definite, but May states that it is unusual to find drops larger than 200 μ on the first stage.

Although there is an overlap in size from slide to slide, the size grading of the sample is of great value in the microscopic analysis, as it enables the most suitable magnification to be chosen for each group.

One of the main advantages of the cascade impactor for the sampling of a jet of mist is that a sample of the spray may be obtained by "isokinetic" sampling, that is, by sampling at such a rate that the air velocities in the sampling tube and in the sampled mist are equal in both magnitude and direction. By following this procedure, discrimination against either small or large particles can be avoided.

There will always be a tendency for some of the larger drops (those over 50-micron diameter) to deposit just inside the leading edge of the sampling tube. However, by using a procedure that permits the entire tube to be washed out and the mass of drops determined, errors from this source can be minimized or avoided. No attempt should be made to converge the sides of the first jet to increase velocity and impaction efficiency, as this would cause serious wall losses of the larger particles. It is, however, permissible to converge the remaining jets, as particles large enough to be thrown out on the walls of these jets would have already been removed by the first impaction.

The best method for obtaining the correct flow rate through the impactor, to insure that stream velocity and sampling-port velocity are equal, is to install a critical-pressure orifice at the impactor outlet. The orifice diameter required to give a flow of 17.5 l/min, as used by May, is about 1.3 mm. By making the last impaction jet sufficiently small, it would be possible to make the last jet perform the function of the critical-pressure orifice, as is done in impingers.

Determination of Size Distribution Among Stages by Mass Methods

Another important advantage of the cascade impactor is that (after calibration) the relative mass of sample on each stage can be obtained by gravimetric, chemical, or colorimetric methods, and the tremendous labor and time involved in microscopic analysis can be avoided. Then, from a calibration of each stage giving the size range of droplets deposited thereon, an integration distribution curve can be drawn. Obviously, a large sample is desirable for an accurate determination of the mass of droplets on each slide, and coalescence of drops is inconsequential when gravimetric or colorimetric methods of analysis are used.

Sampling of Volatile Sprays. All fuel sprays are subjected to evaporation and, in order to carry out a microscopic analysis, the sample must be covered before appreciable evaporation takes place, or some form of detector must be used to leave a permanent record of the original size of the drop.

If the liquid is of low volatility, clean plain glass slides may be used and the microscopic analysis may be carried out before significant evaporation takes place. The size of the original spherical drop can be obtained from the diameter and focal length of the liquid lens, as described later in the section on "Flattening Coefficients."

Another method consists of mounting the drops by totally enclosing them in a matrix of similar density, of high viscosity, but of different refractive index, and in which they are insoluble. May⁽⁴⁻⁵⁴⁾ describes a technique for mounting drops but states that the method is not fool-proof and requires considerable manipulative skill.

The impaction of droplets onto a slide coated with magnesium oxide appears to be a more satisfactory solution of the problem of sampling volatile sprays. The layer of MgO should be thicker than the largest drop expected to impact on the slide. When the drops hit this layer, they penetrate the surface and leave a permanent round impression that may be seen clearly by using strong transmitted light, or brilliant surface illumination at almost glancing incidence. The smallest size detectable is about 3μ , and the layer of MgO is swept away by jets moving at excessively high velocities.

A fourth method for detecting volatile droplets involves coating the sampling slide with a medium which gives, either by chemical or by physical change, a stain or mark where the droplet has hit the slide.

The stain generally has a diameter which is two to three times that of the original drop, so that a spreading factor has to be determined.

Sonkin's Modified Cascade Impactor. Sonkin⁽⁴⁻⁵⁵⁾ modified May's design of the cascade impactor by reducing the cross-section areas of the jets to increase the air velocities. Sonkin's modified impactor is an efficient sampler for the characterization of aerosols having mass median diameters as low as 0.25μ ; however, because the size range studied by Sonkin is of little interest to the subject of fuel-spray analysis, the apparatus is not described here in detail.

Cadle⁽⁴⁻⁵⁶⁾ recently used a plastic model of the Sonkin impactor built from three pieces of machined Lucite cemented together as a sandwich to determine the composition of air-borne particulate material.

Laskin's Modified Cascade Impactor. Laskin⁽⁴⁻⁵⁷⁾⁽⁴⁻⁵⁸⁾ first used May's impactor, which he refers to as the British Cascade Impactor. Then, on the basis of extensive experience with the British instrument, Laskin constructed a modified cascade impactor to suit the requirements of the uranium dust in which he was interested. His impactor was constructed of solid brass, by precision machining methods, rather than of sheet metal.

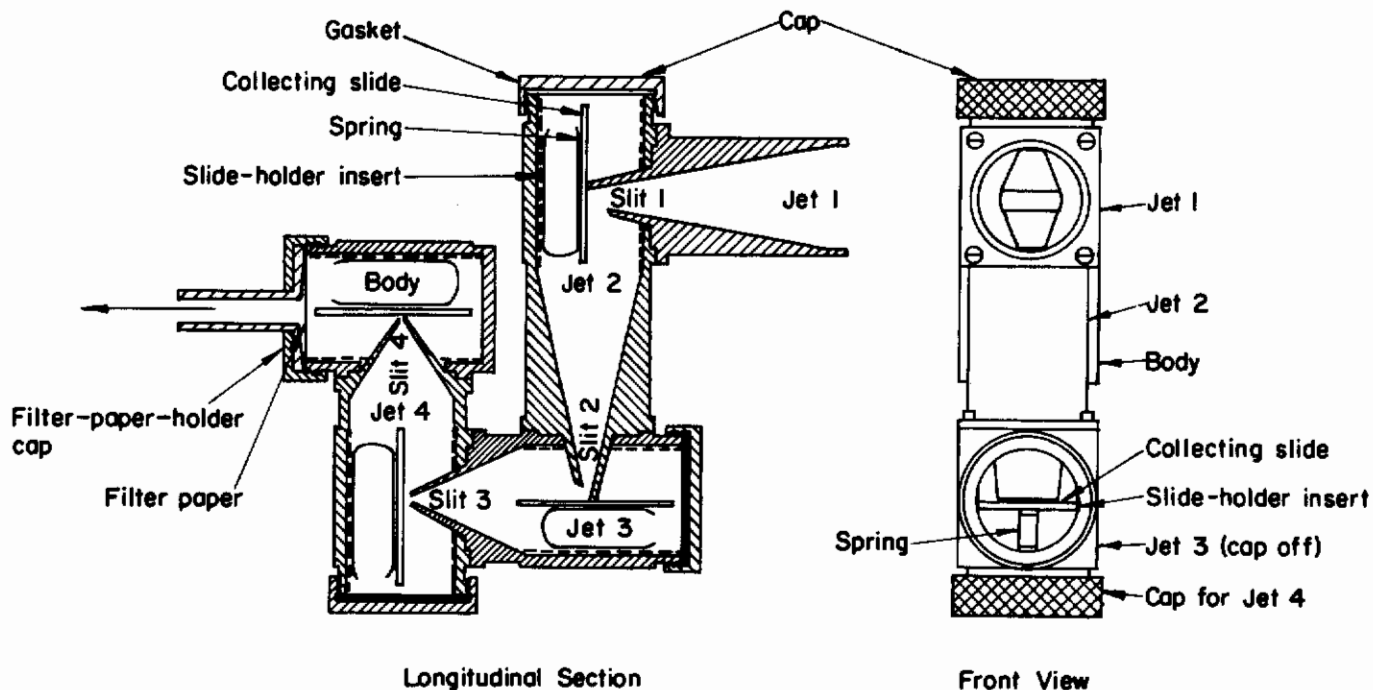


FIGURE 4-17. LASKIN'S MODIFIED CASCADE IMPACTOR
(Laskin)⁽⁴⁻⁵⁷⁾

Figure 4-17 is a drawing of Laskin's modified cascade impactor. The original slit dimensions and internal streamlining of the instrument were patterned after those of the British Cascade Impactor, Figure 4-16, with the exception of Jet 1, which was modified for Laskin's particular conditions. The tapering of the first jet as shown in Figure 4-17 would not be suitable when

sampling the liquid particles of a fuel spray. All parts were machined and interiors were highly polished to minimize internal losses. End losses, representing the portion of the dust distribution that passed through the British instrument, were collected on a filter paper that served as a fifth stage. In this way the entire sample was collected.

Laskin's instrument, as a whole, was of rigid, sturdy construction which would stand the rigors of routine use. It was designed to permit mass production with accuracy limited only by the tolerances of standard machine operation. By modern die-casting methods, exact duplication in large numbers is possible. Uniformity between instruments is desirable, because the calibration constants for one instrument will then be applicable to all others. The procedure for calibrating this instrument for dusts is given in considerable detail by Laskin⁽⁴⁻⁵⁷⁾. For particles of unit density, the mass median diameters for each of the five stages were 13, 5.5, 2.8, 1.9, and 1.2 microns, respectively, from the first to the last stage.

The details of construction of the modified cascade impactor are given in a report by Laskin, Wilson, Lauterbach, Leach, and Falconer⁽⁴⁻⁵⁹⁾.

Battelle Cascade Impactor. Figure 4-18 is an assembly drawing of the Battelle No. 4 cascade impactor now being used at Battelle Memorial Institute by James L. Harp⁽⁴⁻⁶⁰⁾. This impactor consists of six circular jet stages and a seventh filter stage, arranged in tandem fashion. A tandem arrangement was first used by T. Male⁽⁴⁻⁶¹⁾ of the NACA.

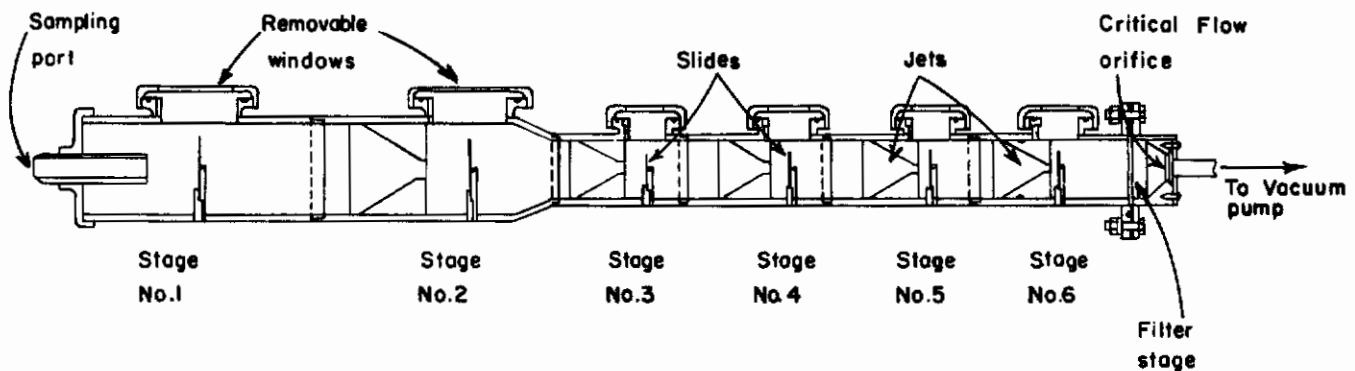


FIGURE 4-18. BATTELLE NO. 4 CASCADE IMPACTOR
(Harp and Pilcher)^(4-53 and 4-60)

The first six stages are designed to cover the size range of 3 to 40 microns. A seventh filter stage removes most of the minus 3 micron material. A vacuum applied at the exit of the impactor draws the sample through the instrument at a fixed rate determined by a critical flow-orifice meter.

The cascade impactor is still being developed at Battelle Memorial Institute, under Air Force sponsorship. It appears promising as a device for accurate measurement of the drop-size distribution of fuel mists having a maximum drop size of about 100 microns.

Cascade Impactor Used for Flight Measurement of Droplet Size. Levine and Klienkecht⁽⁴⁻⁶²⁾ adapted the cascade-impactor method to a study of droplet size of clouds sampled in flight. The air containing the droplets was slowed down from flight speed, by a diffuser, to the inlet-air velocity of the impactor.

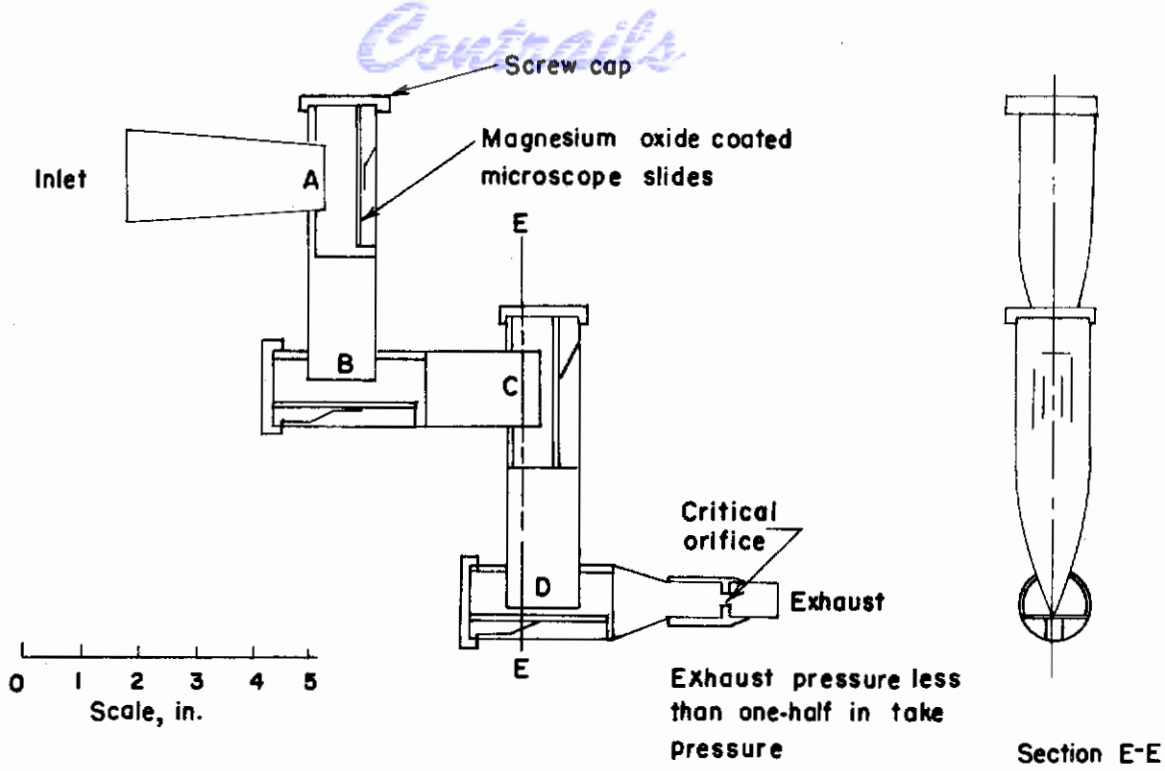


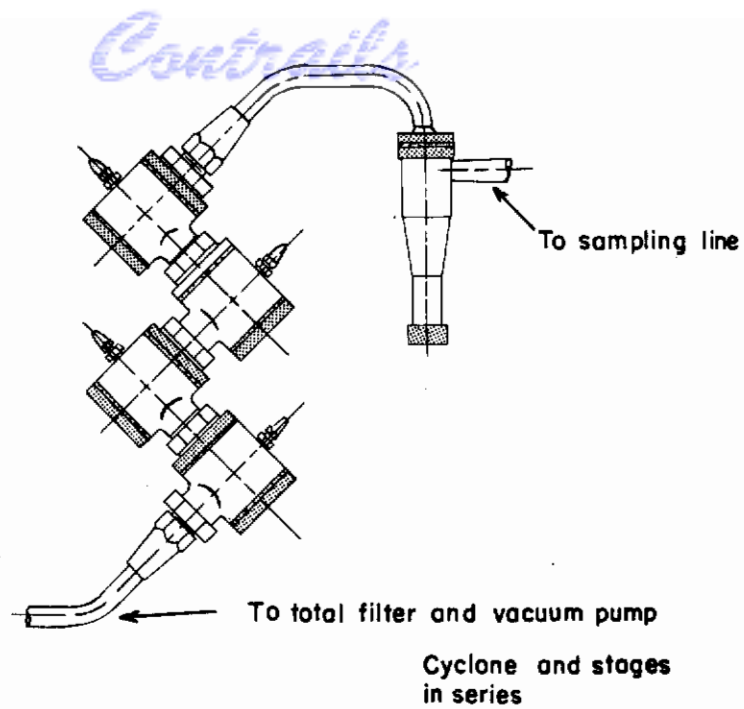
FIGURE 4-19. CASCADE IMPACTOR FOR FLIGHT MEASUREMENT OF DROPLET SIZE
(Levine and Klienknecht)⁽⁴⁻⁶²⁾

Figure 4-19 shows a cross section of the cascade impactor used by Levine and Kleinknecht. It consists of four stages, labeled A, B, C, and D. Air is drawn through the intake by maintaining an exhaust pressure less than one-half the intake pressure. If the size distribution of droplets in the air entering the impactor is narrow, the droplets are caught principally in one or two stages. If most of the droplets are large, they are caught principally on the slides for Jets A and B. Similarly, if small droplets are prevalent, slides for Jets C and D catch most of the droplets. The impactor is suitable for determining drop-size distribution in sprays from nozzles and in natural clouds.

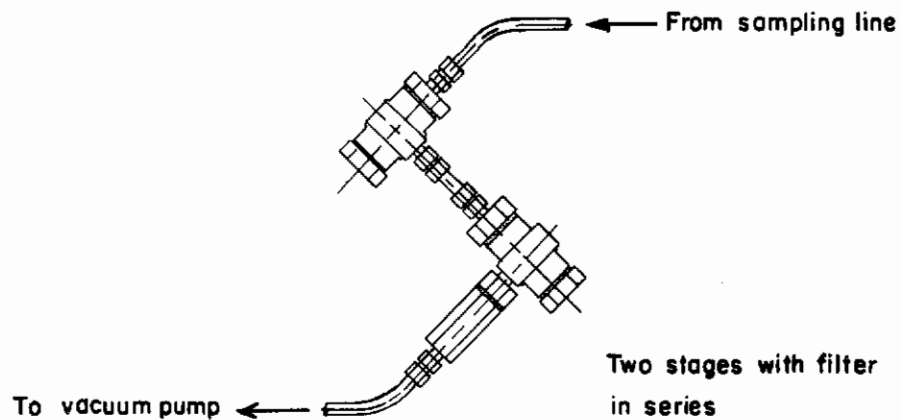
The slides in each stage were coated with a layer of magnesium oxide that was thin compared with the droplet diameter. The thinner coating used by Levine and Klienknecht, compared with that used by May⁽⁴⁻⁵⁴⁾, made it possible to observe impressions made by droplets as small as 4 microns.

Ranz's Cascade Impactor. Ranz and Wong⁽⁴⁻⁶³⁾ designed two types of cascade impactors for the determination of particle size distributions of aerosols. Although these impactors were designed for use with dispersions of particles in sizes of about one micron, the principles involved may be applied to larger sizes of droplets.

Figure 4-20 shows the two impactors in the assembled condition; a detailed description of the component parts is given in the report by Ranz and Wong⁽⁴⁻⁶³⁾. The first type had a 1 2-inch approach-line tube and the second type, which was smaller and more compact, had a 3/8-inch approach-line tube. Rectangular and round jets could be mounted in both types, and the parts were interchangeable, so that several impactors could be mounted in series or in combinations with cyclones and filters. The rectangular jets had cylindrical, convex, inside walls; the round jets had a 60-degree cone as an approach shape. Outside walls of the jets were streamlined at an angle of



Type No.1



Type No.2

FIGURE 4-20. RANZ'S CASCADE IMPACTORS
(Ranz and Wong)⁽⁴⁻⁶³⁾

30 degree, for the first type of impactor, and 45 degrees for the second type, to allow entrainment and to prevent the aerosol stream from spreading before it reached the vicinity of the plate.

The jets were mounted so that the spacing between the jet opening and the impaction plate was from one to three jet widths or diameters. The collectors were microscope slides or flat-bottom glass cups which could be removed from the impactor for analysis. The aerosol particles which escaped impaction were drawn into a filter train which contained two or three separate glass-wool filters.

Theory of Jet Impactors. Ranz and Wong⁽⁴⁻⁶³⁾ developed a theoretical analysis of jet impactors by applying the laws of motion to the movement of the individual particles.

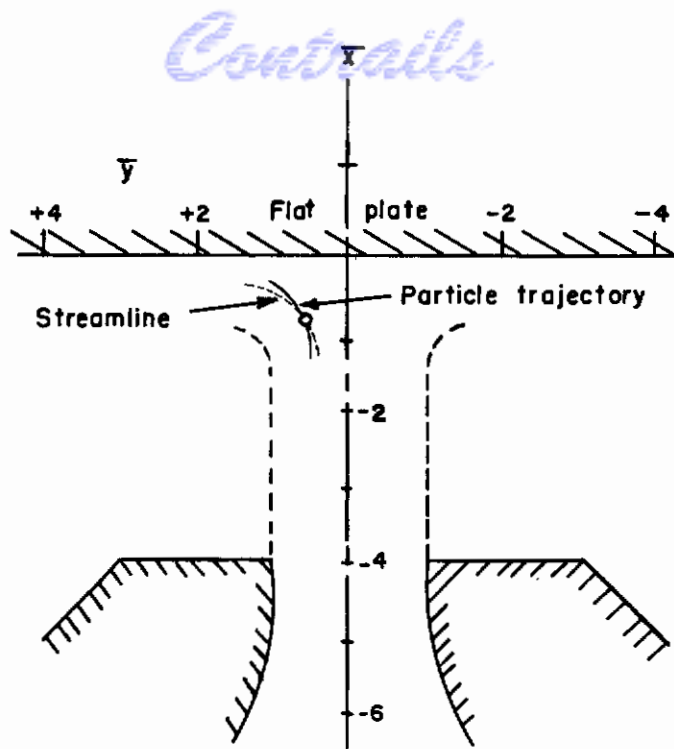


FIGURE 4-21. THEORY OF JET IMPACTORS
(Ranz and Wong) 4-63

Figure 4-21 is a graphical representation of the situation that exists when a jet containing particles moves in a positive x-direction and spreads against a flat plate which is effectively infinite in extent. The particle is subjected to an inertial force which tends to impact it on the surface of the plate. The motion of the particle will not be identical with that of the fluid.

Application of the law of motion to the movement of the particle gives:

$$-\frac{d(\underline{u} - \underline{v})}{z} = d(m\underline{u})/dt$$

where \underline{u} is the velocity of the particle, \underline{v} is the velocity of the air, m is the mass of the particle, and z is the mobility of the particle, which is a function only of the particle diameter and of the physical properties of the fluid.

A small particle will follow the fluid for some distance with \underline{u} equal to \underline{v} . As the plate is approached, \underline{v} changes markedly, to allow the jet to spread, and the particle will follow a trajectory according to the law of motion expressed in the preceding equation. Whether the particle trajectory will reach the surface of the plate depends on: (1) the nearness of its starting point to the axis of flow, (2) the nature of the streamlines along which and across which the particle passes, and (3) the configuration of the flow system.

From a theoretical standpoint, the efficiency of impaction is defined as the ratio of the cross-sectional area of the original aerosol jet from which particles of a given size are removed because their trajectories intersect the surface of the plate to the total cross-sectional area of the jet. All particles which strike the plate are assumed to adhere to its surface, and no particle is assumed to touch the surface unless the trajectory of its center is tangent to or intersects the surface.

Ranz and Wong developed expressions for the efficiency of impaction for simplified flow models of rectangular and round aerosol jets. Their results show that, for a jet operating under a given set of conditions, there is a minimum particle size below which impaction does not occur and a

maximum particle size above which all particles are impacted. Furthermore, the range of particle sizes which are partially impacted is so narrow that an effective separation of particles into two size classes can be accomplished. It is this characteristic which makes the impactor a useful device for determining particle-size distributions.

Problems Related to the Experimental Determination of Drop-Size Distribution

A number of problems arise in the experimental measurement of drop size in addition to the choice of the apparatus to be used. Some of the problems that will be considered here are: (1) the fraction of the area of the slide that should be covered with droplets, (2) automatic scanning devices to reduce the amount of time and labor involved in particle-size counting, (3) collection efficiency, (4) flattening coefficients and impression coefficients, (5) microscopic techniques, and (6) critical impact velocities.

Fraction of Slide Area That Should Be Covered With Droplets. A problem common to all methods of measuring drop-size distribution based on counting and measuring droplets collected on slides is, what fraction of the slide area should be covered? If too many droplets are collected, the probability of error owing to coalescence will be high, and if too few droplets are collected, the sample may not be sufficiently representative of the spray.

Fulton, Nelson, and Yoemans⁽⁴⁻⁶⁴⁾ state that a satisfactory slide for particle-size count should have about 1/500 of its surface covered. This appears unnecessarily low, in view of Armitage's⁽⁴⁻⁶⁵⁾ study of the overlap problem arising in particle counting.

Armitage expressed the probability of overlap in terms of a mean clump size \bar{m} , defined as

$$\bar{m} = \frac{N}{C} = \frac{\text{number of particles falling}}{\text{number of clumps}}$$

The magnitude of the clump factor is determined solely by the ratio of the area of the particles to the area of the plate, and is expressed as

$$\bar{m} = \frac{4\psi}{1 - e^{-4\psi}} = 1 + 2\psi + \dots$$

where $\psi = \pi Nd^2/4A$.

In the above expression, ψ is the ratio of the area of the particles to the area of the plate, d is the diameter of the particles, and A is the area of the plate or slide.

Assuming that the area of the particles is one per cent of the area of the slide, the mean clump size would be 1.02. This would not introduce a serious error in the average drop size, and would permit the counting of five times as many drops per slide as when only 1/500, or 0.2 per cent, of the area of the slide is covered. Purely from the standpoint of ease of counting and measurement, the 0.2 per cent coverage recommended by Fulton et al. may be preferred, but from the standpoint of droplet overlap, a one per cent coverage does not appear excessive.

Automatic Scanning Devices for Measuring Drop-Size Distribution. Three devices are described in the literature for automatically counting from a photomicrograph, the number of droplet images within a given size range. The required apparatus is complicated, but much time can be saved if a large number of spray samples are to be analyzed.

Rupe's Differentiating Droplet Counter. Rupe⁽⁴⁻¹⁹⁾ pointed out that it would have been an endless task to evaluate manually the large quantity of data recorded during his investigation of spray characteristics. Consequently, he developed a semi-automatic counter that could count and separate the drops into size groups.

The three major components that comprise the counter are (1) a scanning device, (2) an optical projection system, and (3) six light-sensitive pickups mounted in three indexing heads. The equipment is complex; reference is made to Rupe's report⁽⁴⁻¹⁹⁾ for a detailed description.

The apparatus has an accuracy of 1 to 2 per cent. A good indication of the counter's reliability was the fact that size-frequency curves could be duplicated by subsequent counting of the same negatives, even though the actual counts were different.

To illustrate the savings in time, the entire set of data for one nozzle was obtained by one operator in about 5 days. By manual methods, the time of two workers for six months would have been required to obtain the corresponding data.

A more recent report by Rupe⁽⁴⁻²⁰⁾ describes a second instrument in which the electronic circuitry was changed considerably in an attempt to obtain a simpler circuit with more stable and reliable operation.

Marshall's Scanning Device. Adler, Mark, Marshall, and Parent⁽⁴⁻⁶⁶⁾ developed an elaborate device that counts and classifies spray droplets by optically scanning a photographic negative of transparent images of droplets of a sample of spray. The negatives are mounted on a rotating drum and are projected by an optical system and focused at a plane of a mask in front of a photomultiplier tube.

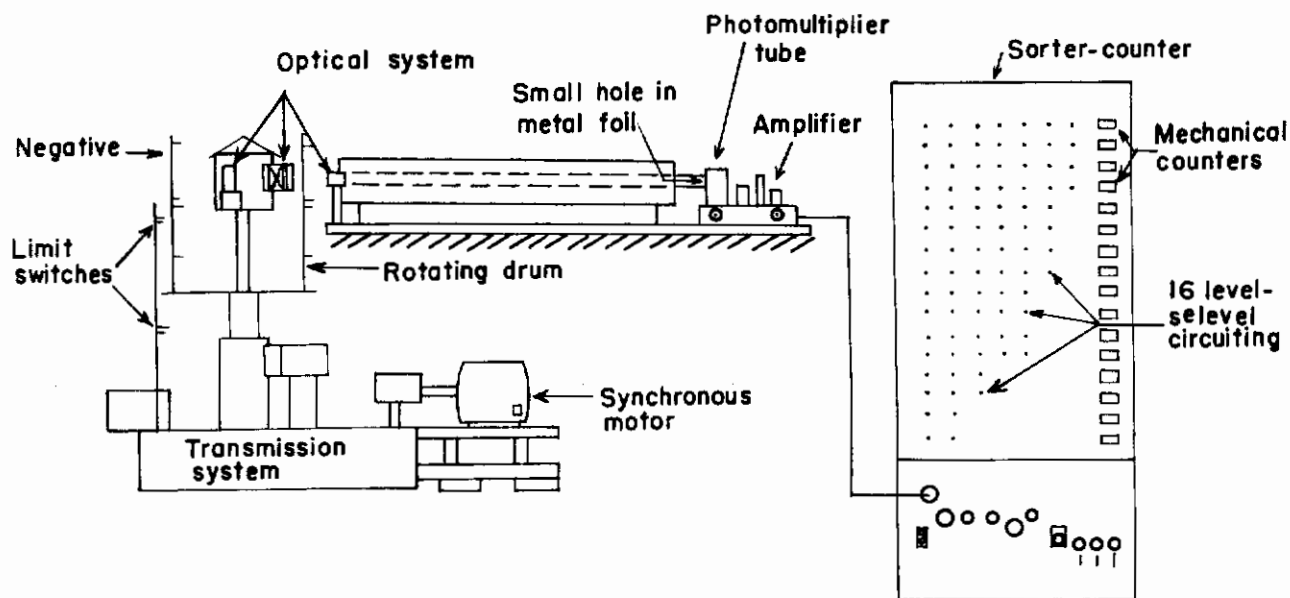


FIGURE 4-22. ELECTRONIC DROP SIZE DISTRIBUTION ANALYZER
(Adler, Mark, Marshall and Parent)⁴⁻⁶⁶

Figure 4-22 is a diagrammatic sketch of the scanning drum and electronic sorter-counter. A small opening is placed in the center of the metal-foil mask in front of the photomultiplier tube. As the images of the drops rotate past this opening, they are simultaneously advanced a small distance at each revolution by the drum. In this manner, the phototube receives a series of light pulses of various durations corresponding to the chords of various lengths created by the passage of each drop image in successive positions across the opening. The light pulses are converted into electrical pulses and are fed into electronic sorter-counter circuits which classify the chords into 15 size classes. A statistical treatment of this chord distribution is then made to give

drop-size distribution. Tables of coefficients were computed to permit rapid conversion of the chord distribution to drop-size distribution. The results of the tests on actual spray samples and on special test negatives demonstrated that Marshall's device could rapidly count and classify drops with acceptable accuracy. The scanning rate could be set as high as 10,000 drops in seven minutes at maximum drum speed.

The advantages of the instrument are: (1) the human element is removed from the counting process, (2) all drops in a run may be scanned, (3) drops may be simultaneously counted and classified into 15 size classes, and (4) counting is about 100 times faster than by manual methods.

The principal limitation of Marshall's analyzer is that it is restricted to the analysis of transparent images on photographic negatives, which requires that the spray be sampled by collection of droplets in cells or on surface-treated slides and then photographed. Successful operation of the instrument depends largely on the preparation of satisfactory negatives.

Pigford's Automatic Drop-Size Counter. Pigford⁽⁴⁻⁶⁷⁾ developed an automatically operated optical device which can scan a transparent photograph of spray droplets and determine the size-frequency curve.

The principal part of the apparatus is a 6-in. -diameter by 10-in. -long glass cylinder around which the photographic negatives are wrapped. This cylinder can be rotated and simultaneously advanced along its axis, so that a parallel light beam of rectangular cross section can be made to traverse a spiral path on the surface of the cylinder. If it is not interrupted by a drop image, the beam of light enters a small right-angle prism located inside the cylinder and passes out from the open end of the cylinder to enter a photoelectric cell. The photocell is connected to an amplifier that activates a self-quenching thyatron circuit which allows a condenser to discharge through a magnetic counter each time the beam is totally obscured. The size-frequency curve is computed statistically from the influence of beam width on the number of counts registered.

Pigford encountered trouble in the operation of the apparatus owing to the tendency of the thyatron circuit to oscillate and give spurious counts. Recently, Skalamera⁽⁴⁻⁷⁰⁾ employed an improved electronic circuit which eliminates the spurious counts.

British Methods for Automatic Counting. Walton⁽⁴⁻⁶⁸⁾ gives an account of the widespread effort being made in England to meet the need for an apparatus to relieve human observers of the tedious work of counting and sizing microscopic particles, and to improve the consistency of results.

Four principles of operation are described:

(1) The "double-scan" method whereby the number of particles cutting the edges of the scan track may be estimated and allowed for by comparing the counts obtained from two scans with tracks of different widths. These two measurements may be made independently by scanning the specimen twice with apertures of different widths, or simultaneously by two such scanning apertures placed side by side.

(2) The "intercept length" method whereby the numbers and lengths of the intercepts of the scanning lines across the particles are recorded. From this information the aggregate area and perimeter of the particles may be obtained. The number and size distribution can be calculated with some difficulty if the particle shape is known.

(3) The "guard spot" method whereby two scanning spots are provided, separated transversely to the direction of motion, one of which controls the counting of the other. The absence of the control signal indicates that the lower or upper edge of a scanned particle has been reached and the particle is then recorded. Its size is not given, although a lower limit to the detection-level may be set. The size distribution may be obtained by repeating the measurements at each of a series of such limits.

(4) The "memory" or "sequential signal" method whereby repeat signals from the same particle in successive scan lines are characterized by their occurrence in a regular sequence at corresponding times or positions. Such sequences of signals are grouped or counted as single particles at the end of the sequence, the size of the particles being obtained from the number of signals in the sequence or from the intercept lengths.

Walton feels confident that automatic counting apparatus to suit many requirements will become available during the next few years.

The BCURA⁽⁴⁻⁶⁹⁾ has developed a method based on repeated counting with scanning apertures of different sizes. An instrument using a "flying spot" technique, similar to television scanning, for surveying the field of view has been investigated by BCURA.

Battelle Semiautomatic Counter. A semiautomatic particle-size counter has been developed by H. P. Munger and J. E. Yocom of the Battelle Memorial Institute. This equipment consists of (1) a projector-enlarger with ground glass for viewing the photomicrographs of aerosols and (2) a special caliper and electrical system for recording the number of drops of each size range. The movable jaw of the calipers determines the position of an electrical pickup on a segmented commutator consisting of conductive segments that correspond to the size classes into which the dispersion is to be divided. Each segment is wired to an electrically operated counter. Each drop or particle must be measured, but the semiautomatic procedure reduces considerably the amount of time and work involved.

Attention is called to the important fact that the final accuracy of the measurement of drop-size distribution is limited by the accuracy with which the spray is sampled, and no correction can be made by automatic scanning devices to compensate for poor sampling.

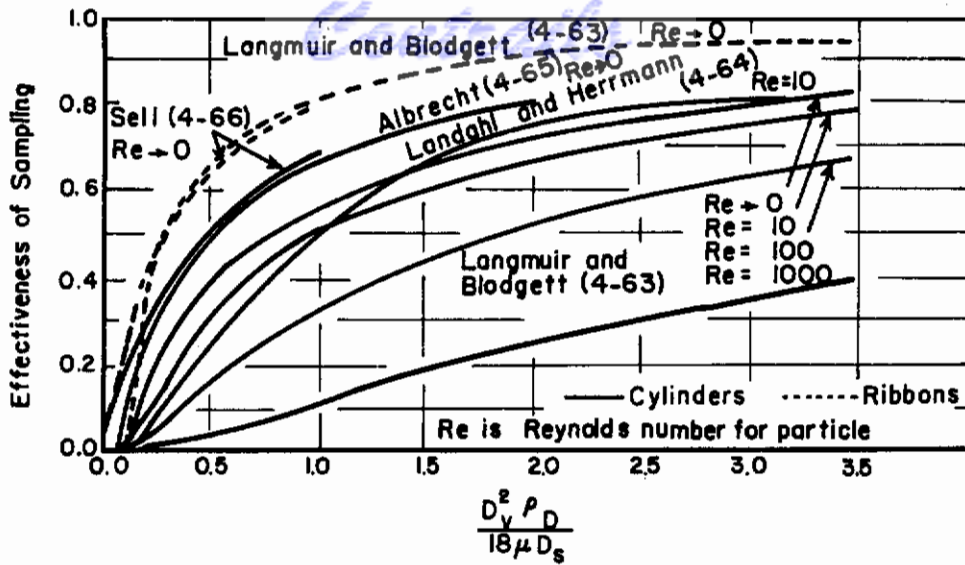
Collection Efficiency. All methods of measuring drop-size distribution that require collection of droplets on a slide or in a cell are susceptible to error owing to discrimination against the smaller size particles. The smallest droplets tend to follow the flow lines around the sampler, rather than collect on the sampler.

Geist, York, and Brown⁽⁴⁻⁴⁷⁾ delineate the problem of sampling bias by pointing out that if all suspended particles maintained their position in the flow lines during deflection, none would be intercepted by a sampler that removed none of the fluid in which the droplets were dispersed. On the other hand, if all the droplets had sufficient inertia to leave their flow lines and to continue in straight paths, the sampler would intercept all droplets whose paths projected into it and collection would be 100 per cent efficient. Actual operation lies between these extremes; larger particles are intercepted and smaller particles tend to follow the flow lines around the sampler. Flow lines directed toward the center of the sampler have a large portion of all sizes of their suspended particles intercepted; flow lines directed toward the edge of the sampler carry all except the largest particles around the sampler.

The effectiveness of sampling increases as the velocity and size of the particles increase and as the width of the sampler decreases.

Figure 4-23 shows the results of several investigations recalculated to a common basis. The ordinate is the calculated effectiveness of sampling. The abscissa is a dimensionless number, defined as the ratio of the maximum horizontal distance traveled by the particle, if injected horizontally into the nonflowing suspension medium with a velocity equal to that of the suspension relative to the sampler, to the distance across the sampler. This abscissa, calculated from Stokes' law, was common to all investigators. The parameter is the Reynolds number.

Although there is a disagreement in the quantitative results of the calculations by the various investigators, there is sufficient qualitative agreement to estimate some limitations of spray-sampling devices.



D = diameter of drop, cm
 v = velocity of carrier gas stream, cm per sec
 ρ_D = density of drop, grams per cc
 μ = viscosity of carrier gas stream, grams per cm-sec
 D_s = controlling distance across sampler, cm

FIGURE 4-23. COMPARISON OF COLLECTION EFFECTIVENESS CALCULATED BY SEVERAL INVESTIGATORS (Geist, York, and Brown)(4-47)

On the basis of the method of Langmuir and Blodgett(4-71), the effectivenesses of a 1-in. ribbon (microscopic slide), a 16-gage wire, and a 24-gage wire were calculated for water drops moving in air.

Figures 4-24, 4-25, and 4-26 show the results. To illustrate the use of these figures, assume a particle velocity of 32 ft per sec and an effectiveness of at least 90 per cent. A 1-inch

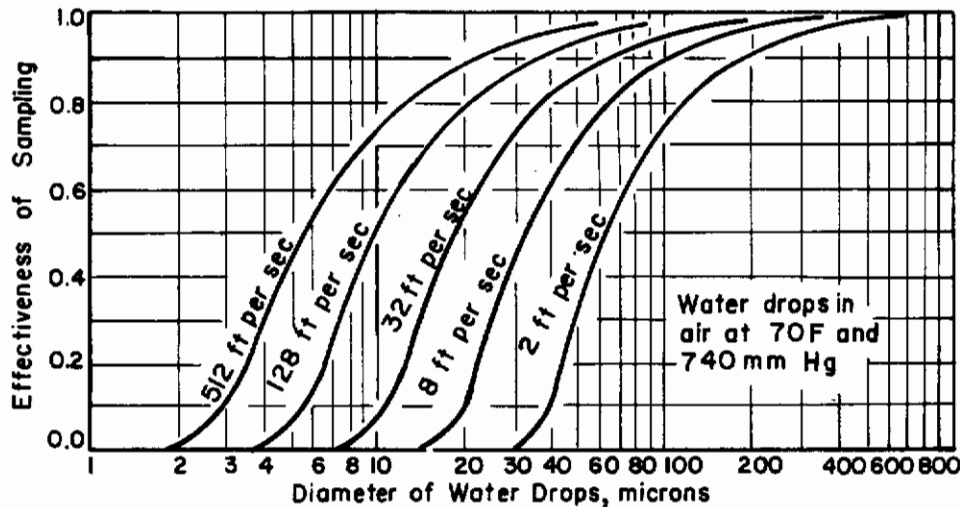


FIGURE 4-24. COLLECTION EFFECTIVENESS OF ONE-INCH MICROSCOPE SLIDE (Geist, York, and Brown)(4-47)

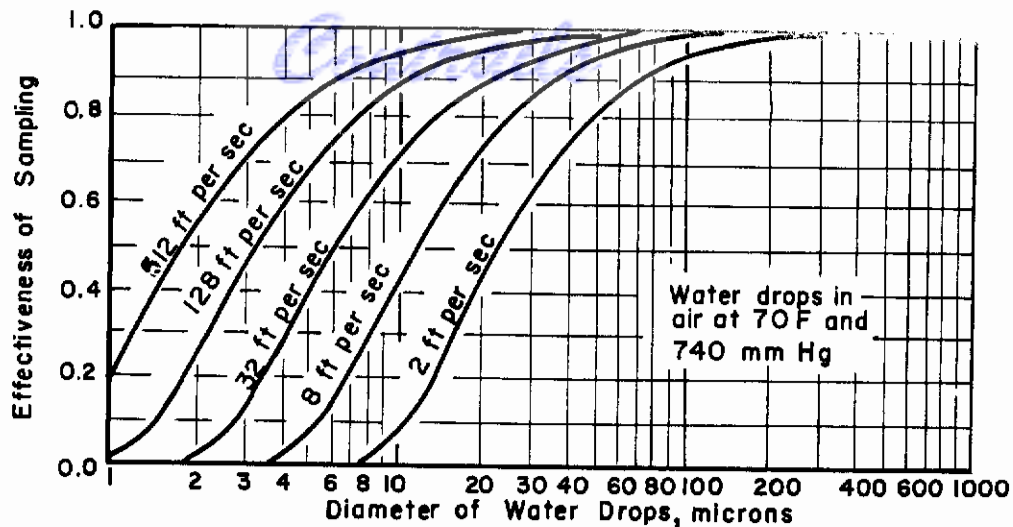


FIGURE 4-25. COLLECTION EFFECTIVENESS OF 16-GAGE WIRE (1295 MICRONS)

(Geist, York, and Brown)(4-47)

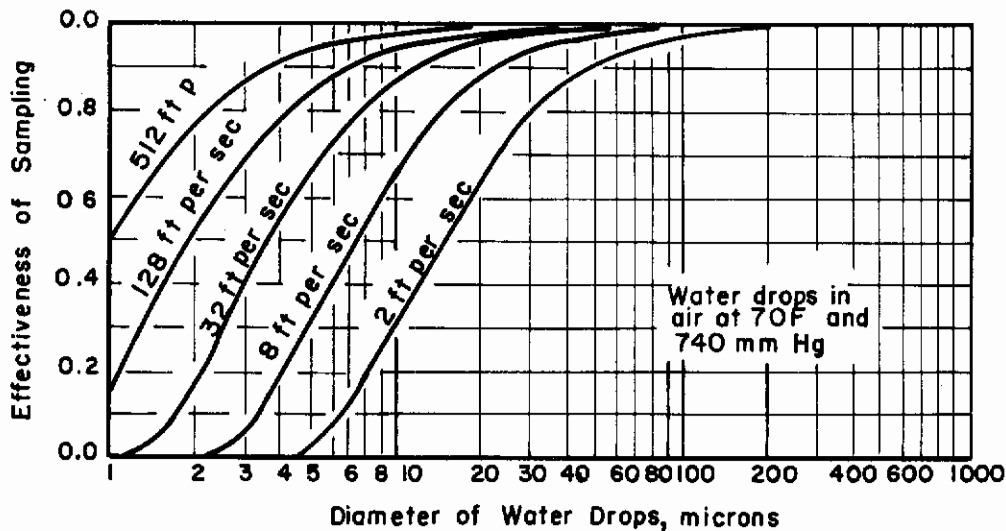


FIGURE 4-26. COLLECTION EFFECTIVENESS OF 24-GAGE WIRE (511 MICRONS)

(Geist, York, and Brown)(4-47)

slide would be an effective interceptor for particles larger than 62 microns, a 16-gage wire (1295 microns) would be effective for particles larger than 20 microns, and a 24-gage wire (511 microns) would be effective for particles larger than 11.5 microns. At a velocity of 32 ft per sec, a 1-inch slide would intercept no particles smaller than 7 microns, a 16-inch wire, no particles smaller than 1.5 microns, and a 24-gage wire, no particle smaller than 1 micron.

These considerations indicate that data on size distribution obtained with large samplers at low velocities are to be questioned for particle sizes smaller than 50 microns.

Houghton and Radford⁽⁴⁻⁸⁾, during their investigation of the particle size of natural fogs, encountered difficulty in obtaining a sufficiently representative sample of fogs having a predominant particle diameter less than 20 microns. To minimize the sampling error, 5-mm-square slides were substituted for the standard 25-mm-square slides. Again, their results could not be considered to be quantitative, but it appeared that more highly representative samples were obtained

on the small slides exposed by impact for drops down to about 5 microns in diameter. It was definitely demonstrated that the 5-mm slides obtained a much truer sample of the fog than did the 25-mm slides.

May⁽⁴⁻⁵⁴⁾ made a theoretical study of the collection efficiency of a stage of a cascade impactor. Dimensional analysis of the system comprising a jet of air issuing from a slot and impacting on a plane surface suggested to May that for geometrically similar systems the condition for dynamical similarity and, therefore, for equal impaction efficiency is given by the expression:

$$\rho D^2 V / \eta L = \text{const.} ,$$

where ρ is the density of the particle (assumed large with respect to air), D is the diameter of the particle (if spherical), V is the velocity of the jet, η is the viscosity of air, and L is a characteristic length of the system (the width of the slot for May's cascade impactor).

Impaction efficiency is taken as the ratio

$$\frac{\text{number of particles hitting plate}}{\text{number of particles entering jet}}$$

It is assumed that all particles hitting the plate, or slide, are retained by it.

Reynolds number was neglected in the above expression; however, in May's cascade impactor, the Reynolds number does not exceed 1400 at any jet, so that streamline flow can be assumed at all jets.

Figure 4-27 shows a plot of experimentally determined mean values of I against the impaction efficiency, where I is a constant for any given impaction efficiency.

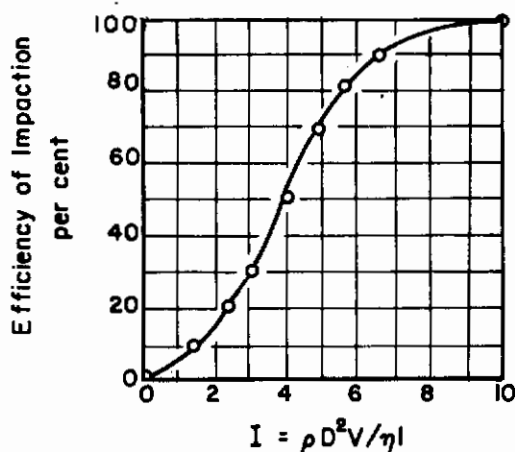


FIGURE 4-27. CURVE FOR ESTIMATING IMPACTION EFFICIENCY OF JETS
(May)⁽⁴⁻⁵⁴⁾

This curve should provide a valuable tool for predicting the performance of any impaction system within the limits prescribed by May. It will also indicate the performance for different sampling rates in the same cascade impactor and indicate the effect of a change in the density of the particle or a change in the viscosity of the air. Laskin⁽⁴⁻⁵⁷⁾ applied May's curve for calculating the expected size counts for the four stages of his cascade impactor (Figure 4-16) and obtained excellent agreement with the experimentally determined values.

May's expression does not take into consideration the ratio of the jet-slide clearance to L , which ratio must be a significant factor influencing the performance of an impactor stage.

Therefore, too much weight should not be given to Figure 4-27 for applications where the ratio of clearance to characteristic length, \underline{L} , of the jet is greatly different from that of May's impactor.

Brun, Demon, and Vasseur⁽⁴⁻⁷⁵⁾ made theoretical calculations of the capture coefficient (ratio of given-sized drops captured to those passed) as a function of air-stream speed, plate width, and drop size. The capture coefficient was found to be higher the narrower the plate, and the coefficient approached unity as the width of the plate approached drop dimensions.

All of these investigations emphasize the importance of using narrow slides wherever drop-lets smaller than 50 microns are involved. The efficiency of collection under a given set of conditions can be predicted with considerable accuracy.

Flattening Coefficient and Impression Coefficient. Another important problem that is encountered when drops are collected on a glass slide is the determination of the coefficient by which the diameters of the flattened drops must be multiplied to obtain the original diameter of the spherical drop. A similar problem exists for the impressions made by drops collected on slides coated with a fragile layer of material, as in the case of MgO-coated slides. For samples collected on glass slides, the term "flattening coefficient" is generally used, and for coated slides, the term "impression coefficient" may be used.

Flattening Coefficient. Houghton and Radford⁽⁴⁻⁸⁾ determined the flattening coefficient by two methods: (1) the height and diameter of individual flattened drops, viewed from the side, was measured; (2) in the second method, an average value of the flattening coefficient was obtained by determining the total weight of a number of flattened drops resting on a slide and then measuring the diameter of the individual drops. From numerous measurements, Houghton and Radford found that the flattening coefficient for water drops resting on a baseline surface is 0.80 ± 0.04 .

May⁽⁴⁻⁵⁴⁾ determined the size of the original spherical drop by measuring the diameter and focal length of the plano-convex liquid lens formed by the flattened drop. The microscope used for the measurement must have a micrometer drum on the fine-focusing adjustment, so that vertical movement of the microscope tube can be estimated in microns.

The original drop diameter ($2r$) can be obtained from the lens diameter ($2A$) and from f' , where f' is the distance between the glass surface and the focal point of the lens. The method applies where the focal point of the lens is below the coverslip, if one has been used. The angle of contact of the liquid, θ , is assumed below 60 degrees, and the surface of the lens is taken to be spherical. May points out that exceptions to these conditions seldom arise in practice.

Let R be the radius of curvature of the liquid lens. From the geometry of the system, it can be shown that

$$\frac{4}{3} \pi r^3 = \frac{\pi R^3}{3} \left[2 - \left(2 + \frac{A^2}{R^2} \right) \sqrt{\left(1 - \frac{A^2}{R^2} \right)} \right].$$

Hence,

$$\frac{r}{R} = \frac{1}{2^{1/3}} \left[1 - \left(1 + \frac{A^2}{2R^2} \right) \sqrt{\left(1 - \frac{A^2}{R^2} \right)} \right]^{1/3} = \psi \frac{A}{R},$$

so that

$$\frac{r}{R} = \frac{R}{A} \psi \left(\frac{A}{R} \right) = \psi \left(\frac{A}{R} \right) \csc \theta.$$

Now, $R = (f' - h)(\mu - 1)$, where h is the thickness of the lens and μ is the index of refraction of the liquid forming the lens. Also, $h = R(1 - \cos \theta)$; hence

$$R = f' \frac{\mu - 1}{1 + (\mu - 1)(1 - \cos \theta)},$$

and

$$\frac{f'}{2R} = \frac{1}{2(\mu - 1)} + \frac{(1 - \cos \theta)}{2}$$

but

$$\frac{f'}{2A} = \frac{f'}{2R} \frac{R}{A} = \frac{f'}{2R \sin \theta}$$

so that

$$\frac{f'}{2A} = \frac{1}{2(\mu - 1) \sin \theta} + 1/2 \tan 1/2 \theta$$

A graphical solution has been worked out by May and is much more convenient to use than the analytical solution.

Figure 4-28 shows the curves for computing original spherical drop diameter from lens diameter. The angle of contact, θ , may be obtained for any likely value of $f'/2A$ for different values of μ . Having obtained the angle of contact θ , the dotted curve in Figure 4-28 makes it possible to evaluate the factor r/A , which is the flattening coefficient.

$$r/A = \frac{\text{Radius of Spherical Drop}}{\text{Radius of Lens}}$$

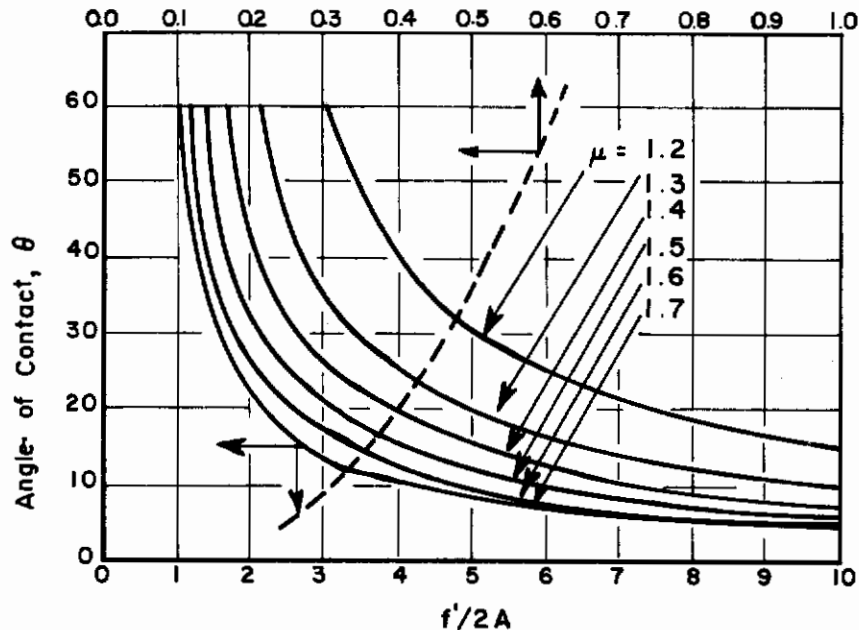


FIGURE 4-28. CURVES FOR COMPUTING ORIGINAL DROP DIAMETER FROM LENS DIAMETER (May)(4-54)

Fuks(4-76) determined the droplet diameter, d , from the lens diameter, D , assuming sphericity of the lens, by use of the formula

$$\frac{d}{D} = \sqrt[3]{\frac{2 + \cos^3 \theta - 3 \cos \theta}{4 \sin^3 \theta}}$$

Figure 4-29 shows the relation of flattening coefficient to contact angle corresponding to the above equation. The curve gives a relation that is in agreement with the dotted curve of Figure 4-28.

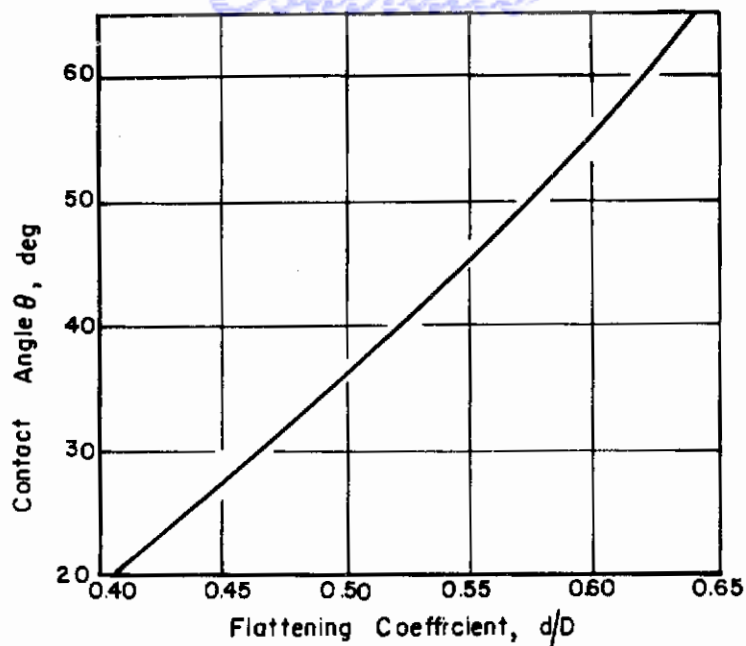


FIGURE 4-29. RELATION BETWEEN FLATTENING COEFFICIENT AND CONTACT ANGLE

(Fuks)⁽⁴⁻⁷⁶⁾

Fuks measured the contact angle with the aid of a microscope mounted in a horizontal position and equipped with a special eyepiece to facilitate the measurement of the angle between the surface of the slide and a line tangent to the base of the lens.

Figure 4-30 is a sketch of a flattened droplet as viewed through a horizontal microscope. The magnitude of the contact angle was practically independent of the size of the lenses, so that measurements were made of large lenses having diameters of 1 to 2 mm to increase precision. For oils resting on a slide coated with a thin layer of basic zinc stearate, the flattening coefficient was almost constant and was equal to about 0.55.

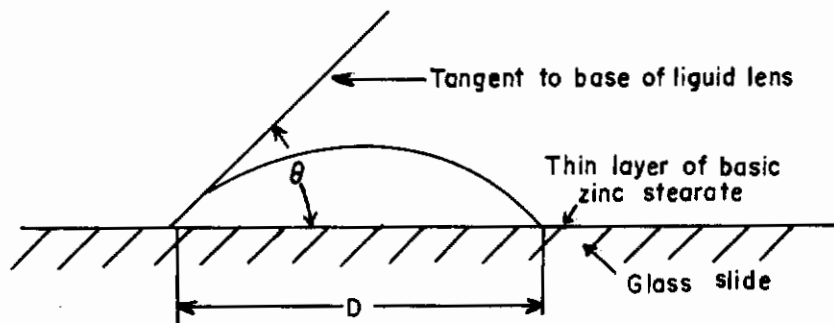


FIGURE 4-30. CONTACT ANGLE, θ , FOR A FLATTENED OIL DROP

Levine and Kleinknecht⁽⁴⁻⁶²⁾ used a simplification of May's method⁽⁴⁻⁵⁴⁾ to determine the flattening coefficient of dibutyl phthalate droplets on clear glass slides. From the focal length, f , of the droplet lens and the index of refraction, n , of dibutyl phthalate, the radius of curvature, r , of the lens was determined from the thin-lens equation $r = (n - 1) f$. The height of the lens, h , is related to r and the lens diameter, $2a$, by

Contrails

$$h = r \left(1 - \sqrt{1 - \frac{a^2}{r^2}} \right) ,$$

and the volume, v , of the lens is

$$v = \frac{1}{6} \pi h (h^2 + 3a^2) .$$

The radius, R , of the spherical droplet before impaction can then be obtained from

$$R = \sqrt[3]{\frac{3v}{4\pi}} .$$

Figure 4-31 shows the plot of actual spherical diameter against the measured flattened diameter for dibutyl phthalate droplets. The curve was based on measurements of the focal lengths of 37 droplet lenses which ranged in diameter from 151 to 8.7 microns.

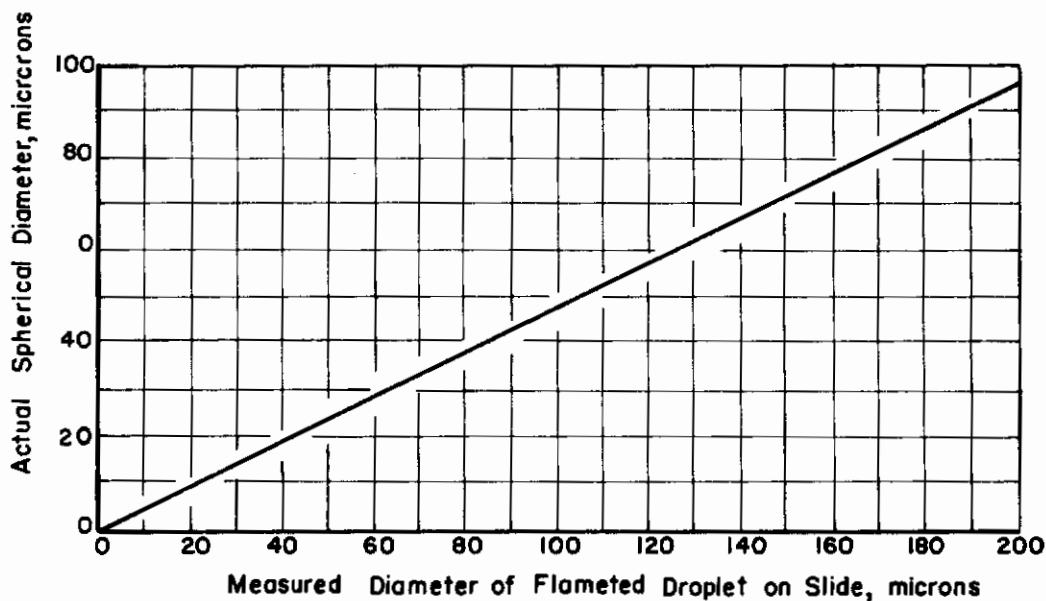


FIGURE 4-31. ACTUAL SPHERICAL DIAMETER AGAINST MEASURED FLATTENED DIAMETER FOR DIBUTYL PHTHALATE DROPLETS
(Levine and Kleinknecht)⁽⁴⁻⁶²⁾

The flattening coefficient is seen to range from 0.45 to 0.48 for dibutyl phthalate droplets having actual spherical diameters of 20 to 100 microns. It is possible, however, that the magnitude of the flattening coefficient will change when the condition of the surface of the glass slide is changed by a variation in the procedure for cleansing the slides. Flattening of the drop results from a balance between gravitational and surface-tension forces, and the latter force will depend upon the condition of the surface of the glass slide. It is, therefore, advisable to determine the flattening coefficient for the specific experimental conditions employed.

Impression Coefficient. Levine and Kleinknecht⁽⁴⁻⁶²⁾ also determined the ratio of the actual spherical diameter to the diameter of the impression made in a thin layer of magnesium oxide. The average value of the impression coefficient for liquids of unit density was about 0.71.

May⁽⁴⁻⁷⁷⁾ made a complete calibration of the method of measuring droplets by the MgO method. He found that, for a size range of from 200 to 20 microns and a wide range of liquids and impact velocities, the ratio of true drop size to impression size was constant at 0.86. The impression coefficient decreased to about 0.72 for 10-micron droplets. Below 10 microns, the magnesium oxide method is of little value, owing to the increasing effect of the grain size, although droplets down to 5 microns, and perhaps smaller ones, can leave an impression at sufficiently high impact velocities.

The results of Levine and Kleinknecht⁽⁴⁻⁶²⁾ and of May⁽⁴⁻⁷⁷⁾, for MgO impression coefficients, are in good agreement for droplets of about 10-micron diameter, namely, 0.71 and 0.72, respectively.

It is of interest to note that K. R. May⁽⁴⁻⁷⁸⁾ developed a magnesium-ribbon "gun" which greatly facilitates the coating of surfaces with MgO produced by burning a 1/8-in. ribbon under the glass slide at such a distance that the tip of the flame just fails to reach the glass.

Stoker⁽⁴⁻⁷⁹⁾ derived a criterion for relating spherical-droplet diameter to the diameter of the track or impression left in a thin layer of soot on which the droplet was collected. He made the assumption that the only significant forces brought into play during the impact are the inertia forces and the forces due to the surface tension of the droplet, and that forces due to viscosity, gravity, and compressibility are of negligible importance. Stoker shows that Weber's number, $\rho d v^2 / \sigma$, is a criterion of dynamical similarity for deformation of the droplet during impact, and that the diameter of the droplet, d , can be determined by the equation

$$\frac{d'}{d} = 0.77 \left(\frac{\rho d v^2}{\sigma} \right)^{1/5},$$

which may be expressed more conveniently as:

$$d = 1.25 \frac{d'}{(\rho d' v^2 / \sigma)^{1/6}},$$

where d' is the track diameter of the droplet, ρ is the density of the droplet, v is the impingement velocity of the droplet, and σ is the surface tension of the droplet.

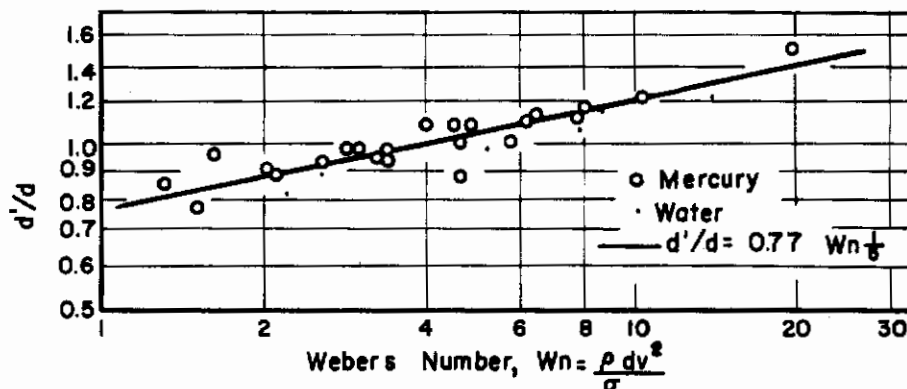


FIGURE 4-32. EXPERIMENTAL RELATIONSHIP BETWEEN WEBER'S NUMBER AND THE RATIO OF TRACK DIAMETER TO DROPLET DIAMETER

(Stoker)⁽⁴⁻⁷⁹⁾

Figure 4-32 shows the experimental relation between the ratio of track diameter to droplet diameter and Weber's number, as determined by Stoker. The experimental data were obtained by allowing droplets of mercury and droplets of water of known diameters to fall from various measured heights onto a soot-coated glass surface and observing the tracks under a microscope. The velocity of impact was taken as the free-fall velocity.

It is apparent from the graph that if Weber's number is about four, the track diameter is equal to the droplet diameter. This would occur, for example, if a water droplet, 5 microns in diameter, struck the coated plate with a velocity of approximately 25 fps.

It is also apparent from the graph that the diameter of the spherical droplet may be either larger or smaller than the diameter of the track or impression. This relation is not in accord with the findings of May⁽⁴⁻⁷⁷⁾, who reported that the ratio of drop size to MgO impression size was constant at 0.86 for droplets larger than 20 microns, and was independent of liquid density and of impact velocity.

Microscopic Techniques. Space will not permit a detailed discussion of microscopic techniques that may be used in the study of drop-size distribution. However, attention will be directed toward a few points of special interest.

Fairs⁽⁴⁻⁸⁰⁾ points out that apart from errors in sampling, the main inaccuracies in particle-size analysis are due to: (1) the uneven dispersion of the sample on the slide, (2) the sizing of an insufficient number of particles, and (3) an inaccurate estimate of the size of nonspherical particles. The resolving power of the microscope lens and the type of light used are important, especially where small particles are concerned. Sodium-vapor illumination greatly improves visibility. Fairs recommended that a special graticule be inserted in the focal plane of the microscope eyepiece for the sizing of particles. Size intervals on Fair's graticule (except for the two lowest) were arranged in a $\sqrt{2}$ progression.

Golitzine⁽⁴⁻²¹⁾ described the apparatus that he used for taking photomicrographs of water droplets. The setup consisted essentially of: (1) a Carl Zeiss 20X microscope, (2) a Leica sliding-focusing copying attachment with a 145-mm length of extension tubing, (3) a Leica camera, without lens, (4) an E. Leitz "Ortholux" lamp housing with 500-watt, 6-amp bulb which transmits light through the droplet sample to the camera, and (5) an E. Leitz, Type RT1, 120/6-volt transformer, 6-amp capacity. Excellent results were obtained.

Brown⁽⁴⁻⁸¹⁾ gives considerable information on microscopic procedures for measuring the size of small particles. The size of the smallest particle determined by the light-field counting method was about 1 micron, and the size of the particles determined by the dark-field counting method was as small as 0.28 micron.

Reference should be made to standard texts on microscopy for more complete general information on microscopic techniques.

Critical Impact Velocity. Rupe⁽⁴⁻⁸²⁾ points out that, in the study of drop-size distribution by the oil-immersion method, droplets of various sizes, traveling at appreciable velocities, must retain their identity as discrete particles while penetrating an air-liquid interface and coming to rest within a collecting cell. Therefore, in order to establish the validity of the collected sample, it was necessary to investigate the possibility of droplet breakup at the point of impact on the oil-air interface. A similar problem must surely exist for the collection of droplets on glass slides or on slides coated with MgO or soot.

Rupe found that, over the range of droplet diameters studied, the critical impact velocity was inversely proportional to the droplet diameter. Consequently, the sampling of water sprays by the kerosine-immersion method⁽⁴⁻¹⁹⁾ is limited by the critical impact velocity.

Figure 4-33 shows the critical impact velocities of water droplets penetrating kerosine-air interface.

Since the slope of the curve as plotted on log-log paper is equal to -1, the expression for the critical impact velocity of water droplets penetrating a kerosine-air interface is simply

$$V_c = \frac{C}{D} ,$$

where V_c is the critical velocity in meters per second, D is the droplet diameter in microns, and C is a constant equal to 1725.

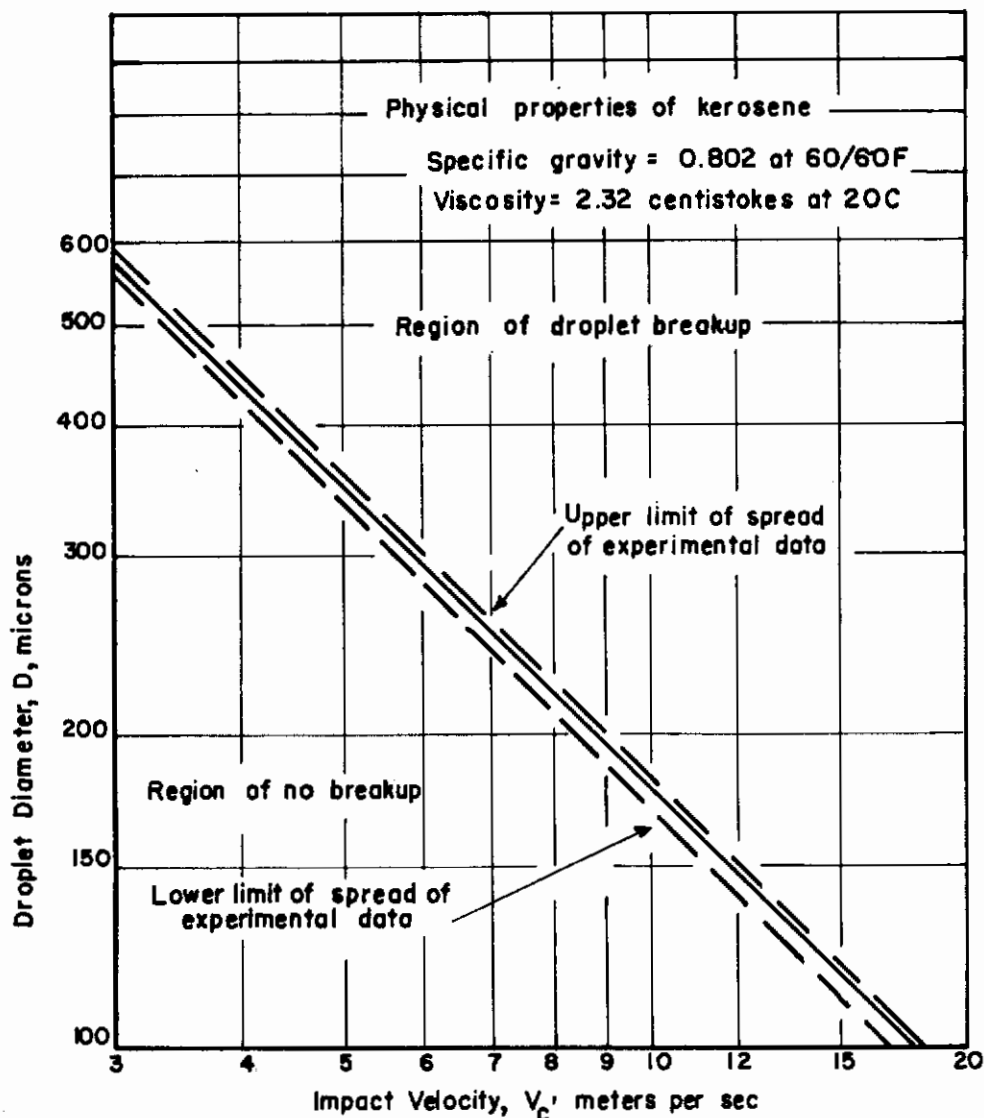


FIGURE 4-33. CRITICAL IMPACT VELOCITIES OF WATER DROPLETS PENETRATING Kerosine-AIR INTERFACE

(Rupe)⁴⁻⁸²

An extremely regular and interesting breakup pattern was observed. Rupe noted in every case, regardless of drop size or critical velocity, that breakup at velocities only slightly higher than critical velocity (about 1 to 2 per cent higher) resulted in two drops, consisting of a comparatively large mass accompanied by a quite small "satellite".

Figure 4-34 illustrates this phenomenon and shows a portion of a collected sample for which approximately half of the droplets exceeded the critical velocity. As the impact velocity was further increased, the "satellite" became larger and larger, until the two drops became of the same size. At this point, another small "satellite" appeared. The diameter ratios of the three drops appeared to be extremely sensitive to small changes in impact velocity. Successive increases in the number of particles formed were observed.

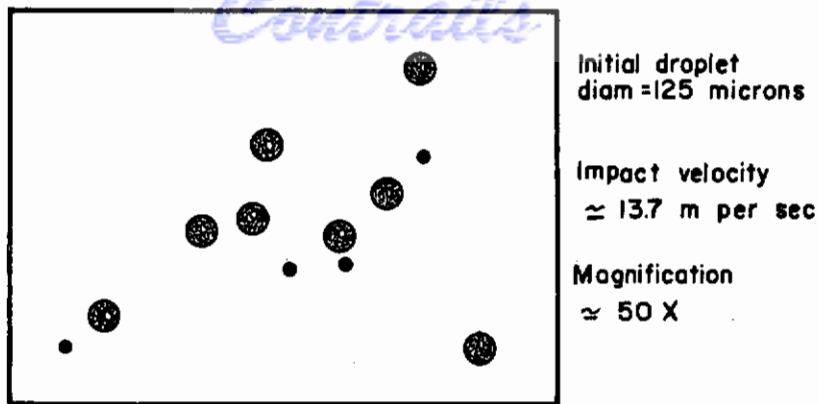


FIGURE 4-34. TYPICAL DROPLET BREAKUP FOR IMPACT VELOCITIES SLIGHTLY HIGHER THAN CRITICAL VELOCITY

(Rupe)⁴⁻⁸²

Rupe made a brief study of droplet impact in glass slides coated with magnesium oxide. He observed that, if a critical impact velocity somewhat lower than the critical velocity for a kerosene-air interface is exceeded, the droplets will strike the surface, flatten out inside the crater which develops, re-form, and bounce away from the surface as discrete droplets. Rupe states that a bouncing droplet may form two or three secondary craters which could be identical with craters formed by similar droplets traveling at a lower velocity or that formed by a smaller droplet traveling at the same velocity.

Golitzine⁽⁴⁻²¹⁾ also observed that droplets impinging on a soot- or vaseline-covered slide splash easily, but that the pattern of splash was quite characteristic, consisting of an empty space with a ring of small droplets around it.

Breakup of droplets on impact is a serious problem that should be investigated in connection with any method of drop-size measurement involving the collection of drops on a clear or coated slide, or in a cell of liquid.

Summary

The analysis of a spray in terms of drop-size distribution is probably the most important single problem involved in the study of atomization of liquid fuels. Research on the mechanism and on methods of atomization, and on nozzle design would be aided greatly by a simple and accurate method for determining the drop-size distribution of the spray.

Of the six classes of experimental methods for determining drop size distribution, the method most generally used consists of collecting a sample of the spray on a glass slide or in a cell containing a special liquid. The droplets are then observed, or photographed, with the aid of a microscope. This method has many variations and is relatively simple, requiring a minimum of apparatus. However, the measuring and counting of hundreds of droplets is obviously a tedious and time-consuming operation. A more valid objection to the simple collection of drops on a glass slide is that it is extremely difficult, if not impossible, to sample the spray without discrimination against the smaller sizes which tend to follow the air stream around the collecting device. Discrimination becomes a serious problem for particles smaller than 20 microns in diameter, and almost no drops smaller than 5 microns will deposit on a slide when ordinary sampling methods are used. No satisfactory correction can be made to compensate for such sampling errors. The magnitude of

error resulting from discrimination against small droplets during sampling can be minimized by using narrow slides. The collection of the spray in a cell containing a confining liquid has two advantages over collection on a slide, (1) the drops remain almost perfectly spherical, provided the density of the confining liquid is only slightly less than that of the sprayed liquid, and (2) evaporation is prevented. A minimum of about 500 to 1000 drops should be measured and counted, and only a small fraction (about one per cent) of the area of the cell or slide should be covered with droplets to reduce the probability of coalescence. The duration of the sampling period is, therefore, extremely important.

The frozen-drop and the wax methods for determining the size distribution of drops in a spray have the advantages that (1) the tedious and time-consuming operations of microscopic counting are eliminated, and (2) sampling errors are less likely because all of a large increment of spray can be collected and handled, employing screens and gravimetric methods of analysis. The chief limitation of these methods is that they do not provide data on the fine particles smaller than 75 microns because no satisfactory screens exist for them. However, air elutriation or sedimentation may be used for analysis of frozen wax particles.

Photographic methods for determining drop-size distribution of fuel sprays have the distinct advantage that no object is placed in the path of the spray which might result in unrepresentative sampling of the droplets. Errors that might result from coalescence or evaporation of droplets after sampling are eliminated. On the other hand, the photographic methods have two definite disadvantages: (1) the droplets smaller than 20 microns cannot be photographed satisfactorily in a fast-moving spray, and (2) the photograph records the spatial rather than the more important temporal distribution of drops. The latter objection can be overcome if drop velocities are known, but data on velocities are not easily obtained. Another serious problem encountered in the photographic method is the determination of whether a droplet is in focus, or out of focus, when it appears near the boundary of the field of focus. Generally speaking, the photographic method is too laborious for routine spray analysis, and it is certainly not ideally suited for extensive research on spray analysis. However, the photographic method may serve as a primary means of calibrating some more simple, indirect method.

Optical methods, based on the scattering of light by dispersed droplets, provide a relatively simple and rapid measure of particle size. However, the optical techniques give data concerning the average drop size or the predominant size only, and size-distribution data cannot be obtained. Also, the optical methods are more suited to the size analysis of aerosols and extremely fine mists than to the analysis of typical fuel sprays. The photometer method, based on a measure of the light absorbed by a spray, is recommended as a rapid means of comparing sprays produced under various injection conditions. The effects of variations of spray-nozzle design or of physical properties of the atomized liquid might be investigated by this indirect method of spray analysis.

Electronic methods of determining drop-size distribution, based upon the electrostatic charge that may be carried by small particles, are extremely rapid and should be applicable to certain problems of spray analysis. However, additional development of electronic methods will be required to improve the stability of the equipment and the reproducibility of the tests. All electronic methods will require calibration against some direct method of determining drop-size distribution.

The size distribution of radioactive compounds may be studied using radioautographic techniques. This method is especially useful in the size range of 0.1 to 10 microns. Inert material cannot be detected, however, and if large particles are present the finer particles tend to be obscured. The method has limited application as a research tool.

The cascade-impactor method offers the most promising solution to the problem of determining drop-size distribution for fine sprays containing drops under 100-micron diameter. This method is based upon the principle that a droplet moving at high velocity will, because of its momentum, impact upon a slide placed in its path. By increasing the velocity of the stream containing the droplets, smaller and smaller sizes will impact. By employing isokinetic sampling, the probability of discrimination against the smaller sizes can be practically eliminated. The greatest efficiency of sampling is achieved in the size range of 50 to 1.5 microns. An important advantage of the cascade impactor is that after calibration, the amount of drops in each size range, collected in

each stage of the cascade impactor, can be obtained by gravimetric, chemical, or colorimetric methods, and the tremendous labor and time required for microscopic analysis can be avoided. The theory of impaction, as it occurs in the cascade impactor, makes it possible to design an instrument to provide impaction of particles of a specified size range in each stage. Any number of stages may be used.

A problem common to all methods of measuring drop-size distribution based on the collection of drops on a slide is deciding how much of the slide area should be covered. A one per cent coverage does not appear excessive from the standpoint of droplet overlap; however, from the standpoint of ease of counting and measuring individual droplets, a coverage of only 0.2 per cent is preferred.

Automatic scanning devices make it possible to count and measure the size of droplets about 100 times as rapidly as by manual methods. Other advantages of the scanning instruments are that the human element, always present in manual methods, is removed, and all of the droplets may be simultaneously counted and classified into a number of size classes. An objection to the scanning devices, besides the fact that they are complicated and expensive to construct and maintain, is that photomicrographic negatives of high definition and contrast are required. Sampling errors that occur during collection of the spray are not minimized by making large counts with scanning devices. The use of a relatively simple semi-automatic particle-size counter may be a compromise solution to the problem of measuring the diameters of large numbers of droplets.

The collection efficiency with which droplets may be sampled by collection on a slide or in a cell depends upon the velocity and size of the particles and upon the width of the sampler. The effectiveness of sampling is increased as the velocity of the particles increases and as the width of the interceptor (glass slide or cell) decreases. Drop-size data based on samples collected on standard glass slides (25 mm wide) are questionable for particles smaller than 50 microns. Slides 5 mm square will collect a much truer sample than standard slides 25 mm x 75 mm. The efficiency of any system of collection by impaction can be predicted with considerable accuracy.

The flattening coefficient, defined as the factor by which the diameter of a flattened drop must be multiplied to obtain the original diameter of the spherical drop, may be determined in several ways. The height and diameter of individual flattened drops, viewed from the side, may be measured, and the flattening coefficient may be computed by solid geometry. Another method is based upon the assumption that the flattened drop is a plano-convex liquid lens. By determining the focal length and diameter of this lens, the flattening coefficient can be computed using an equation for the optics of a plano-convex lens. The flattening coefficient for water drops on a greased surface is about 0.8, and for oil drops on a clean glass surface the flattening coefficient is about 0.5; however, it is highly advisable to determine the flattening coefficient for each specific experimental condition, because the value will change when the properties of the liquid, or the condition of the surface of the slide, are changed.

The impression coefficient, defined as the ratio of the true spherical-drop diameter to the diameter of the impression made in a fragile layer such as MgO, is about 0.86 for drops larger than 20 microns, and about 0.72 for 10-micron droplets, under typical conditions of sampling. The impression coefficient for a wide range of conditions is related to the dimensionless Weber's number.

Satisfactory light-microscopic techniques are available for measuring the size of particles down to about 0.3 micron, provided the resolving power of the microscope lens is sufficiently high. The type of light used and the method of illumination are also important considerations.

Another important factor that must be considered in spray analysis is the possibility that drops break up into two or more droplets upon impact with a glass slide or a liquid-air interface. There exists a "critical impact velocity" which is the particle velocity below which rupture will not occur. The critical impact velocity is inversely proportional to the drop diameter and must be determined for the specific experimental conditions considered.

Much additional development work is required for the extremely rapid electronic method of determining drop-size distribution.

C. C. Miesse and A. A. Putnam

This section on the mathematical representation of drop-size distributions will include the various expressions which have been suggested for this application, their potentialities, and their limitations. It might be hoped that a suitable expression would (1) fit the data adequately, (2) allow for extrapolation, (3) permit easy calculation of mean sizes and other parameters of interest, (4) furnish a means of consolidating large amounts of data, and (5) give an insight into the fundamental mechanism of droplet production. An attempt will be made to make clear the degree to which each of these possibilities can be obtained in the subsequent discussion.

Although each of the investigators who has made an analysis of the breakup of liquid jets has been able to determine, either by means of a valid mechanism or by means of a conjectural model, the size of droplet to be expected as a result of this breakup, none but Baron⁽⁴⁻⁸³⁾ made any attempt to determine the distribution of droplet sizes resulting from secondary atomization of the larger droplets formed originally.

In the absence of any physical mechanism or model upon which to build a theory of drop-size distributions, a number of functions have been uncovered, either by purely empirical or by probability considerations, which have permitted the mathematical representation of experimental drop-size distributions.

The size distributions can be expressed in terms of any of four measurable quantities:

- (1) the incremental number ΔN of droplets within the size range $\left(x - \frac{\Delta x}{2}\right) < x < \left(x + \frac{\Delta x}{2}\right)$;
 (2) the incremental volume (or weight), ΔV , of droplets in this size range; (3) the cumulative number of droplets \underline{N} less than a given size \underline{x} ; and (4) the cumulative volume (or weight) of droplets, \underline{V} , less than a given size \underline{x} . From elementary considerations, it is obvious that the following relation must exist between the number of droplets \underline{N} and the volume \underline{V} :

$$\frac{dN}{dx} = \frac{6}{\pi x^3} \frac{dV}{dx}, \quad (4-1)$$

where \underline{x} is the "effective" diameter which is defined such that an irregularly shaped droplet of effective diameter \underline{x} will produce the same effect, in the phenomenon under consideration, as a spherical droplet of actual diameter \underline{x} .

A relatively simple mathematical function, which is sufficiently flexible for adequate representation of all unimodal experimental distributions is an equation⁽⁴⁻⁷⁶⁾ containing three independent constants:

$$\frac{dN}{dx} = a x^p e^{-bx^n}. \quad (4-2)$$

In the discussion that follows, it will be noted that all except two of the size-distribution functions which have been presented are either specializations of this function, or slight modifications of it.

Each of the various distribution functions which are presented below will be applied to the correlation of the droplet-size data obtained by Houghton⁽⁴⁻⁸⁷⁾, and given in Table 4-2. It is noted that the original data are given in terms of the incremental numerical distribution ΔN ; for this study, the normalized incremental volume distribution $\frac{\Delta V}{\Delta x}$ was obtained by multiplying the normalized incremental numerical distribution, that is, the ratio of ΔN to Δx , by the cube of the mean diameter

Contrails

TABLE 4-2. HOUGHTON'S(4-79) INCREMENTAL NUMERICAL DROP-SIZE DATA AND DROP-SIZE DISTRIBUTION DERIVED THEREFROM

j	2	3	4(a)	5	6	7	8	9	10
Size Range $x_{j-1} - x_j$ μ	Average Diameter D_j μ	Incremental Numerical Distribution, $(\Delta N)_j$	Normalized Incremental Numerical Distribution, $(\frac{\Delta N}{\Delta x})_j$	Normalized Incremental Volume Distribution(b)	Proportional Cumulative Volume Distribution(c)	Cumulative Percentage Oversize, $F_j(x_j)$	Cumulative Percentage Undersize(d)	Inner Percentage Undersize, 100 P _j	
-1	1.5 - 2.5	390,000	390,000	3,120	3,120	99.7	0.3	0	
0	2.5 - 7.5	340,000	68,000	8,500	45,620	95.4	4.6	19.2	
1	7.5 - 12.5	165,000	33,000	33,000	210,620	78.6	21.4	34.9	
2	12.5 - 17.5	40,200	8,040	27,135	346,295	64.8	35.2	45.7	
3	17.5 - 22.5	11,680	2,336	18,688	439,735	55.3	44.7	54.7	
4	22.5 - 27.5	4,970	994	15,531	517,391	47.4	52.6	61.6	
5	27.5 - 32.5	2,160	432	11,664	575,711	41.4	58.6	70.1	
6	32.5 - 37.5	1,730	346	14,835	649,885	33.9	66.1	78.2	
7	37.5 - 42.5	1,080	216	13,824	719,005	26.8	73.2	85.1	
8	42.5 - 47.5	750	130	11,846	778,236	20.8	79.2	91.2	
9	47.5 - 55.0	430	57	7,167	831,986	15.4	84.6	92.3	
10	55.0 - 65.0	350	35	7,560	907,586	7.7	92.3	100.0	
11	65.0 - 75.0	220	22	7,546	983,046	.0	100.0		

(a) Houghton's data.

(b) $10^{-3} D^3 \left(\frac{\Delta N}{\Delta x}\right)_j$

(c) $10^{-3} \sum_{-1}^j D^3 \left(\frac{\Delta N}{\Delta x}\right)_j \cdot \Delta x_j$

(d) $100 - F_j(x_j)$

This expression is linear in $(\log a)$ and $(b \log e)$. If a value of \underline{n} is assumed for a given set of data, it is apparent that \underline{a} and \underline{b} may be determined by plotting

$$\log \left(\frac{1}{x^2} \frac{dN}{dx} \right)$$

against x^n .

Figure 4-35 shows a plot of $\log \left(\frac{1}{x^2} \frac{\Delta N}{\Delta x} \right)$ from Houghton's data, as given in Column 5 of Table 4-2, against $x^{1/4}$. The value of $1/4$ for \underline{n} was found, by trial and error, to allow the data to fall approximately along a straight line. The first row of data, $j = -1$, has not been included because of an uncertainty of the range, Δx , to which these data apply. Since the negative slope is $(b \log e)$, and the zero intercept is $(\log a)$, this process permits a determination of \underline{a} , \underline{b} , and \underline{n} for a given set of data, and thus the characterization of the data by the Nukiyama-Tanasawa equation.

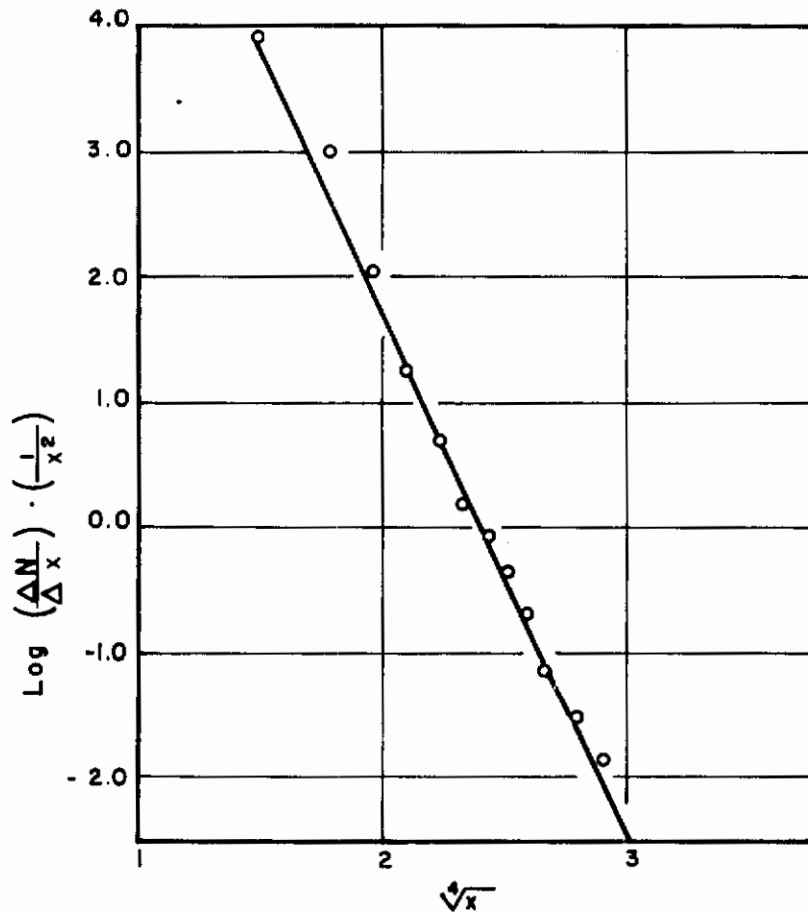


FIGURE 4-35. GRAPH OF NORMALIZED INCREMENTAL NUMERICAL DISTRIBUTION FROM HOUGHTON'S DATA AGAINST $\sqrt[4]{x}$

Better approximations for the values of \underline{a} , \underline{b} , and \underline{n} can be obtained by substituting the value of \underline{n} as obtained by the graphical trial-and-error method outlined above, into Equation (4-11), which can then be used to find solutions for \underline{a} and \underline{b} by the method of least squares. Substitution of the value of \underline{a} thus obtained into the logarithm of Equation (4-11), namely,

$$\log \log \left(\frac{ax^2}{dN} \right) = \log (b \log e) + n \log x \quad , \quad (4-11a)$$

then yields an equation which can be solved readily for \underline{b} and \underline{n} , also by the method of least squares. Alternate use of Equations (4-11) and (4-11a) should be continued until one set of values of the parameters \underline{a} , \underline{b} , and \underline{n} differs from the previous set by less than a preassigned percentage (for example, one per cent).

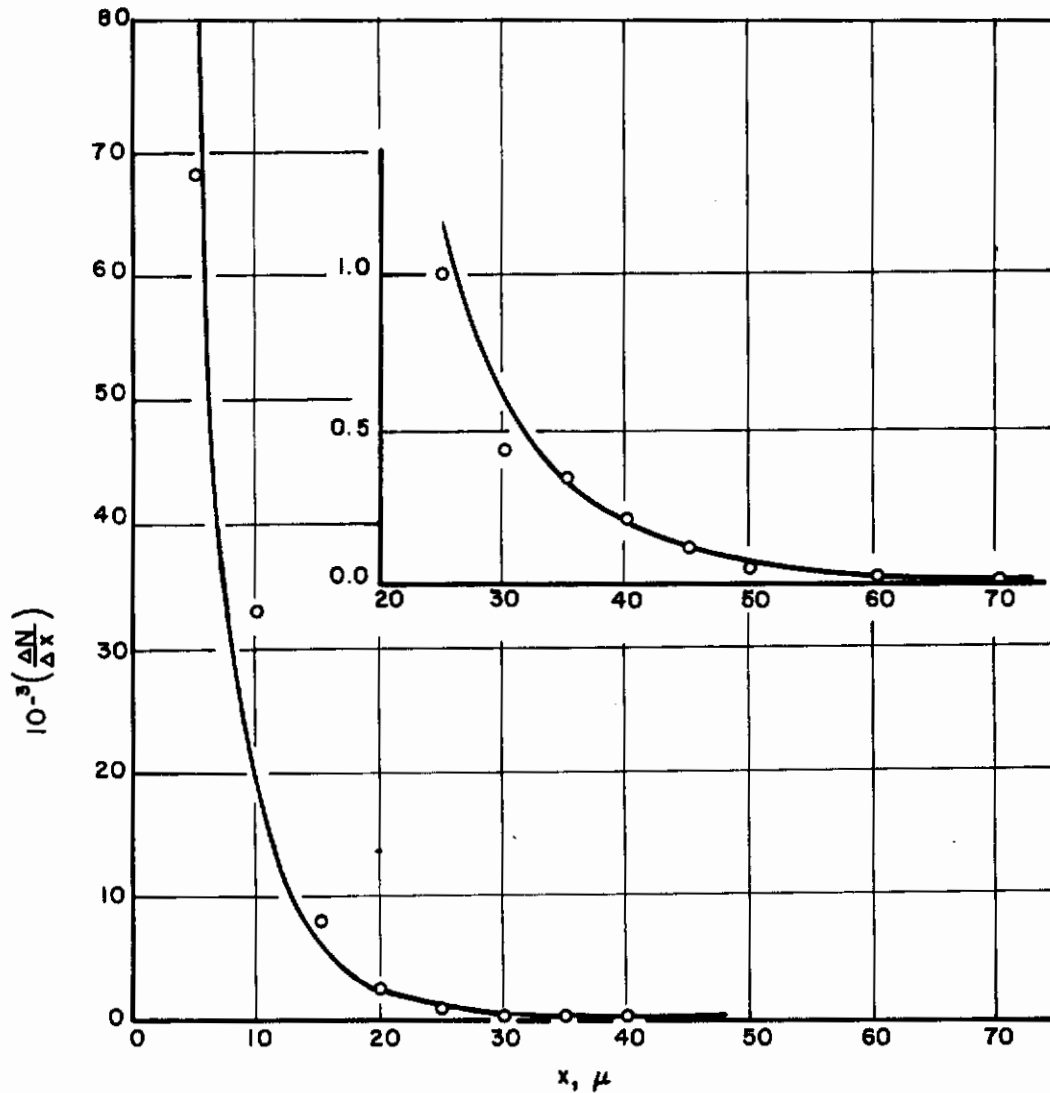


FIGURE 4-36. COMPARISON OF NUKIYAMA AND TANASAWA'S THEORETICAL CURVE WITH NORMALIZED INCREMENTAL NUMERICAL DISTRIBUTION FROM HOUGHTON'S DATA

Figure 4-36 shows a comparison of the theoretical curve thus obtained with the experimental points. It is noted that the correlation thus effected is quite good, especially since only a few applications of the above iteration method were required. It may be noted that a final value of \underline{n} of 0.17 is obtained, as compared with the value of 0.25 obtained graphically from Figure 4-35.

Corresponding changes in \underline{a} and \underline{b} were from 1.12×10^{14} to 1.39×10^{14} and 9.79 to 18.38 respectively. These comparisons clearly indicated that the value of \underline{a} is the least sensitive, and is the proper value to carry over from the use of Equation (4-11) to Equation (4-11a).

Finally, the general equation for mean sizes from the Nukiyama-Tanasawa distribution function is obtained by substituting Equation (4-6) into Equation (4-4). Thus,

$$\bar{x}_{qp}^{q-p} = b \cdot \frac{\left(\frac{q-p}{n} \right) \left[\Gamma_{bx_m}^{n \left(\frac{q+3}{n} \right)} - \Gamma_{bx_o}^{n \left(\frac{q+3}{n} \right)} \right]}{\left[\Gamma_{bx_m}^{n \left(\frac{p+3}{n} \right)} - \Gamma_{bx_o}^{n \left(\frac{p+3}{n} \right)} \right]} \quad (4-12)$$

This simplifies to

$$\bar{x}_{qp}^{q-p} = b \cdot \left(\frac{q-p}{n} \right) \frac{\Gamma \left(\frac{q+3}{n} \right)}{\Gamma \left(\frac{p+3}{n} \right)}, \quad (4-13)$$

when it is assumed that $x_o = 0$ and $x_m \rightarrow \infty$. For small n , Equation (4-13) may be approximated by

$$\frac{q+3}{p+3} \bar{x}_{qp}^{q-p} = \left[\frac{q+3}{bne} \left(\frac{q+3}{p+3} \right)^{\frac{p+3}{q-p}} \right]^{\frac{q-p}{n}} \quad (4-13a)$$

The Rosin-Rammler Equation

Semiempirical Derivation

After many unsuccessful attempts, P. Rosin and E. Rammler⁽⁴⁻⁸⁸⁾ were able to find a general expression which was flexible enough to give adequate representation for the size distributions of all consists of pulverized materials which they investigated. This distribution function is but another specialization of the three-constant expression of Equation (4-2), and is written

$$V = 1 - e^{-bx^n} = 1 - \frac{R}{100}, \quad (4-14)$$

where R is the per cent residue left on the sizing screens.

The validity of Equation (4-14) was subsequently established by a semiempirical inductive derivation. This is presented herein as an example of what might be done in the case of liquid

As a result of grinding tests with bituminous coal, it was found that, for any one test sieve, the per cent residue R varied as a power of the rate of output M for the mill. Thus, it is noted that a change in the value of M will result in a change in the size distribution of the aggregate. This variation, which is expected physically, since a larger period of grinding would result in a larger percentage of fine particles and a smaller percentage retained by any one screen, is expressed by

$$R = cM^p, \quad (4-15)$$

where the values of c and p can be determined by plotting the data on logarithmic coordinates.

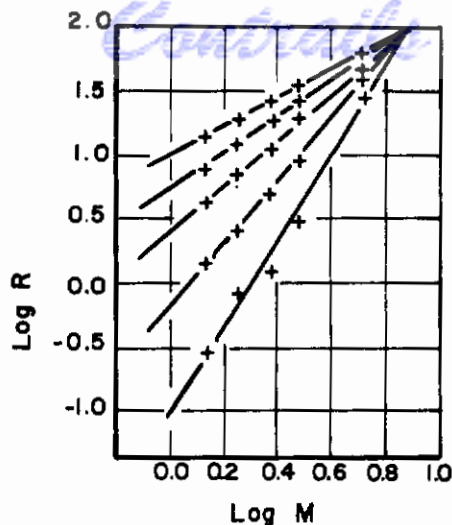


FIGURE 4-37. VARIATION OF THE RESIDUE \underline{R} WITH THE RATE OF OUTPUT \underline{M} FOR VARIOUS SCREENS
(Rosin and Rammler)⁴⁻⁸⁸

Figure 4-37 shows the variation of the residue \underline{R} with the rate of output \underline{M} for various screens, as plotted on logarithmic coordinates. In agreement with Equation (4-15), the data for each sieve fall on a straight line, the linear slope of which is equal to the exponent \underline{p} .

Figure 4-37 also shows a convergence of all the lines on one point, at a value \underline{R} of 100 per cent, and a value \underline{M} of \underline{M}^* . This result is also expected, since at some relatively rapid rate of output \underline{M}^* there will be, obviously, no particle smaller than the largest sieve size considered, and all the particles will be retained in each sieve. This result also gives a relation between \underline{c} and \underline{p} , and Equation (4-15) may be rewritten as

$$\frac{\underline{R}}{100} = \left(\frac{\underline{M}}{\underline{M}^*}\right)^{\underline{p}} \quad (4-16)$$

When the values of \underline{p} obtained from the slopes of the curves of Figure 4-37 were plotted against sieve size \underline{x} on logarithmic coordinates, it was found that \underline{p} varied as a power \underline{n} of \underline{x} . Hence,

$$\underline{p} = \underline{p}_0 \left(\frac{\underline{x}}{\underline{x}_0}\right)^{\underline{n}} \quad (4-17)$$

If only one constant output, \underline{M} , is now considered, and \underline{R}_0 is assumed to be the value of \underline{R} associated with this output, \underline{p}_0 , and with \underline{x}_0 , Equation (4-15) may be rewritten, using Equation (4-17), as

$$\underline{R} = 100 \left(\frac{\underline{R}_0}{100}\right) \left(\frac{\underline{x}}{\underline{x}_0}\right)^{\underline{n}} \quad (4-18)$$

If one lets

$$\underline{b} = \underline{x}_0^{-\underline{n}} \ln\left(\frac{100}{\underline{R}_0}\right) \quad (4-19)$$

Equation (4-18) is the same as Equation (4-14) as originally proposed. From Equation (4-19), it is clear that \underline{b} can also be expressed as

$$\underline{b} = \underline{X}^{-\underline{n}} \quad (4-20)$$

where \underline{X} is the size of the sieve which retains $(100 e^{-1})$ per cent of the total (infinite) consist.

Differentiation of Equation (4-14) yields

$$\frac{dV}{dx} = bnx^{n-1} e^{-bx^n}, \quad (4-21)$$

which, with Equation (4-1), leads to

$$\frac{dN}{dx} = \frac{6bn}{\pi} x^{n-4} e^{-bx^n}; \quad (4-22)$$

this equation is immediately identifiable with the three-constant Equation (4-2). Integration of Equation (4-22) yields

$$N = \frac{6b \binom{3}{n}}{\pi} \left[\Gamma_{bx_0} n \left(\frac{n-3}{n} \right) - \Gamma_{bx_m} n \left(\frac{n-3}{n} \right) \right], \quad (4-23)$$

where the incomplete gamma functions Γ_{α} are as defined by Equation (4-10).

The Bennett Diagram and Inner Percentages

If Equation (4-18) is solved for $\frac{100}{R}$, and if the logarithm of the resultant equation is taken twice, then the following equation linear in \underline{n} and $\log b$, is obtained:

$$\log \log \left(\frac{100}{R} \right) = \log b + \underline{n} \log x + \log \log e. \quad (4-24)$$

Equation (4-24) immediately suggests the plotting of $\log \log \left(\frac{100}{R} \right)$ against $\log x$, from which the value of \underline{n} may be determined as the linear slope of the straight line which most closely fits the data points. This type of graph is called a Bennett⁽⁴⁻⁸¹⁾ diagram, after J. G. Bennett, who first suggested its use.

Curve A of Figure 4-38 is the Bennett-diagram plot of Houghton's data⁽⁴⁻⁷⁹⁾ as transformed to the cumulative volume basis (Column 8 of Table 4-2). It can be seen that Curve A, for which \underline{R} was determined as the per cent of the finite consist, is relatively straight along only a short portion of its extent, but curves sharply to the vertical at the upper and lower size limits of the consist, which precludes a direct evaluation of the parameters \underline{b} and \underline{n} for subsequent use. The reason for this sharp vertical slope at either limit can be seen immediately by consideration of Equation (4-24). Since the per cent of the finite aggregate larger than the upper size limit x_m is zero, the $\log \log \left(\frac{100}{R} \right)$ term becomes infinite, and the curve will turn sharply upward as \underline{x} approaches x_m . Similarly, at the lower limit x_0 , the per cent oversize is one hundred and the corresponding $\log \log \left(\frac{100}{R} \right)$ becomes negatively infinite, which accounts for the sharp downward bend as \underline{x} approaches x_0 .

Curve B shows the straight line which is obtained when the data are transformed to the infinite limits implied by Equations (4-14) and (4-18); the general basis for this transformation will now be described.

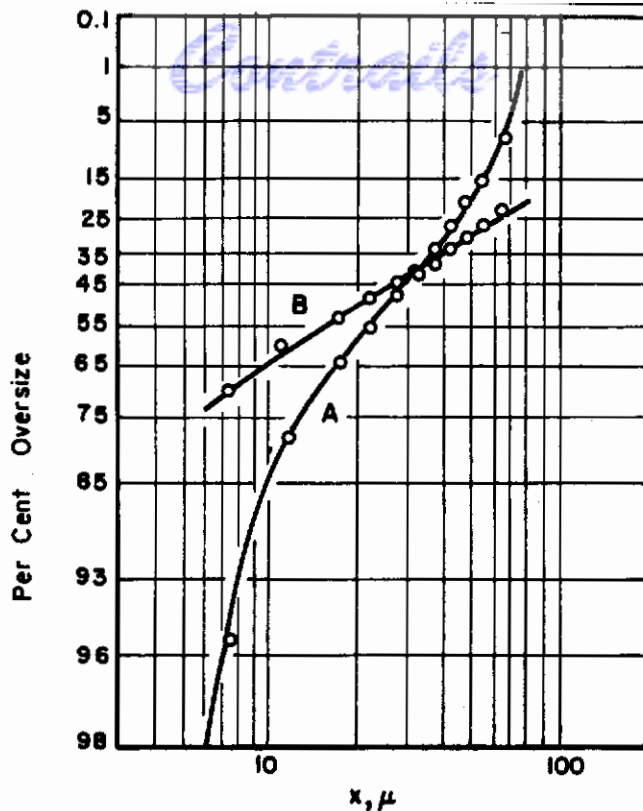


FIGURE 4-38. BENNETT DIAGRAM FOR HOUGHTON'S CUMULATIVE VOLUME DISTRIBUTION; (A) FROM RAW DATA; (B) FROM DATA ADJUSTED TO ACCOUNT FOR UPPER AND LOWER SIZE LIMITS

Consideration of Equations (4-14) and (4-18) reveals that R can be equal to one hundred per cent only for a size x of zero, and that the per cent oversize R can be zero only for infinite values of the size x , thus implying that the size range of the consist extends from zero to infinity. This, however, is never the case physically, and so a means must be found whereby an experimental finite consist can be represented by an equation which implies an infinite consist. This is done by introducing the concept of "inner percentages" which was first defined by B. A. Landry⁽⁴⁻⁹⁰⁾.

The concept of inner percentages is valuable in the sense that it permits the data available to be well fitted over the range covered, with a minimum of parameters, and with parameters which may be easily interpreted. As long as the curves are not used to extrapolate the data beyond a point where the results have physical meaning, or to infer the existence of any such region, there can be no objection to using this concept. On the other hand, as long as data do have limits of range, for various reasons, such a concept is necessary in dealing with the data.

The inner percentage p_i of droplets whose diameters are less than a given value of x_i is defined as the volume (or weight) of droplets whose sizes are less than x_i divided by the total volume (or weight) of droplets in the consist. Thus, the inner percentage of droplets whose diameters are less than x_i is expressed by:

$$p_i = \frac{V_i - V_o}{V_m - V_o} \quad , \quad (4-25)$$

where V_i is the volume of droplets of diameters less than x_i , V_m is the volume of droplets of diameter less than the upper limit x_m , and V_o is the volume of droplets whose diameter is less than the lower limit x_o . In order for the experimental finite consist to be properly represented by Equation (4-18), it is necessary for the experimental inner percentages p_i to be equal to the theoretical inner percentages p_i as found from Equation (4-14), and expressed by

$$P_i = \frac{V_i - V_o}{V_m - V_o} = \frac{e_o - e_i}{e_o - e_m} \quad (4-26)$$

where

$$e_j = e^{-bx_j^n} \quad (4-27)$$

The proper values of \underline{b} and \underline{n} for a given experimental size distribution are those for which the values of P_i most closely approximate the corresponding values of p_i for each range of data. Details of calculation for determining \underline{b} and \underline{n} to fulfill the inner percentage requirements are given subsequently after the presentation of certain prerequisites.

The Effect of the Parameters \underline{b} and \underline{n}

Consideration of Equation (4-24) indicates immediately that a large value of \underline{n} , resulting in a steep slope on the Bennett diagram, corresponds to a highly uniform spray with but a small volume of droplets outside of a small range. Conversely, small values of \underline{n} correspond to a wide distribution of droplet sizes. From Equation (4-20), it can be seen that $(b)^{1/n}$ is a measure of the average size of the particles in the spray, 37 per cent of the droplets (by weight or volume) having diameters greater than $(1/b)^{1/n}$. A small value of \underline{b} means that, on the average, the droplets tend to be large, and conversely.

The effect of \underline{n} on the differential volume and numerical distribution was studied by Hopkins (4-91), who considered Equations (4-21) and (4-22). Differentiation of Equation (4-21) with respect to x yields

$$\frac{d}{dx} \left(\frac{dV}{dx} \right) = bn \left[(n-1) x^{n-2} - bnx^{2n-2} \right] e^{-bx^n} \quad (4-28)$$

which reveals immediately that the diameter x' , at which the greatest differential volume $(dV/dx)_{\max}$ occurs, is then

$$x' = \left(\frac{n-1}{bn} \right)^{1/n} = \left(\frac{n-1}{n} \right)^{1/n} X \quad (4-29)$$

where X is as defined by Equation (4-20). It is noted, from Equation (4-29), that x' has a real value for $n > 1$. Furthermore, x' is always less than X , that is, at least 37 per cent of the volume in the infinite consist must be in droplets greater than x' .

Figure 4-39 shows the variation of $\frac{dV}{dx}$ with x for various values of \underline{n} . The curves on this figure give a graphical representation of the behavior of $\frac{d}{dx} \left(\frac{dV}{dx} \right)$ at $x = 0$ for various values of \underline{n} . This behavior can be determined analytically consideration of Equation (4-28); hence, for

$$\left. \begin{array}{l} n < 1, \frac{d}{dx} \left(\frac{dV}{dx} \right) \rightarrow -\infty ; \\ n = 1, \frac{d}{dx} \left(\frac{dV}{dx} \right) < 0; \\ 1 < n < 2, \frac{d}{dx} \left(\frac{dV}{dx} \right) \rightarrow +\infty ; \end{array} \right\}$$

Contrails

$$n = 2, \frac{d}{dx} \left(\frac{dV}{dx} \right) > 0;$$

$$n > 2, \frac{d}{dx} \left(\frac{dV}{dx} \right) = 0.$$

(4-30)

Bounds on the value of \underline{n} can thus be readily determined for a set of experimental incremental volume data by plotting these data against \underline{x} and by comparing the behavior of the resultant curves at $\underline{x} = 0$ with the criteria of Equation (4-30). If this curve has a real maximum, then this approximate value of \underline{n} may be substituted into Equation (4-29) in order to make a determination of the corresponding approximate value of \underline{b} .

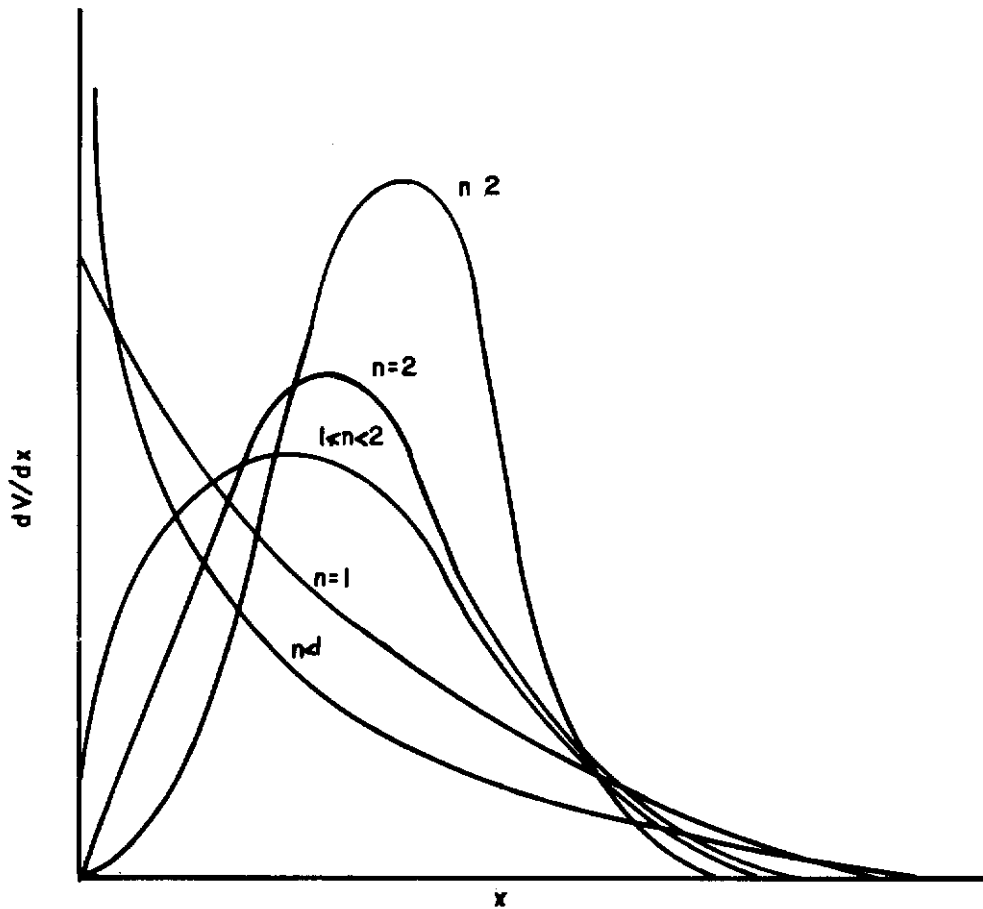


FIGURE 4-39. VARIATION OF dV/dx WITH \underline{x} FOR VARIOUS VALUES OF \underline{n}
(Hopkins)⁴⁻⁹¹

The same type of analysis was then applied to the numerical distribution. Differentiation of Equation (4-22) with respect to \underline{x} yields

$$\frac{d}{dx} \left(\frac{dN}{dx} \right) = \frac{6bn}{\pi} \left[(n-4) x^{n-5} - bnx^{2n-5} \right] e^{-bx^n} , \quad (4-31)$$

which readily indicates that the value x'' of the diameter at which $\frac{dN}{dx}$ is a maximum is

$$x'' = \left(\frac{n-4}{bn} \right)^{1/n} = \left(\frac{n-4}{n} \right)^{1/n} X . \quad (4-32)$$

Hence, x'' has a real value only for $n > 4$. Also, x'' is always less than x' and X .

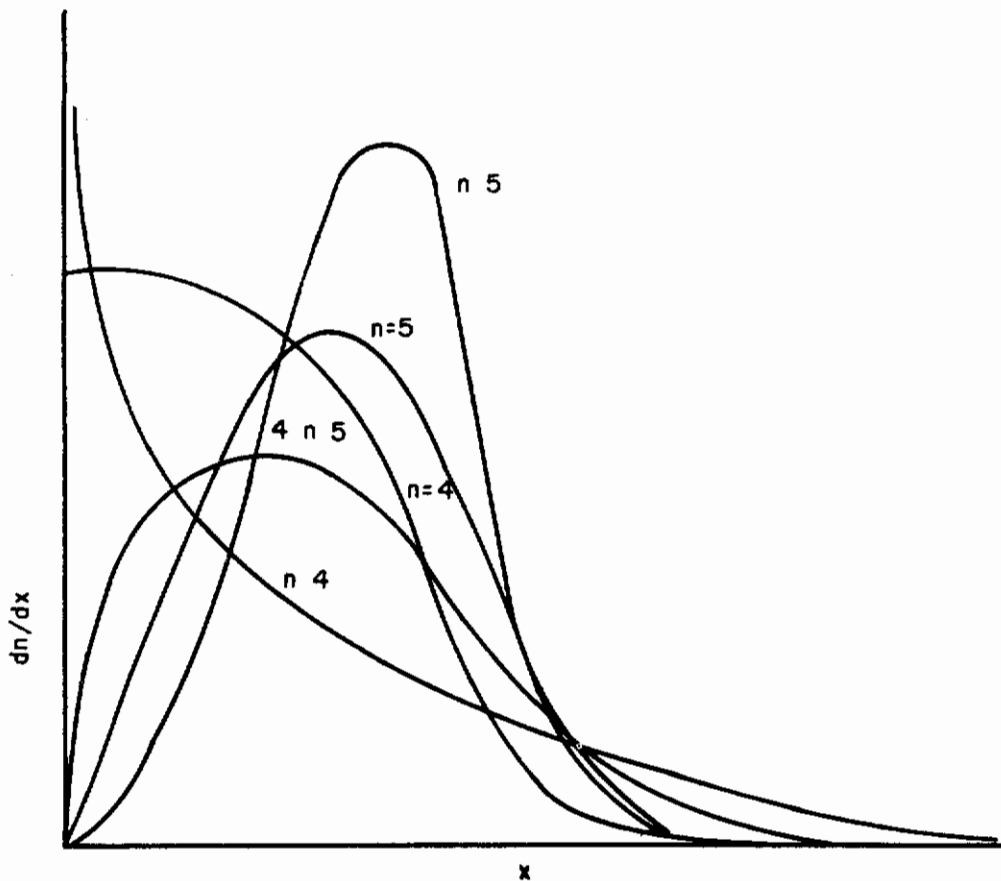


FIGURE 4-40. VARIATION OF $\frac{dN}{dx}$ WITH x FOR VARIOUS VALUES OF n
(Hopkins)⁴⁻⁹¹

Figure 4-40 shows the variation of $\frac{dN}{dx}$ with x for various values of n . Again, the behavior of $\frac{dN}{dx}$ at $x = 0$ for various values of n , which is represented graphically by Figure 4-40, can be determined analytically, from Equation (4-31), to be as follows:

Contrails

$$\left. \begin{aligned}
 n < 4, \frac{d}{dx} \left(\frac{dN}{dx} \right) \rightarrow -\infty ; \\
 n = 4, \frac{d}{dx} \left(\frac{dN}{dx} \right) = 0 ; \\
 4 < n < 5, \frac{d}{dx} \left(\frac{dN}{dx} \right) \rightarrow +\infty ; \\
 n = 5, \frac{d}{dx} \left(\frac{dN}{dx} \right) > 0 ; \\
 n > 5, \frac{d}{dx} \left(\frac{dN}{dx} \right) = 0 .
 \end{aligned} \right\} \quad (4-33)$$

Comparison of Figures 4-39 and 4-40 reveals that the variation of $\frac{dN}{dx}$ with x for $n = a$ corresponds quite closely with the variation of $\frac{dV}{dx}$ with x for $n = a - 3$, except for the curve representing the variation for $a = 4$. For this value of a , $\frac{dN}{dx}$ varies as e^{-x^4} , which is represented by a bell-shaped curve which has a horizontal slope for $x = 0$. On the other hand, for $a - 3 = 1$, $\frac{dV}{dx}$ varies as e^{-x} , the curve which has no horizontal slope for any finite value of x and has a finite negative slope for $x = 0$. The experimentally determined variation of $\frac{dN}{dx}$ with x can also be used to determine an approximate value of n , and, if there is a value x'' of x for which $\frac{dN}{dx}$ has a maximum value, an approximate value for b can be determined by substitution of the approximate values for n and x'' into Equation (4-32).

The Graphico-Analytical Criterion

The following considerations lead to a simple graphical method for determination of the applicability of the Rosin-Rammler function to the set of inner percentages p_i corresponding to any given set of drop-size-distribution data.

Let the theoretical inner percentages p_i , as defined by Equation (4-26), be considered as a continuous function $P(x)$ of x ;

$$P(x) = \frac{e_0 - e^{-bx^n}}{e_0 - e_m} \quad (4-34)$$

Differentiation of Equation (4-34) with respect to x yields

$$\frac{dP}{dx} = \frac{bn}{e_0 - e_m} x^{n-1} e^{-bx^n} = \frac{1}{e_0 - e_m} \frac{dV}{dx}, \quad (4-35)$$

as shown by consideration of Equation (4-21). Consideration of Equations (4-28), (4-29), and (4-35) indicates that $\frac{dP}{dx}$ has one stationary value for $x > 1$, and none for $x \leq 1$. Substitution of Equation (4-29) into the derivative of Equation (4-28) with respect to x indicates that the point x' at which $\frac{dP}{dx}$ has a stationary value is, indeed, a maximum point on the curve of $\frac{dP}{dx}$ against x . Hence, if a given set of drop-size data is to be represented adequately by the Rosin-Rammler function, as given by Equation (4-18), then the experimental inner percentages p_i must be such that the variation of $\frac{\Delta P}{\Delta x}$, or of the incremental volume $\frac{\Delta V}{\Delta x}$, with x must have not more than one maximum point, and no minimum point; that is, it must be unimodal.

The procedure to be followed in determining whether the Rosin-Rammler expression will adequately represent a given set of experimental data is to plot against x the experimentally determined incremental volume distribution $\frac{\Delta v}{\Delta x}$ (or the values of $\frac{\Delta p}{\Delta x}$, as determined graphically from the curve of the experimental inner percentages p against x). If the resultant curve is unimodal, or decreases monotonically from $x = 0$, then the data should be adequately representable by the Rosin-Rammler function. If the resultant curve is truly multimodal, then the Rosin-Rammler function cannot adequately represent the data. Consideration of Equations (4-1) and (4-2) indicates that the same criterion can also determine the applicability of the Nukiyama-Tanasawa function to a given set of experimental data.

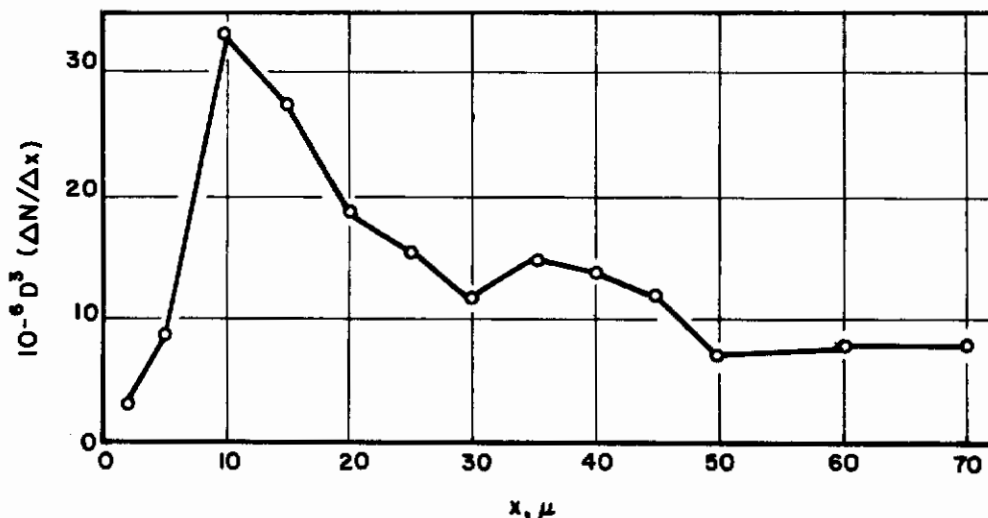


FIGURE 4-41. INCREMENTAL VOLUME DISTRIBUTION FROM HOUGHTON'S DATA

Figure 4-41 shows the variation of Houghton's incremental volume data, from Column 6 of Table 4-2, with x . These data, if the curve through them is extended indefinitely to the right, give a trimodal curve; however, the accuracy of the data do not justify inferring more than a bimodal distribution. Nevertheless, even the bimodal distribution of Houghton's data precludes their perfect representation by either the Rosin-Rammler or the Nukiyama-Tanasawa function.

Iteration Method for Determining b and n for Equivalent Infinite Consist

The method of least squares will now be applied to the problem of determining the values of b and n of the infinite consist corresponding to a given experimental cumulative volume distribution. Since, for a proper representation, $p_i \approx P_i$, Equation (4-26) may be written,

$$P_i = \frac{e_0 - e^{-bx_i^n}}{e_0 - e_m} \quad (4-36)$$

Superficially, Equation (4-36) indicates that there are four unknown quantities to be determined: b , n , e_0 , and e_m . However, e_0 and e_m are functions of the parameters b and n and of the known limits of the data. Let it now be assumed that e_0 and e_m are constants, which can be arbitrarily chosen such that

$$0 \leq e_m \leq e_0 \leq 1.$$

Equation (4-36) can be rewritten as

$$e^{-bx_i^n} = \frac{1}{e_0 - (e_0 - e_m) P_i} = G_i \quad (4-37)$$

If the common logarithm of both sides of Equation (4-37) is taken twice, the following equation results:

$$\log b + n \log x_i + \log \log e = \log \log G_i, \quad (4-38)$$

which is linear in n and $(\log b)$, and, hence, can be solved readily by the method of least squares. At least ten or twelve size-distribution data points should be available for this computation.

The values of \underline{b} and \underline{n} thus obtained are used to determine new values for e_0 and e_m , as defined by Equation (4-27), and the whole process is repeated until two subsequent values of \underline{b} and \underline{n} differ from each other by an amount less than a preassigned limit of accuracy. This method converges to a unique result in no more than eight iterations.

Although the method can be applied with no knowledge of the approximate values for \underline{b} and \underline{n} (let $e_0 = 1$, and $e_m = 0$, for example), several iterations can be avoided by comparing the data with Figures 4-39 and 4-40, to determine an approximate value for \underline{n} . This requires only the plotting of the curves for $\frac{\Delta V}{\Delta x}$ and $\frac{\Delta N}{\Delta x}$ against \underline{x} . In addition, the curve of $\frac{\Delta N}{\Delta x}$ against \underline{x} exhibits a maximum point at $x = x'$, so that the approximate value of \underline{b} , corresponding to the previously determined approximate value of \underline{n} , can be determined by substituting x' and \underline{n} into Equation (4-29). If there is no real maximum value of $\frac{\Delta V}{\Delta x}$, then an appropriate value of \underline{b} can be obtained by substituting the approximate value of \underline{n} , along with the coordinates $\frac{\Delta V}{\Delta x}$ and \underline{x} for a particular point on the curve, into Equation (4-21), which results in a transcendental equation for \underline{b} . These approximate values of \underline{n} and \underline{b} can then be used to determine the first-approximation values of e_0 and e_m , which can be used in the successive iteration method described above.

Houghton's data will now be used to illustrate this method by "decapitation" at the value of x_m of 65μ , and "amputation" at the value of x_0 of 7.5μ . The resulting data, in the form of inner percentage undersize, are tabulated in Column 10 of Table 4-2.

To use the comparison criteria just presented to determine initial values, the data are used in the form shown in Figure 4-42, with allowance made for the decapitation and amputation points. The decapitation and amputated data show a wide scatter and no turning point, in the sense needed for a comparison with the Rosin-Rammler curves. Therefore, no initial choice of \underline{b} and \underline{n} can be made, and the successive iteration outlined above was applied by letting $e_0 = 1$ and $e_m = 0$, as a first approximation. The final values of the parameters were then found to be $n = 0.65861$ and $b = 0.09282$, resulting in Curve B on Figure 4-39.

The method of least squares can also be employed to determine the values of \underline{b} and \underline{n} for a given experimental size distribution if the data are given in terms of the incremental volume $\frac{\Delta V}{\Delta x}$. The logarithm of Equation (4-21) results in the equation,

$$\begin{aligned} \log\left(\frac{dV}{dx}\right) &= \log bn + (n-1) \log x + bx^n \log e \\ &= \alpha + (n-1) \log x + \beta x^n. \end{aligned} \quad (4-39)$$

Hence, if a first approximation for the value of \underline{n} can be obtained by comparing Figures 4-40 and 4-41 with the curves for $\frac{\Delta V}{\Delta x}$ and $\frac{\Delta N}{\Delta x}$ against \underline{x} , the first approximation values for x^n can be determined. Substitution of these approximate values for x^n into Equation (4-39) then yields a series of linear equations for α , β , and $(n-1)$, from which a second value for \underline{n} can be obtained by the method of least squares. By using this new value of \underline{n} , another set of values for x^n is obtained, and the least squares method can be used again to determine a third value for \underline{n} .

This process is then repeated until two successive values of \underline{n} differ by less than a preassigned percentage. The corresponding value of \underline{b} can then be obtained from the value of β which resulted from the last iteration.

This method was not applied to Houghton's data, since the multimodal character of these data, as shown in Figure 4-42, precludes a reasonable representation of the incremental volume distribution by the Rosin-Rammler distribution function.

Mean Diameters for Rosin-Rammler Equation

Substitution of Equation (4-21) into Equation (4-4) yields the following general equation for the various mean sizes of the droplets, as determined by the Rosin-Rammler distribution function.

$$\bar{x}_{qp}^{q-p} = b^{-\frac{q-p}{n}} \left[\frac{\Gamma_{bx_m}^n \left(\frac{q-3}{n} + 1 \right) - \Gamma_{bx_o}^n \left(\frac{q-3}{n} + 1 \right)}{\Gamma_{bx_m}^n \left(\frac{p-3}{n} + 1 \right) - \Gamma_{bx_o}^n \left(\frac{p-3}{n} + 1 \right)} \right], \quad (4-40)$$

which simplifies to

$$\bar{x}_{qp}^{q-p} = b^{-\frac{q-p}{n}} \left[\frac{\Gamma \left(\frac{q-3}{n} + 1 \right)}{\Gamma \left(\frac{p-3}{n} + 1 \right)} \right] \quad (4-41)$$

when it is assumed that $x_o = 0$ and that $x_m \rightarrow \infty$.

Hopkins (4-91) chose a particular Rosin-Rammler equation for an infinite consist, and determined the mean size. Then he determined the mean sizes for various decapitated and amputated portions of this consist. For the range he covered, there was little difference. Basically, this means that once b and n are determined for the infinite consist, the value of x can be computed from the relatively simple Equation (4-41), rather than from Equation (4-40), providing the amount of material outside the cut-off points, as indicated by the infinite-consist equation, is "reasonably small". Hopkins did not investigate the problem sufficiently to lead to a good definition of "reasonably small".

The Weibull Equation

By identifying the distribution function $F(x)$ which determines the quantity of items with dimension $\leq x$ with the probability $P(x)$ of choosing at random an item of dimension $\leq x$, W. Weibull⁽⁴⁻⁹²⁾ arrived at the following general statistical distribution function:

$$F(x) = 1 - e^{-\phi(x)}, \quad (4-42)$$

where the function $\phi(x)$ is to be subject only to the following conditions:

- (1) $\phi(x_o) = 0$; where x_o is the smallest value of x ;
 - (2) $\phi(x) > 0$, for $x > x_o$;
 - (3) $\frac{d\phi(x)}{dx} > 0$.
- (4-43)

Weibull then chooses a simple function $\bar{\phi}(x)$ which would satisfy the conditions of Equation (4-42), namely,

$$\bar{\phi}(x) = \left(\frac{x - x_0}{\bar{x}} \right)^n$$

(4-44)

Weibull made no claims regarding the theoretical basis of either Equation (4-42) or Equation (4-44), but stated that the only merit for the $F(x)$ and the $\phi(x)$ of Equations (4-42) and 4-44 is that these are the simplest mathematical expressions which satisfy the conditions of Equation (4-43).

If Weibull's function is identified with the cumulative volume distribution $V(x)$, then the following equation results:

$$V(x) = 1 - \exp \left\{ - \left(\frac{x - x_0}{\bar{x}} \right)^n \right\}$$

(4-45)

This is seen to be a modification of the Rosin-Rammler Equation (4-21). The difference is that Equation (4-45) allows for the existence of a lower size limit x_0 . This eliminates the necessity for determining one limiting value of the distribution function, namely e_0 . Application of Equation (4-45) to several sets of experimental distribution data indicates that a good correlation is obtained without consideration of the second limiting value e_m of the function, either. Hence, the method of least squares can be used to determine the value of n and \bar{x} directly from the original experimental data for cumulative volume distribution. The equation to which the least-squares method is applied is obtained by taking the logarithm of $1/(1-V)$ twice, where V is defined by Equation (4-45). Thus,

$$\log \log \frac{1}{1-V} = n \log (x - x_0) - \log \bar{x}^n + \log \log e$$

(4-46)

Figure 4-42 is a Bennett diagram of Houghton's cumulative volume distribution data, using Weibull's cut-off method. A cut-off value of x_0 of 7.5μ was chosen as an example, which eliminated the data for $j = -1, 0$ of Table 4-2. Column 8 was then recomputed from Column 7, and used to plot Figure 4-42. It will be noted that the horizontal coordinate is now $(x-x_0)$, rather than \bar{x} , as with the Rosin-Rammler Equation (4-21), or in Figure 4-38.

Figure 4-42 shows that all the data points, except those for 0 and 100 per cent oversize, fall close to the straight line, obtained by the method of least squares, above; this indicates that, at least in some instances, correlation can be obtained by plotting the experimental data directly on a Bennett diagram, the horizontal coordinate of which is $(x-x_0)$. The lower end point, at 100 per cent oversize, is in line with the extrapolated curve, but, because of the coordinates, the lower end point cannot be shown. On the other hand, the upper point, at zero per cent oversize and $(x-x_0)$ of 67.5, is certainly not on the line. (Refer to Figure 4-54b.)

The values of \underline{b} and \underline{n} are not the same as for the same data using the Rosin-Rammler equation and the inner percentage method. This is not unexpected, since the form of the equation has changed. Relative values of \underline{b} and \underline{n} would still have the same interpretation, in comparing sets of data.

Since the argument of the exponential in Weibull's function is $(x-x_0)$, rather than \bar{x} , consideration of Equations (4-4) and (4-45) indicates that the mean diameters, as predicted by Weibull's equation, can be expressed only by a complicated function of incomplete gamma functions:

$$\bar{x}_{qp}^{q-p} = \frac{\sum_{i=0}^{q-3} \frac{(q-3)! x_0^{q-3-i} \bar{x}^i}{(q-3-i)! i!} \Gamma \left(\frac{x_m - x_0}{\bar{x}} \right)^{n \left(\frac{i}{n} + 1 \right)}}{\sum_{i=0}^{p-3} \frac{(p-3)! x_0^{p-3-i} \bar{x}^i}{(p-3-i)! i!} \Gamma \left(\frac{x_m - x_0}{\bar{x}} \right)^{n \left(\frac{i}{n} + 1 \right)}} ,$$

(4-47)

where x_m is the maximum size of droplet. If x_m is assumed to be infinite, the incomplete gamma functions $\Gamma_a(b)$ in Equation (4-47) become the complete gamma function $\Gamma(b)$.

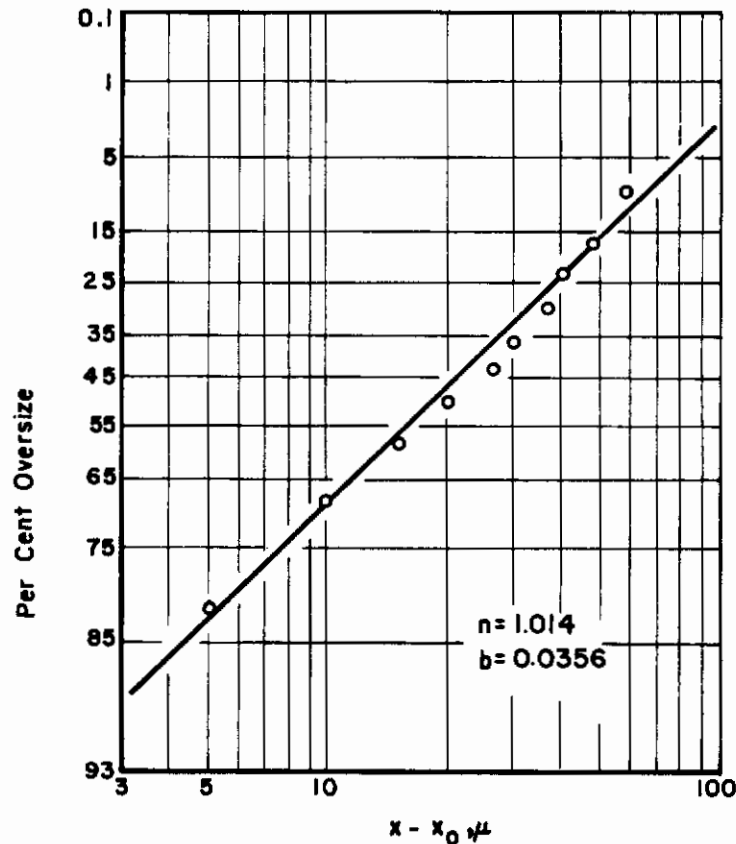


FIGURE 4-42. BENNETT DIAGRAM FOR HOUGHTON'S CUMULATIVE VOLUME DISTRIBUTION, USING $x_0 = 7.5$ FOR WEIBULL'S EQUATION

The Logarithmico-Normal Equation

Application of the methods of statistical analysis to the problem of size distribution has resulted in the logarithmico-normal equation, which has proved to be an effective means of correlating size-distribution data for crushed solids and spray droplets alike. Several theories have been advanced to derive this distribution function from first principles. Most plausible of these theoretical derivations have been those of B. Epstein⁽⁴⁻⁹³⁾ and F. Kottler^(4-94, 4-95).

Statistical Approach

After assuming that any breakage process may be conceived as composed of discrete steps, Epstein made the following assumptions: (a) the probability that a piece will be broken is equal to one, and (b) the proportional size distribution $F_n(x)$ resulting from the n^{th} step in the breakage process, as applied to any piece of size y remaining after the $(n-1)^{\text{st}}$ step, is independent of the size y of the piece.

If it is assumed that the original size distribution $G(y)$ corresponds to the random variable η_1 , and that the first step in the breakage process yields a distribution $F_1(x)$ of pieces obtained from each piece of size y , $F_1(x)$ corresponding to a random variable ζ_1 , then the resultant distribution remaining after the first step of the breakage process will correspond to a random variable $\xi_1 = \eta_1 \zeta_1$, since η_1 and ζ_1 are independent, as assumed in (a) and (b) above. Subsequent steps will result in further size distributions $F_n(\xi)$, each corresponding to an additional random variable ζ_n , which has a multiplicative effect on the random variable ξ_n associated with the resultant distribution after the

n^{th} step. Hence,

Contrails

$$\log \xi_n = \log \eta_1 + \sum_{i=1}^n \log \zeta_i \quad (4-48)$$

By the central-limit theorem of statistics, it can be shown that $\log \xi_n$ is asymptotically normal for $n \rightarrow \infty$, and hence that ξ_n is asymptotically logarithmico-normal. Epstein then proceeded to prove this asymptotic behavior for less restrictive assumptions.

Exponential Law of Decay

Having established that direct application of the Normal Law to the volume distribution of particles was not consistent with physical observations, Kottler(4-94)(4-95) began with a consideration of the exponential law of decay:

$$\frac{dx}{dt} = -kx, \quad (4-49)$$

which, in effect, is a mathematical expression of Epstein's assumption (b), above. Integration of this expression yields

$$t = -\frac{1}{k} \ln \frac{x}{A}, \quad (4-50)$$

where A is the value of x at $t = 0$.

Assuming that the times during which the particles have been comminuted are normally distributed with zero mean and unit variance, the probability z of a volume of particles having the normalized time t connected with them is given by

$$z = \frac{1}{\sqrt{2\pi}} e^{-(t^2/2)} = \frac{1}{\sqrt{2\pi}} e^{-\ln^2(x/A)/2k^2} \quad (4-51)$$

This probability z is also given by

$$z = \left| \frac{dV}{dt} \right| = \frac{kdV}{d \ln(x/A)} = kx \frac{dV}{dx} \quad (4-52)$$

Equating Equations (4-51) and (4-52),

$$\begin{aligned} \frac{dV}{dx} &= \frac{1}{\sqrt{2\pi} kx} e^{-\ln^2(x/A)/2k^2} \\ &= \frac{1}{\sqrt{2\pi} \sigma x} e^{-\ln^2(x/A)/2\sigma^2} \end{aligned} \quad (4-53)$$

where according to the customary probability nomenclatures, A has been identified as the geometric mean size M (which is synonymous with the median for the logarithmico-normal distribution), and k can be identified with the standard deviation, σ .

The cumulative volume distribution V is determined by integration of Equation (4-53) to be

$$\begin{aligned}
 V &= \frac{1}{\sqrt{2\pi}} \int_0^x \frac{1}{\sigma x} e^{-\frac{1}{2\sigma^2} \left(\ln \frac{x}{M}\right)^2} dx \\
 &= \frac{1}{\sqrt{\pi}} \int_{-\infty}^y e^{-y^2} dy \\
 &= \frac{1}{\sqrt{\pi}} \left[\int_{-\infty}^0 e^{-y^2} dy + \int_0^y e^{-y^2} dy \right] \\
 &= \frac{1}{\sqrt{\pi}} \left[\frac{\sqrt{\pi}}{2} + \frac{\sqrt{\pi}}{2} \operatorname{erf}(y) \right],
 \end{aligned}$$

$$V = \frac{1}{2} [1 + \operatorname{erf}(y)], \quad (4-54)$$

where

$$y = \frac{1}{\sigma\sqrt{2}} \ln \frac{x}{M} = -\frac{t}{\sqrt{2}} \quad (4-55)$$

and $\operatorname{erf}(y)$ is the error function, or probability integral, of y . Since $\operatorname{erf}(y)$ is an odd function of y , it follows that $\operatorname{erf}(-y) = -\operatorname{erf}(y)$.

Considerations of Equations (4-1) and 4-53) results in the following expressions for $\frac{dN}{dx}$ and N :

$$\frac{dN}{dx} = \frac{6}{\pi\sqrt{2\pi} \sigma x^4} \exp \left[-\frac{1}{2\sigma^2} \left(\ln \frac{x}{M}\right)^2 \right], \quad (4-56)$$

and

$$N = \frac{3e^{\frac{9\sigma^2}{2}}}{M^3 \pi} \left[1 + \operatorname{erf} \left(y + \frac{3\sigma}{\sqrt{2}} \right) \right], \quad (4-57)$$

where y is as defined by Equation (4-55). Inspection of Equation (4-57) reveals immediately that this equation for N could be readily normalized by setting the coefficient to the left of the bracket equal to one-half. A similar normalization could be effected for the equations for N , as determined for each of the other size-distribution functions.

Log-Probability Coordinates and Goodness of Fit

If Equation (4-54) is solved for y , the following equation, which is linear in $\ln x$, is obtained:

$$\operatorname{erf}^{-1} [2V - 1] = y = \frac{1}{\sigma\sqrt{2}} (\ln x - \ln M), \quad (4-58)$$

where $\operatorname{erf}^{-1} [a]$ is the inverse error function of a . Accordingly, Hazen⁽⁴⁻⁸⁸⁾ and Whipple⁽⁴⁻⁸⁹⁾ have devised a particular type of graph paper, called log-probability paper, on which the ordinate unit is $\log x = 0.434 \ln x$, and the abscissa unit is $\operatorname{erf}^{-1} [2V - 1]$.

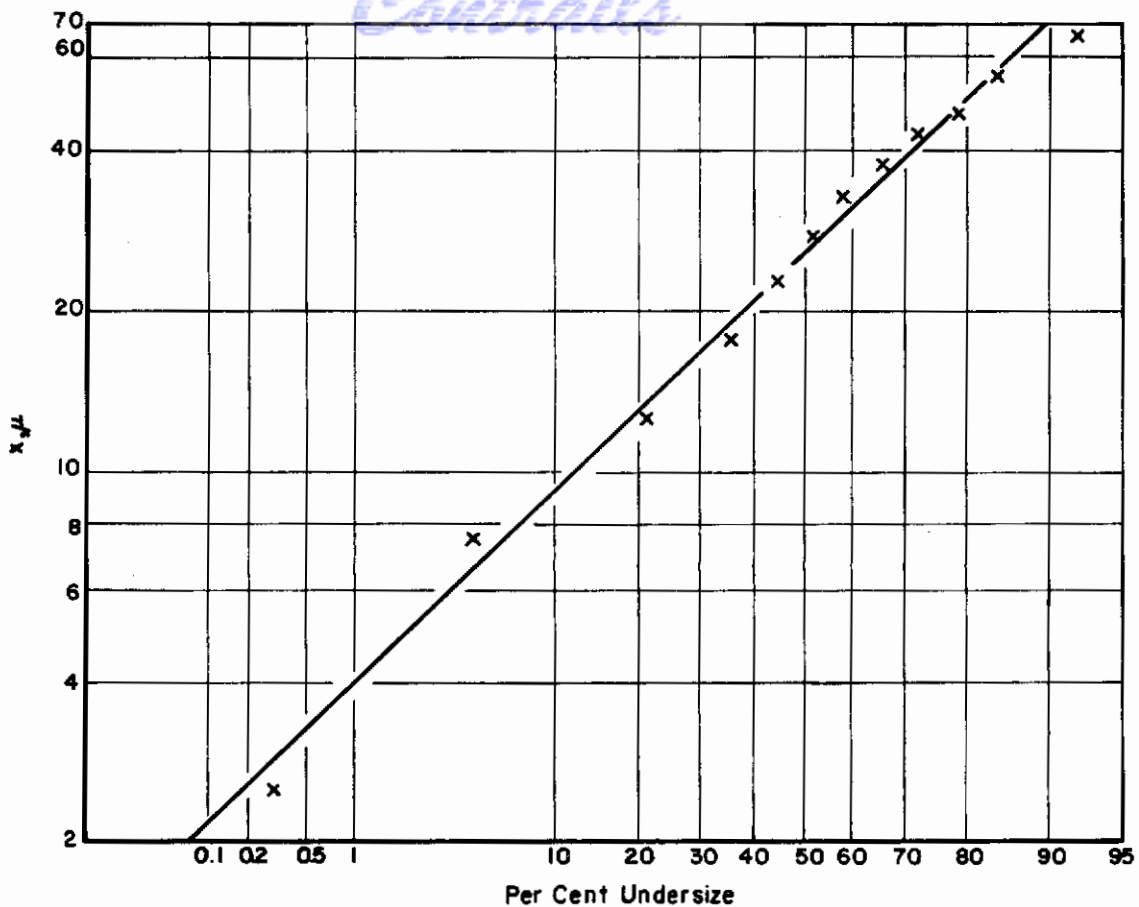


FIGURE 4-43. LOG-PROBABILITY GRAPH OF HOUGHTON'S RAW DATA FOR CUMULATIVE VOLUME DISTRIBUTION

Figure 4-43 is a log-probability graph of Houghton's data, as taken directly from Column 9 of Table 4-2. The straight line which appears to fit these data best has been drawn, and the parameters M and σ have been determined from this line. The value of M can be determined by inspection as the value of \underline{x} at which the straight line crosses the ordinate for which $V = 0.5$, or for which $\text{erf}^{-1} [2V - 1] = 0$. Consideration of Equations (4-55) and (4-58) reveals that the value of σ corresponding to the straight line drawn in this figure can be determined by the equation

$$\sqrt{2} \sigma = \frac{\ln \left(\frac{x_a}{x_b} \right)}{\text{erf}^{-1} [2V_a - 1] - \text{erf}^{-1} [2V_b - 1]}, \quad (4-59)$$

where \underline{a} and \underline{b} are any two points on the line. By a simple change of variable the values of the inverse error functions can be obtained from the Probit tables⁽⁴⁻⁸⁰⁾ of the standardized normal distribution given by

$$y = \frac{1}{\sqrt{2}\pi} \exp(-x^2/2) \quad (4-60)$$

Although the plot of an exact logarithmico-normal distribution will be a straight line on log-probability coordinates, any deviation of the experimental data from the exact logarithmico-normal distribution will be greatly distorted by the log-probability coordinates. Hence, in order to judge the goodness of fit for a particular logarithmico-normal distribution function to a given set of experimental data, it is necessary to compare the experimental deviation δ with some standard error

S associated with the particular logarithmico-normal function. From probability considerations, Urban⁽⁴⁻⁹⁹⁾ showed that the standard error S to be associated with any given value of V is

$$S = \sqrt{\frac{V'(1-V')}{\nu}} \quad (4-61)$$

where ν is the number of data points considered, and V' is the value of the theoretical cumulative volume distribution predicted by the logarithmico-normal function. By using Equation (4-61) it is possible to determine the coordinates V'_E of the standard error band by the equation

$$V'_E = V' \pm S \quad (4-62)$$

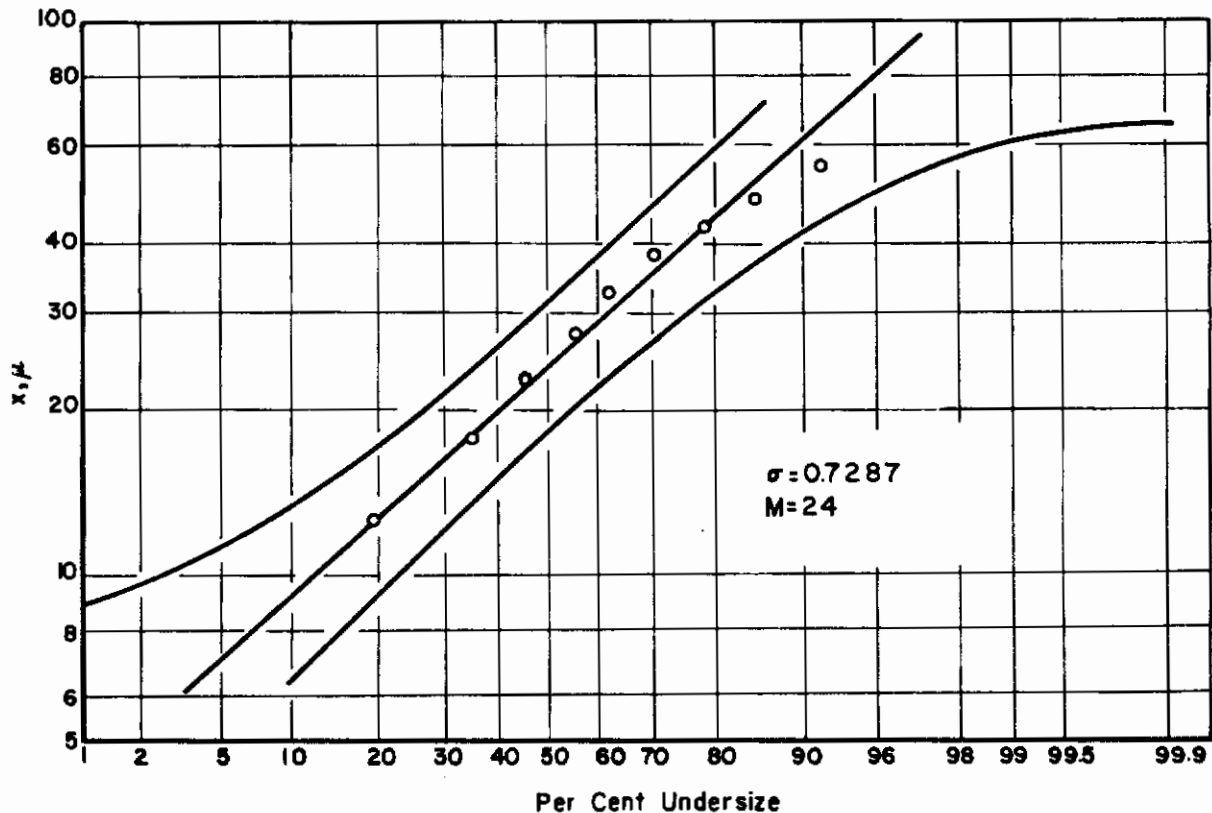


FIGURE 4-44. STANDARD ERROR BAND FOR LOG-PROBABILITY GRAPH OF HOUGHTON'S RAW DATA FOR CUMULATIVE VOLUME DISTRIBUTION

Figure 4-44 shows Houghton's data, decapitated at $x = 65 \mu$ and amputated at $x = 7.5 \mu$, as given in Column 10 of Table 4-2, and the standard error band associated with a mean line through the data points. Inspection of this figure reveals immediately that all of Houghton's experimental data, which have been included, fall inside of the standard error band. Owing to amputation and decapitation at the point $x = 7.5$, the per cent undersize equals zero, and at $x = 65.0$, the per cent undersize equals one hundred. Since these points are both at infinity on a log-probability graph, they do not fall within the error band.

Since the standard error S to be expected varies with the theoretical cumulative volume distribution V' , as seen from Equation (4-61), it is apparent that the logarithmico-normal function which best fits a given set of data (in the least squares sense) will be that function for which the sum of the squares of experimental deviations δ^2 divided by the squares of the standard errors S^2 is a

minimum

Contrails

$$\sum_{i=1}^{\nu} \frac{\delta_i^2}{S_i^2} = \sum_{i=1}^{\nu} \frac{(V_i - V_i')^2}{V_i (1 - V_i')} = \min. \quad (4-63)$$

This sum has been identified with the χ^2 distribution of probability theory by Kottler. The problem thus becomes one of determining the values of the parameters σ and M of Equation (4-53), such that the minimizing conditions of Equation (4-63) are satisfied. Rewriting Equation (4-58) as

$$-\sqrt{2} y = t - \frac{1}{\sigma} \ln M - \frac{1}{\sigma} \ln x = a + b \ln x, \quad (4-64)$$

and recalling from Equation (4-54) that

$$V_i' = \frac{1}{2} \left[1 + \operatorname{erf} \left(\frac{t}{\sqrt{2}} \right) \right],$$

the minimum condition of Equation (4-63) can be expressed by:

$$\frac{\partial}{\partial a} \left(\sum_{i=1}^{\nu} \frac{(V_i - V_i')^2}{V_i' (1 - V_i')} \right) = 0, \quad (4-65)$$

and

$$\frac{\partial}{\partial b} \left(\sum_{i=1}^{\nu} \frac{(V_i - V_i')^2}{V_i' (1 - V_i')} \right) = 0. \quad (4-66)$$

Consideration of Equation (4-54) reveals that Equations (4-65) and (4-66) will be exceedingly nonlinear as they stand. However, by making use of a method suggested by Brunt⁽⁴⁻¹⁰⁰⁾, these equations can be linearized, resulting in two simultaneous linear equations. Brunt's method proceeds as follows: let

$$V = V'(x, a, b) + \delta, \quad (4-67)$$

and let the best-fit values for \underline{a} and \underline{b} be expressed as

$$a = a_0 + a_1 \quad (4-68)$$

and

$$b = b_0 + b_1 \quad (4-69)$$

where a_0 and b_0 are the first approximation values for \underline{a} and \underline{b} , as obtained from the straight line drawn through the experimental points on the logarithmic probability coordinates. Under the assumption that a_1 and b_1 are small compared with a_0 and b_0 , V' can then be expressed by the first three terms of a Taylor series:

$$V'(x, a, b) = (V')_0 + a_1 \frac{\partial (V')_0}{\partial a_0} + b_1 \frac{\partial (V')_0}{\partial b_0}, \quad (4-70)$$

from which

$$V = (V')_0 + a_1 \frac{\partial (V')_0}{\partial a_0} + b_1 \frac{\partial (V')_0}{\partial b_0} + \delta, \quad (4-71)$$

and

$$\delta = V - (V')_0 - a_1 \frac{\partial (V')_0}{\partial a_0} - b_1 \frac{\partial (V')_0}{\partial b_0}, \quad (4-72)$$

where $(V')_0$ is the value of V' obtained from the first graphical approximation. If the denominators of Equations (4-65) and (4-66) are held constant for the differentiation, consideration of Equations (4-65), (4-66), (4-67), (4-71), and (4-72) leads to the following set of equations, which are linear in a_1 and b_1 :

$$\begin{aligned} \frac{\partial}{\partial a} \sum_{i=1}^{\nu} \frac{(V_i - V_i')^2}{V_i' (1 - V_i')} &\approx 2 \sum_{i=1}^{\nu} \frac{1}{V_i' (1 - V_i')} [V_i' - V_i] \frac{\partial V_i'}{\partial a} \\ &\approx 2 \sum_{i=1}^{\nu} \frac{1}{(V_i')_0 [1 - (V_i')_0]} \left[(V_i')_0 - V_i + a_1 \frac{\partial (V_i')_0}{\partial a_0} \right. \\ &\quad \left. + b_1 \frac{\partial (V_i')_0}{\partial b_0} \right] \frac{\partial (V_i')_0}{\partial a_0} = 0, \end{aligned} \quad (4-73)$$

and

$$\begin{aligned} \sum_{i=1}^{\nu} \frac{1}{(V_i')_0 [1 - (V_i')_0]} \left[(V_i')_0 - V_i + a_1 \frac{\partial (V_i')_0}{\partial a_0} \right. \\ \left. + b_1 \frac{\partial (V_i')_0}{\partial b_0} \right] \frac{\partial (V_i')_0}{\partial b_0} = 0, \end{aligned} \quad (4-74)$$

where $\frac{\partial (V_i')_0}{\partial a_0}$ and $\frac{\partial (V_i')_0}{\partial b_0}$ can be determined by consideration of Equations (4-54), (4-55) and (4-63) to be

$$\frac{\partial (V_i')_0}{\partial a_0} = \frac{1}{\sqrt{2\pi}} e^{-\frac{t_0^2}{2}}, \quad (4-75)$$

and

$$\frac{\partial (V_i')_0}{\partial b_0} = \frac{\ln x}{\sqrt{2\pi}} e^{-\frac{t_0^2}{2}}, \quad (4-76)$$

where

$$t_0 = a_0 + b_0 \ln x. \quad (4-77)$$

If a_1 and b_1 are small compared with a_0 and b_0 , respectively, the problem is essentially solved, although further applications of the above method can be made if a closer fit is desired. If, however, the values of a_1 and b_1 as determined by Equations (4-73) and (4-74) are not small compared with a_0 and b_0 , respectively, then the linearizing assumptions of the above method are not correct, and it will be necessary to draw a different straight line which more closely fits the data, as plotted on the log-probability coordinates. It can be seen that this method is of little use if the first graphical approximation was not a good one.

Figure 4-45 shows the best-fit straight-line approximation to Houghton's data, given in Column 10 of Table 4-2, as determined by the above method. Actually, several iterations were made in order to ensure the closest possible fit of the straight line to the experimental data. Comparison of Figures 4-44 and 4-45 show that little was gained over the original fit. No amount of iteration, of course, can change the fact that Houghton's data are not unimodal, and that they have been decapitated and amputated.

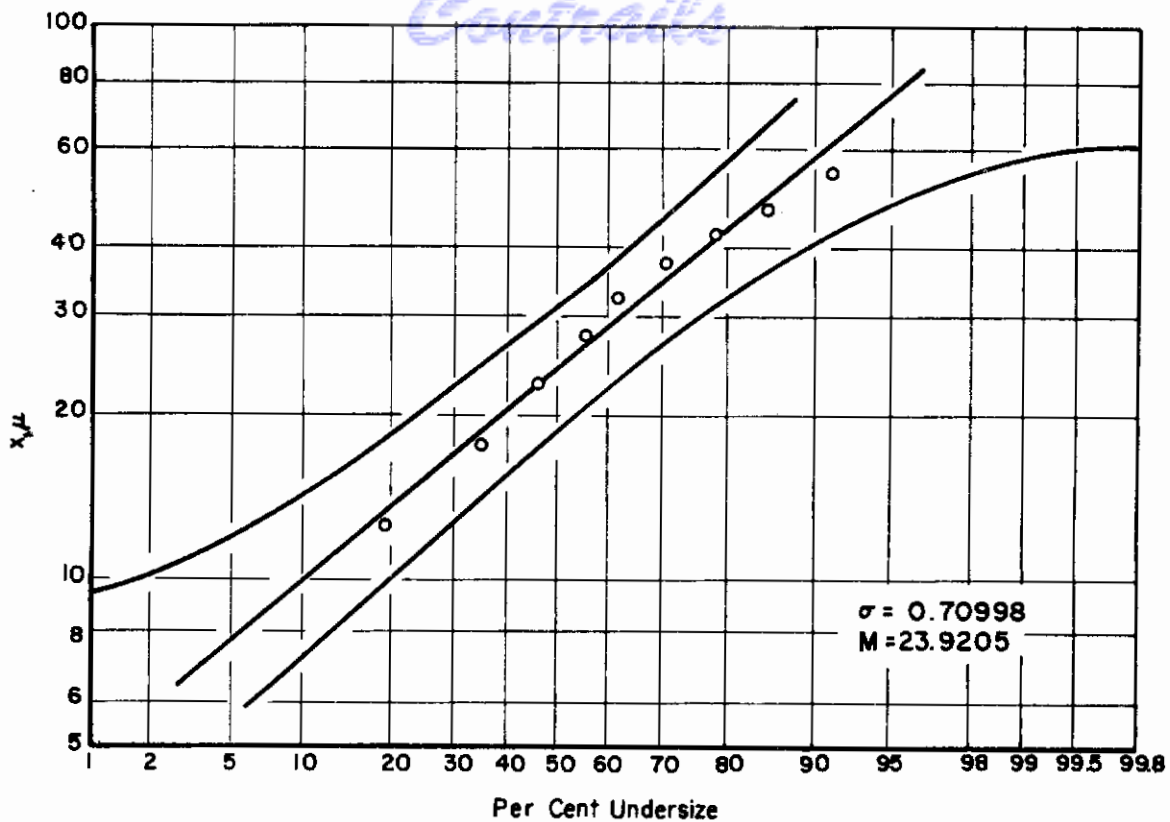


FIGURE 4-45. BEST-FIT STRAIGHT LINE APPROXIMATION TO HOUGHTON'S RAW DATA FOR CUMULATIVE VOLUME DISTRIBUTION AS DETERMINED BY BRUNT'S METHOD

Inner Percentage and the Logarithmico-Normal Equation

In an effort to obtain a better fit to Houghton's data with the logarithmico-normal equation, the effect of upper and lower size limits will be considered. Since the size range for Houghton's data is finite, whereas the logarithmico-normal equation assumes an infinite range of sizes, it again appears advisable to make use of the concept of inner percentages, as described in a previous section. By making use of this concept, a successive iteration method similar to that developed for the Rosin-Rammler Equation (4-18) can be devised for the logarithmico-normal Equation (4-54).

Substitution of Equation (4-54) into Equation (4-26), with consideration of Equation (4-58), yields

$$\begin{aligned} \operatorname{erf}^{-1} [2(V_m - V_o) P_i + 2 V_o - 1] &= \operatorname{erf}^{-1} [G'] \\ &= \frac{2.3026}{\sigma\sqrt{2}} (\log x_i - \log M). \end{aligned} \quad (4-78)$$

Here again, a set of values for V_o and V_m is chosen such that

$$0 \leq V_o < V_m \leq 1, \quad (4-79)$$

and the first-approximation values for σ and M are obtained from Equation (4-59) by the method of least squares. These values of σ and M can then be used to find a new set of values for V_o and

V_m , by using Equation (4-54), and the process can be continued until one set of values for σ and M differs from the previous set by less than a preassigned percentage. As before, this iteration process converges to a unique set of values for σ and M , and a reasonable first guess for the values of V_0 and V_m would be zero and one, respectively.

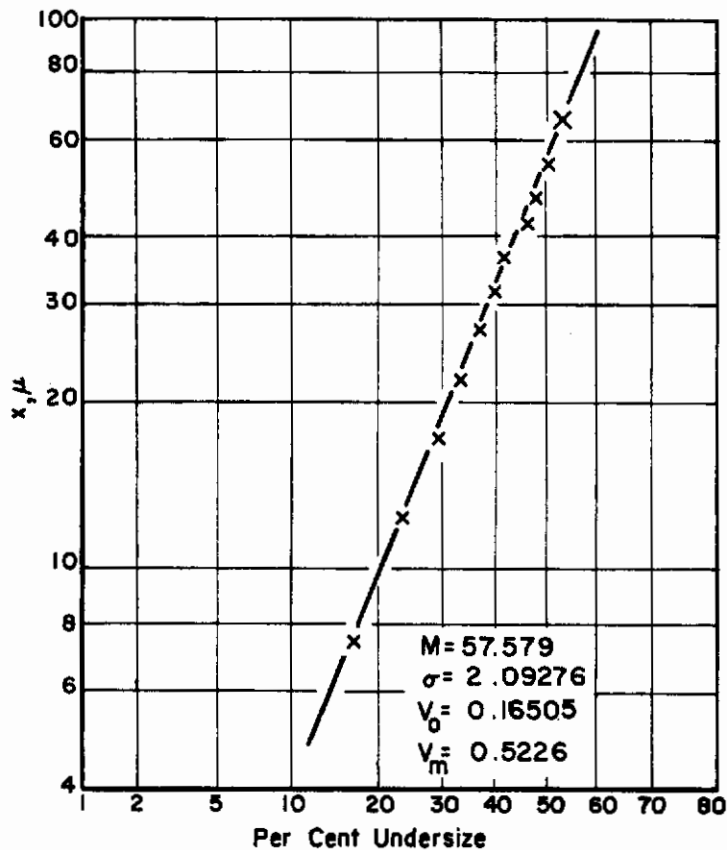


FIGURE 4-46. LOG-PROBABILITY GRAPH OF HOUGHTON'S CUMULATIVE VOLUME DATA, AFTER MAKING ALLOWANCE FOR SIZE LIMITS, USING THE CONCEPT OF INNER PERCENTAGES

Figure 4-46 shows the straight line obtained from Houghton's data given in Column 10 of Table 4-2, as a result of applying the successive iteration method above. The experimental points grouped about this line were obtained by plotting G' against x on the log-probability coordinates. Comparison of Figures 4-45 and 4-46 reveals immediately that the second curve, which makes allowance for the finiteness of the size range, is by far the better fit to the experimental data, and that the concept of inner percentages is again a useful tool in the correlation of drop-size data. It must be kept in mind, however, that this curve shows only 52 per cent undersize at $x = 65 \mu$, or 48 per cent over 65μ . With this large per cent oversize at 65μ , as compared with the value of 7.7 per cent for Houghton's original data, this becomes a case where the mean drop size cannot be approximated by considering the infinite distribution only. The cut-off must be taken into account.

Limited Logarithmico-Normal Equations

A second method for making allowance for x_0 and x_m , the minimum and maximum sizes, respectively, is to modify the logarithmico-normal equation itself. This modification can be effected by redefining the y of Equation (4-55) such that

$$y(x_0) = -\infty$$

and

$$y(x_m) = \infty \quad (4-80)$$

Satisfaction of Equation (4-80) is assumed by letting

$$y = \frac{1}{\sigma\sqrt{2}} \ln \frac{(x-x_0)}{M'(x_m-x)} = \frac{1}{\sigma\sqrt{2}} \ln u' \quad (4-81)$$

which is the argument for Kottler's limited logarithmico-normal function. Consideration of the exponential law of decay, which led to Equation (4-54), indicates that Equation (4-81) can be derived from fundamental considerations only by assuming the following law of decay:

$$\frac{dx}{dt} = -k \frac{(x-x_0)(x_m-x)}{x_m-x_0} \quad (4-82)$$

Although, as mentioned by Kottler, Equation (4-82) is similar to the equation of second-order, or bimolecular, reaction in chemical kinetics, there is no observable extreme value of the rate of decay inside the chemically significant interval. Hence, it appears that Equation (4-81) has no chemically significant interval. Hence, it appears that Equation (4-81) has no physically reasonable theoretical foundation.

Consideration of Equations (4-54) and (4-81) reveals that the following equation is true:

$$M' = \frac{x_{50}-x_0}{x_m-x_{50}} \quad (4-83)$$

where x_a is the value of x for which $V = a$. Also, since $\text{erf}(-y) = -\text{erf}(y)$, it is readily apparent that

$$\frac{(x_m-x_0)}{M'(x_m-x_a)} = \frac{M'(x_m-x_b)}{(x_b-x_0)} \quad (4-84)$$

where

$$b = 1 - a. \quad (4-85)$$

By equating the expressions for M^2 , as obtained from Equations (4-84) and (4-85), the following quadratic equation for the unknown quantities x_m and x_0 , in terms of the experimentally determined values of x_a and x_b , is obtained:

$$\begin{aligned} (x_m-x_a)(x_m-x_b)(x_{50}-x_0)^2 - (x_m-x_{50})^2(x_a-x_0)(x_b-x_0) &= x_0^2 [(x_m-x_{50})^2 - (x_m-x_a)(x_m-x_b)] \\ &\quad - x_0 [x_a x_b (x_m-x_{50})^2 - 2x_{50}(x_m-x_b)] \\ &\quad + x_a x (x_m-x_{50})^2 - x_{50}^2 (x_m-x_a)(x_m-x_b) \\ &= Ax_0^2 - Bx_0 + C = 0 \end{aligned} \quad (4-86)$$

The nonlinearity of Equation (4-86) makes application of the method of least squares inadvisable.

If, however, the minimum size x_0 is assumed to be equal to zero, as was done by Mugele and Evans for their special Upper Limit Function, Equation (4-81) becomes

$$y = \frac{1}{\sigma\sqrt{2}} \ln \frac{x}{M''(x_m-x)} = \frac{1}{\sigma\sqrt{2}} \ln u'' \quad (4-87)$$

from which the following equation for x_m results:

$$\frac{x_m}{x_{50}} = \frac{x_{50} (x_a + x_b) - 2x_a x_b}{x_{50}^2 - x_a x_b} \quad (4-88)$$

The value of x_m can then be determined as the simple average of the values of x_m obtained from Equation (4-88) by letting a equal 5, 10, 15, . . . , 40, and 45.

Having determined x_m by letting $x_o = 0$, the corresponding value of x_o can be readily determined from Equation (4-86) by assuming that $\frac{4AC}{B^2} \ll 1$. From Equation (4-86),

$$\begin{aligned} x_o &= \frac{1}{2} \left[\frac{B}{A} - \frac{B}{A} \sqrt{1 - \frac{4AC}{B^2}} \right] \\ &\approx \frac{1}{2} \left[\frac{B}{A} - \frac{B}{A} \left(1 - \frac{2AC}{B^2} \right) \right] \\ &= \frac{C}{B} \end{aligned} \quad (4-89)$$

Further iteration beyond this first approximation is inadvisable, since it was found that the process is nonconvergent. The best-fit values of σ and M' (or M'') can be determined by substitution of u' (or u'') for u in Equation (4-58), which can then be solved for σ and M' (or M'') by the method of least squares.

Figure 4-47 shows the graph of Houghton's cumulative volume data as given in Column 10 of Table 4-2 against u'' , where x_o is set equal to zero, on log-probability coordinates. Figure 4-48 shows the graph of the same data against u' , where the value of x_o was determined by means of Equation (4-89). The best-fit straight line in each case was determined by the method of least squares. Although each of these straight lines shows better correlation of the data than did the line obtained from the log-normal equation, as shown in Figure 4-45, each is a poorer correlation than that obtained by using the concept of inner percentages, as shown in Figure 4-46.

Mean Diameters for Logarithmico-Normal Equation

From Equations (4-4) and (4-53), the mean diameter for the logarithmico-normal equation is seen to be

$$\bar{x}_{qp} = \left(Me^{(q+p-6)\frac{\sigma^2}{2}} \right)^{q-p} \frac{\Gamma_{m'}(1) - \Gamma_{o'}(1)}{\Gamma_{m''}(1) - \Gamma_{o''}(1)} \quad (4-90)$$

where

$$\left. \begin{aligned} m' &= \frac{1}{\sigma\sqrt{2}} \ln \left(\frac{x_m}{M} \right) - \frac{(q-3)\sigma}{\sqrt{2}} , \\ o' &= \frac{1}{\sigma\sqrt{2}} \ln \left(\frac{x_o}{M} \right) - \frac{(q-3)\sigma}{\sqrt{2}} , \\ m'' &= \frac{1}{\sigma\sqrt{2}} \ln \left(\frac{x_m}{M} \right) - \frac{(p-3)\sigma}{\sqrt{2}} , \\ o'' &= \frac{1}{\sigma\sqrt{2}} \ln \left(\frac{x_o}{M} \right) - \frac{(p-3)\sigma}{\sqrt{2}} . \end{aligned} \right\} \quad (4-91)$$

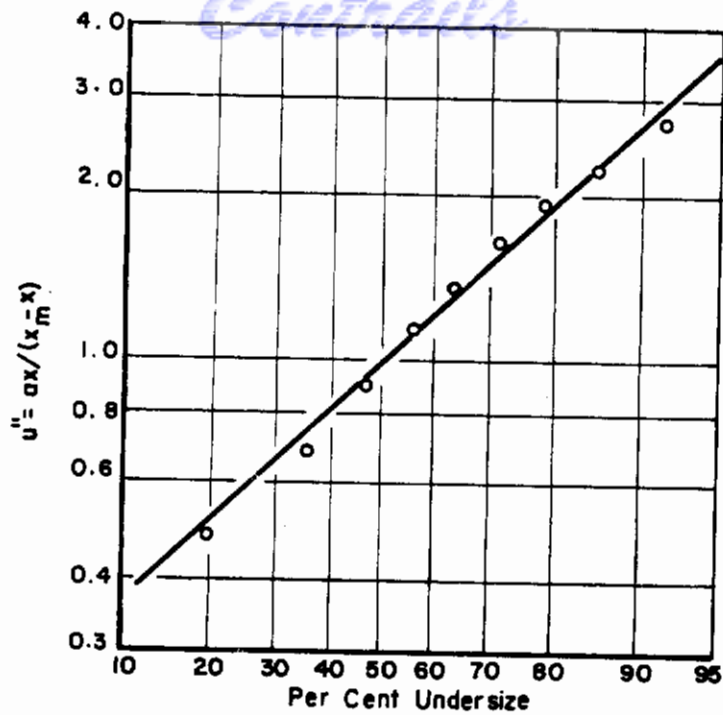


FIGURE 4-47. LOG-PROBABILITY GRAPH OF HOUGHTON'S CUMULATIVE VOLUME DISTRIBUTION DATA USING SPECIAL UPPER LIMIT FUNCTION

$$x_m = 188.2$$

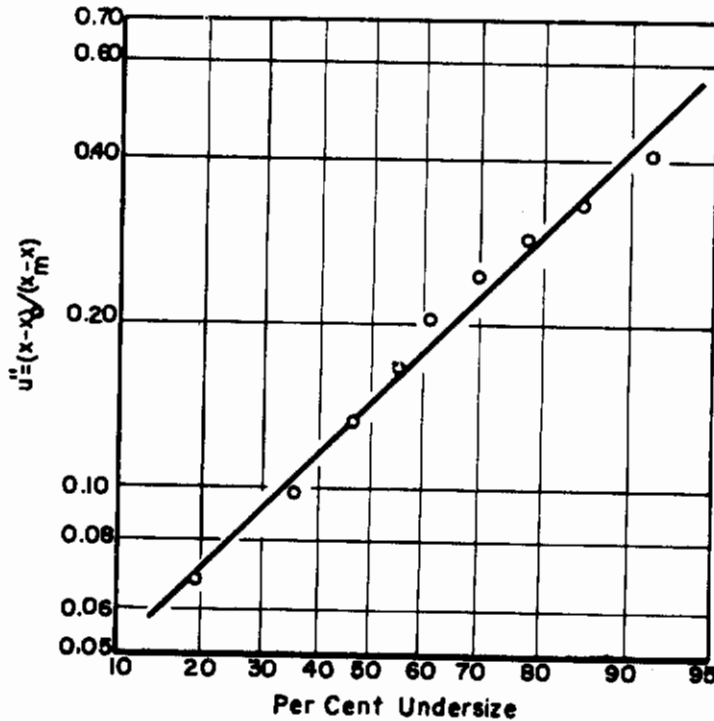


FIGURE 4-48. LOG-PROBABILITY GRAPH OF HOUGHTON'S CUMULATIVE VOLUME DATA USING LIMITED LOGARITHMIC-NORMAL FUNCTION

$$x_m = 188.2 \quad x_0 = 0.74438$$

Consideration of Equations (4-90) and (4-91) reveals that, if x_0 and x_m are set equal to zero and infinity, respectively, the mean size can be determined by the equation

$$\bar{x}_{qp} = Me^{(q+p-6)\frac{\sigma^2}{2}} \quad (4-92)$$

Substitution of Equations (4-54) and (4-81) into Equation (4-4) results in an expression for the mean size which cannot be integrated in closed form for any but a few discrete values of σ . Hence, the limited logarithmico-normal equation, which makes allowance for both x_0 and x_m , offers no advantages whatsoever insofar as the calculation of mean drop sizes is concerned.

However, if only the upper size limit x_m is considered, as in the special upper limit function of Equation (4-88), the general equation for mean drop sizes can be determined by substituting Equations (4-88) and (4-54) into Equation (4-4). The resultant equation then becomes

$$\bar{x}_{pq}^{q-p} = \frac{x_m^{q-p} \sum_{i=0}^{3-q} \frac{(3-q)!}{(3-q-i)! i!} \frac{1}{(M')^i} \exp\left[\frac{(i\sigma)^2}{2}\right]}{\sum_{i=0}^{3-p} \frac{(3-p)!}{(3-p-i)! i!} \frac{1}{(M')^i} \exp\left[\frac{(i\sigma)^2}{2}\right]} \quad (4-93)$$

The Griffith Comminution Function

By applying the theory of probability to the molecular surface energy in an elementary comminuted system, L. Griffith⁽⁴⁻¹⁰¹⁾ obtained an expression for the incremental numerical size distribution which is based on fundamental considerations. He considered an elementary system of N particles with N_i particles in each size range $x_i \leq x < x_i + \Delta x$. The corresponding surface energy per molecule of the particles in each size range was designated as E_i , and the following equations were thus established:

$$\sum_{i=0}^n N_i = N, \quad (4-94)$$

and

$$\sum_{i=0}^n N_i E_i = E, \quad (4-95)$$

where E is the total surface energy of the system.

By assuming that the individual molecules do not possess identity, the number of ways G that the size distribution can occur can be expressed by

$$G = \sum_{i=0}^n \frac{1}{N_i!} \quad (4-96)$$

By further assuming that the size distribution will be that for which G is a maximum, for a given amount of energy, the normalized differential numerical size distribution $\frac{dN}{dx}$ can then be expressed as

Controls

$$\left(\frac{dN}{dx}\right)_i = \frac{N_i}{N} = \frac{p_i e^{-BE_i}}{\sum_{i=0}^n p_i e^{-BE_i}}, \quad (4-97)$$

where p_i is an added probability factor to allow for differential effects of protection on various sizes of particles, and the coefficient B can be determined from the equation*

$$\frac{\sum_{i=0}^n E_i e^{-BE_i}}{\sum_{i=0}^n e^{-BE_i}} = \frac{E}{N}. \quad (4-98)$$

The problem now becomes that of determining expressions for E_i and p_i , as functions of x . By assuming the surface energy g per unit surface area to be independent of x , the surface energy per molecule can be determined as the surface energy of the particle divided by the number of molecules in the particle. Hence,

$$E_i = \frac{6gm}{\rho} \frac{1}{x_i}, \quad (4-99)$$

where m is the mass of a molecule and ρ is the density of the substance.

By postulating that the probability p that a particle class will remain in a certain size range is inversely proportional to the probability that it will be comminuted, Griffith proposed the following expression for the probability p :

$$p = \frac{k}{x^r}. \quad (4-100)$$

Since, in actual practice, the probability of comminution varies from no discrimination to the probability that larger particles will fall into the grinder more rapidly, as predicted by Stokes' law, it is to be expected that

$$0 \leq r \leq 2.$$

Substitution of Equations (4-99) and (4-100) into Equation (4-97) then results in Griffith's equation for incremental numerical size distribution:

$$\frac{dN}{dx} = k' x^{-r} e^{-\frac{b}{x}} \quad (4-101)$$

*See Boltzmann distribution in any statistical mechanics reference.

where

Contrails

$$k' = \frac{k}{\sum_{i=0}^n p_i e^{-BE_i}}, \quad (4-102)$$

and

$$b = \frac{6gm}{\rho}. \quad (4-103)$$

Equation (4-101) is readily linearized by taking the logarithm of both sides:

$$\log \frac{dN}{dx} = \log k' - r \log x - \frac{b \log e}{x}. \quad (4-104)$$

Hence, the best-fit values of k' , r , and b can be determined from experimental data for $\left(\frac{dN}{dx}\right)$ by using the method of least squares.

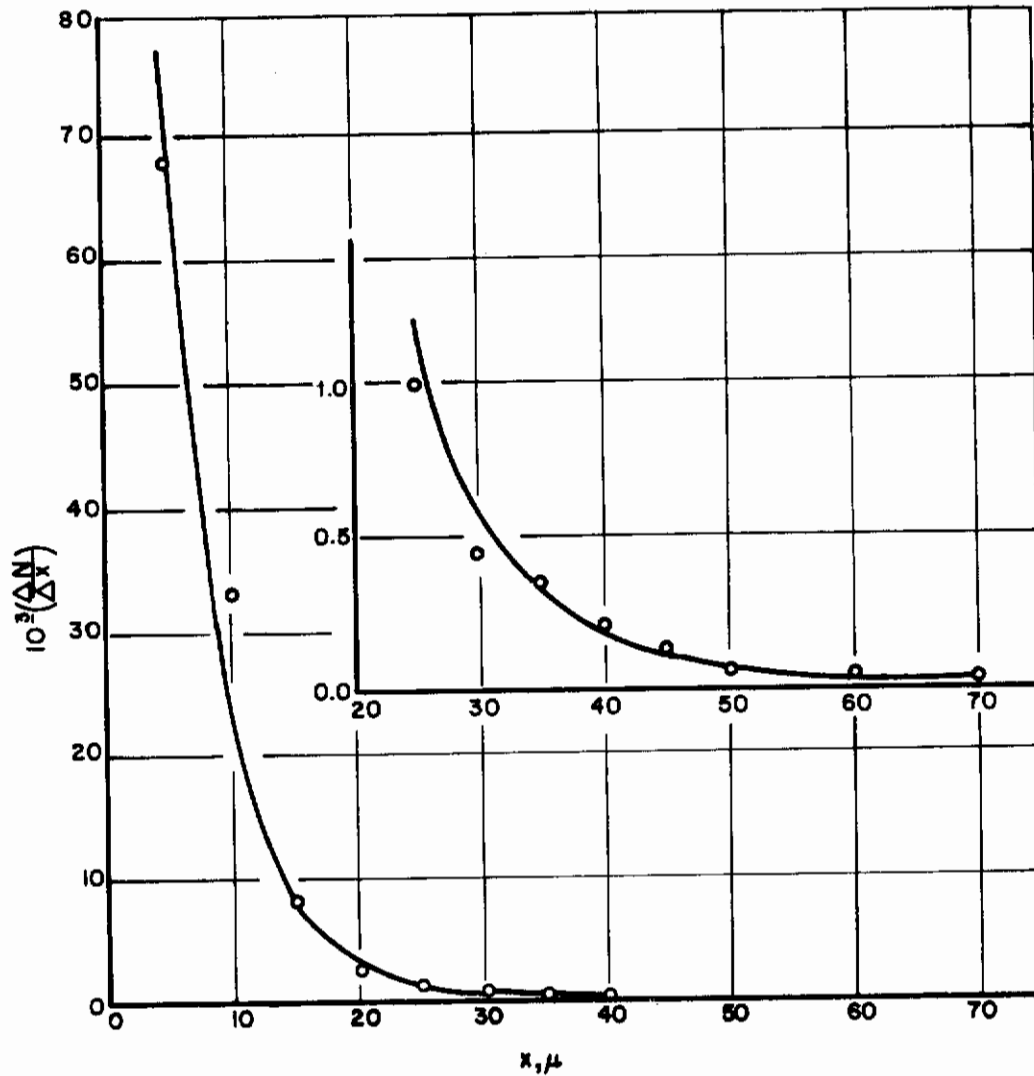


FIGURE 4-49. COMPARISON OF GRIFFITH'S THEORETICAL CURVE WITH NORMALIZED INCREMENTAL NUMERICAL DISTRIBUTION FROM HOUGHTON'S DATA

Figure 4-49 shows the curve obtained, using Equation (4-104), by applying the method of least squares to Houghton's data, given in Column 5 of Table 4-2. It is apparent from this figure that Griffith's distribution function is a valid means of representing incremental numerical size distribution.

Since Equation (4-101) cannot be integrated in closed form, it is not readily applicable to the determination of a cumulative numerical or volume distribution. For the same reason, it cannot be used to determine a general expression for mean sizes.

Roller's Size-Distribution Function

From empirical considerations, P. S. Roller⁽⁴⁻¹⁰²⁾ deduced the following expression for the cumulative volume distribution \underline{V} :

$$V = ax^{1/2}e^{-b/x} \quad (4-105)$$

The corresponding differential distributions are readily determined from Equations (4-1) and (4-105) as

$$\frac{dV}{dx} = a \left(\frac{x^{-1/2}}{2} + bx^{-3/2} \right) e^{-b/x} \quad (4-106)$$

and

$$\frac{dN}{dx} = \frac{3a}{\pi} \left(x^{-7/2} + 2bx^{-9/2} \right) e^{-b/x} \quad (4-107)$$

Consideration of Equation (4-107) indicates immediately that it is impossible to obtain an expression for \underline{N} in closed form. This fact also rules out the possibility of obtaining any expression in closed form for the average size of the droplets.

Inspection of Equations (4-105) and (4-106) indicates at once that Roller's size-distribution function possesses the following general properties, which are confirmed by experimental observation:

$$\left. \begin{aligned} V(0) &= 0, \\ \frac{dV}{dx}(0) &= 0, \end{aligned} \right\} \quad (4-108)$$

and

$$\frac{dV}{dx} = > 0 \text{ for } V = 1.$$

It is readily apparent from Equation (4-105) that the values of \underline{b} and \underline{a} can be determined graphically by plotting $\log(V/x^{1/2})$ against $1/x$. The slope of the best straight line through these points will be equal to $(b \log e)$, and the point at which this line crosses the abscissa, for $x = 1$, will be equal to $\log a$. The best-fit values of \underline{a} and \underline{b} can also be determined analytically by applying the method of least squares to the logarithm of Equation (4-105):

$$\log(V/x^{1/2}) = \log a - b \log e/x \quad (4-109)$$

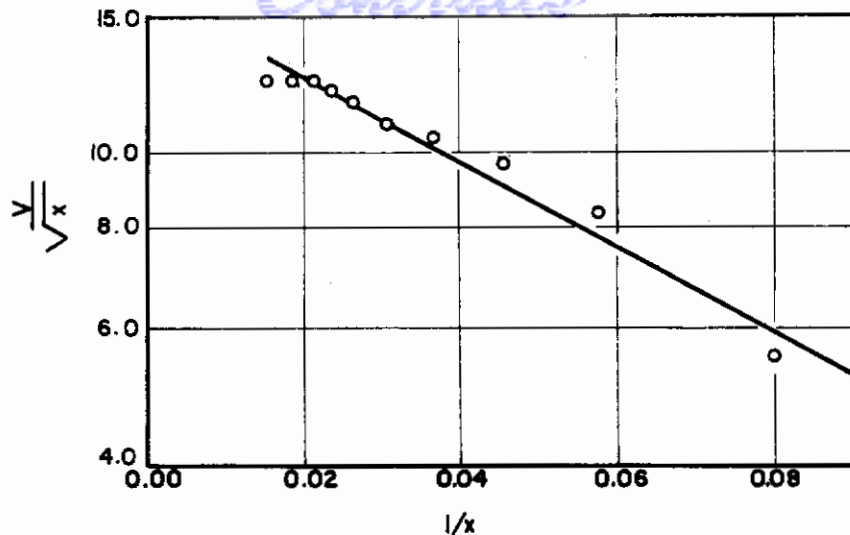


FIGURE 4-50. CORRELATION OF HOUGHTON'S CUMULATIVE VOLUME DISTRIBUTION BY MEANS OF ROLLER'S FUNCTION

Figure 4-50 shows the variation of $\log (V/x^{1/2})$ for Houghton's data (where V is taken from Column 10 of Table 4-2) with respect to $(1/x)$, along with the best-fit straight line as determined by the least squares method outlined above. Inspection of Figure 4-50 indicates that Roller's equation gives about as good a correlation of Houghton's data as the other methods when cut-off limits are not considered.

Since Roller's function, as defined by Equation (4-105), permits no upper limit for V , the iteration method for determining the best values of the parameters by use of the concept of inner percentages, is not applicable to this function. This absence of an upper limit for V makes the iteration process nonconvergent.

Consideration of Equations (4-4) and (4-107) leads to the following complicated expression for the mean diameters, as predicted by Roller's distribution function:

$$\bar{x}_{qp}^{q-p} = b^{q-p} \frac{\Gamma_{b/x_0} (5/2-q) + \Gamma_{b/x_0} (7/2-q) - \left[\Gamma_{b/x_m} (5/2-q) + \Gamma_{b/x_m} (7/2-q) \right]}{\Gamma_{b/x_0} (5/2-p) + \Gamma_{b/x_0} (7/2-p) - \left[\Gamma_{b/x_m} (5/2-p) + \Gamma_{b/x_m} (7/2-p) \right]}. \quad (4-110)$$

Multimodal Size Distribution

Most of the formulae for differential numerical or volume distributions which have been presented cannot be used to fit multimodal data, of which the Houghton's data are a type. Yet, as pointed out on page 1-39 of Chapter 1, several disturbances of different wavelength may contribute to the breakup of a liquid jet. When the phenomenon of secondary atomization occurs, there may then be a different size distribution associated with each of the effective wave-lengths of breakup. The size distribution of the total resultant spray will then be a composite of the various individual size distributions, each associated with a different wavelength of disturbance. Hence, it may be reasoned that multimodal size distributions are, indeed, theoretically to be expected.

However, since it is frequently difficult to determine where one individual distribution "ends" and another "begins", it is difficult to fit a multimodal experimental distribution by a sum of the unimodal expressions given above. Accordingly, the problem has been attacked by considering it to be simply one of curve fitting.

The general function which was found by O'Toole⁽⁴⁻⁹⁵⁾ to represent multimodal distributions best is

$$z = \exp \left[- \sum_{i=0}^{2n} a_i x^i \right], \quad (4-111)$$

where z can be identified either with $\frac{dN}{dx}$ or with $\frac{dV}{dx}$, and where n is the number of maxima observed in the experimental distribution. Three methods for fitting Equation (4-111) to an experimental bimodal size distribution which are described by Dallavalle, Orr, and Blocker⁽⁴⁻¹⁰⁴⁾ are

- (1) The Method of Moments
- (2) The Method of Least Squares
- (3) The Five-Ordinate Method.

Since these are standard methods employed in curve-fitting, they will not be further described here.

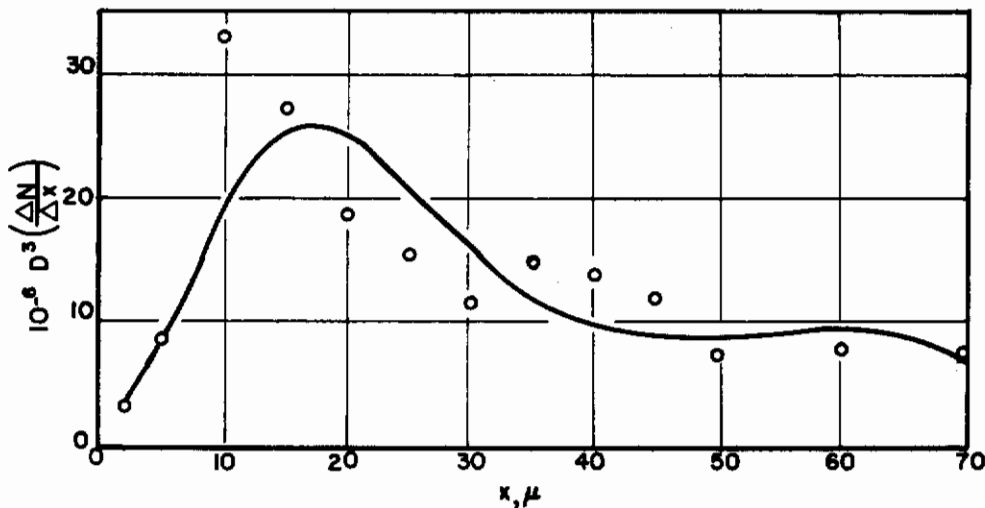


FIGURE 4-51. COMPARISON OF THEORETICAL CURVE OBTAINED, USING O'TOOLE'S METHOD FOR A BIMODAL DISTRIBUTION, WITH NORMALIZED INCREMENTAL VOLUME DISTRIBUTION FROM HOUGHTON'S DATA

Figures 4-51 and 4-52 show the curves obtained by applying the method of least squares to Houghton's data given in Column 6 of Table 4-2, and using the function given by Equation (4-111). Figure 4-51 shows the fit assuming a bimodal-distribution equation; it was mentioned previously that the assumption of a trimodal distribution for these data did not appear compatible with their accuracy. Figure 4-52 shows the fit assuming a trimodal distribution, or, essentially, a distribution function with two more parameters. Figure 4-52 shows better agreement than Figure 4-51, but still not good agreement, although it was obtained at the expense of about twice the labor in fitting. Furthermore, considering that seven parameters were available to fit only 13 points, the agreement may be considered poor indeed.

It may be concluded that this method, considered as a purely empirical one, is of little use, since the fit may be poor, the amount of labor required large, and extrapolation is not, in any sense, justified.

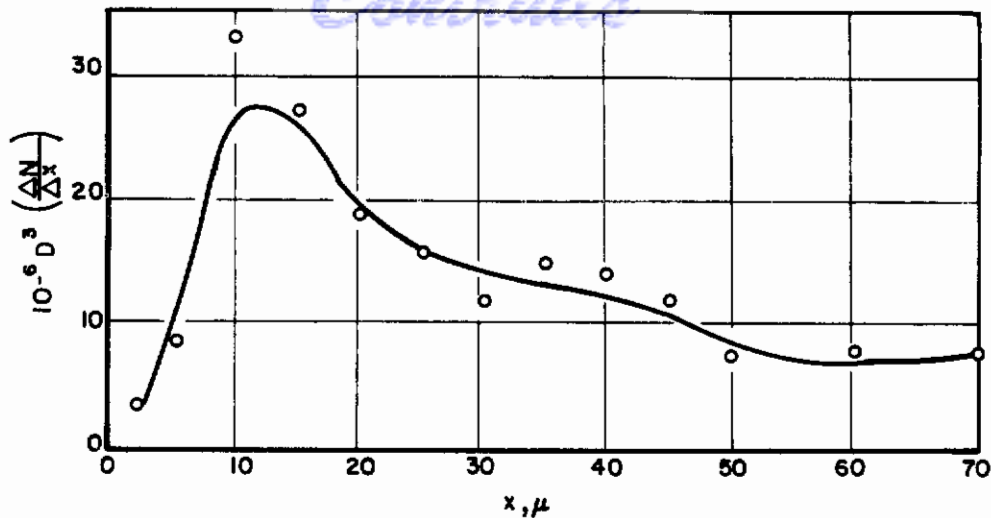


FIGURE 4-52. COMPARISON OF THEORETICAL CURVE OBTAINED, USING O'TOOLE'S METHOD FOR A TRIMODAL DISTRIBUTION, WITH NORMALIZED INCREMENTAL VOLUME DISTRIBUTION FROM HOUGHTON'S DATA

Persistence of Form

Since none of the size-distribution functions described above are based upon fundamental principles, it would seem desirable to devise a method for deriving an expression for drop-size distribution which would conform to some definite physical law. It has been found that a Maxwellian distribution of velocities has a persistence of mathematical form in statistical mechanics. As a mathematical artifice, rather than a physical concept, it can be assumed here as a postulate that the distribution for drop size will show a preservation of form. To this postulate may be added an assumption as to the law of radius change, such as

$$\frac{dr}{dt} = -\frac{k}{r}, \quad (4-112)$$

which is derived for the evaporation of single, stationary droplets (cf. Chapter 8).

G. F. Carrier⁽⁴⁻¹⁰⁵⁾ has examined this problem as follows: Let the number of liquid drops in the system under consideration be N and the number in the radius range of r to $(r + \Delta r)$, at time t , be $N\rho(r,t)\Delta r$, where $\rho(r,t)$ is a density function describing the distribution of drop sizes. Furthermore, let the rate of change of the radius be given by the general relation

$$\frac{dr}{dt} = -g(r) \quad (4-113)$$

If it is supposed that the initial density distribution $\rho(r,0)$ is known, the problem may be defined as that of determining $\rho(r,t)$ from these assumptions. If there are $N\rho(r,t)(r' - r)$ drops in the size range r to r' at time t , there will be the same number of drops in the size range $[r - g(r)\Delta t], [r' - g(r')\Delta t]$ at $(t + \Delta t)$. That is,

$$\rho(r,t)(r' - r) = [\rho(r - g(r)\Delta t, t + \Delta t)] [r' - r - (g(r') - g(r))\Delta t]. \quad (4-114)$$

Dividing both sides of Equation (4-114) by $(r' - r)$ and taking the limit as $r' \rightarrow r$, there results

$$\rho(r, t) = [\rho(r - g(r) \Delta t, t + \Delta t)] [1 - g'(r) \Delta t] \quad (4-115)$$

Dividing by Δt , and passing to the limit as $\Delta t \rightarrow 0$,

$$\frac{\rho(r - g\Delta t, t + \Delta t) - \rho(r, t)}{\Delta t} - \rho g' = 0 \quad ,$$

or

$$\rho_t - g \rho_r - \rho g_r = 0,$$

so that

$$\frac{1}{g} (g\rho)_t - (g\rho)_r = 0. \quad (4-116)$$

Defining

$$\int_{r_0}^r g^{-1}(r) dr = h(r), \quad (4-117)$$

then

$$(g\rho)_t - (g\rho)_h = 0. \quad (4-118)$$

Also, $g\rho$ may be defined in terms of a new function, F , such that

$$g\rho = F [h(r) + t] \quad (4-119)$$

The density distribution may now be written as

$$\rho = \frac{1}{g(r)} F [h(r) + t] \quad (4-120)$$

Suppose that at $t = 0$, $\rho(r, t)$ is given by the function $S(r)$; then

$$S(r) = \frac{1}{g(r)} F [h(r)] \quad (4-121)$$

and, in order to find F , the inverse relation $r(h)$ must be used.

Let $g[r(h)]$ and $S[r(h)]$ be denoted, respectively, by $G(h)$ and $\sigma(h)$. Now Equation (4-121) becomes

$$F(h) = G(h) \sigma(h),$$

and the density function becomes

$$\rho = \frac{1}{g(r)} G [h(r) + t] \sigma[h(r) + t] \quad , \quad (4-122)$$

which reduces, at $t = 0$, to

$$\rho(r, 0) = \sigma[h(r)] = S(r).$$

It is now seen that the types of distribution functions of a self-preserving form are very limited. It may also be noted that if the original distribution has a cut-off at r_0 , the new distribution will have a cut-off at $r_c = r [h(r_0) - t]$.

As an example, the evaporation law of Equation (4-112) will be used, that is, $g(r) = \frac{k}{r}$, and the three-constant equation will be used to express the initial distribution, that is, $S(r) = ar^p e^{-br^q}$. Then

$$h = \int_0^r g^{-1} dr = \frac{r^2}{2k}$$

Also, $r(h) = \sqrt{2kh}$, $G(h) = \sqrt{\frac{k}{2h}}$, and

$$\sigma(h) = a(2kh)^{\frac{p}{2}} e^{-b(2kh)^{\frac{q}{2}}} \quad (4-123)$$

From Equation (4-122), ρ is now

$$\rho = ar (r^2 + 2kt)^{\frac{p-1}{2}} e^{-b(r^2 + 2kt)^{\frac{q}{2}}} \quad (4-124)$$

If the form of the distribution is to be invariant, then the time terms must go into a renormalizing factor, and be separable from r . Thus, p must equal 1 and q must equal 2. Equation (4-124) now becomes

$$\rho = ar e^{-br^2} e^{-b2kt} \quad (4-125)$$

The ratio of the original number of droplets, $\int_0^\infty \rho_0 dr$, to the number of particles, $\int_0^\infty \rho dr$, remaining after evaporation of the smallest droplets gives the renormalizing factor to be applied to ρ , since ρ still relates to the original number of particles.

Making this correction,

$$\bar{\rho} = are^{-br^2} \quad (4-126)$$

which is identical with the original form.

It may be concluded that: (a) the method leading to Equation (4-122) is general, (b) assumption of a form-preserving law greatly limits the available functions and fixes some of the parameters of certain classes of functions, and (c) the further assumption of a decay law may entirely fix one or more parameters of a general distribution equation which meets the requirement of self preservation of form.

Summary

As has been mentioned, none of the expressions for size distribution are based on a fundamental theoretical analysis, although Griffith's comminution function and the logarithmico-normal function are based on plausible conjectures for solid-particle grinding. Consequently, the only bases on which the respective merits of the various expressions can be ascertained are the goodness of fit and the ease with which the parameters can be determined and used in other computations.

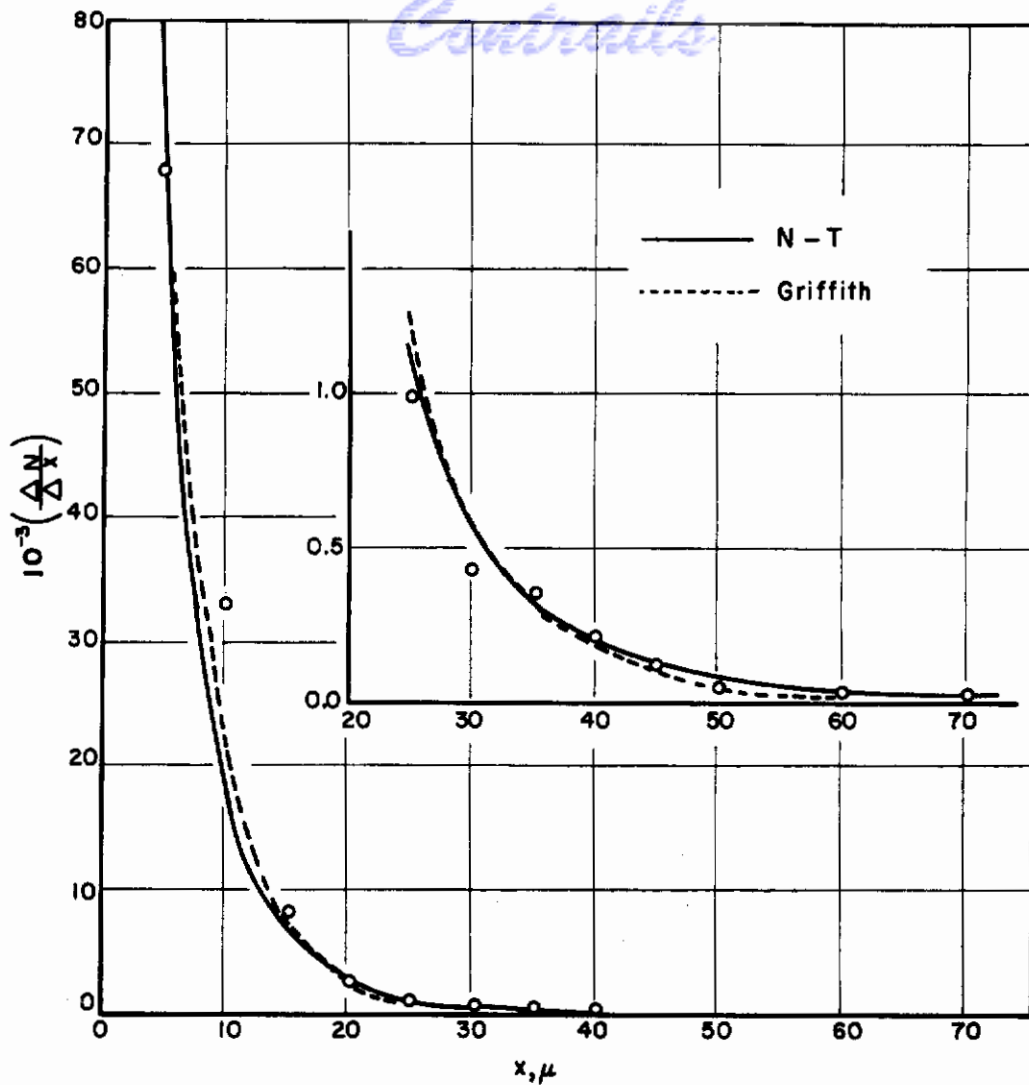


FIGURE 4-53. COMPARISON OF NUKIYAMA-TANASAWA'S AND GRIFFITH'S EMPIRICAL CURVES WITH NORMALIZED INCREMENTAL NUMERICAL DISTRIBUTION FROM HOUGHTON'S DATA

Figure 4-53 shows a comparison of the theoretical curves for the incremental numerical distribution, as given by the Nukyama-Tanasawa function [Equation (4-11)] and by the Griffith comminutive function [Equation (4-104)], for Houghton's data given in Column 5 of Table 4-2. These curves have been reproduced from Figure 4-35 and Figure 4-49, respectively. It is seen that there is little choice between the two curves. One is closer to the data in one region and the other in another region. Without more extensive consideration of the type of randomizing processes that occur in producing and analyzing the data, there is no basis for choice other than convenience.

Figures 4-54a, 4-54b, and 4-54c show a comparison of the various empirical curves for cumulative volume distribution with Houghton's experimental data as given in Column 10 of Table 4-2. From these graphs, it is apparent that each of the curves gives a reasonable correlation for the data in the intermediate size range, but that only those curves (Rosin-Rammler, log-normal) which are obtained by consideration of the concept of inner percentages give a good correlation of the data at either end of the range. However, it has been shown that even these two treatments of the data cannot be used safely as a basis for extrapolation. Of these two curves, it is noted that

the computations involved in the determination of the Rosin-Rammler parameters are less tedious than those involved in the determination of the logarithmico-normal parameters.

Insofar as determining approximate values for the parameters from a plot of the raw data on specialized coordinates is concerned, however, it is noted that a closer approximation is obtained by plotting the data on logarithmico-probability paper, from which the corresponding parameters can be obtained by consideration of the logarithmico-normal equation.

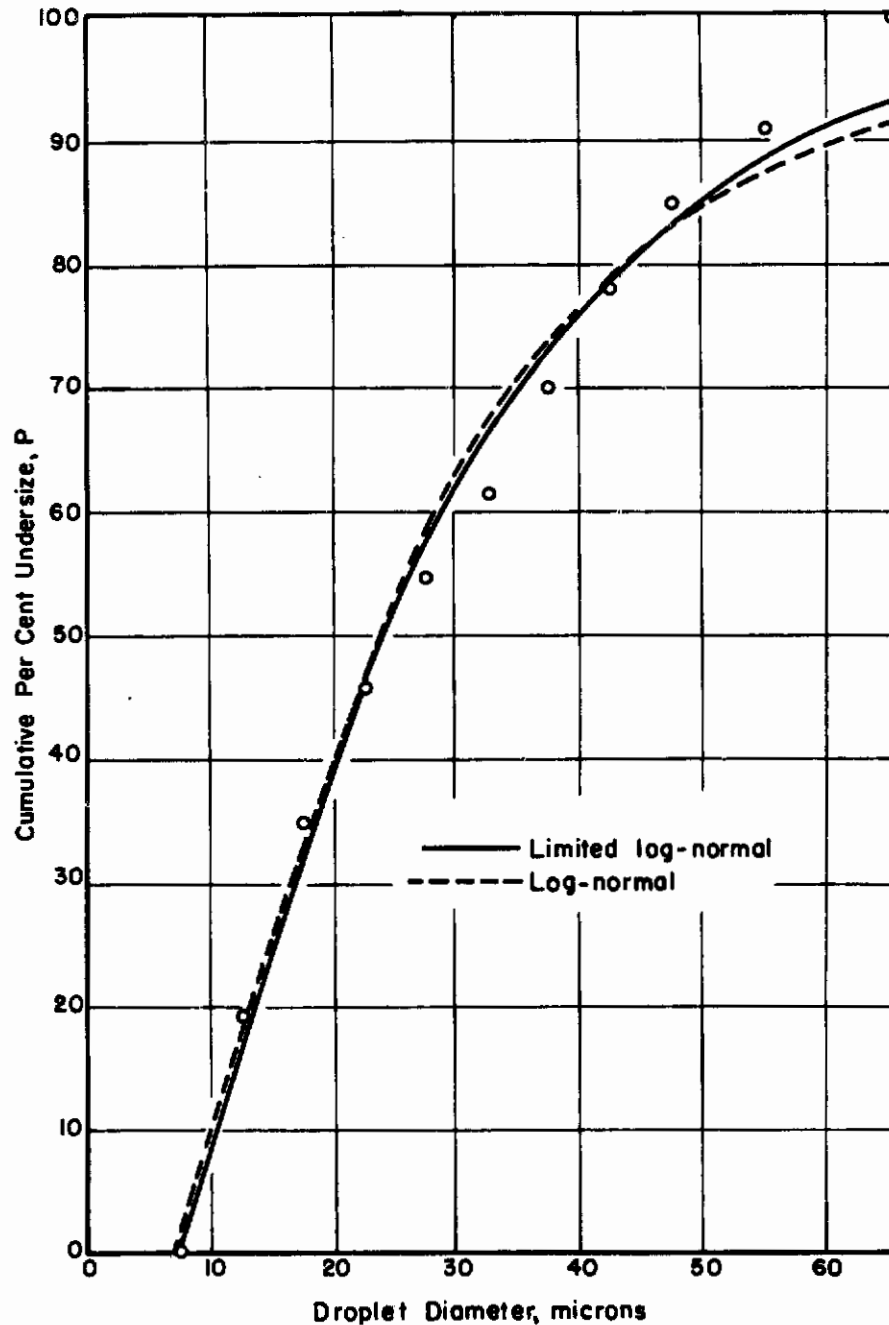


FIGURE 4-54a. COMPARISON OF EMPIRICAL CURVES WITH HOUGHTON'S DATA ON CUMULATIVE PER CENT UNDERSIZE

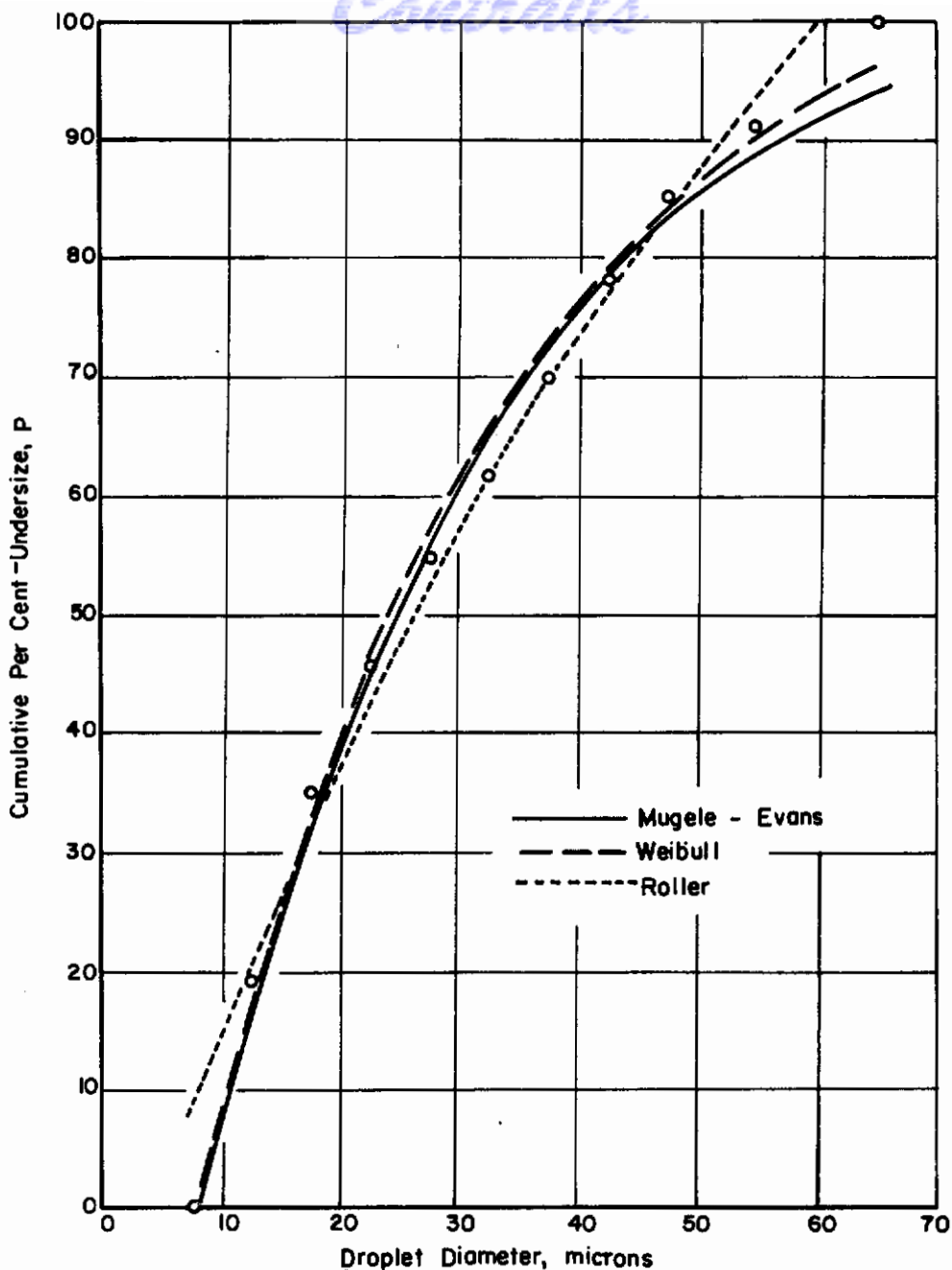


FIGURE 4-54b. COMPARISON OF EMPIRICAL CURVES WITH HOUGHTON'S DATA ON CUMULATIVE PER CENT UNDERSIZE

Determination of the mean sizes is effected most readily by use of Equation (4-92), where the infinite size range is implied for the logarithmico-normal function. A better approximation to the experimental mean sizes can be determined with but little extra effort by use of Equation (4-93), which is derived from the special upper limit function under the assumption of a size distribution which is limited only from above. Full consideration of the upper and lower limits on the size range, however, leads to quite complicated expressions for the mean sizes, which are expressed in terms of incomplete gamma functions. Unfortunately, such a consideration is necessary in many instances.

From this discussion, and from a consideration of other general factors involved, it may be concluded that:

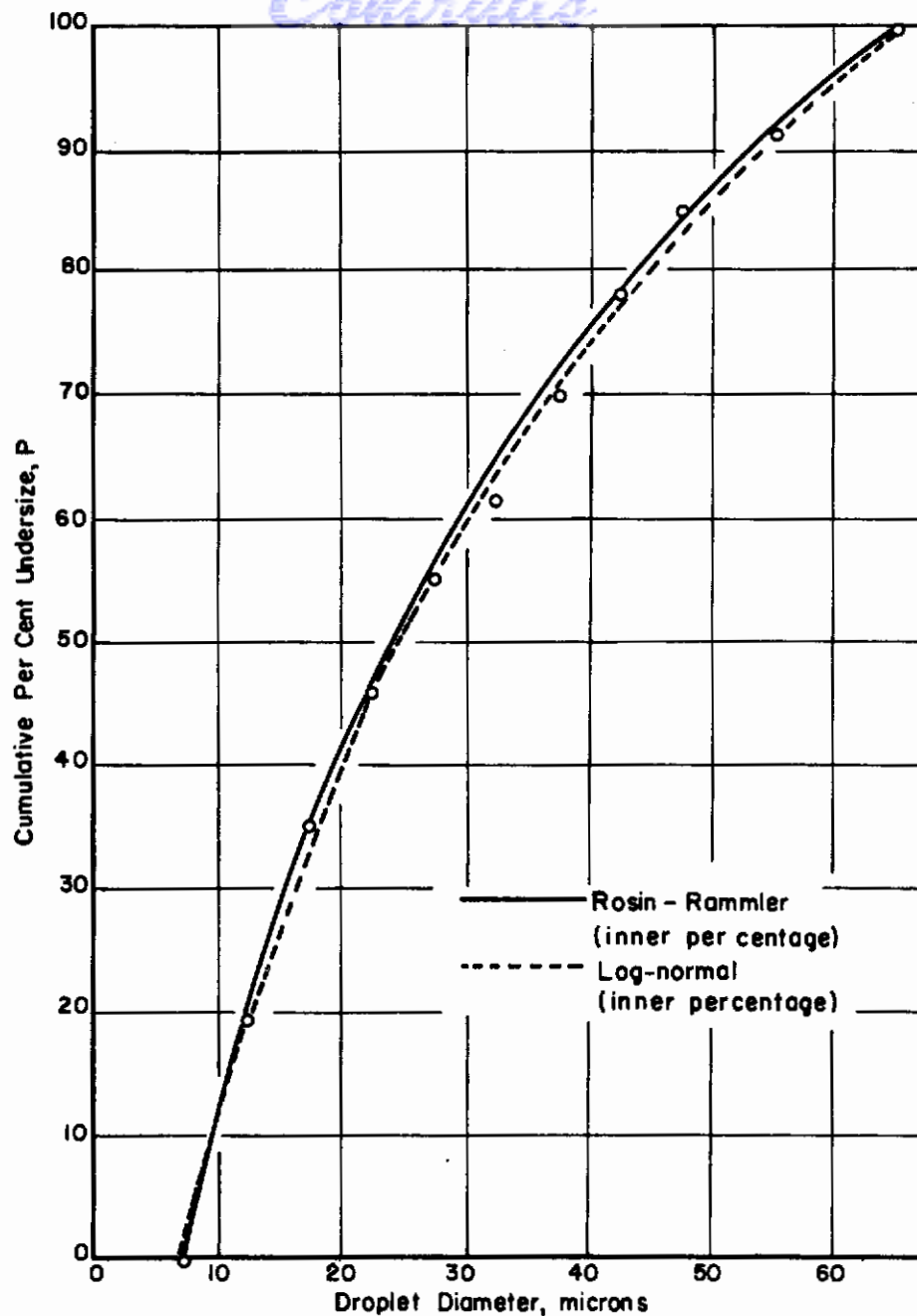


FIGURE 4-54c. COMPARISON OF EMPIRICAL CURVES WITH HOUGHTON'S DATA ON CUMULATIVE PER CENT UNDERSIZE

- (1) None of the distribution curves has a theoretical basis, as regards droplet statistics.
- (2) Two types of cut-off, natural and artificial, are inherent in all the data. Some examples of natural cut-off are an upper size of the order of magnitude of the spray-nozzle diameter and a lower size below which the aggregate of molecules ceases to act as a drop. Artificial cut-offs are given by such factors as limits of observation, on one hand and the size of the sampling instrument, on the other.
- (3) Treatments allowing for decapitation and amputation are desirable, since data are actually decapitated and amputated. However, if the equations are used for extrapolation,

the natural cut-off limits must still be observed, and abnormal percentages outside the artificial limits imposed by the range of data, but inside the natural limits, must be guarded against.

- (4) Sometimes the cut-offs are so extreme relative to the mean size and distribution that, for many practical purposes, an infinite constant may be assumed when using the computed parameter of the curve to determine mean sizes, etc.
- (5) Since none of the curves has a theoretical basis, the important criteria are ease of use, goodness of fit, and, if used for extrapolation, acceptability of extrapolated values.
- (6) Many distributions are multimodal, either because of inaccuracies in the data, in which case the problem is one of statistical judgment, or because of natural factors in the method of producing the spray, in which case methods of combining the appropriate unimodal distribution equations must be devised.

It is clear that as soon as a theoretical equation, even on shaky grounds, is derived for any particular type of spray, then, for this spray, the approach will be revised. The emphasis will shift from fitting data to some distribution equation, with a view of presenting compactly large amounts of data and saying that each parameter varies in a certain manner with the physical conditions, to comparison of the data with the theoretical equation and to an explanation of the differences. It would seem that one should not be led, then, to the reduction of droplet distribution data by means of empirical equations, and to the presentation of only the reduced data.

It may also be concluded that, with the possible exception of developing simple methods of combining unimodal distributions to fit truly multimodal data, further work along the lines of improved data fitting is fruitless. The real need is for the development of distribution equations based on plausible assumptions as to the mechanisms operating in the creation of a spray.

SECTION III - SPRAY PATTERN AND DISTRIBUTION

J. M. Pilcher

In addition to drop-size distribution, the spray pattern or distribution of droplets through the space within the combustion chamber is an important characteristic of a fuel spray. Spray pattern vitally affects combustion efficiency and performance. A common difficulty that may result from nonuniform distribution of droplets is local overheating of the combustion chamber or turbine, which may cause the burnout of parts. The distribution of fuel is important also because, in combination with the velocity distribution, it determines the variation of local air-fuel ratios, and what Rupe⁽⁴⁻¹⁰⁶⁾ has termed combustion-chamber "space efficiency".

Factors Influencing Weight-Flow Distribution

The weight-flow distribution of fuel from swirl-type pressure atomizing nozzles is influenced by the physical properties of the liquid fuel, the operating pressure of the nozzle, and the physical dimensions and configuration of the internal components of the nozzle. Rupe⁽⁴⁻¹⁰⁶⁾ observed that, at low pressures, where the centrifugal forces imparted to the fluid by the tangential slots are low compared with the surface tension, the liquid may take the form of an elongated hollow bulb which is closed at both ends, with the drops forming at, or below, the closure point. As the pressure is increased, the bulb gradually opens up until atomization is occurring approximately half way up the bulb. Further increase in pressure causes the bulb of liquid to open still further, until it stabilizes itself as a hollow cone which is relatively thick at the top and tapers to a fine edge at the open end.

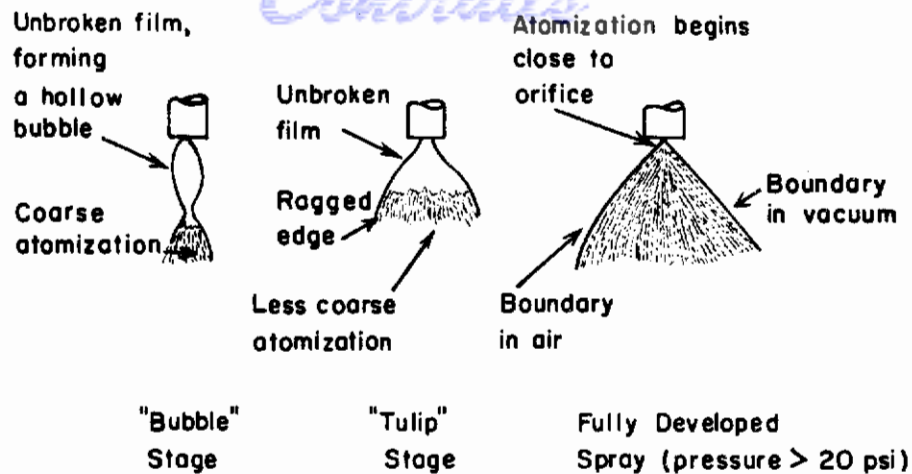


FIGURE 4-55. THREE STAGES OF ATOMIZATION

(Watson)⁴⁻¹⁰⁷

Figure 4-55 shows the three stages of atomization as described by Watson⁽⁴⁻¹⁰⁷⁾. The "bubble" stage occurs at extremely low pressure, where the kinetic energy of the liquid is small compared with the surface tension. As the pressure increases the bubble changes to the form known as the "tulip" stage, with a ragged edge from which fairly coarse droplets of fuel break off. As the pressure is increased further, above 20 psi, the tulip shortens and atomization begins practically at the orifice itself, and the film is virtually nonexistent. The boundary of the fully developed spray, in air, is curved in toward the center of the spray, whereas, in vacuum, the boundary of the spray maintains true conical form.

It is evident from Figure 4-55 that the weight-flow distribution of fuel is materially influenced by fuel pressure. The trend is for more fuel to be distributed further from the axis of the nozzle as pressure is increased. The fineness of droplets, of course, increases as the pressure is increased.

Ganger⁽⁴⁻¹⁰⁸⁾ shows photographs of three similar stages of atomization which he designates as "A", "B", and "C". Stage "A" is called the "bubble" or "olive" form and represents the minimum atomization that can ever be tolerated in service. Ganger describes stage "B" as a "cone of glassy film" extending 5/8 inch from the tip of the nozzle, beyond which there is a cone of coarse drops with the angle not too well defined. For stage "C" the fuel leaves the orifice as droplets rather than as a film, and the cone angle is well defined.

Rupe⁽⁴⁻¹⁰⁶⁾ found that weight-flow distribution changed little with increase in distance from the nozzle, within the region of interest. Fluid characteristics and air velocity also were observed to have negligible effects on weight distribution of liquid atomized at the higher pressures. It may be concluded, therefore, that fuel pressure and nozzle design are the two major factors that determine weight-flow distribution.

Methods for Determining Spray Distribution

Several methods have been developed for measuring the weight-flow distribution from a spray nozzle. The most common method consists of collecting the liquid in a number of glass tubes closed at the bottom and open at the top where the spray enters. In this way, a weight-distribution histogram may be obtained.

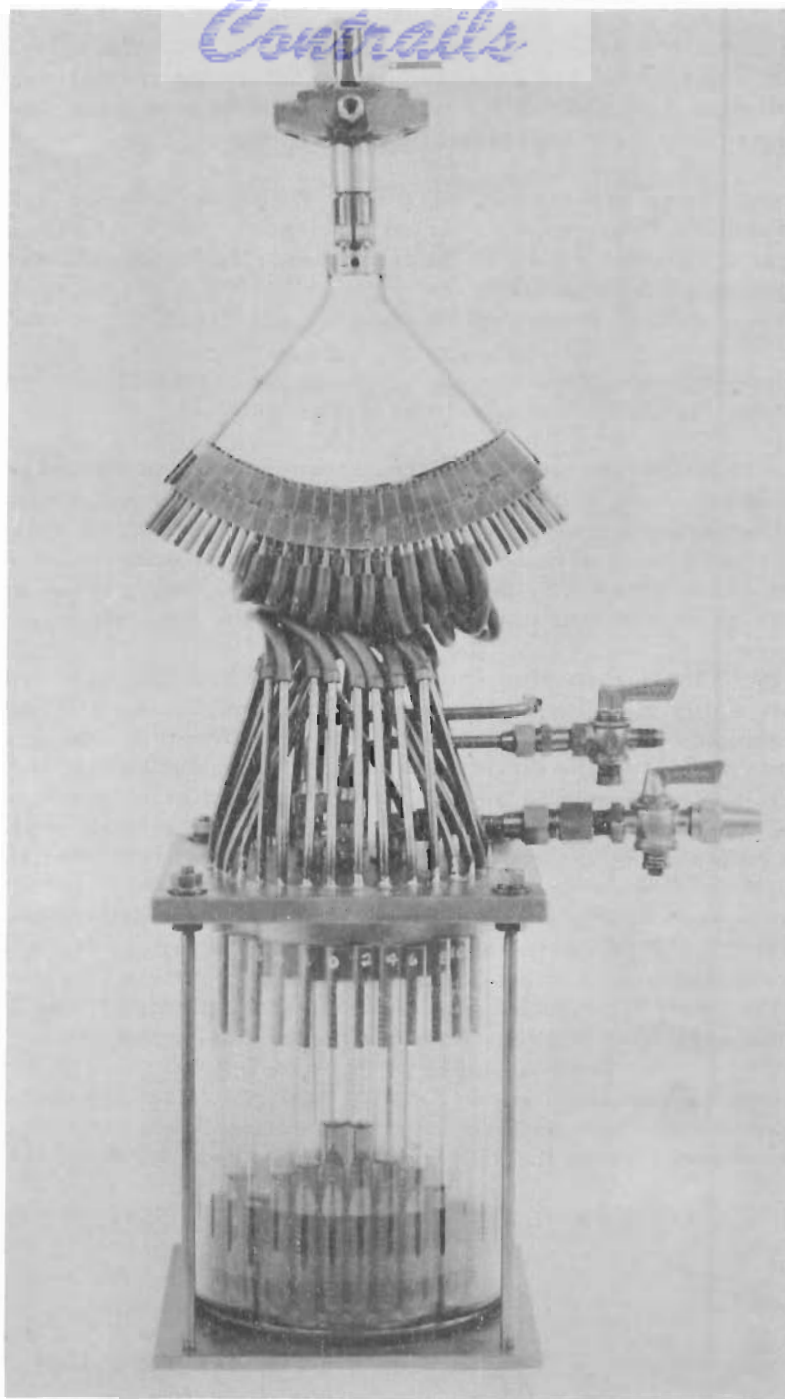


FIGURE 4-56. SPRAY DISTRIBUTION SAMPLER
(The Texas Co.)⁴⁻¹¹⁰

Figure 4-56 is a photograph of a spray distribution sampler or "Nozzle Tester" (4-109) devised by the Texas Company (4-110). It consists of a series of 1/8-in. O. D., 0.084-in. I. D. brass tubes with ends chamfered to form a sharp edge at the outside diameter. These tubes are arranged with their chamfered ends along the arc of a circle of 4-in. radius so that the angle between the center lines of adjoining tubes is 2 degrees. The test nozzle is clamped in such a position that its tip is at the center of the circle. The 32 tubes, covering a 64-degree arc, are individually connected by means of neoprene tubing to an equal number of test tubes, graduated in millimeters.

The test tubes are held in a closed chamber which is connected to a vacuum source. A vacuum of 5 in. of water at the collecting tube has been found satisfactory for a wide range of operating conditions. The period of time during which fuel is collected in the test tubes should be chosen to insure ease of measurement and good reproducibility.

The Texas Company uses kerosene for all tests. With more volatile fuels, such as gasoline, the reproducibility of the test is adversely affected by losses through the ventilating system and the vacuum line attached to the chamber holding the test tubes. Neglecting differences in relative vaporization, the variation in the quantity of fuel collected at the different spray angles is an indication of the distribution of fuel concentration along the arc described by the tube openings.

The distribution of fuel, expressed as cc/min - degree, is useful in evaluating the symmetry of a spray, and in comparing the distribution of several nozzles.

Although the actual histogram is the only true representation of the weight-flow distribution, Rupe⁽⁴⁻¹⁰⁶⁾ has devised two basic criteria which make it possible to plot weight-distribution data as a function of some variable such as pressure. The two criteria are (1) spray angle, and (2) the "peak to center ratio", tentatively defined as the ratio of the maximum unit flow rate to the unit flow rate at the center of the spray. By plotting these two variables, curves may be obtained to compare different nozzles or different liquids atomized with the same nozzle.

Pigford and Pyle⁽⁴⁻¹²⁾, in a study of commercial spray nozzles of the type used in spray absorbers, determined spray distribution by mounting the nozzle above a target painted on a concrete floor. The target consisted of six concentric circles differing in radius by increments of six inches. Radii were painted on the target at angular intervals of 60 degrees. Rates of spray collection were determined by observing the volume of liquid collected in a cylindrical vessel during measured time intervals. The vessel was located successively at various points on the target, usually at six points along each of three equally spaced radii.

Two methods were used by Pigford and Pyle to represent the spray-distribution data. In one, the "spray intensity", f' , expressed as gallons per minute per square foot, was plotted as a function of the angular inclination of a line connecting the spray nozzle with the element of area. In the other method, the spray distribution was represented by plotting \underline{f} , the fraction of the total discharge per unit solid angle at θ degrees from the center line, against θ .

Figure 4-57 shows the relation between \underline{f} and f' , which involves the cosine of the angle θ . For a nozzle which distributes spray uniformly in all directions within the angular limits of the spray cone, \underline{f} is uniform within these limits; f' decreases as $\cos^3 \theta$ toward the edge of the cone.

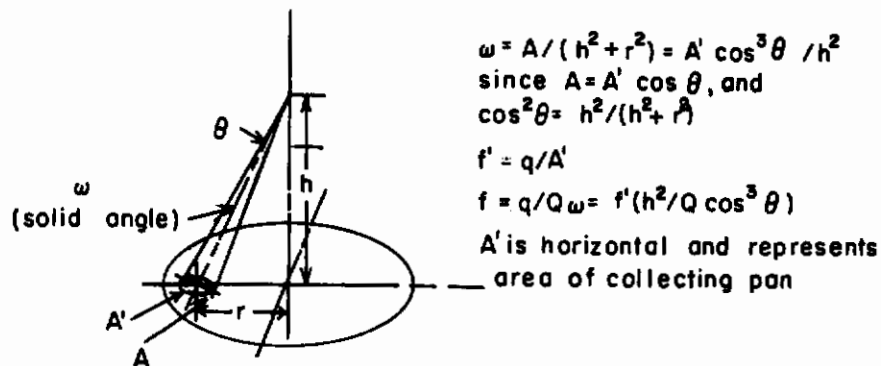


FIGURE 4-57. GEOMETRICAL RELATIONS USED IN REPRESENTING SPRAY DISTRIBUTION

(Pigford and Pyle)⁴⁻¹²

In the case of nozzles for aircraft gas turbines, the spray is generally a hollow cone. An ingenious device known as a rapid spray analyzer has been developed at the Engineering Research Institute of the University of Michigan for the Air Materiel Command of the United States Air Force. This instrument, which can analyze the spray with more convenience than is possible with conventional patternators, is described below. Also, results of tests conducted by the Air Materiel Command of the spray patterns of aircraft fuel nozzles are reviewed.

Rapid Spray Analyzer

Dodge(4-111) and Hagerty and Yagle(4-112), who developed the rapid spray analyzer, set forth the following six basic requirements:

1. The analyzer should survey the spray rapidly; should give quantitative information on the mass distribution of the spray, point by point around the spray periphery; and should give some measure of the mean drop size.
2. The accuracy with which a set of nozzles is matched at all fuel pressures should be determinable.
3. The analyzer should be compact, so that it can be used in combustion chambers to obtain spray information under air- and fuel-flow conditions.
4. The probe or pickup of the instrument should not interfere with air-fuel flow patterns.
5. Permanent graphical records should be taken which would permit ready comparison with a standard performance.
6. The instrument should be easy to operate and to maintain.

The device which Hagerty and his associates have developed meets nearly all of the above requirements.

Figure 4-58 shows the essential parts of the pickup element, which consists of a probe, a cantilevered elastic bar with electric strain gages mounted on it, and a rotating shaft. The probe is a small rod which intercepts a thin slice of the spray. The force exerted by the spray on the probe is transferred to the elastic cantilevered bar and is measured by the electric strain gages. The pickup is rotated at a uniform rate, and the force is measured at every section of the spray. The performance record of the nozzle is recorded on a chart for quick and permanent reference.

Absolute values of the momentum are not actually measured, but, instead, this instrument compares the momentum at one section of the spray with the momentum at all other sections at the same distance from the nozzle tip. Thus, for a perfectly distributed (axially symmetric) spray of absolutely uniform velocity, at a given distance from the tip, the momentum would be the same over the periphery. The measurement of momentum is essentially a measurement of total mass distribution, because the velocities of all sizes of drops close to the nozzle are nearly the same.

In addition to the pickup element, the rapid spray analyzer consists of a motor, cams, contacts and switches necessary for operation of the pickup, a strain analyzer, a recorder, and a control unit. The strain analyzer and recorder are standard items that may be purchased from the Brush Development Company.

Fifty-two working drawings for the entire rapid spray analyzer are available upon request(4-112).

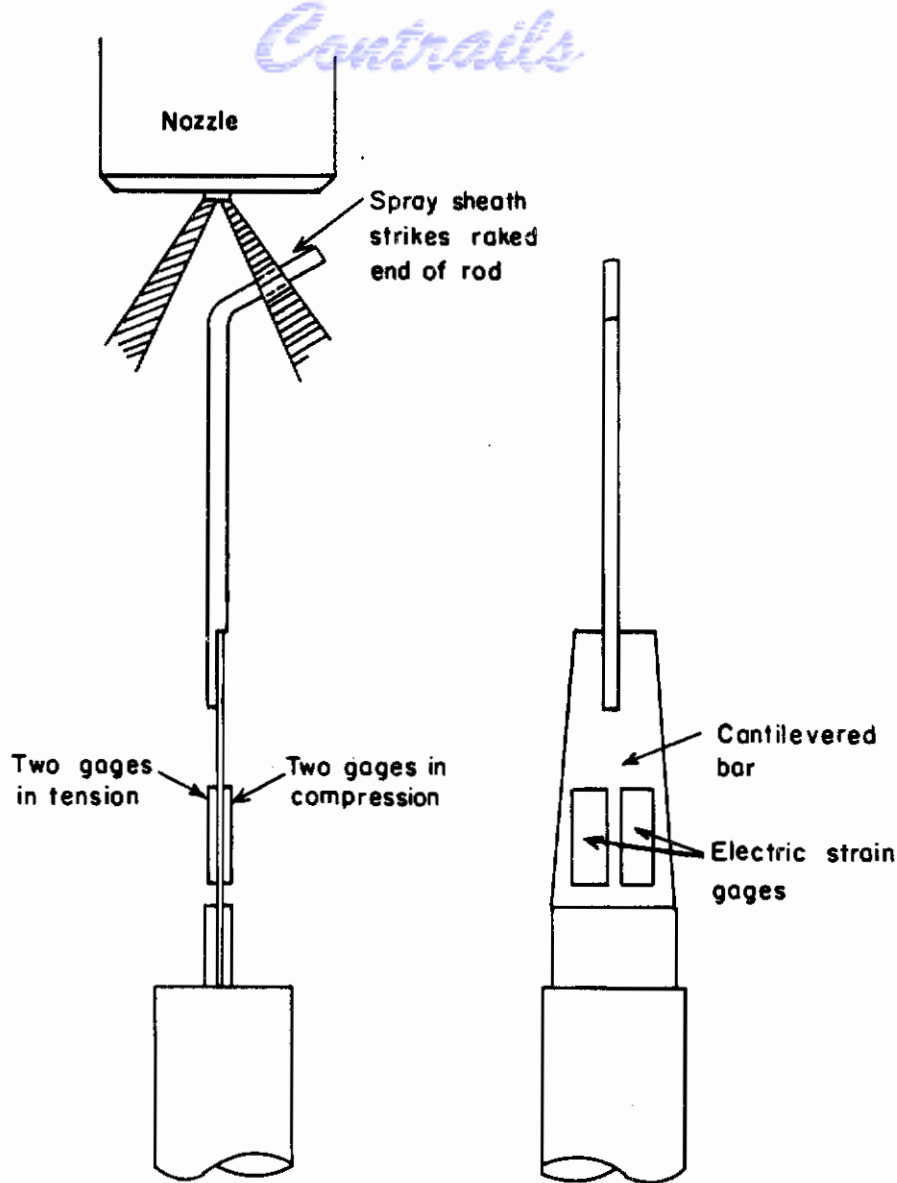


FIGURE 4-58. PICKUP ELEMENT OF THE RAPID SPRAY ANALYZER

(Hagerty and Yagle)⁴⁻¹¹²

The portable model of the rapid spray analyzer is designed to be operated by one person. A distance of one-half inch between the nozzle tip and the end of the straight portion of the probe has been found satisfactory for routine testing of both simplex and duplex nozzles. The present Air Force specifications for testing simplex nozzles call for tests at eight different pressure drops across the nozzle. The complete test may be recorded on a single strip of the recorder chart and, since the operation is automatic, the operator is free to record flow and temperature readings, and to observe the spray itself.

The most obvious applications of the rapid spray analyzer are in nozzle production control, nozzle matching, and the field testing of nozzles.

Rodean(4-113), (4-114), (4-115) of the United States Air Force Air Materiel Command has made extensive application of the rapid spray analyzer. Tests were made of eight duplex fuel nozzles(4-113) using both the segment patternator and the rapid spray analyzer. Rodean reports that a general correlation exists between results with the segment patternator and those with the rapid spray analyzer. He further points out that the great advantage of the rapid spray analyzer is that it is much more sensitive to variations in the spray pattern, since the actual flow is indicated at each point, instead of an average over a segment of the spray.

In a study of the effect of temperature (-85 to +75 F) on spray pattern, as determined by a six-segment patternator, Rodean(4-115) reports no general trend of spray pattern with temperature, but reports that spray pattern varied with each of the five fuel nozzles tested. However, Rodean concluded that the use of the rapid spray analyzer would result in more accurate spray pattern data than those obtained with the segment patternator.

Deposition and Dispersion of Sprays

Alexander and Coldren(4-116), (4-117), (4-118) point out that deposition of a spray on the walls of a duct must be considered in the design and operation of combustion chambers in which liquid fuels are burned. Accordingly, these investigators made a study of the transport of small (average diameter 27 microns) water droplets from a turbulent air stream to the walls of a straight duct to elucidate the mechanism by which sprays are deposited in such systems. They injected the spray axially into an air stream moving at moderate velocities in a straight horizontal circular duct.

From the shapes of the radial profiles of mass velocity of suspended matter, Alexander and Coldren deduced that the major resistance to transfer from the air stream to duct wall resided in a relatively thin layer of gas adjacent to the wall. The problem of mass transfer from the main body of the gas stream to the walls of the confining duct was treated mathematically to yield an equivalent-film coefficient of mass transfer. The coefficient varied with the 1.17 power of the velocity and was 10 to 20 times greater, on a mass basis, than coefficients of common gases under the same conditions.

Brown and Young(4-119), recognizing the fact that combustion performance is influenced by fuel dispersion, conceived the idea of developing a fuel-injection system that would have a fixed fuel pattern for varying fuel and air rates. Then the problems of combustion could be simplified.

Figure 4-59 shows one of the experimental cylindrical jet injectors devised by Brown and Young to study liquid-dispersion patterns. A cylindrical jet of liquid was forced upstream, which resulted in better dispersion than downstream injection.

The droplet-dispersion pattern remained substantially fixed, and the diffusion coefficient did not increase with liquid rate, as when a simple baffled disk was used. The diffusion coefficient increased linearly with air velocity, provided the air-stream velocity was sufficiently high for good atomization. Brown and Young found that the only method for obtaining a fixed droplet-dispersion pattern was to inject the liquid at low velocity (5 to 25 ft per sec), so that the kinetic energy of the emerging jet was negligible. The initial radial component of the droplet velocity was therefore determined by the radial component of air-stream velocity near the nozzle face, which was proportional to the axial component of the air-stream velocity. Hence, the droplet-dispersion pattern was essentially fixed.

The nozzles were mounted in an 8-inch induced-draft duct, and data were obtained over a range of air velocities of from 150 to 285 fps. Diffusion coefficients were calculated assuming point-source injection, whereas the nozzles had diameters of appreciable magnitude. However, small errors from this assumption could be compensated for by assuming the effective point source to be several inches upstream from the nozzle face.

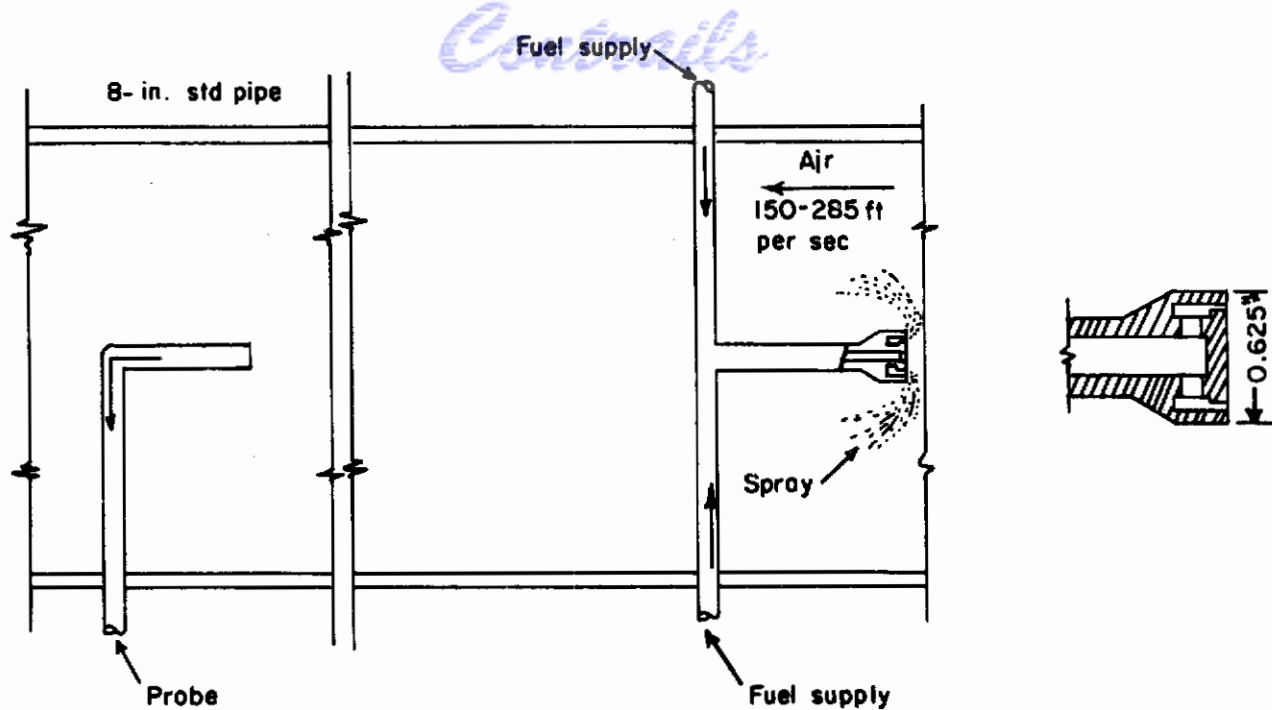


FIGURE 4-59. CYLINDRICAL FUEL INJECTOR FOR STUDY OF SPRAY DISPERSION

(Brown and Young)⁴⁻¹¹⁹

The diffusion coefficient was found to vary as the $3/2$ power of the nozzle disk diameter, and as the first power of the air-stream velocity, resulting in the following empirical equation:

$$E = 0.0025 (d)^{3/2} V$$

where E is the diffusion coefficient in ft^2 per sec, d is the disk diameter in inches, and V is the air-stream velocity in fps. It appears that too much emphasis may be placed on disk diameter in this equation. Brown and Young point out that this equation holds true only when the liquid injection velocity is low enough to prevent penetration of the air stream, and when the air-stream velocity is high enough to overcome the surface tension causing the liquid to adhere to the nozzle body.

Longwell and Weiss⁽⁴⁻¹²⁰⁾ made a valuable contribution to the study of distribution of atomized liquids by investigating the variables that affect the distribution of fuel downstream of simple tube injectors and nozzles. In general, the dispersion of fuel throughout the airstream could be described by a turbulent diffusion process assuming constant eddy diffusivity. The diffusivity used in the diffusion equations must be determined experimentally for any particular equipment; its value is quite sensitive to the nature of the flow and therefore to obstacles in the stream, including the fuel injector and its supporting structure.

For given geometry, the ratio of diffusivity to stream velocity was found to be about constant for vaporized fuels. This would be expected because diffusivity should be proportional to turbulent intensity which, in turn, is proportional to stream velocity in normal pipe turbulence. For nonvolatile fuels, this ratio decreased as velocity increased presumably because the inertia of liquid drops prevented them from closely following the higher velocity random fluctuations in faster flow. Changes in air static pressure from 4 to 55 psia resulted in no change in diffusivity, and similarly there was no effect on diffusivity due to fuel rate. Tests in 6 to 24-inch pipes

showed that duct size has a negligible effect on diffusivity. Because diffusivity should be proportional to the scale of turbulence, which, in turn, is proportional to duct size in normal pipe turbulence, it was theorized that (a) diffusion time was too short, as it often is in practice, for more than about one "cycle" of turbulent air fluctuations, thus causing intensity to determine the effective diffusivity rather than scale, and (b) fully developed normal pipe turbulence may not have existed in the test equipment.

Although eddy diffusivity is a constant of some importance, it is not necessary to know its value with great accuracy in many practical situations. This conclusion follows from the fact that usually much more of the dispersion is a result of the initial spreading caused by the fuel injector and by its supports rather than by subsequent diffusion in the stream. Initial spreading must be taken into account as a boundary condition in the turbulent diffusion equations. A small tube, oriented parallel to the flow, and through which fuel is injected at low velocity, not more than a few feet a second, acts as a point source whether fuel is injected upstream or downstream. The familiar point source equation in turbulent diffusion can then be used. However, if fuel is injected upstream at high velocity in such a tube, the source no longer acts as a point. The fuel jet mushrooms out radially and folds over before passing downstream; the apparent source then closely resembles a disk. Equations and figures were thus given for predicting the distribution downstream from such disks if the disk size and diffusivity were known. Diffusivities were determined experimentally in the same equipment using point source injection. Effective disk sizes for simple tubes pointing upstream were correlated with the several variables. This effective disk size was found to be directly proportional to the actual size of the mushroomed jet as observed spraying in the stream.

Nozzles may also behave as disk sources but a general correlation of disk size with nozzle characteristics and operating conditions is not yet available. In addition, it is important to appreciate that the strut on which the injector is mounted, for any type of injector, may have a significant effect on the resulting distribution.

Solutions for the distribution downstream of a ring source are also given by Longwell and Weiss. The ring source may sometimes be used to simulate injection from a series of nozzles or tubes mounted on a circle. Graphical techniques were developed to account for simultaneous injection from any number of sources, and to account for wall effects and changing duct areas where present.

Summary

The spray pattern, or distribution of droplets through space, vitally affects combustion efficiency and general performance of any engine that burns atomized liquid fuel. The two major factors that determine weight-flow distribution are fuel pressure and nozzle design. As the fuel pressure is increased, for swirl-type nozzles, the geometry of the spray passes through three stages, known as the "bubble" stage, the "tulip" stage, and the "fully developed" spray.

The most common method for determining spray distribution consists of collecting the liquid in a number of glass tubes, so that a weight-distribution histogram is obtained. The resulting spray distribution is represented best by showing the complete histogram. However, results may be expressed more simply in terms of two parameters, (1) spray angle, and (2) "peak to center ratio". Spray distribution may also be reported in terms of the spray intensity plotted as a function of angular inclination.

The rapid spray analyzer, which measures and records the momentum of all sections of the spray, is a marked improvement over the common type of segment patternator that consists of a number of vertical tubes. The rapid spray analyzer is useful in nozzle production control, in nozzle matching, and in the field testing of nozzles. The United States Air Force has made extensive use of the rapid spray analyzer and has found it to be more accurate than the conventional segment patternator.

The major resistance to the deposition of spray on the walls of a duct is offered by a relatively thin layer of gas adjacent to the wall. The equivalent-film coefficient of mass transfer of droplets to the walls varies with the 1.17 power of the stream velocity, and is 10 to 20 times greater than the coefficients of common gases.

With upstream injection, dispersion of liquid is increased considerably over downstream injection. A fixed droplet-dispersion pattern can be obtained by injecting the liquid at low velocity into a high-velocity air stream. Under these conditions the diffusion coefficient varies as the first power of the air-stream velocity.

The dispersion of fuel throughout an air stream may be described by a turbulent diffusion process assuming constant eddy diffusivity. Equations are available for predicting the distribution downstream following injection from a point source, or from a disk, provided disk size and diffusivity are known. The diffusivity must be determined experimentally for any particular equipment.

REFERENCES

- 4-1. Kühn, R., Atomization of Liquid Fuels; NACA Technical Memorandums No. 329, 330 and 331, Sept. 1925. Translated from Der Motorwagen, July 10 and 20, 1924, Oct. 10 and 20, 1924, Nov. 30, 1924, Dec. 10, 1924, Jan. 20, 1925, and Feb. 10, 1925.
- 4-2. Sauter, J., Determining Size of Drops in Fuel Mixtures of Internal Combustion Engines; NACA Technical Memorandum No. 390, Dec. 1926. Translation from Zeitschrift des Vereines deutscher Ingenieure, July 31, 1926.
- 4-3. Lee, Dana W., The Effect of Nozzle Design and Operating Conditions on the Atomization and Distribution of Fuel Sprays; NACA Report 425, 1932.
- 4-4. DeJuhasz, Kalman J., Zahn, O. F., and Schweitzer, P. H., On the Formation and Dispersion of Oil Sprays; Bull. No. 40, Engr. Expt. Sta., The Pennsylvania State College, August 22, 1932, 93 pp.
- 4-5. Woeltjen, A., Ueber die Feinheit der Brennstoffzerstaeubung in Oelmaschinen (On the Fineness of Fuel Atomization in Oil Engines). Dissertation, Technische Hochschule Darmstadt (Germany), 1925, 54 pp., 50 fig.
- 4-6. Sass, F., Kompressorlose Dieselmotoren, Julius Springer, Berlin, 1929, 392 pp., 328 fig.
- 4-7. Nukiyama, S., and Tanasawa, Y., An Experiment on the Atomization of Liquid by Means of an Air Stream (1st Report); Trans. S.M.E. Japan, Vol. 4, No. 14 (Feb. 1938), p. S-13.
- 4-8. Houghton, H. G., and Radford, W. H., On the Measurement of Drop Size and Liquid Water Content in Fogs and Clouds; Papers in Physical Oceanography and Meteorology, published by Mass. Inst. Tech., and Woods Hole Oceanographic Inst., Vol. 6, No. 4, Nov. 1938, 31 pp.
- 4-9. Burdette, Robert C., Some of the Principles Governing the Production of Air-Floated Oil Particles and Their Relation to the Toxicity of Contact Oil Sprays to Insects; Bulletin No. 632, New Jersey Agricultural Experiment Station, New Brunswick, N. J., Jan. 1938, 31 pp.

- 4-10. Doble, S. M., Design of Spray Nozzles; Engineering, Vol. 159, 1945, pp. 21-23, 61-63, 103-104.
- 4-11. Dimmock, N. A., Production of Uniform Droplets; Nature, Vol. 166, No. 4225, Oct. 21, 1950, p. 686.
- 4-12. Pigford, Robert L., and Pyle, Cyrus; Performance Characteristics of Spray-Type Absorption Equipment; Ind. Eng. Chem., Vol. 43, July, 1951, p. 1649.
- 4-13. Merrington, A. C., and Richardson, E. C., The Break-up of Liquid Jets; Proc. of Phys. Soc. (London), Vol. 59, Part I, 1947, p. 1.
- 4-14. Pierce, N. C., Efficiency of Hydraulic Nozzles for Atomization; M. S. Thesis, University of Illinois, 1947, 46 pp.
- 4-15. Limper, Arthur F., Atomization of Liquids by Injection into High Velocity Gas Streams; M. S. Thesis, Univ. of Illinois, 1947, 78 pp. (ATI No. 13087).
- 4-16. Maxwell, R. W., Study of Air Atomization; M. S. Thesis, Mass. Inst. of Technology, May 21, 1948.
- 4-17. Lewis, H. C., Edwards, D. G., Goglia, M. J., Rice, R. I., and Smith, L. W., Atomization of Liquids in High Velocity Gas Streams; Ind. Eng. Chem., Vol. 40, January 1948, p. 67.
- 4-18. Conroy, E. H., Jr., and Johnstone, H. F., Combustion of Sulfur in a Venturi Spray Burner; Ind. Eng. Chem., Vol. 41, Dec. 1949, p. 2741.
- 4-19. Rupe, Jack H., A Technique for the Investigation of Spray Characteristics of Constant Flow Nozzles, Part I; Presented at Conference on Fuel Sprays, Univ. of Michigan, March 30-31, 1949, 14 pp. and 12 fig.
- 4-20. Rupe, Jack H., A Semi-Automatic, Size Differentiating Droplet Counter, Progress Report No. 20-162, Jet Propulsion Lab., Cal. Inst. of Tech., Feb. 26, 1952 (ATI No. 148916), 28 pp.
- 4-21. Golitzine, N., Method for Measuring the Size of Water Droplets in Clouds, Fogs, and Sprays; Note 6, National Aeronautical Establishment, Ottawa, Canada, 1951, 13 pp. and 22 fig.
- 4-22. May, K. R., An Improved Spinning Top Homogeneous Spray Apparatus; Jour. Appl. Phys., Vol. 20, Oct. 1949, p. 932.
- 4-23. Holroyd, H. B., On the Atomization of Liquid Jets; Jour. of the Franklin Inst., Vol. 215, Jan. 1933, p. 93.
- 4-24. Longwell, J. P., Fuel Oil Atomization; D. Sc. Thesis, Mass. Inst. Tech., 1943, 167 pp.
- 4-25. Longwell, J. P., Esso Laboratories, Linden, New Jersey, Private Communication, June 3, 1954.
- 4-26. Taylor, E. H., and Harmon, D. B., Jr., Measuring Drop Sizes in Sprays; Ind. Eng. Chem., Vol. 46, No. 7 (July 1954), pp. 1455-1457.
- 4-27. Joyce, J. R., The Wax Method of Spray Particle Size Measurement; Technical Report No. I. C. T. /7, The Shell Petroleum Co. Ltd., Norman House, Strand, London, W. C. 2, 30 pp. and 20 fig.

- 4-28. Joyce, J. R., The Atomization of Liquid Fuels for Combustion; Jour. Inst. of Fuel, Vol. 22, No. 124, Feb. 1949, p. 150.
- 4-29. Heath, H., and Radcliffe, A., The Performance of an Air Blast Atomizer; National Gas Turbine Establishment Report No. 71, June 1950, 19 pp. and 13 fig.
- 4-30. Wetzel, R. H., Venturi Atomization; Ph. D. Thesis, Chem. Eng. Dept. Univ. of Wisconsin, 1951.
- 4-31. Gilman, S., A Photographic Method of Determining the Size Distribution of Small Particles; M. S. Thesis, Univ. of Pittsburgh, 1942, 16 pp.
- 4-32. Stubbs, H. E., and York, J. L., Photographic Analysis of Sprays; Paper Presented at the Annual Meeting of the Amer. Soc. of Mech. Engrs., Atlantic City, N. J., Nov. 25-30, 1951.
- 4-33. Stehling, Kurt R., Private Communication dated July 30, 1954.
- 4-34. McCullough, S., and Perkins, P. J., Flight Camera for Photographing Cloud Droplets in Natural Suspension in the Atmosphere; NACA Research Memorandum RM E50K01a, June 29, 1951.
- 4-35. Stratton, J. A., Electromagnetic Theory; McGraw-Hill, p. 563, 1941.
- 4-36. Sinclair, D., and LaMer, V. K., Light Scattering as a Measure of Particle Size in Aerosols; Chem. Rev., Vol. 44, April 1949, p. 245.
- 4-37. Durbin, E. J., Optical Methods Involving Light Scattering for Measuring Size and Concentration of Condensation Particles in Supercooled Hypersonic Flow; NACA Technical Note 2441, August 1951, 28 pp.
- 4-38. Anonymous, Tables of Scattering Functions for Spherical Particles; National Bureau of Standards, Applied Mathematics Series 4, Jan. 25, 1948.
- 4-39. Schmidt, J. M., Measurement of Droplet Size by the Diffraction Ring Method; Prog. Report No. 3-18, Jet. Propulsion Lab., Calif. Inst. of Tech., July 27, 1948, 12 pp.
- 4-40. Schmidt, J. M., A Preliminary Investigation of the Atomization of Liquids Injected into an Air Stream; Prog. Report No. 4-101, Jet Propulsion Lab., Calif. Inst. Tech., May 23, 1949.
- 4-41. Sauter, J., Investigation of Atomization in Carburetors; NACA Technical Memorandum No. 518, June 1929. Translation from Zeitschrift des Vereines deutscher Ingenieure; November 3, 1928.
- 4-42. Schmidt, J. M., Application of the Photoelectric Photometer to the Study of Atomization; Prog. Report No. 3-15, Jet Propulsion Lab., Calif. Inst. of Tech., July 30, 1946, 13 pp.
- 4-43. Mehlig, H., Zur Physik der Brennstoffstrahlen in Diesselmaschinen; Automobiltechnische Zeitschrift (Germany), Vol. 37, (1934) pp. 411-421.
- 4-44. Guyton, A. C., Electronic Counting and Size Determination of Particles in Aerosols; Jour. Ind. Hyg. Toxicol., Vol. 28, 1946, p. 133.
- 4-45. Gucker, F. T., Jr., and O'Konski, C. T., Electronic Methods of Counting Aerosol Particles; Chem. Rev., Vol. 44 (1949), p. 373.
- 4-46. Geist, J. M., An Electronic Spray Analyzer for Electrically Conducting Particles, Ph. D. Thesis, Univ. of Michigan, 1950.

- 4-47. Geist, J. M., York, J. L., and Brown, G. G., Electronic Spray Analyzer for Electrically Conducting Particles; Ind. Eng. Chem., Vol. 43, June 1951, p. 1371.
- 4-48. Dodd, E. E., Spray Electrification of Liquid Drops; Bulletin of the Amer. Physical Soc., Vol. 25, No. 6, Paper B-4, Programme of the Los Angeles Meeting at Univ. of Calif., Dec. 28, 1950.
- 4-49. Kunkel, W. B., and Hansen, J. W., A Dust Electricity Analyzer; Rev. Sci. Inst., Vol. 21, 1950, p. 308.
- 4-50. Daniel, J. H., and Brackett, F. S., An Electrical Method for Investigating the Nature and Behavior of Small, Airborne, Charged Particles; Jour. of Appl. Phys., Vol. 22, No. 5., May 1951, p. 542.
- 4-51. Leary, J. A., and Fitzgibbon, F. J., Particle-Size Determination in Radioactive Aerosols by Radio-Autograph; AECD-2791, Technical Information Division, ORE, Oak Ridge, Tennessee, June 7, 1949.
- 4-52. Leary, J. A., Determination of Particle-Size Distributions in Radioactive Aerosols by Radioautograph; Anal. Chem., Vol. 23, No. 6, June 1951, p. 850.
- 4-53. Pilcher, J. M., Characteristics of Sprays and Droplets; Paper presented at Conference on Atomization, Sprays, and Droplets, Sept. 24-25, 1953, Northwestern University.
- 4-54. May, K. R., The Cascade Impactor: An Instrument for Sampling Coarse Aerosols; Jour. of Sci. Instr., (London), Vol. 22, 1945, p. 187.
- 4-55. Sonkin, L. S., A Modified Cascade Impactor; Jour. of Ind. Hygiene, Vol. 28, 1946, p. 269.
- 4-56. Cadle, R. D., Determination of Composition of Air-Borne Particulate Material; Anal. Chem., Vol. 23, No. 1, Jan. 1951, p. 196.
- 4-57. Laskin, S., Measurement of Particle Size; Pharmacology and Toxicology of Uranium Compounds, National Nuclear Energy Series, Division VI, Vol. 1, Book 1, First Edition, 1949, p. 456.
- 4-58. Laskin, S., The Modified Cascade Impactor; Univ. of Rochester, Atomic Energy Project Report UR-129, August 8, 1950.
- 4-59. Laskin, S., Wilson, R. H., Lauterbach, K. E., Leach, L. J., and Falconer, D. W., Production Design of the Modified Cascade Impactor; Univ. Rochester, Atomic Energy Project Report UR-130, Aug. 8, 1950.
- 4-60. Harp, J. L., and Pilcher, J. M., Burning Characteristics of Fuel Mists; Phase 2 of Ignition and Combustion Research under Contract AF-33(038)-12656, E. O. No. 460-35 S. R. -8, USAF, 13th through 16th Quarterly Progress Reports, July 1953 to July 1954.
- 4-61. Male, T., NACA, Cleveland, Ohio, Unpublished work.
- 4-62. Levine, J., and Kleinknecht, K. S., Adaptation of a Cascade Impactor to Flight Measurement of Droplet Size in Clouds; NACA Research Memorandum E51G05, Sept. 18, 1951, 28 pp.
- 4-63. Ranz, W. E., and Wong, J. B., Jet Impactors for Determining the Particle-Size Distributions of Aerosols; A.M.A. Archives of Industrial Hygiene and Occupational Medicine, May 1952, Vol. 5, pp. 464-477.

- 4-64. Fulton, R. A., Nelson, R. H., and Yeomans, A. H., Evaluation of Liquefied-Gas Aerosols; Soap and Sanitary Chemicals, Vol. 27, No. 8, August 1951, p. 129.
- 4-65. Armitage, P., An Overlap Problem Arising in Particle Counting; Biometrika, Vol. 36, 1949, p. 257.
- 4-66. Adler, C. R., Mark, A. M., Marshall, W. R., Jr., and Parent, R. J., A Scanning Device for Determining the Size Distribution of Spray Droplet Images; Chem. Engr. Prog., Vol. 50, No. 1, pp. 14-23 (Jan. 1954).
- 4-67. Figford, R. L., Automatic Determination of Size Distributions of Heterogeneous Liquid Sprays; presented at U. S. Technical Conference on Air Pollution, Washington D. C., May 2, 1950.
- 4-68. Walton, W. H., Automatic Counting of Microscopic Particles; Nature, March 29, 1952, p. 518.
- 4-69. Anonymous, BCURA Studies Dust Assessment in the Field and Laboratory; BCURA Quarterly Gazette, No. 15, 1952. p. 2.
- 4-70. Skalamera, John J., Automatic Analysis of Particle-Size Distribution Data, Master's Thesis Chem. Eng. Dept. Univ. of Delaware (1953).
- 4-71. Langmuir, I., and Blodgett, K. B., Mathematical Investigation of Water Droplet Trajectories; U. S. Army Air Force, Tech. Report 5418, 1946, 65 pp.
- 4-72. Landahl, H. O., and Herrmann, R. G., Sampling of Liquid Aerosols by Wires, Cylinders, and Slides, and the Efficiency of Impaction of the Droplets; Jour. of Colloid Sci., Vol. 4, 1949, p. 103.
- 4-73. Albrecht, F., Theoretische Untersuchungen über die Ablagerung von Staub aus stromender Luft and ihre Anwendung auf die Theorie der Staubfilter, Physik Z., Vol. 32 (1931) p. 48.
- 4-74. Sell, W. Staubausscheidung an einfachen Körpern und in Luftfiltern, Forschungsheft 347, Ausgabe B, Band 2 (August, 1931).
- 4-75. Brun, E., Demon, L., and Vasseur, M., Captation Mécanique de Corpuscules en Suspension dan l'air; Rech. Aero., Paris, Jan. 1948, No. 1, p. 15. English review under title, Mechanical Capturing of Particles in Suspensions in the Air; in Applied Mechanics Reviews, August, 1948, item 1278, p. 228.
- 4-76. Fuks, N. A., Determination of Droplet Size in Oil Fogs; Colloid Jour., USSR, Vol. 11, No. 4, 1949, p. 280.
- 4-77. May, K. R., The Measurement of Airborne Droplets by the Magnesium Oxide Method; Jour. of Sci. Instr., Vol. 27, May 1950, p. 128.
- 4-78. May, K. R., Apparatus for Coating Surfaces with Magnesium Oxide; Jour. of Sci. Instr., Vol. 17, 1940, p. 231.
- 4-79. Stoker, R. L., A Method of Determining the Size of Droplets Dispersed in a Gas; Jour. of Applied Phys., Vol. 17, No. 4, April 1946, p. 243.
- 4-80. Fairs, G. Lowrie, The Use of the Microscope in Particle Size Analysis; Jour. Soc. Chem. and Ind., London, Vol. 62, Oct. 2, 1943, p. 374.
- 4-81. Brown, Carlton E., Fisher, M., and Boyer, F. F., Size of Smallest Particles Determined in Impinger Dust-Counting Methods; Bur. Mines Report of Investigations 4802, July, 1951, 19 pp.

- 4-82. Rupe, Jack H., Critical Impact Velocity of Water Droplets as a Problem in Injector-Spray Sampling; Progress Report No. 4-80, Jet Propulsion Lab., Cal. Inst. Tech., Pasadena, California, September 29, 1950 (ATI No. 96420), 16 pp.
- 4-83. Baron, Thomas, Atomization of Liquid Jets and Droplets; Univ. Illinois, Tech. Report No. 4, February 15, 1949, 24 pp. (Prepared under Contract N6-ori-71, Task Order No. XI, Office of Naval Research, Navy Department.)
- 4-84. Bevans, R. S., Mathematical Expressions for Drop-Size Distributions in Sprays; prepared for Conference on Fuel Sprays, Univ. Mich., Ann Arbor, Michigan, March, 1949.
- 4-85. Mugele, R. A., and Evans, H. D., Droplet Size Distribution in Sprays; Industrial and Engineering Chemistry, Vol. 43, June, 1951, pp. 1317-1324.
- 4-86. Nikiyama, S., and Tanasawa, Y., An Experiment on the Atomization of Liquid (5th report, The Atomization Pattern of Liquid by Means of Air Stream); Summary Section, Trans. SME Japan, February, 1940, Vol. 6, No. 22, p. S-7.
- 4-87. Houghton, H. G., Section on Spray Nozzles; Perry's Chemical Engineers' Handbook, 3rd Edition, McGraw-Hill Pub. Co., Inc., pp. 1170-1175.
- 4-88. Rosin, P., and Rammler, E., The Laws Governing the Fineness of Powdered Coal; Jour. of the Inst. of Fuel, Vol. 7, 1933, pp. 29-36.
- 4-89. Bennett, J. G., Broken Coal; Jour. of the Inst. of Fuel, Vol. 10, 1936, pp. 22-39.
- 4-90. Landry, B. A., Fundamentals of Coal Sampling; Bureau of Mines Bulletin No. 454, 1944, 127 pp.
- 4-91. Hopkins, J. L., The Size Distribution of Droplets in a Fuel Spray; Technical Report No. I. C. T/6, The Shell Petroleum Co. Ltd., Norman House, Strand, London, W. C. 2, (1946) 20 pp. and 7 fig.
- 4-92. Weibull, W., A Statistical Distribution Function of Wide Applicability; Jour. of Applied Mechanics, 1951, p. 293.
- 4-93. Epstein, B., The Mathematical Description of Certain Breakage Mechanisms Leading to the Log-Normal Distribution; Jour. Franklin Institute, Vol. 244, 1947, p. 471.
- 4-94. Kottler, F., The Goodness of Fit and the Distribution of Particle Sizes; Jour. Franklin Institute, Vol. 251, 1951, p. 499 and p. 617.
- 4-95. Kottler, F., The Distribution of Particle Sizes; Jour. Franklin Institute, Vol. 250, 1950, p. 339 and p. 419.
- 4-96. Hazen, A., Storage to be Provided in Impounding Reservoirs from Municipal Water Supply; Trans. Amer. Soc. Civil Eng., Vol. 77, 1914, p. 1539.
- 4-97. Whipple, G. C., The Element of Chance in Sanitation, Jour. Franklin Institute, Vol. 182, 1916, p. 37 and p. 205.
- 4-98. Fisher, R. A., and Yates, F., Statistical Tables; Hafner Publishing Co. Inc., New York, 1949.
- 4-99. Urban, F. M., Die Psychophysischem Massmethoden als grundlagen Empirischer Messungen; Arch. ges. Psychol., Vol. 16, p. 168, (1910).
- 4-100. Brunt, David, The Combination of Observations; Cambridge University Press, London, 1923, p. 75 ff.

- Continuity*
- 4-101. Griffith, L., A Theory of the Size Distribution of Particles in a Comminuted System; Canadian Jour. of Research, Vol. 21, 1943, pp. 57-64.
 - 4-102. Roller, P. S., Law of Size Distribution and Statistical Description of Particulate Materials; Jour. of Franklin Institute, Vol. 223, 1937, p. 609.
 - 4-103. O'Toole, A. L., On the System of Curves of which the Method of Moments is the Best Method of Fitting; Annals of Math. Statistics, Vol. 4, 1933, pp. 1-29.
 - 4-104. Dallavalle, J. M., Orr, C., Jr., and Blocker, H. G., Fitting Bimodal Particle Size Distribution Curves; Ind. Eng. Chem., Vol. 43, No. 6, June 1951, p. 1377.
 - 4-105. Carrier, G. F., Personal Communication, August 17, 1951.
 - 4-106. Rupe, J. H., A Technique for the Investigation of Spray Characteristics of Constant Flow Nozzles, Part II; presented at Conference on Fuel Sprays, University of Michigan, March 30-31, 1949, 7 pp. and 14 fig.
 - 4-107. Watson, E. A., Fuel Systems for the Aero-Gas Turbine; The Engineer, Dec. 19, 1947, p. 576.
 - 4-108. Ganger, Dean R., Practical Observations on Gas Turbine Spray Nozzles, presented at Conference on Fuel Sprays, Univ. Michigan, March 30-31, 1949, 17 pp. and 14 fig.
 - 4-109. Anonymous, Nozzle Tester; Aviation Week, Vol. 53, Aug. 14, 1950, p. 51.
 - 4-110. Anonymous, Fuel Injection Test Procedure; Refining Dept. Tech. and Res. Division, The Texas Company, February 1951.
 - 4-111. Dodge, R. A., Hagerty, W. W., Luecht, J. W., York, J. L., Glass, D. R., Stubbs, H. E., and Yagle, R. A., Continuous Fuel Sprays; AF Technical Report No. 6067, Part 2, November 1950, WADC, Dayton, Ohio, 54 pp.
 - 4-112. Hagerty, W. W., and Yagle, R. A., The Rapid Spray Analyzer; Univ. of Michigan, Engineering Research Institute, Project M-773, Contract No. W-33-038-ac-21230, August 17, 1951, 27 pp.
 - 4-113. Rodean, H. C., Test of Eight J35-A-17 Single Port Duplex Fuel Nozzles; Memorandum Report No. MCREXP-540-74, July 21, 1950, USAF, Air Materiel Command, 68 pp.
 - 4-114. Rodean, H. C., Test of 28 Simplex Fuel Nozzles; Memorandum Report No. MCREXP-540-77, August 25, 1950, USAF, Air Materiel Command, 16 pp.
 - 4-115. Rodean, H. C., Low Temperature Fuel Spray Nozzle Tests; AF Tech. Report No. 6099, October 1950, USAF, Air Materiel Command, 37 pp.
 - 4-116. Alexander, L. G., and Coldren, C. L., Deposition of a Spray on the Walls of a Straight Duct; presented at Conference on Fuel Sprays, Univ. Michigan, March 30-31, 1949, 13 pp. and 6 fig.
 - 4-117. Alexander, L. G., and Coldren, C. L., Transfer of Small Water Droplets from a Turbulent Air Stream to the Walls of a Straight Duct; Tech. Report No. 9, Engr. Expt. Sta., Univ. Illinois, Sept. 15, 1950, 30 pp.
 - 4-118. Alexander, L. G., and Coldren, C. L., Droplet Transfer from Suspending Air to Duct Walls; Ind. Eng. Chem., Vol. 43, June 1951, p. 1325.
 - 4-119. Brown, H. E., and Young, E. C., Droplet Dispersion Characteristics of Low Pressure, Disc Type Nozzles; Report CM-618, Defense Research Laboratory, Univ. of Texas, July, 3, 1950, 19 pp.

4-120. Longwell, J. P., and Weiss, M. A., Mixing and Distribution of Liquids in High-Velocity Air Streams; Ind. Eng. Chem., Vol. 45, p. 667, March 1953.

Contrails

PART I

ATOMIZATION OF LIQUID FUELS

Abramson, B. N., (3-24)

Abramson, B. N., (3-24A)

Adler, C. R., Mark, A. M., Marshall, W. R., Jr., and Parent, R. J., (4-61)

Adler, C. R., Mark, A. M., Marshall, W. R., Jr., and Parent, R. J., A Scanning Device for Determining the Size Distribution of Spray Droplet Images; Chem. Engr. Prog., Vol. 50, No. 1 (January 1954) p 14

Adler, C. R., and Marshall, W. R., Jr., (2-14)

Albrecht, F., (4-65)

Alexander, L. G., and Coldren, C. L., (4-107)

Alexander, L. G., and Coldren, C. L., (4-108)

Alexander, L. G., and Coldren, C. L., (4-109)

Alford, J. S., (3-21)

Altseimer, J. H., Photographic Techniques Applied to Combustion Studies in a Two-Dimensional Transparent Thrust Chamber; J. Amer. Rocket Soc., Vol. 22, No. 2 (Mar - Apr 1952) pp 86-91 and 103

Anderson, W. L., and Thompson, J. K., Development of NRL Photoelectric Particle-Size Meters (OWLS); Naval Research Laboratory, Report 3808, May 28, 1951, 17 pp and figs. ATI No. 107631

Anonymous, Fuel Injection Tests; Automotive Engineer, Vol. 40, March, 1950, p 93-97

Anonymous, (2-18)

Anonymous, (4-33)

Anonymous, (4-62B)

Anonymous, (4-101)

Anonymous, (4-101A)

Armitage, P., (4-60)

Balje, O. E., and Larson, L. V., (1-29)

Baron, T., (1-27) (4-75)

BCURA, BCURA Studies Dust Assessment in the Field and Laboratory, BCURA Quarterly Gazette, No. 15, 1952, p 2

Bender, M., Light Scattering to Determine Particle Size and Molecular Weight and Shape; J. Chem. Education, Vol. 29, (1952) pp 15-23

Bender, M., The Use of Light Scattering for Determining Particle Size and Molecular Weight and Shape; J. Chem. Educ., Vol. 29, No. 1 (Jan. 1952) p 15

Contrails

Bennett, J. G., (4-81)

Bentley, R. A., Cartwright, J., and Gordon, R. L., Photographic Method of Observing the Approximate Size of Liquid Drops Produced by an Atomizer, Brit. J. Appl. Phys., 4, 316 (1953)

Best, A. C., Droplet Size Distribution in Cloud and Fog, Quart. J. Roy. Met. Soc., 7, 418 (1951)

Bevans, R. S., (4-76)

Biles, M. B., An Analysis of Short Length Liquid Sprays; Heat Transfer and Fluid Mechanics Institute, 1949, pp 41-50 (Published by ASME, May 1949)

Binnie, A. M., and Harris, D. P., The Application of Boundary-Layer Theory to Swirling Liquid Flow Through a Nozzle; Quart. J. Mech. and Appl. Math., Vol. III, Part I (1950) pp 89-106

Bolt, J. A., and Saxton, M. F., Atomizing Nozzles; Engineered Products Company, Flint, Michigan, ATI-80930, July 24, 1950

Bolt, J. A., and Saxton, M. F., (3-1A)

Bolt, J. A., Lennox, R. H., and Saxton, M. F., (3-1)

Borodin, V. A., and Dityakin, Y. F., (1-28)

Boshoff, W. H., Characteristics of a Spinning Disk Liquid Sprayer; Proceedings (A) Vol. 166, No. 4, Jan.-Dec. 1952, p 443-449

Bowen, G., and Joyce, J. R., (3-10A)

Brown, C. E., Fisher, M., and Boyer, F. F., (4-73)

Brown, H. E., and Young, E. C., (4-110)

Brun, E., Demon, L., and Vasseur, M., (4-67)

Brun, R. J., Levine, J., and Kleinknecht, K. S., An Instrument Employing a Coronal Discharge for the Determination of Droplet-Size Distribution in Clouds; NACA Technical Note No. 2458, September 1950

Brun, R. J., and Mergler, H. W., Impingement of Water Droplets on a Cylinder in an Incompressible Flow Field and Evaluation of Rotating Multicylinder Method for Measurement of Droplet-Size Distribution, Volume-Median Droplet Size, and Liquid-Water Content in Clouds, NACA Technical Note 2904, March 1953

Brun, R. J., Serafini, J. S., and Moshos, G. J., Impingement of Water Droplets on an NACA 65-212 Airfoil at an Angle of Attack of 4°, NACA RM E52B12

Brunt, D., (4-92)

Buchanan, R. H., Drop Formation in Liquid-Liquid Systems When the Orifice is Wet by the Dispersed Phase; Australian J. Appl. Sci., Vol. 3, pp 233-236, Sept. 1952

Buckland, B. O., and Berkey, D. C., Combustion System for Burning Bunker C Oil in a Gas Turbine; ASME Preprint No. 48-A-109 (1948)

Burdette, R. C., (4-9)

Burgoyne, J. H., and Richardson, J. F., The Inflammability of Oil Mists; Fuel, V. 28, January 1949, p 2-6

Cadle, R. D., and Magill, P. L., (2-9)

Contrails

Cadle, R. D., (4-50)

Caldwell, F. R., and Ruegg, F. W., Seventy-Ninth Report of Progress on the Combustion Chamber Research Program for the Quarter Ending Sept. 30, 1953. Natl. Bur. Stds. Report 1B147, Order NAer 01525, pp 53-68 (ASTIA AD No. 24283)

Carrier, G. F., (4-97)

Castleman, R. A., Jr., (1-5)

Castleman, R. A., Jr., (1-11)

Chelko, L. J., Penetration of Liquid Jets into a High-Velocity Air Stream; NACA, RM E50F21, August 14, 1950

Clarke, J. S., Combustion in Aero Gas Turbines; Engineering, September 15, 1950, pp 230-232

Conroy, E. H., Jr., and Johnstone, H. F., (4-18)

Courshee, R. J., Characterizing Spraying Nozzles; World Crops, March 1954, pp 91-94

Dallavalle, J. M., Micromeritics, 2nd Edition, Pitman Pub. Corp., New York-London, 1948

Dallavalle, J. M., Orr, C., Jr., and Blocker, H. G., (4-96)

Daniel, J. H., and Brackett, F. S., (4-45)

Davies, C. N., Alyward, M., and Leacey, D., Impingement of Dust From Air Jets; Arch. of Ind. Hyg. and Occup. Med., Vol. 4, No. 4 (October 1951) pp 354-397

Davies, C. N., and Alyward, M., The Trajectories of Heavy, Solid Particles in a Two-Dimensional Jet of Ideal Fluid Impinging Normally Upon a Plate; Proc. Phys. Soc. (London) B, 64, pp 889-911 (October 1951)

De Juhasz, K. J., Bibliography of Sprays, August 1948, See also Supplement No. 1 by De Juhasz, K. J., and Meyer, W. E., May 1949. See also the Penn State Bibliography on Sprays (Second Edition) 1953. Published by The Texas Company, Technical and Research Division, 135 East 42nd St., New York, New York

De Juhasz, K. J., Zahn, O. F., and Schweitzer, P. H., (1-15) (4-4)

Diamond, P., and Stehling, K. R., (3-25A)

Dicksee, C. B., How to Bring Together Diesel Fuel and Air; SAE Journal, October 1948, p 43

Dimmock, N. A., (2-21) (4-11)

Doble, S. M., (3-6) (4-10)

Doble, S. M., (3-7)

Doble, S. M., (3-8)

Dodd, E. E., (4-43)

Dodge, R. A., Hagerty, W. W., and York, J. L., (1-36) (3-5)

Dodge, R. A., Hagerty, W. W., Luecht, J. W., York, J. L., Glass, D. R., Stubbs, H. E., and Yagle, R. A., (4-102)

Donnelly, J. J., Spray Formation and Evaporation, Ph. D. Thesis, Univ. Delaware, September 1951

Donnelly, J. J., and Wohl, K., (1-30)

Dorman, R. G., The Atomization of Liquid in a Flat Spray; Brit. J. Appl. Phys., Vol. 3, No. 6, June 1952, p 189

Doumas, M., and Laster, R., Liquid-Film Properties for Centrifugal Spray Nozzles; Chem. Engr. Prog., Vol. 49, pg 10, pp 518-526 (October 1953)

Dreyhaupt, F., British Intelligence Objectives Sub-Committee Final Report 1612

Dunne, B., and Cassen, B., Some Phenomena Associated with Supersonic Liquid Jets; J. Appl. Phys., Vol. 25, No. 5 (May 1954) p 569

Durbin, E. J., (4-32)

Elabd, I. H. A., Analysis of Fuel Sprays by Electrical Methods; Sc. D. Thesis, Univ. Michigan, 1951, Abstracted in Microfilm Abstracts, Vol. XI, No. 2, 1951, pp 310-311

Elmore, W. C., Statistics of Counting, Nucleonics, Vol. 6, 1950, pp 26-34

Ennis, W. B., Jr., and James, D. T., (2-8)

Epstein, B., (4-85)

Erickson, J. L., Thin Liquid Jets; J. of Rational Mechanics and Analysis, Vol. 1, No. 4, Grad. Inst. of Applied Math., Indiana Univ., Bloomington, Ind.

Esso Laboratories, Annual Report on Fundamental Studies of Combustion; (ONR) Report No. RL-9M-47 (66) November 6, 1947, Esso Laboratories Research Division

Fairs, G. L., (4-72)

Falk, D. M., (2-24)

Faust, F. H., and Kaufman, G. T., Editors of Handbook of Oil Burning; Published by Oil-Heat Institute of America, Inc., 978 pp (1951)

Ferlin, J. J., Jr., A Study of Fuel Spray Formation from Nozzles with High L/D Ratio; M. S. Thesis, Univ. California, 1950, 61 pp

Ferrie, F., and Manson, N., Sur L'Etonnage des Microphotographies de Jet Pulverises (The Calibration of Atomized Jets by Microphotographs); Comptes Rendus, Vol. 234, No. 23, June 4, 1952, pp 2254-2256

Field, R. B., Collection of Aerosol Particles by Atomized Sprays; Engr. Expt. Sta., Univ. Illinois, Technical Report No. 5, October 31, 1951

Fisher, R. A., and Yates, F., (4-90)

Fogler, B. B., and Kleinschmidt, R. V., (1-19) (2-5)

Fraser, R. P., Dombrowski, N., and Eisenklam, P., (1-35)

Friedman, S. J., Gluckert, F. A., and Marshall, W. R., Jr., Centrifugal-Disk Atomization; Chem. Engr. Prog., Vol. 48, No. 4, April 1952, pp 181-191

Fuks, N. A., (4-68)

Fulton, R. A., Nelson, R. H., and Yeomans, A. H., (4-59)

Ganger, D. R., (3-2) (4-100)

Garner, F. H., and Henny, V. E., Behavior of Sprays Under High Altitude Conditions, Fuel, Vol. 32, No. 2, April 1953, p 151

Geist, J. M., (4-41)

Geist, J. M., York, J. L., and Brown, G. G., (4-42)

Gelalles, A. G., and Marsh, E. T., (1-44)

Gelalles, A. G., (1-45)

Gelalles, A. G., (1-46)

Giffen, E., and Muraszew, A., The Atomization of Liquid Fuels, John Wiley and Sons, New York (1953)

Giffen, E., Atomization of Fuel Sprays, Engineering, Vol. 174, July 4, 1952, p 6-10

Giffen, E., and Muraszew, A., Fuel Injection in Internal-Combustion Engines. Atomization of Low-Pressure Fuel Sprays, Report No. 1948/5; The Motor Industry Research Association, Middlesex, England, Sept. 1948

Engel, F. C., Fuel Spray Examination Methods, Paper No. 52-A-139, presented at the Annual Meeting of ASME, New York, N. Y., Nov. 30-Dec. 5, 1952

Fraser, R. P., Dombrowski, N., Eisenklam, P., Vibrations as a Cause of Disintegration in Liquid Sheets; Nature, No. 4402, March 13, 1954, p 495

Giffen, E., and Massey, B. S., Some Observations on Flow in Spray Nozzles, Report No. 1950/5. The Motor Industry Research Assoc., Middlesex, Eng., July 1950

Giffen, E., and Massey, B. S., Some Experiments on Spray Atomization with Swirl Atomizers. Report No. 1951/4. The Motor Industry Research Assoc., Middlesex, Eng., June 1951

Giffen, E., and Muraszew, A., Fuel Injection in Internal-Combustion Engines. The Measurement of Atomization in Fuel Sprays. Report No. 1948/4. The Motor Industry Research Association, Middlesex, England, August 1948

Gilman, S., (4-27)

Golitzine, N., (4-20)

Golitzine, N., Sharp, C. R., and Badham, L. G., Spray Nozzles for the Simulation of Cloud Conditions in Icing Tests of Jet Engines; Nat. Aeronautical Est. Canada, Report 14, 1951

Green, H. L., (2-3A)

Green, H. L., Problems in the Atomisation of Liquids; Chap. 5 of Some Aspects of Fluid Flow, being the papers presented at a conference organized by The Institute of Physics at Leamington Spa, on October 25-28, 1950, Edward Arnold Co., (London) 1951, pp 75-86

Contrails

Griffith, L., (4-93)

Gucker, F. T., Jr., and O'Konski, C. T., (4-40)

Gunn, R., A Vertical Shaft for the Production of Thick Artificial Clouds and for the Study of Precipitation Mechanics; J. Appl. Phys., Vol. 23, No. 1, January 1952, p 1

Gunn, S. V., (3-24)

Guyton, A. C., (4-39)

Haenlein, A., (1-9)

Hagerty, W. W., and Yagle, R. A., (4-103)

Hagerty, W. W., Continuous Fuel Sprays, Part 3, AF Technical Report No. 6067 (Pt 3) December 1952, Wright Air Development Center

Harvey, J. F., Marine Steam Oil Atomizers; J. Amer. Soc. of Naval Engrs. Vol. 64, No. 2, May 1952, pp 301-330

Harvey, J. F., and Hermandorfer, A. W., (3-17)

Hatch, T., and Choate, S. P., Measurement of Polarization of the Tyndall Beam of Aqueous Suspension as an Aid in Determining Particle Size; J. of the Franklin Inst., Vol. 210, 1930, pp 793-804

Hawksley, P. G. W., The Physics of Particle Size Measurement: Part I, Fluid Dynamics and the Stokes Diameter; The Brit. Coal Utilization Res. Assoc. Monthly Bulletin, Vol. XV, No. 4 (April 1951) Rev. Series No. 102, p 105

Hawksley, P. G. W., The Physics of Particle Size Measurement: Part II, Optical Methods and Light Scattering, The Brit. Coal Utilization Res. Assoc. Monthly Bulletin, Vol. XVI, Nos. 4 and 5 (April and May 1952) Rev. Series No. 114

Hawksley, P. G. W., Automatic Particle-Sizing by Successive Countings; Nature, Vol. 170, No. 4336, Dec. 6, 1952, p 984

Harp, J. L., and Pilcher, J. M., (4-54)

Hawthorne, W. R., (3-13)

Hazen, A., (4-88)

Heath, H., and Radcliffe, A., (4-26)

Heidmann, M. F., and Humphrey, J. C., (2-26)

Hermans, J. J., Editor, Flow Properties of Disperse Systems, Interscience Publishers, Inc. (1953) (Chaps. 6 and 7) Chap. 6, Liquid Sprays by E. G. Richardson; Chap. 7, Atomization of Liquids, by H. L. Green

Herring, W. M., Jr., Performance of Vaned Disk Atomizers, Ph. D. Thesis, Univ. Wisconsin, 1953

Hinze, J. O., (1-24)

Hinze, J. O., and Milborn, H., (2-15)

Hochschwender, E., (1-32)

Holfelder, O., (1-41)

WADC TR 56-344

VI

Contrails

Holroyd, H. B., (4-22)

Hopkins, J. L., (4-83)

Houghton, H. G., (2-6) (4-79)

Houghton, H. G., and Radford, W. H., (4-8)

Howell, W. E., Boucher, R. J., and Brown, S., Experimental and Statistical Studies of the Drop-Size Distribution in Snow; Quart. Prog. Report, January 23, 1951 on Contribution to the Theory of the Constitution of Clouds, 27 pages (Tech. Report No. 1) Contract AF 19(122)399; Continuation of Contract AF 28(099)25. Unclassified (Mount Washington Observ.)

Inn, E. C. Y., Measurement of Particle Size and Concentration of Homogeneous Aerosols; J. Colloid Sci., 6, 368, (1951)

Jellinek, H. H. G., Size Distributions of Emulsions; J. Soc. of Chem. Ind., Vol. 69, No. 8, p 225 (August 1950)

Joeck, T. D., (2-20)

Johnstone, H. F., and Kleinschmidt, R. V., The Absorption of Gases in Wet Cyclone Scrubbers; Trans. Am. Inst. Chem. Engrs., 34, p 181 (1938)

Jordanides, G., and Chamberlain, N. H., Automatic Particle Sizing by Successive Counting; Nature, 174, No. 4419, July 10, 1954, p 83-84

Joyce, J. R., (1-2) (2-2) (4-25)

Joyce, J. R., (3-18)

Joyce, J. R., (4-24)

Joyce, J. R., Methods of Atomizing Liquid Fuel, J. Inst. of Petroleum, Vol. 39, No. 350, Feb. 1953, p 57

Kenyon, A. S., and LaMer, V. K., Light Scattering Properties of Monodispersed Sulfur Sols. I Monochromatic Ultraviolet Angular Scattering. II Effect of the Complex Index of Refraction Upon Transmittance; J. Colloid Sci., Vol. 4, 1949, pp 163-184

Kesler, G. H., Mass Transport in Spray-Laden Turbulent Air Streams; Ph. D. Thesis, Dept. of Chem. Engrs., Mass. Inst. Tech. (Jan. 1952)

Kircher, H. L., and Med, L., (3-26)

Kobayaski, K., Atomizing Characteristics of Swirl Injection Nozzles, Special Number on Gas Turbines (1951) 203 p, Soc. of Mech. Engr. (Tokyo) Transactions, 17, No. 58

Kolmogorov, A. N., Disintegration of Drops in a Turbulent Flow; Reports of the Academy of Sciences of the USSR (Akademiia Nauk), Vol. 66, No. 5 (1949) p 825 (In Russian)

Kolupaev, P. G., Atomization of Heavy Fuel Oil, Sc. D. Thesis, Mass. Inst. Tech. (1941)

Kottler, F., (4-86)

Kottler, F., (4-87)

Kottler, F., The Logarithmico-Normal Distribution of Particle Sizes: Homogeneity and Heterogeneity; J. Phys. Chem., 56, 422 (April 1952)

Contrails

Kühn, R., (4-1)

Kunkel, W. B., and Hansen, J. W., (4-44)

LaMer, V. K., Inn, E. C. Y., and Wilson, I. B., The Methods of Forming, Detecting, and Measuring the Size and Concentration of Liquid Aerosols in the Size Range of 0.01 to 0.25 Microns Diameter; J. Colloid Sci., 5, 471 (1950)

LaMer, V. K., and Barnes, M. D., Monodispersed Hydrophobic Colloidal Dispersions and Light Scattering Properties; J. Colloid Sci., 1, 71 (1946)

Landahl, H. O., and Herrmann, R. G., (4-64)

Landry, B. A., (4-82)

Lane, W. R., (1-31)

Langmuir, I., and Blodgett, K. B., (4-63)

Lapple, C. E., Fluid and Particle Mechanics; Univ. Book Store, Univ. Delaware, Newark, Delaware (1951)

Lapple, C. E., Mist and Dust Collection in Industry and Buildings; Heating, Piping, and Air Conditioning, July 1944, p 410

Larcombe, H. L. M., (1-26)

Laskin, S., (4-51)

Laskin, S., (4-52)

Laskin, S., Wilson, R. H., Lauterbach, K. E., Leach, L. J., and Falconer, D. W., (4-53)

Lawrence, O. N., (1-7) (2-4) (3-23)

Leary, J. A., (4-47)

Leary, J. A., and Fitzgibbon, F. J., (4-46)

Lee, D. W., (1-39) (4-3)

Lee, D. W., (1-40)

Lee, D. W., and Spencer, R. C., (1-13)

Lee, D. W., and Spencer, R. C., (1-14)

Lenihan, J. M. A., The Shape of a Liquid Jet; Phil. Mag., Vol. 32, (1941) p 393

Levine, J., and Klienkecht, K. S., (4-57)

Lewis, H. C., Edwards, D. G., Goglia, M. J., Rice, R. I., and Smith, L. W., (1-52) (4-17)

Lewis, W., Perkins, P. J., Brun, R. J., Procedure for Measuring Liquid Water Content and Droplet Sizes in Supercooled Clouds by Rotating Multicylinder Method; NACA RM E53D23, June 29, 1953

Limper, A. F., (2-7) (4-15)

Littaye, G., (1-21)

WADC TR 56-344

VIII

Contrails

Littaye, G., (1-22)

Littaye, G., (1-23)

Littaye, M., Étude des Brouillards Obtenus par Pulvérisation Pneumatique, (A Study of Sprays Obtained by Air Atomization); Chaleur et Industrie, No. 258 (1947) p 3.

Longwell, J. P., (1-42) (3-12) (4-23) (4-23A)

Longwell, J. P., and Weiss, M. A., (4-110A)

Lucas, J., (1-1)

Male, T., (4-55)

Marshall, J. S., and Palmer, W. McK., The Distribution of Raindrops with Size, J. Meteorol., 5, 165 (1948)

Marshall, W. R., Jr., and Seltzer, E., (2-13)

Mathewson, C. R., Injection Equipment, SAE Journal, Vol. 54, 1946 (November) No. 11, p 71

Maxwell, R. W., (4-16)

May, K. R., (2-12) (4-21)

May, K. R., (4-48)

May, K. R., (4-69)

May, K. R., (4-70)

McCullough, S., and Perkins, P. J., (4-29)

McEntee, F. J., Jr., (2-3)

McMahon, E., Preliminary Investigation of Fuel Injection and Combustion Problems in Liquid Fueled Rockets; Meteor Report No. BAC-10, Bell Aircraft Corp. in Conjunction with Bur. of Ord. and MIT, June 2, 1947

Mehlig, H., (4-38)

Merrington, A. C., and Richardson, E. G., (1-25) (4-13)

Meyer, W. E., and Ranz, W. E., Sprays, part of Vol. 12 of the Encyclopedia of Chemical Technology, pp 703-721 (1954) The Interscience Encyclopedia, Inc.

Mock, F. C., and Ganger, D. R., (1-6) (3-19)

Mock, F. C., and Ganger, D. R., (1-50)

Monk, G. W., Viscous Energy Dissipated During the Atomization of a Liquid, (Camp Detrick), J. Appl. Phys., Vol. 23, No. 2, (February 1952) p 288

Moshman, J., Critical Values of the Log-Normal Distribution; Oak Ridge Nat. Lab. ORNL-1427 (Physics) December 2, 1952

Mugele, R. A., and Evans, H. D., (4-77)

Muraszew, A., (2-17)

Muraszew, A., Fuel Injection in Internal-Combustion Engines. Fuel Spray Phenomena. Review of Information. Report No. 1947/R/6. The Motor Industry Research Association, Middlesex, England, October 1947

Muraszew, A., Continuous Fuel Injection, Abstracted in Mechanical Engineering, December 1948, p 1009

Northup, R. P., (3-25)

Novikov, I. I., (3-16)

Nukiyama, S., and Tanasawa, Y., (1-49)

Nukiyama, S., and Tanasawa, Y., (4-7)

Nukiyama, S., and Tanasawa, Y., (1-18) (4-78)

Oehler, Th., Der Wasserstrahl and Seine Auflosung in Tropfen, (The Water Jet and its Resolution into Drops); Techn. Mechan. u. Thermodynamik, I. Band Nr. 9, September 1930

O'Konski, C. T., and Doyle, G. J., Light Scattering Studies in Aerosols with a New Counter Photometer; Tech. Report No. 1, Contract No. ONR 222-12, Project No. NR 051-302, Dept. of Chem. and Chem. Engr., Univ. Calif, June 16, 1954

O'Konski, C. T., and Thacher, H. C., Jr., Distortion of Aerosol Droplets by an Electric Field, J. Phys. Chem., 57 955 (1953)

Oschatz, W., Experiments on Fuel Preparation by Injection Nozzles, Deutsche Kraftfahrtforschung No. 57 (1941), 28 pp

O'Toole, A. L., (4-95)

Pai, Shih-I., Fluid Dynamics of Jets; D. Van Nostrand Co.

Panasenkov, N. S., Influences of Turbulence of Liquid Jet on its Atomization; (Zh. tekn. Fiz (J. tech. Phys.) 1951, Vol. 21 (2), 160-166, London, Minist. Supply, June 1952, Libr. Transl. 409, 8 pp)

Park, R. D., (3-4)

Perry, J. H., Chemical Engineers' Handbook, 3rd. Edition, 1950 pp 840-848 and 1170-1174

Pierce, L. J., and Parker, T. B., (3-20)

Pierce, N. C., (4-14)

Pigford, R. L., (4-62)

Pigford, R. L., and Pyle, C., (4-12)

Pilcher, J. M., (4-47A)

Pilcher, J. M., and Terrill, F. B., (2-19)

Plender, P. J., Atomization of Water Sprays in a High-Speed Air Stream, MICRO E 117 Aug. 22, 1952 (United Aircraft Corp. Library)

Pouchot, W. D., and Hamm, J. R., (3-23A)

Primm, G. C., Atomization of Liquid Fuels as Related to the Over-All Operation of Open Hearth Furnaces; National Open Hearth Committee of the Iron and Steel Div. of the AIME Proceedings, Vol. 36, 1953, p 177-179; disc. p 179-180

Probert, R. P., (1-3)

Putte, W. L., v. d. and Bussche, H. K. J. v. d., New Ways of Burning Liquid Fuel; Trans. of the Fuel Economy Conference, The Hague, 1947, Vol. III, pp 1183-1205

Ranz, W. E., and Wong, J. B., (4-58)

Rayleigh, L., (1-8)

Rayleigh, L., (1-37)

Richardson, E. G., Dynamics of Real Fluids, 1950, 1st Ed., Ed. Arnold Company (London)

Renier, E. R., Jr., The Spinning Disk Atomizer as a Source of Homogeneous Drops, M. S. Thesis in Chem. Engr. Dept. MIT (1952)

Rodean, H. C., (4-104)

Rodean, H. C., (4-105)

Rodean, H. C., (4-106)

Roesch, W. C., and Rose, R. F., A Survey of the Literature on the Subject of Atomization; JPL, Calif. Inst. Tech., Prog. Report 1-46, Feb. 1946

Roller, P. S., (4-94)

Romp, H. A., (1-4) (2-1)

Rosin, P., and Rammler, E., (4-80)

Rothrock, A. M., The NACA Apparatus for Studying the Formation and Combustion of Fuel Sprays and the Results from Preliminary Tests; NACA Report 429, 1932, p 549

Rupe, J. H., (4-19)

Rupe, J. H., (4-74)

Rupe, J. H., (4-98)

Rupe, J. H., The Liquid Phase Mixing of a Pair of Impinging Streams, Prog. Report No. 20-195, JPL, Calif. Inst. Tech., August 6, 1953, 68 pp

Rupe, J. H., (4-19A)

Rupe, J. H., (3-26)

Ryan, N. W., (2-25)

Sass, F., (4-6)

Sauter, J., (1-12) (4-36)

Sauter, J., (4-2)

Scheubel, F. N., (1-48)

Contrails

Schmidt, J. M., (1-51)

Schmidt, J. M., (4-34)

Schmidt, J. M., (4-35)

Schmidt, J. M., (4-37)

Schulz, Researches into Spray Nozzles, Orig. Agency; Luftfahrtforschungsanstalt, Hermann Goering (No. FB-1) ATI-47835, No date, 13 pp

Schweiter, P. H., Penetration of Oil Sprays; J. Appl. Phys., Vol. 9 (1938) pp 735-741

Schweiter, P. H., Penetration of Oil Sprays; Penn State Coll. Bull. Eng. Expt. Sta., Series No. 46, Mathematical Supplement, 1937

Schweiter, P. H., (1-16)

Schweiter, P. H., (3-11)

Sell, W., (4-66)

Shafer, M. R., and Bovey, H. L., Laboratory Flow Tests of Fixed Spray Nozzles with Hydrocarbons and with Air; J. Research, Nat. Bur. of Stds., Vol. 43, November 1949, RP 2035

Siestrunck, R., (1-20)

Simons, A., and Goffe, C. R., Photographs of Sprays from Pressure Jets, Aero. Res. Council, R and M, No. 2343 (9975), ARC Tech Report (1953)

Skalamera, John J., (4-62')

Sjenitzer, F., Spray Drying; Chem. Engr. Sci., Genie Chimique, Vol. 1, No. 3, April 1952, p 101

Sinclair, D., and LaMer, V. K., (4-31)

Sleipceovich, C. M., Consiglio, J. A., and Kurata, F., (2-22)

Smulowicz, B., Analysis of the Impactometer, an Instrument for Measuring the Distribution of Raindrop Sizes Encountered in Flight, M. Sc. Thesis, Mass. Inst. of Tech. (1952)

Sohnen, E., and Grigull, U., (3-13A)

Sonkin, L. S., (4-49)

Spanogle, J. A., and Hemmeter, G. T., (2-23)

Stark, W. T., and Constantino, C. S., (3-3)

Stehling, K. R., (3-24B)

Stehling, K. R., (3-24C)

Stoker, R. L., (4-71)

Stone, I., (3-23B)

Stratton, J. A., (4-30)

Straubel, H., (2-22B)

WADC TR 56-344

XII

Contrails

Strehlow, R. A., (2-10)

Stubbs, H. E., and York, J. L., (4-28)

Stubbs, H. E., Canfield, H. H., and Nichols, A., Drop Size Study in the Icing Wind Tunnel, Project M 992-3, Mich. Univ. Eng. and Res. Inst. (1953)

Szlackin, J. A., (1-43)

Tanasawa, Y., An Experiment on the Atomization of Liquid by Means of an Air Stream (6th Report) Characteristics of Crossed Nozzles; Trans. SME Japan, Vol. 6, No. 23, 1940, p S-10

Tanasawa, Y., Outline of the Study on the Atomization of Liquids; Kagaku-Kikai-Kyokai Nenpo, Vol. 7 (1949)

Tate, R. W., and Marshall, W. R., Jr., Atomization by Centrifugal Pressure Nozzles; Part I. Chem. Engr. Prog., Vol. 49, No. 4, p 169 (April 1953). Part II. Vol. 49, No. 5, p 226 (May 1953)

Taylor, E. H., and Harman, D. B., Jr., (4-23B)

Taylor, G. I., (1-38) (3-14)

Taylor, G. I., (3-15)

Tassler, M. C., Film Coefficients for Mass Transfer During Liquid Atomization, Ph. D. Thesis, Univ. Illinois (1952)

The Texas Company, Fuel Spray Pattern; Petroleum Processing, April 1951, Vol. 6, No. 4, p 400

Timbrell, V., Method of Measuring and Classifying Microscopic Spherical Particles, Nature, 170, 318 (1952)

Triebnigg, H., The Pneumatic and Hydraulic Injection in Diesel Engines; Julius Springer, Berlin, 1925

Troesch, H. A., Atomization of Liquids (Eidg Tech. Hochschule, Zurich, Switzerland) Chem. Ing. Tech. 26, 311-20 (1954)

Turner, G. M., and Moulton, R. W., Drop Size Distribution from Spray Nozzles; Chem. Engr. Prog., Vol. 49, No. 4 (April 1953) p 185

Tyler, E., (1-17)

Urban, F. M., (4-91)

Vincent, E. T., Some Considerations Regarding Combustion of High Pressure Sprays; Prepared for Conference on Fuel Sprays, March 30-31, 1949

Vonnegut, B., and Neubauer, R. L., (2-22A)

Walton, W. H., (4-62A)

Walton, W. H., and Prewett, W. C., (2-11)

Watson, E. A., (3-10) (4-99)

Watson, E. A., and Clarke, J. S., (1-47) (3-9)

Weber, C., (1-10)

Contrails

Weibull, W., (4-84)

Weinberg, S., Heat Transfer to Low Pressure Sprays of Water in a Steam Atmosphere, Inst. Mech. Engrs. Proc., 1B, 240 (1952)

Weisenberg, I., Wehrli, R., Dolida, N., and Greenberg, H., (3-27)

Wetzel, R. H., (4-26A)

Wheeler, L. K., and Trickett, E. S., Measurement of the Size Distribution of Spray Particles; Elec. Engr., 1953, Vol. 25 (October) pp 402-6

Whipple, G. C., (4-89)

Wilson, Hewitt, Page, G. A., and Cartwright, V. S., (2-16)

Wilcox, J. D., Design of a New Five-Stage Cascade Impactor; Arch. Ind. Hyg. and Occ. Med. 7, 376-382 (May 1953)

Woeltjen, A., (4-5)

Yeomans, H. A., Directions for Determining Particle Size of Aerosols and Fine Sprays; U. S. Dept. Agriculture Agr. Res. Administration, Bur. Entomology and Plant Quarantine, ET-267, May 1949

York, J. L., (1-33)

York, J. L., Stubbs, H. E., and Tek, M. R., (1-34)

York, J. L., Stubbs, H. E., and Tek, M. R., (1-34A)

Zucrow, M. J., and Beighley, C. M., (3-24D)

CHAPTER 5. BALLISTICS OF A SINGLE DROPLET

ABSTRACT

The methods of classical hydrodynamics are employed to obtain those fundamental results which pertain to the translation and rotation of solid spheres and ellipsoids in an ideal fluid. The extensions of these results to the motion of solid or liquid spheres in real fluids are indicated. The stream functions, velocity potentials, and pressure distributions are obtained only for the simple cases. Stokes' law of drag, internal circulations, and oscillations of viscous spheres are also considered in the classical form. Following the discussion of the classical work, the recent modifications of hydrodynamics due to Oseen's approximation to the Navier-Stokes' equations and Prandtl's theory of the boundary layer are discussed. The various theories regarding the wake formation behind a moving sphere are compared, and a mathematical analysis of droplet deformations is given. Finally, the equations for the motion of a droplet injected into a uniform and curved flow field are developed.

Contrails

BALLISTICS OF A SINGLE DROPLET

by

R. E. Thomas, F. Benington,
A. E. Weller, and J. D. Kettelle, Jr.

The general aim of this chapter is to consider a physical system composed of a single, moving droplet surrounded by a gas. For the most part, the various flow fields which arise from the interactions between the droplet and the gas will be obtained through the general methods of classical hydrodynamics. Every investigator in the field of hydrodynamics is aware of the fact that "drastic" simplifications are often employed in the classical developments. The assumption of zero viscosity is associated with the concept of an "ideal" fluid. The mathematical utility of such a concept is apparent from the resulting simplifications produced in the Navier-Stokes equations. The physical utility lies in the remarkable fact that the correlation between the "ideal" theory and the laboratory data is quite satisfactory in many instances. The failure of the classical theory, however, cannot be attributed merely to the oversimplification involved in the assumption of zero viscosity. Recent mathematical considerations indicate that the ideal fluid is a complete "physical fiction" in the sense that it does not even represent the limiting case of a real fluid whose viscosity approaches zero. Many of the present-day problems and paradoxes arising in the field of hydrodynamics stem from this fact⁽⁵⁻¹⁾. In a sense, it is much more difficult to explain the success of classical hydrodynamics than it is to explain its failure.

The fact that the classical theory does not account for all hydrodynamic phenomena puts a considerable burden on the investigator. Should he assume that the classical methods are applicable to his problem, or should he rely on the more modern methods of dimensional reasoning? From a survey of recent developments in hydrodynamics, he should combine both methods. One of the major endeavors of modern hydrodynamics seems to lie in the attainment of a synthesis of classical results, on one hand, with the theory of modeling and dimensional reasoning on the other. Almost every major advance in the field of hydrodynamics since 1900 has involved a coupling of the classical results with dimensional reasoning.

Thus, the classical results have not been abandoned in the modern approach to hydrodynamics. More properly, the classical results are assumed to be valid in certain specified regions of the flow space. For example, Prandtl⁽⁵⁻²⁾ assumes that the unmodified classical results hold everywhere outside of the "boundary layer", while inside the boundary layer more appropriate simplifying assumptions are made. Consequently, in the physical systems considered in this chapter practically all of the flow volume may be properly treated by classical methods.

These remarks have been made primarily to justify the inclusion of many of the classical results to be found in Part One of this chapter. The material presented in this part is based on several excellent texts on hydrodynamics^(5-3, 4, 5, 6, 7). Some reorganization has been made to afford the simplest and most direct access to those classical results which are applicable to the motion of a droplet in a gas.

In Part Two of this chapter, some of the more recent approximations to the hydrodynamic equations are considered, together with boundary-layer theory, the wake behind a sphere, deformations, oscillations, and trajectories of liquid droplets.

Fundamental Concepts of Potential Flow

In this section several of the fundamental concepts utilized in the classical approach to fluid flow are introduced. These include a brief description of the basic properties of irrotational flow together with a derivation of the Stokes' stream function and the velocity-potential function for axially symmetric flow.

Axially Symmetric Flow

In the classical approach to the problems of three-dimensional flow, one assumes an "axial symmetry", that is, that there exists a line in the flow field such that the flow patterns in any pair of planes containing this line are identical. With respect to a sphere immersed in the fluid, the line of symmetry will be taken as a line through the center of the sphere oriented parallel to the relative velocity of flow at infinity. It will be convenient to use spherical polar coordinates in most of these considerations. These coordinates are related to the usual Cartesian coordinates by the following coordinate-transformation equations:

$$\begin{aligned}x &= r \cos \theta \\y &= r \sin \theta \cos \omega \\z &= r \sin \theta \sin \omega\end{aligned}$$

The x-axis will always be taken in the direction of the fluid flow.

Figure 5-1 shows the position vector, $\vec{P}(r, \theta, \omega)$, of an arbitrary point \vec{P} in the flow field. Let \vec{r} and $\vec{\theta}$ denote unit vectors which are parallel and perpendicular, respectively, to \vec{P} in the meridian plane, $\omega = \text{constant}$. The flow through the space generated by revolving an element of area, $r dr d\theta$, about the axis of flow may be easily obtained as follows. The flow in the $\vec{\theta}$ direction through a cylindrical surface element generated by revolving an element of arc, dr , about the axis of symmetry is given by $F(\theta) = 2\pi v_{\theta} r \sin \theta dr$, where v_{θ} denotes the $\vec{\theta}$ component of the vector velocity \vec{v} . Then Taylor's expansion yields for the first approximation:

$$\begin{aligned}F\left(\theta + \frac{d\theta}{2}\right) - F\left(\theta - \frac{d\theta}{2}\right) &= \frac{\partial F(\theta)}{\partial \theta} d\theta \\&= \frac{\partial}{\partial \theta} \left[2\pi v_{\theta} r \sin \theta dr \quad d\theta \right].\end{aligned}$$

Similarly, the flow in the \vec{r} -direction through a cylindrical surface element generated by revolving an element of arc, $r d\theta$, about the axis of symmetry is given by $F(r) = 2\pi v_r r^2 \sin \theta d\theta$, so that

$$\begin{aligned}F\left(r + \frac{dr}{2}\right) - F\left(r - \frac{dr}{2}\right) &= \frac{\partial F(r)}{\partial r} dr \\&= \frac{\partial}{\partial r} \left[2\pi v_r r^2 \sin \theta d\theta \quad dr \right],\end{aligned}$$

where v_r denotes the \vec{r} component of \vec{v} . Then if there are no sources or sinks in the region (that is, no fluid is created or destroyed), and if the fluid is incompressible, then the flow into the space generated is equal to the flow out of the space, so that

$$\frac{\partial}{\partial \theta} \left[2\pi v_{\theta} r \sin \theta dr \right] d\theta + \frac{\partial}{\partial r} \left[2\pi v_r r^2 \sin \theta d\theta \right] dr = 0 .$$

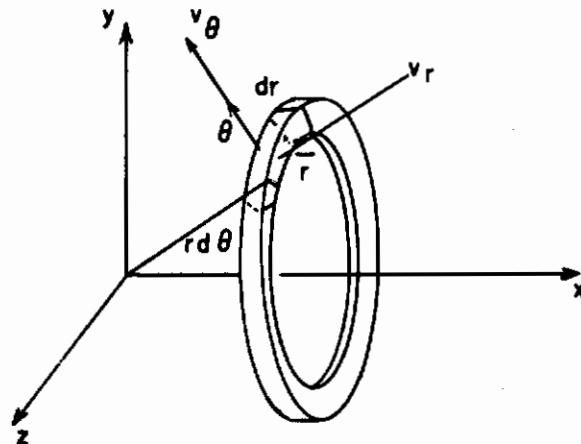
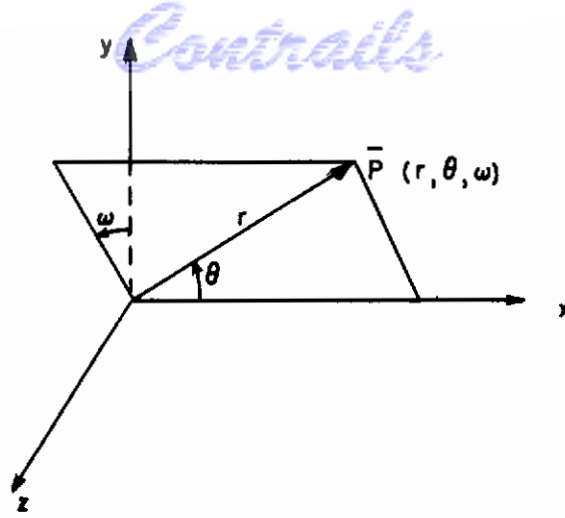


FIGURE 5-1. COORDINATE SYSTEMS FOR AXIALLY SYMMETRIC FLOW

Cancelling $2\pi dr d\theta$ throughout yields

$$\frac{\partial}{\partial \theta} [v_{\theta} r \sin \theta] + \frac{\partial}{\partial r} [v_r r^2 \sin \theta] = 0 ,$$

and this is precisely the condition required for

$$-v_{\theta} r \sin \theta dr + v_r r^2 \sin \theta d\theta$$

to be an exact differential. This expression is defined to be the exact differential of Stokes' stream function, $\psi(r, \theta)$, so that

$$d\psi = -v_{\theta} r \sin \theta dr + v_r r^2 \sin \theta d\theta . \tag{5-1}$$

The relation between the components of the velocity of flow and the stream function is found by alternately setting $dr = 0$ and $d\theta = 0$ in Equation (5-1). This yields

$$v_r = \frac{-1}{r^2 \sin \theta} \frac{\partial \psi}{\partial \theta}$$

$$v_{\theta} = \frac{1}{r \sin \theta} \frac{\partial \psi}{\partial r} .$$

It should be noted that the surfaces represented by $\psi(r, \theta) = \text{constant}$ are surfaces generated by revolving the streamlines in any meridian plane about the axis of symmetry. These stream surfaces are everywhere tangent to the vectors representing the velocity of flow at each point.

Irrotational Flow

If every closed surface in a region, R , can be collapsed to a point without passing outside of R , then R is said to be simply connected. A physical example of a case in which these concepts fail to hold is given by the consideration of an infinite circular cylinder filled with a liquid containing bubbles of a gas. The region, R , consisting of the liquid is not bounded at the ends of the tube, and a sub-region of R containing a bubble cannot be shrunk to zero volume without the boundary passing through the bubble in the process. Thus R is neither closed nor simply connected.

Let R be simply connected and let C be a simple, closed curve in R . The circulation of the fluid with respect to C is obtained by integrating the tangential component of the velocity vector around the curve C . Thus letting \bar{u} denote a unit vector tangent to C and letting ds denote an element of arc along C , the circulation is given by

$$\oint_C \bar{v} \cdot \bar{u} \, ds .$$

If the circulation is zero for every simple closed curve in R , then the fluid flow in R is said to be irrotational. Physically, this means that the angular motion of any incremental volume of fluid is zero. The following properties of irrotational flow should be noted:

- (a) The existence of the Stokes' stream function does not depend on the assumption of irrotational flow.
- (b) In irrotational flow, under conservative forces, the pattern of the fluid flow is completely determined by the boundary conditions.
- (c) Some portions of a fluid medium may undergo irrotational flow while other portions do not.

Vorticity

As a consequence of Stokes' theorem⁽⁵⁻⁸⁾ it follows that

$$\oint_C \bar{v} \cdot \bar{u} \, ds = \int_S (\nabla \times \bar{v}) \cdot \bar{n} \, dS , \quad (5-3)$$

where the integral on the right is taken over the surface, S , enclosed by the curve, C ; dS denotes an element of area, \bar{n} denotes a unit vector which is perpendicular to the surface, and

$$\nabla = \frac{\partial}{\partial r} \bar{r} + \frac{1}{r} \frac{\partial}{\partial \theta} \bar{\theta} + \frac{1}{r \sin \theta} \frac{\partial}{\partial \omega} \bar{\omega} .$$

Thus, in a region which has zero circulation, Equation (5-3) implies that $\nabla \times \bar{v} = \bar{0}$, so that the curl of an irrotational velocity vector is zero. The vector, $\nabla \times \bar{v}$, is called the vorticity vector and is equal in magnitude to twice the angular-velocity vector of rotation at any given point. The subject of fluid motion in which $\nabla \times \bar{v} \neq \bar{0}$ is discussed more fully in Chapter 20.

If there exists a single-valued function of position, $\phi(r, \theta)$, such that $\bar{v} = -\nabla\phi$, then ϕ is called the velocity potential of the fluid flow. In a meridian plane, $\omega = \text{constant}$, this requirement may be written as follows:

$$\bar{v} = v_r \bar{r} + v_\theta \bar{\theta} = -\nabla\phi = -\left[\frac{\partial}{\partial r} \bar{r} + \frac{1}{r} \frac{\partial}{\partial \theta} \bar{\theta} \right] \phi,$$

so that

$$v_r = -\frac{\partial \phi}{\partial r}, \text{ and} \tag{5-4}$$

$$v_\theta = -\frac{1}{r} \frac{\partial \phi}{\partial \theta}.$$

If the velocity is continuous and the circulation with respect to any curve, C , in a region, R , is zero, it follows that the line integral, $\int_A^B \bar{v} \cdot \bar{u} \, ds$, evaluated on some path between the points A and B is independent of the path chosen⁽⁵⁻⁹⁾. In this case the velocity potential, $\phi(P)$, may be defined by the integral, $-\int_0^P \bar{v} \cdot \bar{u} \, ds$, where 0 denotes an arbitrary, fixed origin, and P denotes a variable point in R . Then $d\phi = -\bar{v} \cdot \bar{u} \, ds$, and since $d\phi$ is also given by $\nabla\phi \cdot \bar{u} \, ds$, it follows that $\bar{v} = -\nabla\phi$. Thus, whenever the circulation is zero in a region, R , the velocity, \bar{v} , is the gradient of some scalar function, ϕ . The determination of the velocity potential and its properties constitutes the major considerations of the classical approach to three-dimensional flow. Some of the most important results concerning the nature of the velocity potential are listed in the next section. For a complete treatment of these results, the reader may consult standard text books on hydrodynamics.

General Properties of the Velocity Potential

- (1) As indicated in the last section, the velocity potential exists if and only if the fluid motion is irrotational.
- (2) If a velocity potential exists for a finite volume of fluid for a finite interval of time, then the velocity potential exists for that volume of fluid for all time intervals, provided the density is constant or a function of pressure only⁽⁵⁻¹⁰⁾.
- (3) The existence of a velocity potential indicates that the flow of the fluid could be produced instantaneously from a fluid at rest by the application of a suitable set of impulsive pressures. The impulse pressures are given by $\hat{p} = \rho\phi(r, \theta) + C$, where ρ denotes the density of the fluid and C is an arbitrary constant⁽⁵⁻¹¹⁾.
- (4) The lines of flow in a fluid possessing a velocity potential are orthogonal to the set of surfaces given by the equations $\phi(r, \theta) = \text{constant}$ ⁽⁵⁻¹²⁾.
- (5) The velocity potential is a harmonic function. This means that $\phi(r, \theta)$ is a solution of Laplace's equation⁽⁵⁻¹³⁾ so that

$$\sin \theta \frac{\partial}{\partial r} \left(r^2 \frac{\partial \phi}{\partial r} \right) + \frac{\partial}{\partial \theta} \left(\sin \theta \frac{\partial \phi}{\partial \theta} \right) + \frac{1}{\sin \theta} \frac{\partial^2 \phi}{\partial \omega^2} = 0.$$

In the case of the axially symmetric flow this becomes

$$\frac{\partial}{\partial r} \left(r^2 \frac{\partial \phi}{\partial r} \right) + \frac{1}{\sin \theta} \frac{\partial}{\partial \theta} \left(\sin \theta \frac{\partial \phi}{\partial \theta} \right) = 0 \quad (5-5)$$

- (6) The velocity in any direction, \bar{u} , from an arbitrary point is given by $-\nabla\phi \cdot \bar{u}$ where ϕ denotes the velocity potential at the point and \bar{u} denotes a unit vector in the desired direction(5-14).
- (7) A harmonic velocity potential cannot have a proper maximum or minimum at any point interior to the fluid(5-15). The square of the velocity cannot be a maximum at any point within the fluid(5-16).
- (8) When $\phi(r, \theta)$ is harmonic the volume of fluid crossing a surface is given by $-\iint_S \nabla\phi \cdot \bar{n} \, dS$, where \bar{n} is a unit normal vector to the surface and dS is an element of area(5-17). If the surface is closed, $\iint_S \nabla\phi \cdot \bar{n} \, dS = 0$.
- (9) The mean value of $\phi(r, \theta)$ over the surface of any sphere having no sources or sinks within the boundary is equal to the value obtained at the center of the sphere. This mean value is given by

$$\frac{1}{4\pi r^2} \iint_S \phi(r, \theta) \, dS$$

where the integration extends over the surface of the sphere(5-18).

- (10) The irrotational motion of an infinite fluid completely surrounding a closed surface having fixed boundaries is uniquely determined in case(5-19):

(i) the values of $\phi(r, \theta)$ are specified over the boundary and $\lim_{r \rightarrow \infty} \phi(r, \theta) = \text{constant}$; or

(ii) the values of $\nabla\phi \cdot \bar{n}$ are specified over the boundary and $\lim_{r \rightarrow \infty} \phi(r, \theta) = \text{constant}$.

- (11) If two velocity-potential functions differ only by an additive constant, then they represent the same flow(5-20). The velocity-potential functions may be combined linearly to obtain new velocity-potential functions.

The Velocity Potential in Terms of Surface Zonal Harmonies

Many instances of axially symmetric flow may be treated by assuming that the velocity potential is expressible as the product of two functions, $f(r)$ and $g(\theta)$. The substitution of $f(r)g(\theta) = \phi(r, \theta)$ into Equation (5-5) indicates that $f(r)$ and $g(\theta)$ must satisfy the following equations:

$$r^2 \frac{d^2 f(r)}{dr^2} + 2r \frac{df(r)}{dr} - \lambda^2 f(r) = 0$$

and

$$\frac{1}{\sin \theta} \frac{d}{d\theta} \left(\sin \theta \frac{dg(\theta)}{d\theta} \right) + \lambda^2 g(\theta) = 0 \quad ,$$

where λ^2 denotes a numerical constant. The first equation is Cauchy's differential equation and may be solved by setting $r = e^t$. This substitution yields

$$[D^2 + D - \lambda^2] f(e^t) = 0$$

where D denotes the operator d/dt . Thus, the auxiliary equation is $m^2 + m - \lambda^2 = 0$, and, solving this for m , the following expression for $f(r)$ is obtained:

$$f(r) = A_m r^m + B_m r^{-(m+1)},$$

where A_m and B_m are arbitrary constants and

$$m = \frac{-1 + \sqrt{1 + 4\lambda^2}}{2}.$$

By choosing $\lambda^2 = m(m+1)$ and setting $x = \cos \theta$, the second equation is transformed into Legendre's equation⁽⁵⁻²²⁾

$$(1 - x^2) \frac{d^2}{dx^2} g(\theta) - 2x \frac{d}{dx} g(\theta) + m(m+1) g(\theta) = 0.$$

For integral values of m the solutions of this differential equation are given by the orthogonal set of surface zonal harmonics, $P_m(\cos \theta)$ ⁽⁵⁻²³⁾. Under the above assumptions the velocity potential then has the following form:

$$\phi(r, \theta) = \sum_{m=0}^{\infty} [A_m r^m + B_m r^{-(m+1)}] P_m(\cos \theta). \quad (5-6)$$

The values of A_m and B_m must be obtained from the boundary conditions associated with the particular flow problem under consideration.

Relation Between the Stream Function and the Velocity Potential

When the motion of the fluid is irrotational, Equation (5-4) shows that a velocity potential, $\phi(r, \theta)$, exists such that $v_r = -\partial\phi/\partial r$ and $v_\theta = -1/r \partial\phi/\partial\theta$. Thus from Equation (5-2), the velocity potential is related to the stream function by the equations

$$\frac{\partial\phi}{\partial r} = \frac{1}{r^2 \sin \theta} \frac{\partial\psi}{\partial\theta}$$

and

$$\frac{\partial\phi}{\partial\theta} = \frac{-1}{\sin \theta} \frac{\partial\psi}{\partial r}.$$

(5-7)

It should be noted that the dimensions of $\phi(r, \theta)$ are given by L^2/T , and from Equation (5-7) the dimensions of $\psi(r, \theta)$ are given by L^3/T . Thus, in three-dimensional flow, as compared to two-dimensional flow, it is not possible to interchange the roles of the velocity potential and stream function to obtain additional admissible flow patterns. It is largely for this reason that the complex-variable treatment of two-dimensional flow cannot be immediately applied to three-dimensional flow having axial symmetry.

The classical flow patterns associated with the simple source, sink, and doublet are developed in this section. The velocity potential and stream function associated with these flows are derived by a direct application of Stokes' stream function.

Sources and Sinks

In many simple cases, the velocity potential and stream function may be calculated directly without applying the general solution given by Equation (5-6). Many three-dimensional flow patterns can be easily obtained by superposition of the configurations associated with the creation or destruction of fluid at specified points. A simple source of strength, \underline{m} , is defined to be a point at which a volume of $4\pi m$ units of fluid is created per unit of time. The created fluid is assumed to flow outward from the source in a radial direction, so that $v_\theta = 0$. Analogous definitions hold for the simple sink of strength \underline{m} at which fluid is destroyed.

Flow Due to a Simple Source

From Stokes' stream function, the volume of fluid passing through the surface of a sphere having a simple source for its center is given by the integral $\int_0^\pi 2\pi r^2 v_r \sin \theta d\theta$. By the definition of a simple source, this volume is also given by $4\pi m$, where \underline{m} is the strength of the source. Equating these two expressions shows that the radial velocity, v_r , is given by m/r^2 . Then from Equation (5-4) the velocity potential may be written immediately as

$$\phi(r, \theta) = m/r \quad (5-8)$$

Furthermore, from Equation (5-7) it follows that the stream function is given by

$$\psi(r, \theta) = m \cos \theta \quad (5-9)$$

The velocity potential and stream function for a sink of strength \underline{m} are similarly found to be given by

$$\phi(r, \theta) = -m/r \quad (5-10)$$

and

$$\psi(r, \theta) = -m \cos \theta.$$

Uniform Flow Parallel to an Axis of Symmetry

Figure 5-2 shows a circular disk which is centered on the x-axis. The x-axis is taken to be an axis of radial symmetry for the fluid flow, and the plane of the disk is perpendicular to this axis. Letting U denote the stream velocity in the x-direction, the volume of the fluid passing through the surface of the disk, in unit time, is given by $-\pi r^2 \sin^2 \theta U$. From the definition of Stokes' stream function, it can be shown that this volume of fluid may also be denoted by $2\pi\psi(r, \theta)$. Equating these two expressions for the flow yields

$$\psi(r, \theta) = -1/2 U r^2 \sin^2 \theta \quad (5-11)$$

and from Equation (5-7) it follows that

$$\phi(r, \theta) = -U r \cos \theta \quad (5-12)$$

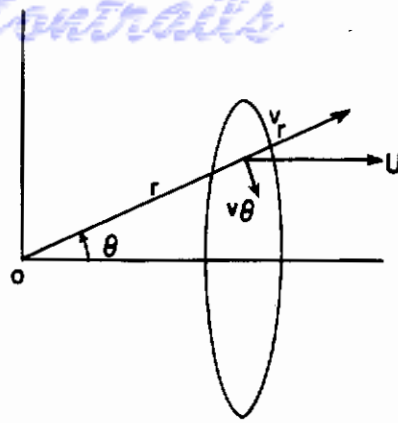


FIGURE 5-2. UNIFORM FLOW THROUGH A DISK

Flow Due to a Doublet

Figure 5-3 indicates a source located at the point $(a/2, 0)$ and a sink at $(-a/2, 0)$. From Equations (5-8), (5-9), and (5-10) and the additive property of potential functions, it follows that the velocity potential and the stream function are given by

$$\phi(r, \theta) = m/r_2 - m/r_1 ,$$

$$\psi(r, \theta) = m \cos \theta_2 - m \cos \theta_1 ,$$

where both the source and sink are assumed to have strength m . Now assume that the strength increases and that the distance between the source and sink decreases in such a manner that

$$\lim_{\substack{a \rightarrow 0 \\ m \rightarrow \infty}} a m = \mu = \text{constant} .$$

The combined source and sink at the origin is called a doublet. Applying the law of sines in Figure 5-3 yields

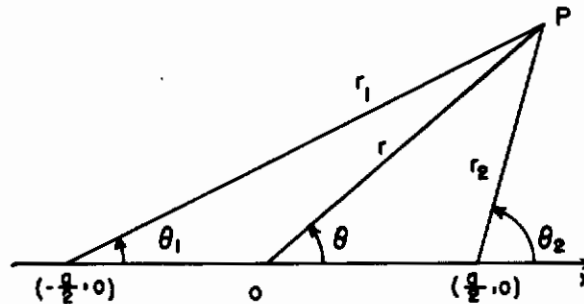


FIGURE 5-3. FORMATION OF A DOUBLET FROM A SOURCE AND A SINK

$$\phi(r, \theta) = \frac{\mu \cos 1/2 (\theta_2 + \theta_1)}{r_1 r_2 \cos 1/2 (\theta_2 - \theta_1)}$$

and

$$\psi(r, \theta) = \frac{\mu r \cos \theta \cos 1/2 (\theta_2 + \theta_1)}{r_1 r_2 \cos 1/2 (\theta_2 - \theta_1)} - \frac{\mu}{2} \left(\frac{1}{r_1} + \frac{1}{r_2} \right) .$$

Then, as a becomes arbitrarily small, θ_1 and θ_2 approach θ , and r_1 and r_2 approach r . Thus the above equations become

$$\phi(r, \theta) = \frac{\mu \cos \theta}{r^2}$$

and

(5-13)

$$\psi(r, \theta) = \frac{-\mu \sin^2 \theta}{r}$$

These equations represent the velocity potential and stream function for a doublet at the origin.

A Solid Sphere in an Ideal Fluid

In this section the fundamental equations relating to the classical flow about a sphere are developed by an application of the Sphere Theorem of Weiss, and the results are interpreted in terms of a Rankine body. The velocity distribution on the surface of the sphere is calculated from the velocity-potential function. The pressure equation and Bernoulli's equation are deduced from the Navier-Stokes equations which are rigorously derived in Chapter 11. From these results the pressure distribution on the surface of the sphere is computed.

The Sphere Theorem

In 1945, Weiss⁽⁵⁻²⁴⁾ proved a theorem which can be readily applied to problems of fluid flow around spheres. The result may be stated as follows:

Theorem. Let $\phi_0(x, y, z)$ denote a velocity potential (in Cartesian coordinates) which defines an irrotational flow of an incompressible, inviscid fluid in a three-dimensional flow field having no rigid boundaries. Suppose, further, that all of the singular points of $\phi_0(x, y, z)$ are outside a sphere of radius a whose center is at the origin. Then, if a sphere, given by $x^2 + y^2 + z^2 - a^2 = 0$, is introduced into the fluid, the new velocity potential, $\phi(x, y, z)$, is given by

$$\begin{aligned} \phi(x, y, z) = & \phi_0(x, y, z) + \frac{a}{r} \phi_0\left(\frac{a^2x}{r^2}, \frac{a^2y}{r^2}, \frac{a^2z}{r^2}\right) \\ & - \frac{2}{ar} \int_0^a \lambda \phi_0\left(\frac{\lambda^2x}{r^2}, \frac{\lambda^2y}{r^2}, \frac{\lambda^2z}{r^2}\right) d\lambda, \end{aligned} \quad (5-14)$$

where $r^2 = x^2 + y^2 + z^2$. An application of this theorem is made in the following section.

Sphere at Rest in a Uniform Stream

From Equation (5-12), the velocity potential in the uniform stream before the introduction of a sphere is given by $\phi_0(r, \theta) = -U r \cos \theta$. Then, by the sphere theorem, Equation (5-14), it follows that the velocity potential after the sphere is introduced may be written as follows:

$$\begin{aligned} \phi(r, \theta) = & -U r \cos \theta - U \frac{a}{r} \left[\frac{a^2 r \cos \theta}{r^2} \right] \\ & + \frac{2}{ar} \int_0^a \lambda \left[U \frac{\lambda^2 r \cos \theta}{r^2} \right] d\lambda. \end{aligned}$$

By evaluating this expression, it is readily found that

$$\phi(r, \theta) = -U \left(r \cos \theta + \frac{a^3 \cos \theta}{2r^2} \right) . \quad (5-15)$$

It may be noted that the resulting velocity potential can be written as $\phi = \phi_1 + \phi_2$, where $\phi_1 = -U r \cos \theta$ is the velocity potential for uniform flow, and $\phi_2 = (-Ua^3/2) \cos \theta/r^2$ is the velocity potential for a doublet of strength $\mu = -Ua^3/2$ which is located at the origin. Thus the flow around a sphere at rest may be considered as equivalent to a superposition of the flow due to a doublet and a uniform flow. The observation that the flow patterns around solids are often mathematically obtainable by a consideration of the flow due to the presence of a suitable array of doublets about the origin has received considerable attention in classical hydrodynamics. The solids which correspond to these arrays of doublets are usually called Rankine's bodies. From the preceding results, the sphere is seen to be the simplest example of a Rankine body.

From Equations (5-11) and (5-13), the stream surfaces corresponding to ϕ_1 and ϕ_2 are, respectively,

$$\psi_1(r, \theta) = -1/2 U r^2 \sin^2 \theta$$

and

$$\psi_2(r, \theta) = \frac{U a^3 \sin^2 \theta}{2r} .$$

Thus, putting $\psi(r, \theta) = \psi_1 + \psi_2$ yields

$$\psi(r, \theta) = -1/2 U r^2 \sin^2 \theta \left(1 - \frac{a^3}{r^3} \right) \quad (5-16)$$

for the stream function associated with a sphere at rest in a uniform stream. From Equation (5-4), the tangential component of the velocity is given by

$$v_\theta = -\frac{1}{r} \frac{\partial \phi}{\partial \theta} = U \left(\sin \theta + \frac{a^3 \sin \theta}{2r^3} \right) . \quad (5-17)$$

On the surface of the sphere, r is equal to a , so that the tangential component of the velocity at the surface is given by

$$v_\theta = \frac{3}{2} U \sin \theta . \quad (5-18)$$

The points on the surface of a body where $v_\theta = 0$ are called the stagnation points. From the preceding equation, the stagnation points on a sphere are found to occur for $\theta = 0$ and $\theta = \pi$. Thus, the tangential velocity is zero at the extreme upstream and downstream points on the surface of the sphere.

The maximum values of the tangential velocity at the surface of the sphere occur for those values of θ which satisfy the equation, $dv_\theta/d\theta = 0$. From Equation (5-18) it is readily found that the critical values of θ are $\pi/2$ and $3\pi/2$. Thus, the maximum tangential velocity occurs on a great circle midway between the stagnation points. The magnitude of this maximum tangential velocity is equal to $3/2 U$.

Sphere Moving Uniformly in a Fluid at Rest

In this case the fluid is assumed to be at rest at infinity. To obtain the appropriate velocity potential and stream function, it is only necessary to combine a uniform flow, U , in the negative direction of the x -axis with the flow of the preceding section. Thus, from Equations (5-15) and

(5-12), it follows that the potential function for a sphere moving in the positive direction of the x-axis is given by

$$\phi(r, \theta) = -\frac{1}{2} U a^3 \frac{\cos \theta}{r^2} . \quad (5-19)$$

By comparing this result with the velocity potential of the doublet, Equation (5-13), it may be inferred that the stream function is given by

$$\psi(r, \theta) = \frac{1}{2} U a^3 \frac{\sin^2 \theta}{r} . \quad (5-20)$$

Navier-Stokes Equations of Motion

The equations of motion of a fluid element in a general tensor form are derived in detail in Chapter 11. The Navier-Stokes equation, Equation (11-19), may be written in the following form:

$$G_j - \frac{1}{\rho} \frac{\partial p}{\partial x_i} \delta_{ij} + \frac{\mu}{\rho} \frac{\partial^2 U_s}{\partial x_r \partial x_i} (-\delta_{ij} \delta_{rs} + \delta_{ir} \delta_{js} + \delta_{is} \delta_{jr} + \frac{1}{3} \delta_{ij} \delta_{rs}) = \frac{\partial U_j}{\partial t} + U_i \frac{\partial U_j}{\partial x_i}, \quad i, j, r, s, = 1, 2, 3,$$

where G_j represents the three components of the external force acting on the fluid element, p denotes the pressure and is proportional to the first scalar invariant of the stress tensor, U_j denotes the component of velocity in the x_j direction, μ denotes the viscosity, and the δ_{ij} satisfy the relations

$$\delta_{ij} = 0 \text{ for } i \neq j$$

$$\delta_{ij} = 1 \text{ for } i = j; i, j = 1, 2, 3 .$$

This general result may be considerably simplified for the present development. Thus, for an ideal fluid the viscosity is zero and the preceding equation becomes

$$G_j - \frac{1}{\rho} \frac{\partial p}{\partial x_i} \delta_{ij} = \frac{\partial U_j}{\partial t} + U_i \frac{\partial U_j}{\partial x_i}; \quad i, j = 1, 2, 3 .$$

Eliminating the δ_{ij} and summing on the repeated indices yields

$$G_j - \frac{1}{\rho} \left[\frac{\partial p}{\partial x_j} \right] = \frac{\partial U_j}{\partial t} + U_1 \frac{\partial U_j}{\partial x_2} + U_2 \frac{\partial U_j}{\partial x_3};$$

$$j = 1, 2, 3 .$$

If the G_j and the U_j are regarded as components of a vector, the preceding equation must be satisfied componentwise. Consequently, the equation may be written in vector form as follows:

$$\bar{G} - \frac{1}{\rho} \nabla p = \frac{\partial \bar{U}}{\partial t} + (\bar{U} \cdot \nabla) \bar{U} ,$$

where \bar{G} represents the vector force, \bar{U} represents the vector velocity, and ∇p is the gradient of the pressure. By the vector identity⁽⁵⁻²⁵⁾,

$$(\bar{U} \cdot \nabla) \bar{U} = 1/2 \nabla(\bar{U} \cdot \bar{U}) - \bar{U} \times (\nabla \times \bar{U}) ,$$

the Navier-Stokes equation becomes

Contrails

$$\bar{G} - \frac{1}{\rho} \nabla p = \frac{\partial \bar{U}}{\partial t} + \frac{1}{2} \nabla (\bar{U} \cdot \bar{U}) - \bar{U} \times (\nabla \times \bar{U}) . \quad (5-21)$$

If it is assumed that the external forces are derivable from a scalar potential function, E , the force \bar{G} may be replaced by $-\nabla E$, so that

$$\frac{\partial \bar{U}}{\partial t} - \bar{U} \times (\nabla \times \bar{U}) = -\nabla \left(\frac{p}{\rho} + \frac{1}{2} \bar{U} \cdot \bar{U} + E \right) . \quad (5-22)$$

Pressure Equation for Irrotational Flow

It has already been shown that the velocity vector of an irrotational motion is the negative gradient of a scalar potential function and the curl of the velocity vector is zero, so that $\bar{U} = -\nabla \phi$ and $\nabla \times \bar{U} = \bar{0}$. Making these substitutions in Equation (5-22) yields

$$\frac{\partial}{\partial t} (-\nabla \phi) = -\nabla (p/\rho + 1/2 \bar{U} \cdot \bar{U} + E) ,$$

or simply,

$$\nabla \left(\frac{p}{\rho} + \frac{1}{2} \bar{U} \cdot \bar{U} + E - \frac{\partial \phi}{\partial t} \right) = 0 . \quad (5-23)$$

This result is known as the pressure equation of the fluid motion. When the velocity potential, ϕ , is known, the velocity, \bar{U} , is determined from $\bar{U} = -\nabla \phi$ and, from Equation (5-23), the pressure distribution may be found. Thus, in principle, the solution to any problem involving irrotational motion is reduced to that of finding the velocity potential.

Bernoulli's Equation

For the case of a fluid motion which is inviscid ($\mu = 0$), incompressible and without sources or sinks ($\nabla \cdot \bar{U} = 0$), irrotational ($\bar{U} = -\nabla \phi$ and $\nabla \times \bar{U} = \bar{0}$) and steady in time ($\partial \phi / \partial t = 0$), the pressure Equation (5-23) becomes

$$\nabla (p/\rho + 1/2 \bar{U} \cdot \bar{U} + E) = 0 ,$$

or

$$p/\rho + 1/2 \bar{U} \cdot \bar{U} + E = \text{constant} . \quad (5-24)$$

This equation is the well-known Bernoulli equation.

Pressure Distribution on the Surface of a Sphere

The velocity potential associated with the irrotational motion of an ideal fluid about a sphere was found to be given by Equation (5-15),

$$\phi(r, \theta) = -U \left(r \cos \theta + \frac{a^3 \cos \theta}{2r^2} \right) .$$

From this, it follows that $\bar{U} \cdot \bar{U} = (\partial \phi / \partial r)^2 + 1/r^2 (\partial \phi / \partial \theta)^2$ is equal to $9/4 U^2 a^2 \sin^2 \theta$ on the surface of the sphere. Thus, by Bernoulli's equation, the following result may be obtained:

$$\frac{p}{\rho} + \frac{1}{2} \left(\frac{9}{4} U^2 a^2 \sin^2 \theta \right) = \frac{p_{\infty}}{\rho} + \frac{1}{2} U^2 ,$$

where p_∞ denotes the pressure at infinity. Consequently, the pressure distribution on the surface of the sphere is given by

$$p - p_\infty = 1/2 \rho U^2 [-5/4 + 9/4 \cos^2 \theta] . \quad (5-25)$$

Motions Derivable From Kinetic Energy

An expression for the kinetic energy of a fluid in irrotational motion due to the uniform motion of a sphere is obtained in this section. The concept of virtual mass is introduced and is employed in the determination of the approximate flow patterns associated with the approach of two spheres and with parallel motion of two spheres. The behavior of a sphere in the vicinity of a wall is deduced from an application of Hamilton's principle and the Euler-Lagrange equations.

Kinetic Energy of a Fluid in Irrotational Motion

The kinetic energy of a volume, V , of fluid is given by the integral $1/2 \int_V \rho \bar{U} \cdot \bar{U} d\tau$, where $d\tau$ denotes an element of volume and the integral is taken throughout the volume. In irrotational flow, $\bar{U} = -\nabla\phi$ so that the kinetic energy may be written as $1/2 \int_V \rho (\nabla\phi) \cdot (\nabla\phi) d\tau$. From the known vector identity (5-26), $\nabla \cdot (\phi\bar{U}) = \bar{U} \cdot (\nabla\phi) + \phi(\nabla \cdot \bar{U})$, and from the divergence theorem, $\int_V \nabla \cdot \bar{U} d\tau = - \int_S \bar{n} \cdot \bar{U} dS$, (where \bar{n} denotes an inwardly directed unit vector normal to the surface element dS), it follows that

$$\int_S \bar{n} \cdot \phi \bar{U} dS = - \int_V \bar{U} \cdot (\nabla\phi) d\tau - \int_V \phi (\nabla \cdot \bar{U}) d\tau .$$

Now replacing \bar{U} by $-\nabla\phi$ and noting that the last integral is zero (since $\nabla \cdot \nabla\phi = 0$), this equation becomes

$$\int_S \bar{n} \cdot \phi (-\nabla\phi) dS = \int_V (\nabla\phi) \cdot (\nabla\phi) d\tau .$$

Since $\nabla\phi = \partial\phi / \partial n \bar{n}$, the last equation implies that the kinetic energy, T , is given by the expression

$$T = 1/2 \rho \int_S \bar{n} \cdot \phi (-\bar{n} \partial\phi/\partial n) dS ,$$

and from $\bar{n} \cdot \bar{n} = 1$, there results

$$T = -1/2 \rho \int_S \phi \partial\phi/\partial n dS . \quad (5-26)$$

This is the general expression for the kinetic energy of a volume of fluid in irrotational motion.

Kinetic Energy of a Fluid Due to the Uniform Motion of a Sphere

For a sphere of radius a , the element of surface area may be taken as $dS = 2\pi a \sin \theta ds$, where ds is an element of arc in a meridian plane. Moreover, the normal velocity, $-\partial\phi/\partial n$, may be expressed also as

$$\frac{\partial\phi}{\partial r} = v_r = \frac{-1}{a^2 \sin \theta} \frac{\partial\psi}{\partial\theta} ,$$

by Equation (5-7). Thus,

Contrails

$$\frac{\partial \phi}{\partial n} dS = \frac{1}{a^2 \sin \theta} \frac{\partial \psi}{\partial s} \frac{\partial s}{\partial \theta} 2 \pi a \sin \theta ds = 2 \pi d\psi ,$$

and the kinetic energy becomes

$$T = -\pi \rho \int_0^\pi \phi d\psi .$$

By utilizing Equations (5-19) and (5-20), this kinetic-energy integral can be expressed as

$$T = \pi/2 \rho U^2 a^3 \int_0^\pi \sin \theta \cos^2 \theta d\theta$$

and the kinetic energy is found to be given by

$$T = 1/3 \pi \rho U^2 a^3 . \quad (5-27)$$

Virtual Mass of a Moving Sphere

From Equation (5-27), the kinetic energy of the irrotational motion due to a moving sphere may be written as $T = 1/4 M^* U^2$, where the mass of the displaced fluid, $4/3 \pi \rho a^3$, is equal to M^* . Thus, the total kinetic energy of the system may be written as

$$T = 1/2 (M + 1/2 M^*) U^2 \quad (5-28)$$

where M denotes the mass of the sphere. The quantity $M' = M + 1/2 M^*$ is called the virtual mass of the sphere. This result indicates that, with respect to kinetic energy, the fluid-sphere system is equivalent to a system consisting only of a sphere which moves with a velocity U and has a mass equal to M' .

The Approach of Two Spheres

Figure 5-4 indicates the approach of two spheres, S_1 and S_2 , having their respective centers, O_1 and O_2 , on the x -axis. As indicated in the figure, U_1 and U_2 are the respective velocities of the spheres; r_1 and r_2 denote the distances of a point, P , from O_1 and O_2 , and θ_1 and θ_2 denote the angles between O_1P and the x -axis and O_2P and the x -axis.

Using the method of images and a zonal harmonic expression of the type given in Equation (5-6), the following approximate form of the velocity potential of the flow is obtained:

$$\begin{aligned} \phi = & \frac{U}{2} \left[\frac{a^3 P_1(\cos \theta_1)}{r_1^2} + \frac{a^3 b^3}{c^3} \frac{P_1(\cos \theta_2)}{r_2^2} \right] \\ & + \frac{U_2}{2} \left[\frac{b^3 P_1(\cos \theta_2)}{r_2^2} + \frac{a^3 b^3}{c^3} \frac{P_1(\cos \theta_1)}{r_1^2} \right], \end{aligned}$$

where a and b denote the radii of the spheres S_1 and S_2 and c denotes the distance between O_1 and O_2 .

By Equation (5-26), the kinetic energy of the liquid due to the motion of the two spheres is given by

$$T = -1/2 \rho \int_{S_1} \phi \frac{\partial \phi}{\partial n} dS_1 - 1/2 \rho \int_{S_2} \phi \frac{\partial \phi}{\partial n} dS_2$$

and, correct to terms in $1/c^3$, this kinetic energy becomes

$$T = 1/4 M_1^* U_1^2 + \frac{2\pi a^3 b^3}{c^3} \rho U_1 U_2 + 1/4 M_2^* U_2^2 , \quad (5-29)$$

where M_1^* and M_2^* denote the mass of the fluid displaced by the spheres S_1 and S_2 , respectively.

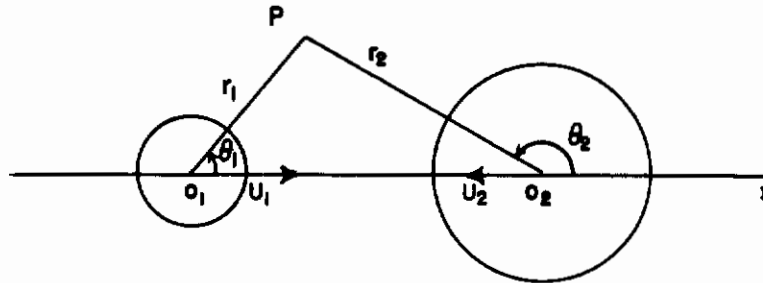


FIGURE 5-4. GEOMETRICAL RELATIONS OF TWO APPROACHING SPHERES

Two Spheres in Uniform Parallel Motion

Using methods similar to those of the preceding section, it may be shown that the approximate kinetic energy of a system composed of two spheres moving in a direction perpendicular to their line of centers is given by the equation

$$T = 1/4 M_1^* U_1^2 + \frac{\pi a^3 b^3 \rho}{c^3} U_1 U_2 + 1/4 M_2^* U_2^2 , \quad (5-30)$$

where U_1 and U_2 denote the respective velocities of the spheres S_1 and S_2 in the line of motion, and the other symbols remain as defined in the preceding section.

Hamilton's Principle and the Euler-Lagrange Equation

By Hamilton's principle, the definite time integral of the kinetic potential has a stationary value for all natural paths of the system in phase space⁽⁵⁻²⁸⁾. By the calculus of variations this principle requires⁽⁵⁻²⁹⁾ that

$$\delta \int_{t_1}^{t_2} (T - V) dt = 0 ,$$

where δ denotes the first variation operator, T denotes the kinetic energy of the system, V denotes the potential energy of the system, and t_1 and t_2 denote the initial and final times of the configuration. Taking the first variation of the above integral yields the Euler-Lagrange equations of motion,

$$\frac{d}{dt} \left(\frac{\partial T}{\partial \dot{q}_i} \right) - \frac{\partial T}{\partial q_i} = Q_i , \quad (5-31)$$

where q_i denotes a generalized coordinate, \dot{q}_i denotes the time derivative of q_i , and Q_i denotes a generalized force. The validity of these equations in the field of hydrodynamics has been thoroughly considered by several writers^(5-1, 30, 31). The equations may be applied to obtain the differential equations of motion of a solid moving through a fluid under the following conditions:

- Continuity*
- (i) The motion of the fluid is due entirely to the motion of the solid.
 - (ii) If the motion of the solid were suddenly stopped, the motion of the fluid would cease at the same instant.
 - (iii) The motion of the fluid is single-valued and irrotational.

Moving Sphere in the Vicinity of a Wall

To apply the Euler-Lagrange equations, the kinetic energy of the system must be computed. In Cartesian coordinates, the kinetic energy may be written as $T = 1/2 (A\dot{x}^2 + B\dot{y}^2)$ where \dot{x} and \dot{y} denote the time derivatives of the position coordinates, and A and B are determined from Equations (5-29) and (5-30).

In Equation (5-29), put $b = a$, so that the approaching spheres have equal radii. If U_1 is equal to U_2 , the resulting flow will be symmetric about a plane perpendicular to the x-axis midway between the spheres. Under these assumptions, no fluid can cross the plane of symmetry so that, mathematically, the symmetry plane is equivalent to a solid wall. Thus, the kinetic energy of a sphere approaching a wall is given by

$$T = 1/4 M^* U^2 \left[1 + \frac{3a^3}{8h^3} \right], \quad (5-32)$$

where h is the distance between the center of the sphere and the wall.

By a similar argument, putting $U_1 = U_2$ and $b = a$ in Equation (5-30) yields the kinetic energy for a sphere moving parallel to a wall. This is given by

$$T = 1/4 M^* U^2 \left[1 + \frac{3a^3}{16h^3} \right]. \quad (5-33)$$

By adding Equations (5-32) and (5-33), the total kinetic energy of a system composed of a sphere moving in the presence of a fixed wall is found to be

$$T = \frac{1}{2} \left\{ \left[M + \frac{1}{2} M^* \left(1 + \frac{3}{8} \frac{a^3}{x^3} \right) \right] \dot{x}^2 + \left[M + \frac{1}{2} M^* \left(1 + \frac{3}{16} \frac{a^3}{x^3} \right) \right] \dot{y}^2 \right\}, \quad (5-34)$$

where the center of the sphere has coordinates (x, y), the wall is given by the equation $x = 0$, and M denotes the actual mass of the sphere.

Substitution of the value of T given by Equation (5-34) into the Euler-Lagrange equations of motion yields

$$\begin{aligned} \frac{d}{dt} \left[M + \frac{1}{2} M^* \left(1 + \frac{3}{8} \frac{a^3}{x^3} \right) \right] \dot{x} + \frac{\dot{x}^2}{2} \left[\frac{9}{16} M^* \frac{a^3}{x^4} \right] \\ + \frac{\dot{y}^2}{2} \left[\frac{9}{32} M^* \frac{a^3}{x^4} \right] = Q_x \end{aligned}$$

and

Contrails

$$\frac{d}{dt} \left\{ \left[M + \frac{1}{2} M^* \left(1 + \frac{3}{16} \frac{a^3}{x^3} \right) \right] \dot{y} \right\} = Q_y .$$

If it is further assumed that the sphere moves at a constant velocity, so that $\ddot{x} = \ddot{y} = 0$, the equations of motion become

$$\frac{9}{64} \frac{M^* a^3}{x^4} (-2 \dot{x}^2 + \dot{y}^2) = Q_x$$

and

$$\frac{-9}{32} \frac{M^* a^3}{x^4} \dot{x} \dot{y} = Q_y .$$

These equations lead directly to the following qualitative statements:

- (i) If the sphere moves in a direction perpendicular to the wall (either toward the wall or away from the wall), then $\dot{y} = 0$ and Q_x is negative. Thus, to maintain uniform motion in a direction perpendicular to the wall, a force toward the wall must be applied to the sphere. Consequently, the sphere behaves dynamically as though it is repelled by the wall.
- (ii) If the sphere moves parallel to the wall so that \dot{x} is zero, it is easily seen that Q_x is positive. Thus, to maintain uniform motion in a direction parallel to the wall, a force directed along the positive x-axis must be applied. Dynamically, the sphere behaves as though it is attracted to the wall.
- (iii) The approach of two equal spheres along their line of centers is accompanied by a force tending to oppose the approach. Thus, a direct collision between two spheres of equal size is not favored.

Flow Past Spheroids

Since the principal modes of oscillation of a liquid droplet are the prolate and oblate spheroids, these forms are given special attention in this section. A brief outline of the classical results pertaining to the irrotational flow associated with the linear translation and rotation of spheroids is presented.

The Motion of Spheroids in a Fluid

The consideration of the flow about an ellipsoid of revolution is important for the investigation of the fluid flow around a liquid globule undergoing oscillations about a spherical shape. In the following sections, the velocity-potential functions and the stream functions associated with the flow about spheroids are presented. It should be noted that, from the knowledge of these functions, an analogous treatment to that given to spheres may be carried out for the spheroids. From the velocity potential, the velocity at every point of the fluid may be obtained by the use of Equation (5-4); the pressure distribution may be derived through Equation (5-23); the kinetic energy and the virtual mass may be calculated from Equations (5-26) and (5-28); and the equations of motion may be obtained from the Euler-Lagrange Equation (5-31).

A prolate spheroid is an ellipsoid of revolution generated by revolving an ellipse about its major axis. The fluid flow past an ellipsoid is best described through the use of ellipsoidal coordinates which are related to the Cartesian coordinates as follows:

$$\begin{aligned} x &= c \cosh u \cos \theta \quad , \\ y &= c \sinh u \sin \theta \cos \omega \quad , \\ z &= c \sinh u \sin \theta \sin \omega \quad . \end{aligned}$$

The surfaces obtained by setting $u = \text{constant}$ are confocal ellipsoids which form a set of surfaces that are everywhere orthogonal to the set of hyperboloids generated by setting $\theta = \text{constant}$. Thus, putting $\alpha = \cos \theta$, $\beta = \cosh u$, and $\gamma = \omega$, the coordinates (α, β, γ) form an orthogonal system. In ellipsoidal coordinates, Laplace's equation, $\nabla^2 \phi = 0$, becomes

$$\begin{aligned} \frac{\partial}{\partial \alpha} \left\{ (1 - \alpha^2) \frac{\partial \phi}{\partial \alpha} \right\} + \frac{1}{1 - \alpha^2} \frac{\partial^2 \phi}{\partial \gamma^2} \\ = \frac{\partial}{\partial \beta} \left\{ (1 - \beta^2) \frac{\partial \phi}{\partial \beta} \right\} + \frac{1}{1 - \beta^2} \frac{\partial^2 \phi}{\partial \gamma^2} \quad . \end{aligned}$$

The solutions to this equation are expressible in terms of the Legendre functions and, in this case, are called ellipsoidal harmonics(5-32). For an axially symmetric flow outside of an ellipsoid, the velocity potential may be written as follows(5-33):

$$\phi(\alpha, \beta) = \sum_{n=0}^{\infty} P_n(\alpha) Q_n(\beta) \quad ,$$

where $P_n(\alpha)$ is Legendre's polynomial of degree n , and

$$Q_n(\beta) = P_n(\beta) \int_{\beta}^{\infty} \frac{d\beta}{[P_n(\beta)]^2 (\beta^2 - 1)} \quad .$$

The corresponding stream function is given by

$$\psi(\alpha, \beta) = \frac{c}{n(n+1)} (1 - \alpha^2) \frac{d P_n(\alpha)}{d \alpha} (\beta^2 - 1) \frac{d Q_n(\beta)}{d \beta} \quad .$$

Thus, if a prolate spheroid moves with velocity U parallel to its major axis, and if $e = 1/\beta_0$ is the eccentricity of a meridian section, it follows from the above equation for $n = 1$ that

$$\psi(\alpha, \beta) = 1/2 A a e \left\{ 1/2 \log \frac{\beta + 1}{\beta - 1} - \frac{\beta}{\beta^2 - 1} \right\} (1 - \alpha^2)(\beta^2 - 1) \quad ,$$

where a denotes the semi-major axis,

$$A = \frac{Ua}{\frac{1}{1 - e^2} - \frac{1}{2e} \log \frac{1 + e}{1 - e}} \quad ,$$

and the boundary conditions are given by $\psi(\alpha, \beta) = 0$ at infinity, and $\psi(\alpha, \beta) = -1/2 U a^2 e^2 (1 - \alpha^2)(\beta^2 - 1)$ at the surface of the ellipsoid. The velocity potential corresponding to this stream function is given by

$$\phi(\alpha, \beta) = A \alpha \left\{ \frac{1}{2} \beta \log \frac{\beta + 1}{\beta - 1} - 1 \right\} .$$

Linear Motion of an Oblate Spheroid

An oblate spheroid is an ellipsoid of revolution obtained by revolving an ellipse about its minor axis. Here the coordinate system employed is related to the Cartesian system as follows:

$$x = c \sinh u \cos \theta \quad ,$$

$$y = c \cosh u \sin \theta \cos \omega \quad ,$$

$$z = c \cosh u \sin \theta \sin \omega \quad .$$

Again, an orthogonal system of ellipsoidal coordinates is obtained by setting $\alpha = \cos \theta$, $\beta = \sinh u$, and $\gamma = \omega$. The surfaces obtained by putting $\beta = \text{constant}$ are oblate spheroids, which are everywhere orthogonal to the hyperboloids of one sheet generated by setting $\alpha = \text{constant}$. In these coordinates, Laplace's equation becomes

$$\begin{aligned} \frac{\partial}{\partial \alpha} \left\{ (1 - \alpha^2) \frac{\partial \phi}{\partial \alpha} \right\} + \frac{1}{1 - \alpha^2} \frac{\partial^2 \phi}{\partial \gamma^2} \\ = \frac{\partial}{\partial \beta} \left\{ (\beta^2 + 1) \frac{\partial \phi}{\partial \beta} \right\} + \frac{1}{\beta^2 + 1} \frac{\partial^2 \phi}{\partial \gamma^2} . \end{aligned}$$

The solutions to this equation for fluid motion outside of the ellipsoid are given by⁽⁵⁻³⁴⁾

$$\phi(\alpha, \beta) = \sum_{n=0}^{\infty} P_n(\alpha) q_n(\beta) \quad ,$$

where

$$q_n(\beta) = P_n(\beta) \int_{\beta}^{\infty} \frac{d\beta}{[P_n(\beta)]^2 (\beta^2 + 1)}$$

and

$$\begin{aligned} P_n(\beta) = \frac{1 \cdot 3 \cdot 5 \cdots (2n - 1)}{n!} \left\{ \beta^n + \frac{n(n - 1)}{2(2n - 1)} \beta^{n - 2} \right. \\ \left. + \frac{n(n - 1)(n - 2)(n - 3)}{2 \cdot 4 (2n - 1)(2n - 3)} \beta^{n - 4} + \dots \right\} . \end{aligned}$$

The stream function corresponding to this velocity potential is given by

$$\psi(\alpha, \beta) = \frac{ae}{n(n + 1)} (1 - \alpha^2) \frac{d P_n(\alpha)}{d\alpha} (\beta^2 + 1) \frac{d q_n(\beta)}{d\beta} .$$

Let $\beta = \text{constant}$ denote an oblate spheroid which moves parallel to its axis through an infinite fluid. If \underline{e} denotes $(\beta^2 + 1)^{-1/2}$ and \underline{a} denotes a semimajor axis, then the preceding equations yield

$$\phi(\alpha, \beta) = A \alpha (1 - \beta \text{arc cot } \beta) \quad ,$$

where

$$A = \frac{-Ua (\beta^2 + 1)^{1/2}}{\beta [(1 - e^2)^{1/2} - 1/e \text{arc sin } e]} \quad ,$$

and

Contrails

$$\psi(\alpha, \beta) = 1/2 \frac{Aa}{\beta} \left[\frac{\beta}{\beta^2 + 1} - \text{arc cot } \beta \right] (1 - \alpha^2) (\beta^2 + 1) .$$

Rotation of an Ellipsoid

The ellipsoidal harmonics appropriate to a rotating ellipsoid in an ideal fluid are expressible as F or $\bar{r} \times \nabla F$ ⁽⁵⁻³⁵⁾, where $\bar{r} = x\bar{i} + y\bar{j} + z\bar{k}$ denotes a position vector in Cartesian coordinates and

$$F = \int_{\lambda}^{\infty} \left(\frac{x^2}{a^2 + \lambda} + \frac{y^2}{b^2 + \lambda} + \frac{z^2}{c^2 + \lambda} - 1 \right) \frac{d\lambda}{k} ,$$

$$x^2 = \frac{(a^2 + \lambda)(a^2 + \mu)(a^2 + \nu)}{(a^2 - b^2)(a^2 - c^2)} ,$$

$$y^2 = \frac{(b^2 + \lambda)(b^2 + \mu)(b^2 + \nu)}{(b^2 - c^2)(b^2 - a^2)} ,$$

$$z^2 = \frac{(c^2 + \lambda)(c^2 + \mu)(c^2 + \nu)}{(c^2 - a^2)(c^2 - b^2)} ,$$

$$k^2 = (a^2 + \lambda)(b^2 + \lambda)(c^2 + \lambda) .$$

Figure 5-5 shows a sketch of the ellipsoid $x^2/a^2 + y^2/b^2 + z^2/c^2 = 1$, which is assumed to rotate with an angular velocity given by $\bar{\omega} = \omega_x \bar{i}$. The velocity of a point on the boundary can be written as $\bar{\omega} \times \bar{r} = -\omega_x z \bar{j} + \omega_x y \bar{k}$. Consequently, the boundary condition is found to be given by $\partial\phi/\partial\lambda = (z \partial y/\partial\lambda - y \partial z/\partial\lambda)\omega_x$, and the velocity potential becomes

$$\phi(x, y, z) = \frac{(b^2 - c^2)^2 abc \omega_x}{2(b^2 - c^2) + (b^2 + c^2)(\beta_0 - \gamma_0)} yz \int_{\lambda}^{\infty} \frac{d\lambda}{(b^2 + \lambda)(c^2 + \lambda)k} ,$$

where $\beta_0 = abc \int_0^{\infty} d\lambda/(b^2 + \lambda)k$ and $\gamma_0 = abc \int_0^{\infty} d\lambda/(c^2 + \lambda)k$. By superposing solutions of a similar form, the velocity potential arising from simultaneous rotations in all three directions may be obtained.

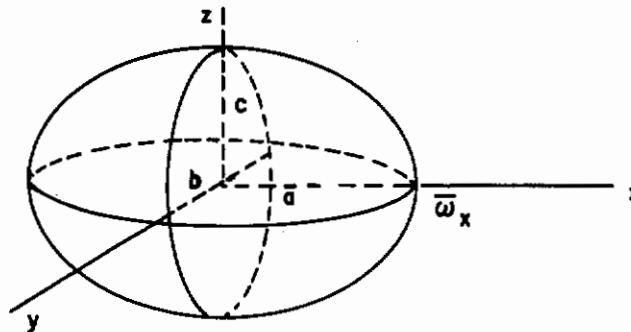


FIGURE 5-5. ROTATION OF AN ELLIPSOID

In the special case of a rotating sphere, $a = b = c$, and the preceding equations show that $\phi(x, y, z) = 0$, so that a rotating sphere does not impart any motion to the surrounding ideal fluid.

In this section, some of the properties of a real fluid are introduced. The stress tensor associated with the flow of a real fluid is presented, together with the concept of kinetic viscosity and Reynolds number. Approximate solutions for the flow of a real fluid past a solid sphere are given for small Reynolds numbers. Stokes' law of drag is derived from the energy-dissipation function, and a correction for "slip" at the surface of the sphere is given. From the drag laws, the terminal velocity of fall is computed, and finally, the simultaneous translation and rotation of a solid sphere at low Reynolds numbers is considered.

Some Properties of Real Fluids

A real fluid is distinguished from an ideal fluid by the fact that the real fluid exhibits a resistance to distortion. This resistance is said to be the result of "internal friction" or viscosity. Some of the more important facts associated with real fluids are given below.

- (1) The viscous forces operating within a fluid cause a positive dissipation of energy when the fluid undergoes any finite internal motion.
- (2) In a real fluid, the stress (or force per unit area of surface) is not necessarily oriented in a direction perpendicular to the element of area dS as in the case of an ideal fluid.
- (3) The stress tensor associated with the motion of a real fluid is fully developed in Chapter 11, and is found to be given by the following matrix:

$$[\psi_{ij}] = \begin{bmatrix} -p + 2\mu \Phi_{11} - 2/3\mu \Phi_{kk}, \mu \left(\frac{\partial U_2}{\partial x_1} + \frac{\partial U_1}{\partial x_2} \right), \mu \left(\frac{\partial U_3}{\partial x_1} + \frac{\partial U_1}{\partial x_3} \right) \\ \mu \left(\frac{\partial U_3}{\partial x_1} + \frac{\partial U_1}{\partial x_3} \right), -p + 2\mu \Phi_{22} - 2/3\mu \Phi_{kk}, \mu \left(\frac{\partial U_2}{\partial x_3} + \frac{\partial U_3}{\partial x_2} \right) \\ \mu \left(\frac{\partial U_3}{\partial x_1} + \frac{\partial U_1}{\partial x_3} \right), \mu \left(\frac{\partial U_2}{\partial x_3} + \frac{\partial U_3}{\partial x_2} \right), -p + 2\mu \Phi_{33} - 2/3\mu \Phi_{kk} \end{bmatrix}$$

where x_1, x_2, x_3 denote Cartesian coordinates, U_1, U_2, U_3 are the respective velocity components, μ denotes the coefficient of viscosity, $\Phi_{11} = \partial U_1 / \partial x_1$, $\Phi_{22} = \partial U_2 / \partial x_2$, $\Phi_{33} = \partial U_3 / \partial x_3$, and $\Phi_{kk} = \Phi_{11} + \Phi_{22} + \Phi_{33} = \partial U_1 / \partial x_1 + \partial U_2 / \partial x_2 + \partial U_3 / \partial x_3$.

- (4) The first scalar invariant (the sum of the diagonal terms) of the stress tensor is defined to be $\psi_{kk} = \psi_{11} + \psi_{22} + \psi_{33}$, so that the pressure, p , for a real fluid is given by the equation

$$p = -\frac{\psi_{kk}}{3}$$

- (5) The force components due to the internal fluid forces are given by $F_j = \partial \psi_{ij} / \partial x_i = \partial \psi_{1j} / \partial x_1 + \partial \psi_{2j} / \partial x_2 + \partial \psi_{3j} / \partial x_3$, $j = 1, 2, 3$.
- (6) To evaluate the relative importance of the viscous forces, the ratio of the viscous stresses to the inertia of the fluid must be considered. The significant quantity in this case is the kinetic coefficient of viscosity, given by $\nu = \mu / \rho$, where μ is the viscosity coefficient of the fluid and ρ is the density of the fluid.

- (7) The coefficient of viscosity in gases has been found to be independent of pressure over wide ranges, but increases with increasing temperatures.
- (8) The stress components across an interface between two dissimilar fluids are continuous, provided the forces due to surface tension are neglected.
- (9) The Navier-Stokes' equations of motion which are developed in Chapter 11, may be expressed componentwise as follows:

$$\frac{\partial U_j}{\partial t} + U_i \frac{\partial U_j}{\partial x_i} = G_j - \frac{1}{\rho} \frac{\partial p}{\partial x_j} + \frac{1}{\rho} \frac{\partial \psi_{ij}}{\partial x_i}, \quad j = 1, 2, 3, \quad ,$$

and, consequently, in vector form, it follows that the fluid motion is governed by the equation

$$\frac{\partial \bar{U}}{\partial t} + (\bar{U} \cdot \nabla) \bar{U} = \bar{G} - \frac{1}{\rho} \nabla p - \frac{\mu}{\rho} \nabla \times (\nabla \times \bar{U}) + \frac{4}{3} \frac{\mu}{\rho} \nabla (\nabla \cdot \bar{U}), \quad ,$$

where it has been assumed that the viscosity is constant throughout the fluid. By the use of the vector identity⁽⁵⁻³⁶⁾, $\nabla \times (\nabla \times \bar{U}) = \nabla (\nabla \cdot \bar{U}) - \nabla^2 \bar{U}$, the preceding equation may be written as follows:

$$\frac{\partial \bar{U}}{\partial t} + (\bar{U} \cdot \nabla) \bar{U} = \bar{G} - \frac{\nabla p}{\rho} + \frac{\mu}{\rho} \nabla^2 \bar{U} + \frac{1}{3} \frac{\mu}{\rho} \nabla (\nabla \cdot \bar{U}). \quad (5-35)$$

If the real fluid is assumed to be incompressible, then $\nabla \cdot \bar{U} = 0$, and the last term of Equation (5-35) may be dropped. If the external forces are assumed to be conservative, then $\bar{G} = -\nabla E$, where E is a scalar function of position. Under these assumptions, the equations of motion may be written in the following convenient forms:

$$\frac{\partial \bar{U}}{\partial t} + (\bar{U} \cdot \nabla) \bar{U} = -\nabla \left(\frac{p}{\rho} + E \right) + \nu \nabla^2 \bar{U}, \quad (5-36)$$

$$\frac{\partial \bar{U}}{\partial t} - \bar{U} \times (\nabla \times \bar{U}) = -\nabla \left(\frac{p}{\rho} + \frac{1}{2} U^2 + E \right) + \nu \nabla^2 \bar{U}. \quad (5-37)$$

- (10) Solutions to the general equations of motion of a real fluid have not been obtained. However, if the equations are subjected to certain simplifying assumptions, solutions are more readily obtained. Usually it is assumed that the quadratic terms in the equations of motion may be neglected. Thus in Equation (5-36), the term $(\bar{U} \cdot \nabla) \bar{U}$ is omitted, so that the resulting differential equation is linear. The approximation which results from a solution of the linearized equation is measured in terms of the Reynolds number, given by

$$Re = \frac{\rho v d}{\mu}, \quad (5-38)$$

where d is some characteristic length, ρ is the fluid density, v is the magnitude of the fluid velocity, and μ is the coefficient of viscosity. This dimensionless quantity is obtained by taking the ratio of the magnitude of the inertia terms (measured by U^2/d) to the magnitude of the viscosity terms (measured by $\mu U/\rho d^2$). If this ratio is small, the Reynolds number is small and the approximation is considered valid.

An approximation may also be obtained by neglecting the terms $\bar{U} \times (\nabla \times \bar{U})$ in Equation (5-37). The resulting solutions are again valid for small values of the Reynolds number.

Steady Flow of a Real Fluid Past a Solid Sphere

If $P(r, \theta)$ denotes a point in a meridian plane, it may be shown⁽⁵⁻³⁷⁾ that whenever the quadratic terms of the equations of motion have been neglected, the stream function, $\psi(r, \theta)$, must satisfy the equation

$$\left[\frac{\partial^2}{\partial r^2} + \frac{\sin \theta}{r^2} \frac{\partial}{\partial \theta} \left(\frac{1}{\sin \theta} \right) \frac{\partial}{\partial \theta} \right]^2 \psi(r, \theta) = 0 \quad ,$$

where the boundary conditions require that $\partial\psi/\partial\theta = \partial\psi/\partial r = 0$ at the surface of the sphere, and $\lim_{r \rightarrow \infty} \psi(r, \theta)$ be equal to $-1/2 U r^2 \sin^2 \theta$. If a solution is assumed to have the form $f(r) \sin^2 \theta$, then $f(r)$ is given by

$$f(r) = A/r + Br + Cr^2 + Dr^4 \quad .$$

The uniform flow at infinity requires that $C = -U/2$ and $D = 0$, so that

$$\psi(r, \theta) = (A/r + Br - 1/2 U r^2) \sin^2 \theta \quad .$$

From Equation (5-2) the velocity components are found to be

$$v_r = U \cos \theta - 2 (A/r^3 + B/r) \cos \theta$$

and

$$v_\theta = -U \sin \theta - (A/r^3 - B/r) \sin \theta \quad .$$

The surface boundary conditions yield $A = -1/4 U a^3$ and $B = 3/4 U a$, where a denotes the radius of the sphere. Thus,

$$\psi(r, \theta) = -1/2 U (1 - 3/2 a/r + 1/2 a^3/r^3) r^2 \sin^2 \theta \quad (5-39)$$

is the appropriate expression for the stream function representing the flow of a real fluid around a sphere at small Reynolds numbers.

Stokes Law of Drag

When the Reynolds number is small the dissipation of energy due to motion of a real fluid is given by

$$F = 1/2 \iiint \Phi \, dx \, dy \, dz \quad ,$$

where

$$\Phi = \mu \left[2 \left(\frac{\partial u}{\partial x} \right)^2 + 2 \left(\frac{\partial v}{\partial y} \right)^2 + 2 \left(\frac{\partial w}{\partial z} \right)^2 + \left(\frac{\partial w}{\partial y} + \frac{\partial v}{\partial z} \right)^2 + \left(\frac{\partial u}{\partial z} + \frac{\partial w}{\partial x} \right)^2 + \left(\frac{\partial v}{\partial x} + \frac{\partial u}{\partial y} \right)^2 \right] \quad .$$

For a sphere it is easily shown that⁽⁵⁻³⁸⁾

$$\Phi = 12 \mu \left(\frac{3A}{r^4} + \frac{B}{r^2} \right)^2 \cos^2 \theta + 36 \mu \frac{A^2}{r^8} \sin^2 \theta \quad ,$$

where A and B are determined by the boundary conditions at the surface of the sphere. If there is no slipping at the surface, then $A = -1/4 U a^3$ and $B = 3/4 U a$, as obtained in the preceding section. Thus the total rate of dissipation of energy is obtained by multiplying Φ by $2\pi r^2 \sin \theta dr d\theta$ and integrating from $\theta = 0$ to $\theta = \pi$ and from $r = a$ to $r = \infty$. These calculations show that $F = 6\pi a \mu U^2$.

If the drag force on the sphere is denoted by D , then DU represents the rate at which work is done when there are no other dissipative forces. If the motion of the sphere is steady, it follows at once that $DU = 6\pi a \mu U^2$, so that

$$D = 6\pi a \mu U \quad (5-40)$$

This important result is known as Stokes' law of drag⁽⁵⁻³⁹⁾. It is usually considered valid for Reynolds numbers between 0.1 and 1.

If it is assumed that the fluid is allowed to "slip" over the surface of the sphere, the Stokes' drag force becomes⁽⁵⁻⁴⁰⁾,

$$D = 6\pi a \mu U \left[\frac{2\mu + \beta a}{3\mu + \beta a} \right], \quad (5-41)$$

where β is the coefficient of sliding friction. For $\beta \rightarrow \infty$ there is no slip and Equation (5-41) reduces to Stokes' law.

Terminal Velocity of Fall for Small Reynolds Numbers

If a sphere is assumed to fall at terminal velocity in a real fluid at small Reynolds numbers, it follows that the downward force due to gravity is equal in magnitude to the sum of the buoyancy force and the drag force. Thus, from Equation (5-41), the following equation holds at the terminal velocity:

$$\frac{4\pi a^3 \rho' g}{3} = \frac{4\pi a^3 \rho g}{3} + 6\pi a \mu U \left[\frac{2\mu + \beta a}{3\mu + \beta a} \right],$$

where ρ' , ρ denote the respective densities of the sphere and the fluid. If this equation is solved for U , the terminal velocity is found to be given by

$$U = \frac{2(\rho' - \rho) a^2 g}{9\mu} \left[\frac{3\mu + \beta a}{2\mu + \beta a} \right] \quad (5-42)$$

If it is assumed that there is no slip between the fluid and the sphere, then $\beta \rightarrow \infty$, and the Stokes' terminal velocity is obtained,

$$U_s = \frac{2(\rho' - \rho) a^2 g}{9\mu} \quad (5-43)$$

Translation and Rotation of a Solid Sphere in a Real Fluid

By using vector methods, Drazin⁽⁵⁻⁴¹⁾ has recently obtained the vector force per unit area acting on a sphere that undergoes simultaneous translation and rotation in a real fluid when the higher order terms are neglected. The force obtained is given by

$$\bar{F} = -1/a (\rho_{\infty} \bar{r} + 3\mu \bar{\omega} \times \bar{r} + 3/2 \mu \bar{U}) ,$$

where p_∞ denotes the pressure at infinity and $\bar{\omega}$ denotes the angular velocity of the sphere. By integrating this expression over the surface of the sphere, the Stokes' drag force given by Equation (5-40) is obtained. This indicates that the drag is independent of the rotation at low Reynolds numbers. The resulting couple about the center of the sphere was found to be given by

$$\bar{C} = 8\pi\mu a^3 \bar{\omega} \quad (5-44)$$

The couple given by Equation (5-44) is often called the Garstang couple, and represents the resistance to rotation offered by a sphere rotating in a real fluid when the Reynolds number, $\rho\omega a^2/\mu$, is small.

Thus, letting k denote the radius of gyration of the sphere, the equations of motion become

$$M d\bar{U}/dt = -6\pi a \mu \bar{U}$$

and

$$M k^2 d\bar{\omega}/dt = -8\pi a^3 \mu \bar{\omega}$$

Further consideration regarding the magnitude of the neglected terms indicates that these results hold only for small Reynolds numbers and very near the surface of the sphere. If the second-order terms cannot be neglected, Lamb⁽⁵⁻⁴²⁾ shows that steady motion is not possible. The rotating sphere behaves like a centrifugal fan that causes the fluid to flow outwards from the equator and inwards toward the poles.

A Liquid Sphere in a Real Fluid

Some of the effects due to the fluid nature of a liquid globule are considered in this section. Corrections to the drag laws and to the terminal velocities are expressed in terms of the viscosity coefficients. The stream functions for the internal circulation of the droplet are given for the "creeping" motions. The equations governing the oscillations of a liquid sphere are given and the effect of these oscillations on the internal circulation is considered.

Linear Motion of a Liquid Sphere in a Real Fluid

When a liquid sphere moves through a real fluid, a finite tangential velocity on the sphere's surface must be taken into account. If it is assumed that the drag experienced by a liquid sphere is proportional to the drag given by Stokes' law, then the actual drag may be written as $R = KD$, where K denotes a proportionality constant and D is given by Equation (5-40). If continuity of the tangential forces and velocities at the surface of the sphere are assumed, then the constant of proportionality is found to be given by⁽⁵⁻⁴³⁾

$$K = \frac{2/3 + \mu'/\mu}{1 + \mu'/\mu},$$

where μ' and μ denote the viscosity coefficient of the fluid sphere and surrounding medium, respectively. If $\mu' \rightarrow \infty$ then the liquid sphere approaches a solid sphere, $K \rightarrow 1$, and Stokes' law is recovered. The above expression for K is a special case of a more general form given by Boussinesq:⁽⁵⁻⁴⁴⁾

$$K = \frac{\beta + (2\mu + 3\mu')a}{\beta + (3\mu + 3\mu')a},$$

where β denotes a surface viscosity due to surface tension.

Terminal Velocity of a Liquid Sphere in a Real Fluid

Contrails

In the range of Stokes' law, the preceding results indicate that the force of drag acting on the liquid sphere is given by

$$R = \frac{2/3 + \mu'/\mu}{1 + \mu'/\mu} (6\pi a \mu U)$$

Thus, the equations of motion for settling under gravity, at terminal velocity, become

$$\frac{4\pi a^3 \rho' g}{3} = \frac{4\pi a^3 \rho g}{3} + \frac{2/3 + \mu'/\mu}{1 + \mu'/\mu} (6\pi a \mu U)$$

and solving for U , it is found that

$$U = \left[\frac{1 + \mu'/\mu}{2/3 + \mu'/\mu} \right] \left[\frac{2(\rho' - \rho) g a^2}{9 \mu} \right]$$

This result is due to Bond(5-45).

Internal Circulation Due to Slow Translation

Under a slow translation, or "creeping motion", the stream function for the internal circulation of a liquid sphere is given by(5-46, 47)

$$\psi'(r, \theta) = - \frac{(\rho' - \rho) a^2 g}{6(3\mu' + 2\mu)} r^2(1 - r^2) \sin^2 \theta$$

and the stream function for the fluid motion outside the sphere is given by

$$\psi(r, \theta) = \frac{(\rho' - \rho) a^2 g}{6(3\mu' + 2\mu)} \left[\frac{\mu' 1 - r^3}{\mu r} - \frac{3\mu' + 2\mu}{\mu} r(1-r) \right] \sin^2 \theta$$

The velocity components may be obtained from these stream functions by Equation (5-2).

Figure 5-6 shows the streamlines within the liquid sphere together with their orthogonal trajectories. These two sets of curves are given by

$$\xi = 4 r^2 (1 - r^2) \sin^2 \theta = \text{constant}$$

and

$$\zeta = \frac{r^4 \cos^4 \theta}{2 r^2 - 1} = \text{constant}$$

Oscillations of a Viscous Sphere

The equations governing the oscillations of a sphere composed of a viscous fluid have been developed by Rayleigh(5-48) and Lamb(5-49). For oscillations between oblate spheroid and a prolate spheroid, Rayleigh obtained an oscillation frequency given by

$$\nu = \frac{4}{\pi} \sqrt{\frac{\sigma}{\rho' d^3}}$$

where d denotes the diameter of a sphere having a volume equal to the volume of the drop, and σ denotes the surface tension. Neglecting internal circulation and the influences of the external gas, it can be shown(5-50) that the amplitude of oscillation of a 3-mm drop of water decreases to

one-half of its initial value in 0.35 second. The energy dissipation within the droplet would cause the amplitude to decrease even more rapidly.

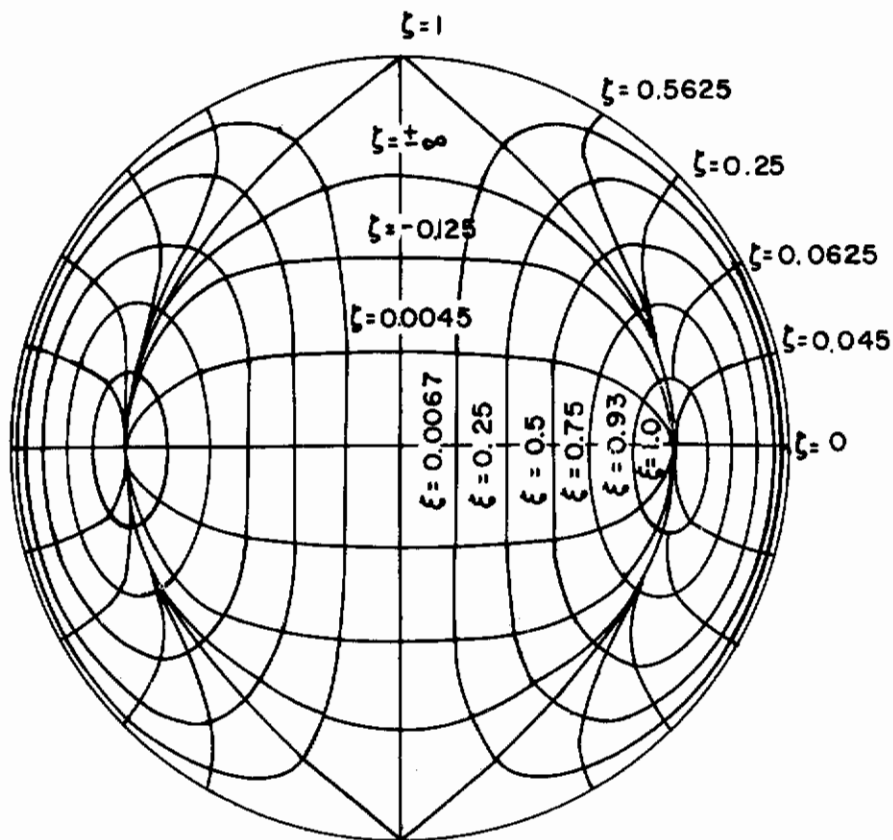


FIGURE 5-6. STREAM LINES AND THEIR ORTHOGONAL TRAJECTORIES IN A VERTICAL PLANE THROUGH THE AXIS OF A FALLING DROPLET

Kronig and Brink⁽⁵⁻⁴⁷⁾

Circulation Due to Oscillations of a Viscous Sphere

The oscillations of a sphere composed of a viscous fluid cause circulation of a different type from that shown in Figure 5-6. If the effects of the external fluid are ignored and no internal eddies are assumed to exist, the lines of flow can be calculated as shown by Lamb⁽⁵⁻⁵¹⁾.

Figure 5-7 shows the streamline configuration for internal motion where the axis of symmetry is taken to be the x-axis. In this case, the maximum velocities occur at a 45° latitude on the surface of the sphere.

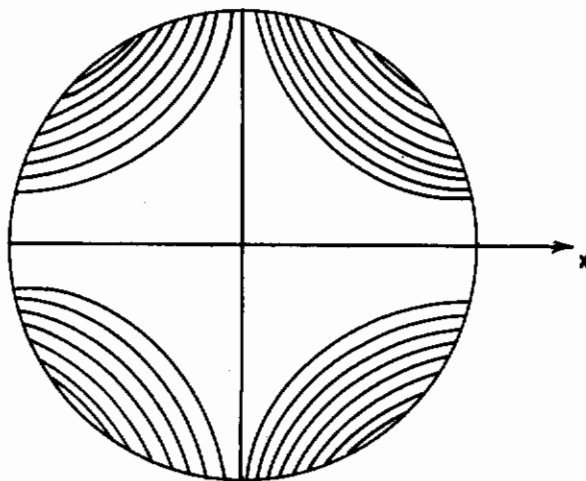


FIGURE 5-7. STREAMLINES DUE TO OSCILLATIONS OF A LIQUID DROPLET

(Lamb)⁵⁻⁵¹

RECENT MODIFICATIONS OF HYDRODYNAMICS

In the first section, the methods of classical hydrodynamics have been applied to some of the problems associated with the motion of a sphere in a fluid medium. If a fluid is assumed to be inviscid, and the motion is assumed to be irrotational, the scope of the results obtainable is somewhat limited. In most instances of practical concern, the attempt to combine irrotational flow with the correct boundary conditions leads to inconsistent mathematical formulations. If the viscous forces are not ignored, the differential equations of motion have greater flexibility, and consequently, the imposition of the correct boundary conditions does not "overdetermine" the equations⁽⁵⁻⁵²⁾. For the viscous fluid, however, the solutions to the Navier-Stokes equations have not been obtained. Furthermore, linearizing of the Navier-Stokes equations leads to approximate solutions which hold, at best, for very small Reynolds numbers and only near the surface of the body.

The modern approach, as suggested by this chapter, aims to rely on the classical results only in a region outside of the body and its "boundary layer". Within the boundary layer the viscous and inertial forces are assumed to be of the same order of magnitude. This approach has developed largely through Prandtl's theory of the boundary layer together with the general considerations of dimensional reasoning.

Modern Approach to Fluid Flow

In this section, Oseen's approximations to the Navier-Stokes equations are given and the corresponding stream function for small Reynolds numbers is presented. Some of the important qualitative features of Prandtl's theory of the boundary layer are discussed and related to classical flow. Finally, theoretical considerations and experimental results pertaining to the formation of the wake behind a moving sphere are presented.

Oseen's Equation of Motion

The validity of Stokes' equation for the drag on a sphere moving in a viscous fluid depends on the assumption that the inertial effects are dominated by the viscous effects. It may be shown that although such an assumption may be valid near the surface of the sphere, it is not valid for portions of a viscous fluid in regions far removed from the sphere⁽⁵⁻⁵³⁾.

In Equation (5-36), Oseen⁽⁵⁻⁵⁴⁾ put $\bar{U} = \bar{U}' + u\bar{i}$, where \bar{i} denotes a unit vector which is parallel to the average velocity, u , and neglected the quadratic terms of the form $(\bar{U}' \cdot \nabla)\bar{U}'$. The hydrodynamic equations may then be written as follows:

$$\frac{\partial \bar{U}'}{\partial t} + u(\bar{i} \cdot \nabla)\bar{U}' = -\nabla(p/\rho + E) + \nu \nabla^2 \bar{U}'$$

At large distances these equations indicate that those quadratic terms arising from the velocity components that are perpendicular to the direction of flow are negligible. The solutions to these equations nearly coincide with the solutions obtained by neglecting the inertia of the fluid in regions very near the surface of the sphere. Thus, the drag on the sphere obtained from Oseen's equations has the same value as that given by Stokes, Equation (5-40). However, in distant regions, the solutions to Oseen's equation differ widely from the Stokes' solutions. The flow pattern is no longer symmetric on the upstream and downstream sides of the sphere.

It should also be noted that the boundary conditions are only approximately satisfied by the solutions to Oseen's equation. The approximation improves as the Reynolds number decreases. By a further refinement of the approximations, Oseen found that the resistance of the sphere was given by $6\pi a \mu U(1 + 3/8 Re)$.

Exact solutions of Oseen's linearized equations of motion were first obtained by Goldstein⁽⁵⁻⁵⁵⁾. At low Reynolds numbers, these solutions were found to agree well with the approximate solutions used by Oseen. An approximating dimensionless expression for the stream function, based on Goldstein's exact solutions, has been obtained by Tomotika and Aoi⁽⁵⁻⁵⁶⁾. For values of the Reynolds number less than unity, the approximating stream function is given by

$$\psi_1 = -\left\{ \frac{3}{4} \left(r_1 - \frac{1}{r_1} \right) - \frac{16 + 3Re}{32} \left(r_1^2 - \frac{1}{r_1} \right) + \frac{3Re}{32} \left(r_1^2 - \frac{1}{r_1} \right) \cos \theta \right\} \sin^2 \theta$$

where $\psi_1 = \psi / Ua^2$ and r_1 is the ratio of the radius of the sphere, a , to the distance of the point considered from the center of the sphere. It may be noted that in the limit, as $Re \rightarrow 0$, the above expression is reduced to a dimensionless form equivalent to Stokes' stream function, Equation (5-39).

Prandtl's Theory of the Boundary Layer

If a body immersed in a fluid is subjected to an impulsive force, the initial motion of the fluid is free from circulation. The classical results regarding the irrotational motions of a viscous fluid are thus applicable to the initial stages of such a motion. The validity of the classical results under these conditions has been experimentally verified by several investigators^(5-57, 58). Experimental evidence also indicates that the fluid in contact with the surface of the solid is at rest relative to the solid at all times. Consequently, when the impulse is applied, the boundary layer consists only of the fluid having immediate contact with the solid. The velocity of any other element of fluid is obtained from the velocity-potential function derived from the classical theory. As the motion continues, however, the number of adjacent layers of fluid between the innermost layer, which has the same velocity as that of the solid surface, and the layer having a velocity given by a velocity potential increases, that is, the boundary layer grows in thickness. In the volume of fluid occupied by the boundary layer, the viscous and inertial effects are assumed to be of comparable magnitude. It may be shown⁽⁵⁻⁵⁹⁾ for the case of a flat plate that the thickness of the boundary layer is directly proportional to the ratio of the distance from the upstream edge to

the square root of the Reynolds number based on that distance. A similar relation may be assumed to apply in the case of a sphere.

In the first section, it was shown that the irrotational motion about a sphere is characterized by the existence of an upstream and downstream stagnation point, together with positions of maximum velocities (and minimum pressures) around the equatorial belt between the stagnation points. According to the classical theory, an element of fluid at the upstream stagnation point is transported by the pressure gradient to a position on the equatorial belt between the two stagnation points. At this point, the fluid element has gained sufficient kinetic energy to continue its motion against the increasing pressure gradient to the downstream stagnation point. In the case of a viscous fluid, however, the fluid element, in traversing between stagnation points, encounters the boundary layer. Here, because of viscosity, some of the energy of the fluid element is dissipated, so that it does not have sufficient energy to move in the direction of increasing pressure to the rear stagnation point. Instead, the fluid element is brought to rest before the completion of its journey at a point on the separation ring. At this point the fluid element leaves the surface of the sphere and becomes part of a vortex sheet that consists of those fluid elements which have had direct contact with the surface of the sphere. The vortex sheet encloses a volume of fluid called the wake. The fluid within the wake undergoes a "recirculation", so that a fluid element at the rear stagnation point moves along the surface towards the front of the sphere until it encounters the separation ring, where it becomes part of the vortex sheet. Additional energy may also be consumed in the vorticity of the wake. This energy must be accounted for in the determination of the velocity potential associated with the irrotational flow outside the wake. In some instances, the fluid motion in the wake may be described as irrotational except at certain isolated vortices. In the two-dimensional flow about an infinite cylinder, for example, the vorticity generated at the surface of discontinuity of velocity collects into isolated vortices in two parallel rows called a Karman vortex street⁽⁵⁻⁶⁰⁾. This subject is considered in more detail in Chapter 20.

The Wake Formation Behind a Sphere

There seems to be little agreement regarding the wake configuration behind a sphere moving in a real fluid. Attempts to generalize the Karman vortex street to three-dimensional flow have not proved successful. For example, Rosenhead⁽⁵⁻⁶¹⁾ has shown that for vortices of finite thickness, a two-dimensional Karman vortex street is always unstable when influenced by three-dimensional disturbances. Levy and Forsdyke⁽⁵⁻⁶²⁾ have proved that a single vortex having a helix for an axis is stable under some conditions, but Jeffreys⁽⁵⁻⁶³⁾ has shown that these conditions cannot be physically realized. A combination of two vortices having helical axes wound on the same cylinder was suggested by Levy^(5-64, 65), but again, difficulties arise in meeting the physical requirements. A wake consisting of a series of vortex rings which drift downstream can also be shown to be unstable.

An investigation by Tomotika and Aoi⁽⁵⁻⁶⁶⁾ has shown that the exact solutions of Oseen's equations, which were obtained by Goldstein, indicate that a stationary vortex ring is formed behind the moving sphere even for Reynolds numbers as small as 0.1.

Experimental evidence regarding the wake formation is also contradictory. Lapple⁽⁵⁻⁶⁷⁾ has indicated that bubbles rising in a liquid may trace a helical course and tend to spiral upwards in agreement with Blanchard's⁽⁵⁻⁶⁸⁾ observation that adjacent droplets spiral into each other. Both of these observations suggest that a helical wake is formed. However, Schmidel⁽⁵⁻⁶⁹⁾ has reported the formation of vortex rings for Reynolds numbers between 500 and 1000. From photographic evidence, Winney⁽⁵⁻⁷⁰⁾ has concluded the existence of a spiral vortex formation for Reynolds numbers between 2000 and 8000. For Reynolds numbers around 10,000, Ermish⁽⁵⁻⁷¹⁾ confirmed Karman's suggestion of intertwined spirals, and Foch and Chartier⁽⁵⁻⁷²⁾ found spiral forms for Reynolds numbers between 100,000 and 300,000.

Figure 5-8 shows sketches of photographs taken by Möller⁽⁵⁻⁷³⁾ of the wake formed behind a sphere over a wide range of Reynolds numbers. It should be noted that in all experiments involving a sphere which is constrained, the resulting wake may be quite different from the wake formed behind a freely moving sphere. In the case of a rising balloon, for example, Lunnon⁽⁵⁻⁷⁴⁾ has

observed that the balloon alternately accelerates and decelerates. The observation seems to suggest that energy-consuming vortices are formed and then discharged, perhaps as a series of vortex rings. If the balloon were constrained, however, such accelerations could not occur.

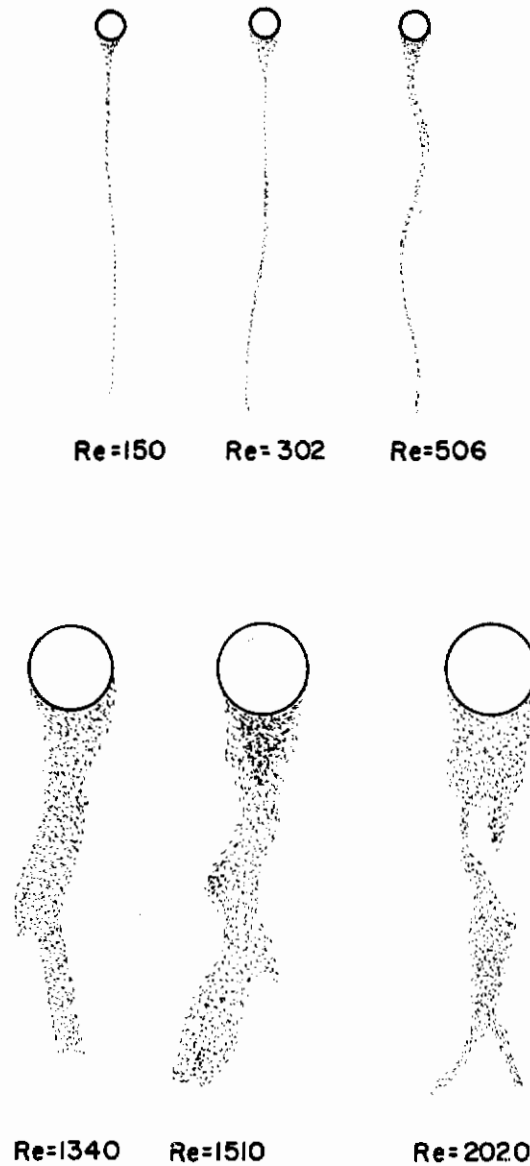


FIGURE 5-8. WAKE FORMATION BEHIND A SPHERE

(Möller)⁵⁻⁷³

Drag on a Solid Sphere Moving in a Real Fluid

The drag force acting on a sphere moving in a real fluid is considered in detail in this section. The drag corrections required by a finite field of flow, by nonviscous flow, by "slip" between the molecules, and by linear acceleration are considered. The empirical formulas of Langmuir, Prandtl, and Kumm which relate the drag coefficient to the Reynolds number are presented and compared with the data of Schiller and Muttray.

Skin Friction, Pressure Drag, and Hydrodynamic Drag

The drag force exerted on a sphere moving in a real fluid is often considered as composed of two components: the drag due to the pressure distribution over the surface of the sphere, and the drag due to the viscous shear. These components of the drag are called the pressure drag and the skin friction, respectively.

In a theoretical investigation based on Goldstein's solution of Oseen's equation, Tomotika and Aoi⁽⁵⁻⁷⁵⁾ found that the ratio of the pressure drag to the skin friction is equal to 1/2 for all Reynolds numbers. Thus, for small Reynolds numbers the pressure drag, D_p , and the skin friction, D_f , are given by the equations

$$D_p = 2\pi a \mu U$$

and

$$D_f = 4\pi a \mu U$$

With the introduction of the boundary layer, the drag force is increased beyond that predicted by Stokes' law, since the actual volume moving through the fluid consists of the sphere together with its boundary layer. At high Reynolds numbers, the drag force may be increased due to the formation of a wake and possible detachment of energy-consuming vortices. Consequently, the magnitude of the drag force is directly influenced by the vortex configuration which occurs in the wake of the moving sphere.

The hydrodynamic drag on a body moving in an infinite fluid field is frequently written as follows:

$$D = C_D (1/2 \rho U^2) A \quad , \quad (5-45)$$

where C_D denotes a dimensionless drag coefficient, and A is the projected area of the body on a plane oriented at right angles to the direction of motion. When the Reynolds number is small, the forces of viscosity dominate the character of the flow. In this case, the drag coefficient is found to be a simple function of the Reynolds number

$$C_D = 24/Re, \text{ where } Re = \rho dU/\mu \quad . \quad (5-46)$$

If this value of the drag coefficient is substituted into Equation (5-45), the usual form of Stokes' law, Equation (5-40), will be obtained. If the velocity is sufficiently increased, any system of vortices will decay into random turbulence. In this case, the drag on a sphere is theoretically proportional to the square of the velocity, as given by Newton's formula⁽⁵⁻⁷⁶⁾

$$D = \pi/4 \rho U^2 a^2 \quad . \quad (5-47)$$

Here the drag may be interpreted as the force due to the loss of pressure on the downstream side, as introduced by the absence of the streamlines in the flow pattern.

Corrections to the Drag Laws

The corrections to the drag of a sphere are generally applied to Stokes' law, Equation (5-40). These corrections arise mainly from the following violations of the hypotheses underlying the development of Stokes' law:

- (1) The fluid field is not infinite in extent.
- (2) The motion is not entirely dominated by the forces of viscosity.

- (3) The fluid is not continuous; for very small spheres, the fluid must be regarded as a discontinuous molecular field.
- (4) The sphere undergoes accelerated motion in the fluid. The corrections due to these causes will be discussed in the sections which follow.

Corrections for a Finite Field of Flow

These corrections include the so-called "wall corrections". For the case of a sphere which settles along the axis of a circular cylinder containing a real fluid, Ladenburg and Faxen⁽⁵⁻⁷⁷⁾ found that the Stokes' drag should be multiplied by the factor k_w , where

$$k_w = (1 + 2.1 d/d') \quad (5-48)$$

Here d and d' denote the respective diameters of the sphere and the cylinder, and the Reynolds number is assumed to be less than one. Clearly, from physical considerations, k_w should become infinite as d/d' approaches one. Consequently, Equation (5-48) is valid only if d/d' is small compared with unity.

For values of d/d' larger than 0.1, an empirical correction has been obtained by Francis⁽⁵⁻⁷⁸⁾:

$$k_w = (1 - d/d')^{-2.5}$$

This correction is valid for small Reynolds numbers and for values of d/d' between 0.13 and 0.97.

In the case of large Reynolds numbers, the drag law given by Newton, Equation (5-47), may be corrected by the factor k_w , where

$$k_w = \left[1 - (d/d')^{3/2} \right]^{-2}$$

This correction factor was first obtained by Munroe⁽⁵⁻⁷⁹⁾. It may be noted that the above wall corrections apply mainly to sedimentation processes where the increased drag is due to the compensating upward flow of fluid.

Corrections Due to the Molecular Structure of the Fluid

A moving sphere whose size is comparable to the mean free path of the fluid molecules may "slip" between the molecules of the fluid. In sedimentation, this causes an increased velocity over the usual Stokes' velocity given by Equation (5-43). To correct for the slip, Cunningham⁽⁵⁻⁸⁰⁾ obtained

$$k_m = \frac{1}{1 + a_m \frac{\lambda}{d}},$$

where λ denotes the mean free path which has not been corrected for any velocity distribution of the fluid molecules. This correction is to be applied to the computed value of the Stokes' drag to obtain the corrected drag. A further refinement of this correction factor has been given by Knudsen and Weber⁽⁵⁻⁸¹⁾.

Table 5-1 shows values of a_m corresponding to values of λ/d , as calculated from data of Millikan⁽⁵⁻⁸²⁾. The value of λ in most gases is of the order of 0.1 of a micron.

TABLE 5-1. VALUES OF a_m FOR VARIOUS
VALUES OF λ/d . Lapple(5-67)

a_m	(λ/d)
1.644	0.01
1.644	0.05
1.645	0.10
1.706	0.3
1.792	0.5
1.931	1.0
2.161	10.0
2.196	∞

Table 5-2 shows a comparison of the motion imparted to a small particle due to collisions with fluid molecules (Brownian movement) with the motion due to gravitational settling. The effects of Brownian movement become quite significant for a particle whose diameter is less than three microns. The average linear displacement, $\Delta s(t)$, in any given direction is given by Lapple(5-67) as

$$\Delta s(t) = \sqrt{\frac{4RTK_m t}{3\pi^2\mu Nd}} \quad (5-49)$$

where R is the gas law constant, T is the absolute temperature, and N denotes Avogadro's number. This result is based on the work of Fletcher. (5-83)

TABLE 5-2. COMPARISON OF BROWNIAN AND GRAVITATIONAL
DISPLACEMENTS FOR SPHERICAL PARTICLES
SUSPENDED IN AIR AND WATER, Lapple(5-67)

Specific Gravity of Particles, 2.0

Particle Diameter, microns	Displacement in 1.0 sec, microns			
	In Air at 70 F, 1 atm		In Water at 70 F	
	Due to Brownian Movement*	Due to Gravitational Settling	Due to Brownian Movement*	Due to Gravitational Settling
0.1	29.4	1.73	2.36	0.005
0.25	14.2	6.30	1.49	0.0346
0.5	8.92	19.90	1.052	0.1384
1.0	5.91	69.6	0.743	0.554
2.5	3.58	400.0	0.471	3.46
5.0	2.49	1550.0	0.334	13.84
10.0	1.75	6096.0	0.236	55.4

*Calculated from Equation (5-49), with $t = 1.0$ sec.

Corrections for Nonviscous Flow

It has already been noted that Stokes' law is mathematically equivalent to the relation $C_D = 24/Re$. This relation holds, however, only for flow which is entirely dominated by the forces of

viscosity, that is, for flow characterized by small Reynolds numbers. For higher Reynolds numbers the inertia forces also become significant and the simple relation given above is no longer valid.

Figure 5-9 indicates the observed relation between the drag coefficient and the Reynolds number over a wide range of Reynolds numbers. Empirically determined functions that approximate the observed data have been calculated by several investigators, and include the following:

$$\text{Langmuir}^{(5-84)} \quad C_D \text{Re}/24 = 1 + 0.197 \text{Re}^{0.63} + 2.6 \times 10^{-4} \text{Re}^{1.38},$$

$$\text{Prandtl}^{(5-85)} \quad C_D = 24/\text{Re} + 1, \quad 0 \leq \text{Re} \leq 100,$$

$$\text{Kumm}^{(5-86)} \quad C_D = 33 \text{Re}^{-2/3}.$$

Engineering approximations are discussed in Perry's Handbook. (5-87)

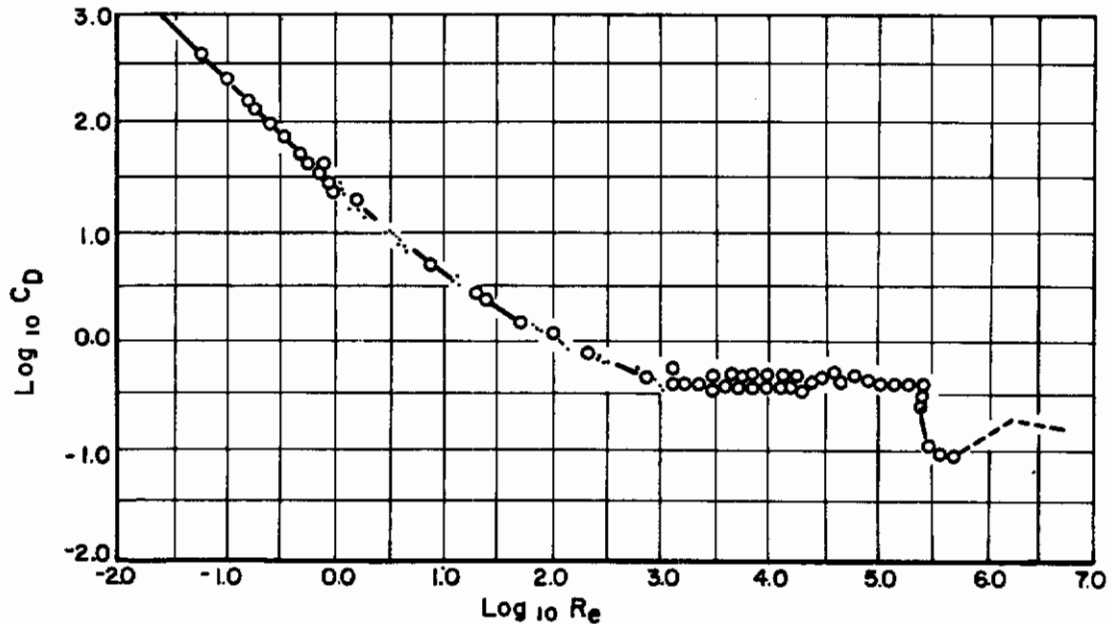


FIGURE 5-9. THE DRAG COEFFICIENT OF SPHERES AS A FUNCTION OF REYNOLDS NUMBER

Goldstein⁽⁵⁻⁷⁾

Table 5-3 shows a comparison of the values predicted by the above equations with the data of Schiller and Muttray⁽⁵⁻⁸⁴⁾. From this table, it is clear that the Langmuir form is the best empirical approximation for the range of Reynolds numbers between 0.2 and 200.0. Rather large deviations are shown by Kumm's equation for most Reynolds numbers.

The dip in the experimental curve relating the drag coefficient to the Reynolds number can be qualitatively explained by assuming that the boundary layer becomes turbulent at this point. The mechanism associated with this phenomenon may be developed as follows. At lower Reynolds numbers, the boundary layer near the separation point is a smooth, well-behaved surface that transmits the viscous forces without amplifying ambient disturbances in the enclosing fluid. At the critical Reynolds number, the boundary layer itself begins to fluctuate rapidly. This permits a much larger transmission of energy to the fluid elements near the surface of the sphere. Consequently, the point of separation moves toward the downstream side of the sphere. Thus, the area

causing the loss of back pressure is reduced so that the back pressure is increased, the velocity is increased, and the drag coefficient is decreased. It should be noted that the Reynolds number at which this phenomenon occurs is strongly affected by the amount of ambient turbulence in the fluid in contact with the sphere. A small wire loop placed on the surface on the upstream side of the sphere can induce this effect and thus lower the resistance. The extreme sensitivity of a sphere to ambient turbulence has led to its utilization as a turbulence indicator. However, it should be noted that the Reynolds number range involved in this turbulent boundary layer phenomena is such that the velocities involved greatly exceed the breakup velocities of droplets.

TABLE 5-3. THE DRAG COEFFICIENT OF SPHERES AS A FUNCTION OF REYNOLDS NUMBER

Reynolds Number, Re	Drag Coefficient, C_D				Per Cent Deviations Between Equations and Experimental Data		
	Schiller & Muttray (Experimental)	Langmuir Equation	Kumm Equation	Prandtl Equation	Langmuir	Kumm	Prandtl
	0	0	0	∞	∞	--	--
0.2	122.4	128.5	97.0	121.	4.90	-20.8	- 1.14
0.6	44.2	45.8	46.4	41.	3.25	4.98	- 7.24
1.0	28.2	28.8	33.0	25.	2.12	17.0	-11.3
2.0	15.4	15.6	20.6	13.	1.30	33.8	-15.6
5.0	7.26	7.43	11.6	5.8	2.34	54.3	-20.1
10.0	4.28	4.44	7.06	3.4	3.74	65.0	-20.6
20.0	2.75	2.79	4.43	2.20	1.45	61.1	-20.0
50.0	1.60	1.62	2.39	1.48	1.25	49.4	- 7.5
100.0	1.10	1.13	1.51	1.24	2.72	37.3	12.7
200.0	0.783	0.834	0.949	1.12	6.52	21.2	43.1
500.0	0.550	0.613	0.516	1.048	11.5	- 6.18	90.6
1000.0	0.447	0.477	0.324	1.024	5.70	-27.5	129.
2000.0	0.393	0.426	0.204	1.012	7.64	-48.1	157.

Corrections for Accelerated Motion

The drag coefficient is a function of the Reynolds number alone only when the motion is steady. Under accelerated motion, dimensional reasoning indicates that the drag coefficient for a liquid sphere is given by

$$C_D = f(\text{Re}, \text{Su}, \text{Wt}, \text{Ac}, \rho/\rho', \mu/\mu') ,$$

where

$$\text{Re} = \rho d U / \mu ,$$

$$\text{Su} = \rho d \sigma / \mu^2 ,$$

$$\text{Wt} = d \left[\frac{4}{3} \frac{|\rho - \rho'|}{\mu^2} \rho g \right]^{1/3} ,$$

$$\text{Ac} = d / U^2 dU/dt .$$

Here, σ denotes the surface tension and the other symbols remain as previously defined.

The experimental data concerned with the accelerated motion of a body in a fluid are limited, and pertain primarily to solid bodies. The dependence of the drag on the acceleration has been considered by Cook⁽⁵⁻⁸⁹⁾ (oscillations of underwater mines), Allan⁽⁵⁻⁹⁰⁾ (steel spheres in water),

Schmidt⁽⁵⁻⁹¹⁾ (balloons in air and wax spheres in water), and Laws⁽⁵⁻⁹²⁾ and Williams⁽⁵⁻⁹³⁾ (water drops in air). The most detailed study of this phenomenon has been made by Lunnon⁽⁵⁻⁹⁴⁾, who experimented with solid spheres of various densities moving in air and water.

From these investigations, it may be concluded that under accelerated motion the drag coefficient is greatly increased for both low and high Reynolds numbers whenever the density of the body approaches the density of the fluid. A quantitative measure of the increases in the drag coefficient for liquid drops is not available, primarily because the drag coefficient fluctuates greatly with the distortion of the liquid drop.

Droplet Deformations and Drag Coefficients

The principal theoretical and experimental results pertaining to the deformation of a liquid droplet are considered in this section. The breakup velocities are expressed in terms of Weber's number and Bond's number. The effects of drop size on surface tension and the effects of surface tension on internal circulation are considered. Finally, the drag coefficients and terminal velocities of liquid droplets, as obtained by Hughes and Gilliland, are presented.

Deformation of a Liquid Drop Moving in a Real Fluid

Hughes and Gilliland⁽⁵⁻⁹⁵⁾ consider the deformation of a liquid drop to be of two basic types: those which consist of oscillations about some equilibrium position, and those which are steady in time. Under steady motion, the pressure distribution on the surface of a liquid sphere is not uniform, so that distortion due to pressure differences is to be expected. Since the static pressure on the surfaces of a deformed sphere has not been theoretically developed, it is not possible to predict the shape which will be assumed by a liquid drop moving in a gas. Most investigators assume that the drop becomes an ellipsoid of revolution with an axis in the direction of the motion. If the semi-major and semi-minor axes are denoted by a and b , then the fineness ratio, $h = b/a$, is a measure of the distortion. For both oblate and prolate spheroids, it can be shown⁽⁵⁻⁹⁵⁾ that the drag correction is small provided $h > 0.8$. Here the uncorrected drag is based on a sphere having a volume equal to that of the spheroid. The symmetry of spheroidal shapes is not confirmed by the photographic studies of Laws⁽⁵⁻⁹⁶⁾ and Henrickson⁽⁵⁻⁹⁷⁾, who showed more distortion on the upstream side than on the downstream side. Williams⁽⁵⁻⁹⁸⁾ has obtained some experimental confirmation of a theoretical result of Saito⁽⁵⁻⁹⁹⁾ which predicted an oblate spheroid for water drops and a prolate spheroid for drops of mercury falling in air.

Disintegration of Liquid Drops

At high relative velocities, the effects of distortion may become so pronounced that the drop breaks up into smaller droplets. This process of disintegration varies considerably under differing conditions. Such phenomena as the "bursting bag" effect and the "umbrella" effect may be produced under extreme conditions⁽⁵⁻¹⁰⁰⁾. The speed of the liquid issuing from an atomizer nozzle insures the "secondary atomization" of the larger drops that are formed initially.

If it is assumed that the viscous drag along the surface of the drop is negligible in determining the shape of the drop, the deformation may be considered to be the result of the interplay between the measure of surface tension, σ/r , which tends to preserve the sphericity, and the deforming pressure forces measured by ρU^2 . The ratio of these quantities is known as Weber's number, $We = \rho r U^2 / \sigma$. The breakup conditions may be determined experimentally, and the critical value of Weber's number associated with these conditions may be computed. For example, Hinze⁽⁵⁻¹⁰¹⁾ found that a droplet of distilled water having a diameter of 1 cm has a breakup velocity of 1220 cm/sec. If it is assumed that the breakup of a 100-micron droplet of distilled water will occur for the same value of the Weber number, then the breakup velocity is easily found to be equal to 12,200 cm/sec, or 400 fps.

The relation between surface tension and the radius of the drop has received considerable attention by several investigators^(5-102, 103, 104, 105). The surface film which produces the surface tension is about 10^{-8} cm in thickness. Thus, for droplets larger than one micron, the thickness of the surface film, δ , is negligible compared with the diameter of the droplet.

Table 5-4, due to Tolman⁽⁵⁻¹⁰³⁾, shows the relation between surface tension, σ , and the ratio of the surface film thickness to the droplet radius, δ/r . The table indicates that for a droplet having a diameter of one micron, $\delta/r = 0.02$, and the uncorrected surface tension, σ_0 , must be multiplied by 0.96 to obtain the correct surface tension.

TABLE 5-4. CHANGE IN SURFACE TENSION WITH RADIUS, Tolman⁽⁵⁻¹⁰³⁾

δ/r	σ/σ_0
0.00	1.00
0.01	0.98
0.02	0.96
0.05	0.91
0.1	0.83
0.2	0.70
0.3	0.60
0.4	0.52
0.5	0.46
0.6	0.41
0.7	0.36
0.8	0.33
0.9	0.30
1.0	0.28

The Effect of Surface Tension on Internal Circulation

The internal circulation due to creeping motion was considered in the first section under the simplification of zero surface tension. The effect of surface tension on circulation has been investigated by Bond and Newton⁽⁵⁻¹⁰⁶⁾. By dimensional considerations, the correction coefficient, k , of the drag law, $R = k(6\pi a\mu U)$, was found to be a function of both μ'/μ and $(\rho' - \rho)a^2g/\sigma$. Thus, the resistance was shown to be a function of surface tension. Furthermore, from the fact that the "skin friction" is equal to 2/3 of the total drag⁽⁵⁻¹⁰⁷⁾, it was shown that the circulation becomes significant whenever the surface tension is small compared with the skin friction.

Mathematical Analysis of Droplet Deformations

J. O. Hinze⁽⁵⁻¹⁰⁸⁾ has made a mathematical investigation of small deformations and oscillations of a droplet moving in a gas. The deformations are considered to be the result of pressures exerted on the surface of the droplet by the surrounding fluid. Specifically, the external pressure distribution acting on the surface of the droplet is assumed to have the following form:

$$p = X(t) P_n(\cos \theta) ,$$

where P_n denotes a Legendre polynomial of order n and $X(t)$ is a given function of time. The distortion is expressed as a function, $\delta(r, \theta)$, which denotes the radial displacement of each fluid element in the droplet from its position in the undeformed state. It is further assumed that the drop

acquires an ellipsoidal form with radial symmetry along the line of motion, so that the deformation may be measured in terms of the one-parameter function, $\delta = \delta(r, 0)$.

For irrotational flow past a sphere, the pressure distribution on the surface of the sphere is given by Equation (5-25). Expressed in terms of Legendre's functions this equation becomes

$$p(\theta) = 1/2 \rho_f U^2 [-1/2 + 3/2 P_2(\cos \theta)]$$

For Reynolds numbers between 10^3 and 2×10^5 , this pressure distribution may be approximated by the following equations:

$$p(\theta) = 1/2 \rho U^2 [-1/2 + 3/2 P_2(\cos \theta)] \text{ for } 0 \leq \theta \leq \pi/3$$

and

$$p(\theta) = -11/32 \rho U^2 \text{ for } \pi/3 \leq \theta \leq \pi$$

By expanding this function in a series of zonal harmonics, the following expression may be obtained:

$$p(\theta) = 1/2 \rho U^2 \left[-0.500 + 0.1915 P_1(\cos \theta) + 0.551 P_2(\cos \theta) + 0.415 P_3(\cos \theta) + 0.178 P_4(\cos \theta) - 0.020 P_5(\cos \theta) + \dots \right]$$

For a steady-state deformation, resulting from a small acceleration of the droplet or from viscous damping of transient oscillations, this pressure causes a maximum deformation given by

$$(\delta/r)_{\max} = -0.095 We \quad (5-50)$$

where the negative sign indicates a flattening of the droplet.

For an analysis of the oscillations resulting from a sudden introduction of the droplet into an air stream, only the cases of very small or very large viscosity of the droplet fluid are amenable to this approach. For large viscosity, $\mu/\sigma\rho r \gg 1$, and the deformation is given by

$$\frac{\delta}{r} = -\frac{\rho U_c^2 r}{\sigma} \left[0.069 \left(1 - e^{-\frac{20}{19} \frac{\sigma}{\mu' r} t} \right) + 0.021 \left(1 - e^{-\frac{35}{22} \frac{\sigma}{\mu' r} t} \right) + 0.005 \left(1 - e^{-\frac{36}{17} \frac{\sigma}{\mu' r} t} \right) + \dots \right]$$

where U_c denotes the velocity corresponding to the critical value of the Weber number. In this case, the oscillation is critically damped so that the maximum deformation does not occur until the steady state is reached. Thus, letting $t \rightarrow \infty$ in the above equation yields Equation (5-50) for the maximum deformation.

When the viscous forces within the droplet are very small, so that $\mu^2/\sigma\rho r \ll 1$, the deformation is measured by

$$\frac{\delta}{r} = \frac{\rho U_c^2 r}{\sigma} \left[0.069 \left(1 - e^{-2 \frac{\mu'}{\rho' r^2} t} \cos \omega_2 t \right) + 0.021 \left(1 - e^{-6 \frac{\mu'}{\rho' r^2} t} \cos \omega_3 t \right) + 0.005 \left(1 - e^{-12 \frac{\mu'}{\rho' r^2} t} \cos \omega_4 t \right) + \dots \right]$$

where $\omega_n^2 = (n-1)(n)(n+2)\sigma/\rho' r^3$. Here the deformation is greatest when $\omega_2 t \approx 0.8\pi$, so that

$$(\delta/r)_{\max} = -0.17 We \quad (5-51)$$

Thus, the deformation resulting from impulsive motion is almost twice as large as that resulting from a gradual increase in velocity.

Equation (5-51) has been found to hold for water droplets having radii as small as 0.1 micron. Experimental values obtained from investigations of falling drops of various liquids indicate that the steady-state critical Weber's number lies between 8 and 15. Breakup will occur for all values of We greater than 15. The equivalent critical range for drops subjected to a sudden blast of air is given by the inequality: $4.5 < We < 8.5$.

Richardson⁽⁵⁻¹⁰⁹⁾ has expressed the deformation of a falling droplet in terms of the Bond number,

$$B = \frac{(\rho' - \rho) d^2 g}{\sigma}$$

Assuming Newton's formula for the terminal velocity,

$$U = 1.74 \sqrt{gd(\rho' - \rho)\rho}$$

the relation between the Bond number and Weber's number is found to be given by

$$We = 1.5B$$

On the basis of a 125-foot droplet fall, Richardson obtained an average value of 12 for the critical Bond number of liquids having a small viscosity. This would indicate a critical Weber's number of 18, which is somewhat higher than the average value of 12 obtained by Hinze. A discrepancy of the same order is found when the experimental data are compared for the various liquids. Richardson also suggests that the deformation of the droplet is significant whenever the Bond number exceeds 0.4, and that the circulation within the droplet has an appreciable effect on the drag coefficient for Bond numbers greater than 1.5.

Table 5-5, due to Lane, shows the minimum breakup velocity corresponding to various droplet diameters under steady-stream and transient-blast conditions. Compared with water, the breakup velocities of dibutyl phthalate and methyl alcohol were decreased by 30 per cent and 43 per cent, respectively. These results indicate that the breakup velocities are directly proportional to the square root of the surface tensions.

TABLE 5-5. CRITICAL VELOCITIES FOR THE BREAKUP OF WATER DROPS, Lane⁽⁵⁻¹⁰⁰⁾

Diameter of Drop, mm	Velocity, m/s	
	In Steady Air Stream	In Transient Air Blast
4.0	12.7	12.0
3.0	14.5	12.1
2.0	17.5	12.6
1.0	24.7	16.0
0.5	35.0	24.0

Table 5-6 shows the values of Weber's numbers computed from the entries of Table 5-5. The nearly constant value of Weber's number in the steady state indicates that this dimensionless

quantity is an appropriate measure of droplet breakup under these conditions. However, the average value of 5.5 is somewhat lower than the value 6.5 which was obtained by Hinze. The marked variation of Weber's number under the transient-blast conditions suggests that further refinements in the theory are needed to cover this case.

TABLE 5-6. THE CRITICAL WEBER NUMBER FOR THE BREAKUP OF WATER DROPS (Based on Table 5-5)

Diameter of Drop, mm	We, Steady Stream	We, Transient Blast
4.0	5.70	5.07
3.0	5.56	3.87
2.0	5.38	2.80
1.0	5.36	2.25
0.5	5.38	2.54
	Average 5.48	

The Drag Coefficient for Liquid Droplets

Direct experimental data from which the value of the drag coefficient may be computed are extremely limited. Laws⁽⁵⁻¹¹⁰⁾ has made accurate measurements on falling drops of water, Watson⁽⁵⁻¹¹¹⁾ used methylsalicylate drops, and Hendrickson⁽⁵⁻¹¹²⁾ used water, nitrobenzene, and n-propanol.

Figure 5-10, due to Hughes and Gilliland⁽⁵⁻¹¹³⁾, shows the result of a theoretical investigation of the variation of the drag coefficient with Reynolds number for various values of $Su = \rho d \sigma / \mu^2$. In order to compare these curves with experimental data, the dimensionless groups C_D , Re , and Su were replaced by

$$Wt = [C_D Re^2]^{1/3},$$

$$Tv = Re/Wt, \text{ and}$$

$$S_d = Su/Wt.$$

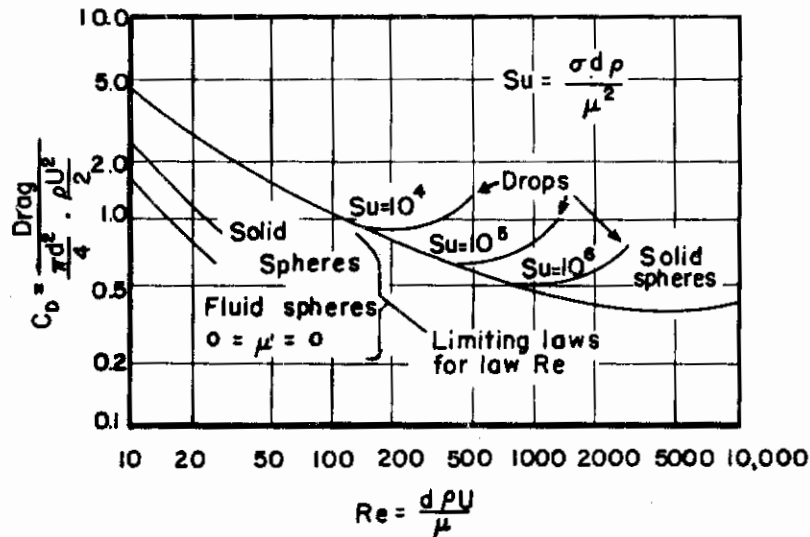


FIGURE 5-10. DRAG COEFFICIENT OF SPHERES AND DROPS

(Hughes and Gilliland)⁵⁻¹¹³

Figure 5-11 shows the data of Laws⁽⁵⁻⁹²⁾ and Watson⁽⁵⁻¹¹¹⁾ as compared with the theoretical curves plotted in terms of the above dimensionless groups. It should be noted that the parameter, S_d , is independent of both the velocity and diameter of the droplet, so that the value of S_d is constant for a given liquid and gas.

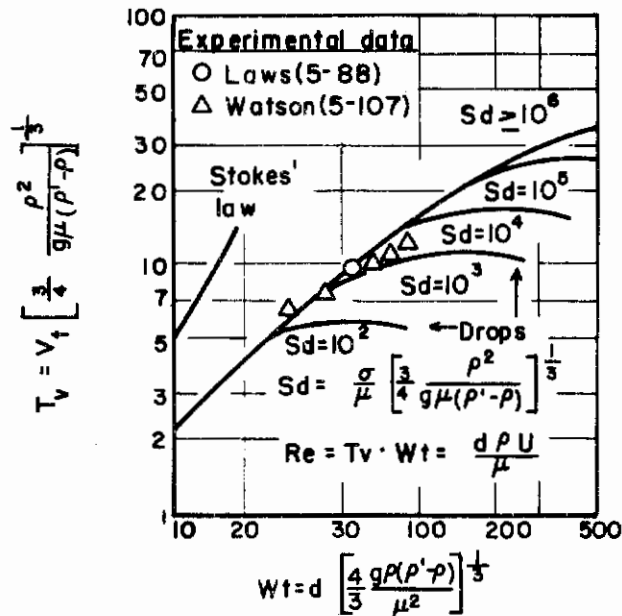


FIGURE 5-11. TERMINAL VELOCITIES OF SPHERES AND DROPS

(Hughes and Gilliland)⁵⁻¹¹³

Oscillations of a Liquid Droplet

The oscillations of a liquid sphere for ideal conditions have been considered in the first section. In the case of a liquid droplet, the external gas exerts considerable influence on the average shape that can be assumed by the droplet. Consequently, the exact nature of the oscillatory motion is difficult to predict. Experimental results of Hendrickson⁽⁵⁻¹¹⁴⁾ indicate that falling drops exhibit oscillations, even after a fall of twenty feet. Williams⁽⁵⁻¹¹⁵⁾ found that the value of the drag coefficient obtained from Laws' data is periodic, so that oscillatory motion is suggested. However, in most cases the average shape of the droplet gives a satisfactory correlation of data, so that considerations of oscillatory motion are of importance primarily in situations where knowledge of the internal circulation is desirable, as in mass transfer by diffusion⁽⁵⁻¹¹⁶⁾.

Equations of Motion

In this section, the equations of motion for a droplet in a gas stream are developed. For the case of small Reynolds numbers, the Stokes' law of drag is utilized. The equations are given for the injection of a droplet into a gas stream when the flow field is uniform and when the flow field consists of curved streamlines.

Equations of Motion of a Droplet in a Gas Stream

From Newton's second law of motion and Equation (5-45), it follows that the equations of motion for a spherical droplet can be written as follows:

$$M' \ddot{x} = -C_D (\rho/2)(U_x - \dot{x})^2 A + E_x \quad , \quad (5-52)$$

$$M' \ddot{y} = -C_D (\rho/2)(U_y - \dot{y})^2 A + E_y \quad ,$$

where U_x and U_y are the Cartesian components of the stream velocity, and E_x , E_y are the components of the external forces acting on the droplet. For a liquid droplet moving in a gas stream, the virtual mass, M' , may be replaced by the true mass, M , in the above equations. It is clear that the solutions to these equations will depend on the particular form of the drag coefficient considered valid for each investigation. Some practical applications of the Stokes, Kumm, and Prandtl forms of the drag coefficient are considered in the following sections.

Equations of Motion for Small Reynolds Numbers

When the Reynolds number is small, the Stokes' relation, $C_D = 24/Re$, is valid, so that Equation (5-52) becomes

$$M\ddot{x} = 6\pi a\mu(U_x - \dot{x}) + E_x$$

and

$$M\ddot{y} = 6\pi a\mu(U_y - \dot{y}) + E_y$$

for a spherical liquid drop moving through a gas. If the fluid character of the droplet must also be considered, it is preferable to write

$$M\ddot{x} = k(6\pi a\mu)(U_x - \dot{x}) + E_x \quad ,$$

$$M\ddot{y} = k(6\pi a\mu)(U_y - \dot{y}) + E_y \quad , \quad (5-53)$$

where

$$k = \left[\frac{2/3 + \mu'/\mu}{1 + \mu'/\mu} \right] .$$

Deformations and the effects of surface tension will invalidate the above equations at higher Reynolds numbers. However, these deviations may be absorbed into the correction factor as long as k is found to be essentially constant over the range of Reynolds numbers considered.

Motion of a Droplet Injected Into a Uniform Gas Stream

In Equation (5-53), choose the x -axis to be parallel with the motion of the gas so that $U_x = U$ and $U_y = 0$. By dividing the resulting equations by $k(6\pi a\mu U)$, the following dimensionless forms may be obtained

$$\frac{d^2\xi}{d\tau^2} + \frac{d\xi}{d\tau} - 1 - \epsilon_x = 0 \quad ,$$

$$\frac{d^2\eta}{d\tau^2} + \frac{d\eta}{d\tau} - \epsilon_y = 0 \quad ,$$

where $\xi = x/TU$, $\eta = y/TU$, $\tau = t/T$, $\epsilon_x = E_x T/MU$, $\epsilon_y = E_y T/MU$, and $T = M/k(6\pi a\mu)$. If E_x and E_y are also constant, these equations have solutions given by

$$\xi(\tau) = \xi(0) + (1 + \epsilon_x)\tau + \left[\frac{d\xi}{d\tau} \Big|_{\tau=0} - 1 - \epsilon_x \right] (1 - e^{-\tau})$$

and

Contrails

$$\eta(\tau) = \eta(0) + \epsilon_y \tau + \left[\frac{d\eta}{d\tau} \right]_{\tau=0} - \epsilon_y \tau (1 - e^{-\tau})$$

Motion of a Droplet in a Field of Curved Streamlines

At low Reynolds numbers, the two-dimensional equations of motion may be written as follows:

$$M \frac{d^2 r}{dt^2} - Mr \left(\frac{d\theta}{dt} \right)^2 = -k(6\pi a \mu) \left(\frac{dr}{dt} - U_r \right) - \frac{M}{R_0} \frac{\rho}{\rho'} U_0^2 + E_r$$

$$Mr^2 \frac{d^2 \theta}{dt^2} + 2Mr \left(\frac{dr}{dt} \right) \left(\frac{d\theta}{dt} \right) = -k(6\pi a \mu) r \left(r \frac{d\theta}{dt} - U_\theta \right) + r E_\theta$$

where r, θ denote the polar coordinates of the droplet, $U_r, U_\theta, E_r, E_\theta$ denote the velocity and external-force components which are parallel and perpendicular to the radial direction, and R_0 denotes the local radius of curvature of the streamlines. If the fluid density is small compared with the droplet density, then the radius of curvature term may be neglected, and the equations can be expressed in the following dimensionless form

$$\frac{d^2 \lambda}{d\tau^2} + \frac{d\lambda}{d\tau} - \left(\frac{\omega^2}{\lambda^3} + \frac{\beta v_\theta^2}{\lambda_0} \right) - v_r - \epsilon_r = 0$$

$$\frac{d\omega}{d\tau} + \omega - \lambda v_\theta - \lambda \epsilon_\theta = 0$$

where $\tau = t/T, \lambda = r/TU, \omega = r^2/TU^2 d\theta/dt, T = M/k(6\pi a \mu), \beta = \rho/\rho', \lambda_0 = R_0/TU, v_\theta = U_\theta/U,$ and $v_r = U_r/U.$

The explicit calculations of a particular trajectory using the preceding equations often require tedious numerical or graphical methods. Lapple and Shepherd⁽⁵⁻¹¹⁷⁾ have given an excellent treatment of the practical calculation of such particle trajectories.

Time Required to Attain Stream Velocity

Kumm⁽⁵⁻¹¹⁸⁾ has calculated the time required for an axially injected drop to attain a given fraction of the stream velocity. In the analysis, the following assumptions are made:

- (1) A gas flows with constant velocity through a tube having a fixed cross-sectional area.
- (2) A drop, initially at rest, is accelerated to its final velocity by the gas stream.
- (3) The velocity component of the drop normal to the gas stream is negligible.
- (4) There is no change in the state of the gas due to the injection of the droplet.
- (5) The drop is assumed to remain spherical in shape throughout the motion.
- (6) The effect of gravitational forces is negligible.

Under these assumptions Equation (5-52) reduces to a single equation given by

$$\ddot{x} = \frac{3\rho(U - \dot{x})^2}{4\rho' d} C_D \quad (5-54)$$

where d is the diameter of the droplet and U is the stream velocity. Using the Kumm relation for the drag coefficient, $C_D = 33 \text{Re}^{-2/3}$, the equation of motion becomes

$$\ddot{x} = \frac{C(U - \dot{x})^{4/3}}{d^{5/3}},$$

where

$$C = \frac{99 \rho^{1/3} \mu^{2/3}}{4 \rho'}$$

The equation for the acceleration of the droplet is readily integrated to yield

$$t = \frac{3d^{5/3}}{C} \left[(U - \dot{x})^{-1/3} - U^{-1/3} \right],$$

and from this equation the position of the droplet is found to be

$$x = Ut + \frac{3d^{5/3}}{2C} \left[\left(\frac{1}{U^{1/3}} + \frac{Ct}{3d^{5/2}} \right)^{-2} - U^{2/3} \right] \quad (5-55)$$

Equation (5-55) is a valid approximation for the droplet trajectory for Reynolds numbers near 0.6 or 500. However, if an accurate trajectory is required over a wide range of Reynolds numbers, it would be preferable to use the Langmuir form for C_D in Equation (5-54) and to evaluate the resulting integral by numerical methods.

Kumm expresses the time and distance necessary for a droplet to reach 90 per cent of the stream velocity in terms of the initial Reynolds number, Re_0 . The following results were obtained:

$$t_{90 \text{ per cent}} = 0.140(\rho' d / \rho U) \text{Re}_0^{2/3}$$

$$x_{90 \text{ per cent}} = 0.0924(\rho' d / \rho) \text{Re}_0^{2/3}$$

These quantities are calculated for a drop-size range from 0.001 to 0.006 in. The distances traveled to attain 90 per cent of the stream velocity were found to be very small under ramjet conditions.

Motion of a Droplet Injected at Right Angles to a Uniform Gas Stream

In a theoretical analysis of the flight path of a fuel droplet in the air stream of a ramjet, Wagner⁽⁵⁻¹¹⁹⁾ has considered the special case of the trajectory of a drop which is injected in a direction at right angles to the motion of air stream. The air stream is assumed to flow at constant velocity, U , through a tube of fixed cross-sectional area. The droplet is assumed to remain spherical and its motion is considered to be independent of gravitational forces.

Relative to a Cartesian coordinate system, (ξ, η) , moving at a velocity, U , with the ξ -axis parallel to the stream velocity, the droplet, just prior to injection, is moving with a velocity $-U$. At the instant of injection, the droplet velocity has a ξ -component equal to $-U$ and an η -component equal to V . Thus the total velocity of the droplet relative to the moving frame of reference is given by $w_0 = \sqrt{U^2 + V^2}$ when $t = 0$. If α denotes the angle that the velocity vector makes with the ξ -axis, then $\alpha = \text{arc tan}(V/-U)$, so that $\sin \alpha = V/w_0$ and $\cos \alpha = -U/w_0$.

The drag force acting on the drop decreases the magnitude of the velocity vector, but over a small time interval does not alter the direction of motion. Consequently, the (ξ, η) -components of

the velocity immediately after injection are given by

$$w_{\xi} = w \cos \alpha = -(w/w_0)U$$

and

$$w_{\eta} = w \sin \alpha (w/w_0)V$$

Upon integrating these velocity components with respect to time, the ξ, η position coordinates of the droplet become

$$\xi = \int_0^t w_{\xi} dt = -U \int_0^t (w/w_0) dt$$

and

$$\eta = \int_0^t w_{\eta} dt = V \int_0^t (w/w_0) dt$$

The transformations to a Cartesian coordinate system (x, y) , which is fixed relative to the flow chamber, are given by the relations $x = \xi + Ut$ and $y = \eta$, so that the (x, y) position coordinates become

$$x = U \int_0^t (1 - w/w_0) dt$$

and

$$y = V \int_0^t (w/w_0) dt$$

(5-56)

In order to integrate these equations of motion, the relation between w and t must be established. For this purpose, Wagner considers a process consisting of the following stages:

- (1) In the first stage, called the preheating period, heat is transferred from the ambient air to the drop. The termination of this period is marked by the attainment of thermodynamic boiling conditions at the surface of the drop. Temperature gradients within the drop and evaporation from the surface of the drop are considered negligible during the preheating period, so that the drop may be assumed to be of constant size during this stage of the process.
- (2) The second stage consists of a period in which the effects of evaporation are significant. The diameter of the drop and its velocity relative to the gas stream both decrease with increasing time.

The preheating period is considered in more detail in the following section. The evaporation period is considered in Chapters 7, 8, 9, and 10.

The Motion of a Droplet During Preheating

From Equation (5-45) and Newton's second law of motion, it follows that the equations of motion for a spherical droplet may be expressed as follows:

$$m dw/dt = -C_D (\rho/2)(\pi d^2/4)w^2$$

Using the Prandtl form of the drag coefficient, $C_D = 24/Re + 1$, the above equation may be written as

$$-\left(\frac{dw}{dt}\right) = \frac{18\mu}{d^2\rho'}w + \frac{3}{4}\left(\frac{\rho}{\rho'd}\right)w^2$$

If the initial Reynolds number is defined to be $Re_0 = \rho w_0 d_0 / \mu$, where w_0 denotes the magnitude of the initial velocity, and d_0 denotes the constant diameter of the droplet, then the vector, w/w_0 , may be replaced by $Re/Re_0 = r$, and the preceding equation becomes

$$-\left(\frac{dr}{dt}\right) = \frac{18\mu}{\rho' d_0^2} r + \frac{3}{4} \frac{\rho w_0}{\rho' d_0} r^2$$

This equation may be integrated to obtain

$$r = (w/w_0) = \left[(Re_0/24 + 1)e^{\frac{18\rho w_0}{Re_0 \rho' d_0} t - Re_0/24} \right]^{-1}, \quad (5-57)$$

and a relation between w and t is thus established. However, further calculations are required to determine a time-dependent heat-transfer equation which involves the drop and airstream variables.

The total quantity of heat, Q , which is transferred to the drop during the preheating period is equal to $(\pi/6) d_0^3 \rho' \Delta H$, and this quantity must be equal to the time integral of the heat transferred to the drop per unit time given by $h\pi d_0^2 \Delta T$, where h denotes the heat-transfer coefficient and ΔT denotes the temperature difference between the drop and the ambient gas. If the preheating time is denoted by t_1 , then the following equation holds:

$$\int_0^{t_1} \pi h d_0^2 \Delta T dt = \pi/6 d_0^3 \rho' \Delta H \quad (5-58)$$

In the integration of Equation (5-58), Wagner assumed that the temperature difference, ΔT , is independent of the time. Thus the nonsteady-state heat-transfer problem is avoided. The approximation seems reasonable when compared with the other simplifying assumptions already introduced into the problem. It may be noted, however, that Tanasawa and Kobayasi⁽⁵⁻¹²⁰⁾ have treated ΔT as time-dependent under nearly the same assumptions as those used by Wagner. The form of ΔT was obtained directly from the transient heat conductivity of a sphere, given by

$$\Delta T = 2(T_g - T_0) \sum_{S=1}^{\infty} \frac{e^{-\nu_S^2 \frac{4Kt}{d_0^2}}}{\nu_S^2 \left(\frac{\lambda'}{\lambda} \right) - \left(1 - \frac{\lambda}{\lambda'} \right)}, \quad (5-59)$$

where d_0 denotes the initial diameter of the drop, T_g , T_0 denotes the temperatures of the gas and the drop at $t = 0$; λ , λ' denote the thermal conductivities of the gas and the liquid, respectively, and K is the thermal diffusivity of the liquid. The variable ν is obtained from the successive roots of the equation

$$\nu = (1 - d_0 h / 2\lambda') \tan \nu$$

Since the time-dependent term in the summation shown in Equation (5-59) is exponential in form, the series will be absolutely convergent. This condition will permit this nonsteady-state form of ΔT to be introduced into Equation (5-58), and the integral of the summation may be taken as the summation over the integral.

If ΔT and d_0 are assumed to be independent of time, then Equation (5-58) may be written as follows:

$$\pi d_0^2 \Delta T \int_0^t h dt = \pi/6 d_0^3 \rho' \Delta H \quad (5-60)$$

This equation may be further simplified by noting that the heat-transfer coefficient between the drop and the ambient gas is given by

$$h = \lambda Nu/d$$

where Nu denotes the Nusselt number for heat transfer and may be expressed as follows⁽⁵⁻¹²¹⁾:

$$Nu = 2.0 + 0.04 Re \quad .$$

These two equations, together with $r = Re/Re_0$, enable Equation (5-60) to be written as

$$\pi d_0 \lambda \Delta T \int_0^{t_1} (2 + 0.04 r Re_0) dt = (\pi/6) d_0^3 \rho' \Delta H \quad . \quad (5-61)$$

After substituting Equation (5-57) into Equation (5-61), dividing by $\pi d_0 \lambda \Delta T$, and then integrating, it is found that

$$\int_0^{t_1} (2 + 0.04 r Re_0) dt = 2t_1 + 0.04 Re_0 \frac{4 \rho' d_0}{3 \rho w_0} \ln \left[\left(\frac{Re_0}{24} + 1 \right) - \frac{Re_0}{24} \exp \left(- \frac{18 \rho w_0}{Re_0 \rho' d_0} t_1 \right) \right] = \frac{d_0^2 \rho' \Delta H}{6 \lambda \Delta T} \quad . \quad (5-62)$$

It may be easily seen that the logarithm term of Equation (5-62) approaches zero. For this limiting case, a characteristic time, t_1^* , may be defined such that

$$t_1^* = \lim_{Re \rightarrow 0} t_1 = \frac{d_0^2 \rho' \Delta H}{12 \lambda \Delta T} \quad .$$

For convenience a dimensionless group, $\tau = t_1/t_1^*$, may be introduced, so that

$$t_1 = \tau t_1^* = \tau \frac{d_0^2 \rho' \Delta H}{12 \lambda \Delta T} \quad . \quad (5-63)$$

Substituting Equation (5-63) into Equation (5-62) yields

$$0.32 \frac{\lambda \Delta H}{\mu \Delta T} \ln \left[\left(\frac{Re_0}{24} + 1 \right) - \frac{Re_0}{24} \exp \left(- \frac{3 \mu \Delta H}{2 \lambda \Delta T} \tau \right) \right] = 1 - \tau \quad . \quad (5-64)$$

This equation can be further simplified by introducing the Prandtl number for air, given by $Pr = \mu C_p / \lambda$, where C_p denotes the specific heat of air at constant pressure. Thus a new lumped parameter, σ , can be defined such that

$$\frac{\mu \Delta H}{\lambda \Delta T} = \frac{Pr \Delta H}{C_p \Delta T} = \sigma \quad ,$$

and Equation (5-64) becomes

$$\frac{0.32}{\sigma} \ln \left[\left(\frac{Re_0}{24} + 1 \right) - \frac{Re_0}{24} \exp \left(- \frac{3}{2} \sigma \tau \right) \right] = 1 - \tau \quad . \quad (5-65)$$

Wagner found a value of 0.6 for σ in the case of a typical fuel (octane) having a boiling point of 126 C.

Figure 5-12 shows a plot of Equation (5-65) from which τ can be read as a function of Re_0 and $\tau(Re_0)$. It may be shown that the velocity at the end of the preheating period is given by

$$w_1 = w_0 r_1 \quad ,$$

where

Contrails

$$r_1 = r_{t=t_1} = \left[\left(\frac{Re_0}{24} + 1 \right) \exp \left(\frac{3}{2} \sigma \tau \right) - \frac{Re_0}{24} \right]^{-1}$$

This equation is also plotted in Figure 5-12. Thus for a given Re_0 , the velocity of the drop at the end of the preheating period may be readily calculated.

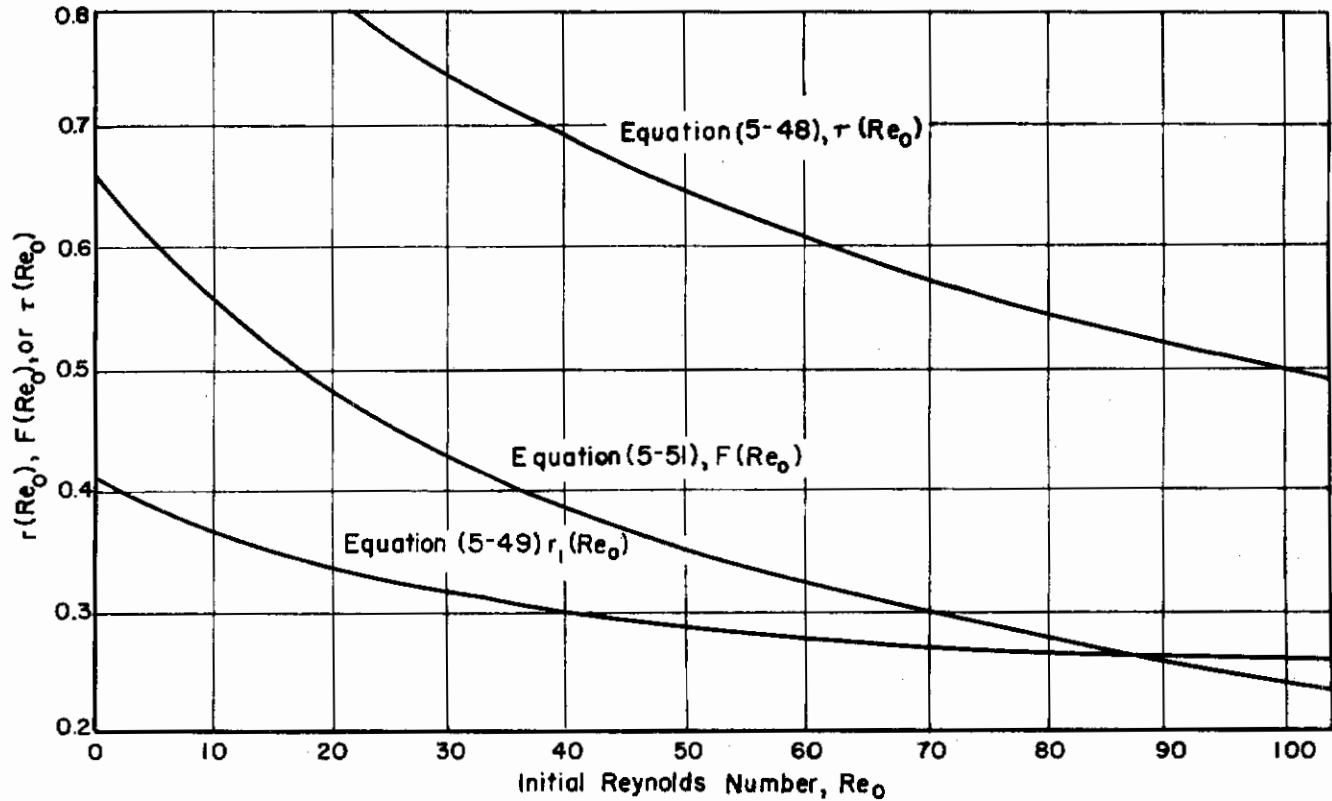


FIGURE 5-12. DIMENSIONLESS PLOT OF THE PREHEATING TIME AND THE VELOCITY AND COORDINATES AT THE END OF THE PREHEATING PERIOD

Finally, equations for the coordinates of the drop at the end of the preheating period are obtained by substituting Equation (5-63) into Equation (5-57). If this result is substituted into Equation (5-56), the integral that defines the position of the drop at the end of the preheating period becomes

$$\begin{aligned} \int_0^{t_1} (w/w_0) dt &= t_1 * \int_0^{\tau} r d\tau \\ &= t_1 * \int_0^{\tau} \frac{d\tau}{\left(\frac{Re_0}{24} + 1 \right) \exp \left(\frac{3}{2} \sigma \tau \right) - \frac{Re_0}{24}} \\ &= t_1 * \left\{ \frac{16}{Re_0 \sigma} \ln \left[\left(\frac{Re_0}{24} + 1 \right) - \frac{Re_0}{24} \exp \left(-\frac{3}{2} \sigma \tau \right) \right] \right\} \end{aligned} \quad (5-66)$$

To facilitate computations, Equation (5-66) can be written in the form

$$F(\text{Re}_0) = \frac{16}{\text{Re}_0 \sigma} \ln \left[\left(\frac{\text{Re}_0}{24} + 1 \right) - \frac{\text{Re}_0}{24} \exp \left(- \frac{3 \sigma \tau}{2} \right) \right]$$

This function is plotted in Figure 5-11 in such a manner that $F(\text{Re}_0)$ can be read as a function of the initial value of Re . From the value of $F(\text{Re}_0)$, the position of the drop at the end of the preheating period can be calculated from

$$x_1 = U t_1^* \left[\tau - F(\text{Re}_0) \right]$$

and

$$y_1 = V t_1^* F(\text{Re}_0)$$

It should be carefully noted that the graphical portion of this analysis is applicable only to liquid having properties similar to those of n-octane. However, the mathematical derivations hold generally within the limitations already discussed. Thus for other fuels, σ may be computed and the new results plotted in the same manner as shown in Figure 5-12.

In contrast to Tanasawa's exact form for ΔT , Wagner's approximate form will tend to give maximum values for the parameters which characterize the termination of the preheating period. It would seem that Tanasawa's form of ΔT would be useful in some particular case, such as those involving a large drop or relatively nonvolatile liquid droplets moving through a steep temperature gradient.

SUMMARY

The purpose of this chapter has been the presentation and discussion of those investigations pertaining to the ballistics of a single droplet. This treatment has been given within the framework of hydrodynamics where classical results of long standing are generally assumed applicable. The assumed validity of these results can often be seriously questioned. In many instances the experimental data are so meager and unreliable that they do not form a satisfactory basis for either the acceptance or rejection of the theory. The need for a large amount of carefully executed experimental work is apparent. In particular, thorough experiments which will furnish reliable data concerning the following phenomena pertaining to the behavior of a liquid droplet are essential: deformation, surface tension, drag, turbulence, acceleration, and wake formation.

Moreover, the inter-relations between these phenomena must also be thoroughly investigated to determine, for example, the effect of turbulence on drag, the effect of oscillation on wake, the effect of deformation on acceleration, and the effect of turbulence on acceleration.

In addition to the vast amount of experimental work required, there is also need for rigorous theoretical investigations. The precise application of hydrodynamic theory has led to many outstanding "paradoxes" which are discussed in some detail in Birkhoff's *Hydrodynamics*. This investigator expresses the opinion that many of the apparent discrepancies between theory and experiment are due to a suppression of mathematical and logical rigor in favor of "physical reasoning". Consequently, the practical investigator should attempt to correlate his data with all the mathematical and logical rigor at his disposal. The utilization of "physical reasoning" in conjunction with the symbolism of mathematics may unjustly verify the underlying theory. Any discrepancy between reliable experimental data and rigorous mathematical theory is a discredit to the theory, not the data.

It should also be noted that most of the results presented in this chapter have been obtained through the use of approximate solutions of the general flow equations. Nisi and Porter⁽⁵⁻¹²²⁾ have pointed out that approximate solutions found to be valid under one set of physical conditions may be

completely invalid under another set of conditions. Thus, a considerable amount of caution must be exercised in every application of the preceding results.

REFERENCES

- 5-1. Birkhoff, G., Hydrodynamics, Princeton Univ. Press, 1950, pp. 19-20.
- 5-2. Prandtl, L., Tietjens, O. G., Applied Hydro- and Aeromechanics, McGraw-Hill Book Co., Inc., 1934, pp. 58-59.
- 5-3. Lamb, H., Hydrodynamics, 6th edition, Cambridge Univ. Press, 1932.
- 5-4. Milne-Thompson, L. M., Theoretical Hydrodynamics, 2nd edition, McMillan Co., 1950.
- 5-5. Streeter, V. L., Fluid Dynamics, McGraw-Hill Book Co., Inc., 1948.
- 5-6. Richardson, E. G., Dynamics of Real Fluids, Edward Arnold and Co., London, 1950.
- 5-7. Goldstein, S., Modern Developments in Fluid Dynamics, Vols. I and II, Oxford Press, 1938.
- 5-8. Phillips, H. B., Vector Analysis, John Wiley and Sons, 1933, p. 62.
- 5-9. Phillips, H. B., Vector Analysis, John Wiley and Sons, 1933, pp. 51-52.
- 5-10. Lamb, H., Hydrodynamics, 6th edition, Cambridge Univ. Press, 1932, pp. 17-18, pp. 36-37.
- 5-11. Lamb, H., Hydrodynamics, 6th edition, Cambridge Univ. Press, 1932, pp. 10-11, p. 18.
- 5-12. Phillips, H. B., Vector Analysis, John Wiley and Sons, 1933, p. 102.
- 5-13. Lamb, H., Hydrodynamics, 6th edition, Cambridge Univ. Press, 1932, p. 112.
- 5-14. Hildebrand, F. B., Advanced Calculus for Engineers, Prentice-Hall, Inc., 1949, p. 298.
- 5-15. Phillips, H. B., Vector Analysis, John Wiley and Sons, 1933, p. 160.
- 5-16. Lamb, H., Hydrodynamics, 6th edition, Cambridge Univ. Press, 1932, p. 39.
- 5-17. Milne-Thompson, L. M., Theoretical Hydrodynamics, 2nd edition, McMillan Co., 1950, p. 51.
- 5-18. Lamb, H., Hydrodynamics, 6th edition, Cambridge Univ. Press, 1932, pp. 39-40.
- 5-19. Lamb, H., Hydrodynamics, 6th edition, Cambridge Univ. Press, 1932, p. 42.
- 5-20. Lamb, H., Hydrodynamics, 6th edition, Cambridge Univ. Press, 1932, p. 18, p. 37.
- 5-21. Sokolnikoff, I. S., and E. S., Higher Mathematics for Engineers and Physicists, McGraw-Hill Book Co., Inc., 1934, pp. 286-287.
- 5-22. Hildebrand, F. B., Advanced Calculus for Engineers, Prentice-Hall, Inc., 1949, pp. 171-174.

- 5-23. Lamb, H., Hydrodynamics, 6th edition, Cambridge Univ. Press, 1932, pp. 114-115.
- 5-24. Weiss, P., On Hydrodynamical Images Arbitrary Irrotational Flow Disturbed by a Sphere, Proc. Camb. Phil. Soc., 40, pp. 259-261, 1945.
- 5-25. Milne-Thompson, L. M., Theoretical Hydrodynamics, 2nd edition, McMillan Co., 1950, p. 43.
- 5-26. Phillips, H. B., Vector Analysis, John Wiley and Co., 1933, p. 38.
- 5-27. Milne-Thompson, L. M., Theoretical Hydrodynamics, 2nd edition, McMillan Co., 1950, p. 51.
- 5-28. Goldstein, H., Classical Mechanics, Addison-Wesley Press, Inc., 1950, pp. 30-31.
- 5-29. Hildebrand, F. B., Methods of Applied Mathematics, Prentice-Hall, Inc., 1952, pp. 147-150.
- 5-30. Lamb, H., Hydrodynamics, 6th edition, Cambridge Univ. Press, 1932, p. 201.
- 5-31. Milne-Thompson, L. M., Theoretical Hydrodynamics, 2nd edition, McMillan Co., 1950, pp. 477-482.
- 5-32. Lamb, H., Hydrodynamics, 6th edition, Cambridge Univ. Press, 1932, pp. 139-140.
- 5-33. Lamb, H., Hydrodynamics, 6th edition, Cambridge Univ. Press, 1932, pp. 140-141.
- 5-34. Lamb, H., Hydrodynamics, 6th edition, Cambridge Univ. Press, 1932, pp. 142-144.
- 5-35. Milne-Thompson, L. M., Theoretical Hydrodynamics, 2nd edition, McMillan Co., 1950, p. 453.
- 5-36. Phillips, H. B., Vector Analysis, John Wiley and Sons, 1933, p. 38.
- 5-37. Lamb, H., Hydrodynamics, 6th edition, Cambridge Univ. Press, 1932, p. 602.
- 5-38. Lamb, H., Hydrodynamics, 6th edition, Cambridge Univ. Press, 1932, p. 603.
- 5-39. Stokes, G. G., Scientific Papers, Univ. Press, Cambridge, 1901.
- 5-40. Basset, A. B., A Treatise on Hydrodynamics, Cambridge; Deighton, Bell and Co., 1888, Vol. II, p. 271.
- 5-41. Drazin, M. P., The General Motion of a Sphere in a Viscous Liquid, Proc. Camb. Phil. Soc., 47, pp. 142-145, 1951.
- 5-42. Lamb, H., Hydrodynamics, 6th edition, Cambridge Univ. Press, 1932, p. 589.
- 5-43. Hadamard, J., Slow Permanent Motion of a Viscous Liquid Sphere in a Viscous Fluid, Comptes Rendus, Vol. 153, 1911, p. 1735.
- 5-44. Dryden, H. L., Hurnaghan, F. B., Batemen, H., Hydrodynamics, National Research Council Bulletin 84, 1932.
- 5-45. Bond, W. N., Bubbles and Drops and Stokes' Law, Phil. Mag. (7), 4, 1927, pp. 889-898.
- 5-46. Rybczynski, W., Concerning the Progressive Motion of a Liquid Sphere in a Viscous Medium; Bull. Acad. Science de Cracovie, Series A, 1911, pp. 40-46.

- 5-47. Kronig, R., and Brink, J. C., The Theory of Extraction from Falling Droplets, Appl. Sci. Res., A2, 1950, pp. 142-154.
- 5-48. Rayleigh, Lord, On the question of the stability of the flow of fluids, Phil. Mag. (5), 34, 1892, p. 177.
- 5-49. Lamb, H., Hydrodynamics, 6th edition, Cambridge Univ. Press, 1932, pp. 639-641.
- 5-50. Hughes, R. R., and Gilliland, E. R., The Mechanics of Drops, Chem. Eng. Prog., Vol. 48, pp. 497-504, 1952.
- 5-51. Lamb, H., Hydrodynamics, 6th edition, Cambridge Univ. Press, 1932, pp. 451-452.
- 5-52. Jeffreys, H., The Wake in Fluid Flow Past a Solid, Proc. Roy. Soc. (London), A128, 1930, pp. 376-393.
- 5-53. Lamb, H., Hydrodynamics, 6th edition, Cambridge Univ. Press, 1932, pp. 608-609.
- 5-54. Oseen, C. W., On the Formula of Stokes and a Related Problem of Hydrodynamics, Arkiv für matematik, Bd. vi. No. 29, 1910.
- 5-55. Goldstein, S., The Steady Flow of a Viscous Fluid Past a Spherical Obstacle at Small Reynolds Numbers, Proc. Roy. Soc. (London), 123A, 1929, pp. 225-235.
- 5-56. Tomotika, S., and Aoi, T., The Steady Flow of a Viscous Fluid Past a Sphere and Circular Cylinder at Small Reynolds Numbers, Quart. J. Mech. Appl. Math., 3, 1950, pp. 140-161.
- 5-57. Milne-Thompson, L. M., Theoretical Hydrodynamics, 2nd edition, McMillan Co., 1950, p. 84.
- 5-58. Prandtl, L., Tietjens, O. G., Applied Hydro- and Aeromechanics, McGraw-Hill Book Co., Inc., 1934, p. 279.
- 5-59. Prandtl, L., Tietjens, O. G., Applied Hydro- and Aeromechanics, Chapter IV, McGraw-Hill Book Co., Inc., 1934, pp. 58-85.
- 5-60. von Karman, T., Rubach, H., Concerning the Mechanism of Fluid and Air Resistance, Phys. Z., Vol. 13, 1912, pp. 49-59.
- 5-61. Rosenhead, L., The Spread of Vorticity in the Wake Behind a Cylinder, Proc. Roy. Soc. (London), A127, 1930, pp. 590-612.
- 5-62. Levy, H., and Forsdyke, A. G., The Steady Motion and Stability of a Helical Vortex, Proc. Roy. Soc. (London), A120, 1928, pp. 670-690.
- 5-63. Jeffreys, H., The Wake in Fluid Flow Past a Solid, Proc. Roy. Soc. (London), A128, 1930.
- 5-64. Levy, H., Aeronautical Research Committee Report, T 2921, March, 1930.
- 5-65. Jeffreys, H., The Wake in Fluid Flow Past a Solid, Proc. Roy. Soc. (London), A128, 1930, p. 391.
- 5-66. Tomotika, S., and Aoi, T., The Steady Flow of a Viscous Fluid Past a Sphere and Circular Cylinder at Small Reynolds Numbers, Quart. J. Mech. Appl. Math., 3, 1950, pp. 140-161.

- 5-67. Lapple, C., Fluid and Particle Dynamics, Univ. of Delaware, 1951, pp. 277-294.
- 5-68. Blanchard, D. C., The Behavior of Water Drops at Terminal Velocity in Air, Trans. American Geophys. Union, Vol. 21, 1950, pp. 836-842.
- 5-69. Schmidel, J., Experimental Investigation of the Motion of a Sphere and Disc in a Viscous Fluid, Physik. Z., 29, 1928, pp. 593-610.
- 5-70. Winny, H. F., Aeronautical Research Committee Report No. 1531, 1932-33, pp. 1-14.
- 5-71. Möller, von W., Experimental Research on the Hydrodynamics of the Sphere, Physik. Z., 39, 1938, p. 80.
- 5-72. Foch, A., and Chartier, C., On the Flow of a Fluid Downstream From a Sphere, Compt. Rend., 200, 1935, pp. 1178-1181.
- 5-73. Möller, von W., Experimental Research on the Hydrodynamics of the Sphere, Physik. Z., 39, 1938, pp. 57-80.
- 5-74. Lunnon, R. G., Fluid Resistance of Moving Spheres, Proc. Roy. Soc. (London), 118A, 1928, pp. 680-694.
- 5-75. Tomotika, S., and Aoi, T., The Steady Flow of a Viscous Fluid Past a Sphere and Circular Cylinder at Small Reynolds Numbers, Quart. J. Mech. Appl. Math., 3, 1950, pp. 140-161.
- 5-76. Newton, I., Principia, Book 2, Prop. 32 (1810).
- 5-77. Schiller, L., Handbook of Experimental Physics, Leipzig, 1932, Vol. IV, Part 2, pp. 337-387.
- 5-78. Francis, A. W., Wall Effect in Falling Ball Method for Viscosity, Physics, Vol. 4, 1933, pp. 403-406.
- 5-79. Munroe, H. S., The English vs. the Continental System of Jigging, Is Close Sizing Advantageous? Trans. Am. Inst. Mining Engrs., Vol. 17, 1888-89, pp. 637-659.
- 5-80. Cunningham, E., On the Velocity of Steady Fall of Spherical Particles Through Fluid Medium (correction to drag), Proc. Roy. Soc. (London), 83A, 1910, p. 357.
- 5-81. Knudsen, M., Weber, S., Resistance to Motion of Small Spheres, Am. Phys., Vol. 36, 1911, pp. 981-994.
- 5-82. Millikan, R. A., Stokes' Law of Fall Completely Corrected, Proc. Nat. Acad. Sci., Vol. 9, 1923, pp. 67-70.
- 5-83. Fletcher, W., A Verification of the Theory of Brownian Movement and a Direct Determination of the Value of N_A for Gaseous Ionization, Phys. Rev., Vol. 33, 1911.
- 5-84. Langmuir, I., and Blodgett, K., A Mathematical Investigation of Water Droplet Trajectories, A. A. F. Tech. Rep. 5418, Air Materiel Command, Wright-Patterson Air Force Base, 1946.
- 5-85. Prandtl, L., Guide to the Theory of Flow, 2nd edition, Braunschweig, 1944, p. 173.
- 5-86. Kumm, E. L., Calculations on the Evaporation Rate of Sprays in Rapidly Moving Gas Streams, Report AL-916, June 23, 1949, North American Aviation, Inc., Aerophysics Laboratory, Project MX-770, RESTRICTED.

- Continued*
- 5-87. Perry, J. H. (editor), Chemical Engineer's Handbook, 3rd edition, pp. 1018-1019.
- 5-88. Schiller, L., Handbook of Experimental Physics, Leipzig, 1932, Vol. IV, Part 2, pp. 269, 304.
- 5-89. Cook, G., An Experimental Determination of the Inertia of a Sphere Moving in a Fluid, Phil. Mag. (6), 39, 1920, pp. 350-352.
- 5-90. Allan, H. S., The Motion of a Sphere in a Viscous Fluid, Phil. Mag. (5), 50, 1900, pp. 323-338 and pp. 519-534.
- 5-91. Schmidt, F. S., On the Accelerated Motion of Spherical Shaped Bodies in a Resisting Medium, Ann. Physik (4), 61, 1920, pp. 633-664.
- 5-92. Laws, J. O., Measurement of the Fall Velocity of Water Drops and Rain Drops, Trans. Am. Geophys. Union, 22, Part III, 1940, pp. 709-721.
- 5-93. Williams, W. E., On the Motion of a Sphere in a Viscous Fluid, Phil. Mag., 29, 1915, pp. 526-552.
- 5-94. Lunnon, R. G., Fluid Resistance of Moving Spheres, Proc. Roy. Soc. (London), 110A, 1926, pp. 302-326. Also reference 5-73.
- 5-95. Hughes, R. R., and Gilliland, E. R., The Mechanics of Drops, Chem. Eng. Prog., Vol. 48, 1952, p. 499.
- 5-96. Laws, J. O., Measurement of the Fall Velocity of Water Drops and Rain Drops, Trans. Am. Geophys. Union, 22, Part III, 1940, p. 709.
- 5-97. Henrickson, F., Jr., Mass Transfer to Drops, S. M. Thesis, Chem. Eng. MIT, Cambridge, Mass., 1941.
- 5-98. Williams, G. C., Heat Transfer, Mass Transfer, and Friction for Spheres, Sc. D. Thesis, Chem. Eng. MIT, Cambridge, Mass., 1942.
- 5-99. Saito, S., On the Shape of the Nearly Spherical Drop Which Falls Through a Viscous Fluid, Sci. Rep. Tohoku Imp. Univ., 2, 1913, p. 179.
- 5-100. Lane, W. R., Shatter of Drops in Streams of Air, Ind. Eng. Chem., Vol. 43, 1951, pp. 1312-1317.
- 5-101. Hinze, J. O., Critical Speeds and Sizes of Liquid Globules, Appl. Sci. Res., Vol. A1, 1949, pp. 273-288.
- 5-102. Hill, T. L., Concerning the Dependence of the Surface Energy and Surface Tension of Spherical Drops and Bubbles on Radius, J. Am. Chem. Soc., 72, 1950, pp. 3923-3927.
- 5-103. Tolman, R. C., The Effect of Droplet Size on Surface Tension, J. Chem. Phys., 17, 1949, pp. 333-343.
- 5-104. Pound, G. M., and LaMer, V. K., Surface Tension of Small Droplets as a Function of Size From Critical Supersaturation Data, J. Chem. Phys., 19, 1951, p. 506.
- 5-105. Koch, F. K. V., On Some Relationships Between Phase Boundary Potential, Adsorption, Surface Tension, and Particle Size, Phil. Mag. (7), 11, 1931, pp. 585-592.
- 5-106. Bond, W. N., and Newton, D. A., Bubbles, Drops, and Stokes' Law, Phil. Mag. (7), 5, 1928, pp. 794-800.

- 5-107. Tomotika, S., and Aoi, T., The Steady Flow of a Viscous Fluid Past a Sphere and Circular Cylinder at Small Reynolds Numbers, *Quart. J. Mech. Appl. Math.*, 3, 1950, pp. 140-161.
- 5-108. Hinze, J. O., Forced Deformations of Viscous Liquid Droplets, *Appl. Sci. Res.*, A1, 1947-48, pp. 263-272.
- 5-109. Richardson, E. G., *Dynamics of Real Fluids*, Edward Arnold and Co., London, 1950, pp. 105-108.
- 5-110. Laws, J. O., Measurement of the Fall Velocity of Water Drops and Rain Drops, *Trans. Am. Geophys. Union*, 22, Part III, 1940, p. 709.
- 5-111. Watson, H. H., cited by Williams (5-98).
- 5-112. Henrickson, F., Jr., Mass Transfer to Drops, S. M. Thesis, Chem. Eng. MIT, Cambridge, Mass., 1941.
- 5-113. Hughes, R. R., and Gilliland, E. R., The Mechanics of Drops, *Chem. Eng. Prog.*, Vol. 48, p. 497.
- 5-114. Henrickson, F., Jr., Mass Transfer to Drops, S. M. Thesis, Chem. Eng. MIT, Cambridge, Mass., 1941.
- 5-115. Williams, G. C., Heat Transfer, Mass Transfer, and Friction for Spheres, Sc. D. Thesis, Chem. Eng. MIT, Cambridge, Mass., 1942.
- 5-116. Kronig, R., and Brink, J. C., The Theory of Extraction from Falling Droplets, *Appl. Sci. Res.*, A2, 1950, pp. 142-154.
- 5-117. Lapple, C. E., Sheperd, C. B., Calculation of Particle Trajectories, *Ind. Eng. Chem.*, Vol. 32, 1940, pp. 605-617.
- 5-118. Kumm, E. L., Calculations on the Evaporation Rate of Sprays in Rapidly Moving Gas Streams, Report AL-916, June 23, 1949, North American Aviation, Inc., Aerophysics Laboratory, Project MX-770, RESTRICTED.
- 5-119. Wagner, C., Calculations of the Flight Path of Fuel Droplets in the Air Stream of a Ramjet, Tech. Report No. 52, Ordnance Research and Development Division, Suboffice (Rocket), Fort Bliss, Texas, February, 1948, CONFIDENTIAL.
- 5-120. Tanasawa, Y., and Kobayaski, K., On the Evaporation Velocity of a Liquid Droplet in a High Temperature Gas, *Tech. Reports of the Tohoku Univ.*, 14, No. 2, 1950, p. 55.
- 5-121. McAdams, W. H., *Heat Transmission*, 2nd edition, McGraw-Hill Book Co., New York, 1942, p. 236.
- 5-122. Nisi, H., and Porter, A. W., On Eddies in Air, *Phil. Mag.*, 46, 1923, pp. 754-768.

Contrails

CHAPTER 6. DYNAMICS OF DISPERSIONS

ABSTRACT

In this chapter the dynamics associated with the injection of liquid droplets into a gas are considered. The treatment is based on the assumption that the injection process may be analyzed by applications of basic results which have been established in the related fields of fixed beds, fluidized beds, and pneumatic transport. The fundamental results pertaining to these systems are developed, and the application of these results to systems of liquid droplets is considered. The problems of sedimentation, flocculation, diffusion, coalescence, and sonic agglomeration are treated briefly. In every case, the results are assumed to be qualitatively valid only in the initial "embryonic" stages of the injection process. Many of the difficulties encountered in dispersion dynamics are pointed out and recommendations for future research are indicated.

Contrails

DYNAMICS OF DISPERSIONS

by

Ralph E. Thomas

The general aim of this chapter is to consider the dynamics of physical systems composed of solid or liquid dispersions in gases. For this purpose, a dispersion is defined to be a distribution of small droplets or particles in a fluid in which the dynamical behavior of a single droplet or particle is significantly influenced by the presence of its neighbors.

The problems of dispersion dynamics do not lend themselves to simple analysis either by the experimentalist or by the theorist. The experimentalist is confronted by an array of variables which is hardly amenable to laboratory control. In considering a simple dispersion of droplets, he must take into account the size distribution of the droplets, coalescence, viscosity, temperature, resistance to motion, evaporation, surface tension, density, pressure, condensation, and electrical charges. The interrelations among these variables are extremely complex. Clearly, the experimentalist must exercise great care if erroneous results and conclusions are to be avoided.

The theoretical side of the picture is no brighter. Although certain mathematical methods (dimensional analysis, statistics, and variational principles) yield some very general results, a complete theoretical development depends to a large extent on first obtaining the exact functional relations which hold among the many variables.

The necessity for distinguishing dispersion dynamics from the dynamics of isolated particles arises from the fact that the equations of motion for an isolated particle simply cannot be applied to a particle in a dispersion. Even in sedimentation under gravity, the mutual influences of the dispersed particles may be extremely large. For example, in a 15 per cent particle concentration by volume, the Stokes' settling velocity of the particles may be reduced by more than 50 per cent (6-1) (6-2). Thus the dispersion as a whole cannot be considered as a physical system composed of a collection of isolated particles.

The mathematical necessity of dealing with the dispersion as a unit has led to the utilization of macroscopic variables which are somewhat analogous to the variables of the "equations of state" employed in thermodynamics. The equations of state of a dispersion are generally expressed in terms of the average pressure gradient occurring in the fluid medium, the superficial velocity of the fluid, and the concentration by volume of the fluid in the dispersion. A mathematical transition between the "equations of state" of a dispersion and the equations of motion of the isolated particle is a delicate matter, even when the problem is simplified by assuming solid particles at rest relative to each other.

Several types of dispersion systems will be considered in this chapter under the headings: fixed beds, sedimentation, fluidized beds, and pneumatic transport. In these systems, the dispersed material is assumed to consist of solid particles. Some of the properties of dispersed liquid droplets will be treated in the discussion sections and in the sections which treat coalescence and sonic agglomeration.

The justification of this chapter must rest on the establishment of a significant relationship between dispersion systems and the injection of liquids into gas streams. To establish such a relation, it is convenient to consider a hypothetical unit volume of space which is situated near the point of injection of the liquid droplets. Initially, it is assumed that the unit volume contains

a large volume concentration of droplets which are moving in a uniform direction and with a uniform injection velocity. At subsequent times, the unit volume is assumed to move with the center of mass of the droplets originally contained in it.

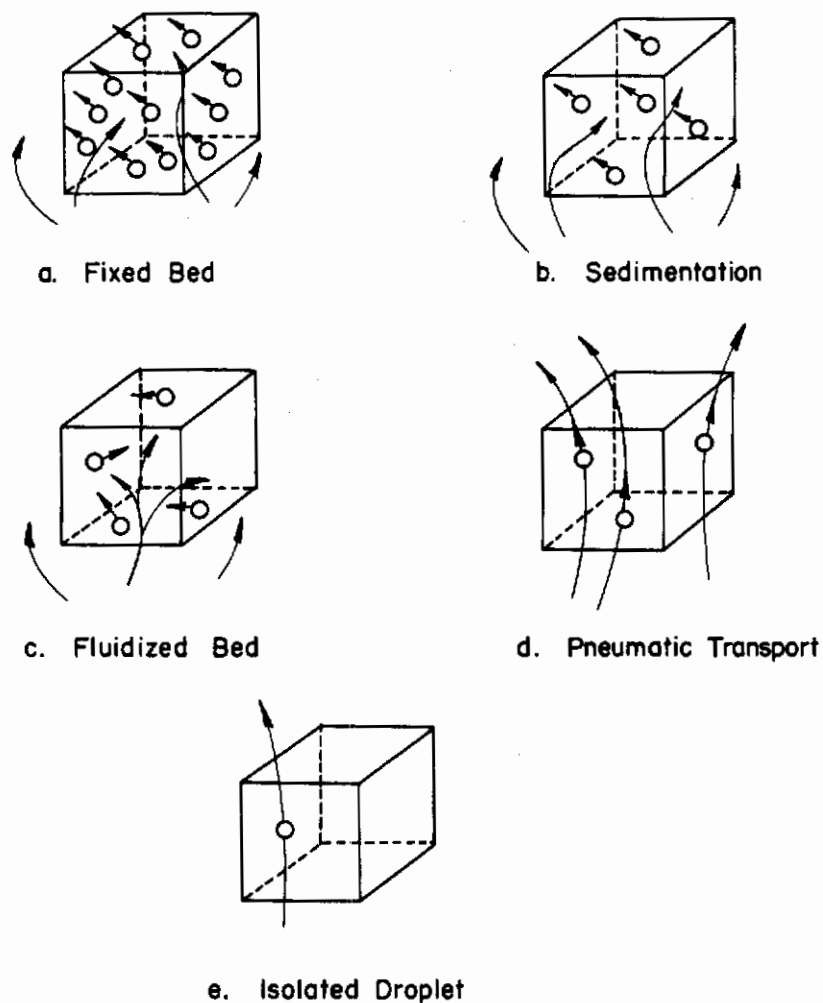


FIGURE 6-1. VARIOUS TYPES OF DISPERSION SYSTEMS ARISING FROM AN INJECTION OF LIQUID DROPLETS IN A GAS STREAM

Figure 6-1a is a sketch of the initial injection conditions. Clearly, the existence of these conditions depends on the type of injector used. Here the small arrows indicate that the droplet velocities are essentially uniform, and the large arrows, representing the directional fluid-stream lines, indicate that the fluid is penetrating between the droplets of the unit volume. This stage may be regarded as a fixed bed which is characterized by fluid flow within a highly concentrated dispersion of droplets which are at rest relative to each other.

In the second stage, Figure 6-1b, the same type of flow is exhibited but at greatly reduced droplet concentrations. This stage of the injection process may be treated as an instance of dispersion sedimentation.

The third stage, Figure 6-1c, indicates a random motion among the droplets and a further decrease in droplet concentration. These conditions are comparable to those of a fluidized bed in which mutually interacting particles are suspended in a fluid medium. In the fourth stage,

Figure 6-1d, the particles are moving in the direction of the fluid flow, and only a slight mutual influence of the droplets is indicated by the small droplet concentration. These conditions are typical of investigations concerned with pneumatic transport. Finally, in Figure 6-1e, the droplet concentration has become sufficiently small so that the behavior of each droplet is unaffected by the other droplets of the spray. Here, the techniques of dispersion dynamics can be replaced by the methods employed in the study of the dynamics of a single, isolated droplet.

It must be understood that the above mechanism of an injected dispersion has not been experimentally established. The theoretical attempt to reduce the injection process to its component parts has led to the sequence outlined above. The study of the subject matter pertaining to each of these components constitutes the major portion of this chapter. It is extremely doubtful whether the equations which are developed in the study of dispersion systems can be successfully applied to a unit volume of spray. It is hoped, however, that the equations may indicate certain qualitative relations which may be expected to hold at some initial "embryonic" stage of the droplet injection process.

For convenience, a nomenclature table follows:

NOMENCLATURE TABLE

A,	transverse cross-sectional area of a circular cylinder.
D,	diameter of a sphere.
D _c ,	diameter of a capillary tube.
D _t ,	diameter of a circular cylinder.
E,	energy density of sonic vibrations.
E(r),	Langmuir's collision efficiency.
$\bar{E}(r)$,	Gunn and Hitschfeld's collection efficiency.
G,	superficial mass velocity of a fluid.
G _s ,	superficial mass velocity of solids in pneumatic transport.
J,	Lapple-Shepherd factor.
K,	numerical constant.
L,	height of a dispersion system.
M,	mass flow rate of fluid in empty tube.
P,	pressure.
ρ ,	permeability.
R,	viscous resistance.
Re,	Reynolds number.
Re*,	modified Reynolds number.

R_H ,	hydraulic radius.
V ,	average relative velocity of fluid with respect to a particle.
V_N ,	Newton's settling velocity.
V_S ,	Stokes' settling velocity.
a ,	specific surface of particles.
a_u ,	upward acceleration in pneumatic transport.
b, b_1, b_2 ,	numerical constants.
c ,	concentration.
c_0 ,	initial concentration.
c_p ,	specific heat at constant pressure.
c_v ,	specific heat at constant volume.
f ,	function of.
f_s ,	Fanning's friction factor.
g ,	acceleration of gravity.
l ,	length of horizontal circular cylinder.
l_m ,	molecular mean free path.
n ,	numerical constant.
p_1, p_2 ,	pressures at $L=0$ and $L=L$, respectively.
r ,	radius of a sphere.
r_p ,	radius of a sphere having same volume as that of the particle.
r' ,	radius of a hypothetical enclosing cylinder.
t ,	time.
u ,	linear fluid velocity per unit cross section.
u_0 ,	linear superficial fluid velocity.
u^* ,	corrected superficial velocity of compressible gas.
u_m ,	superficial fluid velocity at mean pressure.
u_s ,	average final velocity of solids in pneumatic transport.
v ,	terminal velocity of a particle relative to a fixed horizontal plane.
v_s ,	total volume of particles.
v_t ,	total volume of fluid-solid system.

Contracts

γ ,	ratio of specific heats, c_v/c_p .
Δ ,	increment.
δ ,	dimensionless group of Gasterstädt.
ϵ ,	fraction of voids.
μ ,	viscosity of a fluid.
μ_m ,	viscosity of a dispersion system.
ρ_f ,	mass density of fluid.
ρ_g ,	mass density of gas.
ρ_p ,	mass density of a particle or droplet.
τ ,	ratio of actual volume to settled bed volume.
$\phi(\epsilon)$,	shape factor.
ϕ_c ,	Carman's shape factor.

A fixed bed is a physical system composed of solid particles in direct contact with each other and the container walls. The particles are at rest relative to each other and form a porous medium, or packing, through which a fluid is allowed to flow. The subject of fixed beds has received considerable attention because of its engineering importance. Water and chemical filters, absorbing towers, mineral dressing, well drilling, and numerous other industrial operations depend upon a working knowledge of the conditions of flow in a fixed bed. However, completely rigorous and detailed solutions of the hydrodynamic flow equations for fixed beds are still lacking owing to the mathematical difficulties involved. Thus, the equations relating the fluid flow to the physical characteristics of the fixed bed are obtained either by approximate solutions of the hydrodynamic equations or by the correlation of experimentally determined relations with relations arising from qualitative reasoning. A review of this field has been given by Carman⁽⁶⁻³⁾ and by Sullivan and Hertel.⁽⁶⁻⁴⁾

For straight channels, a fluid flow may be characterized as both laminar and viscous, that is, the flow is both nonturbulent and dominated by the forces of viscosity. However, when the channel is curved, or of varying cross section, or is composed of the interstices in a porous medium, the flow may still be laminar but not entirely viscous. This situation arises because inertial forces are involved in the fluid motion along curved streamlines. Consequently, some workers⁽⁶⁻⁴⁾ have criticized the analogous treatment given to flow through fixed beds and flow through straight, uniform channels.

Early investigators⁽⁶⁻⁵⁾⁽⁶⁻⁶⁾ of the laws governing the flow of fluids through fixed beds at low pressures found that the rate of flow is directly proportional to the pressure drop per unit length of the packing. These considerations led to Darcy's⁽⁶⁻⁵⁾ equation,

$$u = \frac{\rho}{\mu} \frac{\Delta P}{L},$$

where permeability, ρ , is expressed in units termed the darcy by Fancher and Lewis⁽⁶⁻⁷⁾ and Barnes⁽⁶⁻⁸⁾. The analogous treatment given to fixed bed flow and flow through straight channels arised from the similarity between Darcy's equation and the Hagen-Poiseuille⁽⁶⁻⁹⁾ equation,

$$u = \frac{D_c^2}{32\mu} \frac{\Delta P}{L}.$$

Using dimensional considerations, two dimensionless groups, $(\Delta P D / Lu_0^2 \rho_f)$ and $(u_0 D \rho_f / \mu)$, are obtained, so that

$$\frac{\Delta P D}{Lu_0^2 \rho_f} = f \frac{u_0 D \rho_f}{\mu} \quad (6-1)$$

The term on the left side of this equation is called the friction factor and is frequently plotted on logarithmic coordinates as a function of the Reynolds number, which appears on the right-hand side.

Figure 6-2, reproduced from Hatfield⁽⁶⁻¹⁰⁾, shows the friction factor plotted against the Reynolds number over a wide range of conditions for fluid flow through beds of porous carbon.

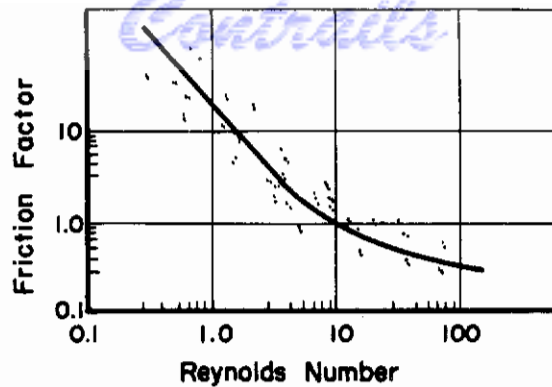


FIGURE 6-2. FRICTION FACTOR AS A FUNCTION OF REYNOLDS NUMBER FOR FLUID FLOW THROUGH POROUS CARBON (Hatfield)⁽⁶⁻¹⁰⁾

Blake⁽⁶⁻¹¹⁾ modified Equation (6-1) by introducing the specific surface of the particles, and dividing the superficial mass velocity, ($u_o \rho_f$), by ϵ . Thus Blake obtained

$$u_o^2 = \frac{\Delta P \epsilon^3}{L \rho_f a} f \left(\frac{G}{\mu a} \right).$$

Burke and Plummer⁽⁶⁻¹²⁾ assumed that the resistance of a fixed bed is given by the sum of the resistances of the individual particles and were led to the following equation:

$$u_o^2 = \frac{\Delta P}{L \rho_f a} \frac{\epsilon^3}{(1-\epsilon)} f \left(\frac{Re (1-\epsilon)}{Da \epsilon} \right).$$

A satisfactory correlation was obtained, but the experimental range was narrow.

A completely empirical approach was taken by Furnas⁽⁶⁻¹³⁾ to obtain

$$u_o^2 = K \frac{\Delta P}{L \rho_f} G^b,$$

where K and b are empirical constants. Chilton and Colburn,⁽⁶⁻¹⁴⁾ and Morse⁽⁶⁻¹⁵⁾ have criticized the Furnas equation on the grounds that the equation is based on flow in both streamline and turbulent states.

Using Fanning's equation⁽⁶⁻¹⁶⁾, Chilton and Colburn⁽⁶⁻¹⁴⁾ obtained

$$u_o^2 = \frac{\Delta P D}{L \rho_f} \frac{1}{K(Re)^n},$$

where for $Re < 40$, $K = 1700$ and $n = -1$, and for $Re > 80$, $K = 76$ and $n = -0.15$.

Carman⁽⁶⁻³⁾ considered the pioneer work of Blake⁽⁶⁻¹¹⁾, Kozeny⁽⁶⁻¹⁷⁾ and others, and, introducing a shape factor, ϕ_c , obtained

$$u_o = \frac{\Delta P \epsilon^3 \phi_c^2 D^2}{180 L(1-\epsilon)^2 \mu}$$

for the region of streamline flow where the modified Reynolds number, $Re^* = u_o \rho_f \phi_c D / \mu(1 - \epsilon)$, is less than 20; and

$$u_o^{1.9} = \frac{\Delta P \epsilon^3 \phi_c^{1.1} D^{1.1}}{2.9 L(1-\epsilon)^{1.1} \mu^{0.1}}$$

for the region of streamline flow where Re^* is greater than 100. The form of these equations has also been obtained by Kozeny⁽⁶⁻¹⁷⁾, Leva,⁽⁶⁻¹⁸⁾ and Hatch⁽⁶⁻¹⁹⁾⁽⁶⁻²⁰⁾.

Figure 6-3, reproduced from Morse⁽⁶⁻¹⁵⁾, shows a comparison between the fixed-bed curves of Carman-Kozeny and Leva, and the experimental data of Wilhelm and Kwauk⁽⁶⁻²¹⁾.

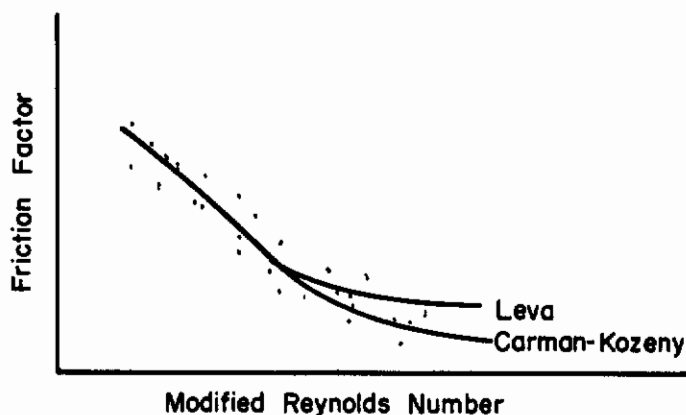


FIGURE 6-3. FIXED-BED DATA OF WILHELM AND KWOUK AS COMPARED WITH CARMAN-KOZENY CURVE AND LEVA CURVE (Morse)⁽⁶⁻¹⁵⁾

The effect of voidage on the flow characteristics has led to considerable disagreement among various workers. The resistance to fluid flow appears to be proportional to $1/\epsilon^n$, but Rose^(6-22, 23, 24) asserts that the exponent, n , is also a function of ϵ . Arthur, Linnet, Raynor, and Sington⁽⁶⁻²⁵⁾ have compared the results of Carman⁽⁶⁻³⁾, Hatch⁽⁶⁻²⁰⁾, Fowler and Hertel⁽⁶⁻²⁶⁾, and Traxler and Baum⁽⁶⁻²⁷⁾ and found that the usual porosity factor, $(1-\epsilon)^2/\epsilon^3$, accounts for the effects of porosity to within experimental error.

A further refinement has been made by Sullivan⁽⁶⁻²⁸⁾. An orientation factor is introduced to permit the study of flow through particles which show a preferred orientation. The evaluation of these orientation factors has received attention in the investigations of Bartell and Osterhoff⁽⁶⁻²⁹⁾, Muskat and Botset⁽⁶⁻³⁰⁾, and others⁽⁶⁻³⁾⁽⁶⁻⁴⁾. Muskat⁽⁶⁻³¹⁾ has also considered the compressibility of the gaseous medium to obtain

$$u^* = u_o \left\{ \frac{p_2^{1+\gamma} - p_1^{1+\gamma}}{(1+\gamma)(p_2 - p_1)p_1^\gamma} \right\}$$

Brinkman⁽⁶⁻³²⁾ has modified Darcy's equation to account for the intermediate ranges of the permeability. He writes

$$\text{grad } P = - \frac{\mu}{P} u + \mu_m \Delta v ,$$

which approximates Darcy's law for small permeabilities and the Navier-Stokes equation for large permeabilities. Using this equation, the force exerted on a sphere by the fluid is found to be

$$R = 6\pi \mu_m u r \left[1 + \lambda r + \lambda^2 r^{2/3} \right]$$

where $\lambda = \left[\frac{\mu}{P \mu_m} \right]^{1/2}$.

Under rather stringent mathematical conditions, Shoumatoff⁽⁶⁻³³⁾ has made a theoretical investigation of the resistance offered by a dispersion to fluid flow. A new shape factor and modified hydraulic radius are introduced so that comparison with other works is not easily made. Transformation equations are developed between the drag equations for individual and massed particles of uniform size. However, some aspects of the development are not fully justified.

Discussion

The evolution of the fixed-bed framework is suggested by the gradual development of the notion of particle size. Beginning with the actual particle diameter, there came various statistical averages, followed by an "effective" particle diameter, the reciprocal of specific surface, the hydraulic radius, and recently, a hydraulic radius modified by a shape factor⁽⁶⁻³³⁾. The Reynolds number has also undergone a series of modifications as shown by the sequence: Re , Re/Da , $Re(1-\epsilon)/Da\epsilon$, and $Re\phi_c/(1-\epsilon)$. These modifications serve as evidence that considerable experimental work must be done before a framework acceptable to most investigators can be established.

Mathematical descriptions involving the use of the hydraulic radius have been carried to a high degree of refinement in the investigations of Blake, Carman, Kozeny, Steinour, and Fowler and Hertel. Iberall⁽⁶⁻³⁴⁾ has termed this line of development the "hydraulic radius" theory in contrast to the "drag" theory as developed by other investigators. Emersleben⁽⁶⁻³⁵⁾, for example, attempted to solve the hydrodynamic equations giving the viscous drag of a fluid on special configurations of parallel fibers. Burke and Plummer⁽⁶⁻¹²⁾ used the drag on spheres to obtain the dependence of the permeability of a porous medium on its porosity. Since experiments have shown better agreement with the results of the hydraulic radius theory, the drag theory has not received much attention. Moreover, the drag theory clearly involves two serious difficulties:

- (1) The solutions of the hydrodynamic equations are extremely difficult to obtain. For example, the hydrodynamic equations for the irrotational flow of a perfect fluid past two spheres have only recently been solved⁽⁶⁻³⁶⁾.
- (2) The statistical assumptions which must be made regarding the number of particles of various shapes which occupy various orientations are difficult to justify and have a tremendous effect on the results obtained.

In this section, the rate of sedimentation of solid particles having an average radius greater than 5 microns will be considered. The particles are assumed to be homogeneously dispersed in a confined, non-flowing liquid. By enclosing the system, certain difficulties are introduced, since the net effect on a particular particle is the combined result of two opposing tendencies. Due to the downward motion of the neighboring particles and the fluid they entrain, there is, together with the force of gravity, an additional downward force acting on a typical particle. Moreover, since the fluid is confined, there is a compensating vertical fluid flow which causes an upward force to be exerted on the particle.

Steinour⁽⁶⁻³⁷⁾ (6-38) considers this problem by expressing the average relative velocity of the fluid with respect to the particle in terms of the average velocity gradient at the surface of a spherical particle, the sphere radius (proportional to the spacing between spheres at constant concentration by volume), and a concentration factor, $\phi(\epsilon)$. The parameter, ϵ , is called the fraction of voids and measures the proportion of fluid in the dispersion as shown by the expression

$$\epsilon = \frac{v_t - v_s}{v_t} .$$

These considerations lead to the following equation for the viscous resistance, R , offered by a single particle,

$$R = \frac{6\pi \mu r_p V}{\phi(\epsilon)} .$$

Thus the usual viscous settling velocity of Stokes has been replaced by $V/\phi(\epsilon)$.

At terminal velocities the total weight of the particles is supported by the fluid. This means that the gradient of the hydrostatic pressure, and hence the buoyancy of the particles is determined by the density of the fluid solid mixture rather than by that of the fluid alone. After taking account of this enhanced buoyancy, and converting from relative velocity of particles and fluid to the velocity of the particles past a fixed reference point, the terminal velocity becomes

$$V = \epsilon^2 \phi(\epsilon) V_s .$$

No complete theoretical solution for the form of the correction factor has been obtained, but analyses aimed toward the solution of this problem have been given by several investigators⁽⁶⁻¹⁾⁽⁶⁻²⁾⁽⁶⁻³⁹⁾.

Some early investigators attempted to correct the Stokes' terminal velocity for the case of a settling dispersion of solid spheres by considering each sphere as moving in a field restricted in some manner by the other spheres. Munroe⁽⁶⁻⁴⁰⁾, for example, supposed that each sphere moved in a virtual cylinder of some "appropriate" radius. Thus, it was only necessary to apply a suitable "wall correction" as in single-particle dynamics. The application of the Munroe⁽⁶⁻⁴⁰⁾, Francis⁽⁶⁻⁴¹⁾, or Ladenburg-Faxen⁽⁶⁻⁴²⁾ wall corrections leads to the following equations:

$$v = V_N \left[1 - (r/r')^{3/2} \right] , \quad \text{(Munroe)}$$

$$v = V_s (1 - r/r')^{2.25} ,$$

(Francis)

$$v = V_s (1 + 2.1 r/r')^{-1} . \quad (\text{Ladenburg-Faxen})$$

From their experiments on the settling velocity of red blood corpuscles, Kermack, McKendrick, and Ponder⁽⁶⁻⁴³⁾ obtained

$$v = V_s \left[1 - 7.1 (1 - \epsilon) \right] .$$

However, this equation seems to indicate that sedimentation will cease for particle concentrations greater than 15 per cent.

Gaudin⁽⁶⁻⁴⁴⁾ adopted the formula

$$v = V_s \epsilon \left[1 - (1 - \epsilon)^{2/3} \right] \left[1 - 2.5 (1 - \epsilon) \right]$$

in which factors were inserted to obtain better correlation with the available data.

Cunningham⁽⁶⁻³⁹⁾ obtained the following expression:

$$v = V_s \left[1 + \frac{3 l_m}{8r} \sqrt{\frac{3\pi}{2}} \right] .$$

This result holds for uniform solid spheres having a diameter smaller than 3 microns in gases, or smaller than 0.01 micron in liquids. An experimental determination of the validity of Cunningham's correction has been made by Millikan⁽⁶⁻⁴⁵⁾.

More recently (1947), Davies⁽⁶⁻⁴⁶⁾ considered the data of Knudsen and Weber⁽⁶⁻⁴⁷⁾, Mattauch⁽⁶⁻⁴⁸⁾, Mönch⁽⁶⁻⁴⁹⁾, and Millikan⁽⁶⁻⁴⁵⁾ and obtained

$$v = V_s \left\{ 1 + l_m/r \left[0.882 + 0.281 \exp(-1.57 r/l_m) \right] \right\}$$

which agrees closely with Cunningham's correction.

Steinour⁽⁶⁻²⁾, from a plot of his experimental data, empirically evaluated the factor $\phi(\epsilon)$, and obtained

$$v = V_s \epsilon^2 10^{-1.82 (1 - \epsilon)} ,$$

where ϵ covers the range, 0.50 to 0.95. This result may be compared with a theoretical equation derived by Burgers⁽⁶⁻¹⁾.

$$v = V_s \left[1 + 6.875 (1 - \epsilon) \right]^{-1} .$$

Figure 6-4 shows a comparison of the results of Steinour with the results of Burgers; v/V_s is plotted as a function of ϵ in each instance.

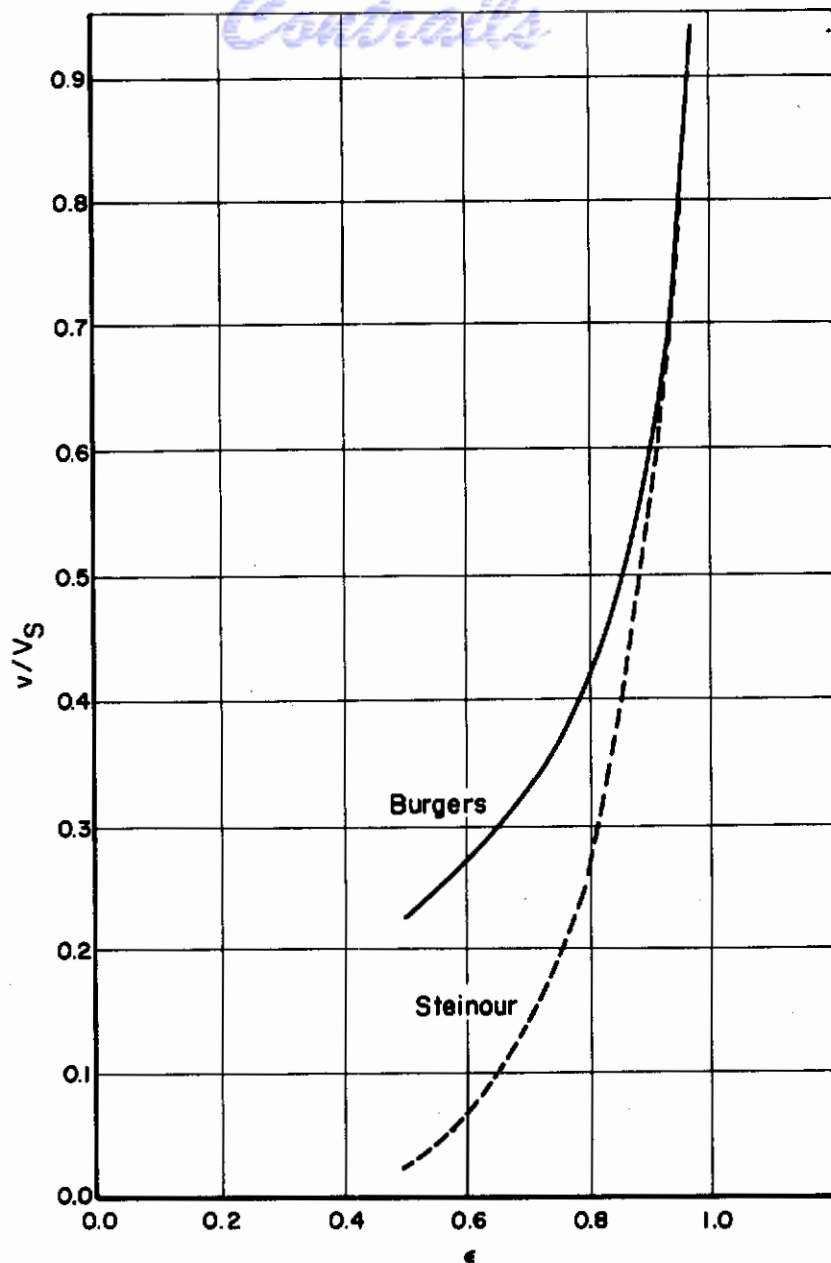


FIGURE 6-4. COMPARISON OF BURGERS' AND STEINOUR'S CORRECTION FOR THE SETTLING VELOCITY OF DISPERSIONS

With certain minor qualifications, considerable empirical confirmation of Steinour's equation has been given by Wilson⁽⁶⁻⁵⁰⁾ who used glass microspheres ranging in size fractions between 3.5 and 15 microns.




Flocculation

Some of the difficulties encountered in determining the sedimentation rates of small particles are due to the formation of loose aggregates of particles, called flocs. Steinour, Powers⁽⁶⁻⁵¹⁾, and Kunkel⁽⁶⁻⁵²⁾ have studied the effects of floc formations on the terminal velocity of fall. In

each investigation, it was found that a floc fell more slowly than the predicted fall velocity of a sphere having the same volume as the component spheres.

Table 6-1, reproduced from Kunkel, shows some typical values of the discrepancy between the actual and theoretical sizes of the flocs as indicated by their fall velocities. The floc formations consisted of several glass spheres which were glued together to form small chains of two, three, etc., up to eight beads. Certain plane arrangements and one cluster of six beads were investigated.

TABLE 6-1. TYPICAL VALUES OF THE DISCREPANCY BETWEEN THE THEORETICAL AND ACTUAL SIZES OF FLOCS AS INDICATED BY THEIR FALL VELOCITIES. (Kunkel)(6-52)

Number of Beads	Arrangement	Mass	Radius of Sphere Having Same Volume	Radius of Sphere Computed by Stokes' Law	Difference, per cent
<u>Linear</u>					
1	o	19.1	1.18	1.20	2
2	oo	39.4	1.51	1.40	7
3	ooo	58.5	1.72	1.50	13
4	oooo	85.1	1.95	1.56	20
8	oooooooo	161.0	2.40	1.64	32
<u>Plane</u>					
3		58.9	1.72	1.53	11
7		137.9	2.28	1.83	20
<u>Space</u>					
6		110.7	2.12	1.85	13

Diffusion

If a dispersion of small particles is not homogeneously distributed in a fluid, a phenomenon called diffusion takes place. Small dispersed particles tend to distribute themselves throughout the available fluid, and, consequently, the sedimentation process may be considerably hindered.

Davies(6-46) has investigated the combined sedimentation-diffusion problem in a nonflowing nonturbulent fluid with particles which are essentially spherical. Using dimensionless groups, the following differential equation is obtained

$$\frac{\partial c}{\partial t} = \alpha \frac{\partial^2 c}{\partial x^2} - \frac{\partial c}{\partial x} \quad (6-2)$$

The steady-state solution to this equation was obtained and checked experimentally by Perrin(6-53). Assuming a constant number of particles in a nonhomogeneous distribution, Mason and Weaver(6-54) obtained a solution to Equation (6-2). The more recent work of Davies(6-46) has led to solutions under a variety of conditions. If the rate of sedimentation is small compared with the rate of diffusion, the solutions take the form of well-known expressions in the theory of heat conduction.

Morton⁽⁶⁻⁵⁵⁾ has considered the settling of a dispersion which is contained in a gas flowing along a horizontal tube. For turbulent flow he obtains

$$\frac{c}{c_0} = \exp \left(- \frac{2 v l}{\pi r u} \right)$$

Figure 6-5 indicates this result by the curve AD which shows the relative concentration as a function of the dimensionless group, lv/ru .

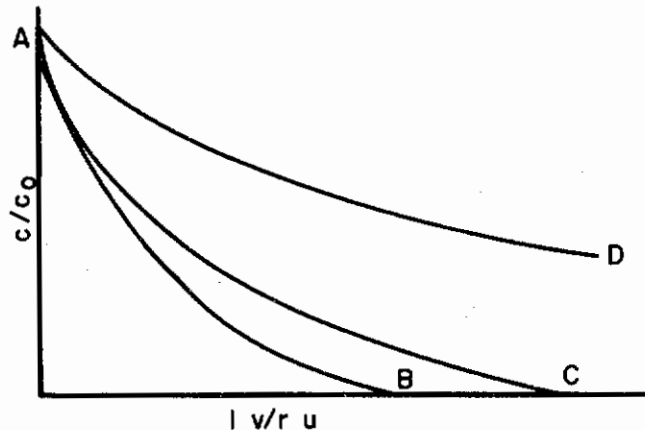


FIGURE 6-5. CONCENTRATION DECAY CURVES OF A SETTLING DISPERSION IN A HORIZONTAL TUBE (Morton)⁽⁶⁻⁵⁵⁾

For non-turbulent flow the particles settle out completely. For instance, the curve AC represents the concentration decay when a Poiseuille type flow is assumed. If the flow velocity is assumed to be constant at all points of the cross section, the decay curve takes the form shown by AB.

Discussion

It may be noted that one can always take the sedimenting particles as a fixed frame of reference so that a sedimentation process and a fixed bed can both be regarded as fluid flow past fixed particles. However, the mathematical expressions describing the sedimentation process must hold over a much wider range of dilutions than those expressions describing flow through a fixed bed. This fact may account for the widespread agreement which has been found to exist among the fixed bed results of Carman, Kozeny, Hatch, Leva, and Sullivan. Differences among these workers arise mainly from considerations involving shape factors, porosity factors, orientation factors, and the experimental determinations of these quantities. By contrast, it may be noted that the equation obtained by Steinour for the sedimentation process has a quite different functional form from that obtained by Burgers.

The results of Steinour and Burgers take direct account of the mutual influence existing among dispersed particles. This is accomplished through the use of the fraction of voids and can be contrasted with the logical uncertainty which must accompany the choice of an "appropriate radius" to account for the effect of a "hypothetical wall".

Physical conditions require a zero settling velocity as a limiting case in highly concentrated dispersions, that is, $\epsilon \rightarrow 0$ must imply $v \rightarrow 0$. From this it is clear that Burgers' result can apply only to dilute dispersions.

Perhaps the most significant feature of the results of Steinour and Burgers lies in the steep slope of the curves for large values of ϵ . Physically, this indicates that, in this region, a small increase in the proportion of solids in the dispersion causes a large decrease in the settling velocity. In fact, a solids concentration of only 5 per cent causes a decrease of more than 25 per cent in the Stokes' velocity. To be within 2 per cent of Stokes' velocity, the concentration must not exceed 0.3 per cent.

From a cursory examination of the results of this section, it would appear that the settling velocity depends only on ϵ and the Stokes velocity. However, this is not the case. The hydraulic radius, or equivalent characteristic linear measure, as well as a functional formulation of the effects of the flow space, must be known, particularly when flocculation is involved. It is to be expected that considerable experimental work will be required before a resolution into these terms can be established.

The simplicity of Kunkel's experiments forms an interesting contrast to the intricate experiments ordinarily associated with dispersion dynamics. The quantitative results which were obtained may be said to apply to the fall velocity of bodies whose elements are spheres, but it does not seem appropriate to make a significant conclusion regarding the fall velocity of a loosely formed floc on the basis of these data. It seems apparent, however, that considerable qualitative information could be gained from similar experiments in which the spheres were not fastened together. Specifically, the envisioned experiments would involve the simultaneous release of various geometrical arrangements of freely falling spheres in a long, vertical column of large diameter containing high specific gravity white oil of known properties. Answers to the following questions might be obtained.

- (1) Do initial horizontal linear arrangements remain linear after release? If not, can it be said, in general, that a linear arrangement becomes planar, or three dimensional?
- (2) Similarly, do initial horizontal planar arrangements remain thus after release? If not, can any general dimensional transformation be predicted?
- (3) Can any distinctive type of behavior be attached to the "outer" or boundary spheres as contrasted with the behavior of the "inner" spheres?
- (4) Is there any tendency to form subclusters, or flocs, and if so, how is this tendency related to the initial arrangements?
- (5) How are the preceding results altered by using spheres of mixed sizes?

It has become increasingly apparent, especially in studies of fluidized beds, that the formation of flocs is an extremely important feature of the mechanics of dispersion systems. However, in the sense of the above proposed experiments, a survey of the literature has shown no basic study of the phenomenon of floc formation. It should also be noted that no quantitative studies have been found concerning the amount of flocculation which may result from turbulence in the fluid.

FLUIDIZED BEDS

When the velocity of flow of the fluid passing through a fixed bed is gradually increased, successive changes take place in the physical system. At a critical "fluidizing velocity" the bed begins to "boil", that is, pockets of continuously agitated, interacting particles are formed. As the velocity of flow is increased beyond the fluidizing velocity, the number and size of the agitated pockets of particles rapidly increase until all the particles are completely supported by the rising fluid and the continuous agitation and interaction between the particles extends throughout the bed. Under these conditions, the bed is said to be fluidized. Although mineral dressing and pneumatic transport of materials have furnished large areas of practical application for fluidization techniques for many years, the subject of fluidized beds must be regarded as in its infancy. Experimental and theoretical developments in this field have increased tremendously since World War II, when the industrial cracking of petroleum by fluidized catalysts was first accomplished. The first major

symposium⁽⁶⁻⁵⁶⁾ on fluid-solid systems was held in December, 1948. Efforts have been made to standardize the terminology and symbolism employed by the research worker⁽⁶⁻⁵⁷⁾. Most investigators of fluidized beds use a terminology which is entirely analogous to that of fixed bed investigators. Thus, the "equation of state" of a fluidized bed involves the pressure gradient, the velocity of fluid flow, and the fraction of voids. It should be noted that the fraction of voids, a constant parameter in fixed-bed flow, serves here as a variable which measures the degree of expansion of the fluidized bed.

Figure 6-6 shows an experimental apparatus suitable for measuring the pressure gradient, fluid velocity, and bed expansion. The apparatus is composed of a vertical glass tube having a wire screen at the lower end for the support of particles. A fluid is passed upward through the screen and bed. The pressure drop is measured by manometers along the vertical tube.

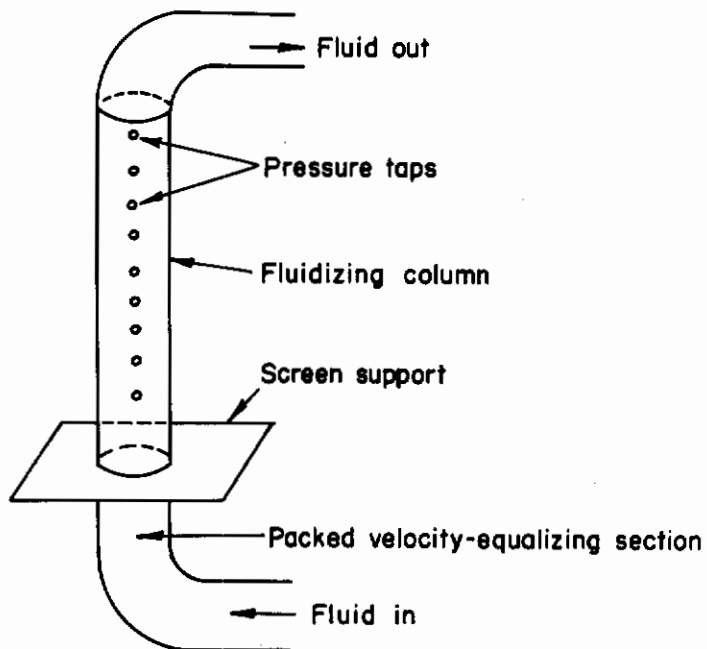


FIGURE 6-6. APPARATUS FOR FLUIDIZATION STUDIES (Wilhelm)⁽⁶⁻⁵⁸⁾

Figures 6-7a and 6-7b, reproduced from the work of Wilhelm⁽⁶⁻⁵⁸⁾, show the characteristic behavior of fluidized beds consisting of uniform, nonagglomerating particles. The curves from A to C represent the fixed-bed stage. A rapid increase of the pressure gradient is indicated as the fluid velocity increases. The "boiling bed" stage is represented by C. The expansion of the bed from D to E has been found to be practically linear⁽⁶⁻²¹⁾ (6-59).

Leva, Grummer, et al⁽⁶⁻⁶⁰⁾ (6-61) used the following equation for a correlation of their data:

$$u_0 \mu \tau = K \left(\frac{\epsilon^3}{(1 - \epsilon)^2} \right)^n$$

This equation is equivalent to the Carman-Kozeny equation for fixed beds when $n = 1$. Thus the exponent, n , measures the deviation of the fluidized bed from the fixed bed. Leva found that $n = 4.5$ for particle diameters of 50 microns. The value of n was found to decrease as the particle size increased, so that for particle diameters of 380 microns, the value 1.0 was obtained for n .

The extensive investigations of Wilhelm and Kwauk⁽⁶⁻²¹⁾ were correlated in terms of different dimensionless groups. However, Morse⁽⁶⁻¹⁵⁾ has put the data of Wilhelm and Kwauk and Leva into the same termed that Carman used so that a comparative study could be made.

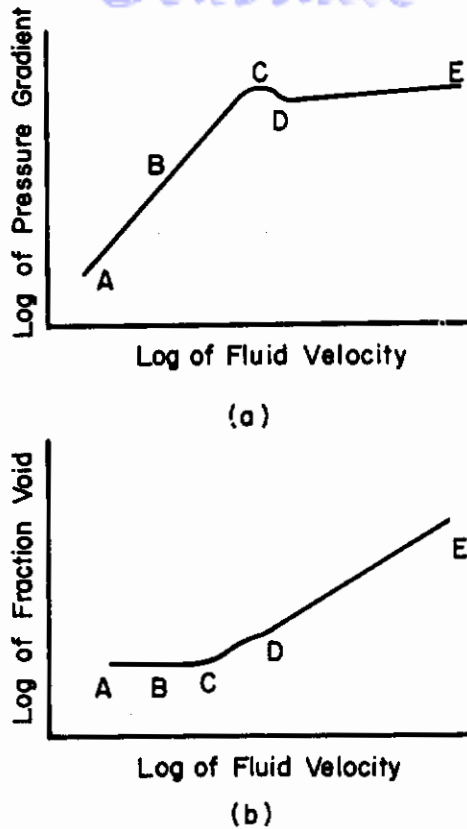


FIGURE 6-7. CHARACTERISTIC BEHAVIOR OF FLUIDIZED BEDS
(Wilhelm)⁽⁶⁻⁵⁸⁾

Figures 6-8 and 6-9, reproduced from Morse⁽⁶⁻¹⁵⁾, indicate some of the results of this investigation.

Figure 6-8 shows the curve through the air-fluidization data of Leva, and Wilhelm and Kwauk along with theoretical curves for fixed beds given by Carman-Kozeny and Leva. The curve for $Re^* < 10$ (about the intersection) represents Leva's data and for $Re^* > 10$ represents the Wilhelm and Kwauk data.

Figure 6-9 shows a more detailed graph of the Wilhelm and Kwauk data for air fluidization at high Reynolds numbers. Comparison with the Carman-Kozeny curve shows practically no correlation.

Ergun and Orning⁽⁶⁻⁶²⁾ have extended Carman's treatment of the flow through a fixed bed by including a turbulence term in the equation of state. Satisfactory correlation was secured with the data of Burke and Plummer⁽⁶⁻¹²⁾ and Oman and Watson⁽⁶⁻⁶³⁾. For spherical particles, the following equation was obtained:

$$\frac{\Delta P}{L} = \left[1 + 96 \frac{b_1}{b_2} \frac{1 - \epsilon}{Re} \right] \frac{b_2}{8} \frac{1 - \epsilon}{\epsilon^3} a_f \rho_f u_m^2$$

where b_1 and b_2 are the intercept and slope obtained by plotting $\Delta P / Lu_m$ against M/A .

Valentine⁽⁶⁻⁶⁴⁾ has made some interesting studies, described by Wilhelm⁽⁶⁻⁵⁸⁾, which qualitatively show that the fluidized bed is a transition state between concurrent upward pneumatic transport and sedimentation.

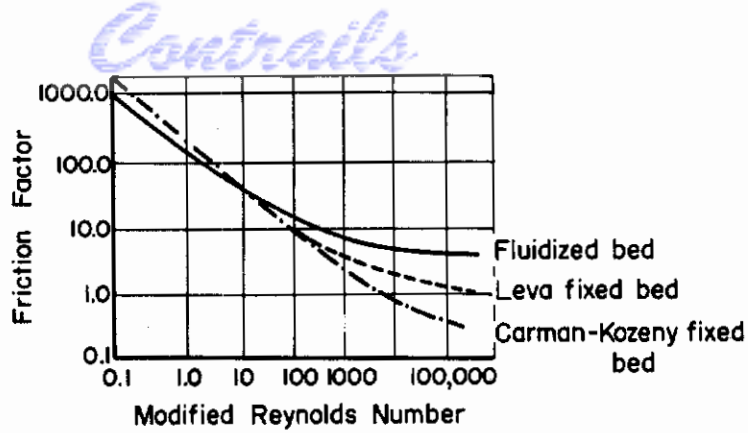


FIGURE 6-8. GRAPH OF FRICTION FACTOR AGAINST MODIFIED REYNOLDS NUMBER FOR FLUIDIZED BEDS (Morse)⁽⁶⁻¹⁵⁾

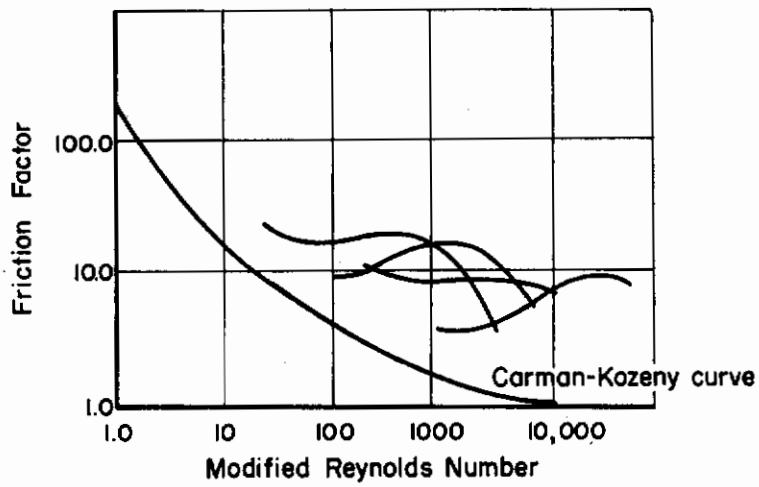


FIGURE 6-9. COMPARISON OF THE AIR FLUIDIZATION DATA OF WILHELM AND KWAUK WITH THE CARMAN-KOZENY CURVE (Morse)⁽⁶⁻¹⁵⁾

Flocculation

Most observers agree^{(6-15) (6-21) (6-58)} that when a gas is used as a fluidizing medium, clumps or aggregates of particles are formed. The resulting "aggregative fluidization" is qualitatively discussed by Morse⁽⁶⁻¹⁵⁾ and is included in the postulational treatment of fluidized beds given by Toomey and Johnson.⁽⁶⁻⁶⁵⁾ A spatially homogeneous fluidization has been termed "particulate fluidization" and is readily achieved by using a liquid as the dispersing medium. In general, both types of fluidization are present to some degree in a fluidized bed. The extreme cases of aggregative fluidization, called "channeling" and "slugging", are described by Parent, Yagol and Steiner⁽⁶⁻⁶⁶⁾.

In addition to the equations of state, many other properties of fluidized beds have been studied in recent years. A brief account of some of these investigations follows.

Density of a Fluidized Bed

Matheson, Herbst, and Holt⁽⁶⁻⁶⁷⁾ have studied the density of a fluidized bed and have found practically linear relations to hold between the bed density and the superficial velocity. The "viscosity" of a fluidized bed has been studied through the use of a Stormer rotating viscosimeter.

Mixing in a Fluidized Bed

The extent of fluid and particle mixing has been studied by Gilliland and Mason⁽⁶⁻⁶⁸⁾. The uniformity of temperature and the mechanism of heat transfer clearly depend on the amount of mixing which occurs in the fluidized bed.

Heat and Mass Transfer

The problems of heat and mass transfer in a fluidized bed have been considered by several investigators. Colburn⁽⁶⁻⁶⁹⁾ introduced the h and k transfer coefficients and the j transfer factors. McCune and Wilhelm⁽⁶⁻⁷⁰⁾ and Hobson and Thodos⁽⁶⁻⁷¹⁾ extended the concept of the j factors. Careful data on heat-transfer rates have been obtained by Mickling and Trilling⁽⁶⁻⁷²⁾ and correlated by Gamson⁽⁶⁻⁷³⁾. Leva, Weintraub, and Grummer⁽⁶⁻⁷⁴⁾ have considered the flow of heat from the container walls to the fluidized bed. Their treatment involves the concepts of "minimum fluid voidage" and "fluidized efficiency". A recent investigation by Leva and Grummer⁽⁶⁻⁷⁵⁾ indicates wide general agreement among the fluidized-bed investigators on the following points:

- (1) Coefficients of heat transfer increase as particle diameter decreases.
- (2) Heat-transfer coefficients are independent of the thermal conductivity of the particles.

Some preliminary investigations into the nature of eddy diffusion in a fluidized bed have been made by McCarter, Stutzmann, and Koch⁽⁶⁻⁷⁶⁾.

Discussion

In the considerations of the previous sections, it has been assumed that the dispersions consist of solid particles. The resulting simplifications are enormous when compared with the complexities involved in dispersion of liquid droplets. In liquid dispersions, the factors of evaporation, surface tension and coalescence cannot be ignored. At the present time, it has not been established that the results obtained under the solid-particle simplifications can be applied to the fluidization of liquid droplets, even as a first approximation.

Perhaps the most significant qualitative result mentioned in this section is concerned with the existence of aggregative fluidization in gaseous media. The definite experimental proof or disproof of the existence of these "clumps" in dispersions of liquid droplets would be of great importance to investigations involving the penetration distance of sprays, the evaporation rates within dispersions, and the burning of droplets at flame fronts.

PNEUMATIC TRANSPORT

When the velocity of fluid flow through a fluidized bed is increased, the bed will expand until most of the particles will be transported out of the system. When the fluidizing medium is a gas, the movement of the dispersion is called pneumatic transport.

A summary of the literature pertaining to pneumatic transport prior to 1940 has been given by Dallavalle(6-77). Cramp's(6-78) investigation takes account of the following forces:

- (1) The force required to support the weight of the particles in a vertical conveyor tube.
- (2) The force required to accelerate the particles from their initial velocity to the transport velocity.
- (3) The force required to overcome friction losses resulting from particle contacts with the conveyor walls.
- (4) The force required to overcome the friction between the fluid and the walls of the container.
- (5) The force required to accelerate the fluid in the conveyor.

Gasterstädt(6-79) introduced the dimensionless group,

$$\delta = \frac{\text{pressure drop in the solids-gas mixture}}{\text{pressure drop without solids at same gas flow rate}}$$

and showed that for a given gas velocity

$$\delta - \frac{1}{\nu} = \text{constant} ,$$

where ν is the solid to gas mass ratio. Segler(6-80) and Vogt and White(6-81) have given some confirmation to Gasterstädt's results, but Farber(6-82) and Zenz(6-83) obtained results which indicate a breakdown of Gasterstädt's treatment at extreme conditions.

Using energy relations and a result of Lapple and Shepherd(6-84), Hariu and Molstad(6-85) express the net acceleration, a_u , on a single particle as follows:

$$a_u = \frac{3\rho g}{4\rho_p D} (\Delta u)^2 J - g - \frac{2f_s u_s^2}{D_t} .$$

The "accelerating distance" of the particle can be calculated by the method of Jennings(6-86). The final result takes the form,

$$\frac{1}{G_s} \left(\frac{dP}{dL} \right) = K \left(\frac{1}{u_s} + \frac{2f_s u_s}{g D_t} + \frac{a_u}{g u_s} \right) .$$

This equation indicates that large pressure gradients will exist at the point of injection since u_s at that point is small.

Discussion

The influence of evaporation in the pneumatic transport of droplets must be regarded as a decisive factor. The total liquid mass in a unit volume of transported droplets will decrease because of evaporation. If a steady droplet flow rate is attained, the total mass of the droplets at any cross section of the conduit will be a function of the distance from the point of injection. Thus, in vertical transport the supporting force diminishes with height until the evaporation of the droplets

is complete. Consequently, the maximum droplet concentration and maximum average-droplet size will occur near the point of injection. Conceivably, in concentrated dispersions, the rate of evaporation may also be a function of height because of the increased vapor content of the gas due to evaporation at lower levels. If the gas flow is constant, some indication of a continual "acceleration" of the droplets may also be evidenced. This effect would stem from the fact that the continuous decrease in the mass of an evaporating droplet would entail a corresponding decrease in the terminal velocity of fall of the droplets. Thus, the relative velocity between the droplet and the gas would diminish with height. To an observer, this phenomenon would appear as a "speeding up" or acceleration of the droplet as it was transported up the column.

The force required for the initial acceleration of small evaporating droplets is difficult to evaluate, even qualitatively. Definite, quantitative results concerning evaporation rates of accelerated droplets in a flowing gas are not yet available. Thus the force of acceleration may or may not be comparable with that involved in the transport of solid particles.

The friction encountered between solid particles and the container walls has no analogue in droplet dispersions. The colliding of droplets with the walls of the column serves to decrease the number of droplets supported by the gas, and, consequently, decreases the average fluid-pressure drop resulting from support of the droplets.

Since the trajectories of the larger droplets may deviate significantly from the lines of flow of the gas, and since the average drop size is a maximum near the point of injection, the amount of liquid deposited on the walls may be assumed to be greatest near the point of injection.

The energy losses due to droplet collisions among themselves can not be considered analogous to the friction loss by colliding particles. The energy relations assumed in droplet collisions demand a satisfactory decision as to whether colliding droplets coalesce or simply "rebound". This question is not easily answered. It will be considered in more detail in the next section.

From these remarks it is clear that the problems of dispersions of liquid droplets are far more intricate than the corresponding problems of solid dispersions. The difficulties of utilizing the results of solid dispersion dynamics in considerations of liquid dispersions are due mainly to problems of evaporation. A satisfactory investigation of the evaporation properties of dispersions of droplets seems to be beyond reasonable establishment at the present time.

It does not seem unreasonable to attempt to establish the existence of pockets or clumps in a dispersion of liquid droplets. If it could be established that evaporation does not dominate this aspect of liquid dispersions, then the segregation features of the solid dispersion might be thoroughly investigated and applied to the liquid dispersion.

COALESCENCE

If a collision of two droplets results in amalgamation, the process by which the single droplet is produced is called direct coalescence. For many years, direct coalescence of cloud droplets was thought to be the major factor involved in the growth of small droplets to droplets of raindrop size (500 microns). More recently, the growth of liquid droplets by direct coalescence has become a subject of much controversy. Direct coalescence has been advocated by Köhler⁽⁶⁻⁸⁷⁾, Findeisen⁽⁶⁻⁸⁸⁾, and Langmuir⁽⁶⁻⁸⁹⁾. Other theories have attempted to explain the growth of liquid droplets by indirect coalescence which features the transfer of liquid vapor from one droplet to another, thereby causing the large droplets to grow at the expense of the smaller ones.

The coalescence controversy derives much of its vigor from the fact that mathematical assumptions utilizing direct coalescence between droplets have led to satisfactory results. However, beginning with the experiments of Dady⁽⁶⁻⁹⁰⁾, no observed case of a droplet collision resulting in coalescence has been reported. Many collisions between droplets have been observed, but in every instance the droplets simply rebounded, or "bounced off" from each other. Swinbank⁽⁶⁻⁹¹⁾ and Gunn and Hitschfeld⁽⁶⁻⁹²⁾ attempt to account for the rebound on the basis of a possible increase in

surface energy during the process of amalgamation. The proposed increase in surface energy serves as a "barrier" to coalescence, and the barrier can be overcome only if the colliding droplets have sufficient kinetic energy. Since the relative kinetic energies of extremely small droplets is small, the direct coalescence of small droplets is not likely to occur. Studies of the noncoalescence of stationary liquid droplets have been made by Deriagin and Prokhorov⁽⁶⁻⁹³⁾. Factors which tend to inhibit the growth of liquid droplets by indirect coalescence have been summarized by Perrie⁽⁶⁻⁹⁴⁾.

From these investigations, maximum droplet accretion may be expected in dispersion systems characterized by turbulent motion, mixed droplet sizes, mixed phases, and non-uniform temperatures. While all of these conditions contribute to indirect coalescence, this type of coalescence process is too slow to be of much practical concern except under severe conditions⁽⁶⁻⁹⁵⁾.

The aerodynamic problem which arises in collision problems involves the trajectories of two approaching droplets. The droplets may collide or the smaller droplet may be deflected around the larger droplet by the gas flow. Langmuir and Bladgett⁽⁶⁻⁸⁹⁾ made an intensive semiempirical study of the trajectories of small droplets in the vicinity of a large droplet. From these studies, Langmuir calculated the collision efficiency, $E(r)$, which may be defined as the ratio of the mass of the dispersed droplets with which the falling drop comes into contact to the mass of the dispersed droplets originally contained in the volume swept out by the falling drop.

Figure 6-10, reproduced from Gunn and Hitschfeld⁽⁶⁻⁹²⁾, shows Langmuir's collision efficiency as a function of the larger, falling-drop radius for various values of the smaller droplet radius.

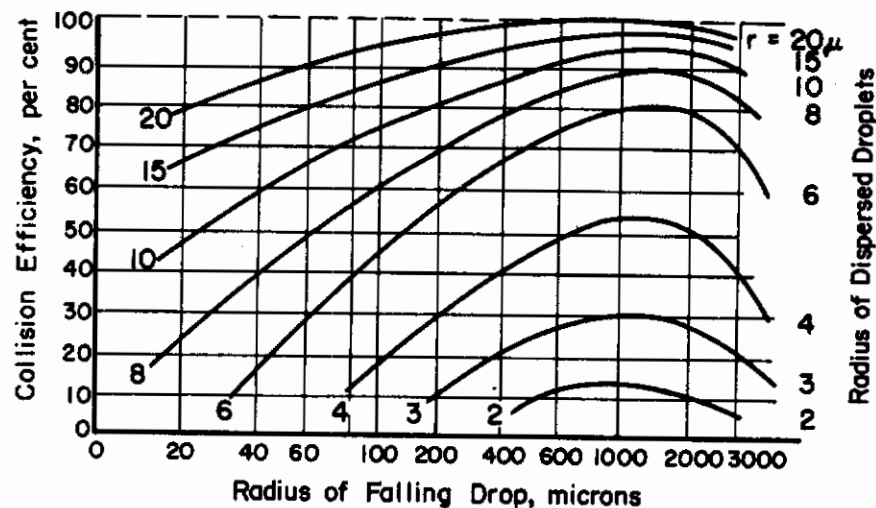


FIGURE 6-10. COLLISION EFFICIENCY AS A FUNCTION OF THE FALLING DROP RADIUS AND THE DISPERSED DROPLET BASED ON LANGMUIR'S ANALYSIS⁽⁶⁻⁸⁷⁾ (Gunn and Hitschfeld)⁽⁶⁻⁹²⁾

Gunn and Hitschfeld⁽⁶⁻⁹²⁾ have carried out an experimental check of Langmuir's results. The methods of Houghton and Radford⁽⁶⁻⁹⁶⁾ and Fuchs and Petrjanoff⁽⁶⁻⁹⁷⁾ were combined to determine the drop-size distributions of heterogeneous dispersions of water droplets in air. Fall-velocity corrections were found to be in agreement with Laws⁽⁶⁻⁹⁸⁾.

Figure 6-11 shows a comparison of Langmuir's theoretical collision efficiency curve, $E(r)$, with Gunn and Hitschfeld's effective collection efficiency curve, $\bar{E}(r)$. From their data Gunn and Hitschfeld conclude that every drop-droplet collision results in direct coalescence.

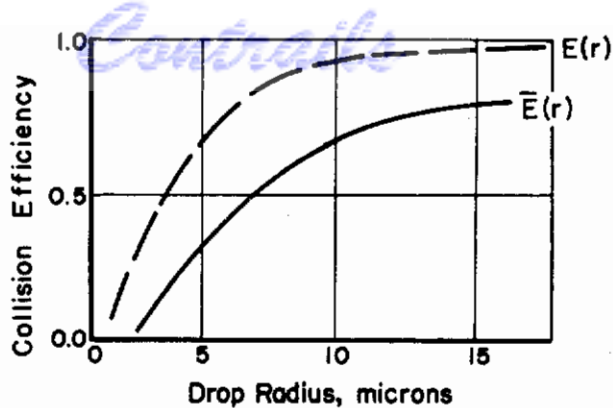


FIGURE 6-11. COMPARISON OF LANGMUIR'S COLLISION EFFICIENCY CURVE, $E(r)$, WITH EXPERIMENTAL COLLECTION EFFICIENCY CURVE, $\bar{E}(r)$, OBTAINED BY GUNN AND HITSCHFELD⁽⁶⁻⁹²⁾

Das⁽⁶⁻⁹⁹⁾ has criticized the results of Langmuir on the basis that Langmuir disregarded the effect of the finite sizes of the smaller droplets. Taking the finite sizes into account yields collision efficiencies greater than 100 per cent, since droplets with centers outside the swept stream may collide with the falling drop.

Discussion

It is apparent that the mechanics of the direct coalescence of two colliding droplets is not understood. The exact nature of the deformation which may act as a "barrier" to direct coalescence has yet to be established. A "barrier" theory, based on surface energies, certainly cannot be established until the transition of surfaces is known. It seems likely that the study of surface energies may yield the most important clues to the amalgamation of motionless droplets, but it is not clear that considerations of surface energy will account for the direct coalescence of colliding droplets. As Swinbank suggests, the relative kinetic energies may be the most important factor. It must be noted, however, that the kinetic-energy proposal of Swinbank does not account for the fact that small droplets have been observed to rest on the surface of a body of the same liquid for several minutes before coalescence occurred. In this process the constant zero kinetic energy can hardly account for the delayed coalescence. Thus, it may not be possible to apply results obtained in coalescence studies of motionless droplets to the coalescence of moving droplets.

The experiments of Gunn and Hitschfeld indicate that the relative size of the colliding droplets are decisive factors in direct coalescence. The steep slope of the collection-efficiency curve shows that a relatively small change in the average drop size in the dispersion produces a large change in the collection efficiency of the larger, falling drop. For dispersions with an average droplet radius less than ten microns, the collection efficiency is exceedingly low. Dispersions with an average droplet radius greater than fifteen microns give collection efficiencies of more than 50 per cent.

Gunn and Hitschfeld substantiate, on the basis of their experiments, the correctness of Langmuir's hypothesis that every drop-droplet collision results in coalescence. However, the calculations of Das show that the actual collection efficiency should be higher than that predicted by Langmuir. Thus, the Gunn-Hitschfeld curve, which is consistently lower than that of Langmuir, differs considerably from the collection efficiencies predicted by Das. This discrepancy may be accounted for by supposing that some of the collisions result in "rebounds" rather than coalescence.

The Das corrections for the finite sizes of the smaller droplets seem essential if investigations of collisions between droplets of the same relative size are to be made. However, the difficulty of

maintaining an appreciable relative velocity between droplets of the same size is an experimental handicap which is only partly overcome by the use of a turbulently flowing gas.

Some direct experimental data concerning the collisions of moving droplets may be obtainable through the use of high-speed photography. If such a study proved feasible, it would seem reasonable to suppose that statistical methods could be utilized to put the problem of "rebound" into probability terms. The establishment of a statistical statement concerning the probable number of rebounds for a given number of collisions may prove extremely useful, even though the actual mechanics of the coalescence process might remain unsolved.

SONIC AGGLOMERATION

Since combustion processes may be accompanied by large sound intensities in the combustion chamber, it seems appropriate to consider the field of sonic agglomeration of dispersions. The fact that high intensity sound waves may increase direct coalescence between droplets and lead to characteristic floc formations may be of significance in those combustion processes which involve dispersions.

Brandt, Heidemann, and Freund⁽⁶⁻¹⁰⁰⁾ have proposed a theory which accounts for sonic agglomeration solely on the basis of the variations of phases and amplitudes existing among the sound waves. The more comprehensive investigations of St. Clair⁽⁶⁻¹⁰¹⁾ indicate that the behavior of the dispersed droplets is due to a combination of the following effects: co-vibrations of the droplets in a vibrating gas, hydrodynamic attraction and repulsion between neighboring droplets, and radiation pressure.

Covibration

Because of the viscous drag force exerted by a gas on a dispersed droplet, the droplet will participate, to some extent, in the vibrations of the gas. At a frequency of 5000 c, a water droplet having a diameter less than 1 micron vibrates with essentially the same amplitude as the gas. If the frequency is increased to 25,000 c, the relative amplitude is about 90 per cent. A reduction of the relative amplitude to 50 per cent requires a frequency of about 90,000 c.

Hydrodynamic Forces

The hydrodynamic forces of attraction and repulsion operating between droplets are significant only when the dispersion is highly concentrated. By the Bernoulli principle, the general effect of an intense sound field on a dispersion of droplets is the creation of repulsive forces between droplets in the direction of vibration and attractive forces in the transverse directions. Experiments conducted by St. Clair⁽⁶⁻¹⁰¹⁾ have shown the production of thin, disc-shaped flocs oriented at right angles to the direction of vibration. In a stable, standing wave, such flocs attained diameters of several centimeters.

Radiation Pressures

Using high-intensity sound waves, it is possible to suspend metal spheres or coins in mid-air by means of the radiation pressure⁽⁶⁻¹⁰¹⁾. This pressure is considered to be the most important effect produced by the sound field. King⁽⁶⁻¹⁰²⁾ shows that a spherical object in a standing wave is acted upon by a radiation force which directs the object toward the velocity antinode.

Figure 6-12, from St. Clair, Spendlove, and Potter⁽⁶⁻¹⁰³⁾, shows the successive changes in concentration of a dispersion which is uniformly distributed at $t = 0$. The concentration curves

are given for $t = 0, 27,$ and 43 seconds for a sound field having an energy density of 1000 ergs per cubic centimeter ($1/3$ watt per cm^2), and a frequency of 10 kc.

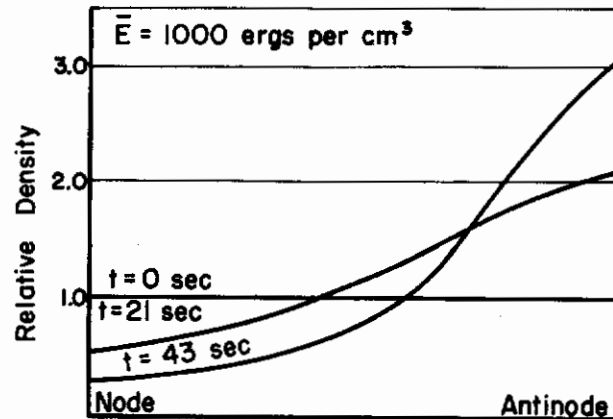


FIGURE 6-12. CALCULATED CHANGE IN CONCENTRATION OF SMOKE PARTICLES DUE TO RADIATION PRESSURE IN A STANDING WAVE FIELD (St. Clair, Spendlove, and Potter)⁽⁶⁻¹⁰³⁾

Discussion

Studies have shown that sound intensities of sufficient energy to produce sonic agglomeration actually occur in combustion chambers. In most combustion systems, the time involved in the complete combustion process is extremely short so that sonic agglomeration is probably not significant. However, it should be noted that the forces which tend to produce agglomeration are present, and some effects arising from these forces in the initial, dense dispersion of droplets occurring near the point of injection may be carried to the flame front. Sound-wave disturbances in these "embryonic" stages of a dispersion may become magnified under the continuing action of the sonic forces as the dispersion progresses towards the flame front. However, no studies have been found concerning the production or transmission of sound-wave disturbances in a dispersion undergoing progressive dilution.

CONCLUDING REMARKS

In the course of this chapter it has been shown that the body of available information concerning the dynamics of dispersions is decidedly limited. Considerable basic research must be carried out before any acceptable mathematical descriptions of dispersion systems can be expected to evolve. Certain specific investigations which were proposed in the preceding discussion sections include the following:

- (a) Basic studies involving the simultaneous release of various geometrical arrangements of spheres in a high specific gravity oil of known properties. The purpose of these studies would be the determination of the relations which exist between the initial and final configuration assumed by a small aggregate of the freely falling spheres. The effects of the mutual influences exerted by the spheres and the tendency to form flocs could be studied. By suitable adaptations, the postulational system of Toomey and Johnson could serve as a theoretical basis underlying the investigation.

- (b) Photographic studies of collision and coalescence among dispersed droplets are suggested as a first step towards obtaining quantitative answers to the problems of "collision with coalescence", "collision with rebound", and the formation of flocs. Statistical analysis of such data would certainly reveal the relative importance of these problems to other problems involved in the injection of liquids into gases.

For immediate answers to specific problems involving dispersion dynamics, the methods of dimensional analysis seem most appropriate. At the outset, each problem should be carefully analyzed to determine whether the system may be regarded as a collection of single droplets or as a dispersion in which each particle significantly influences the behavior of its neighbors. The best measure of this influence is given by the fraction of voids. Considerable care must be exercised in concluding that the fraction of voids is sufficiently close to unity to warrant the use of single-particle dynamics rather than dispersion dynamics. Steinour's results have indicated that in his experiments a void fraction of 0.97 led to a deviation of more than 15 per cent from Stokes' law in gravitational settling.

There are various sources of information regarding developments in the field of dispersion dynamics. The most important general sources include the publications of the petroleum industries, coal industries, chemical industries, and meteorological societies. Perhaps the most complete recent summary of dispersion dynamics has appeared in a German publication⁽⁶⁻¹⁰⁴⁾.

It has been shown that each of the problems that must be solved to obtain a satisfactory treatment of liquid dispersions constitutes an entire field of investigation in itself. Each will require extensive research programs, involving the painstaking collection of data, before sufficient reliable information will be available for a systematic theoretical study of the dynamics of dispersions.

REFERENCES

- 6-1. Burgers, J. M., The Effect of Concentration on the Speed of Sedimentation of Suspensions, Especially Suspensions of Spherical Particles, Proc. Acad. Sci. Amsterdam, Vol. 45, 1942, pp. 9-16.
- 6-2. Steinour, H. H., Rate of Sedimentation. Nonflocculated Suspension of Uniform Spheres, Ind. Eng. Chem., Vol. 36, 1944, pp. 618-624.
- 6-3. Carman, P. C., The Determination of the Specific Surface of Powders, J. Soc. Chem. Ind. (London), Vol. 57, 1938, pp. 225-234.
- 6-4. Sullivan, R. R., and Hertel, K. L., Advances in Colloid Science, Vol. 1, Interscience Publishers, Ind., New York, 1942, pp. 37-48.
- 6-5. Darcy, H. P. G., The Public Fountains of the Village of Dijon, Victor Dalmont, Paris, 1856.
- 6-6. Slichter, C. S., Theoretical Investigation of the Motion of Ground Waters, U. S. Geol. Survey, 19th Annual Rep., Part 2, 1899, pp. 301-384.
- 6-7. Fancher, G. H., and Lewis, J. A., Flow of Simple Fluids Through Porous Materials, Ind. Eng. Chem., Vol. 25, 1933, pp. 1139-1147.
- 6-8. Barnes, K. B., A Method for Determining the Effective Porosity of a Reservoir Rock, Penn State College Min. Ind. Exper. Sta., Bull. No. 10, 1931.
- 6-9. Poiseuille, J., Experimental Investigation of the Movement of Liquids in Capillary Tubes, Inst. de France, Acad. des France, Vol. 9, 1846, pp. 433-543.

- 6-10. Hatfield, M. R., Fluid Flow Through Porous Carbon, Ind. Eng. Chem., Vol. 31, 1939, pp. 1419-1424.
- 6-11. Blake, F. C., The Resistance of Packing to Fluid Flow, Trans. Am. Inst. Chem. Engrs., Vol. 14, 1922, pp. 415-421.
- 6-12. Burke, S. P., and Plummer, W. B., Gas Flow Through Packed Columns, Ind. Eng. Chem., Vol. 20, 1928, pp. 1196-1204.
- 6-13. Furnas, C. C., Flow of Gases Through Beds of Broken Solids, U. S. Bur. Mines Bull., Vol. 307, 1929.
- 6-14. Chilton, T. H., and Colburn, A. P., Pressure Drop in Packed Tubes, Ind. Eng. Chem., Vol. 23, 1931, 913-919.
- 6-15. Morse, R. D., Fluidization of Granular Solids, Ind. Eng. Chem., Vol. 41, 1949, pp. 1117-1124.
- 6-16. Perry, J. H., Chemical Engineers Handbook, 2nd Edition, McGraw-Hill Book Co., New York, 1941, p. 807.
- 6-17. Kozeny, J., Concerning Capillary Conduction of Ground Waters, Math.-naturw. Kl., Vol. 136 (Abt. IIa), 1927, pp. 271-306.
- 6-18. Leva, M., and Grummer, M., Pressure Drop Through Packed Tubes, Parts I, II, and III, Chem. Eng. Prog., Vol. 43, 1947, pp. 549-554, 633-638, 713-718.
- 6-19. Fair, G. M., Hatch, L. P., Fundamental Factors Governing Streamline Flow of Water Through Sand, Journal Am. Water Works Assoc., Vol. 25, 1933, pp. 1551-1565.
- 6-20. Hatch, L. P., Flow Through Granular Media, J. App. Mech., Vol. 62, 1940, pp. A109-A112.
- 6-21. Wilhelm, R. H., and Kwauk, M., Fluidization of Solid Particles, Chem, Eng. Prog., Vol. 44, 1948, pp. 201-218.
- 6-22. Rose, H. E., An Investigation Into the Laws of Flow of Fluids Through Beds of Granular Materials, Proc. Inst. Mech. Eng., Vol. 153, 1945, pp. 141-148.
- 6-23. Rose, H. E., Isothermal Flow of Gases Through Beds of Granular Materials, Proc, Inst. Mech. Eng., Vol, 153, 1945, pp. 148-153.
- 6-24. Rose, H. E., On the Resistance Coefficient - Reynolds Number Relationship for Fluid Flow Through a Bed of Granular Material, Inst. Mech. Eng. (London) J. and Proc., Vol. 153, 1945, pp. 154-161.
- 6-25. Arthur, J. R., Linnett, J. W., Raynor, E. J., and Sington, E. P. C., Flow of an Air Stream Through a Layer of Granules, Trans. Farad. Soc., Vol 46, 1950, pp. 270-281.
- 6-26. Fowler, J. L., and Hertel, K. L., Flow of a Gas Through Porous Media, J. Appl. Phys., Vol. 11, 1940, pp. 496-502.
- 6-27. Traxler, R. N., and Baum, L. A. H., Permeability of Compacted Powders. Determination of Average Pore Size, Physics, Vol. 7, 1936, pp. 9-14.
- 6-28. Sullivan, R., Specific Surface Measurements on Compact Bundles of Parallel Fibers, J. Appl. Physics, Vol. 13, 1942, pp. 725-730.

- 6-29. Bartell, F. E., and Osterhoff, H. J., The Pore Size of Compressed Carbon and Silica Membranes, J. Phys. Chem., Vol. 32, 1928, pp. 1553-1571.
- 6-30. Muskat, M., and Botset, H. G., Flow of Gas Through Porous Materials, Physics, Vol. 1, 1931, pp. 27-47.
- 6-31. Muskat, M., The Flow of Homogeneous Fluids Through Porous Media, McGraw-Hill Book Co., New York, 1937.
- 6-32. Brinkman, H. C., Calculation of Viscous Force Exerted by a Fluid on a Dense Swarm of Particles, Appl. Sci. Research, Vol. 1, 1949, pp. 27-34.
- 6-33. Shoumatoff, N., The Hydrodynamic Resistance of Particles, Am. Soc. Mech. Eng., Paper No. 52-SA-42, Advance Copy, 1952.
- 6-34. Iberall, A. S., Permeability of Glass Wool and Other Highly Porous Media, J. of Res. of the Nat. Bureau of Standards, Vol. 45, 1950, pp. 398-406.
- 6-35. Emersleben, O., The Darcy Filter Formula, Physik Z., Vol. 26, 1925, pp. 601-610.
- 6-36. Sneddon, I. N., and Fulton, J., The Irrotational Flow of a Perfect Fluid Past Two Spheres, Proc. Camb. Philos. Soc., Vol. 45, 1949, pp. 81-87.
- 6-37. Steinour, H. H., Rate of Sedimentation. Suspensions of Uniform Size Angular Particles, Ind. Eng. Chem., Vol. 36, 1944, pp. 840-847.
- 6-38. Steinour, H. H., Rate of Sedimentation. Concentrated Flocculated Suspensions of Powders, Ind. Eng. Chem., Vol. 36, 1944, pp. 901-910.
- 6-39. Cunningham, E., On the Velocity of Steady Fall of Spherical Particles Through Fluid Medium, Proc. Roy. Soc. (London), Vol. 83, (Ser. A), 1910, pp. 357-365.
- 6-40. Munroe, H. S., The English versus the Continental System of Jigging - Is Close Sizing Advantageous?, Trans. Am. Inst. Mining Engrs., Vol. 17, 1889, pp. 637-659.
- 6-41. Francis, A. W., Wall Effect in the Falling-Ball Method for Viscosity, Physics, Vol. 4, 1933, pp. 403-406.
- 6-42. Ladenburg, R., Concerning the Influence of Walls on the Motion of a Sphere in a Viscous Liquid, Ann. Physik, Vol. 23, 1907, pp. 447-458.
- 6-43. Kermack, W. O., McKendrick, A. G., and Ponder, E., The Stability of Suspensions. The Velocities of Sedimentation and Cataphoresis of Suspensions in a Viscous Fluid, Proc. Roy. Soc. Edinburgh, Vol. 49, 1929, pp. 170-197.
- 6-44. Gaudin, A. M., Principles of Mineral Dressing, McGraw-Hill Book Co., New York, 1939.
- 6-45. Millikan, R. A., Law of Fall of a Sphere Through a Gas and the Nature of Molecular Reflection, Phys. Rev., Vol. 22, 1923, pp. 1-23.
- 6-46. Davies, C. N., The Sedimentation and Diffusion of Small Particles, Proc. Roy. Soc. (Ser. A), Vol. 200, 1949, pp. 100-113.
- 6-47. Knudsen, M., and Weber, S., Resistance to Motion of Small Spheres, Ann. Phys., Lpz, Vol. 36, 1911, pp. 981-994.
- 6-48. Mattauch, J., Resistance to Motion of Small Particles Through a Gas, Z. Phys., Vol. 32, 1925, pp. 439-472.

- 6-49. Mönch, G., Resistance of Small Spheres in Motion Through Air, Z. Phys., Vol. 34, 1933, pp. 77-79.
- 6-50. Wilson, B. W., The Sedimentation of Dense Suspensions of Microscopic Spheres, Australian Journal Appl. Sci., Vol. 4, 1953, pp. 274-299.
- 6-51. Powers, T. C., Research Lab., Portland Cement Assoc., Bull 2, 1939.
- 6-52. Kunkel, W. B., Magnitude and Character of Errors Produced by Shape Factors in Stokes' Law Estimates of Particle Radius, J. Appl. Phys., Vol. 19, 1948, pp. 1056-1058.
- 6-53. Perrin, J., Atoms, London, Constable, 1916.
- 6-54. Mason, M., and Weaver, W., The Settling of Small Particles in a Fluid, Phys. Rev. (2), Vol. 23, 1924, pp. 412-426.
- 6-55. Morton, W. B., The Settling of a Suspension Flowing Along a Tube, Proc. Roy. Irish Acad., Vol. 43A, 1935, pp. 1-4.
- 6-56. Symposium on Dynamics of Fluid/Solid Systems, Dynamics of Fluid/Solid Systems, Ind. Eng. Chem., Vol. 41, 1949, pp. 1099-1250.
- 6-57. Symposium on Dynamics of Fluid/Solid Systems, Fluidization Nomenclature and Symbols, Ind. Eng. Chem., Vol. 41, 1949, pp. 1249-1250.
- 6-58. Wilhelm, R. H., Fluidization of Masses of Particles, Research, Vol. 3, 1950, pp. 159-165.
- 6-59. Lewis, W. K., Gilliland, E. R., and Bauer, W. C., Characteristics of Fluidized Particles, Ind. Eng. Chem., Vol. 41, 1949, pp. 1104-1117.
- 6-60. Leva, M., Grummer, M., Weintraub, M., and Pollchik, M., Introduction to Fluidization, Chem. Eng. Prog., Vol. 44, 1948, pp. 511-520.
- 6-61. Leva, M., Grummer, M., Weintraub, M., Pollchik, M., Fluidization of Solid Non-Vesicular Particles, Chem. Eng. Prog., Vol. 44, 1948, pp. 619-626.
- 6-62. Ergun, S., and Orning, A. A., Fluid Flow Through Randomly Packed Columns and Fluidized Beds, Ind. Eng. Chem., Vol. 41, 1949, pp. 1179-1184.
- 6-63. Oman, A. O., and Watson, K. M., Pressure Drops in Granular Beds, Nat. Pet. News, Vol. 36, 1944, pp. R795-802.
- 6-64. Valentine, S., M. S. E. Thesis, School of Engineering, Princeton Univ., Princeton, 1949.
- 6-65. Toomey, R. D., and Johnstone, H. F., Gaseous Fluidization of Solid Particles, Chem. Eng., Prog. 1952, pp. 220-226.
- 6-66. Parent, J. D., Yagol, N., and Steiner, C. S., Fluidizing Processes: Basic Observations From Laboratory Equipment, Chem. Eng. Prog., Vol. 43, 1949, pp. 429-436.
- 6-67. Matheson, G. L., Herbst, W. A., and Holt, P. H., Characteristics of Fluid-Solid Systems, Ind. Eng. Chem., Vol. 41, 1949, pp. 1099-1104.
- 6-68. Gilliland, E. R., and Mason, E. A., Gas and Solid Mixing in Fluidized Beds, Ind. Eng. Chem., Vol. 41, 1949, pp. 1191-1196.
- 6-69. Colburn, A. P., A Method of Correlating Forced Convection Heat Transfer Data and a Comparison With Fluid Friction, Trans. Am. Inst. Chem. Engrs., Vol. 29, 1933, pp. 174-210.

- 6-70. McCune, L. K., and Wilhelm, R. H., Mass and Momentum Transfer in Solid-Liquid Systems, Ind. Eng. Chem., Vol. 41, 1949, pp. 1124-1134.
- 6-71. Hobson, M., and Thodos, G., Paper Presented at Tulsa Regional Meeting, A. I. Ch. E. 1949.
- 6-72. Mickley, H. S., and Trilling, C. A., Heat Transfer Characteristics of Fluidized Beds, Ind. Eng. Chem., Vol. 41, 1949, pp. 1135-1147.
- 6-73. Gamson, B. W., Heat and Mass Transfer, Chem. Eng. Prog., Vol. 47, 1951, pp. 19-28.
- 6-74. Leva, M., Weintraub, M., Grummer, M., Heat Transmission Through Fluidized Beds of Fine Particles, Chem. Eng. Prog., Vol. 45, 1949, pp. 563-572.
- 6-75. Leva, M., and Grummer, M., A Correlation of Solids Turnover in Fluidized Systems: Its Relation to Heat Transfer, Chem. Eng. Prog., Vol. 48, 1952, pp. 307-313.
- 6-76. McCarter, R. J., Stutzmann, L. F., and Koch, H. A., Temperature Gradients and Eddy Diffusivities in Turbulent Fluid Flow, Ind. Eng. Chem., Vol. 41, 1949, pp. 1290-1295.
- 6-77. Dallavalle, J. M., The Theory and Practice of Pneumatic Conveying, Heat. and Ventil., Vol. 39, 1942, pp. 28-32.
- 6-78. Cramp, W., Pneumatic Transport Plants, Chemistry and Industry, Vol. 44, 1925, pp. 207-213.
- 6-79. Gasterstädt, D., An Experimental Investigation of Pneumatic Transport, Z. Verein deut. Ing., Vol. 68, 1924, pp. 617-624.
- 6-80. Segler, G., Pneumatic Transport of Grain, Z. Varien deut. Ing. Vol. 79, 1935, pp. 558-559.
- 6-81. Vogt, E. G., and White, R. R., Friction in the Flow of Suspensions, Ind. Eng. Chem., Vol. 40, 1948, pp. 1731-1738.
- 6-82. Farber, L., Flow Characteristics of Solids-Gas Mixtures in a Horizontal and Vertical Circular Conduit, Ind. Eng. Chem., Vol. 41, 1949, pp. 1184-1191.
- 6-83. Zenz, F. A., Two-Phase Fluid-Solid Flow, Ind. Eng. Chem., Vol. 41, 1949, pp. 2801-2808.
- 6-84. Lapple, C. E., and Shepherd, C. B., Calculation of Particles Trajectories, Ind. Eng. Chem., Vol. 32, 1940, pp. 605-617.
- 6-85. Hariu, O. H., and Molstad, M. C., Pressure Drop in Vertical Tubes in Transport of Solids by Gases, Ind. Eng. Chem., Vol. 41, 1949, pp. 1148-1160.
- 6-86. Jennings, M., Pneumatic Conveying in Theory and Practice, Engineering, Vol. 150, 1940, pp. 361-363.
- 6-87. Köhler, H., Sizes of Water Drops in Clouds and Condensation, Met. Z., Vol. 38, 1921, pp. 359-365.
- 6-88. Findeisen, W., Measurements of Size and Number of Fog Droplets, Gerlands Beitr. Geophysik, Vol. 35, 1932, pp. 295-340.
- 6-89. Langmuir, I., and Bladgett, K., A Mathematical Investigation of Water Droplet Trajectories, A. A. F. Tech. Rep. 5418, Air Materiel Command, Wright-Patterson Air Force Base, 1946.

- 6-90. Dady, G., Contribution to the Study of Precipitation, C. R. Acad. Sci. (Paris), Vol. 225, 1947, pp. 1349-1350.
- 6-91. Swinbank, W. C., Collision of Cloud Droplets, Nature, London, Vol. 159, 1947, pp. 849-850.
- 6-92. Gunn, K., and Hitschfeld, W., Laboratory Investigation of Coalescence Between Large and Small Water-Drops, J. Met., Vol. 8, 1951, pp. 7-16.
- 6-93. Deriagin, B., and Prokhorov, P., On the Cause of the Non-Coalescence of Liquid Drops Upon Contact, C. R. Acad. Sci. USSR, Vol. 54, 1946, pp. 511-514.
- 6-94. Perrie, D. W., Cloud Physics, John Wiley and Sons, Inc., New York, 1950.
- 6-95. Langmuir, I., The Growth of Particles in Smokes and Clouds and the Production of Snow From Supercooled Clouds, Proc. Amer. Phil. Soc., Vol. 92, 1948, pp. 167-185.
- 6-96. Houghton, H. G., and Radford, W. H., On the Measurement of Drop Size and Liquid Water Content in Fogs and Clouds, Pap, Phys. Ocean. Meteor., MIT and Woods Hole Ocean. Inst., Vol. 6, No. 4, 1938, pp. 1-31.
- 6-97. Fuchs, N., and Petrjanoff, I., Microscopic Examination of Fog, Cloud and Rain Droplets, Nature, Vol. 139, 1937, pp. 111-112.
- 6-98. Laws, J. O., Measurement of the Fall-Velocity of Water Drops and Rain Drops, Trans. Amer. Geophys. Union, Vol. 22, pp. 709-721.
- 6-99. Das, P. K., The Growth of Cloud Droplets by Coalescence, Indian J. Met. Geophys., Vol. 1, 1950, pp. 137-144.
- 6-100. Brandt, O., Heidemann, E., and Freund, H., Suspended Matter in a Sound Field, Z. Physik. Vol. 104, 1937, pp. 511-533.
- 6-101. St. Clair, H. W., Agglomeration of Smoke, Fog, or Dust Particles by Sonic Waves, Ind. Eng. Chem., Vol. 41, 1949, pp. 2434-2438.
- 6-102. King, L. V., On the Acoustic Radiation Pressure on Spheres, Trans. Roy. Soc. (London) Vol. 147 (Ser. A), 1934, pp. 233-236.
- 6-103. St. Clair, H. W., Spendlove, M. J., and Potter, E. V., Flocculation of Aerosols by Intense High-Frequency Sound, U. S. Bureau of Mines, Rept. Invest. 4218.
- 6-104. Fluidized Beds in the Chemical Industry, Chemie-Ingenieur-Technik, February, 1952.

Contrails

CHAPTER 7. THE THERMODYNAMICS AND KINETICS
OF EVAPORATION

ABSTRACT

A fundamental discussion is given of the principal factors that enter into both the thermodynamics and kinetics of evaporation. It is shown that both of these aspects of the evaporation process are interrelated through transition energies. Kinetics, however, determine the rate of material transport during the phase change by specifying the energy necessary for the activation of phase transitions having thermodynamic feasibility. Finally, it is demonstrated that the experimentally determined evaporation rates of a wide variety of liquids are in good agreement with the theoretical rates predicted by quantum statistics.

WADC TR 56-344

Contrails

THE THERMODYNAMICS AND
KINETICS OF EVAPORATION

by

F. Benington

One of the important actions preceding the combustion of a liquid fuel is the evaporation of the fuel. Since the degree of fuel vaporization determines, in part, the efficiency of combustion, a knowledge both of the process of evaporation, and of the extent to which it takes place at various points in the combustion chamber is important.

The main purpose of this Chapter is to discuss, from a somewhat fundamental standpoint, the principal factors that enter into both the kinetics and the thermodynamics of evaporation. As will be shown, both of these aspects of evaporation are, to a limited extent, interrelated through transition energies. Thermodynamics, however, is primarily concerned with process-energy changes, matter occupying a position of subsidiary importance. Kinetics, by way of contrast, principally involves the rate of material transport in a chemical reaction or in a phase change and is concerned only with the energy necessary for the activation of a process having thermodynamic feasibility.

Both the vapor pressure and the surface tension of liquid drops are discussed from the standpoint of the chemical potential of Gibbsian thermodynamics. This is the usual method of treating problems of phase transition, to which evaporation properly belongs. A transition is then made to Frenkel's theory of heterophase fluctuations, which concerns the statistical population of nuclei of a new phase growing out of an older phase. This theory is generally applicable to pretransition phenomena in either supercooled or superheated states without regard to the nature of the particular phase change, whether it be condensation or evaporation.

An extension of the Frenkel theory is then made to permit its use to develop the classical kinetics of phase transformation of Volmer, of Becker, and of Zeldovich. In this Chapter, the theory of the condensation process, as developed by these workers, will be presented, in order to preserve the original clarity of their presentation. However, the final rate expression for the condensation rate of a supercooled vapor can readily be applied to the opposite process of the "boil up", or evaporation of a liquid drop, which is of interest here; this is simply accomplished by interchanging the chemical potentials of each phase.

Because this Chapter follows, in most places, a chronological development of evaporation theories, it is natural that the application of Eyring's absolute rate theory should be the last point of discussion. It will be shown that evaporation satisfactorily follows the absolute rate theory for many substances.

THERMODYNAMIC THEORY OF THE EQUILIBRIUM BETWEEN
SUPERSATURATED VAPOR AND A DROP OF LIQUID

Surface phenomena play an important part in processes that are connected with phase changes. These changes include the transition of liquid to gas (evaporation) and gas to liquid (condensation). The theory of phase change, from the thermodynamic standpoint, does not furnish information as to the rate of phase transformation, but gives only the conditions under which two

phases may coexist in equilibrium for any length of time. It is evident that the growth of a new preliquid phase (B), after its initiation in a system, can continue at a finite velocity at the expense of an initial vapor phase (A), only if a nonequilibrium condition exists. The deviation from equilibrium need not be large when the new phase is sufficiently developed. Much larger deviations exist, however, during the initiation of a new phase in the form of "embryonic nuclei". This departure from equilibrium may be described as "metastable", which means that it can exist for a finite length of time. A common example of a metastable state is the superheated liquid, which does not boil although its temperature is above that of the thermodynamic boiling point, which corresponds to an equilibrium between the vapor pressure and the external pressure.

Surface Energy, Vapor Pressure, and Drop Size

If we neglect, for the present, the manner in which a nucleus of phase (B) originates and consider the factors that influence the growth of this phase, we must take into account the fact that the small physical dimensions of the nucleus obviously imply a large ratio of its surface to its volume in comparison with a macroscopic body. Accordingly, the surface energy of the nucleus and the free energy of formation of this surface must constitute an important contribution to the change in the total energy or free energy of a system in which nucleation is taking place. If we consider the surface energy of the nucleus of the (B) phase with respect to a metastable (A) phase, in which the nuclei are suspended as colloidal particles, then the idea of thermodynamic equilibrium between (A) and (B) may be extended according to the treatment of Frenkel⁽⁷⁻¹⁾. According to this theory, the nuclei of (B), of a given shape and size, should remain in equilibrium with the medium (A), in spite of the fact that (A) is not in equilibrium with a fully developed (B) phase.

In the following thermodynamic argument, a drop and its surrounding gas may be regarded as being a closed, isobaric, isothermal system. At equilibrium, the free energy of the system is equal to the work function of the system. Since the work function must vanish under these conditions, then,

$$P_B dV_B + P_A dV_A - \sigma dA = 0 \quad ,$$

where P_i is the pressure of a particular phase; dV_i is the change in volume of a particular phase; dA is the change in surface area of the drop which corresponds to an infinitesimal increase in the drop radius; and σ is the surface tension of the liquid phase measured at a plane surface.

Since a closed system must be at constant volume, it follows that $dV_A = -dV_B$ and that,

$$(P_B - P_A) dV_B - \sigma dA = 0 \quad .$$

By replacing both dV_B and dA by the corresponding drop-radius dependent functions,

$$(P_B - P_A) 4\pi r^2 dr = 8\pi r dr \quad ,$$

gives

$$(P_B - P_A) = \frac{2\sigma}{r} \quad .$$

This equation states that the internal pressure of a spherical drop must exceed the external pressure by $2\sigma/r$, as a condition for mechanical equilibrium of the drop.

In a system of this sort, we may express, conveniently, the total free energy of the system as Φ , the total thermodynamic potential. Then,

$$\Phi = N_A \phi_A + N_B \phi_B + 4\pi r^2 \sigma \quad , \quad (7-1)$$

where the N_i and ϕ_i are respectively the mol numbers and chemical potential of a particular phase. At equilibrium, $\delta\phi = 0$, and also $N_A + N_B = \text{const}$. Therefore, by performing the variations on Equation (7-1),

$$\delta\phi = (-\delta N_B)\phi_A + (\delta N_B)\phi_B + 4\pi(\delta r^2)\sigma = 0 \quad (7-2)$$

Let V_B equal the molecular volume of phase (B); the number of moles, N_B , in this volume is $N_B = 4\pi r^3/3V_B$, and

$$\left(\frac{dN_B}{dr}\right) = \frac{4\pi r^2}{V_B} \quad (7-3)$$

After performing the indicated differentiations in Equation (7-2) and substituting from Equation (7-3), there results:

$$\phi_B - \phi_A + \frac{2\sigma}{r} V_B = 0 \quad (7-4)$$

where, in the limiting case, as $r \rightarrow \infty$, $\phi_A = \phi_B$.

Since $(\partial\phi_i/\partial P)_T = V$, then $d\phi_A = V_B dP$ and $d\phi_B = V_A dP$. By differentiation of Equation (7-4) and by substituting the differentials of the chemical potentials into the result, we have:

$$(V_B - V_A) dP + 2\sigma V_B d(1/r) = 0 \quad (7-5)$$

By assuming that $V_A \gg V_B$ and that the ideal gas law is obeyed, Equation (7-5) becomes:

$$\frac{kT}{P} dP = 2\sigma V_B d(1/r)$$

or

$$kT \int_{P_\infty}^P \frac{dP}{P} = 2\sigma V_B \int_{\infty}^r d(1/r) \quad (7-6)$$

where k is the gas constant per molecule, that is $k = R/N$, where R is the gas constant and N is Avogadro's number; upon integration, Equation (7-6) gives

$$\ln P/P_\infty = \frac{2\sigma V_B}{rkT} \quad (7-7)$$

Shereshefsky⁽⁷⁻²⁾ attempted to verify Equation (7-7) by measuring the vapor pressure of several liquids and their corresponding radii of curvature, in small capillaries. He showed that the lowering of the vapor pressure in the capillaries is much greater than would be predicted by this equation. He concluded that this departure can be attributed to a change in surface tension with drop size. Unfortunately, no account was given of the magnitude of the experimental error and consequently, comparisons cannot be made of this work with other investigations.

From purely theoretical considerations, Tolman⁽⁷⁻³⁾ has shown that considerable change in surface tension with droplet size may be expected; the effect is quite significant for very small droplets. From the classical thermodynamics of Gibbs, the surface tension σ is related to ϕ , the chemical potential of the gas phase by:

$$d\sigma = -\Gamma d\phi \quad (7-8)$$

where Γ is the superficial density of the interphase boundary. The change in chemical potential with the internal pressure of the liquid phase or the vapor phase is:

$$d\phi = \frac{dP'}{\gamma'} - \frac{dP''}{\gamma''} \quad (7-9)$$

where γ' is the liquid density and γ'' the gas density. By combining Equations (7-8) and (7-9), and, then, by combining this result with the differentiated form of $P' - P'' = 2\sigma/r$, there results:

$$\frac{1}{\sigma} \left(\frac{d\sigma}{dr} \right) = \frac{\frac{2}{r^2} [\Gamma/(\gamma' - \gamma'')] }{1 + \frac{2}{r} [\Gamma/(\gamma' - \gamma'')] } \quad (7-10)$$

which expresses the rate of change of surface tension with drop radius.

Tolman then shows that $\Gamma/(\gamma' - \gamma'')$ is related to δ , the thickness of the interphase boundary layer, according to the equation:

$$\frac{\Gamma}{\gamma' - \gamma''} = \delta \left(1 + \frac{\delta}{r} + \frac{\delta^2}{3r^2} \right) \quad (7-11)$$

By substituting Equation (7-11) in Equation (7-10), we have:

$$\ln \frac{\sigma}{\sigma_{\infty}} = \int_{\infty}^r \frac{\left[\frac{2\delta}{r^2} \right] \left[1 + \frac{\delta}{r} + \frac{\delta^2}{3r^2} \right]}{1 + \left[\frac{2\delta}{r} \right] \left[1 + \frac{\delta}{r} + \frac{\delta^2}{3r^2} \right]} dr \quad (7-12)$$

where σ_{∞} is as defined earlier. Although the right-hand side of Equation (7-12) can be integrated to a result containing only elementary functions, it is much more convenient to carry out a numerical integration in the case where this integral is to be applied. However, if we are interested in the case where the phase boundary layer is very thin compared with the radius of the drop, $\delta \ll r$, we can then neglect the terms δ/r and δ^2/r^2 . After making this approximation, Equation (7-12) may be integrated to

$$\sigma/\sigma_{\infty} = (1 + 2\delta/r)^{-1} \quad (7-13)$$

Tolman points out that the most apparent weakness in his theory is in the assumption that δ is invariant with r . This assumption does not seem completely justified, in that δ is probably related to the intermolecular forces in the surface layer, and these forces would be dependent in some manner upon r .

Table 7-1 shows the manner in which σ/σ_{∞} varies with δ/r for both the approximate and exact, numerically integrated solutions of Equation (7-12).

TABLE 7-1. THE EFFECT OF BOUNDARY-LAYER THICKNESS ON SURFACE TENSION FOR SMALL DROPS

δ/r	σ/σ_{∞} (Approx.)	σ/σ_{∞} (Exact)
0	1	1
0.01	0.98	0.98
0.02	0.96	0.96
0.05	0.91	0.91
0.1	0.83	0.83
0.7	0.42	0.36
1.00	0.33	0.28

A comparison of the results in the middle and right-hand columns shows that the deviations between the approximate and the exact results become appreciable as the ratio δ/r becomes large; or, in other words, as r becomes small, which is the important case. Thus for small r 's, the exact solution should be used.

In contrast to Shereshefsky's results, which show considerable departure from Equation (7-7), Thomä(7-4) was able to verify Equation (7-7) for isovaleric acid. He employed an optical interference manometer having a sensitivity of 2×10^{-11} atmospheres to measure the differential liquid vapor pressure between a plane surface and a minute capillary. Adam(7-5), in analyzing Thomä's data, claims that these measurements were within an accuracy of 10 per cent which is probably the experimental error of these very delicate measurements.

Rodebush(7-6) has also examined the behavior of Equation (7-7) from the standpoint of thermodynamics. He concludes that this equation cannot hold below a drop size of 10^{-7} cm (133 water molecules), because it is impossible to speak of saturation pressure when the equilibrium pressure is dependent upon the concentration of molecular clusters present. As long as the saturation pressure is fixed with respect to a single drop, vapor-liquid equilibrium exists. When the aggregates become so small that their concentration becomes significant in determining equilibrium, we are dealing with homogeneous and not heterogeneous equilibrium.

Rodebush substantiates this viewpoint by the following treatment of the entropy of the droplet-vapor system:

The equilibrium between the vapor and molecular clusters may be expressed in terms of S_c , the cluster entropy by:

$$S_c = S_L + \frac{1}{n} (S^*)_{\text{coll}} + S_{\text{vap}} ,$$

where S_L is the entropy/mole of the liquid; $(S^*)_{\text{coll}}$ is the sum of translational and rotational entropies which contribute to the total entropy of an aggregate of n molecules in the gas phase; and S_{vap} is the entropy of vaporization.

The surface entropy can be written as $\Delta H/T$, where ΔH is the heat of vaporization of the liquid. From a comparison of Equation (7-7) with the Clausius-Clapeyron vapor-pressure equation, it is easily shown that:

$$-\frac{\Delta H}{T} = \frac{2\sigma V_B}{rT} .$$

Therefore, the entropy of a cluster may be written as:

$$S_c = S_L + \frac{1}{n} (S^*)_{\text{coll}} - \frac{2\sigma V_B}{rT} ,$$

where the last term shows the effect of surface tension in reducing the entropy of the liquid phase.

Figure 7-1 shows the entropy curves for the liquid S_L and the vapor S_V as a function of radius. The liquid entropy curve shows a minimum at a radius close to 10^{-7} cm. This minimum corresponds to the transition from cluster to drop.

The contribution of surface tension to the maximum decrease of entropy is about two entropy units. This portion of the entropy is small in comparison with the colligative entropy of the cluster. Since the aggregates which represent the liquid phase are in suspension, we may treat them as large molecules in a homogeneous vapor phase; this viewpoint implies that these macromolecules possess translational, rotational, and volume-concentration entropies. It can then be stated that the share of this entropy, per molecule, is $1/n$ of the total entropy, where n is the number of molecules per aggregate. When the number of molecules making up the aggregate is less than 100, this contribution from colligative entropy will more than offset the entropy decrease due to surface tension, and a minimum entropy must occur near a radius of 10^{-7} cm.

Controls

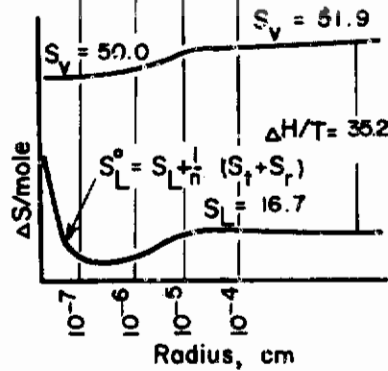


FIGURE 7-1. THE RANGE IN ENTROPY OF A WATER DROP AS A FUNCTION OF ITS RADIUS(7-6)

Heterophase Fluctuations in Phase Change

In the discussions above, reference was made to the concept of a transformation in phase (A) being preceded by the formation of "embryos" of a new phase (B). These embryos may consist of minute droplets or gas bubbles, or crystallites; the number of small embryos fluctuates in time, because some grow into substantial agglomerates of the new phase, while still others dissociate into molecules of the predominating phase (A).

Frenkel(7-7) has developed, through theoretical considerations, a statistical equation which permits the calculation of the number of embryos of a given size. His theory is quite general and is applicable to any phase transition. The two basic assumptions which are necessary for the development of this theory are that: (1) in the range of thermodynamic stability of phase (A), the latter is not homogeneous, but contains embryos of phase (B); and (2) the embryos of phase (B) are increasingly numerous as the rate of transition increases. The distribution function for N_g , the number of embryos consisting of g molecules is:

$$N_g = F \left(\frac{N_A}{F} \right)^g e^{- \left\{ (\Phi_B - \Phi_A)g + \mu g^{2/3} \right\} / kT} \quad , \quad (7-14)$$

where F is the total number of 'molecules' in the generalized sense, that is the nuclei of different sizes which are being treated as molecules of different kinds, N_A is the number of phase (A) molecules; Φ_i is the chemical potential of a particular phase; and μ is a constant proportional to surface energy.

Equation (7-14) may be written in the form:

$$N_g = F \xi^g e^{-\mu g^{2/3} / kT} \quad , \quad (7-15)$$

where

$$\xi = \frac{N_A}{F} e^{-(\Phi_B - \Phi_A) / kT} \quad . \quad (7-16)$$

This is convenient because it is now possible to show how the distribution function varies with temperature and pressure.

Suppose that the temperature T of the system in question is close to the equilibrium temperature T_0 . This, of course, corresponds to an equilibrium pressure P_0 between phases (A) and (B). At equilibrium, $\Phi_A(P_0, T_0) = \Phi_B(P_0, T_0)$, and the difference in chemical potential between the phases may be written in the following approximate form:

$$\Phi_B - \Phi_A = \left[\left(\frac{\partial \Phi_B}{\partial T} \right)_{T=T_0} - \left(\frac{\partial \Phi_A}{\partial T} \right)_{T=T_0} \right] [T - T_0] .$$

Because

$$\left(\frac{\partial \Phi_i}{\partial T} \right)_{T=T_0} = S_i^\circ ,$$

the standard molecular entropy of phase i , we may write

$$\Phi_B - \Phi_A = (S_B^\circ - S_A^\circ)(T - T_0) . \quad (7-17)$$

The entropy of the phase transition is related to λ , the heat of transition by

$$(S_B^\circ - S_A^\circ) = -\lambda/T_0 .$$

Therefore, the temperature dependence of the difference in chemical potential is:

$$\Phi_B - \Phi_A = -\lambda \frac{T - T_0}{T_0} . \quad (7-18)$$

From this relation, it may be seen that in the pretransition state of (A), $\Phi_B > \Phi_A$, that is, $T < T_0$ if $\lambda < 0$, or $T > T_0$ if $\lambda > 0$. Corresponding to the supercooled or superheated state of (A), we have the condition that $\Phi_A > \Phi_B$. This is possible if $T > T_0$ for $\lambda > 0$, or $T < T_0$ for $\lambda < 0$.

By substituting from Equation (7-18) into Equation (7-16), there results:

$$\xi = \left(N_A/F \right) e^{\lambda(T - T_0)/kT_0^2} \approx e^{\lambda(T - T_0)/kT_0^2} ,$$

where

$$N_A \approx F .$$

An examination of the behavior of ξ , the chemical-potential dependent portion of the distribution, with pressure, yields a somewhat more interesting result. If we assume a fixed T while the pressure varies from its corresponding equilibrium value, we may then write:

$$\Phi_B(P, T_0) - \Phi_A(P, T_0) = \left(\frac{\partial \Phi_B}{\partial P} - \frac{\partial \Phi_A}{\partial P} \right)_0 (P - P_0) . \quad (7-19)$$

Since

$$\left(\frac{\partial \Phi_i}{\partial P} \right) = V_L^\circ ,$$

the molecular volume of a phase in an equilibrium state of the phase, Equation (7-19) may be re-written as:

$$\Phi_B - \Phi_A = (V_B^* - V_A^*)(P - P_0) \quad (7-20)$$

Substitution of this form of the chemical potential in Equation (7-16) gives:

$$\xi = \frac{N_A}{F} e^{(V_B^* - V_A^*)(P - P_0)/kT_0} \quad (7-21)$$

If it is supposed that P is smaller than the equilibrium (saturation) pressure P_0 , then, upon substituting the approximate expressions

$$(V_B^* - V_A^*) \cong -V_A^* = \frac{kT_0}{P_0}$$

and $F \cong N_A$ into Equation (7-21), there results:

$$\xi = e^{-(P_0 - P)/P_0} \quad (7-22)$$

In the instance of a supersaturated vapor, a relation between P and g_c , the critical value of g for a minimum N , can be found by equating dN_g/dg , in Equation (7-15), to zero and substituting the above form of ξ . This result may be written

$$\frac{P - P_0}{P_0} = \frac{2}{3} \frac{\mu}{kTg_c^{1/3}}$$

It is of interest to note that this equation is merely an approximate form of Equation (7-7), with P_0 standing for P_∞ , and with $\log(P/P_\infty)$ replaced by $(P/P_\infty) - 1$. It may also be seen that $\mu/3g_c^{1/3}$ corresponds to $2\sigma V_B/r_c$ in Equation (7-7), where r_c is the critical radius of the drop.

The latter relation must follow from the definition of surface energy, $4\pi r^2\sigma = \mu g^{2/3}$, in conjunction with $4\pi r^3 = gV_B$.

Equation (7-7) may be obtained in exact form if $\Phi_B - \Phi_A$, in the pressure dependent case, is replaced by:

$$\Phi_B - \Phi_A = \int_{P_0}^P (V_B - V_A) dP \cong -kT \ln P/P_0$$

An experimental verification of the theory of heterophase fluctuations has not, as yet, been carried out. The principal difficulty that would be encountered in such an investigation is the measuring of a low concentration of liquid embryos in the presence of normal unassociated gas molecules. Frenkel⁽⁷⁻⁷⁾ has suggested that the steady-state concentration of liquid-phase embryos might be measured by the Raman scattering produced by the condensed phase. Landsburg⁽⁷⁻⁸⁾ has already shown, through Raman scattering measurements carried out on vapors at high pressures and near the critical temperature, that embryos can be detected. However, his work lends only qualitative support to the theory of heterophase fluctuations. Frenkel also suggests that a measurement of the extinction of ultrasonic waves might be a satisfactory means for detecting embryonic gas bubbles in a liquid phase; his suggestion is based on the fact that a gas phase possesses a relatively higher compressibility than does the liquid phase. Such measurements would obviously require extremely sensitive and stable sonic-measuring devices.

The application of statistical thermodynamics to a system in a metastable pretransition state can only yield results that are valid over a short time interval. This limitation is imposed because a thermodynamic treatment of the system assumes equilibrium. A second limitation of this particular treatment is imposed by the fact that the system is assumed to consist of ideal rigid spherical molecules. In a more realistic treatment, the interaction forces between real molecules in both the liquid and the gas states would be considered.

Treatment by Classical Statistics

In the kinetic treatment of phase transition, we will extend the previously derived thermodynamic results to predict the rate at which a phase change will take place. Although thermodynamics alone cannot predict this rate, this approach does form a part of the foundation upon which the rate-process equations are constructed.

Although many qualitative speculations have been made concerning the mechanism of evaporation and condensation, Volmer and Weber⁽⁷⁻⁹⁾ appear to be the first workers to have proposed a theoretical treatment of these processes in a supersaturated vapor. In this treatment, Equations (7-15) and (7-16), which express the number of the phase (B) embryos in the quasi-homogeneous system (A) + (B), are used with the provision that all embryos which greatly exceed the critical number g_c are to be eliminated from consideration. The critical number g_c is defined by the maximum of:

$$\Delta\Phi = (\Phi_B - \Phi_A)g + \mu g^{2/3} ,$$

which is

$$g_c = \left(\frac{2}{3} \frac{\mu}{\Phi_A - \Phi_B} \right)^3 .$$

Statistically, the number of phase (B) nuclei is given by:

$$N_{g_c} = F \left(\frac{F}{N} \right)^{g_c} e^{-(\Delta\Phi)_{\max}/kT} ,$$

or approximately by:

$$N_{g_c} = N e^{-\left\{ \frac{\mu g_c^{2/3}}{3 kT} \right\}} . \tag{7-23}$$

In the process of growth, the drops pass through a critical size, which, when exceeded, results in rapid macroscopic condensation. The velocity of this process is proportional to the number of drops of critical size which exist in the system at any instant. This critical number is given by Equation (7-23).

From the standpoint of gas dynamics, the velocity of condensation of the vapor is the product of N_{g_c} by the number of single vapor molecules which strike the total surface of the droplets in the system. This collision number, per unit area, is:

$$\beta = A \left(\frac{kT}{2\pi m} \right)^{1/2} = P (2\pi mkT)^{-1/2} , \tag{7-24}$$

where A is the total number of molecules in the gas phase, (A) , and m is the mass of one molecule of the gas. The condensation velocity, as defined, for the total area of spheres of critical radius is, therefore:

$$Q = 4\pi r_c^2 P N e^{-4\pi\sigma r_c^2/kT} (2\pi mkT)^{-1/2}, \quad (7-25)$$

where the radius of the drop and \underline{g} are related by means of $\mu g^{2/3} = 4\pi r_c^2 \sigma$.

Kaishev and Stranski⁽⁷⁻¹⁰⁾ have derived a somewhat more refined relation than that given by Volmer and Weber. The expressions derived may be applied to: (1) the formation of liquid nuclei in a saturated vapor, (2) the growth of simple cubic-lattice crystals from supersaturated vapor, and (3) the formation of gas nuclei in a superheated liquid. Each of these results is, however, based on Equation (7-25) and its characteristic exponential term.

Farkas⁽⁷⁻¹¹⁾ also extended Volmer and Weber's theory to give a simple expression for computing the rate of liquid nucleus formation in a supersaturated vapor. According to this work, the rate of nucleation is constant as long as the initial conditions remain fixed; the rate of formation is in close agreement with that predicted by Equation (7-25).

Following the early work on the kinetic aspects of phase transition, Becker and Döring⁽⁷⁻¹²⁾ formulated a better approximate theory based upon the earlier treatment of Frenkel⁽⁷⁻¹³⁾. The Becker and Döring work appears to be the most satisfactory approach to the problem in spite of the fact that it is somewhat unrealistic⁽⁷⁻¹⁴⁾. They rejected the purely thermodynamic approach of the early workers and attacked the problem from a kinetic standpoint, taking into account the influence of evaporation on condensation rates. It is of interest to note that their rate equation may be applied either to evaporation or to condensation. In the derivation which is to follow, a condensation process will be used as before.

If α_g is the number of molecules which are evaporated per unit area, per unit time, from the surface S_g of a drop composed of \underline{g} molecules ($g \geq 2$), then $S_g \alpha_g dt$ is the probability that the drop will lose one molecule by evaporation in time dt . Similarly, $S_g \beta dt$ is the probability of the condensation of a single molecule on the same drop. If the system consisting of phases (A) + (B) is in a stable state, then by the principle of detailed balance:

$$N_g S_g \alpha_g = N_{(g-1)} S_{(g-1)} \beta \quad (7-26)$$

It can be shown by a somewhat lengthy proof that,

$$\frac{N_g}{N_{g-1}} \approx \frac{N_A}{F} e^{-\left[(\Phi_B - \Phi_A) + 2/3 \mu g^{-1/3} \right] / kT}, \quad (7-27)$$

where symbols have the same meaning as used previously. By substituting from Equation (7-27) into Equation (7-26), we have:

$$\alpha_g = \frac{F}{N_A} e^{\left[(\Phi_A - \Phi_B) + 2/3 \mu g^{-1/3} \right] / kT} \quad (7-28)$$

If the case where $g \gg 2$ is considered, then the ratio $S_{g-1}/S_g \approx 1$. Also F/N_A will be close to unity if the total number of drops is small. Using these approximations in conjunction with the relation:

$$\frac{2\sigma V_B}{r_g} = \frac{2}{3} \mu g^{-1/3},$$

Equation (7-28) becomes:

$$\alpha_g = \beta e^{(1/kT)(\Phi_A - \Phi_B + \frac{2\sigma V_B}{r_g})} \quad (7-29)$$

It is interesting to note how α_g behaves for drops of the critical size. By substituting from Equation (7-29) and then introducing the pressure-dependent form of the chemical potential,

$$\Phi_B - \Phi_A \approx -kT \log \left(\frac{P}{P_0} \right) ,$$

into this result, we have:

$$\alpha_{g_c} = \beta . \quad (7-30)$$

This result expresses the fact that at critical drop size, the condensation rate is just equal to the evaporation rate.

The validity of the expression for α_g is independent of the existence of equilibrium in the distribution of (B) embryos with respect to their size, as long as the velocities and coordinates of the molecules both in the liquid and in the gas phase preserve a Maxwellian distribution. The relaxation time required for the establishment of this equilibrium is always extremely short in comparison with the time required for the establishment of an equilibrium distribution of embryos with respect to their size.

We may now derive the nonequilibrium (kinetic) equations of evaporation or condensation in a system consisting of phases (A) and (B), using the previously derived equations for both α_g and β . It is now necessary to replace N_g and $N_{(g-1)}$ by the symbols f_g and $f_{(g-1)}$, which denote these numbers in a nonequilibrium distribution. Since Equation (7-26) would not be valid if f_i were substituted for N_i , we must use a new relation between the evaporation and condensation rates. If I_g is taken to be the difference between the number of drops which, by condensation, pass from class (g-1) to class g , and those which pass by evaporation from class g to class (g-1), we may write:

$$I_g = f_{(g-1)} S_{(g-1)} \beta - f_g S_g \alpha_g . \quad (7-31)$$

By substituting α_g from Equation (7-26) into Equation (7-31), I_g , in terms of the collision rate is:

$$I_g = N_{(g-1)} S_{(g-1)} \beta \left(\frac{f_{(g-1)}}{N_{(g-1)}} - \frac{f_g}{N_g} \right) . \quad (7-32)$$

The kinetic expression for the time rate of change of drops passing from one class to another is:

$$\left(\frac{f_g}{t} \right) = I_g - I_{(g+1)} . \quad (7-33)$$

If we consider the drop surface as a function of g , that is, $S(g)$, then for moderately large values of g ,

$$S_{(g-1)} \beta \approx S(g) \beta = D(g) . \quad (7-34)$$

The $D(g)$ term is a measure of the diffusion of the drop through space as a function of the number of molecules which it contains. This diffusion rate is related to the mobility of the drop, q , through Einstein's relation $q = D/kT$, where the diffusion coefficient is:

$$D = \left\{ 4\pi(3^2) V_B^2 g^2 \right\}^{1/3} \beta .$$

By taking into account the approximation used in Equation (7-34) and by treating g as a continuous variable, Equation (7-32) may be written as:

$$I(g) = -N(g) S(g) \beta \frac{\partial}{\partial g} \left[\frac{f(g)}{N(g)} \right] \quad (7-35)$$

where the partial derivative replaces the finite difference. Substitution of $S(g)$ in Equation (7-35) by the diffusion term in Equation (7-34) gives

$$I(g) = -D(g) N(g) \frac{\partial}{\partial g} \left[\frac{f(g)}{N(g)} \right] \quad (7-36)$$

After expansion of the derivative in this equation and rearranging terms,

$$I = -D \frac{\partial f}{\partial g} + Df \left(\frac{\partial \log N}{\partial g} \right) \quad (7-37)$$

Since we have shown generally that $N(g) = Ce^{-\Delta\Phi/kT}$, Equation (7-37) can be written as:

$$I = -D \frac{\partial f}{\partial g} - \frac{D}{kT} f \left(\frac{\partial \Delta\Phi(g)}{\partial g} \right) \quad (7-38)$$

This equation is analogous, in form, to the equation for the diffusion-dependent flow of particles distributed over the g -axis with a density $f(g)$. The thermodynamic potential $\Delta\Phi(g)$ may be likened to an external driving force which brings about the diffusion transport in the system.

A final kinetic equation for $f(g)$, the nonequilibrium distribution function, may be had by re-writing Equation (7-33) as:

$$\frac{\partial f}{\partial t} = I_{(g-1)} - I_g = -\frac{\partial I}{\partial g} \quad ,$$

and by, in turn, substituting this result in the differentiated form of Equation (7-38). This gives,

$$\frac{\partial f}{\partial t} = -\frac{\partial I}{\partial g} = -D \frac{\partial f}{\partial g} + \frac{1}{kT} \frac{\partial}{\partial g} \left(Df \frac{\partial \Delta\Phi}{\partial g} \right) \quad (7-39)$$

Equation (7-39) does not correspond to the simple analogue given for Equation (7-38); the essential difference is that D is now taken as dependent upon g . However, this dependence is weaker than that of $f(g)$, especially when a narrow range of f is taken which is close to the point where $g \approx g_c$.

Becker and Döring obtained a satisfactory solution to this equation by resorting to the sort of approximations used in solving similar equations which arise in connection with electrical networks. In this method, the summations which appear in the general solution of Equation (7-39) are replaced by integrals. This method of solution is complex and involves numerous assumptions. (7-15)

Seven years after the Becker and Döring work, Zeldovich⁽⁷⁻¹⁶⁾ succeeded in solving Equation (7-39) by a simple mathematical technique. The accuracy of his solution is equal to that of the original workers. He considers first the steady-state distribution where $(f/t) = 0$. This is equivalent to writing Equation (7-39) in partially integrated form. Since $I(g)$ must be constant under this assumption, Equation (7-36) must satisfy this condition. Equation (7-36) may be integrated to:

$$f(g) = I N(g) \int_g^G \frac{dg}{N(g) D(g)} \quad (7-40)$$

where G is an arbitrary, finite, upper limit. It is now assumed that all g to be considered lie close to the critical value g_c ; this is equivalent to selecting a range of the independent variable corresponding to the minimum value of $N(g) = Ce^{-\Delta\Phi/kT}$.

By substituting for $N(g)$ in Equation (7-40) the distribution is:

$$f(g) = I e^{-\Delta\phi/kT} \int_g^G \frac{e^{\Delta\phi/kT} dg}{D(g)} \quad (7-41)$$

Now, $e^{\Delta\phi/kT}$ can be shown to possess a sharp maximum at the critical value of g . It is convenient to expand $\Delta\phi$ in a Taylor series about $(g-g_c)$. This yields:

$$\Delta\phi = \Delta\phi_{\max} - \gamma \frac{(g-g_c)^2}{2} \quad (7-42)$$

where

$$\gamma = \left(\frac{\Delta\phi}{g} \right)_{g=g_c} \quad (7-42)'$$

The higher terms of the expansion are neglected since g is selected close to g_c . Upon substituting this expansion in Equation (7-41) and also using $D(g_c)$ for $D(g)$, the distribution becomes:

$$f(g) = \frac{I}{D(g_c)} \exp \left[\frac{\Delta\phi(g_c) - \Delta\phi(g)}{kT} \right] \int_{-(g_c-g)}^{G-g_c} e^{-\gamma\xi^2/2kT} d\xi \quad (7-43)$$

where the dummy variable of integration is $\xi = g - g_c$.

Equation (7-43) may be reduced to an easily integrated form if:

$$G - g_c \gg \sqrt{\frac{kT}{\gamma}} \quad ,$$

and

$$g_c - g \gg \sqrt{\frac{kT}{\gamma}} \quad ,$$

where these intervals are illustrated in Figure 7-2. These inequalities simply place permissible limitations upon the range of g with respect to g_c . Under the conditions of these inequalities, the limits of integration become $\pm \infty$.

Introducing $N(g)/C$ for $e^{-\Delta\phi(g)/kT}$ in Equation (7-43), and using the new limits of integration gives

$$\frac{f(g)}{N(g)} = \frac{I}{CD(g_c)} e^{\Delta\phi(g_c)/kT} \int_{-\infty}^{+\infty} e^{-\gamma\xi^2/2kT} d\xi \quad (7-44)$$

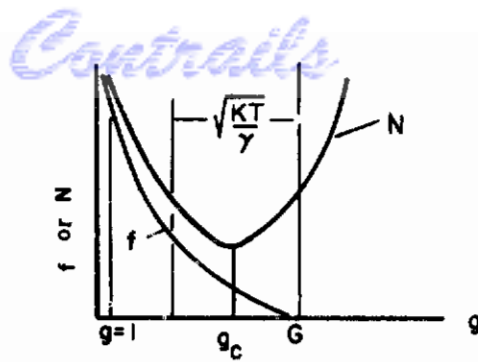


FIGURE 7-2. RELATION OF f AND N to g

The above integral is symmetric in its integrand and may be taken as twice the integral over the limits of 0 to ∞ . This is the familiar Euler integral that appears in many statistical problems; its value is

$$\sqrt{\frac{2\pi kT}{\gamma}}$$

Equation (7-44) may then take the form

$$\frac{f(g)}{N(g)} = \frac{I}{CD(g_c)} e^{\Delta\Phi(g_c)/kT} \left(\frac{2\pi kT}{\gamma}\right)^{1/2} \quad (7-45)$$

Figure 7-2 graphs the behavior of both N and f as functions of g . It may be seen that for $g \ll g_c$, the nonequilibrium distribution $f(g)$ must be nearly equal to $N(g)$. It then follows that this equivalence must hold also in the range $g \approx 1$ to $g \approx g_c - \sqrt{kT/\gamma}$. In other words, when the number of molecules constituting the embryo is considerably less than the critical number for rapid macroscopic growth of a phase, the nonequilibrium and equilibrium distributions are nearly equal.

Figure 7-2 shows also that the equilibrium distribution $N(g)$ becomes a minimum at g_c , then increases for $g > g_c$. The corresponding nonequilibrium distribution $f(g)$ takes a value of $N(g)/2$ at g_c , then vanishes for values of $g \approx G$.

For the range $g \ll g_c$, Equation (7-45) may be set equal to unity. This, with the substitution of $N(g_c)$ for the product of constant C and the exponential term, as was done in connection with Equation (7-33), gives

$$I = D(g_c) C e^{-\Delta\Phi(g_c)/kT} \left(\frac{\gamma}{2\pi kT}\right)^{1/2} = N(g_c) D(g_c) \left(\frac{\gamma}{2\pi kT}\right)^{1/2} \quad (7-46)$$

The coefficient C is thus identified with N , the total number of molecules in the vapor phase.

Finally, Equation (7-46) can be transformed into an expression for Q/N , the ratio between the number of collisions which result in condensation and the number of vapor-phase molecules which are present in the system. Equation (7-46) is first reduced to an equation in r_c , the critical radius. This is accomplished in two steps. First, by combining $D(g_c) = S(g_c)\beta$, $S(g_c) = 4\pi r_c^2$ and $\beta = P(2\pi mkT)^{-1/2}$, the diffusion coefficient becomes

$$D(g_c) = 4\pi r_c^2 P(2\pi mkT)^{-1/2} \quad (7-47)$$

Then, by combining Equation (7-47) with Equation (7-36) and substituting $4/3\pi r_c^2$ for $\Delta\Phi(g_c)$, we have

Contrails

$$\frac{Q}{N} = 2\pi r_c^2 \frac{P}{kT} \frac{\gamma}{m}^{1/2} g_c e^{-4\pi r_c^2 / 3kT} \quad (7-48)$$

The elimination of γ from Equation (7-48) is carried out by differentiating

$$\Delta\phi = -(\phi_A - \phi_B) g + \mu g^{2/3}$$

with respect to g , replacing μ , in the derivative, from

$$g_c = \left(\frac{2}{3} \frac{\mu}{\phi_A - \phi_B} \right)^{2/3}$$

and, again, differentiating with respect to g to give an expression of the form of Equation (7-42) from which,

$$\gamma = 1/3 (\phi_A - \phi_B) / g_c \quad ,$$

which, in turn, is substituted into Equation (7-48) to give the resulting expression

$$\frac{Q}{N} = 2\pi r_c^2 e^{-4\pi r_c^2 / 3kT} \frac{P}{kT} \left(\frac{1}{3} \frac{(\phi_A - \phi_B) g_c}{m} \right) \quad (7-49)$$

This result is practically the same as that resulting from the more elaborate treatment of Becker and Döring. It differs somewhat from Volmer and Weber's expression which is given by Equation (7-25).

The Becker-Döring-Zeldovich theory shows limited agreement with the experimental data of Volmer and Flood⁽⁷⁻¹⁷⁾ which was taken on the adiabatic expansion of air containing water vapor. These workers found a value of 5.03 for P/P_∞ (cf. Equation 7-7) at 261° K for the condensation process; if $\log_e I = 1$ (corresponding to 2.7 nuclei formed/cm²/sec) the theoretical value for $P/P_\infty = 5.14$ for this temperature; however, very small changes in P/P_∞ cause correspondingly large changes in I .

Sander and Damköhler⁽⁷⁻¹⁸⁾ studied the critical supersaturation pressure of air-water vapor as a function of temperature and found that for $\log_e I = 1$, P/P_∞ can be expressed as

$$\log_e P/P_\infty = (780/T) - 1.521 \quad .$$

This result is in reasonably good agreement with the Becker and Döring theory since the latter requires that if I is constant, $\log P/P_\infty$ is proportional to $T^{-3/2}$ providing that the pre-exponential term is nearly independent of T . Sander and Damköhler have also proposed a theoretical expression for I in terms of a number of molecules which are required for a critical nucleus. Their condensation data, however, did not fit this theoretical expression unless the surface energy of water was taken as being less than the value obtained by linear extrapolation from higher temperatures. There is, of course, a possibility that such a nonlinear dependence might exist for the case of supercooling; it may thus be possible to explain these results on the basis of the size of the critical nucleus becoming very small for large values of P/P_∞ . Hence, the variation of the interfacial free energy with the radius of the drop might be considered in light of the arguments presented by LaMer and Pound⁽⁷⁻¹⁹⁾.

By a slight modification in the preceding theory, we may easily demonstrate that by interchanging (A) and (B), Equation (7-49) may be applied to the reverse process of the boiling up of a liquid drop, in which a metastable state exists because of a negative pressure or overheating.

Prior to 1948, no attempt was made to treat the evaporation of droplets from the viewpoint of the Eyring theory of absolute reaction rates. Penner(7-20) first demonstrated that this theory might be applied to the evaporation process to give some useful results. In the most recent development of Penner's work, it is necessary to make certain assumptions regarding the nature of the "activated complex" associated with the process, which will presently be discussed.

In the first treatment of evaporation, Penner develops an expression for calculating the maximum possible rate of isothermal vaporization of a liquid drop. It is first assumed that evaporation is a first order process, that is, that the rate of evaporation is proportional to the number of molecules exposed at the surface of the drop. Two equally important additional assumptions are that a Maxwell-Boltzmann distribution of molecular velocities exists in the liquid and that the molecules that escape from the drop surface have an energy that is in excess of the energy of vaporization ΔE_{vap} . The final rate equation is

$$-\left(\frac{dr}{dt}\right) = e \left(\frac{2\Delta H_{\text{vap}}}{kT\gamma}\right)^{1/2} u e^{-\Delta H_{\text{vap}}/kT}, \quad (7-50)$$

where γ is the specific heat ratio; u is the velocity of sound in the liquid; and e , the base of natural logarithm enters as a coefficient. The variables γ and u in this equation are introduced from the equation for the mean free path of the liquid-phase molecules, Reference (7-21).

When the rates of evaporation, calculated from Equation (7-50), are compared with the corresponding rates calculated from

$$-\left(\frac{dr}{dt}\right) = \frac{p_s}{\rho_L} \left(\frac{M}{2\pi kT}\right)^{1/2}, \quad (7-51)$$

where p_s is the saturation pressure of the liquid; ρ_L is the density of the liquid; and M is the molecular weight; the results agree well with the measured rates found for most nonpolar liquids. Equation (7-51) is based upon the classical kinetic theory of gases, and was first proposed by Knudsen(7-22).

Table 7-2 shows the rates of evaporation for several liquids as predicted by both Equations (7-50) and (7-51) at various temperatures. The column headed Z is the ratio of the rate from Equation (7-51) to the rate from Equation (7-50). The agreement between equations is relatively poor for polar liquids, such as for the alcohol shown and for water; this can probably be attributed to the lack of a correcting term in Equation (7-50) for the degree of association of these compounds. Calculations indicate that the value of Z for water decreases rapidly with increasing temperature, but that Z does not reach unity even at the boiling point.

An examination of the figures given for hydrocarbons shows that for short chain lengths (low molecular weights), the agreement is relatively good, while with longer chains, considerable difference exists between values. Penner attributes these differences to the fact that in deriving his equation, a free-sphere model of the molecule is used; the geometry of higher hydrocarbon molecules does not permit a good spherical approximation to be made. Compact cyclic molecules, such as benzene and cyclohexane, show an agreement which is close to that of the lower paraffins.

The last material tabulated is mercury, which exhibits a large departure. This is to be expected because liquid metals do not behave as perfect liquids in the sense used by Pitzer(7-23).

TABLE 7-2. MAXIMUM POSSIBLE RATE OF DECREASE OF DROPLET RADIUS WITH TIME FOR VARIOUS LIQUIDS

Compound	Temp, C	-dr/dt (7-51), cm/sec	-dr/dt (7-50), cm/sec	Z, ratio
H ₂ O	25	0.342	0.0493	7.0
CH ₃ OH	25	3.01	0.465	6.4
C ₅ H ₁₂	25	23.8	29.4	0.81
C ₆ H ₁₄	25	7.37	4.53	1.6
C ₇ H ₁₆	25	2.29	0.660	3.5
C ₈ H ₁₈	25	0.750	0.0991	7.6
C ₆ H ₆	20	2.56	1.68	1.5
Cyclo-C ₆ H ₁₂	18.4	2.92	1.87	1.6
CCl ₄	20	2.41	1.94	1.2
Hg	20	4.3 x 10 ⁻⁶	16.1 x 10 ⁻⁶	0.27

In a second paper, Penner develops an equation for evaporation rate in terms of absolute rate theory. Briefly, his assumptions and derivations are as follows: The evaporating liquid molecules are assumed to behave as particles moving in a potential box. In this model, it is assumed that the internal contributions to the partition function are the same in both the liquid and in the vapor. The partition function is, then,

$$F = (2\pi mkT)^{3/2} V_f / h^3 \quad (7-52)$$

where V_f is the free volume of the molecules in the liquid, and h is Planck's constant. The free volume is defined as the total volume integral of that portion of the potential energy of the molecule in the liquid which is due to thermal displacements of the center of mass of the molecule from its equilibrium position. Similarly, the partition function of the activated complex, that is, of the association of a molecule with its critical energy is

$$F^* = (2\pi mkT) V_f^{2/3} / h^2 \quad (7-53)$$

The rate of evaporation, in molecules per second, is then

$$K = \left(\frac{kT}{h} \right) \left(\frac{F^*}{F} \right) e^{-\Delta E_{act}/kT} \quad (7-54)$$

where ΔE_{act} is the activation energy per molecule. By substituting the partition functions in Equation (7-54), we have

$$K = V_f^{-1/3} \left(\frac{kT}{2\pi m} \right)^{1/2} \left(e^{-\Delta E_{act}/kt} \right) \quad (7-55)$$

which is identical with the evaporation equation given by Frenkel, Reference (7-24). Calculated evaporation rates, based on Equation (7-55), are much smaller than rates calculated from the Knudsen equation, Reference (7-22).

If we allow for the coordination of one degree of freedom with the reaction coordinate, we can replace F^* by the partition function

$$F^* = (2\pi mkT)^{1/2} V^{2/3}/h^2, \quad (7-56)$$

for a freely moving gas molecule where V is the volume of one molecule.

After making this change, the rate equation becomes

$$K = \left(\frac{V^{2/3}}{V_f} \right) \left(\frac{kT}{2\pi m} \right)^{1/2} e^{-\Delta E_{act}/kT} \quad (7-57)$$

By assuming, as before, that the activation energy for the reaction is ΔH_{vap} , that is, the heat of vaporization, and introducing Kincaid and Eyring's (7-25) term for free volume, Equation (7-57) may be written as

$$-\left(\frac{dr}{dt} \right) = \left(\frac{u^3 m}{kT\gamma} \right) (2\pi\gamma)^{-1/2} e^{-\Delta H/kT}, \quad (7-58)$$

where the variables have the same meaning as in Equation (7-50).

Table 7-3 shows the results of comparative evaporation rates calculated by Equations (7-58) and (7-51). The ratio, Z , is determined in a manner analogous to that in Table 7-2.

The results, as calculated by means of these two equations, are in generally good agreement for sphere-like, nonassociated molecules. This is to be expected, because in the treatment of free volume, a spherical molecular model is assumed.

Penner (7-26) has also shown that the Knudsen Equation, (7-51), and Equation (7-57) may be reduced to nearly identical forms, provided that the right-hand number of the Knudsen equation is multiplied by an accommodation coefficient of the form $e\kappa$, where e is the base of the natural logarithms and κ is the transmission coefficient for activated molecules passing over the potential barrier associated with evaporation. It would seem likely that the discrepancies between calculations made, using the Knudsen and the absolute-rate equation, are due to incomplete specifications of the physical states associated with the partition functions.

In the derivation of the total partition function used in Equation (7-54), it was assumed that the internal contributions both of the activated and of the normal partition functions are essentially equal. This equivalence would not, of course, hold for a liquid-vapor system composed of polar molecules, because a constraint is imposed upon the rotational degree of freedom of a polar molecule in the liquid phase. This constraint arises in connection with the dipole interaction between molecules. Thus, it is necessary to take into account a hindered rotation effect in dealing with polar molecules.

Kincaid and Eyring (7-25) have introduced the "free angle ratio", Φ , as a means of correcting for the hindered rotational effect. This term is defined as the ratio between the liquid rotational partition function and the corresponding partition function for the gas phase. The "free angle" is usually defined as the integral over the angular displacement of the molecule around its center of mass.

TABLE 7-3. COMPARISON OF THE PREDICTED EVAPORATION RATES FOR SEVERAL LIQUIDS BY THE KNUDSEN AND ABSOLUTE-RATE EQUATIONS

Compound	Temp, C	-dr/dt (7-58) cm/sec	-dr/dt (7-51) cm/sec	Z ratio
H ₂ O	20	0.0134	0.254	0.053
CH ₃ OH	25	0.205	3.01	0.068
C ₅ H ₁₂	25	27.2	23.8	1.1
C ₆ H ₁₄	25	5.67	7.37	0.77
C ₇ H ₁₆	25	0.926	2.29	0.40
C ₈ H ₁₈	25	0.159	0.750	0.21
C ₆ H ₆	30	4.42	4.03	1.1
Cyclo-C ₆ H ₁₂	18.4	2.94	2.92	1.0
CCl ₄	20	3.04	2.41	1.3
Hg	20	5.7 x 10 ⁻⁴	4.3 x 10 ⁻⁵	13

Kincaid and Eyring have emphasized the fact that for liquids with hindered rotation, the free-volume free-angle ratio expression,

$$\frac{1}{V_f \phi} = \frac{P_s}{kT} e^{\Delta H_{\text{vap}}/kT} ,$$

should be introduced into Q_i , the internal partition function, so that

$$Q_i = \phi Q_{\text{rot(gas)}} (Q_{\text{vib}}) (Q_{\text{elect}}) .$$

In this expression, the various Q factors refer to the internal-partition functions for rotation, vibration, and electronic degrees of freedom.

Penner (7-26)(7-27) has shown that by the application of this corrected form of the partition function in the derivation of a second rate equation, there results

$$k_{\text{evap}} = k \left(\frac{kT}{2\pi m} \right)^{1/2} \left(\frac{V^{2/3} \phi}{V_f \phi} \right) e^{-\Delta H_{\text{vap}}/kT} ;$$

and by combining this expression with the relation of Kincaid and Eyring, there is obtained a rate equation containing κ , the barrier transmission coefficient. This may be written as

$$k_{\text{evap}} = \kappa V^{2/3} \phi P_s (2\pi m kT)^{-1/2} , \quad (7-59)$$

where the symbols are the same as before.

If \underline{G} is taken as the evaporative weight loss per unit surface per unit time, then,

$$G = 1/S \left(\frac{dV}{dT} \right) = k_e \rho_L / n^{1/3} \quad (7-60)$$

where S is the surface area; V is the volume; ρ_L is the liquid density; and n is the number of molecules per unit volume. Substitution of (7-59) into Equation (7-60) gives

$$G = k\phi (2\pi mkT)^{-1/2} P_S V^{2/3} \rho_L / n^{1/3} \quad (7-61)$$

Since $\rho_L V = m$ and $n^{1/3} V^{1/3} = 1$, Equation (7-61) can be reduced to

$$G = \kappa\phi P_S \frac{m}{2\pi kT}^{1/2} \quad (7-62)$$

Thus, it has been shown that by taking into account the effect of the free-angle ratio on the partition function, the statistical rate equation may be reduced to the Knudsen equation, Equation (7-51), having a coefficient of κ .

Since κ may be taken as nearly unity, a comparison of Equation (7-62) with Equation (7-51) shows that the evaporation coefficient of a polar liquid should be equal to ϕ , the free-angle ratio. This result is confirmed to a surprising extent by the experimental data of Wylle⁽⁷⁻²⁸⁾.

Table 7-4 compares Wylle's experimental evaporation coefficients and the free-angle ratio for a series of polar and nonpolar liquids.

TABLE 7-4. COMPARISON OF EVAPORATION COEFFICIENTS WITH FREE-ANGLE RATIO FOR SEVERAL LIQUIDS⁽⁷⁻²⁸⁾

Liquid	Temp, K	ϵ	ϕ
CCl ₄	273	1	1
C ₆ H ₆	279	0.90	0.85
CHCl ₃	275	0.16	0.54
C ₂ H ₅ OH	273	0.020	0.018
CH ₂ OH	273	0.045	0.048
H ₂ O	283 to 303	0.036 to 0.040	0.04

Wylle calculated the evaporation coefficients, ϵ , from a comparison of experimental rate data with the theoretical rate predicted by Equation (7-51). He used Alty's⁽⁷⁻²⁹⁾ data for water and Baranev's⁽⁷⁻³⁰⁾ data for all the other compounds listed in Table 7-4.

From the foregoing discussions, it may be seen that a consistent theory relating vapor pressure to drop size can be obtained from elementary thermodynamic reasoning or as a by-product from the theory of heterophase fluctuations. Neither approach takes into account the

possible variation of surface tension with drop size, which is proposed by Tolman. This latter influence may, in part, account for the controversial experimental evidence which exists concerning the complete validity of Equation (7-1). In light of Rodebush's reasoning on minimum drop size, it would seem that both Equations (7-7) and (7-12) should be simultaneously examined, by experiment, for a range of drop sizes. The upper size limit for this examination should be close to the region where the Tolman correction becomes small. The lower limit would, of course, be limited by the experimental technique because drops having radii close to 10^{-7} are not directly observable.

It will be shown in Chapter 8 that the surface tension correction is small in comparison with other factors which influence the evaporation of small drops. The most prominent of these factors is the boundary layer of pure vapor which surrounds the drop.

No quantitative data exist supporting the theory of heterophase fluctuations, because of experimental difficulties encountered in measuring the low concentration of embryos. It is felt that an effort should be made to compare this theory with experimental data for the particular case of the cavitation of liquid drops under superheated conditions; no published theories of gross droplet evaporation account for the influence of this metastable state. This may well be an important consideration in the burning of a fuel mist because, according to heterophase theory, drops can move into regions of temperature considerably above the thermodynamic boiling point without instantaneously evaporating. This would be particularly true for a system in which no nucleating foreign particles are present. It would also follow that the lifetime of a moving drop, as predicted by equilibrium theory, would be markedly different from the lifetime at a temperature corresponding to the superheated condition.

It is gratifying to note that the evaporation process can be satisfactorily accounted for by the absolute-rate process theory of Eyring. Penner seems to have accounted for all the factors in this theory excepting the barrier transmission coefficient κ , which he relates empirically both to the free-angle ratio and to the evaporation-accommodation coefficient. It would seem that the absolute-rate theory of evaporation has been developed to the most advanced point possible for a physical process in the absence of a more particular theoretical knowledge of the barrier coefficient.

MULTICOMPONENT EVAPORATION

The absolute rate theory for the evaporation of a single pure component may, in principle, be extended to predicting evaporation rates in multicomponent systems. Schrage⁽⁷⁻³¹⁾ has derived generalized expressions for both evaporation and condensation in multicomponent systems which are based upon the fact that thermodynamic equilibrium between two multicomponent phases requires that their temperatures and the fugacities of each component be the same. Thus, if the properties of the liquid surface are given, n independent equations containing $(n - 1)$ independent composition parameters can be obtained by equating the fugacities of the components. This clearly specifies that a particular gas phase must exist in equilibrium with the specified liquid surface.

The usefulness of Schrage's equations is seriously impaired by the fact that the general form of the required fugacity equations is unknown and therefore little is to be gained by presenting a mathematical derivation of these results.

An examination of the meager literature on the kinetics of multicomponent evaporation shows that no entirely reliable experimental data has been obtained for such systems. Although the works of Miyamoto⁽⁷⁻³²⁾⁽⁷⁻³³⁾ and of Uhara⁽⁷⁻³⁴⁾ present some multicomponent evaporation rate data, this information is not generally useful because some chemical reactions occurred during the evaporation process.

Schrage points out that many extraneous complications arise in connection with multicomponent studies of this sort because the gas does not generally reduce to the uniform state as it

moves away from the phase boundary. Instead, transport occurs through a more complicated diffusion-dependent mechanism. Even for the analysis of an evaporating binary system, it would be necessary to consider the nature of the diffusion mechanism which takes place in both the boundary region and in the region where the interface has a negligible effect on the behavior of the gas phase.

REFERENCES

- 7-1. Frenkel, J., Kinetic Theory of Liquids, 1st Edition, Oxford University Press, London 1946, p. 368-370.
- 7-2. Shereshefsky, J. J., Vapor Pressures in Small Capillaries, J. Am. Chem. Soc., 50, 2966 (1928).
- 7-3. Tolman, R. C., The Effect of Droplet Size on Surface Tension; J. Chem. Phys., 17, 333 (1949).
- 7-4. Thomä, M., Change of Vapor Pressure at a Curved Surface; Z. Physik, 64, 224 (1930).
- 7-5. Adam, N. K., The Physics and Chemistry of Surfaces, Third Edition, Oxford University Press, London 1941, p. 15.
- 7-6. Rodebush, W. H., Nuclei in Condensation and Evaporation; Chem. Rev., 44, 269 (1949).
- 7-7. Reference 7-1, p. 386.
- 7-8. Landsberg, G. S., Intermolecular Forces and the Ramon Effect; Bul. Acad. Sci. (USSR), Ser. Phys. No. 3, 373-82 (1938).
- 7-9. Volmer, M., and Weber, A., Nucleus Formation in Superheated Systems; Z. Phys. Chem., 119, 277-301 (1926).
- 7-10. Kaishev, R., and Stranski, I., Kinetic Derivation of the Rate of Nuclear Formation; Z. Phys. Chem., B26, 317-326 (1934).
- 7-11. Forkas, L., The Velocity of Nucleus Formation in Supersaturated Vapor; Z. Phys. Chem., 125, 236-42 (1927).
- 7-12. Becker, R., and Döring, W., The Kinetic Treatment of Nuclear Formation in Supersaturated Vapors; Ann. der Phys. 24, 719-52 (1935).
- 7-13. Reference 7-1, Chapter VII.
- 7-14. Bradley, R. S., Nucleation in Phase Changes, Quart. Rev. 5, 315 (1951).
- 7-15. Frenkel, J., A General Theory of Heterophase Fluctuations and Pretransition Phenomena; J. Phys. (USSR), 315-24 (1939).
- 7-16. Zeldovich, J., Theory of the Formation of a New Phase - Cavitation; J. Exp. Theor. Physics (USSR) 12, 525 (1942).
- 7-17. Volmer, M., and Flood, H., Formation of Droplets in Vapors; J. Phys. Chem., A170, 273 (1934).
- 7-18. Sander, A., and Damköhler, Übersättigung bei der spontanen Keimbildung in Wasserdampf; Naturwiss., 31, 460 (1943).

- 7-19. LaMer, V. K., and Pound, G. M., Surface Tension of Small Droplets from Volmer and Flood's Nucleation Data; J. Chem. Phys., 17, 1337 (1949).
- 7-20. Penner, S. S., The Maximum Rate of Evaporation of Liquids; J. Phys. and Colloid Chemistry, 52, 367 (1948).
- 7-21. Glasstone, S., Laidler, K. J., and Eyring, H., The Theory of Rate Processes; McGraw-Hill Book Co., Inc., New York (1938).
- 7-22. Knudsen, M., Ann. Physik, 47, 697 (1915).
- 7-23. Pitzer, K. S., J. Chem. Phys., 7, 583 (1939).
- 7-24. Reference 7-1, Chapter I.
- 7-25. Kincaid, J. F., and Eyring, H., Free Volume and Free Angle Ratios of Molecules in Liquids; J. Chem. Phys., 6, 620 (1938).
- 7-26. Penner, S. S., Additions to the Article "Melting and Evaporation as Rate Processes"; J. Phys. Colloid Chem., 52, 1262 (1948).
- 7-27. Penner, S. S., Unpublished work.
- 7-28. Wylle, G., Evaporation and Surface Structure of Liquids; Proc. Roy. Soc. (London), A197.
- 7-29. Alty, T., Maximum Rate of Evaporation of Water; Phil. Mag., 15, 82 (1933).
- 7-30. Baranov, M., Relation Between Surface Energy of Liquids and the Accommodation Coefficient; J. Phys. Chem. (USSR), 13, 1635 (1939).
- 7-31. Schrage, R. W., Interphase Mass Transfer; Chapter IV, Columbia University Press, New York (1953).
- 7-32. Miyamoto, S., Theory of the Rate of Solution of Gas in Liquids; Bull. Chem. Soc., Japan, 7, 8-17 (1932).
- 7-33. Miyamoto, S., A Theory of the Rate of Sublimation; Trans. Faraday Soc., 29, 794 (1933).
- 7-34. Uhara, I., Studies on the Equilibrium Between Dilute Solution and Solute Vapor I, Measurement of the Condensation Coefficient of Solute Vapor at the Liquid Surface of Solvents; Bull. Chem. Soc., Japan, 18, 412-427 (1943).

Contracts

CHAPTER 8. SINGLE-DROPLET EVAPORATION

ABSTRACT

There is first presented the Maxwell theory of droplet evaporation, which is based upon molecular diffusion and conduction of heat under conditions of thermodynamic equilibrium. The Maxwell theory is then modified by introducing the Fuchs' concept of a stagnant boundary layer surrounding the evaporating droplet; the reality of the boundary-layer effect is effectively demonstrated by a comparison of the theory with expounded data. The Fuchs' theory is then extended to include the evaporation of drops in a finite enclosure for the case of both absorbing and reflecting walls. Finally, it is shown that while diffusion transport of small molecules from the boundary layer can be completely described by theory, the opposing thermal-transport process is less completely understood.

Contrails

SINGLE-DROPLET EVAPORATION .

by

F. Benington

The previous chapter has treated the evaporation of liquid drops from the standpoint of both the thermodynamics and the kinetics of the microscopic processes which occur in both the liquid and gas phases. It is now convenient to turn to the subject of the gross macroscopic rate of evaporation of a single droplet, since the underlying basic theory of the microscopic processes has already been established.

In this chapter there is first presented the Maxwell theory of droplet evaporation, which is based upon a balance in thermal and mass transport between the drop and its surrounding gaseous medium. In the development of this elementary theory, it is assumed that molecular diffusion and conduction of heat are alone responsible for evaporation. It is further assumed that a state of thermodynamic equilibrium exists in the system during the entire process.

By introducing the Fuchs concept of a boundary layer surrounding the drop, a more realistic picture of the droplet evaporation process is formed. The reality of the boundary-layer effect is shown by a comparison of the theory with experimental data. It is also shown, from the theoretical standpoint, that a modified form of Fuchs theory is broadly applicable to the evaporation of a wide range of drop sizes, whereas the earlier Langmuir theory is valid only under rather narrow ranges of drop size and of total pressures. The Fuchs theory is then extended to include the evaporation of drops in a finite enclosure for the case of both absorbing and reflecting walls.

A short discussion of the nonstationary evaporation process is presented. Although this problem is one of great mathematical complexity, certain useful results are derived for the assumption of a quasi-stationary state. However, this treatment fails in the instance where a large diminution of drop volume occurs in the period of transient evaporation.

Finally, the process of drop evaporation is examined in the light of present-day knowledge of transport phenomena. It is shown that while diffusion transport for small molecules can be reasonably well explained by theory, the opposing process of thermal transport is less completely understood.

MAXWELL'S EQUATION FOR THE EVAPORATION OF
A SINGLE DROP

The Maxwellian treatment assumes that the rate-governing step in evaporation is a simple diffusion process taking place in an infinite space. In addition to this basic assumption, the following additional assumptions are made:

1. The drop has no motion relative to its surroundings.
2. The evaporative process is isobaric and isothermal.
3. The liquid vapor pressure is small in comparison with the ambient pressure.
4. No convection currents are present in the system.

5. The vapor pressure at the drop surface corresponds to the saturation pressure at the drop temperature.
6. Evaporation takes place as a steady-state equilibrium process.

From Fick's law of diffusion, the mass of gas, i , in moles, which will diffuse across a unit area in unit time is proportional to the concentration gradient of the gas normal to this area. That is,

$$i = D \frac{\partial C}{\partial n} \quad , \quad (8-1)$$

where C is the concentration in moles per unit volume, $\partial C / \partial n$ is the normal concentration gradient, and D is a diffusion coefficient. Now the time dependent rate of diffusion of a gas in spherical coordinates is

$$\frac{\partial C}{\partial t} = D \nabla^2 C = D \left[\frac{\partial^2 C}{\partial r^2} + \frac{2}{r} \frac{\partial C}{\partial r} + \frac{1}{r^2 \sin^2 \theta} \frac{\partial}{\partial \theta} \left(\sin \theta \frac{\partial C}{\partial \theta} \right) + \frac{1}{r^2 \sin^2 \theta} \frac{\partial^2 C}{\partial \phi^2} \right] \quad , \quad (8-2)$$

where r is the polar radius and θ and ϕ are the Eulerian angles. For the case of the spherical drop, the concentration of vapor is uniform at any spherical surface concentric with the drop. Consequently, $\partial C / \partial \theta$ and $\partial C / \partial \phi$ vanish, and Equation (8-2) becomes

$$\frac{\partial C}{\partial t} = D \left[\frac{\partial^2 C}{\partial r^2} + \frac{2}{r} \frac{\partial C}{\partial r} \right] \quad , \quad (8-3)$$

where the concentration varies only radially. Since we have assumed a steady-state diffusion process, the left-hand side of Equation (8-3) may be set equal to zero. A solution to this one-dimensional case is

$$C = A + B/r \quad , \quad (8-4)$$

where A and B are arbitrary constants. The boundary values $C = C_s$ at $r = a$, and $C = C_a$ at $r = \infty$ permit the evaluation of these constants, and Equation (8-4) becomes

$$C - C_a = \frac{a}{r} (C_s - C_a) \quad , \quad (8-5)$$

where C_s is the vapor concentration at the drop surface, C_a is the ambient vapor concentration in the surrounding atmosphere, and a is the radius of the drop.

If Ω is the total mass per unit time, in moles, of gas diffusing outward through a spherical surface of radius r , then

$$\Omega = -4\pi r^2 D \left(\frac{\partial C}{\partial r} \right) \quad . \quad (8-6)$$

From Equation (8-5), the concentration gradient is

$$\frac{\partial C}{\partial r} = - \frac{a(C_s - C_a)}{r^2} \quad . \quad (8-7)$$

Substitution of Equation (8-7) into Equation (8-6) results in

$$\Omega = 4\pi D a (C_s - C_a) \quad . \quad (8-8)$$

If we now assume that the surface and ambient temperatures are nearly equal, that is, $T_s \approx T_a$, and that the vapor obeys the ideal gas law $P = CRT$,

$$\Omega = \frac{4\pi Da}{RT_s} (P_s - P_a) \quad (8-9)$$

Since the time rate of volume change may be written as $dv/dt = -\Omega M/\rho_L$, Equation (8-9) may be written as

$$-\frac{dv}{dt} = \frac{\Omega M}{\rho_L} = \frac{4\pi D M a (P_s - P_a)}{\rho_L R T_s} \quad (8-10)$$

where ρ_L is the liquid density, and M is the molecular weight of the evaporating substance.

According to Equation (8-10), the rate of evaporation is dependent upon P_s , the saturation pressure of the drop. The saturation pressure is, in turn, dependent upon the surface temperature of the drop. As the drop receives heat from its surroundings, the vaporization of the liquid tends to cause cooling to a temperature below the ambient temperature. In the equilibrium process, the inflow of heat balances the latent heat of vaporization of the liquid.

If we consider the conduction of heat only, we have

$$\frac{\partial T}{\partial t} = k \nabla^2 T \quad (8-11)$$

where $k = K/\rho_g c_p$. This equation is similar to the diffusion Equation (8-3), except the diffusion coefficient is replaced by k , the thermal diffusivity of the medium, where K is the thermal conductivity, ρ_g the density, and c_p the heat capacity, all for the gas phase. Equation (8-11) has a steady-state solution similar to Equation (8-5), which is

$$T_a - T = \frac{a}{r} (T_a - T_s) \quad (8-12)$$

where T_a and T_s are the ambient and surface temperatures, respectively.

The flow of heat, Q , through a spherical shell concentric with the evaporating drop is

$$Q = 4\pi r^2 K \frac{\partial T}{\partial r} \quad (8-13)$$

By differentiating Equation (8-12) and using the resulting derivative in Equation (8-13), we have

$$Q = 4\pi K a (T_a - T_s) \quad (8-14)$$

Under equilibrium conditions, the heat transfer to the drop must balance the latent heat of vaporization, ΔH , or

$$Q = \Omega(\Delta H) \quad (8-15)$$

Equating Equations (8-14) and (8-15) gives

$$\Omega(\Delta H) = 4\pi K a (T_a - T_s) \quad (8-16)$$

which, upon eliminating Ω from Equation (8-8), gives

$$T_a - T_s = \frac{D \Delta H}{K} (C_s - C_a) \quad (8-16)$$

If the surface concentration is taken as being much greater than the ambient concentration, then

$$(T_a - T_s) = \frac{D(\Delta H)C_s}{K} \quad (8-17)$$

By applying the gas law, $P_s = C_s RT_s$, Equation (8-17) may be written as

$$(T_a - T_s) = \frac{D(\Delta H)P_s}{KRT_s} \quad (8-18)$$

Correction for Temperature- and Pressure-Dependent Parameters

The next point for consideration is the manner in which D , P_s , and K vary with temperature. The saturation pressure, P_s , is dependent upon temperature in accordance with the Clausius-Clayperon relation,

$$\frac{dP_s}{dT} = \frac{(\Delta H)P_s}{RT_s^2} \quad (8-19)$$

or

$$\ln P_s = - \frac{\Delta H}{RT_s} \quad (8-20)$$

Changes in P_s do not produce correspondingly large variations in K , the thermal conductivity, except at very low pressures(8-2).

Also, the thermal conductivity, K , does not vary widely with temperature. Accordingly, if a temperature, T_m , is taken as a mean value of T_s and T_a , then the variational effect may be expressed as

$$\frac{K_{T_m}}{K_{273}} = \frac{273 + A}{T_m + A} \left(\frac{T_m}{273} \right)^{3/2} \quad (8-21)$$

where K_{T_m} is the thermal conductivity of the vapor at T_m , K_{273} is the thermal conductivity of the vapor at 273 K, and A is Sutherland's constant (empirical) for the particular vapor.

Equation (8-21) has been used as a basis of computing the temperature variation of K as given by the International Critical Tables(8-3); tabular variations and the temperature ranges over which Equation (8-21) is applicable are given for a number of pure hydrocarbons.

The diffusion coefficient for a gas varies with both temperature and pressure in accordance with

$$D = D_o \left(\frac{T}{T_o} \right)^m \frac{P_o}{P} \quad (8-22)$$

where the subscript o refers to standard conditions of P_o and T_o , where D_o is known. If we assume that $P_o/P \approx 1$, then Equation (8-22) becomes $D = D_o(T/T_o)^m$. The exponent m is a parameter which varies from 1.5 to 2.0 for most substances, and depends upon the molecular structure.

At this point, it should be stated that both Equations (8-21) and (8-22) are semiempirical, and that their use depends upon a knowledge of the empirical constants for the substances in question. Both derivations are predicated on an idealized molecular gas model consisting of perfectly

elastic spheres. At a later point a more detailed discussion of molecular diffusion in relation to multicomponent mixtures will be given.

Fuchs(8-4) first introduced the temperature-dependent form of the diffusion coefficient into Maxwell's evaporation equation in connection with studies of the diffusion of water vapor from droplets. This was done as follows:

In the diffusion Equation (8-6), the diffusion coefficient, D , may be taken as a function of the radial coordinate. This follows from the fact that the temperature varies radially and the diffusion coefficient is dependent upon the temperature. The equation may then be written as

$$\Omega = -4\pi r^2 D(r) \frac{dC}{dr} \quad (8-23)$$

Differentiation of Equation (8-12) gives

$$\frac{dr}{r^2} = \frac{dT}{a(T_a - T_s)}$$

which, on substitution into Equation (8-23), yields

$$\Omega = \frac{-4\pi \frac{dC}{dT}}{a(T_a - T_s)D(T)} \quad (8-24)$$

By introducing the temperature-dependent form of the diffusion coefficient from Equation (8-22) into Equation (8-24), and by integrating over appropriate limits, Equation (8-24) is transformed to

$$\Omega = \frac{-\int_{C_s}^{C_a} 4\pi dC}{\int_{T_s}^{T_a} \frac{dT}{a(T_a - T_s)D_s(T/T_s)^m}} \quad (8-25)$$

or

$$\Omega = \frac{4\pi a D_s (m-1) (C_s - C_a) T_a^{m-1} (T_a - T_s)}{T_s (T_a^{m-1} - T_s^{m-1})} \quad (8-26)$$

If we choose $m = 2$, which is the proper value for water vapor, Equation (8-26) reduces to the simple expression

$$\Omega = 4\pi (C_s - C_a) a D_s (T_a / T_s) \quad (8-27)$$

Now, since the temperature and the diffusion coefficient are related by the pressure-independent approximation to Equation (8-22), Equation (8-27) may be written as

$$\Omega = 4\pi a (C_s - C_a) (D_a D_s)^{1/2} \quad (8-28)$$

where the geometric-mean diffusion coefficient taken at surface and ambient conditions is used to replace D_s . Finally, the rate of volume change of the drop is

$$-\frac{dv}{dt} = \frac{\Omega M}{\rho_L} = \frac{4\pi M a (P_s - P_a) (D_a D_s)^{1/2}}{\rho_L R T_s} \quad (8-29)$$

Continued

Several independent workers (8-5, 8-6, 8-7) have checked the formal validity of Maxwell's rate Equation (8-10). Houghton's (8-5) work is of particular interest, since by a special treatment of his data, the evaporation rate of a water drop is found to follow Equation (8-27).

Houghton (8-5) writes the Maxwell equation in the form

$$\frac{dv}{dt} = - \frac{4\pi Dr(\rho_s - \rho_a)}{\rho_L} \quad , \quad (8-30)$$

where ρ_s and ρ_a are the surface and ambient vapor densities. It is of interest to note that Houghton devised this equation by an analogy between droplet vaporization and the electrostatic potential of a sphere. This equation may be transformed into an equation giving the radial evaporation rate, which is

$$\frac{1}{2} \frac{dr^2}{dt} = - \left(D/\rho_L \right) (\rho_s - \rho_a) \quad . \quad (8-31)$$

By integration over appropriate limits

$$\int_{r_0}^r dr^2 = - 2(D/\rho_L) (\rho_s - \rho_a) \int_0^t dt \quad ,$$

or

$$r^2 = - 2 \left(D/\rho_L \right) (\rho_s - \rho_a) t + r_0^2 \quad , \quad (8-32)$$

where r_0 is the initial radius of the drop.

Houghton's (8-5) experimental technique was briefly as follows: Droplets of water were suspended from fibres of various diameters (Wollaston wire, copper wire, and quartz) in order to produce droplets of varying diameter. The fiber holding the drop was suspended in a chamber maintained at a constant temperature, and the change of diameter was noted as a function of time by means of a micrometer microscope. By varying the temperature and the relative humidity of the chamber, $D(\rho_s - \rho_a)$ could be varied. A plot of the experimental values of the square of the radius against time gave a linear relation for fixed conditions of humidity and temperature. In a second treatment of his data, Houghton plotted rdr/dt against $(\rho_s - \rho_a)$ for a series of different humidities. This should, of course, give a linear relation under the assumption that D remains constant, within the series of experiments. However, the curve was nonlinear when the ρ_s corresponding to the ambient temperature was used. When $(\rho_s - \rho_a)$ was corrected for the lowering of the water-drop temperature due to the latent-heat effect, the above linear relation was found to hold. It is easily seen that the slope of these lines should be $-2D/\rho_L$. Houghton subsequently calculated D , the diffusion coefficient of water vapor into air. The values for D were found to be smaller than the corresponding values that have been found by other experimental methods.

Fuchs (8-4) recalculated some of Houghton's data using a geometric-mean value of \underline{D} , that is, $(D_a D_s)^{1/2}$, and found that the diffusion coefficient obtained from this treatment agreed with accepted values to within two to three per cent. This is a direct experimental verification of Equation (8-29).

The Corrections for Both Finite Vapor Pressure and Limited Space of Evaporation

Preceding the derivation of the Maxwell equation, the assumption was made that the vapor pressure of the liquid constituting the drop was small in comparison with the total pressure. At that time, it was also assumed that the evaporation process took place in an infinite space surrounding the droplet.

Fuchs⁽⁸⁻⁴⁾, in his theoretical treatment of evaporation, has discussed the influence of these assumptions upon the form of Maxwell's equation. He assumes that the vapor pressure of the evaporating liquid is not small compared with the total pressure. Since, under equilibrium conditions, the pressure is everywhere the same, there is a decrease in concentration of the vapor which is equal and opposite to the increase in concentration of the air. This produces a convection current which is equal and opposite to the diffusion flux of the vapor. If \underline{U} is the convection current velocity, C' is the air concentration and D' is the diffusion coefficient of air into vapor, then

$$C'U = D' \left(\frac{\partial C'}{\partial r} \right) \quad , \quad (8-33)$$

which determines the velocity of the current. Regardless of which component we assume to be diffusing, $D = D'$, where \underline{D} is the diffusion coefficient which was defined in an earlier section. It then follows that

$$\frac{dC'}{dr} = - \frac{dC}{dr} \quad . \quad (8-34)$$

The convection current velocity is, therefore,

$$U = - \frac{D}{C'} \left(\frac{\partial C}{\partial r} \right) \quad . \quad (8-35)$$

The total outward flux of vapor, Ω , is then dependent upon both the concentration gradient and the convection of the air-vapor mixture. This may be written as

$$\Omega = - 4\pi r^2 \left(D \frac{dC}{dr} - CU \right) \quad . \quad (8-36)$$

By substituting the convection velocity from Equation (8-35) and by introducing the total molar concentration $E = C + C'$, Equation (8-36) becomes

$$\Omega = - \frac{4\pi r^2 DE}{E-C} \left(\frac{dC}{dr} \right) \quad . \quad (8-37)$$

If we now neglect the ambient concentration C_a , which is small compared with the surface concentration, C_s , Equation (8-37) may be integrated to give

$$\Omega = - (4\pi a DE) \ln \left(1 - \frac{C_s}{E} \right) \quad . \quad (8-38)$$

Expanding the \ln term in Equation (8-38) in a series and neglecting higher order terms gives the approximate form

$$\Omega \approx \pi a DC_s \left(1 + \frac{C_s}{2E} \right) \quad . \quad (8-39)$$

If Ω_0 is taken to represent a standard evaporation rate which neglects corrections for finite chamber dimensions or finite vapor pressure, then Ω_0 may be calculated from the previously derived equation, $\Omega = 4\pi Da(C_s - C_a)$, by assuming that $C_a = 0$. That is, $\Omega_0 = 4\pi a DC_s$. By introducing this form into Equation (8-39), we have, finally

$$\Omega = \Omega_0 \left(1 + \frac{C_s}{2E} \right) \quad , \quad (8-40)$$

which shows the necessary correction which must be applied for finite vapor pressures. For water vapor evaporating at 20 C and at atmospheric pressure, the effect of neglecting the finite vapor pressure introduces only a 1.2 per cent error in the rate of evaporation. At higher temperatures this correction becomes more significant.

In the previous derivations of the evaporation-rate equation, it was assumed that an unbounded atmosphere surrounds the drop.

For a drop evaporating in a spherical vessel having absorbing walls, we obtain

$$C = A + \frac{B}{r} \quad ,$$

as before. In such a vessel, the ambient radial boundary is taken to be $r = r_1$, with $C = C_{r_1}$. Also, $C = C_s$ at $r = a$. By evaluating A and B with these boundary conditions, the concentration equation is

$$C - C_{r_1} = \frac{(C_s - C_{r_1}) a}{r} \left(\frac{r_1 - r}{r_1 - a} \right) \quad (8-41)$$

The number of moles evaporating per unit time is then

$$\Omega = \frac{4\pi(C_s - C_{r_1})aD}{1 - \frac{a}{r_1}} = \frac{\Omega_0}{1 - \frac{a}{r_1}} \quad (8-42)$$

Equation (8-42) shows that when the drop diameter is close to the diameter of the vessel, an appreciable correction must be applied. However, if $a \ll r$, the vessel has practically no influence upon the rate of evaporation.

The Nonstationary Evaporation Process

The problem of calculating the rate of evaporation of a drop under nonstationary conditions is one of considerable mathematical complexity. Fuchs⁽⁸⁻⁴⁾ has shown that, in practice, most of the conditions of the process can be treated as being quasi-stationary. This means that the process, at any instant, has the same velocity as that of the stationary state with the boundary conditions corresponding to that particular instant. Fuchs appears to be the only worker who has investigated this phase of the evaporating problem. His treatment will now be presented.

If a drop of radius a is introduced into a region of infinite extent for which, at time zero, the vapor concentration is also zero, then the equation

$$\frac{\partial(Cr)}{\partial t} = D \frac{\partial^2(Cr)}{\partial r^2} \quad (8-43)$$

must be solved using the boundary conditions: $C = 0$ at $t = 0$ for $r > a$, and $C = C_s$ at $t < 0$ for $r = 0$. The solution is

$$C = \frac{2C_s a}{r \sqrt{\pi}} \int_{\frac{r-a}{2\sqrt{Dt}}}^{\infty} e^{-x^2} dx = \frac{C_s a}{r} \operatorname{erfc} \left(\frac{r-a}{2\sqrt{Dt}} \right) \quad (8-44)$$

Writing Ω , the evaporation rate, in terms of the concentration gradient gives

$$\Omega = -4\pi a^2 D \left(\frac{\partial C}{\partial r} \right)_{r=a} \quad (8-45)$$

From differentiation of Equation (8-44) with respect to r , and substitution of the result in Equation (8-45), there results

$$\Omega = 4\pi a D C_0 \left[1 + \frac{a}{\sqrt{\pi D t}} \right] = \Omega_0 \left[1 + \frac{a}{\sqrt{\pi D t}} \right] \quad (8-46)$$

We now wish to show to what extent the evaporation process can be regarded as stationary in accordance with Equation (8-46). If t_1 is the time necessary for the correction term $a/\sqrt{\pi D t}$ to reach a definite value Δ and t_2 is taken as the time necessary for the complete evaporation of a drop, then these times may be written respectively as

$$t_1 = \frac{a^2}{\Delta^2 \pi D} \quad (8-47)$$

and

$$t_2 = \frac{a^2 P_1}{2 M D C_g} \quad (8-48)$$

The ratio of these quantities is

$$\frac{t_1}{t_2} = \frac{2 C_g M}{\Delta^2 \pi D P_1} \quad (8-49)$$

Suppose that $\Delta = 0.01$, $M = 18$, and $C_g = 3.8 \times 10^{-7}$ mole per cm^3 . The ratio is then $t_1/t_2 = 0.04$. This means that if a water drop is caused to evaporate in dry air at 21.7 C, the nonstationary velocity of evaporation exceeds the steady-state rate by only one per cent after 1/20 of the total evaporation time has elapsed.

It is easily seen that for compounds of low velocity and high molecular weight, the approximation to the stationary state is more quickly realized.

In considering the evaporation of multicomponent drops, such as might be encountered in the evaporation of a petroleum distillate, the concentration of the saturated vapor will be a function of time, $C_g(t)$. Fuchs shows that a solution for this condition, corresponding to Equation (8-46), is

$$\Omega = -4\pi a^2 D \left(\frac{\partial C}{\partial r} \right)_{r=a} = 4\pi D a C_g(t) \left[1 + \frac{a}{\sqrt{D\pi t}} \frac{C_s(0) + 2t \int_0^1 C t(1-x^2) dx}{C(t)} \right] \quad (8-50)$$

where $C = dC/dt$. In the original work, the necessary and sufficient conditions for Equation (8-50) to be a good approximation to the stationary state are discussed. The equation is given in a functional form which corresponds to the special form which $C_g(t)$ assumes for the particular system in question.

The function $C_g(t)$ is closely related to the liquid-vapor composition relation for the multicomponent system being considered. If the components in the liquid phase are of nearly the same internal pressure, then the system will follow Raoult's law and hence the vapor composition may be calculated from knowledge of the liquid composition.

Thus far in this discussion, we have treated the evaporative process as taking place in an infinite medium. At this point, we shall treat the question of how a drop evaporates in a vessel having nonabsorbing walls. The importance of this question can be realized by considering the evaporation of a fuel-air dispersion. In applications where a fuel mist is formed in a combustion chamber, evaporation of this kind takes place in the interval prior to combustion. The evaporation of a drop can be considered to take place as though it were in a vessel having nonabsorbent walls of the same material constituting the drop. The volume of the vessel is not that of the combustion chamber but is considered equal to the average free volume enclosing each drop.

Although no completely rigorous solution of this problem has been obtained, Fuchs has worked out a simple approximate solution based on the assumptions that the dispersion contains only a small weight concentration of droplets, and that the drop is situated in a spherical vessel of radius R . The evaporation rate is given by

$$I = 4\pi a D C_s e^{-3Da/R^3} = \Omega_0 e^{-3Da/R^3} \quad (8-51)$$

For small values of a/R , Equation (8-51) gives a good approximation of the stationary state. However, this equation is only applicable in the case where the decrease in volume of drop is very small.

THE VAPOR-CONCENTRATION DISCONTINUITY AT A DROP SURFACE

Up to this point in the discussion, little has been said regarding the values of the vapor concentration at the surface of an evaporating drop. Stefan⁽⁸⁻⁸⁾ and Winkelmann⁽⁸⁻⁹⁾ first recognized the difficulty of assigning a value to this concentration. Fuchs⁽⁸⁻⁴⁾, however, was first to see clearly that the diffusion process does not start directly at the surface of the drop, but rather from the surface of an enveloping sphere of pure vapor; the thickness of this envelope, Δ , is of the order of the mean free path of the "air molecule". This being true, it follows that few air molecules will be present in the spherical shell of thickness Δ . This jump, or step-wise increase in the concentration of vapor, has a vanishingly small value for a plane surface at atmospheric pressure. However, if the evaporation of small drops is being considered, the jump in concentration assumes an important significance, particularly for the case where the diameter of the drop is of nearly the same magnitude as the mean free path of the vapor molecules.

The Case of Evaporation in an Infinite Atmosphere

Fuchs treats the problem of the concentration jump from the standpoint of a drop evaporating in a finite enclosure. It is first assumed that the concentration of vapor is C_1 at a distance $(a + \Delta)$ from the drop center; this concentration is less than the equilibrium value C_s , as may be seen presently. The radial increment Δ is, of course, an equivalent distance, since there must be a concentration gradient within the spherical shell of radii a and $(a + \Delta)$.

The rate at which molecules evaporate into a vacuum is $4\pi a^2 \nu \alpha C_0$, where α is the evaporation coefficient, ν is the collision frequency, and a is the radius of the drop. Now the rate at which molecules arrive at the spherical surface $(a + \Delta)$ is $4\pi a^2 \nu \alpha (C_0 - C_1)$. Under steady-state conditions, this rate of arrival may be equated to the rate at which molecules leave by diffusion, or

$$4\pi a^2 \nu \alpha (C_0 - C_1) = 4\pi (a + \Delta) D C_1 \quad (8-52)$$

Since the time rate of change of the mass of the drop is

$$-\frac{dm}{dt} = 4\pi (a + \Delta) D C_1 m_2 \quad (8-53)$$

where m_2 is the mass of the diffusing molecules, we may eliminate C_1 from Equations (8-52) and (8-53) and arrange the terms of the resulting equation in the form

$$-\frac{dm}{dt} = \frac{4\pi D a C_0 m_2}{\alpha a \nu + \frac{a}{a + \Delta}} \quad (8-54)$$

Fuchs, in his paper, left Δ in an indefinite form. However, Bradley and co-workers⁽⁸⁻¹⁰⁾ interpreted the physical meaning of this factor in the following way: Let the collision area for impact of evaporating and air molecules be A (this will be a mean value for the constituents of air). Let the velocity of the molecules leaving the drop be \bar{u} . Then the number of collisions between air and vapor molecules is $\bar{u} \left(\frac{AP}{RT} \right)$ per second. The reciprocal of this quantity is the time between collisions, so that the distance between collisions is

$$\left(\frac{kT}{A\bar{u}P} \right) \bar{u} = \frac{kT}{A\bar{u}P} = \Delta \quad (8-55)$$

In other words, Δ is taken to be the distance through which a molecule travels from the drop before colliding with an air molecule.

Several workers in the field of droplet evaporation have noted that the linear law for the diminution of droplet surface with time does not hold for droplets of small radius. Speakman and Sever⁽⁸⁻¹¹⁾ found that measurable negative deviations began to occur at a $\approx 1\mu$, while deviations close to 40 per cent occurred at a $\approx 0.1\mu$. They explained this phenomenon as being due to the lowering of the vapor pressure by dissolved nonvolatile impurities. Unfortunately, this interpretation cannot be checked because the curve relations given by these workers do not permit a quantitative comparison with Equation (8-54). Woodland and Mack⁽⁸⁻¹²⁾ observed an opposite behavior in the evaporation of small drops. They report an increase in the rate da^2/dt upon diminishing the size of the drop. No completely satisfactory explanation can be given for this observation. Whytlaw-Gray and Patterson⁽⁸⁻¹¹⁾ have also noted that the rate of evaporation diminishes as the droplet becomes very small, and have commented upon the fact that the effect of Brownian motion increases the experimental error in the measurement of very small drop size.

Although Langmuir⁽⁸⁻¹³⁾ recognized the possibility of the concentration-jump effect, he did not account for it in his work, since many of his observations on evaporating drops were carried out in the size range and at pressures where the equation $-dm/dt = 4\pi a D C_0 m_2$ applies satisfactorily. In the Langmuir expression, the loss per unit area per unit time is $D C_0 m_2 / a$, which becomes infinite as the radius approaches zero. It is evident that Langmuir's equation is not valid either for the evaporation of very small drops at atmospheric pressure or for the evaporation of large drops at very low pressures. It is valid, however, for the evaporation in normal air of drops having radii greater than 10^{-3} cm.

Equation (8-54), unlike Langmuir's, gives the correct vacuum evaporative rate for drops of 1-mm radius, since $\Delta \gg a$ and $a/(a + \Delta)$ vanishes, leaving $-dm/dt = 4\pi a^2 \nu a C_0 m_2$. Under conditions where $a \approx 1$ mm and $P = 1$ atm, $a/(a + \Delta)$ in Equation (8-54) becomes nearly unity and the term $D/a\nu a$ becomes negligible compared with unity if $D = 0.1$, $\alpha = 1$, and $T = 20$ C. In this way, Equation (8-54) can be reduced to Langmuir's equation.

The term $D/a\nu a$ cannot be close to unity if either α or a is of small magnitude. Bradley and co-workers have also noted the behavior of Equation (8-54) for very small values of a . They show that if both \bar{P} and \bar{D} are constant, the rate of evaporation, per unit area, becomes

$$-\frac{dm}{dt} = \frac{D C_0 m_2}{\bar{D} \frac{a^2}{a\nu a + \Delta}} = \nu a C_0 m_2$$

This result predicts that, on a unit-area basis, the rate of evaporation of very small drops, at atmospheric pressure, will be nearly equal to the vacuum rate of evaporation.

As has been pointed out previously, Langmuir's equation predicts an infinite rate of evaporation, per unit area, for $a \rightarrow 0$. On the other hand, the Fuchs equation, on the same basis, predicts evaporation rates less than the Langmuir rate. In the case where α is very small, $D/(a\nu a)$ would be large in comparison with $a^2/(a + \Delta)$ and a great departure from Langmuir's result would be found for $P = 1$ atm and $a = 1$ mm. This is unlikely, for experience has shown that α is nearly unity for most pure liquids.

Table 8-1 summarizes the results of both the Langmuir and Fuchs work on the basis of the surface and mass rates of change of an evaporating drop in vacuo and at atmospheric pressure. Since the diffusion coefficient varies inversely with pressure, $D = Y/P$ is used in the table in order to show the effect of pressure on evaporation rate.

TABLE 8-1. COMPARISON OF LANGMUIR AND FUCHS THEORIES OF EVAPORATION

Equation due to	Decreasing radius (a) at constant pressure			B
	$-\frac{dm}{dt}$	$-\frac{dm}{dt} \frac{1}{4\pi a^2}$ (per unit area)	$-\frac{ds}{dt}$	
Langmuir	$4\pi a D c_0 m_2 \rightarrow 0$ as $a \rightarrow 0$	$\frac{D c_0 m_2}{a} \rightarrow \infty$ as $a \rightarrow 0$	$\frac{8\pi D m_2 c_0}{\rho} \rightarrow \text{constant}$ as $a \rightarrow 0$	
Fuchs	$\frac{4\pi a D c_0 m_2}{\frac{D}{\nu a} + \frac{a}{a+\Delta}} \rightarrow 0$ as $a \rightarrow 0$	$\frac{D c_0 m_2}{\frac{D}{\nu a} + \frac{a^2}{a+\Delta}} \rightarrow \nu c_0 a m_2$ as $a \rightarrow 0$ (vacuum rate)	$\frac{8\pi D m_2 c_0}{\rho} \left\{ \frac{1}{\frac{D}{\nu a} + \frac{a}{a+\Delta}} \right\} \rightarrow 0$ as $a \rightarrow 0$	
Decreasing pressure (P) at constant radius				
	$-\frac{dm}{dt}$	$-\frac{dm}{dt} \frac{1}{4\pi a^2}$	$-\frac{ds}{dt}$	
Langmuir	$\frac{4\pi a Y c_0 m_2}{P} \rightarrow \infty$ as $P \rightarrow 0$	$\frac{Y c_0 m_2}{a P} \rightarrow \infty$ as $P \rightarrow 0$	$\frac{8\pi Y c_0 m_2}{P \rho} \rightarrow \infty$ as $P \rightarrow 0$	
Fuchs	$\frac{4\pi a c_0 m_2}{\frac{1}{\nu a} + \frac{Pa}{Y(a+\Delta)}} \rightarrow 4\pi a^2 \nu c_0 a m_2$ as $P \rightarrow 0$ (vacuum rate)	$\frac{c_0 m_2}{\frac{1}{\nu a} + \frac{Pa^2}{Y(a+\Delta)}} \rightarrow \nu c_0 m_2$ as $P \rightarrow 0$ (vacuum rate)	$\frac{8\pi Y m_2 c_0}{P \rho} \left\{ \frac{1}{\frac{Y}{Pa \nu a} + \frac{a}{a+\Delta}} \right\} \rightarrow \frac{8\pi a \nu a c_0 m_2}{\rho}$ as $P \rightarrow 0$ (vacuum rate)	

The Case of Evaporation Into a Finite Vessel
With Absorbing Walls

Bradley and co-workers(8-10) found that it was necessary to modify Fuchs' expression to put it in a form such that it might be applied to the evaporation of a drop under experimental conditions. Since the expression, as given by Equation (8-54), is derived for the evaporation of a drop in an infinite atmosphere, its form is unsuitable for experimental verification; the following modification assumes that the drop evaporates into a finite vessel having absorbent walls.

In terms of the Fuchs' correction Δ , the rate of change of the mass of the drop is given by

$$-\frac{dm}{dt} \left(\frac{1}{a + \Delta} - \frac{1}{r_0} \right) = 4\pi D C_1 m_2 \quad (8-56)$$

where r_0 is the radius of the vessel. At r_0 , the concentration of vapor is zero. Now, at $(a + \Delta)$, $P_1 = C_1 kT$. Also, the vapor pressure P_1 is taken as being much smaller than the total pressure. By equating the loss of mass by diffusion to the rate of arrival of molecules at $(a + \Delta)$, there results

$$4\pi a^2 \nu a (C_0 - C_1) = \frac{4\pi (a + \Delta) r_0}{(r_0 - a - \Delta)} \quad (8-57)$$

Equation (8-57) is solved for C_1 , the concentration of vapor at $(a + \Delta)$, and this, in turn, is substituted into Equation (8-56). After properly arranging terms, the resulting equation is

$$\frac{dm}{dt} = \frac{4\pi a Y C_0 m_1}{P \left[\frac{Y}{P a \nu \alpha} + a \left(\frac{AP}{aAP + kT} - \frac{1}{r_0} \right) \right]}$$

or, in terms of a , the radius of drop,

$$-a \left(\frac{da}{dt} \right) = \frac{Y C_0 m_2}{\rho P \left[\frac{Y}{P a \nu \alpha} + a \left(\frac{AP}{aAP + kT} - \frac{1}{r_0} \right) \right]} \quad (8-58)$$

By integration, Equation (8-58) reduces to

$$a + H \left[\frac{1}{2}(a + \Delta)^2 - 2\Delta(a + \Delta) + \Delta^2 \ln(a + \Delta) \right] - H \frac{Ha^3}{3r_0} = -Lt + \beta \quad (8-59)$$

where $H = \frac{a \nu P}{Y} = \frac{a \nu}{D}$, $L = \frac{a \nu C_0 m_2}{\rho}$, and $\beta = a$ constant.

In Bradley's experimental work, conditions were selected such that the changes in the radii of the evaporating drops were small. Under these conditions the investigators justifiably treated the equation as if the denominator were constant and carried out the integration after changing from a radius to a surface area variable. This result is

$$(s - s_0) = \frac{-8\pi Y m_2 C_0 t}{\rho P \left[\frac{Y}{P a \nu \alpha} + a \left(\frac{AP}{aAP + kT} - \frac{1}{r_0} \right) \right]} \quad (8-60)$$

If the above derivation were carried out starting with Langmuir's equation, the rate of change of the surface area of the drop, ds/dt , would be found proportional to $1/P$; this would mean that the rate would become infinite as the pressure was decreased. Equation (8-60), however, shows that, as P decreases, ds/dt approaches asymptotically the vacuum rate.

Bradley carried out an extremely precise determination of the rate of evaporation of both dibutyl phthalate and butyl stearate under conditions where Equation (8-60) should be applicable. The evaporation vessel consisted of a glass bulb inside of which was placed a copper-wire basket. The annular space between the wall and the basket was filled with charcoal in order to maintain a vanishingly small concentration of vapor at the wall. This bulb was then attached to a chamber containing a quartz microbalance, the deflections of which could be read by means of a micrometer microscope. From the arm of the balance was suspended a quartz filament carrying the drop of liquid to be evaporated. The entire chamber could be evacuated to any desired pressure by means of a pumping system. The entire evaporation and weighing system was thermostatted at 20 C. Elaborate precautions were taken to assure the absence of moisture and dust from the system.

The decrease in the mass of droplet at fixed pressure, was noted by measuring the balance deflection by means of the micrometer microscope; weight changes of 2.9×10^{-8} g. could be observed in this manner.

In order to examine graphically the data obtained, it was found necessary to write Equation (8-60) in the form:

$$\frac{q_0}{q} = \frac{1}{PW} + \frac{1}{1 + \frac{kT}{aAP}} - \frac{a}{r_0} \quad (8-61)$$

where $q = ds/dt$ at a particular P , $(-8\pi m_2 C_0 t / \rho P) = q_0$, and $W = a \nu \alpha / Y$.

A knowledge of the molecular dimensions permits the calculation of \bar{A} , so that the term $(1 + kT/aAP)^{-1}$ is determined. If $q_0/q - (1 + kT/aAP)^{-1}$ is then plotted against $1/P$, a straight line should result, providing the Fuchs theory is correct; W may then be calculated from the slope of this curve.

Figure 8-1 shows the plot of Bradley's data for the evaporation of dibutyl phthalate drops having radii of 0.5 mm. The variation in drop radii between runs was about five per cent. Graph A shows values of da/dt plotted against $1/F$. This relation shows that Langmuir's equation holds for relatively large values of P , but as P decreases, a marked bending of the curve away from the initial line occurs. In Graph B is shown the effect of replotting the data in accordance with Equation (8-61). It may be noted that the experimental points agree very favorably with the Fuchs theory throughout the range of observations.

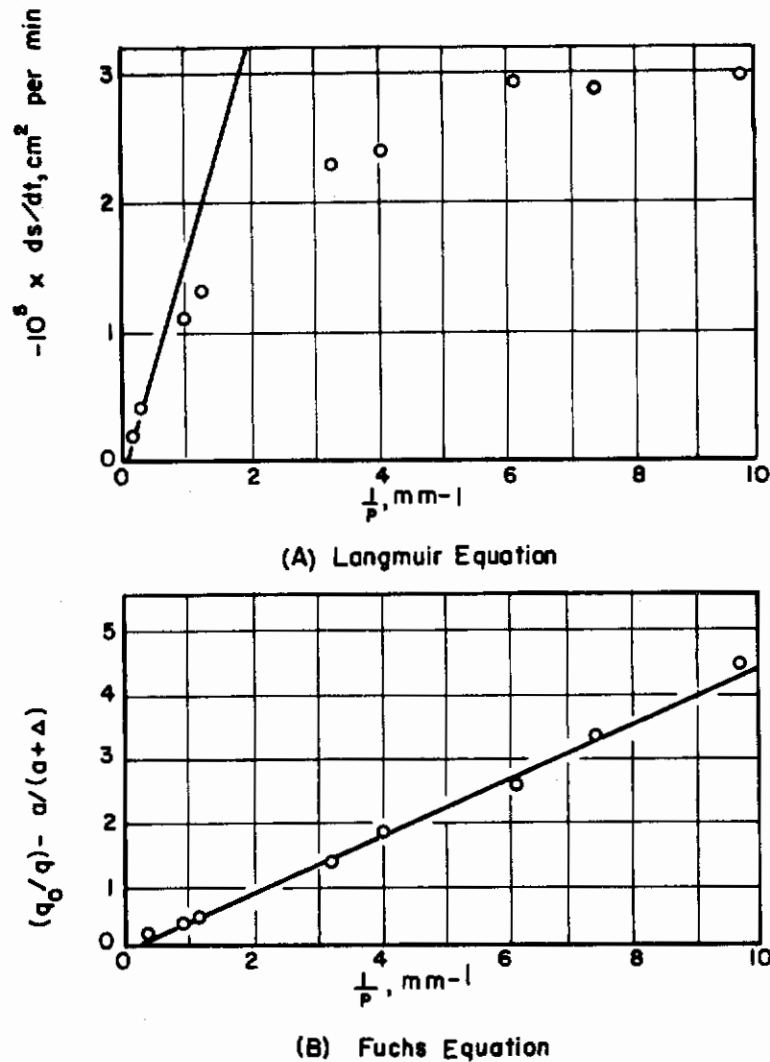


FIGURE 8-1. RATES OF EVAPORATION OF DIBUTYL PHTHALATE DROPS AS A FUNCTION OF PRESSURE

Bradley has also attempted to check the radially dependent Equation (8-59) for a series of experiments in which the radius of the drop varied considerably. The experimental rate was found to differ from the theoretical rate by a factor of two. These workers attribute this departure to the fact that the fibre causes a distortion of the drop shape. Thus, interfacial tension between the drop and the fibre causes heavier drops to be more pear shaped than smaller drops. No attempt has been made to verify this explanation experimentally.

Further work by Birks and Bradley⁽⁸⁻¹⁴⁾ gave better agreement with the Fuchs equation. As a means of establishing more carefully the relation between the droplet radius and the mean-free path of the evaporating molecules, these workers carried out evaporating rate measurements on large droplets ($r = 10^{-2}$ cm) at very low pressures. The recent studies of Moncheck and Reiss⁽⁸⁻¹⁵⁾ show that the evaporation rates of di n-amyl sebacate and of dibutyl phthalate droplets under carefully controlled conditions follow the general form of the Fuchs' equation for $r \approx 5 \times 10^{-5}$ cm.

The Fuchs analysis is, nevertheless, unsatisfactory in many respects because of the ill-defined kinetic model which is described in the original paper; since Δ is not clearly defined, it has not been possible to ascertain the validity of this treatment.

By using a stochastic approach to the evaporation problem, Frisch and Collins^(8-16, 8-17) derived an equation which is similar in general form to Fuchs' result but contains several undetermined parameters. However, the utility of their treatment is severely impaired by the necessity of having to make a number of perhaps unjustifiable assumptions in order to evaluate the parameters.

Moncheck⁽⁸⁻¹⁵⁾ has shown that a more satisfactory solution to the evaporation problem results from the application of non-Maxwellian distribution functions which are appropriate for the treatment of gases in extremely nonuniform states.

The evaporation model is taken as a binary gas mixture containing components 1 and 2 which surround a liquid droplet of component 1. The concentration of each species can be expressed as $C_1(\vec{r}, t)$ and $C_2(\vec{r}, t)$ when the center of the drop is chosen at $r = 0$; \vec{r} denotes a unit vector taken normal to the surface of the drop. The main assumptions are that no temperature or pressure gradients exist in the gas phase and that intermolecular forces can be ignored except during molecular collisions. In addition, it is assumed that no mass motion occurs within the system.

Thus, under these conditions, the Enskog⁽⁸⁻²⁵⁾ nonequilibrium distribution function suffices for expressing

$$f_1(\vec{r}, \mathbf{v}_1) = f^0 \left\{ 1 - D_1(\vec{v}_1) \mathbf{v}_1 \cdot \nabla C_1 \right\} \quad , \quad (8-62)$$

the velocity spectrum of species 1. The equilibrium distribution is denoted by $f^0(\mathbf{v}_1)$ and the vectorial velocity by \vec{v}_1 . The scalar form of $f^0(\mathbf{v}_1)$ can be written as

$$f^0(\mathbf{v}_1) = C_1 (m_1/2\pi kT)^{3/2} \exp(-m_1 \mathbf{v}_1^2/2kT) \quad . \quad (8-63)$$

If Equation (8-62) is integrated over the total velocity space and only the first order perturbation terms retained, then the diffusion coefficient, D_1 , can be defined in terms of an average velocity component $\langle \vec{v}_1 \rangle_{av}$ such that

$$-D_1 \nabla C_1 = C_1 \langle \vec{v}_1 \rangle_{av} = - \left\{ 1/3 \int f^0(\mathbf{v}_1) D_1(\mathbf{v}_1) \mathbf{v}_1^2 d\vec{v}_1 \right\} \nabla C_1 \quad . \quad (8-64)$$

Since the concentrations C_1 and C_2 are only functionally dependent upon r , then the net flux, ϕ , can be expressed as

$$\phi = 4\pi a^2 C_1(a) \langle v_{1n} \rangle_{av} = 4\pi a^2 \left(\frac{\partial C_1}{\partial r} \right)_{r=a} \quad , \quad (8-65)$$

where the subscript n denotes the average velocity component in a direction normal to the drop surface. The net flux is evidently the difference between the condensation flux, ϕ_c , and the evaporation flux, ϕ_v . The former can be taken as

$$\phi_c = 4\pi a^2 \int \alpha(\vec{v}_1) f(\mathbf{v}_1) v_{1n} d\vec{v}_1 \quad , \quad (8-66)$$

where the positive sign (+) indicates that the integration is to be made in the positive direction of V_{1n} . The condensation coefficient, $\alpha(\bar{V}_1)$, is evidently a function of the vectorial value of the velocity \bar{V}_1 . Since α may be taken conveniently as an average coefficient, α_0 , and a first order perturbation average, α_1 , the condensation flux is

$$\phi_c = 4\pi a^2 \left\{ \alpha_0 \int_+ f^0 \cdot V_{1n} d\bar{V}_1 + \alpha_1 (\partial C_1 / \partial r)_a \int_+ f^0 D_1(V_1) V_{1n}^2 d\bar{V}_1 \right\} \quad , \quad (8-67)$$

or since

$$\int V_n^2 F(V) d\bar{V} = 1/3 \int V^2 F(V) d\bar{V} \quad , \quad (8-68)$$

$$\phi_c = 4\pi a^2 \left\{ C_1(a) \alpha_0 \nu + \alpha_1 D/2 (\partial C_1 / \partial r)_a \right\} \quad .$$

The Maxwellian rate at which molecules strike the drop surface is $\nu = (kT/2\pi m_1)^{0.5}$.

By assuming that ϕ_c is independent of ϕ_v so that an equilibrium $\phi = 0$ and $C_1 = C_1^0$, then the evaporation flux is

$$\phi_v = 4\pi a^2 \alpha_0 \nu C_1^0 \quad . \quad (8-69)$$

By combining Equations (8-69) and (8-65) with (8-62), then the radial concentration gradient is

$$(\partial C_1 / \partial r)_a = \alpha_0 \nu [C_1(a) - C_1^0] / D(1 - \alpha_1/2) \quad . \quad (8-70)$$

This result is an unusually useful boundary condition since it is valid at the actual interphase boundary.

Frisch and Collins have pointed out that for the case of a droplet of changing size, the above boundary condition in conjunction with a steady state solution of the Fuchs law equation is a good approximation. Thus, by selecting appropriate forms for $C_1(a)$ and $(\partial C_1 / \partial r)_a$, the rate of change of the droplet radius is

$$da/dt = -m_1 \alpha \nu C_1^0 / \rho(1 - \alpha/2) \left(1 + \frac{\nu a}{(1 - \alpha/2)D} \right) \quad , \quad (8-71)$$

if $\alpha_0 = \alpha_1 = \alpha$. The experimental data of Lennard-Jones and Devonshire(8-18) support this simplification regarding the accommodation coefficients. The above equation can be converted to a form which is equivalent to the case of droplet evaporation under equilibrium conditions but with a correction for a distribution of mean-free paths. Thus $\psi(s)ds$ is the probability of a molecule moving over a path s in a time corresponding to $\Delta t = 1/\nu'$, then the net flux is

$$\phi = \alpha_0 \nu' \int_0^\infty \int_0^\infty \sin^{-1} a/r \int_\beta^\infty 2\pi r^2 \sin \theta V(r, t) \psi(s) ds d\theta dr \quad , \quad (8-72)$$

where $\beta = r \cos \theta (a^2 - r^2 \sin^2 \theta)^{1/2}$. To evaluate this integral, the following reasonable assumptions are made: (1) steady-state conditions, (2) the velocity distribution following each jump is Maxwellian, (3) that $V(r, t) = C_1(a)^{a/r} - C_1^0$, and (4) that $\psi(s)$ is an isotropic function. The resulting rate equation is

$$da/dt = - m_1 \alpha_0 \nu' \langle s \rangle C_1^0 / 4\rho(1 - \alpha_0) / 2 [(1 + \alpha\nu'/2)(1 - \alpha_0/2)] D x \quad (8-73)$$

where x is obtained from the auxiliary equation

$$x = \int_0^{\infty} \psi(s) \left\{ a^2/2 \ln (s^2 + a^2)^{1/2}/a + as/6 (s^2 + a^2)^{1/2} + a^2/3 \left(a - (s^2 + a^2)^{1/2}/s \right) \right\} ds \quad (8-74)$$

By further approximations, $x \approx a \langle s \rangle / 2$ if $a \gg \langle s \rangle$ and $D = (\nu' / 6) \langle s^2 \rangle$ and accordingly

$$\langle s^n \rangle = \int_0^{\infty} s^n \psi(s) ds$$

Thus the approximate form of Moncheck's rate equation is

$$da/dt \approx - \alpha_0 \nu' \langle s \rangle m_1 C_1^0 / 4\rho(1 - \alpha^0)/2 (1 + \alpha_0 \nu' \langle s \rangle a / 4\rho(1 - \alpha_0/2) D) \quad (8-75)$$

Equation (8-75) is identical with Equation (8-71) when $\nu' \langle s \rangle = \langle V_1 \rangle_{av}$, because $\nu = 1/4 \langle V_1 \rangle_{av}$; this is, of course, equivalent to setting $\nu' \langle s \rangle$ equal to the mean-thermal velocity of the molecules.

The simpler rate Equation (8-71) differs from the Fuchs equation by a factor $(1 - \alpha/2)^{-1}$ and therefore the form of the latter equation is correct as long as it is necessary to take into account only the first order perturbation term in the Enskog distribution. Since the successive perturbation functions $f^{(0)}$, $f^{(1)}$, $f^{(2)}$ - are proportional to successive powers of c in the order C , C^0 , C^{-1} -, it is necessary to introduce additional terms as the pressure in the system is decreased. The limit of validity of Equation (8-75) is approached when $\phi(f^{(1)}) = \phi(f^{(0)})$ and where $D/a = 2\nu$. Also, Equation (8-75) does not converge to the vacuum rate of evaporation at the limit $\rho = 0$.

Greenstadt⁽⁸⁻²⁰⁾ has recently given an elegant theoretical treatment of a one-dimensional evaporation problem where the energy distribution of the evaporating molecules is used in a calculation of the corresponding distribution for molecules returning to the liquid surface. The problem is first stated in terms on a nonlinear Holtzmann equation⁽⁸⁻²⁵⁾ for gas transport and then linearized in dimensionless form. The linearized equation is brought into the form of an integral equation of the Fredholm type and is then examined in terms of a Schwinger variational function for the velocity distribution of the molecules returning to the surface. The final integral equation expresses the probability distribution of molecules at the liquid-gas interface during a slow-evaporation process which may be either steady or time dependent. The results of this mathematical analysis are compared with elementary-evaporation theory⁽⁸⁻²¹⁾ for slow evaporation and are found to differ only by correction terms.

DIFFUSION OF DROP EVAPORATION

As has been mentioned earlier, the evaporation of a drop which is at rest relative to the surrounding gas is dependent upon the diffusive transport of molecules from its surface layer to the atmosphere enveloping the drop. The diffusion of a molecular species 1 into species 2 may be expressed as:

$$D_{12} = \frac{2}{3\pi S_{12}^2} \frac{1}{1 + \alpha_{12}} \frac{kT}{P} \left[\frac{2kT(m_1 + m_2)}{\pi m_1 m_2} \right]^{1/2} \quad (8-76)$$

according to the kinetic theory of gases, where S_{12} is the collision radius, α_{12} is a factor dependent upon molecular velocities, and other symbols are as previously defined.

The application of Equation (8-76) to the calculation of the diffusion coefficients of monatomic and diatomic gases presents no particular difficulty. However, in applications to the diffusion of polyatomic molecules, considerable difficulty is encountered because of the complications which arise in connection with evaluating S_{12} . The collision radius is closely related to the geometry and to the mechanical behavior of the molecule which is under consideration. It, therefore, seems apropos to limit the present discussion of diffusion to hydrocarbon vapors, since these molecules possess an homologous behavior with respect to their geometry and molecular dynamics. Furthermore, these compounds are of considerable practical interest because of their widespread use as liquid fuels.

Burk and co-workers⁽⁸⁻²²⁾ have calculated the collision radii of a number of straight-chain paraffins from the collision-area data of Melavin and Mack⁽⁸⁻²³⁾. The later workers calculated collision areas from temperature-viscosity measurements of the hydrocarbon vapors, using Chapman's equation

$$\bar{A} = \frac{0.0868 (1 + \epsilon_\alpha) \rho_0 \bar{V}}{n \eta [1 + C/T]} \quad ,$$

where \bar{A} is the collision area of a molecule, assuming that it behaves as an elastic sphere, ρ_0 is the vapor density at standard conditions, \bar{V} is the average molecular velocity at temperature T, n is the number of molecules/cc, C is the Sutherland constant, and η is the viscosity of the gas; the correction term $(1 + \epsilon_\alpha)$ differs from unity only by one per cent.

Table 8-2 gives the results of Burk's computations. The column headed "a" is calculated by subtracting the ethane-chain length from each of the higher hydrocarbons and dividing the residue by N-2, where N is the number of carbon atoms in the hydrocarbon. A smoothed value of "a" has been taken as 0.23, by assuming that this factor is constant for the paraffin hydrocarbon series. On this basis, the collision radius $(1/2)S_{11}$ may be written

$$(1/2)S_{11} = 0.23 (N-2) + 1.84 \quad . \quad (8-77)$$

Melavin and Mack have remarked that although the Chapman equation predicts that the collision area (and consequently the collision radius) will be independent of the temperature, this may be false to the extent that hydrocarbon molecules are not well approximated by the Sutherland model. Actually, the Sutherland equation is strictly applicable only to monatomic gases.

Bradley and Shellard⁽⁸⁻²⁴⁾ measured the rates of evaporation of three hydrocarbons, n-hexadecane, n-heptadecane, and n-octadecane, into air using the microbalance technique which was described earlier. These experiments were carried out at a number of temperatures, and the diffusion coefficient as a function of temperature was determined for each hydrocarbon.

TABLE 8-2. EXPERIMENTAL COLLISION RADII FOR HYDROCARBONS

Hydrocarbon	Collision Area, Å ²	Radius, Å	"a"
Ethane	10.63	1.84	0.23
Propane	13.53	2.07	0.21
Butane	16.11	2.26	0.21
Heptane	26.7	2.96	0.25
Octane	34.9	3.33	0.26
Nonane	42.5	3.68	--

Table 8-3 shows the self-collision radii for these hydrocarbons as calculated by Bradley, using Jeans⁽⁸⁻²⁵⁾ values for α_{12} . These calculations were made from Equation (8-76) and from Bradley's diffusion data. The tabular values are written as $(1/2)S_{11}$, since Jeans' radius for the "air molecule" (1.87 Å) is subtracted from the calculated value.

TABLE 8-3. RADII OF HYDROCARBON MOLECULES CALCULATED FROM COLLISION EQUATION

Temperature, C	$(1/2)S_{11}$, Å		
	n-C ₁₆ H ₃₄ , $\alpha_{12} = 0.304$	n-C ₁₂ H ₃₆ , $\alpha_{12} = 0.306$	n-C ₁₈ H ₃₈ , $\alpha_{12} = 0.308$
14.97	4.53	4.40	4.56
16.97	4.52	--	--
20.01	4.51	4.37	4.55
24.98	4.49	4.34	4.53
29.98	4.46	4.31	4.50
34.88	4.22	4.29	4.47
39.94	--	4.27	4.44

Bradley and Shellard compare their values of $(1/2)S_{11}$ with those calculated from Equation (8-77). This equation gives for n-C₁₆H₃₄, 5.03 Å and for n-C₁₈H₃₈, 5.52 Å. These values do not compare favorably with those given in this table. These investigators state that it is unrealistic to treat a flexible molecule, such as a hydrocarbon, as though it were an elastic sphere. A further point of criticism of Equation (8-77) lies in the assumption that the radius of a hydrocarbon molecule increases uniformly by 0.23 Å per additional CH₂ group, an assumption contrary to the generally accepted theory of higher hydrocarbon geometry.

Bradley and Shellard made comparisons of their experimental radii for the three hydrocarbons with radii calculated from the Eyring Equation⁽⁸⁻²⁶⁾ for the mean square of the distance between the centers of the end carbon atoms. The calculated results did not agree with the experimental values. Application of both the free-rotation correction of Taylor⁽⁸⁻²⁷⁾ and the Van der Waal radius correction for each methylene group in the chain also failed to account for this discrepancy between theory and experiment. In all these theoretical treatments, no account is taken of the intramolecular forces, which favor strongly the molecule's assuming a compact form by coiling of the chain.

Bradley and Shellard⁽⁸⁻²⁴⁾ found, by constructing helical-coil molecular models, with the ends of the hydrocarbons set at a statistical distance apart to allow for free rotation, that it was possible to account for the average experimental molecular diameters of the three long-chain hydrocarbons studied. The models assumed a nearly spherical form, which serves to demonstrate that the effect of statistical coiling will be more pronounced with increasing hydrocarbon-chain length. Hydrocarbons up to n-nonane would have scarcely more than one helical turn.

The discussion of the diffusion of hydrocarbon molecules shows that a proper choice of collision radius for any complex polyatomic molecule presents numerous difficulties. Thus, the diffusion coefficients which are based upon theoretical collision radii are always open to question on the ground that all theories lead to widely differing radii. It would seem obvious that the most satisfactory diffusion coefficients for use in evaporation studies of complex molecules would be those obtained from transport experiments carried out under conditions similar to those of evaporation.

One of the most notable recent contributions to the theory and calculation of diffusion coefficients has been made by Hirschfelder and co-workers(8-28, 8-29, 8-30), at the University of Wisconsin. Their work is based upon the fact that the transport properties of gases depend upon the forces between the molecules which are to be considered. The force between molecules may be written as the potential-energy function

$$E(r) = 4\epsilon \left[-\left(\frac{r_0}{r}\right)^6 + \left(\frac{r_0}{r}\right)^{12} \right] \quad , \quad (8-78)$$

in which r is the molecular separation, ϵ is the maximum energy of attraction (force constant), and r_0 is the collision diameter for low-energy head-on collisions. The force constant can be calculated by means of the relations

$$r_0 = (8.33 \times 10^7)(V_c)^{1/3} \quad , \quad (8-79)$$

$$\epsilon = 0.75 kT_c \quad , \quad (8-80)$$

or

$$\epsilon = 1.39 T_b \quad , \quad (8-81)$$

where T_c and T_b are, respectively, the critical temperature and the normal boiling point and V_c the critical volume of the molecular species in question. All of the above equations are a direct consequence of the Lennard-Jones and Devonshire theory of gases and liquids(8-32, 8-33).

From Equation (8-78) may be derived an expression for χ , the angle of deflection of two colliding molecules. This, in turn, is related to the "reduced" collision cross section $S^{(1)}(K)$ by

$$S^{(1)}(K) = \left\{ 4 \left[2 - \frac{1 + (-1)^l}{1 + 1} \right] \right\} \int_0^\infty \left[1 - \cos^{(l)} \chi \right] \beta d\beta \quad , \quad (8-82)$$

where K is the relative kinetic energy of the molecules at large separation and along a line of centers, β is the distance of closest approach, and l is a constant which is equal to 2 for most gas-diffusion problems. For the case of the rigid sphere model of the last section, $S^{(1)}(K) = 1$. Hirschfelder's approach to the diffusion problem is much more realistic than that of the earlier discussion, since it is not based upon ideally elastic collisions.

Hirschfelder has transformed Equation (8-82) to the collision integral(8-26)

$$W^{(1)}(n;x) = 1/8 \left[2 - \frac{1 + (-1)^l}{1 + 1} \right] x^{n+2} \int_0^\infty e^{-xK} K^{n+1} S^{(1)}(K) dK \quad , \quad (8-83)$$

where $x = \epsilon/kT$.

This integral has been tabulated numerically(8-22) as $W^{(1)}(n;x)$ for $x = 0.3$ to 400, l ranging from 1 to 4, and n ranging from 1 to 6. In order to use this collision integral, it is necessary to know only the values of ϵ/k and r_0 , which in many instances, can be computed from critical data.

Hirschfelder's(8-29) final equation for binary diffusion to the first approximation is

$$D_{12} = \frac{0.00092916 T^{3/2} \left[M_1 + M_2/M_1 M_2 \right]^{1/2}}{P(r_{12})^2 W^{(1)}(1; kT/\epsilon_{12})} \quad , \quad (8-84)$$

where D_{12} is the binary diffusion coefficient, cm^2/sec , M_i is the molecular weight of the i th component, P is the pressure in atmospheres, r_{12} is the collision diameter in \AA , and ϵ_{12} is the maximum energy of attraction between the unlike molecules.

In most cases, Equation (8-84) gives results which compare excellently with experimental data and which represent a great improvement over the Sutherland assumption; this is particularly so for nonpolar gas mixtures. Because the collision integrals are set up in terms of interaction energies and collision diameters, Equation (8-84) should be applicable to the diffusion of gases at both very high and very low temperatures. Under the latter condition, quantum mechanical energy corrections would be necessary because the theory is based upon classical gas dynamics.

This treatment does not permit the calculation of the diffusion coefficients in the instance where both compounds are polar molecules. However, Equation (8-84) may be applied to binary mixtures of polar and nonpolar gases because the energy of interaction is the same as that of a nonpolar gas mixture.

Curtiss(8-30) has extended this theory in such a manner that it may be applied to calculating the diffusion coefficient of one molecular species into any number of other species. Although the basic mathematical analysis underlying the treatment is complex, the resulting equations are simple and may be readily applied. It is, however, necessary to know all the possible binary intermolecular diffusion coefficients for the system, as well as the concentration of each component. The final useful equation is in determinant form.

The calculation of accurate diffusion coefficients for multicomponent systems would, of course, be directly useful in the study of the evaporation and combustion of drops of liquid hydrocarbon fuels because many molecular species are usually present in such a system.

HEAT TRANSFER AND DROP EVAPORATION

It was pointed out at the beginning of this chapter that the rate of evaporation of a drop is dependent both upon the absorption of thermal energy and upon the outward diffusion of the molecules constituting the drop. In deriving the Maxwell equation for evaporation, it was assumed that the reception of heat by the drop took place through conduction alone. The effects of thermal radiation and of free convection were neglected. In this section there will be discussed the mechanism of heat transfer by all these processes and also the probable extent to which each mechanism affects drop evaporation.

The reversible absorption of heat in any constant-volume system is given by

$$\frac{dq}{dt} = \left(\frac{\partial E}{\partial T} \right)_v = c_v dT \quad , \quad (8-85)$$

where q is the heat absorbed, E is the energy change corresponding to a change in temperature, and c_v is the heat capacity at constant volume. For a drop of radius a , the total heat absorption becomes

$$\frac{dq}{dt} = (4\pi a^2)(Z)\alpha' c_v dT \quad , \quad (8-86)$$

where Z is the number of collisions/unit area/unit time, and α' is the thermal-accomodation coefficient of the surface. Neglecting, for the moment, the absorption of radiation, Equation (8-86) expresses the absorption of heat by conduction alone. The pressure-dependent collision number, Z , is $p/(2\pi m_1 k T_g)^{1/2}$, using the nomenclature of Chapter 7, and dT may be taken as $(T_g - T_d)$, the difference in temperature between the gas and the drop. Now if the gas is assumed to be polyatomic, c_v must be the sum of contributions of the translational, rotational, and vibrational heat capacities. The translational and rotational contributions are, respectively, $1/2k$ and $3/2k$ per molecule. Since the vibrational contribution depends upon the vibrational energy levels of the particular molecule, it will be neglected in the approximate form $c_v = 2k$.

By substituting these expressions for dT , c_v , and Z in Equation (8-86), there results, upon rearrangement,

$$\frac{dq}{dt} = 4\pi a^2 \alpha' p \left(\frac{2kT_g}{\pi m_1} \right)^{1/2} \frac{T_g - T_d}{T_g} \quad (8-87)$$

B

The rate of heat loss for a drop of mass m is

$$\left(\frac{dq}{dt} \right) = \left(\frac{dm}{dt} \right) c_v (T_g - T_d) - \frac{\Delta H}{M} \left(\frac{dm}{dt} \right) \quad (8-88)$$

where M is the molecular weight. This equation states that the rate of heat loss is equal to the rate of mass transport of thermal energy away from the drop plus the amount of heat, ΔH , which is necessary for vaporizing the liquid at the mass-transport rate. If the process is assumed to be at steady state the first term on the right can be dropped, and Equations (8-87) and (8-88) may be combined to give

$$-\frac{\Delta H}{M} \left(\frac{dm}{dt} \right) = 4\pi a^2 \alpha' p \left(\frac{2kT_g}{\pi m_1} \right)^{1/2} \frac{T_g - T_d}{T_g} \quad (8-89)$$

In the steady state, the absorption of heat by the drop is balanced by an equal and opposite loss of heat resulting from evaporative cooling. The extent of self-cooling is, under this condition, equal to $(T_g - T_d) = \delta T$, or

$$\delta T = -\frac{\Delta H}{4a^2 p M \alpha'} \left(\frac{m_1 T_g}{2\pi k} \right)^{1/2} \left(\frac{dm}{dt} \right) \quad (8-90)$$

If it is assumed that the drop behaves as a black body and absorbs E_r calories of thermal radiation per unit time, then the rise in temperature due to radiation is

$$\delta T_r = \frac{E_r}{mc_v} \quad (8-91)$$

Equation (8-90) becomes, on adding Equation (8-91),

$$\delta T = \frac{E_r}{mc_v} - \frac{\Delta H}{4a^2 p M \alpha'} \left(\frac{m_1 T_g}{2\pi k} \right)^{1/2} \left(\frac{dm}{dt} \right) \quad (8-92)$$

since E_r always produces a temperature rise in the drop.

Conduction of Heat

It may be deduced from the kinetic theory of gases that the total rate of transport, Γ , of a disturbance G per gas molecule is

$$\Gamma = 1/3 n \lambda \bar{v} \left(\frac{\partial G}{\partial x} \right) \quad (8-93)$$

where λ is the mean free path of the molecule, n is the number of molecules in the volume considered, and \bar{v} is the average molecular velocity. For an ideal gas, the energy is directly proportional to the absolute temperature, T . The proportionality factor is c_v , the heat capacity at constant volume. If G is the mean energy per molecule, then $G = m_1 c_v T$. Assuming that the temperature varies along the x -coordinate,

$$\frac{\partial G}{\partial x} = m_1 \frac{\partial (c_v T)}{\partial x} = m_1 c_v \left(\frac{\partial T}{\partial x} \right) \quad (8-94)$$

Combining Equations (8-93) and (8-94) results in

$$\Gamma = 1/3 n m_1 \lambda \bar{v} c_v \left(\frac{\partial T}{\partial x} \right) \quad (8-95)$$

By definition, the thermal conductivity is the quantity of heat transported per unit area per unit time, through a unit temperature gradient. If $(\partial T/\partial x) = 1$, then Γ becomes the thermal conductivity K , or,

$$K = 1/3 n m \lambda \bar{v} c_v = \frac{2}{3\pi\sigma^2} \left(\frac{kT}{\pi m} \right)^{1/2} m c_v \quad (8-96)$$

where σ is the molecular diameter. It may be easily shown that Equation (8-89) can be reduced to a simple form containing K . Thus, the outward transport of mass (diffusion) is counterbalanced by the inward transport of heat (thermal conductivity).

In the previous section, it was shown that the simple kinetic-molecular picture for diffusion is inadequate for explaining the mass transport of polyatomic molecules in a multicomponent system. Similarly, the conduction of heat in the evaporation of a multicomponent drop cannot be satisfactorily accounted for by this elementary theory. Unfortunately, a completely satisfactory theory for thermal conduction in polyatomic gases has not yet been developed. Hirschfelder⁽⁸⁻²⁹⁾ has proposed that the thermal conductivity of a gas may be written as

$$k = \left(\frac{H\eta}{vM} \right) \left[c_v + \frac{9}{4} R \right] \quad (8-97)$$

Here, η is the gas viscosity and H and v are functions of kT/ϵ ; the ratio H/v is approximately equal to one. The bracketed factor comes directly from the Eucken assumption which states that during a collision, thermal equilibrium is instantaneously established between the translational energy and the energies associated with the internal degrees of freedom of the molecule. Chapman and Cowling⁽⁸⁻³³⁾ have discussed the Eucken assumption and have concluded that it is not completely justifiable because it assumes that the transport of translational energy is not affected by the existence of internal energy in the system. This could only be true if exchange between translational energy and internal energy occurred so rarely that it might be neglected, which is of course unlikely. A second point of criticism is that in accordance with this mechanism, the transport of internal energy would take place by molecular diffusion from one part of the gas system to another, each molecule transporting with it the mean internal energy of the region from which it originated. In other words, the mean free path of the transport would not be that associated with viscosity, but rather that appropriate for self-diffusion.

Hirschfelder compared thermal conductivities calculated from Equation (8-97) with the conductivity measurements of Johnston and co-workers⁽⁸⁻³⁴⁾ for He, CH₄, NO, CO₂, and O₂. It was found that agreement was satisfactory only for helium, the other gases showing marked departures from the theoretical values. It is not surprising that helium falls into good agreement, because it possesses no internal degrees of freedom. The comparison indicates that the Eucken assumption is not valid for polyatomic molecules. A satisfactory theory which will take into account the mechanism of energy transfer from translation into rotation and vibration is still to be found. Hirschfelder states that until an adequate theory is proposed, there is little use in trying to apply the complicated Chapman-Enskog relations to the problem of calculating the heat conductivity of multicomponent gas mixtures.

It would appear that the direct accurate experimental measurement of thermal conductivity is difficult in comparison with the measurement of the other gas-transport properties. For this reason, it is nearly impossible to construct even an empirical formulation expressing the thermal conductivity of polyatomic gas molecules.

It is possible, however, to apply Equation (8-97) to gases at very high temperatures because the molecules then behave in a more nearly classical manner. Equation (8-97) may then be used in combustion calculations, providing that data are available from which both the viscosity and the heat capacity of the gas mixture may be calculated.

In the earlier general discussion of heat transfer, it was indicated that a portion of the energy transmitted to an evaporating drop is received through the absorption of radiant energy. As will be shown later, the estimated amount of thermal energy received by this mechanism is small compared with that received by conductive heat transfer. It is, of course, possible for certain wavelength radiations to produce exothermic chemical reactions in the liquid phase as a result of photochemical activation. However, a discussion of this case more properly belongs to the subject of chemical kinetics and falls out of the scope of this treatment of heat transfer.

Penner(8-35) has treated the problem of radiant heat reception by drops under the assumption that both the drop and the surrounding gases behave as black bodies. The drop is considered to act as a receiver of radiant energy in a volume which is filled continuously with emitters of radiant energy. The radiation incident upon one sq cm of receiver surface per second is

$$\int_{\lambda} I_{\lambda}^1 d\lambda = \int_{\lambda} I_{\lambda}^* \left(1 - \exp \left[-k_{\lambda} \rho l \right] \right) d\lambda \quad , \quad (8-98)$$

where I_{λ}^1 is the energy in cal/sec which is emitted by one sq cm of a black body at the temperature of the radiating gases in the wavelength interval λ to $\lambda + d\lambda$, I_{λ}^* is the corresponding energy absorbed by the receiver in the same units, k is the average mass-absorption coefficient in the wavelength range, and l is the radiation path over which the emitters can be "seen" by the receiver.

Avery(8-36) has used Equation (8-98) in connection with the estimation of radiant energy transfer in solid-propellant rockets. In both his work and in Penner's, it is assumed that in a closed vessel uniformly filled with emitters throughout the path length l , the radiant energy

$\int_{\lambda} I_{\lambda}^* d\lambda$ incident on a small volume element of the receiver is equal to the sum of $\int_{\lambda} I_{\lambda}^1 d\lambda$ and of the radiant energy reflected from the wall and transmitted through l . The reflected energy is neglected in Penner's treatment because the reflection coefficient of an oxidized-steel combustion chamber is close to 0.2. By neglecting this effect, there will be introduced an error of about 10 per cent in the estimation of radiant energy transfer.

The maximum temperature rise in a spherical drop can be estimated in the following manner: It is first assumed that all of the incident radiation, from an emitter at temperature T , I_T , is incident on a small volume element dV at the same time and in a direction normal to the surface of dV . For a sphere of radius a , the absorbed radiation E_r is

$$E_r = \int_{\lambda} I_{\lambda}^1 \left(1 - e^{-2K_{\lambda}a} \right) \left(4\pi a^2 \right) d\lambda \quad , \quad (8-99)$$

where K_{λ} is the absorption coefficient of the receiver. If K_{λ} is chosen as being K , the average coefficient for a wide wavelength band, then Equation (8-99) may be integrated to give

$$E_r = \left(1 - e^{-2Ka} \right) 4\pi a^2 I_T \quad . \quad (8-100)$$

Equation (8-91) gives the increment of increase in drop temperature due to the absorption of radiant energy. This may now be written in terms of Equation (8-100), as

$$\Delta T = \frac{E_r}{Mc_p} = \frac{3(1 - e^{-2Ka})I_T}{a\rho_a c_p} \quad . \quad (8-101)$$

If a is small, then $e^{-2Ka} \approx 1 - 2Ka$ and Equation (8-101) becomes

Controls

$$\Delta T = \frac{6KI_T}{\rho_a c_p} \quad (8-102)$$

When the wavelength dependence of K is to be considered, Equation (8-102) should be replaced by

$$\Delta T = \frac{6}{\rho_a c_p} \int_{\lambda} K_{\lambda} J_{T\lambda} d\lambda \quad (8-103)$$

Penner's numerical value for ΔT has been worked out only for the case of a droplet in motion. A detailed discussion of this case will be given in Chapter 9, where the more important problems of heat transfer and drop motion will be discussed.

CONCLUDING REMARKS

It would appear from the foregoing discussion that the general theory of single droplet evaporation in a quiescent gas has been developed to the point where there is good agreement with experimental data. On the other hand, it has been shown that the evaporation process is strongly dependent upon the transport quantities of heat transfer and molecular diffusion. These quantities are, in turn, related to the molecular structures of both the liquid-phase and the gas-phase molecules.

Although the theory of molecular diffusion has been developed to the extent that it may be applied to the calculation of diffusion coefficients for multicomponent systems, it is limited to those systems which contain no more than one polar component. In order to accurately predict diffusion coefficients in systems containing several polar gases, it would first be necessary to develop suitable potential-energy forms for the interaction of pairs of polar molecules. Secondly, collision integrals would have to be evaluated from these potential-energy relations before the desired diffusion coefficients could be computed.

Further theoretical work on the collision geometry of large molecules appears to be needed in view of the fact that Bradley was unable to calculate, through purely theoretical considerations, the collision diameters of long-chain hydrocarbons. It is, at present, difficult to ascertain the best approach to this problem because of its inherent complexity. Adequate mathematical tools seem to be lacking for the problems connected with the geometrical behavior of long-chain molecules in the gas phase. It may be possible that from an examination of the theoretical techniques used in treating the diffusion of linear polymers in solution, a better understanding could be obtained of gas-phase diffusion of large hydrocarbon molecules.

While diffusive transport is relatively well understood, the mechanism of thermal conductivity in polyatomic gases is still in a somewhat puzzling state. Although it may be possible to develop a theory which obviates the necessity of using the Eucken assumption, no good experimental data are available for the thermal conductivities of polyatomic gases. This lack of data is undoubtedly connected with the fact that the measurement of this quantity over a temperature range, by available techniques, is exceedingly difficult. An improved experimental method for measuring heat conduction in gases is sorely needed.

Various speculations have been made concerning the effective magnitude of thermal radiation in moving-droplet evaporation. No experimental work appears to have been carried out for either static or moving drops. It would appear that further work is needed to determine the influence of radiation on the evaporation of liquid-fuel mists.

Continuity
REFERENCES

- 8-1. Maxwell, J. C., Diffusion, Sci. Papers, 2, 639, 1890.
- 8-2. Kennard, E. H., Kinetic Theory of Gases, McGraw-Hill Book Company, 1st edition, New York, 1938, p 182.
- 8-3. International Critical Tables, McGraw-Hill Book Company, 1st edition, New York, 1929, Vol. 5, p 214.
- X 8-4. Fuchs, N., Concerning the Evaporation of Small Drops in a Gas Atmosphere, NACA Technical Memorandum No. 1160, 1947.
- 8-5. Houghton, H. G., A Study of the Evaporation of Small Drops, Physics, 4, 419, 1933.
- X 8-6. Toplay, B., and Whytlaw-Gray, R., Experiments on the Evaporation Rates of Small Drops, Phil. Mag., 4, 873, 1927.
- X 8-7. Namekawa, T., and Takahashi, T., Note on the rate of Evaporation of Small Water Drops, Memoirs, Coll. Sci., Kyoto Imp. Univ., 20, 139, 1937.
- 8-8. Stefan, G., Wien Ber., 65, 323, 1872; 68, 385, 1873; 83, 343, 1881.
- 8-9. Winkelmann, A., A Series of Articles Published in Wien Ann., 1884-1889.
- X 8-10. Bradley, R. S., Evans, N. G., and Whytlaw-Gray, R., The Rate of Evaporation of Small Droplets, Proc. Roy. Soc., A186, 368, 1946.
- 8-11. Patterson, H. S., and Whytlaw-Gray, R., Smoke, Arnold, Ltd., London, 1932, p 181.
- X 8-12. Woodland, D., and Mack, E., The Effect of Surface on Surface Energy Thickness of Saturated Vapor Films, Jour. Am. Chem. Soc., 55, 3149, 1933.
- 8-13. Langmuir, I., The Dissociation of Hydrogen into Atoms, (Jour. Am. Chem. Soc., 37, 426, 1915.)
- X 8-14. Birks, J., and Bradley, R. S., The Rate of Evaporating Drops II, Proc. Roy. Soc., London, A198, 226, 1949.
- X 8-15. Moncheck, L., and Reiss, H., Studies of Evaporation of Small Drops, J. Chem. Phys., 22, 831, 1954.
- X 8-16. Frisch, H. L., and Collins, F. C., Diffusional Processes in the Growth of Aerosol Particles, J. Chem. Phys., 20, 1797, 1952.
- 8-17. Frisch, H. L., On Diffusion Controlled Phase Growth, Z. Elektrochem., 56, 324, 1952.
- 8-18. Lennard-Jones, J. E., and Devonshire, A. F., The Interaction of Atoms and Molecules with Solid Surfaces, Proc. Roy. Soc., London, A156, 6, 1936.
- 8-19. Frisch, H. L., and Collins, F. G. J., Chem. Phys. (in press).
- X 8-20. Greenstadt, J., Variational Formulas in Evaporation Theory, Phys. Rev., 93, 1140, 1954.
- 8-21. Dieterici, G., Kinetic Theory of Liquids, Ann. Physik N. F., 66, 826, 1898.
- 8-22. Burk, R. R., Laskowski, L., and Lankelme, H. P., Kinetics of the Thermal Decomposition of Straight Chain Paraffins, Jour. Am. Chem. Soc., 63, 3248, 1941.

- 8-23. Melavin, R. M., and Mack, E., The Collision Areas and Shapes of Carbon Chain Molecules in the Gaseous State, Normal Heptane, Normal Octane, Normal Nonane, Jour. Am. Chem. Soc., 54, 888, 1932.
- 8-24. Bradley, R. S., and Shellard, A. D., The Rate of Evaporation of Drops - Vapor Pressures and Rates of Evaporation of Straight Chain Paraffin Hydrocarbons, Proc. Roy. Soc., 239, 1949.
- 8-25. Jeans, J., An Introduction to the Kinetic Theory of Gases, Cambridge University Press, 1940.
- 8-26. Eyring, H., The Resultant Electric Moment of Complex Molecules, Phys. Rev., 38, 746, 1932.
- 8-27. Taylor, W. J., Average Length and Radius of Normal Paraffin Hydrocarbon Molecules, Jour. Chem. Phys., 16, 257, 1948.
- 8-28. Hirschfelder, J. O., Byrd, R. B., and Spatz, E. L., The Transport Properties of Gases and Gas Mixtures, Chem. Phys., 44, 205, 1944.
- 8-29. Hirschfelder, J. O., Byrd, R. B., and Spatz, E. L., The Transport Properties of Non-Polar Gases, Jour. Chem. Phys., 16, 968, 1948.
- 8-30. Curtiss, C. F., and Hirschfelder, J. O., Transport Properties of Multicomponent Gas Mixtures, Jour. Chem. Phys., 17, 550, 1949.
- 8-31. Lennard-Jones, J. E., and Devonshire, A. F., Critical Phenomena in Gases I; Proc. Roy. Soc., A163, 53, 1937. Critical Phenomena in Gases II - Vapor Pressure and Boiling Point, Roy. Soc., A165, 1, 1938.
- 8-32. Corner, J., Zero Point Energy and Lattice Dimensions, Trans. Faraday Soc., 35, 711, 1939.
- 8-33. Chapman, S., and Cowling, T. G., The Mathematical Theory of Non-Uniform Gases, Cambridge Univ. Press, Teddington, 1939.
- 8-34. Johnston, H. L., and Grilly, E. R., Accommodation Coefficients for Heat Conduction Between Gas and Bright Platinum for Nine Gases, Jour. Chem. Phys., 14, 233, 1946.
- 8-35. Penner, S. S., and Weinbaum, S., Some Considerations of the Effect of Radiation on the Performance of Liquid Fuel Rockets, Jour. Opt. Soc. of Am., 38, 599, 1948.
- 8-36. Avery, W. H., Studies of Radiation Phenomena in Rockets, OSRD Report No. 3880, 1944.

Contrails

CHAPTER 9. EVAPORATION OF A "MOVING"
DROPLET

ABSTRACT

The evaporation of a rigid liquid sphere under conditions of ambient-gas motion is described in terms of a set of simultaneous differential equations which relate heat and mass transfer to the hydrodynamic variables of gas flow in the region of the liquid surface. The principal differences between heat and mass transfer are shown to be related to the mechanism of propagation of a thermal or concentrative disturbance through a gradient in the transport path. The similarity in mechanism, in conjunction with reasonable simplifying hydrodynamical assumptions, permits some approximate solutions to the fundamental equations to be made after each equation is reduced to a dimensionless form. The resulting solution is, nevertheless, limited in their usefulness because of the buildup assumptions which were necessary in their formulation.

Contrails

EVAPORATION OF A "MOVING" DROPLET

by

F. Benington

THEORETICAL RESULTS

In the previous chapter, equations were derived which adequately described the evaporation of a single droplet in a quiescent gaseous medium. Under the conditions imposed, molecular diffusion and heat transfer played the all-important role in determining the evaporation rate of the liquid. Thus, linear transport equations having radial symmetry sufficed to describe the evaporation process under equilibrium conditions. In contrast to this simple case, the evaporation of a liquid surface under conditions of ambient gas motion is described in terms of a set of differential equations which relate both heat and mass transport to the hydrodynamic variables which must be considered in the description of this dynamic process. The condition of gas-stream motion thus introduces a number of mathematical complexities into the problem of determining the rate of evaporation of a droplet.

An examination of the differential equations for heat and mass transfer shows that there is a great similarity between these two processes. The principal difference between these transport quantities is connected with the mechanism of propagation of a thermal or concentration disturbance through a gradient in the transport path. This similarity in mechanism, in conjunction with simplifying hydrodynamical assumptions, permits some approximate solutions to the fundamental equations to be made after each equation has been reduced to a dimensionless form. Such solutions are, nevertheless, limited in their usefulness because of the assumptions which are necessary in their formulation.

Certain results from the convection of heat from solid objects immersed in a moving stream of fluid have long been thought to be applicable to the transfer of mass under analogous conditions. In 1905, Boussinesq⁽⁹⁻¹⁾ solved the heat-flow equations for arbitrary solids of revolution and concluded that the convective heat transfer was proportional to $U^{1/2}$, where U is the mean stream velocity. He assumed that the thermal conductivity of the medium was small and that the only important temperature gradient was that normal to the surface of the solid. Similarly, King⁽⁹⁻²⁾ arrived at the same result for the heat loss from an infinite cylinder immersed in a moving gas stream. Several other investigators have also verified the conclusion that heat convection is proportional to the square root of the stream velocity.

Jeffreys⁽⁹⁻³⁾ derived an expression for the rate of evaporation of a liquid from a plane surface, using an analogy between his mass-transfer equation and Boussinesq's corresponding equation for heat transfer. He concluded that the mass-transfer rate was proportional to $U^{1/2}$. Namekawa and Takahasi⁽⁹⁻⁴⁾ have also verified the general validity of this proportionality from the measurement of the evaporation rate of single water droplets.

Although there have been numerous experimental researches upon the problem of liquid surface evaporation in moving air streams, there is only meager reference to the fundamental air dynamics of this problem. For the most part, nearly all workers have employed the method of dimensionless parameters to obtain evaporation equations which are useful in practice. Powell⁽⁹⁻⁵⁾ has analyzed the evaporation results of many of these workers and has shown their results to be in fair agreement for evaporation from plane surfaces.

The first mathematical approach to the problem of evaporation from a plane surface was made by Millar⁽⁹⁻⁷⁾ in 1937. His fundamental attack was made possible by the theoretical treatment of eddy transfer developed by Sverdrup⁽⁹⁻⁷⁾, in conjunction with the Von Karman⁽⁹⁻⁸⁾ expression for skin friction. The equation for the evaporation of a sphere in a moving gas stream

remained unsolved until 1938 when Frössling⁽⁹⁻⁹⁾ developed his semiempirical result which forms the basis of nearly all present day analyses of single-drop and spray-evaporation equations.

There is, at present, no completely rigorous solution to the equations for convective mass and heat transfer from spheres. However, it would seem that any expression for predicting the convective evaporation rate in this case should fulfill the following two conditions: (1) that at $U = 0$, the evaporation rate would follow the Maxwellian diffusion rate equation, and (2) that for stream velocities greater than 0, the evaporation rate should be a function of the square root of the stream velocity since it is reasonable to assume a linear velocity gradient across the boundary layer.

Evaporation From a Plane Surface

Before turning to the formulation of the evaporation problem for the moving sphere, an account will be given of the evaporation of a liquid from a plane surface. This case is of interest since it represents one of the few analytical solutions involving dynamic evaporation that may be found in the literature. Moreover, evaporation from a plane is also of interest since it represents the limiting case for a sphere of infinite radius under the conditions of air flow parallel to the surface.

Jeffreys⁽⁹⁻³⁾, in treating evaporation from a plane, has given substantially the following discussion: Let ρ be the density of the ambient gas mixture at any point above the liquid surface, and let V be the fraction of this density due to the evaporating substance. The air stream direction is taken as being directed along the x -coordinate, parallel to the liquid surface; the velocity has a component u in the x -direction at some point above the surface. The air-flow velocity components in the y - and z -directions are v and w , where y is perpendicular to x and lies in the plane of the liquid surface; z is taken as being normal to the liquid surface. For an air flow of moderate velocity, the flow profile in the z -direction is assumed to increase rapidly from zero at $z = 0$ to perhaps $u/2$ at a point which is a millimeter or so above the surface. If the vapor has a lower density than air, the density, V , will decrease rapidly through this layer from some value $V = V_0$ to a decidedly smaller value outside of the boundary layer. It is assumed that diffusion occurs through the mechanism of "eddy diffusion" and that the transport coefficient is given by A . By analogy to heat conduction or molecular diffusion, the time-dependent transport equation may be written as

$$\frac{\partial V}{\partial t} = \frac{\partial}{\partial x} \left(A \frac{\partial V}{\partial x} \right) + \frac{\partial}{\partial y} \left(A \frac{\partial V}{\partial y} \right) + \frac{\partial}{\partial z} \left(A \frac{\partial V}{\partial z} \right) \quad (9-1)$$

Also, the velocity components are related through

$$\frac{\partial V}{\partial t} = u \frac{\partial V}{\partial x} + v \frac{\partial V}{\partial y} + w \frac{\partial V}{\partial z} \quad (9-2)$$

If the density gradient changes only in the z -direction, and A is constant, then, under steady state conditions, Equations (9-1) and (9-2) reduce to

$$u \frac{\partial V}{\partial x} = A \frac{\partial^2 V}{\partial z^2} \quad (9-3)$$

or with $A/u = h^2$

$$\frac{\partial V}{\partial x} = h^2 \frac{\partial^2 V}{\partial z^2} \quad (9-3)$$

The integrated form of Equation (9-3) is

$$V = V_0 \left(1 - \frac{2}{\sqrt{\pi}} \int_0^{z/2h \sqrt{x}} e^{-q^2} dq \right) \quad (9-4)$$

where q is a variable of integration. If the air stream approaching the upstream edge of the surface is free of vapor molecules, then $V = 0$ at $x < 0$ and, evidently, for the interface where $z = 0$

$$\frac{\partial V}{\partial z} = \frac{V_0}{h\sqrt{\pi x}}$$

Therefore, the rate of evaporation per unit area of surface is

$$A\rho \frac{\partial V}{\partial z} = \rho V_0 \sqrt{\frac{Au}{\pi x}} \quad (9-5)$$

For a strip having a width dy and extending over $x = 0$ to x_1 , the right hand side of Equation (9-5) becomes

$$\rho V_0 dy \int_0^{x_1} \left(\frac{Au}{\pi x} \right)^{1/2} dx = 2 \rho V_0 \left(\frac{Aux_1}{\pi} \right)^{1/2} dy$$

or for the entire rectangular area, the total evaporation is

$$2 \rho V_0 \left(\frac{Au}{\pi} \right)^{1/2} \int x_1^{1/2} dy \quad (9-6)$$

if cross-wind diffusion is neglected.

Jefferys has concluded that Equation (9-6) may be applied to the evaporation at a smooth surface whose maximum dimension ranges from about 20 cm to 5000 meters, under the condition of "eddy diffusion". This solution appears to express only the convective part of the evaporation, since the rate of evaporation vanishes at zero stream velocity. A complete solution should give a finite rate of evaporation in terms of molecular diffusion for $u = 0$.

W. G. L. Sutton⁽⁹⁻¹⁰⁾ extended Jefferys' work by considering the behavior of the eddy-diffusion coefficient in Equation (9-1) under the conditions of turbulent motion of the air stream. In his development of this problem, \underline{u} and \underline{A} are taken as potential functions of \underline{z} , the coordinate normal to the evaporating surface. In nonturbulent flow systems, \underline{A} is the ordinary molecular

diffusivity, whereas, under turbulent air-stream motion, this quantity must be treated as a variable. The molecular diffusivity is relatively unimportant in comparison with the mass transport which occurs as a result of the turbulent eddies which are large compared with the mean free path of the vapor molecules.

In the steady-state, two-dimensional case, the operator $\partial/\partial z$ in Equation (9-1) acts on $A(z)$ as well as upon $\partial V/\partial z$, or

$$\bar{u} \frac{\partial V}{\partial x} = \frac{1}{\rho} \frac{\partial}{\partial z} \left[A(z) \frac{\partial V}{\partial z} \right] \quad (9-7)$$

where \bar{u} is a mean stream velocity in the x -direction and the other variables are as defined previously. By assuming that the density of the air is virtually independent of z , the density, V , in Equation (9-7), may be replaced by C , the mass of vapor per unit volume of air, so that

$$\bar{u} \frac{\partial C}{\partial x} = \frac{1}{\rho} \frac{\partial}{\partial z} \left[A(z) \frac{\partial C}{\partial z} \right]. \quad (9-8)$$

Sutton deduced the form of $A(z)$ using Taylor's⁽⁹⁻¹¹⁾ theory of diffusion by continuous gas movement. The dependence of $A(z)$ upon \bar{u} and z is

$$A(z) = \left| \frac{(1/2 \pi k^2)^{1-n} (z-n)^{1-n} n^{1-n}}{(1-n)(2n-2)^2 - 2n} \right| \rho \bar{u}^{(1-n)} z^{(1-n)} \quad (9-9)$$

which is based upon

$$\frac{\bar{u}}{\bar{u}_1} = \left(\frac{z}{z_1} \right)^{n(2-n)}$$

as an expression for the variation of the air-flow component \bar{u} along the z -coordinate; \bar{u}_1 is a known mean velocity at a height z_1 above the evaporating surface. The Von Karman constant is k and has been assigned a value of 0.4 by Nikuradse⁽⁹⁻¹²⁾; ν is the kinematic viscosity of the gas, and n is a number characteristic of the degree of turbulence.

O. G. Sutton⁽⁹⁻¹³⁾ obtained a solution for Equation (9-8) under the assumption that the vapor is of constant density at the surface. This result gives the functional form of $E(\bar{u}, x_0)$, the evaporation rate from a unit width of an infinite strip of length x_0 from the upstream edge of the surface. The evaporation rate may be written in terms of the definite integral

$$E(\bar{u}, x_0) = \int_0^{\infty} \bar{u} (C_x = x_0) dz = K \bar{u}^{(2-n)/2+n} x_0^{2/(2+n)}, \quad (9-10)$$

where K is defined below.

If lateral diffusion is neglected, then for a rectangular area of downstream length x_0 and of width y_0 , Equation (9-10) becomes

$$E(x_0, y_0) = K \bar{u}_1^{(2-n)/(2+n)} x_0^{2/(2+n)} y_0. \quad (9-11)$$

Similarly, for a circular area of radius r

$$E(r) = K' \bar{u}_1^{(2-n)/(2+n)} r^{(4+n)/(2+n)}. \quad (9-12)$$

The quantities K and K' , taken as independent of \bar{u}_1 , x_0 and \bar{r} , are defined by

$$K = C_0 \left(\frac{2+n}{2-n} \right)^{(2-n)/(2+n)} \left(\frac{2+n}{2\pi} \right) \sin \frac{2\pi}{2+n} \Gamma \left(\frac{2}{2+n} \right) a^{2/(2+n)} z_1^{-n^2/(4-n^2)}$$

and

$$K' = \frac{2^{2+n} K \pi^{1/2} \Gamma \left(\frac{3+n}{2+n} \right)}{\Gamma \left[\frac{8+3n}{2(2+n)} \right]}$$
(9-13)

The quantity C_0 in Equation (9-13) is obtained from

$$C = C_0 \left\{ 1 - \frac{1}{\pi} \sin \frac{2\pi}{2+n} \Gamma \left(\frac{2}{2+n} \right) \Gamma \left[\frac{\frac{n}{\bar{u}_1} z^{(2+n)/(2-n)}}{\frac{(2+n)^2}{2-n} a z_1^{n/(2-n)} x}, \frac{n}{2+n} \right] \right\}$$
(9-14)

which is a formal solution to Equation (9-8). The following auxiliary quantities appearing in Equation (9-14) are defined as:

$$a = \left[\frac{(1/2\pi k^2)^{1-n} (2-n)^{1-n} n^{1-n}}{(1-n)(2n-2)^{2-2n}} \right]^\nu z_1^{n^2/(2-n)}$$
(9-15)

$$C_0 = \lim_{z \rightarrow 0} C(x, z) \text{ for } 0 < x < x_0$$

$$\Gamma(P) = \int_0^\infty x^{P-1} e^{-x} dx; \quad \Gamma(\theta, P) = \int_0^\theta x^{P-1} e^{-x} dx$$

The rate of evaporation from a liquid surface may now be calculated from Equations (9-11) or (9-12) with auxiliary equations (9-13) and (9-15) in combination with numerical values of n , \bar{u}_1 , z_1 , C_0 and ν . The concentration variable, C_0 , is identical with the saturated vapor density at $z = 0$. By assuming the perfect-gas law to be valid, C_0 may be evaluated from

$$C_0 = P_s M / RT$$
(9-16)

where P_s is the saturation vapor pressure, M is the molecular weight of the liquid, and T is the absolute temperature.

Pasquill⁽⁹⁻¹⁴⁾ carried out a series of experiments in which the evaporation of bromobenzene was measured at a number of different stream velocities. Calculations of the theoretical evaporation rate in accordance with Sutton's theory were made using the values $T = 290$ K, $M = 157$, $k = 0.4$, $\nu = 0.147$ cgs units and $z_1 = 1$ cm. The value for n , in this calculation, was taken as being 0.238.

Table 9-1 shows a comparison of Pasquill's measured rates with the rates predicted by the Sutton theory.

Continued

TABLE 9-1. COMPARISON OF CALCULATED AND OBSERVED EVAPORATION RATES

(Bromobenzene)

\bar{u}_1 (meters/sec)	1	2	4	5	6	7	8	9
E_{theory} (g/min/mm Hg) ^(a)	0.28	0.48	0.84	1.00	1.16	1.31	1.45	1.59
$E_{\text{Expt'l}}$ (g/min/mm Hg)	0.25	0.43	0.76	0.76	1.06	1.20	1.34	1.48

(a) From Equations (9-11), (9-13), and (9-15).

It may be seen from Table 9-1 that the values of E_{theory} compare well with the observed evaporation rates. However, Pasquill further compared Sutton's theoretical rate equations for the evaporation of a number of pure liquids which had been measured by Wade⁽⁹⁻¹⁵⁾; the evaporation of water was used as a basis of comparison.

Table 9-2 shows Pasquill's calculated results in terms of $ET/(P_s - P_a)$, the value of which is taken as being unity for water. By multiplying this quantity by $1/M$, a constant should result if the above theory adequately describes the evaporation of these liquids. The variation in $ET/M(P_s - P_a)$ shown in this table indicates that considerable discrepancy exists between theory and experiment. Pasquill deduced that the molecular-diffusion coefficient is more likely to play an important role in turbulent transport than is the viscosity. The effect of substituting D , for ν in $A(z)$, is shown in the last column of Table 9-2. It may be seen that this substitution results in a more satisfactory agreement between experimental and theoretical evaporation rates.

TABLE 9-2. RATES OF EVAPORATION OF VARIOUS LIQUIDS RELATIVE TO WATER

Liquid	$ET/(P_s - P_a)$	M. W.	$ET/[M(P_s - P_a)]$	D	$ET/[M(P_s - P_a)D^{2n/(2+n)}]$
Water	1.00	18	1.00	0.275	1.00
Acetone	2.52	58	0.78	0.094	0.99
Benzene	3.54	78	0.82	0.099	1.02
Ethyl acetate	3.10	88	0.63	0.093	0.80
Toluene	3.44	92	0.67	0.092	0.86
Aniline	3.82	93	0.74	0.069	0.98
Trichlorethylene	4.18	131	0.57	0.079	0.75
Methyl sulfate	5.09	152	0.60	0.054	0.84
Carbon tetra- chloride	5.00	154	0.58	0.071	0.79
Bromobenzene	6.72	157	0.77	0.068	1.02

Contrails
Evaporation From a Spherical Drop
in a Moving Gas Stream

The problem of predicting the evaporation rate of a moving spherical droplet received little or no attention before Frössling's⁽⁹⁻⁹⁾ work in 1938. Since that time, there have been a number of investigations, both theoretical and experimental, concerning the evaporation of moving droplets under a variety of experimental conditions. Nearly all of this subsequent work, in part, is based upon Frössling's original analyses, and consequently his treatment of the problem will be presented in some detail.

It will be assumed that the evaporating drop retains a spherical shape throughout the evaporation process. The problem is treated only for the stationary state because the transient problem is extremely difficult to solve. Fortunately, both the velocity and the evaporation rate of the drop can be assumed to be independent of the time under this assumption.

Although diffusion is important under these conditions of evaporation, there is also imposed the important mechanism of the transport of vaporized molecules into the moving gas stream by the "shedding" of the saturated vapor boundary layer which surrounds the moving drop. This latter kind of transport takes place through the mechanism of viscous flow. The problem is first set up in terms of the Navier-Stokes equation, the continuity equation, and appropriate boundary conditions for the flow of gas in the region of the drop surface.

First, the velocity field is defined by the equation

$$\begin{aligned} u \left(\frac{\partial u}{\partial x} \right) + v \left(\frac{\partial u}{\partial y} \right) + w \left(\frac{\partial u}{\partial z} \right) &= - \frac{1}{\rho} \left(\frac{\partial P}{\partial x} \right) + \frac{\mu}{\rho} \nabla^2 u \\ u \left(\frac{\partial v}{\partial x} \right) + v \left(\frac{\partial v}{\partial y} \right) + w \left(\frac{\partial v}{\partial z} \right) &= - \frac{1}{\rho} \left(\frac{\partial P}{\partial y} \right) + \frac{\mu}{\rho} \nabla^2 v \\ u \left(\frac{\partial w}{\partial x} \right) + v \left(\frac{\partial w}{\partial y} \right) + w \left(\frac{\partial w}{\partial z} \right) &= - \frac{1}{\rho} \left(\frac{\partial P}{\partial z} \right) + \frac{\mu}{\rho} \nabla^2 w \end{aligned} \quad (9-17)$$

under the condition that

$$\frac{\partial u}{\partial x} + \frac{\partial v}{\partial y} + \frac{\partial w}{\partial z} = 0$$

The variables in these equations are the same as those used in the previous section; P is the total pressure and, μ , the absolute viscosity. Equations (9-17) are valid only under the conditions of incompressible flow and in the absence of gravitational field.

The corresponding concentration field of vaporized molecules which surround the drop may conveniently be defined in terms of the molecular-diffusion equation under flow conditions. Jefferys⁽⁹⁻³⁾ has given this equation as

$$u \left(\frac{\partial C}{\partial x} \right) + v \left(\frac{\partial C}{\partial y} \right) + w \left(\frac{\partial C}{\partial z} \right) = D \cdot \nabla^2 C \quad (9-18)$$

The concentration of vapor molecules in the gas phase, as before, is C and the diffusion coefficient is D .

Assuming that the gas flow is unidirectional and of velocity U , the boundary conditions for Equations (9-17) and (9-18) may be set down as: $u = U$; $v = w = 0$; $C = 0$ for large values of x , y , and z . Also, $C = C_m$ at the surface of a drop of diameter d ; this surface is defined by the equation $x^2 + y^2 + z^2 = d^2/4$.

Contrails

Since the evaporation rate is a function of the concentration gradient along a unit vector \bar{n} taken normal to a surface element of the drop, dF , the total rate of mass flux, dm/dt is, generally,

$$\left(\frac{dm}{dt}\right) = -D \iint_F \left(\frac{\partial C}{\partial \bar{n}}\right) dF \quad (9-19)$$

Frössling reduced Equations (9-18) and (9-19) to a nondimensional form by means of the following transformations of variables:

$$\left. \begin{array}{l} x = x_1 d \\ y = y_1 d \\ z = z_1 d \\ \bar{n} = \bar{n}_1 d \end{array} \right\}, \quad \left. \begin{array}{l} u = u_1 U \\ v = v_1 U \\ w = w_1 U \end{array} \right\}, \quad \text{and} \quad \left. \begin{array}{l} P = P_1 \rho U^2 \\ C = C_1 C_m \\ F = F_1 d^2 \end{array} \right\} \quad (9-20)$$

The new subscript variables in Equation (9-20) are now dimensionless in form. In addition to these variables, it is also necessary to define the Reynolds number as $Re = \rho v d / \mu$ and the Schmidt number, Sc , is defined by

$$Sc = \rho D / \mu \quad (9-21)$$

The substitution of the quantities defined by Equations (9-20) and (9-21) into Equation (9-19) leads to

$$\left(\frac{dm}{dt}\right) = D C_m d \iint_{F_1} \left(\frac{\partial C_1}{\partial \bar{n}_1}\right) dF_1 \quad (9-22)$$

Since the magnitude of the velocity components u_1 , v_1 , and w_1 , as well as the pressure P , are now functions of Re , x_1 , y_1 , and z_1 , the dimensionless diffusion equation must be of the form $C_1 = \theta(Re, Sc, x_1, y_1, z_1)$. If C_m is expressed by the ideal-gas law, then $C_m = MP/RT$ and Equation (9-22) can now be integrated with respect to the surface variables to give

$$\left(\frac{dm}{dt}\right) = D \frac{MP d}{RT} \cdot f(Re, Sc) \quad (9-23)$$

Thus, for any pure liquid, f will depend only upon the Reynolds number. A solution to Equation (9-23), from which the form of $f(Re, Sc)$ can be obtained, is only possible for the extreme cases where $Re \gg 1$ or $Re \ll 1$. For the latter condition, $f(Re, Sc) = 1$, and the evaporation rate will be of the same form as the Fuchs Equation (8-29) for droplet evaporation into a stagnant atmosphere, which was presented in Chapter 8.

By applying the Prandtl(9-16) boundary-layer theory to the case of evaporation under the condition where the Reynolds number is much greater than unity, a nontrivial solution to Equation (9-23) is possible. The result of this treatment is useful for computational purposes.

According to the boundary-layer theory, gas viscosity effects are present only in the thin layer surrounding the drop. The thickness of this layer decreases with increasing values of Re ; also, the gas velocity in the boundary layer rapidly increases from zero, at the gas-liquid interface, to a value which approaches the stream velocity outside of the boundary layer. A condition of potential flow is assumed to exist in the region exterior to the boundary layer.

Shedding of the boundary layer takes place at a point downstream from the leading surface of the drop; the position of shedding is known as the separation point. When once the pressure distribution outside of the drop is specified, it is then theoretically possible to compute the velocity distribution in the boundary layer and also the position of the separation point. The two alternative

methods which may be used to make this calculation are either through the use of experimentally measured pressure-distribution data or by computing a potential flow pattern for a given form of the vortex wake by the Oseen-Zeilon asymptotic theory⁽⁹⁻¹⁷⁾.

The geometry of the boundary layer is most important in determining both heat and mass transfer. The strong dependence of the latter rate upon the nature of the boundary layer is clearly seen from the fact that this layer exists as a stagnant film immediately above the gas-liquid interface. The immobility of this film gives rise to a steep concentration gradient of the evaporating molecules from the increasing shear force of the gas stream with increasing values of the Reynolds number.

In examining the behavior of $f(Re, Sc)$, Frössling essentially has followed the method of Boltze⁽⁹⁻¹⁸⁾ for treating the velocity boundary layer about a rotating sphere immersed in a moving stream of fluid. Through neglecting higher order terms in Equation (9-17) and by further assuming steady state conditions,

$$\left. \begin{aligned} u \left(\frac{\partial u}{\partial x} \right) + v \left(\frac{\partial u}{\partial y} \right) + w \left(\frac{\partial u}{\partial z} \right) &= -\bar{u} \left(\frac{\partial \bar{u}}{\partial x} \right) + \frac{\mu}{\rho} \left(\frac{\partial^2 u}{\partial y^2} \right) \\ \text{and} \quad \frac{\partial (r' u)}{\partial x} + \frac{\partial (r' v)}{\partial y} &= 0 \end{aligned} \right\} \quad (9-24)$$

Figure 9-1 shows the geometrical relations between the variables which appear in Equation (9-24). The length of a vector normal to the drop surface is given by \underline{y} . The corresponding length of a meridian curve taken from the stagnation point to the base of \underline{y} is equal to \underline{x} . The velocity components \underline{u} and \underline{v} are taken as being, respectively, parallel and perpendicular to the wall enclosing the airstream. The radial distance from the axis of rotation of the drop is r' .

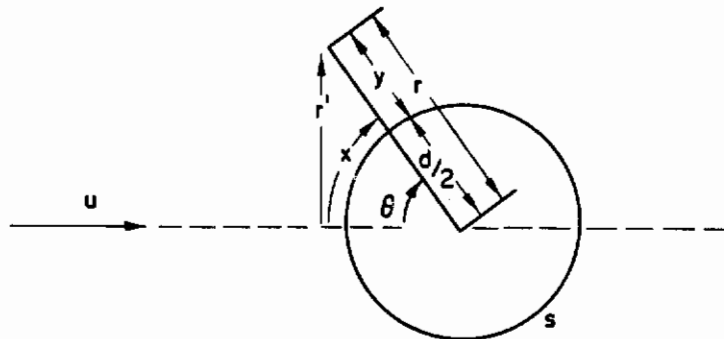


FIGURE 9-1. GEOMETRIC REPRESENTATION OF DROPLET EVAPORATION VARIABLES

The concentration-velocity relations, given by Equation (9-18) may be written in compact form as

$$\underline{U} \cdot \nabla c = D \cdot \nabla^2 c \quad (9-25)$$

For the three-dimensional case possessing radial symmetry, Equation (9-25) may be expanded in spherical coordinates to

$$\frac{u}{r} \left(\frac{\partial c}{\partial \theta} \right) + v \left(\frac{\partial c}{\partial r} \right) = D \left[\frac{1}{r^2} \frac{\partial}{\partial r} \left(r^2 \frac{\partial c}{\partial r} \right) + \frac{1}{r^2 \sin \theta} \frac{\partial}{\partial \theta} \left(\sin \theta \frac{\partial c}{\partial \theta} \right) \right] \quad (9-26)$$

if the polar axis passes through the center of the drop and is oriented in such a manner that it is directed against the direction of gas flow. The general radius vector is \underline{r} , and θ is the angle

between the direction of flow and \underline{r} . If y is now taken as the thickness of the boundary layer for sphere of radius r_0 , then Equation (9-26) becomes

$$u \left(\frac{\partial c}{\partial x} \right) + v \left(\frac{\partial c}{\partial y} \right) = D \left(\frac{\partial^2 c}{\partial y^2} + \frac{2}{r_0} \frac{\partial c}{\partial y} + \frac{\partial^2 c}{\partial x^2} + \frac{1}{r_0} \frac{\partial c}{\partial x} \cot \frac{x}{r_0} \right) \quad (9-27)$$

where $r = d/2 + y$ and $x = (d/2)\theta$, and assuming that $y \ll r_0$, which corresponds to a thin boundary layer ($Re \gg 1$). For points which are not too close to the stagnation point, that is, for the condition $\cot(2x/d) \ll 1$ or $2x/d \gg \epsilon^2$, where $\epsilon = y/d$, the dimensionless boundary layer thickness, Equation (9-27) is reduced to:

$$u \left(\frac{\partial c}{\partial x} \right) + v \left(\frac{\partial c}{\partial y} \right) = D \frac{\partial^2 c}{\partial y^2} \quad (9-28)$$

The continuity Equation (9-24) can also be written in simplified form, if the term $v/(d/2 + y) \approx 2v/d$ is neglected. That is

$$\frac{\partial u}{\partial x} + \frac{\partial v}{\partial y} + \frac{2u}{d} \cot \frac{2x}{d} = 0 \quad (9-29)$$

The simplified boundary layer problem has not been reduced to solving Equations (9-24) (first equation), (9-28) and (9-29) subject to the conditions that

$$\left. \begin{array}{l} u = v = 0 \\ c = c_m \end{array} \right\} \text{ at } y = 0 \quad ,$$

and

$$\left. \begin{array}{l} u = U_1 \\ c = 0 \end{array} \right\} \text{ for } y \rightarrow \infty \quad .$$

By taking a new set of variables

$$\left. \begin{array}{l} x = x' d \\ y = \frac{d}{Re^{1/2}} y' \end{array} \right\} , \quad \left. \begin{array}{l} u = U u' \\ v = \frac{U}{Re^{1/2}} v' \end{array} \right\} , \text{ and } \quad \left. \begin{array}{l} c = c_m c' \\ U_1 = U U_1' \end{array} \right\}$$

and, in turn, by substituting in Equations (9-24), (9-28), and (9-29), these equations become,

$$\left. \begin{array}{l} u' \frac{\partial u'}{\partial x'} + v' \frac{\partial u'}{\partial y'} = U_1' \frac{\partial u_1'}{\partial x'} + \frac{\partial^2 u_1'}{\partial y_1'^2} \\ \frac{\partial u'}{\partial x'} + \frac{\partial v'}{\partial y'} + 2u' \cot 2x' = 0 \\ u' \frac{\partial c'}{\partial x'} + v' \frac{\partial c'}{\partial y'} = \frac{1}{Sc} \left(\frac{\partial^2 c'}{\partial y_1'^2} \right) \end{array} \right\} \quad (9-30)$$

and

where U_1 is the velocity of potential flow along the boundary layer. The boundary conditions for these equations may now be written as:

Continuity

$$\left. \begin{aligned} u' = v' = 0 \\ c' = 1 \end{aligned} \right\} \text{ at } y = 0$$

and

$$\left. \begin{aligned} u' = U_1' \\ c' = 0 \end{aligned} \right\} \text{ for } y' \rightarrow \infty$$

If the gas velocity is of sufficiently large magnitude that the quadratic resistance law for flow is obeyed, then the terms U_1' and $U_1' (\partial U_1' / \partial x')$ will be almost independent of Re since both of the terms are independent of x' . Frössling cites the experimental and theoretical work of Luthander and Ryberg⁽⁹⁻¹⁹⁾ as proof of this point. Similarly, it follows that for large Re , u' and v' are functions of x' and y' alone. The same is also true for the separation points,

$$(\partial u' / \partial y')_{y' = 0} = 0,$$

which lie along a circle at $\theta = \theta_a \cong 80^\circ$ on the sphere.

An examination of the diffusion expression in Equation (9-28) shows that $c' = f(x', y', Sc)$ or, in terms of the previously defined dimensionless quantities, \underline{c} , \underline{x} , \underline{y} , it follows that a new concentration function may be written as

$$c/c_m = \Phi \left(\frac{x}{d}, \frac{y Re^{1/2}}{d}, Sc \right). \tag{9-31}$$

The evaporation rate through the boundary layer on the upstream side of the circle of separation is then

$$\frac{dm}{dt} = -D \iint_S \left(\frac{\partial c}{\partial y} \right)_{y=0} dS = -D c_m \int_0^{\theta_a} \left[\frac{\partial}{\partial y} \Phi \left(\frac{x}{d}, \frac{y Re^{1/2}}{d}, Sc \right) \right]_{y=0} \frac{\pi d^2}{2} \sin \theta d\theta.$$

The bracket quantity in this expression may now be evaluated through

$$\left[\frac{\partial}{\partial y} \Phi \left(\frac{x}{d}, \frac{y Re^{1/2}}{d}, Sc \right) \right] = \frac{Re^{1/2}}{d} \left[\frac{\partial}{\partial \xi} \Phi \left(\frac{x}{d}, \xi, Sc \right) \right]_{\xi=0} = \frac{Re^{1/2}}{d} \Phi_1 \left(\frac{x}{d}, Sc \right).$$

However, $x/d = \theta/2$ so that

$$\frac{dm}{dt} = -D c_m Re^{1/2} d \int_0^{\theta_a} \frac{\pi}{2} \Phi_1 \left(\frac{\theta}{2}, Sc \right) \sin \theta d\theta.$$

But the integral is a function of the Schmidt number only, and

$$\frac{dm}{dt} = -2\pi D \frac{MP}{RT} d [\psi(Sc)] (Re)^{1/2}. \tag{9-32}$$

Most of the evaporation at large values of Re occurs ahead of the separation line, so that Equation (9-32) should express approximately the total evaporation over the entire sphere.

Since Equation (9-32) should be of the form

$$\frac{dm}{dt} = -2\pi D \frac{MP}{RT} d$$

for $Re = 0$, then, evidently,

$$\frac{dm}{dt} = -2\pi D \frac{MP}{RT} d \left[1 + \left(\psi (Sc) \right) (Re)^{1/2} \right] \quad (9-33)$$

should be the final form.

Frössling evaluated $\psi (Sc)$ from experimental data and found that $0.276 Sc^{1/3}$ expressed this function satisfactorily. A further discussion of this result will be presented in connection with experimental work on single-droplet evaporation.

Ranz⁽⁹⁻²⁰⁾, in discussing Frössling's analysis, points out that Equation (9-33) takes into account only mass transfer in the evaporation of a drop. Thus, this equation is only applicable to the evaporation of substances of low volatility. It was soon evident, in the evaporation of volatile materials, that heat-transfer rates would play an important part in the over-all mechanism, through the latent heat of evaporation of the liquid. Ranz has shown that, by its analogy to mass transfer, the heat transfer coefficient for the case of a moving drop is of the form

$$Nu = -1/2 \int_0^\pi \left(\frac{\partial T}{\partial r} \right)_{r=1} \sin \theta d\theta = Nu' [Re, (Re, Pr)] \quad (9-34)$$

which is of the same general form as the last integral given in the Frössling development. In this dimensionless expression, the groups Nu , Nu' , and Pr are

$Nu = dh_c/k$, the Nusselt group for heat transfer,

$Nu' = k_G M_m d P_f / D_v \rho$, the mass-transfer analogue of Nu , and

$Pr = c_p \mu/k$, the Prandtl number,

where h_c is the average heat-transfer coefficient by convection and conduction per unit area of interface per unit temperature difference across the transfer path; k is the thermal conductivity, k_G is the coefficient of mass-transfer analogous to h_c , M_m is the average molecular weight of the gas mixture in the transfer path, P_f is the average partial pressure of the nondiffusing component usually a log mean value, and D_v is the diffusivity of the vapor in the transfer path. Other variables are as previously defined.

Similarly, the mass-transfer rate can be put in the form

$$Nu' = -1/2 \int_0^\pi \left(\frac{\partial P_f}{\partial r} \right)_{r=1} \sin \theta d\theta = Nu \left[Re, \left(Re, Sc, \frac{P_f}{\pi} \right) \right], \quad (9-35)$$

where π is the function denoting the total pressure in this system.

Under conditions when the diameter of the drop is extremely small, the Reynolds number approached zero and the mass- and heat-transfer rates in dimensionless form are related by

$$Nu = Nu' = 2. \quad (9-36)$$

By examining these dimensionless groups in terms of their fundamental variables, it can be shown that the rate of decrease of surface area for an evaporating droplet is constant; this fact has been confirmed by Frössling⁽⁹⁻⁹⁾, Fuchs⁽⁹⁻²¹⁾, Langmuir⁽⁹⁻²²⁾, and by Williams⁽⁹⁻²³⁾.

From the connection between Equations (9-33) and (9-35), the mass-transfer correlation for forced convection in an airstream is

$$Nu' = 2.0 + k_1 Sc^{1/3} Re^{1/2}, \quad (9-37)$$

and by analogy with Equation (9-34), the corresponding heat-transfer correlation is

$$\text{Nu}'' = 2.0 + k_2 \text{Pr}^{1/3} \text{Re}^{1/2} \quad (9-38)$$

Equations (9-37) and (9-38) both conform to the condition implied by Equation (9-36) for the evaporation of a drop in a stagnant-gas atmosphere.

Under the actual condition of zero relative velocity between the drop and its surroundings, the conditions of simple heat conduction and molecular diffusion expressed by Equation (9-38) are not really valid, since a density gradient exists across the transport path. Ranz has accounted for this effect, and has shown that, under this condition, Equations (9-37) and (9-38) reduce, respectively, to

$$\text{Nu}' = 2.0 + k_1 \text{Sc}^{1/3} \text{Gr}^{1/4}$$

and

$$\text{Nu} = 2.0 + k_2 \text{Pr}^{1/3} \text{Gr}^{1/4}$$

which are in accordance with the standard empirical correlations of McAdams⁽⁹⁻²⁴⁾. The Grashof group, Gr, is equal to $d^3 \rho^2 g \beta \Delta T / \mu^2$, where ΔT is the temperature drop across the film, and β is the thermal coefficient of expansion of the gas phase.

Kronig and Bruijstein⁽⁹⁻²⁵⁾ examined theoretically the heat and mass transfer from spheres in a moving fluid medium for the condition that $\text{Re} \ll 1$. This case is important, since the results should be applicable to the evaporation of very small droplets of high stream velocities. Also, this work partially fills in a gap in the Frössling theory since this latter work is valid only for the condition $\text{Re} = 0$ or $\text{Re} \gg 1$. Their approach to the transfer problem is somewhat unique in that a perturbation method, furnished a solution.

In the Kronig treatment, a sphere of radius r_0 is considered as having a large thermal conductivity in comparison with the fluid stream. The temperature of the sphere is maintained at a unit value while the ambient stream temperature is set equal to zero. The Peclet number, Pe , is equal to $(\text{Re})(\text{Pr})$; since it is assumed that $\text{Re} \ll 1$, Pe will be of small magnitude because Pr is generally close to unity for gases. If the radial coordinate r is taken as a multiple of unit r_0 and, if the velocities are also multiples of the unit average homogeneous stream velocity U_0 , then the thermal transport by both conduction and convection is

$$\nabla^2 T - \epsilon U \cdot \text{grad } T = 0 \quad (9-39)$$

and $\epsilon = 1/2 \text{Pe}$. Equation (9-39) is analogous to Equation (9-3) for the diffusion of evaporating molecules, where ϵ is replaced by $1/h_2$.

The radial and angular components, u_r and u_θ , are chosen such that the polar axis of the drop coincides with the direction of flow of the medium well away from the drop. Since Re is small, the Stokes⁽⁹⁻²⁶⁾ components may be used here. That is

$$\left. \begin{aligned} u_r &= \left(1 - \frac{3}{2r} + \frac{1}{2r^3} \right) \cos \theta \\ u_\theta &= \left(1 - \frac{3}{4r} - \frac{1}{2r^3} \right) \sin \theta \end{aligned} \right\} \quad (9-40)$$

with $\cos \theta = v$. The boundary conditions, $T = 1$ for $r = 1$, and $T = 0$ for $r = \infty$, should be satisfied by all solutions to Equation (9-39).

The temperature distribution about a point source of heat located at the coordinate origin is

$$T = \frac{1}{r} e^{-\epsilon/2 r (1-v)} \quad (9-41)$$

for the steady state. Since the temperature field about a finite sphere should at least resemble Equation (9-41) and, because T vanishes for $r = \infty$, Kronig expressed T as

$$T = \theta e^{-\epsilon/2 r (1-v)} , \quad (9-42)$$

where θ is a new dependent variable. A new differential equation in θ is obtained by substituting Equations (9-42) and (9-40) into (9-39). That is,

$$\left[\nabla^2 + \epsilon \left(-\frac{\partial}{\partial r} - \frac{1}{r} + J \right) + \epsilon^2 Q \right] \theta = 0 \quad (9-43)$$

with

$$J = \left(\frac{3}{2r} - \frac{1}{2r^3} \right) v \frac{\partial}{\partial r} + \left(\frac{3}{4r^2} + \frac{1}{4r^4} \right) (1 - v^2) \frac{\partial}{\partial v}$$

and

$$Q = \frac{3}{8r} + \frac{1}{84r^3} - \left(\frac{3}{4r} - \frac{1}{4r^3} \right) v + \left(\frac{3}{8r} \frac{3}{8r^3} \right) v^2 .$$

The boundary condition corresponding to Equation (9-43) in the new variable θ is

$$\theta = e^{\epsilon/2 (1-v)}, \text{ for } r = 1 . \quad (9-44)$$

If the parameter ϵ is small, as has been supposed, a perturbation method offers a possible route to the solution of Equation (9-43) by the following procedure. Suppose θ to be expressible by

$$\theta = \theta_0 + \epsilon \theta_1 + \epsilon^2 \theta_2 \dots + \epsilon^n \theta_n . \quad (9-45)$$

Introducing Equation (9-45) into Equation (9-43) and equating similar powers of ϵ gives

$$\begin{aligned} \nabla^2 \theta_0 &= 0 \\ \nabla^2 \theta_1 &= - \left(-\frac{\partial}{\partial r} - \frac{1}{r} + J \right) \theta_0 \\ \nabla^2 \theta_2 &= - \left(-\frac{\partial}{\partial r} - \frac{1}{r} + J \right) \theta_1 - Q \theta_0 \\ &\dots \end{aligned} \quad (9-46)$$

In order to satisfy Equation (9-43) for all values of ϵ , the boundary conditions from Equation (9-44) must also be in the form of Equation (9-45) or

$$\left. \begin{aligned} \theta_0 &= 1 \\ \theta_1 &= 1/2 (1 - v) \\ \theta_2 &= 1/8 (1 - v)^2 \\ &\dots \end{aligned} \right\} \text{ for } r = 1 \quad (9-47)$$

With the zeroth approximation, θ_0 set equal to $1/r$, the temperature field for a sphere in a stationary medium, the following successive coefficients are found for Equation (9-45) to the second approximation:

$$\begin{aligned}
 \theta_0 &= 1/r \\
 \theta_1 &= 1/2r + (-3/4r + 3/8r^2 - 1/8r^3) v \\
 \theta_2 &= 1/2 \log r - \frac{49}{960 r} + \frac{31}{128 r^2} - \frac{179}{2688 r^3} - \frac{\log r}{32 r^3} + \frac{1}{2240 r^5} \\
 &\quad + (-3/8 - 3/16r + 3/8r^2 - 1/16r^3) v \\
 &\quad + (1/16 + 9/32r - 57/128r^2 + 235/896r^3 + \frac{3 \log r}{32 r^3} \\
 &\quad - 3/64r^4 + 5/448r^5) v^2
 \end{aligned}
 \tag{9-48}$$

The solution given by Equations (9-48) and (9-45) indicates that the temperature field vanishes everywhere excepting in the direction $v = 1$ where T in the second approximation, becomes negatively infinite because of the presence of the $(-1/2 \log r)$ term in θ_2 . However, $D \leq T \leq 1$ must hold everywhere in the medium, so that the perturbation solution fails only for large r close to the line where $v = 1$.

The heat transfer in the immediate neighborhood of the sphere must take place principally by conduction since the velocity of the gas vanishes at the surface of the drop. Consequently, the heat transfer is proportional to the average radial temperature gradient. By combining Equations (9-44), (9-45), and (9-48) and by taking the radial derivative of the temperature, there results

$$\left(\frac{\partial \bar{T}}{\partial r} \right)_{r=1} = - \left(1 + 1/2 \epsilon + \frac{581}{960} \epsilon^2 . . . \right) . \tag{9-49}$$

This equation is also proportional to the Nusselt group, Nu , which must satisfy the condition $Nu = 2.0$ for $Re = 0$ which was discussed in connection with Equation (9-36). Upon taking twice the value of the right-hand side of Equation (9-49) and introducing Pe for $1/2 \epsilon$, there results

$$Nu = 2 + 1/2 Pe + \frac{581}{1920} Pe^2 + \tag{9-50}$$

Similarly, the mass-transfer equation corresponding to Equation (9-39) is

$$\nabla^2 C + \xi \bar{U} \cdot \text{grad } C = 0 ,$$

and the corresponding mass-transfer solution for analogous boundary conditions is

$$\left(\frac{\partial C}{\partial r} \right)_{r=1} = - \left(1 + 1/2 \xi + \frac{581}{960} \xi^2 . . . + \right) . \tag{9-51}$$

As in heat transfer, the Nusselt number, Nu' , defined in connection with Equation (9-34), must also follow the condition $Nu' = 2.0$ and $Re = 0$. This group can be introduced into Equation (9-15) after replacing ξ by Pe_m , or

$$Nu' = 2 + 1/2 Pe_m + \frac{581}{1920} Pe_m^2 . . . + \tag{9-52}$$

The Peclet number for mass transfer, Pe_m , contains D , the molecular diffusion coefficient in place of the thermal conductivity which occurs in Pe .

Kronig has commented on the fact that Fuchs⁽⁹⁻²¹⁾ claimed that gas motion would have no effect upon an evaporation-rate expression which is linear in ϵ . This erroneous conclusion was based upon taking a concentration field as being proportional to $1/r$ and attempting to solve the mass-transfer equation to a low degree of approximation.

A comparison of the Frössling⁽⁹⁻⁹⁾ and the Ranz and Marshall⁽⁹⁻²⁰⁾ correlations with the correlation of Kronig and Bruijsten⁽⁹⁻²⁵⁾ suggests that extrapolation of the experimental data to zero velocity (Nu against $Re^{1/2}$) may not be correct. Kramers⁽⁹⁻²⁷⁾ correlated accurate measurements on the heat transfer from spheres to a moving fluid at $Re > 10$ and found that although the linear relation satisfied the experimental data, extrapolation to $Re = 0$ gave a limiting $Nu > 2.0$.

Figure 9-2 shows qualitatively the relative behavior of Kramers' and Kronig's data for low values of Re or Pe . It may be seen that the Kronig correlation behaves correctly at $Pe = 0$ and is concave upward during a rapid rise at low values of Pe . It is obvious that an inflection point must exist in higher approximations of this correlation if it is to agree with the Kramers data at higher values of Pe or Re .

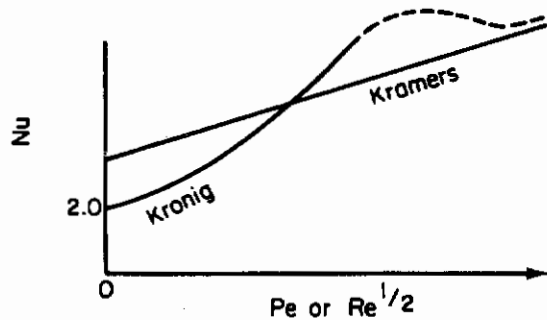


FIGURE 9-2. COMPARATIVE BEHAVIOR OF THE KRONIG AND KRAMERS CORRELATIONS

Williams⁽⁹⁻²³⁾ has made studies of the evaporation of liquid drops of various materials over a range of Re from nearly zero to over 400. He concludes that the mass-transfer rate, in terms of Nu' , is best expressed by three different correlations, depending upon the range of Re . That is

$$\left. \begin{aligned} Nu' &= 2 \text{ for } Re < 4 \\ Nu' &= 1.50 Sc^{1/3} Re^{0.35} \text{ for } 4 < Re < 400 \\ Nu' &= 0.43 Sc^{1/3} Re^{0.56} \text{ for } Re > 400 \end{aligned} \right\} \quad (9-53)$$

Since these results have been deduced from empirical considerations and are a discontinuous function of Re , little can be said regarding their theoretical significance.

Evaporation of Drops in a High-Temperature Gas Stream

The rate of evaporation of a drop may be explicitly expressed as a function of Nu' and is

$$\left(\frac{dm}{dt} \right) = \frac{2\pi r MPD_v}{RT} \left(\frac{P_f}{P_{Lm}} \right) Nu' \quad (9-54)$$

where p_{Lm} is the log mean pressure of the diffusing component and other variables are the same as before. Thus, Equation (9-54) may be used to calculate evaporation rates of drops under conditions of the different values of Re which correspond to a particularly appropriate form of Nu' .

Both Ranz and Marshall⁽⁹⁻²⁰⁾ and Ingebo⁽⁹⁻²⁸⁾ have commented that Equation (9-54) does not validly express the evaporation rate for droplets of volatile materials which are introduced into a high-temperature gas stream. This may be deduced from the fact that in Equation (9-54), no account is taken of either the sensible heat transported by the vapor molecules or of the thermal diffusion through large thermal gradients. It is evident that p_{Lm} has a large effect upon the

evaporation rate, inasmuch as small changes in the surface temperature produce correspondingly large changes in this parameter. Therefore, a knowledge of the surface temperature of the drop is required for calculations of evaporation at high gas temperature. Under the latter condition, the measurement of surface temperature is extremely difficult, particularly for small drops.

Evaporation-rate equations may, however, be derived from either partial-pressure differences, as in the instance of Equation (9-54), or from the corresponding temperature differentials, ΔT , which act as the driving forces in a thermal balance equation. Ingebo⁽⁹⁻²⁸⁾ has obviated the necessity of measuring the surface temperature by deriving an evaporation equation based on thermal driving forces, in which ΔT is approximated as being the difference between the gas stream temperature and the boiling point of the liquid. Wagner⁽⁹⁻²⁹⁾ considered this approximation to be conservative and has applied it to his own work on droplet evaporation.

The heat balance for a drop surrounded by a vapor film can be written as

$$h_c A (T_g - T_s) = \frac{dm}{dt} \left[\lambda_l - C_p (T_l - T_s) \right] \quad (9-55)$$

where A is the drop area, λ is the latent heat of vaporization of the liquid, and other variables are as defined previously; subscripts g , s , and l refer, respectively, to the gas phase, surface, and liquid phase conditions. Ingebo has assumed that $\lambda_l \gg C_p (T_l - T_s)$, so that

$$h A (T_g - T_s) = \lambda_l \frac{dm}{dt} \quad (9-56)$$

The approximation that $\lambda_l \gg C_p (T_l - T_s)$ is clearly inconsistent with the assumption that $(T_l - T_s)$ be large since λ_l cannot be very much larger than $C_p (T_l - T_s)$ for high ambient gas temperatures. In Equation (9-56), h , the film coefficient, is taken as a function of the heat transferred by both the gas and diffusing vapor as a result of bimolecular collisions. From kinetic arguments it can be shown that h is a function of k_g , the thermal conductivity of the gas, and also of the ratio k_g/k_v where k_v is the thermal conductivity of the vapor. Since h must also be a function of the momentum and the heat-transfer group,

$$\frac{hd}{k_g} = \gamma \left(\frac{k_g}{k_v} \right)^m \text{Re}^n \text{Sc}^q \quad (9-57)$$

where γ is a proportionality constant and the quantities m , n , and q are undetermined exponents. Ingebo ran a series of experiments in which $k_g \text{Sc}/k_v$ was held constant by varying the mass flow of air about a drop of methanol maintained at constant air stream temperature. In this way, the exponent n was found to be 0.6. Mc Adams⁽⁹⁻³⁰⁾ cites the data of Williams which verify this result for $20 \leq \text{Re} \leq 150,000$.

An examination of Sc and k_g/k_v shows that both quantities may vary with the gas temperature and also with the properties of the vapor. In light of this fact, Ingebo concluded that an experimental determination of m and q would not be practical. A new correlation group ($\text{Re} \cdot \text{Sc}$), representing the ratio of turbulent momentum transfer to molecular mass transfer was then introduced into Equation (9-57); experimental data showed that the best values of the exponents m and q were, respectively, 0.5 and 0.6, or that

$$\frac{hd}{k_g} = \gamma (\text{Re} \cdot \text{Sc})^{0.6} \left(\frac{k_g}{k_v} \right)^{0.5} \quad (9-58)$$

The proportionality constant, γ , was evaluated by experiment and the resulting expression for h was substituted into the heat-balance Equation (9-56) with the result

$$\frac{dm}{dt} = \frac{k_g \Delta T}{\lambda_l} \pi d \left[2.0 + 0.303 (\text{Re} \cdot \text{Sc})^{0.6} \right] \left(\frac{k_g}{k_v} \right)^{0.5} \quad (9-59)$$

Ingebo's equation was found to correlate with the evaporation rates of nine different liquids having latent heats of vaporization which ranged from 50 to 500 g-cal/gm for a temperature range of 30-500 C; Re values varied from 1600 to 5700.

Pigford⁽⁹⁻³¹⁾ has pointed out that Ingebo's correlation is somewhat different from other experimentally determined equations in having both a more pronounced dependence of Reynolds and Prandtl numbers as well as a factor containing the ratio k_g/k_v . It is also noteworthy that this expression does not take into account the effect of mass transfer away from the evaporating surface upon the conduction of heat toward the surface.

It is of interest to compare the behavior of the evaporation rate as a function of the temperature as calculated by Equation (9-59) and by the Frössling Equation (9-33). In the range of large Re, the two rates appear to be convergent with decreasing temperature. In the limiting case where Re is zero, the Frössling correlation leads to $Nu = 2.0$ while, for Equation (9-59), $Nu = 2 (k_g/k_v)^{0.5}$. Since the latter result is applicable only to the situation where the diameter of the droplet is greater than the mean free path of the evaporating molecules, it is somewhat analogous to the form of the evaporation rate given by Fuchs for the existence of a vapor concentration discontinuity in the region of the drop (compare to Chapter 8, pages 8-10).

A more realistic treatment of the evaporation of droplets at elevated temperatures has been presented by Godsave⁽⁹⁻³²⁾. His approach is dependent upon solving the heat conduction for a droplet of radius, r_1 , surrounded by a concentric spherical flame front of radius, r_2 ; the surface temperatures are T_1 and T_2 , respectively. Thus, the one dimensional conduction equation is

$$k \left(\frac{d^2 T}{dx^2} \right) - \frac{dx}{dt} \left(\frac{dT}{dx} \right) + \frac{1}{C_p} F = 0, \quad (9-60)$$

where heat supplied by the local heat source (cal sec⁻¹ cm⁻³) of strength F , and $k = K/C_p \rho_g$; K is the mean thermal conductivity of the vapor bounded by the temperature limits T_1 and T_2 . Equation (9-60) possesses the general form of an equation which has already been discussed by Tanford and Pease⁽⁹⁻³³⁾ in their analysis of the temperature distribution behind a plane flame front taken normally to a stream of premixed gas.

Since both the mass and the thermal distributions are spherically symmetric about the origin, then Equation (9-60) may be written in terms of a radius, r , such that

$$k \left(\frac{d^2 T}{dr^2} \right) + \left(\frac{2k}{r} - \frac{dr}{dt} \right) \frac{dT}{dr} + \frac{F}{C_p \rho_g} = 0. \quad (9-61)$$

Since $T = T_1$ at $r = r_1$ and $T = T_2$ at $r = r_2$, Equation (9-61) can be conveniently integrated to give T in terms of a lumped parameter

$$B = \left(\frac{dm}{dt} C_p \right) / 4\pi K$$

By differentiating Equation (9-61) and putting $\Delta T = T_2 - T_1$ with $r = r_1$, the thermal gradient at the surface during evaporation is

$$\left(\frac{dT}{dr} \right) = \frac{E \Delta T}{e^{-E/r_2} - e^{-E/r_1}} \left(\frac{e^{-E/r}}{r^2} \right) \quad (9-62)$$

The Nusselt number for a drop of r_1 as a function of the parameter E is

$$Nu = \frac{2 r_1 k}{K} = (2 r_1) \frac{1}{\Delta T} \left(\frac{dT}{dr} \right)_{r_1} = \frac{2E}{r_1} \left\{ \exp E (1/r_1 - 1/r_2) - 1 \right\}^{-1} \quad (9-63)$$

In the limiting case of total evaporation where $\left(\frac{dm}{dt}\right) \rightarrow 0$, E also vanishes and therefore

$$Nu_o = \frac{2 r_2}{r_2 - r_1} \quad (9-64)$$

which is the Nusselt number for a sphere of radius r_1 surrounded by a concentric sphere of radius r_2 . As the radius of the outer sphere r_2 tends to infinity, then $Nu_o \rightarrow 2$ which is the limiting value for Nu in the case of a sphere immersed in a stagnant, infinite medium.

Godsave's final rate equation for evaporation and combustion is then

$$\left(\frac{dm}{dt}\right) = \log_{10} \left[1 + \frac{C_p \Delta T}{(\Delta H - a)} \right] / \left[0.4343 \frac{C_p}{4\pi K} \left(\frac{1}{r_1} - \frac{1}{r_2} \right) \right] \quad (9-65)$$

where $a = R_a / \left(\frac{dm}{dt}\right)$; the radiation constant $R_a = \alpha_a \alpha_f \sigma T^4$ with α_a and α_f denoting the absorptivities of the droplet and flame front.

By using a pseudo-stationary and steady state assumption, Ranz⁽⁹⁻³⁴⁾ has also arrived at an expression for the evaporation rates of droplets at high-ambient gas temperatures. Although Ranz equation is essentially the same as Godsave's it is somewhat better form for computation purposes. Thus, if

$$\left(\frac{dm}{dt}\right) = \frac{4\pi r_1 k_{av}}{(C_p)_{av}} N \quad (9-66)$$

is the rate of evaporation, N can be calculated implicitly from

$$N = \frac{k_1 (C_p)_{av} (T_2 - T_1)}{k_{av} \lambda_1} \left[\frac{N}{\exp(N - N/r_2) - 1} + \frac{r_1 \sigma (T_2^4 - T_1^4)^\alpha}{K_1 (T_2 - T_1)} \right] \quad (9-67)$$

The constants used in Ranz expressions are:

λ_1 = latent heat of vaporization taken at the temperature T_1 (cal/gm)

k_{av} = average thermal conductivity for air at $(T_2 - T_1)/2$ (cal/sec cm °K)

K_1 = volume average conductivity of vapor and air at estimated surface conditions (cal/sec cm °K)

$(C_p)_{av}$ = heat capacity of vapor for evaporating substance at $(T_2 - T_1)/2$ (cal/gm °K)

Tanasawa and Kobayashi⁽⁹⁻³⁵⁾ have, in a manner similar to Ingebo, used the thermal-balance approach in the derivation of a droplet evaporation equation which applies to extremely small drops after injection into the hot gas. In this treatment, these investigators have assumed conditions such that the Reynolds number is vanishingly small; the problem is then reduced to solving the simultaneous equation of heat and mass transfer while ignoring the free- and forced-convection effects. The solutions to Tanasawa's equations express the transient, transport processes, and, in computations, some convergence problems arise in connection with their use.

Tanasawa first considers that the over-all period from injection to complete evaporation may be broken down into the following two intervals.

- (1) A preheating period, in which the drop, of initial radius r_0 and of uniform temperature T_0 , is injected into the hot gas at a temperature T_g . The duration of this interval is defined as the time, t_1 , which is required for the surface of the drop to reach a temperature T_s .
- (2) An evaporation period during which the radius of the drop diminishes due to mass loss until complete evaporation has taken place. This period is of duration t_2 , and the surface temperature of the drop, T_s , remains constant throughout this interval.

In the first interval, the radially dependent temperature of the drop is given by the solution to the heat-conduction equation for a sphere⁽⁹⁻³⁶⁾ of uniform initial temperature, T_0 , after immersion in a fluid maintained at a higher uniform temperature, T_g . That is,

$$rT = 2 r_0 (T_0 - T_g) \sum_{S=1}^{\infty} \frac{[\beta_s^2 + (1-r_0\alpha)^2]^{1/2}}{\beta_s \left[\beta_s^2 \left(\frac{1}{r_0\alpha} \right) - (1-r_0\alpha) \right]} \left(\exp - \frac{\beta_s^2 kt}{r_0^2} \right) \sin \frac{\beta_s r}{r_0} \quad (9-68)$$

The values of β_s are given by the successive roots of the equation

$$\beta = (1 - r_0\alpha) \tan \beta \quad .$$

The thermal diffusivity of the liquid phase is k , and α is related to the coefficient of heat transfer, h , by $\alpha = h/k_l$, where k_l is the thermal conductivity of the liquid.

By assuming r_0 small, the Nusselt heat-transfer group, $Nu = (2 r_0\alpha)/k$, is approximately 2.0, and thus,

$$r_0\alpha = \frac{Nu}{2} \frac{k_a}{k_l} \approx k_a/k_l \quad . \quad (9-69)$$

The expression for the duration of the preheating period, t_1 , is arrived at by substituting Equation (9-69) into Equation (9-68) under the conditions that $r = r_0$, $t = t_1$, and $T = T_s$. The resulting expression is

$$\frac{(T_g - T_s)}{(T_g - T_0)} = 2 \sum_{S=1}^{\infty} \frac{1}{\beta_s^2 \left(\frac{k_l}{k_a} \right) - \left(1 - \frac{k_a}{k_l} \right)} \exp - \frac{\beta_s^2 kt_1}{r_0^2} \quad . \quad (9-70)$$

Unfortunately, Equation (9-70) converges slowly for small values of the ratio k_a/k_l . This ratio usually lies between 0.1 and 1.0 for most systems in which k_a values are taken as those of air. In this range, the approximation

$$\frac{(T_g - T_s)}{(T_g - T_0)} \sim e^{\xi^2} (1 - \text{erf } \xi) + (k_l/k_a) \left[(1 - 2\xi^2) e^{\xi^2} (1 - \text{erf } \xi) - 1 + \frac{2\xi}{\pi^{1/2}} \right] \quad , \quad (9-71)$$

which is given by Goldstein⁽⁹⁻³⁷⁾, gives quite satisfactory results; the parameter ξ is

$$\left(\frac{\kappa t_1}{r_0^2} \right) \quad .$$

Table 9-3 shows numerical values of $(T_g - T_s)/(T_g - T_0)$ for values of both $(\kappa t_1/r_0^2)$ and k_a/k_l as calculated from Equation (9-71). If F_1 is a value of $(\kappa t_1/r_0^2)$ corresponding to a given temperature and thermal-conductivity ratio, then

defines the first period.

TABLE 9-3. NUMERICAL VALUES OF TEMPERATURE RATIO AS A FUNCTION OF $(\kappa t_1/n_0)$ AND (k_a/k_l)

(Tanasawa and Kobayashi)⁽⁹⁻³⁵⁾

$k_a/k_l \backslash \kappa t_1/n_0$	0.1	0.2	0.3	0.4	0.5	0.6	0.7	0.8	0.9	1.0
0.00010	0.9989	0.9977	0.9966	0.9955	0.9943	0.9932	0.9921	0.9910	0.9898	0.9887
0.00025	0.9982	0.9964	0.9946	0.9928	0.9910	0.9892	0.9875	0.9857	0.9839	0.9822
0.00050	0.9973	0.9949	0.9923	0.9898	0.9873	0.9848	0.9822	0.9797	0.9773	0.9748
0.0010	0.9962	0.9927	0.9891	0.9855	0.9819	0.9784	0.9748	0.9713	0.9678	0.9644
0.0025	0.9941	0.9883	0.9826	0.9769	0.9712	0.9656	0.9600	0.9545	0.9491	0.9437
0.0050	0.9914	0.9833	0.9750	0.9668	0.9588	0.9509	0.9431	0.9354	0.9277	0.9202
0.010	0.9876	0.9758	0.9689	0.9524	0.9410	0.9298	0.9189	0.9081	0.8975	0.8872
0.025	0.9795	0.9600	0.9408	0.9222	0.9042	0.8867	0.9697	0.8532	0.8372	0.8216
0.050	0.9694	0.9404	0.9124	0.8857	0.8596	0.8358	0.8123	0.7899	0.9683	0.7477
0.10	0.9528	0.8315	0.7612	0.6985	0.6426	0.5925	0.5475	0.5071	0.4707	0.4378
0.25	0.9106	0.7198	0.6152	0.5293	0.4574	0.3971	0.3464	0.3035	0.2671	0.2360
0.50	0.8455	0.5395	0.4029	0.3041	0.2319	0.1785	0.1388	0.1089	0.0861	0.0687
1.0	0.7303	0.2272	0.1130	0.0577	0.0302	0.0162	0.0089	0.0050	0.0029	0.0017
2.5	0.4698	0.0538	0.0136	0.0036	0.0010	0.0003	0.0001	0.0000	0.0000	0.0000
5.0	0.2252	0.0030	0.0002	0.0000	0.0000	0.0000	0.0000			
10	0.0518	0.0000	0.0000							
25	0.0000									

Tanasawa treats the evaporation period (2), described above, as a stepwise process in time. As evaporation takes place, both the diameter of the drop and surface temperature decrease as a result of heat dissipation. The total evaporation period can thus be taken as the sum of the conductive and evaporative time increments, Δt_c and Δt_e , respectively, such that each interval is independent of the other.

Figure 9-3 shows the manner in which the drop diameter was changed under this assumption.

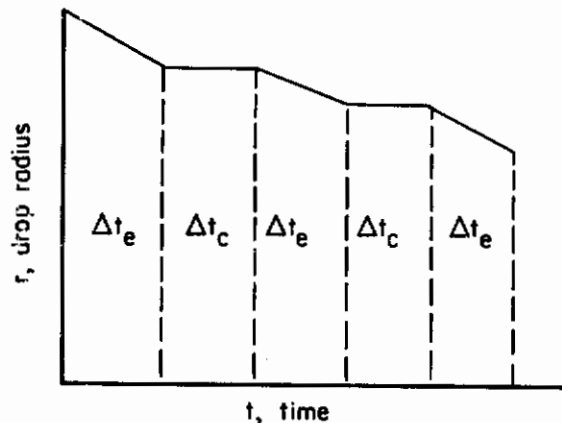


FIGURE 9-3. INCREMENTAL REPRESENTATION OF CONDUCTION AND EVAPORATION IN SECOND PERIOD
(Tanasawa and Kobayashi)⁽⁹⁻³⁵⁾

It may be seen, in the limiting case where Δt_e and Δt_c approach zero, that a smooth radius-time function results. For this limiting case, the evaporation increment is

$$dt_e = -\frac{\lambda Pe}{k_a (T_g - T_s)} r dr, \quad (9-73)$$

whereas the conductive increment is

$$dt_c = -\frac{1}{\kappa} F_2 r dr \quad (9-74)$$

or

$$dt_2 = dt_e + dt_c = -\frac{1}{\kappa} \left\{ \frac{\lambda}{C_p (T_g - T_s)} \frac{k_\ell}{k_a} + F_2 \right\} r dr. \quad (9-75)$$

The term F_2 in Equation (9-75) is an expression for the transient heat flow in the interval t_2 , which is subject to similar convergence conditions as in Equation (9-70). For small values of the thermal conductivity ratio, the analogous Goldstein approximation is

$$F_2 = \frac{\left(\frac{k_a}{k_\ell} \right) (T_g - T_s) / (T_g - T_o)}{G}, \quad (9-76)$$

where

$$G = \left\{ \left(\frac{1}{\sqrt{\pi}} - \xi \right) \xi + \sum_{n=1}^{\infty} \left[\frac{2n}{(2n-1)\sqrt{\pi}} - \xi \right] \xi^{2n+1} \right\} \left(\frac{\kappa t_1}{r_o^2} \right)^{-1} + \left(\frac{\kappa t_1}{r_o^2} \right)^{-1/2} \left\{ \left(1 - \frac{4}{\sqrt{\pi}} \xi \right) \xi + \sum_{n=1}^{\infty} \left[(2n+1) - \frac{(2n+2)^2}{(2n+1)\sqrt{\pi}} \xi \right] \xi^{2n+1} \right\} \quad (9-77)$$

Table 9-4 gives values of \underline{G} calculated from Equation (9-77) for practical ranges of the thermal properties of air and various liquid components. Double linear interpolation is a satisfactory means of calculating intermediate values of the tabular arguments for use in approximate work; more accurate results may be obtained by calculating \underline{G} from Equation (9-77).

The evaporation velocity of a drop can now be calculated from

$$\frac{dr}{dt_2} = -\frac{\kappa C_p (T_g - T_s)}{(k_\ell/k_a) \lambda + F_2 (T_g - T_s) C_p} \left(\frac{1}{r} \right). \quad (9-78)$$

Equation (9-78) is, of course, in agreement with the well known experimental observation that the time rate of change of r^2 is constant during evaporation.

Finally, the total evaporation time, t , is

$$t = t_1 + t_2 = \frac{r_o^2}{\kappa} \left\{ F_1 + F_2 \left[1 - \left(\frac{r}{r_o} \right)^2 \right] \right\}, \quad (9-79)$$

and the droplet lifetime after injection is

$$t_0 = \frac{r_0^2}{\kappa} (F_1 + F_2) \quad (9-80)$$

TABLE 9-4. VALUES OF \underline{G} AS A FUNCTION OF (k_a/k_l) AND $(\kappa t_1/n_0^2)$
(Tanasawa and Kobayashi)⁽⁹⁻³⁵⁾

k_a/k_l $\kappa t_1/n_0^2$	0.1	0.2	0.3	0.4	0.5	0.6	0.7	0.8	0.9	1.0
0.00010	0.0174	0.0174	0.0175	0.0175	0.0175	0.0175	0.0175	0.0175	0.0175	0.0175
0.00025	0.0273	0.0273	0.0273	0.0274	0.0274	0.0274	0.0275	0.0275	0.0275	0.0275
0.00050	0.0382	0.0382	0.0383	0.0383	0.0384	0.0385	0.0385	0.0386	0.0386	0.0387
0.0010	0.0532	0.0533	0.0534	0.0535	0.0536	0.0537	0.0538	0.0539	0.0540	0.0542
0.0025	0.0817	0.0819	0.0822	0.0825	0.0827	0.0830	0.0832	0.0835	0.0838	0.0840
0.0050	0.1107	0.1113	0.1118	0.1123	0.1128	0.1133	0.1138	0.1143	0.1148	0.1153
0.010	0.1487	0.1497	0.1506	0.1515	0.1525	0.1534	0.1544	0.1553	0.1563	0.1573
0.025	0.2113	0.2134	0.2155	0.2176	0.2197	0.2218	0.2239	0.2260	0.2281	0.2303
0.050	0.2641	0.2675	0.2710	0.2746	0.2781	0.2817	0.2853	0.2889	0.2926	0.2963
0.10	0.3109	0.3159	0.3215	0.3268	0.3323	0.3378	0.3434	0.3490	0.3548	0.3605
0.25	0.3385	0.3452	0.3521	0.3590	0.3661	0.3732	0.3804	0.3878	0.3952	0.4027
>0.50	0.3400	0.3469	0.3538	0.3609	0.3680	0.3753	0.3827	0.3901	0.3976	0.4053

Figure 9-4 plots the radius of drops of various pure liquids as a function of time in accordance with Equation (9-79). All drops have an initial radius of 50μ and a value of $T_0 = 20\text{ C}$. The injection takes place into an air stream at $T_g = 1000\text{ C}$ and it is assumed that the surface temperature, T_s , is equal to the normal boiling point of the liquid at one atmosphere pressure.

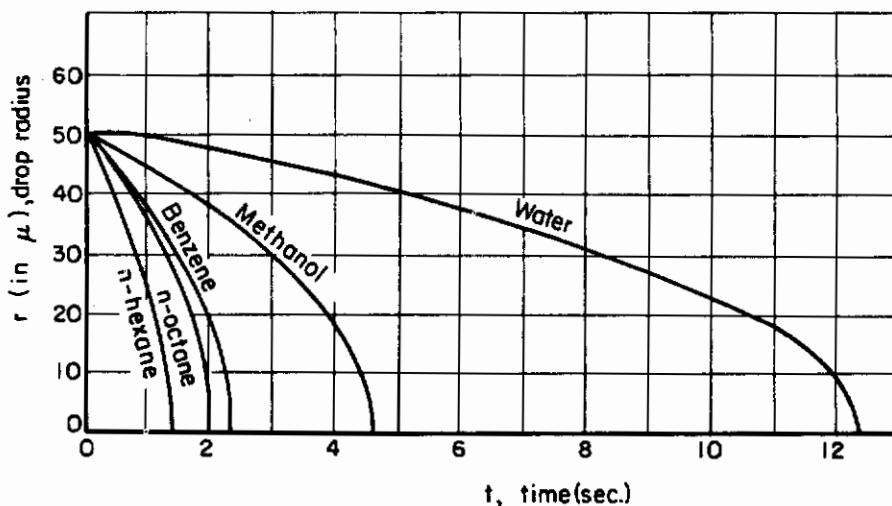


FIGURE 9-4. DROPLET RADIUS AS A FUNCTION OF TIME FOR FIVE LIQUIDS
(Tanasawa and Kobayashi)⁽⁹⁻³⁵⁾

The mathematical approach used by Tanasawa permits a calculation of the comparative rates of evaporation of isothermal drops and conducting drops. The isothermal case is given by Equation (9-73) and the conductive case by Equation (9-79).

Figure 9-5 shows the comparative rates of evaporation for water, methanol and n-octane under the same initial conditions which were used in constructing the curves shown in Figure 9-4.

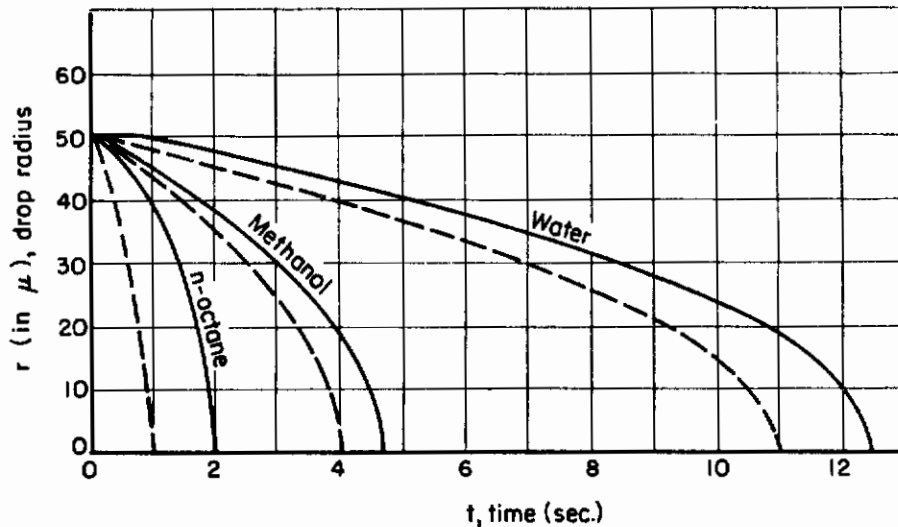


FIGURE 9-5. COMPARISON OF EVAPORATION DATES OF SEVERAL LIQUIDS UNDER ISOTHERMAL AND CONDUCTIVE BEHAVIOR

(Tanasawa and Kobayashi)⁽⁹⁻³⁴⁾

From Figure 9-5 it may be seen that conduction is not a particularly important contribution for small drops of methanol or water since the comparative required times for evaporation differ only by about 10 per cent. In contrast, n-octane shows a corresponding difference of about 100 per cent. It may then be concluded that the ratio (λ/k_f) is the dominant factor in determining whether conduction is important under these evaporation conditions; when this ratio is large, the conductive contribution to the evaporation rate is small, whereas, for small values of this ratio, conduction is important.

In the limiting case where $Re = 0$, both the Ingebo and Tanasawa equations show a strong dependence upon the thermal conductivity of the evaporating medium. The precise difference in the form of the two equations can probably be attributed to the fact that Ingebo's derivation is semi-empirical whereas Tanasawa's approach is theoretical. The parabolic form of the drop radius-time function needs no particular comment, since it has been verified in numerous experimental investigations.

The Lifetime of Small Droplets at High Temperatures

Both Wagner⁽⁹⁻²⁹⁾ and Kumm⁽⁹⁻³⁸⁾ have followed the method of Tanasawa in assuming that the lifetime of a droplet can be divided into a preheating and evaporation period; as in the earlier work, both investigators assume no mass loss in the preheating period.

Wagner has approached the problem of calculating the lifetime of the droplet at high temperatures by means of the heat balance Equation (9-55). Like Ingebo, Wagner made the inconsistent assumption that $C_p (T_\lambda - T_g) \ll \lambda$, and thus ignored the heat capacity term. In addition to this assumption, the Nusselt number for heat transfer is taken as being

$$Nu = 2 + 0.04 Re$$

in accordance with McAdams. Since Re is vanishingly small for small droplets, the coefficient of heat transfer can be written as

$$h = \frac{k_a}{2r} \text{Nu} = \frac{k_a}{r}$$

By substituting these values in Equation (9-55) and by taking $r = 0$ for $t = t_0$, Wagner's life-time equation is given by

$$t_0 = \frac{\lambda_\ell \rho_\ell r_0^2}{2 k_a (T_g - T_s)} \quad (9-81)$$

This is, of course, identical with the equation which could be derived from Ingebo's work.

Kumm⁽⁹⁻³⁸⁾ has criticized the Wagner-Ingebo approximation,

$$\lambda_\ell \gg C_p (T_g - T_s) ,$$

since it implies that the heat required to raise the liquid vapor to the ambient temperature is negligible. He has, therefore, included the heat-capacity term in his derivation but essentially follows the method given by Wagner. The resulting lifetime is

$$t_0 = \frac{\rho_\ell C_p r_0^2}{2 k_a \ln \left[1 + \left(\frac{C_p (T_g - T_s)}{\lambda_\ell} \right) \right]} \quad (9-82)$$

Equation (9-82) is consistent with the lifetime equations which are given by Godsave⁽⁹⁻³²⁾ and by Colburn and Drew⁽⁹⁻³⁹⁾ where t_0 is shown to be dependent upon the evaporation rate of the droplet.

Table 9-5 compares the calculated lifetimes of n-hexane drops, after injection into air at 1000 F, in accordance with the various equations already discussed in this section. The initial size of drop is taken as 50 microns and the initial drop temperature is 20 C.

TABLE 9-5. COMPARISON OF PREDICTED DROPLET LIFE FOR n-HEXANE
(Initial Diameter, 50 μ)

Investigator	Equation Number	t_0 (sec)	Comments
Kumm	(9-82)	2.38×10^{-3}	Isothermal drop
Wagner	(9-81)	1.98×10^{-3}	Isothermal drop
Tanasawa	(9-80)	1.42×10^{-3}	Transient heat conduction in drop

Both the Kumm and Wagner equations, which assume an isothermal drop, predict a longer lifetime than does the Tanasawa equation. It would thus appear that the transient heat conduction may be important in any precise prediction of droplet lifetime. The sizeable difference between the isothermal treatments also suggests that the approximation $\lambda_\ell \gg C_p (T_g - T_s)$ may not be completely justified for the evaporation for all substances at high temperatures.

Regarding the derivation of his equation, Kumm states that his results will give the maximum lifetime of a droplet; it is of interest to note that this value of t_0 for n-hexane is the highest shown in Table 9-5.

Continuity

Hartwig⁽⁹⁻⁴⁰⁾ has made a similar theoretical study of the rate of evaporation of liquid drops injected into hot gases; his work is an extension of Penner's⁽⁹⁻⁴¹⁾ investigation of the evaporation of isothermal drops. Hartwig accounted for thermal gradients within the drop in the case of two thermal models. In the first model, the drop was considered as an isothermal core surrounded by an isothermal shell. The second approximation utilized the actual temperature profiles in drops as established by the usual heat balance between thermal conduction with the drop, convective heat transfer to the drop, and the cooling produced by the latent heat of vaporization at the gas-liquid interface.

The results of the shell-model approximation were found to be in quite satisfactory agreement with available experimental data on the evaporation of isothermal drops of aniline at high temperature. Numerical solutions for the evaporation rate indicated that the mass transport is virtually independent of the chosen thickness of the isothermal shell. In the conduction model, the surface temperature was found to be consistently lower than the value found for the isothermal-shell model. Thus, the conduction model gave somewhat different results from the isothermal-shell model. Since Hartwig's work leads to nonintegrable equations in the case of both models, it was necessary to resort to numerical methods for obtaining solutions. These will not be given here since they are applicable only to the evaporation of a single substance under a fixed set of conditions; instead, the reader is referred to the excellent original work, from which the numerical methods are available for application to other particular evaporation problems.

El Wakil, Uyehara, and Meyers⁽⁹⁻⁴²⁾ have recently made theoretical calculations to determine whether the case where single fuel droplets are evaporating under conditions which are met in jet engines. On the basis of experimental data and a careful analysis of a few necessary assumptions, these workers have drawn the following conclusions:

- (1) At high air temperatures, the nonsteady state evaporation is usually of major importance. Large droplets can be expected to reach the combustion zone before steady state conditions are attained.
- (2) During the nonsteady state evaporative process, the bulk of the heat arriving at the gas-liquid interface goes into sensible heat rather than into latent heat of vaporization. This is particularly true for low-volatility fuels.
- (3) The rate of mass transfer usually increases with time during the "warm-up" period.
- (4) The mass transfer rate usually decreases with time at high air densities in spite of the fact that the droplet is constantly receiving heat.

Evaporation of Droplets Under Special Cases of Motion

In this section there will be treated two special cases of droplet evaporation under dynamic conditions. In the first case, single-droplet evaporation is examined during the period immediately after injection at a high initial velocity into a relatively slow-moving gas. The aerodynamic drag forces rapidly decelerate the drop and give rise to the second condition, where the evaporating drop moves in accordance with the free-fall equations. This treatment of evaporation arises in connection with the spray drying of solutions of a nonvolatile solute contained in a volatile solvent, the latter usually being water.

Free Fall

It is first convenient to reduce Equation (9-33), which expresses the evaporation rate of a moving droplet, to a dimensionless form containing the droplet relative velocity, v_d . Following Sjenitzer⁽⁹⁻⁴³⁾, this equation may be written in terms of the pressure gradient, Δp , taken radially from the drop surface as

$$\frac{dm}{dt} \text{ (kmol/sec)} = 2\pi D_v d \frac{\Delta P}{RT} \left[1 + 0.276 \text{Re}^{0.5} \text{Sc}^{0.33} \right] \quad (9-83)$$

For low values of p , the factor $(\Delta P/RT)$ can be written in terms of ΔH , the absolute-humidity difference between the drop surface and the ambient gas, or

$$\frac{\Delta P}{RT} \cong \Delta H \frac{\rho_G}{M} \quad (9-84)$$

where M is the molecular weight of the evaporating liquid. If L is the weight of the drop at any time and L_0 is the initial weight, then $L/L_0 = x$ will be the weight fraction of the original drop remaining after t seconds; also, $L_0 = (\pi/6) d^3 \rho_L$. The evaporation rate,

$$\frac{dx}{dt} = \frac{12 D_v \Delta H}{d^2} \left(\frac{\rho_G}{\rho_L} \right) \left[1 + 0.276 \text{Re}^{0.5} \text{Sc}^{0.33} \right],$$

is obtained by making the substitutions in Equation (9-83). The relative velocity of the drop may be expressed in terms of a characteristic length, ℓ , such that $\ell/t = v_d$, or

$$\frac{dx}{d\ell} = \frac{12 D_v \Delta H}{v_d d^2} \left(\frac{\rho_G}{\rho_L} \right) \left[1 + 0.276 \text{Re}^{0.5} \text{Sc}^{0.33} \right] \quad (9-85)$$

Equation (9-85) may be used to compute the fractional evaporation per unit length of free-fall path after establishing the form of v_d under this condition.

The resistance to the motion of a falling drop is

$$F = c_d \pi \left(\frac{d}{2} \right)^2 \frac{1}{2} \rho_L v_d^2 \quad (9-86)$$

where c_d is the drag coefficient for the spherical drop. A second condition for the force on a moving sphere under free fall is that

$$F = g \left(\frac{\pi}{6} \right) d^3 (\rho_L - \rho_G) \quad (9-87)$$

The resistive force, F , is constant if the droplet has reached a constant settling rate, since there is no acceleration of the particle. Under this condition, Equations (9-86) and (9-87) may be combined to give

$$v_d^2 = \frac{4g d (\rho_L - \rho_G)}{3\rho_G c_d} \quad ,$$

or, in terms of the Reynolds number.

$$c_d \text{Re}^2 = \frac{4g d^3 \rho_G (\rho_L - \rho_G)}{3\mu^2} \quad (9-88)$$

Figure 9-6 shows a plot of Re against $c_d \text{Re}^2$ for experimentally measured drag coefficients. Thus, by computing $c_d \text{Re}^2$ from the right-hand side of Equation (9-88) and by reading the corresponding value of Re from Figure 9-6, the steady, free-fall velocity can be calculated from $\text{Re} = v_d \rho_L d / \mu$. This value is then applied to Equation (9-85) for calculating the fractional evaporation per unit length of fall.

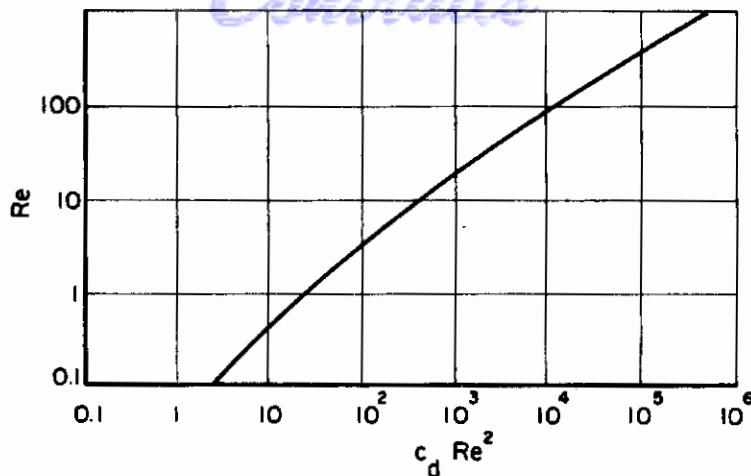


FIGURE 9-6. EXPERIMENTAL VALUE OF THE DRAG COEFFICIENT AS A FUNCTION OF THE REYNOLDS NUMBER

(Sjenitzer)⁹⁻⁴³

Both Marshall and Seltzer⁽⁹⁻⁴⁴⁾ and Duffie and Marshall⁽⁹⁻⁴⁵⁾ have given equations for calculating the lifetime of a liquid drop moving under free fall at terminal velocity in accordance with Stokes law. Their lifetime equation is

$$t_o = \frac{\rho_L \lambda}{2\Delta T} \int_0^{d_o} \frac{d(d)}{h} \quad (9-89)$$

where d_o is the initial drop diameter and h is the film coefficient which was defined in connection with Equation (9-56). It is now desired to know how h varies with the drop diameter d . This may be obtained from the dimensionless correlation.

$$Nu = 2 \left[1 + 0.276 (Pr)^{1/3} (Re)^{1/2} \right] = \frac{hd}{k_v} \quad (9-90)$$

By solving Equation (9-90) for h and substituting the result in Equation (9-89)

$$t_o = \frac{\rho_L \lambda}{4\Delta T k_v} \int_0^{d_o} \frac{d \cdot d(d)}{\left[1 + 0.276 (Pr)^{1/3} \left(\frac{dv_d \rho_G}{\mu} \right)^{1/2} \right]} \quad (9-91)$$

If, as before, the drop is assumed to be moving at terminal velocity in accordance with Stokes law, then

$$v_d = \frac{g (\rho_L - \rho_G) d^2}{18\mu} \quad (9-92)$$

The lifetime Equation (9-91) assumes the form

$$t_o = \frac{\rho_L \lambda d_o^2}{8\Delta T k_v} \left[1 - \frac{2}{d_o^2} \int_0^{d_o} \frac{B d^{5/2} d(d)}{1 + B d^{3/2}} \right] \quad (9-93)$$

with

$$B = 0.276 \left(\frac{C_{p\mu}}{k_v} \right)^{1/3} \left[\frac{g(\rho_L - \rho_G) \rho_G}{18\mu^2} \right]^{1/2}$$

Equation (9-93) may now be integrated in a series form to give

$$t_o = \frac{\rho_L \lambda d_o^2}{8\Delta T k_v} \left[1 - \sum_{j=1}^{\infty} (-1)^{j-1} \frac{4}{3j+4} B^j d_o^{3j/2} \right] \quad (9-94)$$

Under the condition that $d_o^{3/2} < 1/B$ for convergence, the original work of Marshall and Seltzer shows graphs for t_o as a function of d_o with ΔT as a parameter. However, these results are for the evaporation of water and will not be given here.

In the case of zero relative velocity, Equation (9-94) is identical with the lifetime equation of Ligebo⁽⁹⁻²⁸⁾ and of Wagner⁽⁹⁻²⁹⁾. The Stokes law behavior is usually accepted as being valid for $Re < 2.0$.

Tsuji⁽⁹⁻⁴⁶⁾ has also derived an expression for calculating the evaporation rates of freely falling drops. He also assumes that the Frössling rate equation satisfactorily describes the evaporation process in the absence of large thermal gradients. Tsuji does not give a derivation of his equation nor does he present the assumptions under which it is supposed to be valid. The equation given for the free-fall velocity of the drop shows this quantity as a function of the condensation or evaporation accommodation coefficient taken at the drop surface; this coefficient is described in the work of Alty and Mackay⁽⁹⁻⁴⁷⁾. It is difficult to compare Tsuji's results with those of other workers without having more complete information regarding the basis of his analysis.

A further discussion of droplet evaporation under free-fall conditions will be given in connection with the analysis of experimental investigations on droplet evaporation.

Rapid Droplet Deceleration

Before droplets reach a steady velocity in a gas stream, they often have a high initial velocity as a result of the conditions of injection or atomization. In the retardation of motion, the kinetic energy of the drop is, in part, dissipated in overcoming air resistance. The influence of the gravitational field may be neglected in this case because the flight time under consideration is very small and, furthermore, the free-fall path in this interval is negligible.

Sjenitzer⁽⁹⁻⁴³⁾ has derived equations in dimensionless form for expressing both the distance and "braking time" for a high-speed drop. His results are sufficiently generalized to be of use in calculating actual evaporation rates. Wagner⁽⁹⁻²⁹⁾ has carried out a similar analysis using an analogous approach. Since his results are applicable only to the evaporation of n-octane drops, Sjenitzer's treatment will be discussed.

Suppose that an injected droplet loses kinetic energy through drag forces in the air stream; then, according to Newton's second law,

$$-m \frac{dv_d}{dt} = c_d \left(\frac{\pi}{8} \right) \rho_G v_d^2 d^2$$

or

$$1/3 d^3 \rho_L \frac{dv_d}{dt} = \frac{1}{4} c_d \rho_G v_d^2 d^2 \quad (9-95)$$

because $m = (\pi/6) d^3 \rho_L$. The dimensionless form of the velocity and time can be written as

$$Re = \frac{d v_d}{\mu} \rho_G \text{ and } \theta = \frac{t}{\frac{4}{3} \left(\frac{\rho_L}{\rho_G} \right) \frac{d^2}{\mu}}$$

which, upon introduction into Equation (9-95), gives

$$d\theta = - \frac{d(Re)}{c_d Re^2} \quad (9-96)$$

If the time interval, Δt , is defined such that it represents the time during which velocity decreases from $(v_d)_1$ to $(v_d)_2$ for a corresponding change of Re_1 to Re_2 , then

$$\Delta t = \frac{4}{3} \left(\frac{\rho_L}{\rho_G} \right) \left(\frac{d^2}{\mu} \right) \int_1^2 d\theta = \frac{4}{3} \left(\frac{\rho_L}{\rho_G} \right) \int_{Re_1}^{Re_2} \frac{d(Re)}{c_d Re^2} \quad (9-97)$$

Thus, from values of the integral

$$\theta = \int_{Re_1}^{Re_2} \frac{d(Re)}{c_d Re^2} \quad (9-98)$$

it is possible to calculate the time interval for the "braking" of the droplet.

The distance corresponding to Δt is obviously $\Delta \ell = \int_1^2 v_d dt$ or

$$\Delta \ell = \frac{4}{3} d \left(\frac{\rho_L}{\rho_G} \right) \int_1^2 Re d\theta = \frac{4}{3} d \left(\frac{\rho_L}{\rho_G} \right) \int_{Re_1}^{Re_2} \frac{d(Re)}{c_d Re} \quad (9-99)$$

Similarly, the "braking distance" can be evaluated from Equation (9-99) and numerical values of the integral

$$\sigma = \int Re d\theta = \int \frac{d Re}{c_d Re} \quad (9-100)$$

Figures 9-7 and 9-8, respectively, show the reduced time, θ , and the reduced distance, σ , as a function of the Reynolds number. These graphs have been constructed for use in calculating both Δt and $\Delta \ell$ in accordance with Equations (9-97) and (9-99) for a moving drop of any liquid.

In calculating the evaporation of a droplet during the "braking period", it is convenient to consider only the second term in Equation (9-83), since this portion corresponds to the quantity of evaporation, E , which is associated with the motion of the drop. This may be written as

$$E = 2\pi d D_v \frac{\Delta P}{RT} \left(0.276 Sc^{1/3} \int_1^2 Re^{1/2} dt \right) \quad (9-101)$$

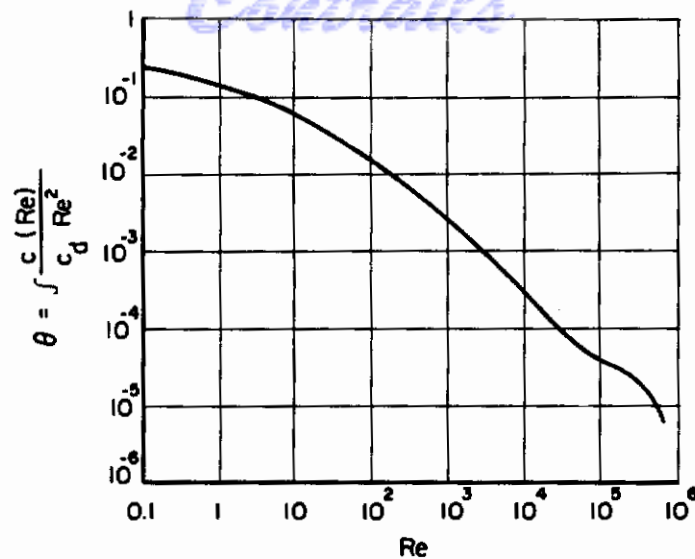


FIGURE 9-7. GRAPHICAL VALUES OF THE REDUCED TIME AS A FUNCTION OF THE REYNOLDS NUMBER (Sjenitzer)⁹⁻⁴³

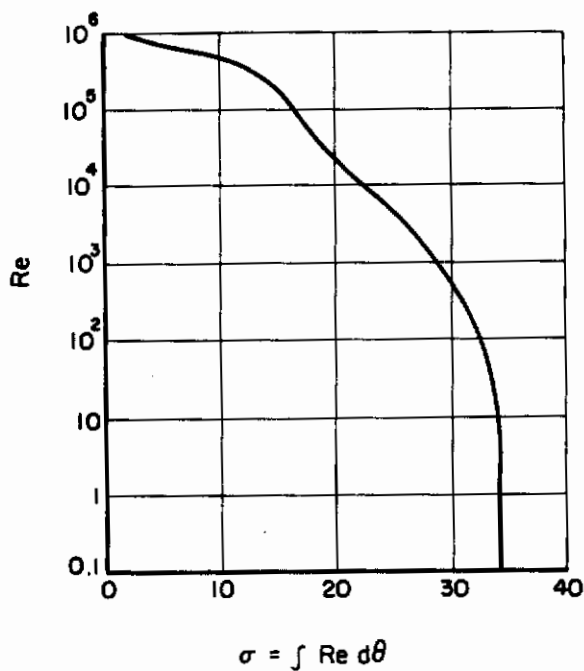


FIGURE 9-8. GRAPHICAL VALUES OF THE REDUCED DISTANCE AS A FUNCTION OF THE REYNOLDS NUMBER (Sjenitzer)⁹⁻⁴³

By introducing the reduced time into Equation (9-101) from Equation (9-90), there results

$$E = 0.276 \frac{8\pi}{3} d^3 \left(\frac{\rho_L}{\rho_G} \right) \left(\frac{D_v}{\mu} \right) \left(\frac{\Delta p}{RT} \right) Sc^{1/3} \int_{Re_1}^{Re_2} \frac{d(Re)}{c_d Re^{1.5}} \quad (9-102)$$

The fractional evaporation, \underline{x} , can be found by dividing \underline{E} by $(\pi/6) (\rho_L/M)d^3$ and by introducing Δp from Equation (9-84). Then,

Contrails

$$x = 4.42 \Delta H Sc^{-0.67} \int_{Re_1}^{Re_2} \frac{d(Re)}{c_d Re^{1.5}} \quad (9-103)$$

expresses the fractional evaporation during braking.

Figure 9-9 gives Sjenitzer's graph for computing the integral shown in Equation (9-103); these values, in conjunction with calculated values for ΔH and Sc , permit the calculation of the fractional evaporation in accordance with Equation (9-103).

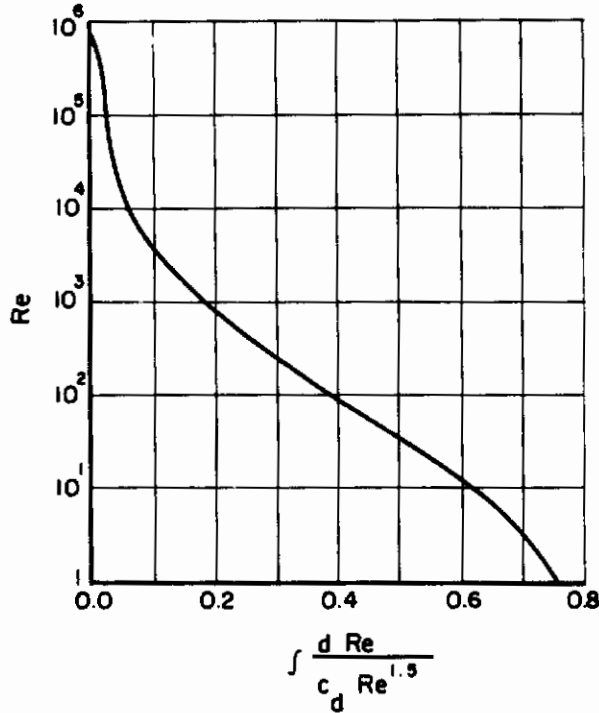


FIGURE 9-9. GRAPHICAL SOLUTION TO $\int \frac{d Re}{c_d Re^{1.5}}$
(Sjenitzer)⁹⁻⁴³

Figure 9-9 shows that the evaporation during rapid deceleration is independent of the initial velocity and is only dependent upon the final Reynolds number. Thus, there is little to be gained in choosing too high initial velocity from the standpoint of increasing evaporation during this period. However, increasing the initial velocity does increase the "braking distance" of the droplet. In the case of very small droplets, the braking evaporation is insignificant compared with evaporation due to free fall.

The Contribution of Radiant Heat Transfer to Droplet Evaporation

Thus far, in the present treatment of moving droplet evaporation, heat transfer has been considered as taking place only by conduction and convection; radiant heat transfer has been neglected. However, when a liquid droplet is injected into a combustion chamber or piston-type engine, it is subjected to a condition under which radiant heat transfer to the evaporating droplet may take place from a hot wall, hot gas, or a flame. Penner⁽⁹⁻⁴⁸⁾ has given a mathematical treatment of this problem which permits an approximate calculation of the radiant heat transfer to the drop.

Figure 9-10 shows a quadrant of a cylindrical combustion chamber appropriately labelled with the variables used in the analysis of this problem.

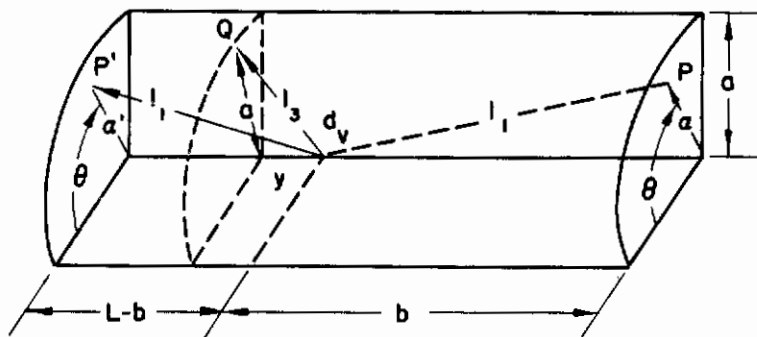


FIGURE 9-10. QUADRANT OF A CYLINDRICAL COMBUSTION CHAMBER WITH A VOLUME ELEMENT dV MOVING ALONG ITS AXIS

(Penner and Weinbauer)⁹⁻⁴⁸

Consider a moving gaseous volume element, dV , moving at a fixed velocity, \underline{v} , along the axis of the combustion chamber. In order to calculate the temperature rise in this element, it is necessary to calculate I_T , the radiant energy incident on dV during its residence time in the chamber. The volume element is taken as being a distance $(L - b)$ from the upstream end of the cylinder. In accordance with Figure 9-10, the distances l_1 , l_2 , and l_3 are taken such that

$$l_1 = [a^2 + b^2]^{1/2}$$

$$l_2 = [a'^2 + (L - b)^2]^{1/2}$$

$$l_3 = [a^2 + y^2]^{1/2}$$

The radiant energy incident upon dV when it has reached a distance b from the exit end of the combustion chamber is

$$\bar{I}'_{\lambda}(b) = \bar{I}_{\lambda}^0 [1 - \exp[-k_{\lambda}\rho\bar{\ell}]] = (I_{\lambda}^0/A) \int_A [1 - \exp(-k_{\lambda}\rho\ell)] dA \quad (9-104)$$

where the bar denotes an average value, dA is an element of the chamber-wall area, I^0 is the energy emitted by 1 cm^2 of the wall, assuming it to behave as a black-body radiator, ρ is the gas density, and ℓ is the length of the radiation path. The quantity k_{λ} is the average mass-absorption coefficient of the gas at wavelength λ .

From the definitions of the various l_i and from Equation (9-104), it can be shown that

$$\begin{aligned}
 I'_\lambda(b) = & 4 I_\lambda^0 / (2\pi a^2 + 2\pi aL) \int_0^{\pi/2} d\theta \left\{ \int_0^a \left(1 - \exp \left[-k_{\lambda\rho} (a^2 + b^2)^{1/2} \right] \right) ada + \right. \\
 & \int_0^a \left(1 - \exp \left[-k_{\lambda\rho} [a'^2 + (L - b)^2]^{1/2} \right] \right) a' da' + \int_0^b \left(1 - \exp \left[-k_{\lambda\rho} (a^2 + y^2)^{1/2} \right] \right) ady + \\
 & \left. \int_0^{L-b} \left(1 - \exp \left[-k_{\lambda\rho} (a^2 + y^2)^{1/2} \right] \right) ady \right\} . \quad (9-105)
 \end{aligned}$$

Also, the radiant flux received over all wavelengths at a fixed position along the flow axis is

$$I'(b) = \int_\lambda I'_\lambda(b) d\lambda .$$

Since the volume element dV is moving at a constant rate, v , evidently

$$\left. \begin{aligned}
 b &= L \text{ at } t = 0 \\
 b &= 0 \text{ at } t = L/v \\
 b &= L - vt \text{ at all } t
 \end{aligned} \right\} \quad (9-106)$$

are boundary conditions. Thus, $0 \leq b \leq L$. The total radiant energy incident upon the receiver, I_T , is then

$$I_T = \int_0^{L/v} I'(b) dt . \quad (9-107)$$

By combining Equations (9-105), (9-106), and (9-107) and noting the conditions of axial symmetry, there results, upon integration with respect to θ ,

$$\begin{aligned}
 I_T = & [2/a(a + L)] \int_\lambda I_\lambda^0 d\lambda \int_0^{L/v} dt \left\{ \int_0^a \left(1 - \exp \left[-k_{\lambda\rho} [a^2 + (L - vt)^2]^{1/2} \right] \right) ada + \right. \\
 & \left. \int_0^{L - vt} \left(1 - \exp \left[-k_{\lambda\rho} (a^2 + y^2)^{1/2} \right] \right) ady \right\} , \quad (9-108)
 \end{aligned}$$

under the black-body-radiator assumption. A further necessary condition is that

$$\lim_{\ell \text{ or } k_\lambda \rightarrow \infty} I_T = (L/v) \int I_\lambda^0 d\lambda .$$

If it is assumed that the injected drop moves along the axis of the cylinder and that the lifetime path is $(L - b)$ in length, then the lifetime is

$$t = (L - b)/v ,$$

and L/v , the upper limit in Equation (9-108), can be replaced by $(L - b)/v$.

Continuity

The increment of temperature rise due to radiation, ΔT_r , which is derived approximately from Equation (9-108), is

$$\Delta T_r = (3/C \rho r) \int_{\lambda} I_T (1 - e^{-2K_{\lambda}r}) d\lambda \quad (9-109)$$

for a drop of radius r . The quantity K_{λ} is an average absorption coefficient for the evaporating liquid, taken over a wavelength interval λ to $(\lambda + d\lambda)$. In this approximation it is assumed that all radiation is incident in a direction normal to the drop surface.

Droplet Deformation and Evaporation

Practically no consideration has been given to the possible influences of hydrodynamical surface roughening and of secondary atomization upon the rate of evaporation of single moving droplets. The lack of analysis of these possible influences is probably dictated by the mathematical complexities associated with a theoretical approach and to the difficulties which would be encountered in experimental measurements. Norris⁽⁹⁻⁴⁹⁾ has followed the pattern of investigation of Sverdrup and Miller⁽⁹⁻⁵⁰⁾ in attempting to analyze the influence of surface roughening of a plane liquid surface upon the rate of evaporation of the liquid. Although his analysis, as it stands, cannot be applied to evaporation from a spherical surface, it appears to indicate that hydrodynamically rough surfaces undergo up to four times as much evaporation as do smooth surfaces under similar conditions. In this analysis, it is assumed that the surface areas under consideration are large.

It would seem that a possible approach to the influence of surface roughening on evaporation would be through Hinze's⁽⁹⁻⁵¹⁾ treatment of the forced deformation of viscous-liquid spheres. Hughs and Gilliland⁽⁹⁻⁵¹⁾ have discussed the influence of elasto-viscous deformation on the drag coefficient of a moving droplet. In Hinze's work, the effect of viscosity is considered in the solution to the linearized hydrodynamical equations, with boundary conditions given for the external pressure distribution under conditions of rotational symmetry and a vanishing tangential stress.

Secondary atomization may also occur through the mechanism which has been proposed both by Triebnigg⁽⁹⁻⁵³⁾ and by Heyler⁽⁹⁻⁵⁴⁾. The former investigator states that the critical size of a moving drop is determined by the balance between hydrostatic-pressure forces over the drop surfaces and the surface-tension pressure at the gas-liquid interface. This may be written as

$$c_d \frac{1}{2} \rho_g U^2 = \frac{2\sigma}{r} \quad , \quad (9-110)$$

where σ is the surface tension of the liquid.

If it is assumed that the tangential forces at the surface of the drop can be neglected, then the deformation of the drop is determined by the air-velocity pressure, $\rho_g U^2$, and the surface-tension pressure, σ/r . A combination of these pressures in dimensionless form is known as the Weber number,

$$We = \frac{\rho_g U^2 r}{\sigma} \quad . \quad (9-111)$$

Secondary atomization occurs when the value of We exceeds a certain critical value $We_{(cr)}$. However, this critical value depends upon time and, consequently, the viscosity of the liquid plays an important part in determining the secondary atomization. Hinze⁽⁹⁻⁵¹⁾ has discussed this point and an outline of his analysis is given in Chapter 5.

Experimental work on droplet break-up indicates that under free-fall conditions,

while, under the condition where the drop is injected axially into a moving gas stream,

$$2.5 < We_{(cr)} < 8.5 .$$

From Equation (9-83), the mass rate of evaporation can be written in terms of the droplet surface area, s , as

$$\frac{dm}{dt} = - 2 D_v \sqrt{\pi s} \frac{\Delta p}{RT} \left\{ 1 + 0.276 Re^{1/2} Sc^{1/3} \right\} .$$

Since Re and We are related by

$$\left(\frac{\sigma}{\mu_g U} \right) We = Re ,$$

evidently,

$$\frac{dm}{dt} = - 2 D_v \sqrt{\pi s} \frac{\Delta p}{RT} \left\{ 1 + 0.276 \left(\frac{\sigma}{\mu_g U} \right)^{1/2} We^{1/2} Sc^{1/3} \right\} . \quad (9-112)$$

Thus, the droplet evaporation process should proceed in accordance with Equation (9-112) as long as $We < We_{(cr)}$. When $We_{(cr)}$ is reached, secondary atomization takes place and the total evaporation rate increases because an increase in s occurs also.

Evaporation From Multicomponent Drops

In practical applications, most liquid fuels consist of several molecular species having different volatilities, diffusion coefficients, and thermal conductivities. The evaporation of multicomponent drops of such fuels is therefore dependent upon concentration gradients in both the liquid and gas phases. A theoretical approach to the multicomponent-droplet-evaporation problem for the condition where the Reynolds number is greater than zero is therefore complicated by the necessity of solving simultaneously the hydrodynamical equations and the multicomponent-diffusion equations for both phases. No complete treatment of this problem for the general case of i components exists, and the present discussion is, of necessity, limited to a few fairly well known aspects of multicomponent evaporation.

Examination of Equation (9-83) shows that both D_v and Δp will vary with time, since the composition of the mixture constituting the drop will change as the more volatile compounds evaporate. The first discussion given here will be limited to the evaporation of an ideal binary mixture of hydrocarbons; extensive phase-behavior data on more complex systems of hydrocarbons is given in the excellent review by Hadden⁽⁹⁻⁵⁵⁾.

By assuming that the partial pressure of the hydrocarbon mixture is negligible in the ambient air, the factor Δp may then be taken as the total pressure of the two components at the surface of the drop. For an ideal solution, an equilibrium constant k_i may be written so that $pk_i = p^o$, where p is the total hydrocarbon pressure and p^o is the vapor pressure of a single component. Nederbragt⁽⁹⁻⁵⁶⁾ has derived an equation for calculating k in binary hydrocarbon mixtures where p , V , T data are available for the particular system. Thus, the Gibbs free energy, G , for a gas mixture composed of N_i moles of a component with i carbon atoms may be written as

$$G = (\Sigma N_i) \int V dp + RT \Sigma N_i \ln \frac{N_i}{\Sigma N_i} \quad (9-113)$$

or the partial molal free energy is

$$\frac{\partial G}{\partial N_i} = \int V dp + (\sum N_i) \frac{\partial}{\partial N_i} \left[\int V dp + RT \ln \frac{N_i}{\sum N_i} \right] \quad (9-114)$$

From the phase rule, $\int V dp$ is determined, for a binary mixture, by pressure, temperature, and a third parameter which may be chosen as the average number of carbon atoms, \bar{i} . Then,

$$\frac{\partial}{\partial N_i} \int V dp = \frac{\partial \bar{i}}{\partial N_i} \frac{\partial}{\partial i} \int v dp, \quad (9-115)$$

where

$$\bar{i} = \frac{\sum N_i i}{\sum N_i}$$

and

$$\frac{\partial \bar{i}}{\partial N_i} = \frac{i - \bar{i}}{\sum N_i}$$

The partial molal free energy is now given by

$$\int V dp + (i - \bar{i}) \frac{\partial}{\partial i} \int V dp + RT \ln \frac{N_i}{\sum N_i}$$

Since $\partial G / \partial N_i$ is identical in both phases, the equilibrium constant is now

$$\begin{aligned} \ln \left(\frac{N_i}{\sum N_i} \right)_{\text{gas}} - \ln \left(\frac{N_i}{\sum N_i} \right)_{\text{liquid}} = \ln K = - \left[\int \frac{V}{RT} dp + (i - \bar{i}) \frac{\partial}{\partial i} \int \frac{V}{RT} dp \right]_{\text{gas}} + \\ \left[\int \frac{V}{RT} dp + (i - \bar{i}) \frac{\partial}{\partial i} \int \frac{V}{RT} dp \right]_{\text{liquid}}, \end{aligned} \quad (9-116)$$

which applies only under conditions of equilibrium evaporation.

While the form of Δp is simple for this case, the corresponding form of D_v , the diffusion coefficient, is more complicated. The subject of calculating multicomponent-diffusion coefficients has been extensively treated by Hirschfelder and co-workers (9-57), (9-58), (9-59); a discussion of these calculations is given in Chapter 8 in connection with the expression for transport quantities.

The evaporation of a single component from a moving, two-component-liquid drop has been treated by Kronig and Brink (9-60). The circulation currents, which are caused by the viscous forces at the liquid-vapor boundary, give rise to an evaporation rate which is different from the case of the evaporation of a stationary droplet. Under simplifying assumptions which permit the solution to the hydrodynamical equations of flow, these workers were able to solve the evaporation problem by an eigenvalue method.

Kronig assumes that the quadratic terms in the velocity equations be ignored in accordance with the treatment given by Hadamard (9-61). Let a drop of radius a , density ρ_l and viscosity μ_l be permitted to fall through a gaseous medium of density ρ_g and of viscosity μ_g . The Stokes stream function for the liquid is then

$$\psi_l = - \frac{g (\rho_l - \rho_g)^2 a^2}{6 (3\eta_l + 2\eta_g)} r^2 (1 - r^2) \sin \theta, \quad (9-117)$$

and the corresponding stream function in the surrounding gas phase is

Contrails

$$\psi_G = \frac{g (\rho_l - \rho_g)^2 a^2}{6(3\eta_l + 2\eta_g)} \sin^2 \theta \left[\frac{\eta_l}{\eta_g} \frac{1 - r^3}{r} - \frac{2\eta_l + 2\eta_g}{\eta_g} r (1 - r) \right], \quad (9-118)$$

where r , θ , and an additional angular coordinate, ϕ , constitute a system of polar coordinates with the origin at the center of the drop.

The radial- and angular-velocity components, v_r and v_θ , associated with the stream functions are

$$\left. \begin{aligned} v_r &= \frac{1}{r^2 \sin \theta} \frac{\partial \psi}{\partial \theta} \\ v_\theta &= \frac{1}{r \sin \theta} \frac{\psi}{r} \end{aligned} \right\} \cdot \quad (9-119)$$

The equation which represents a family of stream lines inside the drop in a plane containing the polar axis is

$$\xi = 4 r^2 (1 - r^2) \sin^2 \theta \quad (9-120)$$

since ξ differs from ψ_G by a constant factor only. The set of trajectories orthogonal to the streamlines defined by ξ are given by

$$\zeta = \frac{r^4 \cos^4 \theta}{2r^2 - 1} \quad (9-121)$$

A plot of both the ζ and ξ curves is given in Figure 5-5 in Chapter 5.

If ξ and ζ are taken as a set of orthogonal curvilinear coordinates, a line element in the liquid region, ds , may be conveniently defined as

$$ds^2 = ds_\xi^2 + ds_\zeta^2 + ds_\phi^2$$

with components

$$\left. \begin{aligned} ds_\xi &= \frac{a d\xi}{8r \sin \theta \Delta^{1/2}} \\ ds_\zeta &= \frac{a(2r^2 - 1)^2 d\zeta}{4r^3 \cos^3 \theta \Delta^{1/2}} \end{aligned} \right\} \cdot \quad (9-122)$$

and

$$ds_\phi = ar \sin \theta d\phi$$

The auxiliary parameter, Δ , is $(1 - r^2) \cos^2 \theta + (2r^2 - 1)^2 \sin^2 \theta$.

By following a particular liquid particle over a given streamline in the drop in a closed cycle and, in turn, comparing the time for this circulation with the time required for the concentration of the evaporating component in the drop to fall to $1/e$ of its original value, it is possible to obtain the ratio of the circulation rate to the diffusion rate over a path normal to the streamline. Thus, the concentration, c , is independent of ζ and also of ϕ , for reasons of symmetry. Since $c = c(\xi, t)$, the excess of the volatile component diffusing into a region bounded by ξ and $\xi + d\xi$ per unit time is equal to the increase per unit time of the amount of the volatile component in this region. The equation of transport is

$$\int_{s_\zeta} \int_{s_\phi} D_v \frac{\partial}{\partial s_\xi} \left(\frac{\partial c}{\partial s_\xi} ds_\zeta ds_\phi \right) ds_\xi = \frac{\partial}{\partial t} \int_{s_\zeta} \int_{s_\phi} c ds_\xi ds_\zeta ds_\phi . \quad (9-123)$$

From symmetry considerations, it is sufficient to integrate Equation (9-123) with respect to s_ζ (half of the streamline) and ϕ . After introducing line elements defined by Equation (9-122) into Equation (9-123) and carrying out the indicated integration, the differential equation for $c = c(\xi, t)$ is

$$\frac{\partial}{\partial \xi} \left[p(\xi) \frac{\partial c}{\partial \xi} \right] = \frac{a^2}{16 D} q(\xi) \frac{\partial c}{\partial t} \quad (9-124)$$

with

$$p(\xi) = \int \frac{(2r^2 - 1)^2 \sin^2 \theta}{r \cos^3 \theta} d\zeta \quad (9-125)$$

and

$$q(\xi) = \int \frac{(2r^2 - 1)^2}{4r^3 \cos^3 \theta \Delta} d\zeta$$

The integrals given by Equation (9-125) are conveniently evaluated in terms of known functions in the following way: the factors $\cos^3 \theta$ and $\sin^2 \theta$ are first eliminated through Equations (9-120) and (9-121) so that both integrands contain only r, ξ, ζ . In the resulting expression, ζ is replaced by r as a variable of integration, since

$$\zeta = \left[r^2 (1 - r^2) - 1/4\xi \right]^2 / (1 - r^2)^2 (2r^2 - 1)$$

results from eliminating θ from Equations (9-120) and (9-121). The integrated forms of Equations (9-125) which result are

$$p(\xi) = \frac{2}{3} \left(1 + \xi^{1/2} - 1/2 \right) \left[(4 - 3\xi) E \left(\frac{1 - \xi^{1/2}}{1 + \xi^{1/2}} \right)^{1/2} - (4\xi^{1/2} - 3\xi) K \left(\frac{1 - \xi^{1/2}}{1 + \xi^{1/2}} \right)^{1/2} \right] \quad (9-126)$$

and

$$q(\xi) = 2 \left(1 + \xi^{1/2} \right)^{-1/2} K \left(\frac{1 - \xi^{1/2}}{1 + \xi^{1/2}} \right)^{1/2}$$

The functions \underline{K} and \underline{E} are complete elliptic integrals of the arguments shown in parentheses and are defined and tabulated by Jahnke and Emde⁽⁹⁻⁶²⁾. A short table of $p(\xi)$ and $q(\xi)$ for numerical arguments in the range $0 \leq \xi \leq 1$ is given in Kronig's paper.

The assumption is now made that the time of circulation, t_c , is small in comparison to the corresponding diffusion time, t_d . The circulation time is evidently

$$t_c = 2 \int \frac{ds_\zeta}{v} , \quad (9-127)$$

from previous considerations. The total velocity is obtained from

$$v^2 = v_r^2 + v_\theta^2 . \quad (9-128)$$

By substituting Equation (9-119) into Equation (9-128) and, in turn, by substituting this result into Equation (9-127), there results an integral in ψ which may be evaluated after replacing ψ by the form given in Equation (9-117). The circulation time is then

$$t_c = \frac{6(3\eta_\ell + 2\eta_g)}{g|\rho_\ell - \rho_g|a} q(\xi) \quad (9-129)$$

The modulus of the density difference is used in Equation (9-129) in order that t_c will always be a positive quantity.

The concentration of the volatile component present in the drop is given by the series solution to the diffusion equation; that is,

$$c(r, t) = \frac{2c_o}{\pi r} \sum_{n=1}^{\infty} \frac{(-1)^{n+1}}{n} \exp\left(-n^2 \frac{\pi^2 D_\ell t}{a^2}\right) \sin n\pi r, \quad (9-130)$$

with $c = c_o$ for $t = 0$ and $r = 1$. The mass of the droplet as a function of time may be written as

$$M(t) = \int_0^1 4\pi a^3 r^2 c dr \quad (9-131)$$

with the initial mass as

$$M(o) = c_o \frac{4\pi a^3}{3} \quad (9-132)$$

Substituting Equation (9-131) into Equation (9-130) and taking the ratio $M(t)/M(o)$ gives

$$\frac{M(t)}{M(o)} = \frac{6}{\pi^2} \sum_{n=1}^{\infty} \frac{1}{n^2} \exp\left(-n^2 \frac{\pi^2 D_\ell t}{a^2}\right),$$

from which it may be seen that the exponent takes the value 0.550 when $M(t)/M(o) = e^{-1}$. The diffusion time is then

$$t_d = 0.056 \frac{a^2}{D_\ell} \quad (9-133)$$

The ratio of the circulation and diffusion time is now

$$t_c/t_d = \frac{6(3\eta_\ell + 2\eta_g) D_\ell}{0.056 g|\rho_\ell - \rho_g|a^3} q(\xi) \quad (9-134)$$

Kronig has presented the following conclusions regarding his theory:

- (1) Since the time of diffusion is dependent both upon D_v and D_ℓ , the assumption that $t_c \ll t_d$ cannot be realized when D_v is infinitely large. This follows from the fact that, under this condition, c must vanish at the drop.
- (2) The circulation time decreases as $1/a$ while the diffusion time increases as a^2 for increasingly large drop sizes. It is then evident that a large drop size favors the basic assumption regarding the relative magnitudes of t_d and t_c . However, an upper size limit for the drop must exist in order that the quadratic terms may be justifiably neglected in the hydrodynamical equations.

- (3) The function $q(\xi)$ in Equation (9-132) can be shown to diverge logarithmically for the streamline $\xi = 0$, which corresponds to the liquid-vapor boundary at the drop surface. Therefore, there will always exist a layer in which the inequality $t_d \gg t_c$ will not be valid. As the drop size is increased, this layer assumes less relative importance. From Equation (9-134), $t_c/t_d < 1$, or

$$q(\xi) < \frac{0.0093 g |\rho - \rho_g| a^3}{(3\eta + 2\eta_g) D_f}$$

If it is assumed that the drop is large enough to follow validly the above assumptions, then Equation (9-124) may be solved for the rate of evaporation. The boundary values necessary for the solutions are:

- (1) $\xi = 0$, when $c = 0$, if the drop moves through a gas in which the concentration of the diffusing substance is initially zero.
- (2) $\xi = 1$ for all finite c .
- (3) Inside the drop, $c = c_0$ at $t = 0$.

Assuming that Equation (9-124) has a solution of the form

$$c(\xi, t) = \Xi(\xi) T(t)$$

then, by separating variables

$$\frac{d}{d\xi} \left[p(\xi) \frac{d\Xi}{d\xi} \right] + \mu q(\xi) \Xi = 0 \quad (9-135)$$

and

$$\frac{dT}{dt} + \mu \frac{16 D_f}{a^2} T = 0 \quad (9-136)$$

Equation (9-136) is immediately solvable and

$$T = \exp \left(-\mu_n \frac{16 D_f t}{a^2} \right) \quad (9-137)$$

A solution to Equation (9-135) is of the Sturm-Liouville type and requires a treatment by the method of normalized eigenvalues. The eigenvalues corresponding to the solution are designated by μ_n and the corresponding eigenfunctions by $\Xi_n(\xi)$. The generalized solution to Equation (9-135) is

$$c(\xi, t) = c_0 \sum_{n=1}^{\infty} A_n \Xi_n(\xi) \exp \left(-\mu_n \frac{16 D_f t}{a^2} \right) \quad (9-138)$$

The coefficients A_n , upon introducing the boundary values, are defined by

$$A_n = \int_0^1 q(\xi) \Xi_n(\xi) d\xi \quad (9-139)$$

The total mass of the vaporizing component as a function of time is

$$M(t) = \iiint c ds_\xi ds_\zeta ds_\phi$$

which reduces to

$$M(t) = \frac{\pi a^3}{2} \int_0^1 q(\xi) \cos \xi \quad (9-140)$$

from symmetry considerations and the boundary conditions prescribed above.

Introducing Equation (9-138) into Equation (9-140) gives

$$M(t) = \frac{\pi a^3 c_0}{2} \sum_{n=1}^{\infty} A_n^2 \exp\left(-\mu_n \frac{16 D_l t}{a^2}\right)$$

or

$$\frac{M(t)}{M(0)} = \frac{3}{8} \sum_{n=1}^{\infty} A_n^2 \exp\left(-\mu_n \frac{16 D_l t}{a^2}\right) \quad (9-141)$$

by introducing $M(0)$ from Equation (9-132).

The eigenvalues μ_n and their corresponding eigenfunctions $E_n(\xi)$ are obtained by the method of Ritz⁽⁹⁻⁶³⁾. If the solution to this problem is confined to $n = 2$, then

$$\mu_1 = 1.678, \quad \mu_2 = 9.83,$$

and the normalized eigenfunctions are

$$E_{(1)} = 0.828 \xi + 0.401 \xi^2$$

and

$$E_{(2)} = 4.23 \xi - 5.62 \xi^2$$

Introducing these values into Equation (9-136) with $c = e^{-1}$ and $t = t_d'$ gives

$$t_d' = 0.022 \frac{a^2}{D_l} \quad (9-142)$$

for the time in which the concentration of the volatile component falls to e^{-1} of its original value.

Equation (9-142) represents the case where evaporation takes place by both convection and diffusion, while Equation (9-133) corresponds to the evaporation for a stationary drop. It is interesting to note that the convective rate is about 2.5 times as fast as the stationary rate.

Kronig, Van Der Veen, and Ijzerman⁽⁹⁻⁶⁴⁾ further examined the diffusion-circulation theory for the conditions where the droplet moves slowly in a gravitational field. Thus, $t_c \gg t_d$, and the concentration will differ only slightly from that of the stationary droplet. The diffusion and hydrodynamical equations discussed earlier were solved by the perturbation method⁽⁹⁻⁶⁵⁾. The perturbations were considered as being produced by small variations in the dimensionless parameter

$$\beta = \frac{g(\rho_l - \rho_g) a^3}{6(3\eta_l + 2\eta_g) D_l} \quad (9-143)$$

The final result for the second approximation, is

Contrails

$$\frac{t'_d}{t_d} = 1 - 0.00121 \beta^2 + \dots, \quad (9-144)$$

which is valid only when β is of the order of 0.05 mm or less; this is implied by the necessary condition that $\beta^2 \ll 1$ which arises in connection with the perturbation calculations. The quantity t'_d/t_d is the ratio between the diffusion times for the moving and stationary cases.

A few experimental studies have been made concerning the effect of internal circulation on mass transfer from two-component droplets to a surrounding liquid medium. Garner⁽⁹⁻⁶⁶⁾ and Garner and Skelland⁽⁹⁻⁶⁷⁾ studied the diffusion of water into droplets of several immiscible organic liquids containing anhydrous cobalt chloride; as the water diffused into the organic phase, the color gradually changed from an initial deep blue to pink. By making colored motion pictures of the falling droplets, it was possible to ascertain by the color changes, the internal flow pattern of the droplet. Under conditions of inward diffusion, internal circulation was observable at Reynolds numbers as low as 64 to 71. Circulation began at higher Reynolds numbers as the viscosity of the liquid phase of the droplet was increased.

Spells⁽⁹⁻⁶⁸⁾ has shown that the pattern of internal flow in droplets is in good agreement with the hydrodynamical predictions of Hadamard⁽⁹⁻⁶¹⁾ and of Rybczynski⁽⁹⁻⁶⁹⁾ as long as the droplet remains spherical.

EXPERIMENTAL RESULTS

The measurement of droplet evaporation in a moving gas stream has been the subject of a number of experimental investigations. In nearly all instances these measurements were carried out on droplets which were suspended from filaments in the gas stream rather than by methods which would permit the observation of the drop under free-fall conditions. This technique of measurements appears to be due to Frössling⁽⁹⁻⁹⁾ and has been used by most other workers. The drop is picked up on the filament suspension and placed in the air stream which is maintained at a fixed temperature and linear velocity. The time rate of change of the drop diameter is obtained from successive photographs of the drop, and the evaporation rate is calculated from these rate data in conjunction with the heat and mass-transfer coefficients which are discussed in the previous section.

Sources of Error in Experimental Measurements of Drop Evaporation

Frössling has carefully described the principal sources of error which arise in connection with the measurement of droplet evaporation by the above method. Since these errors apply generally to such evaporation studies, they will be fully described in this section.

Deviations From Spherical Shape

From the theoretical investigations of Rayleigh and of Lenard⁽⁹⁻⁷⁰⁾, it may be concluded that moving drops are subject to surface vibrations of various orders (n). If t_n is the vibration time of a drop having a mass m and surface tension σ , then, for small amplitudes,

$$t_n = \left(\frac{3\pi}{n(n-1)(n+2)} \cdot \frac{m}{\sigma} \right)^{1/2} \quad (9-145)$$

From Equation (9-145) it may be shown that the drop is spherical when $n = 1$ and ellipsoidal for $n = 2$; more complicated shapes arise for $n > 2$. Frössling⁽⁹⁻⁷¹⁾ has shown that when the droplet radii exceed 0.03 cm, the vibrations are so slow and their amplitude so small that no appreciable

distortion occurs which would effect the evaporation rate. For radii close to 0.1 cm, appreciable deviations from spherical shape can be expected because the amplitudes of the surface waves are larger than in the case of smaller drops.

Generally, spheres of viscous liquids having radii less than 0.75 mm should follow approximately the same laws which apply to the evaporation of rigid spheres under free-fall conditions of motion.

The Compressibility of the Surrounding Gas

In the derivation of the flow Equation (9-17), Frössling assumed that the gas atmosphere surrounding the drop was incompressible. In his experimental measurements of droplet evaporation, the stream velocities were less than 12 meters per second; this velocity corresponds to an upper limit of the dynamic pressure of 0.7 mm Hg. According to Krell⁽⁹⁻⁷²⁾, the radially-dependent pressure variations are of the order of magnitude of the dynamic pressure and, in the range of low velocities, the compressibility of the gas stream may be neglected at the leading point of a small droplet.

Effect of Turbulence

Frössling carried out a series of experiments on the evaporation of drops of nitrobenzene at several low intensities of stream turbulence and at a constant stream velocity of 1 meter per second. It was considered that the effect of turbulence at this velocity was negligible for drops having an upper size limit of 0.6 mm. The average deviation of the experimental results attributed to turbulence was not greater than 1.6 per cent.

A discussion of evaporation of droplets at higher levels of turbulence is given in Chapter 10.

Transient Conditions

The transient condition of evaporation for a static droplet has been analyzed by Fuchs⁽⁹⁻²¹⁾; this problem was fully discussed in Chapter 8. Frössling has justifiably concluded from Fuch's analysis that the deviations attributable to transient conditions should be smaller than the corresponding deviations for the static case. This conclusion is based upon the fact that the concentration gradient is always large in the dynamic case of evaporation.

Vapor Pressure at the Drop Surface

In nearly all evaporation experiments, the existence of a saturated vapor layer at the surface of the drop is taken as a limiting condition. Frössling⁽⁹⁻⁹⁾ analyzes the correctness of this assumption as follows.

The mass of vapor molecules striking each unit area of the drop surface is $\frac{\partial^2 m}{\partial A \partial t}$ per second. From kinetic considerations, this derivative may be written as

$$\frac{\partial^2 m}{\partial A \partial t} = \left(\frac{\alpha}{1 - \frac{\alpha}{2}} \right) \left(\frac{M}{2\pi RT} \right)^{1/2} (p_s - p_o) ,$$

where α is the accommodation coefficient of the surface for evaporating molecules (see Chapter 7 for a discussion of the significance of this factor). The saturation pressure at the surface is p_s , and p_o is the partial pressure of the vapor in the ambient gas stream. The surface area of the droplet is taken as A .

The accommodation coefficient, α , in air may possibly differ from the vacuum value because of the presence of the adsorbed air on the drop surface which may act as a "barrier" to the transport of molecules by the normal diffusion process. However, few values of α have been measured under these conditions so that it becomes difficult to assess completely the significance of this factor.

The Nusselt group for mass transfer, Nu' , may be written as

$$Nu' = \left(\frac{\partial^2 m}{\partial A \partial t} \right) \frac{d}{D_v c_m}$$

or, in terms of the concentration variables corresponding to the pressures,

$$\frac{\alpha}{1 - \frac{\alpha}{2}} \left(\frac{M}{2\pi RT} \right)^{1/2} (p_s - p_o) = \frac{D_v (c_o - c') Nu'}{d}$$

The relative correction necessary for incomplete saturation at surface is $(p_s - p_o)/(p_o - p')$, or

$$(p_s - p_o)/(p_o - p') = \left(\frac{2 - \alpha}{2\alpha} \right) \left(\frac{2\pi M}{RT} \right)^{1/2} \frac{D_v Nu'}{d} = \gamma Nu'$$

Since Nu' varies across the surface of the drop, the average value, $\overline{Nu'}$, is conveniently taken as being

$$\overline{Nu'} = \frac{1}{A} \left\{ \int Nu' dA - \gamma \int \overline{Nu'}^2 dA \right\}$$

Thus, the relative correction (ω) to be applied to the evaporation rate of a moving drop is

$$\omega = \gamma \frac{\int \overline{Nu'}^2 dA}{\int Nu' dA}$$

From a plot of Nu' against $\cos \theta$, where θ is the angular coordinate of the drop, Frössling concludes that the maximum correction is $4/3 \overline{Nu'}$.

Using Alty and Mackay's⁽⁹⁻⁴¹⁾ value of $\alpha = 0.036$ for water, Frössling showed that his form for the correction factor, ω , is at least approximately correct.

Effect of Drop Curvature on Vapor Pressure

In Chapter 7, there was discussed the influence of drop curvature upon the vapor pressure of very small liquid drops following the Thompson vapor-pressure equation. Since Schreiber⁽⁹⁻⁷³⁾ criticized the Thompson law from the standpoint of its being thermodynamically incorrect, Frössling calculated the vapor-pressure correction by a modified equation and concluded that drop curvature had a negligible effect for drops of an observable size.

Deviations From the Ideal-Gas Law

In the Frössling equation, c_m is calculated from the ideal-gas law in spite of the fact that the vapor is nearly saturated. However, a comparison of the computed values for c_m for water vapor

with the experimentally determined values from Landoldt-Bornstein⁽⁹⁻⁷⁴⁾ demonstrated that the maximum error is about 0.5 per cent at $T < 40$ C. In the evaporation of higher boiling compounds, the relative error should be even less than this amount.

Self-Cooling of the Drop

In Frössling's evaporation experiments, the evaporation rates were corrected to those corresponding to the measured air stream temperature. Thus, by balancing the cooling of the drop due to the latent heat of vaporization against the heating of the drop by convection, conduction, and radiation, by conduction of heat through the suspension, and by frictional effects, it was possible to calculate the maximum temperature reduction in the droplet, T_{max} , relative to the surrounding gas under both static and dynamic conditions of evaporation.

Table 9-6 shows the calculated values of T_{max} compared with the measured values which were obtained by allowing liquid droplets of aniline and nitrobenzene and solid spheres of naphthalene to evaporate on a thermocouple junction. Measurements were taken both in still and moving air.

The calculated and measured temperature reductions agree quite well. The self-cooling is greater for aniline droplets for which the latent heat of vaporization is the largest of the three compounds studied. The effect of this reduction in drop temperature causes about a 2 per cent decrease in the rate of change of the droplet diameter with time, during evaporation. In the cases of nitrobenzene and naphthalene, the self-cooling error is negligible relative to the magnitudes of other experimental errors.

TABLE 9-6. MEASURED AND CALCULATED SELF-COOLING EFFECTS IN DROPLETS UNDER STATIC AND DYNAMIC CONDITIONS OF EVAPORATION. Frössling⁽⁹⁻⁹⁾

Compound	Static Evaporation		Evaporation at Large Re	
	T_{max} , C	$T_{measured}$, C	T_{max} , C	$T_{measured}$, C
Aniline	0.42	0.32	0.16	0.49
Nitrobenzene	0.12	0.12	0.19	0.21
Naphthalene	0.048	--	0.074	--

Correlations of Experimental Measurements

Frössling's measurements were carried out on evaporating drops of nitrobenzene, aniline, water, and naphthalene in an airstream maintained at an ambient temperature of 20 C. The measurements of the rate of change of the square of the drop diameter as a function of time were carried out in accordance with the method described at the beginning of this section. The corrections which were discussed above were applied to these observations.

Figures 9-11 and 9-12 show the correlations of the time rate of change of d^2 with $Re^{1/2}$ for aniline and nitrobenzene, respectively. The experimental data behaves in accordance with Equation (9-33) with the factor ψ (Sc) taken as being a constant which is characteristic of the evaporating substance. Equally satisfactory correlations were also obtained for water and for naphthalene.

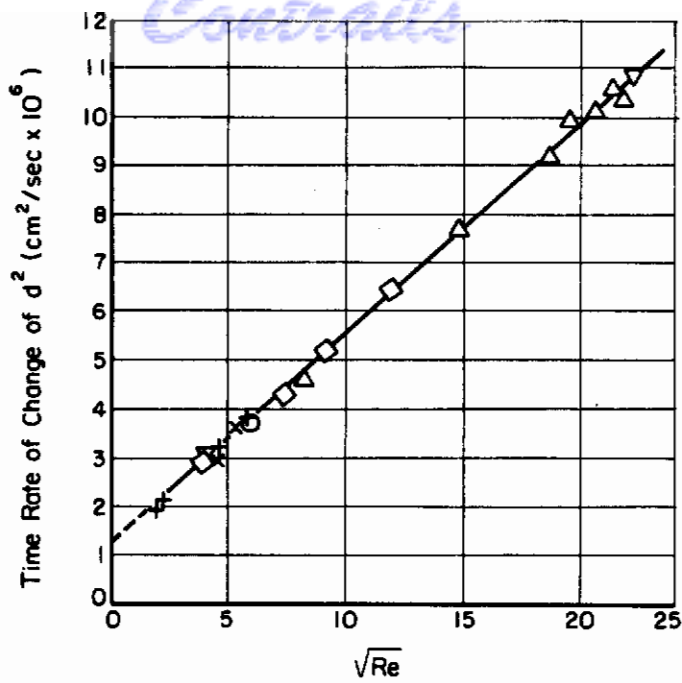


FIGURE 9-11. CORRELATION OF CORRECTED EVAPORATION RATE OF ANILINE AGAINST $Re^{1/2}$
(Frössling)⁹⁻⁹

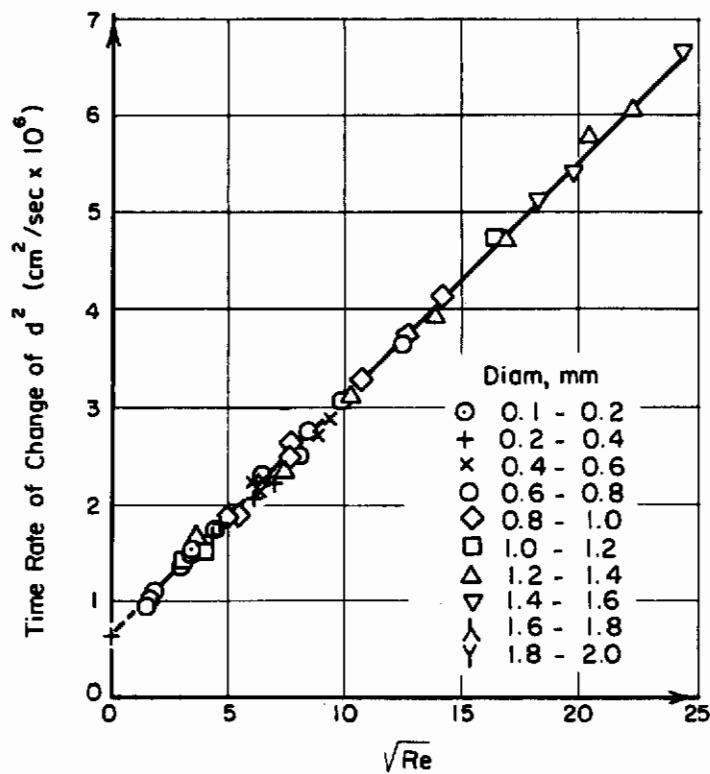


FIGURE 9-12. CORRELATION OF CORRECTED EVAPORATION RATE FOR NITROBENZENE AGAINST $Re^{1/2}$
(Frössling)⁹⁻⁹

Table 9-7 shows values ψ (Sc) taken in the form $k' (Sc)^{1/3}$ from the slopes of the evaporation-data graphs for all compounds studied. The value $k' = 0.276$ has since been verified by other investigators for the evaporation of a wide variety of substances

TABLE 9-7. NUMERICAL DATA USED IN THE DETERMINATION OF THE EVAPORATION CONSTANT $k' = 0.276$

(All units CGS., values at 20 C and 760 mm Hg)

Substance	$k' (Sc)^{1/3}$	D_v	(η_g / ρ_g) (air)	$(Sc)^{1/3} = \frac{\eta_g}{\rho_g D_v}^{1/3}$	k'
Nitrobenzene	0.378	0.0560	0.150	1.390	0.272
Naphthalene	0.387	0.0593	0.150	1.363	0.284
Aniline	0.358	0.0702	0.150	1.288	0.278
Water	0.228	0.2530	0.150	0.842	0.272
Mean = 0.276					

Ranz(9-75) has also made measurements of the evaporation rates of suspended drops of benzene, water, and aniline. His method of measurement differed from Frössling's in that a constant drop diameter was maintained at a feed rate which was just sufficient to keep the value of D_p constant. Air, at a measured rate of flow, was passed through a heating chamber filled with copper turnings which acted as a temperature stabilizer for the gas stream. The uniformly-heated gas stream was then passed through a calming section of pipe and then through a divergent nozzle of the type described by Mache and Hebra(9-64); the nozzle opening was covered with a 140-mesh screen in order to produce a uniform velocity profile which was everywhere equal to the average volumetric velocity. Velocity profiles were examined by hot-wire anemometry.

Droplets were suspended in an airstream from a glass capillary filament which had been pretreated with a silicone polymer to insure uniform contact conditions and to prevent "creeping". Uniform and reproducible droplets were produced by forcing a measured volume of the liquid from a precision microburette which was directly attached to the capillary suspension. Drops in the size range of 600-1000 microns could be produced with this device.

Since droplet self-cooling effects had to be accounted for in the correlation of the experimental data, temperature measurements of the airstream and also in the bulk of the droplet were made by using manganin-constantan thermocouples. During high-temperature-evaporation experiments, drop diameters were measured by cinematography. At lower temperatures, the change in the diameter of the drop was measured directly from a projected magnification of the drop image on a microscope camera screen.

Ranz(9-20) computed the transport quantities necessary for testing the agreement of his experimental data with Equations (9-37) and (9-38) by the best available methods. Heat capacities at constant pressure were calculated by the statistical-mechanical method of Curtiss and Hirschfelder(9-77), viscosities on the basis of the Lennard-Jones intermolecular-potential theory(9-78), and the thermal conductivities were taken from the experimental data of Taylor and Johnson(9-79). The multicomponent diffusion coefficients, D_v , were determined in accordance with the numerical methods described by Hirschfelder and co-workers(9-57) (9-58) (9-59).

Ranz(9-75) presented his evaporation data in a different manner from that used by Frössling; instead of presenting the data as $(d(d)^2/dt)$ against $Re^{1/2}$, the heat- and mass-transfer correlations

corresponding to Equations (9-37) and (9-38) were plotted. This is evidently in agreement with Frössling's correlation since, for heat transfer,

$$Nu = - 1/4 \frac{\lambda_f P_f}{\Delta T_k} \left(\frac{d(d)}{dt} \right)$$

and for mass transfer

$$Nu' = - 1/4 \frac{P_f M_m P_f}{\Delta P D_v \rho_m} \left(\frac{d(d)}{dt} \right)$$

The variables shown in these expressions are as defined previously with the subscripts m and f referring to these quantities, respectively, as the mean value and the value in the transport path.

Figure 9-13 shows the mass-transfer correlations for evaporating water drops in a moving airstream for temperature ranges of 85-221 C. Both the Ranz and Frössling data are presented, and it may be seen that the agreement between the results of both investigators is good. Ranz concludes (1) that there is no effect of diameter which is not included in Re, since the correlation is equally good over the range of drop diameters studied, and (2) that the assumption of a drop temperature corresponding to the temperature of adiabatic saturation (in lieu of the actual wet bulb temperature), at least in the case of water, is justified.

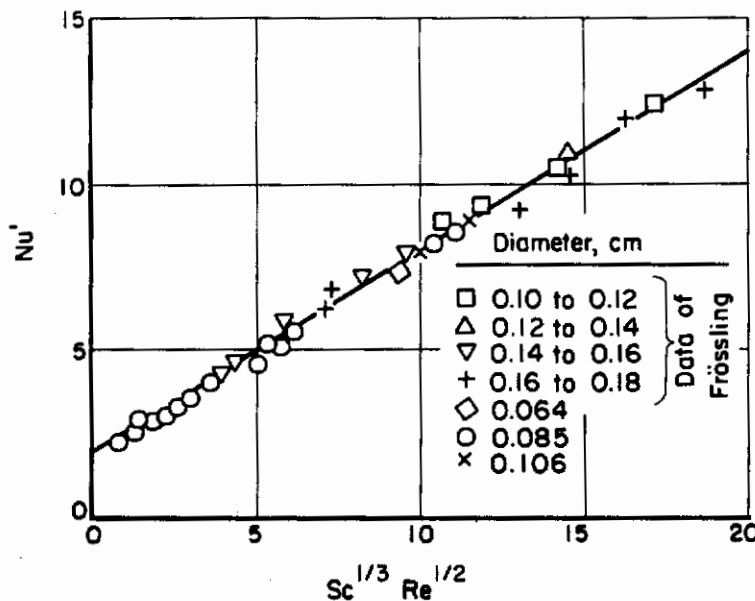


FIGURE 9-13. MASS TRANSFER FOR EVAPORATING WATER DROPS

(Ranz)⁹⁻⁷⁵

Figure 9-14 shows Ranz' data for evaporating benzene drops having an average diameter of 0.110 cm. Air temperatures between 20.4 and 24.4 C were used in these evaporation measurements. The corresponding range of drop temperatures was 3.5 to -0.94 C which, of course, indicates that the benzene drops were supercooled below the liquidus point in all these experiments. Again, the agreement with the mass-transfer correlation is excellent. In the measurements of the drop diameters of these relatively large benzene drops, it was observed that the vertical diameter exceeded the horizontal diameter by about 8 per cent. Average values were used in computing the mass-transfer rates.

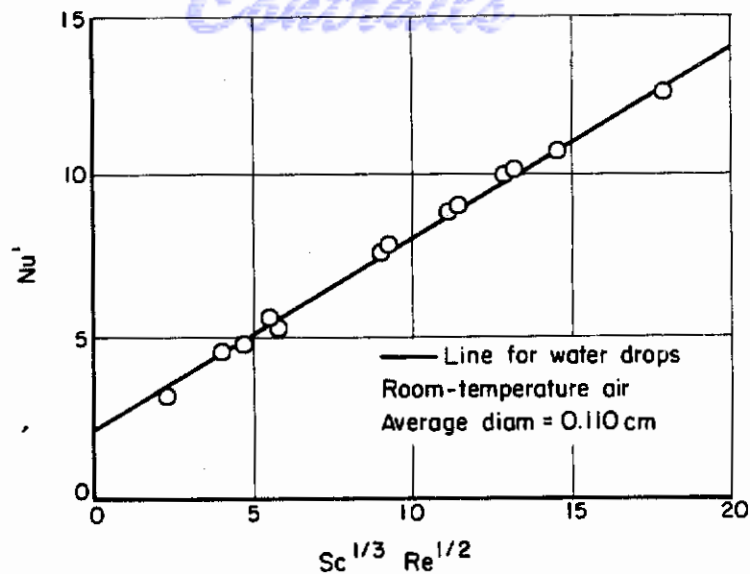


FIGURE 9-14. MASS-TRANSFER CORRELATION FOR EVAPORATING BENZENE DROPS

(Ranz)⁹⁻⁷⁵

In the discussion which follows the derivation of Equation (9-38), it is pointed out that, at $Re = 0$, simple theory would indicate that Nu (heat transfer) should equal 2.0. However, in the evaporation of actual volatile liquid drops at $Re = 0$, the free-convection transfer of both mass and heat should follow the correlations

$$Nu' = 2.0 + k_1 Sc^{1/3} Gr^{1/4}$$

and

$$Nu = 2.0 + k_2 Pr^{1/3} Gr^{1/4} \quad , \quad (9-146)$$

where Sc is the Schmidt number, Gr is Grashaf number, and Pr is the Prandtl number.

Figure 9-15 shows Ranz' data for the evaporation of water drops in still air compared with the free-heat-convection correlation given by Equation (9-146). Also shown are the data of Elenbas⁽⁹⁻⁸⁰⁾ for convective heat transfer from a silver sphere cooling in air as well as the data of Meyer⁽⁹⁻⁸¹⁾ for convective heat transfer from water drops. All data are in good agreement with the convective correlation given by Equation (9-146). Ranz points out that little consideration has been given to the convective errors whose magnitudes depend largely upon the experimental conditions under which evaporation measurements are made.

→ Ranz⁽⁹⁻⁷⁵⁾ has shown that the Frössling heat- and mass-transfer correlations are generally in remarkable agreement with the experimental results of many other investigators. In fact, extrapolations up to five times beyond the range of the Ranz experiment show excellent agreement with the results of other workers who investigated the range of high Reynolds numbers.

Figure 9-16 shows a composite correlation of both heat and mass transfer using the data of Kramers⁽⁹⁻²⁷⁾, Maisel and Sherwood⁽⁹⁻⁸²⁾, Frössling⁽⁹⁻⁹⁾, and of Ranz⁽⁹⁻⁷⁵⁾. In preparing this correlation, Ranz corrected the Maisel and Sherwood values for D_v to the more accurate values used in his own calculations. The data of Kramers are definitely above the correlation line at low values of Re ; Ranz attributes this to the effect of free convection.

Ranz has commented upon the extrapolation of the Frössling mass- and heat-transfer correlations to higher airstream temperatures. For the temperature range 300-500 C, the heat-transfer correlation seems to be the preferred relation because the thermal conductivity values are better known than are the diffusion coefficients which are associated with mass-transfer

calculations. The principal difficulty which is encountered in these high-temperature problems is that of calculating the correct transport quantities over the average transport path.

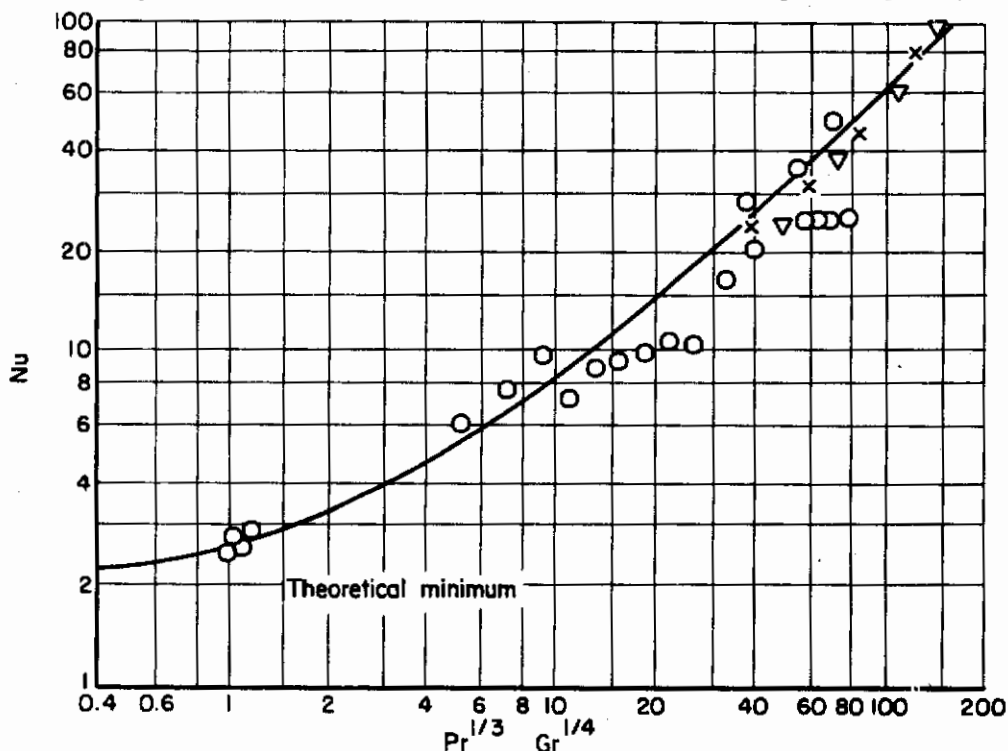


FIGURE 9-15. FREE CONVECTION OF HEAT FROM SPHERES.
CORRELATION LINE $Nu = 2.0 + 0.60 Pr^{1/3} Gr^{1/4}$
(Ranz)⁹⁻⁷⁵

In the previous section, there was discussed the semiempirical correlation of Ingebo⁽⁹⁻²⁸⁾, which is applicable to evaporation at high temperatures. Ingebo compared his correlation Equation (9-59) with data taken on the evaporation of nine liquid substances, of widely differing volatilities for a wide range of the Reynolds number and at temperatures of from 30 to 500 C. The technique which was employed by Ingebo in obtaining evaporation data was somewhat different from the methods which were employed by Frössling and by Ranz.

Figure 9-17 shows schematically the apparatus used by Ingebo. Compressed air at 200 psi was passed through the reducing valve into an electrically heated chamber; the flow rate was measured by means of a rotameter on the upstream side of the heating chamber. The exit gas was then passed through a calming section followed by a 200-mesh screen before entering the test section. Instead of using a suspended drop for the evaporation measurements, Ingebo used a porous cork sphere, having a diameter of 0.688 cm, which was kept wetted with the evaporating liquid by means of a hypodermic syringe. The tip of the needle was located at the center of the sphere and the liquid was forced through the pores of the sphere by manually depressing the plunger of the syringe.

The surface temperature of the wetted cork sphere was measured by means of a 40-mil iron-constantan thermocouple which was mounted flush with the surface of the sphere. Similarly, measurement was also made of the temperature at the center of the sphere to determine the rate at which sensible heat was transferred to the sphere during measurements of the evaporation rate.

Vaporization rates were measured in accordance with the following procedure.

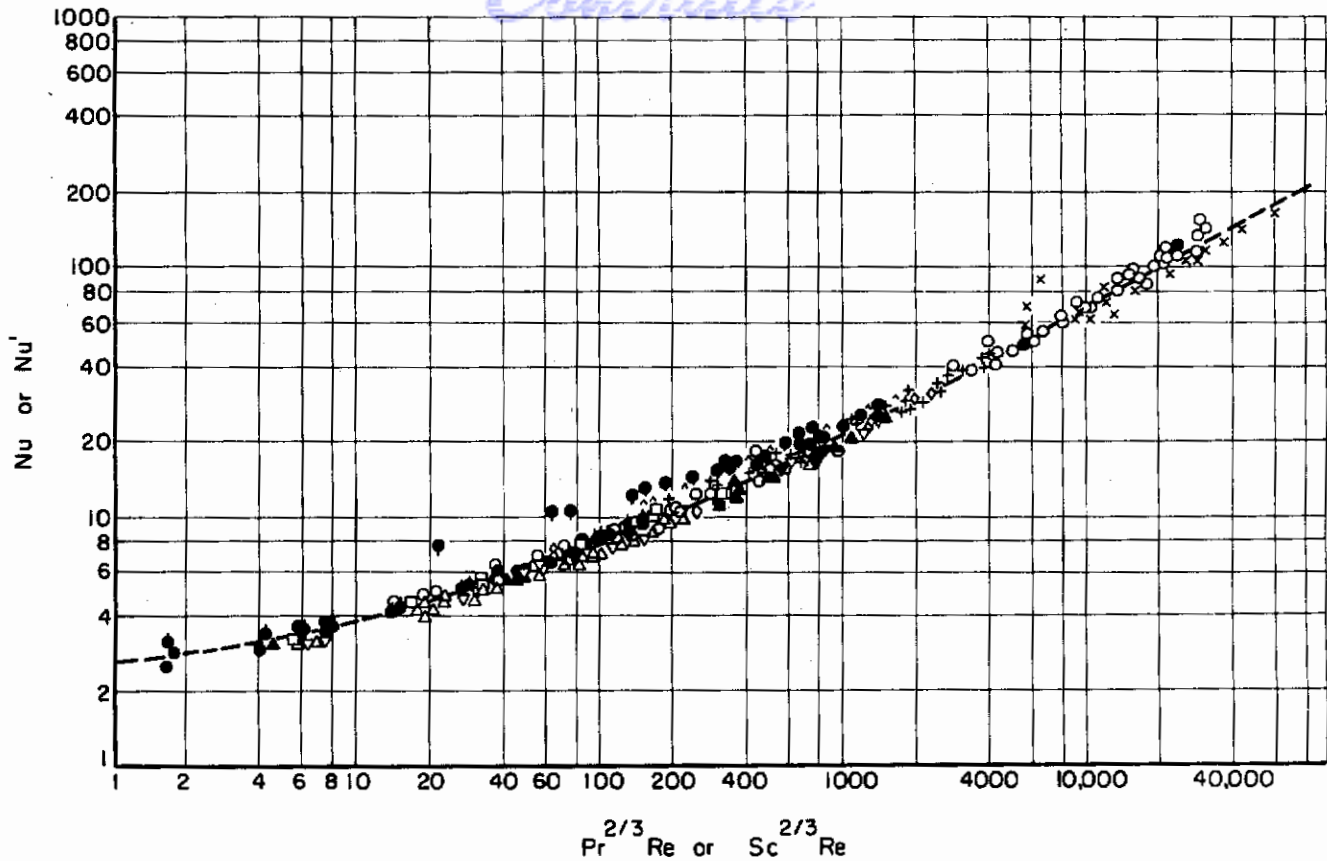


FIGURE 9-16. COMPOSITE HEAT AND MASS TRANSFER CORRELATIONS FOR SPHERES
(Ranz)⁹⁻⁷⁵

- (1) Removing the test tube which normally covered the sphere to prevent evaporation.
- (2) Holding the sphere in the airstream in a test section for a period of two minutes while keeping the surface wetted by manually depressing the syringe plunger.
- (3) Replacing the test tube over the sphere.

Airstream and sphere temperatures were obtained in the usual way. The total evaporation from the sphere during the exposure was obtained by weighing the syringe, cork sphere, and test-tube combination before and after evaporation.

The transport quantities used in the correlation computations were taken from handbook values. It is not apparent from Ingebo's report how the values were obtained for the high-temperature cases. It would appear that Ranz has given considerably more attention to the matter of accurately calculating the transport quantities than has Ingebo.

The theoretical implications of the Ingebo correlation have already been presented in connection with the discussions regarding Equation (9-59). This equation may conveniently be written in terms of the dimensionless groups, which have already been defined, in the following expression

$$Nu = \left[2 + 0.303 (Re) (Sc)^{0.6} \left(\frac{k_g}{k_v} \right)^{0.5} \right]$$

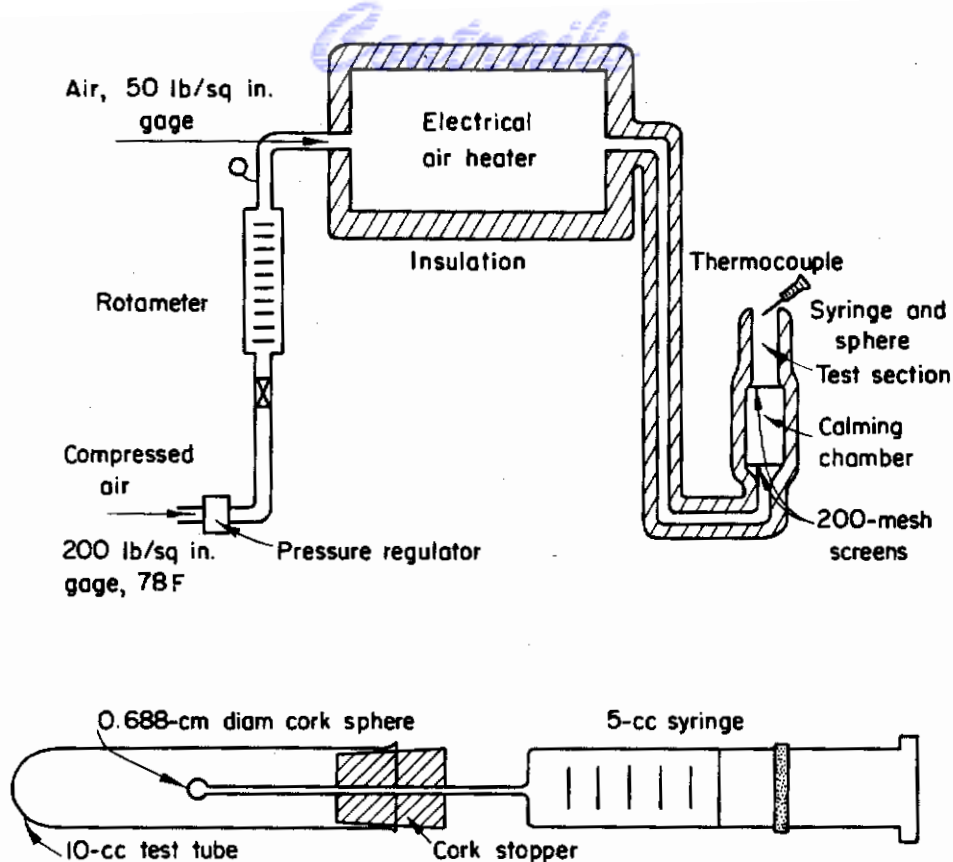


FIGURE 9-17. SCHEMATIC DIAGRAM OF VAPORIZATION APPARATUS
(Ingebo)⁹⁻²⁸

Figure 9-18 shows the Ingebo experimental data for the evaporation rates of nine compounds in accordance with the dimensionless groups appearing in Equation (9-59). Also shown are the Frössling evaporation data for both water and nitrobenzene. It is interesting to note that the Frössling data correlate quite well with Equation (9-103). It would appear that Ingebo's data tend to diverge quite markedly with increasing values of $(Re)(Sc)^{0.6}(k_g/k_j)^{0.5}$. This may possibly be connected with the uncertainties in the calculated transport quantities at high temperatures. A recalculation of these quantities might possibly yield a stronger correlation for the higher temperature evaporation data.

It would seem that Ingebo's experimental method may be open to some question from the standpoint of the accuracy of measurement of surface temperature in the evaporating liquid film; this would be particularly so if the film thickness were small in comparison to the dimension of the thermocouples. The possible errors introduced in this measurement are not clearly discussed in Ingebo's report. Also, the discontinuity in the thermal conduction path in passing from the liquid film to the cork sphere may possibly have influenced the surface temperature readings.

It would seem that further experimental work would be needed to justify completely the statement that there is a sameness for the evaporation processes in a wetted porous sphere and in liquid drops.

The evaporation studies of Gohrbandt⁽⁹⁻⁸³⁾, which were carried out by cinematographically recording the change in size of suspended camphor spheres in an airstream at 30-500 C and over a range of Re of 100-2000, indicate that mass rate of evaporation is at least proportional to $Re^{1/2}$. In an extension of these studies to higher gas temperatures, Gohrbandt⁽⁹⁻⁸⁴⁾ has concluded that the evaporation rate of liquid spheres is proportional to a factor of the form $(1 + K Re^{1/2})$. He concludes that a general form of this type is valid for both high and low air temperatures, but that K is a function of the temperature. Since Gohrbandt's experimental data

are not available at this time, it is not possible to make a comparison of the evaporative-rate correlations by the Ingebo and Frössling equations; the temperature dependence of K could lead to agreement with either result.

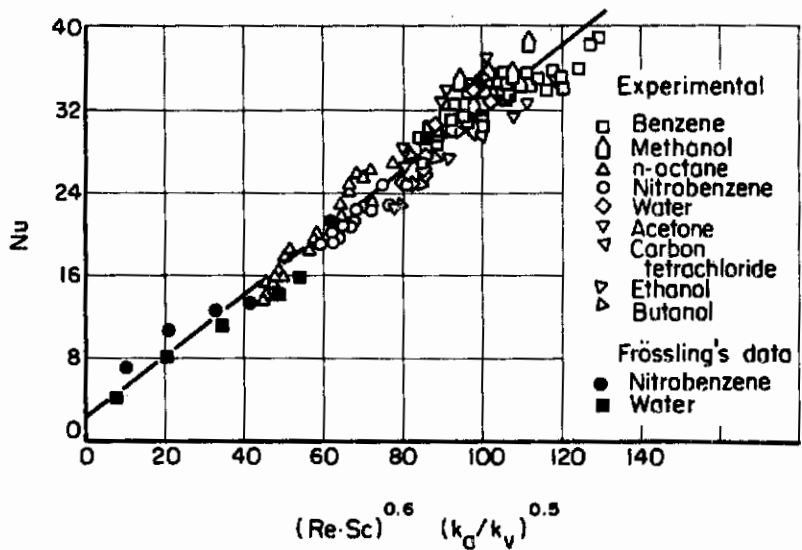


FIGURE 9-18. CORRELATION OF EVAPORATION RATES FOR NINE LIQUIDS (Ingebo)⁹⁻²⁸

Johnstone and Eads⁽⁹⁻⁸⁵⁾ have derived an expression for calculating the time which would be required to evaporate completely a liquid droplet. This expression is based upon the Frössling correlation and it is assumed that the temperature of the drop is constant throughout the evaporation period; this assumption is equivalent to assuming that the droplet vapor tension is also invariant. The difference between the droplet surface and ambient air temperatures, Δt , was calculated from the expression

$$\Delta t = \text{const} \left(\frac{\partial \ln p}{\partial t} \right) \left(\frac{Nu'}{Nu} \right)$$

rather than by the direct measurement used by Ingebo. It was found that the ratio (Nu' / Nu) was practically constant for all experimental measurements. These workers have also shown that the Frössling equation can be used to predict accurately the evaporation rate of small sulphur droplets at moderately high temperatures (150-200 C). The high rates of evaporation of sulfur above 200 C prevented a further study of evaporation at higher temperatures with this material.

At the present time, considerable experimental work is under way at the National Gas Turbine Establishment, in England, on the problem of the evaporation and combustion of freely falling droplets. Topps⁽⁹⁻⁸⁶⁾ has done some preliminary work on the evaporation of pure hydrocarbons and fuel-oil droplets having diameters of 300-500 μ . These studies are being made under free-fall conditions and at high temperatures and pressures. Although a complete analysis of this work is not as yet available, Topps⁽⁹⁻⁸⁷⁾ has indicated that heat transfer in the moving drops is strongly related to the skin friction during transit in the high-temperature region; this approach is discussed by Goldstein⁽⁹⁻⁸⁸⁾.

The process of droplet evaporation for materials of relatively low volatility is comparatively well accounted for by the Frössling correlation. This is particularly so under conditions where the thermal and concentration gradients are not large. The problem of droplet evaporation for volatile compounds in a high-temperature environment appears to need further experimental investigation. In this connection, new techniques are sorely needed for measuring rapid rates of droplet evaporation, and further theoretical work seems to be required on the problems

associated with selecting proper values for the transport quantities in the transfer path between the droplet and the gas stream.

In all the work discussed, the processes of simultaneous heat and mass transfer have been treated as if they were virtually independent phenomena. This is clearly not the case, since the vaporizing molecules give up a portion of their sensible heat to the gas molecules present in the transfer path and thus materially change the rate of sensible heat transfer. This complicated dependence appears to require an extended treatment beyond that given by Ackerman⁽⁹⁻⁸⁹⁾ in 1936.

Although some thought has been given to several simplified and interesting problems in connection with the evaporation of multicomponent drops, no work on the generalized hydrodynamical and diffusion problems for multicomponent drops under motion has as yet appeared. The mathematical aspects of this portion of the evaporation problem appear to be extremely complex, but any result of such an investigation, even though meager, should be of considerable importance.

REFERENCES

- 9-1. Bossinesq, M. J., Calcul de Pouvoir Refroidissant des Courants Fluides; J. de Math., Series 2, 1 (1905) 285.
- 9-2. King, L. V., Convection of Heat From Small Cylinders; Trans. Roy. Soc. (London), Series 4, 214 (1914) 347.
- 9-3. Jefferys, H., Some Problems of Evaporation; London Phil. Mag., 35 (1918) 273.
- 9-4. Namekawa, T., and Takahasi, T.; Note on the Rate of Evaporation of Small Water Drops; Mem. Coll. Sci., Kyoto Imp. University, 20 (1937) 139.
- 9-5. Powell, R. W., and Griffiths, E., Evaporation of Water From Plane and Cylindrical Surfaces; Trans. Inst. Chem. Eng., 13 (1935) 175.
- 9-6. Millar, F. G., Evaporation From Free Water Surfaces; Canadian Meteor. Service Memoirs, 112 (1937) 43.
- 9-7. Sverdrup, H. V., On the Ratio Between Heat Conduction From the Sea Surface and the Heat Used for Evaporation; Annals. N. Y. Acad. Sci., 44 (1945) 81.
- 9-8. Von Karman, T., Turbulence and Skin Friction; J. Inst. Aero. Sci., 1 (1934) 1.
- 9-9. Frössling, N., Über die Verdunstung Fallender Tropfen; Gerl. Beitr. Geophysik, 52 (1938) 170.
- 9-10. Sutton, W. G. L., On the Equation of Diffusion in a Turbulent Medium; Proc. Roy. Soc., 182 (1943) 48.
- 9-11. Taylor, G. I., Diffusion by Continuous Movements; Proc. Lond. Math. Soc., 20 (1921) 196.
- 9-12. Nikuradse, J., Laws of Turbulent Flow in Smooth Tubes; Fors. V.D.I., 356 (1932) 36.
- 9-13. Sutton, O. G., Wind Structure and Evaporation in a Turbulent Atmosphere; Proc. Roy. Soc., 146 (1934) 701.
- 9-14. Pasquill, F., Evaporation from a Plane, Free-Liquid Surface Into a Turbulent Airstream; Proc. Roy. Soc., 182 (1943) 75.
- 9-15. Wade, L., Paper Presented at Meeting of the Institute of Chemical Engineers, January (1942).

- Continued*
- 9-16. Prandtl, L., Wein-Harms Handbuch d. Exptl. Physik, Akademische Verlag., Leipsig (1930), 4, 1, 279.
 - 9-17. Oseen, C. W., Hydrodynamik, Akad. Verlag., Leipzig (1927).
 - 9-18. Bolze, E., Grenzsichten in Rotations körpern in Flüssigkeiten mit Kleiner Reiburg; Dissertation, Univ. Gottingen (1908).
 - 9-19. Luthander, S., and Ryberg, A., Experemantelle Untersachung über den Luftwiderstand bei einer Umeine mit der Windrichtung Parallele Achse Rotier eu deu Kugel, Physik, Zeit 36, 552 (1935).
 - 9-20. Ranz, W. E., and Marshall, W. R., Evaporation from Drops, Part I; Chem. Eng. Progress, 48 (1952) 141.
 - 9-21. Fuchs, N., Concerning the Evaporation of Small Drops in a Gas Atmosphere; NACA Technical Memorandum No. 1160, 1947.
 - 9-22. Langmuir, I., Evaporation of Small Spheres; Phys. Rev., 11 (1918) 368.
 - 9-23. Williams, G. C., Ph. D. Dissertation, Mass. Inst. of Technology (1943). Also available in abridged form in PB Report No. 6538.
 - 9-24. McAdams, W. H., Heat Transmission, McGraw-Hill Book Co., New York (1942).
 - 9-25. Kronig, R., and Bruijstein, J., On the Theory of Heat and Mass Transfer From a Sphere in a Flowing Medium at Low Values of Reynolds Number; App. Sci. Res., A2 (1951) 439.
 - 9-26. Lamb, H., Hydrodynamics, 6th Edition, Dover Publications, New York (1932).
 - 9-27. Kramers, H., Heat Transfer From Spheres to Flowing Media; Physica, 12 (1946) 61.
 - 9-28. Ingebo, R. D., Vaporization Rates and Heat Transfer Coefficients for Pure Liquid Drops; NACA Research Memorandum No. E51c19 (1951).
 - 9-29. Wagner, C., Calculation of the Flight Rate of Fuel Droplets in the Air Stream of a Ramjet; Tech. Report No. 52, Ordnance Research and Development Division, Suboffice (Rocket), Fort Bliss, Texas, February (1948).
 - 9-30. McAdams, W. H., Heat Transmission, 2nd Edition, p. 273, McGraw-Hill Book Co., New York (1942).
 - 9-31. Pigford, R. L., Mass Transfer; Ind. Eng. Chem., 45 (1953) 957.
 - 9-32. Godsave, G. A. E., Studies of the Combustion of Drops in a Fuel Spray - The Burning of Single Drops of Fuel; Fourth Symposium on Combustion, p 818, Williams and Wilkins Co., Baltimore, 1953.
 - 9-33. Tanford, C., and Pease, R. N., (a) Equilibrium Atom and Free Radical Concentrations in Carbon Monoxide Flames; J. Chem. Phys., 15, 431 (1947). (b) Theory of Burning Velocity, I, Temperature and Free Radical Concentrations near the Flame Front, Relative Importance of Heat Conduction and Diffusion; J. Chem. Phys., 15, 433 (1947). (c) Theory of Burning Velocity, II, The Square Root Law for Burning Velocity; J. Chem. Phys., 15, 861 (1947).
 - 9-34. Ranz, W. E., Private Communication, May 1954.
 - 9-35. Tanasawa, Y., and Kobayashi, K., On the Evaporation Velocity of a Liquid Drop in a High Temperature Gas; Tech. Reports of Tohoku Univ., 15 (1950) 55, 14 No. 2.

- 9-36. Carslaw, H. S., Introduction to the Mathematical Theory of the Conduction of Heat in Solids; Dover Publications, New York (1945).
- 9-37. Goldstein, S., Calculation of the Surface Temperature of Simple Bodies; Z. fur. angew. math. u. Mechanik, 14 (1934) 158.
- 9-38. Kumm, E. L., Calculations on the Evaporation Rate of Sprays in Rapidly Moving Gases; Report AL-916, June 23, 1949, North American Aviation, Inc., Aerophysics Laboratory, Project MX-770.
- 9-39. Colburn, H. P., and Drew, T. B., Heat Transfer and Fluid Friction During Flow Across Banks of Tubes, Trans. ASME, 76 (1954) 841.
- 9-40. Hartwig, F. W., The Evaporation of Liquid Drops in a Hot Gas; B. Sc. Thesis, Cal. Inst. of Technology (1952).
- 9-41. Penner, S. S., Evaporation of Liquid Droplets in a Rocket Motor; Progress Report No. 9-13, Project No. TU2-1, JPL, Cal. Inst. of Tech., September 5, 1947.
- 9-42. El Wakil, M. M., Uyehava, O. K., and Myers, P. S., A Theoretical Investigation of the Heating-Up Period of Injected Fuel Droplets Vaporizing in Air; NACA Tech. Note 3179, May 1954.
- 9-43. Sjenitzer, F., Spray Drying; Chem. Eng. Sci., 3 (1952) 101.
- 9-44. Marshall, W., and Seltzer, E., Principles of Spray Drying; Chem. Eng. Progress, 46 (1950) 501.
- 9-45. Duffie, J. H., and Marshall, W. R., (a) Properties of Spray-Dried Materials; Chem. Eng. Prog., 49, 417 (1953). (b) Factors Influencing the Properties of Spray Dried Materials; Chem. Eng. Prog., 49, 480 (1953).
- 9-46. Tsuji, M., On the Rate of Evaporation of Falling Drops; Meteor. Soc. of Japan, (2nd Series) [28(4)] (1950) 121.
- 9-47. Alty, T., and Mackay, C. A., The Accommodation Coefficient and Evaporation Coefficient of Water; Proc. Roy. Soc., 149 (1935) 104.
- 9-48. Penner, S. S., and Weinbaum, S., Some Considerations of the Effect of Radiation on the Performance of Liquid Fuel Rockets; J. Opt. Soc. Am., 38 (1948) 599.
- 9-49. Norris, R., Evaporation from Extensive Surfaces of Water Roughened by Waves; Roy. Meteor. Soc. Quart. Journal, 74 (1948) 1.
- 9-50. Sverdrup, H. V., Oceanography for Meteorologists; Prentice-Hall, Inc., New York (1953).
- 9-51. Hinze, J. O., Critical Speeds and Sizes of Liquid Globules; App. Sci. Res., A1 (1949) 273.
- 9-52. Hughs, R. R., and Gilliland, S. R., The Mechanics of Drops; Chem. Eng. Prog., 48 (1952) 497.
- 9-53. Triebnigg, A., Der Einblase und Einspritzvorgang bei Diesel-maschinen; Vienna (1929).
- 9-54. Heyler, M., L'Injection Mechanique In Combustible dans les Moteurs Diesel; III^e Congress du Chauffage Industriel, Paris (1929).
- 9-55. Hadden, S. T., Vapor-Liquid Equilibrium in Hydrocarbon Systems; Chem. Eng. Prog., 44 (1948) 37.

- Control*
- 9-56. Nederbragt, G. W., Gas-Liquid Equilibrium in Hydrocarbon Systems; App. Sci. Res., A1 (1949) 237.
- 9-57. Hirschfelder, J. O., Byrd, R. B., and Spotz, E. L., The Transport Properties of Gases and Gas Mixtures; Chem. Rev., 44 (1944) 968.
- 9-58. Hirschfelder, J. O., Byrd, R. B., and Spotz, E. L., The Transport Properties of Non-Polar Gases; J. Chem. Phys., 16 (1948) 968.
- 9-59. Curtiss, C. F., and Hirschfelder, J. O., Transport Properties of Multicomponent Gas Mixtures; J. Chem. Phys., 17 (1949) 550.
- 9-60. Kronig, R., and Brink, J. C., On the Theory of Extraction from Falling Drops; App. Sci. Res., A2 (1949) 142.
- 9-61. Hadamard, J. C., Translatory Motion of a Fluid Sphere in a Viscous Medium; Comp. Rendus, 152 (1911) 1735.
- 9-62. Jahnke, E., and Emde, F., Tables of Functions with Formulae and Curves; Dover Publications, New York (1943).
- 9-63. Margenau, H., and Murphy, G. M., The Mathematics of Physics and Chemistry; D. Van Nostrand Co., Inc., New York (1943).
- 9-64. Kronig, R., Van Der Veer, B., and Ijzerman, P., On the Theory of Extraction from Falling Drops II; App. Sci. Res., A3 (1952) 103.
- 9-65. Pauling, L., and Wilson, E. B., Introduction to Quantum Mechanics; McGraw-Hill Book Company, New York.
- 9-66. Garner, F. H., Diffusion Mechanism in the Mixing of Fluids; Trans. Inst. Chem. Eng., 28, 88 (1950).
- 9-67. Garner, F. H., and Skelland, A. H. P., Liquid-Liquid Mixing as Affected by the Internal Circulation in Drops; Trans. Inst. Chem. Eng., 29, 315 (1951).
- 9-68. Spells, K. E., A Study of Circulation Patterns Within Liquid Drops Moving Through Liquids; Proc. Phys. Soc. (London) B65, 541 (1952).
- 9-69. Rybczynski, W., Translatory Motion of a Fluid Sphere in a Viscous Medium; Bull Acad. Sci., Cracovie 1, 40 (1911).
- 9-70. Lenard, P., Wein-Harms, Handbuch für Expt'l. Physik VI, 184, Akademische Verlag, Leipzig (1930).
- 9-71. Frössling, N., Constant Velocity of a Falling Sphere; Gerl. Beitr. Geophysik, 51 (1937) 169.
- 9-72. Krell, O., Druckverteilung an der Luftumstroemten Kugel; Z. für Lufttechnik und Motorlufts, 22 (1931) 97.
- 9-73. Schreber, K., Equation Between the Osmotic Pressure and the Rise in Boiling Point After Arrhenius; Z. Elektrochem., 32 (1926) 149.
- 9-74. Landolt-Bornstein, Phys. Chem. Tabellen III, 2421; J. Springer, Berlin (1931).
- 9-75. Ranz, W. E., and Marshall, W. R., Jr., Evaporation from Drops II; Chem. Eng. Prog., 48 (1952) 173.
- 9-76. Mache, H., and Hebra, A., Measurement of the Rate of Burning of Explosive Gas Mixtures; Sitzber. Akad. Wiss. Wein, 11a (1941) 157.

- Continued*
- 9-77. Curtiss, C. F., and Hirschfelder, J. O., Thermodynamic Properties of Air; Reports No. CM-472 and CM-518, Univ. of Wisconsin Naval Res. Laboratory (1948).
 - 9-78. Chapman, S., and Cowling, T. G., The Mathematical Theory of Non-Uniform Gases; Cambridge Univ. Press, New York (1939).
 - 9-79. Taylor, W. J., and Johnston, H. L., An Improved Hot Wire Cell for Accurate Measurement of the Thermal Conductivity of Gases over a Wide Range of Temperature, J. Chem. Phys., 14 (1946) 219.
 - 9-80. Elenbaas, W., The Dissipation of Heat by Free Convection of Spheres and Horizontal Cylinders; Physica, 9 (1942) 285.
 - 9-81. Meyer, P., Heat Transfer to Small Particles by Natural Convection; Trans. Inst. Chem. Eng., 15 (1937) 127.
 - 9-82. Maisel, D. S., and Sherwood, T. K., Effect of Air Turbulence on the Rate of Evaporation of Water; Chem. Eng. Progress, 46 (1950) 172.
 - 9-83. Gohrbandt, W., The Evaporation of Spheres in a Hot Gas Stream; Nat. Gas Turbine Estab. Memo. No. 110, April (1951).
 - 9-84. Gohrbandt, W., Unpublished Work, Nat. Gas Turbine Estab. (1952).
 - 9-85. Johnstone, H. F., and Eads, D. K., Vaporization of Small Sulphur Drops; Ind. and Eng. Chem., 42 (1950) 2293.
 - 9-86. Topps, J. E. C., An Experimental Study of the Vaporization and Combustion of Falling Drops; Nat. Gas Turbine Estab. Memo No. 105, February (1951).
 - 9-87. Topps, J. E. C., Unpublished Work, Nat. Gas Turbine Establishment (1952).
 - 9-88. Goldstein, S. (Editor), Modern Developments in Fluid Dynamics; Oxford University Press, New York (1938).
 - 9-89. Ackermann, G., Heat and Material Transfer Under Large Temperature and Partial Pressure Differences; Forsch. Ing. Wes., 8, V.D.I. Forsch No. 382 (1937).

Contrails

CHAPTER 10. SPRAY EVAPORATION

ABSTRACT

An analysis of dynamic-spray evaporation is given which is based upon the aerodynamic and transport aspects of single-droplet evaporation developed in Chapter 9. It is assumed that these semiempirical relations are valid for the evaporation of individual droplets of varying size which constitute the ensemble of the spray. Thus, the evaporation rates for individual drops are integrated to obtain a total evaporation rate; droplet-interaction effects are ignored in this treatment. A drop-size distribution function is introduced into the analysis to account for the spectrum of drop sizes which may be present in a real spray. It is, of course, necessary to make numerous assumptions regarding the time-dependent behavior of the size distribution in order to circumvent the mathematical difficulties which are associated with this problem.

Contrails

SPRAY EVALUATION

by

F. Benington

In studying the combustion of any liquid fuel that is dispersed in a gaseous oxidant by spray injection, it is important to know what parameters most markedly influence the course of the evaporation of the fuel spray. On the basis of the information presented in earlier chapters, it can be seen that free-stream turbulence, drop-size distribution, and the relative velocity between the drops and the air stream are among the most important parameters in determining spray-evaporation rates.

The aerodynamic and transport aspects of single-droplet evaporation under conditions of ambient gas motion have already been developed in Chapter 9. In the present chapter, it is assumed that these semiempirical relations are valid for the evaporation of the individual drops of varying size which constitute the ensemble of the spray. Thus, the evaporation rates for individual drops are integrated to attain a total evaporation rate without considering any interaction effects upon the total rate. It will be necessary to revert to the use of a drop-size distribution function in order to determine the total evaporation rate because a real spray is made up of a spectrum of drop sizes. Unfortunately, it is necessary to make numerous assumptions regarding the time-dependent behavior of the distribution function in order to circumvent certain mathematical difficulties associated with this problem.

Adequate caution and judgment should be exercised in attempting to apply the results of this chapter to any real spray system. In this respect, it would first be well to re-examine the assumptions of Chapter 9 in addition to those which will be presented herein. This is clearly indicated, since spray evaporation is based upon the single-droplet treatment.

Although many factors enter into both the geometry and intensity of the turbulence and velocity fields for particular combustion chambers, no attempt has been made to examine these factors because of both mathematical difficulties and the limited usefulness of this kind of result. Rather, the treatment will be restricted to general considerations.

SIZE DISTRIBUTION OF DROPLETS IN A SPRAY

The subject of drop-size distribution in sprays was analyzed and discussed in detail in Chapter 4. However, a few remarks in this connection bear repetition at this point in order to lend an adequate continuity to this development.

The production of a dispersed system of liquid drops in a gaseous medium is usually accomplished by injecting the liquid phase into the gaseous phase by means of a spray nozzle or injector. The resulting liquid-phase dispersion contains droplets of various sizes in different abundances, the most plentiful size lying between the maximum and minimum sizes. Bevans⁽¹⁰⁻¹⁾ has summarized the most useful mathematical expressions for describing particle- and drop-size distributions and has compared their relative utility for describing liquid sprays. The following mathematical forms are considered useful in this respect in that all were found to fit the data of Kolupaev⁽¹⁰⁻²⁾ on the size consists of oil sprays:

$$\text{Rosin-Rammler (10-3)} \quad \frac{dN}{d\delta} = a\delta^{q-4} e^{-b\delta^q}, \quad (10-1)$$

$$\text{Nukiyama-Tanasawa (10-4)} \quad \frac{dN}{d\delta} = a\delta^2 e^{-b\delta^q}, \quad (10-2)$$

and the logarithmico-normal equation described by Epstein⁽¹⁰⁻⁵⁾, which will not be used in this discussion. In Equations (10-1) and (10-2), a , b , and q are constants, δ is the drop diameter, and N is the number of drops of diameter greater than δ . Both equations are empirical and the constants must be determined by experiment.

In the section which follows, in the course of developing the rate equations for the evaporation of a dynamic spray, use will be made of the mean drop diameter $\bar{\delta}$. Equation (10-1) is not satisfactory for calculating $\bar{\delta}$ if $q < 3$ since $\bar{\delta} = 0$ under this condition; this arises from the fact that Equation (10-1) gives an infinite number of infinitesimal drops for $q < 3$. However, Equation (10-2) is free from this limitation and may be conveniently used to determine $\bar{\delta}$.

Neither of the distribution functions which have been given accurately describe a real spray since both predict the existence of a size range of from zero to infinity. Clearly, any real spray must possess a finite upper bound of drop size. Both equations do, however, predict that the frequency of occurrence of particles rapidly approaches zero as the particle size is increased beyond the size of greatest probability.

THE EFFECT OF DROP SIZE AND STREAM VELOCITY UPON THE MASS RATE OF SPRAY EVAPORATION

A careful search of the literature has shown that little work has been done in the field of developing theoretical equations for expressing the rate of spray evaporation under conditions of motion. This is not surprising in that any such theory would have as a basis the evaporation rate of a single droplet in a moving gas stream. As has been shown already, no analytical solution for the single-droplet problem has ever been obtained. Therefore, any solution to the spray evaporation would be, at best, an approximation in light of the existing theory.

Fledderman⁽¹⁰⁻⁶⁾ has attempted to develop an equation for predicting the total evaporation rate of a unidirectional spray by applying the Frössling⁽¹⁰⁻⁷⁾ equation to each drop in the ensemble constituting the spray. The steady-state evaporation of a single droplet is given by:

$$\frac{dm}{dt} = -2\pi D \frac{Mp}{RT} \left[1 + 0.276 (Sc)^{1/3} (Re)^{1/2} \right] \delta, \quad (10-3)$$

where m is the mass of the drop, D is the diffusion coefficient, p is the saturation pressure, t is the time, T is the temperature, R is the gas constant, M is the molecular weight, Sc is the Schmidt group, Re is the Reynolds number, and δ is the drop diameter. If the spray consists of droplets of the same mass m , then the rate of evaporation of the i^{th} drop is

$$\frac{dm_i}{dt} = -2\pi D \frac{Mp}{RT} \left[1 + 0.276 (Sc)^{1/3} (Re_i)^{1/2} \right] \delta_i \quad (10-4)$$

where $(Re_i) = \frac{u_r \delta_i}{\nu}$, where u_r is the relative velocity of the drop along the x axis, and ν is the gas viscosity.

It is assumed that u_r is the same for all drops at a given value of \underline{x} and that each drop evaporates without any interaction with its neighbors. Suppose that dN_i is the number of drops whose diameters lie in the range $\delta_i + d\delta$, then $m_i dN_i$ is the total mass of the drops within this size group. For each size group, the evaporation rate is

$$\frac{d}{dt} [m_i dN_i] = -A [1 + B (Re_i)^{1/2}] \delta_i dN_i, \quad (10-5)$$

where

$$A = \frac{2\pi D M_p}{RT},$$

and

$$B = 0.276 (Sc)^{1/3}.$$

The total rate of evaporation for the entire consist is now obtained by summing the indices for all the sizes from 0 to \underline{N} . Then

$$\frac{d}{dt} \left[\sum_0^N m_i dN_i \right] = -A \left\{ \sum_0^N [1 + B (Re_i)^{1/2}] \delta_i dN_i \right\}. \quad (10-6)$$

If the distribution is considered as being a continuous function, the summation signs in Equation (10-6) can be replaced by integrals. Equation (10-6) may then be written as

$$\frac{d}{dt} \int_0^N m dN = -A \int_0^N [1 + B (Re)^{1/2}] \delta dN. \quad (10-7)$$

By taking M_t as being the total mass of the spray at some value of \underline{x} ,

$$-\frac{dM_t}{dt} = A \int_0^N [1 + B (Re)^{1/2}] \delta dN \quad (10-8)$$

where

$$\int_0^N m dN = M_t.$$

By eliminating Re from Equation (10-8) we have

$$-\frac{dM_t}{dt} = A \int_0^N \delta dN + C u_r^{1/2} \int_0^N \delta^{3/2} dN \quad (10-9)$$

with

$$C = AB/(\nu)^{1/2}.$$

The distribution function is now introduced into Equation (10-9) by substituting dN from Equation (10-2) which results in

$$-\frac{dM_t}{dt} = A a \int_{\infty}^0 \delta^3 e^{-b\delta^q} d\delta + Ca u_r^{1/2} \int_{\infty}^0 \delta^{7/2} e^{-b\delta^q} d\delta ,$$

or

$$\frac{dM_t}{dt} = A a \int_0^{\infty} \delta^3 e^{-b\delta^q} d\delta + Ca u_r^{1/2} \int_0^{\infty} \delta^{7/2} e^{-b\delta^q} d\delta . \quad (10-10)$$

Both of the integrals in Equation (10-10) can be reduced to the form

$$\Gamma(n) = \int_0^{\infty} \xi^{(n-1)} e^{-\xi} d\xi$$

where $\Gamma(n)$ is the standard gamma function whose properties are described elsewhere⁽¹⁰⁻⁸⁾. By substituting $\xi = b\delta^q$, these integrals reduce to the incomplete gamma functions. That is

$$\int_0^{\infty} \xi^{(4/q-1)} e^{-\xi} d\xi = \frac{\Gamma(4/q)}{qb^{4/q}}$$

$$\int_0^{\infty} \xi^{(9/2q-1)} e^{-\xi} d\xi = \frac{\Gamma(9/2q)}{qb^{(9/2q)}} . \quad (10-11)$$

Substituting Equation (10-11) into (10-10) gives the mass evaporation rate as

$$\frac{dM_t}{dt} = A a \left[\frac{\Gamma(4/q)}{qb^{4/q}} \right] + Ca u_r^{1/2} \left[\frac{\Gamma(9/2q)}{qb^{(9/2q)}} \right] . \quad (10-12)$$

The constant a in Equation (10-12) may be evaluated by integrating the distribution function as given in Equation (10-2). That is

$$N = -a \int_0^{\infty} \delta^2 e^{-b\delta^q} d\delta = -a \left(\frac{\Gamma(3/q)}{qb^{(3/q)}} \right)$$

or

$$a = - \frac{N q b^{3/q}}{\Gamma(3/q)} . \quad (10-13)$$

Eliminating a between Equations (10-12) and (10-13) gives

$$-\frac{dM_t}{dt} = A N \frac{\Gamma(4/q)}{b^{1/q} \Gamma(3/q)} + C N (u_r)^{1/2} \frac{\Gamma(9/2q)}{b^{(3/2q)} \Gamma(3/q)} . \quad (10-14)$$

Equation (10-14) can, at least in principle, be solved for the mass rate of evaporation providing A , C , and N are constant and, in addition, if b and q are known functions of the time. However, there is no theoretical means of arriving at values for b and q , nor is there a sufficiency of evaporation data from which the time dependent variations of b and q may be determined. Carrier⁽¹⁰⁻⁹⁾

has, in fact, pointed out that the form of distribution functions may not be preserved in time during spray evaporation; this analysis is presented in Chapter 4⁽⁴⁻⁹⁷⁾.

It should again be recalled that in the application of the Frössling equation to spray evaporation, it is assumed that u_r is a constant. York⁽¹⁰⁻¹⁰⁾ has pointed out that it is fairly certain that a distribution of the velocities exists among drops in a real spray. Whether or not this velocity distribution arises during spray formation is not evident. However, if it is recalled that the drag coefficient is related to the drop diameter through Reynolds number, it would seem that there is a reasonable possibility that a velocity distribution could develop after spray formation. Furthermore, it would seem probable that the existence of a marked spread in spray-droplet velocities would greatly influence the results which might be calculated from Equation (10-14).

Fledderman has pointed out that Equation (10-14) is much too complicated in form to be checked by the existing limited experimental data. Since neither theoretical considerations nor experimental data are available for evaluation \bar{b} and \bar{q} as functions of the time, Equation (10-14) may be conveniently put in the form

$$-\frac{dM_t}{dt} = \text{constant } \bar{\delta} + \text{constant } u_r^{1/2} \bar{\delta}^{3/2} \quad , \quad (10-15)$$

where

$$\left. \begin{aligned} \frac{\Gamma(4/q)}{b^{1/q} \Gamma(3/q)} &= c_0 \bar{\delta} \\ \frac{\Gamma(9/2q)}{b^{3/2q} \Gamma(3/q)} &= (c_0 \bar{\delta})^{3/2} \end{aligned} \right\} \quad \text{and} \quad (10-16)$$

where c_0 is a constant.

Since

$$b^{-1/q} \left[\frac{\Gamma(9/2q)}{\Gamma(3/q)} \right]^{2/3} = c_0 \bar{\delta} \quad ,$$

then

$$\frac{\Gamma(4/q)}{\Gamma(3/q)} = \left[\frac{\Gamma(9/2q)}{\Gamma(3/q)} \right]^{2/3} \quad (10-17)$$

Graphical examination of Equation (10-17) shows that this relation is not generally valid for arbitrary values of q . This is, however, a satisfactory approximation for the moderately wide range of q which is of interest in this treatment. Fledderman has also shown that at experimentally determined values of q of 1.0 and 0.5, Equation (10-17) is in error by respectively 6.2 and 12.5 per cent; thus the validity of Equation (10-17) decreases with increasing values of q .

If it is assumed that Equation (10-15) holds approximately for any value of x , then

$$-\frac{dM}{dt} = c_0 N \left[A \bar{\delta} + C u_r^{1/2} C_0^{1/2} \bar{\delta}^{3/2} \right] \quad (10-18)$$

THE MEAN SPRAY-VELOCITY APPROXIMATION

Fledderman points out that it is preferable to determine u_r as a function of time from experimental data. However, in the absence of such data, it is necessary to resort to the concept of a mean spray velocity corresponding to \bar{m} , the mass of the mean drop which is characteristic of the spray. If m_i is the initial mass of this drop, then from

$$\mu = \frac{m_i - m}{m_i} = 1 - \frac{m}{m_i} \quad ,$$

$$\frac{d\mu}{dx} = \frac{1}{m_i} \frac{dm}{dx} \quad ,$$

and, since

$$\frac{dm}{dt} = \frac{dm}{dx} \cdot \frac{dx}{dt} = u_d \frac{dm}{dx} \quad ,$$

where u_d is the relative velocity of the drop, it follows that

$$\frac{dm}{dt} = - m_i u_d \frac{d\mu}{dx} \quad . \quad (10-19)$$

The Frössling equation for the mean drop may now be written as

$$m_i u_d \left(\frac{d\mu}{dx} \right) = \frac{2\pi DMP}{RT} \left[1 + 0.276(Sc)^{1/3} (Re)^{1/2} \right] \bar{\delta} \quad . \quad (10-20)$$

By introducing Equation (10-19) into Equation (10-20), and by using

$$Re = (U - u_d) \bar{\delta} / \nu$$

as a mean Reynolds number where U is the stream velocity, there results, on squaring,

$$A_1 u_d^2 + B_1 u_d + C_1 = 0 \quad , \quad (10-21)$$

a quadratic expressing u_d , the mean spray velocity, whose constants are given by

$$\left. \begin{aligned} A_1 &= \frac{13.1}{(Sc)^{2/3}} \left[m_i \frac{d\mu}{dx} \frac{RT}{2\pi DMP} \left(\frac{1}{\bar{\delta}} \right) \right]^2 \\ B_1 &= \frac{26.2}{(Sc)^{2/3}} \left[m_i \frac{d\mu}{dx} \frac{RT}{2\pi DMP} \left(\frac{1}{\bar{\delta}} \right) \right] - \frac{\bar{\delta}}{\nu} \\ C_1 &= \frac{13.1}{(Sc)^{2/3}} - \frac{U\bar{\delta}}{\nu} \end{aligned} \right\} \quad (10-22)$$

A further discussion of these equations will be given later in this chapter in connection with experimental data on evaporation.

A second theory of spray evaporation has been developed by Probert(10-11), using the Rosin-Rammler law of drop-size distribution. In this development, emphasis is placed upon the effect of size distribution on the evaporation of single-droplet rather than on the mechanism of the moving-droplet evaporation rate used in Fledderman's theory. Probert states that his theory is valid only for the evaporation of small drops of relatively low vapor-pressure liquids. This development is as follows:

As was pointed out above, the Rosin-Rammler equation is satisfactory for describing the size consist of oil sprays produced by atomization. This may be written as

$$R = e^{- (\delta/\bar{x})^n} \quad , \quad (10-23)$$

where R is the weight or volume fraction of the spray composed of drops where diameters are greater than δ , \bar{x} is a constant called the size consist, and n is a constant called the distribution constant. The constants \bar{x} and n completely define the spray and are characteristic of both the atomizer and the liquid being atomized.

If R in Equation (10-23) is measured in volumetric units, then the volume fraction of the injected spray in which the drops may be taken as having a diameter δ is

$$dR = - n \frac{\delta^{(n-1)}}{\bar{x}^n} e^{-(\delta/\bar{x})^n} d(\delta) \quad . \quad (10-24)$$

By assuming that the volumetric rate of injection is V , then the number of drops per unit volume injected and of size δ is

$$\frac{dR}{(\pi/6)\delta^3} = \frac{6}{\pi} (-n) \frac{\delta^{(n-4)}}{\bar{x}^n} e^{-(\delta/\bar{x})^n} d(\delta) \quad , \quad (10-25)$$

and the number of drops of size δ injected per second is

$$\frac{6}{\pi} (-n) \frac{\delta^{(n-4)}}{\bar{x}^n} e^{-(\delta/\bar{x})^n} V d\delta \quad . \quad (10-26)$$

It has already been established that the rate of evaporation of a single drop is proportional to its diameter (see Chapter 7), or

$$\frac{d}{dt} (\delta_t^3) = - K\delta_t \quad , \quad (10-27)$$

where δ_t is the diameter at time t , and K is a constant which depends upon the nature of the liquid being evaporated and upon its surroundings. Then Equation (10-27) may be written

$$3\delta_t d\delta_t = - Kdt$$

or upon integrating over the limits δ_0 to δ_t ,

$$\delta_t^2 - \delta_0^2 = - 2/3 Kt$$

or simply

$$\delta_t = \sqrt{\delta_0^2 - \lambda t} \quad (10-28)$$

where λ will be called the evaporation constant. Thus, after t seconds, a drop of diameter δ will have decreased to $\sqrt{\delta^2 - \lambda t}$ and the volume of each drop is then $(\pi/6)(\delta^2 - \lambda t)^{3/2}$.

By combining Equations (10-28) and (10-26), the volume of the drops having an initial diameter δ is now

$$(-n) \frac{\delta^{(n-4)}}{\bar{x}^n} e^{-(\delta/\bar{x})^n} (\delta^2 - \lambda t)^{3/2} V d\delta \quad .$$

If the evaporation process has taken place over a period of τ seconds, then the drops which were initially of size $\sqrt{\lambda\tau}$ are just disappearing and only drops of $\delta > \sqrt{\lambda\tau}$ contribute to the remaining spray volume. The total remaining volume is then

$$\int_{\sqrt{\lambda\tau}}^{\infty} (-n) \frac{\delta^{(n-4)}}{\bar{x}^n} (\delta^2 - \lambda\tau)^{3/2} e^{-(\delta/\bar{x})^n} V d\delta$$

or the volume fraction remaining is

$$V_f = \int_{\sqrt{\lambda\tau}}^{\infty} (-n) \frac{\delta^{(n-4)}}{\bar{x}^n} (\delta^2 - \lambda\tau)^{3/2} e^{-(\delta/\bar{x})^n} d\delta \quad (10-29)$$

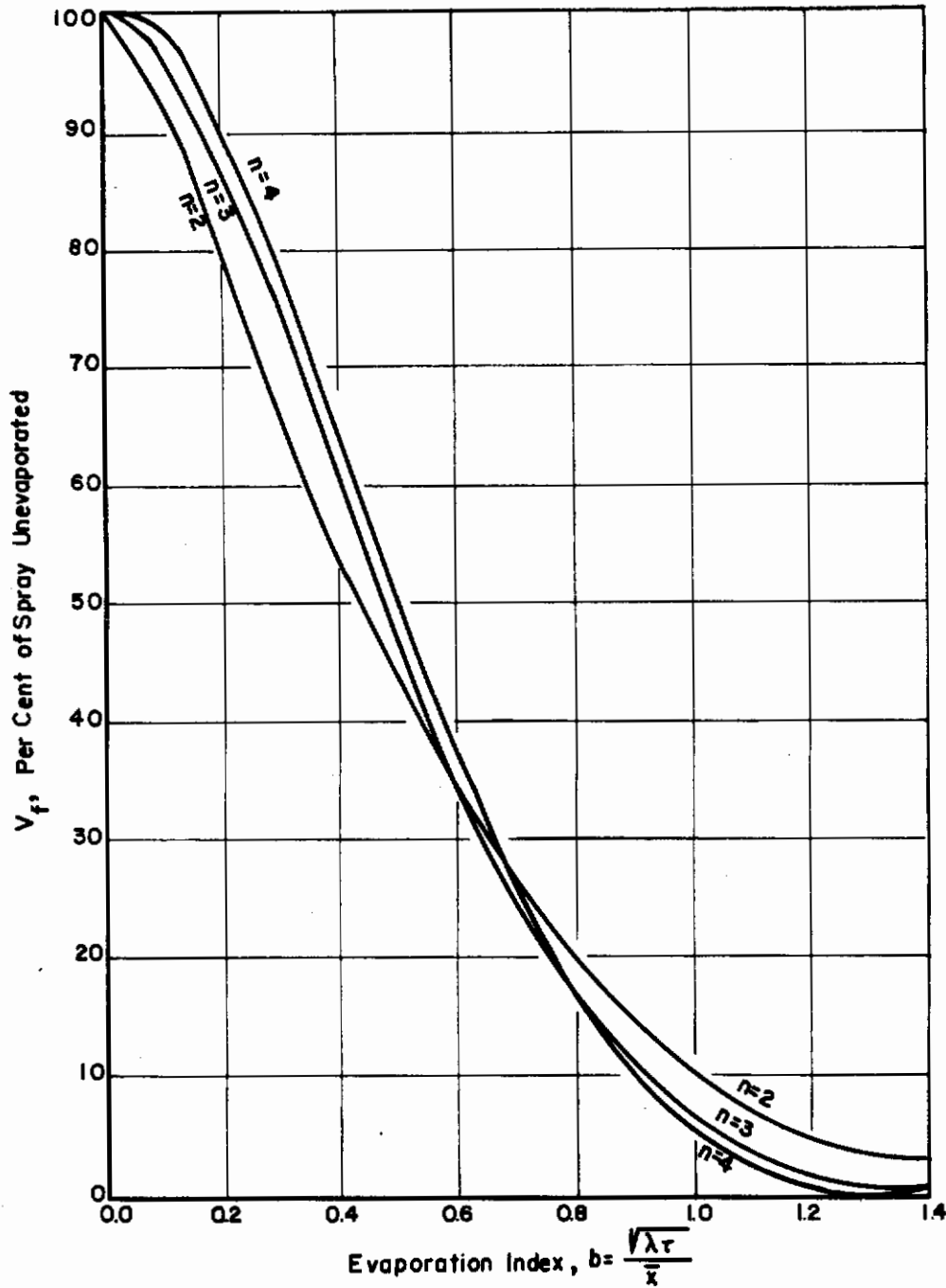


FIGURE 10-1. PER CENT OF SPRAY UNEVAPORATED AS A FUNCTION OF EVAPORATION INDEX (Probert)¹⁰⁻¹¹

Unfortunately, Equation (10-29) cannot be integrated in terms of elementary functions nor can a satisfactory series expansion solution be made. However, by transforming the variables of integration by the substitution of $\delta/\bar{x} = b \sec \theta$, where $b = \sqrt{\lambda\tau/\bar{x}}$, Equation (10-29) may be reduced to

$$V_f = 3 \int_0^{\pi/2} e^{-(b \sec \theta)^n} \sin^2 \theta \cos \theta \, d\theta \quad (10-30)$$

Probert has numerically integrated this expression, and the results are shown in Figure 10-1 as a plot of V_f against b for $n = 2, 3, 4$. He states that this particular range of n was selected because, in practice, it has been found that all atomizing nozzles give sprays having values of n lying within this range.

It is interesting to note that these curves show a fallacy which arises in connection with comparing fuels on their initial rates of evaporation upon injection. It appears that the time for evaporation of a given quantity of the liquid is more sensitive to changes in δ than to changes in n . On the other hand, the distribution constant, n , does show its effect in the way it markedly influences the time necessary to evaporate the last few per cent of the spray. A small mean-drop diameter corresponds to a small value of n which, in turn, is reflected in a high initial rate of evaporation. However, after the evaporation of about 75 per cent of the liquid, the effect of n becomes inverted and the rate of evaporation becomes small for large values of n . Probert concludes that for rapid evaporation, \bar{x} should be as small as possible, and n correspondingly large. This would appear to be so, even though a large n means a slower initial rate.

It should be pointed out that Probert's model for an evaporating spray is static in that no variables connecting drop motion with evaporation are included in the equations which are presented. In the static system described by Probert, it would seem that the individual drop evaporation rate would be influenced to some extent by its surrounding neighbors which are also undergoing evaporation. Fuchs⁽¹⁰⁻¹²⁾ has considered the importance of this influence in the development of his equations for the evaporation of a single drop in a fuel spray under static conditions. In spite of the fact that a completely rigorous solution for the single-drop case is not possible, it can be shown, in dispersions containing a small weight per cent of droplets, that the single-drop equation rate is given by Equation (8-51) which was presented in Chapter 8.

TURBULENCE AND SPRAY EVAPORATION

A comparison of the static and dynamic cases of droplet evaporation shows that in the latter instance there is a strong dependence upon u_r , the relative velocity of the drop in the airstream. Fleddermann⁽¹⁰⁻¹³⁾ has given some attention to the problem of determining the influence of u_r upon the evaporation rates of sprays under conditions of turbulent flow; his rate equations, in their present state of development, seem generally valid for the evaporation of moving sprays, but are not useful for computational purposes because they are a set of nonintegrable equations.

The volume rate of spray evaporation can be written as

$$\frac{dV}{dt} = - \sum_{i=1}^N \Xi(T) \delta_i (1 + \xi \delta_i^{1/2} u_{r_i}^{1/2}) \quad (10-31)$$

for an ensemble of N drops having diameter classes specified by δ_i . The variable Ξ is taken as an evaporation coefficient which is dependent upon the scale and nature of the turbulence present in the stream. Equation (10-31) cannot be integrated in its present form because the time dependent variation of u_{r_i} is not known; that is, as $t \rightarrow \infty$, $u_{r_i} \rightarrow 0$. To date, there is no definite data from which either the distribution or the decay forms of u_{r_i} may be determined. An approximate solution can, however, be made under the assumption that all u_{r_i} are equal and that they decay at equal rates.

If the evaporation process is taking place in a turbulent air stream, then there are localized fluctuating velocities, u_j , superposed upon the free-stream velocity \underline{U} . A complete discussion of the mathematical aspects of velocity component correlations is presented in Chapter 12 and will not be treated in detail in this discussion. It will first be considered how Equation (10-31) is influenced by the turbulent-velocity fluctuations u_1 , u_2 , and u_3 , where u_1 lies in the direction of \underline{U} , and u_2 and u_3 lie in the direction of \underline{y} and \underline{z} axes of the stream. The instantaneous relative velocity of the drop, u_r , is given by

$$u_r = \left\{ (U + u_1 - u_d)^2 + u_2^2 + u_3^2 \right\}^{1/2} \quad (10-32)$$

where u_d , the drop velocity, lies in the same direction as \underline{U} . Equation (10-32) may be conveniently written as

$$u_r = (U - u_d + u_1) \left[1 + \frac{u_2^2 + u_3^2}{(U - u_d + u_1)^2} \right]^{1/2} \quad (10-33)$$

If the values of the fluctuations u_j are restricted to values such that

$$u_j < 0.2 (U - u_d) \quad , \quad (10-34)$$

then the square root term in Equation (10-33) will be positive and approximately unity. Under this assumption, the square root term, designated u_{23}^2 , can, for the present, be neglected, then

$$u_r = \bar{u}_r + u_1 \quad (10-35)$$

where \bar{u}_r is the average relative velocity.

The mean evaporation rate for the spray can now be written as

$$\frac{\overline{dV}}{dt} = - \sum_{i=1}^N \Xi(T) \delta_i \left[1 + \xi \delta_i^{1/2} \frac{1}{(\bar{u}_{r_i} + u_1)} \right]^{1/2} \quad (10-36)$$

where $\Xi(T)$ is the turbulent evaporation coefficient containing turbulent transport quantities. From theoretical considerations, Taylor⁽¹⁰⁻¹⁴⁾ has shown that the diffusion coefficient, under turbulent flow conditions, is the sum of the laminar diffusion coefficient and of a turbulent coefficient which is proportional to

$$(u')^2 = (\bar{u}_1^2 + \bar{u}_2^2 + \bar{u}_3^2)$$

Schubauer⁽¹⁰⁻¹⁵⁾ has also verified this relation experimentally. For normally encountered ranges of u' , the turbulent coefficient is predominant and $\Xi(T)$ should approximately be proportional to u' and also should be larger than the corresponding laminar coefficient. The mean evaporation rate for the spray should then be proportional to u' , or

$$\frac{\overline{dV}}{dt} = - \sum_{i=1}^N \Xi(T) \delta_i \left[1 + \xi \delta_i^{1/2} \bar{u}_{r_i}^{1/2} \left\{ 1 + \frac{1}{2} \frac{(u')}{\bar{u}_{r_i}} - \frac{1}{8} \frac{(u')^2}{\bar{u}_{r_i}^2} + \frac{3}{48} \frac{(u')^3}{\bar{u}_{r_i}^3} \dots \right\} \right] \quad (10-37)$$

since for the particular case $(u')^2 = \bar{u}_1^2$. Fledderman states that this equation would appear to define the mean rate of evaporation at the time of injection because \bar{u}_{r_i} is initially of large magnitude. As the spray traverses downstream, \bar{u}_{r_i} will generally tend to decrease while u' will either increase or decrease, depending upon the character of the flow.

It would also seem probable that at some point in the stream

$$u' \approx \bar{u}_{r_i}$$

and consequently u_{23_i} would become an appreciable factor in determining the average rate of evaporation. Thus, the possibility that the fluctuations of u' may be sufficiently negative to cause

$$u_{r_i} = \bar{u}_{r_i} + u_1 \quad (10-38)$$

to become also negative, leads to the necessity of writing

$$|\bar{u}_{r_i} + u_1|$$

in order that \bar{u}_{r_i} be positive always. These considerations lead, finally, to an evaporation equation of the form

$$\frac{d\bar{V}}{dt} = - \sum_{i=1}^N \Xi(T) \delta_i \left[1 + \xi \delta_i^{1/2} \frac{1}{(u_{23_i} |\bar{u}_{r_i} + u_1|)^{1/2}} \right] \quad (10-39)$$

It can be concluded that the primary effect of turbulence upon spray evaporation will be upon $\Xi(T)$. The preceding discussion is, of course, based upon $u_r^{1/2}$ being a factor in Re , and, under the assumption that

$$u_1, u_2, u_3, \ll (U - u_d) \quad ,$$

the effect of turbulence through Re will be negligibly small.

If Equation (10-39) is to be used in calculating the rate of evaporation of a spray moving under laminar flow conditions, the distribution of δ_i and u_{r_i} , as well as the decay law for u_{r_i} , must be known. In a turbulent field, a necessary additional requirement is a knowledge of the magnitude of

$$|\bar{u}_{r_i} + u_1|$$

This latter quantity requires the distribution of u' over the turbulent field as well as the fluctuations of u' .

Even if the above data for completely specifying the turbulent field were available, it is probable that Equation (10-39) could not be integrated to yield an analytical result. Either a justifiable simplification of the equation or the use of numerical techniques would seem to be the only practical approach to calculating average evaporation rates under turbulent flow conditions.

MASS AND HEAT BALANCE IN DYNAMIC- SPRAY EVAPORATION

No completely adequate treatment of the detailed heat and mass balance in a dynamic spray has been developed to date. It may be inferred from the previous section that the transport quantities which enter into $\Xi(T)$, for the turbulent case of evaporation, would be extremely difficult to determine by either theory or experiment. Even for the case of spray evaporation under laminar flow conditions, it has not been possible to specify completely heat and mass balance by other than approximate equations which utilize average values for the necessary parameters. In setting up approximate heat-and-mass-transfer balances, the equations for the corresponding transport quantities in the single moving droplet case are utilized.

Johnstone and co-workers⁽¹⁰⁻¹⁶⁾ have treated the related problem of heat transfer from a cylindrical wall to a cloud of free-falling particles in connection with designing "flash" heating units for finely divided solids. While heat transfer by convection, conduction, and radiation are discussed in this treatment, no consideration is given to mass transfer. In order to solve the Fourier-Poisson equation for an "average" heat-transfer coefficient, it was assumed that the axial velocity of the particle is such that all of the streamlines of constant flow are parallel to the surface of the spherical particle. The forms of the resulting velocity components are comparable with those given by Prandtl⁽¹⁰⁻¹⁷⁾ for both potential and viscous flow about a sphere. The resulting expressions give an average heat-transfer coefficient which is free of the usual Peclet number limitation ($Pe > 13,000$) associated with ideal flow conditions.

This heat-transfer problem has also been studied by Drew⁽¹⁰⁻¹⁸⁾, by Levêque⁽¹⁰⁻¹⁹⁾, and Boussinesq⁽¹⁰⁻²⁰⁾. In the latter treatment of the problem, the flow was assumed to be irrotational and expressible as a potential function. Under these conditions, a solution to the Fourier-Poisson equation for moving spheres is possible only if certain terms in the general solution can be neglected. Ignoring these terms is only justified for $Pe > 13,000$. It would therefore seem that the Boussinesq analysis would be of little value in predicting heat transfer to dynamic-spray systems. On the other hand, the Johnstone analysis should be applicable to the case where a low-volatility spray undergoes heating during the pre-evaporation period (see Chapter 5) where no mass transfer occurs.

The absorption of radiant energy by clouds of moving particles has been the subject of numerous investigations. Haslam and Hottel⁽¹⁰⁻²¹⁾ have shown that the geometry of the radiant surface enclosing the particle is an important consideration in the calculation of total radiation absorption. Also, Jakob⁽¹⁰⁻²²⁾ and Nusselt⁽¹⁰⁻²³⁾ have independently arrived at mathematically identical equations for the absorptivity of gases. All of these analyses lead to the same expression for cloud absorptivity E_c .

The coefficient of radiant heat transfer, h_r , can now be calculated from the wall and particle temperatures, which are respectively T_w and T_p . This is

$$h_r = \frac{0.172 E_c}{\sigma} \frac{\left[\left(\frac{T_w}{100} \right)^4 - \left(\frac{T_p}{100} \right)^4 \right]}{(T_w - T_p)} \quad (10-40)$$

where σ is the ratio of particle area to wall area.

On the basis of the similarity between the heat- and mass-transfer process, a mass-transfer coefficient, k_g , can be deduced from the form of the heat-transfer coefficient, h_g . However, all of these results which are based upon the Frössling equation for single drops have been applied to spray evaporation by assuming an average uniform droplet diameter.

Fledderman has calculated both heat- and mass-transfer coefficients for sprays of n-hexane in air at a stream velocity of 50 ft/sec using extrapolated values of μ , $\bar{\delta}$, and Re obtained from his experimental data.

Table 10-1 shows values of k_g and h_g calculated from the correlation of Frössling⁽¹⁰⁻⁷⁾, McAdams⁽¹⁰⁻²⁴⁾, and of Kramers⁽¹⁰⁻²⁵⁾. Although there is considerable disagreement among the values for k_g and h_g , all pairs of values lead to fairly consistent results for the average drop temperature. Thus, it may be concluded from a graph of average drop temperature against the upstream distance from the spray nozzle, that

$$A = 2\pi Mp/RT$$

is essentially a constant in Equation (19-4), since the average drop temperature rapidly approaches the wet-bulb temperature condition for the moving stream.

Correlation	$k_g, (\text{lb mol})/(\text{hr})(\text{ft}^2)(\text{atm})$	$h_g, \text{Btu}/(\text{hr})(\text{ft}^2)(^\circ\text{R})$
Frössling	18.7	272
McAdams	15.8	230
Kramers	24.0	349

It should be clearly seen that this analysis is not applicable to the calculation of heat and mass transfer in the cases of large concentration and thermal gradients between the stream and the spray particles. It has already been stated by Ranz(10-26) that, under these conditions, the Frössling correlation for mass and heat transfer must be modified in accordance with the diffusion equations of Colburn and Pigford(10-27).

In Chapter 8, there was some discussion of the heat- and mass-transfer equation derived by Ingebo(10-28). These equations were found to be valid for the evaporation of fluid spheres of high volatility under large thermal gradients. It should be possible to repeat Fledderman's analysis under the assumption that an averaged Ingebo correlation would best express spray evaporation under conditions of high concentrations and thermal gradients. Since no experimental data, such as Fledderman's, have been obtained on the evaporation of sprays at high temperatures, it would be necessary to make such additional observations before any new equation could be verified.

THE EFFECT OF A CYLINDRICAL DUCT UPON
SPRAY EVAPORATION

In the case where a spray is injected into a cylindrical duct or combustion chamber, the wall of this enclosure can act as a sink for droplets in that it will be wetted by the spray. Also, spray deposited will tend to evaporate under the influence of both the wall temperature and stream flow near the wall.

The problem of spray deposition on the wall of a cylindrical duct has been treated by Alexander and Coldren(10-29) under the assumption that the droplets behave statistically like gas molecules and undergo radial diffusion to the wall. If the stream velocity, U , is radially uniform, then the diffusion equation governing this transport is

$$\left(\frac{\partial C}{\partial t}\right)_r = \alpha \left(\frac{1}{r} \frac{\partial C}{\partial r} + \frac{\partial^2 C}{\partial r^2}\right) \quad (10-41)$$

where α is the diffusivity of the spray, and C is the concentration of liquid particles in the gas phase. The left-hand side of this expression represents the mass transport of drops across a cylindrical surface. The volume element is considered as moving with the air stream in the x-direction of flow; the axial diffusion of drops from the ends of the moving element is neglected. The general solution to Equation (10-41) is

$$C = \sum_1^{\infty} A_n e^{-a_n^2 \alpha t} J_0(a_n r) \quad (10-42)$$

If the wall is taken as a sink for droplets, then $C = 0$ at $r = D/2$, where D is the diameter of drop. From this boundary condition and Equation (10-42), evidently, $J_0(a_n D/2) = 0$ determines the values of successive a_n .

The mass of suspended droplets remaining in the moving element is

$$m = 2\pi U \int_0^{D/a} C(r, t) r dr \quad (10-43)$$

Substituting Equation (10-42) into Equation (10-43) gives, upon integration,

$$m = \pi U D \sum_1^{\infty} A_n e^{-a_n^2 \alpha t} J_1(a_n D/2) \quad (10-44)$$

By neglecting higher terms in this summation and by differentiating with respect to t , there results

$$\frac{dm}{dt} = -\pi U D A_1 a_1^2 \alpha e^{-(a_1^2 \alpha t)} J_1\left(\frac{a_1 D}{2}\right) \quad (10-45)$$

or by combining Equations (10-44) and (10-45) the rate is

$$\frac{dm}{dt} = -a_1^2 \alpha m \quad (10-46)$$

Since $t = x/U$, then dm/dt may be expressed as $U dm/dx$ and Equation (10-46) may be written as

$$\frac{d \ln(m/m_0)}{dx} = -\frac{a_1^2 \alpha}{U} \quad (10-47)$$

where m_0 is the mass rate of spray injection. Thus, if Equation (10-47) is valid, a plot of the logarithm of the mass fraction of the liquid remaining in the spray against the downstream distance from the nozzle, x , should be a linear relation having a slope given by $-(a_1^2 \alpha)/U$.

Alexander and Coldren found this linear relation to be valid for expressing wall wetting at reasonable distances downstream from the point of injection. In a series of experiments in which water drops were injected into a cylindrical duct under turbulent flow conditions, the percentage of undeposited spray was measured by collection at a number of axial positions in the test section of the duct. It was found that the rate of water injection had little effect upon the deposition of the spray.

Figure 10-2 shows the experimental results of Alexander and Coldren plotted in accordance with Equation (10-47) for five different air velocities; no specific values for these velocities are given in the original work excepting for the curve marked 263 fps. However, it may be seen that the slopes of the straight-line portions of these curves tend to decrease with increasing air velocity. The departure from linearity at the upstream portions of each curve is attributed to neglecting the higher terms in the summation which is given by Equation (10-44). A second departure from linearity for the velocity $U = 263$ fps at $x = 70-90$ cm has not been explained, in spite of the fact that this is stated to be a reproducible effect.

The following equation for the spray diffusivity of water droplets was obtained from the slopes of curves given in Figure 10-2:

$$\alpha = 0.77 U^{0.6}$$

It is interesting to note that α can be calculated by using the entire curve shown in Figure 10-2. This, however, requires that $C = f(r)$ be known for $t = 0$, since A_n in Equation (10-42) would require evaluation. Calculated values for α , in the case of water sprays, range from 20 to 30 in.²/sec.

Longwell and Weiss⁽¹⁰⁻³⁰⁾ have also made studies of the effect of a cylindrical duct upon the mixing and distribution of liquids in high-velocity air streams. They have concluded that the distribution which results from injecting a liquid fuel into a high-velocity gas stream can be predicted

with good accuracy. By using the principles of turbulent diffusion, these investigators have shown that wall effects and changing duct dimensions can be accounted for by means of simple graphical techniques. The predicted distributions had a maximum error of 20 per cent (at any fuel concentration) and an average error of less than seven per cent when compared to experimentally measured distributions.

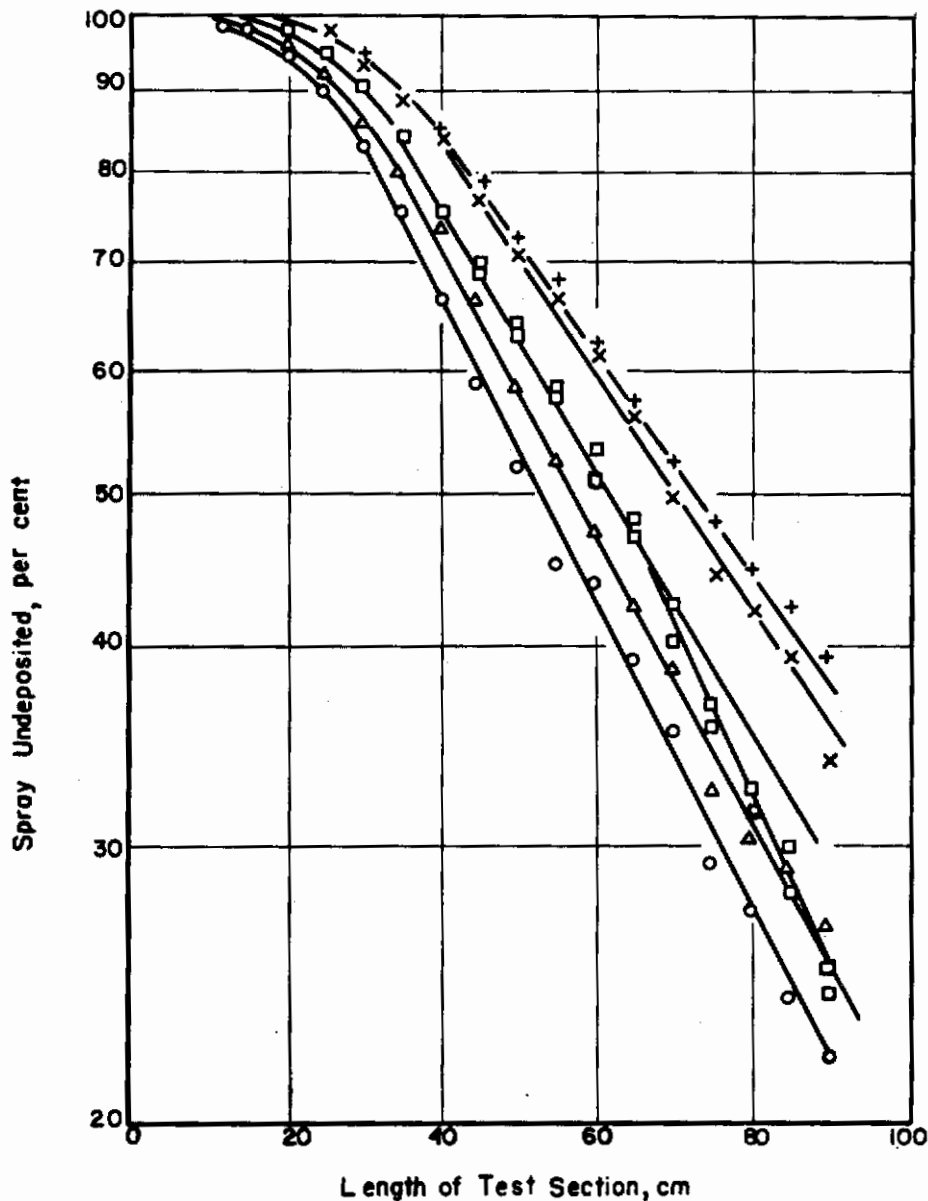


FIGURE 10-2. DEPOSITION OF SPRAY ON THE WALLS OF A STRAIGHT DUCT AT HIGH LEVELS OF TURBULENCE (Alexander and Coldren)¹⁰⁻²⁹

Sherwood and co-workers⁽¹⁰⁻³¹⁾ have made similar diffusivity measurements on carbon dioxide injected into rapidly moving air streams. The analysis of data taken close to the point of injection, where the duct would have a small effect on the divergence of the stream, showed that α varies directly with the stream velocity.

The evaporation of a continuous cylindrical liquid film into a moving gas stream, under viscous and turbulent flow conditions, has been studied by Gilliland and Sherwood(10-32). These workers collected a large volume of data on the rates of evaporation for nine different liquids of varying volatility. Each liquid was permitted to flow at a fixed rate down the internal wall of a cylindrical duct, while air was passed either countercurrently or in parallel to the direction of fluid flow. From measured evaporation rates, flow rates, and wall temperatures, a dimensionless correlation was obtained from evaporation rates in terms of the Reynolds and Schmidt numbers. The mass-transfer coefficient, K_c , was found to be

$$\frac{K_c D}{D_v} = 0.023 (Re)^{0.83} (Sc)^{0.44} \quad (10-49)$$

for $2000 \leq Re \leq 20,000$ and for pressures of from 110 to 2330 mm Hg. In Equation (10-49), D is the internal diameter of the duct, and D_v is the diffusion coefficient for the particular vapor being examined. Equation (10-49) is similar, in form, to the corresponding general heat-transfer equation which is given by McAdams(10-33). It has been suggested that, in using this correlation, some correction be made for the resistance of the moving liquid film.

Maisel and Sherwood(10-34) point out, from a more nearly theoretical treatment of mass transfer under turbulent flow conditions, that $(Sc)^{2/3}$ should be replaced by $(Sc)^{0.44}$; similar conclusions have also been reached by Chilton and Colburn(10-35). The latter workers point out, however, that the narrow range of Sc (0.60 to 2.4 in most experiments) does not permit a conclusive differentiation between these exponents.

Gilliland and Sherwood(10-32) have also considered the evaporation from a wetted cylindrical wall under viscous flow conditions, that is for $Re < 2000$. Under these conditions, mass transfer takes place presumably by a diffusion process. Solutions to the differential equation for diffusive transport are

$$\frac{P_2 - P_1}{P_w - P_1} = 1 - 4 \sum \frac{1}{a_n^2} \exp \frac{-a_n^2 D_v \rho L}{W} \quad (10-50)$$

for rodlike flow, and

$$\begin{aligned} \frac{P_2 - P_1}{P_w - P_1} = 1 - 0.10238 e \left(-14.623(\pi/4) \frac{D_v \rho L}{W} \right) \\ - 0.0122 e \left(-89.22(\pi/4) \frac{D_v \rho L}{W} \right) \end{aligned} \quad (10-51)$$

for parabolic flow. P is the partial pressure of the diffusing gas; subscripts 1 and 2 refer, respectively, to the inlet and outlet positions, while subscript w refers to the liquid-vapor boundary. The mass rate of gas flow is W , and L is the length of the cylindrical section. The coefficients a_n are the successive roots of the equation $J_n(x) = 0$.

Both Equation (10-50) and Equation (10-51) were found to be only in fair agreement with experimental data taken on the evaporation of liquids under isothermal, viscous flow. It may be seen that both the theoretical and empirical relations which are given in this section are only applicable at moderately low temperatures. Thus, their application may not be satisfactory in cases where the temperature of the wall or gas is high or, in general, under conditions of steep thermal gradients.

In situations where high wall temperatures are encountered, there will, of course, be no wetting by sprays. The wall will then act as a flash evaporator for the spray droplets. It would seem that the matter of predicting the rate of evaporation of the spray by a hot wall would be an extremely complex problem even under favorable conditions of symmetry.

EXPERIMENTAL MEASUREMENTS OF SPRAY-
EVAPORATION RATES

At the beginning of this chapter, it was pointed out that the measurement of spray evaporation in a moving gas stream is made difficult by the necessity of having a rather complete knowledge of the drop-size distribution at several points along the air stream. Since satisfactory techniques for measuring drop-size distribution have been developed only recently, little has been done in the way of experimental work on the evaporation of dynamic spray.

The earliest significant experimental work on spray evaporation is largely concerned with the ignition and combustion of liquid fuels in compression-ignition engines. Since the bulk of these investigations lead only to qualitative results, a full treatment will not be given here. Rather, some of the more important conclusions resulting from these experimental investigations will be discussed in brief.

In 1921, Wollers and Ehmcke⁽¹⁰⁻³⁶⁾ carried out vaporization studies on a variety of fuel oils in connection with their work on the diesel engine. Their tests were made by injecting a fuel spray into a preheated bomb at relatively high pressures and then determining the evaporation rates of the fuel sprays from pressure-time and pressure-temperature data. These measurements, in conjunction with ignition-point determination, lead these investigators to the conclusion that ignition in the diesel engine does not require fuel vaporization. Unfortunately, the result of this investigation was misinterpreted by a number of other investigators, who concluded that not only did vaporization have no effect on the combustion process, but that ignition started in the liquid phase. Alt⁽¹⁰⁻³⁷⁾, discussing the influence of vaporization on combustion and ignition, stated that "if vaporization were important for ignition, then the higher the ignition point above the boiling point, the better the fuel would be for compression ignition engine". This conclusion is obviously in error since, in actuality, the closer the ignition temperature of the fuel is to the boiling point, the greater becomes the ease of ignition.

Rothrock and Waldron⁽¹⁰⁻³⁸⁾ reinvestigated the problem of vaporization and its relation to combustion in the compression-ignition engine. They used high-speed cinematography as a means of measuring the variation of fuel-spray vaporization with engine speed. Two main conclusions can be drawn from their data. First, considerable vaporization of the injected fuel spray occurs between injection and combustion in a high-speed compression-ignition engine. Secondly, fuel vaporization markedly influences the rate of combustion of the fuel.

Selden and Spencer⁽¹⁰⁻³⁹⁾ investigated the evaporation of fuel-oil sprays which were produced by injecting the fuel into a bomb pressurized by an inert gas. Initial temperatures ranging from 150 to 350 C were attained by placing the bomb in a constant-temperature bath. The apparatus and measurement technique used are described in the earlier work of Cohn and Spencer⁽¹⁰⁻⁴⁰⁾. The fuel, maintained at a constant temperature, was injected into the heated bomb which had previously been pressurized with nitrogen, carbon dioxide, or air. The charged weight of fuel could be varied accurately by changing the injection pressure and the duration of the injection period (0.002 to 0.006 sec). Pressure-time traces were made by recording the movement of an optical-type differential-pressure indicator with a synchronous motor-driven drum camera.

Figure 10-3 shows five typical pressure-time traces for experiments in which an initial fuel-vapor concentration was present in the bomb prior to the injection of the fuel spray. The AB interval on each trace corresponds to an interval during which the rate of heat transfer to the spray is practically constant. It may be concluded that, in this interval, some evaporation of the fuel takes place. This follows from the fact that, if the total heat transferred to the spray merely served to cause a heating of the fuel, there would not be a decrease in pressure during the interval AB which is shown in Figure 10-3. As increasingly more fuel is injected into the same gas charge, under the condition that thermal equilibrium is established between injections, the saturation and partial pressures of the liquid fuel should gradually approach the same value. This effect is closely responsible for the apparent diminution in pressure change in the AB interval as the cumulative number of injections is increased from 1 to 23. These results also show that the fraction of the heat transferred to the fuel or to the vapor, which causes evaporation, is an appreciable part of the total heat transfer in the interval AB.

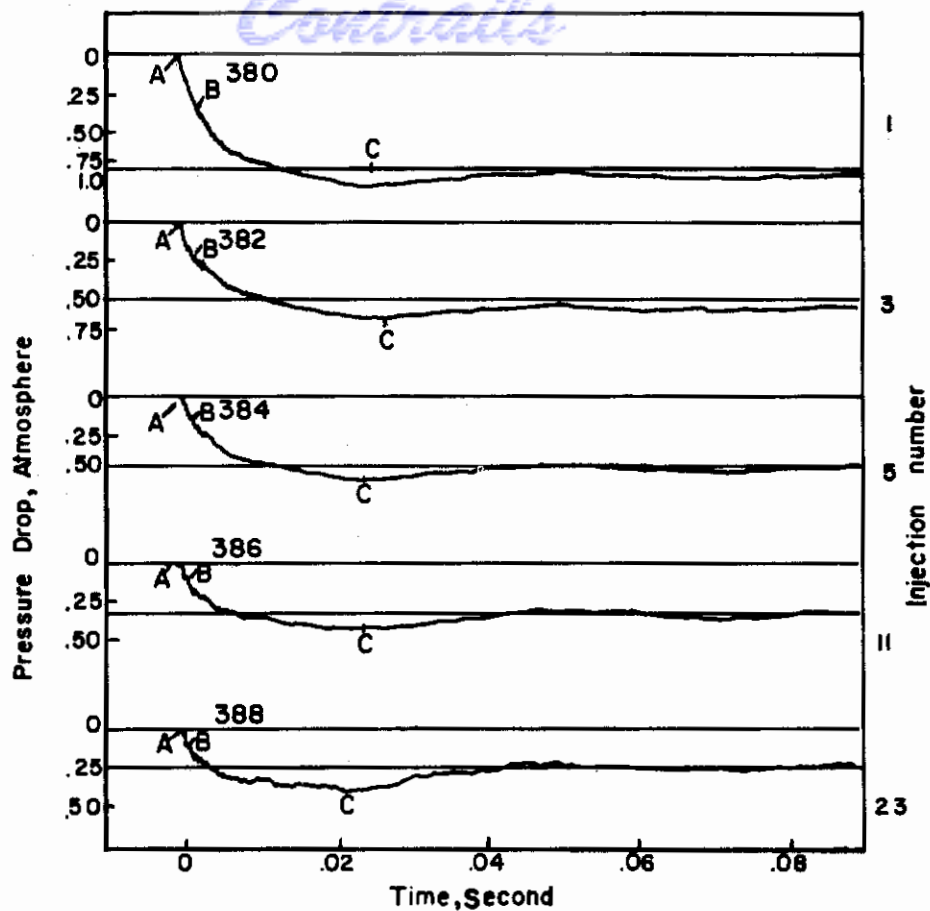


FIGURE 10-3. PHOTOGRAPHIC TRACE OF PRESSURE-TIME RELATION FOR SUCCESSIVE INJECTIONS OF OIL SPRAYS INTO A HEATED BOMB

(Selden and Spencer)¹⁰⁻³⁹

This study of the injection of the liquid fuel into a compressed gas furnished considerable data concerning the initial heat exchange between the gas and the fuel spray. Although qualitative evidence was given for the fact that the fuel vaporization takes place immediately after injection starts, no actual rates of vaporization can be obtained from this experimental data. In a discussion of their results, Selden and Spencer consider both the temperature decrease in the spray due to a Joule-Thompson effect and the heat transfer due to radiation; they conclude that neither contribution is of significant magnitude for consideration under their experimental conditions. The conclusion regarding the negligible effect of radiation on spray evaporation has also been confirmed by the experimental work of Wolfhard and Parker⁽¹⁰⁻⁴¹⁾ and by the theoretical findings of Penner and co-workers⁽¹⁰⁻⁴²⁾.

Previous work on the role of evaporation in the compression-ignition engine has not contributed significantly to the knowledge of the mechanism of spray evaporation in a moving gas stream. These investigations do, however, leave little doubt that both mass and heat transfer occur between a gas and a fuel spray in the diesel engine in accordance with the qualitative findings of Wentzel⁽¹⁰⁻⁴³⁾ and of Dreyhaupt⁽¹⁰⁻⁴⁴⁾.

The matter of liquid-fuel characteristics affecting vaporization in engines has been the subject of an experimental investigation of Gilbert and co-workers⁽¹⁰⁻⁴⁵⁾. They conclude that the quality of an air-fuel mixture is determined by (1) the air temperature, (2) the liquid-fuel temperature, (3) the air-fuel ratio, (4) the fraction of the fuel vaporized, and by (5) the total pressure for

any particular liquid fuel. Turbulence level is also considered to be an important factor since transport quantities and the degree of mixing are strongly dependent upon this parameter. All these factors which influence mixture quality are intimately related to the evaporation process and have been discussed separately in earlier parts of this section.

As a result of studying the combustion of fuel sprays, Godsave⁽¹⁰⁻⁴⁶⁾ has concluded that the evaporation of a fuel spray is controlled by two distinct rate-determining mechanisms. At relatively low temperature, the evaporation is governed by diffusion where vapor pressure is the predominant parameter, whereas, under conditions of elevated temperatures, heat-transfer rate to the spray is the most important quantity. In the latter mechanism, the dominant parameter is the quantity of heat required to raise the temperature of the fuel to the surface equilibrium temperature. Clearly, each mechanism is an extreme case, and at intermediate temperatures both will be operative to a relative extent depending upon the temperature.

EVAPORATION OF A SPRAY IN A MOVING GAS STREAM

An examination of the literature on experimental measurements of spray evaporation shows that no completely satisfactory determinations have been carried out under conditions where a liquid spray is injected into a moving gas stream. Thus, most of the equations which were discussed in the theoretical part of this chapter have not, as yet, been verified by experiment.

Streamline Flow

Fledderman⁽¹⁰⁻⁶⁾ has, however, carried out a limited number of spray-evaporation measurements on n-hexane injected into a moving air stream under both streamline and turbulent flow conditions. His measurements were neither sufficient in number nor were they carried out under a wide enough range of conditions to permit a complete examination of the theoretical considerations developed earlier.

This experimental work was confined to measuring the evaporation of a spray of n-hexane droplets at a number of axially located points in a transport-test section of a small wind tunnel. Since these measurements were carried out using ambient air at slightly above room temperature, they may not be applicable to the evaporation of a spray in a high-temperature gas stream. However, the technique and results are of sufficient interest to warrant some detailed description.

The necessary data for calculating the evaporation which had taken place in the spray during its motion through the test section was obtained by simultaneously collecting spray samples with a probe and photographing the spray at a number of positions along the section; the stream velocity was maintained constant during these measurements.

The spray was photographed under conditions of optimum illumination and magnification; the film was then developed under rigorously controlled conditions in order to obtain an average optical density of 1.9. This optimum value was determined by photographing droplets of known size to give a series of negatives, each developed to a different optical density. A graph of the ratio of measured to actual drop size against the optical density indicated a convergence to the ratio of 1.9. From such photographs, it was then possible to calculate $m(\delta)$, the mass of droplets having diameters between δ and $\delta + d\delta$ at a given position, by means of a tedious counting technique.

The total mass of the spray passing a given position in the test section was measured by means of a series of collection probes on a test rack which was positioned normal to the direction of the air flow. Since individual probes collected only a fraction of the total spray, a fictitious spray density was used in the computation of the total mass of spray. This density is defined as the ratio of the mass collected to the area of the inlet of the probe. The spray pattern was reasonably symmetrical, and spray densities lying in the same transverse plane were averaged to give the mean

spray density in the annulus whose center fell on the axis of the spray cone. The product of the annulus area by the mean density gave the mass of spray passing through the annulus during the run time. The sum of the masses passing through each annulus then gave the total mass of spray passing through a particular cross section of the test section. The mass value was then corrected for evaporation and for the collection efficiency of the probe.

The method for calculating the collection efficiency of the probe was based on the theoretical analyses of Langmuir and Blodgett⁽¹⁰⁻⁴⁷⁾. These workers developed an expression for the maximum total efficiency of deposition of fog particles on the stagnation point of a sphere. This efficiency, $\bar{\beta}_0$, is calculated from the integral

$$\bar{\beta}_0 = \int_0^{\infty} \beta_0(\delta) \frac{m(\delta)}{M} d\delta$$

where M is the total mass collected at a given position, and $m(\delta)$ is obtained, as explained earlier from photographic measurements. The function $\beta_0(\delta)$ is obtained from charts which are given in Langmuir and Blodgett's report.

Fledderman assumed that the drop diameters changed with the evaporation and calculated β_0 from the values of $m(\delta)$ corresponding to a measured spray mass of m_0 . The mean drop diameter, $\bar{\delta}_0$, corresponding to $\bar{\beta}_0$ was then obtained from the Langmuir and Blodgett chart. Thus, the mean drop diameter of the spray was taken as that diameter corresponding to the same collection efficiency for the entire spray.

It was then assumed that the whole spray was composed of droplets of a size $\bar{\delta}_0$. In this way, the change in the mass of the spray from station to station, corresponding to a diameter change from $\bar{\delta}_0$ to $\bar{\delta}$, would be given by

$$\bar{\delta} = \bar{\delta}_0 \left(\frac{M}{M_0} \right)^{1/3} \quad (10-52)$$

On the basis of this mean diameter, $\bar{\beta}_0$ was calculated for all stations by the summation

$$\bar{\beta}_0 = \sum \beta_0(\delta_i) m(S_i)$$

Figure 10-4 shows Fledderman's evaporation data plotted as μ , the spray-evaporation ratio, against x , the downstream distance for various air velocities; these data were taken under streamline flow conditions. Values of $(d\mu/dx)$, $\bar{\delta}$, and m_1 were next obtained from Figure 10-4 in conjunction with Equation (10-52). These data were used to calculate u_d , the mean spray velocity, as a function of the downstream distance x , from Equation (10-21). In making these calculations, the quantities ν , Sc , and $RT/2\pi DM_p$ were assumed to be of constant value over the range of x in which the measurements were made.

Figure 10-5 shows the change in the mean spray velocity, u_d , as a function of x for three stream velocities. From the values of u_d , Fledderman also calculated both the average drag coefficient of the spray and the magnitude of the hexane-vapor velocity taken in a direction normal to the air stream. Since these subjects are connected with cloud ballistics, they are not discussed here.

Turbulent Flow

Fledderman⁽¹⁰⁻⁶⁾ also has carried out a series of experiments on the evaporation of n-hexane sprays under varying intensities of stream turbulence. The techniques used in the measurements of evaporation were identical with those described under the streamline flow experiments.

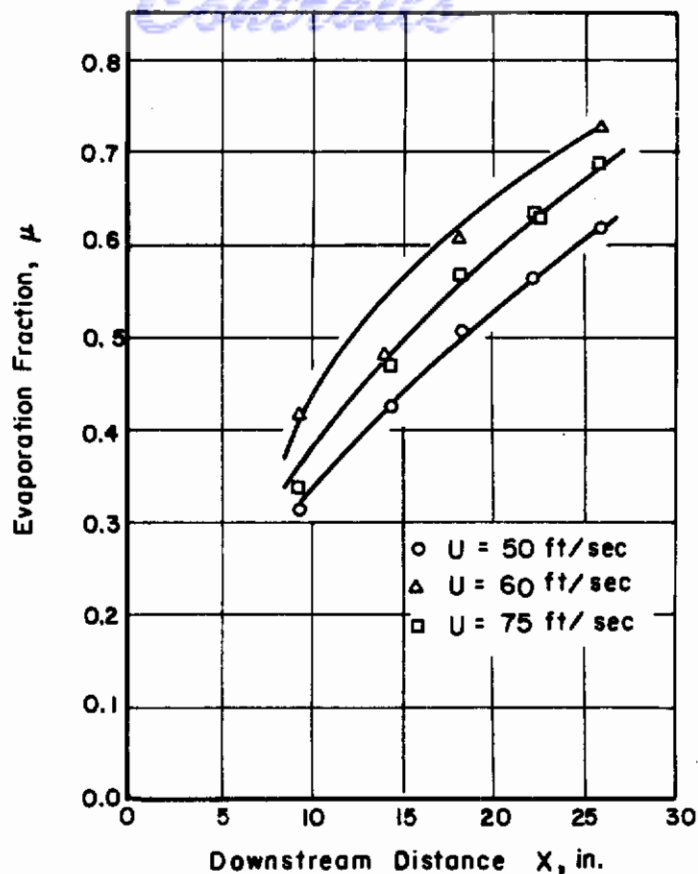


FIGURE 10-4. EVAPORATION FRACTION AS A FUNCTION OF DOWNSTREAM DISTANCE AT VARIOUS STREAM VELOCITIES

(Fledderman and Hanson)¹⁰⁻⁶

In the course of these experiments, varying degrees of turbulence were produced by placing wire screens of different mesh openings in the upstream entrance to the test section. Evaporation measurements were made under five different turbulence fields. The effect of turbulence upon the total evaporation was expressed as a comparison of μ values at various turbulence numbers, σ ; the latter quantities were calculated from the expression

$$\sigma = \frac{100 \sqrt{u^2}}{U}$$

by assuming isotropic turbulence conditions. The fluctuating velocity component, U , was measured at points along the test section by means of a Bureau of Standards hot-wire anemometer⁽¹⁰⁻⁴⁸⁾.

Figure 10-6 shows the variation in the evaporation coefficient, u , with downstream distance in the test section at five different levels of turbulence. These data were obtained at $U = 50$ fps and at an ambient air temperature of 20 C. Because σ varies with x , it was not convenient to show the quantitative effect of turbulence in this plot. However, these curves show generally that μ increases with increasing σ , since the level of turbulence increases for any x from the lower to the upper curve shown.

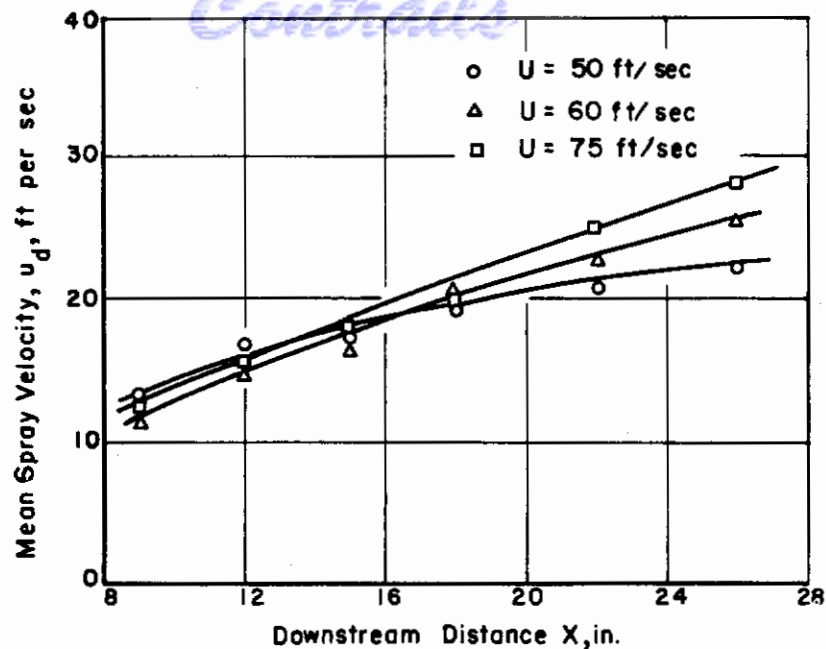


FIGURE 10-5. MEAN SPRAY VELOCITY AS A FUNCTION OF DOWNSTREAM DISTANCE

(Fledderman and Hanson)¹⁰⁻⁶

Table 10-2 shows more clearly the quantitative relation of σ and μ for $x = 12$ in. and $U = 50$ fps. The data indicate, as does Figure 10-6, that the trend is for μ to increase with increasing σ . Also, it would appear that a decrease in L , the scale of turbulence, (see Chapter 12 for definition) produces an increase in evaporation. It would, however, seem hazardous to make this conclusive in light of the relatively large scatter in Fledderman's experimental data and also because μ is actually an integrated evaporation coefficient measured from the injection point to some value of x . The effect of turbulence number upon evaporation would seem to indicate turbulence tends to affect the diffusion coefficient rather than to operate through the Reynolds number.

TABLE 10-2

Screen	Turbulence Scale, L , in.	Turbulence Number, σ , per cent	μ
2.5 mesh + streamers	0.107	6.67	0.496
2 mesh, 0.148-in. wire	0.079	2.55	0.474
None	0.103	0.34	0.395

It is evident that much more work is necessary on the subject of single-droplet evaporation under turbulent conditions before any firm conclusions can be drawn regarding the evaporation of turbulent sprays.

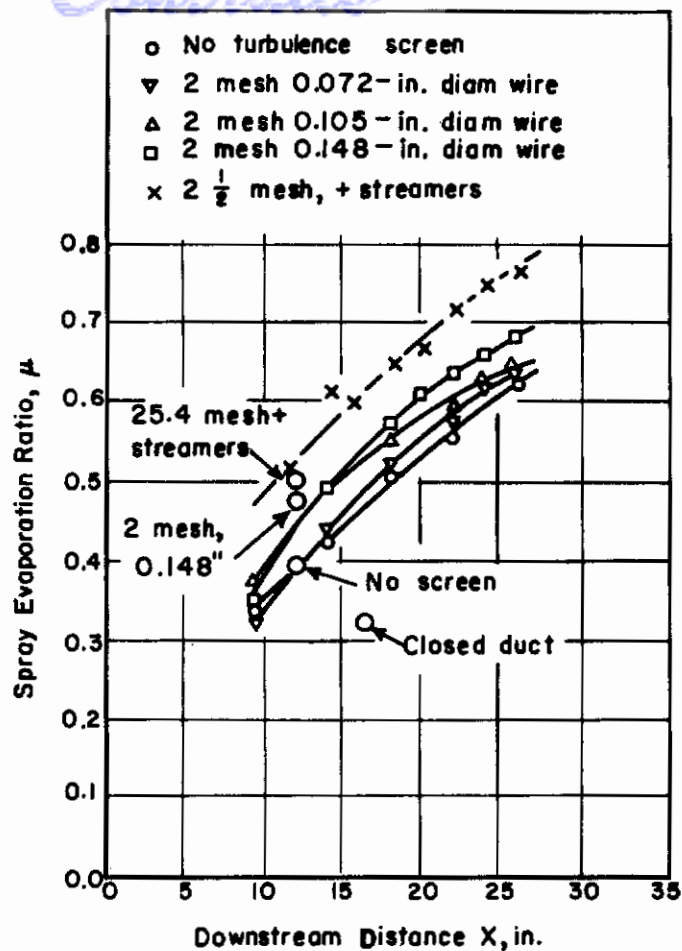


FIGURE 10-6. SPRAY EVAPORATION AS A FUNCTION OF DISTANCE FROM NOZZLE UNDER TURBULENT FLOW CONDITIONS

(Fledderman and Hanson)¹⁰⁻⁶

CONCLUDING REMARKS

The problem of spray evaporation appears to have received considerably more attention from the standpoint of theory than experiment. The reason for the conspicuous lack of experimental data can be traced to the inherent difficulties associated with measuring spray evaporation under both streamline and turbulent flow conditions.

All available theoretical developments of the spray-evaporation problem can be criticized on a multiplicity of points. The principal objection is that dynamic-spray evaporation is either treated from the standpoint of the behavior of some statistically average droplet in the ensemble, following an empirical evaporation law for a moving droplet, or from a consideration of the entire drop ensemble following the Maxwellian evaporation law for a static drop. Although neither of these treatments can be examined for its respective merit by a comparison with existing experimental data, it would seem that each possesses a certain unreal quality in light of certain physical considerations in the behavior of real sprays. The assumption of the Maxwellian law holding for the evaporation of the ensemble entirely neglects the role of boundary layer transport under conditions of motion and assumes that radial diffusion is the predominant parameter in determining bulk evaporation. Each

of these mechanisms also neglects the possible influence of both secondary atomization, in accordance with Hinze's theory⁽¹⁰⁻⁴⁹⁾, and surface deformation on the rate of evaporation of the spray. Although the effect of secondary atomization may be small for drops of small diameter, the total effect of droplet-surface deformation may materially contribute to a higher evaporation rate than that which would be predicted for a smooth surface. Norris⁽¹⁰⁻⁵⁰⁾ has concluded that evaporation from a hydrodynamically rough surface must be about four times as great as from a smooth surface.

In all the discussions which have been presented, the evaporation of individual drops has been considered as taking place in an infinite medium. In other words, each drop is assumed to evaporate independently of its neighbors. Fuchs⁽¹⁰⁻¹²⁾ has shown clearly that this condition is not realized in the case of an evaporating fuel-air dispersion under static conditions. It may be inferred from his analysis that the interaction of concentration gradients from nearest neighbors may have considerable influence on each surrounded drop. A detailed theoretical analysis of this aspect of spray evaporation, for the dynamic case, is necessary in order to examine completely the validity of this assumption.

It would appear that much theoretical and experimental work is needed regarding the heat and mass transfer from single drops, under high-temperature conditions, before any radical development can be made in the theory of spray evaporation in combustion chambers. Because of the unmanageable nature of the differential equations for heat and mass transfer under flow conditions, it would seem likely that the best approach to this problem lies in the direction of the correlation of the dimensionless groups which might be assembled from high-temperature evaporation data.

The problem of the evaporation of a spray under turbulent conditions is, of course, formidable from the mathematical standpoint. There is much to be learned about the evaporation of single droplets under turbulent conditions before any progress is remotely possible for the case of the spray. It would seem more than likely that this area would remain relatively unexplored for the longest time because of the huge amount of basic analysis which seems to be a prerequisite to further fundamental exploration.

Finally, it would seem that the most fruitful theoretical approach to the question of heat and mass transfer under turbulent conditions might be to attempt the development of new mathematical techniques for application to this kind of nonlinear problem.

REFERENCES

- 10-1. Bevans, R. S., Mathematical Expressions for Drop-Size Distributions; Paper presented at the Conference on Fuel Sprays, Univ. of Michigan, Ann Arbor, Michigan, March 30-31, 1949.
- 10-2. Kolupaev, P. G., Atomization of Heavy Fuel Oil; D.Sc. Thesis, Chemical Engineering MIT, 1941.
- 10-3. Rosin, P., and Rammler, E., The Laws Governing the Fineness of Powdered Coal; J. Inst. Fuels, Vol. 7, 1933, p. 29.
- 10-4. Nukiyama, S., and Tanasawa, Y., An Experiment on the Atomization of Liquids (Third Report); Trans. Soc. Mechanical Engr., Vol. 5, 1939, p. 63.
- 10-5. Epstein, B., Logarithmico-Normal Distribution in the Breaking of Solids; Ind. and Eng. Chem., Anal. Edition, Vol. 11, 1939, p. 334.
- 10-6. Fledderman, R. G., and Hanson, A. R., The Effects of Turbulence and Wind Speed on the Rate of Evaporation of a Dynamic Spray; Report No. CM 667, Project M604-3, Contract NOrd 7924, Task UMH-3D, U. S. Navy Department, BuORD, June 20, 1951, Univ. of Michigan.

- Centrals*
- 10-7. Frössling, N., The Evaporation of Falling Drops; Gerlands Beit. d. Geophysik, Vol. 52, 1938, p. 170.
 - 10-8. Whittaker, E. T., and Watson, G. N., A Course in Modern Analysis; p. 235, American Edition, The Mac Millan Co., New York City, 1943.
 - 10-9. Carrier, G. F., Private Communication, August 17, 1951.
 - 10-10. York, J. L., Photographic Analysis of Sprays; Ph.D. Thesis, 1949, Univ. of Michigan.
 - 10-11. Probert, R. P., The Influence of Spray Particle Size and Distribution in the Combustion of Oil Drops; London Phil. Mag., Vol. 37, 1946, p. 94.
 - 10-12. Fuchs, N., Concerning the Evaporation of Small Drops in a Gas Atmosphere; NACA Technical Memo. 1160, 1947.
 - 10-13. Fledderman, R. G., The Influence of Turbulence Upon the Rate of Evaporation of a Dynamic Spray; Ph.D. Thesis, Univ. of Michigan, 1950.
 - 10-14. Taylor, G. I., Statistical Theory of Turbulence; Proc. Roy. Soc., Vol. A151, 1935, p. 421.
 - 10-15. Schubauer, G. B., A Turbulence Indicator Utilizing the Diffusion of Heat; NACA Technical Report 524, 1935.
 - 10-16. Johnstone, H. F., Pigford, R. L., and Chapin, J. H., Heat Transfer to Clouds of Falling Particles; Trans. A. I. Ch. E., Vol. 37, 1941, p. 95.
 - 10-17. Prandtl, L., and Tietjens, O. G., Fundamentals of Hydro and Aeromechanics; McGraw-Hill Book Co., New York City, 1934, p. 151.
 - 10-18. Drew, T. B., Mathematical Attacks on Forced Convection Problems; Trans. A. I. Ch. E., Vol. 26, 1931, p. 26.
 - 10-19. Levêque, A., Exchange of Heat by Circulation of a Viscous Liquid in Tranquil Motion Through a Cylindrical Tube; Compt. Rendus, Vol. 185, 1927, p. 1190.
 - 10-20. Boussinesq, J., Calcul du Pouvoir Refroidissant des Courants Fluids; J. Math. Pures et Appl., Vol. 1, 1905, p. 285.
 - 10-21. Haslam, R. T., and Hottel, H. C., Combustion and Heat Transfer; Trans. ASME, Vol. 50, 1928, p. 9.
 - 10-22. Jakob, M., Heat Insulation and Heat Exchange, Part 5. General Principles of Heat Flow; Der Chemie Ingenieur, Vol. 1, 1933, p. 293.
 - 10-23. Nusselt, W., Radiation From Gases Flowing in Pipes; Z. Ver. Deut. Ing., Vol. 70, 1926, p. 763.
 - 10-24. McAdams, W. H., Heat Transmission; McGraw-Hill Book Co., New York City, 1942.
 - 10-25. Kramers, H., Heat Transfer From Spheres to Flowing Media; Physica, Vol. 12, 1946, p. 61.
 - 10-26. Ranz, W. E., and Marshall, W. R., Evaporation From Drops; Chem. Eng. Progress, Vol. 48, 1952, p. 141.
 - 10-27. Colburn, A. P., and Pigford, R. L., Chemical Engineers Handbook, Section 8; Third Edition, McGraw-Hill Book Co., New York City, 1950.

- 10-28. Ingebo, R. D., Vaporization Rates and Heat Transfer Coefficients for Pure Liquid Drops; NACA Technical Note 2386, 1951.
- 10-29. Alexander, L. G., and Coldren, C. L., Deposition of a Spray on the Walls of a Straight Duct; Paper presented at the Conference on Fuel Sprays, Univ. of Michigan, March 30-31, 1949.
- 10-30. Longwell, J. P., and Weiss, M. A., Mixing and Distribution of Liquids in High-Velocity Air Streams; Ind. and Eng. Chem., Vol. 45, 1953, p. 667.
- 10-31. Towle, W. L., and Sherwood, T. K., Eddy Diffusion. Mass Transfer in the Central Portion of a Turbulent Air Stream; Ind. and Eng. Chem., Vol. 31, 1939, p. 457.
- 10-32. Gilliland, E. R. and Sherwood, T. K., Diffusion of Vapors Into Air Streams; Ind. and Eng. Chem., Vol. 26, 1934, p. 516.
- 10-33. McAdams, W. H., Heat Transmission, McGraw-Hill Book Company, New York City, 1933.
- 10-34. Maisel, D. S., and Sherwood, T. K., Evaporation of Liquids Into Turbulent Gas Streams; Chem. Eng. Progress, Vol. 46, 1950, p. 131.
- 10-35. Chilton, T. H., and Colburn, A. P., Mass Transfer Coefficients; Ind. and Eng. Chem., Vol. 26, 1934, p. 1183.
- 10-36. Wollers and Ehmcke, The Process of Evaporation of Fuels, The Formation of Oil Vapor and the Behavior of Oil Vapors and Oil Gases During Combustion in the Diesel Engine; Kruppsche Monats., Vol. 2, 1921, p. 1.
- 10-37. Alt, O., Combustion of Liquid Fuels in the Diesel Engine; NACA Technical Memo. No. 281, 1924.
- 10-38. Rothrock, A. M., and Waldron, C. D., Fuel Vaporization and Its Effect on Combustion in a High-Speed Compression-Ignition Engine; NACA Report No. 435, 1932.
- 10-39. Selden, R. F., and Spencer, R. C., Heat Transfer to Fuel Sprays Injected Into Heated Gases; NACA Report No. 580, 1937.
- 10-40. Cohn, M., and Spencer, R. C., Combustion in a Bomb With a Fuel Ignition System; NACA Report No. 544, 1935.
- 10-41. Wolfhard, H. G., and Parker, W. G., Evaporative Process in a Burning Kerosine Spray; J. Inst. Petroleum Tech., Vol. 35, 1949, p. 118.
- 10-42. Penner, S. S., Effect of Radiation on the Rate of Burning of Solid Fuel Propellants; J. Appl. Physics, Vol. 19, 1948, p. 392.
- 10-43. Wentzel, W., Ignition Processes in the Diesel Engine; Forschung, Vol. 6, 1935, p. 105.
- 10-44. Dreyhaupt, F., Systematic Theoretical Analysis of the Reactions During Diesel Ignition; Motortech. Zeit., Vol. 4, 1942; Vol. 5, 1943, p. 59; Vol. 5, 1943, p. 373.
- 10-45. Gilbert, M., Howard, J. N., and Hicks, B. L., An Analysis of the Factors Affecting the State of Fuel and Air Mixtures; NACA Technical Note No. 1078, 1946.
- 10-46. Godsave, G. A. E., The Combustion of Drops in a Fuels Spray; National Gas Turbine Establishment Memorandum No. M95, October, 1950.

- Control*
- 10-47. Langmuir, I., and Blodgett, K. B., A Mathematical Investigation of Water Drop Trajectories; Army Air Force Technical Report No. 5418, General Electric Company, February 19, 1946.
- 10-48. Anon., Description and Instruction Manual for the Portable Turbulence Measuring Apparatus, Model 1940.
- 10-49. Hinze, J. O., Critical Speeds and Sizes of Liquid Globules; Appl. Sci. Research, Vol. A1, 1949, p. 273.
- 10-50. Norris, R., Evaporation From Extensive Surfaces of Water Roughened by Waves; Roy. Meteorol. Soc. Journal, Vol. 74, 1948, p. 1.

Contrails

CHAPTER 11. THE EQUATIONS OF FLUID DYNAMICS

ABSTRACT

In this chapter, which is introductory to Chapter 12, the basic equations of fluid flow are derived in Cartesian tensor notation. Included are the continuity equation, the equation for the dissipation of energy by viscosity, the energy equation for a viscous fluid, and the Navier-Stokes equation.

Contrails

THE EQUATIONS OF FLUID DYNAMICS

by

A. E. Weller

In this chapter the fundamental equations of fluid dynamics will be derived. Although the derivations of these equations may be found in almost any textbook on fluid dynamics, they are presented here to ensure retaining the continuity of subject and notation in the applications of these equations in Chapter 12.

The equations will be derived in the Cartesian tensor notation that will also be used in the following chapter. While not as compact as the Gibbs dyadic notation, nor as generalized as the Einstein tensor notation, the Cartesian tensors lead to equations the meaning of which can be seen without additional reduction. Accordingly, this chapter will begin with a brief intuitive discussion of Cartesian tensors.

CARTESIAN TENSOR NOTATION

The quantities known as vectors have associated with them both a magnitude and a direction. In general, such a quantity may be considered as the sum of three similar quantities having the directions of three rectangular Cartesian space coordinates,

$$\vec{V} = \vec{V}_1 + \vec{V}_2 + \vec{V}_3 ,$$

where the subscripts denote the directions of the coordinate axes and the summation denotes a vector sum. These three quantities are called the components of the vector \vec{V} . With the agreement that such a symbol is to take on all possible values of the subscript, we may write the vector \vec{V} as V_i . The arrow, used to distinguish the quantity as a vector, may be dropped, since the subscript also performs this function. Thus, the same vector quantity can be expressed in vector form as \vec{V} or in Cartesian tensor form as V_i .

If the coordinate system is transformed to a new set of rectangular Cartesian coordinates, then the component V_1 in the new system is

$$V_1 = \bar{V}_1 \cos \alpha + \bar{V}_2 \cos \beta + \bar{V}_3 \cos \gamma , \tag{11-1}$$

where the barred quantities are the components in the old coordinate system, and α , β , and γ are the angles between the new x_1 axis and the old \bar{x}_1 , \bar{x}_2 , \bar{x}_3 axes. The above direction cosines will be denoted as

$$\cos \alpha = l_{11} ,$$

$$\cos \beta = l_{12} ,$$

$$\cos \gamma = l_{13} .$$

Obviously, there are six other such cosines, l_{21} , l_{22} , l_{23} , l_{31} , l_{32} , and l_{33} . In general, we can designate these quantities by the symbol l_{ij} . The convention is adopted that whenever a

subscript is repeated in an expression, the expression is to be summed over all possible values of that index. Then Equation (11-1) can be written

$$V_1 = l_{1i} \bar{V}_i = l_{11} \bar{V}_1 + l_{12} \bar{V}_2 + l_{13} \bar{V}_3 . \quad (11-2)$$

Since the equations for the other components of \underline{V} are of the same form, Equation (11-2) can be generalized to

$$V_j = l_{ji} \bar{V}_i .$$

Since the axes are mutually perpendicular, componentwise multiplication of the direction cosines gives

$$l_{j1} l_{j2} = 0 ,$$

$$l_{j1} l_{j1} = 1 ,$$

or

$$l_{ij} l_{ik} = \begin{cases} 0 & \text{if } j \neq k \\ 1 & \text{if } j = k \end{cases} .$$

The value of the product, $l_{ij} l_{ik}$, is independent of the subscript i . Thus, i is called a dummy index, and the product $l_{ij} l_{ik}$ may be written more simply as

$$l_{ij} l_{ik} = \delta_{jk} , \quad (11-3)$$

where

$$\delta_{jk} = \begin{cases} 0 & \text{if } j \neq k \\ 1 & \text{if } j = k \end{cases} .$$

The transformation of vectors under a change of coordinates requires the use of direction cosines. These quantities have two subscripts which refer to two directions, the directions of the old and new axes. Such quantities can be arrived at in another way. Consider the product of two vectors,

$$A_i B_r .$$

This product may be considered as a new quantity,

$$C_{ir} = A_i B_r ,$$

with two directions, i and r , associated with it. Such quantities are called tensors of rank two. In this sense, a vector is a tensor of rank one. The direction cosines, l_{ik} , are not tensors, since the two subscripts refer to different coordinate systems. However, the subscripts in the quantity δ_{jk} refer to the same coordinate system, so that δ_{jk} is a tensor of rank two.

Suppose that a transformation of coordinates is made from the old \bar{x}_j axes to the new x_i axes. Then, the vectors, \bar{A}_i and \bar{B}_r , are transformed by the equations

$$A_i = l_{ij} \bar{A}_j ,$$

$$B_r = l_{rk} \bar{B}_k .$$

Thus

$$A_i B_r = l_{ij} l_{rk} \bar{A}_j \bar{B}_k ,$$

or

$$C_{ir} = l_{ij} l_{rk} \bar{C}_{jk} .$$

More generally, a tensor may be defined to be a quantity which transforms according to the preceding equation. This concept can be extended to tensors of rank n , $F_{ij\dots n}$,

$$F_{ij\dots n} = l_{ir} l_{js\dots} l_{nw} \bar{F}_{rs\dots w} .$$

From this definition it is obvious that the product of two tensors is a tensor.

In rectangular Cartesian coordinates,

$$\frac{\partial x_i}{\partial \bar{x}_j} = \frac{\partial \bar{x}_j}{\partial x_i} ,$$

so that

$$A_{ij} = l_{ir} l_{js} \bar{A}_{rs} ,$$

and

$$\bar{A}_{rs} = l_{ir} l_{js} A_{ij} .$$

In generalized coordinates the transformations

$$A_i = \frac{\partial x_i}{\partial \bar{x}_j} \bar{A}_j ,$$

and

$$A_i = \frac{\partial \bar{x}_j}{\partial x_i} \bar{A}_j$$

may lead to different results.

In the rectangular Cartesian coordinate systems used in the following developments, it is unnecessary to distinguish between these different types of tensors. This permits a simplification of the notation.

In the use of vectors, two types of products frequently arise: the scalar product and the vector product. The scalar product is defined as

$$\vec{A} \cdot \vec{B} = A_i B_i .$$

Since the index in this equation is repeated, it disappears from the final result so that the product is a scalar quantity.

The vector product is defined as the vector,

$$\vec{A} \times \vec{B} = \overrightarrow{(A_2 B_3 - A_3 B_2)_1} \overrightarrow{(A_3 B_1 - A_1 B_3)_2} \overrightarrow{(A_1 B_2 - A_2 B_1)_3} .$$

To express this vector as a general product, it is necessary to introduce the skew symmetric unit tensor, e_{ijk} , such that e_{ijk} is zero if any two indices are equal. Otherwise, e_{ijk} is equal to $(-1)^n$ where n is the number of permutations necessary to place the indices in the order 1, 2, 3.

Then, the vector product of \vec{A} and \vec{B} becomes

$$\vec{A} \times \vec{B} = A_i B_j e_{ijk} . \quad (11-4)$$

THE EQUATION OF CONTINUITY

One of the fundamental equations of fluid dynamics expresses the physical law of the conservation of matter. Consider a fluid composed of a number of identifiable constituents. The mass density of the fluid will equal the sum of the mass densities of all of the constituents at any point,

$$\rho = \rho^1 + \rho^2 + \dots + \rho^i , \quad (11-5)$$

where superscripts refer to the constituents.

The mass flow rate of the i th constituent through some element of a surface within the stream will be denoted by

$$q_r^i l_r dS ,$$

where dS is the area of the element and l_r are the direction cosines of its normal. The total flow rate of the entire fluid through the surface is

$$q_r l_r dS = \rho V_r l_r dS .$$

A velocity associated with each constituent of the mixture may be defined by the equation

$$V_r^i = \frac{q_r^i}{\rho^i} .$$

Since the total mass flow rate must equal the sum of the mass flow rates of all the constituents, it follows that

$$\rho V_r = \rho^1 V_r^1 + \rho^2 V_r^2 + \dots + \rho^i V_r^i . \quad (11-6)$$

Consider a small parallelepiped having dimensions dx_r , dx_s , dx_t , with center at the origin. Expanding the flux of the constituent in a series about the origin, the difference in the mass flow rates through the two faces normal to the x_r -axis is given by

$$\left[\rho^i V_r^i + \frac{\partial}{\partial x_r} (\rho^i V_r^i) \frac{dx_r}{2} + \dots \right] dx_s dx_t - \left[\rho^i V_r^i - \frac{\partial}{\partial x_r} (\rho^i V_r^i) \frac{dx_r}{2} + \dots \right] dx_s dx_t = \frac{\partial}{\partial x_r} (\rho^i V_r^i) dx_r dx_s dx_t .$$

The net outward flux of the i th constituent from the volume must equal the rate of decrease of the constituent within the volume. Letting Γ^i represent the net rate of increase per unit volume of the i th constituent from the sources and sinks in the volume element, and $\partial \rho^i / \partial t$ the rate of increase of density within the volume, it follows that

$$\frac{\partial}{\partial x_r} (\rho^i V_r^i) dx_r dx_s dx_t = - \frac{\partial \rho^i}{\partial t} dx_r dx_s dx_t - \Gamma^i dx_r dx_s dx_t .$$

Similar equations may be written for each of the constituents of the mixture. When these equations are added, it follows from Equations (11-5) and (11-6) that,

$$\frac{\partial}{\partial x_r} (\rho V_r) = - \frac{\partial \rho}{\partial t} - \Gamma . \quad (11-7)$$

This is the equation of continuity.

THE NAVIER-STOKES EQUATION

The application of Newton's second law of motion to a fluid leads to the classical momentum equation of fluid mechanics, generally known as the Navier-Stokes equation. Newton's second law relates the rate of change of momentum of a given mass to the forces acting upon the mass. In tensor notation,

$$f_j = \frac{dV_j}{dt} , \quad (11-8)$$

where f_j is the total force acting on a unit mass of the fluid, including both external forces such as gravity and internal shear and pressure stresses exerted by other parts of the fluid; V_j is the velocity and dV_j/dt is the acceleration of the fluid element.

In a Cartesian coordinate system the acceleration is given by

$$\frac{dV_j}{dt} = \frac{\partial V_j}{\partial t} + \frac{\partial V_j}{\partial x_i} \frac{dx_i}{dt} .$$

Now dx_i/dt is equal to V_i , so that this equation may be written

$$\frac{dV_j}{dt} = \frac{\partial V_j}{\partial t} + V_i \frac{\partial V_j}{\partial x_i} . \quad (11-9)$$

In general, the fluid can have three types of motion; a rigid-body translation, a rigid-body rotation, and a pure deformation. The first two types of motion may be treated by classical methods of mechanics. However, the fluid elements tend to resist deformation. This internal resistance, which is found to be proportional to the rate of deformation, greatly complicates the equations of motion.

For a rigid-body translation, the velocities at all points must be the same, so that

$$\frac{\partial V_j}{\partial x_i} = 0 .$$

Therefore, terms containing this derivative must account for the pure rotation and pure deformation.

Consider two points in the fluid separated by a distance, dx_i , with the coordinate system fixed in relation to one of the points. If the distance between them changes, the fluid will be deformed or strained. The velocity of the second point with respect to the first is given by

$$dV_j = \frac{\partial V_j}{\partial x_i} dx_i . \quad (11-10)$$

This velocity represents a combination of rotational velocities and rates of deformation. For pure rotation, the velocity, R_j , is given by

$$R_j = \omega_k x_l e_{klj} ,$$

where ω_k is the angular velocity, x_l are the coordinates of the point, and e_{klj} , is the skew symmetric unit tensor. The space rate of change of this motion will be

$$\frac{\partial R_j}{\partial x_i} = \frac{\partial \omega_k}{\partial x_i} x_l e_{klj} + \omega_k \frac{\partial x_l}{\partial x_i} e_{klj} . \quad (11-11)$$

For a pure rotation, there can be no change of the angular velocity with respect to the space coordinates. Thus the first term on the right must be zero. Also,

$$\frac{\partial x_l}{\partial x_i} = \delta_{il} ,$$

where δ_{il} is defined in Equation (11-3). Equation (11-11) then becomes

$$\frac{\partial R_j}{\partial x_i} = \omega_k e_{kij} . \quad (11-12)$$

The angular velocity for a pure rotation is given by the expression

$$\omega_k = 1/2 \frac{\partial V_s}{\partial x_r} e_{rsk} .$$

Equation (11-12) can thus be written

$$\frac{\partial R_j}{\partial x_i} = 1/2 \frac{\partial V_s}{\partial x_r} e_{rsk} e_{kij} .$$

Since this equation gives the space variation of velocity for a pure rotation, it can be subtracted from Equation (11-10) to give the velocity associated with the pure strain, dD_j . This yields

$$dD_j = dV_j - dR_j ,$$

or

$$dD_j = \frac{\partial V_j}{\partial x_i} dx_i - 1/2 \frac{\partial V_s}{\partial x_r} e_{rsk} e_{kij} dx_i .$$

Because of the skew symmetric properties of the e tensor, this equation can be written

$$dD_j = \frac{\partial V_j}{\partial x_i} dx_i - 1/2 \left(\frac{\partial V_j}{\partial x_i} - \frac{\partial V_i}{\partial x_j} \right) dx_i .$$

Therefore,

$$dD_j = 1/2 \left(\frac{\partial V_j}{\partial x_i} + \frac{\partial V_i}{\partial x_j} \right) dx_i ,$$

and

$$\frac{dD_j}{dt} = 1/2 V_i \left(\frac{\partial V_j}{\partial x_i} + \frac{\partial V_i}{\partial x_j} \right) = 1/2 V_i (\delta_{js} \delta_{ir} + \delta_{is} \delta_{jr}) \frac{\partial V_r}{\partial x_s} .$$

Contrails

Also,

$$\frac{dR_j}{dt} = 1/2 \frac{\partial V_r}{\partial x_s} e_{rst} e_{tij} V_i = 1/2 V_i \frac{\partial V_r}{\partial x_s} (\delta_{js} \delta_{ir} - \delta_{is} \delta_{jr}) .$$

Two tensors of second rank, Φ_{ij} and Ω_{ij} , are defined by the following equations

$$\Phi_{ij} = 1/2 \frac{\partial V_r}{\partial x_s} (\delta_{js} \delta_{ir} + \delta_{is} \delta_{jr}) ,$$

$$\Omega_{ij} = 1/2 \frac{\partial V_r}{\partial x_s} (\delta_{js} \delta_{ir} - \delta_{is} \delta_{jr}) .$$

Φ_{ij} is called the rate-of-strain tensor, and Ω_{ij} is called the rotation tensor. Then,

$$\frac{dR_j}{dt} = V_i \Omega_{ij} ,$$

$$\frac{dD_j}{dt} = V_i \Phi_{ij} ,$$

and

$$V_i \frac{\partial V_j}{\partial x_i} = V_i \Phi_{ij} + V_i \Omega_{ij} .$$

Returning to Equation (11-8), it is necessary to specify the forces acting on a particle of fluid. These will include both the external forces and the internal forces due to pressure and the strain.

Consider a small surface, S , within the fluid. The force per unit area which the fluid on one side of the surface exerts upon the fluid on the other side is known as the stress. The component of the stress perpendicular to the surface is called the normal stress, σ . The component of the stress tangent to the surface is called the shearing stress, τ . Each stress has two directions associated with it, the direction in which the stress acts and the orientation of the surface, defined by the direction of the surface normal. The stresses are therefore components of a tensor of second rank, say ψ_{ij} , where the first subscript denotes the direction of the surface normal and the second the direction in which the stress acts.

The following argument shows that the stress tensor, ψ_{ij} , is symmetric. Consider a small rectangular volume of fluid with sides, dx_r , and with one corner at the origin of the coordinate system. The moments tending to rotate this volume about the x_k -axis are $\psi_{ij} (dx_j dx_k) dx_i$, and $-\psi_{ji} (dx_i dx_k) dx_j$. The sum of these moments must equal the moment of inertia, I , times the angular acceleration about the x_k -axis. Thus,

$$(\psi_{ij} - \psi_{ji}) dx_i dx_j dx_k = I \frac{d\omega_k}{dt} ,$$

where

$$I = \rho dx_i dx_j dx_k \frac{dx_i^2 + dx_j^2}{12}$$

so that

$$\psi_{ij} - \psi_{ji} = \rho \frac{dx_i^2 + dx_j^2}{12 dt} d\omega_k$$

The right-hand member of this equation is an infinitesimal of second order, and as the fluid element becomes vanishingly small, there results

$$\psi_{ij} - \psi_{ji} = 0,$$

or

$$\psi_{ij} = \psi_{ji},$$

so that ψ_{ij} is symmetric. Hence, it makes no difference which subscript is chosen to indicate the direction of the stress or the orientation of the surface.

The mean value of the normal stress, ψ_{ii} , is the pressure, p . Denoting by ϵ_{ij} the difference between the stresses and the pressure,

$$\psi_{ij} = -p\delta_{ij} + \epsilon_{ij},$$

where the minus sign is introduced for the convention of having the positive direction as the direction of the surface normal. Summing this equation over $i = j$, there results

$$\psi_{11} + \psi_{22} + \psi_{33} = -3p + (\epsilon_{11} + \epsilon_{22} + \epsilon_{33}).$$

Since the pressure is the mean value of the normal stresses,

$$\epsilon_{11} + \epsilon_{22} + \epsilon_{33} = 0.$$

The functions ϵ_{ij} must be functions of the rate of strain, Φ_{kl} . Assuming that the ϵ_{ij} may be represented by linear functions,

$$\epsilon_{ij} = \mu_{ijkl} \Phi_{kl},$$

where μ_{ijkl} is a tensor of fourth rank and contains the fluid viscosity. Since ϵ_{ij} and Φ_{kl} are both symmetric, μ_{ijkl} must be symmetric in both ij and kl , so that

$$\mu_{ijkl} = \mu_{jikl} = \mu_{ijlk}.$$

If the fluid is isotropic, this tensor must be independent of the orientation of the axes. A transformation to a new set of coordinates yields

$$\mu_{mnpq} = l_{im} l_{jn} l_{kp} l_{lq} \mu_{ijkl}.$$

Since

$$l_{im} l_{jn} \delta_{ij} = \delta_{mn},$$

and

$$l_{im} l_{kp} \delta_{ik} = \delta_{mp},$$

the form of μ_{ijkl} can remain unchanged only if it is composed of constants multiplied by the delta tensors.

Therefore, μ_{ijkl} must be of the form,

$$\mu_{ijkl} = a \delta_{ij} \delta_{kl} + b \delta_{ik} \delta_{jl} + c \delta_{il} \delta_{jk} . \quad (11-13)$$

However, μ_{ijkl} can be symmetric in ij and kl only if b equals c . Hence,

$$\mu_{ijkl} = a \delta_{ij} \delta_{kl} + b(\delta_{ik} \delta_{jl} + \delta_{il} \delta_{jk})$$

so that

$$\epsilon_{ij} = a \delta_{ij} \Phi_{kk} + b(\Phi_{ij} + \Phi_{ji})$$

and since Φ_{ij} is symmetric,

$$\epsilon_{ij} = a \delta_{ij} \Phi_{kk} + 2b \Phi_{ij} . \quad (11-14)$$

Summing this equation over $i = j$ yields

$$\epsilon_{11} + \epsilon_{22} + \epsilon_{33} = 3a(\Phi_{11} + \Phi_{22} + \Phi_{33}) + 2b(\Phi_{11} + \Phi_{22} + \Phi_{33}) = 0 ,$$

from which it follows that

$$a = -2/3 b .$$

The viscosity is so defined that for a two-dimensional flow between flat plates, with the flow in the x_1 direction, and V_2 equal to zero,

$$\psi_{21} = \mu \frac{\partial V_1}{\partial x_2} ,$$

where μ is the absolute viscosity. Comparing this and similar equations for two-dimensional flow in differing directions, it is found that

$$b = \mu ,$$

and

$$a = -2/3 \mu .$$

Therefore, Equation (11-14) becomes

$$\epsilon_{ij} = -2/3 \mu \Phi_{kk} \delta_{ij} + 2 \mu \Phi_{ij} ,$$

and the stress tensor is given by

$$\psi_{ij} = -(p + 2/3 \mu \Phi_{kk}) \delta_{ij} + 2 \mu \Phi_{ij} . \quad (11-15)$$

The forces acting on an element of fluid can now be determined. Consider a rectangular volume of fluid with sides dx_s centered at the origin. If F_j is a component of the internal force per unit volume, then

Continuity

$$F_j dx_i dx_j dx_k = (\psi_{ij} + 1/2 \frac{\partial \psi_{ij}}{\partial x_i} dx_i) dx_j dx_k - (\psi_{ij} - 1/2 \frac{\partial \psi_{ij}}{\partial x_i} dx_i) dx_j dx_k ,$$

so that

$$F_j = \frac{\partial \psi_{ij}}{\partial x_i} . \quad (11-16)$$

By including the external force per unit mass of fluid, G_j , the total force acting on the fluid element becomes

$$F_j = \rho G_j + \frac{\partial \psi_{ij}}{\partial x_i} .$$

Multiplying Equation (11-8) by the density, ρ , yields

$$\rho f_j = \rho \frac{dV_j}{dt} . \quad (11-17)$$

Since

$$\rho f_j = F_j ,$$

Equation (11-17) can be written as

$$\rho G_j + \frac{\partial \psi_{ij}}{\partial x_i} = \rho \frac{dV_j}{dt} ,$$

and expansion of this equation in terms of Equations (11-9) and (11-15) yield

$$\rho G_j - \frac{\partial p}{\partial x_j} - 2/3 \frac{\partial}{\partial x_i} (\mu \phi_{kk}) \delta_{ij} + 2 \frac{\partial}{\partial x_i} (\mu \phi_{ij}) = \rho \frac{\partial V_j}{\partial t} + \rho V_i \frac{\partial V_j}{\partial x_i} .$$

By expanding ϕ , and combining similar terms, the following result is attained

$$\rho G_j - \frac{\partial p}{\partial x_j} + \frac{\partial}{\partial x_i} \left[\mu \frac{\partial V_s}{\partial x_r} (-2/3 \delta_{ij} \delta_{rs} + \delta_{ir} \delta_{js} + \delta_{is} \delta_{jr}) \right] = \rho \frac{\partial V_j}{\partial t} + \rho V_i \frac{\partial V_j}{\partial x_i} . \quad (11-18)$$

If the viscosity does not vary from point to point, then

$$\rho G_j - \frac{\partial p}{\partial x_j} + \mu \frac{\partial^2 V_s}{\partial x_r \partial x_i} (-2/3 \delta_{ij} \delta_{rs} + \delta_{ir} \delta_{js} + \delta_{is} \delta_{jr}) = \rho \frac{\partial V_j}{\partial t} + \rho V_i \frac{\partial V_j}{\partial x_i} . \quad (11-19)$$

This is the familiar form of the Navier-Stokes equation. If the viscosity does vary, Equations (11-18) or (11-19) must be used cautiously, since the assumption of isotropy in Equation (11-13) will not be correct.

THE DISSIPATION OF ENERGY BY VISCOSITY

It was shown in Equation (11-16) that the force caused by internal stresses acting upon an element of fluid is given by

$$F_j = \frac{\partial \psi_{ij}}{\partial x_i} .$$

The rate at which work is done by these stresses may be expressed as

$$\frac{dw}{dt} = \frac{\partial}{\partial x_i} (\psi_{ij} V_j), \tag{11-20}$$

and the portion of this work which is converted into kinetic energy of the fluid becomes

$$F_j V_j = V_j \frac{\partial \psi_{ij}}{\partial x_i} .$$

By subtracting this result from Equation (11-20), the rate at which energy is dissipated by viscosity per unit volume is found to be given by

$$W = \frac{dw}{dt} - F_j V_j = \psi_{ij} \frac{\partial V_j}{\partial x_i} .$$

From Equation (11-15) it follows that

$$W = -p \frac{\partial V_i}{\partial x_i} - 2/3 \mu \left(\frac{\partial V_i}{\partial x_i} \right)^2 + \mu \left[\left(\frac{\partial V_r}{\partial x_s} \right) \left(\frac{\partial V_r}{\partial x_s} \right) + \frac{\partial V_r}{\partial x_s} \frac{\partial V_s}{\partial x_r} \right] .$$

If the fluid is incompressible and without sources or sinks, this result becomes

$$W = \mu \left[\left(\frac{\partial V_r}{\partial x_s} \right)^2 + \frac{\partial V_r}{\partial x_s} \frac{\partial V_s}{\partial x_r} \right] . \tag{11-21}$$

In this chapter the fundamental equations of fluid dynamics have been derived in the Cartesian tensor notation. These equations will be used in the studies of turbulent flow in Chapter 12.

Contracts

CHAPTER 12. TURBULENCE

ABSTRACT

This chapter reviews the literature on turbulence and turbulent flow. The review is divided into two main sections, the phenomenological theories of turbulence, which include the mixing-length theories and Reichardt's hypothesis, and the statistical theory of turbulence. Experimental data from the literature are included in both sections for comparison with the various theories. An extensive bibliography of the literature on turbulence, jets, and wakes is included.

Topics covered under phenomenological theories are the eddy viscosity concept, Prandtl's mixing-length theory, Taylor's vorticity-transport theory, Reichardt's hypothesis, and recent attempts to generalize Reichardt's hypothesis in the study of turbulent jets.

In the section on the statistical theory, consideration is given to Taylor's original development of the theory through the concept of velocity correlations and scale, Von Karman's extension of this work and his generalized correlation tensor, the decay of turbulence and the propagation of the correlations, Loitsianskii's invariant and Batchelor's extension of this work, the spectrum of turbulence, Kolmogoroff's theory of local isotropy, and Taylor's theory of turbulent diffusion based on the auto-correlations.

Contrails

TURBULENCE

by

A. E. Weller

Turbulence has been defined by G. I. Taylor as "... an irregular motion which in general makes its appearance in fluids, gaseous or liquid, when they flow past solid surfaces or even when neighboring streams of the same fluid flow past or over one another". (12-1) This definition may be expanded somewhat, particularly in respect to the expression, "irregular motion". An essential feature of turbulent motion is that the fluctuations are random. Hence, vortex trails and pulsations are not examples of turbulence since they exhibit a certain regularity. The use of the word "random" implies that a time or frequency limit be chosen in the definition, since any random motion will appear regular over a sufficiently small time interval. For example, the motion of the molecules in a gas will appear regular over a time interval small in comparison with the mean free path divided by the molecular velocity. Practically, this means that there is a difficulty in defining exactly where turbulence begins and ends. More will be said of this in a later section.

The importance of turbulence in fluid mechanics can not be overstated. Turbulence may increase the resistance to flow by several magnitudes, greatly increase the rate of heat transfer through a fluid and produce mixing or diffusive effects. In practical engineering problems, fluid flow is nearly always in the turbulent region; non-turbulent flow requires prohibitively small velocities and corresponding large flow areas.

In the field of combustion, the importance of turbulence has long been recognized. The application here is one of providing increasing combustion intensities. Since turbulence produces mixing effects, local regions of rich or lean mixtures tend to be eliminated, allowing a more efficient utilization of combustion space. Also, it has been found experimentally that turbulence greatly increases effective flame speed, thus allowing higher velocities and through-puts in a given size combustion chamber.

REYNOLDS NOTATION

The actual velocity at a point in a turbulent fluid is a complex function of time, $U = U(t)$. Due to the random nature of the velocity variation with time, it is difficult to measure the flow parameters and express them as functions of time. Even if this were possible, the resulting complication of the equations of motion would present a formidable obstacle. Fortunately, it is possible to simplify this situation by introducing the notation devised by Reynolds. Using this notation, and averaging the equations of motion with respect to time, most of the parameters are replaced by their mean values.

In the Reynolds notation, each parameter is assumed to be representable by the sum of a mean and a fluctuating component. Thus the flow may be written as

$$U(t) = \bar{U} + u' \tag{12-1}$$

where the bar denotes a time average and the prime denotes a fluctuating random component of velocity. As would be expected, the mean velocity is defined by

$$\bar{U} = \overline{U(t)} = \frac{1}{T} \int_0^T U(t) dt \quad ,$$

where \underline{T} is a suitable time interval. It now follows from Equation (12-1) that

$$\overline{u'} = \frac{1}{T} \int_0^T u' dt = 0 \quad , \quad (12-2)$$

provided $\overline{\overline{U}} = \overline{U}$. However, as mentioned in the introduction, the above equations do not furnish a value for the time interval, \underline{T} . Excellent discussions of this problem have been given by Feng-Kan Chuang (12-2) and by Dryden (12-3, 12-4). In the final analysis, the problem appears to be insoluble. However, in most practical cases, no difficulty is encountered, provided that a second averaging does not change the value of the mean velocity, so that

$$\frac{1}{T} \int_0^T \left[\frac{1}{T} \int_0^T U(t) dt \right] d\tau = \frac{1}{T} \int_0^T U(t) dt \quad , \quad (12-3)$$

for all values of \underline{T} greater than some limiting value. If this requirement is not fulfilled, then the separation of the instantaneous motion into a mean and a fluctuating component is much more difficult. A possible approach in such cases is to limit the discussion to the high frequency, small scale components as part of the mean motion. This is similar to the approach taken by Kolmogoroff. In the sections that follow, the mean values will be restricted to a negligible change over the period of averaging, so that the requirement of Equation (12-3) is satisfied.

The notation of Equation (12-1) may be extended with the same significance to other flow parameters and to the fluid properties. Thus, for example,

$$U(t) = \overline{U} + u' \quad ,$$

$$U_i(t) = \overline{U}_i + u'_i \quad ,$$

$$\rho(t) = \overline{\rho} + \rho' \quad ,$$

and

$$p(t) = \overline{p} + p' \quad ,$$

where $U_i(t)$ denotes the component of the velocity in the x_i direction, $\rho(t)$ denotes fluid density and $p(t)$ denotes fluid pressure.

It was pointed out that the mean value of a fluctuating quantity is zero whenever a second averaging leaves the mean unchanged. However, the mean square and the mean product of fluctuating quantities are not zero. Thus in the case of turbulent velocity the random components satisfy the inequalities:

$$\overline{u'^2} \neq 0 \quad ,$$

and

$$\overline{u'_1 u'_2} \neq 0 \quad .$$

If the Reynolds notation is introduced into the continuity equation, Equation (11-7), there results

$$\frac{\partial}{\partial x_i} \left[(\overline{\rho} + \rho') (\overline{V}_i + v'_i) \right] = - \frac{\partial \overline{\rho}}{\partial t} - \frac{\partial \rho'}{\partial t} - \overline{\Gamma} - \Gamma' \quad . \quad (12-4)$$

On averaging this equation with respect to time, all terms containing a single primed quantity vanish, and the equation becomes

$$\frac{\partial}{\partial x_i} (\overline{\rho V}_i) + \frac{\partial}{\partial x_i} (\overline{\rho' v'_i}) = - \frac{\partial \overline{\rho}}{\partial t} - \overline{\Gamma} \quad .$$

If the fluid is incompressible, $\rho' = 0$, then the mean motion satisfies the equation of continuity. It follows from this result and Equation (12-4) that the divergence of the fluctuating velocity must be zero if the fluctuating source strength is zero. If the turbulence is isotropic, then, as will be shown later, $\overline{\rho'v'_i}$ is zero, and again the mean motion will satisfy the equation of continuity. If the fluid is compressible or the turbulence nonisotropic, then the situation becomes more complex.

Consider the Navier-Stokes equation in the following form,

$$\rho G_j + \frac{\partial}{\partial x_i} \psi_{ij} = \rho \frac{\partial V_j}{\partial t} + \rho V_i \frac{\partial V_j}{\partial x_i}$$

For an incompressible fluid under non-fluctuating external forces, $\bar{\rho} = \rho$ and $\bar{G}_j = G_j$. Thus, the introduction of Reynolds notation into all but the last term yields

$$\rho G_j + \frac{\partial}{\partial x_i} \bar{\psi}_{ij} = \rho \frac{\partial \bar{V}_j}{\partial t} + \overline{\rho V_i \frac{\partial V_j}{\partial x_i}} \quad (12-5)$$

where $\bar{\psi}_{ij}$ is identical with ψ_{ij} except that the instantaneous velocities have been replaced by their mean values.

The last term in Equation (12-5) may be written as

$$\overline{\rho V_i \frac{\partial V_j}{\partial x_i}} = \frac{\partial}{\partial x_i} (\overline{\rho V_i V_j}) - \bar{V}_j \frac{\partial}{\partial x_i} (\overline{\rho V_i})$$

If there are no sources or sinks, and the mean motion is steady, then the last term on the right drops out, so that

$$\overline{\rho V_i \frac{\partial V_j}{\partial x_i}} = \frac{\partial}{\partial x_i} (\overline{\rho V_i V_j}) \Big|_{\bar{\Gamma}} = \frac{\partial \bar{V}_j}{\partial t} = 0$$

Introducing the Reynolds notation, the left side becomes

$$\overline{\rho V_i \frac{\partial V_j}{\partial x_i}} = \frac{\partial}{\partial x_i} (\rho \bar{V}_i \bar{V}_j) + \frac{\partial}{\partial x_i} (\overline{\rho v'_i v'_j})$$

The first term on the right may be written as

$$\frac{\partial}{\partial x_i} (\rho \bar{V}_i \bar{V}_j) = \rho \bar{V}_i \frac{\partial \bar{V}_j}{\partial x_i}$$

Introducing these expressions into Equation (12-5), the Navier-Stokes equation becomes

$$\rho G_j + \frac{\partial}{\partial x_i} \bar{\psi}_{ij} = \rho \bar{V}_i \frac{\partial \bar{V}_j}{\partial x_i} + \frac{\partial}{\partial x_i} \left[(\overline{\rho v'_i v'_j}) \right]$$

for the mean steady-state flow of an incompressible fluid without sources or sinks.

The term in brackets represents a transport of momentum by the turbulent fluctuations and is equivalent to a stress. A turbulent stress tensor, Ψ_{ij} , can be defined by

$$\Psi_{ij} = - (\overline{\rho v'_i v'_j})$$

and the Navier-Stokes equation written as

$$\rho G_j + \frac{\partial}{\partial x_i} (\bar{\psi}_{ij} + \Psi_{ij}) = \rho \bar{V}_i \frac{\partial \bar{V}_j}{\partial x_i} \Big|_{\bar{\Gamma}} = \frac{\partial \bar{V}_j}{\partial t} = 0$$

Continuity

The stresses, Ψ_{ij} , are known as the Reynolds stresses.

Thus, except for the addition of a new stress tensor, the Navier-Stokes equation for turbulent flow retains its original form with the instantaneous values replaced by their means. Experimentally, it is found that the Reynolds stresses may be several hundred times as great as the viscous stresses. (12-5) The discovery of the Reynolds stresses explained the large stresses found in turbulent flow. However, unless the values of the indicated products can be determined, no further progress can be made.

PHENOMENOLOGICAL THEORIES OF TURBULENCE

The first step toward evaluation of the turbulent stresses was made by Boussinesq in the late 19th century. He assumed that the net effect of turbulence was equivalent to an increase in the viscosity, and introduced a "coefficient of mechanical viscosity", ϵ , now known as the eddy viscosity, which corresponds to the ordinary kinematic viscosity, ν . (12-5) The stress tensor then takes the form:

$$(\bar{\psi}_{ij} + \Psi_{ij}) = - (p + 2/3 \epsilon \bar{\rho} \bar{\Phi}_{kk}) \delta_{ij} + 2 \epsilon \bar{\rho} \bar{\Phi}_{ij}$$

At best, this is only a slight improvement. The quantity, ϵ , must be determined by experiment. Also, since ϵ depends upon the dynamic conditions of the flow and is nearly independent of the fluid properties, it will vary with the space coordinates. Generally, then, the isotropy of the fluid properties required in the derivation of the stress tensor is not satisfied in practice. Also, since a space variation makes calculations very difficult, most treatments using this approach assume a constant value of ϵ .

Prandtl's Mixing Length Theory

To proceed farther, it is necessary to relate the values of the Reynolds stresses with the measurable quantities of the mean flow. When visual observations of turbulent flow are made, either by optical methods or by introducing foreign particles into the fluid, it is found that fairly well-defined bodies of fluid, called eddies, move about in a random fashion as recognizable units for considerable intervals of time. A comparison of this motion to the motion of the molecules in a gas is suggestive. The eddies can be treated somewhat as the molecules of a gas, and the concept of a mean free path can be introduced. The analogy seems quite logical, since the Reynolds stresses, resulting from a transfer of momentum by the turbulent fluctuations, are a counterpart of the viscous stresses, caused by a transfer of momentum by the fluctuating molecular motion.

Consider, for example, a two-dimensional, incompressible flow in the x_1 -direction, such that

$$\bar{U}_1 = \bar{U}_1(x_2) \quad ,$$

$$\bar{U}_2 = \bar{U}_3 = 0 \quad ,$$

$$u'_3 = 0 \quad ,$$

and

$$\frac{\partial \bar{U}_1}{\partial x_1} = 0 \quad ,$$

In this case, all of the Reynolds shear stresses except one,

$$\Psi_{12} = -\rho \overline{u'_1 u'_2} \quad ,$$

vanish. Consider an eddy, located in a layer of fluid where the mean velocity is \bar{U}_1 . Due to the turbulent motion, this eddy moves in the x_2 direction to a layer of fluid where the mean velocity is different, say $\bar{U}_1 + d\bar{U}_1$, and loses its identity because of mixing with the fluid at this new level. Associated with this mixing process is a velocity fluctuation (12-5, 12-6, 12-7) having an absolute value given by

$$|u'_1| = \ell \frac{\partial \bar{U}_1}{\partial x_2} \quad , \quad (12-6)$$

where ℓ , is called the mixing length, is the distance that the eddy travels in the x_2 -direction before mixing occurs.

From the equation of continuity, the x_2 component of the fluctuating motion is expected to have the same magnitude as u'_1 so that

$$|u'_2| \propto \ell \frac{\partial \bar{U}_1}{\partial x_2} \quad . \quad (12-7)$$

That is, the motion induced by the eddy in the x_1 direction is expected to cause an inrush of fluid from layers above and below the level considered. The turbulent stress can then be written

$$\Psi_{12} = -\rho \overline{u'_1 u'_2} = -\rho \ell^2 \left(\frac{\partial \bar{U}_1}{\partial x_2} \right)^2 \quad ,$$

where ℓ^2 is the mean value, and the constant of proportionality in Equation (12-7) has been absorbed in the undetermined length. Since the sign of the stress must change with the sign of $\partial \bar{U}_1 / \partial x_2$, this result is more correctly written as

$$\Psi_{12} = -\rho \ell^2 \left| \frac{\partial \bar{U}_1}{\partial x_2} \right| \frac{\partial \bar{U}_1}{\partial x_2} \quad .$$

Neglecting viscous stresses in comparison with the turbulent stress, the Navier-Stokes equation becomes

$$-\frac{\partial p}{\partial x_1} = \frac{\partial}{\partial x_2} \left(\rho \ell^2 \left| \frac{\partial \bar{U}_1}{\partial x_2} \right| \frac{\partial \bar{U}_1}{\partial x_2} \right) \quad , \quad (12-8)$$

and, if ℓ is independent of x_2 ,

$$-\frac{\partial p}{\partial x_1} = 2\rho \ell^2 \frac{\partial \bar{U}_1}{\partial x_2} \frac{\partial^2 \bar{U}_1}{\partial x_2^2}$$

It might be asked what has been gained by replacing an unknown eddy viscosity, ϵ , by an unknown length, ℓ . The answer is that the length ℓ may be intuitively expected to be related in some simple manner to the lengths that characterize the flow geometry, such as the distance from a boundary. If only one such length exists, the mixing length may be supposed to be proportional to it.

The development above corresponds to that of Prandtl's momentum transfer theory. (12-6, 12-7) G. I. Taylor pointed out (12-8) that local pressure gradients affect the transfer of momentum. Consequently the neglect of these gradients in Prandtl's theory may introduce errors into the above equations. Moreover, similar momentum and temperature profiles are

predicted by the application of Prandtl's theory to the flow field of a heated jet. Experimental evidence has shown that this prediction is not true so that further refinements in Prandtl's theory are required.

Taylor's Vorticity Transport Theory

Taylor developed a treatment of turbulence which differs from Prandtl's theory in that vorticity rather than momentum is the property transferred. The advantage of this assumption is that local pressure gradients do not affect the transfer of vorticity if the motion is confined to two dimensions.

The Navier-Stokes equation for an incompressible two-dimensional flow in the x_1 direction is given by Equation (11-19). If the effects of viscosity are neglected⁽¹²⁻⁸⁾ this equation becomes

$$-\frac{1}{\rho} \frac{\partial \bar{p}}{\partial x_1} = \bar{U}_1 \frac{\partial \bar{U}_1}{\partial x_1} + \bar{U}_2 \frac{\partial \bar{U}_1}{\partial x_2} + \overline{u'_1} \frac{\partial u'_1}{\partial x_1} + \overline{u'_2} \frac{\partial u'_1}{\partial x_2}$$

Upon introducing the component of fluctuating vorticity,

$$\eta' = 1/2 \left(\frac{\partial u'_2}{\partial x_1} - \frac{\partial u'_1}{\partial x_2} \right) ,$$

the preceding equation yields

$$-\frac{1}{\rho} \frac{\partial \bar{p}}{\partial x_1} - 1/2 \frac{\partial}{\partial x_1} \left(\overline{u'^2_1} + \overline{u'^2_2} \right) = -2 \overline{u'_2 \eta'} + \bar{U}_1 \frac{\partial \bar{U}_1}{\partial x_1} + \bar{U}_2 \frac{\partial \bar{U}_1}{\partial x_2}$$

For this type of flow, the following equations hold:

$$\begin{aligned} \frac{\partial \bar{U}_1}{\partial x_1} &= 0 , \\ \bar{U}_2 &= 0 , \\ \frac{\partial \overline{u'^2_1}}{\partial x_1} &= \frac{\partial \overline{u'^2_2}}{\partial x_1} = 0 , \end{aligned}$$

so that

$$\frac{1}{\rho} \frac{\partial \bar{p}}{\partial x_1} = 2 \overline{u'_2 \eta'}$$

If it is assumed that vorticity is carried by eddies in the same manner as the transport of momentum in the Prandtl theory, an eddy moving over a distance, l_T , has a vorticity differing from its surroundings by the amount,

$$d\eta = \eta' = -l_T \frac{\partial}{\partial x_2} \left(-1/2 \frac{\partial \bar{U}_1}{\partial x_2} \right) = 1/2 l_T \frac{\partial^2 \bar{U}_1}{\partial x_2^2} , \quad (12-9)$$

since the vorticity of the mean motion is $-(1/2)\partial \bar{U}_1 / \partial x_2$. The change in vorticity is positive because a decreasing vorticity is characterized by a negative second derivative.

Thus, the Navier-Stokes equation becomes

$$2 \overline{u'_2 \eta'} = \overline{u'_2} \ell_T \frac{\partial^2 \overline{U}_1}{\partial x_2^2}$$

As before, the following equations hold:

$$\left| u'_1 \right| = \ell_T \frac{\partial \overline{U}_1}{\partial x_2},$$

and

$$\left| u'_2 \right| \propto \ell_T \frac{\partial \overline{U}_1}{\partial x_2},$$

so that the equation of motion becomes

$$\frac{1}{\rho} \frac{\partial \overline{p}}{\partial x_1} = \ell_T^2 \frac{\partial \overline{U}_1}{\partial x_2} \frac{\partial^2 \overline{U}_1}{\partial x_2^2}$$

This equation is similar to Equation (12-8) of Prandtl's theory. In the event that ℓ is independent of x_2 the equations are identical except for a constant, which can be absorbed in the undetermined length ℓ or ℓ_T . This constant factor is important however in the equations describing heat transfer due to the fluctuating motion.

Consider the case of a two-dimensional jet. If pressure gradients within the jet are neglected and ℓ is assumed constant at any cross sections, then the equation obtained from Prandtl's theory is

$$\overline{U}_1 \frac{\partial \overline{U}_1}{\partial x_1} + \overline{U}_2 \frac{\partial \overline{U}_1}{\partial x_2} = 2 \ell^2 \frac{\partial \overline{U}_1}{\partial x_2} \frac{\partial^2 \overline{U}_1}{\partial x_2^2} \quad (12-10)$$

The equation obtained from the vorticity transport theory is

$$\overline{U}_1 \frac{\partial \overline{U}_1}{\partial x_1} + \overline{U}_2 \frac{\partial \overline{U}_1}{\partial x_2} = \ell_T^2 \frac{\partial \overline{U}_1}{\partial x_2} \frac{\partial^2 \overline{U}_1}{\partial x_2^2},$$

which is identical with Equation (12-10) with the Prandtl mixing length, ℓ , replaced by the equivalent Taylor mixing length, ℓ_T . Hence, the two theories yield the same solutions for mean velocity distributions.

The equations for heat transfer in the two cases are (12-6, 12-9)

$$Q = \rho C_p \ell^2 \frac{d\overline{U}_1}{dx_2} \frac{d\overline{T}}{dx_2},$$

and (12-8, 12-9)

$$Q = \rho C_p \ell_T^2 \frac{d\overline{U}_1}{dx_2} \frac{d\overline{T}}{dx_2},$$

where the heat flux, Q , is the energy transferred across a unit area in a unit time. The substitution of the Prandtl mixing length into the latter equation yields

$$Q = 2 \rho C_p \ell^2 \frac{d\overline{U}_1}{dx_2} \frac{d\overline{T}}{dx_2}$$

Experimental data obtained by Fage and Falkner(12-10) for the distribution of temperature and velocity in the wake behind a heated cylinder indicate that heat spreads more rapidly than momentum. The experimental data are in fair agreement with profiles calculated from the vorticity transport theory. (12-11) However, neither theory yields acceptable profiles for the temperature distribution in heated jets. (12-12)

Figure 12-1 shows the results of the various mixing-length theories and some experimental data of the temperature distributions in the wake of a heated body of revolution.

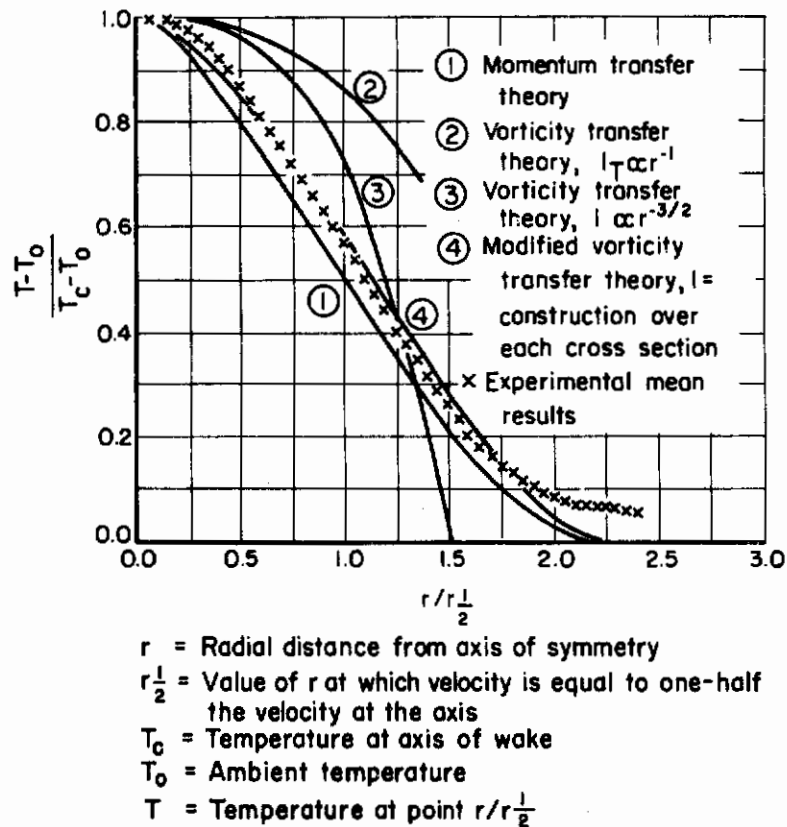


FIGURE 12-1. A COMPARISON OF THE MIXING LENGTH THEORIES WITH EXPERIMENTAL DATA OF THE TEMPERATURE DISTRIBUTION IN THE WAKE OF A HEATED BODY OF REVOLUTION Goldstein(12-7), Vol. 11, p. 590

It has been pointed out that the true test of a turbulence theory is not in predicting the mean velocity distribution, but in predicting the distribution of the fluctuating motion itself. (12-13, 12-14) In this respect, both mixing length theories fail. The most obvious discrepancy is at the center of a jet or wake, where $\partial \bar{U}_1 / \partial x_2$ equals zero. If the mixing length is finite, then the fluctuating motion must fall to zero on the axis of symmetry, but this is definitely not true. Also, experimental evidence indicates that the mixing length is not constant over a cross section of a jet or wake, as has been assumed in the classical treatments of this problem. (12-9, 12-16)

Various modifications including the introduction of a second mixing length have been made with the aim of eliminating these objections to the mixing length theories. These modifications greatly complicate the task of obtaining solutions to the equations of motion, and there is little physical argument to justify them.

Continuity

Another objection to the mixing length theories is contained in Equations (12-6) and (12-9). These equations assume that the mixing length is small in comparison with the range of x_2 . This is not true. Typical values of the mixing length range from about one tenth of the width in a jet or wake to about four tenths of the distance from the wall in pipe turbulence, for measurements near the wall, and sixteen per cent of the radius at the center. (12-5, 12-13, 12-14)

Perhaps the most fundamental objection to the mixing length theories is that they imply the turbulent motion to be discontinuous. The classical model of a fluid is continuous, and the equations of motion are based upon this assumption. While incorrect in the final analysis, since all fluids are composed of discrete molecules, the assumption is very good in all cases where the dimensions of the container are large in comparison with the mean free path of a molecule and the number of molecules is large. Measurements made with the hot-wire anemometer suggest that the turbulent fluctuations may be regarded as continuous. The introduction of the concept of discontinuous mixing into equations of motion based upon a continuous model of the fluid can hardly be expected to produce accurate results.

Squire(12-13) points out that the integration of the equations of motion based upon the mixing length theories tends to mask the disagreement with experiment, and the experimental data are not sufficiently accurate to compare with the equations in differential form. He also demonstrates that most of the results obtained from the mixing length theories can be obtained from simple dimensional analysis, without any assumption concerning the mechanism of turbulence. Evidently, the results obtained from the mixing length theories depend primarily upon the assumption of dynamic similarity and not upon the proposed mechanism. Von Karman's mixing length theory(12-15) owes its success entirely to the similarity concept involved.

These criticisms of the mixing length theories show that the proposed physical mechanism is incorrect. However, for problems in which only the mean velocity, temperature, or concentration distributions are required, they provide a reasonable approximation to fact and lead to equations of flow in a form which can be solved.

Reichardt's Hypotheses

The phenomenological approach taken by Reichardt to the theory of turbulence differs from that of the mixing length theories in that no attempt is made to provide a physical model. Reichardt(12-17) observes that the mean profiles of momentum flux in the free turbulence shown by jets and wakes, can be approximated by error functions, and that the profiles are similar at all cross sections beyond a certain distance from the origin of the jet or wake. The error functions are found to be solutions to the equations of motion provided the relation,

$$\overline{UV} = -\Lambda \frac{\partial \overline{U^2}}{\partial r} \quad , \quad (12-11)$$

holds where

$$\Lambda = \frac{b}{2} \frac{db}{dx} \quad ,$$

\underline{U} and \underline{V} denote instantaneous velocities in the \underline{x} and \underline{r} directions, \underline{x} denotes the distance along the axis of symmetry, \underline{r} denotes the radial distance from the axis of symmetry, and \underline{b} is a function of \underline{x} alone.

Although there is no physical basis for Equation (12-11), Reichardt points out that this is not necessary for the success of a method which is required to yield acceptable solutions only for the mean profiles of momentum flux.

If viscous effects and pressure gradients are assumed to be negligible, then the equation of motion for an axially symmetric jet in cylindrical coordinates is given by

Continuity

$$\frac{\partial \bar{U}^2}{\partial x} + \frac{1}{r} \frac{\partial}{\partial r} (r \bar{U}V) = 0$$

A substitution using Equation (12-11) yields

$$\frac{\partial \bar{U}^2}{\partial x} - \Lambda \frac{\partial}{\partial r} \left(r \frac{\partial \bar{U}^2}{\partial r} \right) = 0$$

A solution to this equation is the error function,

$$\bar{U}^2 = \frac{K}{b^2} e^{-\left(\frac{r}{b}\right)^2} \tag{12-12}$$

It is possible to generalize Reichardt's hypothesis to include any transportable property. If it is assumed that molecular transport is negligible, that there is no generation of the property, and that a steady state exists, then a generalized transport equation can be written as (12-2, 12-18)

$$\frac{\partial}{\partial x_i} (\bar{H}U_i) = 0$$

where \bar{H} is the concentration of the quantity being considered. In cylindrical coordinates, this equation takes the form,

$$\frac{\partial \bar{H}U}{\partial x} - \frac{1}{r} \frac{\partial}{\partial r} (r \bar{H}V) = 0$$

In analogy to Equation (12-11) it is assumed that

$$\bar{H}V = -\Lambda_H \frac{\partial \bar{H}U}{\partial r} \tag{12-13}$$

and consequently, the equation of motion becomes

$$\frac{\partial \bar{H}U}{\partial x} - \frac{H}{r} \frac{\partial}{\partial r} \left(r \frac{\partial \bar{H}U}{\partial r} \right) = 0$$

Solutions to this equation are of the same form as Equation (12-12), and may be written as

$$\bar{H}U = \frac{K_H}{b_H^2} e^{-\left(\frac{r}{b_H}\right)^2} \tag{12-14}$$

where

$$\Lambda_H = \frac{b_H}{2} \frac{db_H}{dx}$$

It will be noted that the solutions obtained are in the form

$$\bar{U}^2 = \bar{U}^2 + \bar{u}'^2$$

or

$$\bar{H}U = \bar{H} \bar{U} + \bar{H}'u'$$

The momentum flux profiles at all cross sections beyond a certain distance from the origin of the jet or wake have been observed to be similar. That is, they are functions of a single variable, η , so that

$$\frac{\overline{U^2}(x, r)}{\overline{U^2}(x, 0)} = f(\eta) \quad , \quad (12-15)$$

where

$$\eta = \frac{r}{x}$$

From Equation (12-12) it follows that

$$\frac{\overline{U^2}(x, r)}{\overline{U^2}(x, 0)} = e^{-\left(\frac{r}{b}\right)^2} \quad , \quad (12-16)$$

and, finally, the identification of Equation (12-15) with Equation (12-16) requires that

$$b = Cx \quad ,$$

where C denotes a constant of proportionality. If the generalized flux profiles are also similar, then

$$b_H = C_H x \quad , \quad (12-17)$$

and substitution of Equation (12-17) into Equation (12-14) yields

$$\overline{HU} = \frac{K_H}{C_H^2 x^2} e^{-\frac{\eta^2}{C_H^2}}$$

The constant, K_H , can be evaluated by writing the equation for the conservation of \overline{HU} . If A_0 is the area of the jet orifice, then

$$2\pi \int_0^\infty \frac{K_H}{C_H^2 x^2} e^{-\frac{\eta^2}{C_H^2}} x^2 \eta d\eta = \overline{HU}(0, 0) A_0$$

A change in the independent variable to η^2/C_H^2 , followed by an integration and evaluation of this equation yields

$$K_H = \frac{\overline{HU}(0, 0) A_0}{\pi}$$

The solution to the equation of motion is then given by

$$\overline{HU} = \frac{\overline{HU}(0, 0) A_0}{\pi C_H^2 x^2} e^{-\frac{\eta^2}{C_H^2}} \quad , \quad (12-18)$$

where it has been assumed that all profiles are similar and that these profiles may be represented by error functions. The assumption of similarity requires that the jet originate from a point source, otherwise, the equation will apply only at cross sections at distances from the origin large

in comparison with the size of the origin. Experimentally, it is found that the above requirement is approximately met when the profile is at least ten orifice diameters downstream from the jet orifice.

If Equations (12-13) and (12-17) are substituted into the equations of motion, there results

$$\frac{\partial \overline{HU}}{\partial x} - \frac{C_H^2 x}{2r} \frac{\partial}{\partial r} \left(r \frac{\partial \overline{HU}}{\partial r} \right) = 0$$

Since this equation is linear in \overline{HU} , a linear combination of solutions describes the flow field formed by any number of point-source jets. (12-17) In particular, for a jet whose source has finite area, it follows that

$$\overline{HU} = \int_0^{A_0} \frac{\overline{HU}(y_0, z_0)}{\pi C_H^2 x^2} e^{-\frac{\eta^2(y_0, z_0)}{C_H^2}} dA, \quad (12-19)$$

where $\overline{HU}(y_0, z_0)$ and $\eta(y_0, z_0)$ indicate that these quantities may vary in the plane of the jet origin. For a round jet with a flat profile at the origin, $\overline{HU}(y_0, z_0)$ is constant and

$$\eta^2(y_0, z_0) = \frac{R^2 + D^2 - 2RD \cos \phi}{x^2},$$

where R is the radial distance from the axis of symmetry, D is the distance of the point source from the axis of symmetry, and ϕ varies from zero to 2π . Also, because

$$dA = D dD d\phi,$$

Equation (12-19) becomes

$$\overline{HU} = \int_0^{R_0} \int_0^{2\pi} \frac{\overline{HU}(0, 0)}{\pi C_H^2 x^2} e^{-\frac{R^2}{C_H^2 x^2} - \frac{D^2}{C_H^2 x^2} - \frac{2RD}{C_H^2 x^2} \cos \phi} D dD d\phi,$$

where R_0 is the radius of the jet source. This equation can be expanded into a power series and integrated to yield

$$\overline{HU} = \frac{\overline{HU}(0, 0)}{\pi C_H^2 x^2} e^{-\frac{R^2}{C_H^2 x^2}} \left[\pi C_H^2 x^2 \left(1 - e^{-\frac{R_0^2}{C_H^2 x^2}} \right) + \dots \right]$$

It will be noted that for the limiting case where $x \gg R_0$, this equation reduces to Equation (12-18) with A_0 equal to πR_0^2 .

The linearization of the equations of motion and the degree of simplicity obtained are the chief virtues of Reichardt's hypothesis. The accuracy of the solutions is not great, particularly near the edge of a jet or wake, but reasonably good approximations are obtained near the axis of symmetry.

Figures 12-2 and 12-3 compare the equations obtained from Reichardt's hypothesis with experimental data.

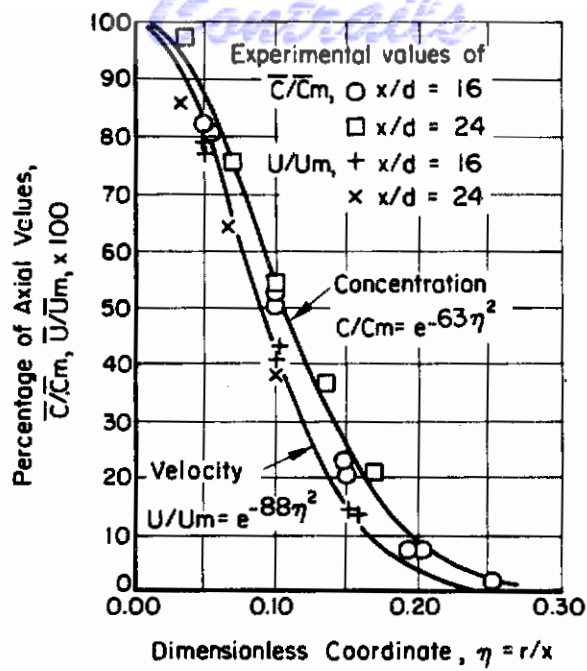


FIGURE 12-2. VELOCITY AND CONCENTRATION PROFILES IN A JET OF NITROGEN

Keagy and Weller(12-20)

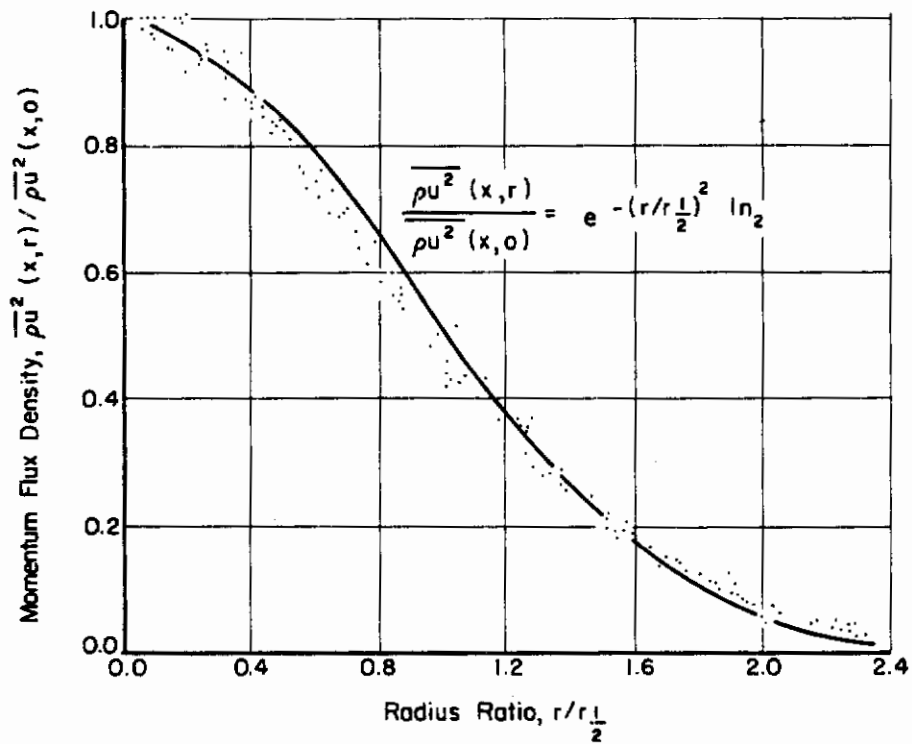


FIGURE 12-3. MOMENTUM FLUX DENSITY PROFILES IN A JET OF AIR

Alexander, Baron, and Comings(12-18)

As in the other phenomenological theories, Reichardt's hypothesis does not yield information concerning the fluctuating motion. Hence, it suffers from the same criticism as that directed against the mixing length theories. Additionally, it is based upon the assumption that the mean value profiles may be represented by error functions, and in the more extended form, that all profiles are similar at distances from the origin large in comparison with the size of the orifice. Both of these assumptions are untrue in detail. Forstall and Shapiro⁽¹²⁻¹⁹⁾ have indicated that a cosine function yields as good an approximation to the measured profiles as does the error function, and Batchelor⁽¹²⁻¹⁴⁾ reports that the profiles in the wake behind a cylinder are not exactly similar at distances up to six hundred diameters behind the cylinder. Keagy and Weller⁽¹²⁻²⁰⁾ measured the velocity and concentration profiles in round jets of nitrogen, carbon dioxide, and helium expanding into air and found that, while error functions give reasonable approximations to the profiles, the axial variations do not agree with Equation (12-18).

Even with these objections, Reichardt's hypothesis has much to recommend it. The linearization permits the treatment of flow near the origin of the jet or wake and the interaction of two or more jets. Neither of these cases can be conveniently handled by the mixing-length theories. At the same time, the mathematical labor required to obtain solutions is greatly reduced. Reichardt's hypothesis, as originally formulated, applied only to free turbulence. Recently, however, attempts to extend this hypothesis to flow patterns where the effects of walls or other solid boundaries are present have been made with reasonable success.^(12-21, 12-22)

THE STATISTICAL THEORY OF TURBULENCE

In the early investigations of turbulent flow it was suggested that turbulent motion consists of eddies of a more or less definite size moving through the bulk of the fluid. This idea, combined with concepts borrowed from the kinetic theory of gases, led Prandtl and Taylor to introduce a mixing length, which is analogous to the mean free path in a gas.

This approach tacitly implies that turbulent motion is discontinuous and that eddies can preserve their identity. That is, the original momentum, vorticity, or some other property of an eddy can be continuously identified over a considerable length of time before mixing occurs and the eddy merges with its surroundings. This conception might have some merit if the "eddy density" were quite low, but this is untrue. Also, since molecular diffusion is the only process by which such eddies can lose their individual properties to their surroundings, the physical properties of the fluid should have a pronounced effect upon the magnitude of the mixing length. However, in these theories it is assumed that the mixing length is independent of molecular transport properties.

The idea of an eddy, however, is a convenient intuitive concept. If a turbulent flow field is examined by some method which makes the streamlines visible, eddy-like bodies of fluid having vaguely defined boundaries, can be seen. Still, the eddies constitute a continuous part of the flow field so that any attempt to define the diameter of an eddy by simple measurements must fail. One method of defining a length scale which is connected with the average size of the eddies was discovered by G. I. Taylor. According to Taylor⁽¹²⁻²³⁾, "It is clear that whatever we may mean by the diameter of an eddy a high degree of correlation must exist between the velocities at two points which are close together when compared with this diameter. On the other hand, the correlation is likely to be small between the velocities at two points situated many diameters apart".

Following this line of thought, Taylor introduced the correlation coefficient, R_y . This is the correlation between fluctuating velocities at two points separated by a distance, y , perpendicular to the direction of the fluctuating velocities. Symbolically, the correlation coefficient is given by

$$R_y = \frac{\overline{u_1 u'_1}}{\sqrt{\overline{u_1^2}} \sqrt{\overline{u'_1^2}}}$$

where the u 's denote fluctuating velocities, the primes denote values at a second point, and the bars denote a time mean value of the form given in Equation (12-2).

The correlation coefficient can have values between plus and minus one. If the two velocities have a perfectly random phase relationship, then the correlation coefficient is zero. A correlation coefficient of zero does not necessarily mean, however, that the fluctuations are unrelated.

The value of the correlation coefficient at a given separation, y , can sometimes be considered as a measure of the fraction of eddies having a diameter equal to or greater than that distance. If the correlation coefficient approaches zero sufficiently rapidly as y tends to infinity, then a length l_2 may be defined as

$$l_2 = \int_0^{\infty} R_y dy$$

This length may be considered as a measure of the average diameter of the eddies and is known as the Eulerian scale. The tendency at present is to avoid the identification of such quantities with physical properties of the turbulence.

Figure 12-4 is a plot of a measurement of R_y as a function of the distance, y . Such measurements can be made by squaring and averaging the added outputs of two hot-wire anemometers located a distance, y , apart. This yields

$$\overline{(u_1 + u'_1)^2} = \overline{u_1^2} + \overline{u'_1^2} + 2 \overline{u_1 u'_1}$$

The values of $\overline{u_1^2}$ and $\overline{u'_1^2}$ can be found separately by measuring the outputs of hot-wire anemometers with a thermo-milliammeter. Subtraction of these values from $\overline{(u_1 + u'_1)^2}$ gives the quantity, $2 \overline{u_1 u'_1}$. An alternate method is to square the sum and difference of the outputs from the two wires and subtract to give the value, $4 \overline{u_1 u'_1}$. Other methods are also available.

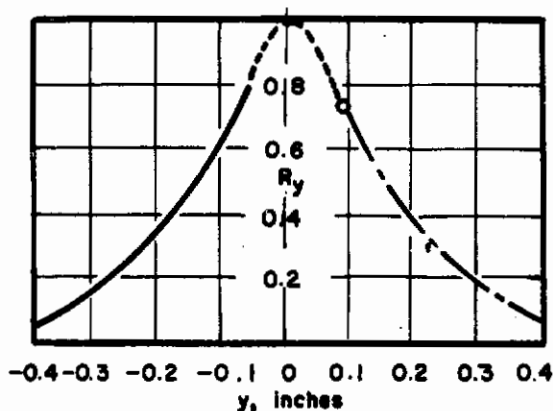


FIGURE 12-4. MEASURED VALUES OF THE CORRELATION COEFFICIENT, R_y , BEHIND A GRID

Mesh Spacing 0.9 x 0.9 in., $\overline{u^2} = 0.1015 \text{ ft}^2/\text{sec}^2$
(Taylor)12-23

Taylor's correlation coefficient may be generalized to express the correlation between velocities in any direction at two points. Since these correlation coefficients involve the product of two vector velocities, they may be regarded as components of a tensor of rank two, (12-24) and written as follows:

$$R_{ij} = \frac{\overline{u_i u'_j}}{\sqrt{\overline{u_i^2}} \sqrt{\overline{u'_j^2}}}$$

In this expression $\overline{u_i^2}$ and $\overline{u_j^2}$ refer to mean square value of the i th and j th components, and do not signify the contracted product, $\overline{u_i u_i}$, or $\overline{u_j u_j}$.

Isotropic Turbulence

The simplest type of turbulence to investigate is that which is isotropic and homogeneous. In homogeneous isotropic turbulence, the mean value of any function of the fluctuating velocity components and their derivatives at a particular point or pair of points is unaltered by a rotation of the coordinate system or by a reflection of the axes in a plane through the origin. Equivalently, these values are independent of the direction cosines of the velocity components. Homogeneous isotropic turbulence is usually called "isotropic".

In isotropic turbulence, the Reynolds shear stresses are zero. Consider the product, $\overline{u_i u_j}$. A rotation of the axes 180 degrees about the x_i axis yields

$$U_i = u_i \quad ,$$

$$U_j = -u_j \quad ,$$

so that

$$\overline{u_i u_j} = -\overline{U_i U_j} \quad .$$

The assumption of isotropy requires that

$$\overline{u_i u_j} = \overline{U_i U_j} \quad ,$$

and consequently, $\overline{u_i u_j}$ is zero unless i equals j .

Experimental evidence has shown that all turbulent motion tends toward isotropy. Fage and Townend(12-35) found that the turbulence in the central portion of a pipe is approximately isotropic. Similarly atmospheric turbulence is found to approach the condition of isotropy at sufficiently large distances from the ground. The turbulence generated in a stream by means of a grid of bars becomes isotropic a short distance downstream of the grid. Recent measurements, however, indicate that the final approach to isotropy is very slow, and that, in fact, complete isotropy may never be reached. (12-26)

The Correlation Tensor

In isotropic turbulence, the correlation tensor is capable of being expressed in analytic form. Consider two points, P and P' , connected by the line, \underline{r} , in the coordinate system, x_k . If the axes are transformed to an x_r -system with X_i coincident with \underline{r} , then

$$U_i = \ell_{is} u_s \quad ,$$

$$U'_t = \ell_{jt} u'_j \quad ,$$

and where the U_r denote velocity components in the new system and ℓ_{kr} denote the direction cosines between the old and new axes. In the new coordinate system, only the correlations, $\overline{U_1 U'_1}$, $\overline{U_2 U'_2}$, and $\overline{U_3 U'_3}$ exist, since by rotations of the X_r -axes, all other correlations may be shown to be zero. Also, since $\overline{U_2 U'_2}$ and $\overline{U_3 U'_3}$ differ only by a rotation of the axes, they must be equal. These two remaining correlations are scalars and may be represented as functions of time and the scalar distance between the two points:

Controls

$$f(r, t) = \frac{\overline{U_1 U'_1}}{\overline{U^2}},$$

$$g(r, t) = \frac{\overline{U_2 U'_2}}{\overline{U^2}} = \frac{\overline{U_3 U'_3}}{\overline{U^2}}.$$

(12-20)

Here $\overline{U^2}$ is the common value of $\overline{U_i^2}$, since in isotropic turbulence this value is independent of direction and position.

In terms of the correlations in the X_r -system, the correlation tensor is expressible as

$$R_{ij} = \frac{\overline{u_i u'_j}}{u^2} = l_{ir} l_{js} \frac{\overline{U_r U'_s}}{\overline{U^2}},$$

$$= l_{i1} l_{j1} f(r, t) + (l_{i2} l_{j2} + l_{i3} l_{j3}) g(r, t).$$

Therefore,

$$R_{ij} = l_{i1} l_{j1} [f(r, t) - g(r, t)] + \delta_{ij} g(r, t),$$

where

$$\delta_{ij} = l_{i1} l_{j1} + l_{i2} l_{j2} + l_{i3} l_{j3}.$$

The direction cosines are given by

$$l_{i1} = \frac{\xi_i}{r},$$

where the ξ_i denote the components of \underline{r} in the x_k coordinate system, so that the correlation tensor becomes

$$R_{ij} = \frac{\xi_i \xi_j}{r^2} [f(r, t) - g(r, t)] + \delta_{ij} g(r, t) \quad (12-21)$$

The correlation tensor is symmetric since the component tensors, $\xi_i \xi_j$, and δ_{ij} , are symmetric.

If the turbulent fluid is incompressible and without sources or sinks, the continuity equation may be written

$$\frac{\partial \overline{u_i}}{\partial x_i} + \frac{\partial u_i}{\partial x_i} = 0,$$

where $\overline{u_i}$ is the mean velocity and u_i is the fluctuating velocity. The mean motion satisfies the equation of continuity in this case, so that

$$\frac{\partial \overline{u_i}}{\partial x_i} = 0.$$

Consider the point, P , in the correlation tensor to be fixed at the origin of a coordinate system. If the point P' is allowed to vary, the components of \underline{r} can be introduced as coordinates. The continuity equation at P' then becomes

$$\frac{\partial u'_j}{\partial \xi_j} = 0.$$

Multiplication of this equation by $u_j/(u^2)$, which is independent of the location of P , yields

$$\frac{\partial \frac{u_i u'_j}{u^2}}{\partial \xi_j} = 0$$

Taking the mean value of both sides and expanding according to Equation (12-21) gives

$$\frac{\partial R_{ij}}{\partial \xi_j} = \frac{\partial}{\partial \xi_j} \left\{ \frac{\xi_i \xi_j}{r^2} \left[f(r, t) - g(r, t) \right] + \delta_{ij} g(r, t) \right\} = 0$$

Differentiation of the right side of this equation followed by a grouping of terms and a contraction yields

$$\frac{\partial R_{ij}}{\partial \xi_j} = 2 \frac{\xi_i}{r^2} [f - g] + \frac{\xi_i}{r} \frac{\partial f}{\partial r} = 0$$

Finally, multiplication of this equation by r^2/ξ_i , gives

$$2 [f - g] + r \frac{\partial f}{\partial r} = 0 \quad (12-22)$$

Equation (12-22) is a relation between the two correlations, $f(r, t)$ and $g(r, t)$. The correlation tensor can therefore be completely expressed in terms of one scalar function and its derivative.

Since $f(r, t)$ and $g(r, t)$ are independent of the orientation of \underline{r} , they must be even functions of \underline{r} ,

$$f(r, t) = f(-r, t) \quad ,$$

$$g(r, t) = g(-r, t) \quad .$$

On expanding these functions in a series in \underline{r} about the point, \underline{P} , only even powers of \underline{r} are obtained, so that

$$\left. \begin{aligned} f(r, t) &= 1 + \frac{f''(0)}{2!} r^2 + \frac{f^{iv}(0)}{4!} r^4 + \dots \\ g(r, t) &= 1 + \frac{g''(0)}{2!} r^2 + \frac{g^{iv}(0)}{4!} r^4 + \dots \end{aligned} \right\} \quad (12-23)$$

If these results are used to substitute into Equation (12-22) and coefficients of corresponding values of \underline{r} are equated, then

$$2 f''(0) = g''(0) \quad ,$$

$$3 f^{iv}(0) = g^{iv}(0), \text{ etc.}$$

Then for small values of \underline{r} , the following results are valid:

$$f(r, t) = 1 + \frac{1}{2} f''(0) r^2 \quad , \quad (12-24)$$

$$g(r, t) = 1 + f''(0) r^2 \quad , \quad (12-25)$$

and

Correlations

$$R_{ij} = -\frac{1}{2} \xi_i \xi_j f''(0) + \delta_{ij} \left[1 + f''(0) r^2 \right] \quad (12-26)$$

The Microscale of Turbulence

Since $f''(0)$ has the dimensions of the reciprocal of a length squared, a length, λ , can be defined as

$$\lambda^2 = -\frac{1}{f''(0)} = -\frac{2}{g''(0)} \quad (12-27)$$

Both $f''(0)$ and $g''(0)$ are measures of the curvature of the correlation curve at the origin, and therefore must be connected with the mechanism by which the correlation coefficient decreases from one. Because the smallest eddies must be responsible for the behavior of the correlation coefficient near $r = 0$, G. I. Taylor(12-23) proposed that the length λ , be taken as a measure of the average size of the smallest eddies. He proposed the name microscale for this length.

Correlations Between Derivatives of Velocities

The correlation tensor can be used to find the correlations between space-derivatives of the fluctuating velocities(12-27), such as

$$\frac{\partial u_i}{\partial x_r} \frac{\partial u_j}{\partial x_s}$$

The correlation between first derivatives can be found as follows. If x_r are the coordinates of the point where u_i is measured, and x'_s are the coordinates of the point where u_j' is measured, then

$$\frac{\partial u_i u_j'}{\partial x_r} = \overline{u^2} \frac{\partial R_{ij}}{\partial x_r}$$

The components of the line, \underline{r} , joining the two points are given by

$$\xi_r = x'_r - x_r$$

and since x_r is independent of x'_r , it follows that

$$d\xi_r = -dx_r$$

Therefore,

$$\frac{\partial u_i u_j'}{\partial x_r} = -\overline{u^2} \frac{\partial R_{ij}}{\partial \xi_r}$$

The fluctuations at either point are independent of the location of the other point so that differentiation with respect to x_r and x'_s yields

$$\frac{\partial^2 u_i u_j'}{\partial x_r \partial x'_s} = \frac{\partial u_j' \partial u_i}{\partial x'_s \partial x_r} = -\overline{u^2} \frac{\partial^2 R_{ij}}{\partial \xi_r \partial \xi_s}$$

If the two points are made to coincide, the distinction between the primed and unprimed quantities vanishes, and

$$\overline{\frac{\partial u_i}{\partial x_r} \frac{\partial u_j}{\partial x_s}} = -u^2 \left. \frac{\partial^2 R_{ij}}{\partial \xi_r \partial \xi_s} \right|_{r=0}$$

It follows from Equation (12-26) that the second partial derivative of the correlation tensor at $r = 0$ is given by

$$\left. \frac{\partial^2 R_{ij}}{\partial \xi_r \partial \xi_s} \right|_{r=0} = f''(0) \left[2\delta_{rs} \delta_{ij} - \frac{1}{2} (\delta_{is} \delta_{jr} + \delta_{js} \delta_{ir}) \right],$$

so that all the desired correlations are expressed in terms of $f''(0)$ and a numerical constant. The same method can be applied to higher derivatives.

Triple Correlations

In a manner similar to the correlation coefficient, the correlations between three fluctuating velocities can be considered, two at one point and one at another. This triple correlation may be defined by

$$\frac{\overline{u_i u_j u_k'}}{(\overline{u^2})^{3/2}},$$

or

$$\frac{\overline{u_i' u_j' u_k}}{(\overline{u^2})^{3/2}}.$$

The triple correlations form the components of a tensor of third rank, T_{ijk} . (12-27, 12-28)

Assume for the moment that the line r joining the two points is directed along the x_1 -axis in a homogeneous isotropic turbulence field. After elimination of those correlations which change sign with rotation about the x_1 axis, there remains

$$\overline{u_1 u_1 u_1'} = (\overline{u^2})^{3/2} k(r, t),$$

$$\overline{u_2 u_2 u_1'} = (\overline{u^2})^{3/2} h(r, t),$$

and

$$\overline{u_1 u_2 u_2'} = (\overline{u^2})^{3/2} q(r, t).$$

In a manner analogous to that used in connection with the double correlation tensor, the triple correlation tensor may be shown to be a function of the three scalar correlations, $k(r, t)$, $h(r, t)$, and $q(r, t)$, of the form

$$T_{rst} = \left[k - h - 2q \right] \frac{\xi_r \xi_s \xi_t}{r^3} + \delta_{rs} \frac{\xi_t}{r} h + \delta_{rt} \frac{\xi_s}{r} q + \delta_{st} \frac{\xi_r}{r} q,$$

where ξ_r, ξ_s, ξ_t denote the components of \underline{r} .

As in the case of the correlation R_{11} , the equation of continuity can be used to obtain relations between the three triple correlations, \underline{k} , \underline{h} , and \underline{q} , provided the fluid is incompressible. These relations are given by

$$\underline{q} = -\underline{h} - \frac{1}{2} r \frac{\partial \underline{h}}{\partial r} \quad , \quad (12-28)$$

and

$$\underline{k} = -2\underline{h} \quad . \quad (12-29)$$

Consider the correlation

$$\overline{(u^2)^{3/2}} \underline{k} = \overline{u_1^2 u_1'} \quad .$$

By expansion of u_1' in terms of ξ_1 , the component of \underline{r} in the x_1 direction, \underline{k} , may be shown to be given by

$$\begin{aligned} \overline{(u^2)^{3/2}} \underline{k} = & \overline{u_1^3} + \frac{1}{3} \frac{\overline{\partial u_1^3}}{\partial \xi_1} \xi_1 + \frac{1}{2} \overline{u_1^2} \frac{\overline{\partial^2 u_1}}{\partial \xi_1^2} \xi_1^2 \\ & + \frac{1}{6} \overline{u_1^2} \frac{\overline{\partial^3 u_1}}{\partial \xi_1^3} \xi_1^3 + \dots \quad . \end{aligned}$$

If the x_1 axis is reflected in the x_2, x_3 plane, all terms containing even powers of ξ_1 must vanish since the velocity terms change in sign. Also $\overline{\partial u_1^3 / \partial \xi_1}$ is zero because u_1^3 is zero everywhere. Therefore, the series development for \underline{k} must start with the cubic term,

$$\frac{1}{6} \overline{u_1^2} \frac{\overline{\partial^3 u_1}}{\partial \xi_1^3} \xi_1^3 \quad .$$

The series development in terms of \underline{r} has the same form:

$$\underline{k} = \frac{1}{6} k'''(0)r^3 + \frac{1}{120} k^{(V)}(0)r^5 + \dots \quad .$$

Thus, from Equations (12-28) and (12-29) it follows that

$$\underline{k}(0) = \underline{h}(0) = \underline{q}(0) = 0 \quad .$$

Figure 12-5 shows some experimental measurements of \underline{h} for flow behind a grid at various Reynolds numbers and at various distances downstream. (12-29)

Correlations Between Scalars and Velocities

Consider the correlation between a fluctuating scalar, \underline{p} , at a point, \underline{P} , and a fluctuating velocity, u_1' , at a point, \underline{P}' , denoted by

$$\overline{\underline{p} u_1'}$$

with the line, \underline{r} , joining points, \underline{P} and \underline{P}' . A transformation from the x_i coordinates to the X_r coordinates, where X_1 lies along \underline{r} , yields

$$\overline{\underline{p} v_{r'}} = \overline{\underline{p} u_1'} \ell_{ir} \quad .$$

If the turbulence is isotropic, a rotation of axes about X_1 shows that

$$\overline{p V_2'} = \overline{p V_3'} = 0$$

The correlation, $\overline{p V_1'}$, can be written (12-27) as follows:

$$p V_1' = \sqrt{p^2} \sqrt{u^2} S(r)$$

where $S(r)$ is a scalar function of the distance between the points. In terms of the original coordinates the correlation becomes

$$\overline{p u_i'} = \sqrt{p^2} \sqrt{u^2} S(r) l_{i1} \quad (12-30)$$

If the fluid is incompressible, then

$$\frac{\partial \overline{p u_i'}}{\partial \xi_i} = 0$$

because p does not depend upon the coordinates of the point, P' . A substitution using Equation (12-30) yields

$$\frac{\partial}{\partial \xi_i} [S(r) l_{i1}] = 0$$

Changing from the direction cosines to the components of \underline{r} , (12-28) and introducing the variable

$$\Sigma = \frac{S(r)}{r}$$

there results

$$\Sigma \frac{\partial \xi_i}{\partial \xi_i} + \xi_i \frac{\partial \Sigma}{\partial \xi_i} = 0$$

A contraction followed by an integration gives

$$\Sigma = \frac{C}{r^3}$$

so that

$$S(r) = r \Sigma = \frac{C}{r^2}$$

Since $S(r)$ must be regular at $r = 0$, it follows that

$$C = 0$$

and hence,

$$\overline{p u_i'} = 0$$

Thus, the correlation between a fluctuating scalar at \underline{P} and a fluctuating velocity at P' is equal to zero.

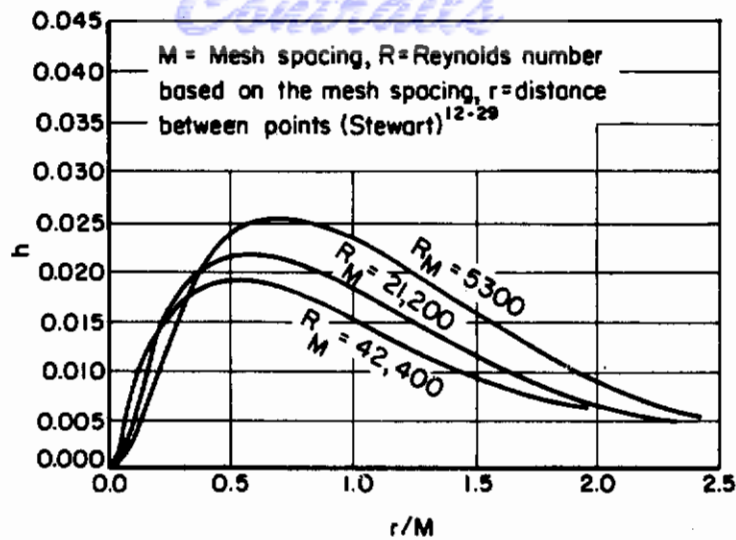


FIGURE 12-5. MEASURED VALUES OF THE TRIPLE CORRELATION COEFFICIENT, h , BEHIND A GRID

The Correlation Between Fluctuating Density and Fluctuating Velocity

By the same method used in the preceding section, the correlation between the fluctuating density ρ , at a point P , and the fluctuating velocity, u_i' , at a second point P' , may be investigated.

The resulting equation takes the form:

$$\frac{\partial \overline{\rho u_i'}}{\partial \xi_i} = \sqrt{\rho^2} \sqrt{V_1'^2} \left[\frac{\partial S(r)}{\partial r} + 2 \frac{S(r)}{r} \right]$$

However, the equation of continuity can no longer be used to reduce this expression, because $\partial u_i' / \partial \xi_i$ is not necessarily zero. However, it may be shown that

$$\overline{\rho u_i} = 0$$

that is, the correlation is zero for $r = 0$, but this result is obtainable by a simple rotation of axes.

The Propagation of the Correlation

The Navier-Stokes equation for the fluctuating motion of incompressible isotropic turbulence can be written from Equation (11-19) as

$$\nu \left(\frac{\partial^2 u_j}{\partial x_1^2} + \frac{\partial^2 u_j}{\partial x_2^2} + \frac{\partial^2 u_j}{\partial x_3^2} \right) = \frac{1}{\rho} \frac{\partial p}{\partial x_j} + u_i \frac{\partial u_j}{\partial x_i} + \frac{\partial u_j}{\partial t}$$

Multiplication of this equation by u'_k , which is independent of the coordinates of the unprimed quantities, followed by a substitution using the equation of continuity yields

$$\nu \delta_{rs} \frac{\partial^2 u_j u'_k}{\partial \xi_r \partial \xi_s} = - \frac{1}{\rho} \frac{\partial}{\partial \xi_j} (\rho u'_k) - \frac{\partial}{\partial \xi_i} (u_i u_j u'_k) + u'_k \frac{\partial u_j}{\partial t}$$

In terms of mean values this result becomes

$$\sqrt{\overline{u^2}} \nu \delta_{rs} \frac{\partial^2 R_{ijk}}{\partial \xi_r \partial \xi_s} = -(\overline{u^2})^{3/2} \frac{\partial T_{ijk}}{\partial \xi_i} + \overline{u'_k} \frac{\partial u_j}{\partial t}$$

Similarly, starting with the equation at the point P', and using the relation, $\overline{u_j u'_i u'_k} = -\overline{u_i u_j u'_k}$, there results,

$$\overline{u_j} \frac{\partial u'_k}{\partial t} + (\overline{u^2})^{3/2} \frac{\partial T_{ikj}}{\partial \xi_i} = \nu \delta_{rs} \overline{u^2} \frac{\partial^2 R_{ijk}}{\partial \xi_r \partial \xi_s}$$

The sum of these two results, expressed in terms of \underline{h} , \underline{f} , and \underline{r} , yields the von Kármán-Howarth relation, (12-27)

$$\frac{\partial \overline{fu^2}}{\partial t} + (\overline{u^2})^{3/2} \left[\frac{8}{r} h + 2 \frac{\partial h}{\partial r} \right] = 2\nu \overline{u^2} \left[\frac{\partial^2 f}{\partial r^2} + \frac{4}{r} \frac{\partial f}{\partial r} \right] \quad (12-31)$$

From this equation, it can be seen that the behavior of \underline{f} , the double correlation, cannot be found without some knowledge of the triple correlation, \underline{h} ; \underline{h} cannot be found without knowing the fourth-order correlation; and a similar result holds for higher order correlations.

The Decay of Isotropic Turbulence

From the power series development of \underline{f} and \underline{h} about the point, P, and from Equation (12-22) it follows that Equation (12-31) can be written as

$$\frac{d\overline{u^2}}{dt} = -\frac{10\nu \overline{u^2}}{\lambda^2} \quad (12-32)$$

This equation was first obtained by von Kármán and Howarth, (12-27) If there is a mean stream velocity, \underline{U} , such that

$$\frac{d}{dt} = U \frac{d}{dx},$$

then

$$U \frac{d\overline{u^2}}{dx} = -10\nu \frac{\overline{u^2}}{\lambda^2}$$

This result corresponds to G. I. Taylor's equation for the decay of turbulence behind a grid.

The decay of turbulence may be approached in another manner, (12-4, 12-19) The turbulent energy per unit volume of the fluid for isotropic turbulence is equal to $\frac{3}{2} \rho \overline{u^2}$ and the rate of dissipation of the turbulent energy is given by

$$\overline{W} = -\frac{3}{2} \rho \frac{d\overline{u^2}}{dt} \quad (12-33)$$

If the fluid is incompressible, the mean rate of energy dissipation is given by the time average of Equation (11-21) so that

$$\overline{W} = \mu \left[\overline{\left(\frac{\partial u_r}{\partial x_s} \right)^2} + \overline{\frac{\partial u_r}{\partial x_s} \frac{\partial u_s}{\partial x_r}} \right]$$

From Equations (12-24) and (12-25) it follows that

$$\overline{W} = -15\mu \overline{u^2} f''(0) ,$$

or, in terms of the microscale from Equation (12-27), the rate of decay of isotropic turbulence is given by

$$\overline{W} = 15\mu \frac{\overline{u^2}}{\lambda^2} . \quad (12-34)$$

This equation combined with Equation (12-33) yields a result which is identical to the von Kármán-Howarth relation.

Some Properties of the Microscale

From dimensional reasoning, the rate of dissipation of energy in turbulence should be proportional to the quantity, $\rho(\sqrt{\overline{u^2}})^3/L$, where L is a dimension defining the scale of the turbulence. If L is chosen to be the Eulerian scale, l_2 , then

$$\overline{W} = 15 \frac{\mu \overline{u^2}}{\lambda^2} \propto \frac{\rho(\sqrt{\overline{u^2}})^3}{l_2} , \quad (12-36)$$

for which the relation

$$l_2 \frac{\lambda^2}{2} = C \frac{\nu}{l_2 \sqrt{\overline{u^2}}} ,$$

is obtained where C is constant for a particular system. The substitution of a Reynolds number of turbulence, defined by

$$N_o = \frac{l_2 \sqrt{\overline{u^2}}}{\nu} ,$$

gives

$$\frac{\lambda}{l_2} = \sqrt{\frac{C}{N_o}} . \quad (12-37)$$

This equation cannot be expected to hold at very low values of N_o , since λ would then increase without limit. Although correlation curves can be drawn for which λ is greater than l_2 , such curves have not been obtained experimentally. However, Taylor⁽¹²⁻³⁰⁾ reported one measurement of λ/l_2 equal to 0.86.

The Decay of the Scale and Intensity of Turbulence

From the relations given in Equation (12-36) and in Equation (12-33) there is obtained,

$$-\frac{d\sqrt{\overline{u^2}}}{dt} = A \frac{\overline{u^2}}{l_2} ,$$

where A is constant. The assumption that the turbulence is carried by a stream of uniform velocity, U , with $\frac{d}{dt}$ replaceable by $U \frac{d}{dx}$ implies

Continued

$$\frac{d}{dx} \left(\frac{U}{\sqrt{u^2}} \right) = \frac{A}{\ell_2} \quad (12-38)$$

The quantity $\sqrt{u^2}/U$ is called the intensity of turbulence.

Integration of Equation (12-38) shows that

$$\frac{U}{\sqrt{u^2}} - \frac{U}{\sqrt{u_0^2}} = A \int_{x_0}^x \frac{1}{\ell_2} dx \quad (12-39)$$

Hence, it is necessary to know the law of decay of the scale of turbulence before the decay of the intensity can be found. Taylor assumed that ℓ_2 was a constant, but when experimental data became available, it was found that the scale increased as the turbulence decayed. Taylor then tried a linear law of decay for the scale, but the resulting form of Equation (12-39) did not agree well with experimental data.

A relation between the scale and the distance, $x - x_0$, can be obtained from dimensional analysis. If it is assumed that the rates of decay of $\sqrt{u^2}$ and ℓ_2 depend only upon the values of $\sqrt{u^2}$ and ℓ_2 , then it follows that (12-4, 12-31)

$$\frac{d}{dx} \left(\frac{U}{\sqrt{u^2}} \right) = \frac{A}{\ell_2} \quad (12-40)$$

and

$$\frac{d\ell_2}{dx} = B \frac{\sqrt{u^2}}{U} \quad (12-41)$$

where $\frac{d}{dt}$ has been replaced by $U \frac{d}{dx}$.

Equation (12-40) is identical with Equation (12-38). This is expected since both equations are based on the same set of assumptions. However, Equation (12-41) is a new relation.

If Equation (12-40) is differentiated and ℓ_2 eliminated by use of the original equation, there results

$$\frac{U}{\sqrt{u^2}} \frac{d^2}{dx^2} \left(\frac{U}{\sqrt{u^2}} \right) + \frac{B}{A} \left[\frac{d}{dx} \frac{U}{\sqrt{u^2}} \right]^2 = 0$$

where the elimination of $d\ell_2/dx$ has been accomplished by the use of Equation (12-41). The first and second integrals of this equation are given by

$$\frac{d}{dx} \left(\frac{U}{\sqrt{u^2}} \right) = C_1 \left(\frac{U}{\sqrt{u^2}} \right)^{-\frac{B}{A}} \quad (12-42)$$

and

$$\frac{U}{\sqrt{u^2}} = \left[\left(\frac{U}{\sqrt{u_0^2}} \right)^{\frac{A+B}{A}} + C_1 \frac{A+B}{A} (x - x_0) \right]^{\frac{A+B}{A}} \quad (12-43)$$

respectively.

Equations (12-40) and (12-42) may be used to eliminate C_1 in Equation (12-43) so that

$$\frac{\sqrt{u_0^2}}{\sqrt{u^2}} = \left[1 + \frac{\sqrt{u_0^2} (A + B)}{\ell_{20} U} (x - x_0) \right] \frac{A}{A + B} \quad (12-44)$$

If this equation is differentiated and substituted into Equation (12-40), there results for the decay of the scale,

$$\frac{\ell_2}{\ell_{20}} = \left[1 + \frac{\sqrt{u_0^2} (A + B)}{\ell_{20} U} (x - x_0) \right] \frac{A}{A + B} \quad (12-45)$$

From Equations (12-40) and (12-32), it is possible to show that the constant, C , in Equation (12-37) is given by

$$C = \frac{5}{A} ,$$

so that

$$\frac{\lambda}{\ell_2} = \sqrt{\frac{5}{A N_0}}$$

This result is free from the arithmetic error in Dryden's derivation. (12-4)

Equations (12-40) and (12-41) can also be obtained by expressing the von Kármán-Howarth relation in terms of the variable, $\eta = r/\ell_2$, to give

$$\begin{aligned} - \frac{1}{\sqrt{u^2}} \frac{d\ell_2}{dt} \eta \frac{df}{d\eta} + \frac{\ell_2}{(u^2)^{3/2}} \frac{du^2}{dt} f + 2 \left(\frac{dh}{d\eta} + 4 \frac{h}{\eta} \right) \\ = \frac{2}{N_0} \left(\frac{d^2 f}{d\eta^2} + \frac{4}{\eta} \frac{df}{d\eta} \right) \end{aligned} \quad (12-46)$$

Dryden⁽¹²⁻⁴⁾ reasoned from Equation (12-46) that if the correlations, f and h , retain the same form for all times, then the coefficients in this equation must be constants, since the coefficient of the third term is constant and f and h are assumed to be functions of η alone. Hence, it follows that

$$\frac{d\ell_2}{dt} = B \sqrt{u^2} ,$$

$$\frac{1}{2} \frac{du^2}{dt} = -A \frac{(u^2)^{3/2}}{\ell_2}$$

and

$$\frac{\ell_2 \sqrt{u^2}}{\nu} = N_0 .$$

The first two of these equations correspond to Equations (12-40) and (12-41). The third relation requires that the product, $\ell_2 \sqrt{u^2}$, be constant. Therefore, A and B must be equal.

Von Kármán, making the additional assumption that N_0 is so large that the third term of Equation (12-46) is negligible, eliminated u^2 from the first two of these equations to obtain (12-27)

$$l_2 \frac{d^2 l_2}{dt^2} = - \frac{5}{\alpha\beta} \left(\frac{dl}{dt} \right)^2$$

Von Kármán's solution to this equation contains an algebraic error. When corrected, his results become

$$l_2 = l_{20} \left(\frac{t}{t_0} \right)^{\frac{\alpha\beta}{5 + \alpha\beta}}, \quad (12-47)$$

$$\sqrt{u^2} = \sqrt{u_0^2} \left(\frac{t}{t_0} \right)^{-\frac{5}{5 + \alpha\beta}}, \quad (12-48)$$

and

$$\lambda^2 = (5 + \alpha\beta) \nu t, \quad (12-49)$$

where $\alpha = 5/A$ and $\beta = B$.

If $\alpha\beta = 5$, then von Kármán's solution corresponds to that obtained by Dryden.

A reference dimension may be introduced into Equations (12-44) and (12-45) or Equations (12-47) and (12-48). Von Kármán found that if M/d , where M is the mesh size of the turbulence generating grid and d is the bar diameter, is not too small, then the use of the bar diameter, d , results in a single equation for all grids. (12-32) Dryden (12-4) evaluated Equations (12-44) and (12-45) for his data and found that

$$\left(\frac{U}{\sqrt{u^2}} \right)^2 = 400 \left[1 + 0.04 \left(\frac{x}{d} - 80 \right) \right], \quad (12-50)$$

$$\left(\frac{l_2}{d} \right)^2 = 0.264 \left[1 + 0.04 \left(\frac{x}{d} - 80 \right) \right], \quad (12-51)$$

where $A = B = 0.2056$. These equations fit his data with fair accuracy, but do not fit the data obtained by others. A possible explanation of this discrepancy is the effect of free stream turbulence in the various wind tunnels. (12-4)

Figure 12-6 includes a plot of Equation (12-50).

Figure 12-7 includes a plot of Equation (12-51).

Figure 12-8 and 12-9 show the decay of λ . Note that one set of data follows the relation $\lambda^2 \propto \nu t$, while the other set does not.

Von Kármán also considered self-preserving correlations in which f is a function of the variable, $\chi = r/\sqrt{\nu t}$, alone. With this assumption,

$$\frac{\partial^2 f}{\partial r^2} = \frac{\partial}{\partial \chi} \left(\frac{1}{\sqrt{\nu t}} \frac{\partial f}{\partial \chi} \right) \frac{\partial \chi}{\partial r},$$

$$\frac{\partial^2 f}{\partial r^2} = \frac{1}{\nu t} \frac{\partial^2 f}{\partial \chi^2} \quad (12-52)$$

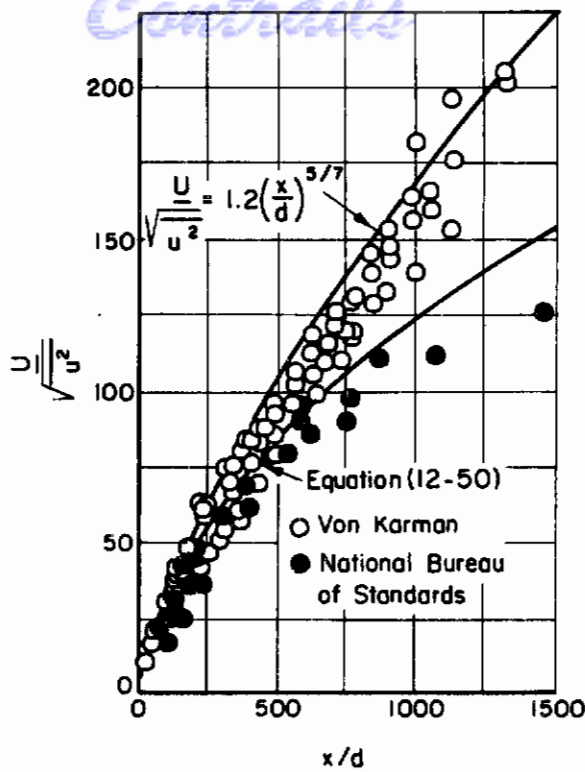


FIGURE 12-6. THE DECAY OF TURBULENT INTENSITY BEHIND A GRID

Dryden 12-4

An evaluation of Equation (12-52) at r equals zero followed by a substitution into Equation (12-23) for

$$\frac{1}{\lambda^2} = - \left(\frac{\partial^2 f}{\partial r^2} \right)_0$$

yields

$$\frac{d\overline{u^2}}{dt} = - 10 \frac{\overline{u^2}}{t} a$$

where

$$a = - \left(\frac{\partial^2 f}{\partial \chi^2} \right)_0$$

This equation may be integrated directly to yield

$$\frac{\sqrt{\overline{u^2}}}{\sqrt{\overline{u_0^2}}} = \left(\frac{t}{t_0} \right)^{-5a}$$

Note that if

$$a = \frac{1}{5 + \alpha\beta} = \frac{A}{5(A + B)}$$

this equation corresponds to Equation (12-48). With a different choice of the arbitrary constants this result corresponds to Equation (12-44).

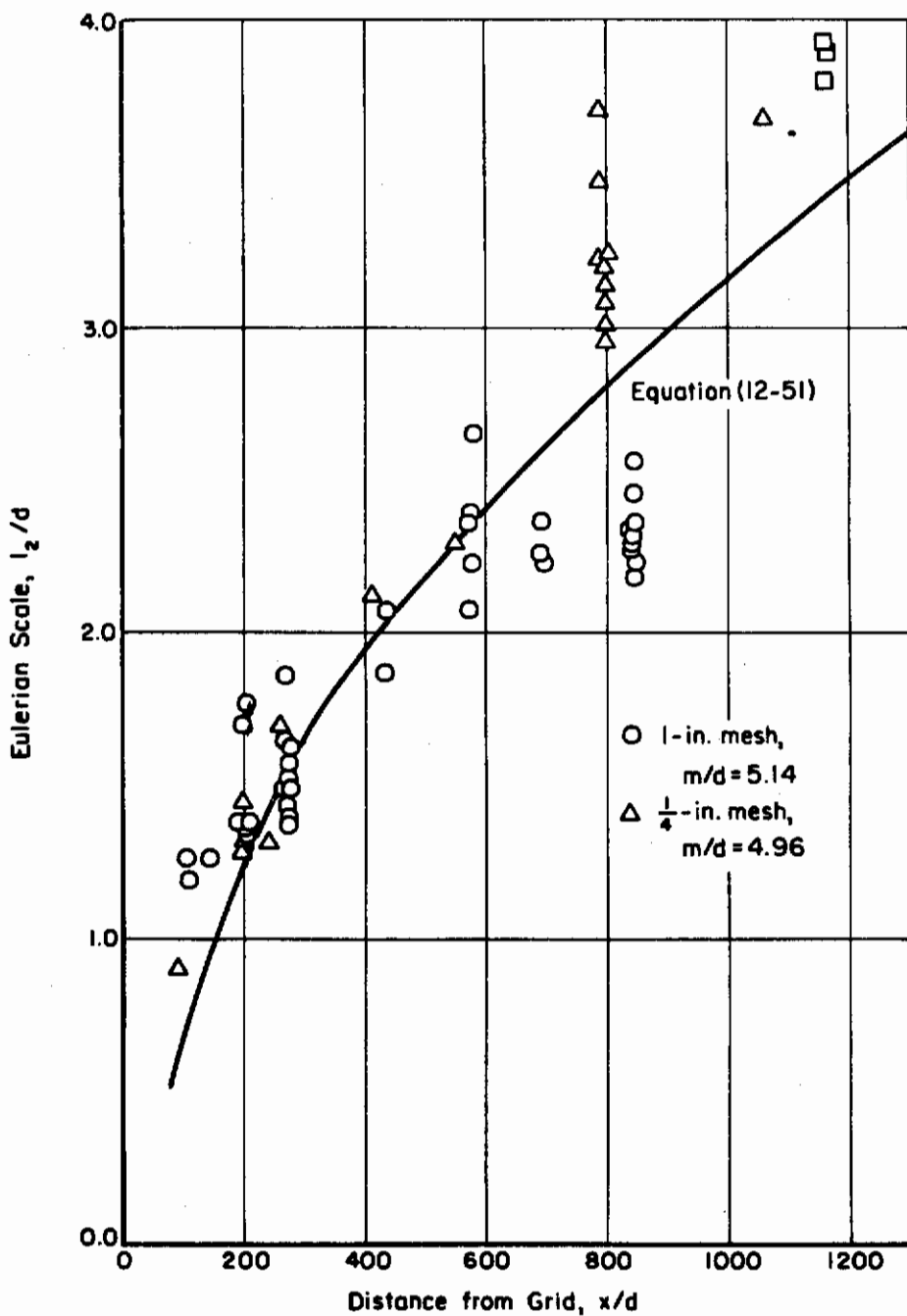


FIGURE 12-7. THE DECAY OF THE TURBULENT SCALE

Dryden, Schubauer, and Skramstad(12-33)

From Equation (12-52) it follows that

$$\left(\frac{\partial^2 f}{\partial x^2}\right)_0 = \frac{1}{\nu t} \left(\frac{\partial^2 f}{\partial X^2}\right) = \frac{a}{\nu t}$$

$$\lambda^2 = \frac{1}{a} \nu t$$

This equation is identical with Equation (12-49) if

$$a = \frac{1}{5 + \alpha\beta}$$

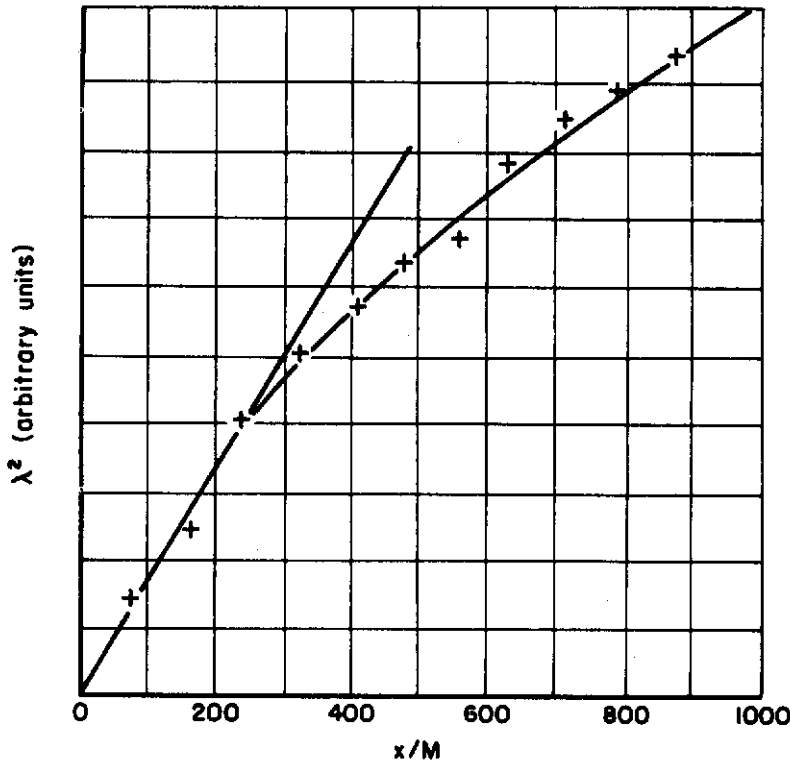


FIGURE 12-8. DECAY OF THE MICROSCALE, λ

Lin(12-34)

The identity of the equations obtained when assuming either $f = f(r/\ell_2)$ or $f = f(r/\nu t)$ suggests that $\ell_2 \propto \nu t$. If Dryden's result that $A = B$ is general, then

$$\frac{\ell_2}{\ell_{20}} = \left(\frac{t}{t_0} \right)^{1/2}$$

and

$$\ell_2 \propto \sqrt{\nu t}$$

Hence, the two assumptions are equivalent and a single law of decay is obtained for turbulence having self-preserving correlation coefficients. For this law, both the scale and microscale increase as the square root of the time, while the fluctuating velocity decreases as the reciprocal of the square root of time. This type of turbulence is characterized by a constant value of the product, $\ell_2 \sqrt{u^2}$.

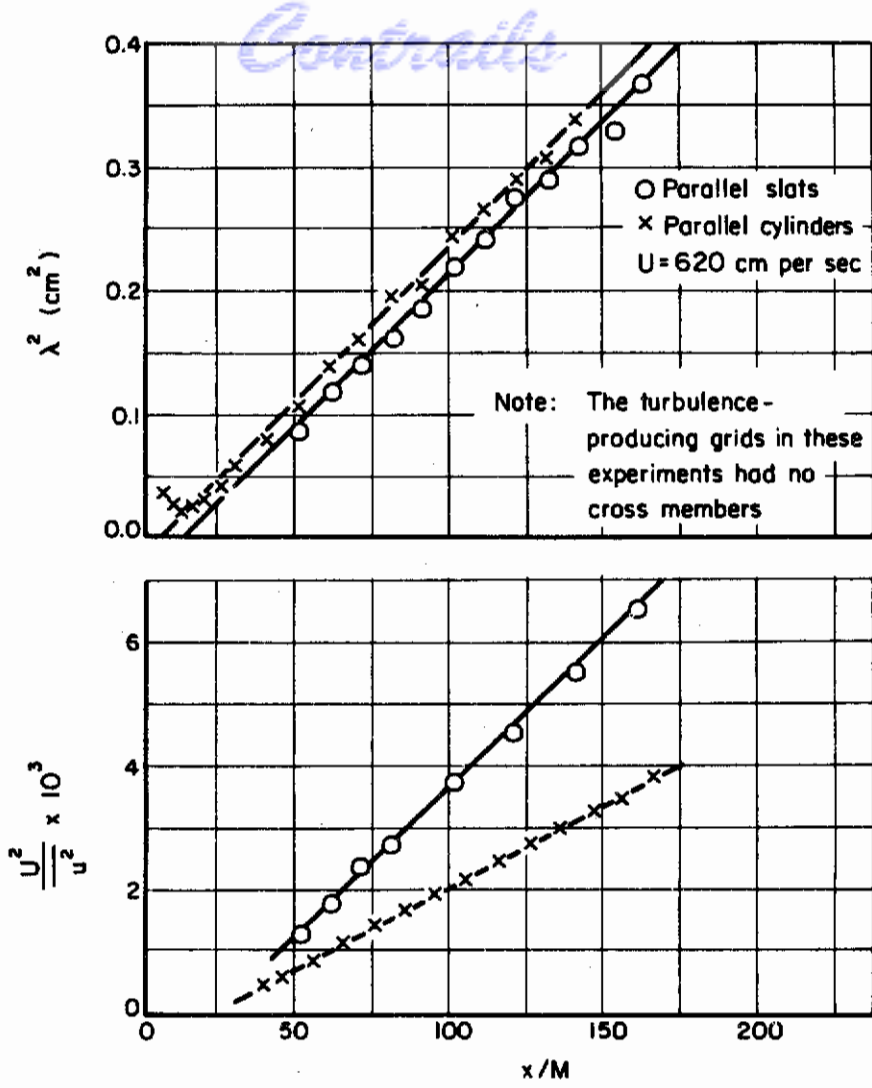


FIGURE 12-9. DECAY OF TURBULENCE BEHIND GRIDS OF DIFFERING SHAPES

Stewart and Townsend(12-35)

It is interesting to note that the assumption of a simple power law of decay in which $\overline{u^2}$ decays as t^{-n} yields the results:(12-36)

$$\frac{\overline{u^2}}{u_0^2} \propto \left(\frac{t}{t_0}\right)^{-n}$$

and

$$\frac{\lambda}{\lambda_0} \propto \left(\frac{t}{t_0}\right)^{1/2}$$

For self-preserving turbulence, the scale and microscale must be proportional so that

$$l_2 \propto \sqrt{vt}$$

and the two cases of self-preserving turbulence are seen to be identical.

If the von Kármán-Howarth relation, Equation (12-31), is multiplied by r^m and integrated by parts between the limits of 0 and ∞ , then

$$\begin{aligned} \frac{d}{dt} \overline{u^2} \int_0^{\infty} f r^m dr &= -2 (\overline{u^2})^{3/2} \left[h r^m \right]_0^{\infty} \\ &+ (2m - 8) (\overline{u^2})^{3/2} \int_0^{\infty} h r^{m-1} dr \\ &+ 2 \nu \overline{u^2} \left[\frac{\partial f}{\partial r} r^m \right]_0^{\infty} \\ &- 2 \nu \overline{u^2} (m-4) \int_0^{\infty} \frac{\partial f}{\partial r} r^{m-1} dr \end{aligned} \quad (12-53)$$

If m is equal to four, and if $h r^4$ and $(\partial f / \partial r) r^4$ tend to zero as $r \rightarrow \infty$, then

$$\overline{u^2} \int_0^{\infty} f r^4 dr = \Lambda = \text{constant},$$

where Λ is the Loitsianskii invariant and remains constant throughout the process of decay. (12-28)

The assumption that $(\partial f / \partial r) r^4$ and $h r^4$ converge to zero as $r \rightarrow \infty$ seems physically sound, but experimental measurements of the behavior of f and h at large values of r are too crude to establish this assumption. (12-29, 12-37)

Batchelor (12-36) has shown that if experimental evidence concerning the signs of f and k are introduced into Equation (12-53), then

$$\frac{\partial}{\partial t} (\overline{u^2} \int_0^{\infty} f r^m dr) \begin{cases} > 0 \text{ if } m > 4, \\ = 0 \text{ if } m = 4, \\ < 0 \text{ if } m = 3, 2, 1, 0. \end{cases}$$

A length, L_* , which may be considered as a scale of turbulence, may be defined as

$$L_*^5 = \int_0^{\infty} f r^4 dr,$$

with the result that

$$\overline{u^2} L_*^5 = \Lambda$$

This relation was first obtained by L. G. Loitsianskii. (12-28)

For self-preserving turbulence, all lengths based upon correlation coefficients must be proportional, and therefore,

$$\overline{u^2} l_2^5 = \text{constant} \quad (12-54)$$

This is in contradiction with the previous result,

$$\overline{u^2} \ell_2^2 = \text{constant} ,$$

unless

$$N_0 = 0, t = \infty .$$

Thus, completely self-preserving turbulence is possible only at very large values of the decay time. Batchelor has made an unsuccessful attempt to show that \underline{f} does indeed become self-preserving at large values of t .

Dryden's data for a one-inch grid(12-33) fit Equation (12-54) better than the constant Reynolds number relation derived from Equations (12-50) and (12-51).

It may be noted that neither Dryden's solution to the decay problem, Equations (12-44) and (12-45), nor von Kármán's solution, Equations (12-47), (12-48), and (12-49) are capable of simultaneously satisfying the Loitsianskii invariant and the relation, $\ell_2 \sim \nu t$, demanded by the assumption of self-preserving correlations. It is known, however, that the Loitsianskii invariant depends largely on the largest eddies present, and during the time scale involved here, these eddies scarcely decay at all.

Partially Self-Preserving Turbulence

Experimentally, it has been found that the expansion of \underline{f} in terms of r/λ is independent of t to terms of fourth degree, and that $k(r/\lambda)$ is independent of t to the term of third degree. (12-38) Hence, \underline{f} and \underline{k} must be self-preserving for small values of r/λ .

An apparent consequence of the self-preservation of \underline{f} near the origin is that the microscale, which depends only upon the behavior of \underline{f} at the origin, must follow the decay law derived from the assumption of completely self-preserving turbulence, namely,

$$\lambda \propto \sqrt{\nu t} .$$

From this, Batchelor's power law of decay,

$$\overline{u^2} \propto t^{-n} ,$$

may be derived by integrating the expression for energy decay given by Equation (12-32). Unfortunately, the scales, ℓ_2 , and L_* , cannot be expected to be proportional to λ in the case of partially self-preserving turbulence. Therefore, the Loitsianskii invariant cannot be used to determine the value of the exponent \underline{n} ; in fact, the invariant cannot be extended to any scale other than L_* . However, if λ maintains exactly the same form as it has in completely self-preserving turbulence, then the solution for $\overline{u^2}$ is independent of whether or not the turbulence is self-preserving. The Loitsianskii invariant then shows that the correct value of \underline{n} is 5/2, so that

$$\lambda^2 = 4 \nu t, \overline{u^2} \propto t^{-2.5}, L_* \propto t^{-1/2} ,$$

and ℓ_2 asymptotically approaches $t^{-1/2}$ as $t \rightarrow \infty$, provided the turbulence becomes self-preserving at large t . Unfortunately, the variation of $\overline{u^2}$ found experimentally does not agree at all with this scheme. The exponent, \underline{n} , is found to lie much closer to 1.5 than 2.5. This may be a result of nonequilibrium conditions among the eddies large enough to contribute to the Loitsianskii invariant. The solution which most closely fits this value is von Kármán's Equation (12-48), with $\alpha\beta = 2$, as required by the Loitsianskii invariant. This gives the value 1.43 to \underline{n} . The law of decay is then given by

$$\overline{u^2} \propto t^{-10/7}, \lambda^2 \approx 7 \nu t, L_* \propto t^{2/7} .$$

As noted above, however, this solution does not make L_* or l_2 proportional to λ , even though the turbulence is assumed self-preserving in the derivation of these equations.

Figure 12-6 includes a plot of the above relation for the decay of $\overline{u^2}$, and shows that the decay of the scale does not fit the available data. Although this solution was originally obtained for the case of turbulence characterized by a large Reynolds number, the modification above might be expected to hold over a somewhat greater range. The scale, l_2 , will vary in some undetermined manner, probably approximating the variation of L_* .

Turbulent Diffusion

The mixing length theories of turbulence are basically an attempt to describe the diffusive nature of turbulence. A particle of fluid, an eddy, is pictured to move in a random manner through the bulk of the fluid and thus carry its properties to other sections of the fluid. The defects in this picture have been pointed out in preceding sections. A theory of turbulent diffusion free from the objections raised against the mixing length theories was introduced by G. I. Taylor(12-39). Consider the integral,

$$\int_0^{t_1} \overline{u_{t_1} u_{t_2}} dt_2 \quad ,$$

where u_{t_1} is the velocity in a given direction of a particle of fluid at time t_1 and u_{t_2} is its velocity at time t_2 . The quantity $\overline{u_{t_1} u_{t_2}}$ is the auto-correlation of the velocity, u , and an auto-correlation coefficient may be defined as

$$R_e = \frac{\overline{u_t u_{t+\theta}}}{\sqrt{\overline{u_t^2}} \sqrt{\overline{u_{t+\theta}^2}}} \quad (12-55)$$

If the turbulence is homogeneous and stationary in time, then

$$\overline{u_t^2} = \overline{u_{t+\theta}^2} = \overline{u^2} \quad ,$$

and the integral may be written as

$$\int_0^{t_1} \overline{u_{t_1} u_{t_2}} dt_2 = \overline{u^2} \int_0^{t_1} R_{t_2-t_1} dt_2 \quad (12-56)$$

The velocity, $u_t + \theta$, can be expanded in a series about t , multiplied by u_t , and averaged to give

$$\overline{u_t u_{t+\theta}} = \overline{u^2} R_\theta = \overline{u^2} + u_t \frac{du_t}{d\theta} \theta + u_t \frac{d^2 u_t}{d\theta^2} \frac{\theta^2}{2!} + \dots \quad (12-57)$$

If it is assumed that the mean squares of all derivatives of u_t with respect to time have constant values,

$$\overline{\left(\frac{d^n u_t}{d\theta^n} \right)^2} = \text{const.} \quad ,$$

then it may be shown that (12-39, 12-40)

$$u_t \frac{d^{2n+1}}{d\theta^{2n+1}} (u_t) = 0$$

Consequently, (12-57) may be written as

$$\overline{u^2} R_\theta = \overline{u_t^2} + u_t \frac{d^2 u_t}{d\theta^2} \frac{\theta^2}{2!} + u_t \frac{d^4 u_t}{d\theta^4} \frac{\theta^4}{4!} + \dots$$

which shows that R_θ is an even function of θ .

Because R_θ is even and u_{t_1} is independent of t_2 , it follows that Equation (12-56) can be written as

$$\int_0^{t_1} \overline{u_{t_1} u_{t_2}} dt_2 = u_{t_1} \int_0^{t_1} u_{t_2} dt_2 \quad (12-58)$$

The integral on the right is obviously the distance, \underline{X} , traveled by the particle of fluid in time, t_1 , so that

$$\int_0^{t_1} \overline{u_{t_1} u_{t_2}} dt_2 = \overline{u_{t_1} X}$$

or

$$\int_0^{t_1} \overline{u_{t_1} u_{t_2}} dt_2 = \frac{1}{2} \frac{d}{dt} (\overline{X^2})$$

A second integration and substitution yields

$$\overline{X^2} = 2 \overline{u^2} \int_0^T \int_0^{t_1} R_\theta d\theta dt_1 \quad (12-59)$$

The auto-correlation coefficient, R_θ , must be equal to one when θ equals zero. If time intervals so short that R_θ does not differ appreciably from one are considered, then

$$\sqrt{\overline{X^2}} = \sqrt{\overline{u^2}} T \quad (12-60)$$

and the diffusing quantity is seen to spread at a rate proportional to the root mean square fluctuating velocity, $\sqrt{\overline{u^2}}$. If R_θ falls toward zero sufficiently rapidly as the time separation increases, a length, ℓ_1 , may be defined as

$$\ell_1 = \sqrt{\overline{u^2}} \int_0^\infty R_\theta d\theta$$

and the spread of the diffusing quantity will be given by

$$\overline{X^2} = 2 \ell_1 \sqrt{\overline{u^2}} T$$

In molecular diffusion, the mean square displacement of a molecule is given by

$$\overline{X^2} = 2 DT$$

where \underline{D} is the diffusion coefficient. Hence, for large values of the time interval, turbulent diffusion in a homogeneous stationary field may be described by the same equations as molecular diffusion, with a diffusion coefficient equal to $\ell_1 \sqrt{u^2}$. Further discussions are given by Batchelor(12-41), Uberoi(12-42), and others.

The length, ℓ_1 , may be considered as a measure of the scale of turbulence when the flow is described in the Lagrangian manner. Its role in turbulent diffusion is similar to that of the mean free path in molecular diffusion. In this respect, it is somewhat similar to the mixing length. It differs from the mixing length in that the concept of mixing, a molecular process, does not arise in its definition.

It might be expected that the Lagrangian scale, ℓ_1 , would be related in some manner to the Eulerian scale, ℓ_2 , defined by the equation,

$$\ell_2 = \int_0^{\infty} R_y dy \quad ,$$

where the correlation, R_y , is the same as g , given in Equation (12-20). In particular, where the turbulence is expected to have a definite scale, as in the turbulence generated by a grid in an air stream, both ℓ_1 and ℓ_2 might be supposed to be some definite fraction of the grid mesh or bar diameter. (12-23) For turbulence behind such grids, G. I. Taylor found ℓ_2 to be approximately twice ℓ_1 (12-23). However, no general relation is known connecting the two scales and more recent measurements fail to confirm Taylor's findings. (12-42)

Kolmogoroff's Theory of Local Isotropy

Much of the difficulty encountered in attempts to determine a law of decay for the turbulent energy and a law of propagation of the correlation is due to the fact that most of the turbulent energy is contained in the large eddies while dissipation of the energy takes place in the smallest eddies.

Two methods for separating the effects of the various sizes of eddies have been devised. The first and most obvious method consists of the introduction of a spectral function expressing the fraction of energy contained in the eddies of each size. This approach was pioneered by Taylor. (12-30) A second interesting approach was suggested by Kolmogoroff, (12-43, 12-44) and will be considered first.

The essential point of Kolmogoroff's theory is the use of velocity differences, or relative velocities, as the relevant quantities rather than the velocities themselves. If the reference velocity is taken at a point \underline{P} in the four-dimensional space (x_1, x_2, x_3, t) and if P' is some other point, then a typical velocity difference will be

$$w_i = u_i(P') - u_i(P) \quad .$$

Kolmogoroff then restricts the two points to lie in a domain, \underline{G} . If nonzero averages formed from the w_i 's are independent of the reference point \underline{P} , the turbulence is called locally homogeneous in the domain \underline{G} . If in addition, the nonzero averages formed from w_i 's are independent of rotations and reflections of the coordinate axes, the turbulence is called locally isotropic within the domain \underline{G} . Note that since \underline{G} is a four-dimensional domain, local isotropy requires that the turbulence be steady in time, in contrast to the ordinary isotropy of Taylor.

Kolmogoroff argues for the existence of locally isotropic turbulence in the following manner. The turbulence consists of eddies or disturbances ranging in scale from a length characteristic of the mean flow to some much smaller length, at which scale the flow is laminar. This may be viewed as a series of flows, each carrying a disturbance of the next smaller order of scale. Thus, if the Reynolds number of any of these flows is sufficiently high, the flow is unstable and incites

disturbances of the next smaller scale, the process continuing until the Reynolds number becomes sufficiently small for the flow to be stable. At all scales smaller than this, the flow is laminar.

The largest eddies obtain their energy originally from the mean flow, and therefore are subjected to nonisotropic influences. It might be suspected, however, that these nonisotropic influences would gradually be lost as the turbulent energy is passed to successively smaller eddies. It would then be possible to define the spatial extent of \underline{G} so that the velocity differences between any two points in \underline{G} exhibit isotropy. The requirement of steadiness may be met by limiting the temporal extent of \underline{G} . If the flow is assumed to change appreciably in a time interval, \underline{T} , then clearly the temporal extent of \underline{G} must be less than \underline{T} . It seems reasonable to assume that the characteristic period of an eddy decreases with size of eddy. Hence, the smaller eddies will undergo a great many periods during the interval \underline{T} , and their motion will appear approximately steady for time intervals considerably smaller than \underline{T} . Thus, there are two requirements on the extent of \underline{G} : (1) that it be small enough for the w_i 's to exhibit isotropy, and (2) that it be small enough for the period of the largest eddies contained in \underline{G} to be considerably smaller than \underline{T} . The two conditions do not appear to be related, hence the condition giving the smaller dimension is determinate. Batchelor has pointed out that if the unsteadiness is entirely due to the decay of the turbulence, the period, \underline{T} , will be of the order ℓ/v , where ℓ and v are a length and velocity characteristic of the turbulence. Since it is the largest eddies which contribute most to the turbulent flow, this time will be of the order of the period of the largest eddies. (12-45)

Experimental evidence and the many relations derived between the microscale and the integral scale suggest that the effect of increasing the Reynolds number of the mean flow is to produce smaller eddies, while leaving the larger eddies unchanged in scale. Therefore, as the Reynolds number of the mean flow increases, the eddies responsible for the viscous dissipation of energy become smaller, and the characteristic period of eddies of a given size decreases. This suggests that local isotropy is most likely to exist at high Reynolds numbers, since otherwise there may be no eddies small enough to be contained in \underline{G} .

Correlation in Locally Isotropic Turbulence

In locally isotropic turbulence, the velocity correlations are formed from the velocity differences, w_i . The typical double correlation is given by

$$\overline{w_i' w_i''} = [u(P') - u(P)] [u(P'') - u(P)]$$

If the turbulence is isotropic in the customary sense, these correlations may be expressed in terms of the usual correlations. The above double correlation can be expressed in terms of correlations involving only two points each, as shown by

$$\begin{aligned} \overline{w_i' w_j''} + \overline{w_i'' w_j'} &= \overline{(u_i' - u_i)(u_j'' - u_j)} + \overline{(u_i'' - u_i)(u_j' - u_j)} \\ &= \overline{u_i' u_j'' - u_i' u_j - u_i u_j'' + u_i u_j} \\ &\quad + \overline{u_i'' u_j' - u_i'' u_j - u_i u_j' + u_i u_j} \end{aligned}$$

By rearranging the terms and making use of the linear nature of the averaging operation (12-2) and spatial homogeneity, there results

$$\overline{w_i' w_j''} + \overline{w_i'' w_j'} = \overline{w_i' w_j'} + \overline{w_i'' w_j''} - \overline{w_i''' w_j'''} ,$$

where $w_k''' = u_k'' - u_k'$.

If the correlations, $\overline{w_i' w_j''}$, are symmetrical in the indices, then

$$\overline{w_i' w_j''} = 1/2 (\overline{w_i' w_j'} + \overline{w_i'' w_j''} - \overline{w_i''' w_j'''}) ,$$

which is the required result. If the turbulence is isotropic in the usual sense, then $\overline{u_i' u_j'} = \overline{u_i u_j'}$, etc. and the two correlations may be identified term by term. However, Batchelor has given a general proof for the case where the fluid is incompressible. (12-45)

As in the case of ordinary isotropy, the second-order correlations may be expressed in a form analogous to Equation (12-21):

$$\overline{w_i' w_j'} = \frac{\xi_i \xi_j}{r^2} B_{dd}(r) - B_{nn}(r) + \delta_{ij} B_{nn}(r) \quad ,$$

where B_{dd} and B_{nn} are the scalar correlations between the relative velocity components parallel and normal to the line joining the two points. The equation of continuity also yields a relation between B_{dd} and B_{nn} :

$$B_{dd} - B_{nn} = -1/2 r \partial B_{dd} / \partial r \quad .$$

It should be noted, however, that in contrast to the functions, f and g , B_{dd} and B_{nn} are zero at r equal zero.

The third-order correlation in locally isotropic turbulences may be shown to be expressible in terms of a single scalar,

$$B_{ddd}(r) = \overline{(u_d' - u_d)^3} \quad .$$

When the turbulence is isotropic in the ordinary sense, the two sets of correlations are related by the equations:

$$\begin{aligned} B_{dd} &= 2 \overline{u^2} [1 - f] \quad , \\ B_{nn} &= 2 \overline{u^2} [1 - g] \quad , \\ B_{ddd} &= 6 (\overline{u^2})^{3/2} k \quad . \end{aligned} \quad (12-61)$$

Similarity Hypotheses in Locally Isotropic Turbulence

In order to proceed further, Kolmogoroff proposed two similarity hypotheses, which are mathematical expressions of the physical mechanism suggested by his theory. Kolmogoroff's first hypothesis is that in locally isotropic turbulence, the statistical properties are determined solely by the energy dissipation per unit mass, ϵ , and the kinematic viscosity, ν .

This hypothesis is justified by the consideration of the energy transfer through the successive scales of eddies. At the largest scale, where the Reynolds number is high, the energy dissipated by viscosity is negligible, hence these eddies must pass on to the next smaller scale an amount of energy, ϵ . Otherwise, there would be an accumulation or deficit of energy in some scale as the decay progressed. Therefore, the characteristics of the largest eddies are determined entirely by ϵ . The only additional parameter required to determine the characteristics of the smaller eddies is the viscosity, ν .

Thus, if the correlations are functions of r , the distance separating the two points, then they must also be functions of r/η , where η is a length formed from ϵ and ν , given by

$$\eta = \left(\frac{\nu^3}{\epsilon} \right)^{1/4} \quad .$$

The only physical length with which η may be reasonably identified is the scale of the eddies responsible for the dissipation. Similarly, the characteristic velocity formed from ϵ and ν , $(\nu\epsilon)^{1/4}$, must be identified with the characteristic velocity of the smallest eddies.

From the first hypothesis, the second-order correlation, $B_{dd}(r)$, must have the form

$$B_{dd}(r) = (\nu\epsilon)^{1/2} \beta_{dd}(r/\eta) ,$$

where β_{dd} is a universal function, and similarly,

$$B_{ddd}(r) = (\nu\epsilon)^{3/4} \beta_{ddd}(r/\eta) .$$

Because β_{dd} must exhibit the same dependence on r as does B_{dd} , it follows that β_{dd} is an even function of r and equals zero at $r = 0$. Hence, for values of r small compared with η ,

$$B_{dd}(r) \propto (\nu\epsilon)^{1/2} (r/\eta)^2 .$$

Kolmogoroff's second hypothesis is that if the spatial separations of the three points are large compared to η , the statistical properties are dependent only on ϵ . This hypothesis is justified by the previous discussion since the large eddies determine the statistical properties at large values of r .

The universal functions, β_{dd} and β_{ddd} , must therefore have a functional dependence on r such that for large values of r the correlations are independent of ν . Thus

$$\beta_{dd}(r/\eta) = C(r/\eta)^{2/3} ,$$

where C is a constant, and

$$B_{dd}(r) = C(\epsilon r)^{2/3} . \tag{12-62}$$

It follows that

$$B_{nn}(r) = 4/3 B_{dd}(r) ,$$

and for $r \ll \eta$ there is obtained, (12-46)

$$B_{nn}(r) = 2B_{dd}(r) .$$

The function, β_{ddd} , for large values of r becomes

$$\beta_{ddd}(r/\eta) \propto r/\eta$$

and

$$B_{ddd}(r) \propto \epsilon r . \tag{12-63}$$

Proceeding in a similar fashion, it can be shown that the m -order correlation varies as $r^{m/3}$ for large values of r . For small values of r , the velocity differences are proportional to the product of the spatial derivative and r ; hence, the m -order correlation involving two points varies as r^m .

The Navier-Stokes Equation for Locally Isotropic Turbulence

Equation (12-31) which is the Navier-Stokes equation for turbulence with ordinary isotropy, may be written in terms of B_{dd} and B_{ddd} provided the turbulence is also locally isotropic. Using Equations (12-61) and (12-29), the result is

$$3 \frac{\partial}{\partial t} (\overline{2u^2} - B_{dd}) = \frac{\partial B_{ddd}}{\partial r} + 4 \frac{B_{ddd}}{r} - 6\nu \left(\frac{\partial^2 B_{dd}}{\partial r^2} + \frac{4}{r} \frac{\partial B_{dd}}{\partial r} \right) .$$

The equation must hold regardless of whether the turbulence has ordinary isotropy.

From the point of view of local isotropy, the correlations do not vary with time. Therefore, from Equation (12-33), the above equation can be written as

$$-4\epsilon = \frac{\partial B_{ddd}}{\partial r} + \frac{4}{r} B_{ddd} - 6\nu \left(\frac{\partial^2 B_{dd}}{\partial r^2} + \frac{4}{r} \frac{\partial B_{dd}}{\partial r} \right) \quad (12-64)$$

From Equation (12-34), it follows that

$$\epsilon = \frac{15}{2} \nu \left(\frac{\partial^2 B_{dd}}{\partial r^2} \right)_0$$

and the power-series development for B_{dd} yields

$$\frac{\partial B_{dd}}{\partial r} = \frac{2}{15} \frac{\epsilon r}{\nu}$$

for small values of r .

If the skewness factor for the parallel component of the relative-velocity distribution is introduced,

$$S(r) = \frac{\overline{(u_d' - u_d)^3}}{[\overline{(u_d' - u_d)^2}]^{3/2}} = \frac{B_{ddd}(r)}{[B_{dd}(r)]^{3/2}}$$

then Equations (12-62) and (12-63) imply that

$$S(r) \propto \frac{\epsilon r}{C^{3/2} \epsilon r} = C^{-3/2}$$

for $r \gg \eta$. The constant of proportionality may be determined from Equation (12-64), noting that for large values of r , the terms involving B_{dd} vary as $r^{-4/3}$ and the terms in B_{ddd} , which is proportional to (ϵr) , predominate. Therefore,

$$B_{ddd}(r) = -4/5 \epsilon r$$

and

$$S(r) = -4/5 C^{-3/2}$$

From this relation, $S(r)$ is independent of r and equals a constant for large values of r . Townsend(12-47) found $S(r)$ to be nearly constant and approximately equal to -0.38, but more recent measurements by Stewart(12-29) indicate that $S(r)$ is not constant for large values of r , and in addition varies with the Reynolds number.

Figure 12-10 shows the results of Stewart's measurements. For small values of r , the theory predicts

$$S(0) = \frac{B_{ddd}(0)}{[B_{dd}(0)]^{3/2}} \propto \frac{(\nu\epsilon)^{3/4} (r/\nu)^3}{[(\nu\epsilon)^{1/2} (r/\eta)^2]^{3/2}} = \text{const},$$

but this is not confirmed by Stewart's results.

Comparison of Kolmogoroff's Theory With Experiment

Figure 12-11 shows the results of the first experimental investigation of local isotropy made by Corrsin.(12-48) The shear correlation, R_{12} , was measured as a function of frequency and was

found to decrease toward zero with increasing frequency in a turbulent jet. This indicates that the motion approached isotropy at the scales corresponding to the higher frequencies.

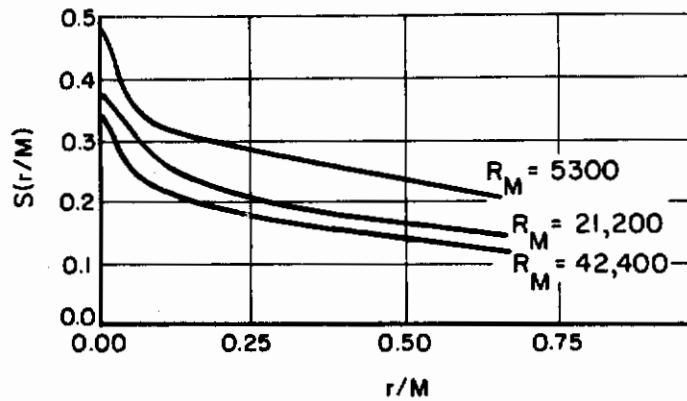


FIGURE 12-10. STEWART'S MEASUREMENTS OF $S(r)$

Stewart(12-29)

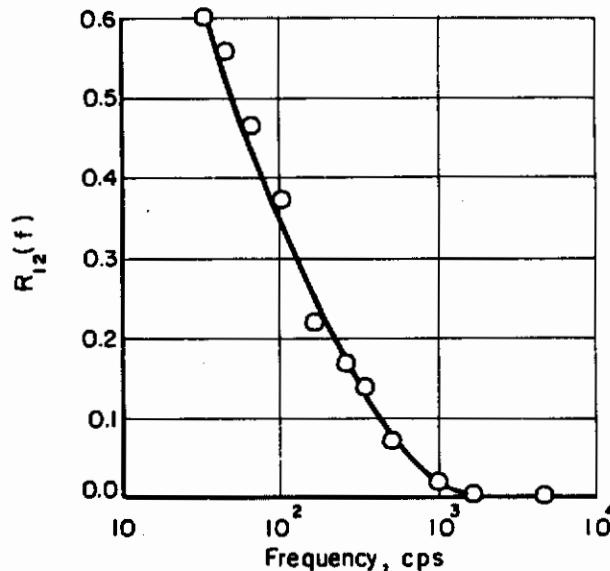


FIGURE 12-11. THE SHEAR CORRELATION, R_{12} , AS A FUNCTION OF FREQUENCY

Corrsin(12-48)

Because most of the experimental work in turbulence has been conducted in the field of isotropic turbulence downstream of a grid in a wind tunnel, it is desirable to compare Kolmogoroff's theory with this type of turbulence.

The isotropic nature of such a turbulent field is well confirmed for reasonably small values of \underline{r} . However, when \underline{r} becomes comparable to ℓ_2 , the integral scale, the turbulence becomes somewhat anisotropic. The spatial extent of \underline{G} must therefore be chosen smaller than ℓ_2 .

The time interval over which the turbulence will change appreciably, as pointed out before, is of the order $\ell_2 / \overline{u^2}$, the period of the largest eddies. From the decay rate of isotropic turbulence given by Equation (12-32) it follows that

$$\Delta t = - \frac{\Delta \overline{u^2}}{\overline{u^2}} \frac{\lambda^2}{10\nu}$$

Batchelor(12-45) selects a ten per cent change in $\overline{u^2}$ as appreciable, so that \underline{T} is equal to $\lambda^2/100\nu$. The ratio of the period of the largest eddies to \underline{T} is given by

$$\frac{100\nu \ell_2}{\sqrt{\overline{u^2}} \lambda^2} = 100 \frac{\ell_2}{\lambda} \frac{1}{R_\lambda}$$

From Equation (12-37), this ratio is expected to be nearly constant, and experimental measurements suggest that it is of the order unity. Under these conditions, only eddies small compared to ℓ_2 have periods small compared to \underline{T} , and local isotropy can be assumed to apply over the range where $r \ll \ell_2$.

From the definition of η and Equation (12-32), there is obtained,

$$\eta = \frac{\nu^{1/2} \lambda^{1/2}}{(15)^{1/4} (\overline{u^2})^{1/4}}$$

so that

$$\frac{\ell_2}{\eta} = \frac{\ell_2}{\lambda} (\sqrt{15} R_\lambda)^{1/2}$$

Here it is seen that the Reynolds number must be large in order that η be sufficiently small for Kolmogoroff's second hypothesis to be applied.

Over the range where the second similarity hypothesis can be applied, the second-order and third-order correlation coefficients can be written as

$$1 - f(r) = \frac{C}{2} \left(\frac{15}{R_\lambda} \frac{r}{\lambda} \right)^{2/3}$$

and

$$k(r) = - \frac{2}{R_\lambda} \frac{r}{\lambda}$$

where $\eta \ll r \ll \ell_2$.

Figure 12-12 is a comparison of the relation for $g(r)$ with Dryden's experimental data. (12-33) The value of ℓ_2/M for the experimental curve is about 0.24, so that the theory would seem to be verified over the small expected range.

The second test to which Kolmogoroff's theory has been subjected is the comparison of $S(0)$ and $S(r)$ with the expected constant values predicted by the theory. As pointed out previously, the more recent measurements of S do not provide agreement with the theory. Either the similarity hypotheses are wrong, or more likely, the state of equilibrium proposed by Kolmogoroff does not exist at the highest Reynolds numbers that have been used in the experiments. There is evidence that this is the case, at least for the very large eddies. (12-26) It might be expected that complete equilibrium is not obtained at any scale.

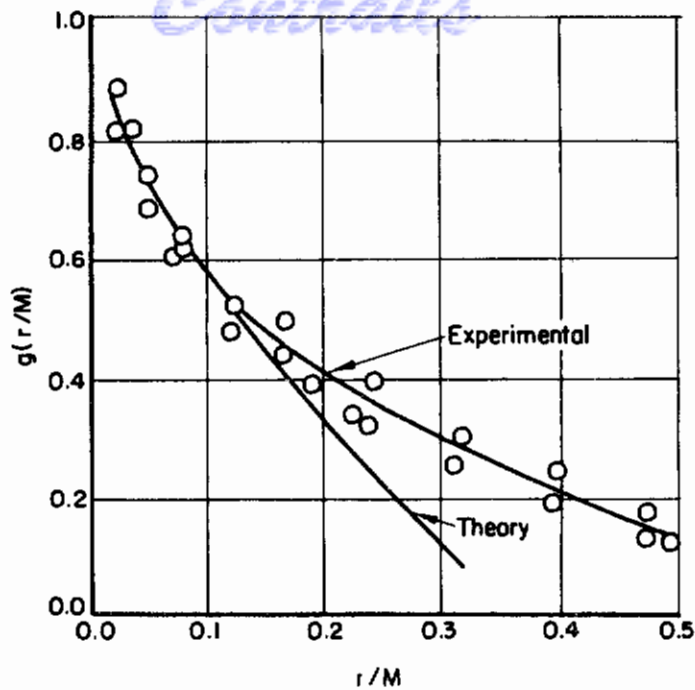


FIGURE 12-12. COMPARISON OF KOLMOGOROFF'S THEORY WITH EXPERIMENT

Batchelor⁽¹²⁻⁴⁵⁾

The Spectrum of Turbulence

As an alternative to defining a correlation coefficient in such a way that the various sizes of eddies may easily be considered separately, a spectral function may be introduced. This function represents the contribution of the eddies of certain size or characteristic frequency to the statistical parameter being considered. In the following paragraphs the spectrum of u^2 , or the energy spectrum, will be considered.

The auto-correlation, defined in Equation (12-55) may be expressed as a Fourier integral,

$$\overline{u(t) u(t + \theta)} = \overline{u^2} R_\theta(\theta) = \overline{u^2} \int_0^\infty F(\omega) \cos \omega \theta \, d\omega \quad (12-65)$$

Setting the time displacement, θ , equal to zero, in which case $R_\theta = 1$, there results,

$$\overline{u^2} = \overline{u^2} \int_0^\infty F(\omega) \, d\omega \quad ,$$

so that,

$$\int_0^\infty F(\omega) \, d\omega = 1 \quad .$$

Now, $F(\omega) \cos \omega \theta \, d\omega$ represents the contribution to R_θ of those components of the motion having a characteristic frequency between ω and $\omega + d\omega$. Therefore, $F(\omega)$ represents the contribution of those components to the turbulent energy, $\overline{u^2}$, and $F(\omega)$ is the energy spectrum.

Equation (12-65) may be formally identified with the Fourier cosine transform, that is, R_θ is the Fourier cosine transform of the energy spectrum $F(\omega)$. Taking the inverse transform, there results

$$F(\omega) = \frac{2}{\pi} \int_0^{\infty} R_\theta(\theta) \cos \omega \theta \, d\theta \quad (12-66)$$

Thus, if either R_θ or $F(\omega)$ is known, the other may be calculated. It is possible to measure both of these quantities experimentally. The auto-correlation may be measured either by the diffusion method based on Equation (12-59) or by recording the output of a hot-wire anemometer on magnetic tape and correlating the output obtained from two pickup heads, whose physical displacement along the tape corresponds to a time displacement in the original signal. (12-26, 12-49) The energy spectrum may be measured by passing the output of the hot-wire anemometer through band pass filters. (12-30, 12-33, 12-50)

The relation between the energy spectrum and the auto-correlation is quite simple. However, a real objection which may be made is whether the auto-correlation coefficient can be represented by such an integral. It seems fairly certain that R_θ is sufficiently well behaved for such a representation; indeed, the assumption that the turbulent motion is continuous is sufficient. Moreover, this same question, in some form, must be answered for any of the developments that have been used. Taylor's original derivation of the relations between the spectrum and the correlation suffers from a lack of mathematical rigor, (12-30) but this has been corrected in the many derivations that have followed. (12-2, 12-37, 12-40)

In the field of turbulence encountered in wind tunnel experiments the auto-correlation may be related to the spatial correlation, $f(r)$. In such a case, the turbulence is carried in a uniform stream of velocity, \underline{U} , and by a Newtonian transformation $\theta = r/U$, it follows that

$$\overline{u^2} R_\theta = \overline{u(t) u(t + \theta)} = \overline{u(x) u(x + r)} = \overline{u^2} f(r)$$

This can be true only for small values of \underline{r} , since turbulent diffusion causes the particles to move away from the streamlines originally occupied. The smallness of \underline{r} is determined primarily by the turbulent intensity, in accordance with Equation (12-60) and the turbulence Reynolds number, R_λ . (12-42, 12-51)

Under the assumption that turbulent diffusion can be neglected, Equation (12-66) can be written in terms of \underline{r} rather than θ so that

$$F(\omega) = \frac{1}{U} \frac{2}{\pi} \int_0^{\infty} f(r) \cos \frac{\omega r}{U} \, dr$$

Since $f(r)$ is nearly independent of the mean velocity, \underline{U} , $UF(\omega)$ must be a function of ω/U . The ratio, ω/U , can be considered as the wave number of the eddies whose frequency is ω . Thus, the "wavelength", or characteristic dimension, is given by $\lambda = 1/k = U/\omega$, so that

$$F(k) = \frac{2}{\pi U} \int_0^{\infty} f(r) \cos kr \, dr \quad (12-67)$$

where \underline{k} is the wave number. Taylor, using the data of Simmons and Salter, (12-50) calculated $f(r)$ from the inversion transform of Equation (12-67) and compared this with measured values of $f(r)$.

Figure 12-13 shows that the agreement between the calculated and measured values of $f(r)$ is remarkably good.

Once the change of variables from frequency to wave numbers has been made, the obvious step is to identify the wave number with the size of an eddy, so that large wave numbers correspond to small eddies, and small wave numbers to large eddies. This step must be made with caution, since $f(r)$ is a one-dimensional correlation whereas turbulence is a three-dimensional

phenomenon. The size of an eddy must really be identified with $k_i k_i$, where k_i is the wave-number vector. This leads to the three dimensional spectrum introduced by Heisenberg. (12-52) By analogy with the one-dimensional case a spectral tensor, Φ_{ij} , may be defined by

$$\Phi_{ij}(k) = \frac{1}{8\pi^3} \int \int \int_{-\infty}^{\infty} R_{ij}(r) e^{-i k_s r_s} dV(r) \quad ,$$

where $dV(r)$ is an element of volume in physical space. The inverse transform leads to

$$R_{ij}(r) = \int \int \int_{-\infty}^{\infty} \Phi_{ij}(k) e^{i k_s r_s} dV(k) \quad ,$$

where $dV(k)$ is an element of volume in wave-number space. In the particular case where the indices are equal,

$$\overline{u_1^2} + \overline{u_2^2} + \overline{u_3^2} = \int \int \int_{-\infty}^{\infty} \Phi_{ii}(k) e^{i k_s r_s} dV(k)$$

and Φ_{ii} is seen to be the spectrum of the total turbulent energy.

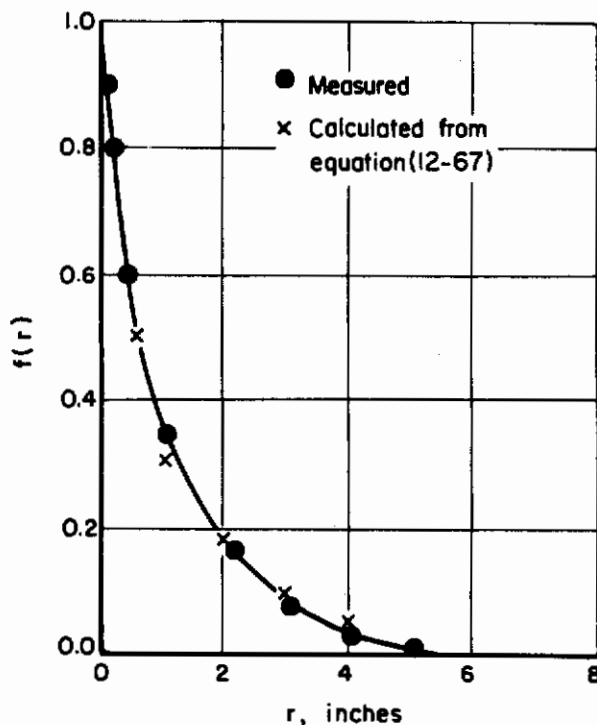


FIGURE 12-13. COMPARISON OF $f(r)$ CALCULATED FROM THE SPECTRUM WITH EXPERIMENTAL DATA

Taylor (12-30)

One advantage of a properly formed three-dimensional spectrum, lies in the fact that its value at $k = 0$ is zero. Taylor's one-dimensional spectrum does not have this property. In fact, from Equation (12-67) it follows that

$$F(0) = \frac{2l_2}{\pi U}$$

Physically, this appears to be due to the one-dimensional nature of the spectrum, since motions having a wave number of zero in the particular direction may have a finite wave number in some other direction and hence make a contribution to the energy. (12-2)

If the discussion is confined to isotropic turbulence, then a relation may be obtained between the one-dimensional and three-dimensional spectra. Moreover, the one-dimensional spectrum can be measured experimentally. Because of these facts, the following remarks refer to the one-dimensional spectrum. (12-53)

Applications to the Dynamics of Turbulence

Because a relation exists between the correlation and the spectrum, nothing really new can be expected from an investigation of the spectrum. However, the spectrum is often a more convenient way to represent the turbulent field. For example, Kolmogoroff's theory may be stated in spectral terms.

If the Fourier transform of Equation (12-31) is taken, there results

$$\frac{\partial E}{\partial t} + T(k) = -2\nu k^2 E(k) \quad ,$$

where

$$E(k) = 3/2 \overline{u^2} F(k) \quad ,$$

and

$$E = \int_0^{\infty} E(k) dk \quad .$$

The term, $T(k)$, represents the transfer of energy from one wave number to another. Kolmogoroff's similarity hypotheses can be applied directly (12-34) to yield

$$E(k) = (\nu\epsilon)^{1/2} e(k\eta) \eta \quad ,$$

$$T(k) = (\nu\epsilon)^{3/2} t(k\eta) \quad ,$$

where k is large, and e and t are universal functions. For small values of k the second hypothesis applies, and

$$E(k) \propto \epsilon^{2/3} k^{-5/3} \quad ,$$

and

$$T(k) \propto \epsilon k^{-1} \quad .$$

The corresponding properties of the correlations may be obtained by taking the inverse transforms of the above equations.

The Generation of Turbulence

It is found experimentally that laminar flow becomes unstable as the Reynolds number is increased. Small disturbances in the flow are amplified and extract energy from the mean flow whenever the Reynolds number exceeds some critical value. Although the initial development of the disturbance has been studied extensively, (12-54, 12-55) little is known about the process by which the energy extracted from the mean flow by these disturbances is finally transformed to the

random energy of turbulence. Since the linearized equations of motion fail to predict such a development, the explanation presumably lies in the nonlinear terms of the Navier-Stokes equation. The actual generation of turbulence in a boundary layer appears to be a sporadic process. Recent attempts to understand this process have produced some interesting intuitive notions, but have not been successful in producing quantitative results. (12-56, 12-57)

The production of turbulence can be delayed or prevented by several methods. For example, the boundary layer may be stabilized by addition or removal of fluid; the Reynolds number may be restricted to values below the critical value; or the oncoming flow may be freed from disturbances. In general, the elimination or reduction of regions of shear motion from which the turbulence can obtain energy will delay the onset of turbulence.

In some instances turbulence is deliberately generated in a flow system to increase mixing effects, diffusive effects, or to increase the flame speed in a combustion reaction. The production of turbulence by a physical device is accompanied by a pressure drop in excess of that which exists for laminar flow. This effect is generally undesirable. Dryden, (12-3) reasoning from the mixing-length theories, has suggested that the maximum mixing effect is obtained for a given pressure drop if the scale is large and the fluctuating velocity is small. However, if only a short time is available for mixing, then a high intensity must be employed because Equation (12-60) shows that the rate of diffusion is proportional to u^2 and is independent of the scale. Also, if the scale is large in comparison with the dimensions of the system, then the mixing will tend to be spotty. Recent investigations of these effects have been reported by Taylor. (12-58)

The effect of turbulence on flame speed is not understood. The most important parameter seems to be the fluctuating velocity, although some data indicate that turbulent flame speed is nearly independent of all turbulence parameters provided that turbulence is present in excess of some small critical value.

The scale and intensity of turbulence can be varied independently over wide ranges. For isotropic turbulence generated by grids in a wind tunnel, the intensity can be varied from less than 0.1 to about 5.0 per cent of the mean speed. The scale may be varied to upper limits set by the dimensions of the apparatus. If the grid is replaced by a perforated plate, strongly anisotropic turbulence is generated having intensities up to approximately 20 per cent of the mean speed.

CONCLUDING REMARKS

Of the existing theories of turbulence the statistical theory may provide a complete understanding of turbulence. However, in its present form, the statistical theory is not adapted for use in solving practical problems. Also, at present, the statistical theory is little better than a phenomenological theory. The equations of fluid motion should provide a complete solution to the problems of turbulence if mathematical methods were sufficiently powerful to solve them. The simplification effected by averaging the equations permits a partial treatment by the existing methods of mathematics, but a complete solution cannot be based on mean values alone. Basically, the element lacking is a correct physical mechanism of turbulence, and until this mechanism is discovered, a complete solution cannot be obtained in terms of the statistical theory. Once the correlation functions are introduced, the equations of motion lead to a system containing more unknown functions than equations. In the case of the Navier-Stokes equation for incompressible flow, one equation in two unknowns is obtained. Thus, before the equations can be solved, an additional physical law must be postulated. The self-preservation concept, in which the correlation functions depend on one variable, is not sufficient. Recent modifications of this concept by Lin (12-59, 12-60) show promise, but are not yet entirely satisfactory.

Moreover, Krzywoblocki (12-61) has pointed out that the extension of the present statistical theory to turbulence in a compressible fluid may be very difficult. The use of the continuity equation in its incompressible form, $\partial u_i / \partial x_i = 0$, permits a vast simplification of the equations involved. He suggests that without this simplification, little progress can be made.

On the other hand, the mixing-length theories propose a physical mechanism of turbulence and thus obtain a nearly complete solution to the turbulence problem. However, the proposed mechanism cannot be correct.

Reichardt's hypothesis is purely phenomenological and makes no attempt to provide a mechanism. Hence it is useful only in the restricted range for which it was proposed, and in this instance numerical answers can be obtained only by experiment. However, it does offer the most convenient way of solving the equations of motion. In application to combustion problems, some success has been achieved with the phenomenological theories. This success is shown, for example, by the prediction of the length of flames burning in a jet. In those applications which have supposedly used the statistical theory, the actual application was phenomenological in character.

In Chapters 1, 5, 10, 15, 16, and 19, the effect of turbulence upon flames, atomization, ballistics, and evaporation are considered. The understanding of these combined processes is far from complete, and this reflects the lack of knowledge in the separate fields. In this respect, however, the statistical theory of turbulence is a useful tool. The experimental work done in connection with the statistical theory has provided a basis for the generation of turbulence with controllable characteristics and permits an accurate description of the turbulent motion in terms of statistical parameters. Even though the relations between these parameters and the effect of turbulence upon various phenomena is not understood, even empirically, their measurement allows a comparison between the work of different experimenters. Hence, the statistical theory has laid the groundwork for future empirical studies of the effect of turbulence upon other phenomena taking place in turbulent fluid streams.

As pointed out by Squire, (12-13) the measurement of mean values provides little information concerning turbulence. Therefore, any serious investigation into the field of turbulence must necessarily include measurements of the fluctuating motion. At the present, the only method of obtaining these measurements directly is by the use of a hot-wire anemometer, an expensive and delicate instrument.

Before turbulence studies can be unconditionally recommended, it is necessary to consider whether the results of such studies are likely to be applicable to combustion research. At present it appears that no direct application is likely. The suspected generation of turbulence by flames suggests the possibility of strong interactions between combustion phenomena and flow phenomena. Such considerations prohibit the direct application of results obtained in cold-flow turbulence studies to combustion systems. Indirectly, such studies may well be indispensable in establishing a firm understanding of the fluid dynamics of the turbulence.

A wider, and perhaps a temporarily more productive field, would be concerned primarily with the gross effect of turbulence upon the various phenomena of combustion. Again, much work has been done, but the results of various investigators are often conflicting. At present, the most pressing problems in this field appear to be the role of turbulence in flame holding by bluff objects, and the effect of turbulence on flame speed. There is a strong possibility that these two problems are related.

Consequently, it is difficult to recommend a positive program of research in the field of turbulence. A great amount of work is presently being done in this field, but much of it is of little worth. A factor which severely hampers future research in this field is the lack of interested and qualified men. There are few men in this country who are both informed and active in the field.

REFERENCES

- 12-1. Von Kármán, Th., Turbulence; J. Roy. Aero. Soc., Vol. 41, 1937, p. 1109.
- 12-2. Chuang, Feng-Kan, On the Statistical Theory of Turbulence; Ph. D. Thesis, Calif. Inst. Tech., 1950.

- 12-3. Dryden, H. L., Turbulence and Diffusion; Ind. Eng. Chem., Vol. 31, 1939, pp. 416-425.
- 12-4. Dryden, H. L., A Review of the Statistical Theory of Turbulence; Quart. Appl. Math., Vol. 1, 1943, pp. 7-42.
- 12-5. Bakhmeteff, B. A., Mechanics of Turbulent Flow; Princeton Press, 1936.
- 12-6. Durand, W. F. (Ed.), Aerodynamic Theory; Vol. 3, Division G, 1934, reprinted 1943, p. 119.
- 12-7. Goldstein, S. (Ed.), Modern Developments in Fluid Dynamics; Oxford Press, 1938, Vol. 1 Chapt. 5, pp. 191-233.
- 12-8. Taylor, G. I., The Transport of Vorticity and Heat in Turbulent Motion; Proc. Roy. Soc. Lond., Vol. 135. Series A, 1932, pp. 685-702.
- 12-9. Abramovich, G. N., The Theory of a Free Jet of a Compressible Gas; Central Aero-Hydrodynamical Institute of Moscow, Report 377, 1939; NACA TM 1058.
- 12-10. Fage, A., and Falkner, V. M., Note on Experiments of the Temperature and Velocity in the Wake of a Heated Cylindrical Obstacle; Proc. Roy. Soc. Lond., Vol. 135, Series A, 1932, p. 702.
- 12-11. Reference 12-7, Vol. 2, pp. 663-665.
- 12-12. Reference 12-7, Vol. 2, pp. 672-673.
- 12-13. Squire, H. B., Reconsideration of the Theory of Free Turbulence; RAE Farnborough, Report No. Aero. 2023, Mar., 1945; Abst. in Phil. Mag., Vol. 39, 1948, pp. 1-20.
- 12-14. Batchelor, G. K., On the Theory of Free Turbulence; J. Aero. Sci., Vol. 17, 1950, pp. 441-445.
- 12-15. Von Kármán, Th., Mechanische Ähnlichkeit und Turbulenz; NACA TM 611, 1931.
- 12-16. Tollmien, W., Calculation of Turbulent Expansion Processes; ZAMM, Vol. 6, pp. 468-478; NACA TM 1085.
- 12-17. Reichardt, H., A New Theory of Free Turbulence; ZAMM, Vol. 21, pp. 257-264; J. Roy. Aero. Soc., Vol. 47, 1943, pp. 167-176.
- 12-18. Alexander, L. G., Boron, T., and Comings, E. W., Transport of Momentum, Mass, and Heat in Turbulent Jets; Univ. of Ill. Engineering Exp. Station, Tech. Report No. 8, Part 1, Contract N6-ori-71, Task Order No. XI, ONR, Sept. 1, 1950, Correction Sheet, May, 1951.
- 12-19. Forstall, W., Jr., and Shapiro, A. H., Momentum and Mass Transfer in Coaxial Gas Jets; Meteor Report No. 39, Mass. Inst. of Tech., Dept. of Mech. Eng., July, 1949.
- 12-20. Keagy, W. R., and Weller, A. E., A Study of Freely Expanding Inhomogeneous Jets; Heat Transfer and Fluid Mechanics Inst., 1949.
- 12-21. Alexander, L. G., Comings, E. W., Grimmet, H. L., and White, E. A., Transfer of Momentum in Jet of Air Issuing Into a Tube; Tech. Rep. No. 11, Univ. Ill. Eng. Exp. Sta., 1952, 50 p.
- 12-22. Alexander, L. G., and Kivnick, A., Simultaneous Transport of Heat and Momentum in a Ducted Jet; Tech Rep. No. 12, Univ. Ill. Eng. Exp. Sta., 1952, 27 p.

- 12-23. Taylor, G. I., Statistical Theory of Turbulence; Proc. Roy. Soc. Lond., Vol. 151, Series A, 1935, pp. 421-478.
- 12-24. Von Kármán, Th., The Fundamentals of the Statistical Theory of Turbulence; J. Aero. Sci., Vol. 4, 1937, pp. 131-138.
- 12-25. Fage, A., and Townend, H. C. H., Examination of Turbulent Flow with an Ultramicroscope; Proc. Roy. Soc. Lond., Vol. 135, Series A, 1932, p. 656.
- 12-26. Batchelor, G. K., and Stewart, R. W., Anisotropy of the Spectrum of Turbulence at Small Wave Numbers; Q. J. Mech and Appl. Math., Vol. 3, 1950, pp. 1-8.
- 12-27. Von Kármán, Th., and Howarth, L., On the Statistical Theory of Isotropic Turbulence; Proc. Roy. Soc. Lond., Vol. 164, Series A, 1938, pp. 192-215.
- 12-28. Loitsianskii, L. G., Some Basic Laws of Isotropic Turbulent Flow; Central Aer-Hydrodynamical Inst. of Moscow, Report No. 440, 1939; NACA TM 1079.
- 12-29. Stewart, R. W., Triple Velocity Correlations in Isotropic Turbulence; Proc. Camb. Phil. Soc., Vol. 47, 1951, pp. 146-157.
- 12-30. Taylor, G. I., The Spectrum of Turbulence; Proc. Roy. Soc., Lond., Vol. 164, Series A, 1938, pp. 476-490.
- 12-31. Dryden, H. L., The Theory of Isotropic Turbulence; J. Aero. Sci., Vol. 4, 1937, pp. 273-280.
- 12-32. Von Kármán, Th., Some Remarks on the Statistical Theory of Turbulence; Proc. Fifth Inter. Congr. of Appl. Mech., Cambridge, Mass., 1938, p. 347.
- 12-33. Dryden, H. L., Schubauer, G. B., Mock, W. C., and Skramstad, H. K., Measurements of Intensity and Scale of Wind-Tunnel Turbulence and Their Relation to the Critical Reynolds Number of Spheres; NACA Report 581, 1937.
- 12-34. Lin, C. C., On the Law of Decay and the Spectrum of Isotropic Turbulence; Proc. 7th Int. Cong. for Appl. Mech., Lond., Sept., 1948.
- 12-35. Stewart, R. W., and Townsend, A. A., Similarity and Self-Preservation in Isotropic Turbulence; Phil. Trans., Vol. 243, 1951, pp. 359-386.
- 12-36. Batchelor, G. K., Energy Decay and Self-Preserving Correlation Functions in Isotropic Turbulence; Quart. Appl. Math., Vol. 6, 1948, pp. 97-116.
- 12-37. Goldstein, S., Statistical Theory of Turbulence; Lecture Series No. 6, The Institute for Fluid Dynamics and Applied Mathematics, University of Maryland, 1950, 43 p.
- 12-38. Batchelor, G. K., and Townsend, A. A., Decay of Vorticity in Isotropic Turbulence; Proc. Roy. Soc., Vol. 190, Series A, 1947, pp. 534-550.
- 12-39. Taylor, G. I., Diffusion by Continuous Movements; Proc. Lond. Math. Soc., Vol. 20, 1921, p. 196.
- 12-40. Frenkiel, F. N., Introduction to Some Topics on Turbulence; Lecture Series No. 3, The Institute for Fluid Dynamics and Applied Mathematics, University of Maryland, 1950.
- 12-41. Batchelor, G. K., Diffusion in a Field of Homogeneous Turbulence, I. Eulerian Analysis; Austral. J. Sci., Vol. 42, 1949, pp. 437-450.
- 12-42. Uberoi, M. S., and Corrsin, S., Diffusion of Heat From a Line Source in Isotropic Turbulence; NACA TN 2710, 1952, 90 p.

- 12-43. Kolmogoroff, A. N., The Local Structure of Turbulence in Incompressible Viscous Fluid for Very Large Reynolds Numbers; C. R. (Doklady) Acad. Sci. U. R. S. S., Vol. 31, 1941, pp. 301-305.
- 12-44. Kolmogoroff, A. N., Dissipation of Energy in the Locally Isotropic Turbulence; C. R. (Doklady) Acad. Sci. U. R. S. S., Vol. 32, 1941, pp. 16-18.
- 12-45. Batchelor, G. K., Kolmogoroff's Theory of Locally Isotropic Turbulence; Proc. Camb. Phil. Soc., Vol. 43, 1947, pp. 534-559.
- 12-46. Agostini, L., and Bass, J., Les Theories de la Turbulence; Publications Scientifiques et Techniques du Ministere de l'Air, No. 237, 1950.
- 12-47. Townsend, A. A., Experimental Evidence for the Theory of Local Isotropy; Proc. Camb. Phil. Soc., Vol. 44, 1948, pp. 560-565.
- 12-48. Corrsin, S., An Experimental Verification of Local Isotropy; J. Aero. Sci., Vol. 16, 1949, pp. 756-757.
- 12-49. Favre, A., Mesures Statistiques de la Correlation dans le Temps; Proc. Seventh Int. Cong. for Appl. Mech., Lond., 1948.
- 12-50. Simmons, L. F. G., and Salter, C., An Experimental Determination of the Spectrum of Turbulence; Proc. Roy. Soc. Lond., Vol. 165, Series A, 1938, pp. 73-89.
- 12-51. Lin, C. C., On Taylor's Hypothesis and the Acceleration Terms in the Navier-Stokes Equations; Q. Appl. Math., Vol. 10, 1953, pp. 295-306.
- 12-52. Heisenberg, W., Zur Statischen Theorie der Turbulenz; Zeits. fur Phys., Vol. 124, 1948, pp. 628-657.
- 12-53. Dryden, H. L., The Turbulence Problem Today; Proc. First Midwestern Conf. Fluid Dynamics, Univ. of Ill., 1950, Edward Brothers, 1951, pp. 1-20.
- 12-54. Tollmien, W., General Instability Criterion of Laminar Velocity Distributions; NACA TM 792, 1936.
- 12-55. Schubauer, G. B., and Skramstad, H. K., Laminar-Boundary-Layer Oscillations and Transition on a Flat Plate; NACA Tech. Rep. No. 909, 1948, pp. 327-357.
- 12-56. Munk, M. M., Mechanism of Turbulent Fluid Motion; Aero Digest, Vol. 64, 1952, p. 32. See also, On Turbulent Fluid Motion; J. Aero. Sci., Vol. 18, 1951, pp. 442-446, and On the Mechanism of Turbulent Fluid Motion; Proc. Second Midwestern Conf. Fluid Mech., 1952, Eng. Exp. Sta., Ohio State Univ., pp. 19-33.
- 12-57. Theodorsen, T., Mechanism of Turbulence; Proc. Second Midwestern Conf. Fluid Mech., 1952, Eng. Exp. Sta., Ohio State Univ., pp. 1-18.
- 12-58. Taylor, G. I., The Dispersion of Matter in Turbulent Flow Through a Pipe; Proc. Roy. Soc. Lond., Vol. 223A, 1954, pp. 446-468.
- 12-59. Lin, C. C., Note on the Law of Decay of Isotropic Turbulence; Proc. Nat. Acad. Sci., Vol. 34, 1948, pp. 540-543.
- 12-60. Lin, C. C., and Von Karman, Th., On the Concept of Similarity in the Theory of Isotropic Turbulence; Rev. Mod. Phys., Vol. 21, 1949, pp. 516-519.
- 12-61. Krzywoblocki, M. S. v., On the Foundations of Certain Theories of Turbulence; J. Franklin Inst., Vol. 252, 1951, pp. 409-412.

CHAPTER 13. HYDRODYNAMIC RECIRCULATION

ABSTRACT

This chapter is concerned with recirculating flow as encountered in combustion systems. Most of the work recorded in the literature has been carried out on isothermal-flow systems, and such systems are discussed first. Examples are given (1) of the stable flow pattern around a bluff body at low Reynolds numbers, (2) of the unstable flow pattern around a bluff body at high Reynolds numbers, and (3) of the unstable flow pattern typical of a closed system with one or more entries and exits. The theoretical and empirical developments associated with these systems are also outlined. The changes made in these flow patterns by the presence of a flame are next discussed. It becomes evident that the literature is not in agreement on many factors concerning the recirculation systems, including the stabilizing or nonstabilizing effect of the flame on the flow system. Following the discussion of the experimental phase of the recirculation research, the types of recirculation encountered in practice are illustrated by the use of typical combustion units. Basic similarities in the flow patterns are noted. Some concluding remarks are made about possible avenues of future work.

Contrails

HYDRODYNAMIC RECIRCULATION

by

H. Einbinder and A. A. Putnam

This chapter is concerned with recirculating flows as applied to combustion systems. Because of their importance in flame holding (see Chapter 16), special attention is given to the eddies produced behind bluff bodies.

In many practical applications, such as ram jets and afterburners, it is desirable to maximize the rate at which energy is released by combustion. If a bluff body is introduced into the gas stream, to serve as a flame holder, the velocity of the oncoming fuel-air mixture can be increased to several hundred feet per second, even though the normal burning velocity may be only a few feet per second. The flame-holding properties of such bluff bodies are intimately associated with the recirculation region of hot burned gas in their wakes. This is indicated by the fact that streamlined bodies, for which the recirculation region is a minimum, are extremely poor flame holders⁽¹³⁻¹⁾.

In the first section of this chapter, discussion is limited to recirculation in the absence of heat sources, or adiabatic flow; the effect of combustion on recirculation is considered in the second section. Next, a number of practical combustion systems which employ recirculating flows are described; and finally, some concluding remarks based on the previous discussion are presented.

RECIRCULATION IN ADIABATIC FLOW

Although interest centers on recirculation in combustion systems when the flow is diabatic (heat sources are present), it is natural to begin with the simpler situation with heat sources absent for several reasons: first, because a large body of experimental and theoretical work has been done on this type of flow whereas the diabatic case remains largely unexplored; and second, because the flow is a function of only a single dimensionless parameter, the Reynolds number, whereas the combustion process may introduce additional significant dimensionless parameters.

A typical picture of recirculating flow is shown in Figure 13-1. The white tracks are the flow streamlines which are traced by injecting aluminum particles into the fluid.

To illustrate the hydrodynamic phenomena encountered as the Reynolds number is varied, consider the flow of a real fluid perpendicular to the axis of an infinite circular cylinder. Due to the viscous forces, the fluid in contact with the cylindrical surface is at rest, whereas at large distances from the cylinder, the fluid moves with the undisturbed flow velocity. As a result of these two conditions, a region of recirculating flow is set up behind the cylinder.

At low Reynolds numbers, two stable symmetric vortices are formed in the wake. As Re is increased, the vortices move further downstream, until a critical value is reached ($Re_c \approx 50$) when they become unstable to asymmetric disturbances. The vortices are then shed alternately from opposite sides of the cylinder and move downstream in parallel lines* with a definite frequency and spacing between them. This system of vortices, known as a vortex street, persists downstream until the vorticity in the street diffuses into the main body of the fluid. As Re is further increased, the vortex street is damped out more rapidly because of the increase in the rate of vortex diffusion.

*In a system bounded by parallel walls or in an ideal inviscous fluid.

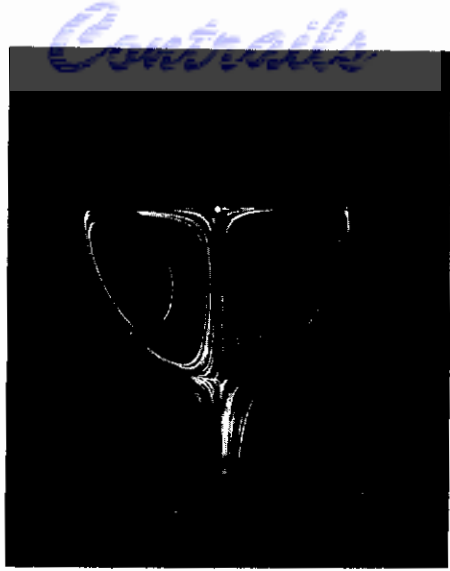


FIGURE 13-1. FLOW BEHIND A FLAT PLATE AT A LOW REYNOLDS NUMBER

(Camichel and Dupin)¹³⁻²

The photographs of Figure 13-2 show the characteristic rolling up into eddies of the vortex layer created at the surface of the cylinder forming a vortex street downstream. When $Re > 2500$, the vortex street is no longer observed, but vortices continue to shed regularly until the entire wake becomes turbulent ($Re > 10^5$). A high concentration of turbulent energy in a discrete frequency range has been observed for Re up to 2×10^6 (13-4).

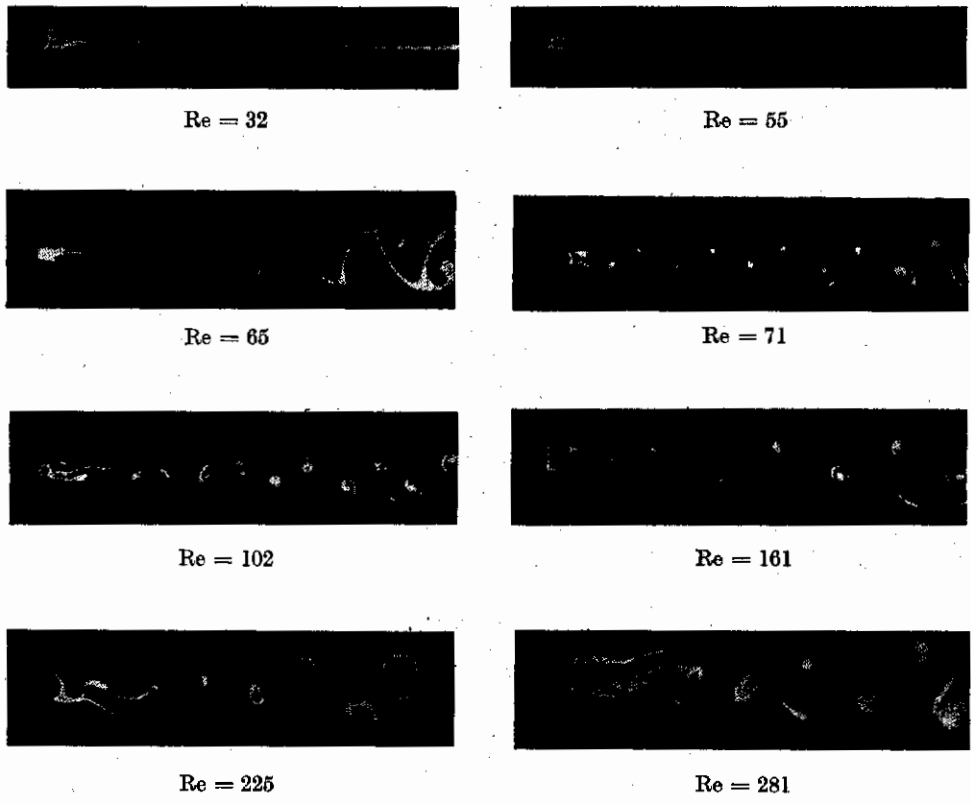


FIGURE 13-2. THE FORMATION AND DISCHARGE OF VORTICES FROM A CYLINDER

(Homann)¹³⁻³

Figure 13-3 is useful in considering these phenomena from another point of view. The cylinder is assumed to start from rest so that no vorticity is present at the beginning of the motion. If the flow is considered to be irrotational (and hence, potential), the flow is identical on the upstream and downstream sides of the cylinder. At the surface of the cylinder, the fluid velocity is zero at the stagnation points A and A'; whereas it is a maximum at B and B' where the streamlines are parallel to the main flow. By Bernoulli's theorem $p/\rho_0 + u^2$ is a constant along a streamline; therefore, the pressure is a maximum at A and A' and a minimum at B and B'. Now consider the effect of viscosity. Viscous forces oppose the motion of the fluid in the boundary layer adjacent to the surface of the cylinder. On the upstream side, from A to B and A to B', this retarding effect does not change the character of the motion because the pressure gradient in the initially irrotational flow acts in the direction of the fluid motion. On the downstream side the viscous forces cause the fluid particles to lose all their kinetic energy before reaching A'. As a result, the pressure gradient turns the fluid particles back thereby forming a region of reverse flow between the boundary and the external flow. Since new fluid is continually undergoing this process, the region of reverse flow broadens out, pushing the external flow progressively farther away from the boundary until it separates from the surface of the cylinder. These separation points are located 80° from the forward stagnation point A (see Figure 13-14). When the boundary layer becomes turbulent ($Re > 10^5$), the separation points shift to the downstream side of the cylinder. Experimental observations indicate that flames are anchored to flame holders at these separation points(13-5).

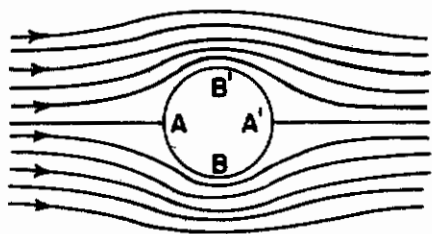


FIGURE 13-3. FLOW OF A NONVISCIOUS FLUID AROUND A CYLINDER

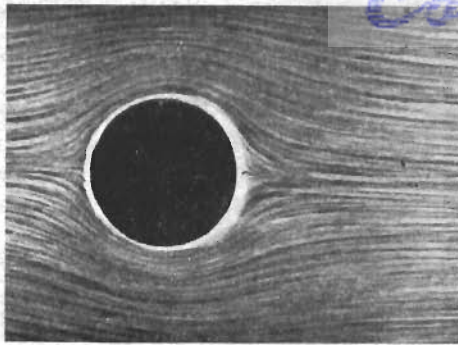
The series of photographs of Figure 13-4 record the temporal development of the flow behind a cylinder set in motion with constant acceleration. Initially there is no boundary layer present, so that the flow is irrotational as shown in (a). The growth of the boundary layer until unstable vortices are shed can be traced in the sequence of pictures from (a) to (f).

The Stationary Regime

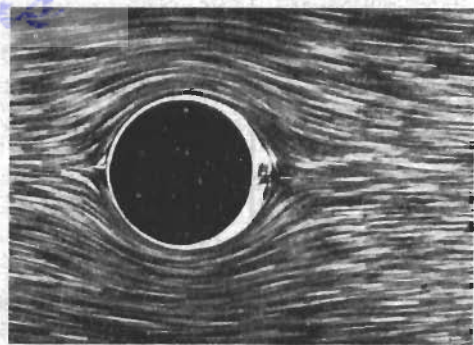
In the region of low Reynolds numbers, the streamlines followed by the fluid particles are independent of time. The motion of the fluid is governed by the Navier-Stokes equations which, for incompressible flow, can be written in dimensionless vector form by introducing a characteristic velocity U_0 and length L associated with the motion. The equation of motion becomes

$$\frac{\partial \bar{q}}{\partial \tau} + (\bar{q} \cdot \nabla) \bar{q} = -\nabla p + \frac{1}{Re} \nabla^2 \bar{q} \tag{13-1}$$

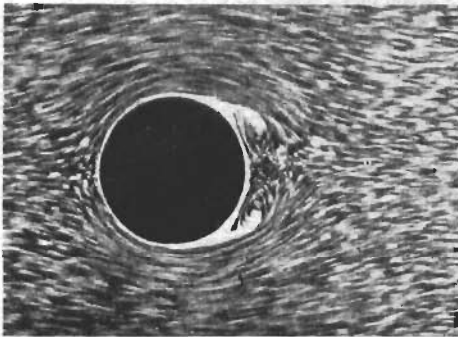
where the dimensionless velocity, pressure, time, and Reynolds number are given by $\bar{q} = \bar{U}/U_0$, $p = p/\rho_0 U_0^2$, $\tau = U_0 t/L$, and $Re = \rho_0 U_0 L/\mu$, respectively, with ρ_0 , and μ denoting fluid density and viscosity. The spatial coordinates in the differential operator ∇ are $x = X/L$, $y = Y/L$, and $z = Z/L$ (see Chapter 11).



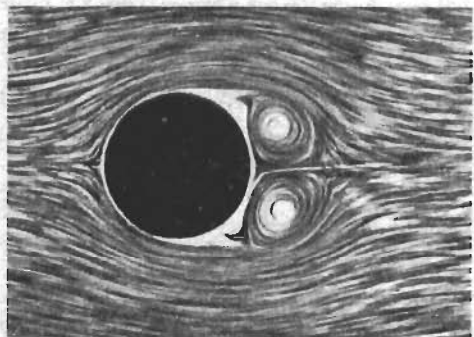
a) Potential flow immediately after starting



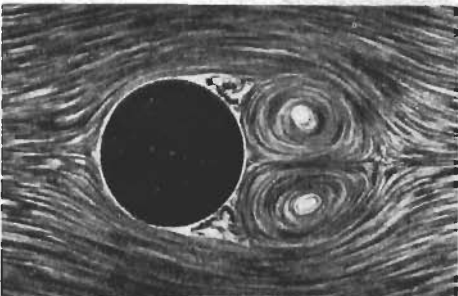
b) Accumulation of material in the boundary layer



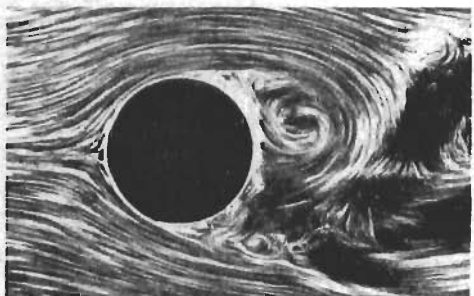
c) Formation of pair of vortices flow separates from cylinder



d) The eddies grow in size



e) The eddies continue to grow in size



f) They become unstable and the flow becomes asymmetric

FIGURE 13-4. FORMATION OF VORTICES BEHIND A CYLINDER MOVING FROM REST WITH CONSTANT ACCELERATION

(Prandtl and Tietjens)¹³⁻⁶

Equation (13-1) indicates that the motion about geometrically similar bodies will be identical in terms of corresponding dimensionless variables provided their Reynolds numbers are equal⁽¹³⁻⁷⁾. Therefore, the motion about such similar bodies can be discussed as a function of this single dimensionless parameter.

In the stationary regime where $\partial \bar{q} / \partial \tau = 0$, the essential difficulty in solving the equations of motion arises from nonlinear terms, $(\bar{q} \cdot \nabla) \bar{q}$, due to the inertial forces. Because of this difficulty, Stokes⁽¹³⁻⁷⁾ neglected these forces entirely in treating slow stationary motion ("creeping motion"), and replaced Equation (13-1) by

$$\nabla^2 \bar{q} = Re \nabla p, \tag{13-2}$$

which is valid only if $Re \ll 1$.

Since the fluid is taken to be incompressible and no heat sources are present, the equation of continuity requires that

$$\nabla \cdot \bar{q} = 0 \quad (13-3)$$

Thus, a stream function ψ can be introduced, which for two-dimensional motion is

$$u = \partial\psi/\partial y \text{ and } v = -\partial\psi/\partial x \quad .$$

Equation (13-2) then becomes

$$\nabla^4 \psi = 0 \quad (13-4)$$

This biharmonic equation must be solved subject to the boundary conditions that the normal and tangential velocities of the fluid vanish at the surface of the body.

For the sphere, the solution of Equation (13-4) yields the dimensionless stream function⁽¹³⁻⁹⁾

$$\psi = 1/2 \left[1 - \frac{3}{2r} + \frac{1}{2r^3} \right] r^2 \sin^2 \theta \quad , \quad (13-5)$$

where for a sphere of radius a , $r = R/a$.

This leads to Stokes' celebrated formula for the drag force on a slowly moving sphere, which has found wide application in the study of droplet ballistics (see Chapter 5). The corresponding stream function for nonviscous flow is⁽¹³⁻⁹⁾

$$\psi = 1/2 \left[1 - \frac{1}{r^3} \right] r^2 \sin^2 \theta \quad . \quad (13-6)$$

The principal difference between these two stream functions arises from neglecting the inertial forces in Equation (13-5), which are predominant at large distances from the sphere, and ignoring the viscous forces in Equation (13-6), which are important near it. Therefore, Stokes' approximation, which may be classed as a boundary-layer theory, does not represent the motion at large distances, but is valid in the neighborhood of the sphere.

Since the flow pattern obtained from Equation (13-5) is identical on the upstream and downstream sides of the sphere, Stokes' approximation fails to show the characteristic formation of a vortex ring in the wake. Moreover, when applied to find the flow about a slowly moving cylinder, an infinite value for the drag force is obtained.

To obtain a flow field with vortex motion behind an obstacle, it is necessary to employ Oseen's approximation, which takes some account of the inertia forces and also linearizes the equations of motion. If the field at infinity flows with constant velocity U_0 in the positive x direction, then, introducing a unit vector \bar{i} in the x direction, the velocity of the fluid can be written in dimensionless form as $\bar{i} + \bar{q}$, where \bar{q} is the vector velocity produced by the presence of the body in the fluid. At large distances from the body, \bar{q} becomes vanishingly small. Oseen's linearized equations are obtained by neglecting all terms of second and higher order in \bar{q} , in the Navier-Stokes equation. For the x component the equation of motion becomes

$$\frac{\bar{q}}{x} = -\nabla p + \frac{1}{\text{Re}} \nabla^2 \bar{q} \quad . \quad (13-7)$$

With $k = 1/2 \text{ Re}$, this equation and the equation of continuity⁽¹³⁻³⁾ are satisfied by

$$\bar{q} = -\nabla \theta + \frac{1}{2k} \nabla^2 \psi - i \times \quad (13-8)$$

and

$$p = \partial\phi/\partial x , \tag{13-9}$$

provided that

$$\nabla^2 \chi - 2k \frac{\partial \chi}{\partial x} = 0 \tag{13-10}$$

and

$$\nabla^2 \phi = 0 . \tag{13-11}$$

Analytical solutions of these equations have been given by Goldstein⁽¹³⁻¹⁰⁾ for the sphere and by Flaxen⁽¹³⁻¹¹⁾ for the circular cylinder, while the corresponding flow fields about these bodies have been treated in detail by Tomotika and Aoi⁽¹³⁻¹²⁾; in a later reference⁽¹³⁻¹³⁾ Tomotika and Aoi extended their work to cover an elliptic cylinder and a flat plate.

In dimensionless spherical coordinates, the general solution of Equations (13-10) and (13-11) is given by

$$\chi = e^{kr} \cos \theta \sum_{m=0}^{\infty} (2m+1) B_m \left[\frac{\pi}{kr} \right]^{1/2} K_{m+1/2}(kr) P_m(\cos \theta) , \tag{13-12}$$

$$\phi = \sum_{n=0}^{\infty} A_n \frac{P_n(\cos \theta)}{r^n} , \tag{13-13}$$

where $K_{m+1/2}(kr)$ is the modified Bessel function of order $m+1/2$, $P_m(\cos \theta)$ is the Legendre polynomial of order m , and A_n and B_m are constants of integration fixed by the boundary conditions. The flow field about a sphere can be determined from this general solution. For small Reynolds numbers, the approximate dimensionless stream function is found to be

$$\psi = - \left[\frac{3}{4} (r - 1/r) - \frac{16 + 3 \text{Re}}{32} (r^2 - 1/r) + \frac{3 \text{Re}}{32} (r^2 - 1/r^2) \cos \theta \right] \sin^2 \theta . \tag{13-14}$$

Figure 13-5 shows the flow field about a sphere for $\text{Re} = 1$ as calculated by Tomotika and Aoi⁽¹³⁻¹²⁾. For $\text{Re} = 0$, Equation (13-14) reduces to Stokes' solution given by Equation (13-5).

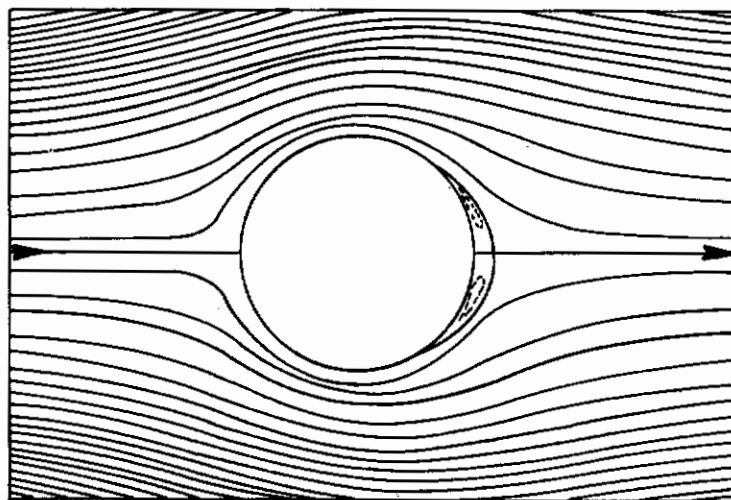


FIGURE 13-5. CALCULATED STREAMLINES ABOUT A SPHERE FOR $\text{Re} = 1$ (Tomotika and Aoi)⁽¹³⁻¹²⁾

In accordance with experimental observation a stationary vortex ring is formed behind the sphere. This vortex ring is always present, even when Re is small, although in this case it has a weak strength and is confined to the boundary layer.

In dimensionless cylindrical coordinates, the general solution of Equations (13-10) and (13-11) is

$$\chi = e^{kr} \cos \theta \sum_{m=0}^{\infty} B_m K_m(kr) \cos m \theta \quad (13-15)$$

and

$$\phi = A_0 \log r - \sum_{n=0}^{\infty} \frac{A_n \cos n \theta}{n r^n} \quad (13-16)$$

where, as before, A_n and B_m are constants of integration. The corresponding approximate non-dimensional stream function for flow about a cylinder is given by

$$\psi = [A(r - 1/r) - Br \log r] \sin \theta + [C(r^2 - 1/r^2) - Dr^2 \log r] \sin 2 \theta \quad (13-17)$$

where

$$A = 1/2 B = \frac{1}{2(\log Re - 2.0023)}, \quad C = \frac{-Re}{16}, \quad \text{and } D = -BC.$$

The flow about a cylinder corresponding to $Re = 4$, shown in Figure 13-6, is calculated by Tomotika and Aoi⁽¹³⁻¹²⁾, using the exact expression for the stream function involving modified Bessel functions.

Figure 13-7 shows that the regions of recirculating fluid lie within a parabolic region behind the cylinder. The recirculation regions are shown by the shaded areas for a series of Reynolds numbers. In agreement with observation, this region grows in size with increasing Reynolds number.

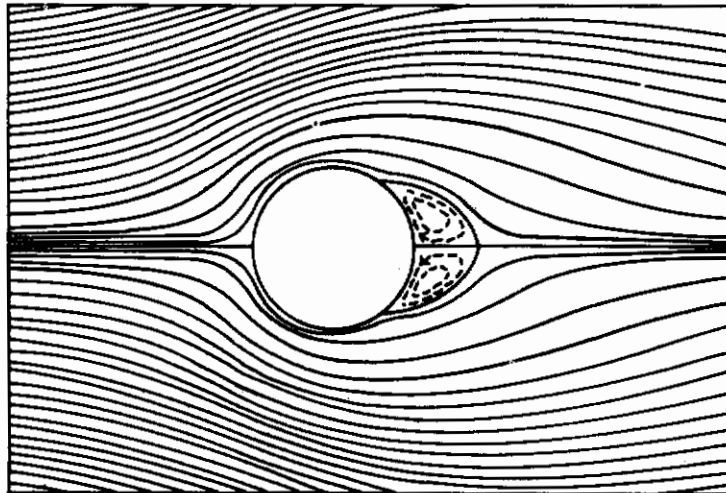


FIGURE 13-6. CALCULATED STREAMLINES ABOUT A CYLINDER FOR $Re = 4$

(Tomotika and Aoi)⁽¹³⁻¹²⁾

A comparison of the experimental and the calculated drag coefficients shows that Oseen's approximation holds for spheres when $Re \leq 2$ and holds for cylinders when $Re \leq 10$ ⁽¹³⁻¹²⁾. Thus, the approximation becomes inaccurate much below the critical Reynolds number for vortex shedding.

When Oseen's approximation is no longer valid, the flow can be calculated numerically by successive approximations similar to relaxation methods. The streamlines found in this way by Thom⁽¹³⁻¹⁴⁾ for the flow about a circular cylinder at $Re = 20$ are in good agreement with photographs of the actual flow⁽¹³⁻¹⁵⁾. The principal drawback of this direct numerical approach, aside from the great labor involved, is the necessity for recomputing the entire flow field for each desired value of the Reynolds number.

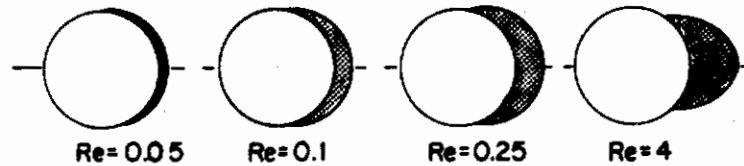


FIGURE 13-7. RECIRCULATING REGION BEHIND A CYLINDER FOR VARYING REYNOLDS NUMBERS

(Tomotika and Aoi)⁽¹³⁻¹²⁾

The Shedding of Vortices

Two possible mechanisms have been advanced for the blow-off of a flame attached to a bluff body as the velocity of the oncoming gas stream is increased. The first mechanism assumes that the recirculation region of hot, unburned gas behind the flame holder is unable to transfer heat rapidly enough to ignite the cold, unburned gas and thereby release enough energy to the downstream portion of the recirculation zone to maintain its temperature^{(13-16, 17, 18)*}. This explanation is general enough to cover both stable and shedding vortex systems.**

According to the second mechanism, the hot vortices become hydrodynamically unstable, are shed downstream, and thereby prevent the ignition of unburned gas^{(13-17, 20)***}. A variation on this mechanism would involve a premature transition from a laminar to a turbulent boundary layer on the flame holder; however, it is difficult to envision such an occurrence caused by heat addition downstream unless an oscillation mechanism is also proposed⁽¹³⁻²³⁾. Whether any variation of either or both of these mechanisms is the cause of blow-off is still an open question.

The behavior of the vortices can be studied by means of the close analogy that exists between the diffusion of the vorticity ζ in a viscous fluid and the diffusion of heat. The diffusion of vorticity is governed by the Equation (13-9)

$$\frac{d\bar{\zeta}}{d\tau} = (\bar{\zeta} \cdot \nabla) \bar{q} + \frac{1}{Re} \nabla^2 \bar{\zeta} \quad (13-18)$$

If the motion is started from rest, then $\bar{q} = 0$ and this equation becomes

$$\frac{d\bar{\zeta}}{d\tau} = \frac{1}{Re} \nabla^2 \bar{\zeta} \quad (13-19)$$

which has the same form as the equation for heat conduction.

*A homogeneous reactor theory recently advanced⁽¹³⁻¹⁹⁾ is a variation on this mechanism, but the aerodynamic problem does not enter into the formulation directly.

**There is some indication that vortex shedding when a flame is held might take place at a greater downstream distance from the holder.

***There is experimental evidence that when the flame is about to blow off, the downstream end of the recirculation region becomes unstable and moves upstream^(13-21, 22).

In the stationary regime, the vorticity produced at the solid boundary is just balanced by that which diffuses out of the recirculating region into the main body of the fluid. When a critical Reynolds number, Re_c , is reached, the additional vorticity produced by a small disturbance in the boundary layer exceeds the amount which the recirculating region can lose by diffusion; thus, the vortices in the wake become unstable and are shed downstream. According to Kovasznay⁽¹³⁻²⁴⁾, $Re_c = 40$ for a circular cylinder. By reducing the turbulent disturbances upstream, this instability can be inhibited, and symmetric stationary vortices can be observed in a metastable region where $Re > Re_c$.

Table 13-1 shows some experimental results of Thom⁽¹³⁻¹⁴⁾ which indicate that the presence of channel walls inhibits the shedding of vortices. The critical Reynolds number is based on the fluid velocity at large distances from the cylinder, while the corrected Re_c takes into account blockage, that is, the increase in stream velocity of the fluid passing around the cylinder owing to the decrease of cross-sectional area of the flow caused by the channel walls. After this correction is made, the inhibiting effect of the channel walls on vortex shedding becomes even more pronounced.

TABLE 13-1. CRITICAL REYNOLDS NUMBERS FOR THE SHEDDING OF VORTICES FROM CIRCULAR CYLINDERS AS A FUNCTION OF THE RATIO OF THE CHANNEL WIDTH, D , TO ITS DIAMETER, d (Thom)⁽¹³⁻¹⁴⁾.

Re_c	Re_c (Corrected)	D/d
30	31	40
46	48	20
62	68	10

For axially symmetric systems, the stationary vortex ring set up in the wake becomes unstable for a definite Re_c , above which irregular vortex loops are shed downstream with a random pitch and vorticity⁽¹³⁻²⁵⁾. Jefferys⁽¹³⁻²⁶⁾, after considering possible configurations, concludes that there is no regular arrangement of rings serving as a generalization of the two-dimensional vortex street. This is confirmed by Möller's photographs⁽¹³⁻²⁷⁾ of the irregular vortex forms produced in the wake of a sphere.

When Re_c is reached for a circular disk set normal to the main flow, the transverse diameter of the vortex ring is about 1.5 times the diameter of the disk. The corresponding Re is given by Stanton and Marshall⁽¹³⁻²⁵⁾ as $Re_c = 195$, while Simmons and Dewey⁽¹³⁻²⁸⁾ find $Re_c = 100$. The variation in the values of Re_c is probably due to differences in the turbulence initially present, since Re_c is a function of the magnitude of these initial disturbances.

The Vortex Street

Once the critical Reynolds number is exceeded for two-dimensional flow about an obstacle, vortices are shed with a regular frequency downstream, forming a vortex street as shown in Figure 13-8, where a is the distance between vortices in the same row and h is the distance between vortex rows. In an unbounded fluid, these trails of diffuse vortices tend to diverge downstream. In practice, however, this spreading is prevented by the presence of channel walls which compress the flow laterally, leading to the formation of parallel vortex rows⁽¹³⁻²⁹⁾.

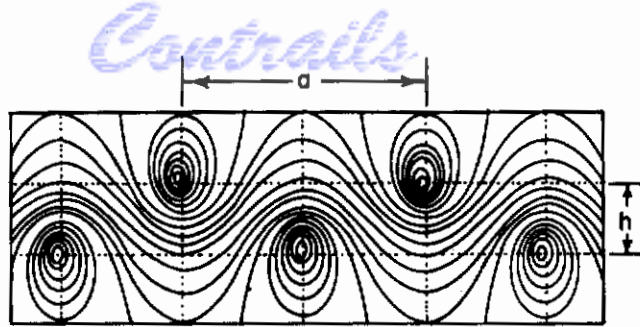


FIGURE 13-8. THE VORTEX STREET

Because of its hydrodynamic importance, the vortex street has been the subject of extensive investigation. Its theoretical treatment has been discussed in detail in several standard texts^(13-8, 9, 15). In view of its possible importance in determining the stability of combustion systems, a general survey of the principal features of the vortex street is given here.

In a theoretical analysis of this phenomena, Karman⁽¹³⁻³⁰⁾ replaced this system of diffuse vortices by an infinite double row of concentrated line vortices moving in an inviscid fluid, as shown in Figure 13-9. By dividing all lengths by a and all velocities by U_0 , the undisturbed stream velocity, the relations for the Karman vortex street can be expressed in dimensionless form. Each vortex of dimensionless strength, $\kappa = k/aU_0$, has no velocity due to vortices in its own row and a velocity of $1/2 \kappa \tanh(\pi r)$ due to those of the opposite row, where $r = h/a$ is the spacing ratio. Thus at large distances downstream from the obstacle, the vortex street moves with a velocity relative to the undisturbed fluid of

$$\bar{q}_s = \kappa/2 \tanh(\pi r) \quad (13-20)$$



FIGURE 13-9. THE KARMAN VORTEX STREET

The spacing ratio, r , can be determined from stability considerations. Thus, Karman⁽¹³⁻³⁰⁾ showed that such a configuration of vortices would be unstable for two-dimensional disturbances when each vortex is given an initial infinitesimal displacement unless

$$\sinh(\pi r) = \sqrt{2}, \text{ or } r = 0.36 \quad (13-21)$$

This spacing ratio should hold in the neighborhood of a bluff body. By displacing only a pair of vortices and holding the others fixed, Karman obtained instability unless

$$\sinh(\pi r) = 1, \text{ or } r = 0.28 \quad (13-22)$$

This ratio should be valid at large distances downstream^(13-31, 32). However, the Karman vortex street is unstable for three dimensional disturbances⁽¹³⁻³³⁾.

A symmetric double row, with the vortices of one row opposite to those of the other, will move forward as a whole along its length, but is unstable to two-dimensional disturbances. A double row with vortices of one row neither exactly opposite nor half-way between those in the other, will maintain its form, but will not move forward, and will not be stable in presence of disturbances⁽¹³⁻³⁴⁾. Some progress has been made in studying the stability of a system consisting of two pairs of vortex streets, but numerical evaluation of the mathematical results and comparison with experiment is still required⁽¹³⁻³⁵⁾.

Actually, r is always observed to be nearer to 0.36 than to the value given by Equation (13-22)(13-36, 37). Experiments(13-29) show that, despite irregularities in the vortex street, the longitudinal spacing, a , remains constant downstream. This is expected, since the velocity of the vortices along the street mask those due to instabilities which may be present(13-38). Normal to the street, these growing disturbances are not masked, and divergence of the two parallel rows of vortices is produced. As a result, h is not constant unless the fluid is bounded by channel walls.

For a cylinder of diameter d , as Re is increased several times larger than Re_c (13-29), a and h decrease until they approach limiting values given by $a/d \approx 5$ and $(h/d) \approx 1.7$. However, the spacing ratio, $r = h/a$, remains constant. The dimensionless velocity of the vortex street increases with Re until it reaches a limiting value of $q_s = 0.23$. From Equation (13-25), this implies that κ reaches the limiting value of 6.9. Results similar to those given here for cylinders hold for the vortex street set up behind other two-dimensional bodies(13-27).

The stability of the Karman vortex street in a channel of finite breadth has been treated theoretically by Glauert(13-40) and Rosenhead(13-41). The latter(13-29) has shown experimentally that wall effects are negligible if the channel is at least four times larger than the diameter of the obstacle.

Two important dimensionless parameters may be associated with the vortex street. The first is the Strouhal Number, S , which is a measure of the rate of vortex shedding. It is defined as

$$S = fd/U_0 \tag{13-23}$$

where f is the frequency with which vortices are shed from a body of diameter d , and U_0 is the undisturbed stream velocity. The variation of S with Reynolds number for a circular cylinder is shown in Figure 13-10, from which it can be seen that S tends asymptotically to a constant value of approximately 0.20 for large Re . Over a range of Reynolds numbers of interest, it follows from Equation (13-23) that the frequency of vortex shedding is a linear function of the main-stream velocity. Rayleigh(13-42) derived an empirical equation for S for circular cylinders from an analysis of the experimental data of Strouhal. This equation, which has been found to be in good agreement with later observations, is given by

$$S = 0.195 (1 - 20.1/Re) \tag{13-24}$$

For other two-dimensional bodies(13-32), the limiting value of S varies from about 0.15 to 0.30.

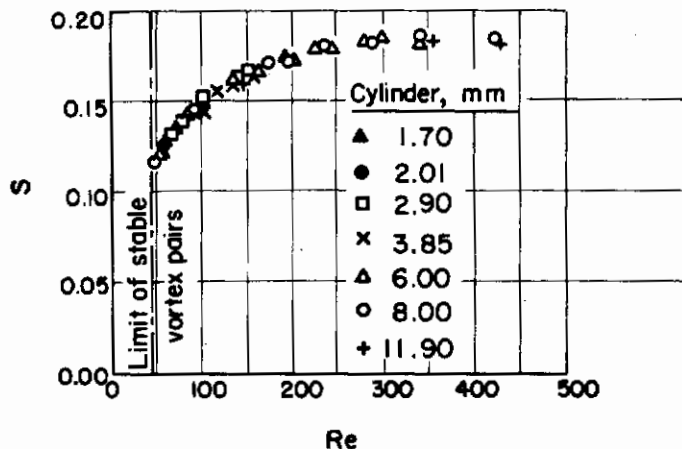


FIGURE 13-10. VARIATION OF STROUHAL NUMBER WITH REYNOLDS NUMBER FOR A CIRCULAR CYLINDER

(Camichel and Dupin)(13-2)

If S is defined using the distance between the free vortex layers behind an obstacle instead of the width of the obstacle, then for $Re \gtrsim 300$, for all obstacles, S equals 0.28, approximately(13-43).

This relation holds even after the entire boundary layer becomes turbulent and the drag coefficient takes a sudden drop (about $Re = 4 \times 10^5$ for cylinders)⁽¹³⁻⁴⁾.

Roshko⁽¹³⁻⁴³⁾ also indicates that there are three vortex shedding regions. For $40 < Re < 150$, the vortex shedding is stable, and the energy is dissipated by viscous processes. For $150 < Re < 300$, one finds an unstable region. For $Re > 300$ turbulence is also generated in the shear layer between the oncoming flow and the recirculation region. According to Roshko, it follows that Equation (13-24) should be replaced by two separate equations, one for $Re < 150$, and one for $Re > 300$.

Spivock⁽¹³⁻⁴⁴⁾ studied the vortex shedding frequency of two parallel cylinders. He found that the cylinders act independently, as far as frequency is concerned, when they are far apart. As the gap to diameter ratio, g/d , is decreased below one, the frequency, f , (and thus the Strouhal number, fd/U) jumps slightly and then decreases, rapidly at first and then more slowly, to a minimum value at $g/d = 1/11$. This is followed by a small increase to the Strouhal number associated with a cylinder having twice the original diameter when the gap becomes zero. At the same time as these changes occur in the primary frequency, a frequency associated with shedding through the gap becomes apparent. This frequency equals the primary frequency at $g/d = 1$, increases for $g/d < 1$, and levels off near $g/d = 1/2$. Below $g/d = 1/2$, the gap frequency drops to about $1/2$ the primary frequency and remains constant until it ceases at very small value of g/d . This final jump seems to indicate a change in shedding mechanism at this gap distance.

A second dimensionless ratio, K , can be introduced as a measure of the vorticity transported downstream by the vortex street. It is defined as

$$K = \kappa \bar{f}$$

where $\bar{f} = af/U_0$ is the dimensionless frequency with which the vortices are shed. By substitution of the value $r = 0.36$, given by Karman's stability analysis, Equation (13-20) becomes

$$\kappa = 2 \sqrt{3/2} \bar{q}_s \quad (13-25)$$

This result allows the strength of an individual vortex to be calculated from the velocity of the street. Simple kinematical considerations show that \bar{f} must be related to the dimensionless velocity of the vortex street according to

$$\bar{f} = 1 - \bar{q}_s \quad (13-26)$$

Multiplying these two equations together yields an equation for the vorticity transport parameter

$$K = 2.45 \bar{q}_s (1 - \bar{q}_s) \quad (13-27)$$

The maximum value of K occurs when $\bar{q}_s = 1/2$, for which

$$K_{\max} = 0.61 \quad (13-28)$$

Younger, Gabriel, and Michelson⁽¹³⁻³⁹⁾ made an extensive series of observations on the vortex street behind a series of flame-holding shapes. Since \underline{S} and \underline{K} are constant over the range of Reynolds numbers considered, their results can be usefully summarized in Figure 13-11, which gives the \underline{S} and \underline{K} values associated with various two-dimensional obstacles. It can be seen that by varying the body shape, \underline{S} can be doubled and \underline{K} increased by 60 per cent. However, these results have no immediate relation to flame-holder design because, (1) they refer to the cold flow, and (2) little is known about the relation between vortex shedding and blow-off so that optimum values of \underline{S} and \underline{K} may or may not exist for flame holding.

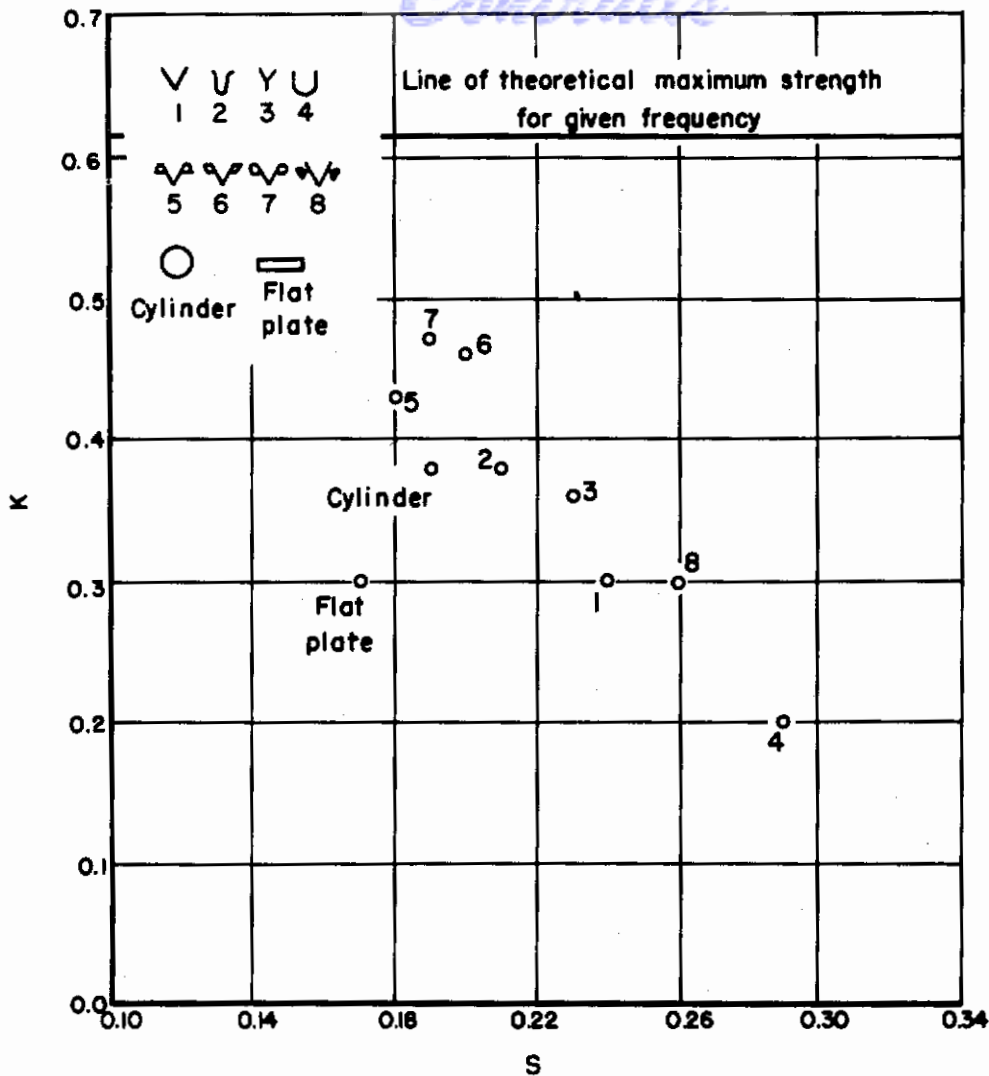


FIGURE 13-11. VORTICITY TRANSPORT PARAMETER PLOTTED AGAINST STROUHAL NUMBER

(Younger, Gabriel, and Michelson)⁽¹³⁻³⁹⁾

The drag on a body due to the vortex street can be calculated if the vortex spacing, a , and the velocity of the street, \bar{q}_s , are known. Heisenberg⁽¹³⁻⁴⁵⁾ attempted to calculate these quantities theoretically for the wake behind a flat plate, and obtained

$$\bar{q}_s = 0.23, a/d = 5.5, \text{ and } S = 0.14. \quad (13-29)$$

These values are in fair agreement with observation, although there is considerable variation among reported values. However, the assumptions underlying Heisenberg's theory cannot be justified⁽¹³⁻¹⁵⁾, so that a and \bar{q}_s must be found by direct measurement.

Nothing has been mentioned to this point about the mechanism which determines the frequency at which vortices are shed. Birkhoff⁽¹³⁻³⁸⁾ and Hanin⁽¹³⁻⁴⁶⁾ have advanced related theories of a conventional nature, while Shaw⁽¹³⁻²³⁾ has advanced an acoustic theory, for explaining the frequency of vortex shedding. The theories of Birkhoff and Hanin are discussed first.

Birkhoff pictures the wake behind an obstacle as swinging from side to side. The theoretical lift coefficient, by the Kutta-Joukowski theory, is then $2\pi\alpha$, where α is the angle of incidence of the wake with the mean stream direction. From Newton's second law, the force is equal to the acceleration of the mass involved; thus

$$-pd'l' \ddot{\alpha} = (2\pi\alpha) (\rho v^2/2) ,$$

(13-30)

where d' is the width of the wake and l' is the average length of the wavering portion of the wake. The frequency becomes

$$f = v/2 \sqrt{\pi d'l'} ,$$

(13-31)

and

$$S = 1/2 \sqrt{\pi} (d/k'l')^{1/2} ,$$

(13-32)

where $k = d'/d$. For $k = 4/3$ and $l' = 3d/2$, it follows that $S = 0.2$. Based on the width of the wake, d' , and the assumption that $l' = k'd'$, f becomes invariant with changes in other conditions, as noted experimentally by Roshko⁽¹³⁻⁴³⁾. Using the same basic assumptions, Hanin⁽¹³⁻⁴⁶⁾ made a more detailed analysis of this problem for the case of a flat plate.

Shaw⁽¹³⁻²³⁾ assumes that acoustic pressure waves are set up and move around the obstacle in such a manner that the pressure waves are in phase at the two separation lines on the obstacle, and are out of phase at the upstream central edge. The breaking away supplies the energy to this pressure-wave pattern. The frequency is high compared to the shedding frequency. For a cylinder, Shaw gives the frequency of $f_a = 3c/2\pi d$ for the appropriate wave system. Now when a vortex is shed, it is assumed to continue to oscillate at this frequency and send waves upstream. Since each pair of vortices does this, the vortex-shedding frequency is assumed to be 1/2 of the beat frequency, or

$$f = 1/2 (3c/2\pi d) (v - v_s)/c ,$$

(13-33)

where v_s is the velocity of the vortices relative to the main stream. It is clear that the assumption is also made that the maximum amplitude of the frequency, f_a , which now varies in amplitude because of the beat, initiates a discharge of the larger of the pair of vortices.

Since

$$S = fd/v = 0.239 (1 - v_s/v) ,$$

(13-34)

the possibility of agreement of this result with observation is clear. Shaw relates $(1 - v_s/v)$ to a theoretical equation for the drag coefficient, and from drag data computes S for $100 < Re < 10^6$. The agreement is excellent, considering all the factors involved. Thus, although the former theories are more logical, it would appear that this theory merits experimental investigation. If the theory is correct, the results may have considerable bearing on the blow-off mechanism of flame holders in certain regions.

Flow Within Closed Chambers

Thus far, only the flow about an obstacle in a uniform stream has been considered. However, in many combustion systems, the flow of gases takes place within a closed chamber to which the gases are admitted through one or more entrances and are expelled through one or more exits.

The complexity of the aerodynamics of such systems is illustrated by the fact that the optimum design of ports in the open-hearth furnace is still a matter of dispute⁽¹³⁻⁴⁷⁾. The flow may also lead to significant secondary effects. An example occurs in open-hearth furnaces⁽¹³⁻⁴⁸⁾ where erosion of the walls is caused by the abrasive action of particles which are thrown against the walls by large eddies set up by the blast of air directed against the molten charge.

Chesters and his co-workers^(13-49, 50) have published a series of striking photographs of a two-dimensional flow in various closed systems, as a preliminary to the study of the three-dimensional flow within furnaces⁽¹³⁻⁵¹⁾. First, they confirmed that when the volume flow rate of a

Contrails

jet normally incident on a second jet is increased until it is $3/4$ of the latter, the flow becomes unstable. This supports the empirical observation that the fuel and air jets in gas furnaces should not be directed at right angles to each other.

The photographs of Figure 13-12 show the unstable flow produced when liquid enters along the major axis of an ellipse and leaves through two symmetrically placed exits. As is evident from the photographs, there is a regular oscillation in flow - the "swinging jet" - so that most of the liquid is discharged through one of the exits while the other one remains relatively dry.

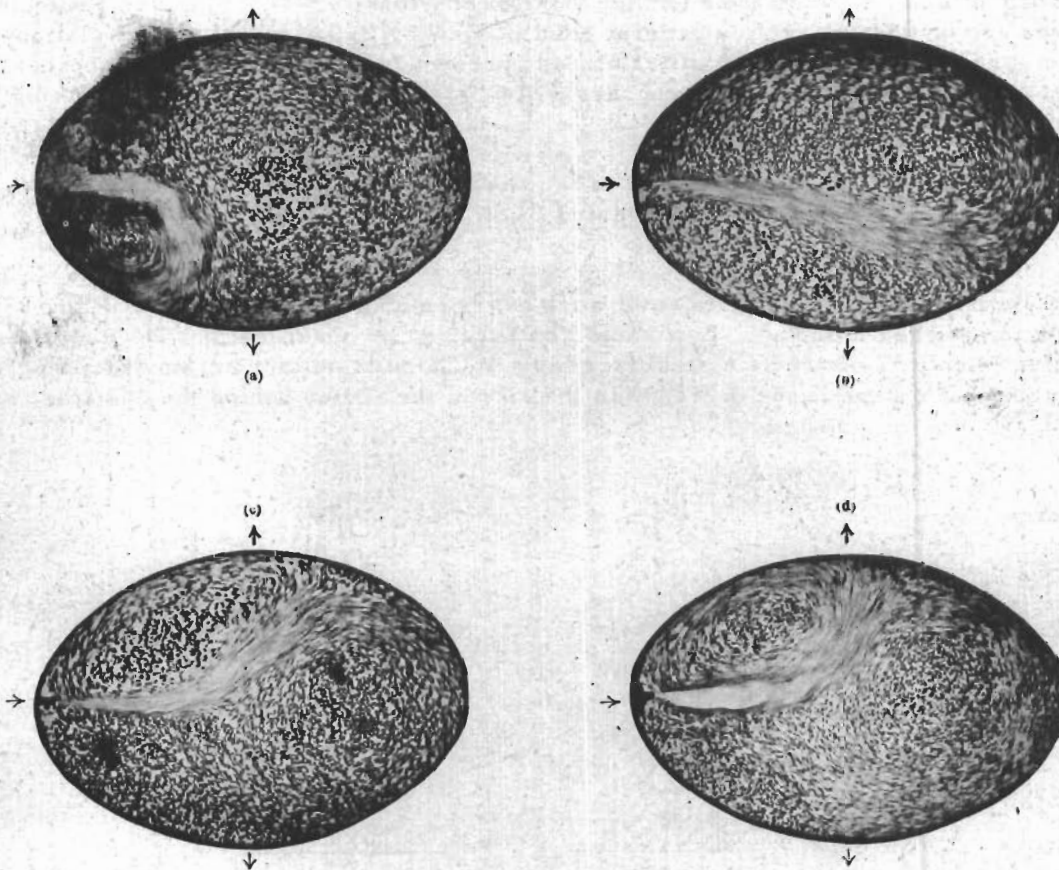


FIGURE 13-12. FLOW PATTERNS IN AN ELLIPSE, SINGLE ENTRY WITH A DOUBLE EXIT. FOUR POSITIONS OF THE UNSTABLE "SWINGING" JET

(Chesters and Philip)(13-49)

Other flows are comparatively stable. An example is a jet located at the midpoint of one of the sides of an equilateral triangle and directed toward the opposite corner, with exits at the other two corners. Here the presence of converging walls appears to inhibit the growth of instabilities in the flow.

At present, no general criteria exist which predict the relative stability of different configurations of exits and entrances.

RECIRCULATION IN DIABATIC FLOW

Thus far, all the flows discussed have been restricted to an incompressible fluid without heat sources. Heat addition through combustion can exert a profound influence on the nature of the flow because the fluid is no longer barotropic, that is, $\rho \neq F_1(p)$, so that Helmholtz's theorem on the conservation of vorticity for an inviscid fluid is no longer valid⁽¹³⁻⁵²⁾. As a result, vorticity can be produced when the fluid passes through the flame front. Some theoretical results have been

obtained for the steady rotational flow of an ideal gas having an equation of state of the form, $\rho = F_1(p) F_2(s)$, where $F_2(s)$ denotes a function of the specific entropy of the gas. A unified treatment of important results through 1949 has been given by Prim(13-53). The development is based on a substitution principle together with certain generalizations of Crocco's theorems(13-53) relating vorticity to pressure.

Tsien(13-55) has treated the influence of combustion on the flow field when a flame is attached to a stabilizer in a two-dimensional channel. He treats the flame as infinitely thin, but includes compressibility effects, extending the earlier work of Scurlock(13-56). The laws governing such diabatic flows are considered from a general point of view by Hicks(13-57). The relations derived are complex, and in view of the difficulties already present in the case of no heat sources it is doubtful that much further theoretical progress will be made in the near future in treating these more general flows.

Flow Behind Bluff Bodies

Only a limited amount of experimental work has been done on the flow field behind bluff bodies when a flame is attached to them*. Lewis and Von Elbe(13-58) observed that the flow about the end of a blunt wire when it is acting as a stabilizer for a V-flame is quite different from that in adiabatic flow. The principal change is the decrease in the size of the eddies behind the obstacle, as shown in Figure 13-13.

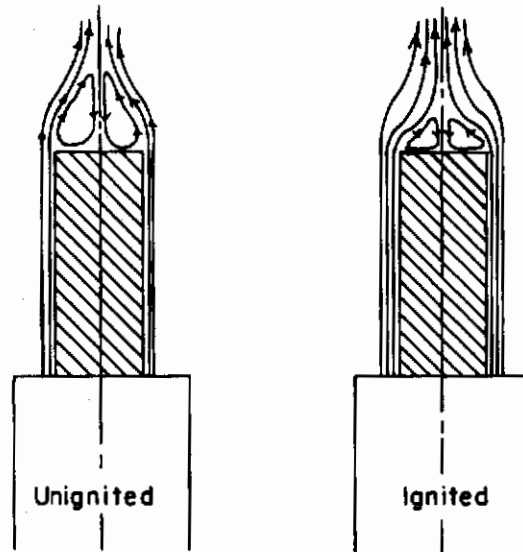


FIGURE 13-13. STREAMLINES ABOVE A WIRE WITH A FLAT END,
WIRE DIAMETER 0.21 CM

(Lewis and Von Elbe)(13-59)

Many of the observations on the diabatic flow behind bluff bodies have been made by the combustion group at MIT(13-1, 5, 21, 56, 60). These observers report that the most important influence of the flame is to inhibit the shedding of vortices, thus greatly extending the domain of Reynolds numbers for which a stable recirculation region exists. Since $Re = UL/\nu$ and $\nu \cong (T/T_0)^{7/4}$, there is a large decrease in the Reynolds number due to the increase in kinematic viscosity caused by the rise in temperature when the gas passes through the flame front, but the

*See Chapter 16 for treatment of combustion aspects of this problem.

stabilizing effect of the flame is much greater than this decrease in Re would indicate. However, these observations contradict those of Nicholson and Field⁽¹³⁻²⁰⁾, who claim that vortices are continuously shed from the flame holder into the wake, so that no stable recirculation region exists.

No adequate explanation has been given for this increase in hydrodynamic stability. Scurlock⁽¹³⁻⁵⁶⁾ has attributed it to a decrease in eddy size caused by the increase in the stagnation pressure in the burned gases behind the stabilizers, as shown in Figure 13-14.

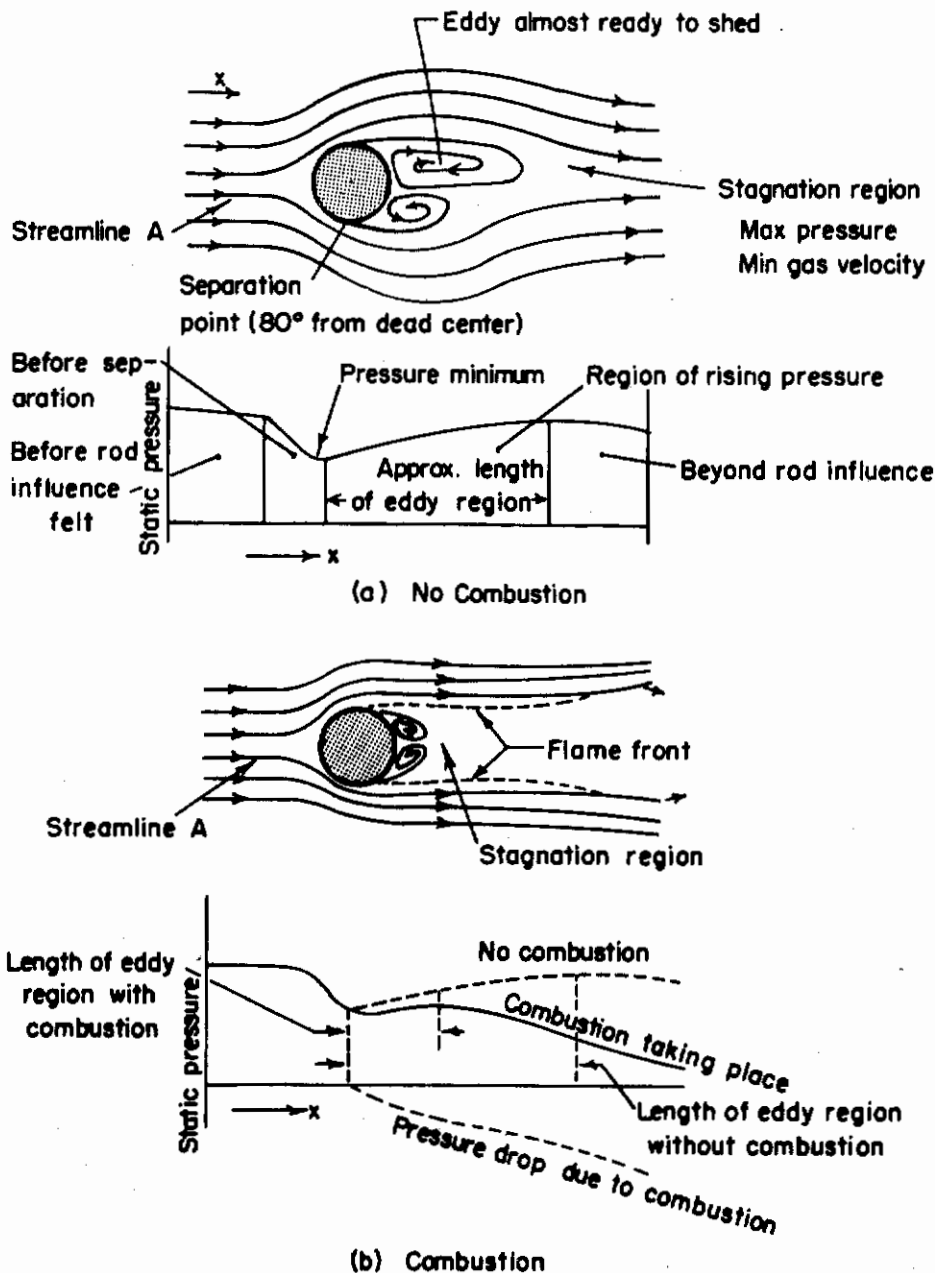


FIGURE 13-14. FLOW ABOUT A ROD

Evidence for the existence of a stable eddy region behind a flame holder can be derived from several sources⁽¹³⁻⁵⁹⁾. First, shadow photographs indicate that the stabilized flame is laminar. Second, it is observed that when a probe is placed at a short distance ahead of the flame, the front is violently disturbed by the eddies emanating from the probe; but if the latter is moved close enough to the front, the flame soon becomes attached to the probe which acts as a second stabilizer. When

this occurs, the flame is no longer violently disturbed, indicating that eddies are no longer being shed from the probe.

Finally, when a probe containing NaCl is inserted in the wake and moved to within an eddy length of the stabilizer, the entire recirculation region behind the flame holder suddenly becomes filled with an intense yellow light due to the incandescent sodium⁽¹³⁻⁶¹⁾.

Unfortunately, no detailed studies have been made on the dependence of this eddy length on Reynolds number or on flame-holder shape, although some evidence suggests that the eddy length is about 1-1/2 to 2 times the flame-holder diameter⁽¹³⁻²¹⁾. From a study of flame widths for stabilizing shapes, Scurlock⁽¹³⁻⁵⁶⁾ has tentatively concluded that the width of the eddy region for gutters is less than for cylinders with the same characteristic dimension. On the other hand, because the blowout limits are about the same, he concludes that the corresponding eddy lengths are approximately equal.

Putnam⁽¹³⁻⁶²⁾ presents data showing that the stability limits of a series of flame holders of a single diameter increases with an increase in the angle between the flow axis and the flame at the point of contact with the flame holder. The result is attributed to an increase in size of recirculation zone.

Vortex Shedding Behind Flame Holders

When a flame is attached to a flame holder, vortices may be shed downstream by two mechanisms. The first mechanism is related to an instability of the boundary layer which leads to the formation of the Karman vortex street. This mechanism is shown by the schlieren photograph of Figure 13-15. The observed frequency is in approximate agreement with the calculated frequency based on the flow velocity of the unburned gas. However, the vortices apparently propagate along the flame front which serves as an interface between the hot and cold gases, rather than directly downstream. It also may be noted that the vortex spacing increases rapidly downstream.

The second cause of vortex shedding, which has been investigated experimentally by Scurlock⁽¹³⁻⁵⁶⁾, is due to the velocity gradients produced across the flame front. These are shown schematically in Figure 13-16.

In a classic paper, Rayleigh⁽¹³⁻⁶⁴⁾ showed that a discontinuity of velocity across two adjacent streamlines is unstable and will roll up into a series of vortices⁽¹³⁻⁶⁵⁾. In a real fluid, where no discontinuities in velocity can exist, hydrodynamic stability is a function of the velocity gradient and the Reynolds number of the flow⁽¹³⁻⁶⁶⁾. In general, increases in velocity gradient and Re favor instability.

From Figure 13-16, it can be seen that there are two regions with high velocity gradients which would serve as a source of vortices. One region is at large distances downstream due to the expansion and acceleration of the unburned gases in the confined system. The other region occurs in the neighborhood of the flame holder where there is a large difference in velocity between the unburned gas in the main stream and the relatively stagnant hot gas in the recirculating region. Scurlock⁽¹³⁻⁵⁶⁾ has taken shadowgraphs, as shown in Figure 13-17, which vividly demonstrate the development of vortices from the latter region. The small insert Photograph 5-1-93 shows very clearly the dark region behind the flame holder associated with the hot recirculating gases. All the disturbances are symmetric, except in Photograph 4-2-91, where turbulence has been introduced into the unburned gas by inserting a mesh upstream. This is in contrast to the asymmetric pattern of the vortex street.

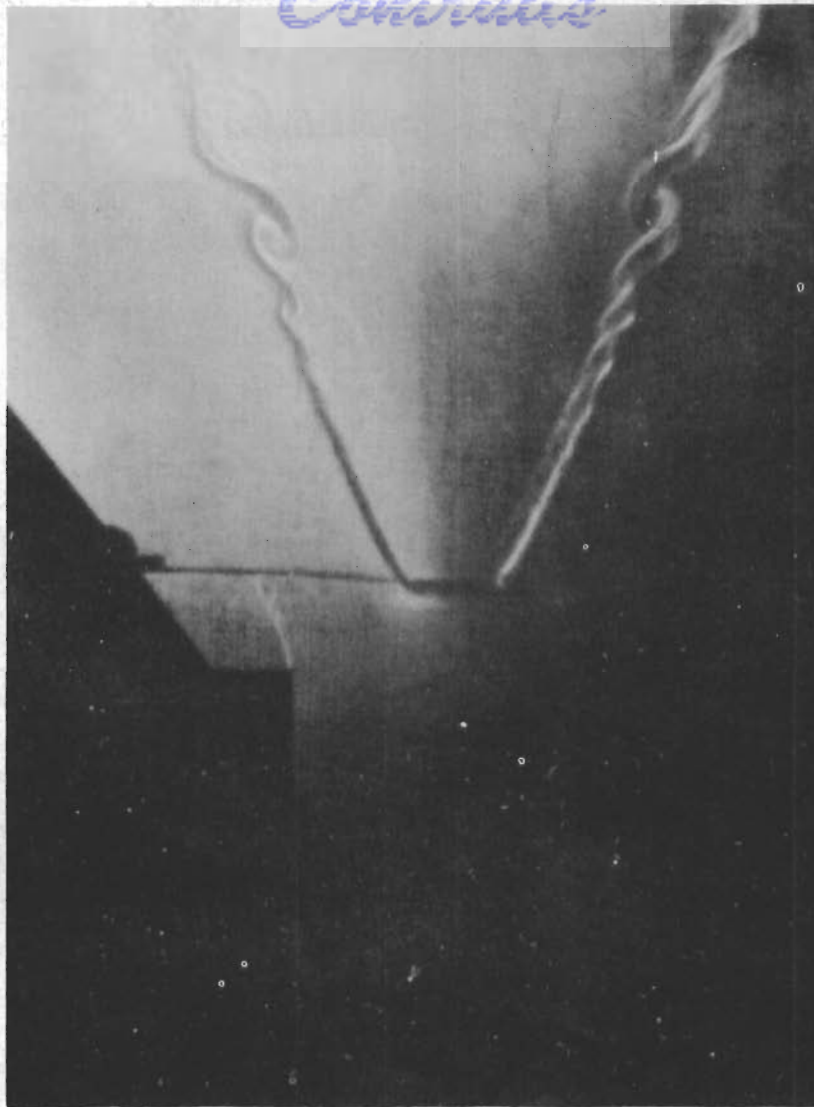
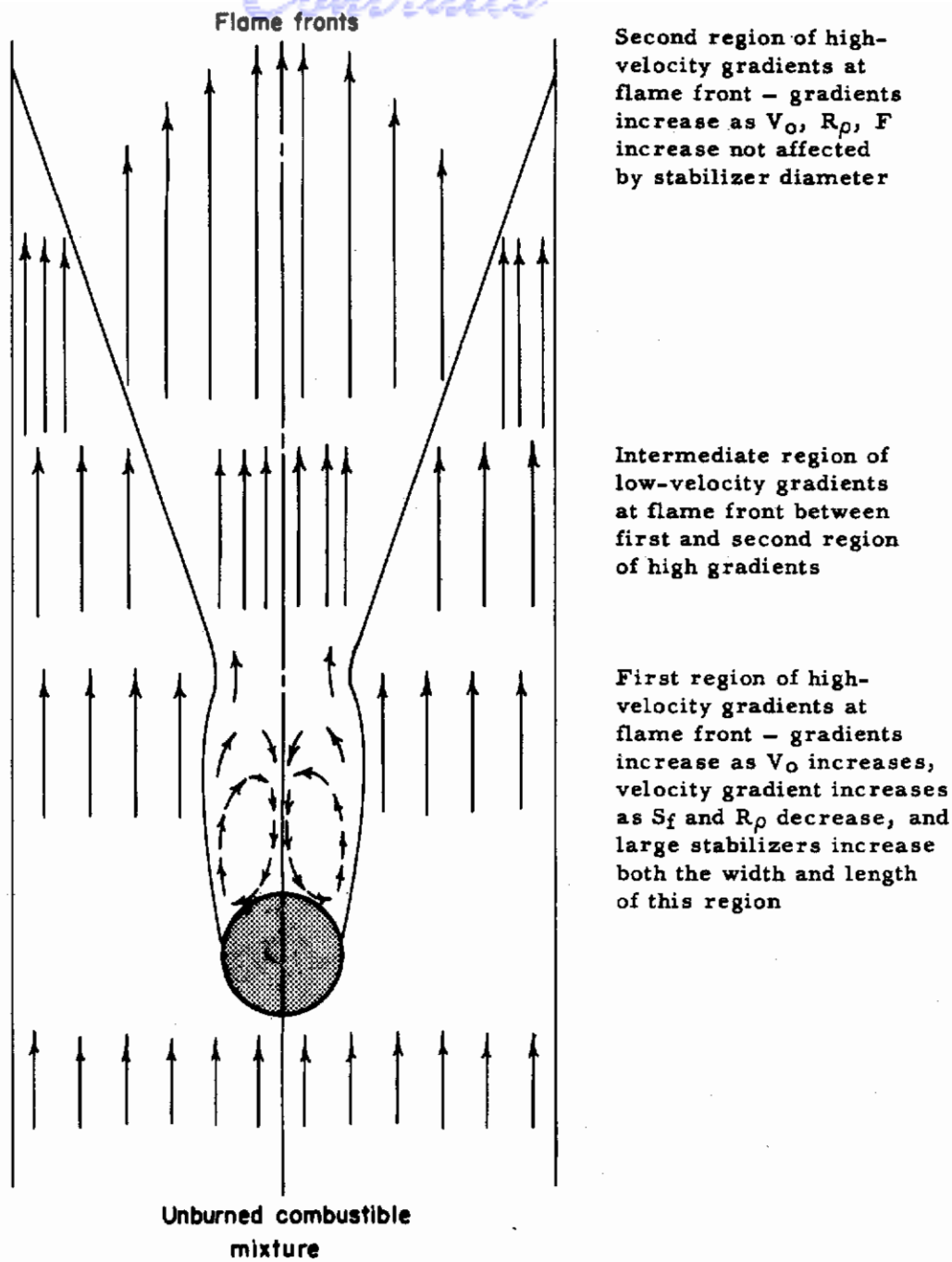


FIGURE 13-15. VORTEX SHEDDING FROM A FLAT PLATE WITH AN ATTACHED LEAN-PROPANE FLAME ($Re \approx 9,000$)

(Putnam and Kleider)⁽¹³⁻⁶³⁾

Finally, the importance of oscillations in distorting the flame front should be noted^(13-67, 68, 69, 70). Since most experiments are conducted on flames in confined chambers, the unstable flame front may set up a resonant pulsation in the system which can exert a profound influence on the combustion process. An example of this phenomenon is the "singing flame" obtained by placing a long tube over a Bunsen flame. Such resonant pulsations lead to a symmetric distortion of the flame front, as shown in the shadowgraph of Figure 13-18.



Second region of high-velocity gradients at flame front - gradients increase as V_0 , R_ρ , F increase not affected by stabilizer diameter

Intermediate region of low-velocity gradients at flame front between first and second region of high gradients

First region of high-velocity gradients at flame front - gradients increase as V_0 increases, velocity gradient increases as S_f and R_ρ decrease, and large stabilizers increase both the width and length of this region

FIGURE 13-16. SCHEMATIC DIAGRAM OF THE FLOW PATTERN BEHIND A FLAME HOLDER, SHOWING THE HIGH-VELOCITY GRADIENTS NEAR THE FLAME

(Scurlock)(13-56)

Since little work has been done on diabatic flows, the experimental observations which have been given here must be regarded as only a brief survey of the principal facts known about this largely uncharted field.

Contrails



V = 24.3
1/f = 12.57
d = 0.038"



V = 25.2
1/f = 11.87
d = 0.038"



V = 24.1
1/f = 12.50
d = 0.498"



V = 49.1
1/f = 11.84
d = 0.498"

FIGURE 13-17. SHADOWGRAPHS OF THE VORTEX FORMATION BEHIND ROD FLAME HOLDERS. V IS THE MAIN STREAM VELOCITY IN FT PER SEC; d , THE DIAMETER OF THE ROD, AND $1/f$ IS THE MASS AIR-FUEL RATIO

(Scurlock)(13-56)



FIGURE 13-18. SHADOWGRAPH OF V-FLAME IN COMBUSTION CHAMBER. $d = 0.125$ IN., $V = 15$ FT PER SEC

(Dunlap)(13-67)

Aerodynamic investigation of combustion systems presents many difficulties largely due to the high temperatures involved. For this reason, attempts have been made to simulate combustion by another physical process which can be studied more easily in the laboratory. Such a process of modeling a combustion system, as well as the associated fields of dimensional analysis and similarities as applied to combustion, are discussed in detail by Weller and Thomas⁽¹³⁻⁷¹⁾.

The principal effect of combustion as far as the aerodynamic flow is concerned is the decrease in density of the burned gas and its increase in kinematic viscosity due to the rise in temperature caused by burning. The decrease in density can be as much as 1/7 for stoichiometric mixtures, with a corresponding increase of thirty times in the kinematic viscosity. Several attempts have been made to model these effects. One method of representing the gas dynamic aspects of flow through a plane combustion front is by the application of the water channel analogy with a flux source simulating combustion⁽¹³⁻⁷²⁾. Another method consists of simulating the increase in kinematic viscosity due to combustion by injection of a Methocel solution into water, whose effect is to increase the viscosity of the water without changing any of its other properties⁽¹³⁻⁷³⁾.

However, to date, simulation has been successfully applied to combustion systems only in studying the flow caused by the buoyant forces created by variations in density. Thus, Groume-Grjmailo⁽¹³⁻⁷⁴⁾ investigated the stratification due to buoyancy of gas within furnaces by using streams of colored paraffin and water. Another example is the work of Rosin⁽¹³⁻⁷⁵⁾, who made an interesting study of the flow of hot gases up chimneys of open fireplaces. He replaced the bed of coal by salt briquettes which were dissolved by flowing water to simulate the flow of air. By setting the model upside down, the increase in density of the saturated salt water solution is partly analogous to the decrease in the density of the burned gases. This model is open to criticism since the change in density corresponds to an increase of only 40 per cent, whereas the density of the burned gases may fall to 1/3 or 1/4 its cold value. However, using this simulation technique, Rosin was able to show many of the relevant features of the flow in chimneys. In particular, he showed that efficiency is seriously impaired when, due to sharp protrusions, a standing vortex is set up in the throat of the chimney. On the basis of this study, he suggested an improved chimney design to eliminate such defects.

Finally, it may be noted that, because of difficulties in modeling the flow of hot gases, almost all research on the flow patterns in furnaces^(13-47, 48, 51, 74, 75) has been limited to cold flow. As a result, it is questionable how far these results apply to the flow of hot gases within furnaces.

RECIRCULATION IN PRACTICAL COMBUSTION SYSTEMS

In this section some useful types of recirculation regions in combustion systems are considered.

Spin-Stabilized Burner

Figure 13-19 shows a typical spin-stabilized domestic oil burner. This type of stabilization is to be found in most domestic and commercial oil burners, although the spin may be produced by various other burner designs. The entering air is swirled at A by vanes and the swirling air passes outward through the nozzle. The spinning air mass is discharged in a hollow-cone dispersion, entraining air from the center region to create a low-pressure area at the center. From B hot gas flows downstream into this low-pressure area and ignites the fresh combustible mixture. A secondary recirculation pattern may be set up in the surrounding gases at C and D, depending on furnace design. The hollow cone of fuel oil droplets usually has such an angle that the fuel moves together with the fresh gases.

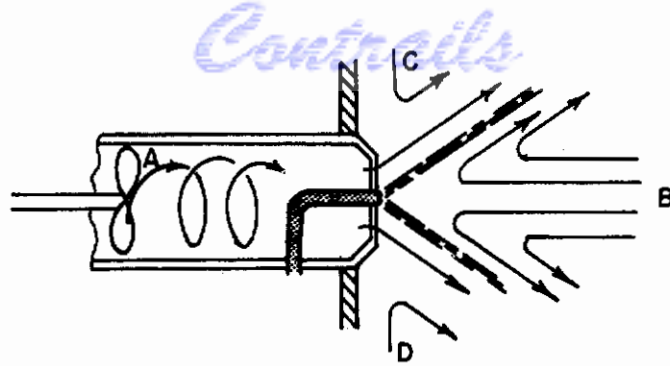


FIGURE 13-19. SPIN-STABILIZED OIL BURNER

Baffle Flame Holder

Figures 13-13, 13-14, and 13-16 amply illustrate the recirculation pattern behind simple obstacles. Because of shearing forces, the flow over the edges causes the gases behind an obstacle to rotate. This rotation is more like a rotating solid body than like a vortex, in which the tangential velocity decreases outward from the center of rotation. The recirculation volume may be roughly spherical in shape, as behind the axially symmetric flame holder of Figure 13-13, or may be cylindrical, as behind the rod in Figure 13-16, or behind the V gutters found in some ram jets and afterburners. For annular gutter flame holders, it follows that the recirculation region is doughnut shaped.

The fuel is usually injected upstream of these units, so that a combustible mixture, in the vapor phase, flows by the flame holder. However, some of the fuel may not evaporate before reaching the flame holder, and, consequently, may deposit on the baffle side of the flame holder. The stability limits and combustion processes associated with the baffle flame holders are discussed in more detail in Chapter 16. It should be noted, however, that in combustion systems in use, the baffles usually have a V or U section. They are usually in multiple form, forming a grid or set of annular rings. In ram-jet application, the blockage area is relatively high, usually about 40 to 60 per cent. For afterburners, the blockage is somewhat less, and is, on occasion, decreased further by staggering the holders.

Asymmetric Flame Holder

Figure 13-20 shows an asymmetric flame holder, in which the air is supplied through an opening at A. A recirculation is set up in the region, B, bounded on the top by the combustion-chamber wall, C. The fuel is sprayed in roughly parallel to this air jet and just above it. If one pictures two of these units placed back to back at the wall, C, and the wall removed, the pattern of flow is seen to be similar to that for the symmetric baffle flame holder. The location of the injected fuel approximately along the interface between the hot, recirculating gases and the fresh gases corresponds to that in the spin-stabilized burner.

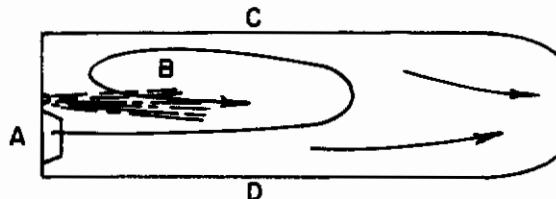


FIGURE 13-20. ASYMMETRIC FLAME HOLDER

Figure 13-20 is also a good illustration of the behavior of an orifice-type flame holder. In this case the unit is considered to be symmetric about the lower wall, D, and the wall removed. However, with orifice-type flame holders, as with baffles, it is common to inject the fuel upstream, or use gaseous fuel, so that a combustible mixture is supplied to the burner.

Can-Type Combustor

Figure 13-21 shows a typical can-type combustor. The air moves radially inward from the first rows of orifices at a high velocity and impinges at the center. Part of the air moves upstream along the axis, outward along the dome, and downstream along the wall. Some air is admitted in slots along the wall to prevent carbon deposits and to cool the metal wall. The fuel is injected in a hollow-cone spray pattern, thus giving an over-all flow pattern which somewhat resembles that found in the swirl-type oil burner. Additional air is admitted through orifices and slots further downstream. Secondary recirculation is also set up between pairs of orifices in the same row, as might be expected, and thus the over-all flow pattern is highly conducive to large-scale mixing.

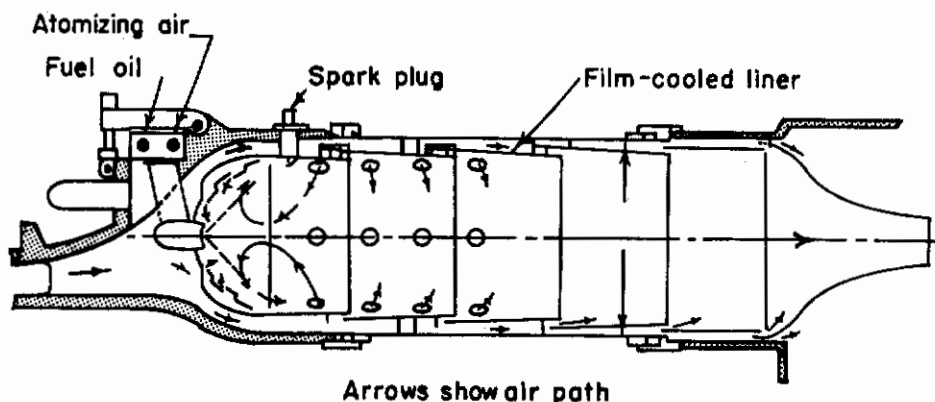


FIGURE 13-21. COMBUSTOR FOR GENERAL ELECTRIC 4800-HP LOCOMOTIVE GAS TURBINE, FOR RESIDUAL FUEL OIL

Controlled Recirculation Burner

Figure 13-22 is a schematic diagram of a controlled recirculation burner. The fuel oil enters the burner through a pressure atomizing nozzle, and is vaporized by the hot, recirculated products of combustion. By so designing the recirculation chamber that the pressure increases downstream, hot, burned gas is drawn through the chamber and is ejected into the unburned fuel-air mixtures. Burning takes place downstream, where the velocity of the oncoming gas decreases due to the divergence of the channel walls.

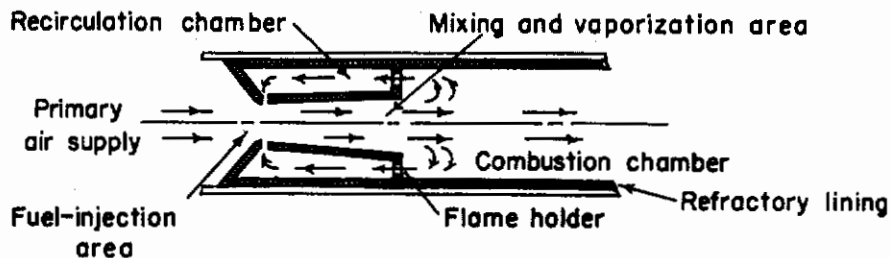


FIGURE 13-22. SCHEMATIC DIAGRAM OF HIGH-VELOCITY BURNER

(Peskin)(13-76)

Figure 13-23 shows a section of the Curtiss-Wright J-65 engine. This unit illustrates some variations on the scheme of controlling the flow of gases for specific purposes. The fuel flows at a rather low pressure onto a hot surface, where it vaporizes and is mixed with a turbulent stream of primary air. Burning begins before the gases leave the J-shaped tube. Secondary air is supplied by sets of air jets which contribute to mixing.

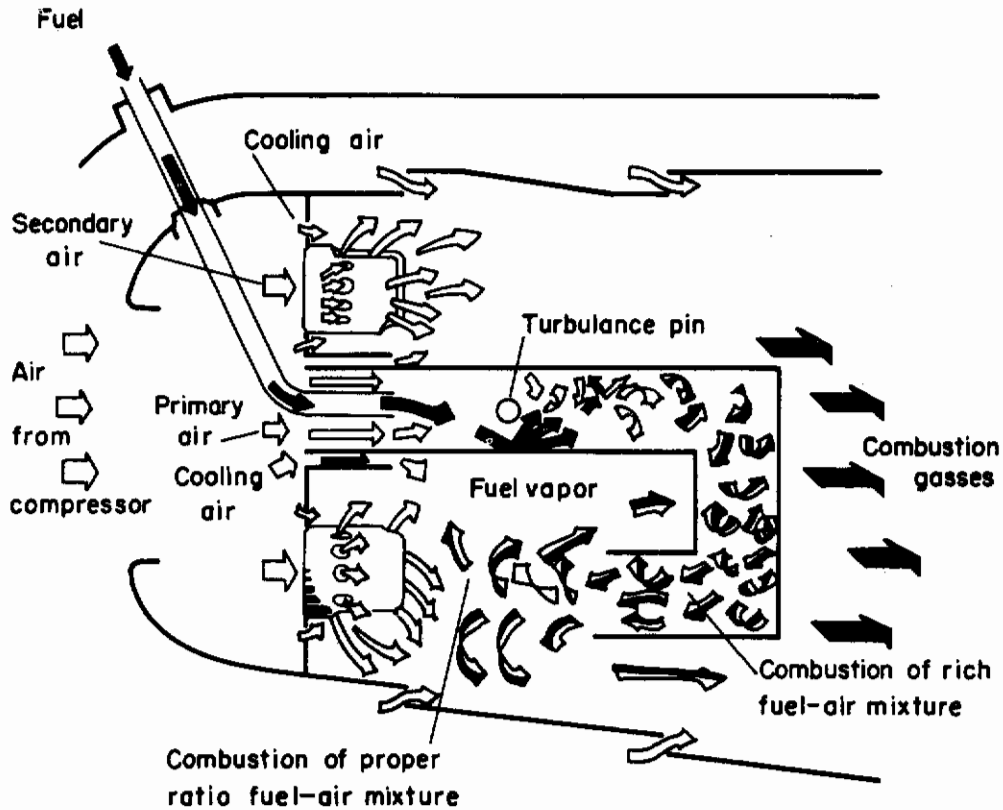


FIGURE 13-23. THE COMBUSTION CHAMBER OF THE CURTISS-WRIGHT J-65

(Reproduced from Curtiss-Wright Drawing)

CONCLUDING REMARKS

In view of the enormous difficulties in the way of further theoretical advances, work in the immediate future should be concentrated on a broad program of experimental research. Such a program can be divided into two phases: one phase should be concerned with adiabatic flow and the other phase should be concerned with diabatic flow.

Adiabatic Flow

The recirculation pattern which has been discussed in the previous section is comparable to rotation of a solid body; only after the breaking away of the recirculation pattern, or part of it, from the region of generation of circulation does the pattern start to degenerate into a vortex, wherein the tangential velocity is inversely proportional to the radius. Thus, in a combustion

system, the fully developed vortex street which has been investigated quite extensively for two-dimensional flow probably never develops. Not only are the flows often three dimensional, but the region in which the recirculation is initially generated is the region of greatest interest relative to flame holding*. It appears that theories to explain vortex shedding frequencies need specific experimental confirmation. The influence of laminar and turbulent momentum interchange must be evaluated; the rate of approach of the actual flow field to that of classical fluid dynamics should be determined; and, finally, the critical range in which various modes of recirculation occur should be ascertained. In connection with the study of three-dimensional flow fields, as opposed to two-dimensional flow fields, the difficulty of visualization of a three-dimensional flow field has always been an obstacle. However, this might be overcome by extensive application of stereoscopic-photographic techniques, which would allow the shedding of vortex rings behind axial symmetrical flame holders to be studied.

Diabatic Flow

Because little is known about the flow fields which occur behind bluff bodies when the flame is attached to them, general studies should be undertaken to determine the nature of these diabatic flows. The large difference in gas density between the recirculation zone and the oncoming gases is the most obvious complication. It may even be that flow with a flame present is more similar to cavitation flows behind an obstacle moving in water, than to the adiabatic flow discussed in this chapter. In any case, the change in flow patterns and critical Reynolds numbers when flames are present should be studied thoroughly. Also important to some theories of flame holding and stability is the size of the recirculation zone, and the transport properties across the boundaries. Finally, measurements of the change in drag on the stabilizer caused by the presence of the attached flame should be made; in afterburners and ram jets the relation between drag and flame-holding ability is extremely important, as well as the question of whether there is an optimum shape producing minimum drag for a given range of operation.

REFERENCES

- 13-1. Williams, G. C., Basic Studies on Flame Stabilization; J. Aero. Sci., Vol. 16, 1949, p 714.
- 13-2. Camichel, C., and Dupin, P., Flow of a Viscous Liquid About an Obstacle - Curves α , β - Alternating Vortices of Bernard-Karman; J. Rheology, Vol. 3, 1932, p 413.
- 13-3. Homann, P., Influence of Large Viscosities on the Flow About Cylinders and Spheres; Forsch. Ing.-Wes., Vol. 7, 1936, p 1.
- 13-4. Delaney, N. K., and Sorensen, N. E., Low-Speed Drag of Cylinders of Various Shapes, NACA TN 3038, Nov., 1953.
- 13-5. Mikol, E. P., Flames of Fuel Gases Issuing and Burning in the Wakes of Cylinders; Meteor Report No. 67, MIT, June, 1949.
- 13-6. Prandtl, L., and Tietjens, O. G., Applied Hydro- and Aeromechanics, McGraw-Hill Book Company, New York, 1934, p 279.

*The further history of the vortex may be of importance in flame spreading, as discussed extensively in Chapter 15.

- 13-7. Birkhoff, G., Hydrodynamics, A Study in Logic, Fact, and Similitude, Princeton University Press, Chap. 3, 1950.
- 13-8. Lamb, H., Hydrodynamics, Dover Publications, New York, 1945, p 594, 225, 680.
- 13-9. Milne-Thomson, L. M., Theoretical Hydrodynamics, Macmillan Company, New York, 1950, p 523, 413, 505, 338.
- 13-10. Goldstein, S., The Steady Flow of Viscous Fluid Past a Fixed Spherical Obstacle at Small Reynolds Numbers; Proc. Roy. Soc., (London) Vol. 123A, 1929, p 225.
- 13-11. Flaxen, H., Exact Solution of Oseen's Differential Equation for the Case of Translatory Motion of a Cylinder; Nova Acta Regiae Societatis Scientiarum Upsaliensis, Volumen extraordinem, 1927, p 1.
- 13-12. Tomotika, S., and Aoi, T., The Steady Flow of Viscous Fluid Past a Sphere and Circular Cylinder at Small Reynolds Numbers; Quart. J. Mech. Appl. Math., Vol. 3, 1950, p 140.
- 13-13. Tomotika, S., and Aoi, T., The Steady Flow of a Viscous Fluid Past an Elliptic Cylinder and a Flat Plate at Small Reynolds Numbers, Quart. J. Mech. and App. Math, Vol. 6, 1953, p 290.
- 13-14. Thom, A., The Flow Past Circular Cylinders at Low Speeds; Proc. Roy. Soc., (London) Vol. A141, 1933, p 651.
- 13-15. Goldstein, S., Modern Development in Fluid Dynamics, Oxford University Press, London, 1938, Vol. 1, Chap. 2, p 64; Vol. 2, Chap. 13; p 546.
- 13-16. Putnam, A. A., and Carrier, G. F., A Model of the Flame-Holding Mechanism, Battelle Memorial Institute, Technical Report No. 15033-2, May, 1953.
- 13-17. Longwell, J. P., Flame Stabilization by Bluff Bodies and Turbulent Flames in Dusts, Fourth Symposium on Combustion, Williams and Wilkins, Baltimore, Md., 1953.
- 13-18. Spalding, D. B., Theoretical Aspects of Flame Stabilization, Aircraft Engineering, Sept., 1953, p 264.
- 13-19. Longwell, J. P., Frost, E. E., and Weiss, M. A., Flame Stability in Bluff Body Recirculation Zones, Ind. Eng. Chem., 45, 1953, p 1629.
- 13-20. Nicholson, H. M., and Field, J. F., Some Experimental Techniques for the Investigation of the Mechanism of Flame Stabilization in the Wakes of Bluff Bodies; Third Symposium on Combustion, Flame and Explosion Phenomena, Williams and Wilkins Co., Baltimore, 1949, p 21.
- 13-21. Longwell, J. P., Combustion Problems in Ram Jet Design, J. Aero. Sci., Vol. 16, 1949, p 707.
- 13-22. Kutzko, G. G., Battelle Memorial Institute, Unpublished Schlieren Motion Pictures.
- 13-23. Shaw, R. A., The Solution of the Problem of a Cylinder Shedding a Periodic Wake; Fluid Motion Subcommittee, Aeronautical Research Council 12, 696 FM 1395, Nov., 1949.
- 13-24. Kovaszny, L. S. G., Hot Wire Investigation of the Wake Behind Cylinders at Low Reynolds Number; Proc. Roy. Soc., (London) Vol. A198, 1949, p 174.
- 13-25. Stanton, T. E., and Marshall, D., Eddy Systems Behind Discs, Proc. Roy. Soc., (London) Vol. A130, 1931, p 295.

- 13-26. Jeffreys, H., The Wake in Fluid Flow Past a Solid; Proc. Roy. Soc., (London) Vol. A128, 1930, p 376.
- 13-27. Möller, W., Experimental Study of the Hydrodynamic Motion of the Sphere, Phys. Z., Vol. 39, 1938, p 57.
- 13-28. Simmons and Dewey, British A.R.C. Rep. and Mem., No. 1334, 1931.
- 13-29. Rosenhead, L., and Schwabe, M., An Experimental Investigation of the Flow Behind Circular Cylinders in Channels of Different Breadths; Proc. Roy. Soc., (London) Vol. A129, 1930, p 115.
- 13-30. Von Karman, T., Göttinger Mach., p 509, 1911, (Translated in de Bothezat, G., An Introduction to the Laws of Air Resistance); NACA Rep No. 28, 1920.
- 13-31. Von Karman, T., Göttinger Mach., 1912, p 225.
- 13-32. Von Karman, T., and Rubach, H., On the Mechanism of Liquid and Air Resistance, Phys. Z., Vol. 13, 1912, p 49.
- 13-33. Rosenhead, L., The Spread of Vorticity in the Wake Behind a Cylinder, Proc. Roy. Soc., (London) Vol. A127, 1930, p 590.
- 13-34. Rosenhead, L., Double Row of Vortices With Arbitrary Stagger; Proc. Camb. Phil. Soc., Vol. 25, 1929, p 132.
- 13-35. Coddington, E. A., The Stability of Infinite Differential Systems Associated With Vortex Streets, J. Math and Physics, Vol. 30, 1951, p 171.
- 13-36. Bernard, H., On the Inexactness for a Real Liquid of Karman Theory on the Stability of Alternating Vortices; Comptes Rendus, Vol. 128, 1926, p 1523.
- 13-37. Fage, A., and Johansen, F. C., The Structure of Vortex Sheets, Phil. Mag., Vol. 5, 1928, p 417.
- 13-38. Birkhoff, G., Formation of Vortex Streets, J. App. Physics, Vol. 24, No. 1, 1953, p 98.
- 13-39. Younger, G., Gabriel, D. S., and Michelsen, W. R., Experimental Study of Isothermal Wake-Flow Characteristics of Various Flame-Holder Shapes, NACA RM E51K07, 1952.
- 13-40. Glauert, H., The Karman Vortex Street in a Channel of Finite Breadth, Proc. Roy. Soc., (London) Vol. 120A, 1928, p 34.
- 13-41. Rosenhead, L., The Karman Vortex Street in a Channel of Finite Breadth, Phil. Trans. Roy. Soc., (London) Vol. A228, 1929, p 275.
- 13-42. Rayleigh, W., Aeolian Tones, Phil. Mag., Vol. 29, 1915, p 443.
- 13-43. Roshko, A., On the Development of Turbulent Wakes From Vortex Streets, NACA TN 2913, March, 1953.
- 13-44. Spivock, H. M., Vortex Frequency and Flame Pattern in the Wake of Two Parallel Cylinders at Varied Sporing Normal to an Air Stream, J. Aero. Sci., Vol. 13, 1946, p 289.
- 13-45. Heisenberg, W., The Absolute Dimension of the Karman Vortex Motion, Phys. Z., 23, 1922, p 363.

- 13-46. Hanin, M., Generation of Vortices Behind a Flat Plate, submitted to Office of Scientific Research, U. S. Air Force Research and Development Command, Baltimore, Md., under Contract No. AF 33(038)-21406, 1953.
- 13-47. Leys, J. A., and Leigh, E. T., Pressure and Flow Distribution in a Model of a Venturi-Type Open-Hearth Furnace, J. Iron Steel Inst., Vol. 165, 1950, p 301.
- 13-48. Newby, M. P., Experiments on the Gas and Fluid Flow in Side-Blown Converter Model, J. Iron Steel Inst., Vol. 162, 1949, p 452.
- 13-49. Chesters, J. H., and Philip, A. R., Open-Hearth Furnace Models, Part I, Flow Patterns in Ducts, J. Iron Steel Inst., Vol. 162, 1949, p 385.
- 13-50. Howes, R. S., and Philip, A. R., Open-Hearth Furnace Models, Part II, Flow Visualization and Photography, J. Iron Steel Inst., Vol. 162, 1949, p 392.
- 13-51. Halliday, I. M. D., and Philip, A. R., Open-Hearth Furnace Models, Part III, Flow Patterns in Model Furnaces, J. Iron Steel Inst., Vol. 162, 1949, p 401.
- 13-52. Vanzonyi, A., On Rotational Gas Flows, Quart. Appl. Math., Vol. 3, 1945, p 29.
- 13-53. Prim, R. C., Steady Rotational Flow of Ideal Gases, J. Rational Mechanics and Analysis, Vol. 1, 1952, p 425.
- 13-54. Crocco, L., A New Stream Function for the Investigation of Rotational Flow of Gases, Z.A.M.M., Vol. 17, 1937, p 1.
- 13-55. Tsien, H. S., Influence of Flame Front on the Flow Field, J. Appl. Mech., Vol. 18, 1951, p 188.
- 13-56. Scurlock, A. C., Flame Stabilization and Propagation in High Velocity Gas Streams, Meteor Report No. 19, May, 1948.
- 13-57. Hicks, B., Aerodynamic Effects of Heat Released by Combustion of Steadily Flowing Gases; Third Symposium on Combustion, Flame and Explosion Phenomena, Williams and Wilkins Co., Baltimore, 1949, p 21.
- 13-58. Lewis, B., and Von Elbe, G., Stability and Structure of Burner Flames, J. Chem. Phys., Vol. 11, 1943, p 75.
- 13-59. Williams, G. C., Hottel, H. C., and Scurlock, A. C., Flame Stabilization and Propagation in High Velocity Gas Streams, Third Symposium on Combustion, Flame and Explosion Phenomena, Williams and Wilkins Co., Baltimore, 1949, p 21.
- 13-60. Williams, G. C., and Shipman, C. W., Some Properties of Rod-Stabilized Flames of Homogeneous Gas Mixtures, Fourth Symposium on Combustion, Williams and Wilkins Co., Baltimore, 1953, p 733.
- 13-61. Kutzko, G. G., Battelle Memorial Institute, Private Communication.
- 13-62. Putnam, A. A., The Effect of Boundary Layer Thickness on Flame Stability, Fuel, Vol. 33, No. 3, 1954, p 555.
- 13-63. Putnam, A. A., and Kleider, C. L., Battelle Memorial Institute, Private Communication.
- 13-64. Rayleigh, W., On the Instability of Jets, Proc. London Math. Soc., Vol. 10, 1879, p 4; reprinted from his Scientific Papers, Cambridge University Press, London, Vol. 1, 1899, p 361.

- 13-65. Rosenhead, L., Formation of Vortices From a Surface of Discontinuity, Proc. Roy. Soc., (London) Vol. A134, 1931, p 170.
- 13-66. Lin, C. C., On the Stability of Two Dimensional Parallel Flows, Quart. Appl. Math., Vol. 3, 1945-46, pp 117, 218, 277.
- 13-67. Dunlap, R. A., Resonance of a Flame in a Parallel-Walled Combustion Chamber, UMM-43, Project MX 833, Univ. of Michigan, March, 1950.
- 13-68. Putnam, A. A., and Dennis, W. R., A Study of Burner Oscillations of the Organ-Pipe Type, Trans. ASME, Vol. 75, No. 1, 1953, p 15.
- 13-69. Putnam, A. A., and Dennis, W. R., Organ-Pipe Oscillations in a Flame-Filled Tube, Fourth Symposium on Combustion, Williams and Wilkins Co., Baltimore, 1953, p 566.
- 13-70. Blackshear, P. L., Jr., Driving Standing Waves by Heat Additives, Fourth Symposium on Combustion, Williams and Wilkins Co., Baltimore, 1953, p 553.
- 13-71. Weller, A. E., and Thomas, R. E., Similarities in Combustion, WADC Technical Report 55-132, October, 1955.
- 13-72. Oppenheim, A. K., Gasdynamic Analysis of the Development of Gaseous Detonation and Hydraulic Analogy, Fourth Symposium on Combustion, Williams and Wilkins Co., Baltimore, 1953, p 471.
- 13-73. Reynolds, D., Phase 3 of Combustion and Ignition Research Under contract to OAF, Seventh Quarterly Progress Report, Battelle Memorial Institute, April, 1952.
- 13-74. Groume-Orjmailo, The Flow of Gases in Furnaces, John Wiley and Sons, New York, 1923.
- 13-75. Rosin, P. O., Aerodynamics of Domestic Open Fires, J. Inst. Fuel, April, 1939, p 198.
- 13-76. Peskin, L. C., High Velocity Burners Cut Fuel Cost and Furnace Size, Iron Age, Vol. 168, Aug. 9, 1951, p 63, Aug. 16, 1951, p 104.

CHAPTER 14. LAMINAR FLAME PROPAGATION

ABSTRACT

The propagation rate of a laminar flame through a combustible mixture is often considered a primary variable in combustion studies. This rate has been used as a correlation parameter in studies of flame stability, quenching, and ignition, flame oscillations, and turbulent flame speed. Yet, for a given mixture, the value of burning velocity is often a source of considerable disagreement. The mechanism from which a rate results is also a subject of considerable debate.

In this chapter on laminar flame propagation, the various theories of flame propagation are outlined first. Methods of measuring burning velocity are then covered, and their limitations and advantages noted. Following this discussion, the physical effect on burning velocity of temperature, pressure, mixed fuels, and non-hydrocarbon fuels is considered. Finally, the two most prominent classes of theories of burning velocity, the thermal theories and the species diffusion theories, are compared on the basis of the experimental results considered in the previous two sections.

Contrails

LAMINAR FLAME PROPAGATION

by

A. Levy

There has been much debate as to how important the burning velocity of a laminar flame is in determining the performance of a high-duty combustor. However, at the least, it appears that the stability limits of a flame bear some resemblance to burning velocity curves. At the other extreme, it might eventually be found necessary to know the burning velocity characteristics of a fuel to evaluate many of the properties of a combustor.

From a more fundamental viewpoint, the burning velocity is the connecting link between applications of high-temperature combustion and studies of the kinetics of combustion. If a theory of the mechanism of combustion fails to predict burning velocities in agreement with observations, the theory is immediately open to question.

The importance of theories and experimental studies of burning velocity has been recognized to such an extent that excellent treatments of the subject are available in many books and reviews. To name a few, there are the older and more recent texts by Lewis and von Elbe⁽¹⁴⁻¹⁾⁽¹⁴⁻²⁾, the older text by Jost⁽¹⁴⁻³⁾, and a recent text by Gaydon and Wolfhard⁽¹⁴⁻⁴⁾.

The contents of the five combustion symposia^(14-5, 6, 7, 8, 9), and the AGARD text⁽¹⁴⁻¹⁰⁾ contain many references to studies of burning velocity. Among the references which are of special bibliographic value are the reviews of the current literature on combustion by Lewis and von Elbe which have been appearing in *Industrial and Engineering Chemistry*; only the two most recent articles are listed among the references at the end of this chapter⁽¹⁴⁻¹¹⁾.

Because of this extensive literature, the emphasis has been placed in this chapter not so much on the details of the studies of burning velocity as on the over-all picture. The various theories are covered first, then the various techniques of measuring burning velocity are discussed. The effects on the rate of combustion of various physical factors such as pressure are covered next. Finally, the literature in which the various theories of combustion are compared is reviewed.

THEORIES OF FLAME PROPAGATION

A sound theory of flame propagation would explain the relation between burning velocity and the fundamental physical and chemical properties of fuels. However, since the first attempts in the late 19th Century, all attempts to develop such a theory have led to failure. This situation results from both an insufficient knowledge of the chemical processes occurring in the flame and the complex nature of the problem with its associated mathematical difficulties.

Theories of flame propagation are divided mainly into two groups; (1) thermal theories, which are developed using thermal transport properties and (2) radical-diffusion theories, which use diffusive transport properties. There is also a third group of theories which combines the two main groups above, and which may be classified as comprehensive theories.

An excellent review of these three groups of flame propagation theories has been prepared by Evans(14-12). Evans' review presents not only the basic equations of the various theories, but the assumptions which form the basis of the theories. In the following pages only the more general points of these theories shall be discussed.

Thermal Theories

The thermal theories are based on an assumed balance of thermal energy in the combustion zone and are developed from a generalized temperature distribution in the flame zone as shown in Figure 14-1.

The flame front is considered to be stationary at $x = 0$, and the reaction zone extends a distance δ . The rate of change of heat content may be expressed as

$$\frac{\partial(\rho H)}{\partial t} = \text{div}(\lambda \text{ grad } T) - \rho v \text{ grad } H + rQ \quad (14-1)$$

where ρ is the density of the gases, H is the heat content, λ is the coefficient of thermal conductivity, T is the temperature, v is the velocity of the gas, r is reaction rate, and Q is heat of reaction. Setting all time derivatives to zero, one obtains

$$\frac{d^2T}{dx^2} - \frac{F \rho c_p}{\lambda} \frac{dT}{dx} + \frac{rQ}{\lambda} = 0. \quad (14-2)$$

The burning velocity or flame speed, F , has replaced the gas velocity v , and the assumption of constant specific heat, c_p , has permitted H to be eliminated. This equation is fundamental to the thermal theories; variations in the thermal theories result from different assumptions introduced to make a solution feasible.

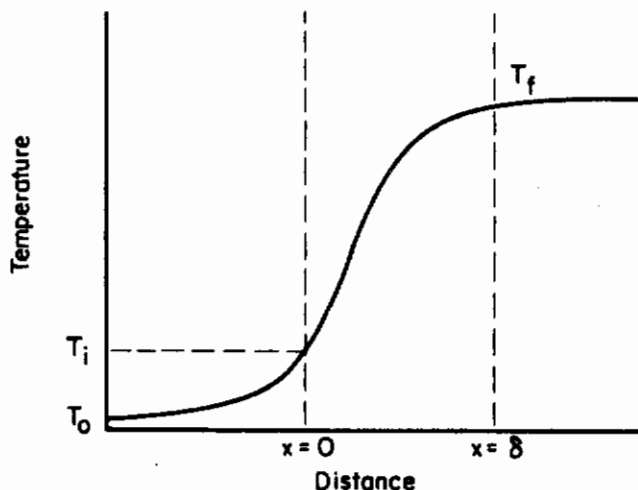


FIGURE 14-1. A GENERALIZED TEMPERATURE DISTRIBUTION
ACROSS THE FLAME FRONT

The boundary conditions are:

$$T = T_0 \text{ at } x = -\infty, \quad (14-3)$$

where T_0 is the initial temperature of the gases, and

$$T = T_f \text{ at } x = +\infty, \quad (14-4)$$

where T_f is the temperature of the burned gases.

Before proceeding further, the significance of T_i , often called the ignition temperature, must be stated. The ignition temperature only exists as a hypothetical formulation serving as an aid in solving and identifying some point in the combustion process. It is not a fundamental constant nor special factor for any fuel. It is generally considered the point at which the hot, fast reaction begins. On the general plot in Figure 14-1, T_i may be either high or low, depending on the particular theory.

In solving Equation (14-2), two important assumptions which strongly influence any solution of the equation are usually introduced. These are (1) below T_i , no reaction occurs; and (2) above T_i , the reaction proceeds at a constant rate. Concerning the first assumption, the combustion reaction is a continuous process, going from a slow oxidation to a cool flame region under proper conditions, and finally to the hot-flame, fast reaction. To say that no reaction occurs is equivalent to saying that there is no slow oxidation. But slow oxidations and cool flames do occur, do have exothermic heats of reaction, and, therefore, contribute to raising the gases to the ignition temperature T_i , in addition to the heating effect due to conduction from the flame front. Concerning the second assumption, kinetic studies show that the rate of oxidation is a function of temperature, pressure, and concentration; therefore, the rate is a function of distance within the flame front. Until the mechanism of hydrocarbon combustion is better understood, however, it is possibly preferable and certainly easier to obtain formal mathematical solutions to Equation (14-2) by considering the term rQ/λ to be constant.

For $T < T_i$, Equation (14-2) is solved with rQ/λ equal to zero. For $T \geq T_i$, rQ/λ takes a constant value. At T_i , the temperature and heat flow of the two equations are equated. This results in the equation:

$$\frac{T_i - T_0}{T_f - T_0} = \frac{1 - e^{-\alpha \delta}}{\alpha \delta}, \quad (14-5)$$

where $\alpha = F \rho c_p / \lambda$. Assuming $T_f \gg T_i$ and replacing α by its original expression one obtains the burning velocity equation,

$$F = \sqrt{\frac{\lambda r}{\rho c_p a_0} \frac{T_f - T_0}{T_i - T_0}}, \quad (14-6)$$

where a_0 is a mole concentration term obtained from the rate equation

$$r = - \frac{da}{dx} \frac{dx}{dt} = \frac{a_0}{\delta} F. \quad (14-7)$$

Equation (14-6) is the form of solution arrived at by many of the early workers⁽¹⁴⁻¹³⁾ using the approach given.

Two simple developments along the same lines as the general derivation can now be given. In each one the heat release in the flame zone is equated to the heat conducted to the unburnt gas. Using the temperature representation of Figure 14-1, the heat due to conduction for $x < 0$ can be represented as $\bar{c}_p v (T_i - T_0)$, where \bar{c}_p is an average heat capacity for the unburned gases. For $x > 0$, the heat of reaction available for conduction across the flame front can be said to be proportional to $(T_f - T_i)$, or equal to $k(T_f - T_0)$. Equating the two heat terms, and solving for v ,

$$v = F = \frac{k}{\bar{c}_p} \frac{(T_f - T_i)}{(T_i - T_0)} \quad (14-8)$$

This is the form arrived at by Mallard and LeChatelier⁽¹⁴⁻¹³⁾. Crussard⁽¹⁴⁻¹³⁾ assumes that the heat of reaction is proportional to $(T_f - T_i)/v$. This yields a square-root expression similar to the general Equation (14-6):

$$v = F = \sqrt{\frac{k}{c_p} \frac{T_f - T_i}{T_i - T_o}} \quad (14-9)$$

(Similar developments, leading to the above relation, have been worked out by Daniell, Dahmkohler, and Jahn(14-13)).

The burning velocity equations are all similar, since the approaches used are so nearly alike. In addition to relating the burning velocity to the thermal properties of the system, the equations do give some indication of the stability limits. As these developments are made only on a thermal basis, the amount of heat liberated by the reaction will be a maximum near stoichiometric mixtures, and will decrease as the gas mixtures get richer or leaner. The final temperature T_f , therefore, must also decrease, and the ignition temperature T_i can only rise. As a result, a condition is reached on either side of stoichiometric where T_f approaches T_i , and when the point is reached where $T_f < T_i$, the equations lose their significance. This condition can be taken to indicate extinction of the flame.

The Russian workers Zeldovich, Frank-Kamenetsky, and Semenov disagree with the above work on the grounds that Equation (14-6) indicates a low ignition temperature and that there has been no attempt to relate T_i to the induction period(14-14). At atmospheric pressure, induction periods of one-tenth to several seconds may occur before ignition. In a flame traveling at 100 cm/sec across a reaction zone about 0.1 mm in depth, the induction period cannot exceed 10^{-4} sec. As a result of this, the authors claim that the ignition temperature could not be very low, but on the contrary, must be rather close to T_f . Another reason for this point of view is that for any of the three equations given, if $T_i = T_o$, the burning velocity becomes infinite.

Semenov says that the ignition temperature can be lower than T_f only by an amount not exceeding RT_f^2/E . In other words, if one has a flame at $T_f = 2400$ K, and $E = 40,000$ calories per mole, $RT_f^2/E = 270$ K, and T_i would be about 2130 K, or quite close to T_f .

Using the view that $T_i \approx T_f$, the second term in Equation (14-2) drops out, giving:

$$\frac{d^2T}{dx^2} + \frac{rQ}{\lambda} = 0. \quad (14-10)$$

Semenov and Zeldovich(14-14) solve this equation for zero, first and second order reactions after first introducing an Arrhenius expression for the rate term. A detailed analysis of this method may be found in the Evans' review and also in a review by Markstein and Polanyi(14-15).

A solution for a zero order reaction follows:

$$F = \sqrt{\frac{2\lambda}{\rho c_p a_o} S e^{-E/RT_f} \frac{RT_f^2}{E(T_f - T_o)}}, \quad (14-11)$$

where S is a collision factor term.

There are experiments that indicate that Semenov's idea of a high ignition temperature is probably not correct. The values of T_i as measured (mostly in low-pressure flames because of the wider reaction zone available) are usually within the range of 700 C to 900 C(14-16). On the other hand, a recent study by Bartholomé, Dryer, and Leseman(14-17) gives support to the high ignition temperature that Semenov prefers. On the basis of an experimental study(14-18), Bartholomé concluded that in a methane-air system, the chemical reaction starts at very high temperatures in the range of the flame temperatures, about 2000 C. These authors feel that too much emphasis has been put on the diffusion theory when there are many situations where the old theory, as presented by Mallard and LeChatelier(14-13), holds better.

In order to avoid the introduction of the questionable idea of an ignition temperature, Bartholomé proposes integrating the complicated differential equations arising from a heat and

material balance on an integrating machine. Bartholomé sets up a rate expression for the methane-oxygen reaction based on work by Sachsse⁽¹⁴⁻¹⁹⁾ and introduces the rate expression into the general thermal equation. He is left with the following equation

$$\frac{d^2T}{dx^2} = \frac{w c_p}{\lambda} \frac{dT}{dx} - \frac{q}{\lambda} \left(\frac{q_0 F}{qR} \right)^{3/2} w^{-3/2}, \quad (14-12)$$

the solution of which is obtained on a computer. The mole rate, w , is determined by trial and error and q is a heat of reaction. The criterion of the solution is that d^2T/dx^2 approaches zero asymptotically as $x \rightarrow \infty$.

Burning velocities calculated by this method are much higher than experimental values, although the method does lend support to the idea of a high ignition temperature.

Species Diffusion Theories

Since the basic equations of diffusive transport are similar to those of thermal transport, the developments involved in both theories are similar. A major difference in the results is in the predicted effect of pressure on burning velocity. The effect is negligible in thermal theories, but important in diffusion theories.

In leading up to a development of an argument of the diffusion theory, Gaydon and Wolfhard⁽¹⁴⁻²⁰⁾ first developed a thermal theory with the purpose of indicating some of its shortcomings. They start from the same type of setup as shown in Figure 14-1. They call the region $x < 0$ the preheating zone, δ_{pr} ; the region of fast reaction is called δ_r . Using an average rate \bar{r} , the number of molecules oxidized n_c is expressed in the equation:

$$n_c F = \int_0^{\delta_r} \bar{r} dx = \bar{r} \delta_r. \quad (14-13)$$

They say that there is some average temperature gradient in the reaction zone,

$$\left(\frac{dT}{dx} \right)_{ign} = \frac{T_f - T_i}{\delta_r} f, \quad (14-14)$$

where the averaging factor, f , lies between 1 and 2.

The flow of heat at the point of ignition is:

$$\lambda \frac{dT}{dx} = c_p \rho F (T_i - T_0), \quad (14-15)$$

so that

$$\frac{\lambda (T_f - T_i)}{\delta_r} f = c_p \rho F (T_i - T_0). \quad (14-16)$$

Solving for F , after substituting for δ_r in Equation (14-13), the thermal-theory expression is obtained for burning velocity:

$$F = \sqrt{\frac{f \lambda r}{c_p \rho n_c} \frac{(T_f - T_i)}{(T_i - T_0)}}. \quad (14-17)$$

Gaydon and Wolfhard compute the time a molecule spends in the reaction zone from

Continued

$$t_r = \frac{\delta_r}{V_r} \approx \frac{\delta_r}{F} \left(\frac{T_o}{T_r} \right) \approx \frac{\delta_r}{F \left(\frac{T_f + T_i}{2 T_o} \right)} \quad (14-18)$$

where V_r is the gas velocity in the reaction zone. Using Wolfhard's⁽¹⁴⁻²¹⁾ previous observation that the luminous zone of an acetylene flame is $2/3 \delta_r$, they determine that an acetylene-oxygen flame at one atmosphere pressure has $\delta_r = .003$ cm. From Equation (14-18) it follows that $t_r = 4 \times 10^{-7}$ second. Considering an induction region with a temperature rise from 500° to 900° C, the induction period for acetylene-oxygen flame could not be greater than about 10^{-7} second. This value Gaydon and Wolfhard consider too small to permit a thermal explanation.

Gaydon and Wolfhard then use a diffusion development in the following manner.

A molecule will diffuse over a distance $x^2 = 2 Dt$ in time t ; if it is assumed that a distance $x = 2 \delta_r$ is required to reach ignition, then the velocity of molecules in the flame zone can be expressed as

$$V_r = \frac{D}{2 \delta_r}, \quad (14-19)$$

where D is the diffusion coefficient. The equation for burning velocity becomes, by use of Equation (14-13) and by correcting V_r to F by a temperature term,

$$F = \frac{D_r}{2n_c} \frac{T_o}{T_r}. \quad (14-20)$$

Since the number of molecules reacting is proportional to pressure, and since the diffusion coefficient is inversely proportional to pressure, this equation states that, as long as the rate of reaction is second order with respect to pressure (that is, is a bimolecular reaction), the burning velocity will be independent of pressure.

As will be shown subsequently, this conclusion does not agree with some of the other theories; however, this is unimportant, since the mechanisms of many of the hydrocarbon reactions are specific within themselves in their sensitivity to pressure effects. Thus, the relative order of the chain-starting, chain-propagating, and chain-breaking reactions would determine the over-all pressure dependency of the flame reaction. It is more significant that there are many reactions for which the independence of burning velocity with pressure is pronounced.

It has been shown above that a condition can arise where a reaction may be initiated faster than it can be accounted for by any thermal process. This condition was recognized long before Gaydon and Wolfhard's work. Also, there have been many kinetic experiments which showed that introduction of free radicals could produce reaction in systems at much lower temperatures than the ignition temperatures. As a result of this, Lewis and von Elbe⁽¹⁴⁻²²⁾ proposed, in 1934, a theory of diffusion of radicals. They based their theory on the idea that free radicals were the important elements in flame propagation, through their chain-branching and chain-propagating reactions in the burning mechanism. Therefore, their theory states qualitatively that the free radicals produced in the reaction zone are able to diffuse, in a counterflow direction, into the unburned gas, in sufficient quantity to propagate the reaction. This means that an energy "surge" is not required to support the combustion, and since only a small number of atoms or radicals is necessary in the unburned region, and since these atoms and radicals require negligible energies of activation, the total energy level may be considered constant throughout the entire flame zone. There is some difference of opinion regarding this idea of constant energy level throughout every boundary. Zeldovich⁽¹⁴⁻²³⁾, for example, does not agree entirely with Lewis and von Elbe. He feels that the energy level will be constant at the beginning and at the end of the reaction, but in the reaction zone itself, thermal and diffusive properties may enter which will raise or lower the energy level, depending upon the properties of the gas. Only under ideal conditions does Zeldovich consider the energy as constant throughout each phase of the reaction zone. He says that the

increase in energy due to heating is compensated for by the loss of chemical energy that the diffusing gas takes with it. The similarity to the Lewis and von Elbe statement is obvious, but the difference is not quite so obvious.

According to Zeldovich, the theoretical combustion temperature will depend to a large extent on the diffusive- and thermal-transport properties. One might also explain the occurrence of stability limits by the same method. If an added constituent increases the diffusive-to-conductive ratio, it will promote combustion, and if it reduces the ratio, it will inhibit it. In other words, Zeldovich feels that both properties are important in combustion, but diffusion will play a larger role, owing to the presence of hydrogen in most hydrocarbon oxidations. Zeldovich proceeds to explain his argument on mathematical grounds. For an idealized case where molecules are similar in physical properties and $\lambda = D c \rho$, he shows that the total energy is constant, in agreement with Lewis and von Elbe. It follows from his argument that when $D c \rho \neq \lambda$ the energy may not remain constant throughout, but will be constant only at $\chi = \pm \infty$.

Lewis and von Elbe apply their theory to the relatively simple (in terms of its kinetics) decomposition flame of ozone. The derivation is based on the equality of the number of ozone molecules entering the reaction zone and the number reacting in any unit time. Steady-state conditions are applied and equations are set up for each component, ozone, oxygen molecules, and oxygen atoms, of the following form

$$\left(\frac{\partial N_{O_2}}{\partial t}\right)_D + \left(\frac{\partial N_{O_2}}{\partial t}\right)_V + \left(\frac{\partial N_{O_2}}{\partial t}\right)_c = 0 \quad (14-21)$$

where D , V , and c refer to diffusion, mass flow, and chemical reaction rates. These three equations are then combined with an equation of state and an energy balance of the chemical and thermal energies for the slow reaction,

$$E_{O_3} N_{O_3} + E_O N_O = (N_{O_2} + 1.5 N_{O_3} + 0.5 N_O) \bar{c}_p (T_f - T_i) . \quad (14-22)$$

After approximating a diffusion coefficient for the ternary system, a rate equation can be obtained for the formation of oxygen. The rate equation is then substituted into the following flame equation

$$F N_{O_3} = \int_{x=0}^{x=\delta} \frac{1}{1.5} \left(\frac{\partial N_{O_3}}{\partial t}\right) dx . \quad (14-23)$$

Bechert⁽¹⁴⁻²⁴⁾ has also analyzed the ozone flame, using a rather simplified theory based mainly on the activation energy parameter and applying only the laws of conservation of matter, momentum and energy. His method accounts for the diffusion of atoms and radicals into the flame front by adjusting the energy of activation parameter from a measured flame-speed value. This value of E is somewhat smaller than the energy value ordinarily measured for the over-all reaction. It does, however, agree more with the energy values proposed by Fenn and Calcote⁽¹⁴⁻²⁵⁾.

Fenn and Calcote have shown that many of the discrepancies to date might be the result of using too high an activation energy in burning velocity calculations. Analyses of studies such as these show that there is no satisfactory agreement yet between the parameters governing flame propagation and reaction kinetics.

Bechert's method avoids the necessity of bringing the chemical mechanism into the problem and permits one to treat the problem merely on the basis of physical parameters.

Table 14-1 compares some of the final results of the methods of Lewis and von Elbe and of Bechert. At low temperatures the latter method's results are in much better agreement with the experimental data. The first column, m , refers to the molar ratio of oxygen to ozone.

TABLE 14-1. COMPARISON OF CALCULATED BURNING VELOCITIES WITH EXPERIMENTAL RESULTS FOR THE OZONE REACTION

<u>m</u>	Temperature, K		Burning Velocity, cm/sec		
	Initial	Final	Exptl.	Lewis & von Elbe	Bechert
3054	300	1239	55.0	253.	71.7
3054	427	1343	158.	451.	158.
1497	302	1922	160.	333.	369.
1016	468	2044	747.	664.	747.

When Equation (14-21) is put into more familiar terms, the close similarity to Equation (14-2), which is the general differential equation relating burning velocity to the other variables, becomes quite obvious:

$$D \frac{d^2(\text{NO}_2)}{dx^2} - \frac{d}{dx} (\text{NO}_2\text{F}) + \frac{d(\text{NO}_2)}{dt} = 0. \quad (14-24)$$

The significance of this similarity is that Figure 14-1 can be labeled not solely as a temperature-distribution curve, but also as a potential curve where one may substitute temperature, or radical concentration, or any other potential that might be considered the driving force in the combustion.

The similarity in the techniques of Bartholomé, of Lewis and von Elbe, and of Zeldovich should be noted. All attempts to solve the rate part of the equation with an appropriate Arrhenius expression, or by means of Lewis and von Elbe's conservation of energy, turn out to be a specific case of Zeldovich's general treatment.

The development due to Tanford and Pease⁽¹⁴⁻²⁶⁾ is probably one of the more controversial ones -- not because of the method of development so much as because the results imply a specific pressure effect on burning velocity, which is not always corroborated experimentally. Tanford⁽¹⁴⁻²⁷⁾ has investigated the CO-H₂ flame from the standpoint of calculating the concentrations of H and O atoms and of OH radicals. He set up the differential equation for heat transfer and material transport, and showed that temperature falls off rapidly as distance from the flame front increases. Since the hydrogen-atom concentration is a negative exponential of temperature, this concentration would fall off still more rapidly than would temperature, whereas the non-equilibrium concentration of hydrogen atoms, caused by diffusion from the flame front, would fall off more slowly. On this basis, he concludes that the diffusion of radicals is more important in the combustion process than the concentration of radicals from thermal dissociation.

Figure 14-2 represents a correlation of H, O, and OH concentrations with the burning velocity of a CO-H₂ flame. It was the opinion of the investigators at the time that correlation for the hydrogen atoms was better than that for the O or OH species. It was also shown that the diffusion process must be more important than the thermal process in producing hydrogen atoms in the flame zone.

A detailed derivation is omitted here. However, using standard concepts an equation similar to Equations (14-2) and (14-24) is developed,

$$D \frac{\partial^2 c}{\partial x^2} + u \frac{\partial c}{\partial x} + Ac = 0, \quad (14-25)$$

where *c* refers to the concentration of atoms or radicals, *u* is a gas velocity or burning velocity, and *A* is a proportionality constant arising from the approximate rate of production of hydrogen atoms as a first-order reaction.

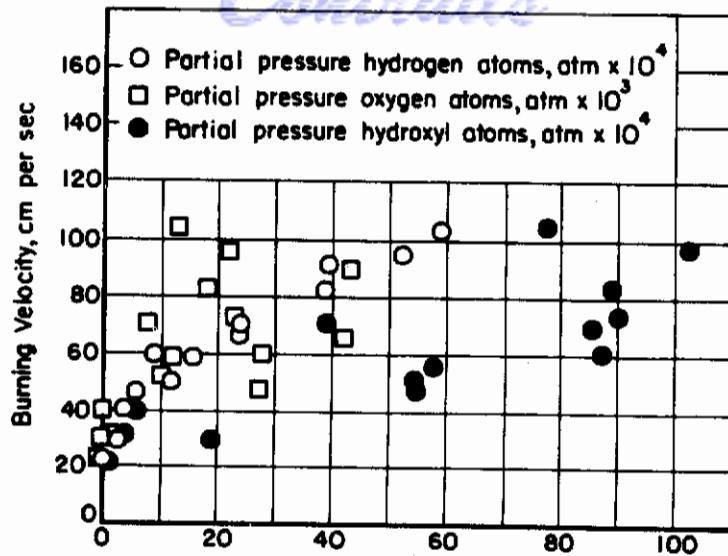


FIGURE 14-2. CORRELATION BETWEEN BURNING VELOCITY AND FREE-RADICAL CONCENTRATION (Tanford) (14-27)

Solving this equation requires calculation of the concentrations of the atoms or radicals. It is necessary, therefore, to use some average temperature for the flame front and combustion zone, so that the partial pressures of the radicals will be known at the boundary $x = 0$. For the boundary $x \rightarrow -\infty$, the concentration of radicals is assumed to approach zero, as does the rate of formation of radicals. The concentration, c , then becomes

$$c = c_1 \exp\left(\frac{Bux}{D}\right), \quad (14-26)$$

where c_1 is the concentration of active radicals at $x = 0$, and where B approaches 1 as A approaches zero. Having a relation for the radical concentration, and making an assumption relative to the production of products by the radicals, the flow rate may be related to the original concentration of radicals in the flame.

The final equation of the development is

$$F = \left[\sum \frac{k_i C p_i D_i}{Q B_i} \right]^{1/2} \quad (14-27)$$

where c is the concentration of combustible, Q is the mole fraction of potential combustion products, k_i is a rate constant, p_i is an equilibrium partial pressure at the flame front, D_i is a relative diffusion coefficient with respect to other active species, the subscript i refers to the species under consideration, and B_i is a term (approximately unity) depending on the rate of radical recombination. Since the mole fraction of active radicals due to dissociation will vary with the square root of pressure, the burning velocity F will vary inversely with the fourth root of the pressure.

It is this last result which causes the many discussions related to this theory. As will be shown later, the experimental evidence does not support the conclusions of this development in the majority of cases reported.

Van Tiggelen⁽¹⁴⁻²⁸⁾ has developed a burning velocity theory based on the chain branching reactions of the combustion system and on the diffusion of active centers produced in these reactions. He has applied his theory with fair success to the combustion of methane, hydrogen, and ammonia. The final equation which is arrived at has the following form

$$F = \frac{4 T_0 \sqrt{2 R(O_2)} \exp(E/RT_m)}{\pi \sqrt{3 m p T_m}} \quad (14-28)$$

where T_0 and T_m are the initial and the flame temperatures, m is the molecular weight of the active species, p is pressure, (O_2) refers to the oxygen concentrations, and R is the gas constant. The theory affords another method of checking the activation energy of these systems since this term appears in the final equation, in a somewhat similar manner to the Semenov-developed equations. Therefore, a study of the variation of burning velocity with temperature would permit one to determine the activation energy, E , in the above equation.

Wave-Propagation Theory

Manson⁽¹⁴⁻²⁹⁾ has introduced a new idea as a possible means for flame propagation in his scheme of wave propagation whereby active particles are pushed forward into the flame front. The development is based on the small pressure drop in the immediate vicinity of the reaction zone, explained by a phenomenon of projection of active centers (usually hydrogen atoms).

$$\Delta p = \frac{1}{2} \frac{T_1}{T_2} (p_H)_2 \quad (14-29)$$

The subscripts 1 and 2 represent the unburned and burned gases, respectively, and p_H represents the partial pressure of hydrogen atoms at the temperature T_2 .

Momentum considerations lead to a relation between pressure drop and flame speed; replacing the pressure drop by the concentration term,

$$F \approx \mu \left[\frac{(p_H)_2}{2 \rho (1 - \mu)} \right]^{1/2} \quad (14-30)$$

where μ is the ratio of densities in the burned gases to the unburned gases, and ρ is density of the unburned gases.

Manson has recently extended this theory of flame propagation to predict the effect of pressure on burning velocity⁽¹⁴⁻³⁰⁾. The equation

$$F = F_0 (p_0/p)^n \quad (14-31)$$

expresses this effect where the exponent n varies from 0.25 on the rich side to 0.40 on the lean side when hydrocarbons are burned in air. The coefficient becomes less for mixtures burning in oxygen, and is independent of pressure between 0.1 and 5 atmospheres.

Theories Combining Thermal and Diffusion Mechanisms

Before entering into the more comprehensive flame propagation theories it should be pointed out, although it may be quite obvious from the number of existing theories, that the thermal and radical diffusion problem is far from resolved. Often one finds that any arguments used to defend one theory can readily be applied with a minimum of assumptions to defend the other theory. In this regard reference is made to two excellent papers -- the first by Hoare and Linnett⁽¹⁴⁻³¹⁾, defending the thermal theories, and the second by Simon⁽¹⁴⁻³²⁾, defending the diffusion theories. Hoare and Linnett show that the carbon monoxide flame reaction can be explained thermally by combining calculations on ignition and flame temperature. Their arguments are based on the fact that reactions causing higher flame temperature and faster reaction rates reflect themselves in all the thermal flame propagation equations with an increase in burning velocity. Simon's review of

the diffusional process in flame-propagating reactions presents a rather complete picture of the correlation of these phenomena which tend to point out the limitations of the theories today. The result of her review is that a unique answer to the problem does not exist yet, although she favors a diffusion mechanism.

As one studies the arguments for either the thermal or diffusion mechanisms, it becomes apparent that the actual combustion process probably depends on both mechanisms to some extent. Thus, the more refined theories are expected to have some aspects of each type of mechanism.

There have been at least four developments in this class, those of Hirschfelder and Curtiss⁽¹⁴⁻³³⁾, of von Karman and Penner⁽¹⁴⁻³⁴⁾, of Boys and Corner⁽¹⁴⁻³⁵⁾, and of Friedman and Burke⁽¹⁴⁻³⁶⁾. The Hirschfelder and the von Karman developments combine the effects of conduction and diffusion, and are similar. The latter theory bases its analysis on a constant enthalpy process in which an extended steady-state process for chain reactions is used. The former theory attempts to consider the physical problems caused by diffusion of active centers in these chain reactions.

The Hirschfelder-Curtiss Analysis

The Hirschfelder-Curtiss development is the most general of these comprehensive developments, and likewise the most complex. Since the momentum equation may be omitted due to the negligible pressure drop across the flame front*, only three classes of equations must be set up and solved; these are the equations of state, of energy, and of the continuity of chemical component.

The development requires an idealized porous-plug flameholder so that the boundary conditions are fixed at a finite distance upstream of the flame. Although this assumption seemed rather idealized when first proposed, recently it has almost been achieved in practice, as reported in the flat-flame studies of Spalding⁽¹⁴⁻³⁷⁾. Spalding describes a flat-flame burner in which the flame is held on a water-cooled porous plate. This permits him to maintain flames composed of stoichiometric as well as the weak, limit flame mixtures.

Solving these equations must be done by complex, numerical methods. Therefore few flame systems have been analyzed in detail. The decomposition flames of azo-methane, nitric oxide, ethylene oxide, hydrazine, and ozone have been worked out however.

Any attempt to condense this complex mathematical development would only prove inadequate. Reference is therefore made to Hirschfelder's text⁽¹⁴⁻³³⁾ for a complete treatment, and to the Evans' review⁽¹⁴⁻¹²⁾ for a shorter mathematical development.

Hirschfelder and collaborators are extending their numerical method to the hydrogen-bromine flame⁽¹⁴⁻³⁸⁾. In the hydrogen-bromine flame one has the almost ideal flame system since the mechanism of this reaction has been thoroughly worked out for at least low temperatures. If the Hirschfelder method is applicable to the relatively high temperatures of the flame reaction, it should be possible to work out the details of this flame reaction with relatively good accuracy.

The Von Karman-Penner Theory⁽¹⁴⁻³⁴⁾

In principle the von Karman and the Hirschfelder developments are similar. The principal tenet of the former is that the cumbersome calculations of Hirschfelder's treatment may be substantially reduced by neglecting the influence of the chemical reactions. Von Karman outlines his theory in the light of the ozone reaction and shows where his calculations yield flame speeds close to Hirschfelder's and to the experimental values.

* Note that this is equation used by Manson⁽¹⁴⁻²⁹⁾.

Boys and Corner have treated the problems of thermal and species distribution separately for the one-dimensional flame, and then combined the results. In their development the authors analyze a generalized case for a single exothermic reaction. They treat three cases: (a) a first-order rate from a unimolecular mechanism, (b) a second-order rate from a bimolecular mechanism, and (c) a second-order rate from low-pressure unimolecular mechanisms.

Reference is made to the authors' paper and to the Evans' review for details of the mathematical development.

The Friedman and Burke Development(14-36)

This development is not a comprehensive one in the sense that the preceding three developments were. However, it is discussed here because patterns of heat release and species formation are related to the burning velocity and flame thickness.

The starting point of this development is in general heat-balance equation, Equation (14-2). A parallel equation is used for the species diffusion case,

$$\frac{d^2c}{dx^2} - \frac{F}{D} \frac{dc}{dx} + \frac{W}{D\rho_c} = 0, \tag{14-32}$$

where W replaces the heat-release term and represents the rate of species formation. These two equations are transformed to a dimensionless basis, four possible forms of heat release and species formation are presented (Figure 14-3), and relations between variables are investigated.

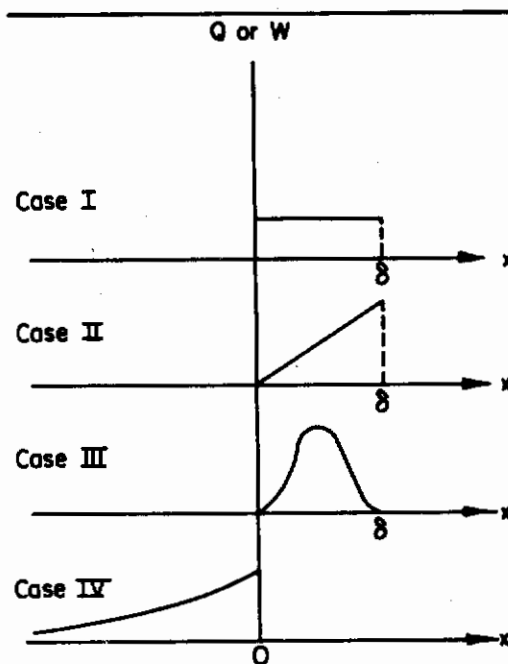


FIGURE 14-3. HEAT RELEASE AND SPECIES-FORMATION PATTERNS (Friedman and Burke) (14-36)

In a more recent paper these authors⁽¹⁴⁻³⁹⁾ have obtained numerical solutions with the aid of an electronic calculator for the differential equations describing a hypothetical model of a laminar flame. They have set their equations up for a first order irreversible reaction and have taken into account the temperature dependence of thermal conductivity and diffusion.

Continued
Empirical Equations for Burning Velocity

The combustion group at the Cleveland Laboratory of the National Advisory Committee for Aeronautics has obtained the fundamental burning velocities of some 50 hydrocarbons mixed with air using the tube method⁽¹⁴⁻⁴⁰⁾. Hibbard and Pinkel⁽¹⁴⁻⁴¹⁾ have correlated these data for the maximum flame velocities with the equation

$$F = N_A K_A + N_B K_B + \dots + \dots + \dots, \quad (14-33)$$

where the N's are concentrations of various types of C-H bonds and the K's are empirically derived flame-speed coefficients.

Table 14-2 presents a summary of their data; the increasing coefficients signify larger effects on increasing burning velocities.

TABLE 14-2. COEFFICIENTS FOR CALCULATING MAXIMUM BURNING VELOCITY (Hibbard and Pinkel) (14-41)

Type of C-H Bond	Coefficient K_i
Methane	35.2×10^{-19}
Primary	42.5
Tertiary	45.4
Secondary	47.5
Cyclohexyl	50.5
Alkene	80.7
Aromatic	84.3
Configurated diene	86.1
Allene	123.0
Alkyne	223.9

Simon⁽¹⁴⁻⁴²⁾ has taken the Gerstein data and shown that the Tanford-Pease equation may be modified so that the H, O, and OH radicals are given equal weight as chain carriers, which seems to agree with the Linnett and Wheatley data (see Figure 14-8); by this hypothesis, most of the calculated burning velocities agree within ± 5 per cent of the experimental values. The method is interesting in that a calculated rate constant, k , obtained from the data, shows no significant change for the various hydrocarbons. This suggests that the oxidation mechanisms for all the hydrocarbons must be similar, and also gives weight to the opinion that efforts in studying the kinetics of the simpler hydrocarbons will lead to results applicable to hydrocarbons of higher molecular weight and more complex structure. This is also borne out by the fact that most of the hydrocarbons give burning velocities falling within a narrow range.

THE MEASUREMENT OF BURNING VELOCITY

There are three basic methods of measuring burning velocity. In one the burning velocity is defined as a measured flame area divided by a measured flow rate through that area. In the second, the burning velocity is defined as the product of the flow velocity and the size of the angle between the flow line and flame front. In the third method, particle traces are used in the gases. Although these methods should lead to the same result, the controversies over the correct area to use, or the correct flame front position (visible, shadow, or schlieren cone) and angle to use, or the proper correction for particle drag and acceleration, have resulted in as much disagreement among experimentalists as among theorists. For this reason, Figure 14-4 is a fitting introduction to this

section, before proceeding with a discussion of the work of various investigators. It adequately illustrates the typical disagreements found in data from various types of experiments.

Bunsen Burner Methods

In the original studies by Gouy⁽¹⁴⁻⁴³⁾ and Michelson⁽¹⁴⁻⁴⁴⁾ on bunsen-type burners, four simplifying assumptions were introduced. They are:

1. The flow in the tube is streamline and the velocity distribution of the gases across the tube is parabolic.
2. There is a sharp, instantaneous boundary between the burned and unburned gases.
3. The burning velocity is constant across the entire flame front.
4. The motion of the gas is parallel to the axis of the burner tube right up to the flame front.

It was quickly realized by these workers, by Ubbelohde⁽¹⁴⁻⁴⁵⁾, and by Stevens⁽¹⁴⁻⁴⁶⁾ that assumptions three and four could not be maintained. All noted that the rounded tip and curved base of the Bunsen cone were deviations from the idealized conditions, and only by considering the entire area of the cone were they able to obtain logical results.

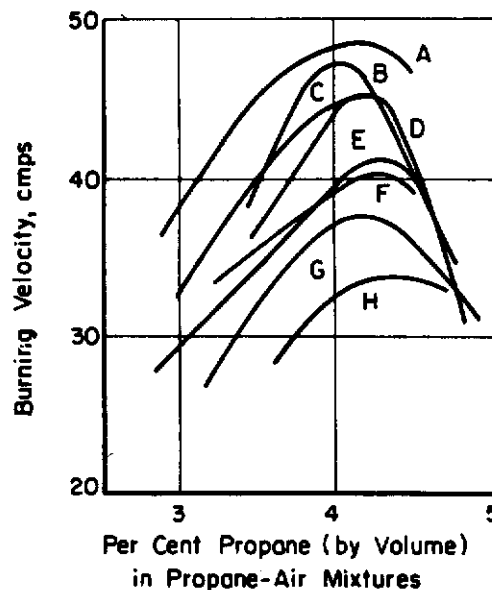


FIGURE 14-4. BURNING VELOCITIES OF PROPANE-AIR MIXTURES AS OBTAINED BY SEVERAL WORKERS

(Garner, Long, and Ashforth) (14-54)

Smith and Pickering⁽¹⁴⁻⁵⁰⁾ measured burning velocity from the flame angle at 0.707 of the radius from the axis of the burner. They chose this point because it permitted measurements on a flatter region of the flame cone, and because at this distance for parabolic flow, the flow velocity is equal to the average flow velocity.

Smith(14-55) and later Lewis and von Elbe(14-56) adapted a particle-track technique for measuring burning velocities. By injecting magnesium oxide and stannic chloride hydrate dusts into the gas streams, it was also possible to study temperature distribution, as well as variation of burning velocity along the flame cone.

Figure 14-5 illustrates the variation of burning velocity along the surface of the flame cone(14-56). This variation is characteristic of Bunsen flames; the increase at the tip of the cone is due to the increased curvature of the flame surface, while the decrease at the edges is due to the cooling effect of the wall of the tube and dilution with the surrounding atmosphere.

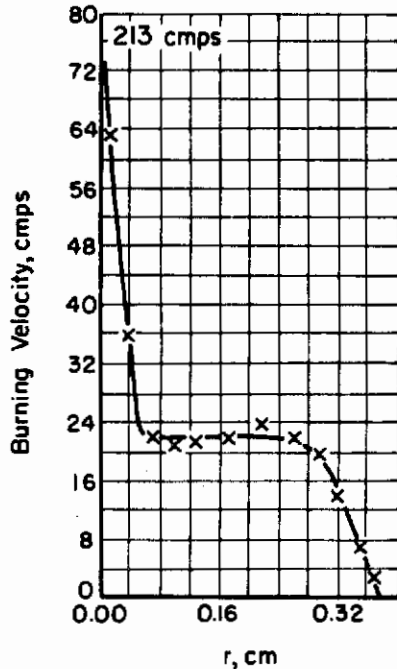


FIGURE 14-5. VARIATION OF BURNING VELOCITY WITH THE DISTANCE r FROM AXIS OF BURNER TUBE (Lewis and von Elbe)(14-56)

Anderson and Fein(14-49) and, more recently, Fristrom and co-workers(14-57) have applied the particle-track technique to obtain temperature profiles. Essentially the method is one of determining gas-particle velocities on both sides of the flame front. Then by combining these velocities into equations of state and of continuity one calculates the flame temperature. Details of this method are described rather well in the paper of Anderson and Fein. Flame speed measurements of propane-air flames are also presented in their paper.

Culshaw and Garside(14-53) use the total area method on the inner edge of the luminous cone. As shown in Figure 14-4 their values are decidedly lower than the other values; however, this may be the result of using burners under one-cm diameter.

Singer(14-58) has applied the slot-burner technique to eliminate some of the controversial rim effects. The advantage of such a burner is that it applies a truncated cone method of measurement to flow with a uniform velocity profile; thus it is easier to calculate a value of burning velocity. Also, when one plots burning velocity as a function of position of measurement, one obtains a decidedly larger portion of the burner which has a constant burning velocity, that is the plateau of the type in Figure 14-5 is extended.

Efforts have also been made to analyze the tip effect on measurements of burning velocity rather than to just lose them in some experimental averaging technique(14-59)(14-60). These analyses generally involve consideration of the flow lines and the heating up of the central flame mixture in the cone. Lichty concludes from his analysis that natural gas has a tip burning velocity of about 64-87 cm/sec.

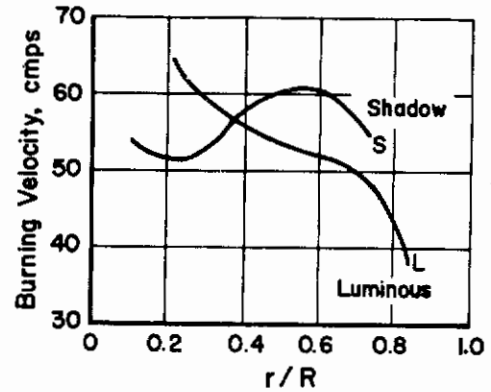


FIGURE 14-6. VARIATION IN BURNING VELOCITY WITH THE METHOD AND POSITION OF MEASUREMENT (Garner, Long, and Ashforth)(14-47)

Harris, Grumer, von Elbe, and Lewis⁽¹⁴⁻⁵¹⁾ have compared the angle method to the area method in measuring the burning velocity of propane flames. They report agreement by the two methods when the angle is measured at one-half the radius, rather than at 0.707 the radial distance chosen by Smith and Pickering.

Besides the difficulty in the methods of measurement, there is also difficulty in deciding where to apply the method. The Bunsen cone affords three possibilities in this respect, the visible, schlieren, and shadow cones. Figure 14-6 exemplifies this predicament rather well. The schlieren curve, which is not shown in the figure, is closer to the shadow curve than to the luminous curve.

Sherratt and Linnett⁽¹⁴⁻⁶¹⁾ have investigated this problem, and in agreement with Anderson and Fein, show that the outer edge of the shadow cone must correspond to the maximum temperature gradient in the flame. In a later study Grove, Hoare, and Linnett⁽¹⁴⁻⁶²⁾ use the sharp inner edge of the shadow cone and obtain burning velocities for ethylene and air which are only four per cent less than those reported by Sherratt and Linnett.

Sherratt and Linnett have shown that the flow lines are refracted before the luminous zone; however, Garner and associates believe that the shadow zone also includes the zone of heat conduction back from the flame. Therefore, they chose a point between these two zones. An interesting feature of their analysis is that they obtain this boundary line by extrapolating the flow lines across the shadow and luminous zones to a point of intersection. Using this cone as the start of the reaction zone, one can tie in the temperature measurements of Klaukens and Wolfhard, and the approximations of Gaydon and Wolfhard⁽¹⁴⁻²⁰⁾, which concluded that $2 \delta_T \approx 3 \delta_L$. The significance is only qualitative, but does show why such great emphasis has been placed on attempting to obtain absolute values of burning velocity and flame-zone thickness. As a point of interest, it might prove fruitful to compare this extrapolated cone to the schlieren cones. It is to be expected that the two cones would take a position very close to one another, and might even coincide with one another over a good part of their surface.

Garner's results in Figure 14-4⁽¹⁴⁻⁴⁷⁾ which are higher than the other results were obtained by the angle method. In a recent review in which he compares the luminous, schlieren, and shadow techniques⁽¹⁴⁻⁶³⁾ of measuring burning velocity, Garner and his associates confirm their older results.

Albright⁽¹⁴⁻⁶⁴⁾ has compared luminous- and shadow-burning velocities for the less-volatile, liquid hydrocarbons. An interesting feature of this work is that in contrast to Figure 14-6, three intersections are obtained, at r/R values of 0.1, 0.45 and 0.48. Since the hydrocarbons were completely vaporized it is difficult to explain the variation with the single intersection obtained in Garner's propane studies.

Broeze⁽¹⁴⁻⁵²⁾ is a proponent of the schlieren cone for measuring flame speeds. Broeze bases his preference on the coincidence of the schlieren cone with the reaction zone on studies he made by passing smokes through the flame. Using ammonium chloride smoke in the proper amount, that is, not enough to lengthen the flame or to reduce the burning velocity, he observes that the smoke vanishes sharply at a position about one mm ahead of the luminous zone. A pure zinc oxide smoke also showed this, but not as distinctly. Comparison of these positions with the schlieren positions shows that the smoke disappears at about 0.1 mm beyond the schlieren zone.

A strong argument in favor of the schlieren-cone technique is that it is difficult to explain such sharp temperature and density changes at the flame surface by heat conduction, and therefore it must be concluded that a large change in the reaction rate is occurring here. An objection to the schlieren technique is that it can be too sensitive to give a well-defined flame cone⁽¹⁴⁻⁴⁹⁾⁽¹⁴⁻⁶⁵⁾ and for this reason some workers prefer using the shadow-cone technique.

Wohl⁽¹⁴⁻⁶⁶⁾ and his associates have studied the flame burning from a nozzle, which has a different flow pattern than a tube. As a result, their data agree qualitatively with the observations of Bartholome. The nozzle flames show greater stability than the burner flames under all conditions. Wohl reports that the nozzle flame will remain seated on the burner at lower velocities and can be lifted off the burner to a stable position at higher velocities than the tube flame. The reader

is referred to Chapter 16 for a discussion of this point in relation to the velocity gradient at the wall.

Wohl's results on butane flames may be generalized by saying that schlieren-measured burning velocities average about two per cent higher than luminous burning velocities, and about three per cent higher than shadow-measured burning velocities.

A new photographic technique employing phase-contrast photographs has been used by Van Steenis(14-67). This technique, called the Zernicke method, is an adaptation of the schlieren technique. The flame outline is obtained by changing the phase of a central light 90° with respect to the defraction images. Except for this one paper, this technique has not been critically tested.

As a final remark on studies of burning velocity with Bunsen burners, reference is made to two papers by W. Jost(14-68)(14-69). In these papers the bunsen flame is analyzed with respect to the aerodynamic problems and the chemical reactions which influence these flames. Problems such as edge or rim effects are discussed in relation to flat flames, floating flames and other flame deformations.

Propagation in Tubes

In the tube propagation method of measuring burning velocity, the flame is timed as it passes two points along the tube. The relation for the burning velocity is

$$F = (U_o - U_g) \frac{A_t}{A_f} ; \quad (14-34)$$

where U_o is the observed flame speed and U_g is the velocity of unburned gas ahead of the flame, and A_t/A_f is the ratio of tube area to flame area(14-70). This latter term is difficult to calculate correctly, since the flame does not maintain a constant shape during its propagation. Hoare and Linnett(14-71) have, for example, observed ethylene-air flames propagating down a tube by taking three pictures of the flame simultaneously from different points of vantage. Their pictures show that the flames are hemispherical for certain composition limits and tipped for others. As a result the computation of the flame front area is decidedly more troublesome than in the bunsen method. The tube method does have an advantage, however, in that one can measure the flame speed of small quantities of gas by this technique.

The tube technique is subject to geometric influences, since varying the length and the diameter of the tube affects the turbulence. Behrens(14-72) has observed that burning velocity measurements in a 12-meter tube, 3.8 to 21.-mm diameter, yield higher burning velocities for methane, ethane, benzene, and hydrogen than are obtained in bunsen burners. He attributes this to a turbulence in the gas stream. He also observes a discontinuity as the burning velocity increases with changing composition in ethylene and acetylene flames. This phenomenon is attributed to soot formation which makes it easier for the free radicals to recombine; thus, setting free their dissociation energy and increasing the thermal conductivity of the system.

The Bubble Method

In this method, the gas mixture is centrally ignited and the rate of propagation of the expanding flame front is measured. The main problem in this method is no longer one related to flame shapes but it is the calculation of the correct expansion ratio of the gases as the flames move out in all directions. This was the major problem at the time of Stevens' original work on this method in 1923(14-46) and is still the major problem(14-73). Stevens' original calculation yields the equation

$$F = S \phi$$

where S is called the space velocity and ϕ is the expansion ratio equal to V_0/V_f , the ratio of initial to final volumes. Essentially, all the methods of calculation resemble this.

The reliability of the soap-bubble technique is good as can be seen from the table below, taken in part from Strehlow and Stuart's paper⁽¹⁴⁻⁷³⁾. Propylene and propane flames also show good agreement of results between burner or soap bubble techniques⁽¹⁴⁻⁷⁹⁾. Such good agreement does not always result, however. Acetylene burning velocities by the two methods show good agreement on the lean side, but on the rich side agreement is poor⁽¹⁴⁻⁷⁷⁾⁽¹⁴⁻⁷⁸⁾. This may be attributed to several factors, including solubility of the acetylene in the bubble material and the easy soot-forming characteristics of acetylene.

TABLE 14-3. A COMPARISON OF BURNING VELOCITY MEASUREMENTS

Per cent Ethylene in Air	F (Strehlow and Stuart)	F (Other Investigators)	
6.5	62.4 cm/sec	61.1(14-74)	
7.0	66.2	65.6(14-75)	65.5(14-74)
7.5	68.6	67.8(14-74)	68.3(14-70)
8.0	65.8	67.2(14-75)	67.5(14-74)

Simon and Wong⁽¹⁴⁻⁷⁸⁾ have analyzed the disturbed surface of the soap-bubble flame and claim that it causes high burning velocities in methane-oxygen flames that are obtained by the burner technique.

With the increased knowledge of the effect of water vapor on many oxidation reactions, current experiments appear to be concentrating on non-aqueous bubble methods in contrast to earlier studies where the more convenient soap-bubble was used as the containing medium. Price and Potter⁽¹⁴⁻⁸⁰⁾ have used the non-aqueous bubble technique on CO-O₂ mixtures. Using a rubber balloon they determined the flame speed of CO-O₂ - H₂O mixtures; different concentrations of the water vapor were obtained by varying the temperature of their system.

Mention should be made here of the constant-volume "bubble" or "bomb" method. In this method, both the change in flame diameter and the pressure rise with time, in the bomb, are recorded. From the two records, the burning velocity can be computed, at least in principle. However, since the small difference of two large numbers enters into this computation, it has been found more satisfactory to make some assumptions on the constancy of the ratio of specific heats during combustion, and develop equations leading to independent computation of burning velocity from the pressure measurements and from the flame photographs. The values of burning velocity computed by the two independent methods were found by Manton, von Elbe and Lewis⁽¹⁴⁻⁸¹⁾ to check each other and compare favorably with measurements by other methods for stoichiometric ethylene-, methane-, and propane-air mixtures.

Flat Flame Method

Referring to Figure 14-4, it is seen that the burning velocity curves stop abruptly at values well above $F = 0$. This raises the question as to whether burning velocity actually goes to zero as the composition becomes leaner or richer, or whether it does have a finite lower value.

Some progress toward an experimental answer to these questions has been made by Powling⁽¹⁴⁻⁸²⁾, who has designed a burner capable of stabilizing slow-burning flames. In this

burner, the burner rim is replaced with a stream of nitrogen. Using this technique, he has reported burning velocities for propane as low as 5.4 cm/sec, and a lean limit of 2.12 per cent propane; this is the lowest value yet observed for propane mixtures. It also appears from his data for pentane and butane that the burning velocity may approach zero at the lower limit. Egerton and Thabet⁽¹⁴⁻⁸³⁾ have applied this burner technique to methane, propane, pentane, heptane, ethylene, acetylene and benzene flames in the 5-10 cm/sec burning velocity region, and have also used it to determine the limits of combustion.

Mache and his group⁽¹⁴⁻⁸⁴⁾, measuring the burning velocity of methane-air flames over the entire range of flammability, obtained a curve which suggests a continuous approach to zero at both the lean and rich limits.

One of the shortcomings of the Powling flat-flame burner is that it is incapable of holding fast burning flames. Spalding⁽¹⁴⁻⁸⁵⁾ has attempted to overcome this drawback by passing his gaseous mixture through a porous metal, water-cooled plate. The flame seeks an equilibrium position above this plate under these conditions so that the burning velocity equals the gas velocity. Spalding has been able to measure the burning velocities of stoichiometric and lean propane-air mixtures by this technique.

Remarks on the Measurement of Burning Velocity

It would be desirable to conclude this section with a recommended method of measuring the burning velocity. However, such a recommendation cannot be made. Returning to the four assumptions of Gouy and Michelson, in their original studies, it can be seen that in some of the experimental approaches all four assumptions (or their equivalents) have been violated. The Poiseuille flow distribution across the tube may hold, but such a velocity distribution does not produce a flame cone with sufficiently straight sides to be measured accurately. By burning the flame off an accelerating nozzle, the flow distribution can be such that an almost flat flow profile is obtained. This changes the gradient at the walls and tends to straighten out the curved surface of the flame cone.

The results of kinetic studies and of photographic records show that an infinitely thin reaction surface cannot be assumed. The reaction zone has a finite depth which is a function of the reaction rate and flame speed among other things.

Figures 14-5 and 14-6 have shown how the burning velocity will vary along the flame front; furthermore, burning velocity varies differently for each flame surface measured. Powder tracks have shown that the gas stream will remain parallel to the axis of the burner up to the shadow cone, but at the schlieren cone some bending outward is noticeable, owing to expansion and back-pressure effects, and at the luminous cone the deviation is pronounced.

The schlieren cone is probably the best surface to be measured, that is, this is the one more nearly coincident with $x = 0$ on Figure 14-1, but techniques must still be improved to make the cone-area measurements more accurate. Probably the most precise experimental measurements can be made by the shadow technique, but this cone is not considered the truest cone in terms of the reaction zone.

But the important objective in all this work is not to obtain absolute values of burning velocity. A great deal of work remains before these absolute values can be related to kinetic data. Until this is accomplished, burning velocity measurements should be considered important only as relative measurements for stability studies and for preliminary kinetic studies. Burning velocity is tied in with these studies, because it reflects the effect of such fundamentals as reaction rates, reaction-zone thickness, flame temperature, pressure, and ignition limits.

The Effect of Temperature

Considering the equation for burning velocity

$$F = \sqrt{\frac{\lambda r}{\rho C_p a_0} \frac{T_f - T_0}{T_i - T_0}}, \quad (14-6)$$

one would not expect burning velocity to vary in any simple manner with temperature since $\lambda \propto T^{.84}$, $C_p \propto T^{.09}$, $\rho \propto T^{-1}$ and the reaction rate varies as $e^{-E/RT}$ in a typical case. An example of the temperature variation for natural gas-air flames is shown in Table 14-4 from investigations of Sherratt and Linnett(14-61) and Johnston(14-86).

TABLE 14-4. EFFECT OF TEMPERATURE ON BURNING VELOCITY OF STOICHIOMETRIC MIXTURES OF NATURAL GAS AND AIR

Temperature, C	Flame Speed, cm/sec	
	Sherratt & Linnett	Johnston
16	28.0	
52	37.6	
58.3		42.7
88	50.9	
175		104
309		148
483		250

Broeze reports that propane and butane each yield burning velocity data directly proportional to T_0 in the range 20 C to 200 C(14-52). Sachsse(14-87) obtains a similar linearity for propane-air mixtures over the larger range 20 C to 500 C. Passauer(14-88) reports propane burning velocities proportional to T_0^2 . Dugger(14-89) has applied the Semenov equation for a bimolecular reaction-rate controlling step for the propane-air flame and obtains experimental and theoretical curves in the range 29 C to 343 C which agree quite well. His data place the temperature relation between the first and second power of the initial gas temperature.

Dugger also applies the Tanford-Pease Equation (Eq 14-27) to his results to determine the temperature effect. He assumes that only p_i , C , and D_i are temperature-dependent and obtains a relation which falls 35 per cent low at the higher temperatures. This is not too serious, however, since the assumptions are much stronger in applying the Tanford-Pease equation, as equilibrium concentrations of the free radicals H, O, and OH are calculated at a specific flame temperature, it is assumed that equilibrium conditions are attained in the reaction zone, that no reaction is occurring before ignition and that there is no large chain-branching term. Dugger has extended these studies to other hydrocarbons and to lower temperatures. In general his results show that the burning velocity data can be correlated in an equation of the form

$$F = A + BT^n, \quad (14-36)$$

where constants A, B, and n are determined from the data, and T is the absolute temperature. He has also been able to obtain linear correlations between burning velocity and H-atom concentrations at the flame temperature(14-90).

Dixon-Lewis(14-91) has investigated the effect of preheat on the burning velocity. He gives experimental evidence which suggests that the effect of preheat on burning velocity is independent of the effect of temperature on the reaction rate.

The pressure effect on flames is a highly controversial one, both from the theoretical and the experimental point of view. The extent of the divergencies is best seen in Tables 14-5 and 14-6 where the theoretical and experimental effects respectively are shown.

Table 14-6 is taken from Simon's⁽¹⁴⁻³²⁾ review.

The results in Simon's table present a rather complete summary of the situation as regards the pressure effect. It is difficult to expand on this to any extent due to the wide discrepancy which exists. Lewis⁽¹⁴⁻⁹²⁾ has pointed out that the major problem today in checking for the correct theory to explain these phenomena may be in the experimental technique. He makes this quite apparent in the figure reproduced below from his discussion.

Figure 14-7 is interesting in that it shows the pressure effect to be dependent on burning velocity. Up to $F = 50$ cm/sec burning velocity increases with decreasing pressure, then it remains independent of pressure up to $F = 100$ cm/sec, following which the burning velocity decreases with decreasing pressure.

Ubbelohde and Koelleker⁽¹⁴⁻⁴⁵⁾ found that the burning velocities of methane, benzene, carbon monoxide, and acetylene, all increased as the pressure was reduced. However, they did note an odd effect with acetylene; a six per cent mixture of acetylene and air gave burning velocity data varying more than those from a 12 per cent mixture, as the pressure was changed. Khitrin and associates⁽¹⁴⁻⁹³⁾ were able to fit their results to the following equation on the same series of gases, including acetylene:

$$F = \frac{k_1 \sqrt{P + k_2}}{P} \quad (14-36)$$

where P is the total pressure and the k 's are empirical constants. Their equation is based on data above one atmosphere. Khitrin did run one series of soap-bubble tests where he found no variation with pressure for a carbon monoxide-air flame. However, this is a good example of the care necessary in setting up an experiment because, in this instance, the water vapor played an important role in affecting the reaction.

Garside, Forsyth, and Townend⁽¹⁴⁻⁹⁴⁾ and Linnett and Wheatley⁽¹⁴⁻⁹⁵⁾ observed a progressive increase of ethylene-air burning velocities with reduced pressures. Interestingly enough, Linnett and Wheatley obtain even more conclusive correlations of atom concentration with burning velocity than Tanford and Pease obtained in their original correlation on CO flames. Figure 14-8 summarizes their correlation.

Garner, Long and Ashforth⁽¹⁴⁻⁴⁷⁾ also obtained good agreement with the Tanford-Pease relation for benzene and n-heptane flames at reduced pressures, although their results show the variation to be closer to the inverse third root of the pressure.

Most of these studies have covered the pressure effect at pressures only mildly above atmospheric, if at all, and for the most part well below atmospheric. Egerton and Lefebvre⁽¹⁴⁻⁹⁶⁾ have recently measured velocities of methane, propane, ethylene and propylene from one-half to nine atmospheres. They obtained pressure exponents of 0.5 for methane and 0.3 for the other gases. These variations were not independent of composition, however, since richer mixtures were observed to be affected less by pressure variations.

Edse⁽¹⁴⁻⁹⁷⁾ has studied H_2-O_2 flames up to 100 atmospheres pressure on extremely small burner tubes. At 14.6 atmospheres he obtained burning velocities of 3500 cm/sec and concludes from measurements of the pressure drop across the flame front that flame velocities of turbulent flames are not larger than those of laminar flames.

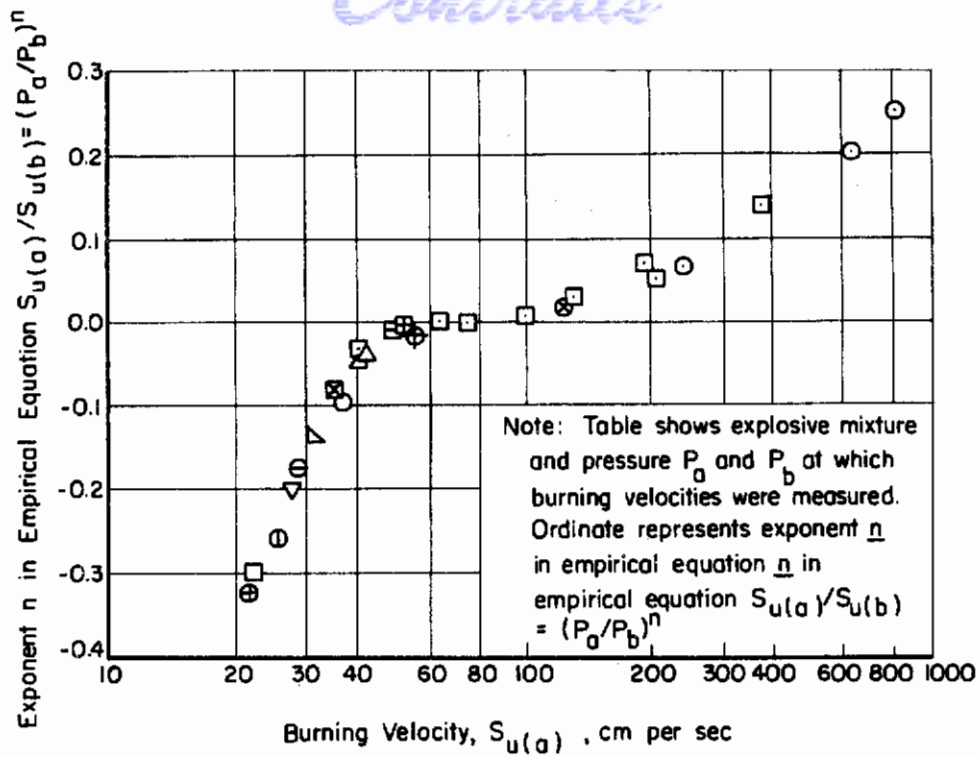
Confidential

TABLE 14-5. THE VARIATION OF BURNING VELOCITY PRESSURE
AS PREDICTED BY DIFFERENT THEORIES

Author		Relation of Burning Velocity to Pressure
Crussard, Jouget and Daniell ⁽¹⁴⁻¹³⁾	m = 1	F = k
	m = 2	F = kP ^{1/2}
Semenoff, Zeldovich and Frank-Kamenetsky ⁽¹⁴⁻¹⁴⁾	m = 1	F = kP ^{-1/2}
	m = 2	F = k
Tanford and Pease ⁽¹⁴⁻²⁶⁾		F = kP ^{-1/4}
Hirschfelder and Curtiss ⁽¹⁴⁻³³⁾	1 < m < 2	F = kP ^{(m-2)/2}
Boys and Corner ⁽¹⁴⁻³⁵⁾		F = kP ^{(m-2)/2}
	Case (a) unimolecular decomposition,	m = 1
	Case (b) bimolecular reaction,	m = 2
	bimolecular reaction,	m = 3
Case (c) unimolecular decomposition (low pressure, m = 2)		F = k
Gaydon and Wolfhard ⁽¹⁴⁻²⁰⁾		F = k

TABLE 14-6. THE VARIATION OF BURNING VELOCITY WITH PRESSURE
AS DETERMINED EXPERIMENTALLY⁽¹⁴⁻³²⁾

Mixture	Method	Pressure Dependence
Methane-air	Bunsen burner	$u \propto p^{-0.2}$
5.9 % Methane-air	Flat flame	$u \propto p^{-0.49}$
6.2 % Methane-air	Flat flame	$u \propto p^{-0.49}$
2.3 % Propane-air	Flat flame	$u \propto p^{-0.30}$
2.4 % Propane-air	Flat flame	$u \propto p^{-0.29}$
Butane-air	Bunsen burner	Slight change
Butane-air	Bunsen burner	$u \propto p^{+n}$
n-Pentane-air (stoic.)	Bunsen burner	$u \propto p^{-0.36}$
Octane-air (stoic.)	Bunsen burner	$u \propto p^{-0.39}$
1, 3-Butadiene-air	Bunsen burner	$u \propto p^{-n}$
Ethylene-air (stoic.)	Bunsen burner	$u \propto p^{-0.13}$
9 % Ethylene-air	Bunsen burner	$u \propto p^{-0.40}$
9 % Ethylene-air	Bunsen burner	$u \propto p^{-n}$
3.15 % Ethylene-air	Flat flame	$u \propto p^{-0.31}$
Ethylene-air	Bunsen burner	$u \propto p^{-n}$
Ethylene-air	Soap bubble	No change
Acetylene-air	Bunsen burner	No change
2.7 % Acetylene-air	Flat flame	$u \propto p^{-0.47}$
Acetylene-air (max.)	Bunsen burner	Slight change
Acetylene-air	Bunsen burner	Max. at 200 mm
Acetylene-oxygen	Bunsen burner	No change
Benzene-air	Bunsen burner	$u \propto p^{-0.31}$



Mixture	Press, atm		Mixture	Press, atm	
	P_a	P_b		P_a	P_b
$C_2H_4 + 3 O_2$	0.10	0.05	$CH_4 + 2 O_2$	0.25	0.10
$C_2H_4 + 3 O_2 + 3 N_2$	1.0	0.5	$CH_4 + 2 O_2 + 2 N_2$	1.0	0.5
$C_2H_4 + 3 O_2 + 5.56 N_2$	1.0	0.5	$CH_4 + 2 O_2 + 3.72 N_2$	1.0	0.1
$C_2H_4 + 3 O_2 + 9.5 N_2$	1.0	0.25	$CH_4 + 2 O_2 + 6.35 N_2$	1.0	0.25
$C_2H_4 + 3 O_2 + 11.3 N_2$	1.0	0.04	$CH_4 + 2 O_2 + 7.5 N_2$	1.0	0.1
$C_2H_4 + 3 O_2 + 13.5 N_2$	1.0	0.25	$CH_4 + 1.67 O_2 + 6.27 N_2$	1.0	0.25
$C_2H_4 + 3 O_2 + 11.3 A$	1.0	0.10	$CH_4 + 2.41 O_2 + 9.05 N_2$	1.0	0.25
$C_2H_4 + 3 O_2 + 11.3 He$	1.0	0.10	$CH_4 + 2.5 O_2 + 9.4 N_2$	1.0	0.25
$C_2H_4 + 2.06 O_2 + 7.75 N_2$	1.0	0.25			
$C_2H_4 + 2.5 O_2 + 9.4 N_2$	1.0	0.10	$C_3H_8 + 4.16 O_2 + 15.6 N_2$	1.0	0.25
$C_2H_4 + 3.6 O_2 + 13.6 N_2$	1.0	0.10	$C_3H_8 + 5 O_2 + 18.8 N_2$	1.0	0.25
$C_2H_4 + 4.35 O_2 + 16.4 N_2$	1.0	0.25	$C_3H_8 + 6.02 O_2 + 22.6 N_2$	1.0	0.25
$C_2H_4 + 5 O_2 + 18.8 N_2$	1.0	0.25	$C_3H_8 + 6.25 O_2 + 23.5 N_2$	1.0	0.25

FIGURE 14-7. CHANGE OF BURNING VELOCITY WITH PRESSURE
(Discussion by Bernard Lewis)⁽¹⁴⁻¹⁰⁾

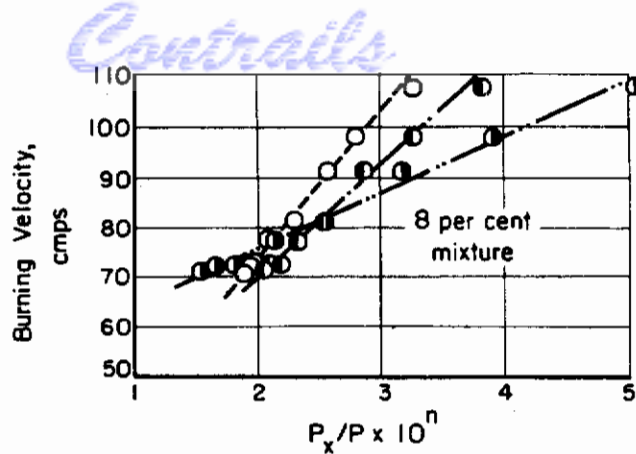


FIGURE 14-8. VARIATION OF THE BURNING VELOCITY OF AN 8 PER CENT ETHYLENE-AIR MIXTURE WITH THE FRACTION OF ACTIVE RADICALS

(Linnett and Wheatley)⁽¹⁴⁻⁹⁵⁾

Effect of Mixed Fuels

Of special interest in studies of burning velocity is a method of predicting the burning velocity of mixtures of various hydrocarbons and air.

D. B. Leason⁽¹⁴⁻⁹⁸⁾ has studied the effect of additives such as benzene, iso-octane ethers, acetane, hydrogen, and carbon monoxide, on propane-air flames, and concludes that it is difficult to increase the burning velocity markedly with additives. This is substantially the conclusion reached by Kurz⁽¹⁴⁻⁹⁹⁾ and by Egerton and Thabet⁽¹⁴⁻⁸³⁾. Leason does show, however, that the effect of the additives on burning velocity is still dependent on the concentration of active species in the flame zone by comparing a part of burning velocity of the mixture against $(6.5 P_H + P_O + P_{OH})$.

Kurz⁽¹⁴⁻¹⁰⁰⁾, however, has also shown that the burning velocity of propane-air mixtures is reduced more by hydrogen-sulfide additions than can be accounted for from flame temperature calculations. Even on the basis that the burning velocity of the mixture may be some averaged burning velocity of the two gases, the burning velocity for the $H_2S - C_3H_8$ mixture is low. It is postulated that the flame reaction is inhibited by S_2 molecules reacting with the active centers in the flame.

Non-Hydrocarbon Systems

The mixture of primary interest among the non-hydrocarbon fuel systems is the hydrogen-bromine flame. As was pointed out earlier this appears to be the ideal system from which to study the flame reaction. The reaction mechanism is well-established⁽¹⁴⁻¹⁰¹⁾, the thermodynamic data have been accurately determined⁽¹⁴⁻¹⁰²⁾, and the reaction is relatively simple in that it involves only chain-propagating steps with no complicating chain-branching steps. Due to the complex nature of hydrocarbon oxidations, none of these facts exist for even the simplest hydrocarbon system.

Experimental investigations on this reaction have been directed by R. C. Anderson⁽¹⁴⁻¹⁰³⁾. Table 14-7 compares some observed burning velocities with those values calculated with the aid of the Mallard-Le Chatelier equation⁽¹⁴⁻¹⁰⁴⁾. It is of interest to note that the experimental burning velocities peak at mixtures rich in hydrogen, rather than at the stoichiometric point predicted by

thermal considerations. Attempts to relate the experimental values to a Tanford-Pease calculation were even less encouraging(14-105).

TABLE 14-7. BURNING VELOCITY OF VARIOUS HYDROGEN-BROMINE MIXTURES AND COMPARISON WITH THERMAL THEORY

(R. C. Anderson)(14-104)

Br ₂ , mole per cent	F, cm/sec, Observed	F, cm/sec, Calculated (T = 300 C)
20	2.8	0.6
31	15.8	5.2
40	10.	6.7
50	7.2	7.0
60	5.8	2.6

In recent studies Anderson and co-workers have investigated the effects of burner size, burner position, and temperature(14-106). Although definite conclusions could not be drawn, Anderson favors atomic hydrogen diffusion as the controlling process. In studying the stability of these flames, it is observed that there is a strong tendency for flame shape to be characteristic of the composition of the mixture(14-107).

Kokochashvili(14-108) also observed an influence of composition on the shape of the flame front advancing down a tube. Some of his work suggests that two separate mechanisms are necessary to explain ignition and propagation. He observes, for example, that ignition is achieved more easily with excess halide plus hydrogen, while the maximum rate of reaction is with excess hydrogen plus halide. Kokochashvili offers some explanation on the basis of a strictly thermal explanation.

Of interest in the theoretical treatment of these flames is a recent thesis study under the direction of S. S. Penner(14-109). The results of the calculations show that the calculated burning velocities are about twice Anderson's experimental values, while Hirschfelder's calculations(14-102) are about four times higher. Of possible major importance in these considerations is the question, Can the steady-state assumption used in the low-temperature kinetics be applied to the flame reaction? On the basis of Mileson's work(14-109) the assumption is valid, whereas Hirschfelder feels that it may not be valid at high temperatures and in fact the standard mechanism may also include the bimolecular reaction $H_2 + Br_2 \rightarrow 2HBr$ at flame temperatures.

Ausloos and Van Tiggelen(14-110) have directed their attention to combustion of ammonia mixtures. They observed a maximum burning velocity for NH₃ - O₂ (54 per cent NH₃) of 113 cm/sec. Burning velocities were also obtained for NH₃ - H₂ - O₂ mixtures.

Murray and Hall(14-111) have studied the hydrazine flame. They have shown that the hydrazines probably decompose before the flame zone and that one is burning an NH₃ - H₂ mixture in the actual flame zone.

Cyanogen flames are of interest due to their similarity to CO-flames, and also due to their high flame temperatures. Their similarity to CO-flames is borne out by the strong water-vapor effect which they exhibit. It is of interest that although the hydrogen atom has been thought to be of prime importance in CO-flames, the hydroxyl radical has been shown by Brokaw and Pease(14-112) to be more important in cyanogen flames. This conclusion results from finding no difference in burning velocity of cyanogen mixtures using D₂O and H₂O.

The decomposition flame of ethylene oxide is another flame which is of interest to investigators because the kinetics have been studied extensively. The flame reaction has been studied by

Burden and Burgoyne⁽¹⁴⁻¹¹³⁾, Friedman and Burke⁽¹⁴⁻¹¹⁴⁾, and Gerstein, McDonald and Schalla⁽¹⁴⁻¹¹⁵⁾. There is some question as to whether the decomposition may be expressed as going to CH_4 and CO or to C_2H_4 , CO , and H_2 . As a result, calculations of the adiabatic flame temperature and calculations of the burning velocity are somewhat questionable.

Ausloos and Van Tiggelen⁽¹⁴⁻¹¹⁰⁾ have directed their attention to combustion of ammonia mixtures. They observed a maximum burning velocity for $\text{NH}_3 - \text{O}_2$ (54 per cent NH_3) of 113 cm/sec. Burning velocities were also obtained for $\text{NH}_3 - \text{H}_2 - \text{O}_2$ mixtures.

Murray and Hall⁽¹⁴⁻¹¹¹⁾ have studied the hydrazine flame. They have shown that the hydrazines probably decompose before the flame zone and that one is burning an $\text{NH}_3 - \text{H}_2$ mixture in the actual flame zone.

Cyanogen flames are of interest due to their similarity to CO -flames, and also due to their high flame temperatures. Their similarity to CO -flames is borne out by the strong water-vapor effect which they exhibit. It is of interest that although the hydrogen atom has been thought to be of prime importance in CO -flames, the hydroxyl radical has been shown by Brokaw and Pease⁽¹⁴⁻¹¹²⁾ to be more important in cyanogen flames. This conclusion results from finding no difference in burning velocity of cyanogen mixtures using D_2O and H_2O .

The decomposition flame of ethylene oxide is another flame which is of interest to investigators because the kinetics have been studied extensively. The flame reaction has been studied by Burden and Burgoyne⁽¹⁴⁻¹¹³⁾, Friedman and Burke⁽¹⁴⁻¹¹⁴⁾, and Gerstein, McDonald and Schalla⁽¹⁴⁻¹¹⁵⁾. There is some question as to whether the decomposition may be expressed as going to CH_4 and CO or to C_2H_4 , CO , and H_2 . As a result, calculations of the adiabatic flame temperature and calculations of the burning velocity are somewhat questionable.

COMPARISON OF THERMAL AND DIFFUSION THEORIES

Following this review of laminar flame propagation from both the theoretical and experimental side, it would be fitting to conclude with a convincing discussion of the mechanism by which the flame propagates. This cannot be done at present. The information is not available to judge the relative importance of the two schools of thought -- heat conduction and radical diffusion -- as will be apparent in this concluding section.

The protagonist of the radical-diffusion theory questions the thermal theory on the basis of observed lack of effects of promoters on flame speed. Such promoters lower the ignition temperature, but do not change the burning velocity⁽¹⁴⁻¹¹⁶⁾, whereas the purely thermal theory would predict a change in burning velocity with a change in ignition temperature. Likewise Gaydon and Wolfhard have found, in their study of low-pressure flames, that the concentration of OH radicals observed from spectroscopic measurements is much higher than can be attributed to equilibrium concentrations at the flame temperature.⁽¹⁴⁻⁴⁾

Townend⁽¹⁴⁻¹¹⁷⁾, on the other hand, has stated that the application of theories based on diffusion of radicals (especially hydrogen atoms) is rendered obscure by the lack of quantitative evidence pertaining to the quenching reactions undergone by such radicals. Probably there is good basis for Townend's arguments since most of the quenching problems have been discussed in relation to the thermal theory. However, it appears that there is sufficient evidence of an indirect manner, to show that quenching can also be explained by radical diffusion theory. This is based on low-pressure flame studies, where it is found necessary to increase the diameter of the burner with decrease in pressure to maintain a stable flame.

Hoare and Linnett⁽¹⁴⁻¹¹⁸⁾, although not rejecting the diffusion theory, do show that their results on ethylene and carbon monoxide flames can be explained just as well by the thermal theory as by the diffusion theory. They lend support to the thermal theory in two ways. The burning velocities for C_2H_4 -air have been obtained with nitrogen and with carbon dioxide present. In both

cases, the burning velocity is decreased, but to a greater extent with CO₂. This is explained on the basis that the heat capacity of CO₂ is greater than that of nitrogen.

Another explanation is obtained in the following manner. The rate of heat release for a reaction is written in terms of the equilibrium constant and activation energy as

$$H = k \frac{P_{CO} P_{H_2O}}{P_{O_2}} e^{-E/RT_i}, \quad (14-38)$$

so that

$$T_i = \frac{E}{R \ln \frac{P_{CO} P_{H_2O}}{P_{O_2}} - \ln \frac{H}{K}} \quad (14-39)$$

where T_i is a sort of "ignition" temperature, E is the activation energy, and R is the gas constant. The rate term has been chosen on the basis of kinetic results. The term H/K was chosen so that T_i equalled about 1000 K, and an equilibrium flame temperature T_f was calculated. The ratio of temperature terms $\frac{T_f - T_0}{T_i - T_0}$ was then plotted against the observed burning velocities and, except for a few points, very good agreement was obtained.

The authors also show, that both the ethylene and carbon monoxide reactions obey the Tanford-Pease relation on the basis that the relative concentration of active radicals can be approximated as being equal to the sum of the relative diffusion coefficients for each radical times its equilibrium concentration, $(6\frac{1}{2}) P_H + (1) P_O + (1) P_{OH}$. On plotting radical concentration against burning velocity, curves are obtained which are similar to those obtained by Tanford and Pease for atomic hydrogen in the CO flame (compare Figures 14-2 and 14-8).

Walker and Wright⁽¹⁴⁻¹¹⁹⁾ have attempted to analyze the maximum burning velocities of 36 hydrocarbon-air mixtures in terms of Semenov's thermal equation and Tanford and Pease's diffusional equation. The results from both equations indicate that all the hydrocarbons burn with the same mechanism. The Semenov equation, however, gives somewhat better correlation with experimental results, and when lower activation energies are used as suggested by Fenn's studies⁽¹⁴⁻²⁵⁾ the correlations become still better.

Dugger and Simon⁽¹⁴⁻¹²⁰⁾ have also made this type of correlation. Besides the Semenov and Tanford-Pease equations, Manson's equation was also investigated. With respect to the first two equations, their results are similar to Walker and Wright's. The Manson equation, however, although rather simple to use, gives a poorer correlation with experimental data on burning velocity. This type of correlation has also been applied to iso-octane, propane, and ethylene flames with similar results⁽¹⁴⁻¹²¹⁾.

Clingman, Brokaw, and Pease⁽¹⁴⁻¹²²⁾ have attempted to relate methane-inert gas burning velocities to the diffusion and the thermal theories. In both cases it is observed that the data do not agree well with the individual theories, suggesting that no one theory, but possibly a combination of thermal and diffusion processes are necessary.

It is quite apparent, therefore, that there is no final statement that can be made on laminar-flame theories. The problem of whether the mechanics of flame propagation is related to heat transfer or diffusion of free radicals and atoms into the flame front, or to both, is not the principal obstacle. As can be seen from the marked similarity in the equations used in any of these developments, the final equations that must be solved are, basically, the same.

Possibly the most basic problem is finding the true relation for the variation of temperature and active species in the reaction zone. If this were accomplished the rather loosely defined ignition temperature might take on a more specific role in these developments. In any case, the final analysis requires a correlation between the theory and experiment.

In conclusion, the evidence indicates that a middle-road approach is best, and that laminar flame propagation is probably a combination of thermal conduction and species diffusion phenomena.

REFERENCES

- 14-1. Lewis, B. and von Elbe, G., *Combustion, Flames, and Explosion of Gases*, Academic Press, New York, 1951, 795 pages.
- 14-2. Lewis, B. and von Elbe, G., *Combustion, Flames, and Explosion of Gases*, The University Press, Cambridge, England, 1938, 415 pages.
- 14-3. Jost, W. (translated by H. O. Croft), *Explosion, and Combustion Processes in Gases*, McGraw-Hill, New York, 1946, 621 pages.
- 14-4. Gaydon, A. G., and Wolfhard, H. G., *Flames*, Chapman and Hall, 1953, 340 pages.
- 14-5. First Combustion Symposium, *Ind. Eng. Chem.*, Vol. 20, 1928, pp. 998-1057.
- 14-6. Second Combustion Symposium, *Chem. Rev.*, Vol. 21, 1937, pp. 209-460; and Vol. 22, 1938, pp. 1-310.
- 14-7. Third Symposium on Combustion and Flame and Explosion Phenomena, Williams and Wilkins, Co., Baltimore, 1949, 748 pages.
- 14-8. Fourth Symposium (International) on Combustion, Williams and Wilkins, Co., Baltimore, 1953, 926 pages.
- 14-9. Fifth Symposium (International) on Combustion, Reinhold and Co., New York, (In press).
- 14-10. Selected Combustion Problems, Advisory Group for Aeronautical Research and Development, NATO, Paris, Butterworths Scientific Publications, London, 1954, 534 pages.
- 14-11. Lewis, B. and von Elbe, G., *Combustion*, *Ind. Eng. Chem.*, Vol. 43, 1951, p. 1925; Vol. 45, 1953, p. 1921; (cf. Chemical Abstracts for earlier reviews in this journal).
- 14-12. Evans, M. W., Current Theoretical Concepts of Steady-State Flame Propagation; *Chemical Reviews*, Vol. 51, 1952, p. 363.
- 14-13. Crussard, L.; *Compt. rend.*, Vol. 158, 1914, pp. 125, 340.
Daniell, P. J; *Proc. Roy. Soc.*, Vol. A126, 1930, p. 393.
Nusselt, W.; *Ver. deut. Ing.*, Vol. 59, 1915, p. 872.
Mallard, E., and LeChatelier, H. L., *Ann. Mines*, Vol. 4 (8), 1883, p. 274.
Dahmkohler, G.; *Z. Elektrochemie*, Vol. 46, 1940, p. 601.
Jahn, G., *Der Zundvorgang in Gasgemischen*; Oldenbourg, Berlin, 1934.
- 14-14. Semenov, N. N, *Thermal Theory of Combustion and Explosions. III. The Theory of the Normal Propagation of Flames*, *Progress of Physical Sciences, USSR*; Vol. 24, 1940, p. 433.
Zeldovich, Ya. B., and Frank-Kamenetskii, D. A., *Theory of Thermal Propagation of Flame*; *Acta Physicochem. URSS*, Vol. 9, 1938, p. 341.
Zeldovich, Ya. B., and Semenov, N. W., *Jour. Exptl. and Theor. Phys. USSR*, Vol. 10, 1940, p. 116.
- 14-15. Markstein, G. H., and Polanyi, M., *Flame Propagation - A Critical Review of Existing Theories*; *Bumblebee Report No. 61*, April 1947, p. 5.
- 14-16. Klaukens, H., and Wolfhard, H. G., *Measurements in the Reaction Zone of a Bunsen Flame*; *Proc. Roy. Soc.*, Vol. A193, 1948, p. 512.

- 14-17. Bartholomé, E., Dreyer, H. J., and Lesemen, K. J., Determination of Flame Speed of a Hot Flame by Solution of an Eigenvalue Problem, Using an Electronic Integration; Z. für Elektrochemie und angew. Phys. Chem., Vol. 54, 1950, p. 246.
- 14-18. Bartholomé, E., and Hermann, C., Theory of Flame Velocities; Z. Elektrochemie, Vol. 54, 1950, p. 246.
- 14-19. Sachsse, H., Induction Time and Ignition Temperature in Methane - Oxygen Mixtures; Z. Phys. Chem., Vol. (B) 33, 1936, p. 229.
- 14-20. Gaydon, A. G., and Wolfhard, H. G., Influence of Diffusion on Flame Propagation; Proc. Roy. Soc., Vol. A196, 1949, p. 105.
- 14-21. Wolfhard, H. G., The Properties of Stationary Flames at Low Pressures; A. Tech. Phys., Vol. 24, 1943, p. 206.
- 14-22. Lewis, B., and von Elbe, G., On the Theory of Flame Propagation; Jour. Chem. Phys., Vol. 2, 1934, p. 537.
- 14-23. Zeldovich, Ya. B., Theory of Flame Propagation; Jour. Phys. Chem., USSR, Vol. 22, 1948, p. 27, (NACA Translation, TM 1282, June 1951).
- 14-24. Bechert, K., Theory of Propagation of Combustion with Application to Combustion of Ozone; Portugal, Physi., Vol. 3, 1949, p. 29; Theory of Burning Velocity in Combustible Mixtures; Z Naturforsch., Vol. 3A, 1948, p. 584; Z. Elektrochem., Vol. 54, 1950, p. 239.
- 14-25. Fenn, J. B., and Calcote, H. F., Activation Energies in High Temperature Combustion; "Fourth Symposium (International) on Combustion", Williams and Wilkins, Baltimore, 1953, p. 231.
- 14-26. Tanford, C., and Pease, R. N., Theory of Burning Velocity, II. The Square Root Law for Burning Velocity; Jour. Chem. Phys., Vol. 15, 1947, p. 861.
- 14-27. Tanford, C., Theory of Burning Velocity, I. Temperature and Free Radical Concentration Near the Flame Front, Relative Importance of Heat Conduction and Diffusion; Jour. Chem. Phys., Vol. 15, 1947, p. 433.
- 14-28. Van Tiggelen, A., Chemical Theory of the Speed of Flame Propagation; Bull. Soc. Chim. Belges, Vol. 58, 1949, p. 259; The Kinetic Study of Combustion and Flame Reaction. The Rate of Flame Propagation; Acad. Roy. Belg., Classe Sci. Mem., Vol. 27, 1952, p. 3.
- 14-29. Manson, N., Hydrodynamical Theory of Flame Vibration; Proc. 7th Int. Congress of App. Mech., Vol. II, 1948, p. 187; Jour. Chem. Phys., Vol. 17, 1949, p. 837.
- 14-30. Manson, N., Effect of Pressure on the Fundamental Burning Velocity in Gaseous Mixtures; Fuel, Vol. 32, 1953, p. 186.
- 14-31. Hoare, M. F., and Linnett, J. W., Mechanism of Flame Propagation; Jour. Chem. Phys., Vol. 16, 1948, p. 747.
- 14-32. Simon, D., Diffusion Processes as Rate-Controlling Steps in Laminar Flame Propagation; AGARD text, London, 1954, p. 59.
- 14-33. Hirschfelder, J. O. and Curtiss, C. F., Theory of Flame Propagation; "Third Symposium on Combustion, Flame and Explosion Phenomena", Williams and Wilkins, 1949, p. 121; Jour. Chem. Phys., Vol. 17, 1949, p. 1076; Jour. Phys. and Coll. Chem., Vol. 55, 1951, p. 774; "Fourth Combustion Symposium, Williams and Wilkins, Baltimore, 1953, p. 190; J. Phys. Chem., Vol. 57, 1953, p. 403; n. b., A complete description of all these papers is given in "Molecular Theory of Gases and Liquids" by J. O. Hirschfelder, C. F. Curtiss, and R. B. Bird; John Wiley, New York, 1954.

- 14-34. Von Karman, T. and Penner, S. S., Fundamental Approach to Laminar Flame Propagation; AGARD text, London, 1954, p. 5.
- 14-35. Boys, S. F., and Corner, J., Structure of the Reaction Zone in a Flame; Proc. Roy. Soc., Vol. A197, 1949, p. 90.
Corner, J., Effect of Diffusion of the Main Reactants on Flame Speeds in Gas; Proc. Roy. Soc., Vol. A198, 1949, p. 388.
- 14-36. Friedman, R., and Burke, E., on the One-Dimensional Theory of Flame Structure; Jour. Aer. Sci., Vol. 18, 1951, p. 239.
- 14-37. Spalding, D. B., New Method for Measuring Flame Speed; Research (London), Vol. 6, No. 9, 1953, pp. 52S.
- 14-38. Campbell, E. F. and Hirschfelder, J. O., Review of the Reaction Kinetics and Transport Properties of a Hydrogen-Bromine Flame, University of Wisconsin, NRL Report CF-2108, November 17, 1953, 59 pages.
- 14-39. Friedman, R. and Burke, E., A Theoretical Model of a Gaseous Combustion Wave Governed by a First Order Reaction; Jour. Chem. Phys., Vol. 21, 1953, p. 710.
- 14-40. Gerstein, M., Levine, O., and Wong, E. L., Determination of Fundamental Burning Velocities of Hydrocarbons by a Revised Tube Method; Jour. Amer. Chem. Soc., Vol. 73, 1951, p. 418; also Ind. Eng. Chem., Vol. 43, 1951, p. 2770.
- 14-41. Hibbard, R., and Pinkel, B., Correlation of Maximum Fundamental Flame Velocity with Hydrocarbon Structure; Jour. Amer. Chem. Soc., Vol. 73, 1951, p. 1622.
- 14-42. Simon, D. M., Theoretical Consideration of the Burning Velocities of Hydrocarbons; Jour. Amer. Chem. Soc., Vol. 73, 1951, p. 422.
- 14-43. Gouy, M., Ann. Chim. Phys., Vol. 18, 1879, p. 27.
- 14-44. Michelson, W., Wiedemanns Ann, Vol. 37, 1889.
- 14-45. Ubbelohde, L. and Hofsass, J., Gasbeleucht, Vol. 56, 1913, p. 1253. Ubbelohde, L. and Koelliker, ibid., Vol. 56, 1916, p. 49.
- 14-46. Stevens, F. W., The Rate of Flame Propagation in Gaseous Explosive Reactions; NACA Report 186, 1923; Jour. Amer. Chem. Soc., Vol. 48, 1926, p. 1896.
- 14-47. Garner, F. H., Long, R., and Ashforth, G. K., Determination of Burning Velocities in Benzene-Air Mixtures; Fuel, Vol. 28, 1949, p. 272; also, Jour. Chem. Phys., Vol. 18, 1950, p. 1112, and Fuel, Vol. 29, 1950, p. 284.
- 14-48. Bartholomé, E., On a Method for Measuring Flame Velocity; Z. Elektrochemie, Vol. 53, 1949, p. 191.
- 14-49. Andersen, J. W., and Fein, R. S., Measurement of Burning Velocities and Flame Temperatures of Bunsen Flames; Jour. Chem. Phys. Vol. 17, 1949, p. 1268; Vol. 18, 1950, p. 441.
- 14-50. Smith, F. A. and Pickering, S. F., Measurements of Flame Velocity by a Modified Burner Method; Jour. Res. Bur. of Stand., Vol. 17, 1936, p. 7.
- 14-51. Harris, M. E., Grumer, J., von Elbe, G., and Lewis, B., Burning Velocities, Quenching and Stability Data on Nonturbulent Flames of Methane and Propane with Oxygen and Nitrogen; Third Symposium on Combustion, Flame, and Explosion Phenomena, Williams and Wilkins Co., Baltimore, 1949, p. 80.

- 14-52. Broeze, J. J., Theories and Phenomena of Flame Propagation, Third Symposium on Combustion, Flame and Explosion Phenomena, Williams and Wilkins Co., Baltimore, 1949, p. 146.
- 14-53. Culshaw, G. W. and Garside, J. E.; Inst. Gas. Engrs., Comm. No. 346, 1948.
- 14-54. Garner, F. H., Long, R., and Ashforth, G. K., Burning Velocities of Propane-Air Mixtures; Fuel, Vol. 30, 1951, p. 63.
- 14-55. Smith, F. A., Problems of Stationary Flames; Chem. Rev., Vol. 21, 1937, p. 389.
- 14-56. Lewis, B. and von Elbe, G., Stability and Structure of Burner Flames; Jour. Chem. Phys., Vol. 11, 1943, p. 75.
- 14-57. Fristrom, R. M., Prescott, R., Neumann, R. K., and Avery, W. H., Temperature Profiles in Propane-Air Flame Fronts, Fourth Symposium (International) on Combustion, Williams and Wilkins, Baltimore, 1953, p. 267.
- 14-58. Singer, J. M., Burning Velocity Measurements on Slot Burners; Comparison with Cylindrical Burner Determinations; Fourth Symposium (International) on Combustion, Williams and Wilkins, Baltimore, 1953, p. 353.
- 14-59. Renouard, P., Deviation of the Burning Velocity of a Gas in a Flame Radius of Curvature of the Blue Cone at its Tip; Compt. Rend., Vol. 233, 1951, p. 235.
- 14-60. Lichty, L. C., Evaluation of Flame Speed at the Burner Flame Tip; Ind. Eng. Chem., Vol. 44, 1952, p. 1395.
- 14-61. Sherratt, S., and Linnett, J. W., Determination of Flame Speed in Gaseous Mixtures; Trans. Far. Soc., Vol. 44, 1948, p. 596.
- 14-62. Grove, J. R., Hoare, M. F., and Linnett, J. W., Shadow Cast by a Bunsen Flame, Its Production and Usefulness; Trans. Far. Soc., Vol. 46, 1950, p. 745.
- 14-63. Garner, F. H., Long, R., and Thorley, B., A Comparison of Schlieren, Shadow and Luminous Methods of Determining Burning Velocities, "Fourth Symposium (International) on Combustion", Williams & Wilkins, Baltimore, 1953, p. 386.
- 14-64. Albright, R., Heath, D., and Thena, R., Flame Velocities of Liquid Hydrocarbons; Ind. Eng. Chem., Vol. 44, 1952, p. 2490.
- 14-65. Nicholson, H. M., and Field, J. P., Some Experimental Techniques for the Investigation of the Mechanism of Flame Stabilization in the Wakes of Bluff, Bodies; Third Symposium on Combustion, Flame and Explosion Phenomena, Williams and Wilkins Co., Baltimore, 1949, p. 44.
- 14-66. Wohl, K., et al., Methods of Determining Burning Velocities and Stability Measurements of Tube and Nozzle Flames; Meteor Report UAC-49, December, 1950.
- 14-67. Van Steenis, J., Determination of the Velocity of Burning; Nature, Vol. 170, 1952, p. 1068.
- 14-68. Jost, W., Bunsen Burners; Naturwissenschaften, Vol. 39, 1952, p. 418.
- 14-69. Jost, W., and Seig, L., Anomalous Burner Flames, Z. Naturforsch., Vol. 6A, 1951, p. 403.
- 14-70. Gerstein, M., Levin, O., and Wong, E. L., Determination of Fundamental Burning Velocities of Hydrocarbons by a Revised Tube Method; Jour. Amer. Chem. Soc., Vol. 73, 1951, p. 418; also Ind. Eng. Chem., Vol. 43, 1951, p. 2770.

- 14-71. Hoare, M. F. and Linnett, J. W., Burning Velocity Determinations X. Flame Propagation Along Horizontal Tubes; Trans. Far. Soc., Vol. 49, 1953, p. 1038.
- 14-72. Behrens, H., Flame Propagation in Tubes I., Z. Elektrochem., Vol. 55, 1951, p. 330; ibid, II., p. 695.
- 14-73. Strehlow, R. A. and Stuart, J. G., An Improved Soap Bubble Method of Measuring Flame Velocities; "Fourth Symposium (International) on Combustion", Williams and Wilkins, Baltimore, 1953, p. 329.
- 14-74. Conen, H. R., Linnett, J. W., V. Use of Schlieren Photography in Determining Burning Velocities by the Burner Method; Trans. Far. Soc., Vol. 47, 1951, p. 981.
- 14-75. Pickering, H. S. and Linnett, J. W., VI Use of Schlieren Photography in Determining Burning Velocities by the Soap-Bubble Method, Trans. Far. Soc., Vol. 47, 1951, p. 989.
- 14-76. Linnett, J. W., Pickering, H. S. and Wheatley, P. J., IV. Soap-Bubble Method of Determining Burning Velocities; Trans. Far. Soc., Vol. 47, 1951, p. 974.
- 14-77. Aoki, H., and Hirasawa, H., Combustion of Mixtures of Acetylene and Air in a Soap Bubble; Oyo Butusuri (J. Applied Physics) Vol. 20, 1951, p. 15; Chem. Abstracts, Vol. 46, 1952, p. 1851h.
- 14-78. Simon, D. M. and Wong, E. L., Burning Velocity Measurements, Jour. Chem. Phys., Vol. 21, 1953, p. 936.
- 14-79. Gray, K. L., Linnett, J. W. and Mellish, C. E., IX. Propylene + Air and Propane + Air Mixtures; Trans. Far. Soc., Vol. 48, 1952, p. 1155.
- 14-80. Price, T. W. and Potter, J. H., Flame Velocities in CO-O₂ Mixtures; ASME Trans., Vol. 75, 1953, p. 91, "Fourth Symposium (International) on Combustion", Williams and Wilkins, Baltimore, 1953, p. 363.
- 14-81. Manton, J., von Elbe, G., Lewis, B., Burning Velocity Measurements in a Spherical Vessel with Central Ignition; "Fourth Symposium (International) on Combustion", Williams and Wilkins, Baltimore, 1953, p. 358.
- 14-82. Powling, J., A New Burner Method for the Determination of Low Burning Velocities and Limits of Inflammability; Fuel, Vol. 28, 1949, p. 25.
- 14-83. Egerton, A. C., and Thabet, S. K., Flame Propagation: The Measurement of Burning Velocities of Slow Flames and the Determination of Limits of Combustion; Proc. Roy. Soc., Vol. 211A, 1952, p. 445.
- 14-84. Mache, H., Kozak, W., and Zappe, A., The Burning Velocity of Methane-Air Mixtures Near the Limits of Flammability; Monatsh., Vol. 83, 1952, p. 171.
- 14-85. Spalding, D. B., New Method for Measuring Flame Speed; Research (London), Vol. 6, No. 9, 1953, p. 52S.
- 14-86. Johnston, W. C., Flame Propagation Rates at Reduced Pressures; Jour. Soc. Auto. Eng., Vol. 55, Dec., 1947, p. 62.
- 14-87. Sachsse, H., The Temperature Dependence of the Flame Velocity and the Temperature Fall in the Forepart of a Flame; Z. Physik. Chem., Vol. 180 A, 1937, p. 305.
- 14-88. Passauer, H., Effect of Preheating Gas and Air on Flame Temperature and Rate of Flame Propagation; Gas und Wasserfach, Vol. 73, 1930, pp. 313, 343, 369, and 392.

- 14-89. Dugger, G. L., Effect of Initial Temperature on Flame Velocities of Propane-Air Mixtures, J. Amer. Chem. Soc., Vol. 72, 1950, p. 5271; Vol. 73, 1951, p. 2398.
- 14-90. Dugger, G. L., and Heimel, S., Flame Speeds of Methane-Air, Propane-Air, and Ethylene-Air Mixtures at Low Initial Temperatures; Nat'l. Adv. Comm. Aeron., Tech. Note No. 2624, 1952, 25 pp.; cf also NACA Tech Note No. 2680, 1952, 25 pp.; NACA Res. Memo E52J24, 1953, 23 pp.
- 14-91. Dixon-Lewis, G., Effect of Preheat on Burning Velocity; Fuel, Vol. 30, 1951, p. 287; -- and Wilson, M. J. G., Trans. Far. Soc., Vol. 47, 1951, p. 1106.
- 14-92. Lewis, B., Discussions on D. M. Simon paper (Ref. 14-32), AGARD text, p. 176.
- 14-93. Khitrin, L., The Influence of Pressure on the Speed of Normal Flame Propagation; Tech. Phys., USSR, Vol. 3, 1936, pp. 926, and 1034.
- 14-94. Garside, J. W., Forsyth, J. S., Townend, D. T. A., Stability of Burner Flames; Jour. Inst. Fuel, Vol. 18, 1945, p. 175.
- 14-95. Linnett, J. W., and Wheatley, P. J., The Effect of Pressure on the Burning Velocity of Ethylene-Air Mixtures; Trans. Far. Soc., Vol. 45, 1949, p. 1152.
- 14-96. Egerton, A. C. and Lefebvre, A. H., Flame Propagation, The Effect of Pressure Variations on Burning Velocities; Proc. Roy. Soc., Vol. 222A, 1954, p. 206.
- 14-97. Edse, R., Studies on Bunsen Burner Flames at High Pressures with Hydrogen-Oxygen Mixtures; Ohio State University Eng. Expt. Station Bulletin No. 149, 1952, p. 441.
- 14-98. Leason, D. B., The Effect of Additions in the Burning Velocity of Propane-Air Mixtures; "Fourth Symposium (International) on Combustion", Williams and Wilkins, Baltimore, 1953, p. 369.
- 14-99. Kurz, P. F., Flame Stability with Mixed Fuels, Ind. Eng. Chem., Vol. 45, 1953, p. 2072.
- 14-100. Kurz, P. F., Influence of Hydrogen Sulfide on Flame Speed of Propane-Air Mixtures; Ind. Eng. Chem., Vol. 45, 1953, p. 2361.
- 14-101. Kassel, L. S., "The Kinetics of Homogeneous Gas Reactions", The Chemical Catalogue Company, Inc., New York, 1932, Chapter 11; also Bodenstein, M. and Lind, S. C., Zeit. Physik Chem., Vol. 57, 1906, p. 116.
- 14-102. Campbell, E. S. and Hirschfelder, J. O., Review of the Reaction Kinetics and Transport Properties of a Hydrogen Bromine Flame; University of Wisconsin NRL Report, CF-2108, November 17, 1953, 58 pages.
- 14-103. Anderson, R. C., Hydrogen-Bromine Flames; University of Texas, DRL - 320, CM-773, October 16, 1953.
- 14-104. Anderson, R. C., Calculations of Burning Velocities for Hydrogen-Bromine Mixtures: I. Mallard-LeChatelier Equation; Univ. Texas Report CF-1328, DRL-220, Sept., 1949.
- 14-105. Anderson, R. C., Calculations of Burning Velocities for Hydrogen-Bromine Mixtures: II. Square Root Laws; Univ. Texas Report CF-1409, DRL 291, March, 1950.
- 14-106. Cooley, S. D. and Anderson, R. C., Flame Propagation Studies Using the Hydrogen-Bromine Reaction; Ind. Eng. Chem., Vol. 44, 1952, p. 1402; also Jour. Amer. Chem. Soc., Vol. 74, 1952, p. 739.

- 14-107. Phillips, V. D., Brotherton, T. D., and Anderson, R. C., Physical Characteristics and Stability of Some Low Temperature Flames: The Hydrogen-Bromine System, "Fourth Symposium (International) on Combustion", Williams and Wilkins, Baltimore, 1953, p. 701.
- 14-108. Kokochashvili, V. I., The Combustion of Hydrogen-Bromine Mixtures; Zhur. Fiz. Khim., Vol. 25, 1951, p. 444; also Vol. 23, 1949, p. 21.
- 14-109. Mileson, D. F., The Thermal Theory of Laminar Flame Propagation for Hydrogen-Bromine Flames; Calif. Inst. Tech., Tech Report No. 6, Contract No. DA-495-Ord 446, July 1954.
- 14-110. Ausloos, P. and Van Tiggelen, A., Flame Propagation Velocities of Gaseous Mixtures Containing Ammonia; Bull. Soc. Chim. Belges, Vol. 60, 1951, p. 433.
- 14-111. Murray, R. C. and Hall, A. R., Flame Speeds in Hydrozine Vapor and in Mixtures of Hydrazine and Ammonia with Oxygen; Trans. Far. Soc., Vol. 47, 1951, p. 743.
- 14-112. Brokaw, R. S. and Pease, R. N., The Effect of Water in the Burning Velocities of Cyanogen-Oxygen-Argon Mixtures; Jour. Amer. Chem. Soc., Vol. 75, 1953, p. 1454.
- 14-113. Burden and Burgoyne, Proc. Roy. Soc., Vol. 199A, 1949, p. 328.
- 14-114. Friedman, R. and Burke, E., Burning Velocity of Ethylene Oxide Decomposition Flames; Jour. Chem. Phys., Vol. 21, 1953, p. 165.
- 14-115. Gerstein, M., McDonald, G. E., and Schalla, R. L., Decomposition Flame Studies with Ethylene Oxide, "Fourth Symposium (International) on Combustion", Williams and Wilkins, Baltimore, 1953, p. 375.
- 14-116. Egerton, A. C., and Powling, J. Limits of Flame Propagation at Atmospheric Pressure; Proc. Roy. Soc., Vol. A193, 1948, pp. 172 and 190.
- 14-117. Townend, D. T. A., The Mechanism of Flame Propagation, Fuel, Vol. 29, 1950, p. 64.
- 14-118. Hoare, M. F., and Linnett, J. W., Mechanism of Flame Propagation; Jour. Chem. Phys., Vol. 16, 1948, p. 747; Trans. Far. Soc., Vol. 47, 1951, p. 179.
- 14-119. Walker, P. L. and Wright, C. C., Hydrocarbon Burning Velocities Predicted by Thermal Versus Diffusional Mechanisms; Jour. Amer. Chem. Soc., Vol. 74, 1952, p. 3769; Vol. 75, 1953, p. 750.
- 14-120. Dugger, G. L. and Simon, D. M., Prediction of Flame Velocities of Hydrocarbon-Air Flames, "Fourth Symposium (International) on Combustion", Williams and Wilkins, Baltimore, 1953, p. 336; also Simon, D. M., Reference 14-32.
- 14-121. Dugger, G. L., and Graab, D., Flame Velocities of Hydrocarbon-Oxygen-Nitrogen Mixtures; "Fourth Symposium (International) on Combustion", Williams and Wilkins, Baltimore, 1953, p. 302.
- 14-122. Clingman, W. H., Brokaw, R. S. and Pease, R. N., Burning Velocities of Methane with Nitrogen-Oxygen, Argon-Oxygen and Helium-Oxygen Mixtures; "Fourth Symposium (International) on Combustion", Williams and Wilkins, Baltimore, 1953, p. 310.

CHAPTER 15. TURBULENT FLAMES OF PREMIXED GASES

ABSTRACT

The survey of literature on turbulent flames in premixed gases is divided into the following sections: the theory of turbulent flames, flame instability, experiments on turbulent flames, and concluding remarks. The theories of turbulent flame propagation, which are discussed first, fall naturally into three groups — those in which the scale of turbulence is considerably smaller than the flame thickness, those in which the scale of turbulence is considerably larger than the flame thickness, and those in which the scale of turbulence and the flame thickness are about the same. The theories pertaining to each of these classes are discussed in turn, and their similarities and differences noted. The various treatments of flame instability which might lead to flame-generated turbulence are covered next. Following this evaluation of the mathematical aspects of the turbulent flame phenomena, the experimental data reported in the literature are discussed. Certain factors common to these data are pointed out. In the final section, all of the work is summarized briefly and some deductions are made as to why there is so much disagreement in this field of research.

Contrails

TURBULENT FLAMES OF PREMIXED GASES

by

A. A. Putnam

The commonly observed Bunsen-type flame has a smooth, relatively thin and sharp flame front. The edges of the front are held near the burner wall where the flow velocity is low. The flame front is maintained by the spreading inward of the flame into the unburned gases, at a burning velocity of about one foot per second for hydrocarbon-air mixtures. As the exit velocity from the burner is increased, the flame elongates. As an example, for a burner tube of one-inch diameter and a mean gas velocity of about 4 ft/sec, the flame is about 2 inches long. Applying this proportionality to a high-duty combustion chamber, where velocities can be as high as 200 ft/sec, a combustion chamber length of better than 8 ft is indicated. This, of course, assumes that the flame speed, characteristic of the laminar conditions at low flow rates, does not change with flow rate.

However, for the Bunsen-type flame just mentioned, as the velocity is increased so as to exceed a critical Reynolds number, turbulence is generated, the flame loses its well-defined shape, becoming thick and diffuse in appearance, and the rate of increase, with velocity, of the mean length of flame decreases. Thus, even though the tip of the flame may extend as far as would be computed assuming laminar conditions (this point is not established in the literature), the bulk of the combustion will take place sooner, and high combustion efficiency, that is, high degree of completion of the burning, may be obtained with shorter distances. This latter situation is typical of high-duty combustors.

It is clear that the study of the effective flame speed under turbulent conditions, or of "turbulent flame speed", to fix the relative position of the flame, and the study of the total thickness of the flame under these conditions, are both of great practical importance. Historically, two approaches have been used. One of these concerns itself with the mechanism involved in the increase of apparent flame speed by turbulence. This leads to various mathematical expressions to describe the mechanism. The other approach is purely empirical and concerns itself with experiments on various types of burner equipment having known amounts of turbulence present, and with the direct or indirect correlation of turbulent flame speed with design characteristics.

Such a separation of the available information is followed in this chapter. In the theoretical section, the cases in which the scale of turbulence is smaller than, or about the same size as, or larger than the flame thickness are considered separately. The associated topic of flame instability is covered immediately after the theoretical discussion of flame turbulence, to afford further background for the discussion of the test data. The third section, on the test data reported in the literature, is followed by a section in which the problems of the turbulent flame are discussed more generally.

THEORY OF TURBULENT FLAMES

Small-Scale Turbulence

Shelkin⁽¹⁵⁻¹⁾ presented the first turbulent flame-speed equations which would reduce to the proper form when there was no turbulence. For this study, he presupposed two general types of turbulence, one in which the scale of turbulence is much smaller, and one in which the scale is

much larger than the thickness of the laminar flame front. He also discussed the transition regions between these two types.

In the first region, where l_2 , the Taylor scale based on length*, is much less than δ , the laminar flame thickness, Shelkin assumes that the only effect is an increase in the transfer rates. Assuming a thermal theory of flame propagation (the argument is the same for a diffusion theory), the new transport term becomes $\Gamma + \alpha\epsilon$, where Γ is the thermal diffusivity, ϵ is the turbulent transport coefficient, and α is close to 1; α is not included in most treatments, but is included here so that easier comparisons may be made. Since, as shown in Chapter 14, the various theories of flame propagation indicate that the transport term enters under a square root, the ratio of the turbulent burning velocity to the normal burning velocity is

$$\frac{F_t}{F} = \sqrt{\frac{\Gamma + \alpha\epsilon}{\Gamma}} = \sqrt{1 + \frac{\alpha\epsilon}{\Gamma}} \quad (15-1)$$

This equation satisfies the limiting condition of no turbulence, and for high-turbulence intensity becomes

$$\frac{F_t}{F} = \sqrt{\frac{\alpha\epsilon}{\Gamma}} \quad (15-2)$$

The approximation expressed by Equation (15-2) was derived earlier by Damköhler⁽¹⁵⁻²⁾, who used Prandtl's turbulence arguments as a basis for his derivation. Damköhler also used Prandtl's mixing coefficient, $l |\overline{u'}|$, for ϵ , where l is the Prandtl mixing length and $|\overline{u'}|$ is the time average value of the absolute fluctuating velocity.

Whereas Shelkin concludes that the presence of small-scale turbulence is implausible because of the small thickness of the flame front, Wohl⁽¹⁵⁻³⁾ considers that small-scale turbulence might occur in association with large-scale turbulence. Whether this factor should be considered would depend, first, on the initial turbulence spectrum, second, on the time available for the small-scale turbulence to decay, and third, on the thickness of the laminar flame, δ , which may be quite large at lower pressures.

Wohl assumes that the probability, w , of the occurrence of a scale $l_1 < \delta$, in turbulence of an average scale l_1 , is given by

$$w = 1 - e^{-(\delta/l_1)} \approx \delta/l_1 \quad (15-3)$$

Thus, the exchange coefficient of Shelkin's equation, Equation (15-1), should be reduced by this probability, so that

$$\frac{F_t'}{F} = \sqrt{1 + \frac{\alpha\epsilon}{\Gamma} \frac{\delta}{l_1}} \quad (15-4)$$

As ϵ may be defined as the product of the Taylor time-based length l_1 , and the root mean square fluctuating velocity**, u' , Equation (15-4) becomes

$$\frac{F_t'}{F} = \sqrt{1 + \frac{\alpha\delta u'}{\Gamma}} \quad (15-5)$$

*An extensive discussion of the various turbulence parameters used in this chapter is given in Chapter 12.

**The derivation of this relation is given in the section, Turbulent Diffusion, in Chapter 12.

It is shown by Wohl⁽¹⁵⁻³⁾, Friedman⁽¹⁵⁻⁴⁾, and others that $\delta \approx \Gamma/F$, so that Equation (15-5) may be written as

$$\frac{F_t'}{F} = \sqrt{1 + \frac{\alpha u'}{F}} \quad (15-6)$$

For small-turbulence intensities, this reduces to

$$F_t' = F + (\alpha/2)u' \quad (15-7)$$

while for high intensities,

$$F_t' = \sqrt{\alpha u' F} \quad (15-8)$$

In summation, for small-scale turbulence by itself, an improbable case, Equation (15-1) is available. For correcting the burning velocity for the small-scale component of normal turbulence, Equation (15-6) can be used.

Large-Scale Turbulence

Moderate Intensity

The second type of turbulence considered by Shelkin is that in which the characteristic length of the turbulence is much greater than the thickness of the flame front. In this case, the effect is assumed to be only one of distorting the flame front, and thus increasing the product of the burning velocity and the burning area.

Figure 15-1 shows a time exposure and an instantaneous schlieren photograph of a turbulent flame made by Karlovitz, et al.⁽¹⁵⁻⁵⁾. That the concept of the earlier workers regarding large-scale turbulence was justified, is clearly shown by the instantaneous schlieren photograph.



a. Time Exposure



b. Instantaneous Schlieren

FIGURE 15-1. PHOTOGRAPHS OF A TURBULENT NATURAL GAS - AIR FLAME

Re = 10,000; Burner Tube Radius = 15.8 mm
(Karlovitz, Denniston, and Wells)⁽¹⁵⁻⁵⁾

This picture of the effect of turbulence is similar to that observed earlier by Markstein⁽¹⁵⁻⁶⁾ in his studies of the effect of acoustical oscillations on flames. He found that the flame speed computed from the visible upstream surface was greater than the laminar burning velocity, while the burning velocity computed from the area of the distorted front, shown by instantaneous photographs, agreed with the laminar burning velocity. Because of the periodicity of the acoustic disturbance and the resulting orderliness of the distorted front, Markstein could make this computation.

Figure 15-2 shows a laminar, uniform flame front, distorted locally in conical surfaces, that is ordinarily used in the development of an equation for turbulent flame speed based on the concept outlined above. The depth of penetration, h , of these cones is assumed to be proportional to $(u' t)$, where t is the time available for penetration. The time, t , is of the order of the time taken for the flame to spread from both sides to the center of the base of the cone. Thus $t \sim l_1/2F$. Damköhler used l for l_1 , and Shelkin used l_2 for l_1 . However, since the entire argument is qualitative in nature, this makes no real difference. The depth of penetration, therefore, varies with $(u' l_1)/(2F)$. The total area of a cone is

$$\pi (l_1/2) \sqrt{(l_1/2)^2 + h^2} ,$$

the ratio of the cone surface to base area is

$$\sqrt{1 + 4 (h/l_1)^2} .$$

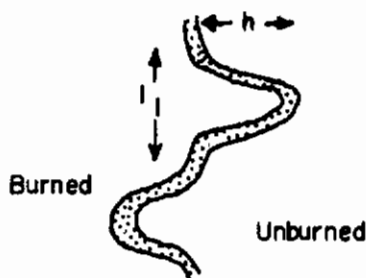


FIGURE 15-2. SCHEMATIC DIAGRAM OF DISTORTED FLAME FRONT

(Shelkin)⁽¹⁵⁻¹⁾

Therefore, since the product of laminar burning velocity and total area equals the product of the turbulent burning velocity and the projected area,

$$F_t/F = \sqrt{1 + 4 (h/l_1)^2} = \sqrt{1 + \beta^2 (u'/F)^2} , \quad (15-9)$$

where β is about 1. For the case where $u' \gg F$, this reduces to

$$F_t = \beta u' \quad (15-10)$$

which corresponds to Damköhler's equation for this region. For $u' \ll F$,

$$F_t/F = 1 + (\beta^2/2) (u'/F)^2 . \quad (15-11)$$

Wohl has indicated that it is equally satisfactory to use a cylinder, instead of a cone, as a model of the distorted front. This leads to the relation

$$F_t/F = 1 + 4 h/l_1 = 1 + 2 \beta u'/F . \quad (15-12)$$

Further consideration indicates that some of the flat region surrounding the cylinder or cone should be included; however, this correction can be included in β by reducing its value.

Wohl considered that the time required to destroy the cylinder might be that time required for the turbulent flame to sweep the cylinder base. Thus, the depth of penetration would vary with $u' l_1 / F_t$ instead of with $u' l_1 / F$, and

$$F_t / F = 1 + 2 \beta u' / F_t \quad . \quad (15-13)$$

Solving for F_t ,

$$F_t / F = 1/2 (1 + \sqrt{1 + 8 \beta u' / F}) \quad . \quad (15-14)$$

For small values of u' / F ,

$$F_t / F = 1 + 2 \beta u' / F \quad , \quad (15-15)$$

which is identical with Equation (15-12), while for large values of u' / F ,

$$F_t = \sqrt{2 \alpha u' F} \quad . \quad (15-16)$$

If the conical shape is considered, rather than the cylindrical shape, the smaller limit is the same as Equation (15-11), whereas the larger limit is of the same form as for that of the cylinder.

One further step may be taken at this time: Wohl's small-scale turbulence correction to the burning velocity given by Equation (15-8) may be made. This means that the burning velocity of Equation (15-16) should be corrected for small-scale turbulence. Therefore,

$$F_t = \sqrt{2 \beta u' F_t'} = (2\beta)^{1/2} (\alpha)^{1/4} u'^{3/4} F^{1/4} \quad . \quad (15-17)$$

In a later paper, Wohl, et al., also considers the possibility that the time available for propagating a distortion might be determined by the rate, U , at which an eddy passes through the mean flame front; thus the depth of penetration would vary with $u' l_1 / U$, and, in place of Equations (15-12) or (15-13), (based on cylindrical distortion), one has

$$F_t / F = 1 + 2 \beta u' / U \quad . \quad (15-18)$$

The corresponding modification for Equation (15-9) (based on conical distortion) is

$$F_t / F = \sqrt{1 + (\beta u' / U)^2} \quad . \quad (15-19)$$

Because u' is normally considerably less than U , and β is of the order of one, it is seen that F_t / F would not be larger than, say, about 5. This much is in agreement with observations made on uniform, open-flow systems.

Karlovitz developed a turbulent-flow speed theory as a result of observing the instantaneous photographs of a turbulent Bunsen flame, which shows a highly distorted but continuous front, as shown in Figure 15-1.

Basically, Karlovitz starts with Wohl's Equation (15-12). However, since the depth of penetration, h , varies linearly with time for only small intervals of time, and some recession takes place at longer intervals of time, for most of the time the depth of penetration is less than $(u' t)$. To determine the variation of h , or as redefined, the root mean square displacement, $\sqrt{X^2}$, with time, Karlovitz starts with the turbulence equations of Taylor, uses the correlation coefficient, R_t , which, as discussed in Chapter 12, is on a Lagrangian basis. The scale of turbulence is, therefore, given by

Conclusions

$$l_1 = u' \int_0^{\infty} R_t dt \quad , \quad (15-20)$$

and the characteristic time is

$$t_c = \int_0^{\infty} R_t dt \quad . \quad (15-21)$$

The variation of the root mean square displacement is given by

$$d(\overline{X^2})/dt = 2 u'^2 \int_0^t R_t dt \quad . \quad (15-22)$$

For small intervals of time, $t \ll t_c$, $R_t \approx 1$, and

$$\sqrt{\overline{X^2}} = u' t \quad , \quad (15-23)$$

whereas, for large intervals of time, $t \gg t_c$, $\int_0^t R_t dt$ reaches a definite limiting value, t_c , and

$$(\overline{X^2}) = 2 u'^2 t_c t = 2 l_1 u' t \quad . \quad (15-24)$$

Assuming the form of e^{-t/t_c} for R_t , for intermediate values, where $t \sim t_c$,

$$\overline{X^2} = 2 l_1 u' t \left\{ 1 - (t_c/t) \left[1 - e^{-t/t_c} \right] \right\} \quad . \quad (15-25)$$

The time, \underline{t} , over which a given element exists is of the order of l_1/F . It is realized that this \underline{F} should be corrected for small-scale turbulence if any such effect exists; Equation (15-8) as developed by Wohl can be used. However, in the subsequent treatment, this factor is omitted.

The additive flame speed caused by the turbulence, F_t'' , is

$$F_t'' = \sqrt{(\overline{X^2})}/t \quad . \quad (15-26)$$

By means of Equation (15-25) and the definition of t_c as given by combining Equations (15-20) and (15-21), $\sqrt{(\overline{X^2})}$ and \underline{t} may be eliminated from the equation defining F_t'' . Adding F_t'' , as just defined, to the burning velocity, \underline{F} , and rearranging terms, yields

$$F_t/F = 1 + \left\{ 2 u' / F \right\}^{1/2} \left\{ 1 - (F/u') \left[1 - e^{-u'/F} \right] \right\}^{1/2} \quad , \quad (15-27)$$

in the general case.

For $u'/F \ll 1$, Equation (15-27) reduces to

$$F_t/F = 1 + u'/F \quad , \quad (15-28)$$

and in the case of very strong turbulence, $u'/F \gg 1$,

$$F_t/F = 1 + \sqrt{2} u'/F \approx \sqrt{2} u'/F$$

(15-29)

Figure 15-3, showing the advance of the flame in a distorted front, was used by Karlovitz to point out that, while the turbulence tends to increase the distortion to the front, the normal type of flame propagation tends to eliminate the distortion, in the manner illustrated.

Finally, it may be seen that Wohl's cylinder-based derivation and Karlovitz' derivation lead to the same results at the two limits of very weak and very intense turbulence. It follows that, if Wohl's correction for small-scale turbulence is made to either equation, the identity of form is still retained.

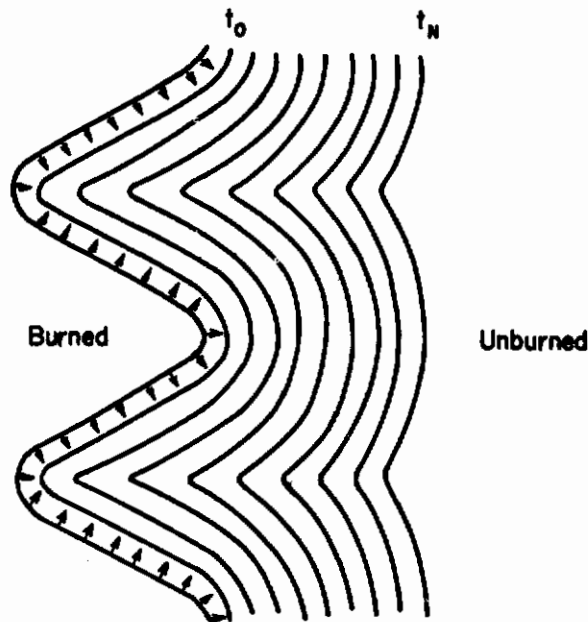


FIGURE 15-3. ADVANCE OF FLAME IN DISTORTED FRONT

(Karlovitz, Denniston, and Wells)(15-5)

Wohl, et al., points out that in most combustors, the flame is held in a small region, and the distortion of the flame increases as the flame spreads out from the holding region. Scurlock and Grover⁽¹⁵⁻⁷⁾ elaborate on Karlovitz' result to take account of this fact. To do this, they retain the correlation coefficient R_t and introduce, also, the correlation coefficient R_y . Although the use of these coefficients is not technically correct, the resulting form of equation is reasonable. As a consequence of this treatment, Karlovitz' Equation (15-25) is modified by replacing l_1 (note that $t_c = l_1/u'$) by l_1' , where

$$l_1/l_1' = 1 + F/2u' \quad (15-30)$$

It may be noted that Scurlock's later use of the time term as determined by the flame-propagation rate along the mean flame front indicates that F of Scurlock's Equation (15-30) should be replaced by F_t .

Scurlock and Grover also made a more exact computation of the effect of the advancing flame front than did Karlovitz, and thus allow for the tendency of the front to decrease the total flame area. The final equation, however, is so complicated that a numerical solution is necessary for each set of conditions.

Figure 15-4 shows the result of these computations, with reasonable values assumed for the ratio of l_1/l_2 and some other arbitrary constants of the formulated equations. It is seen that the

ratio of turbulent to laminar burning velocity increases with time* to a maximum depending on the ratio of rms fluctuating velocity to the laminar burning velocity. An increase of scale, l_2 , increases the time to reach the maximum.

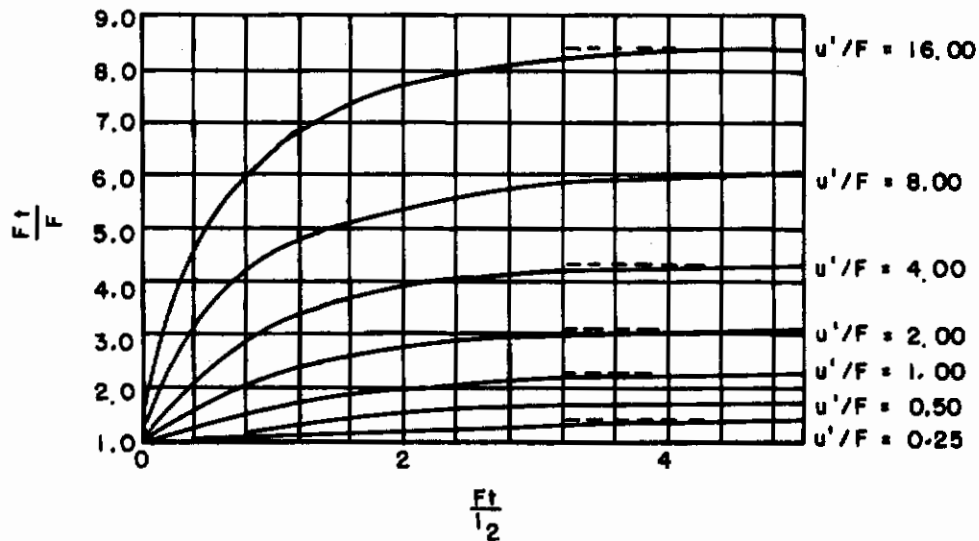


FIGURE 15-4. COMBINED EFFECT OF EDDY DIFFUSION AND FLAME PROPAGATION

(Scurlock and Grover)(15-7)

Before passing on to the considerations of high intensity turbulence, one other point considered by Scurlock and Grover might well be mentioned. They computed the distortion of the flame produced by a single eddy passing through the flame front.

Figure 15-5 shows the result of this computation. As the ratio of eddy-spin velocity to burning velocity increases, the amount of distortion increases. At the highest rotary velocity, the flame spirals in on itself. It is not clear in this figure, but is noted by Markstein that the distortion caused by the eddy propagates along the flame front even after the eddy has passed through and beyond the front; and, in an actual flame the distortion may not only propagate along the front, but may even expand in size.

High-Intensity Turbulence

In considering the turbulent flame as a distorted laminar front, some thought must be given to the possibility that the flame will be distorted so rapidly that the front will break. This will partially destroy the continuity of the flame, and allow unburned gases to pass through, at least temporarily.

*Time is computed from the flame-propagation rate along the front from the region of holding; thus

$$t = \int_0^L ds/U \cos \beta$$

where L is the distance along the front, U is the stream velocity at any point s on the front, and β is the angle between the front and the stream direction.

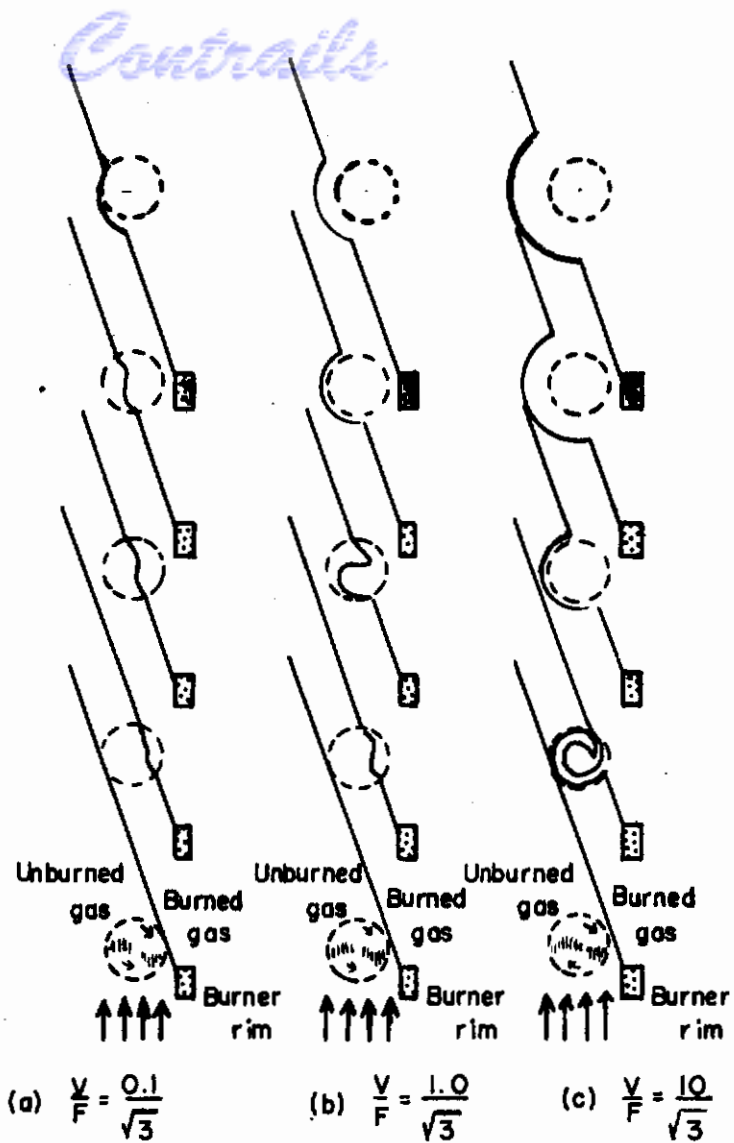


FIGURE 15-5. DISTORTION OF STABILIZED FLAMES DURING PASSAGE OF SINGLE EDDIES

(Scurlock and Grover)(15-7)



FIGURE 15-6. SCHEMATIC DIAGRAM OF HIGHLY TURBULENT FLAME

(Shelkin)(15-1)

Figure 15-6* shows the idea that Shelkin uses as a basis for his discussion of the range of $l_1 \gg \delta$ and $u' \gg F$, in which he assumes that the turbulence would be so violent that the front would be broken. Shelkin considers flame speed to be proportional to the square root of the exchange coefficient divided by a reaction time; in the case of the discontinuous front, the exchange coefficient is ϵ or $l_1 u'$.

An elementary volume $(l_1)^3$ will break up over the duration of time, l_1/F , that the flame takes to traverse the distance l_1 at normal burning velocity. In this time, the total path traveled at the fluctuating velocity is

$$L = (l_1/F) u' \quad (15-31)$$

The ratio L/l_1 indicates the number of traverses of the front through the volume $(l_1)^3$, so that the flame-front area per unit volume is

$$(L/l_1) l_1^2 / l_1^3 = u' / F l_1 \quad (15-32)$$

and the time of combustion of the unit volume is $F l_1 / u'$ divided by F , or l_1 / u' . Combining this time with the exchange coefficient in the manner previously indicated,

$$F_t \sim \sqrt{l_1 u' / l_1 / u'} = u' \quad (15-33)$$

This is the same as Shelkin's relation for the continuous, disturbed flame front (Equation (15-10)). It may also be noted that this is the same basic idea as in Wohlenberg's⁽¹⁵⁻⁹⁾ paper (cf Chapter 19).

Shelkin assumes, among other things, that the time to burn an elemental volume is the same as the travel time through the front; that is, that every elemental volume starts to burn at the front. Wohl⁽¹⁵⁻¹⁰⁾ makes a somewhat different approach to the high-turbulence intensity problem. If a mass is followed through the front, starting at time $t = 0$ at the front, new eddies are assumed to be generated in the mass at a frequency $\nu \sim u' / l_1$. Therefore, the number of eddies generated by the time t , is $kt(u' / l_1)$, and the total surface of the eddies is $k' t (u' / l_1)$, where k and k' are assumed to be independent of the time elapsed since a unit mass has entered into the combustion zone. The rate of burning at time t is, therefore, the product of the burning velocity and the surface area or $Fk' t(u' / l_1)$. The average distance, $d\delta$, that the flame propagates during the time, dt , is $Fk' t(u' / l_1) dt$. Integrating, the time, t_c , to travel the thickness of the flame, δ' , and thus complete combustion, is given by the relation

$$\delta' = (Fk' u' / l_1) (t_c^2 / 2) \quad (15-34)$$

However, the turbulent flame speed is also given by

$$F_t = \delta' / t_c \quad (15-35)$$

so that, eliminating δ' ,

$$t_c = (F_t / F) (2l_1 / u' k') \quad (15-36)$$

Using the approximate general formula, previously used by Shelkin, that

$$F_t \sim \sqrt{\epsilon / t_c} \quad (15-37)$$

and substituting $u' l_1$ for ϵ , yields

*This model may also be representative of the region of a turbulent flame away from the holder, where the continuous front has been largely torn apart. This tearing is discussed later.

$$F_t \sim \sqrt{k' (u')^2 F / 2F_t} \quad (15-38)$$

or, taking all F_t to one side,

$$F_t \sim (k')^{1/3} (u')^{2/3} F^{1/3} \quad (15-39)$$

One point open to question here is the assumption of k' as invariant. Some consideration of the problem of defining k' more exactly indicates that it is conceivable that it would vary with the time that a unit mass has been in the combustion zone, especially if the flame itself acts as a turbulence generator. Further elaboration of this equation would appear profitable after obtaining test data of a type needed.

Karlovitz, et al, (15-11, 12) approached the problem of the turbulent flame in a region of high intensity turbulence by first considering a laminar flame propagating into a stream of changing velocity. Based on the ignition temperature concept an increase in the flow velocity across the stream causes the burning velocity to decrease in order to allow time for the increased flow of gases to come to the ignition temperature*. Karlovitz' resulting equation is not integrable in a closed form, but he calculates some particular values.

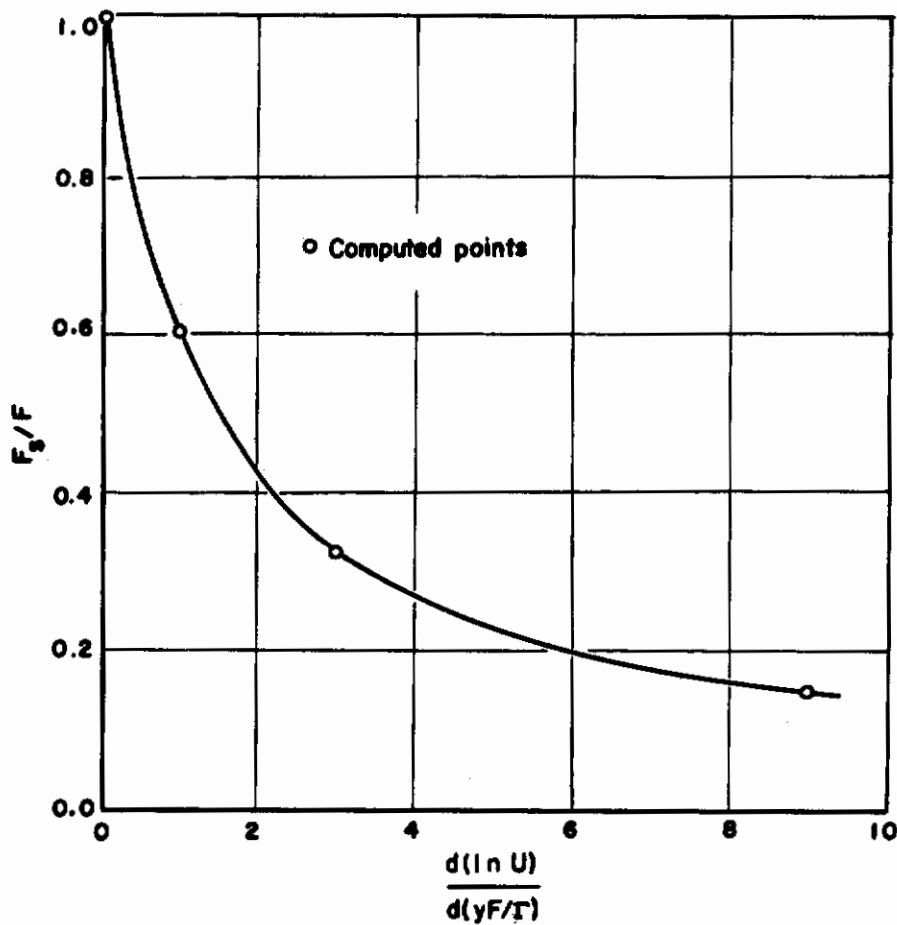


FIGURE 15-7. BURNING VELOCITY OF STRETCHED FLAME AS A FUNCTION OF VELOCITY GRADIENT

*With uniform flow velocity, each streamline can be considered in self-equilibrium, but in a region of changing velocity, heat must be treated as being supplied from each stream to the adjacent one.

Figure 15-7 shows Karlovitz' results. The ratio of reduced burning velocity, F_s , to the normal burning velocity, F , is a function of the rate of change of the log stream velocity with respect to the dimensionless distance across the stream. The decrease in F_s may be interpreted to mean that the flame front becomes less stable and more apt to break.

Karlovitz(15-12) extends this result to the turbulent flame by considering the rate of the stretch of the flame front in a segment of a turbulent flame. Essentially, the abscissa of Figure 19-7 becomes

$$\alpha(u'/F)(\Gamma/l_1F)$$

where α is the order of magnitude of 1. Thus, as the intensity increases, or the scale or burning velocity decreases, the flame front will be more likely to develop holes. Such holes have been observed by Karlovitz using ionization probes.

Summary of High Intensity Turbulence Equations

For turbulence of high intensity, four expressions have been derived, which are expressible in the general form

$$F_t \sim (u')^{1-m} F^m, \quad 0 \leq m \leq 1/2, \quad (15-40)$$

and a fifth expression is given approximately by

$$F_t = u' F/U \quad (15-41)$$

These expressions may indicate general relations to be sought in experimental work.

Transition Region of Turbulence

Shelkin also discusses, in a qualitative manner, the transition region between small-scale turbulence and large-scale turbulence. Again using the ratio of exchange coefficient to reaction time as a basis, (Equation (15-37)) and assuming the Arrhenius law for reaction time,

$$t \sim \exp(E/RT), \quad (15-42)$$

Shelkin indicates that, with a mixing length of the order of size of the flame-front thickness, in any one region, gases are pulled in from distances $\pm l_2$, so that, with turbulence

$$t \sim 1/2 \left\{ \exp \left[E/R(T + l_2 dT/dx) \right] + \exp \left[E/R(T - l_2 dT/dx) \right] \right\} \quad (15-43)$$

When $(T_c - T_0)/\delta$ is substituted for dT/dx , it is seen that T and $(l_2/\delta)(T_c - T_0)$ are of the same order of magnitude. Thus, the second part of Equation (15-43) becomes more dominant than the first, because of the relative magnitude of the difference and sum terms, and

$$t \sim \exp \left\{ E/R \left[T - (l_2/\delta)(T_c - T_0) \right] \right\}, \quad (15-44)$$

and becomes larger as l_2 increases. The increase of l_2 is more than balanced by the increase in t (in the ratio (l_2/t) , and thus the reaction rate decreases.

However, the time magnitude of the effect must also depend on the velocity of mixing, and eventually the time will depend only on $1/u'$, as indicated for large-scale turbulence, rather than the relation given by Equation (15-44).

Delbourg's (15-13) treatment is difficult to classify in terms of the previous discussion. The direct addition of laminar- and turbulent-transport coefficients is used when these transport terms are believed to be of similar nature, as in Shelkin's Equation (15-1) for small-scale turbulence. However, Delbourg apparently believes that since the thickness of the front will increase with turbulence, such a treatment is valid as long as the scale is smaller than the turbulent flame thickness, which may be considerably larger than the laminar flame thickness; thus, Delbourg's treatment may be considered to refer definitely to the transition region, and also to the large scale turbulence region if the scale involved is sufficiently greater than the laminar flame thickness.

Delbourg uses a classical one-dimensional derivation of flame speed, replacing the laminar-transport coefficients with turbulent-transport coefficients. The reaction considered is monomolecular, although he indicates that similar results are obtained from other orders of reaction. The ignition temperature, a controversial term to begin with, is considered constant, even under the turbulent conditions; this assumption perhaps requires justification.

The fuel concentration is first determined, neglecting laminar diffusion; second-order and higher terms in the expansion are dropped. Also, a dimensionless group containing a distance term apparently is lost from the first-order term. The solution for fuel concentration as a function of distance is used in the determination of the temperature distribution. In this case, the transport term is the sum of the laminar and turbulent coefficients.

The final step is to apply Nikuradse's classical data on pipe turbulence to the computation of the variation of flame speed across a pipe section. The average turbulent flame speed, on a volume flow basis, is found to be given by

$$F_t/F = 0.128 Re^{0.4}, Re > 3000 \quad (15-45)$$

Because the laminar-diffusion terms were dropped at certain stages in the analysis, this solution is not applicable to small intensities of turbulence. However, if the picture presented is correct for some types of turbulent flames, and the assumptions mentioned can be shown to be reasonable, the general form of the resulting equation should be valid for large intensities, even though the numerical constants are incorrect.

A similar treatment for the secondary, vapor-phase reaction in a solid fuel fired rocket is given by Corner (15-14).

FLAME INSTABILITY

Any flame instability of a laminar flame will cause an increase in surface area and an increase in apparent flame speed, and, at the same time, will cause a deviation of the accelerated flow of the burning gases from the usually considered one-dimensional case for laminar flow. If the damping is not sufficient, a flame may act to increase its own speed and thickness, both directly, through increasing the surface of burning, and indirectly, by generating turbulence. It follows that the stability of the flame, in itself, deserves consideration.

• Landau (15-15) and Darrieus (15-16) independently derived a criterion for the instability of a laminar flame front, assuming (1) that the characteristic size of instability was much larger than the flame thickness, (2) that the burning velocity was much smaller than the speed of sound, (3) that viscous forces could be neglected, and (4) that the burning velocity was invariant with curvature of the front. The result is that, if the gases expand upon burning, which they normally do for deflagration flames, the flame is unstable for all perturbations. This result does not disagree with observations on turbulent flames, since in high-velocity or turbulent regions, where viscous effects can, in a certain sense, be neglected, the observed flame front is definitely unstable. However, the question is not answered as to whether the observed instability is caused by the

turbulence already present, or by the flame. It also does not give an explanation for such phenomena as the rotating pyramids of rich propane flames on a Bunsen burner*.

Markstein⁽¹⁵⁻¹⁸⁾ refines Landau's approach by assuming that the burning velocity and the temperature at the front varies with the curvature of the front. The derivation of the equation defining the unstable regions is presented for the case where only the burning velocity varies with curvature, that is, where

$$F = F_0 (1 + \mu L/R) \quad , \quad (15-46)$$

where L is a characteristic length of the order of the thickness of the combustion zone, R is the radius of curvature, and the parameter μ is normally considered positive; that is, the flame speed is considered to increase as the flame becomes concave toward the unburned gases. It may be noted that the term μ brings in the chemical aspects of the problem, as well as transport effects, notably differential diffusion. The expansion ratio, f , and the ratios

$$T_b^0/T_u^0, u_b^0/u_u^0, \rho_u^0/\rho_b^0$$

are all assumed to be equal. The pressure drop across the flame is given by

$$p_u^0 - p_b^0 = \rho_u^0 (u_u^0)^2 (f - 1) \quad . \quad (15-47)$$

Also, for a steady flame condition,

$$u_u^0 = F_0, u_b^0 = fF_0 \quad . \quad (15-48)$$

In these expressions, u denotes velocity, p , pressure, ρ , density, and the subscripts u and b refer to unburned and burned gas regions, respectively.

On these steady-state conditions are imposed the small time-dependent perturbations denoted by primes. Neglecting second-order terms, the momentum and continuity equations for the perturbations become

$$\frac{\partial u'_u}{\partial t} + F_0 \frac{\partial u'_u}{\partial x} = - \frac{1}{\rho_u^0} \frac{\partial p_{u'}}{\partial x} \quad ,$$

$$\frac{\partial v'_u}{\partial t} + F_0 \frac{\partial v'_u}{\partial x} = - \frac{1}{\rho_u^0} \frac{\partial p_{u'}}{\partial y} \quad ,$$

and

$$\frac{\partial u'_u}{\partial x} + \frac{\partial v'_u}{\partial y} = 0 \quad (15-49)$$

for the unburned gas**. A similar set of equations is obtained for the burned gas region.

The particular solution is sought that will satisfy the boundary conditions that the perturbation amplitudes approach zero at $x \rightarrow \pm \infty$, and be periodic in y and exponential in t . The latter conditions are met by the form

$$g(y, t) = \exp [i 2\pi y/\lambda + \beta t] \quad , \quad (15-50)$$

*Reference 15-17 contains a review of the literature relating to such flame phenomena.

**These may be derived easily from Equations (11-7) and (11-19).

where λ is the wavelength of the perturbation. If the real part of β is positive, it is seen that the disturbance grows and the system is unstable. Since Equation (15-49) has constant coefficients, the solution must also be exponential in x . A substitution of such a form into Equation (15-49) leads to the result that the expression in x will take one of the forms

$$e^{2\pi x/\lambda}, e^{-2\pi x/\lambda}, \text{ or } e^{-\beta x/u^0}$$

Only the first form will satisfy the boundary conditions at $x = -\infty$ in the unburned gases, whereas the last two forms satisfy the boundary conditions at $x = +\infty$ in the burned gas*.

The solution to Equation (15-49) can now be written as

$$\left. \begin{aligned} u'_u/F_0 &= A_1 f_1(x) g(y, t) \\ v'_u/iF_0 &= A_1 f_1(x) g(y, t) \\ p'_u/\rho_u^0 F_0^2 &= -(\alpha f + 1) A_1 f_1(x) g(y, t) \\ u'_b/F_0 &= [A_2 f_2(x) + A_3 f_3(x)] g(y, t) \\ v'_b/iF_0 &= [-A_2 f_2(x) - \alpha A_3 f_3(x)] g(y, t) \\ p'_b/\rho_u^0 F_0^2 &= (\alpha - 1) A_2 f_2(x) g(y, t) \end{aligned} \right\} \quad (15-51)$$

where

$$\left. \begin{aligned} \alpha &= \beta\lambda/2\pi f F_0 \\ f_1(x) &= e^{2\pi x/\lambda} \\ f_2(x) &= e^{-2\pi x/\lambda} \\ f_3(x) &= e^{-2\pi\alpha x/\lambda} \end{aligned} \right\} \quad (15-52)$$

Figure 15-8 is a sketch of the laminar, unstable flame front considered by Markstein. The movement of the flame front in the x -direction, at the point (ξ, η) , is given by

$$d\xi/dt = u_u - F \cos \phi = u_b - fF \cos \phi \quad (15-53)$$

where ϕ is the angle between the disturbed and average flame fronts. Similarly, the movement in the y direction is given by

$$d\eta/dt = v_u + F \sin \phi = v_b + fF \sin \phi \quad (15-54)$$

For small values of ϕ ,

$$\sin \phi \approx \phi \approx \partial \xi / \partial y \quad (15-55)$$

Since ξ is dependent on y and t in the same manner as the other perturbations, ξ may be defined by

$$\xi = (\lambda A_4 / 2\pi) g(y, t) \quad (15-56)$$

*Markstein(15-20) has pointed out that "it is really not necessary to require this term ($\exp(-\beta x/u^0)$) to vanish at $+\infty$, since it corresponds to vorticity generated in the flame, that can reach $+\infty$ only after an infinite time. On the other hand, in the stable case, $\beta < 0$, the boundary conditions also would permit the term to be included in the unburned gas, but physically this would not make sense for the stability analysis. It is, however, of interest in the corresponding analysis of a turbulent flame, where the upstream vorticity is essential".

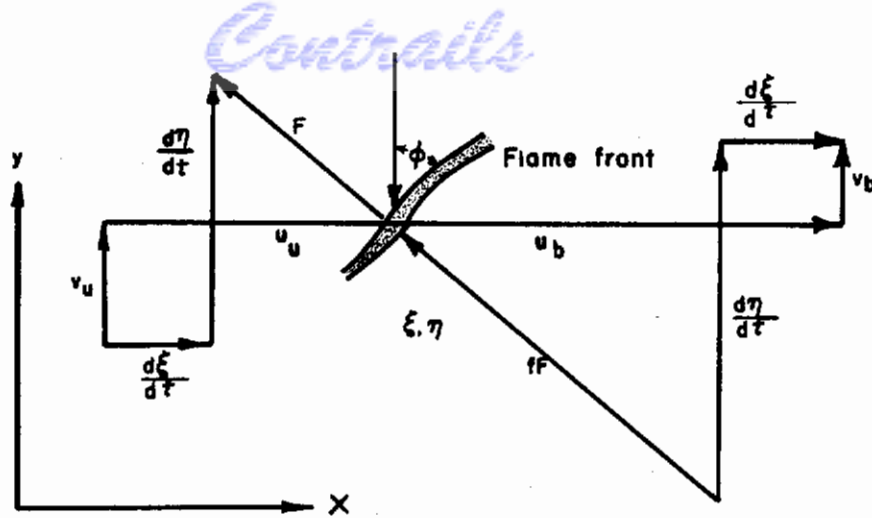


FIGURE 15-8. SCHEMATIC DIAGRAM OF LAMINAR UNSTABLE FLAME FRONT
(Markstein)(15-18)

Solving for $\partial^2 \xi / \partial y^2$, noting that the radius for curvature of the flame front, R , is approximately $-1/(\partial^2 \xi / \partial y^2)$, and substituting into the Equation (15-46) for F yields

$$F = F_0 [1 + \sigma A_4 g(y, t)] \quad , \quad (15-57)$$

where

$$\sigma = 2\pi\mu (L/\lambda) \quad . \quad (15-58)$$

The final boundary condition for the boundary between the unburned and burned gases comes from the generalized version of Equation (15-47), which, upon expansion and dropping of the second-order terms, becomes

$$P_{u'} - P_{b'} = P_u^0 F_0^2 (f - 1) [2\sigma A_4 g(y, t)] \quad . \quad (15-59)$$

At the flame-front position, where $x \approx 0$, Equations (15-53), (15-54) and (15-59) now become a set of linear homogeneous equations in $A_1, 2, 3, 4$:

$$\begin{aligned} A_1 - (\alpha f + \sigma) A_4 &= 0, \quad , \\ A_2 + A_3 - f(\alpha + \sigma) A_4 &= 0 \quad , \\ A_1 + A_2 + \alpha A_3 - (f - 1) A_4 &= 0 \quad , \\ (\alpha f + 1) A_1 + (\alpha - 1) A_2 + 2\sigma (f - 1) A_4 &= 0 \quad . \end{aligned} \quad (15-60)$$

A nontrivial solution for the system may be obtained for the two values of α given by

$$\begin{aligned} \alpha &= [1/(1+f)] [-(1+\sigma) - (1+f - 1/f + \sigma^2 - 2\sigma f)^{1/2}] \quad , \\ \alpha &= [1/(1+f)] [-(1+\sigma) + (1+f - 1/f + \sigma^2 - 2\sigma f)^{1/2}] \quad , \end{aligned} \quad (15-61)$$

For $\alpha = 1$, $f_3(x) = f_2(x)$ from Equation (15-52), and the solution is trivial.

As indicated earlier for β , which is proportional to α , (Equation (15-52)), a negative value of α indicates a stable solution; therefore, the solution of α with the negative sign on the square root is discarded as a possible unstable solution. This leaves only the term with a positive sign on the square root to be considered. When the entire term is positive, an unstable condition exists.

It follows from Equation (15-61) that the condition for instability is satisfied whenever

$$(f - 1)/f > 2\sigma = 4\pi \mu(L/\lambda) \quad , \quad (15-62)$$

or whenever

$$\lambda > [f/(f - 1)] 4\pi \mu L \quad . \quad (15-63)$$

This indicates that whenever μ is positive, the normal condition, disturbances of wavelengths below some certain value will not increase in amplitude. From Equation (15-63), for Landau's condition of $\mu = 0$, all wavelengths are unstable. This is to be expected, since the solution reduces to Landau's for such a condition.

The value of λ at which the maximum instability occurs is obtained by setting $d\alpha/d\sigma$ equal to zero. As a result of maximizing Equation (15-61) one obtains

$$\alpha^3 - [(9f-1)/4]\sigma^2 + [(f+1)(3f-2)/2f]\sigma - (f-1)(f^2 + f-1)/4f^2 = 0 \quad . \quad (15-64)$$

For an expansion ratio, f , or 5, σ is about 0.2, or

$$10 \pi \mu L/\lambda \approx 1 \quad , \quad (15-65)$$

Markstein shows that, for equal diffusion coefficients, including thermal diffusivity,

$$\mu L = \Gamma / F_0 \quad , \quad (15-66)$$

where Γ is the diffusion coefficient; thus the wavelength of maximum instability is

$$\lambda \approx 10 \pi \Gamma / F_0 \quad . \quad (15-67)$$

Markstein ran tests on combustible mixtures of several different molecular-weight fuels over a wide range of pressures. By controlling the amount of nitrogen added to any fuel mixture, cellular flames could be stabilized in a vertical tube at $400 < Re < 600^*$. These cells were convex toward the unburned gases, with the joining portion of the cell edges pointing downstream. It was found that the size** of the cell varied roughly with the reciprocal pressure and with the cube root of the reciprocal molecular weight of the fuel. The observed deviations from these approximate variations appear to be explicable from (1) the variation of F_0 with molecular weight and pressure, (2) the exact variation of Γ with molecular weight, and (3) the edge corrections when cells are not small compared to the tube diameter. Thus, the experimental results and the theory appear to check quite well.

Friedman⁽¹⁵⁻²²⁾, comparing his results on quenching distance with the cellular-flame results, points out that they are similar in several ways, namely; the dimensionless group obtained from Equation (15-67) correlates the quenching distance data very well; quenching distance and cell diameter are of the same order of magnitude; their variation with pressure, diluent, and mixture ratio appear to be the same.

Markstein also points out that his flames were only unstable on the rich side, unless hydrogen was added. In this instance, unstable flames were obtained on the lean side. No cells were obtained for methane. These results are similar to those of Manton, et al⁽¹⁵⁻²³⁾, and others. Manton, in flame-speed tests by the bomb method, found nonisotropic (distorted) propagation of the flame with a fuel-rich mixture when the fuel had a diffusion rate less than that of oxygen, and with a fuel-lean mixture when the fuel had a larger diffusion rate than that of oxygen.

*An apparatus for studying "cells" above a slot burner is described in Reference 15-21. This is adjusted to give traveling and vanishing cells whose smallest size is to be correlated with Equation (15-63).

**Square root of cross-sectional area of combustion tube, divided by number of cells.

Continued

These observations might be explained on the following basis: consider a stable flame from a fuel-rich mixture with a low fuel diffusion rate; if the flame front advances slightly, the relative time for diffusion is reduced and the mixture at the critical point of burning (say, the ignition temperature) becomes relatively more lean, with a resulting increase in flame speed. Such an increase in flame speed would lead to a further acceleration of the flame and an unstable condition. Similarly, an initial deceleration would lead to further decreases and instability. If the rates of diffusion are reversed, by the same line of reasoning, the process becomes stabilizing.

Once some curvature has been imparted to the flame front, preferential diffusion leads to a segregation of the faster and slower diffusing gases. For instance, for the rich, heavy hydrocarbon flames, the flame tends to be leaner at the upstream point of the flame (when the higher flame speed is required to maintain the cups) and richer in the interstices of the cups. For some flames, this leads to smoke streamers from the cup interstices.

Another possible stabilizing effect is that of flame propagation itself, as discussed previously in reference to Figure 15-3. However, Markstein⁽¹⁵⁻²⁴⁾ shows that this effect, by itself, cannot stabilize a flame.

Markstein also carried out the solution for the effect of gravity on the stability of the flame. For a downward propagating flame in a vertical tube, the effect is stabilizing, increasing with decreasing burning velocity. It not only increases the lower limit of the unstable region, but also puts an upper limit on the size of the cells.

Einbinder⁽¹⁵⁻²⁵⁾ used this gravitational phenomenon in interpreting Markstein's experimental observations on the presence or absence of cells as follows: the combustion process is assumed to be thermal for rich, slowly burning hydrocarbon flames; this leads to a relatively thin flame, to small cells, and to a relatively small gravity effect; these cells were observed in the experimental equipment. On the lean side, the combustion mechanism changes to the radical type; this leads to a relatively thick flame, to large cells, and to a large damping effect of the gravitational forces. For the flow velocity used in Markstein's tests, the gravity effect was sufficient to eliminate the cells completely for lean hydrocarbon flames.

Einbinder also points out that experiments should be made over a much greater range of variables, particularly flow velocity, in order to provide convincing experimental confirmation of his theory, or any alternate theory, and also to provide basis information on the mechanism of flame propagation.

It may be that for a large enough system, or a flow already unstable, insufficient stabilization will take place at any composition. Thus, this sort of flame generated disturbance may always be present in high duty combustion systems.

Markstein^(15-26, 27) has extended his theory to explain the alternate appearance and disappearance of the cells when an organ-pipe type oscillation is set up in the combustion system. The new cells grow from the boundary interstices of the old cells, and the frequency of repetition of the cell pattern is half that of the oscillation. The occurrence of such phenomena, if not recognized, can considerably complicate turbulent flame speed experiments.

Einbinder has extended Markstein's theoretical treatment of cellular flames by including the effect of viscosity, using the Navier-Stokes Equation (11-7), and by setting up the boundary conditions between the burned and unburned gases for a finite flame thickness, then allowing the thickness to approach zero. Viscosity is found to decrease the computed cell size by approximately 30 per cent. Markstein⁽¹⁵⁻²⁰⁾ points out that this result not only is contrary to expectations, but is contrary to some unpublished results obtained with a less involved analysis. He indicates that the difficulty may be connected with the assumed boundary conditions.

Tsien⁽¹⁵⁻²⁸⁾ and Ball⁽¹⁵⁻²⁹⁾ show that the curves flame front generates vorticity. Some indication of this process is given by the pictures of actual vortex generation taken by Williams,

et al(15-30)*. Near the flame holder the vortices curl downstream and inward towards the locally retarded region behind the flame holder, while at greater distances from the flame holder, where the burned gases are moving at higher velocity, the direction of rotation of the generated vortices reverses.

Tsien's equation gives the generated vorticity as approximately equal to $(V/R) [(f-1)/f]$, where V is the stream velocity and R is the radius of curvature of the streamline at the front. In the distorted front present in a turbulent stream, R can be small and also vary in sign. This could lead to the production of eddies of the scale of the original distortion, and thus to a maintenance of the turbulence in the stream in the vicinity of the front.

Karlovitz approached the problem of flame instability from a different point of view, along the lines first mentioned by Semenov(15-31). When the flame front is distorted, the burned gases are accelerated away from the front in various directions, depending on the instantaneous surface positions. Over some distance and time, these directions are random, and may be interpreted as turbulence. The fluctuations of intensity and of direction of the jets of burned gas lead to continuous distortion of the front, and may thus be self-perpetuating.

Figure 15-9 shows the front, with the unburned gas considered as stationary. The forward component of the velocity is $(f-1) F \cos \phi$, and the average value of this component, \bar{u} , is given by

$$\begin{aligned} \bar{u} &= \overline{(f-1) F \cos \phi} = (f-1) \overline{F \cos \phi} \\ &= (f-1) F \frac{\int_0^A \cos \phi \, dA}{A} = (f-1) F S/A \quad , \end{aligned} \quad (15-68)$$

where A is the actual area and S is the projected area. Since

$$SF_t = AF \quad , \quad (15-69)$$

then

$$\bar{u} = (f-1) F^2/F_t \quad . \quad (15-70)$$

It should be noted that the value of \bar{u} that Karlovitz obtains is the average along the line of the front and not downstream from the front.

Karlovitz, still considering the unburned gases stationary, divides the kinetic energy of the burned gases into two portions, that going to supply the average velocity of the gas, \bar{u} , and the remainder to be considered as generating random turbulence. Thus, assuming the generated turbulence to be isotropic, it follows that

$$3u'^2 + [(f-1) F^2/F_t]^2 = [(f-1)F]^2 \quad (15-71)$$

For large values of F_t/F ,

$$u' \cong (1/\sqrt{3})(f-1) F \quad (15-72)$$

is the intensity of the generated turbulence.

*The possibility cannot be ignored that these vortices are only vortices generated at the flame holder, expanding, and moving downstream.

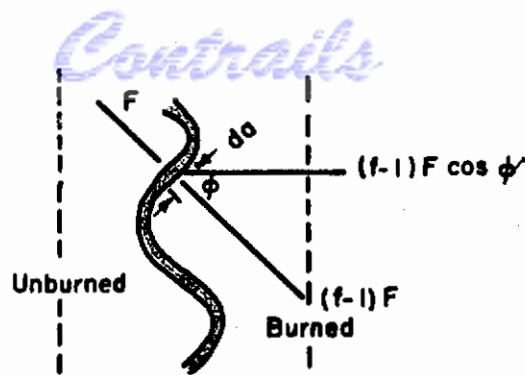


FIGURE 15-9. SCHEMATIC DIAGRAM OF TURBULENT FLAME FRONT

(Karlovitz, Denniston, and Wells)(15-5)

It might be preferable to base the derivation on a fixed position of the distorted laminar flame front, rather than on a stationary condition for the unburned gas. Although the front is constantly moving, owing to the turbulence, its average position, in the system where the flame is held, is fixed, and it appears that the front may be considered as distorted, but in an average stationary position.

Scurlock and Grover(15-7) carry out this type of derivation, in which the average position of the flame front, rather than the unburned mass of gas, is considered stationary. Other of their assumptions also differ from those of Karlovitz. They obtain the result

$$u \approx [(K_m/3)f(f-1)(U^2 - F^2)]^{1/2}, \quad (15-73)$$

where K_m is a function of f , and U is the velocity of the unburned stream; for an unconfined flame, U is identified as F_t , while for a confined flame, U is the stream velocity and is greater than F_t . It is readily seen that this result differs considerably from that of Karlovitz, essentially in the approximate replacement of F of Equation (15-72) by $U\sqrt{K_m}$.

Figure 15-10 gives K_m as a function of the expansion ratio, f , as computed by Scurlock(15-32) for another use. It should be noted that the computation strictly applies to $F_t/F = \infty$. Scurlock and Grover indicate that these values of K_m are the maximum possible for a given value of f , and the fact that $F_t/F \neq \infty$ has been compensated for by including F^2 in Equation (15-73). However, F_t/F is rarely over 5, and this correction factor may not be assumed to be even approximately correct without further justification. Furthermore, there is no evidence given that the K_m of Figure 15-10 is a maximum. That this entire treatment deserves expansion, clarification, and close comparison with that of Karlovitz is well illustrated by the comment in Reference 15-8. From either Karlovitz's equation or that of Scurlock and Grover, it appears that the flame-generated turbulence may far exceed the turbulence initially present. Thus, the only function of the initial turbulence might be either to start the process or to indicate that conditions are such that flame-generated turbulence can start and grow. However, neither of these models seems quite realistic. It would appear that by the time the jets from the distorted flame have degenerated into turbulence, the turbulence would be in the order of a mixing length from the front. With the turbulence at this distance behind the flame front, it is difficult to see how the flame front could any longer be affected.

On the other hand, if the jets are to be considered as generating vortices (which should tie in with Tsien's work mentioned above), then the term u' , used as characterizing homogeneous turbulence, is not the proper term to characterize vorticity.

After considering the difficulties produced by attacking the problem of flame-generated turbulence on the basis of an energy balance, it is well to consider the extension which Markstein(15-33) is making to his theory, treated in the first part of this section. Markstein uses only mass and momentum balances in his study of unstable flames. In Reference 15-33 he considers this system subjected to a sinusoidal shear wave. For the steady state solution, the equations fail for wavelengths above the critical size (see Equation 15-63). For wavelengths

above about half the critical size, the shear wave is amplified. Below this size, it is not amplified. Although the potential flow disturbances may be large in the front, they die off rapidly. The transient solution, more applicable to the actual case in which flames are held from boundary, has not been obtained.

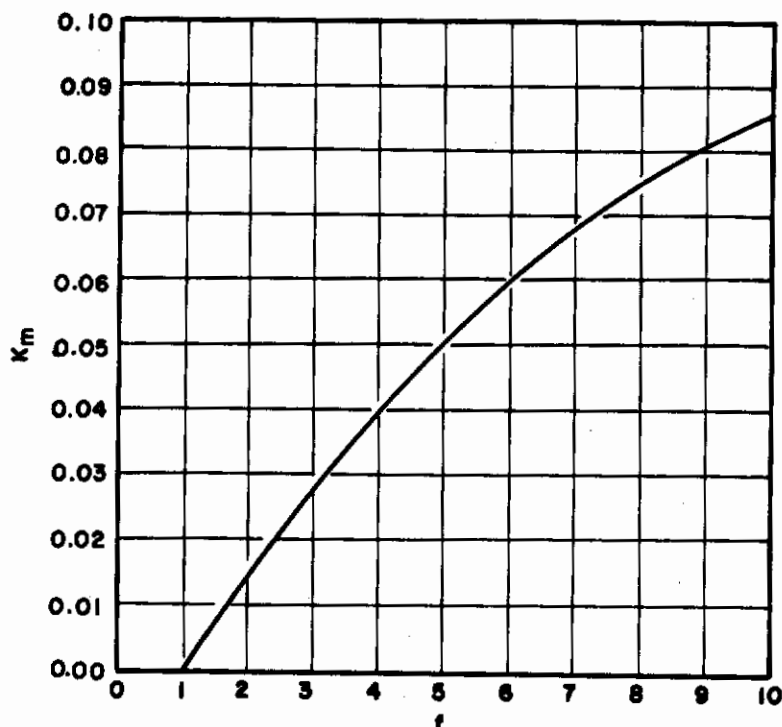


FIGURE 15-10. PLOT OF K_m AS A FUNCTION OF f
(Scurlock and Grover)⁽¹⁵⁻⁷⁾

EXPERIMENTS ON TURBULENT FLAMES

Experimental studies of turbulent flames have, in general, shown little relation to the theoretical predictions. Only recently have attempts been made to explain the differences, both by observing flames instantaneously rather than on a time average, and by formulating theories to conform to the observations. Thus, far more experimental work is required for a complete understanding of the processes involved in turbulent flames.

Coward and Hartwell⁽¹⁵⁻³⁴⁾, in 1932, presented a set of data for the speed of uniform movement of various methane-air flames ignited at the open end of long tubes of various diameters. For diameters up to 10 cm, the flame fronts had the normally observed parabolic shape, and the speed of uniform movement was found equal to the product of the normal burning velocity and the ratio of flame-front area to the cross-sectional area of the tube. However, for tube diameters of 20 cm and over (with one possible exception at 20 cm) the front was formed for multitudinous cups of the type observed by Markstein in his studies of flame stability. The cup diameters appear to agree with those indicated by an extrapolation of Markstein's data on other fuels.

The two types of results described may also be separated at a Reynolds number, based on the speed of uniform movement of the flame, of $Re = 7500$. This indicates that a turbulence phenomenon is present. The speed of uniform movement in the turbulent region appears to vary with the square root of the product of the diameter and the laminar burning velocity.

Unger(15-35) enlarged upon Coward and Hartwell's method by measuring the difference between flash-back velocity and stream velocity, with continuous flow, in tubes of 2, 3, and 4 cm diameter. The tests were conducted with city gas-air mixtures for Re from 1000 to 13,000. For those tests of $Re > 2400$, at which a definite break occurred in the data, Unger found that the results could be expressed in the form

$$F_t \sim d^{0.4} Re^{0.6} \quad (15-74)$$

Small second-order terms have been dropped from Unger's original expression. Unger also gives a similar equation for the results with $Re < 2400$, but this is not pertinent to the discussion. Unger notes two other differences between the laminar and turbulent regions. The photograph of the laminar flame showed smooth, though curved, flame surfaces, while the flames from the photographs in the turbulent region appeared rough and distorted. The response of an ionization probe as the laminar flame passed was smooth, as compared with an irregular response when a turbulent flame passed.

Damköhler(15-2) studied flames held on the ends of long pipes, with fully developed pipe turbulence present. Turbulent burning velocities of propane-oxygen mixtures were obtained by the area method for both the inner and outer flame surfaces. It was noted that the burning velocity computed from the outer surface agreed quite well with the laminar burning velocity in most instances; therefore, the ratio of outer to inner surface area was assumed to be the same as the ratio of turbulent to laminar burning velocity. As will be discussed later, there is no apparent reason for this observation to be generally true.

Damköhler shows his rather limited data in two separate plots; one with F_t/F plotted against Re gives a straight line at high Re ; one with F_t/F plotted against \sqrt{Re} gives a straight line at low Re . From these plots, several deductions have been made in the past. However, all the data on the 0.1385-cm and the 0.218-cm-diameter tubes were for $900 < Re < 5000$, while the data on the 0.272-cm-diameter tube were for $13,000 < Re < 18,000$; thus, the two sets do not overlap. Furthermore, the plots show that the curves representing the two lower sets of data are displaced, relative to each other.

Figure 15-11 shows the ratio of burning velocities plotted against the product of the diameter squared and the stream velocity, which product, incidentally, is proportional to the volume flow rate. The data still do not overlap on this plot, but the fit to a straight line is excellent, with no consistent deviations. The corresponding equation is of the form

$$F_t/F \sim v^{1/3} d^{2/3} \quad (15-75)$$

Since this equation is not dimensionally correct, it is apparent that all the pertinent factors have not been included.

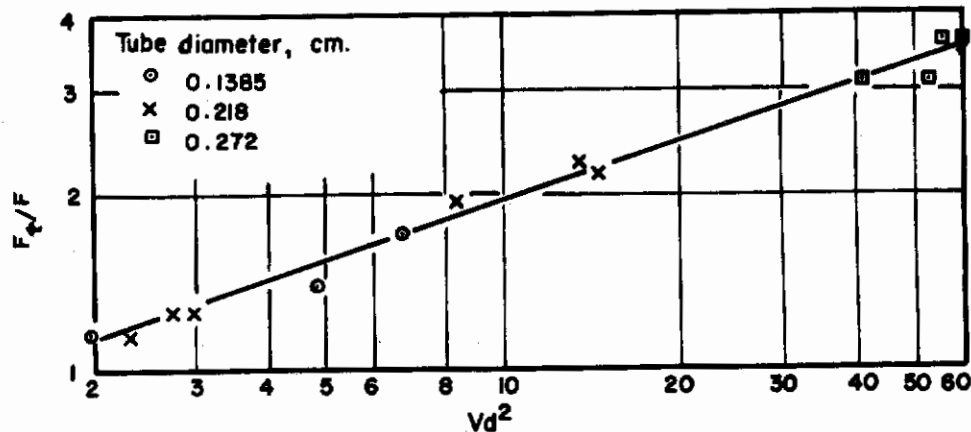


FIGURE 15-11. DAMKÖHLER'S TURBULENT BURNING VELOCITY DATA

Again, no exactly corresponding theoretical equation is found, although there is some similarity to Damköhler's small-scale equation and Delbourg's⁽¹⁵⁻¹³⁾ equation in that Equation (15-75) predicts variation of turbulent flame speeds with diameter. In fact, Delbourg, in his treatment, notes that Damköhler's data may be fitted by his derived Equation (15-75) with only a change in the multiplying factor. He, also, qualitatively explains the difference in the values of the multiplying factors. However, as noted before, the data plotted in this manner show a definite deviation with diameter, indicating a more powerful influence than postulated by Delbourg.

Manson⁽¹⁵⁻³⁶⁾ reported tests on a mixture of one-half acetylene and one-half oxygen discharged through orifices from 1 to 1.4 mm in diameter, at Re from 3000 to 12000. The turbulent flame speeds, measured by the area method, fit the curve,

$$F_t \sim v^{1/4} d^{1/4} \sim Re^{1/4} \quad , \quad (15-76)$$

with small scatter. There was no apparent additional effect of diameter, but the range of diameter used was small. Manson also stated that photographs of the flame front showed a uniform flame thickness up to Re of 7000, but a badly defined surface at Re > 9000. Not only does the equation agree in form with Delbourg's theory, with the exponent of 1/4 not being too far from Delbourg's exponent of 0.4, considering that Delbourg developed his theory for pipe turbulence, but the comments on flame thickness are those one might expect from Delbourg's theory.

Williams and Bollinger⁽¹⁵⁻²⁷⁾ carried out tests similar to those of Damköhler, but varied the Re over the much wider range of 2000 to 35,000. Four tube diameters, from 1/4 in. to 1-1/8 in., and three fuels, acetylene, ethylene, and propane, were used, all with air. Because of the difficulty of defining either the minimum or maximum surface areas, the flame speed was computed from the area of the mean surface through the flame. The equation obtained, giving the best fit to all the data, is

$$F_t/F = 0.176 d^{0.256} Re^{0.238} \sim v^{1/4} d^{1/2} \quad . \quad (15-77)$$

This equation is very similar to the equation found to fit Damköhler's data, with 1/4 powers replacing the 1/3 powers. And again, it is seen that there is an influence of diameter greater than that given by Re alone.

Scurlock and Grover attempted to use their theory, including the effect of eddy diffusion, flame propagation, and flame generated turbulence, to explain the result obtained by Williams and Bollinger. Although they computed values of F_t/F of the correct order of magnitude, they could not explain the strong effect of burner diameter.

Wright⁽¹⁵⁻²⁷⁾ used the Mache-type burners, with dimensions 1 x 12 cm, 2 x 12 cm, 3 x 12 cm, and 2 x 2 cm, rather than a Bunsen type. This allowed for variation of the scale and intensity of turbulence by the installation of various grids ahead of the converging section, whereas other investigators had confined their work to fully developed pipe turbulence. Furthermore, since the suppression of the component of turbulence parallel to the stream was almost inversely proportional to the contraction ratio, while the component normal to the stream direction, v' , was little affected by the contraction, the relative influence of the two turbulence components could be determined.

Wright presents three conclusions as the result of tests on propane-air mixtures, over a range of velocities of 150 to 500 cm/sec. First, the ratio of turbulent to laminar burning velocity is a function only of the ratio of v' to the laminar burning velocity. It may also be noted that the v' component of turbulence is closely normal to the flame front.

Second, the effect of low-level turbulence is relatively more important than that of high level turbulence. Third, within the accuracy of the data, there is no distinction in the effect between different kinds of grids or different sizes of burners.

Wright shows two sets of data. One, for one grid and nozzle, and two velocities, is closely fitted by the function

Continued

$$F_t/F - 1 \sim (v'/F)^{0.8} \quad (15-78)$$

for v'/F varying from 0.4 to 5. The second set includes all the data, without distinction. Wright suggests, for these data in which the scatter is large, an average curve of F_t/F against v'/F , for $v'/F > \sim 0.3$, which may be expressed as

$$F_t/F - 1.2 = 1.04 v'/F \quad (15-79)$$

This latter curve, at higher values of v'/F where 1.2 may be considered to be essentially the same as 1, agrees in form with Shelkin's large-scale equation based on cylindrical-flame distortion. However, a somewhat better fit to the data may be obtained by Karlovitz's Equation (15-27), if u' of Equation (15-27)* is increased by a factor of 1.8. From the excellence of the set of data for the one nozzle and grid, and the wide scatter for all the data when grouped together, it appears that some factor or factors not eliminated from consideration by Wright's conclusions must be present; the equations given above, therefore, probably do not include all the pertinent variables.

Bowditch's⁽¹⁵⁻³⁹⁾ approach is the same as Wright's. However, he used only a 2 x 6-in. accelerating nozzle and a stoichiometric mixture of propane and air. Turbulence generating grids of from two to six mesh were placed in the throat, rather than upstream of the throat, and various lengths of downstream extensions were employed to change the intensity of turbulence at the front. Pilot flame holders along the edges permitted the study of velocities from 30 to 70 fps.

Like Wright, Bowditch found no effect of scale. However, Bowditch's turbulent flame speed data, when converted to the form of F_t/F as a function of u'/F , gives values of F_t/F about three times those given by Wright for corresponding values of u'/F . This may possibly indicate that the higher Re of Bowditch's data permits less relative damping of flame-induced oscillations, and thus a greater effect of these oscillations.

Bowditch made measurements on contorted fronts pictured by high-speed shadowgraphs and found, for the low-intensity turbulence of a six-mesh grid, a ratio of distorted to mean area of 1.6, whereas, for the high intensity from a two-mesh grid, the ratio was 1.5 for the same total flow rate. Since the turbulent flame speed had increased by 25 per cent, this indicated a decrease in distorted-surface area of 25 per cent; this is contrary to what would be predicted for an increased turbulent burning velocity, by the distorted flame-front theory. Bowditch ascribes this to the increase of flame speed on curved surfaces of the type encountered at the tip of the Bunsen flame. This seems to touch upon ideas advanced by Delbourg in obtaining Equation (15-45), and also upon ideas of Wohl in deriving Equation (15-39). However, it is questionable whether shadowgraphs including a six-in. section have sufficient sharpness to permit such a computation as Bowditch makes, and it is not considered that the distorted-surface theory is disproved by these observations.

Hottel, et al.⁽¹⁵⁻⁴⁰⁾ generated various sizes and degrees of turbulence in a one-in. jet of natural gas and air, by destroying the pipe turbulence with fine-mesh screen and generating the desired turbulence by grids at various distances upstream of the exit and downstream of the fine mesh. The scale of turbulence, in general, was smaller than that used by Wright in his tests, but did not become so small as to be less than the thickness of the laminar flame. Since the flow was aspirated by a steam ejector, the noise level was high and the measurements of turbulence intensity had to be corrected for the component of the unidirectional sound waves in the average plane of the flame front.

Hottel, et al., measured the minimum and maximum areas of long-exposure flame photographs, and the depth of penetration and diameter of the distortions in instantaneous photographs, which look much like Karlovitz' photographs. From the instantaneous pictures, they found that the average diameter of perturbations equaled roughly five times the turbulence probe separation at a correlation coefficient, R_y , of 1/2. The correlation with the usual scale, l_2 , which includes the effect of the negative correlation region, was not as good.

* u' and v' are not distinguished in Equation (15-27).

For one turbulence generator, with 0.1-in. -diameter drilled holes, at two burning velocities, the depth of the perturbations was found to be proportional to the ratio, u'/F . Hottel, et al., from a comparison of these tests and others with 8-mesh screen and 0.05-in. -diameter drilled holes, inferred that the scale of turbulence did not affect the depth of penetration. However, a close inspection of the data shows that curves through the later mentioned data are not of the same shape or slope as those for the data for 0.1-in. drilled holes, and, thus, the conclusion that scale does not affect the penetration distance is not justified.

Hottel, et al., found that the turbulent burning velocity measured from the time exposures could not be correlated in the form of F_t/F as a function of u'/F , as found by Wright. Therefore, they substitute into Shelkin's Equation (15-9) their results, that h varies only with u'/F , and that the diameter of the perturbation is five times their turbulence scale. The final equation, after some manipulation, is

$$\sqrt{(F_t/F)^2 - 1} = \alpha u' / l_3 F \quad , \quad (15-80)$$

where l_3 is the probe separation at $Re = 1/2$. From the turbulent burning-velocity test, the value of the left-hand side was computed. Hottel, et al., shows this term plotted against $u' / l_3 F$; no value of α in Equation (15-80) gives a satisfactory fit; a right-hand side of the form $\alpha (u' / l_3 F) + 0.55$ gives a somewhat better fit, but the scatter is still large. Furthermore, these data seem to follow separate curves for each scale, and the curves tend to fall off at higher values of $u' / l_3 F$. The one conclusion that may possibly be drawn from the tests is that they, like the data of Wright, seem to indicate a larger than expected effect of the turbulence in the oncoming stream at low-turbulence levels.

Hottel, et al., also indicate that the burning velocities computed from the outer flame boundary are near to, but slightly less than, the corresponding laminar burning velocities.

Karlovitz studied natural gas-air and acetylene-air flames at the end of pipes, with fully developed pipe turbulence present. Provision was made for a small piloting flame around the rim of the tube, and for a protective air mantle moving with the speed of the tube gases. The flame front was defined as being along the line of greatest density of exposure on time exposure films. From the angle of this line with the oncoming stream, the turbulent burning velocity was computed as a function of radial distance. In general, the turbulent velocity rose rapidly from the laminar burning velocity near the wall, and finally leveled off near the axis. Whereas Hottel, et al., used instantaneous photographs to determine the parameters to substitute into the classical turbulent-burning velocity equations, Karlovitz used his instantaneous photographs as a guide in developing new equations. However, the measured burning velocity turns out to be far greater than those predicted by the derived expressions.

Karlovitz, therefore, reversed the usual procedure and calculated the turbulence intensity required by Equation (15-27) to produce the maximum observed burning velocity. The maximum value of the turbulent intensity, in the region of the axis, was found to agree qualitatively with that computed from Equation (15-72). In fact, the intensity derived from the data varied from 40 per cent to 140 per cent of the value given by Equation (15-72), as Re varied from 10,000 to 50,000.

In a subsequent paper⁽¹⁵⁻¹²⁾, Karlovitz, et al., reports the development of an ionization probe to measure the number of times the flame front of a turbulent flame sweeps a given point, and also the per cent time the probe is within the flame. The number of passes as a function of the flame penetration of the probe had a Gaussian distribution. From this distribution, Karlovitz⁽¹⁵⁻⁴¹⁾ computed $\sqrt{X^2}$ for his bunsen-type flame at $Re = 25,000$. With a 3.15 cm burner tube, $\sqrt{X^2}$ increased from 0.071 cm at 2.5 cm above the burner rim to 0.15 cm at 5.0 cm, and 0.25 cm at 9.0 cm. Defining $\sqrt{X^2}$ as $l_2 (F_t - F)/F$ (see Equation 15-26), the corresponding values of l_2 were 0.23, 0.13, and 0.10 cm. This indicated a decreasing scale with increasing height of flame. This does not seem to agree with the photographs. Furthermore, if Wohl's criticisms on the use of t as the time to sweep the distance, l_2 , with a laminar flame is valid, a turbulent burning velocity should be used to determine the sweep time. This would lead to a value of l_2 , little different from $\sqrt{X^2}$. This is a more reasonable result.

Scurlock and Grover, in comparing their theory with Karlovitz's test results on turbulent burner velocity, found that the predicted variation of F_t/F as a function of radius was invariably low when only eddy diffusivity and flame propagation were taken into account. When they also included the effect of their flame induced turbulence, the agreement was good up to about one-half the distance in from the wall. They showed no computed results for the critical core region, but the trend of the theoretical curves seemed to be to fall low by about 40 per cent.

These results would be most promising if it were not for the fact that Karlovitz, et al, and Scurlock and Grover, give explanations of the observed values of F_t based on two dissimilar equations for predicting the magnitude of the flame generated turbulence. In view of this fact, however, one realizes that any reasonable theory of flame turbulence will put one in the "right field"; with a sufficiency of arbitrary parameters, a good fit may be obtained.

Kleder, et al⁽¹⁵⁻⁴²⁾, using an apparatus patterned after that of Hottel, studied by the schlieren method propane-air flames from Re of 1,800 to 41,000 and pressures from 6 in. Hg to 26 in. Hg. They conclude that, in the region away from the tip of the flame, the flames' main action is to provide a temperature interface to show up the turbulence in the oncoming stream. Some indications of flame smoothing were seen, in the sense that small grain turbulence did not show up with the flame present.

Kleder, et al, imply that the correct way to consider the turbulent flame might be to consider first the stream turbulence (and large vortices, if they are present). This flame is assumed to be a front of small, but finite, thickness. This limits the minimum curvature which the flame can follow. Otherwise, the flame merely waves like a flag in the breeze. Complications are produced by possible jet action on elements concave toward the burned gases, and some tearing in high velocity gradient regions, but these factors might be treated by perturbation techniques. Preferential diffusion effects might also be treated as a perturbation on the "grain" of turbulence present.

Wohl, et al, studied butane flames burning from long tubes 1.01 and 2.55 cm inside diameter. A small annulus of pilot flames of a stoichiometric mixture of butane and oxygen was used to hold the main flame. Screens of 100 mesh, 10 mesh, and 4 mesh were placed at 5 cm from the tube end. The system was also used with no screens present which gave high turbulence. As found by previous investigators, the turbulent burning velocity, obtained from the mean area of maximum luminosity surface, varied roughly in the same manner as the laminar burning velocity. However, the composition of maximum flame velocity was shifted significantly to the rich side for the butane-air flame. Since Wohl also found a shift to the lean side for tests made with methane as a fuel, he concludes this is evidence of a strong effect of the Markstein instability phenomenon. Increased intensity of turbulence had the usual effect of increasing the turbulent burning velocity.

Wohl expressed his test result in a form similar to his theoretical Equation (15-18), that is, in the form

$$F_t/F - 1 = k [(u'/U) + \gamma] \quad (15-81)$$

However, although γ was only 0.01

$$k = 2.8 \alpha (U/540)^\beta ,$$

where α increased from 1 to 9.6 and β decreased from 1.6 to 0.5 in changing the per cent theoretical fuel from 80 to 130. The change in the value of α might be explained on the basis of the Markstein instability effect, but it is difficult to justify the value of β of about 1, if the original equation is the proper one to use in this instance.

Scurlock and Grover, using their theory, computed turbulent burning velocities to correspond to Wohl's data. The theoretical curves all peaked nearer stoichiometric than the experimental curves. Neglecting flame generated turbulence gave a theoretical result in fair agreement with measured average burning velocities at 540 cm/sec flow velocity for pipe turbulence, 10 mesh screen turbulence, and 100 mesh screen turbulence. Including their flame generated turbulence in the computation gave better predictions in the first instance, higher but about as good predictions in the second instance, and predicted turbulent burning velocities much too high in the third instance.

At an average velocity of 1495 cm/sec, including the flame generated turbulence improved the agreement for the pipe turbulence; with a four mesh screen the theoretical predictions, with or without the effect of flame generated turbulence included, were close together and much too low.

In a later report on his work, Wohl showed that F_t , for a butane-air flame, first increased extremely rapidly with average flow velocity, and then increased in a slow linear manner with flow velocity. F_t also increased from 100 mesh screen to no screen to 4 mesh screen as reported before. This result is in line with the reports of other experimenters that the effect of the initial stream turbulence seems to be much greater than expected.

Williams, et al., studied the turbulent flame in a 1 in. x 3 in. rectangular, closed system, with a flame holder across the 1 in. width. Using a 0.188 in. diameter rod 9 inches from the accelerating nozzle and turbulence generating grid for a flame holder, and Cambridge city gas as a fuel, they found no significant effect of approach stream turbulence (no screen, 3 mesh, 8 mesh) on the flame width. However, with a 0.038 in. flame holder two inches from the chamber entrance and turbulence generating grid, Scurlock found a definite increase in flame width (nearly a factor of two) as the turbulent intensity increased from 2.8 per cent to 6.5 per cent. These tests indicate that only when approach stream turbulence is below a certain level can it be neglected, as compared to other factors in a closed combustion system.

In the tests on the 0.188 in. rod, Williams, et al., measured the flame width four inches from the holder. Usually the width increased with velocity. However, at very lean mixtures the velocity effect reversed. As will be discussed later, this is probably related to a low burning velocity, which results in the influence of the holder and holding process predominating to a greater distance downstream.

Figure 15-12 shows a turbulent flame speed Williams, et al., calculated from their measured flame widths, using a relation derived on the basis of a line flame holder. Tests at 50 fps with rod sizes from 0.026 inches to 0.498 inches showed no effect of rod size on the width, except at very rich and very lean mixtures, as just mentioned. This indicates that either the rod was not producing the turbulence which affected the flame or that the effects produced by the rod were not critical as to size. The latter possibility may be related to the absence of scale effects in some of the theories of turbulent burning velocities.

The calculated flame-speed curves for turbulent burning velocity are of the general shape of the laminar burning velocity curves. However, their order appears strange; the 50 fps curve was more peaked than the others, and reached the same maximum as the 220 fps curve, at $F_t = 10$ fps. It is also shown by Williams, et al, that values of turbulent burning velocity calculated from Equation (15-9) (with $\beta = 1/2$) did not go above 4 fps, as compared with the maximum value computed from flame width data of 13 fps. This may be the result of using the outer flame boundary rather than the line of most intense luminosity to compute burning velocity.

Williams, et al., indicate another possibility, however. They point out that near the holder, in an enclosed stream, the cold gases move faster than the hot gases; this produces a vortex street with rotation inward at the downstream side. Away from the holder, the hot gases eventually reach the higher velocity; the generated vortices then rotate in the opposite direction. Since the turbulent burning velocities are larger with an enclosed flame than an open flame, in general, and this rotational factor is a main difference between the two types of systems, it is possible that the flame stretching caused by the vortex street is an important factor in determining the turbulent burning velocity in a closed system. This idea can explain the high value of burning velocities computed from the data. It also makes the very lean flame results shown in Figure 15-12 at least appear possible, since as the velocity increases, the relative influence of the two types of vortex generation would change at a given distance from the flame holder.

In studying turbulent flames in an enclosed system, Wohl, et al., used a 1.5 x 2.0 in. cross section duct. The plate holder was across the 2 inch width. The fuel was propane. For a 0.247 in. width holder, the turbulent burning velocity, given by the upstream visible surface of the flame, was found to be represented by

$$F_t/F - 1 = 26.2 (u' / U) + 1.40 (U/24)^{1.12} \quad , \quad (15-82)$$

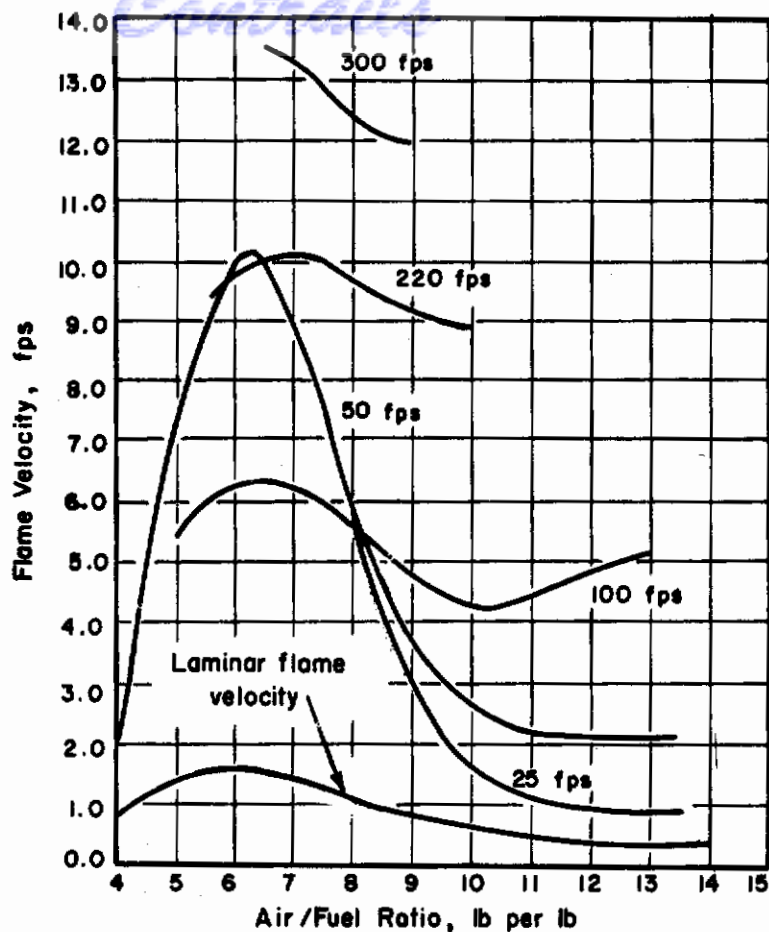


FIGURE 15-12. TURBULENT FLAME VELOCITIES CALCULATED FROM MEASURED FLAME WIDTH

(Williams, Hottel, and Scurlock)⁽¹⁵⁻³⁰⁾

using two different values of $100 u' / U$ of < 0.4 and 9.0 . The spreading of the flame by the high degree of turbulence is clearly evident in the photographs taken at a stream velocity of about 50 fps. With a small amount of turbulence, the upstream front is sharp and the downstream front nearly so; with nine per cent turbulence, the flame becomes fuzzy and spreads out in both directions.

Wohl's results agree in essential details with Scurlock's, as to what occurs in a turbulent confined stream. As seen from the equation, u' / U has little effect, compared to the term containing U alone, when it is small, but an increasing effect as u' / U increases.

In a later paper, Wohl points out that the line of the most intense luminosity and the line of 50 per cent consumption of oxygen did not coincide in the enclosed flame, although they did coincide in an open flame. Using the 50 per cent consumption line to define the mean flame front, Wohl found that the turbulent burning velocity first increased with an increase in flow velocity and then decreased. This he suggests is a result of disruption of the front (as per Karlovitz' holes).

Kumagai and Kimura⁽¹⁵⁻⁴³⁾ report the most encouraging data on turbulent burning velocities, as far as agreement with theory is concerned. They forced two different meshes through a town gas-air mixture at various velocities, and ignited the mixture after the passage of the mesh. Their data on turbulent-burning velocity fit the curves given by Shelkin's Equation (15-9) with little scatter. When u' was computed from the mesh velocity as the average velocity through the grid, β^2 was found to be approximately 1 for the smaller mesh, of 0.11 mm wire spaced on 0.46 mm centers, and about 2 for a grid about four times larger. Both values are reasonable for β^2 , according to Shelkin's theory. Kumagai and Kimura explained the lesser value of turbulent-burning

velocity obtained with the smaller grid at the same mesh velocity, on the basis of a more rapid decay of smaller scale turbulence. This appears quite reasonable, since an approximate calculation shows that the intensity will decay about 50 per cent in the smaller grid in the same time as it decays 30 per cent in the larger grid; using these decayed intensities, a constant value of β^2 of about 4 is obtained. This is again quite reasonable. Of course, this explanation requires that the time for decay is of the correct value, and thus there is no positive proof that there is not another effect of scale.

This interpretation of the work of Kumagai and Kimura points up the necessity of knowing the scale and intensity of turbulence in the region the flame is traversing at the time it passes. (This same fact is pointed out clearly by Fehling⁽¹⁵⁻⁸⁾.) However, this apparatus does eliminate the effects of boundaries and, with this done, the results start to compare closely with theory.

Leason⁽¹⁵⁻⁴⁴⁾ used an apparatus similar to that of Unger in order to eliminate the possibility of flame-generated turbulence. Various turbulence-generating screens were placed about half way in a vertical 5.4-cm-diameter by 125-cm-long tube. Combustible mixtures of propane or ethane, and air were flowed up through the tube at low Re; thus, the turbulence generated by the screens could be expected to fade out rapidly, and in a manner calculable from the literature. The flame was flashed downward in the tube and the rate of the propagation was measured. Photographs showed flames in the region immediately behind the screen, that appeared like those of Coward and Hartwell for $Re > 7500$, and showed smooth front flames, also like those of Coward and Hartwell at $Re < 7500$, in the region far downstream from the grids.

Leason assumed that the turbulent and the smooth propagation rates were in the same ratio as the turbulent and laminar burning velocities; that is, that the relative shape of the parabolic front remained the same. For low values of u' , an area ratio based on the distortion of a flame front by a vortex was used, but at higher u' , Leason used Equation (15-9) with $\beta = 2$. However, he found that his data could not be fitted by these equations.

Leason next assumed a statistical distribution of turbulence scales, and assumed that flame speed was changed by the small-scale components in the manner indicated by Equation (15-2). With a suitable distribution function, and making this correction, Leason was able to fit his data. Further, some later data on another type of equipment were also matched. From this, Leason concluded that small scale turbulence did have an effect and could be accounted for.

Some comments should be made on this work. There is an indication that only part of the data are shown; however, for this part of the data, an equally satisfactory fit may be obtained by using Equation (15-9), with a value of $\beta = 4$, or Equation (15-12), with a value of $\beta = 5/8$. Either value is reasonable. Other equations, such as that developed by Karlovitz, may be equally satisfactory. On the other hand, Wohl's simple correction term for small-scale turbulence, given by Equation (15-6), which is a correction similar to that made by Leason and gives another variable, allows a better fit of the data. Finally, it appears from the photographs that there is large-scale distortion, which may be a normal characteristic of flame instability.

Buttner, et al⁽¹⁵⁻⁴⁵⁾, conducted experiments on a propane-air mixture, using a converging-jet nozzle of 0.422-in. diameter. To generate turbulence, an axially mounted rod, 0.086-in. diameter, extending downstream to the burner throat, was rotated at speeds up to about 8000 rpm.

As the speed of rotation was increased, the flame front was observed to become more diffuse and somewhat changed in shape. The increase in flame speed was somewhat greater than the square of the rpm.

From a consideration of all the turbulent-burning velocity tests as a whole, several remarks can be made. First, in every instance, the scale of the turbulence at the flame front was at least twice, and usually much more than twice, the laminar flame thickness of the mixture considered. Thus, there are no results corresponding to small-scale turbulence theory, and it is only barely possible that transition region turbulence was encountered. However, if Delbourg is correct in assuming that comparison should be made between scale and turbulent flame thickness, his theory might be applicable to some test results. On the other hand, all the instantaneous photographs of turbulent flames that have been taken show a distorted flame front of the type idealized in

Figure 15-2 and shown in the photograph of Figure 15-1. Thus the evidence to date is that the increase of flame speed by turbulence is brought about by a distortion of the normal flame surface, with, possibly, a contribution to the normal burning velocity through the small-scale components of the turbulence, although the possibility that other types of turbulent flames exist is given some support and cannot be excluded.

The data on turbulent-burning velocity, with fully developed pipe turbulence, indicate a dependence of the turbulent-burning velocity on pipe diameter which is at least as great as that due to velocity, and in the tests over the widest range of diameters, a variation of flame speed with pipe diameter that is twice that due to velocity. Stating this another way, this burning velocity appears to vary, not with velocity, but perhaps with Re , and more likely with volume-flow rate. The usual treatment of the distorted front gives no variation with scale, or indirectly, with diameter; Delbourg's theory gives a variation with only Re ; and no theory gives a variation with volume-flow rate; therefore, it appears that there is complete disagreement between theory and tests. This may be related entirely to the interpretation of stream turbulence, as far as the flame is concerned, and the absence of consideration of boundary effects.

In the tests with turbulence generators such that uniform turbulence of a measurable scale is generated across the stream, Wright, Leason, and Bowditch indicate no variation of flame speed with scale, and Hottel indicates some depressing effect as the scale increases. Considering the scatter of the data in all cases, it may be concluded that there may be some variation of flame speed with scale in these tests, but certainly not the large variation indicated by the pipe turbulence tests. Furthermore, the distorted-flame-front equations appear to be the most suitable for interpreting these data.

There is little in the tests that refers to the problem of flame thickness. Two investigators noted that the burning velocity, determined from the downstream surface of the flame, was very close to the laminar burning velocity; however, the position of this surface is greatly dependent on the time of exposure. There is an indication in the tests that the burning velocity measured at the mean surface varies with a higher power of scale or diameter than those measured at the upstream surface; this would indicate that flame thickness increases less rapidly than expected from a simple scaling of the thickness with diameter. This observation is somewhat akin to Hottel's result, that the depth of penetration, which should be related to flame thickness, did not increase with scale in his tests, as expected from the simple theory. It may be concluded that even less is known experimentally about turbulent flame thickness than about turbulent flame speed.

CONCLUDING REMARKS

The theory and test results which have been discussed separately may now be considered from a more general viewpoint. This will allow some deductions to be made as to the cause of the differences and discrepancies, and enable one to plan better for future studies. In the first place, Markstein showed self-induced instability of a flame, both theoretically and in tests. Tsien and Ball proved that conditions of the front would induce vorticity. Karlovitz and Scurlock derived an equation for the flame-generated value of u' . Karlovitz' tests indicated that turbulent flame speed could not be explained by the pre-flame stream turbulence, but agreed qualitatively with the velocity expected for the flame-induced u' . Wright indicated that, at low values of stream turbulence, there appeared to be another source of turbulence. Bowditch's tests at higher Re show this even more strongly. Furthermore, to include the effect of F on u' in the general Equation (15-40), which sums up most of the theories of large-scale turbulence, would increase the exponent of F and decrease that of the pre-flame u' , and bring the theory into better agreement with the observations. The evidence is, then, that flame-induced turbulence is a very important factor in the turbulent flame phenomenon, especially at the lower values of stream turbulence. Therefore, future work should include not only the study of high-intensity uniform turbulence in the oncoming stream, generated by grids and the like, but also the effect of flame-induced turbulence, from the range where the stream turbulence is small, up to the range where flame-induced turbulence becomes of less importance.

Hottel and others observed that the flame front grows in thickness as the distance from the wall increases. Karlovitz' pictures show that, at least for the type of turbulence in which the instantaneous front is highly distorted but apparently of the laminar type, the flame is fixed at one edge and the distortions grow from this edge, much like a flag waving in the breeze. After a certain distance, the distortions become so great and irregular that no more conclusions may be drawn as to growth. It appears that this region of regular distortion constitutes a type of boundary layer, which may be treated separately from the core of the gases. The existence of such a layer may also permit an explanation of the difference between results with pipe-generated and screen-generated turbulence, since the scale of the pipe-generated turbulence increases gradually from the wall to the axis of the tube, whereas the screen-generated turbulence is constant nearly to the wall.

There is an interesting possibility in the matching of Markstein's natural wave lengths of instability with the scale of stream turbulence produced by grids, or similar turbulence generators. That such a matching may occur is indicated by Wohl's tests on the flame from the end of a pipe, in which a trend of size of distortion with mixture ratio was observed. Such matching may lead to an amplifying of the turbulence above normally expected values, and an increase in turbulent burning velocity. At the same time, because the grid position could be controlled, the intensity of turbulence could also be minimized at the region of flame holding, so that the unstabilizing effects of turbulence on flame holding could be minimized.

When the flame is enclosed, the shear forces between the confined hot and cold gases generate vorticity. These vortices stretch the flame front by a large amount, and thus increase the turbulent-burning velocity. This phenomenon, which appears to be a principal factor in determining the turbulent-burning velocity of the confined flame, is nearly absent in the unconfined flame. Though this phenomenon might be considered flame generated turbulence, it is not the same as that considered in Markstein's treatment. It also does not appear that it should be treated by the mathematics used in describing and investigating homogeneous turbulence. It would appear that this flame stretching, resulting from shear forces between the hot and cold gases, is a separate and distinct problem, and should be dealt with as such.

In many of the treatments of turbulence, the Re number is used. However, the effect of only two terms in this dimensionless group has been studied, diameter and velocity. There has been little study of diffusivity and kinematic viscosity, which are affected greatly by pressure and temperature. In fact, this comment is not confined to the use of the Re number; it is applicable to the study of turbulent flames in general. With pressures and temperatures varying considerably in the usual type of air-supplied combustors, and increasing to very large values in rockets, these factors need considerable study.

In the theoretical work, almost all the emphasis has been placed on turbulent-burning velocity; in the experimental work, although emphasis has also been on burning velocity, there has been some indirect comments on observed flame thickness. These are the two most obvious properties of pre-mixed flame, but they may not be the most fundamental. Thus, some consideration should be given as to whether the study of the turbulent flame should not include other factors.

In the laminar, one-dimensional approach to flame theory, the mass velocity from cross section to cross section of the flow stream remains constant. Thus, if the cross-sectional area of the flame is known, the mass velocity of the flame is equal to the mass flow through the section divided by the sectional area, and it makes no difference how or where the area is measured. This reasoning has led to the wide use of burning velocity as an important parameter.

However, in any actual system, some region of the flame surface, and usually most of the flame front, will have some curvature. This leads to three sources of error. First, the cross-sectional area, parallel to the flame front, of the stream tube will vary with distance into the flame; thus, the proper area to use is indeterminate. Second, the burning velocity depends on the curvature of the flame front, and thus, the supposedly constant characteristic of the combustible mixture becomes a function of the configuration and gas dynamics of the apparatus. Third, the variable curvature leads to selective diffusion of the fuel and oxygen, and a variation of composition over the flame surface.

The thickness of the laminar flame cannot be measured accurately. Here, the points at which to start and to stop the measurement of the thickness must be defined. Next, the measurement itself must be made, and finally the thickness is also a function of the flame parameters that were found to influence burning velocity.

In the turbulent case, these difficulties are magnified. Instead of a relatively thin laminar front, the front becomes thick and diffuse. Thus, Damköhler was lead to measuring the upstream and downward surface area of the flame, while Williams and Bollinger measured a mean area. The connection of either of these measurements with the fundamental properties of the gas and system is vague. If, instead of the time picture, the instantaneous picture of those flames is considered, the front appears to be composed of highly distorted laminar flame surfaces. Computing the average value of the enveloping upstream and downstream areas, and the degree of combustion through the average front, becomes a statistical problem. Furthermore, the laminar-burning-velocity problem is revived when the distorted surface itself is considered.

On the other hand, if Delbourg's type of turbulent flame exists, or if the small-scale component must be separately treated, as by Leason, the instantaneous picture will not be helpful, but the same type of problems as in fundamental studies of burning velocity will be encountered.

Turbulent flame thickness, on the distorted laminar flame basis, also is a statistical problem. On the basis of Delbourg's theory, the treatment would follow that for the laminar front. Some statements have been made to the effect that the area computed from the downstream extent of the flame is about the same as that computed using laminar burning velocity. This should allow, with the measurement of turbulent flame speed, a computation of average flame thickness. However, as mentioned before, it seems very improbable that such a simple connection between the downstream extent of the turbulent flame and the laminar-burning velocity should be a fundamental phenomenon.

Thus, it may be concluded that both turbulent-burning velocity and turbulent flame thickness, as now measured, are not fundamental properties of the mixture and its turbulence, but are affected greatly by the configuration of the system. The method of computing the position and extent of the turbulent flame in a combustion system is not known. The interaction of flow turbulence, flame-generated turbulence, unstable wavelengths of the flame front, and wall effects must be studied. Several possible types of turbulent flames have been outlined; tests in the future should definitely indicate which type is occurring. Instantaneous (spark) as well as time exposures should be studied. Turbulence should be measured in the flame.

With the results of such tests, it should be possible to redefine or rederive the necessary equations to describe observed phenomenon.

Comair
REFERENCES

- 15-1. Shelkin, K. I., On Combustion in a Turbulent Flow; NACA TM No. 1110, Feb. 1947, (Translated from Journal of Technical Physics (USSR) Vol. 13, No. 9, 10).
- 15-2. Damköhler, G., The Effect of Turbulence on the Flame Velocity in Gas Mixtures; NACA TM No. 1112, April, 1947, (Translated from Zeitschrift für Electrochemie und Angewandte Physikalische Chemie, Vol. 46, No. 11, Nov. 1940).
- 15-3. Wohl, K., Shore, L., von Rosenberg, H., Weil, C. W., The Burning Velocity of Turbulent Flames, Fourth Symposium on Combustion, Williams and Wilkins, Baltimore, Md., 1953, p 620.
- 15-4. Friedman, R., and Johnston, W. C., The Wall Quenching of Laminar Propane Flames as a Function of Pressure, Temperature, and Air-Fuel Ratio; Journal of Applied Physics, Vol. 21, 1950, p 791.
- 15-5. Karlovitz, B., Denniston, D. W., Jr., and Wells, F. E., Investigation of Turbulent Flames; Journal of Chemical Physics, Vol. 19, No. 5, May 1951, p 541.
- 15-6. Markstein, G. H., Interaction of Flame Propagation and Flow Disturbances; Third Symposium on Combustion, Flame and Explosion Phenomena, Williams and Wilkins, Baltimore, Md., 1949, p 162.
- 15-7. Scurlock, A. C., and Grover, J. H., Propagation of Turbulent Flames, Fourth Symposium on Combustion, Williams and Wilkins, Baltimore, Md., 1953, p 645; also, Experimental Studies on Turbulent Flames, Selected Combustion Problems, Butterworth Scientific Publications, London, 1954, p 215.
- 15-8. Discussions on Turbulent Flames, Selected Combustion Problems, Butterworth Scientific Publications, London, 1954, p 263.
- 15-9. Wohlenbert, W. J., Influence of Reaction Interface Extension in Gaseous Fuel Combustion, Trans. ASME Vol. 70, 1948, p 143.
- 15-10. Wohl, K., Private Communication.
- 15-11. Karlovitz, B., Open Turbulent Flames, Fourth Symposium on Combustion, Williams and Wilkins, Baltimore, Md., 1953, p 60.
- 15-12. Karlovitz, B., Denniston, D. W., Jr., Knapschaefer, D. H., Wells, F. E., Studies of Turbulent Flames, *ibid.*, p 613.
- 15-13. Delbourg, P., Influence of Turbulence on the Mechanism of the Combustion Reactions in the Gas Phase; Revue De L'Institut Français Du Petroile et Annales Des Combustible Liquids, Vol. 4, No. 9, Sept. 1949, p 530.
- 15-14. Corner, J., The Effect of Turbulence on Heterogeneous Reaction Rates; Transactions Faraday Society, Vol. 13, 1947, p 635.
- 15-15. Landau, L., On the Theory of Slow Combustion; Acta Physicochemica URSS, Vol 19, No. 1, 1944.
- 15-16. Darrieus, G., Le Mecanique des Fluides, Dunod, Paris, 1941, p 15.
- 15-17. Markstein, G. H., Instability Phenomena in Combustion Waves, Fourth Symposium on Combustion, Williams and Wilkins, Baltimore, Md., 1953, p 44.

- 15-18. Markstein, G. H., Experimental and Theoretical Studies of Flame-Front Stability; Journal of Aeronautical Sciences, Vol. 18, No. 3, March 1951, p 199.
- 15-19. Lessen, M., On the Stability of Laminar Flame Fronts, Journal of Aeronautical Sciences, Vol. 19, No. 12, 1952, p 852.
- 15-20. Markstein, G. H., Private Communication.
- 15-21. Markstein, G. H., and Somers, L. M., A Slot Burner Method for Studying Combustion Wave Instability, Journal of Chemical Physics, Vol. 21, No. 5, 1953, p 941.
- 15-22. Friedman, R., A Possible Relation Between Cellular Flame Structure and Quenching; Journal of Aeronautical Sciences, Vol. 18, July 1951, p 499.
- 15-23. Manton, J., von Elbe, G., and Lewis, B., Nonisotropic Propagation of Combustion Waves in Explosive Gas Mixtures and the Development of Cellular Flames, Journal Chemical Physics, Vol. 20, Jan. 1952, p 153.
- 15-24. Markstein, G. H., Nonisotropic Propagation of Combustion Waves, Journal Chemical Physics, Vol. 20, No. 6, 1952, p 1051.
- 15-25. Einbinder, H., The Hydrodynamic Stability of Flame Fronts, *ibid.*, Vol. 21, No. 3, 1953, p 480.
- 15-26. Markstein, G. H., Interaction of Flow Pulsation and Flame Propagation, Journal Aeronautical Science, Vol. 18, No. 6, June 1951, p 428.
- 15-27. Markstein, G. H., and Somers, L. M., Cellular Flame Structure and Vibration Flame Movement in N-Butane-Methane Mixtures, Fourth Symposium on Combustion, Williams and Wilkins, Baltimore, Md., 1953, p 527.
- 15-28. Tsien, H. S., Influence of Flame Front on the Flow Field, Journal of Applied Mechanics, Vol. 18, No. 2, June 1951, p 189.
- 15-29. Ball, G. A., Combustion Aerodynamics - A Study of a Two-Dimensional Flame, Harvard University, Department of Engineering Sciences and Applied Physics, Cambridge, Mass., p 162.
- 15-30. Williams, G. C., Hottel, H. C., and Scurlock, A. C., Flame Stabilization and Propagation in High Velocity Gas Streams, Third Symposium on Combustion, Flames, and Explosion Phenomena, Williams and Wilkins, Baltimore, Md., 1949, p 21.
- 15-31. Semenov, N. M., Thermal Theory of Combustion and Explosion, Part 3. Theory of Normal Flame Propagation, NACA TM 1026, (Translated from Progress of Physical Sciences (USSR), Vol. 24, No. 4, 1940).
- 15-32. Scurlock, A. C., Flame Stabilization and Propagation in High Velocity Gas Streams, Meteor Report No. 19, Fuels Research Laboratory, MIT, July 1948.
- 15-33. Markstein, G. H., Interaction of a Plane Flame Front with a Plane Sinusoidal Shear Wave, Journal Aeronautical Science, Vol. 20, No. 8, 1953, p 581.
- 15-34. Coward, H., and Hartwell, F. J., Studies in the Mechanism of Flame Movement, Journal of Chemical Society, 1932, p 1996, 2676.
- 15-35. Unger, W., Determining the Rate of Ignition of Flowing Air-Gas Mixtures, Forschung auf dem Gebiete des Ingenieurwesens, Vol. 15, No. 1, Jan.-Feb. 1944.

- Continued*
- 15-36. Manson, N., Propagation des Detonations et des Deflagrations Dans Les Melanges Gazeus, L'Office National D'etudes et de Recherches Aeronautique et des L'Institut Francais des Petroles, Paris, 1947, p 144.
 - 15-37. Williams, D. T., and Bollinger, L. M., The Effect of Turbulence on Flame Speed of Bunsen Type Flames, Third Symposium on Combustion, Flame, and Explosion Phenomena, Williams and Wilkins, Baltimore, Md., 1949, p 176.
 - 15-38. Wright, F. H., Measurements of Flame Speed and Turbulence in a Small Burner, Progress Report 3-21, Jet Propulsion Laboratory, California Institute of Technology.
 - 15-39. Bowditch, F. W., Some Effects of Turbulence on Combustion, Fourth Symposium on Combustion, Williams and Wilkins, Baltimore, Md., 1953, p 674.
 - 15-40. Hottel, H. C., Williams, G. C., and Levine, R. S., The Influence of Isotropic Turbulence on Flame Propagation, *ibid.*, p 636.
 - 15-41. Karlovitz, B., A Turbulent Flame Theory Derived from Experiments, Selected Combustion Problems, Butterworth Scientific Publications, London, 1954, p 248.
 - 15-42. Kleder, C. L., Weller, A. E., and Putnam, A. A., Technical Report No. 15035-4, Battelle Memorial Institute, Columbus, Ohio, April 1955.
 - 15-43. Kumagai, S., and Kimura, I., The Effect of Turbulence of Flame Propagation in Gases, Fourth Symposium on Combustion, Williams and Wilkins, Baltimore, Md., 1953, p 667.
 - 15-44. Leason, D. B., Turbulence and Flame Propagation in Premixed Gases, *Fuel*, Vol. 30, No. 9, Oct. 1951, p 233.
 - 15-45. Buttner, H. J., Bowditch, F. W., Floyd, W. W., The Flame Propagation Velocity of Air Propane Mixtures in a Controlled Turbulence Bunsen Burner, *The Texas Journal of Science*, Vol. I, No. 3, Sept. 30, 1949.

Contracts

CHAPTER 16. THE STABILITY LIMITS OF THE PREMIXED FLAMES

ABSTRACT

Three conditions are considered in the discussion of the stability limits of premixed flames. The flammability limits of a static mixture are considered first because they would appear to be limiting cases. These limits are affected by composition, pressure, and chamber size in a manner that seems related to certain phenomena observed in studies of flame stability. The stability of flames in low velocity streams is next examined, both from an experimental and theoretical point of view. Related phenomena such as quenching are also discussed. Finally, flame stability in a high-velocity stream is covered; it appears to depend on a different mechanism than stability in a low-velocity stream. However, because of the limited amount of variables, the various theories of high-velocity flame stability, and of low-velocity flame stability, all lead to similar correlation terms.

Contracts

THE STABILITY LIMITS OF THE
PREMIXED FLAME

by

Arthur Levy and A. Putnam

In the preceding two chapters the principal topics have been the propagation of laminar and turbulent premixed flames. Little mention has been made of the limits that other properties of the combustible mixture, and the combustor itself, places on the possibility of maintaining a stable propagating flame front. The present chapter will cover these factors.

Regardless of how large a volume of quiescent mixture of fuel and oxidant is present, a propagating flame cannot be produced beyond certain limits of composition of this mixture. Even in a quiescent mixture, such limits are reduced as the size of the confining chamber becomes small. The effects of mixture composition and chamber size will be discussed first.

In low velocity burners, such as the Bunsen type, the flame may blow-off if the velocity is too high, flash back if the velocity is too low, or just go out if the velocity is reduced and the burner is below a minimum size. This minimum size for flash-back, the quenching distance, has been found to be relative to the size effect in the extinction of the quiescent mixture. The stability limits of the low velocity burners will be the second topic for consideration.

For burners with high flow velocities, the flames are held by obstacles in the stream. Blow-off of this type of flame will be covered in the later sections of this chapter.

FLAMMABILITY LIMITS OF STATIC MIXTURE

Absolute Limits

Numerous investigations have been made using static mixtures of various compositions of fuel and oxidant to determine the limiting compositions within which a flame will maintain itself and continue to propagate. An excellent review of this subject with special emphasis on the more recent progress was made by Sir Alfred Egerton in his Fourth Symposium survey paper⁽¹⁶⁻¹⁾.

Coward and Jones⁽¹⁶⁻²⁾ have reviewed the majority of the results of flammability limits up to 1952, and present a great deal of the limit data in tabular form. Their review includes a bibliography of 368 references.

Coward and Jones have also defined a "standard-limit procedure": In the procedure, the mixture is placed in a vertical glass tube at least 2 in. in diameter, 54-in. long, and closed at both ends. Just prior to ignition, the lower end is opened. The mixture is then ignited by a naked coal-gas flame about one inch long. A mixture is judged to be flammable when the mixture flame will traverse the entire length of the tube under repeated tests.

For the purposes of this discussion, it will be assumed that the procedure gives essentially the absolute limits for most combinations of fuel and oxidant.

Recent studies on the flammability limits of hydrocarbon-air mixtures have been made in this country by Zabetakis, Scott, and Jones⁽¹⁶⁻³⁾. In England, Burgoyne and co-workers⁽¹⁶⁻⁴⁾ have made similar studies.

Table 16-1 presents a portion of the data obtained by the latter group.

It is well known today that the walls may exert an influence on the branching and recombination processes occurring in propagation. However, White⁽¹⁶⁻⁵⁾ has shown in his early studies that for most conditions, at atmospheric pressure, a tube having a diameter of five cm will have no visible effect on the upward propagation, and that a tube one and a half meters long is sufficient to allow the products to cool behind the flame front and to allow the criteria of continued propagation to be determined.

Egerton and Powling⁽¹⁶⁻⁶⁾ have studied the ignition limit problem in the light of present-day knowledge of the role of free radicals in combustion processes. They have investigated the problem from two points of view: (1) the role of a promoter and (2) the influence of changes in physical properties of the mixtures. It was felt that since flame speed is low at the limits, there might be reactions occurring in the preflame period which would promote or inhibit combustion. There would be a considerable advantage in the use of a promoter if it would widen the limits of a fuel, increase flame speed, and thus permit complete combustion in a smaller volume. Some of the additives tried were diethyl peroxide, ethylnitrate, nitrogen peroxide, acetaldehyde, methyl iodide, ozone, and ethyl alcohol.

TABLE 16-1. FLAMMABILITY LIMITS OF VARIOUS FUELS

(Burgoyne and Williams-Leir)⁽¹⁶⁻⁴⁾

Combustible	Supporter	Limit, per cent	
		Lower	Upper
H ₂	Air	4.19	74.6
H ₂	O ₂	4.65	93.9
CH ₄	Air	5.26	14.3
C ₂ H ₆	Air + N ₂	3.1	12.5
C ₃ H ₈	O ₂	2.4	57
n-butane	Air	1.93	9.05
Isobutane	Air	1.80	8.44
n-pentane	Air	1.62	--
Isopentane	Air	1.61	--
n-hexane	Air	1.46	--
n-heptane	Air	1.26	--
n-octane	Air	1.12	--
C ₂ H ₄	O ₂	3.10	79.9
C ₃ H ₆	Air	2.40	10.3
C ₃ H ₆	O ₂	2.10	52.8

Table 16-2 gives the data for methane-air mixtures. These data are typical also of the effect of promoters on other hydrocarbon and hydrogen mixtures with air. Except in the case of methyl iodide, there appears to be a reduction in the lower limit, and no effect on the upper limit. The results obtained with the iodide are consistent with its chain-breaking characteristics. The fact that there is not a significant change in the limits seems to indicate that the promoter introduces active centers into the mixture at lower temperatures without changing the manner of propagation. It might be concluded that the promoters are able to extend the lower limit values slightly because these limits will be determined by the minimum number of chains available. Thus an inhibitor would be expected to affect both limits, but a promoter would be expected to affect only the lower limit, in agreement with the data in Table 16-2.

TABLE 16-2. FLAMMABILITY LIMITS FOR METHANE-AIR MIXTURES WITH ADDITIVES

(Egerton and Powling)⁽¹⁶⁻⁶⁾

Additive	Additive, per cent	Lower Limit, per cent	Upper Limit, per cent
None	0.0	5.26	14.3
(C ₂ H ₅) ₂ O ₂	0.5	4.16	13.9
(C ₂ H ₅)ONO ₂	0.5	4.47	14.1
NO	0.5	4.93	14.9
O ₃	0.47	5.07	14.5
C ₂ H ₅ OH	0.53	4.54	--
CH ₃ I	0.5	6.29	12.3

More recently, Coleman⁽¹⁶⁻⁷⁾ has shown that small additions of fluorinated and brominated hydrocarbons exerted more than a dilution effect near the limits. Larger additions, however, had only the normal dilution effect.

Egerton and Powling⁽¹⁶⁻⁸⁾, after the above study, replaced the nitrogen in the air with other inert diluents, such as carbon dioxide, argon, and helium. It has generally been agreed by other workers that the order of decreasing extinguishing power is CO₂ > N₂ > A. The position of the helium varies. Coward and Hartwell⁽¹⁶⁻⁹⁾ place helium before argon, Posthumus⁽¹⁶⁻¹⁰⁾ places helium before the CO₂, and Heiningen⁽¹⁶⁻¹¹⁾ places the helium after the CO₂. The data of Posthumus are probably of limited value here since his experiments were made in a 1.6-cm tube. Heiningen used a 2.2-cm tube and Coward and Hartwell used a 5-cm tube. Egerton and Powling also used a 5-cm tube and obtained the result, CO₂ > N₂ > A, in agreement with the results of Coward and Hartwell. The results indicate that the flame is propagated only if a certain minimum temperature can be reached in the flame boundary. The specific heats of the mixture and the heat of combustion are used to determine whether the flame propagates; the effect of heat conductivity remains uncertain. Only in the case of helium is heat conductivity high enough to show a strong influence; with CO₂, N₂, and A the thermal conductivity decreases slightly in the same order, but the change is fairly small. The evidence lends support to the view that the limits, although determined by a minimum temperature, represent a minimum rate of oxidation at the flame front and that the flame is propagated mainly by active centers.

The effects of inert gas are apparent in all phases of combustion work, and will be referred to later in this chapter with respect to flame stabilization and quenching. Mellish and Linnett⁽¹⁶⁻¹²⁾

have studied these effects in detail and have shown that in most instances the $\text{CO}_2 - \text{N}_2 - \text{A}$ order holds.

The flammability limits of pure hydrocarbon-air mixtures have been measured at reduced pressures for several hydrocarbons for the purpose of determining some systematic change as a function of the molecular structure⁽¹⁶⁻¹³⁾. A series of 18 pure hydrocarbons were investigated in a Coward-Jones type of apparatus. The results with the paraffins show that all the lean limits, when expressed as per cent of stoichiometric fuel, are about the same, while the rich limits occur in the following order; hexane > pentane > butane > propane > ethane > methane. The effect of branching appears to be minor except in the cases where 2,2-dimethyl butane is compared to n-hexane. In these instances, the rich limit on the unbranched paraffin is greater, but the lean limits are practically identical. The limit data for unsaturated hydrocarbons, such as propene-1, butene-1, and pentene-1, are confusing in that they do not seem to behave in any ordered manner. Butene and pentene show wider limits than their parent paraffins, but propane and hexene show narrower limits than their parent paraffins. To explain such anomalous results would require knowledge of the chemical kinetics of the specific reactions. It is observed that the odd-numbered chains behave differently from the even-numbered chains; further study might show some difference in the point of breakage of the CH bond in each case.

Due to the lack of knowledge on the processes involved, there has been no successful kinetic application to the calculation of the flammability limits for mixtures of gases in these static systems. Coward⁽¹⁶⁻¹⁵⁾ has extended LeChatelier's rule for calculating limits of mixtures. The rule states that knowing the limits l_1, l_2 , etc., for the individual gases in a mixture and the per cent P_1, P_2 , etc., of each gas present, the limits for the mixture (upper or lower) are expressed as

$$L = \frac{100}{\frac{P_1}{l_1} + \frac{P_2}{l_2} + \dots} \quad (16-1)$$

Burgoyne and Williams-Leir⁽¹⁶⁻¹⁶⁾ have applied this rule in their study on the effect of methyl bromide as an extinguisher. Their results may be summarized by saying that methyl bromide reduced limits in the following order of increasing susceptibility, $\text{H}_2 > \text{C}_2\text{H}_4 > \text{C}_6\text{H}_6 > \text{cyclo-hexane} > \text{n-hexane} > \text{CO} > \text{CH}_4$. Application of the LeChatelier rule to the methyl bromide-coal gas-air system gives reasonable agreement, within 10 per cent. It would be expected that this rule would hold fairly well for gases with similar properties, but not well for gases that exhibit effects such as cool flames. In the case of the analysis above, the coal gas contains mostly methane and hydrogen plus some nitrogen, carbon dioxide, and air. The CO and C_2H_4 present, which do not behave like hydrogen and methane, total about 15 per cent. Therefore, the 10 per cent error in the limit rule is reasonable.

Cassan⁽¹⁶⁻¹⁷⁾ has examined the LeChatelier principle to determine if the principle could be used to calculate the effect of inert gases. In effect the method merely divides the inert gases among the other gases.

Generally all applications of this principle hold as long as effects are additive. For this reason the behavior of mixtures of gases on the lean side is readily interpreted; on the rich side, however, the principle becomes somewhat clouded due to interactions which occur in the competition for the insufficient oxygen supply.

Table 16-3 shows how the flame-zone temperatures and the ignition temperatures vary, at the lower limit, for several hydrocarbon-air mixtures.

TABLE 16-3. IGNITION AND FLAME TEMPERATURES FOR SEVERAL
PARAFFIN HYDROCARBONS AT THE LOWER LIMIT

(Townend and Maccormac)(16-18)

Hydrocarbon	Lower Limit, per cent	Flame Temperature, C	Ignition, Temperature, C
Methane	5.26	1255	650
n-butane	1.93	1445	480
n-pentane	1.62	1485	470
n-hexane	1.46	1568	275
n-heptane	1.26	1569	255
n-octane	1.12	1575	245

It is apparent that the ignition temperature of the n-paraffins decreases with increasing chain length, and that the temperature in the flame zone increases slightly with chain length. Since the flames of the paraffins of higher molecular weight are progressively more difficult to propagate, it appears that the conditions for propagation do not depend so much on ignition temperature or stability characteristics as they do on the ability to provide reaction centers into the unburned mixture.

An interesting question raised by much of the recent work on the flat-flame burner is whether this flat-flame method will eventually supersede the "standard tube method". As Egerton shows in his review⁽¹⁶⁻¹⁾ the flat-flame method yields lower flame temperatures at the lower limit than the tube method. The almost constant flame temperatures by the new method, in contrast to the increasing temperatures for higher hydrocarbons by the tube method, may indicate that the flat-flame method yields results more consistent with the oxidation properties of hydrocarbons. More results by the flat-flame method are required to substantiate this hypothesis, however.

Limiting Effect of Chamber Size

It was noted previously that test chambers below a certain size have a deleterious effect on the flammability limits. As the pressure is reduced below atmospheric, this effect of size becomes increasingly apparent.

Figure 1 shows this effect of chamber size, as obtained by Simon, Belles, and Spakowski⁽¹⁶⁻¹⁹⁾. As expected, the larger the tube diameter, the lower the minimum pressure at which the flame can propagate. By use of a proportionality factor on the diameter, these investigators found that their data could be correlated with the data of other investigators on the variation of minimum quenching distance with pressure. Since flammability limits represent the limit of flame propagation processes, the authors attempt to correlate their results in terms of the Tanford-Pease diffusion mechanism. However, as in all these arguments, diffusion and heat conduction are practically inseparable, and although a good correlation was obtained, the argument cannot be resolved.

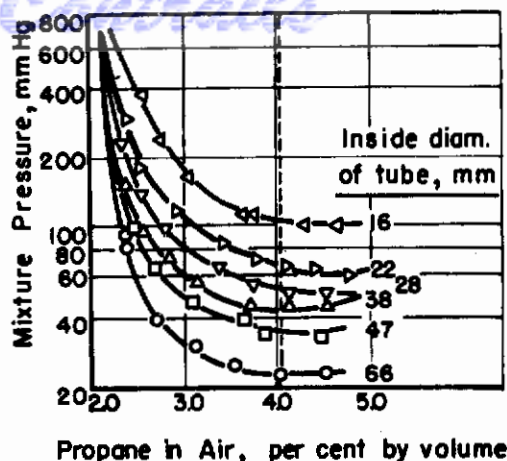


FIGURE 16-1. EFFECT OF TUBE DIAMETER ON PRESSURE FLAMMABILITY LIMIT (LOW CONCENTRATION PART OF TOTAL CURVES)

Simon, Belles, and Spakowski(16-19)

Zabetakis and co-workers at the Bureau of Mines have also investigated low-pressure flammability limits. A concise report of test results with methane, ethane, propane n-butane, and iso-butane at pressures of 400, 200, 100, and 70 mm Hg, indicates the regions of flammability of these hydrocarbon-air mixtures.(16-20) Zabetakis and Richmond have also considered the importance of, and difference between, ignitability and propagation at low pressures.(16-21) At extremely low pressures, 25 mm Hg and less, the energy of the ignition source can be important in determining whether the flame will propagate part way or all the way up the tube. DiPiazza, Gerstein, and Weast(16-13) observed a similar result in their studies.

Figure 16-2 shows another characteristic feature of the limits of ignition of hydrocarbon mixtures at reduced pressures. There is a normal lean lobe characterized by a blue flame which fills the tube, while the rich lobe shows a green-to-yellow flame which does not fill the tube. The nature of the two lobes has been investigated by Spence and and Townend(16-14). In earlier studies Townend postulated that two processes were occurring and associated one lobe (on the rich side) with the cool flame and the other lobe with the normal flame. Under suitable pressure conditions he was able to obtain a cool flame in the normal, hot-flame region. Townend's cool-flame postulation is further borne out by the fact that methane, which does not have any cool flame, has only one lobe; also, the flames in the rich lobe propagate up the tube very slowly whereas the lean flames propagate up the tube at a faster and more definite rate.

Delbourgo and Laffitte(16-22) have studied this double-lobe phenomenon in ethane, propane, butane, and pentane flames, using electrical ignition to start the flame. Except for ethane, they observe the characteristic two-lobe pressure effect. Although these earlier studies showed no double-lobe effect for ethane, a later study did show the start of an irregularity in ethane flames.(16-23) The latter results are consistent with Gerstein's earlier findings.(16-13)

An interesting feature of Delbourgo and Laffitte's study is the choking-off of the second, rich side lobe as the mixture is diluted with nitrogen. This is shown by Figure 16-3.

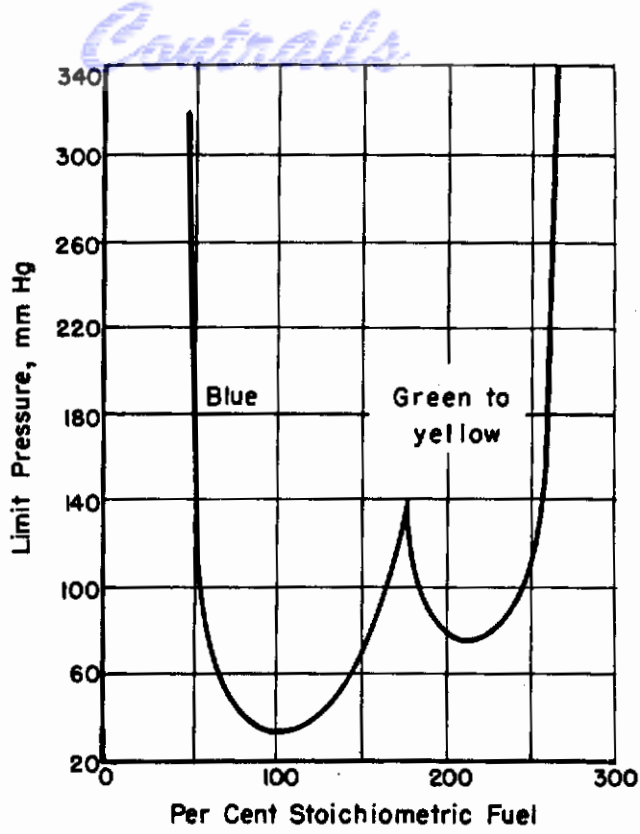


FIGURE 16-2. LIMIT CURVE FOR PROPANE-AIR AS A FUNCTION OF PRESSURE

DiPiazza, Gerstein, and Weast(16-13)

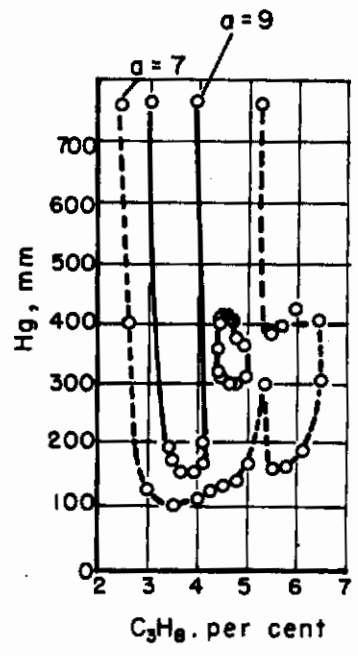


FIGURE 16-3. FLAMMABILITY REGION OF PROPANE ($O_2 + aN_2$) MIXTURES

Laffitte and Delbourgo(16-23)

The principal contributions to the work on low velocity flame stability in this country have been made by Lewis and von Elbe(16-24 thru 31) and their associates at the Bureau of Mines. In Europe, large contributions have come from the British workers, Garside, Forsyth, and Townend. (16-31,32). The following discussion will draw heavily on the contributions of these workers.

The flash-back of a mixture through a small space and the minimum size of space through which such flash-back may occur are closely related. The minimum energy required to ignite a mixture and the measured space within which a mixture can be ignited are also related. And finally, the minimum ignition space is related to the minimum quenching distance. When blow-off is considered, it is found that an additional factor of diffusion with the surroundings enters the problem; however, there is still a close relation with the mechanisms involved in the other limiting phenomena. For this reason it is difficult to separate the discussion of the theories of flame stability according to the limit involved. Therefore, the theories will be discussed in a group. This will be followed by a discussion of the test result pertaining to the various limits.

Theories of Flame Stability

Figure 16-4 shows the three positions of a flame front which must be considered in the analysis of flash-back (and blow-off). Curve 1 shows the conditions where the combustion wave gets close to the rim of the burner. When this occurs the gas velocity exceeds the burning velocity and tends to drive the front back to the equilibrium position, Curve 2. Curve 3 is the reverse case, and the opposite effect tends to occur here; that is, the burning velocity, which is now in excess both because quenching effects are less and because the flow velocities are somewhat less, drives the front back to the equilibrium position. At the equilibrium position, the burning velocity equals the gas velocity at one point along the front.

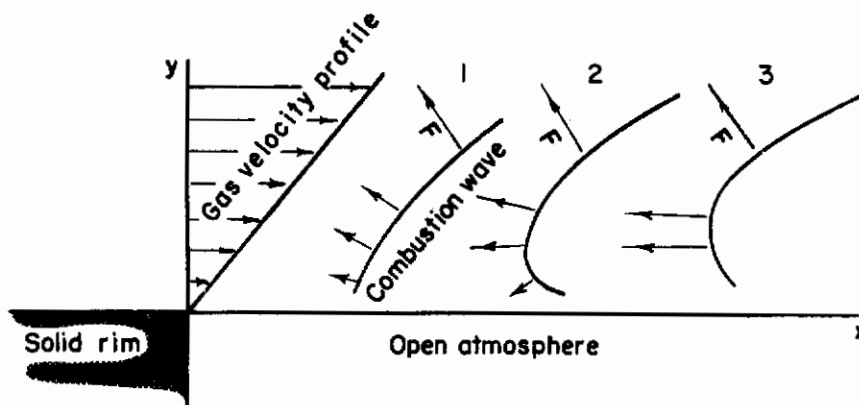


FIGURE 16-4. STABILIZATION OF A COMBUSTION WAVE
IN LAMINAR FLOW

Lewis and Von Elbe(16-29)

The laminar gas-velocity profile in a pipe is described by the Poiseuille equation

$$U = 2 V(R^2 - r^2)/\pi R^4 , \tag{16-2}$$

where \underline{V} is volume flow rate, \underline{R} the radius of the tube, and \underline{r} the variable distance from the axis of the tube. The slope of this curve near the wall is called the critical velocity gradient \underline{g} and given by

$$g = \lim_{r \rightarrow R} - \frac{dU}{dr} = 4V/\pi R^3 \quad (16-3)$$

Conditions leading to flash-back and blow-off are related to the boundary velocity gradient. If V is reduced, g is decreased so that the equilibrium position, Curve 2, moves nearer to the burner exit. A condition is eventually reached on reducing g where the burning velocity becomes greater than the gas velocity, U , and flash-back occurs. Blow-off occurs similarly but in the opposite direction of the above effects. As g increases, the flame moves farther from the rim until eventually dilution from surrounding air becomes too great and the flame is blown off the burner.

Figure 16-5 is the model used by Lewis and von Elbe to develop the relations between quenching and flash-back. A combustion wave is considered to be propagating in a quiescent gas between two parallel plates, whose separation is only slightly greater than the critical quenching distance. In line with the treatment of stationary flames, the wave is considered at rest and the unburned gas moves forward into this wave. The unburned gas enters at a rate equal to the flame speed under the above conditions. T_u is the temperature isotherm of the unburned gas. T_1 and T_o are the temperature isotherms at the beginning and end of the reaction zone. To obtain an equation of the heat flow across the dead space y_o , the heat flow in front of the reaction zone is considered. This is obtained through the standard heat-balance equation used in computing burning velocity (Cf Chapter 14),

$$\frac{d^2T}{dx^2} - F \left(\frac{\rho C_p}{\lambda} \right) \frac{dT}{dx} + \frac{q}{\lambda} = 0 \quad (16-4)$$

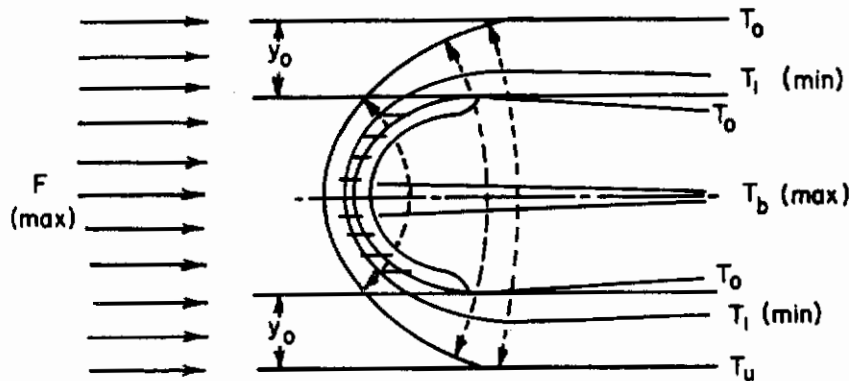


FIGURE 16-5. TEMPERATURE PROFILES BETWEEN COOLING SURFACES

Lewis and Von Elbe(16-29)

To make the problem tractable, however, the authors assume (a) from T_u to T_1 , $q = 0$, and (b), from T_1 to T_o , q is constant while the left hand term of Equation 16-4 is zero. To account for the loss of heat to the walls, a loss occurring at right angles to the flow direction, they derive the equation

$$- \frac{d^2T_b}{dy^2} = a^2 \frac{(T_1 - T_u)(T_b^o - T_b)}{(T_b^o - T_b + T_1 - T_u)} \quad (16-5)$$

where T_b , T_b^o denotes the flame temperature and the maximum flame temperature, respectively and

$$a = c_p \rho F / \lambda$$

By assuming that $T_1 - T_1^o = T_b^o - T_b$, T_b can be determined as a function of distance from the wall. Along a streamline, then, the net heat release can be determined from the value of T_b , and, by use of Eq. 16-4, the burning velocity near the wall, F' , can be obtained as a function of y . The

final equations relate a dimensionless burning velocity, a dimensionless distance, and a dimensionless temperature. For the axially symmetric system (a tube), this result for the two-dimensional system can be suitably modified.

Numerical calculations are found to be necessary in using these equations to determine either the minimum flame propagation distance between the walls (quenching distance) or the critical velocity gradient for flash-back. For example, to determine the flash-back gradient, the ratio of burning velocity at the dimensionless distance, \underline{D} , from the wall to the normal burning velocity is plotted against the distance. The slope of a straight line through (0, 0) which just contacts this curve is the critical gradient.

From this critical gradient and the burning velocity, a critical distance for flash-back can be computed.

Table 16-4 gives calculated and observed values for these distances. It is noted that the agreement is good on the lean side, but progressively poorer on the rich side.

TABLE 16-4. COMPARISON OF EXPERIMENTAL AND THEORETICAL VALUES OF FLASH-BACK AND QUENCHING DISTANCES FOR PROPANE-AIR MIXTURES

(Harris, Grumer, Lewis, and von Elbe)⁽¹⁶⁻³⁰⁾

Propane Concentration, Fraction of Stoichiometric	H, 10 ⁵ Cal.		F/gf, cm.		d, cm.		2R, cm.	
	Exp. *	Calc.	Exp.	Calc.	Exp.	Calc.	Exp.	Calc.
		Minimum Value						
0.70	53	88	0.20	0.22	0.55	0.40	0.85	0.94
0.75	37	78	0.17	0.26	0.41	0.46	0.66	1.1
0.90	14	52	0.10	0.18	0.24	0.33	0.31	0.78
1.00	9.2	38	0.081	0.14	0.21	0.27	0.28	0.64
1.10	6.8	35	0.071	0.14	0.20	0.26	0.28	0.62
1.28	5.9	99	0.058	0.19	0.21	0.37	0.37	0.88
1.40	6.2	370	0.058	0.36	0.24	0.65	0.49	1.5
1.50	7.0	1100	0.068	0.57	0.28	1.0	0.66	2.3

*M. V. Blanc, P. D. Guest, G. von Elbe, and B. Lewis, Third Symposium on Combustion, Flame, and Explosion Phenomena, Madison, Wisconsin, p. 363.

Before considering other flash-back studies, it is well to note that Lewis and von Elbe⁽¹⁶⁻²⁹⁾ have also presented a theory of blow-off, using a similar development to that above. Heat flow is assumed to occur only in the direction of stream flow. Considering a streamline of Figure 16-4 passing through a point where the flow velocity and burning velocity are equal,

$$c_p \rho F(T - T_u) = \lambda \left(\frac{\partial T}{\partial x} - E \right) \quad , \quad (16-6)$$

where the integration constant, E , is the temperature gradient at $x = 0$. This equation can be integrated between $x = 0$ and $x = x_1$, giving a relation for x_1 . The minimum value of x_1 , for which the equation is satisfied is the stable condition. Carrying out this minimizing process and making some substitutions yield

$$2 \ln \left[\frac{(2(1 + \tau) - A)}{(1 - A)} \right] = A(1 + 2\tau)/(1 - A) \left[2(1 + \tau) - A \right] \quad , \quad (16-7)$$

where A is the ratio of the burning velocity at the point of holding, F_1 , to the normal burning velocity, F , and

$$\tau = (T_1^0 - T_u) / (T_b^0 - T_1^0) .$$

If data are available for F and the T 's are functions of the mole fractions of fuel, it is only necessary to account for the diffusion of secondary air into the mixture as it approaches blow-off. If it is assumed that diffusion occurs only in the y direction, and that a molecule will travel a distance equal to $\sqrt{Dt_1}$ in the time t_1 , where t_1 is given by F_1/x_1 , then the change in the fuel concentration will be a function of $F_1/g\sqrt{Dt_1}$. The gradient, g , can now be computed by numerical processes as a function of the diluted concentration, and the maximum value of the gradient, which occurs at blow-off, can be obtained. The authors have applied their theory to some methane-air data. The computed curve is of the same shape as the experimental curve, but lower by a factor of about three. This is probably caused by the expansion and slowing down of the stream as it emerges from the tube. This has the effect of giving a larger and slower moving stream, which would not blow-off as soon as calculations based on the flow velocity in the tube and tube diameter would indicate.

Wohl⁽¹⁶⁻³⁴⁾ considers a fundamental distance, Δ , associated with the combustion process. He then discusses in some detail the manner in which Δ is related to each of the observables, dead space, quenching distance, penetration distance (calculated from flash-back data), and a distance calculated from blow-off data.

Putnam and Smith⁽¹⁶⁻³⁵⁾ considered the extinction region where the flame over a port smaller than the critical quenching diameter goes out as the flow velocity is reduced. In this case, the predominant loss of heat is not to the walls but to the volume of gas around the combustible mixture. Essentially, they obtain the result that, at extinction,

$$Qc_p \rho / \delta \lambda$$

is constant for a given mixture. Q is the volume flow rate of combustible and δ is a critical distance similar to quenching distance. The limited amount of data available appear to confirm this relation.

Experimental Results

Garside, Forsyth and Townend^(16-32, 33), in their studies on ethylene-air mixtures, show that the normal burning velocity for any concentration remains constant down to pressures as low as 20 cm of mercury. The dead space, however, which they define as the distance between the burner wall and the luminous boundary of the flame, was shown to vary with flame area, pressure, temperature, mixture composition, and burner size. The dead space is not quite constant with change in the rate of flow of mixture, so that dead space increases with increase in size of flame, more so at lower pressures. It is necessary therefore to refer all comparisons of dead space to a standard flame area. The dead space was also found to increase as the pressure decreased, and to decrease as the temperature was raised. At constant pressure the effect of an increase in diameter of burner is to cause some decrease in dead space.

Before it was even realized that dead space* was important in flash-back studies, it was realized from the similarity of the shapes of flame-speed curves and flash-back curves (as plotted against fuel-air compositions), that these two were closely related. As a consequence of the low-pressure ethylene studies, the role of dead space (or a similar measurement) became more

*It has been brought to the attention of the authors that Garside confused dead space with depth of penetration of quenching. Dead space, as defined by Garside is not directly involved at the flash-back limit and only becomes directly applicable at blow-off when the ambient atmosphere is entrained into the flame. (The author is grateful to J. Grumer, Bureau of Mines, for bringing forth this point).

apparent. If a plot is made of the reciprocal of dead space against concentration of ethylene at various values of pressure, a series of curves similar to the flash-back curves is obtained. The author's conclusions may be summarized by saying that the tendency toward flash-back is proportional to the ratio of burning velocity to dead space; that is, at constant burning velocity, the mixture with the smaller dead space will flash back more easily and at constant dead space, the faster burning gas will flash back first.

These workers have studied the problem of blow-off also, and although their study is not so complete as the flash-back study, they note that the blow-off tendency decreases as the burner diameter is increased. They note, without comment, that above a certain diameter (not given) blow-off appears independent of diameter. This may only be an illusion caused by the smaller improvement at larger diameters. It might also be related to a change in flow pattern as the Reynolds number increases.

The velocity gradient theory has also been the basis of a development which permits a correlation of blow-off and flash-back data in terms of dimensionless parameters⁽¹⁶⁻³⁶⁾; in this case the dimensionless parameter is the Peclet number, $DV\rho c_p/\lambda$, based on burning velocity and on jet velocity, where either velocity is represented by the quantity V , D is the diameter of the burner, and ρ , c_p and λ refer to the unburned gas. The advantage of such a development is that a representation of flash-back data may be accomplished for several burner pressures and fuels. In this manner the Peclet number for the jet is found to vary as the square of the Peclet number for the flame for high flow velocities.

This development in terms of dimensionless parameters, and that of Lewis and von Elbe, also hold for the case of laminar flow where the flame is held from the end of an axially symmetric rod, but has blown-off at the outer stream boundary.

It has also been shown that the velocity gradient principle may be applied to turbulent flames⁽¹⁶⁻³⁷⁾. The blow-off of seated propane-air flames has been obtained as a function of fuel/air ratio, Reynolds number, and tube diameter. In the region studied, with Re varying between 1000 and 20,000, the blow-off tendency is shown to decrease as the diameter of the tube is increased, which agrees with the studies made in the laminar range⁽¹⁶⁻³²⁾. The velocity gradient at the wall correlates with the fuel/air ratio for blow-off in fully developed flow in pipes, whether laminar and turbulent. Similarly a new velocity term, U_w , called the velocity at the inner boundary of the laminar film is introduced from the theory of turbulent flow; the velocity gradient at the wall is given by $U_w^2/N^2\nu$, where N is a constant equal to 10 and ν is the kinematic viscosity. The authors correlate this velocity term in a similar manner to the velocity gradient term. However, although interesting, the new velocity term U_w does not add anything to the general picture and is limited to conditions of blow-off in the turbulent region, whereas the velocity gradient correlation covers both laminar and turbulent flow, even though the theoretical development has been for laminar flow. Probably such a correlation, above Reynolds number = 2300, is just fortuitous, since the velocity profile changes so markedly between $Re = 2000$ and $Re = 3000$.

Reiter and Wright⁽¹⁶⁻³²⁾ have studied the stability of mixtures of propane plus hydrogen with air in the laminar region. Their work is to be compared with that of Bollinger and Williams⁽¹⁶⁻³⁷⁾. For the case of only propane and air, the velocity gradient correlations of the two groups fall very close to one another (See Figure 16-6). This helps to confirm further the theory of Lewis and von Elbe, since Reiter and Wright used different size tubes, made of different material (Pyrex) and with different cooling (air cooling instead of water cooling) than other workers. Using a tube 0.57 cm in diameter, the comparison is good up to a critical velocity gradient of 6000 second^{-1} ; above this the blow-off data of these workers tend to depart from those of Bollinger and Williams. This occurs at $Re = 2200$, so the departure is not astonishing and probably represents the rule rather than the exception, even though the Bollinger and Williams data hold at such high Reynolds numbers.

The effect of adding hydrogen to propane is nonlinear both for flash-back and blow-off. The effect of hydrogen is to extend the velocity gradient over which the burner will operate satisfactorily. Although the authors call this effect a "marked effect", if one considers that a small amount of propane, 10 per cent of the fuel, can reduce the velocity gradient at blow-off as much as 80 per cent, it would appear that the more marked effect is that the small amount of propane can quench

the reaction as much as it does. In general, the effects noted are more pronounced in flash-back than in blow-off.

Wright^(16-39,40) has followed this work with stability studies on methane-CO and propane-CO flames. Grumer, et al.,⁽¹⁶⁻⁴¹⁾ have also investigated these mixtures in their stability studies on mixed-fuel combinations.

Wohl⁽¹⁶⁻⁴²⁾ and his associates have studied the stability of butane-air flames above tubes and nozzles. They obtain the same type of curves of velocity gradient as a function of fuel concentration as other investigators. Also as the turbulent region is approached their blow-off curve tends to flatten out in the same manner as Reiter and Wright show for propane flames. Since the velocity gradient at the nozzle wall will be greater than at the tube wall, it would be expected that flash-back and blow-off would require smaller flow velocities for the nozzle. This was confirmed in the study. It was also shown that lifted flames (held in a position of one to two diameters above the exit port) were more stable when held above a nozzle than above a tube. The stability of flames burning off a nozzle was extended toward both the high and low velocities and toward lower fuel concentrations. More detailed analysis of these flames is given in Wohl's Fourth Symposium paper.⁽¹⁶⁻³⁴⁾

Figure 16-6 is a compilation of the stability data of the several investigations reported above on methane, propane, and butane. That a relation exists between velocity gradient and fuel/air ratio is evident.

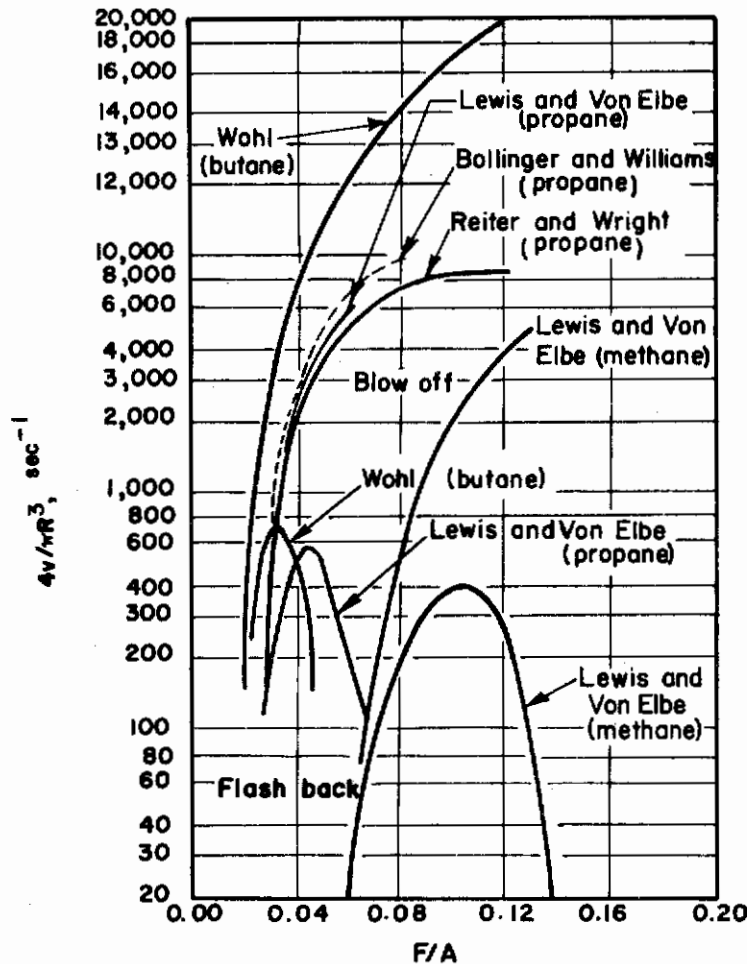


FIGURE 16-6. CRITICAL VELOCITY GRADIENTS FOR METHANE, PROPANE, AND BUTANE

Clusins and Schumacher⁽¹⁶⁻⁴²⁾ have also studied lifted flames above burner tubes. They studied the lifted butane flame in terms of the effect that hydrogen or oxygen had as an additive;

they observed that the flame drops back to the burner tube as soon as the burning velocity was increased.

One of the practical uses of flame stability studies is to determine whether various fuels can be interchanged, and what effects they have on each other. Grumer, Harris, and Schultz⁽¹⁶⁻⁴¹⁾ have been concerned with this type of problem at the Bureau of Mines. Their work applies the velocity-gradient theory to a mixture of fuels. By comparing the stable regions of the mixed fuels to those of the standard fuels (i. e. propane), the limits within which fuels may be interchanged are readily established.

Kurz⁽¹⁶⁻⁴⁴⁾ has studied the effect of various hydrocarbon mixtures such as isobutane-ethylene under varying flow velocities; he observed that on the lean side (with respect to the total fuel concentration) the blow-off and flash-back limits are readily predicted from a knowledge of these limits for the two fuels burning alone, and a use of the Le Chatelier principle. Kurz's and Grumer's general results are quite similar, in that they both show that fuels are compatible on the lean side, but are not compatible on the rich side. In the case of hydrogen sulfide mixtures the fuels are not compatible under any circumstance; but this is to be expected because of the inhibiting power of sulfur in chain propagating reactions.⁽¹⁶⁻⁴⁵⁾

The stability of flames burning off short ports, or odd-shaped ports, is complicated by the change in the velocity profile of gases passing through the ports. As a result the critical velocity gradient is more difficult to determine. Wilson and Hawkins⁽¹⁶⁻⁴⁶⁾ have correlated the blow-off of ethylene and propane flames from short circular ports with some success, while Grumer and co-workers⁽¹⁶⁻⁴⁷⁾ have made successful correlations on non-circular ports.

The stability of the flat flame has been investigated by Holland.⁽¹⁶⁻⁴⁸⁾ Since flame stability has been shown to be dependent on the burner orifice, it is to be expected that the stability of flat flames would depend upon the degree of spread in the gas stream. Holland has also shown that the flat flame is rather unstable while streamline flow is maintained, but is rather stable if slight turbulence is introduced.

Putnam and Smith,⁽¹⁶⁻³⁵⁾ Calcote,⁽¹⁶⁻⁴⁹⁾ and Calcote and Pease⁽¹⁶⁻⁵⁰⁾ have made studies of the effect on various flame stability parameters of applying an electric field. Putnam used the field as a means of extending the extinction region discussed previously. Calcote made a more detailed study of the various effects. However, a quantitative answer has not been given to the question of whether the effects are a result of the back pressure produced by the ion current, or an increase in burning velocity as a result of the localized ion current.

Quenching Distance

As becomes evident in Wohl's discussion of the problem of flame stability,⁽¹⁶⁻³⁴⁾ quenching distance is probably a fundamental parameter important to the development of a generalized theory of flame stability. However the relation of quenching to blow-off is not as yet entirely clear. The Lewis and von Elbe treatment does show the possibility of such a relation and as has been shown the blow-off data can be correlated fairly well using the velocity gradient. However, the added difficulty of the diffusion of secondary air into the flame is more than a minor problem and tends to blur the relation of quenching distance to blow-off data.

From the studies mentioned, four methods of measuring quenching distance or a similar distance have developed. These are: (1) measurement of the dead space between the base of the flame and the burner rim, (2) determination of the minimum tube diameter or minimum distance between two parallel plates when flash-back occurs, (3) determination of minimum distance between parallel plates at which spark ignition will occur, and (4) determination of the ratio of normal burning velocity to velocity gradient.

Friedman⁽¹⁶⁻⁵¹⁾ and Johnston⁽¹⁶⁻⁵²⁾ have studied the quenching problem on oxyhydrogen flames and on propane-air flames using the second method of plane-parallel plates. By applying

a simplified picture of the heat generation and heat flow in this gap to the Mallard-LeChatelier equation, Friedman expressed the quenching distance X as

$$X = \frac{\lambda}{F c_p \rho} \left(\frac{1}{f} \cdot \frac{T_f - T_i}{T_i - T_o} \right)^{1/2}, \quad (16-8)$$

where f is a dimensionless geometrical ratio with values between 0 and 1 and the other symbols take on their usual meanings (See Chapter 14). The critical gaps for stoichiometric oxyhydrogen mixtures with various amounts of nitrogen vary from 0.2 mm to 1.16 mm as the nitrogen increases from 15 to 68 mole per cent. In order to calculate the heat flow to the wall, it is necessary to assume a certain flame thickness, d , so that before the flame-speed equation is introduced the critical distance X is expressed as

$$X = \sqrt{\frac{k}{f F c_p \rho} d}. \quad (16-9)$$

This equation suggests a method of determining the reaction-zone thickness experimentally where the variation of the flame speed of a mixture with pressure is known. As in all these procedures, of course, the accuracy will be limited by the precision with which the geometrical factor f is known.

Friedman also suggests a free-radical analogue of Equation 16-8; he has applied it to the case described above of inert gases in an oxyhydrogen mixture. This mixture does not turn out to be the best choice, however, since the possibility of gas-phase quenching is introduced which further complicates the diffusion problem. The work of L. Seig⁽¹⁶⁻⁵³⁾ on the narrowing of the limits of oxyhydrogen mixtures with combustible and noncombustible additives establishes the fact quite well. However to use a radical diffusion analogue in the quenching distance problem demands a greater knowledge of the kinetics of the effects reported by Seig and others. In this sense the state of knowledge on quenching is about like that of all flame propagation. It is quite likely that radical diffusion must exist, but it will require a concentrated effort to handle the complicated mathematical problems of chemical kinetics, diffusion, and heat transfer simultaneously.

Friedman and Johnston find that the minimum quenching distance for propane flame is 1.2 in. at 35 mm mercury pressure. On the basis of Figure 5 in Reference 16-24, this would correspond to a diameter of 1.6 in. in a tube. Gerstein⁽¹⁶⁻¹³⁾ in his study of the effect of pressure on the flammability limits of various hydrocarbons reports a low-pressure limit for propane-air of 34 mm Hg in a 2-in. diameter tube⁽¹⁶⁻⁵⁴⁾. Thus it appears that quenching must have an important effect on the flammability limits at low pressures. Simon⁽¹⁶⁻⁵⁵⁾ has attempted to correlate all these facts. Table 16-5 shows the results of her study. Although the calculated pressures do not agree with experimental ones at smaller quenching distances, results suggest rather definitely that wall quenching limits propagation in a tube.

TABLE 16-5. APPLICATION OF QUENCHING THEORY TO MINIMUM PRESSURE FOR IGNITION

(Simon)⁽¹⁶⁻⁵⁵⁾

Tube Diameter, mm	Plane Parallel Distance, mm	Minimum Pressure, mm Hg	
		Expt'l	Calc.
10	7.4	500-700	160
18.3	13.5	170-200	83
33	24.4	49	44
58	43.0	25	23
89	66.	12	14

HIGH VELOCITY FLAME STABILIZATION

High-duty combustion, under conditions of steady flow, is dependent upon flow velocity and the flame-holding system. The main interest in flame holders lies in their ability to permit stable combustion over wide limits of air flow and fuel concentrations. Under conditions where the flow velocity may be as high as 600 fps it is necessary to anchor a stable pilot flame at some point, whereupon the stable flame front will originate from this point. A common method is to place a suitably designed object in the stream, the result being that the gas mixture, in the wake of this object, is slowed down to a velocity which will support a stable flame. Flame holders may have a variety of shapes: flat plates, rods, wedges, cylinders, tubes, etc. The important point is that they provide regions of low velocity from which the flame may be held.

It is of interest to note how the use of flame holders came about. Work was in progress, at the Bureau of Standards, for the investigation of the use of hot objects to serve as a point of ignition in high-velocity combustion⁽¹⁶⁻⁵⁶⁾. It was observed that the flame sometimes left the hot object and stabilized itself at a point downstream. The stabilization occurred at a point of sudden enlargement in the piping. This enlargement had not been intended to serve any special purpose.

In this section, the various test results on flame-holding will be discussed first. This will be followed by a review of research on problems related to flame stability. Finally, the various theories of flame stability will be considered briefly.

Experimental Studies

Scurlock⁽¹⁶⁻⁵⁷⁾ studied homogeneous mixtures of propane and air and of city gas and air in a rectangular combustion chamber of a 3 x 1-in. cross section, at flow velocities of 30 to 350 ft/sec, at atmospheric pressure, and at 300 to 340 K. Scurlock used rods, wedges, and flat plates as baffles, which extended across the full width of the combustion chamber. The rod diameters were varied from 1/16 to 1/2 in.

To explain his results he postulated a theory of blow-off (to be discussed later) which indicated a correlating equation of the form

$$V/W^n = \phi(\text{composition}), \quad (16-10)$$

where V is the velocity at blow-off, W is the width of the flame holder, n is a constant parameter, and ϕ is a function of composition. Scurlock found n to be about 0.45 for his data.

Figure 16-7 shows the rough correlation obtained by Scurlock for propane-air mixtures with various sizes of flame holders. He has also attempted to correlate the data of Longwell⁽¹⁶⁻⁵⁸⁾ and of Lewis and von Elbe⁽¹⁶⁻²⁴⁾ on this basis, with poor results. This is not surprising, since Longwell shows an excellent correlation of his own data with $n = 1$. Moreover, the correlation of Lewis and von Elbe's data which pertain to the laminar flow range given in Reference 16-39 also indicates that $n = 1$.

The term $V/W^{0.45}$ in Equation 16-10 is dependent on the type of fuel as noted in tests with propane and with city gas.

DeZubay⁽¹⁶⁻⁶⁰⁾ makes some attempt to determine the effect of this dependence. Table 6 is taken from DeZubay's discussion of Longwell's review of the topic of flame stabilization⁽¹⁶⁻⁶⁰⁾.

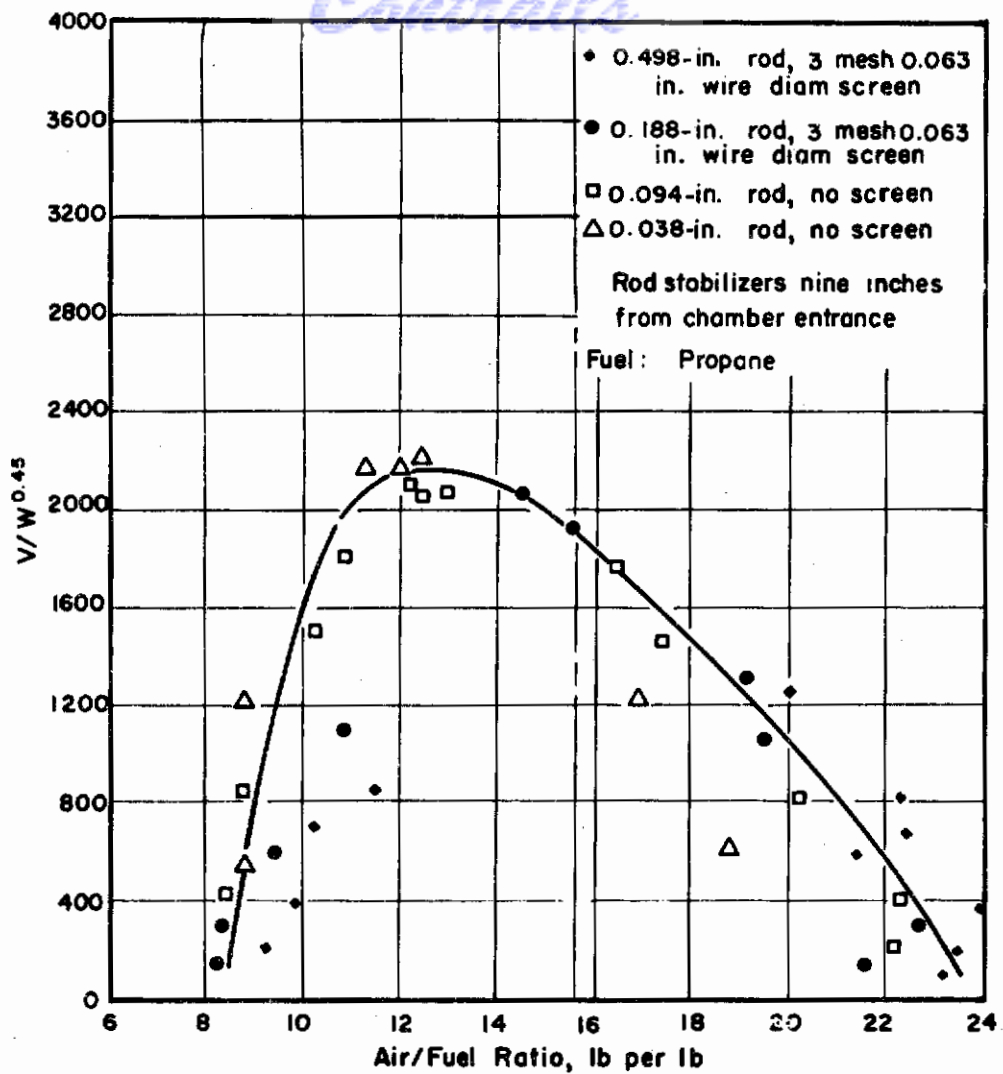


FIGURE 16-7. CORRELATION OF BLOWOUT DATA FOR PROPANE AND AIR

Scurlock(16-57)

TABLE 16-6. THE VARIATION OF STABILITY PARAMETER, V/D^n , WITH DIFFERENT FUELS(16-61)

Fuel	Stability Parameter
Naphtha	V/D
Propane	$V/D \cdot 85$
Hydrogen	$V/D \cdot 74$

Scurlock found that heating the stabilizer extends the stability limits and cooling narrows them. Similar effects have been noted with respect to quenching distances. He also found that the stability limits are unaffected by the outer walls within a range of ratios of duct width to stabilizer dimension of about 10 to 80. However, smaller ratios of duct to holder size have been used by many investigators, and may have considerable effect on the correlation between holder size and blow-off velocity. Because of the interaction of the flame on the holder and the spreading of the flame in a confined system, the length of the combustion chamber is also of importance. It should also be noted that the stability limits decrease with increase in intensity of initial turbulence.

Haddock⁽¹⁶⁻⁶²⁾ used a nonleaded gasoline of wide distillation range, 116 to 308 F, and high vapor pressure. The flame was stabilized on cylindrical rod flame holders and on an equilateral triangle arrangement of three 2-in. disks in a plane perpendicular to the air stream. The air velocities were as high as 300 ft/sec.

Haddock related the parameters of chamber velocity, mixture temperature, and fuel concentration to blow-off conditions. Because he used a three-disk-type of flame holder, it is difficult to compare his data with other work. This holder has 20 per cent area blockage. In terms of a one-disk holder in the 7.75-inch duct, this would be equivalent to a 3-1/2-inch flame holder. The ratios of duct width to stabilizer dimension is only about 2.3, and as Scurlock has shown above, below a ratio of 10 the walls influence the results. Haddock reports no appreciable change in flame stability over a 200 F temperature range. He finds also that on a qualitative basis, longer chambers are needed to contain the flames from the leaner mixtures, whereas shorter ones suffice for stoichiometric mixtures. This of course is in agreement with all flame-propagation data which indicate that the slightly richer than stoichiometric mixtures always exhibit maximum flame speeds.

In a latter investigation, Haddock⁽¹⁶⁻⁶³⁾ investigated blow-off using an apparatus more like that of Scurlock. He studied the blow-off characteristics of a completely vaporized and mixed hydrocarbon fuel in a 1 x 4-in. combustion chamber, using cylindrical flame holders varying in diameter from 0.127 to 0.494 in.; the flame holders were made of steel and were cooled by water. He finds that cooling the flame holder influences results only slightly, but that confining the flame to a constant-area channel tends to reduce blow-off velocities. Blow-off velocity was found to vary with the 1.2 power of the initial gas temperatures and with the square root of the diameter of the flame holder. The latter point agrees with Scurlock's correlation on city gas and propane flames.

Russi, Cornet, and Cornog⁽¹⁶⁻⁶⁴⁾ varied flame-holder temperature from 500 to 2000 F. Gas velocities were only up to 60 fps. Their results showed a widening of the stable flame region (in terms of air-fuel ratios) as the temperature was raised. However, at the lowest velocities of 20 feet per second the heat effect was not as clear; at this velocity there was virtually no effect on stability over the entire temperature range. Williams⁽¹⁶⁻⁶⁵⁾ covered a range of velocities up to 350 fps. The results of both of these studies indicate that the higher the flame-holder temperature, the wider the stability limits.

Longwell⁽¹⁶⁻⁵⁸⁾ used axially symmetric baffles of various shapes. These baffles varied from 0.75 to 2.87 inches in diameter and the flow velocities were as high as 900 fps. The fuel was petroleum naphtha. The limits were not changed much unless the downstream side of the baffle was rounded. This effect was observed by Scurlock, too, and indicates the role of the eddy region in flame holding. Longwell also found that whether the baffle was open or closed at the downstream end was not important. Longwell has correlated his blow-off data by plotting the ratio r/V , radius of holder to velocity of stream, against the air/fuel ratio. He bases his analysis on the mixing time as the limiting factor and says that this should be proportional to the volume of critical reaction zone and inversely proportional to the velocity.

By introducing sodium into the flame at several positions downstream from the flame holder, Longwell has been able to determine the approximate length of the reverse eddy zone. The length of the eddy zone is found to extend out about 1.7 baffle diameters downstream from the baffle.

An investigation of the effect of pressure has been carried out by DeZubay. His tests were run in a 2-3/4-in. duct with flat disks 1/4 in. to 1 in. in diameter. Propane-air mixtures were used at flow velocities varying from 40 to 550 fps, and at pressures of 3, 5, 7, and 15 psia. The

blow-off velocity was found to vary as $P^{0.95}d^{0.85}$, and consequently, the fuel/air ratio at blow-off is a function of $V_o/P^{0.95}d^{0.85}$. This is in close agreement with Longwell's analysis (air/fuel ratio proportional to the ratio of radius to blow-off velocity).

Figure 16-8 relates the results of these four investigations. Also included are some data taken from Lewis and von Elbe's investigation(16-24) of the blow-off properties of propane-air mixtures. The solid line is taken from DeZubay's study (Figure 4, Reference 16-66). The other curves on this plot have been obtained by converting the various test results to DeZubay's correlation factor $V_o/P^{0.95}d^{0.85}$.

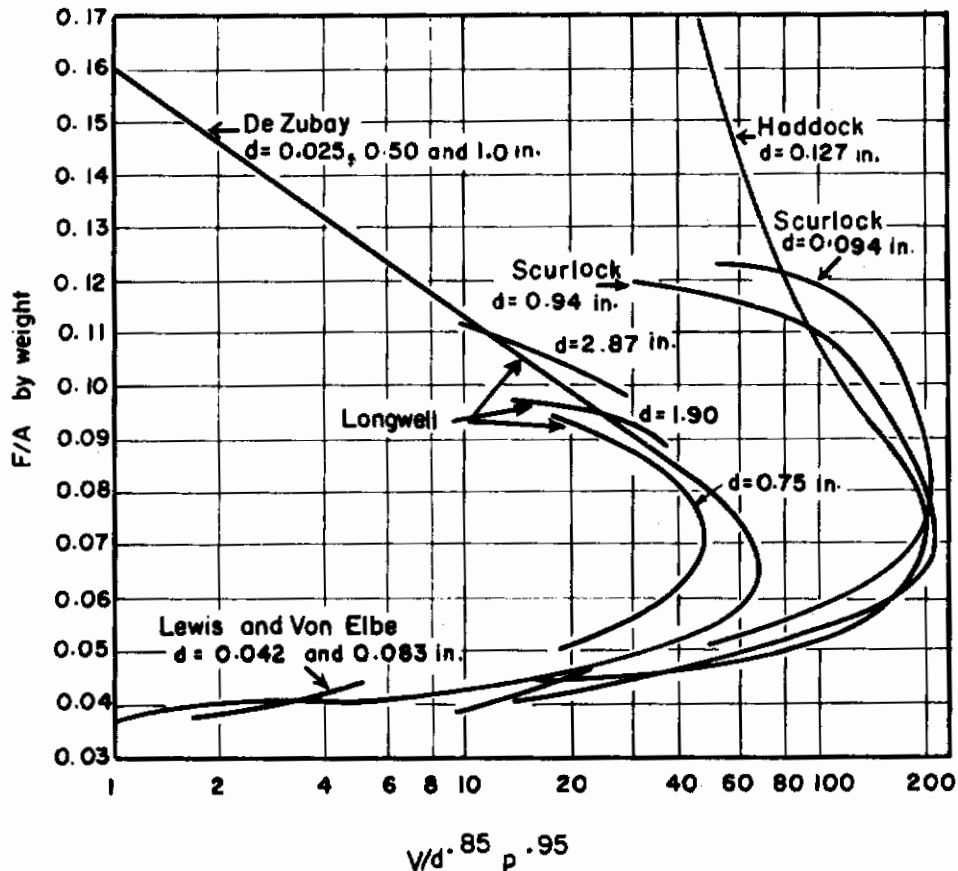


FIGURE 16-8. CORRELATION OF BLOW-OFF DATA FOR VARIOUS FUELS USING THE DEZUBAY FACTOR, $V/d^{.85} p^{.95}$

In a later paper DeZubay(16-67) presents further propane data and also includes some data on hydrogen-air mixtures. He finds the blow-off velocity varies less rapidly with pressure and diameter of holder with hydrogen air mixtures than with propane.

Barrère and Mestre(16-68) present some excellent data on a series of flame holders in a confining duct. The holders vary from 3 to 8 mm in diameter, and have the shape of disks, spheres, hollow hemispheres, and hollow cones. The results are similar to those of other investigators. They also show an increase in stability limits by a change in temperature of the oncoming stream from 551°K to 873°K, and a decrease in stability limits by an increase of the downstream length of the combustion chamber.

Weir, et al,(16-69) and Kutzko(16-70) investigated the blow-off limits of spheres and disks, respectively, in an open system, using propane as the fuel. Both investigations show that the distance of the flame holder above the nozzle could be neither too high nor too low without introducing extraneous effects. Kutzko indicates that the size of flame holder must be less than 3/8 the

jet diameter to prevent interaction of the holding region with the air surrounding the jet. It should be noted that corresponding difficulties have been observed in studies in closed systems.

These tests show that the size of flame holder is unimportant in determining blow-off limits at low velocities on the rich side. This result is probably caused by preferential diffusion. As the Reynolds number increases, the effect of preferential diffusion becomes less, and the stability curves move toward the lean side. The stability curves for the smaller diameter holders may contact or even overlap the stability curves for the larger holders, on the rich side. On the lean side, the curves are correspondingly spread farther apart. It should be noted that Spalding and Tall⁽¹⁶⁻⁷¹⁾, in obtaining their excellent correlation of blow-off data from many sources, made such a shift adjustment in processing the data.

Kutzko also shows that when the flame holder becomes so small as to approach the quenching distance in size, the ratio of the flame holder size to the quenching distance becomes an important factor. Therefore results obtained from the study of very small holders are of little value for extrapolation to full scale.

Putnam⁽¹⁶⁻⁷²⁾ points out that as the angle of the flame at the line of flame holding, relative to the axis, increases, the limits of stability are extended for a given diameter of flame holder. He also indicates that the boundary-layer thickness at the downstream end of the flame holders, where the flame is held, apparently is not an important factor in determining blow-off limits.

Hottel, et al⁽¹⁶⁻⁷³⁾, made a study of stabilization of flames in air-fuel spray mixtures on rod flame-holders. The results of this study, which are discussed in detail in Chapter 18, can be interpreted in terms of the previous results pertaining to homogeneous mixtures.

Wakelin, et al,⁽¹⁶⁻⁷⁴⁾ injected fuel in a series of radial jets from an obstruction on the axis of the 1-inch diameter combustion chamber. The air received an intense swirl just before it passed this region. This created an intense mixing and a uniform composition in the combustion region. The swirl probably increased the holding ability of the obstruction, also.

With this equipment, they studied the flame-stability characteristics of vaporized fuels in an attempt to determine the fuel properties that are important in combustion chamber analysis and design. They investigated the following fuels: isobutane, SPB2, iso-octane, neohexane, benzene, toluene, xylene, cumene and cyclohexane. Their results show that there is no systematic effect of chain length or aromatic structure on flame stability. Also there was found to be no correlation with the ease of oxidation of the fuels as measured by spontaneous ignition tests, and equally absent was the evidence of any effect due to additives.

For most of the fuels tested, the stability limits obtained in the quartz tube, at air flows of 2500 cc/sec for lean mixtures, and 1000 cc/sec for rich mixtures, correlated well with the static ignition limits. But this good correlation does not establish that the ignition limit is the controlling feature, since the factors of flame temperature and flame speed are also related to ignition limits. Acetylene was also studied, and the correlation here was not as good, suggesting that flame speed must be an important factor also.

Mikol⁽¹⁶⁻⁷⁵⁾ studied the problem of burning of propane and of city gas in the wake of cylinders in a system in which the gas entered through a slot in the downstream side of a cylindrical flame holder. The flame holder was set transverse to the air stream and all mixing and combustion occurred downstream. Blow-off data were obtained on flame holders 1/2, 3/4, and 1-1/2 in. in diameter, and it was observed that stability could be attained over a 100-fold variation in gas flow. Quantitatively this type of set-up is so different from other arrangements that results can not be compared. High-speed pictures, taken of the burning gases, indicate discrete and discontinuous masses of burning gas. Although it is possible that the burning is continuous and that the discontinuous regions represent discontinuities in luminosity, it appears more probable that, due to the manner of fuel injection, mixing was not efficient with the result that "ribbons of gas" peeled at the proper concentrations for combustion and only these zones were burning. The pictures indicate recirculation regions three to five diameters long. This is appreciably higher than the value reported by Longwell and is probably due to the action of the gas jet in extending the eddy region by reducing the reverse flow about the cylinder.

The author has attempted to correlate these data by means of Scurlock's correlation but was unsuccessful. The data likewise do not correlate with DeZubay's work. The reason for this is that the rich limit blow-off is strictly a mixing phenomenon. Therefore, as the fuel rate is increased, blow-off becomes dependent upon the velocity of the gas jet as well as on the usual factors of flame-holder dimension and gas temperature.

Related Experimental Studies

Williams and Shipman(16-76) have studied propane-air flames in a 1 x 3-in. rectangular duct. Flame holder size was varied from 0.1 to 0.5 inches diameter, and gases were analyzed in the wake of the flame holder both for the total pressure variation and for concentration changes. The authors note that, although a minimum concentration of active species may be necessary to maintain a flame, other factors are equally important in determining stability limits. From pictures and measurements of the flames, they present the additional argument that blow-out occurs from turbulent decay of the flame, caused when the recirculating gases are replaced by cool gases.

These investigators also showed, from their measurements of composition, that preferential diffusion takes place between the oncoming stream and the recirculation zone behind the holder. This argument serves as a logical basis for the explanation previously mentioned for the composition shift of the stability limits with flame-holder size.

Wilkerson and Fenn(16-77) investigated the ability of various cone-shaped flame holders to mix the heat from the pilot zone with the fresh gases. This was accomplished by making thermocouple traverses in the gas stream and determining from this a mixing factor, $K = q/4\pi xT$, where q is the rate of heat input, x is a distance along the burner axis downstream from the igniter, and T is the temperature measured at this distance. The mixing factor was then correlated with the pilot heat and with an Arrhenius-type reaction rate to obtain a combustion efficiency, defined by the geometry of the system.

Wright and Becker(16-78) studied the ignition of a stream of combustible composition by a central core of hot gases. They showed that the stream could be ignited in this manner. There were two zones apparent in the flame, an initial zone with a weak flame confined to the mixing region, and a zone containing the propagating flame. The position of the initial flame showed little dependency on the fuel/air ratio or stream velocity; however, the flame rapidly moved closer to the beginning of the interfaces as the temperature of the hot core increased.

The intense propagating flame moved rapidly upstream with increasing richness of mixture, decreasing velocity, and increasing core temperature.

There is no doubt that these phenomena are related to the process that occurs between the oncoming gas stream and the recirculating region behind a flame holder. However, a correlation of the results from the two types of tests has not yet been made.

A mathematical study of the reaction interface between a hot gas stream and a cold combustible mixture has been carried out by Marble and Adamson(16-79). Although a comparison of these results with the results of Wright and Becker is not given, the conclusions appear to be compatible. These studies border on the classical studies of ignition delay. Because of this, and because of the spontaneous ignition theories of combustion stability advanced by Lloyd and Mullins, (16-80, 81) it is necessary to review some of the work on ignition lag.

One of the older investigations of ignition is that of Wullmer and Lehman(16-82) who streamed the gas mixture over a heated wire and showed that ignition occurred more readily at lower flow velocities, and at large diameter wires when the flow velocity was kept constant. Silver(16-83) showed that ignition in a static system could be achieved by shooting small heated spheres into the gas mixture. He showed that the larger the diameter of the spheres, the lower the surface temperature necessary. Paterson(16-84) extended the study from the low velocity of 12 fps to 200 fps, and found that as the velocity was increased it was necessary to raise the surface temperature. In a more recent study the ignition problem has been examined in the velocity range 50-500 fps for

heated cylindrical rods. Most of the data taken by Mullen and his associates was on pentane-air mixtures at the stoichiometric fuel concentration. (16-85) The system was set up in such a way that obstacles could be placed in the stream to cause a turbulent effect. However, no measurements of the turbulence were made. The results were expressed in terms of the surface temperature of the rod T_r necessary for ignition. Their results may be summarized as follows:

- (a) Insertion of screens..... T_r raised
- (b) Increasing inlet temperature of gases..... T_r reduced
- (c) Increasing rod diameter..... T_r reduced
- (d) Increasing pressure..... T_r reduced
- (e) Use of platinum rod instead of stainless steel..... T_r raised
- (f) Polished, as against dull rods..... no change
- (g) Increasing humidity..... T_r raised.

In comparing the effect of fuel types it was found that the ease of ignition based on the surface temperature of the rod measurement occurred in the following order among some of the fuels investigated: (1) hydrogen, (2) acetylene, (3) carbon disulfide, (4) ethylene oxide, (5) propylene oxide, (6) pentane, (7) methanol. This order was obtained at a flow velocity of 160 fps.

An upward concavity exists in all of the curves of surface temperature as a function of stream velocity which Mullen and his group obtained. Mullen explains this concavity on a "chemical basis", as he terms it, such that the ignition temperature is related to an ignition lag, the higher the ignition temperature the shorter the ignition lag. This relationship may be expressed by an Arrhenius-type rate equation,

$$tP^n e^{-E/RT_{ig}} = \text{constant}, \quad (16-11)$$

where t is the time required for ignition under the conditions of pressure, P , and ignition temperature T_{ig} . The exponent, n , is a constant, generally between zero and two.

The lag time in the ignition, following reasoning similar to that used by Longwell (16-58) to explain blow-off, is proportional to the size of the critical reaction zone and inversely proportional to the feed rate, V ,

$$t \propto \left(\frac{\text{rod area}}{\text{rod perimeter}} \right) \propto \left(\frac{1}{V} \right). \quad (16-12)$$

This becomes then

$$t \propto \frac{D}{V}, \quad (16-13)$$

where D is the diameter of the ignitor rod. The ignition temperature is proportional to D/V , and to the temperature difference between the rod and the gas, as shown by

$$T_{ig} \propto \frac{D}{V} (T_r - T_o). \quad (16-14)$$

According to Equation 16-11 a plot of $\log t$ against $1/T$ is linear, everything else remaining constant; therefore a plot of $\log (D/V)$ against $V/D(T_r - T_o)$ should be linear. Mullen's plot gives good linear correlations for each rod diameter, but there appears to be a further influence of rod diameters which causes a change in slope from one diameter to another. Differences found for the various fuels can be explained fairly well by their reactivity which is reflected in the exponential,

However, the influence of the thermal properties of the fuels must also be considered, otherwise the behavior of hydrogen can not be explained.

Strickland-Constable(16-86) considers the ignition delay time to be related to the steady state combustion process. He uses a thermal mechanism which assumes no reactions before the ignition temperature is reached, although a similar result could probably be obtained using a radical mechanism.

The delay period, \bar{P} , at constant temperature, is expressed as

$$\bar{P} = ke^{-E/RT} \quad (16-15)$$

In a time dt only a fraction of the delay, dt/ \bar{P} , is completed. For both the constant temperature case of an ignition study, and the varying temperature case of a propagating flame

$$\int_0^{\bar{P}} \frac{dt}{\bar{P}} = 1. \quad (16-16)$$

From this point, the thermal flame-speed equations are applied. Two equations are obtained, one being Equation 16-16 in terms of the distance x along the reaction path and another in terms of temperatures as a function of this distance, x. By a trial and error procedure, a value of T_i , the ignition temperature, is chosen; T is obtained as a function of x and this is substituted into an equation of the form of Equation 16-16. When the area integrates to unity, the conditions are correct, under the assumptions of the development.

Using data of Coward(16-87) and of Lloyd(16-88) on methane and kerosene, respectively, ignition temperatures of 1180 C and 1420 C are obtained. These temperatures appear quite high. The conditions of the development must dictate this, for if some reaction had occurred before the ignition temperature was reached, the temperature would be lower. It is difficult to see how they could be lowered much, however, in a strictly thermal development, whereas the inclusion of radical diffusion into this treatment could result in more reasonable values.

A generalized extension of this development can be worked out in terms of dimensionless parameters. The general expression used is

$$F^2 \left(\frac{c\rho k}{\lambda} \right) = \psi \left(\frac{E}{RT}, \frac{T_i}{T_o} \right), \quad (16-17)$$

where k is the delay constant in the delay period given by Equation 16-15. The treatment is similar to the above in that the data must be correlated in terms of the k, E, and T_i values. However, it has the advantage over the preceding treatment in that a trial and error solution is not necessary, and the variation of the term (cρ/λ) with temperature through the flame front can be included. Such a treatment for methane results in $T_i \cong 1200$ C, which is comparable to the value obtained by Strickland-Constable. It should be mentioned that the reverse process, where burning velocity is computed from ignition temperature data, is necessarily very inaccurate.

Mullins(16-89) has made a rather thorough study of the ignition of fuels under conditions where the fuel is injected into a duct through which are passed the hot exhaust gases from a combustion chamber. The effects of fuel atomization are readily reproduced and the chemical characteristics of many liquid fuels may be examined. Ignition delays of the order of those experienced in gas turbine combustion (0.5 to 30 milli-seconds) were determined for many fuel sprays, including, ethers, alcohols, esters, cyclo-compounds, kerosene, and others. In general air/fuel ratio and air velocity had only minor effects on ignition delay; spray-particle size, fuel temperature and air turbulence had some noticeable effect. Pre-heating of the fuel reduced ignition delay; Mullins believes that this reduction exceeds that due to change in physical properties. In tests with

additives, ethyl nitrate was reported as the only additive which appreciably reduced ignition delay. On ascending the homologous series of normal alcohols, Mullins reports an increase in ignitability. These studies are related to Mullins' other work on vitiated air flames, and are also of general importance in droplet combustion (Chapter 18).

Theories of Flame Holding

Spalding and Tall⁽¹⁶⁻⁷¹⁾ have presented an excellent review of the various theories and experimental results pertaining to flame holding; this review is used as a basis for the following comments.

Two basically different theories have been advanced to explain the flame holding action of high velocity flame holders. The more recent of these theories, advanced by Longwell⁽¹⁶⁻⁹⁰⁾ and DeZubay⁽¹⁶⁻⁶⁷⁾, is that of the homogeneous reactor. It is assumed that the mixing is so intense in the reaction zone that the mixture is homogeneous. Equilibrium is at the point where the difference in mass of fuel entering and leaving the zone equals the rate of consumption by chemical reaction. These investigators obtain

$$A/vP^n = \phi \text{ (composition, temperature) } , \quad (16-18)$$

where A is the entering gas mass flow rate, v is the reactor volume, P is the pressure, n is a constant equal to two for a bi-molecular reaction, and ϕ is a function of the composition and temperature.

Spalding and Tall, however, by identifying the reaction zone with the thin reaction zone in a laminar flame, are able to obtain the relation

$$(Vd/\Gamma) = K (Fd/\Gamma)^2 , \quad (16-19)$$

where V is the blow-off velocity, d is the characteristic distance, $\Gamma = \lambda/c_p\rho$, and K is a constant.

In a previous paper, Spalding⁽¹⁶⁻⁹¹⁾ had considered three models of the general type advanced by earlier investigators. In the first, continuous recirculation of the burned and unburned gas is assumed within the reaction zone. Extinction occurs when the supply of fresh gases reduces the temperature of the mixture to a point that the reaction can no longer keep pace with the supply.

For the second model, the reaction zone is treated as a pair of standing vortices. These are fed with unburned combustible by turbulent diffusion. When the temperature profile is such that the reaction rate cannot keep up with the turbulent diffusion, extinction occurs.

In the third model, Spalding considers a jet of burned gas mixing with the fresh gas. Again extinction is assumed to occur when the mixing becomes too intense relative to the reaction rate. It should be pointed out that this third model is also considered in detail by Lees⁽¹⁶⁻⁹²⁾. The connection of the model with other work at C. I. T., covered in the previously discussed References 16-78 and 16-79, is clear.

Similarities in these approaches can be seen, and, indeed, the same mathematical relation comes out of each model. It is also not surprising that the relation is the same as that obtained by Spalding and Tall for the homogeneous reactor.

Spalding and Tall finally point out that a dimensional analysis is sufficient to arrive at Equation 16-19. Since there are only a limited number of relevant variables, this result also had to follow.

Before continuing with the review of the work by Spalding and Tall, other methods of approach to this same problem by other investigators will be outlined. Scurlock⁽¹⁶⁻⁵⁷⁾, to explain his results, postulated the mechanism of flame stabilization as follows. The cold unburned gases approach the rods, separate on their way around the rod and then come in contact with hot gases

in the eddy region. A rapid transfer of heat and chain carriers occurs along this contact surface; ignition temperature is reached and burning takes place. The chain carriers resulting from this combustion then move into the eddy region where they become available to continue the cycle. The recirculating hot gases in the eddy region are thus the continuous source of ignition. The rate of heat supply, H , necessary for continuous ignition should be a function of the same properties that hold in the case of laminar flames; thus the following expression is considered

$$H \propto \frac{V_o^e \lambda}{F} (T_{ig} - T_o) , \quad (16-20)$$

where V_o is the average stream velocity raised to an arbitrary power, e , and the other symbols have their usual meanings. If the eddy region is assumed to be at the final reaction temperature, T_f , one can expect the heat transfer to increase as $(T_f - T_o)$ increases and as the length of the heat-transfer surface increases. This latter surface is proportional to the characteristic dimension, d , of the stabilizer. The rate of heat transfer to unburned gas in the eddy region, H_{tr} , is expressed as

$$H_{tr} \propto \left(\frac{dV_o}{\nu} \right)^g \lambda (T_f - T_o) , \quad (16-21)$$

where ν is the kinematic viscosity, and g is an exponent. On the basis that at blow-off the two rates are equal, the two expressions are equated to give the following equation:

$$\frac{V_{BO}^{e-g}}{dg} = \frac{K}{\nu^g} \frac{F(T_f - T_o)}{(T_i - T_o)} = \phi(f) , \quad (16-22)$$

where V_{BO} is the chamber velocity at blow-off, e and g are exponents, and $\phi(f)$ is a function of the air/fuel ratio.

Scurlock postulates the condition of blow-off on the basis of these thermal equations. As the air/fuel ratio increases more energy is required for ignition and the eddy region then becomes cooler, until the region cannot transfer enough heat from the burned gases to ignite the oncoming mixture.

Putnam and Carrier⁽¹⁶⁻⁹³⁾ assumed a model of the flame holding mechanism in which the heat transfer to the unburned gases near the holder was balanced against the heat transferred to the recirculation gases farther downstream, after the gases had ignited and were burning. Following the indications of photographs that the interface between the unburned gases and the recirculation zone appeared smooth and thin, they assumed that the process is controlled by laminar diffusion. Modifications to this assumption are possible in considering the final results. This development showed that

$$(F/V) (FL/\Gamma) \quad (16-23)$$

is essentially constant, with only slight variations resulting from variations in the composition. Here L is the length of the recirculation zone. This result is the same as that given in Equation 16-19.

Following their analysis of the various theories of blow-off, Spalding and Tall correlate other available data on blow-off. The effects of preferential diffusion are accounted for by shifting the blow-off curves so that peak values occurred at values corresponding to maximum burning velocities. After this transformation (Vd/Γ) was plotted against (Fd/Γ) .

Figure 16-9 shows the resulting plot. The axially symmetric holders fall on one curve and the two-dimensional holders fall on a parallel curve. At the high end, the slope is 2:1 as predicted by their theory. At the lower end, the slope is about 1.4:1, which corresponds to 0.4 for the

exponent in Scurlock relation. A simple qualitative explanation of the 1.4 values is based on the fact that d should not be the diameter of the obstacle but a value related to the length of the recirculation zone. Below a certain Reynolds number (which varies directly with the vertical coordinate), the length of the recirculation zone gradually increases. This leads to a change in the slope.

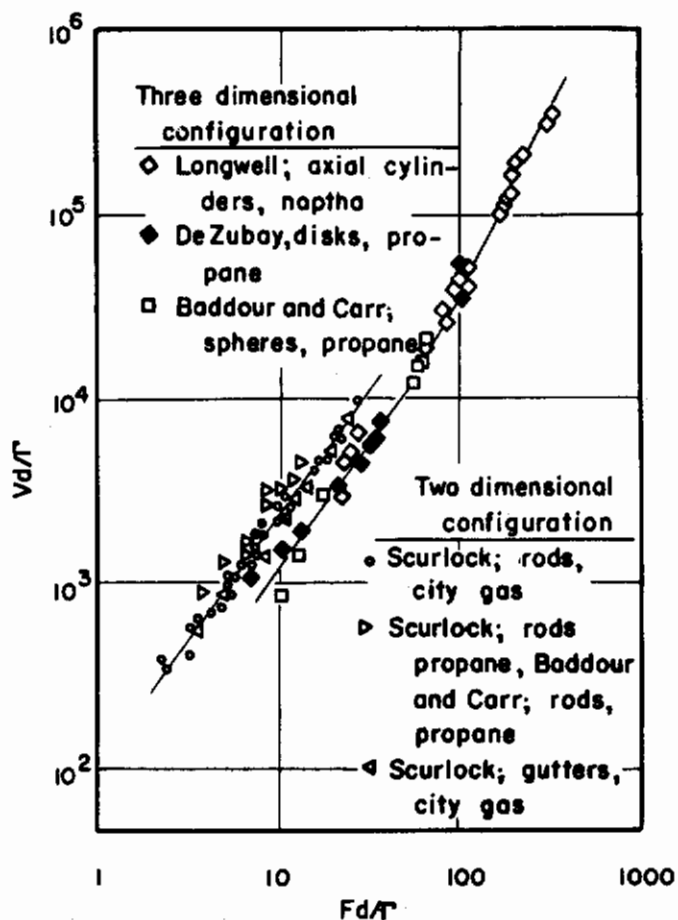


FIGURE 16-9. CORRELATION CURVES FOR FLAMES STABILIZED BY A BLUFF BODY IN A PREMIXED GAS STREAM

Spalding and Tall(16-71)

Spalding and Tall also point out that at very low values of (Fd/Γ) , the characteristic value of the quenching distance is approached. This will result in another break in the curve, this time to a steeper slope.

Using the homogeneous reactor theory as a basis, Spalding and Tall study the effects of radiation losses. They point out that radiation losses result in a lower limit to the stable range of operation. Furthermore, as the operating pressure decreases, these losses become more important and finally result in a lower limit to the pressure at which the reactor may be operated. These results apply not only to the recirculation zone, but to the entire combustor considered as a homogeneous reactor.

Lloyd and Mullins^(16-80, 81) advance the spontaneous ignition concept as being the important factor in flame holding as contrasted to the previous terms which assume a steady state phenomena. Considering that the factor (V/d) , which correlates much blow-off data, can be considered as a reciprocal time, that the homogeneous reactor concept can be considered on a sufficiently small scale to be isolated islands of unburned mixtures being ignited by temperature effects, and that

ignition delay and burning velocity can be related, it is not difficult to see that good arguments can be advanced in favor of this mechanism proposed by Lloyd and Mullins. Spalding, in his discussion of their work, points out that two characteristics of ignition delay times are an exponential variation with temperature, and a relation independent of air/fuel ratio; these two characteristics do not appear to be found in studies of flame holding. In both of these cases, however, the mixing rate may be the controlling rate factor, whereas the actual ignition of the gases would still be controlled by the spontaneous process as contrasted to the continuous propagation of other theories.

Concluding Remarks

The preceding discussion has shown that there may be limits of fuel/air mixtures beyond which a flame will not propagate. However, the effects of chamber size seem to prevail in most experiments on the limits of combustion, and there may be no absolute limit. When a continuous flow combustion system is considered, the limits of combustion are found to depend on a characteristic velocity of the fuel, termed burning velocity, and a characteristic length, such as quenching distance. Using these concepts, qualitative explanations of the observed phenomena are possible, but in some instances quantitative explanations are not satisfactory.

At high velocities, where flames are stabilized by bluff bodies, the limits depend on the velocity and size of the stabilizer. The exact dependence is a function of many variables, several of which are often ignored or unrecognized. There is considerable evidence, however, that the detailed mechanism of flame holding may change as the Reynolds number increases. At the lower velocities, the recirculation region is longer. A long, smooth, thin luminous region surrounds the upstream side of the recirculation zone. As the velocity increases, the recirculation zone tends to become smaller. The thin luminous zone also tends to shorten. It has been observed in some cases that blow-off is preceded by a rapid destruction of this zone from the downstream end. However, there is some evidence that the entire zone can be turbulent and the flame will still persist. A detailed study of the characteristics of the flame holding mechanism itself as a function of size of holder, fuel composition, stream velocity, and stream turbulence is definitely needed.

On the theoretical side, the various theories all seem to lead to the same result; however, this is not surprising since only a limited number of parameters are considered. This leads to only a limited number of dimensionless groups to correlate the data, regardless of the actual theory put forth.

Possibly the most suitable manner in which to conclude the discussion of the flame holding problem, is to point out that each investigator evaluates the various aspects of the problem, and develops a model, on the basis of his own background. Thus, each model may contain some aspects of the true picture, but none is entirely correct.

Comair
REFERENCES

- 16-1. Egerton, A. C., Limits of Inflammability, "Fourth Symposium on Combustion", Williams and Wilkins, Baltimore, Md., 1953, p. 4.
- 16-2. Coward, H. F., and Jones, G. W., Limits of Flammability of Gases and Vapors; U. S. Bureau of Mines Bulletins No. 279 (1938) and No. 503 (1952).
- 16-3. Zabetakis, M. G., Scott, G. S., and Jones, G. W., Limits of Flammability of Paraffin Hydrocarbons in Air; Ind. Eng. Chem., Vol 43, 1951, p. 2120; also, *ibid*, Vol. 45, 1953, p. 2079; and Bureau of Mines Reports of Investigations No. 4829, 1951.
- 16-4. Burgoyne, J. H., and Neale, R. F., Limits of Inflammability and Spontaneous Ignition of Some Organic Combustibles in Air; Fuel, Vol. 32, 1953, pp. 5 and 17; also, Burgoyne, J. H. and Williams-Leir, G., Fuel, Vol. 27, 1948, p. 118.
- 16-5. White, A. G., Limits for the Propagation of Flame in Inflammable Gas-Air Mixtures; J. Chem. Soc., 1924, p. 2387.
- 16-6. Egerton, A., and Powling, J., Limits of Flame Propagation at Atmospheric Pressure, I. The Influence of Promoters; Proc. Roy. Soc., Vol. A193, 1948, p. 172.
- 16-7. Coleman, E. H., Effects of Fluorinated Hydrocarbons on Inflammability Limits of Combustible Vapors; Fuel, Vol. 31, 1952, p. 445.
- 16-8. Egerton, A., and Powling, J., Limits of Flame Propagation at Atmospheric Pressure, II. The Influence of Changes in Physical Properties; Proc. Roy. Soc., Vol. A193, 1948, p. 190.
- 16-9. Coward, H. F., and Hartwell, F. J., Extinction of Methane Flame by Diluent Gases; J. Chem. Soc., 1926, p. 1522.
- 16-10. Posthumus, K., Explosion Regions of Gas Mixtures in Which One or Two Gases are Endothermic; Rev. Trav. Chem. Pays Bas, Vol. 49, 1930.
- 16-11. Van Heiningen, J., Explosion Limits. I. Influence of Argon, Nitrogen, Helium, and Carbon Dioxide on Combustion Limits of Hydrogen, Carbon Monoxide, Methane and Butane in Air; *Ibid*, Vol. 55, 1936, p. 65.
- 16-12. Mellish, C. E., and Linnett, J. W., The Influence of Inert Gases on Some Flame Phenomena; "Fourth Symposium on Combustion", Williams and Wilkins, Baltimore, Md., 1953, p. 407.
- 16-13. DiPiazza, J. T., Gerstein, M., and Weast, R. C., Flammability Limits of Pure Hydrocarbon-Air Mixtures; Ind. Eng. Chem., Vol. 43, 1951, p. 2721.
- 16-14. Spence, R., and Townend, D. T. A., The Cool Flame and Two-Stage Ignition Systems in Ether-Air Mixtures at Room Temperature; Nature, Vol. 155, 1945, p. 330.
- 16-15. Coward, H. F., et al, The Dilution Limits of Inflammability of Gaseous Mixtures; J. Chem. Soc., Vol. 115, 1919, p. 27.
- 16-16. Burgoyne, J. H., and Williams-Leir, G., Influence of Incombustible Vapors on Limits of Inflammability of Gases and Vapors in Air; Proc. Roy. Soc., Vol. A193, 1948, p. 525.
- 16-17. Casson, H., Practical Calculation of Flammability Limits of Gaseous Mixtures; Chaleur et Industrie, Vol. 34, March 1953, p. 77.
- 16-18. Townend, D. T. A., and Maccormac, M., The Inflammation of Hydrocarbon-Air Mixtures; J. Inst. Petroleum, Vol. 25, 1939, p. 459.

- 16-19. Simon, D. M., Belles, F. E., and Spakowski, A. E., Investigation and Interpretation of the Flammability Region for Some Lean Hydrocarbon-Air Mixtures; "Fourth Symposium on Combustion", Williams and Wilkins, Baltimore, Md., 1953, p. 126.
- 16-20. Scott, G. S., Zabetakis, M. G., and Furno, A. L., Flammability of Mixtures of Individual Paraffin-Hydrocarbon Gases with Air and Added Nitrogen at Sub-atmospheric Pressures; U. S. Bureau of Mines, Rept of Investigation No. 4839, 1952.
- 16-21. Zabetakis, M. G., and Richmond, J. K., The Determination and Graphic Representation of the Limits of Flammability of Complex Hydrocarbon Fuels at Low Temperatures and Pressures; "Fourth Symposium on Combustion", Williams and Wilkins, Baltimore, Md., 1953, p. 121.
- 16-22. Delbourgo, R., and Laffitte, P., The Flammability Regions of Ethane, Propane, and Butane; Compt. rend., Vol. 233, pp 958, 1612 (1951); Nature, Vol. 167, 1951, p. 985.
- 16-23. Laffitte, P., and Delbourgo, R., Ignition by Condenser Sparks. Regions of Flammability of Ethane, Propane, N-Butane, and N-Pentane, "Fourth Symposium on Combustion", Williams and Wilkins, Baltimore, Md., 1953, p. 114.
- 16-24. Lewis, B., and von Elbe, G., Stability and Structure of Burner Flames; J. Chem. Phys., Vol. 11, 1943, p. 75.
- 16-25. Von Elbe, G., and Mentser, M., Further Studies of the Structure and Stability of Burner Flames; J. Chem. Phys., Vol. 13, 1945, p. 89.
- 16-26. Blanc, M. V., Guest, P. G., von Elbe, G., and Lewis, B., Ignition of Explosive Gas Mixtures by Electric Sparks, Part I; J. Chem. Phys., Vol. 15, 1947, p. 798.
- 16-27. Lewis, B., and von Elbe, G., Ignition of Explosive Gas Mixtures by Electric Sparks, Part II, J. Chem. Phys., Vol. 15, 1947, p. 803.
- 16-28. Lewis, B., and von Elbe, G., Ignition and Flame Stabilization in Gases; Trans. ASME Vol. 70, 1948, p. 307.
- 16-29. Von Elbe, G., and Lewis, B., Theory of Ignition, Quenching and Stabilization of Flames of Nonturbulent Gas Mixtures; "Third Symposium on Combustion, Flame, and Explosion Phenomena", Williams and Wilkins, Baltimore, 1949, p. 68.
- 16-30. Harris, M. E., Grumer, J., von Elbe, G., and Lewis, B., Burning Velocities, Quenching, and Stability Data on Nonturbulent Flames of Methane and Propane with Oxygen and Nitrogen; *ibid*, p. 80.
- 16-31. Lewis, B., and von Elbe, G., "Combustion, Flames, and Explosions of Gases", Academic Press, New York, 1951, Chapter VII.
- 16-32. Garside, J. E., Forsyth, J. S., and Townend, D. T. A., Stability of Burner Flames; J. Inst. Fuel, Vol 18, 1945, p. 175.
- 16-33. Forsyth, J. S., and Garside, J. E., The Mechanism of Flashback of Aerated Flames; "Third Symposium on Combustion, Flame, and Explosion Phenomena", Williams and Wilkins, Baltimore, 1949, p. 99.
- 16-34. Wohl, K., Quenching, Flashback, Blow-off — Theory and Experiment; "Fourth Symposium on Combustion"; Williams and Wilkins, 1953, p. 68.
- 16-35. Putnam, A. A., and Smith, L. R., On the Extinction Limit of Laminar Flames; "Fourth Symposium on Combustion", Williams and Wilkins, Baltimore, Md., 1953, p. 708.

- Compendium*
- 16-36. Putnam, A. A., and Jensen, R. A., Application of Dimensionless Numbers to Flash-Back and Other Combustion Phenomena; "Third Symposium on Combustion, Flame, and Explosive Phenomena", Williams and Wilkins, Baltimore, Md., 1949, p. 89.
 - 16-37. Bollinger, L. M., and Williams, D. T., Experiments on Stability of Bunsen-Burner Flames for Turbulent Flow; NACA Tech. Note 1234, June, 1947.
 - 16-38. Reiter, S. H., and Wright, C. C., Stability of Burner Flames With Propane-Hydrogen Mixtures; Ind. Eng. Chem., Vol. 42, 1950, p. 691.
 - 16-39. Walker, P. L., and Wright, C. C., Stability of Bunsen Flames for Binary and Ternary Mixtures of Methane, Carbon Monoxide, and Water Vapor; Fuel, Vol. 31, 1952, p. 37; Stability and Burning Velocity of Bunsen Flames with Propane - Carbon Monoxide Mixtures, Ibid, p. 45.
 - 16-40. Levy, A., and Kurz, P. F., An Analysis of the Stability of Carbon Monoxide-Hydrocarbon-Air Flames; J. Am. Chem. Soc., Vol. 77, 1955, p. 1459.
 - 16-41. Grumer, J., Harris, M. E., and Schultz, H., Predicting Interchangability of Fuel Gases; Ind. Eng. Chem., Vol. 44, 1952, p. 1554, Ibid, p. 1547.
 - 16-42. Wohl, K., et al, Methods of Determining Burning Velocities and Stability Measurements of Tube and Nozzle Flames; Meter Report UAC-49, December, 1950.
 - 16-43. Clusius, K., and Schumacher, E., Flames, III, Free-Floating Butane Flames; Helv. Chim. Acta., Vol. 34, 1951, p. 1415.
 - 16-44. Kurz, P. F., Flame Stability Studies on Shielded Bunsen Burners; Ind. Eng. Chem., Vol. 46, 1954, p. 746; also, Ibid, Vol. 45, 1953, p. 2072.
 - 16-45. Kurz, P. F., Influence of Hydrogen-Sulfide on Flame Speed of Propane-Air Mixtures, ibid, Vol. 45, 1953, p. 2361.
 - 16-46. Wilson, C. W., and Hawkins, N. G., Blow-Off of Flames from Short Burner Ports; Ibid, Vol. 43, 1951, p. 2029.
 - 16-47. Grumer, J., Harris, M. E., and Schultz, H., Flame Stabilization on Burners With Short Ports or Non-Circular Ports; "Fourth Symposium on Combustion", Williams and Wilkins, Baltimore, Md., 1953, p. 695.
 - 16-48. Holland, B. H., The Structure and Stability of Flat Burner Flames; J. Inst. Fuel, Vol. 26, 1953, p. 282.
 - 16-49. Calcote, H. F., Electrical Properties of Flames - Burner Flames in Transverse Electric Fields; "Third Symposium on Combustion, Flame and Explosion Phenomena", Williams and Wilkins, Baltimore, Md., 1949, p. 245.
 - 16-50. Calcote, H. F., and Pease, R. N., Electric Properties of Flame-Burner Flames in Longitudinal Electric Fields; Ind. Eng. Chem., Vol. 43, 1951, p. 2726.
 - 16-51. Friedman, R., The Quenching of Laminar Oxyhydrogen Flames by Solid Surfaces; "Third Symposium on Combustion, Flame, and Explosion Phenomena", Williams and Wilkins, Baltimore, 1949, p. 110.
 - 16-52. Friedman, R., and Johnston, W. C., The Wall-Quenching of Laminar Propane Flames as a Function of Pressure, Temperature, and Air/Fuel Ratio; J. Applied Physics, Vol. 21, 1950, p. 791.

- 16-53. Seig, L., Narrowing the Ignition Limits of Hydrogen Air Mixtures by Means of Additives; Ang. Chem., Vol. 63, 1951, p. 143.
- 16-54. Jones, G. W., and Spolan, I., Inflammability of Gasoline Vapor-Air Mixtures at Low Pressures; U. S. Bureau Mines, R. I. 3966, 1946.
- 16-55. Simon, D. M., A Comparison of Quenching Distance and Inflammability Limit Data for Propane-Air Flames; J. Applied Physics, Vol. 22, 1951, p. 103.
- 16-56. Caldwell, F. R., et al, Combustion in Moving Air; SAE Quart., Vol. 3, 1949, p. 327.
- 16-57. Scurlock, A. C., Flame Stabilization and Propagation in High Velocity Gas Streams; Meteor Report No. 19, MIT, May, 1948; also, Williams, G. C., Hottell, H. C., and Scurlock, A. C., Flame Stabilization and Propagation in High Velocity Gas Streams, "Third Symposium on Combustion, Flame, and Explosion Phenomena", Williams and Wilkins, Baltimore, Md., 1949, p. 21.
- 16-58. Longwell, J. P., Chenevey, J. E., Clark, W. W., and Frost, E. E., Flame Stabilization by Baffles in a High Velocity Gas Stream; "Third Symposium on Combustion, Flame, and Explosion Phenomena", Williams and Wilkins, Baltimore, 1949, p. 40.
- 16-59. Putnam, A. A., and Jensen, R. A., Application of Dimensionless Numbers to Flash-Back and Other Combustion Phenomena; "Third Symposium on Combustion, Flame, and Explosion Phenomena", Williams and Wilkins, Baltimore, 1949, p. 89, Figure 11.
- 16-60. DeZubay, E. A., Discussion of Reference 16-61.
- 16-61. Longwell, J. P., Flame Stabilization by Bluff Bodies and Turbulent Flames in Ducts; "Fourth Symposium on Combustion", Williams and Wilkins, Baltimore, 1953, p. 90.
- 16-62. Haddock, G. W., Study of Combustion of Homogeneous Hydrocarbon-Air Mixtures in Channeled Flow; J. P. L., C. I. T., Progress Report 4-124, May, 1950.
- 16-63. Haddock, G. W., Flame Blow-Off Studies of Cylindrical Flame Holders in Channeled Flow; J. P. L., C. I. T., Progress Report 3-24, May, 1951.
- 16-64. Russi, M. J., Cornet, I., and Cornog, R., The Influence of Flame Holder Temperature on Flame Stabilization; "Fourth Symposium on Combustion", Williams and Wilkins, Baltimore, 1953, p. 743.
- 16-65. Williams, G. C., Basic Studies on Flame Stabilization; J. Aero. Sci., Vol. 16, 1949, p. 714.
- 16-66. DeZubay, E. A., Flame Stability of Bluff Bodies; Aero Digest, Vol. 61, July, 1950, p. 54.
- 16-67. De Zubay, E. A., A Study of Flame Stability Based on Reaction Rate Theory, ASME Preprint 54-SA-27, June, 1954.
- 16-68. Barrère, M. and Mestre, A., Stabilization des Flamme par des Obstacles, "Selected Combustion Topics", Butterworths, London, 1954, p. 426.
- 16-69. Weir, A. Jr., Rogers, D. E., and Cullen, R. E., Blow-Off Velocities of Special Flame Holders, University of Michigan Report UMM-74, September, 1950.
- 16-70. Kutzko, G. G., Investigation of Limits of Flame Stability of Disk Flame Holders in a Free Stream.
- 16-71. Spalding, D. B., and Tall, B. S., Flame Stabilization in a High Velocity Gas Stream and the Effect of Heat Losses at Low Pressures, The Aeronautical Quarterly, Vol. V, 1954, p. 195.

- Continued*
- 16-72. Putnam, A. A., Effect of Boundary-Layer Thickness on Flame Stability; Fuel, Vol. 33, No. 3, July 1954, p. 355.
 - 16-73. Hottell, H. C., May, W. G., Williams, G. C., and Maddocks, F. E., Jr., Flame Stabilization in Air-Fuel Spray Mixtures; "Fourth Symposium on Combustion", Williams and Wilkins, Baltimore, 1953, p. 715.
 - 16-74. Wakelin, R. J., Jeron, R., and Baldwin, R. R., Study of Flame Stability Characteristics of Different Vaporized Fuels in Small Scale Combustion Chambers; Fuel, Vol. 30, 1951, p. 82.
 - 16-75. Mikol, E. P., Flames of Fuel Gases Issuing and Burning in the Wake of Cylinders; Meteor Report No. 67, M.I.T., June, 1949.
 - 16-76. Williams, G. C. and Shipman, C. W., Some Properties of Rod Stabilized Flames of Homogeneous Gas Mixtures; "Fourth Symposium on Combustion", Williams and Wilkins, Baltimore, 1953, p. 733.
 - 16-77. Wilkerson, E. C. and Fenn, J. B., Effect of Flame Holder Geometry on Combustion Efficiency, Ibid, p. 749.
 - 16-78. Wright, F. H. and Becker, J. L., Combustion in the Mixing Zone Between Two Parallel Streams, J. P. L., C. I. T., Progress Report 3-25, June, 1952.
 - 16-79. Marble, F. E., and Adamson, T. C., Jr., Ignition and Combustion in a Laminar Mixing Zone, "Selected Combustion Problems", Butterworths, London, 1954, p. 111; also Jet Propulsion, Vol. 24, No. 2, p. 85.
 - 16-80. Lloyd, P., and Mullins, B. P., The Problem of Combustion at High Altitudes, "Selected Combustion Problems", Butterworths, London, 1954, p. 405.
 - 16-81. Mullins, B. P., Combustion in Vitiated Air, Ibid, p. 447.
 - 16-82. Wullner and Lehman, Ann. Min. Belg., Vol. 6, 1886, p. 9.
 - 16-83. Silver, R. S., Ignition of Gaseous Mixtures by Hot Particles; Phil. Mag. (7), Vol. 23, 1937, p. 633.
 - 16-84. Paterson, S., The Ignition of Inflammable Gases by Hot Moving Particles; Ibid, Vol. 28, 1939, p. 1; Vol. 30, p. 437.
 - 16-85. Mullen, J. W., Fenn, J. F., and Irby, M. R., The Ignition of High Velocity Streams of Combustible Gases by Heated Cylindrical Rods; "Third Symposium on Combustion, Flame, and Explosion Phenomena", Williams and Wilkins, Baltimore, 1949, p. 317.
 - 16-86. Strickland-Constable, R. F., The Burning Velocity of Gases in Relation to the Ignition Delay Period; Ibid, p. 229.
 - 16-87. Coward, H. F., Ignition Temperature of Gases; J. Chem. Soc., 1934, p. 1382.
 - 16-88. Lloyd, P., Spontaneous Ignition of Liquid Fuel in Hot Gas Stream; 6th International Congress for Applied Mechanics.
 - 16-89. Mullins, B. P., The Spontaneous Ignition of Fuels Injected into a Hot-Air Stream; Fuel, Vol. 32, 1953, Part I p. 211, Part II p. 234, Part III p. 327, Part IV p. 343, Part V p. 363, Part VI p. 451, Part VII p. 467, Part VIII p. 481.
 - 16-90. Longwell, J. P., Frost, E. E., and Weiss, M. A., Flame Stability in Bluff Body Recirculation Zones; Ind. Eng. Chem., Vol. 45, 1953, p. 1629.

- 16-91. Spalding, D. B., Theoretical Aspects of Flame Stabilization; "Aircraft Engineering", September, 1953, p. 264.
- 16-92. Lees, L., Fluid-Mechanical Aspects of Flame Stabilization, "Jet Propulsion", Vol. 24, No. 4, 1954, p. 234.
- 16-93. Putnam, A. A., and Carrier, G. F., A Model of the Flame Holding Mechanism, Battelle Tech. Report 15033-2, WADC, 1953.

Contrails

CHAPTER 17. IGNITION OF COMBUSTIBLE MIXTURES

ABSTRACT

Spark ignition of inflammable gas mixtures has been the subject of extensive experimental and theoretical research for over a hundred years. Weaknesses in early research techniques resulted in conclusions at variance with present knowledge. Recent workers have been successful in correlating ignition test data with significant variables, and with theories, so that the factors in ignition of static gas mixtures are well defined. Important variables are: (a) properties of the gas mixture, including fuel properties, and proportions of fuel, oxygen, and diluents, (b) imposed conditions of pressure and temperature, and (c) spark conditions, including energy and duration of the discharge, and shape and spacing of the electrodes.

Contrails

IGNITION OF COMBUSTIBLE MIXTURES

by

H. R. Hazard

The precise sequence of events leading to ignition of combustible gas mixture by an electric spark or other small source of energy is not yet clearly understood. In spite of sporadic research in spark ignition for the past 150 years, the known variables of spark ignition were related empirically for the first time in the work of Lewis, von Elbe, and associates, published in 1947. In most of the earlier work experimenters observed the effects of one or more variables, but failed to consider others which also affected their data, with the result that a great mass of confusing, contradictory, and incorrect information on spark ignition is widely distributed through the various technical journals.

As an ignition source for studying the mechanism of ignition, an electric spark has the following advantages:

1. The energy interchange from electrical circuit to gas is nearly instantaneous; the discharge duration can be varied from about 0.01 microsecond upward at will.
2. The energy source is highly concentrated; a large amount of energy can be introduced into a small spark gap.
3. Precise measurement of the rates of energy discharge and the total energy of discharge can be made.
4. All of the energy measured passes into the gas to be ignited, so that large corrections are eliminated.

The greatest disadvantage of the electrical spark for ignition research is the uncertainty as to the exact mechanism by which electrical energy causes ignition, and how electrical factors affect results. This objection appears minor compared to the advantages of spark ignition as a research tool.

Ignition sources other than electric sparks have been used, to a certain extent, for study of ignition processes. These include hot particles injected into the explosive mixture, wires or large metal strips heated to known temperatures, and fine fusible wires. In general, these ignition sources have not been so satisfactory as electric sparks, because the rate at which heat was added to the explosive mixture was low, the corrections involved were usually much larger than the energy required for ignition, and interpretation of data was difficult.

At the present time, the most comprehensive and authoritative study of all phases of ignition is that of Lewis and von Elbe published in their 1951 edition of "Combustion, Flames and Explosions of Gases"⁽¹⁷⁻¹⁾. In this Chapter, the data of Lewis and von Elbe has been used as a criteria for evaluation of the data of other experimenters.

HISTORY OF RESEARCH ON SPARK IGNITION

The earliest significant research on spark ignition of gases was that of Sir Humphry Davy, who published the results of his investigations in 1816. Ninety-six years later, H. F. Coward⁽¹⁷⁻²⁾

remarked that "in spite of the interest attaching to the phenomenon of ignition our knowledge of the subject has not increased much since the investigations of Sir Humphry Davy were published in 1816". In this review, the ignition research which took place before 1912 will be ignored, as the state of knowledge at that time was not sufficient to be of particular interest.

The study of ignition during the past 50 years has been carried on through the efforts of a few key personalities, with the help of more numerous collaborators. Because of the small number of research investigations for which results have been published, the general nature of each of them is described below with comments on the value of the test data and the general conclusions of the experimenters. Ignition theories are discussed separately.

H. F. Coward, 1912-1927

H. F. Coward and associates^(17-2, 3, 4) determined the least igniting pressures of gas mixtures using both inductance sparks and capacitance sparks. The use of least igniting pressure as a criterion of ignition requires that ignition occur under quenching conditions, so that all data are limited in this respect. In a variety of experiments it was found that optimum spark lengths existed for various gas mixtures and pressures, that the amount of gas burned in passing a spark under conditions which did not cause ignition was related to spark energy, that ignition was independent of the size and shape of the container, and that all gas burned except for the film at the wall. The work was performed carefully and the results well interpreted.

W. M. Thornton, 1912-1924

Thornton^(17-5, 6, 7, 8) systematically varied electrical and chemical factors, publishing a large mass of data on the effects of spark parameters and gas properties. These data now appear more confusing than enlightening. It is obvious that his data were affected to a variable degree by quenching effects in small spark gaps, making them useless for any present correlation work.

R. V. Wheeler, 1914-1924

Wheeler^(17-9, 10, 11, 12) used fixed spark gaps to determine the least igniting current (in the primary of an inductance coil) for mixtures of various gases at various pressures. In addition, he used "break sparks"⁽¹⁷⁻¹³⁾, in which electrodes in contact were suddenly separated, determining the ignition energy. His energy values were 10 to 20 times those of later experimenters because of quenching effects. Finally, Morgan and Wheeler⁽¹⁷⁻¹⁴⁾ collaborated in experiments in which methane-air mixtures were ignited by inductance sparks using variable spark gaps. It was found that the spark length for minimum ignition energy varied with methane content. Although no energy values were published, the spark lengths reported were similar to recent values⁽¹⁷⁻¹⁾. The significance of the data was completely misinterpreted in a thermal theory in which the effect of spark length was discussed in terms of the concentration of heat in the ignited gas, and the resulting temperature gradients through the gas, involving loss of heat from the source. Loss of heat to the electrodes was not suspected. Although Wheeler's results and techniques were superior to those of previous experimenters, they appear to have little current importance.

J. D. Morgan, 1916-1934

Morgan^(17-15, 16) determined minimum ignition energies for mixtures of coal gas and air using several induction coils with different core arrangements. He found that, although input energy to the coils varied considerably, the output energy for ignition was identical for all

arrangements. In research toward verifying a thermal theory of ignition⁽¹⁷⁻¹⁷⁾, he passed a rapid series of sparks through lean mixtures of carbon monoxide and air, and found that the amount of gas burned was proportional to the heating effect of the arc. He also achieved similar results using a heated wire. The work was crude compared to that of later experimenters, and appears of little value. An attempt to relate thermal and electrical theories of ignition⁽¹⁷⁻¹⁸⁾ was inconclusive. All of the work of Morgan is reviewed in a book published in 1944⁽¹⁷⁻¹⁹⁾.

C. C. Patterson and N. Campbell, 1918

Patterson and Campbell⁽¹⁷⁻²⁰⁾ did a large amount of research on the electrical characteristics of spark circuits and their influence on ignition. In an attempt to control current and duration of sparks from a capacitor, they found that the discharge consisted of a series of sparks of similar voltage and current with time intervals between. Spark duration was shown to be below 50 microseconds. (Values of 0.01 to 1 microsecond are now accepted.)

Experiments with induction coils showed that they produced a series of "capacity sparks" from the characteristic capacitance of the circuit. Ignition, if obtained at all, was obtained with the first spark, which had somewhat higher voltage than successive sparks. Experiments with spark voltage, capacitance, electrode geometry, and electrode material showed variations to be expected under quenching conditions. In a final application of their results, it was shown that the power output of an aircraft engine in dynamometer tests was exactly the same using spark energy of 1.4 millijoules per spark as it had been with the standard ignition system supplying 90 millijoules per spark.

The approach of Patterson and Campbell to the ignition problem was sound, and they published considerable practical information on spark circuits, but the actual data on ignition is of little value because it was obtained under quenching conditions which mask the effect of other variables.

Bone, Frazier, and Witt, 1927

Bone, Frazier, and Witt⁽¹⁷⁻²¹⁾ studied the effect of spark energy on the speed of flame propagation from a spark gap. They found that the velocity of flame propagation was independent of spark energy, although the flame following a high-energy spark was much brighter than that from a low-energy spark.

G. I. Finch and Associates, 1931-1937

G. I. Finch and his several associates conducted an extensive research program to determine the effect of electrical factors on spark ignition. From this work, Bradford and Finch⁽¹⁷⁻²²⁾ arrived at their excitation theory of ignition, which is of interest because it is the only theory which showed that specific electrical factors could be more important in determining the igniting power of a spark than the total energy discharged. Careful analysis of their data indicates that it was obtained under quenching conditions which mask the effect of other variables. Although they have demonstrated that electrical factors such as discharge current, frequency, and duration of inductance sparks can affect igniting power slightly when large quenching effects are present, their interpretation of the data appears extremely questionable.

Finch and Thompson⁽¹⁷⁻²³⁾ observed that the frequency of a capacitance discharge spark, controlled by variables in the electric circuit, influenced the igniting power of the spark to a greater degree than discharge energy or duration. They concluded that specific molecular activation, rather than thermal effects, caused ignition. Ignition energies were about 10,000 times as great as those of recent experimenters⁽¹⁷⁻¹⁾, a result of quenching conditions.

Bradford, Finch, and Prior^(17-24, 25) studied the effects of attenuation of the capacitance and inductance components of coil discharges on their igniting power. They found that the capacitance component contributed nothing to ignition, but that any attenuation of the inductance component reduced igniting power. Careful analysis of the data for these tests shows that the ignition energies observed for the capacitance component of the spark alone were not much higher than those found by recent experimenters; however, as inductance energy was added, the ratio of discharge energy to present accepted values of minimum ignition energy increased from about 10 to about 10,000, indicating that the inductance energy as applied under the test conditions was not effectively used. It is concluded that the work of Finch and associates contributes little to current understanding of ignition, except that it raises a question as to why an inductance spark will sometimes cause ignition under quenching conditions when a capacitance spark of similar energy may not.

H. W. Thompson, 1932

Thompson⁽¹⁷⁻²⁶⁾ used least igniting pressure as a tool to study the reaction mechanism of hydrogen-oxygen mixtures. Mixtures of hydrogen and oxygen were diluted by 12 gases of different physical properties, and ignited by sparks from an induction coil in a fixed spark gap. It was found that the partial pressure of the reactants decreased as the diffusion coefficient of the diluent decreased and as the proportion of the diluent increased. These data were taken as evidence that combustion took place by a chain reaction mechanism. The concept of least igniting pressures appears satisfactory for the type of comparisons made by Thompson, although it is not satisfactory for determining the relation of minimum ignition energy to pressure.

G. Mole, 1936

Mole⁽¹⁷⁻²⁷⁾ proposed a theory of ignition based on the concept of a local ignition source containing active particles which increase in number by chain branching and disappear after a short life. If the number of active particles increases without limit, ignition results.

H. G. Landau, 1937

Landau⁽¹⁷⁻²⁸⁾ developed a theory based on the assumption that the chemical reactions in a small volume surrounding an ignition source are of the chain type. He assumed that the ignition source introduced an initial concentration of active particles, which increased by chemical reaction and were lost by diffusion. If the reaction proceeded so that temperature at the ignition source increased without limit, ignition occurred. In an extension of this theory⁽¹⁷⁻²⁹⁾, a mathematical treatment for ignition from ellipsoidal sources, having as limits a sphere and a cylinder of infinite length, was developed. Landau's theory appears to be of academic interest, as the variables used cannot be measured by conventional means.

H. Herzing, 1937

Herzing⁽¹⁷⁻³⁰⁾ investigated the effects of spark length, spark energy, and fuel-air proportions on the ignition of pentane, heptane, hexane, and air, using sparks from an induction coil to determine least igniting pressures. He was able to plot the usual U-shaped curve of least igniting pressure against mixture ratio, determine an optimum spark length, measure a slight effect of initial gas temperature, and show that the most ignitable mixture was richer for higher molecular weight fuels. Although these experiments were not of particular significance, they again demonstrated the importance of spark length in determining ignition energy.

Viallard^(17-31, 32, 33, 34) measured the minimum energy for ignition of diethyl ether and air, in various proportions, at atmospheric pressure. From his data, he observed that energy for ignition could be represented by the relation: $H=CV^x$, where H is minimum ignition energy, C is capacitance, V is voltage, and x is a constant for each shape of electrode. Viallard concluded that the important variable in ignition was not energy, because discharge energy varies with CV^2 , while his constant, x , varied from 2 to 9, being lowest for pointed electrodes and highest for large spherical electrodes. Lewis and von Elbe (Ref 17-1, p 425) have examined the work of Viallard closely to determine the reason for the variable nature of the voltage exponent, and have concluded that the experiments were conducted using low voltages and high capacitances in such a way that quenching effects caused the variation. With short spark length, where quenching is significant, pointed electrodes minimize quenching effects; the data with other electrode shapes merely show the relative quenching effects in short arcs. Viallard's work appears to contribute little toward an understanding of theoretical aspects of ignition.

A. Hayakawa and R. Goto, 1941

Hayakawa and Goto⁽¹⁷⁻³⁵⁾ investigated ignition of hydrogen-oxygen and hydrogen-air mixtures by electric sparks, relating spark voltage to ignition pressure. Their work does not appear to be significant.

Y. Toryama, S. Saito, and R. Saito, 1942-1943

Toryama, Saito, and Saito^(17-36, 37, 38) observed that energy required for ignition was reduced when a suitable inductance was included in the discharge circuit, that ignition energy was not affected by electrode material, and that blunt electrodes required more energy than pointed electrodes. These data are all typical for short spark gaps in which quenching is a factor. In later experiments they found that energy required for ignition depended on spark length.

J. W. Linnett and Associates, 1945-1949

Linnett^(17-39, 40) studied the effects of diluent gases on the limiting igniting pressures of stoichiometric mixtures of hydrogen and oxygen, and of hydrogen and nitrous oxide. Diluent gases were selected to cover a range of diffusivities and thermal conductivities in an attempt to distinguish between the effects of diffusion and those of thermal conduction. From data with hydrogen-oxygen mixtures, it was concluded that the effect of small quantities of diluent gas was to inhibit diffusion of chain carriers from the ignition center, improving ignition; the effect of large quantities of diluent was thermal, extreme dilution lowering the temperature resulting from the initial ignition processes, slowing the reaction and making ignition more difficult. The theory developed by Linnett⁽¹⁷⁻³⁹⁾, which is based on the previous theory of Mole⁽¹⁷⁻²⁷⁾, appears to explain the data satisfactorily. This theory is based on the assumption that ignition occurs if the rate of formation of chain carriers exceeds the rate of loss of chain carriers by diffusion to surrounding gas.

From the data on nitrous oxide-hydrogen mixtures it was concluded that the ignition of this mixture was thermal in character, and was governed largely by thermal properties of the mixture. In comparing the results with different diluents it was found that the relation of the ratio of ignition energy/heat capacity to heat capacity was a straight line for mixtures with each diluent gas, which was in accord with the requirement of a thermal theory of ignition, that the temperature at the ignition source should increase without limit. Thermal conductivity appeared to outweigh thermal capacity in importance. The data and conclusions of Linnett are of interest because of his success in delineating conduction and diffusion effects in ignition.

Boyle and Llewellyn^(17-41, 42) attempted to clarify the effects of various variables influencing accidental ignition of solvent vapors and dusts by electric sparks. Their results were of good accuracy, agreeing quite closely with the most recent data, and their conclusions regarding the important ignition variables were correct. Variables investigated included circuit capacitance, circuit resistance, electrode configuration and spacing, and initial gas temperature. One result on which other experimenters had reported little was the effect of circuit resistance on minimum ignition energy. It was found that the principle result of adding resistances from 10,000 to 500,000 ohms was to slightly raise the voltage required for spark discharge raising the discharge energy slightly. Data were not exact enough to measure the effect of initial gas temperatures up to 200 F, although later experimenters have shown an effect⁽¹⁷⁻⁵⁴⁾.

Llewellyn⁽¹⁷⁻⁴²⁾ reported minimum ignition energies for dust clouds in air. It was found that spark duration, varied by circuit resistance, greatly influenced ignition energy; minimum energy was obtained with a spark duration of about 2000 microseconds. Values of minimum ignition energy for dusts and vapors are compared in Table 1. Ignition of dusts required 15 to 2500 times the energy required for the least ignitable vapor. The experimental method used for these tests may have resulted in quenching, leaving some doubt as to whether the values tabulated are actually minimum values.

TABLE 17-1. MINIMUM IGNITION ENERGIES FOR EXPLOSIVE
 DUST CLOUDS AND VAPOR-AIR MIXTURES

Explosive material	Particle size, microns	Ignition energy, millijoules
Aluminum	90	55
Magnesium	40	25
Ferro-manganese	100	250
Zinc	100	150
Silicon	50	2500
Acaroid resin	20	60
Calcium silicide	10	700
Methyl methacrylate	10-100	17
Carbon disulphide	(Vapor)	0.15
Heptane	(Vapor)	1.10

B. Lewis, G. von Elbe, P. G. Guest, M. V. Blanc, and W. Roth, 1944-1952

The most comprehensive and authoritative work on spark ignition yet published was that conducted at the Bureau of Mines under the direction of Lewis and von Elbe. This work, for the first time, quantitatively related several variables of spark ignition which had been previously observed in qualitative form by other experimenters. A complete description of this work has been published in book form⁽¹⁷⁻¹⁾, but all but the most recent of the several different investigations have also been described fully in technical journals^(17-43, 44, 45, 46). As the information is already widely available, only the most important features of this work will be outlined here.

The technique and apparatus used in this work have been described by Blanc, Guest, von Elbe, and Lewis^(17-43, 44), and by Lewis and von Elbe⁽¹⁷⁻¹⁾. The apparatus consisted of an explosion bomb containing a spark gap, a bank of capacitors, and a high-voltage power source

Continued

isolated from the spark gap circuit by a rotary charge conveyer or, interchangeably, a 10^{11} -ohm resistor. The explosion bomb was 5 inches in diameter, constructed of stainless steel, and arranged so that gas mixtures at any selected pressure could be ignited. The spark gap had one fixed electrode and one movable electrode which could be accurately positioned with a micrometer screw. For measurement of quenching distances and minimum ignition energy, the electrodes were fitted with flush 1-in.-diam. glass flanges, which sharply delineated the quenching distance. Electrodes of other shapes were also used to obtain comparative data. The electrical circuit included the spark gap, a bank of air capacitors continuously variable from 1 micro-microfarad to 5000 micro-microfarads, and a voltmeter. Provisions were made to insert external resistances and inductances in series with the spark gap for a few tests. For the smallest capacitance values the electrodes alone served as the capacitor.

To determine the minimum ignition energy of a selected gas mixture, the test bomb was charged to the test pressure, the electrode spacing was set at a reasonable value, the circuit capacitance was adjusted, and the charge in the capacitor was gradually built up until discharge occurred. The capacitance was varied in successive tests to find the minimum value at which ignition could be obtained. The process was then repeated for different electrode spacings to determine the optimum spacing at which ignition energy reached a minimum. This spacing also corresponded to the quenching distance when glass-flanged electrodes were used. Using this technique, a large mass of accurate data on quenching distances and minimum ignition energies for many gas mixtures over a wide range of pressures was determined. These data are presented in full in Reference (17-1), and in less detail in References (17-43) and (17-44).

Figure 17-1 shows the relation of ignition energy to spark-gap geometry for a mixture containing 8.5 per cent methane in air, at a pressure of 0.33 atmosphere. The values of ignition energy for the glass-flanged electrodes were constant as the electrode spacing was reduced from 0.35 in. to 0.25 in., but at 0.24 in. the mixture could not be ignited with any energy input. For a spark-gap configuration in which the positive electrode was tipped by a 1/16-in. sphere, and the negative electrode had a glass flange, it will be noted that ignition was obtained with electrode spacings down to 0.15 in., but that ignition energy increased as electrode spacing decreased, because of quenching from the electrodes. With pointed electrodes, ignition could be obtained with still smaller spark gaps, and the rate at which ignition energy increased below the quenching distance would be less. However, regardless of electrode shape, the minimum ignition energy would be obtained with an electrode spacing of 0.25 in. The value of minimum ignition energy was not affected by electrode shape, nor were the values of ignition energy for electrode spacings greater than the quenching distance. This explains why some experimenters found a very great effect of electrode shape on ignition energy, while others found no effect, and also why published values of ignition energy for specific mixtures and pressures vary so widely.

Figure 17-2 shows minimum ignition energies and quenching distances for various mixtures of propane, oxygen, and nitrogen at pressures of 1 to 0.2 atmospheres. Ignition energy was increased by reduction of pressure or by diluting a propane-oxygen mixture with nitrogen. The curves for quenching distances are similar to those for ignition energy.

Figure 17-3 shows the relation of quenching distance to absolute pressure for methane, propane, butane, hexane, heptane, and ethane in air.

Figure 17-4 shows the relation of minimum ignition energy to absolute pressure for methane and other gases in air. In general, the ignition energies for the hydrocarbon compounds are similar, but that for hydrogen is much lower.

Figure 17-5 shows the relation of minimum ignition energy to quenching distance for hydrocarbon-nitrogen-oxygen mixtures at various pressures. It appears significant that the minimum ignition energy should be proportional to the square of the quenching distance over such a wide range of values, and with so little deviation. This relation was used as the basis for the 1951 treatment of the Lewis and von Elbe theory of minimum ignition energy.

The effects of circuit resistance, inductance, and discharge voltage on ignition energy were investigated over a narrow range of values and found negligible. When resistances up to 30 ohms were placed in the discharge circuit, no effect on minimum ignition energy could be measured.

Contrails

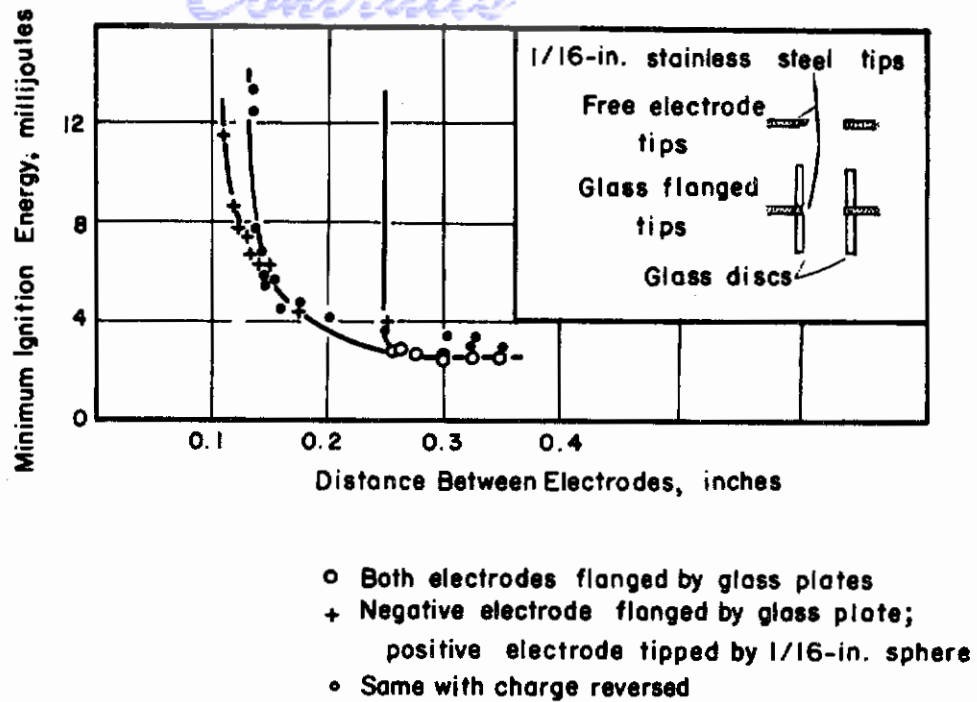


FIGURE 17-1. RELATION OF MINIMUM IGNITION ENERGY TO SPARK-GAP SPACING AND SHAPE FOR MIXTURE CONTAINING 8.5 PER CENT METHANE IN AIR, AT 250 mm Hg ABSOLUTE.

Lewis and von Elbe(17-1), p 395

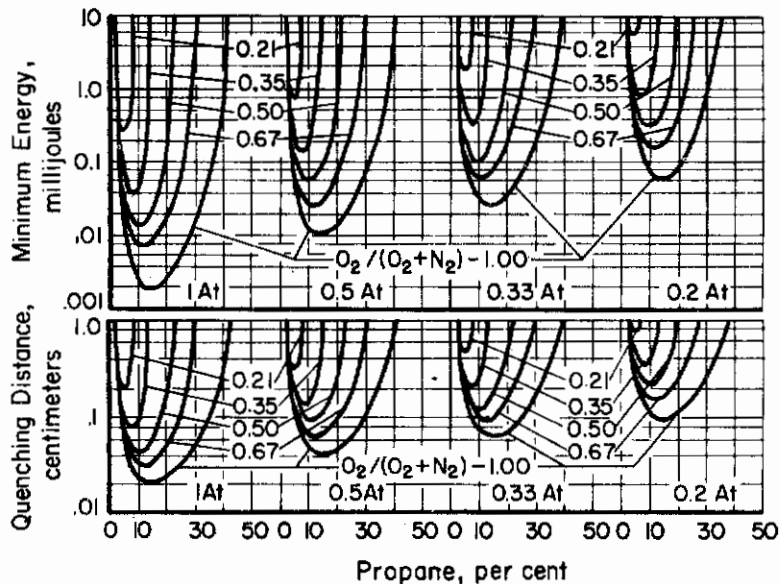


FIGURE 17-2. MINIMUM SPARK IGNITION ENERGIES IN MILLIJOULES OF PROPANE, OXYGEN, AND NITROGEN AT ONE ATMOSPHERE PRESSURE AND LOWER, AND QUENCHING DISTANCES BETWEEN FLANGED ELECTRODES FOR THE SAME MIXTURES. CURVES CORRESPOND TO CONSTANT RATIOS OF OXYGEN AND NITROGEN.

Lewis and von Elbe(17-1), p 412

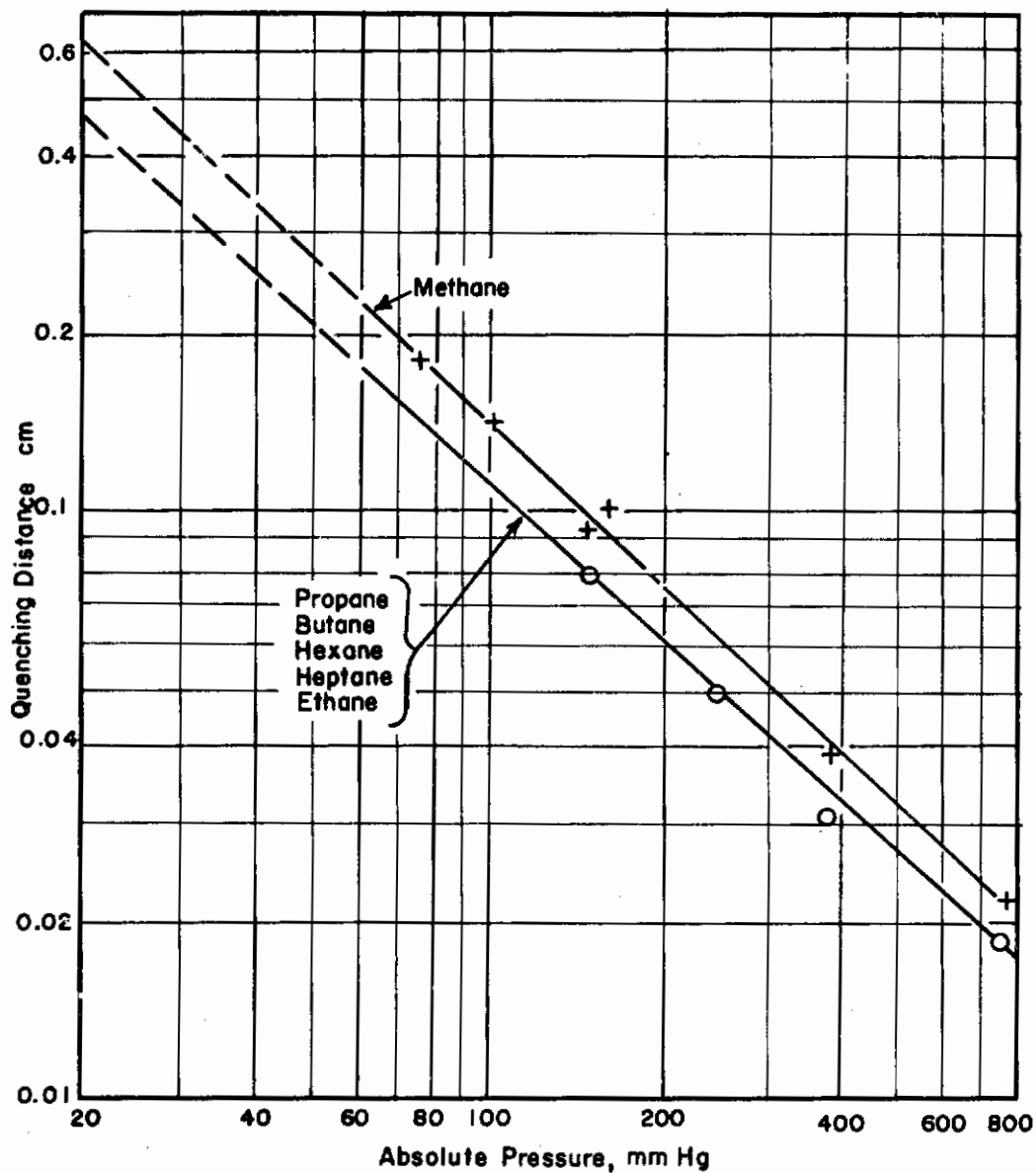


FIGURE 17-3. RELATION OF QUENCHING DISTANCE TO STATIC PRESSURE FOR METHANE, PROPANE, BUTANE, HEXANE, HEPTANE, AND ETHANE WITH AIR

Lewis and von Elbe⁽¹⁷⁻¹⁾, p 408-413

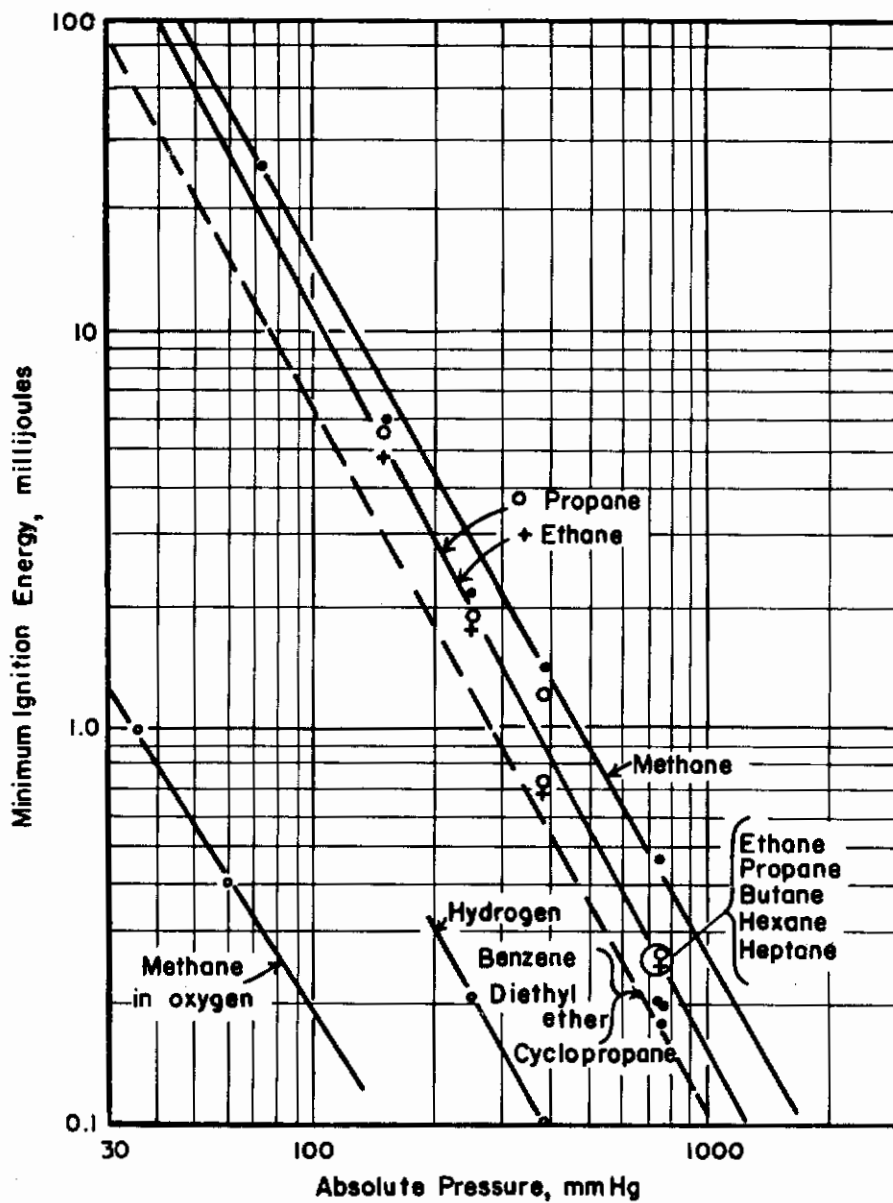


FIGURE 17-4. RELATION OF MINIMUM IGNITION ENERGY TO STATIC PRESSURE FOR HYDROCARBON FUELS IN AIR

Lewis and von Elbe(17-1)

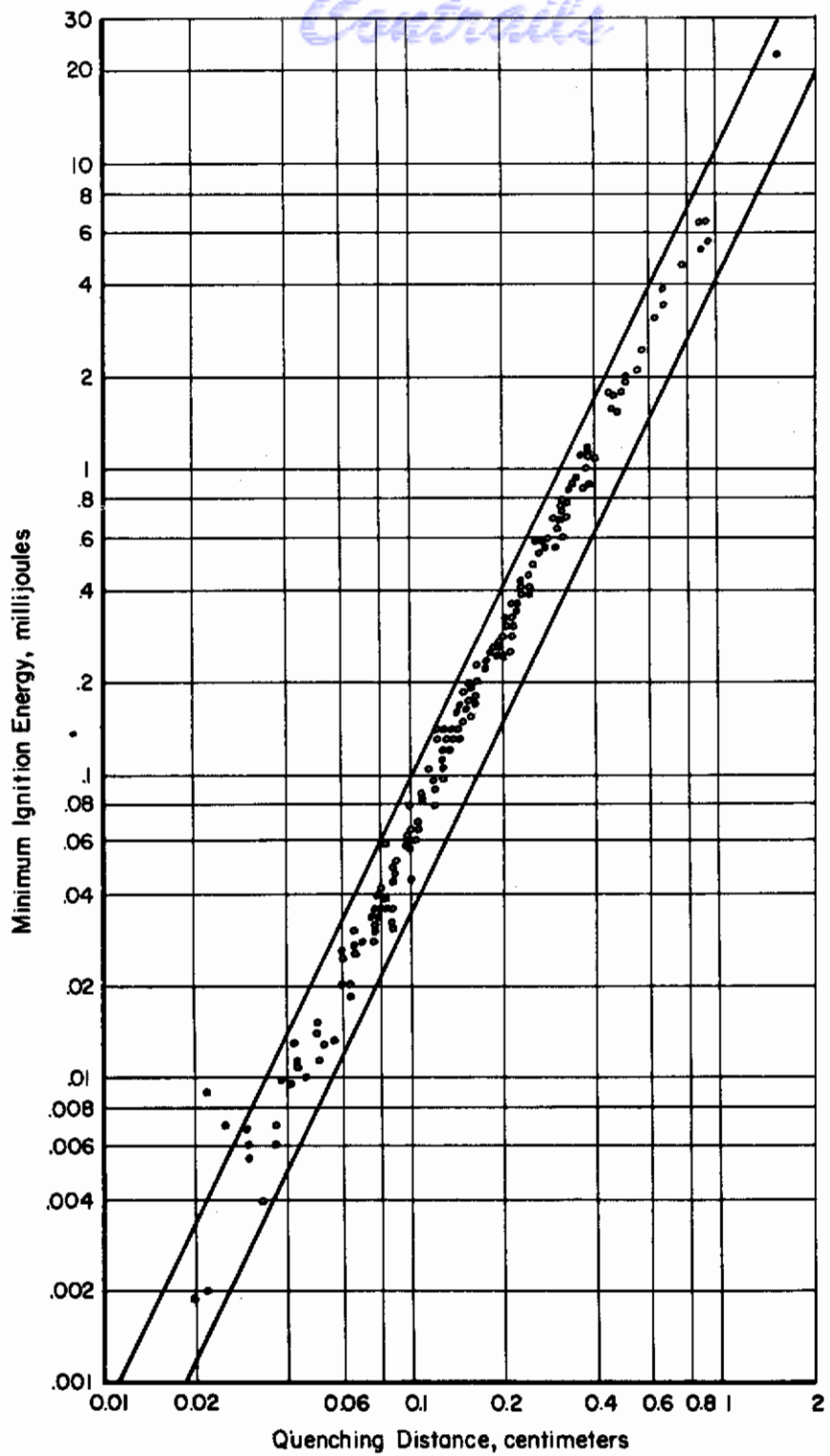


FIGURE 17-5. RELATION OF MINIMUM IGNITION ENERGY TO QUENCHING DISTANCE FOR HYDROCARBON-OXYGEN-NITROGEN MIXTURES

Lewis and von Elbe(17-1), p 415

Insertion of inductances made from a few turns of heavy copper wire also resulted in no measurable effect. In a few tests, the discharge voltage was increased above the breakdown voltage of the spark gap by using a quick-acting switch between the capacitors and the spark gap. It was found that very small increases in minimum ignition energy, which could not be readily duplicated, occurred with high voltages; these were attributed to turbulence in the spark gap, which was greater at high voltages, and which would affect somewhat the shape of the initial flame and, consequently, the energy losses from the flame. A much more detailed study of the effects of electrical factors on spark structure and ignition characteristics is now in progress, using a two-channel oscillograph to measure voltage and current, and high-speed (2500 frames per sec.) photography to show spark configuration.

Roth, Guest, Lewis and von Elbe^(17-1,46) made calorimetric measurements of the heat generated by electric sparks and the rate at which energy was absorbed by electrodes, and found that all of the energy stored in the capacitance of the spark circuit was available for ignition in the spark gap at the moment of discharge, but that heat loss to the electrodes occurred at an appreciable rate from the moment of discharge.

H. Morris, 1949

Humbert Morris⁽¹⁷⁻⁴⁷⁾, in a discussion of the data of Blanc, Guest, Lewis and von Elbe, pointed out two approximate relations not discussed by Lewis and von Elbe, as follows: For the optimum spark-gap width, the number of gas molecules in the effective part of the spark gap is independent of pressure and characteristic of the gas mixture. The effective part of the minimum ignition energy per molecule of gas varies with the square of the partial pressure of oxygen. These relations may prove of interest in future study of ignition theory.

R. Friedman and E. Burke, 1949

In discussing the 1947 theory of spark ignition advanced by Lewis and von Elbe, Friedman and Burke⁽¹⁷⁻⁴⁸⁾ point out that the loss of energy from the ignition center by diffusion can be equal to or even greater than the loss by thermal conduction, and suggest that a theory which considers only thermal mechanisms of energy transfer is fundamentally weak. They also observe that the correlation of minimum ignition energy with the square of the measured quenching distance is better than with the quenching distance calculated by the Lewis and von Elbe theory. In the 1951 treatment of their theory of minimum ignition energy, Lewis and von Elbe show that the relation of minimum ignition energy to the square of the quenching distance is consistent with their theory.

C. C. Swett, Jr., 1948-1951

Swett, at the NACA Lewis Laboratory, investigated the ignition of flowing propane-air mixtures at low pressures and temperatures. His work included a study of sparks in high-velocity air streams, a study of energy required to ignite flowing propane-air mixtures, a study of the effects of electrode parameters on ignition energy, and a study of the effects of turbulence on ignition.

In a study of spark discharges in an air stream^(17-49,50), an oscilloscope was used to measure energy, average power, and discharge time under various conditions of air velocity, electrode spacing, electrode diameter, pressure, temperature, and spark duration. It was found that average power increased with pressure, velocity, and electrode spacing, and that electrode diameter and air temperature had negligible effect. Air velocities up to 570 fps were used with pressures from about 5 to 25 in. Hg and temperatures as low as -70 F. Spark energy varied from 50 to 250 millijoules per discharge, and discharge time varied from 200 to 700 microseconds. Air velocity caused the discharge to blow downstream and to terminate after a short time.

In a second investigation(17-49,51), Swett determined the minimum energy requirements to ignite flowing combustible mixtures of propane and air in the pressure range of 2 to 4 in. Hg. Spark duration was varied from 1.5 to 25,000 microseconds, gas velocity was varied from 5 to 54 fps, and fuel/air ratio was varied over a wide range. At a pressure of 3 in. Hg, the minimum ignition energies for velocities of 5 to 54 fps occurred at fuel/air ratios of 0.08 to 0.095. The energy required for ignition increased almost linearly with increasing gas velocity in the range of 5 to 54 fps. For a spark duration of 600 to 800 microseconds, minimum ignition energies for a velocity of 5 fps and pressures of 2, 3, and 4 in. Hg absolute were 57, 32, and 14 millijoules, respectively. At a gas velocity of 54 fps, corresponding values were 84, 58, and 42 millijoules, respectively. When extrapolated to zero velocity, these values are in good agreement with those of Lewis and von Elbe. When the spark duration was varied from 25,000 microseconds to 1.5 microseconds, the energy required for ignition was lowest for sparks lasting 125 to 1000 microseconds. At 3 in. Hg and 54 fps, ignition energy was 150, 35, and 500 millijoules for spark duration of 1.5, 125, and 25,000 microseconds, respectively.

In a third investigation(17-52), the effects of electrode spacing, configuration, and material on the energy required for ignition of a flowing propane-air mixture were determined. In addition, the energy distribution along the spark length was determined, and previous measurements of the effect of spark duration were confirmed. Data were obtained at a pressure of 3 in. Hg absolute, a temperature of 80 F, a mixture velocity of 5 fps, and a fuel/air ratio of 0.0835 by weight. It was found that the energy required for ignition decreased as the electrode spacing was increased, with the minimum energy at a spacing of 0.65 in. for large electrodes. Small-diameter electrodes or pointed electrodes required less energy for ignition than large-diameter electrodes if the spacing was less than 0.65 in. At larger spacings no difference was noted.

Significant effects of electrode material on ignition energy were ascribed to differences in the type of discharge produced; glow discharges, which required higher energy for ignition than arc-glow discharges, were usually produced by all electrodes except those coated by cesium oxide. With pure glow discharges, the ignition energy was constant for electrodes of lead, cadmium, brass, aluminum, and tungsten.

In determining energy distribution along a glow discharge, it was found that one-third to one-half the spark energy was concentrated in a small region near the cathode electrode, and the remainder was uniformly distributed across the spark gap.

A detailed comparison of long-duration sparks and short-duration sparks showed that the ignition energy for long-duration sparks was much less than that for short-duration sparks. At zero stream velocity, and with a spark duration of about 1 microsecond, 22 to 24 millijoules were required for ignition, compared with a value of 22.7 published by Lewis and von Elbe(17-1). For a velocity of 5 fps, the ignition energy for a 1-microsecond spark was 34 to 36 millijoules. For a spark duration of 600 microseconds, however, the ignition energy with a mixture velocity of 5 fps was only 10.7 to 19.6 millijoules, depending on whether a glow or arc-glow discharge was formed. Photographs showed a distinct difference between long-duration sparks and short-duration sparks; with short-duration sparks, fairly large luminous zones surrounded the spark near each electrode, but with long-duration sparks, only one luminous zone appeared, and this was downstream from the spark. This appeared to indicate that the energy distribution in the sparks was different, but there was no means of measuring the energy distribution in the 1-microsecond spark.

In a later publication(17-53), Swett attempted to correlate his data for ignition energy as a function of stream velocity by assuming that, as the spark was blown downstream, only that portion of the total energy dissipated in a length equal to the spark gap spacing was effective. If the rate of dissipation in the spark is constant and uniform across the gap, this leads to the relation:

$$\Delta H = \Delta H_0 \left(\frac{2V\theta}{S \ln \left(\frac{2V\theta + S}{S} \right)} \right)$$

where ΔH is the required energy for ignition, H_0 is the ignition energy for zero stream velocity,

V is the stream velocity, θ is the discharge duration and S is the gap spacing. However, the correlation appears to be of a form which does not effectively explain the data. The effects of velocity and discharge duration appear to be independent to at least a first approximation.

In an investigation of the effect of turbulence on ignition energy⁽¹⁷⁻⁵³⁾, Swett found that the fluctuating velocity was the important factor and that the integral scale had no measurable effect. This suggests a diffusion mechanism similar to that given by Equation (12-60).

The work of Swett is of particular interest because, for the first time, the effects of flow variables on minimum ignition energy were investigated and the effect of duration of the spark discharge was explored. The fact that a spark may take more than one form, thus requiring more or less energy for ignition, had not previously been demonstrated. The relations of electrode size and spacing to minimum ignition energy under flow conditions proved similar to those previously found under static conditions.

H. F. Calcote and Associates, 1949-1952

Under the direction of H. F. Calcote, determinations of minimum ignition energy have been made for a large number of chemical compounds. An attempt was made to correlate minimum ignition energy with molecular arrangement rather than physical properties of the gas mixture, with some success. The data are in good agreement with the 1951 Lewis and von Elbe theory of minimum spark ignition energy.

Calcote, Gregory, Barnet, and Gilmer⁽¹⁷⁻⁵⁴⁾ have reported minimum ignition energies for 74 chemical compounds, in stoichiometric proportions with air at atmospheric pressure. In addition, they have reported data relating minimum ignition energy to quenching distance for 16 compounds, and the effect of fuel/air ratio for 12 compounds. Comparative data showed that minimum ignition energies measured using flanged electrodes, as described by Blanc, Guest, von Elbe, and Lewis⁽¹⁷⁻⁴³⁾, were higher than those measured using plain electrodes by a predictable amount. Otherwise, the data are in good agreement with those of Lewis and von Elbe where comparison is possible. Minimum ignition energy varied approximately with the square of the quenching distance (actually with the 2.48 power over a relatively narrow band of values), for the compounds for which quenching distance was measured.

Figure 17-6 shows the relation of minimum ignition energy to absolute pressure for a number of compounds in air, as determined by Calcote, et al. Some data from Lewis and von Elbe are included for comparison. In comparing minimum ignition energies with molecular weight and arrangement of compounds, the following conclusions were drawn:

1. Hydrocarbon ignition energies decreased in the order: alkanes, alkenes, and alkynes.
2. An increase in chain length, or chain branching, increased ignition energy.
3. Conjugation generally lowered the ignition energy.
4. For long chains, the effect of structural variation was small, but for short chains the effects were much larger.
5. Negative substituent groups resulted in increasing ignition energy in the order: mercaptan, alcohol, chloride, and amine group. The effect of chlorides and amine groups were particularly large.
6. Primary amines increased ignition energy more than secondary or tertiary amines.
7. Ethers and thioethers increased ignition energy.
8. The peroxide group lowered the ignition energy greatly.

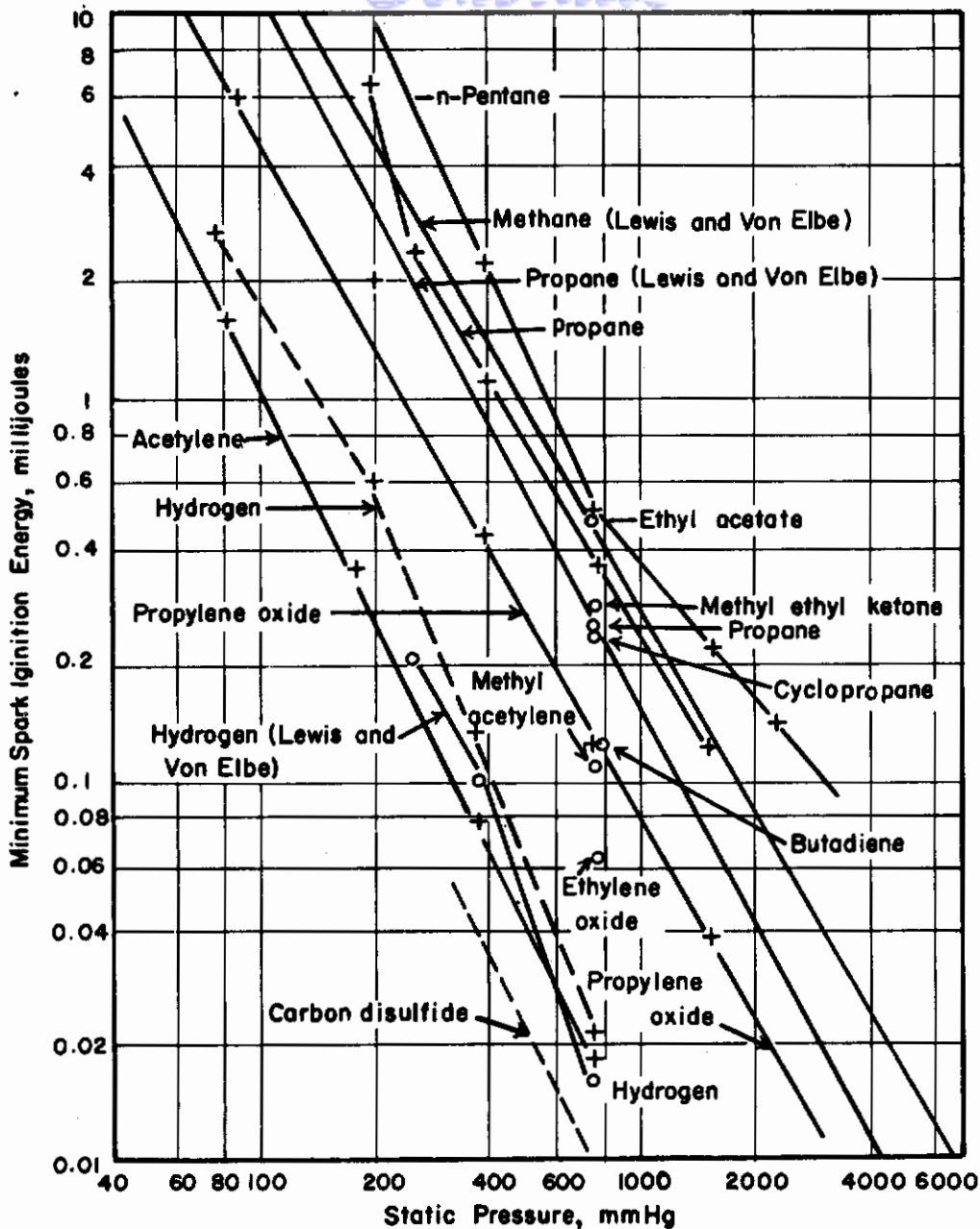


FIGURE 17-6. RELATION OF MINIMUM IGNITION ENERGY TO STATIC PRESSURE FOR A NUMBER OF COMPOUNDS IN AIR

Experiment, Inc. (17-54), Lewis and von Elbe (17-1)

9. Esters and ketones increased ignition energy greatly, but aldehydes raised ignition energy only slightly.

10. Ignition energies for three-cornered rings were very low, particularly with the oxygen ring.

11. Six-membered saturated compounds had relatively high ignition energies, but those of five-membered rings were about average.

12. Ignition energies for aromatics were similar to these for linear hydrocarbons containing the same number of carbon atoms.

The data presented appear to be precise and reliable, and should be of great value in evaluating future ignition experiments and theories because of the wide range of chemical and physical properties of compounds for which data were obtained.

Gregory, King, Calcote⁽¹⁷⁻⁵⁵⁾ have reported an investigation of the effect of initial gas temperature on minimum ignition energy. Ignition energies were determined for hydrogen, acetylene, carbon disulphide, propylene oxide, propane, n-pentane, n-heptane, and iso-octane, at temperatures from -50 C to 250 C. In all instances, ignition energy decreased as temperature increased. For iso-octane, ignition energy decreased from 2.8 millijoules to 0.46 millijoule as temperature was raised from 25 C to 175 C. When ignition energy was plotted against temperature on semilogarithmic coordinates, the data fell on straight lines having different elevations and slopes for different compounds, indicating a relation of the form $H = Ae^{BT}$, where H is the ignition energy, A and B are constants which are different for different compounds, and T is initial temperature.

A paper by Fenn⁽¹⁷⁻⁵⁶⁾ discusses the relation of lean flammability limit to minimum spark ignition energy.

Y. B. Zeldovich and N. N. Simonov, 1949

Zeldovich and Simonov⁽¹⁷⁻⁵⁷⁾, working at the Academy of Science, USSR, Moscow, have developed a theory of ignition based on original data. The original publication, in Russian, has not been obtained, but the following information is available from Chemical Abstracts:

If a gas explosion is induced by a spark of energy E , ignition follows the law:

$$E = Qk \lambda^3 \eta u^3 C_p \rho^2 ,$$

where Q is the heat of reaction, k is a constant, η is the coefficient of utilization of the ignition energy, u is the linear velocity of flame propagation, C_p is the heat capacity, λ is the thermal conductivity, and ρ is the thermal diffusivity of the reaction products.

The coefficient of utilization of spark energy was determined by discharging condensers at the lowest discharge voltage through NH_3 gas, measuring the amount of NH_3 decomposed, and assuming that 23,000 cal/mol were required for decomposition. This coefficient was independent of the number of sparks and of the length of the spark gap, but varied with the capacitance, being proportional to the (-0.24) power of capacity, and varied slightly with pressures from 40 to 760 mm.

The equation was applied to data for mixtures with oxygen of CO , H_2 , and $CO-H_2$. The minimum ignition energy of these mixtures was determined at pressures of 50 to 760 mm, and the value of k determined as 12, which infers that the calculated radius of the sphere raised to flame temperature by the spark was larger than the width of the heated zone in a stationary flame, by a factor of 3. This factor of 3 is also satisfied by the experiments of Lewis and von Elbe, whose theory Zeldovich believed to be incorrect. Photographs of spark ignition show radii of luminous spheres to be 1.3 times the calculated radius for CO_2-H_2O mixtures, and 0.7 times the calculated radius for CO_2-H_2O mixtures.

From the above information, there appears to be considerable room for question about the validity of the theory. Only CO and H_2 in O_2 were examined, quenching effects from the electrodes appear to have been ignored, the ignition energy varied with capacitance, and the "minimum voltage for ignition" was used. From these considerations, the theory would appear to be of little value. However, Zeldovich is an experienced worker in the field of ignition and combustion research, and was familiar with the work of Lewis and von Elbe. Consequently, it appears reasonable to reserve judgement of this work until it can be evaluated in greater detail.

Olsen and Gayhart(17-58, 59, 60), of the Applied Physics Laboratory, have investigated the use of high-speed-flash schlieren photography for study of the early stages of ignition and flame propagation in high-velocity gas streams, and the use of explosive grains of powder as ignition sources. In initial qualitative studies, test and analytical techniques suitable for quantitative measurements were developed.

The technique for study of early stages of ignition was based upon photographing a succession of identical sparks, at increasing intervals following the spark discharge, to obtain a series of pictures showing the growth of the small "kernel" of heated gas formed by a spark. The spark was produced by the discharge of a condenser through the spark gap, triggered by an auxiliary spark from a small induction coil. The schlieren photographs were obtained using GE FT-108 flash tube, producing a light flash of about 1 microsecond duration. A timing circuit introduced a preselected time interval between the spark discharge and the light flash. In a typical series of pictures, this time interval was increased from 20 microseconds to 65 microseconds in steps of 5 to 10 microseconds. Steps of 5 microseconds would produce a series of pictures equivalent to motion pictures of a single spark taken at 200,000 frames per sec.

It was found that after the shock wave separated from the heated kernel about 2 microseconds after the 1/4-microsecond discharge; the kernel expanded according to the adiabatic expansion law. Four microseconds after the discharge, the pressure behind the shock wave was approximately 2.5 atmospheres. For a 250 millijoule spark, pressure equilibrium was reached in about 16 microseconds. Photographs taken at intervals longer than 30 microseconds showed that the kernel developed into a torus, with the volume increasing slowly. Calculations indicated that a considerable portion of the spark energy, as high as 30 per cent, was dissipated as work against the atmosphere by the expanding kernel. The same general sequence of events was observed for sparks in air, in oxygen, and in a propane-air mixture.

The use of explosive particles as ignition sources was also studied. This has the advantage of eliminating the quenching effects of spark electrodes from consideration, and of permitting variation of the chemical species introduced into the ignition zone by the ignition source. In preliminary tests, a Bunsen burner was ignited using small grains of black powder suspended by a wire of 0.0015-inch diameter, and exploded by a concentrated light beam. In tests with grains of different sizes, it was found that powder grains larger than 25 micrograms, providing combustion energy of 75 millijoules or more, caused ignition. This energy is probably about 100 times the minimum ignition energy measured using spark ignition, but the technique may be developed to give comparable data.

A. J. Metzler, 1952

Metzler(17-61), at the NACA Lewis Laboratory, has reported minimum ignition energies for ethane, ethylene, acetylene, n-hexane, cyclohexane, and benzene, and correlated minimum ignition energy for these fuels with flame speed. Mixtures of fuel vapor in air were ignited in a bomb under static conditions at pressures from 50 to 100 mm Hg, and fuel/air ratios were varied over a sufficient range to determine the mixture for minimum ignition energy. Data were for a temperature of 100 F and a spark duration of 1000 microseconds, and are in general agreement with data of Lewis and von Elbe(17-45), and of Calcote(17-54). When minimum ignition energy was plotted against pressure on log-log coordinates, data fell on straight lines having a slope of -1.76; data of Lewis and von Elbe, by comparison fell on lines with a slope of -1.84.

An excellent correlation between minimum ignition energy and flame velocity at atmospheric pressure was found. On a log-log plot all data fell on a straight line having a slope of -0.8. Further correlation of data along these lines was recommended.

Hazard⁽¹⁷⁻⁶²⁾ has published a comprehensive review of research on spark ignition which discusses critically all important published results of research on spark ignition since 1900.

A. E. Weller, 1953-1955

Weller⁽¹⁷⁻⁶³⁾ has in progress an investigation of ignition of fuel mists by electric sparks. In this work fuel droplets of uniform size are produced by a spinning-disc atomizer, entrained in air, and passed through a spark gap within a time interval of the order of 10 milliseconds. This minimizes the evaporation of liquid fuel, so that essentially only fuel drops and air are present in the spark gap. Preliminary data indicate that the energy required to ignite kerosine drops is very much greater than the energy required to ignite kerosine vapor. Occasional ignition could be obtained with ignition energy of 20 millijoules; increasing ignition energy to 160 millijoules raised this frequency to 25 per cent, and energy of 4 joules was required for ignition frequency of 100 per cent. Tests in which a drop of kerosine was deliberately placed on the electrodes showed a marked increase in ignition frequency. Following considerable refinement of equipment, which appears necessary, it is planned to continue this investigation to obtain data on effect of drop size, fuel/air ratio, electrode spacing, and fuel properties on energy required for ignition.

IGNITION THEORIES

The relative importance of mass diffusion and of thermal conductivity as mechanisms for energy transport in flame fronts has been a controversial subject for many years. Because the laws for the two mechanisms are the same, and the diffusion and conduction coefficients for individual materials usually vary in a similar manner, it has proved extremely difficult to devise experiments which show conclusively the extent to which each of the two mechanisms affects flame propagation. Since ignition is a special case of flame propagation, ignition theories also fall into two groups, those in which the diffusion mechanism is considered as the important consideration, and those in which thermal mechanisms are considered most important. The theories of Mole and Linnett represent the first group, and the theories of Taylor-Jones, Morgan, and Wheeler, Lewis and von Elbe, and of Fenn fall in the second group. The theory of Landau considers both processes, but eliminates diffusion processes in the derivations. Both the Lewis and von Elbe theory, and the Linnett theory have been supported by test data, but a final conclusion regarding the relative importance of the diffusion and conduction processes, and their proper treatment in an ignition theory, does not appear possible at this time.

The empirical correlation of minimum ignition energy with quenching distance is excellent, and it now appears possible to predict minimum ignition energies for gas mixtures under any required conditions, either by use of the empirical correlation or by use of the Lewis and von Elbe theory of minimum ignition energy.

At the present time, there are eight theories which have been formulated to describe ignition from electric sparks. The authors of these theories, and their dates of publication, are listed below:

<u>Date of Publication</u>		<u>Date of Publication</u>			
1.	1922	Taylor-Jones, Morgan, and Wheeler	5.	1947	Lewis and von Elbe
2.	1936	Mole	6.	1951	Lewis and von Elbe
3.	1937	Landau	7.	1949	Zeldovich and Simonov
4.	1945	Linnett, Raynor, and Frost	8.	1952	Fenn

The thermal theory of Taylor-Jones, Morgan, and Wheeler is based on the assumption that the requirement for ignition is the heating of a critical volume of gas to a critical temperature. The most effective ignition source would heat only this volume to the required ignition temperature with no loss of heat to surrounding gas before ignition.

The activation theory of Mole describes a mechanism in which a local source of ignition introduces into a small volume of gas a number of active particles, and assumes that if these active particles multiply without limit, ignition results.

The Landau theory assumes that an ignition source introduces a number of active particles into a small volume, and these multiply by chain branching or are lost by diffusion. A heat-generating reaction proceeds at a rate proportional to concentration of active particles, and heat is lost by conduction. If the temperature at the ignition source increased without limit, ignition results.

Linnett and associates obtained qualitative data relating the effects of diffusivity and thermal conductivity of gas mixtures to the relative difficulty of ignition, and extended the general method of Mole to evaluate these data. Equations relating ignition to diffusion characteristics of gases appeared to explain the data satisfactorily.

The 1947 theory of Lewis and von Elbe attempted to relate the minimum spark-ignition energy to the physical properties of the gas mixture, including conductivity, flame speed density, and quenching distance. The correlation of minimum ignition energy with these variables was good.

The 1951 theory of Lewis and von Elbe was based on the experimentally determined relation $E = Cd^2$, where E is the minimum ignition energy, C is a constant, and d is the quenching distance. It was shown that this empirical relation is consistent with physical properties of the gas mixture.

The Thermal Theory of Taylor-Jones, Morgan, and Wheeler

The thermal theory of Taylor-Jones, Morgan, and Wheeler was based upon the premise that the fundamental requirement for ignition is that a critical volume must be heated to a critical ignition temperature. An attempt was made to relate this premise to experimental data by analyzing the temperature gradients around ignition sources in which the volume of heat source and the rate of heat supply were varied.

In comparing this theory to experimental results, qualitative verification was assumed from the following facts: Ignition energy was lowest for a critical spark-gap length, and increased when the spark gap was lengthened or shortened. (The increase in energy when the spark gap was shortened, however, is now explained as resulting from loss of energy to the spark electrodes, and not as the result of an overly "concentrated" energy source. The dispersion of energy over a volume larger than the critical volume increases ignition energy regardless of the theory assumed). Capacitance sparks of extremely short duration required less energy than inductance sparks of extremely long duration.

It is now possible to examine the theory on a quantitative basis, rather than to rely on qualitative observations. If we apply the theory to the data of Lewis and von Elbe (Reference 17-1), a discrepancy is immediately apparent. These data show that the minimum ignition energy varies with the square of the quenching distance (see Figure 17-5), which may be assumed to be a linear function of the diameter of the critical spherical volume of the thermal theory. The variables in a thermal theory would include specific heat, ignition temperature, and critical volume, which would vary with the cube of the quenching distance. However, the quenching distance is proportional to the thermal conductivity of the gas in the spark gap, and, therefore, to the rate of heat loss from the ignition source. In order for the thermal theory to be consistent with the relation of ignition energy with the square of the quenching distance, it would be necessary that the variation of diameter of the initial sphere be less than proportional to the quenching distance. The required ignition temperature might also be increased as the conductivity increased, as the rate of heat loss over the "sufficient time" for ignition would be greatly increased.

The principal objection to this theory is the fact that it is based upon the idea of a fixed ignition temperature, which is not in accord with present knowledge of chain-branching mechanisms. For nonchain-branching reactions, which are rare, the thermal theory may be adequate.

Mole's Activation Theory of Spark Ignition, 1936

Mole's "activation" theory of spark ignition⁽¹⁷⁻²⁷⁾ is an attempt to express mathematically the views of Finch and his collaborators that ignition is the result of some specific activation of molecules, rather than a mere heating of the gas around the spark. While the conclusions of Bradford and Finch were fundamentally unsound, the theory developed by Mole appears to be of more lasting interest.

Mole's theory assumes that an ignition source introduces active particles at a constant rate into a small volume of gas around the source. Some of these combine and produce additional active particles; others are deactivated by an unspecified process. The concentration, or number of active particles at any time depends upon the rate of activation from the ignition source, the rate of activation from combination, the rate of deactivation, and the initial level of activation. A critical activation level is required for ignition. It is shown that the limits of inflammability are reached when the number of new active particles produced by combination become less than the number of active particles combining, so that the concentration of active particles decreases rather than increases.

In a further analysis, Mole attempts to show why a low-frequency discharge would be more effective than a high-frequency ignition source, as follows: During the first part of a single current pulse, active particles are formed from the discharge effects only. These particles, however, contribute energy, by combination, at a rate which increases with time so that the longer the continuous discharge proceeds, the more rapid is the increase in concentration of active particles. Above some critical concentration, ignition will result. When a current pulse ends, the concentration of active particles drops off, slowly at first, then more rapidly. If the current pulses are very short, as in high-frequency discharges, most of the active particles must come from the discharge pulses, as they are terminated before combustion contributes a major proportion. With lower frequencies and, thus, with longer current pulses, the concentration of active particles at the end of each pulse is greater because of the added concentration from combustion after the initial part of the current pulse. The general level of activation around the ignition source gradually builds up during successive pulses until one pulse finally increases the level above the critical value.

The work of Finch and Thompson⁽¹⁷⁻²³⁾ shows an effect of frequency which Mole considered as experimental verification of his theory. Actually, a capacitance-discharge spark of extremely short duration and of much less energy than that used by Finch and Thompson will cause ignition. Whether the slight extension of the quenching limit found by Finch and Thompson can be explained by Mole's theory is open to question. Mole's treatment would predict that a single pulse of energy large enough to cause ignition would be most effective, as only a low residual excitation level would be present at the start of each of a succession of pulses. The theory does not consider the effect of temperature rise from the reaction on the rates of chain branching and diffusion, or the diffusion mechanism, or the loss of heat by conduction from the ignition center. However, the treatment of the chain-branching mechanism appears sound and of interest for further theoretical application. Some of the actual variables involved, such as the rate at which the ignition source produces active particles, cannot be measured by present experimental techniques, so that experimental proof of the theory is difficult.

Landau's Theory of Ignition by Chain Branching, 1937

Landau's ignition theory^(17-28, 29) is based on the assumption that a spark introduces both heat and chain carriers into the ignition center, and that if the chain carriers multiply in such a manner that the temperature in the ignition center does not fall, ignition results.

In order to treat the problem mathematically, the following physical assumptions were made: In a combustible gas mixture contained in a large vessel, there is an arrangement for rapidly releasing energy within a small volume at a distance from the walls, as by passing an electric spark. It is assumed that this energy instantaneously heats a small spherical volume and also creates active particles. A heat-generating reaction follows, which is assumed to proceed at a rate proportional to the concentration of active particles; this concentration varies with distance and with time, because the active particles are diffusing through the gas and are, in addition, increasing in number at a rate proportional to their concentration, through chain branching. Since the theory is concerned with the resulting temperatures, the chemical reaction enters the picture only insofar as it generates heat; the mechanism of reaction is of importance only in that the reaction proceeds at a rate proportional to the concentration of active particles.

The small sphere surrounding the ignition source loses heat by conduction and gains heat through chemical reaction. Both the rate of the heat-generating reaction and the rate of chain branching increase with increasing temperature, so that any decrease in temperature would slow them down, resulting in a further decrease of temperature, and eventual termination of the process. Thus, the criterion for ignition is that the temperature at the center of ignition shall not fall.

In deriving the equations to describe this process, it is assumed that the diffusion coefficient of the active particles is equal to the thermometric conductivity of the gas through which they diffuse; this is not exact, but does not introduce a large error and greatly simplifies the derivation. The effects of pressure changes, the presence of burned combustion products, and the effect of temperature changes on the rates of chain branching and on the heat-releasing reaction are not considered, on the basis that they would not greatly change the conclusions, but would complicate the derivation.

The critical ignition condition, as derived, is:

$$\frac{4(T_1 - T_0)k}{Qn_0 R^4} < \frac{aC}{D}$$

where T_0 is initial temperature of the gas, T_1 is the initial temperature of the sphere after spark discharge, R is the radius of the critical sphere, n_0 is the number of active particles per unit volume produced by the ignition source, Q is the heat generated per reaction of one active particle per unit time, k is the thermal conductivity, a is the branching coefficient, D is the diffusion coefficient, and C is the constant.

The physical interpretation of this equation is difficult. If n_0 , Q , and L are assumed to vary exponentially with temperature, then the equation becomes:

$$\frac{T_1 - T_0}{R^4} = C \frac{1}{kD} e^{-\frac{E}{RT_1}}$$

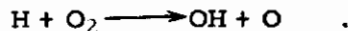
Landau found that if T_1 was chosen as the minimum temperature of a solid spherical particle which would just cause ignition, then $\log T_1 - T_0/R^4$ plotted against $1/T$ yielded straight lines. He interpreted this as a confirmation of his theory. Comparison of Landau's theory with modern spark ignition data does not seem possible.

Correlations of Ignition Data by Linnett, Raynor, Frost, and Nutbourne, 1945

Experiments by Linnett, Raynor, and Frost⁽¹⁷⁻³⁹⁾ showed that the minimum igniting pressure of a stoichiometric oxygen-hydrogen mixture was lowered by the addition of small amounts of chemically inert gas. The effectiveness of inert gases in lowering the ignition pressure was correlated with the diffusion coefficients of the inert gases, those with small diffusion coefficients being most effective in lowering the minimum ignition pressure. It was concluded that the inert

gases promoted ignition by reducing the diffusion of active particles from the ignition source, and thus aiding the increase of activation level in this region. It was also found that larger additions of inert gases raised the ignition pressure, and that the order of this effect for the different gases was in the order of their heat capacities. Thus, for greatly diluted mixtures, thermal factors outweighed other considerations.

The correlations of data were based upon the Mole treatment of the chain-branching mechanism, plus clever manipulation of diffusion equations to compare relative effects of different diluent gases. The result indicated that at equal hydrogen and oxygen pressures the slowest reaction, which controls the rate of chain branching, was



In experiments in which various gases were added to a stoichiometric oxygen-hydrogen mixture, the rates at which hydrogen atoms and oxygen atoms would diffuse from the small sphere surrounding the spark were examined. The diffusion rates of hydrogen atoms and oxygen atoms were found to be similar and in fair agreement with observed data. It was not possible to decide what diffusing particle limited the process. The general conclusion regarding the ignition of hydrogen and oxygen was that the minimum igniting pressure in the presence of small amounts of nitrogen, argon, carbon dioxide, hydrogen, and oxygen can be interpreted approximately by a modification of the theory of Mole, and, therefore, that this theory contains the essential features of the problem. However, in detail, there were some anomalies which resulted from the simplifications introduced, such as the ignoring of the temperature level in the zone of ignition. However, the fact that the temperature could be ignored suggests that the changes in temperature resulting from the introduction of small amounts of inert gases were of secondary importance compared to other factors. When large quantities of diluent gases were added, the least igniting pressure was increased, the increases caused by various gases being related to thermal conductivities rather than to diffusion characteristics, indicating that the ignition mechanism had changed and was thermal in nature.

Mixtures of nitrous oxide and hydrogen with inert gases were used by Linnett and Nutbourne (17-40) to study the mechanism of ignition for gases which react by a nonbranching-chain mechanism. Using a constant value of ignition energy, the least ignition pressures of stoichiometric mixtures of nitrous oxide and hydrogen to which helium, carbon monoxide, nitrogen, and argon were added was determined. It was found that addition of any diluent gas raised the least igniting pressure, and that the effect varied with the thermal conductivity and heat capacity of the mixture. The data were correlated to show that the relation of the ratio, ignition energy/heat capacity, to heat capacity was a straight line for each diluent gas, and that the slopes of these lines were proportional to the thermal conductivities of the gas mixtures. From this, it was concluded that ignition of gases which react by a nonbranching chain mechanism is thermal in nature and can be explained in terms of thermal properties of the gas mixture.

Since ignition and combination of many hydrocarbon fuels are known to proceed by chain-branching processes, the conclusions of Linnett that the diffusion coefficients of the fuel-oxidant mixture, and not the thermal conductivity, correlate with the incidence of ignition appears of fundamental importance. Because the equations for conduction are similar to those for diffusion, it is only by comparisons of mixtures in which diffusion and conduction coefficients vary differently that the effects of each can be separated. The work of Linnett and associates appears to be the only conclusive comparison between conduction effects and diffusion effects. However, they also show that thermal effects can predominate if the fuel and oxidant mixture is greatly diluted, or if the chemical reaction proceeds by a nonbranching-chain mechanism. Although proof of the Mole or Landua theories does not appear possible, they provide a basis for data correlations such as those of Linnett.

The Lewis and von Elbe Theory of Minimum Ignition Theory: The 1947 Theory

The 1947 ignition theory of Lewis and von Elbe(17-45) is a special case of their wave theory of flame propagation. A thermal combustion wave from an instantaneous point source of heat is

assumed, and diffusion processes are neglected on the basis that they can be excluded to permit study of such transitory states as ignition, though this would not be permissible for study of a steady-state combustion process. This ignition process is described by Lewis and von Elbe as follows:

"When a mass element passes through a combustion wave, it at first gains heat by conduction from preceding hotter elements and later loses heat by conduction to succeeding cooler elements. Correspondingly, the sum h of the thermal and chemical energy per unit mass at first increases above the level h_0 for the unburned or adiabatically burned gas, and later decreases to the same level. It follows that in a unit-area segment of a plane combustion wave the excess energy

$$\int_{x_u}^{x_b} \rho(h - h_0) dx$$

is stored, where x_u and x_b denote reference points before and behind the wave. This energy is acquired at the expense of the energy content of the burned gas as the flame grows from a small sphere to its final size. The energy that is thus lost by the burned gas is insignificant except at the flame origin. Here, the excess energy must be furnished by the ignition source. It is the function of the latter to initiate the reaction by producing a high local concentration of heat and chain carriers, and to furnish at least as much energy as is necessary to satisfy the excess energy requirement of the smallest flame that is capable of self-propagation. Such a flame may be visualized as a burning sphere of the smallest volume consistent with the condition that the rate of heat production should equal the rate of heat conduction to the surrounding unburned gas, and the minimum ignition energy is the integral

$$\int_0^{\infty} 4 \pi r^2 \rho(h - h_0) dr.$$

The calculation of this energy is made possible by assuming a simplified, partly linear temperature gradient in the combustion wave. This approximate gradient closely circumscribes the actual gradient. The resulting temperature and energy distribution can be calculated numerically from data on the flame diameter, the burning velocity, the initial and flame temperature, the heat conductivity, density and specific heat of the unburned gas. In a calculation of this kind, no issue arises concerning a "thermal" or "kinetic" theory of flame propagation. The issue arises only when, conversely, an attempt is made to calculate the burning velocity and the width of the reaction zone from speculative values of the ignition temperature and the rate of the chemical reaction. No data are available for the diameters of the smallest self-propagating flames; however, they are smaller than the readily measurable flame quenching distances between plane parallel plates by a factor of about 2."

The equation derived for the above conditions was:

$$H = 4\pi r_1^2 \frac{\mu_u}{S_u} \left(\frac{T_u}{T_a} \right)^{1/2} (T_b - T_u) \left(\frac{a^0}{a} \right)^2 \frac{1 + 1.3 ar_1}{1 + a^0 r_1 \left[1 - (3/ar_1)^{1/3} \right]}$$

in which terms are as follows: H is the minimum ignition energy; r_1 is the diameter of smallest self-propagating flame; μ is the temperature gradient; S is the burning velocity in a plane wave; T is the temperature;

$$a = \frac{c_p \rho_u S_u}{\mu}$$

where c_p is the specific heat, ρ_u is the density, μ is the temperature gradient; T_a is the temperature average of T_0 and T_1 ; subscript \underline{b} refers to burned gas; subscript \underline{u} refers to unburned gas; and superscript \underline{o} refers to conditions in a plane combustion wave.

This equation has been used to calculate the diameters of minimum ignition spheres. The calculated diameters were, in general, in agreement with the assumption that the diameter is half of the quenching distance.

The 1951 Lewis and von Elbe Theory of Minimum Ignition Energy

As shown in Figure 17-5, the correlation of minimum ignition energy with the square of the quenching distance is excellent over a very wide range of energies and distances. The 1947 Lewis and von Elbe theory does not predict this, but the authors have reconciled the general form of the theory with the data correlation in the following manner:⁽¹⁷⁻¹⁾

The final equation for minimum ignition energy was derived from an initial equation:

$$H = 4 \pi r_{\min.}^2 h_c,$$

which shows that minimum ignition energy is proportional to the critical value h_c of the excess enthalpy per unit area, and the surface of the combustion wave, which varies with $r_{\min.}^2$, the minimum flame radius. The minimum flame radius is of the order of half the quenching distance, so that the right side of this equation is approximately $\pi d^2 h_c$. Since chemical energy must be released in the wave for ignition to occur, the value of h_c must be greater than that of h_o , the enthalpy of the temperature wave alone, so that the original equation can be modified to the approximate form:

$$H \approx \pi d^2 h_o \approx \pi d^2 (\mu/S_u^o) (T_b^o - T_u).$$

This equation has been checked against the test data of Lewis and von Elbe (Reference 17-1), and those of Calcote⁽¹⁷⁻⁵⁴⁾, and a very good correlation found. Lewis and von Elbe accept this as evidence that the theory, though strongly simplified, is basically correct.

The Lewis and von Elbe theory of minimum ignition energy permits calculation of minimum ignition energy from physical properties of the gas mixture. At the present time, it is the only theory which permits accurate quantitative prediction of any of the fundamental variables of ignition and, thus, is probably the most valuable theory for any practical solution of ignition problems. The data correlation relating minimum ignition energy to the square of the quenching distance is also of great value both for practical applications of ignition and as a basis for future theoretical treatment of ignition mechanisms.

Fenn's Reaction Rate Theory

Fenn⁽¹⁷⁻⁵⁶⁾ attempted to relate all of the known factors influencing ignition by using a theory based on a second-order reaction with the assumption that the ignition requirement was for the rate of heat generation to be at least equal to the heat loss. From these assumptions, it can be shown that to a good approximation the activation energy is given by

$$E = \alpha T_f (\text{lean})$$

where \underline{E} is the activation energy, $T_f (\text{lean})$ is the adiabatic flame temperature at the lean limit and α

is a constant. The final equation for ignition energy takes the form

$$\log \left(\frac{H N_o^3}{T_f - T_o} \right) = L + 2 \log T_o - 2 \log p_o + \frac{0.65 \alpha T_f \text{ (lean)}}{RT_f}$$

where \underline{H} is the minimum ignition energy, N_o is the mole fraction of oxygen, T_f is the adiabatic flame temperature, T_o and p_o are the initial temperature and pressure, \underline{R} is the gas law constant, \underline{L} is an undetermined constant, and α is a constant.

Fenn found that this equation gave a reasonable correlation of the data with $\alpha = 16$ and activation energies ranging from about 16 Kcal/mole for hydrogen to 26 Kcal/mole for propane.

The Zeldovich and Simonov Theory

The Zeldovich and Simonov theory of ignition is based on original data on ignition of mixtures of oxygen with CO and H₂. If a gas explosion is induced by a spark of energy \underline{E} , ignition follows the law:

$$E = Qk \lambda^3 \eta u^3 C_p^3 \rho^3$$

where \underline{Q} is the heat of reaction, \underline{k} is a constant, η is the coefficient of utilization of ignition energy, \underline{u} is the linear velocity of flame propagation, C_p is the heat capacity, λ is the thermal conductivity, and ρ is the thermal diffusivity of the reaction products.

The value of \underline{k} was determined as 12π , which infers that the calculated radius of the sphere raised to flame temperature by the spark was larger than the width of the heated zone in a stationary flame, by a factor of 3. This factor of 3 also fits the data of Lewis and von Elbe. Photographs of spark ignition show radii of luminous spheres to be 1.3 times the calculated radius for CO-H₂-O₂ mixtures, and 0.7 times the calculated radius for CO₂-H₂O mixtures.

CONCLUDING REMARKS

Ignition of Gas Mixtures

Several studies of ignition of gas mixtures are currently under way. The general objectives of these studies are to learn more about the effects of electrical variables on ignition, to observe photographically the very early stages of ignition and connect these observations with other data, and to investigate the ignition of flowing gas streams.

At the Bureau of Mines, experiments to relate electrical factors to the spark structure and the minimum ignition energy are in progress. Sparks from electrical circuits giving widely different discharge characteristics will be studied using a two-channel oscillograph to record discharge voltage and current, and an Eastman high-speed motion-picture camera (2500 frames per sec.) to take schlieren pictures of the early stages of spark growth.

In a second project at the Bureau of Mines, ignition in flowing gas streams is under study. The effects of Reynolds' number, electrode variables, and spark-discharge characteristics will be studied. A similar project has been carried on at the NACA Lewis Flight Propulsion Laboratory by Swett. From these two projects, an understanding of the effects of flow on ignition of gases can be expected.

At the Applied Physics Laboratory of Johns Hopkins University, the early stages of ignition are under study using spark-schlieren photography in a system by which successive sparks can be photographed at intervals corresponding to very high-speed motion pictures. The success of this work in extending present knowledge of spark ignition will depend to a large degree on how closely it can be correlated with past work, and coordinated with other work such as that at the Bureau of Mines.

Ignition of Liquid-Fuel Mists

The problem of ignition of fuel mists is complicated by the wetting of electrodes, the energy absorbed as heat of vaporization of liquid droplets, the partial vaporization of droplets, and the extreme heterogeneity of the combustible mixture in small regions. Such variables as fuel volatility, the extent of fuel vaporization, the droplet size consist in the fuel mist, and flow conditions will be very important. It is probable that the minimum ignition energy for fuel-air mists will depend on the above variables to such a degree that theories or empirical data correlations suitable for homogeneous gas mixtures will not be applicable.

The only past work on ignition of hydrocarbon-fuel mists is that done in combustion systems of turbojet engines and ramjets. Because of the many uncontrollable variables in these studies, information of theoretical value has not been obtained.

At the present time a study of ignition of fuel mists is in progress at Battelle Memorial Institute. Preliminary results indicate that the variables important in ignition of fuel mists containing little or no vapor may be considerably different from those for gases, and that energies required for ignition are much higher than for gas mixtures.

It appears that the most productive and potentially useful field for future research on spark ignition will be in connection with study of ignition of fuel mists, in experiments planned to determine the important variables and correlate them on an empirical or theoretical basis. Although the theoretical aspects of this work appear complex and difficult, the practical usefulness of the results, as applied to engine ignition problems, appears to be large enough to justify research.

REFERENCES

1. Bernard Lewis and Guenther von Elbe, "Combustion, Flames and Explosions of Gases", Academic Press, Inc., 125 East 23rd Street, New York 10, N. Y., 1951, pp 391-425.
2. H. F. Coward, C. Cooper, and C. H. Warburton, "The Ignition of Electrolytic Gas by the Electric Discharge", Jour, Chem. Soc., Vol 101, 1912, p 2278.
3. H. F. Coward, Charles Cooper, and Julius Jacobs, "The Ignition of Some Gaseous Mixtures by the Electric Discharge", Jour. Chem. Soc., Vol 105, 1914, p 1067.
4. H. F. Coward and E. G. Meiter, "Chemical Action in the Electric Spark Discharge - The Ignition of Methane", Jour, Am. Chem. Soc., Vol 49, 1927, p 396.
5. W. M. Thornton, "The Electrical Ignition of Gaseous Mixtures", Proc. Roy. Soc. (London), Vol 90, 1914, pp 272-297.
6. W. M. Thornton, "The Ignition of Gases by Condenser Discharge Sparks", Proc. Roy. Soc., Vol 91, 1914, p 17.
7. W. M. Thornton, "The Reaction Between Gas and Pole in the Electrical Ignition of Gaseous Mixtures", Proc. Roy. Soc., Vol 92, 1915.

8. W. M. Thornton, "Ignition of Gases by Impulsive Electric Discharge", Proc. Roy. Soc., Vol 92, 1915, p 381.
9. Richard Vernon Wheeler, "'Stepped' Ignition", Jour. Chem. Soc., Vol 111, 1917, p 130.
10. R. V. Wheeler, "The Influence of Pressure on the Ignition of a Mixture of Methane and Air by the Impulsive Electric Discharge", Jour. Chem. Soc., Vol 111, 1917, p 411.
11. R. V. Wheeler, "The Ignition of Gases, Part I - Ignition by the Impulsive Electric Discharge, Mixtures of Methane and Air", Jour. Chem. Soc., Vol 117, 1920, p 903.
12. R. V. Wheeler, "The Ignition of Gases, Part III - Ignition by the Impulsive Electric Discharge, Mixtures of the Paraffins With Air", Jour. of the Chemical Society, Vol 125, p 1858.
13. R. V. Wheeler, "The Ignition of Gases, Part V - Ignition by Inductance Sparks, Mixtures of the Paraffins With Air", Jour. Chem. Soc., Vol 127, 1925, pp 14-26.
14. J. D. Morgan and R. V. Wheeler, "Phenomena of the Ignition of Gaseous Mixtures by Induction Coil Sparks", Jour. Chem. Soc., Vol 119, 1921, pp 239-251.
15. E. Taylor-Jones, J. D. Morgan, and R. V. Wheeler, "On the Form of the Temperature Wave Spreading by Conduction From Point and Spherical Sources With a Suggested Application to the Problem of Spark Ignition", Phil. Mag., Vol 43, 1922, p 359.
16. J. D. Morgan, "The Ignition of Explosive Gases by Electric Sparks", Jour. Chem. Soc., Vol 115, 1919, pp 94-104.
17. J. D. Morgan, "Some Further Experiments on the Combustion of Inflammable Gases by Electric Sparks", Phil. Mag., Vol 11, 1931, p 158.
18. J. D. Morgan, "An Experiment Relating to the Thermal and Electrical Theories of Spark Ignition", Phil. Mag. Vol 18, 1934, p 827.
19. J. D. Morgan, "Principles of Ignition", Pitman, London, 1944.
20. Clifford C. Patterson and Norman Campbell, "Some Characteristics of the Spark Discharge and its Effects in Igniting Explosive Mixtures", Proc. Physical Society of London, Vol 31, 1918-19, pp 168-227.
21. Bone, Frazier, and Witt, "The Initial Stages of Gaseous Explosions, Part III - The Behavior of an Equimolar Methane-Oxygen Mixture When Fired by Sparks of Varying Intensities", Proc. Roy. Soc. (London), Vol A114, 1927.
22. B. W. Bradford and G. I. Finch, "The Mechanism of Ignition by Electrical Discharges", Chem. Reviews, Vol 21, 1937, pp 221-243.
23. G. I. Finch and H. H. Thompson, "The Effect of Frequency on the Condensed Discharge Ignition of Carbonic-Oxide-Air Detonation Gas", Proceedings of the Royal Society of London, Vol 134, 1931, p 343.
24. B. W. Bradford, G. I. Finch, and A. M. Prior, "The Coil Ignition of Some Explosive Gas Mixtures", Jour. Chem. Soc., Vol 136, 1933, p 227.
25. B. W. Bradford, G. I. Finch, and A. M. Prior, "The Ignition of Some Explosive Mixtures by Modified Coil Discharge", Jour. Chem. Soc., Vol 137, 1934, p 75.
26. H. W. Thompson, "The Explosive Combination of Hydrogen and Oxygen - The Function of Walls in Gaseous Reactions", Trans. of the Faraday Society, Vol 28, 1932, p 299.

27. G. Mole, "The Ignition of Explosive Gases", Proceedings of the Physical Society, Vol 48, 1936, p 857.
28. H. G. Landau, "The Ignition of Gases by Local Sources", Chem. Reviews, Vol 21, 1937, p 245.
29. H. G. Landau, "The Ignition of Gases by Local Sources II Ellipsoid Sources", Jour. of Chem. Physics, Vol 7, 1939, p 112.
30. H. Herzing, "Ignition Limits of Hydrocarbons", Z. Ver Deut. Ing., Vol 81, 1937, p 1502. Also Chem. Abstracts, Vol 32, p 87422.
31. Rodolphe Viillard, "Sur l'inflammation des melanges gazeux par l'etincelle electrique: melanges air diethylether", Comptes Rendus, Vol 207, 1938, p 1405.
32. Rodolphe Viillard, "Data on Ignition of Combustible Gases by Electric Sparks - Necessary Minimum Energy for Ignition of Combustible Gas Mixture by Means of the Electric Spark", Jour. Chim. Phys., Vol 40, 1943, pp 54-61.
33. Rodolphe Viillard, "Data on Ignition of Combustible Gas Mixtures by an Electric Spark; Minimum Energy Necessary for the Ignition of Combustible Gas Mixtures by the Electric Spark II New Experiments"; Jour. Chim. Phys., Vol 40, 1943, pp 101-108.
34. Rodolphe Viillard, "Ignition of Gas Mixtures by Electric Sparks; Minimum Ignition Energies", Jour. Chim. Phys., Vol 16, 1948, p 555.
35. A. Hayakawa and R. Goto, "Explosive Reactions of Gases II Spark Ignition of Oxyhydrogen Gas at Low Pressures", Rev. Phys. Chem., Japan, Vol 15, 1941, p 117. See CA 36, 47445, CA 33, 64594.
36. Y. Toriyama and S. Saito, "Ignition of Inflammable Gases", Jour. Inst. of Electrical Engineers, Japan, Vol 62, 1942, p 427.
37. Yotsuo Toriyama, Seikichi Saito, and Ryoji Saito, "Explosion of Methane Gas by Electric Sparks", Oyo Butsuri (Applied Physics) Japan, Vol 12, 1943, p 463. (Chemical Abstracts, Vol 41, Column 5307 h).
38. Y. Toriyama and S. Saito, "Ignition of Methane", Jour. Inst. Elec. Engrs., Japan, Vol 63, 1943, p 85.
39. J. W. Linnett, E. J. Raynor, and W. E. Frost, "The Mechanism of Spark Ignition", Trans. Faraday Society, Vol 41, 1945, p 487.
40. J. W. Linnett and D. M. Nutbourne, "The Spark Ignition of Nitrous Oxide-Hydrogen Mixtures", Third Symposium on Combustion, Flame, and Explosion Phenomena, Williams and Wilkins, Baltimore, Md., p 336.
41. A. R. Boyle and F. J. Llewellyn, "The Electrostatic Ignitibility of Various Solvent Vapour-Air Mixtures", Jour. Soc. Chem. Ind., Vol 66, 1947, pp 99-102.
42. F. J. Llewellyn, "Incendiary Action of Electric Sparks in Relation to Their Physical Properties", Trans. Inst. Rubber Industries, Vol 23, 1947, p 29.
43. M. V. Blanc, P. G. Guest, Guenther von Elbe, and Bernard Lewis, "Ignition of Explosive Gas Mixtures by Electric Sparks. I. Minimum Ignition Energies and Quenching Distances of Mixtures of Methane, Oxygen, and Inert Gases", Jour. Chem. Physics, Vol 15, 1947, p 798.

44. Bernard Lewis and Guenther von Elbe, "Ignition of Explosive Gas Mixtures by Electric Sparks. II. Theory of the Propagation of Flame From an Instantaneous Point Source of Ignition", Jour. Chem. Phys., Vol 15, 1947, p 803.
45. M. V. Blanc, P. G. Guest, Guenther von Elbe, and Bernard Lewis, "Ignition of Explosive Gas Mixtures By Electric Sparks III. Minimum Ignition Energies and Quenching Distances of Mixtures of Hydrocarbons and Ether With Oxygen and Inert Gas", Third Symposium on Combustion Flame and Explosion Phenomena, Williams and Wilkins, Baltimore, 1949.
46. W. Roth, P. G. Guest, G. von Elbe, and B. Lewis, "Heat Generated by Electric Sparks", Jour. Chem. Phys., Vol 19, Dec., 1951, p 1530.
47. Humbert Morris, "Ignition of Gas Mixtures by Electric Sparks", Third Symposium on Combustion Flame and Explosion Phenomena, Williams and Wilkins Company, Baltimore, 1949, p 361.
48. R. Friedman and Edward Burke, "Spark Ignition of Gas Mixtures", Jour. Chem. Phys., Vol 17, p 667.
49. Clyde C. Swett, Jr., "Effect of Gas Stream Parameters on the Energy and Power Dissipated in a Spark and on Ignition". Third Symposium on Combustion Flame and Explosion Phenomena, Williams and Wilkins Co., Baltimore, 1949.
50. Clyde C. Swett, Jr., "Investigation of Spark Gaps Subjected to Altitude and Air-Velocity Conditions", NACA Research Memorandum No. E8117, November, 1948.
51. Clyde C. Swett, Jr., "Spark Ignition of Flowing Gases I. Energies to Ignite Propane-Air Mixtures in Pressure Range of 2 to 4 Inches Mercury Absolute", NACA Research Memorandum No. RM E9E17, August 4, 1949.
52. Clyde C. Swett, Jr., "Spark Ignition of Flowing Gases, Part 2 - Effect of Electrode Parameters on Energy Required to Ignite a Propane-Air Mixture", NACA Research Memorandum No. E51J12, December 18, 1951, 26 pages.
53. Clyde C. Swett and Richard H. Donlon, "Spark Ignition of Flowing Gases III. Effect of Turbulence Promoters on the Energy Required to Ignite a Propane-Air Mixture", NACA RM E52J28, January, 1953.
54. H. F. Calcote, C. A. Gregory, Jr., C. M. Barnet, and R. B. Gilmer, "The Effect of Molecular Structure on Minimum Spark Ignition Energy", Ind. and Eng. Chem., Vol 44, 1952, p 2656-2662.
55. C. A. Gregory, Jr., T. R. King, and H. F. Calcote, "The Temperature Coefficient of Minimum Spark Ignition Energy", presented at ACS Joint Symposium on Combustion Chemistry, April 10, 1951.
56. J. B. Fenn, "Lean Flammability Limit and Minimum Spark Ignition Energy", Ind. and Eng. Chem., Vol 43, No. 12, 1951, pp 2865-2868.
57. Y. B. Zeldovich and N. N. Simonov, "Theory of the Spark Ignition of Explosive Gas Mixtures", Zhur. Fiz. Khim., Vol 23, 1949, pp 1361-1374.
58. H. L. Olsen and E. L. Gayhart, "Preliminary Studies on the Ignition and Propagation of Flames in High-Speed Gas Streams", The Johns Hopkins University, Applied Physics Laboratory, Silver Spring, Maryland, CM-632, February 8, 1951.
59. H. L. Olsen, R. B. Edmonson, and E. L. Gayhart, "Energy Relationships for Electric Spark Phenomena in Argon", The Johns Hopkins University, Applied Physics Laboratory, CM-689, September, 1951.

60. H. L. Olsen, R. B. Edmonson, and E. L. Gayhart, "Microchronometric Schlieren Study of Gaseous Expansion from an Electric Spark", Journal of Applied Physics, Vol 23, 1952, pp 1157-1162.
61. Allen J. Metzler, "Minimum Ignition Energies of Six Pure Hydrocarbon Fuels of the C₂ and C₆ Series", NACA RM E52F27, Aug. 1952.
62. H. R. Hazard, "A Review of Research on Spark Ignition", Battelle Technical Report No. 1503-7, to WADC under Contract No. AF 33(038)-12656, March 13, 1952.
63. A. E. Weller, "Eighteenth Progress Report on Ignition and Combustion Research, Phase 7, Ignition Research", Sept. 13, 1954, prepared by Battelle Memorial Institute under Contract No. AF 33(038)-12656.

CHAPTER 18. DROPLET COMBUSTION

ABSTRACT

The combustion process in a liquid fuel-vaporized fuel-air mixture is far more complex than that in a homogeneous fuel-air mixture. Part of the combustion may take place between the vaporized fuel and extremely small droplets, and the air, and proceed in the manner of a premixed flame. On the other hand, fuel in large droplet form may burn as individual diffusion-type flamelets. The discussion of the burning of droplets is therefore introduced by a short review of the information in Chapters 4 and 10 on some of the effects of the size distribution of the droplets. The various theories of droplet combustion, which are closely related to theories of evaporation, are then considered. The chapter is concluded with a review of the experimental results on flammability limits and propagation rates in fuel mists, and the effect of the physical properties of fuel sprays in flame stability limits in high velocity streams.

Contracts

DROPLET COMBUSTION

by

A. Levy

Most of the work in fundamental combustion research has been done with homogeneous gas mixtures. This type of combustion, as compared to the combustion of a heterogeneous mixture, is more amenable to theoretical analysis, is less complex on an experimental basis, and gets results more readily interpreted. But many common forms of combustion do not occur in homogeneous systems. The combustion chamber of jet planes, for example, utilizes a heterogeneous mixture of liquid fuel, vaporized fuel, and air, the fuel being carried and supplied in liquid form. It is therefore necessary to understand the burning process of heterogeneous systems.

The new combustion problems which arise when liquid fuels are burned result from the necessity of vaporizing the fuel and bringing it into intimate contact with the oxidant. There is little doubt but that combustion can occur only in the gas phase, and then vaporization may occur. However, the optimum method of obtaining this vaporization and then of obtaining the desired mixing of the vapors is dependent on the geometry of the combustion chamber.

As will become apparent in the subsequent discussion, the number of variables encountered in heterogeneous combustion is far larger than the number encountered with homogeneous combustion. Yet the number of results available are far less. As a consequence, it is extremely difficult to bridge the gap between the fundamental work in this phase of combustion and the application.

THE EFFECT OF SIZE DISTRIBUTION

The more specific details of the processes of atomization, evaporation, and mixing were covered in earlier chapters. The application of these studies to combustion will be investigated in this chapter. In agreement with the chronological sequence of the life of the fuel droplets in the combustion chamber, the effects of atomization and of size distribution are covered first. Theory and experiments in homogeneous gas systems show that combustion is supported within a certain range of fuel-to-air ratios. It is therefore necessary to introduce the liquid fuel into the system in such a manner that such ratios may be easily achieved. The two ways in which this can be done are by vaporization and by atomization. In the former process, the liquid fuel would be completely vaporized and the combustion process is reduced to the simple, homogeneous problem. In the latter case, the fuel must be broken up into small enough droplets that a heterogeneous mixture of fuel drops, fuel vapor, and air is obtained. The first method would be practical if the fuels used for combustion were of high quality, so that no solid residue was left behind to coat or obstruct the vaporizing chamber. But with the heavier grades of liquid fuels that are used, this may be impractical. Therefore, liquid fuels are introduced into the combustion chamber by means of spray nozzles or atomizers. The purpose of these devices is, of course, to break up the liquid stream into many fine drops.

No atomizer produces a strictly uniform distribution of droplets; but more important, investigation of droplet combustion suggests that a uniform-sized spray may not be desirable, for it has been shown that the spread of drop sizes in a spray depends upon the number of small drops

required to produce enough vapor for ignition purposes. (18-1) Then, if there are a sufficient number of small drops to propagate a stable gas flame, the larger drops vaporize and support combustion. How large the larger drops should be is determined by the heat necessary to vaporize the fuel in the time available, by the number of small drops present, and by the length of the combustion chamber. The vaporization of large drops cools the flame, so that the small drops must be present to feed sufficient fuel to the flame until the larger ones produce enough vapor. The oil-fired open-hearth steel furnace is a good example where a large size of drop is desirable, that combustion may be maintained over a large distance. In the case of the turbojet combustion chamber, the fuel droplet would necessarily be much smaller since the chamber is much shorter and the flow velocity is much higher.

The computation of the combustion volume of a flame, as this may be related to size of drop, is too complicated to perform with any accuracy. In the absence of better data, Gibbs (18-2) has taken data by Houghton from Perry's Handbook (18-3) and has related the combustion volume to the degree of atomization, by assuming that the fuel will react at a rate faster than the rate of vaporization. From the data used, a nominal distribution of large drops of 10 microns to 500 microns in diameter gives a surface of 1.52 sq ft per cu in. of oil. A drop distribution of 2 to 70 microns yields 56.2 sq ft per cu in. Knowing the time rate of volume formation of combustion products and the vaporization time for a volume of oil, it is found that the coarse atomization requires 1.42 cubic feet of combustion space compared with 0.038 cubic foot of space for the fine spray. Such a large difference in size of combustion chamber is an important consideration in selecting a proper fuel-injection system.

Probert (18-4) has investigated this topic in more detail (see Chapter 10). His analysis involves the burning of a cloud of drops whose size distribution conforms to the Rosin-Rammler relation

$$\frac{R}{100} = e^{-\left(\frac{x}{\bar{x}}\right)^n} \quad (18-1)$$

where R is the per cent residue by weight or volume greater than diameter x , \bar{x} is the size factor, that is, a measure of the degree of atomization such as the droplet size when $R = 37$ per cent, and n is the diversity factor, that is, a measure of the range of size distribution, a high n factor signifying a small dispersion of sizes about the mean,

Probert defines the best spray as one which evaporates the fastest; he uses a mean diameter term which is representative of the over-all rate of evaporation. A volume of liquid with the smallest drops would evaporate the fastest; or in Probert's terms, if all the drops in this liquid were laid end to end, they would give the longest line. Therefore, the mean diameter is defined as the diameter of a droplet which evaporates at the same rate per unit volume as the volume made up of drops of that size. Now, this diameter would be representative of a spray at the moment of injection, but with combustion proceeding simultaneously, the rate of evaporation of the drops would be different. It stands to reason that, with steady burning, the fuel is being injected at the same rate that it is being consumed or evaporated. Probert compares this volume of fuel to the volume initially injected into the chamber and calls this ratio the specific volume. The specific volume and mean diameter are evaluated in terms of gamma functions and are expressed as

$$\text{specific volume} = \frac{\bar{x}^2}{2\lambda} \Gamma\left(1 + \frac{2}{n}\right), \quad (18-2)$$

and

$$\text{mean diameter} = \bar{x} \sqrt{\frac{\Gamma\left(1 + \frac{2}{n}\right)}{2}}; \quad (18-3)$$

λ is the evaporation constant. It is apparent that the diversity factor, n , has very little influence

on these quantities so that the mean diameter can be expressed as $\bar{x} / \sqrt{2}$.

Figure 18-1 is taken from Probert's analysis and is best explained in his words: These curves "clearly show how misleading it is to rate fuel sprays on their initial rates of evaporation when injected. For although the times of evaporation of a given quantity are much more sensitive to changes in \bar{x} than in n , yet the distribution constant n does have a great effect on the time necessary to evaporate the last few per cent of the spray. A small value of n gives a small mean diameter of the injected spray and correspondingly a high initial rate of evaporation, but after about 75 per cent of the liquid has been evaporated the effect of n is inverted. It is now seen that \bar{x} should be as small as possible, and n large, for quick evaporation of the whole spray, even though a large value of n means a slower initial rate of evaporation".

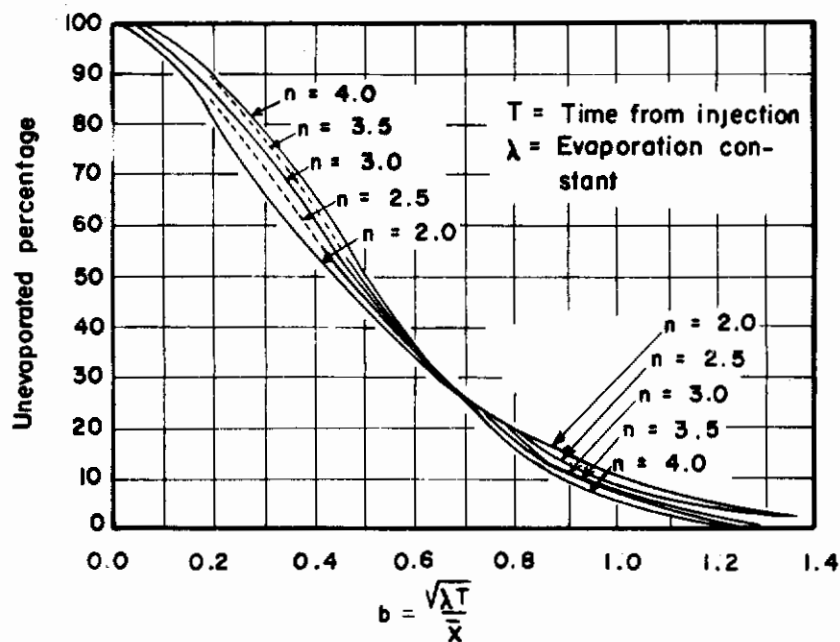


FIGURE 18-1. THE INFLUENCE OF THE DISTRIBUTION FACTOR ON THE EVAPORATIVE PROCESS

(Probert) (18-4)

THEORY OF DROPLET COMBUSTION

The theory of the combustion of liquid drops has not, until recently, been extensively investigated, partly because of the complexities of the heterogeneous system and partly because the early work on liquid-fuel combustion was only in a developmental stage. It has generally been concluded, as a result of recent studies^(18-5, 18-6), that the earlier assumptions tying together the burning process and the evaporative process are good. Godsave, at the National Gas Turbine Establishment, in England, has confirmed this in a series of preliminary experiments whereby a drop of hydrocarbon fuel was suspended from a fine silica wire and ignited. The rate of decrease of the drop, followed photographically, was found to vary directly with the first power of the radius. According to all the classical theories of evaporation (see Chapter 8), the rate of evaporation in unit weight per second of a drop, into still air, should be proportional to the first power of the radius and to the difference in the vapor pressure at the surface of the drop and in the surrounding air. Godsave's⁽¹⁸⁻⁵⁾ experiments confirm the proportionality with radius in the range of 1000 to 2000 microns, and Kumagai and Isoda's⁽¹⁸⁻⁶⁾ experiments confirm the results in the range of 300 to 1300 microns. In agreement with views put forward earlier

by Lloyd⁽¹⁸⁻⁷⁾, the results show that in the case of the burning drop the vapor pressure does not exert any noticeable effect on the burning rate. As a result of this, Lloyd has suggested, and many others have agreed, that the burning rate for liquid-fuel droplets depends upon the transfer of heat required to raise the temperature of the drop to the boiling point and to supply the heat of vaporization.

Figure 18-2 gives a schematic presentation of the distribution of the vapor around the drop according to Gudkov-Belyakov⁽¹⁸⁻⁸⁾, who uses this model in refuting all the old theories which claimed that combustion of liquid droplets could possibly take place in the liquid phase. He does this by comparing the heating qualities of colliding molecules in the liquid phase with those in the vapor phase, and shows how rapidly the vapor-phase molecules receive their energy and are ready to react with oxygen.

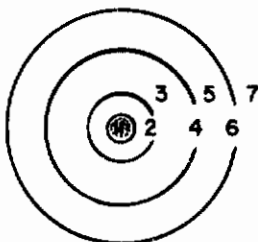


FIGURE 18-2. THE DISTRIBUTION OF VAPOR SURROUNDING A DROP

(Gudkov-Belyakov)⁽¹⁸⁻⁸⁾

In Figure 18-2 the Droplet 1 is at the lowest temperature, and molecules leave its surface to move out into the surrounding environment. At Boundary 2, the surface is almost entirely vapor molecules, but at Boundaries 3, 4, 5, and 6, air is rapidly diffusing in and mixing with the vapor. According to the author's picture, the vapor and air are within the combustion limits, so that for a "still-air" system spontaneous ignition could occur between Boundaries 3 and 6. Although this representation is probably accurate before ignition in the "still-air" system, any relative velocity will distort the pattern. After combustion the pattern is not correct for at least two reasons. First, even with a stationary droplet, buoyancy effects produced by the combustion will create a relative air velocity. Second, combustion will not occur over such a wide range of inflammability limits, but instead will occur at the stoichiometric fuel-air concentration.

Some early experiments of K. Neuman⁽¹⁸⁻⁹⁾, who was a proponent for liquid-phase combustion, are of interest in contrasting the early lines of reasoning to what is known today. Neuman studied the delay of spontaneous ignition in still and in turbulent air as a function of the temperature of the liquid. He reported that turbulence heated the liquid fuel more rapidly and the delay period was shorter. Consequently, "the preliminary vaporization of fuel was not imperative". However, below 382 C he reports that the ignition delay was even greater than that for still air, thereby refuting his own theory.

Before going into the various developments of the theory of heat transfer to the drop during the combustion process, the work of another Russian worker will be discussed. G. N. Khudyakov⁽¹⁸⁻¹⁰⁾ has studied the combustion of liquid fuel while in simulated flight. To do this, a drop was attached to a filament in a stream of air. However, it was found necessary to keep the drop spherical during this process; consequently, a metal sphere, 15.7-mm. diameter, was attached in such a way that fuel could continually be supplied to its surface. In this manner the drag on a drop was obtained during combustion and without combustion by measuring the deflection of the filament. Defining the drag coefficient C as

Contrails

$$C = \frac{2F}{S\rho V^2} \quad (18-4)$$

where F is the drag on the drop, V is the velocity of the air stream, ρ is the density of the air, and S is the projected area of a drop, it was found that the coefficient was reduced from the range 0.54 to 0.62 without combustion, to the range 0.48 to 0.52 with combustion. In other words, everything else being equal, the burning drop will travel farther than the nonburning one.

It was found that combustion takes place behind the drop in the form of a burning tail, in much the same manner as the tail behind a flame holder. Even at 24 meters per second, the burning tail does not break away from the drop. Another similarity to the flame holder is that experiments show that eddies exist behind the drop; also, although the pressure behind the drop decreases, it decreases less for the burning drop because of the presence of combustion products, which explains the decreased drag on the burning drop. Because of the flame-holder type of action, the evaporation of the fuel will not occur in the same manner for all sides of the drop. The eddies behind the drop form a low-pressure reverse-flow region where the fuel vapors become concentrated and are mixed with air and burn. Since burning occurs on this side, more intensive evaporation also occurs here. Khudyakov has presented a good physical picture of the burning drop with air rushing past it. However, it must be realized that for most of the drops in the air stream of the combustion chamber, the drops are so small (less than 50 microns) that they rapidly assume the air-stream velocity.

Lloyd^(18-7, 18-11) has reviewed the relation of fuel properties to burning processes in gas turbines, and comes to the conclusion that basic information on droplet combustion is too meager for exact analysis.

Wolfhard and Parker⁽¹⁸⁻¹²⁾ have investigated the burning of a kerosene in air. When a fine kerosene spray was projected from a nozzle, it was found that the ignited spray held a stationary position at some distance from the nozzle. Since schlieren photographs were not very helpful in studying these flames, the authors resorted to a theoretical treatment of the heat transfer to the spray. By applying Stokes' law to the droplets and considering the drops to range in size from 10 to 100 microns in diameter, the authors show that the smallest drops quickly come to rest, relative to the air, and then move with air velocity. In tests that were run, the flame front was held about 2.5 cm from the nozzle. If the air velocity is about 25 cm per sec at the flame front, this means that the small drops must reach this position within 0.1 second. Can a 10-micron drop evaporate in this time? From Frossling's calculations (see Chapter 9), a water drop, which has a much higher vapor pressure than kerosene, would have a decrease in diameter of only about 10 per cent during this time. Also, there would be no significant increase in evaporation due to the radiation from the flame front. Therefore, it appears that, since the drop cannot evaporate in the relatively long trip to the flame front, processes occurring at the flame front must be important.

The authors then assume, for kerosene, a thickness of reaction zone of about 2.1 mm. The drops must be able to vaporize and diffuse in the short time corresponding to this narrow zone. Assuming that the kerosene goes through this zone at about 20 cm per sec, the authors show that there is sufficient heat conducted to the drops to evaporate them completely in this small zone.

If one considers a cubic centimeter of air with sufficient 100-micron drops to support combustion, then the situation can be described as a single droplet in a cube of air 0.135 cm on a side. To find the time necessary for a molecule to diffuse to the edge of this cube, the familiar Einstein diffusion equation is applied,

$$x^2 = 2Dt \quad (18-5)$$

Assuming $D \approx 1$ in a flame,

Contrails

$$t = \frac{(0.068)^2}{2} = 0.0023 \text{ second.} \quad (18-6)$$

This would be more than sufficient time for the evaporation to take place, since the drop cannot pass through the flame front this fast. Therefore, it is concluded that small droplets can vaporize directly in the narrow preheating zone of the flame front.

The authors show this to be true by mixing kerosene spray with butane. With no combustion the drops are readily visible in the entire gas stream leaving the burner tip. During combustion the drops are visible only in the inner cone, and on the other side of the cone the product gases are entirely free of drops.

A similar study has been made of the burning of fuel mists off a hemispherical flame holder (18-13). In studies where a low flash point, kerosene-type fuel MIL-F-5624, formerly called ANF-58, was used, it was observed by high-speed motion pictures of the inverted flame that a large number of drops do go through the flame front, presumably because they are too large to evaporate in the flame front.

In this study an attempt was made to relate an apparent flame speed to the burning mist. This is a most difficult problem, however, because one is working with an inverted flame, so that the simple laminar flow lines no longer exist. Also, in such a situation a varying fuel/air ratio exists. Since the mist is introduced several diameters upstream, the fuel/air ratio at the flame holder becomes a function of the drop-size distribution. Likewise, the heat removed from the flame is also a function of the size of the drops that are large enough to pass through the front.

A similar example of a study with fuel mists which becomes very complicated as a result of the role of the drop-size distribution is the experiments of Lloyd's where the variation of ignition lag was studied (18-14). A spray was injected into a chamber and was carried forward by heated air. The ignition lag was measured as a function of the air temperature and the drop size. In such a process two delays are involved, the physical delay of evaporation and mixing and the chemical delay associated with preflame reactions. Three combustion zones occur in such a process:

(a) There is the preflame zone where intermediate oxidation products are formed. Cool-flame radiation from the activated formaldehyde occurs here also.

(b) There is the flame front where the fast reaction occurs. The delay here is a function of the temperature, pressure, and reaction mechanism.

(c) There is the main flame where the unevaporated fuel eventually vaporizes and ignites. This flame region depends upon the drop-size distribution for its total flame length. To date, there has not been sufficient effort placed on the burning in this last region.

A general theory for the conduction of heat in a moving medium has been developed by Godsave (18-15) along with his experimental study on single-drop evaporation. The development has been used to derive general equations for the temperature distribution and heat transfer in the preflame region. The solutions to these equations are then applied to the case of the burning of a single fuel droplet.

Two cases of burning drops are considered. There is the linear case where reference is made to the premixed stream of vapor and air that is burning; and there is the spherical case where reference is made to the flame formed about each drop of liquid fuel. In the ideal case the drop is surrounded symmetrically by the spherical flame front. The latter case is more nearly a direct application of Godsave's experimental study, and the former case is more nearly an application of Lloyd's and Pilcher's studies.

The analyses are interesting in their similarity to the approach of Tanford and Pease (18-16) in their development of flame-propagation equations (see Chapter 14). Although the linear case refers to the premixed flame and the spherical case refers to the diffusion flame, the temperature distribution in the two cases will depend upon the three basic processes of conduction, gas motion, and local energy changes; the difference in the two cases will result, of course, from the extent of the dependence on each process.

The three factors which determine the temperature distribution are:

- (1) The conduction of heat due to the instantaneous temperature gradient at any point.
- (2) The motion of the gas, which successively removes a layer of gas and replaces it at any point by an adjacent layer at a different temperature.
- (3) The heat-energy changes due to (a) chemical reaction, and (b) radiation effects.

Two situations exist, (a) the simple case where thermal conductivity, λ , is constant, and (b) the case where λ is not constant in the space concerned. For the simple case, the ordinary equation of heat conduction, relating temperature to time, holds,

$$\frac{\partial T}{\partial t} = k \left(\frac{\partial^2 T}{\partial x^2} + \frac{\partial^2 T}{\partial y^2} + \frac{\partial^2 T}{\partial z^2} \right) \tag{18-7}$$

where $k = \lambda / (c\rho)$, c and ρ are the heat capacity and density, respectively, and where x , y , and z are the space coordinates.

When λ is not constant and the medium is in motion, and there is a local source, F , supplying a unit quantity of heat in time ∂t , the generalized equation is

$$\begin{aligned}
& c\rho \left(\frac{\partial T}{\partial t} + \frac{dx}{dt} \frac{\partial T}{\partial x} + \frac{dy}{dt} \frac{\partial T}{\partial y} + \frac{dz}{dt} \frac{\partial T}{\partial z} \right) \\
& = \left(\frac{\partial}{\partial x} \frac{\lambda \partial T}{\partial x} + \frac{\partial}{\partial y} \frac{\lambda \partial T}{\partial y} + \frac{\partial}{\partial z} \frac{\lambda \partial T}{\partial z} \right) + F.
\end{aligned}
\tag{18-8}$$

At equilibrium,

$$\frac{\partial T}{\partial t} = 0. \tag{18-9}$$

For the linear case where conduction occurs along one axis only, Equation (18-8) becomes

$$\frac{dx}{dt} \frac{dT}{dx} = k \frac{d^2 T}{dx^2} + \frac{1}{c\rho} F. \tag{18-10}$$

For the spherical case where the vapor is flowing symmetrically outward, the equation in polar coordinates may be written

$$k \frac{d^2 T}{dr^2} + \left(\frac{2k}{r} - \frac{dr}{dt} \right) \frac{dT}{dr} + \frac{1}{c\rho} F = 0. \tag{18-11}$$

If ϵ is defined as the fraction of reaction completed, that is, $\epsilon = 1$ at the flame front, and $\epsilon = 0$ infinitely far away from the flame front, and then F may be expressed in terms of the total heat release, Q , and the linear gas velocity, u ,

$$F = - Q \frac{d\epsilon}{dx} \rho u. \tag{18-12}$$

When this is applied to the linear case, Equation (18-10), the same relation arrived at by Tanford and Pease results,

$$\frac{d^2T}{dx^2} + \frac{c\rho u}{\lambda} \frac{dT}{dx} - \frac{Q\rho u}{\lambda} \frac{d\epsilon}{dx} = 0. \quad (18-13)$$

The solutions are obtained by using the same assumptions as suggested by Tanford and Pease. The rate of heat transfer, \underline{H} , in the flame region, $0 < x < \delta$, for example, is

$$H = c\rho u (T - T_0) + \frac{Q}{\delta} (x - \delta) \rho u. \quad (18-14)$$

As shown in Chapter 14, this implies that \underline{T} and dT/dx are continuous at $x = \delta$.

In the spherical case, where no dilution of the vapor is assumed as the drop approaches the flame front, the radial mass flow of vapor, dm/dt , is

$$\frac{dm}{dt} = 4\pi r^2 \rho \frac{dr}{dt}. \quad (18-15)$$

In the case of a diffusion flame about each drop, the simple analysis is complicated by diffusion of fuel and air to stoichiometric concentrations before burning, and by the occlusion of combustion products with the fresh gases. The effect of this is to change the value of the constants in Equation (18-11), so that they no longer represent values for pure gases. Instead of noting this change with primes, the symbols will be used unchanged, although it must be recognized that this limitation exists. For steady-state conditions, material and heat balances exist for the diluent gases. Now if fuel is passing through the volume element, $4\pi r^2 dr$, the amount of heat released in time dt will be

$$\left[4\pi r^2 \rho \frac{dr}{dt} dt \right] \left[- Q \frac{d\epsilon}{dr} dr \right].$$

Hence \underline{F} , which is the heat release per unit volume, will be

$$F = - Q \frac{d\epsilon}{dr} \left(\frac{M}{4\pi r^2} \right),$$

where $M = dm/dt$. Equation (18-11) becomes

$$\frac{d^2T}{dr^2} + \left(\frac{2}{r} - \frac{Mc}{4\pi r^2 \lambda} \right) \frac{dT}{dr} - Q \frac{M}{4\pi r^2 \lambda} \frac{d\epsilon}{dr} = 0. \quad (18-16)$$

This is analogous to the linear equation.

The solution depends upon the assumption that all the heat is released at the flame surface, that is, that $d\epsilon/dr$ vanishes everywhere but at the flame front. The temperature distribution is given as

$$T = \frac{T_2 - T_1}{e^{-D/r_2} - e^{-D/r_1}} e^{-D/r} + \frac{T_1 e^{-D/r_2} - T_2 e^{-D/r_1}}{e^{-D/r_2} - e^{-D/r_1}}, \quad (18-17)$$

where the Subscripts 1 and 2 refer to equilibrium conditions on the surface of the drop and at the flame front, respectively, and $D = Mc/4\pi\lambda$.

The heat-flow balance at the drop surface is

$$M \Delta H = \lambda 4\pi r_1^2 \left(\frac{dT}{dr} \right)_{r=r_1} \quad (18-18)$$

$$M \Delta H = \frac{4 \pi \lambda D \Delta T}{\exp \left[D \left(\frac{1}{r_1} - \frac{1}{r_2} \right) \right] - 1}, \quad (18-19)$$

where ΔH is the amount of heat necessary to raise the fuel to the liquid surface equilibrium temperature and to evaporate it. The importance of the temperature gradient at the surface is apparent in Equation (18-18). The rate of evaporation is proportional to the temperature gradient there; however, it must also be pointed out that as M increases with an increase in dT/dr , the result is an eventual decrease in dT/dr so that an equilibrium state is reached. In Equation (18-18), therefore, the values are equilibrium values.

Equation (18-19) is then the burning rate as normally defined. After substituting for D , the final burning-rate equation is

$$\frac{dm}{dt} = \frac{\log \left[1 + c \frac{\Delta T}{\Delta H} \right]}{0.4343 \frac{c}{4\pi\lambda} \left(\frac{1}{r_1} - \frac{1}{r_2} \right)}. \quad (18-20)$$

It has been mentioned earlier that the heat-release term includes radiation effects besides the chemical effects. However, this has been omitted in this development since, besides being an additional complicating factor, it is not a large effect until the temperature rises to a high value. Also, the radiation that might be absorbed by hydrocarbons in the vapor phase is not significant until the flame front is approached.

The change in size of the drop has not been included in this investigation, but it can be assumed that the evaporation rate determined by a steady-state process cannot be too different from the process where the drop is continuously decreasing in size. The effect of gas motion relative to the drop has been excluded also because of its complications. To include this, it would be necessary to apply the Navier-Stokes equations for viscous flow in a form appropriate to the boundary conditions.

In the light of all these approximations, the relations expressed by the final burning-rate equation can be summarized by stating that to increase the burning rate it is necessary, alternatively or simultaneously, to

- (a) Increase flame temperature.
- (b) Decrease reaction zone thickness, that is, increase diffusion rate of the fuel, or increase reaction rate, or decrease r_2 .
- (c) Increase thermal conductivity.
- (d) Decrease latent heat of evaporation of the fuel.

If Equation (18-20) is written in the form

$$\frac{dm}{dt} = \frac{k}{\left(\frac{1}{r_1} - \frac{1}{r_2} \right)} \quad (18-21)$$

$$= \frac{k (r_2 r_1)}{r_2 - r_1}, \quad (18-22)$$

and if $r_1 + x$ is substituted for r_2 , then

$$\frac{dm}{dt} = k r_1 \left(\frac{r_1 + x}{d} \right), \quad (18-23)$$

where x is the distance over which the vapor diffuses to the flame front. The relation is thus obtained that the burning rate becomes proportional to the radius as r becomes small compared to the reaction-zone thickness while, for relatively large sizes of drops ($r_1 = 1000$ microns), the proportionality does not hold. This latter point is in contradiction to the experimental results obtained by Godsave, where he observed the burning drops to evaporate at a rate proportional to the radius for drops as large as 2000 microns. (18-17) A way out of this difficulty is to assume that x varies with r , which seems to be the case. The constant of population apparently varies with the fuel. (18-18)

Godsave observes in his studies in which he attempts to analyze the experimental results in terms of his heat-transfer development that the life of the drop is determined by an evaporation constant, Λ . This evaporation constant is identical with that used by Probert (18-4). In general, Godsave's studies bear out the fact that burning of the single fuel drop is in principle a physical problem in which sufficient heat is supplied to the drop to cause evaporation, and the chemical reaction occurs at a distance relatively far removed from the drop surface. [A good summary of these studies is presented by Godsave in his Fourth Combustion Symposium paper (18-19).]

Goldsmith and Penner (18-20) have also examined the problem of single-drop combustion. Their analysis is an extension and generalization of Godsave's work. However, it differs by the fact that integrated forms of the energy and continuity equations are used, thereby removing the necessity of using the rather invalid approximations of constant thermal conductivity and specific heat of the fuel. The analysis also yields expressions for the temperature and the radius of the combustion surface which were not obtainable by Godsave's approach.

Details of the analysis are omitted here. However, it is of interest to note that the theory predicts that r_c/r_e (combustion radius divided by drop radius) should be constant for fixed values of the physico-chemical parameters; as seen in the table below such appears to be the case, where the fuels are similar. That the calculated ratios are all too high is ascribed to the strong convective currents for the large drops actually tested.

TABLE 1. COMPARISON OF CALCULATED AND OBSERVED COMBUSTION RADII (Goldsmith and Penner) (18-20)

Fuel	Observed, r_c/r_e	Calculated, r_c/r_e
Benzene	2.97	11.8
n-Heptane	3.03	10.3
Toluene	2.59	11.5

Further experimental confirmation of the constancy of r_c/r_e is shown in Hall and Diederichsen's studies. (18-21) These investigators observed the combustion of suspended drops with a continuous drum camera trace and report an approximately constant distance between drop and flame. They also studied this as a function of pressure and report that the distance varies as $P^{-1/2}$ in the region 1 to 20 atmospheres. The mass burning rates varied in proportion to the first power of the drop diameter in this work, which is in accord with other investigators, and as $P^{1/4}$.

Spalding (18-22) has also studied the combustion of liquid fuels in a gas stream. His reasons for such a study are aptly stated "...conceptions proper to homogeneous combustion, such as flame speed, mixture formation and flame temperature are often wrongly applied to the heterogeneous conditions obtained in burning fuel sprays." Spalding has applied the film concept of heat and matter transfer to the combustion of fuel drops.

Figure 18-3 shows the appropriate temperature and partial pressure curves as they appear in the double-film concept. Although the kinetics of hydrocarbon oxidations reveal many slow, rate-determining steps, the same assumption prevails here as for all diffusion-flame studies, the reaction is assumed to proceed at a rate such that it offers no resistance to the over-all process. In other words, as soon as the fuel and air are in the proper proportions, reaction occurs. The reaction surface is located at B in the Figure. Fuel diffuses between A and B, while oxygen diffuses between B and C. As Zeldovich proves in his study (see Chapter 19), the partial pressures of the two reactants are zero at B. The heat of the reaction at B must be dissipated by conduction "assuming that radiation is negligible", and this is done in heating the fuel and the main gas stream. When the temperature and concentration curves are known and the two distances, AB and BC, can be approximated, the burning process can be explained by means of four equations: (a) the relation for diffusion across CB, (b) the number of molecules of fuel and oxygen reaching B, and (c) and (d) the two heat-conductivity equations across AB and CB. The four equations, after the analysis of G. Ackerman⁽¹⁸⁻²³⁾, for diffusion of gases and for heat transfer, are:

(a) Diffusion of oxygen from C to B,

$$\frac{G_o}{4\pi x_B} = \int_B^C \frac{DP}{RT} \cdot \frac{dP_o}{P + \left(\frac{G_f}{G_o} - 1\right) P_o} \quad (18-24)$$

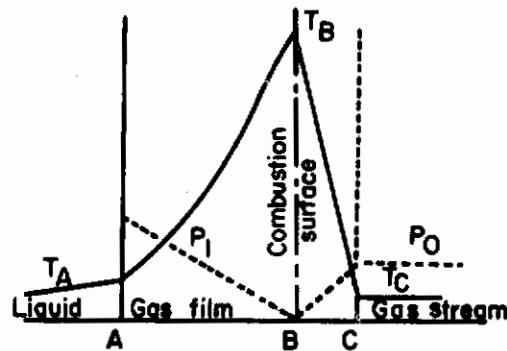


FIGURE 18-3. THE TEMPERATURE AND CONCENTRATION GRADIENTS IN THE DOUBLE LAYER FILM

(Spalding) ⁽¹⁸⁻²²⁾

(b) The stoichiometric relation,

$$G_f = \frac{G_o}{r_o} = \frac{G_p}{r_p} \quad (18-25)$$

(c) Heat conduction from B to C

$$\frac{G_f}{4\pi x_B} = \int_{T_C}^{T_B} \frac{\lambda dT}{H - Q - \int^T \frac{c_p - c_o}{c_p - c_o} dT} \quad (18-26)$$

(d) Heat conduction from B to A

$$\frac{G_f}{4\pi} \left(\frac{1}{x_A} - \frac{1}{x_B} \right) = \int_{T_A}^{T_B} \frac{\lambda dT}{L + Q + \int^T c_f dT} \quad (18-27)$$

where the following nomenclature applies:

- G matter-transfer rate
- D diffusion coefficient
- T absolute temperature
- λ thermal conductivity
- R universal gas constant
- P total pressure
- p partial pressure
- H calorific value of liquid
- L latent heat of vaporization
- Q heat used for heating up drop
- x distance from center of drop
- c_p specific heat, constant pressure
- r number of mols per mol of fuel

and suffixes A, B, and C refer to positions of Figure 18-3 and o, p, and f refer to oxygen, combustion products, and fuel, respectively.

The procedure is to calculate the flame temperature, T_B , from Equations (18-24, 18-25, and 18-26) for various values of T_C and partial pressure of oxygen. Then for a value of T_B , the burning-rate equation is

$$\frac{G_f}{4\pi x_A} = \int_{T_A}^{T_B} \frac{\lambda dT}{L + Q + \int^T c_f dT} + \int_{T_C}^{T_B} \frac{\lambda dt}{H - Q - \int^T c_p - c_o dT} \quad (18-28)$$

The rate of burning according to this equation is proportional to the radius of the drop. It has been pointed out by the NACA staff (private communication) that when a mean heat capacity is introduced into Spalding's equation (18-27), Godsave's equation (18-20) is obtained.

Returning to the combustion surface, B, in Figure 18-3, one finds that B must take on a finite thickness in practice due to interdiffusion of the reactants, and this in turn reduces the rate of reaction. Spalding uses this fact to determine the stability of burning droplets on a theoretical basis. (18-24) As he states, there is a maximum intensity of reaction which a flame may possess, and if the rate of mass transfer exceeds this quantity, the flame is extinguished. The rate of mass transfer, as developed in his more recent paper (18-24), is dependent only on the Transfer Number, which Spalding defines as the temperature or concentration gradient between the fuel surface and an infinite distance into the gas stream.

Spalding checks his theory with experiments on burning fuels from the surface of spheres under conditions of natural and forced convection. (18-25) He observes that the flame around the leading face of the sphere of liquid fuel is extinguished when the air velocity exceeds a critical value which is proportional to the diameter of the sphere. This is in accord with his theoretical development. The temperature dependence of the extinction velocity yields a heat of activation of 40,000 kcal/mole. This agrees well with Dugger's values for propane-air flame speed mixtures (15-53), but disagrees with Fenn's lower activation energy values (14-25).

It was shown in Chapter 16 (see Table 16-3) that a certain minimum temperature has to be maintained in a reaction zone. (18-26) This minimum varies from 1255 C for methane to 1575 C for n-octane. Spalding has shown that the minimum temperature for kerosene is just below 2000 C. (18-27) At this point the diffusion process probably is no longer rate determining because the chemical process becomes too slow. Accordingly, all points below $T_B = 1800$ C are assumed to signify extinction.

Figure 18-4 illustrates this, and also brings forth another point which is often misinterpreted. It is often said that when cold dilution air is introduced too early into the chamber, combustion is stopped by chilling. However, the curve shows that air at 0 C will only exert a "chilling" effect if the oxygen content is reduced below 16 per cent. In other words the chilling phenomenon is a combined effect of temperature and composition.

One other effect that becomes apparent in this treatment is that of the dissociation of CO_2 at the flame surface. In the case of solid-particle combustion, this effect is enough to double the rate of burning. With liquid fuels, however, two effects counteract each other.

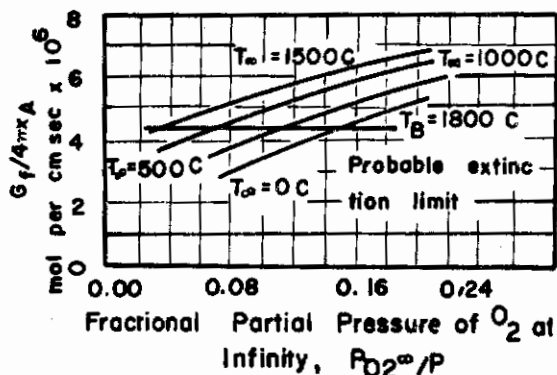


FIGURE 18-4. THE COMBUSTION RATE OF KEROSENE SPRAYS

(Spalding) (18-22)

The diffusion distance for oxygen to the carbon monoxide is reduced from what it is to the regular flame surface (see Figure 18-3); however, the reduced temperature resulting from the dissociation greatly reduces the rate of the vaporization process so that the net increase in burning rate, for liquid fuels, is actually small. With solid-particle combustion, there is obviously no vaporization to be affected by the reduced temperature.

How can one relate these rate equations to the practical burning problems? Figure 18-4 shows that, even though some oxygen is used up, as long as the temperature of the main gas stream is raised, combustion will proceed. In turbojet applications the air will be heated to about 1000 C so that the oxygen content can fall almost to 8 per cent before extinction would occur.

The effect of a large unevenness in drop-size distribution (low n value in the Rosin-Rammler expression) is that the large drops may have insufficient air surrounding them. This may cause smoke due to hydrocarbon cracking and formation of carbon particles.

The effect of turbulence on droplet combustion would probably be to increase the rate of combustion due to additional heating by convection. However, in the case of small droplets, turbulence would not be likely to have a large effect, since the relative velocity of the air would not be very much greater than that of the drop, and would tend to move the drop with it.

By applying the foregoing equations, the burning time for a kerosene drop, t_b , is expressed by the equation

$$t_b = 146 d_o^2 \text{ sec} , \quad (18-29)$$

where d_0 , the initial droplet diameter, is expressed in cm.

It follows, if a chamber is two feet long and is sweeping air through at 50 fps, that a drop must burn within 0.04 second. Therefore, any drop greater than 200 microns will not be completely burned in such a chamber and combustion efficiency will be reduced. This combustion time may possibly be increased due to reverse-flow conditions, although ignition delay will affect the combustion time adversely. This suggests that, for a kerosene-type of fuel, the upper size limit of the drops should be about 200 microns. This of course is only an approximate value, and for other fuels with lower vapor pressures, a smaller size drop is probably necessary for the upper limit.

Figure 18-5 compares the times for complete evaporation of kerosene sprays using Spalding's, and Wolfhard and Parker's analyses. The calculations have been performed only for drops up to 200 microns in diameter. For drops larger than 10 microns the Spalding calculations yield longer burning times by a factor of about 8. Considering the approximations of both developments, this is a relatively good check of the theories.

Actually these curves serve as a means of defining the upper limits of complete burning times for kerosene droplets. The curves may also be applied to the studies of Pilcher(18-13) where it was observed that a large number of drops passed through the flame front not completely burned. The fuel used in this investigation was a kerosene-type fuel; if the same burning velocity is assumed for the vaporized fuel as for kerosene, a flame-front thickness of about 2 mm can be estimated. The droplets coming from the nozzle had a velocity of approximately 470 cm/s; therefore they passed through the flame zone in about 0.004 second. From the curves of Figure 18-5, it can be estimated that the drops passing through the flame front were, on the average, larger than 80 microns in diameter.

Topps substantiates Spalding's studies by showing that when drops of the size 300-500 microns fall through an atmosphere at temperatures greater than the boiling point of the drops (400 to 950 K), the rate of evaporation is mainly dependent upon the heat transfer to the drops(18-26). In terms of simple heat-transfer theory his studies suggest that in gas-turbine practice there is less advantage to be gained from fine atomization than expected.

Topps'(18-26) data on combustion rate do not agree with the theoretical derivations made considering evaporating moving drops without combustion (see Chapter 7); however, if the $1/2$ power of the Reynolds number, given by theory, is changed to 1.2, an equation in line with Topps' results would be obtained. When it is considered that the heat effects due to combustion change not only the flow pattern around the droplet but also the drag, this change in power is not unreasonable. Thus, it may be concluded that no radical disagreement has been found yet between theory and tests in this phase of combustion work, but considerably more work is required to tie the theory and tests together.

THE STABILIZATION OF FLAMES IN MISTS AND SPRAYS

As for the burning of single drops, there are two cases to be considered: (a) the case where the fuel spray is completely volatilized by the time it reaches the flame front, and (b) the case where the drops remain liquid until they reach the flame front. The former case is, for the most part, similar to the stability of homogeneous gas mixtures. A limiting factor however may be the degree of mixing of fuel vapor and air by the time the mixture reaches the flame front.

In the second case, numerous factors will influence the stability of the fuel-mist flame. Some of these are: (a) spray drop size and distribution, (b) fuel volatility, (c) air/fuel ratio, (d) air-stream velocity, (e) flame-holder size and temperature, (f) combustion-chamber dimensions and temperature, (g) air-stream temperature, and (h) total pressure. These are probably the more important factors, although several others may be indirectly related to the above. It is almost impossible to determine the individual effect of each of these variables but, as more studies are carried out, it is hoped that relations may eventually be obtained among all of them.

From a theoretical standpoint, since combustion occurs in the gas phase, the same parameters as determined the stability in the gas phase determine the limits of combustion for a heterogeneous mixture.

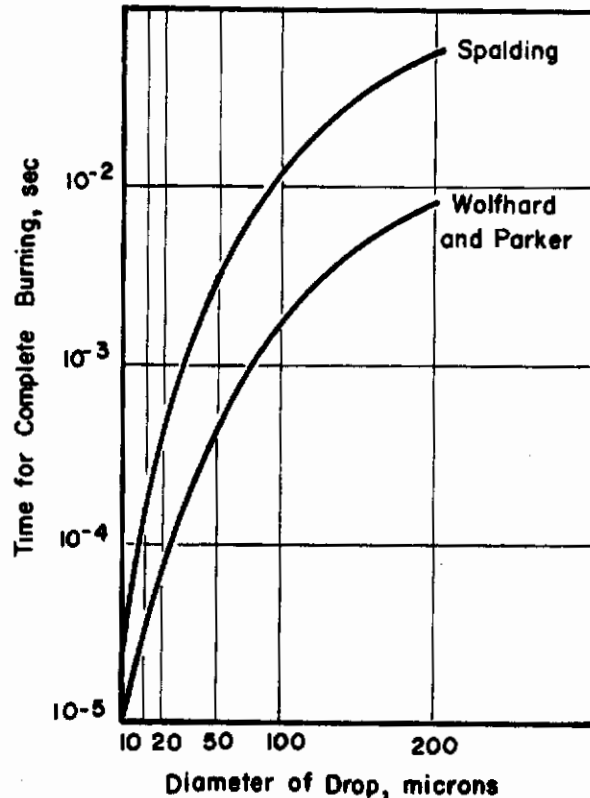


FIGURE 18-5. COMPARISON OF THE SPALDING AND THE WOLFHARD AND PARKER ANALYSES FOR THE BURNING RATES OF KEROSENE DROPLETS

In 1923, Haber and Wolff reported on some ignition studies of mists⁽¹⁸⁻²⁸⁾. Their study at that time was for the purpose of determining whether the intensity and duration of combustion were sufficient to vaporize the fuel and transform the mixture into a homogeneous one. The fuels used were petroleum (180-200 C fraction), tetrahydronaphthalene (tetralin), and quinoline, and the drop sizes ranged from 1 to 100 microns. Their observations covered the lower explosion limit of the mist, the limiting mist for complete combustion, and the rate of propagation in the mist.

The lower explosion limit proved to be independent of the homogeneity of the mixture. Whether the fuel was completely vaporized or whether it burned as a liquid-gaseous mixture, the explosion limit was the same for petroleum and for tetralin. This is understandable since, at the lower limit, the rate of propagation is quite low, and sufficient time exists to raise the drop to its vaporization temperature and to form a homogeneous mixture with air; hence, a homogeneous gas flame is being propagated near the lower limit.

The heat of vaporization absorbed by the liquid fuel is a minor part of the heat of combustion of the vaporized fuel. Since the heat of vaporization is about 10,000 calories per mole for low-boiling fuels (B. P. around 200 C), whereas the heat of combustion of the high molecular weight hydrocarbons is as much as 1.4×10^6 calories, the loss due to vaporization is less than one per cent, usually less than the experimental error.

In homogeneous combustion, when the gases are present in stoichiometric ratio, reactions go essentially to completion to form carbon dioxide and water vapor. In heterogeneous mists, the reactions are not as efficient. First, it is not practical to establish a stoichiometric relation

between total fuel and air since the fuel/air ratio only has significance in the gas phase where the burning proceeds. As a result, the same weights of fuel sprays will give varying fuel-air ratios in the gas phase depending upon the mean drop size of the spray. Secondly, some of the fuel in the larger drops will crack thermally before vaporization and will eventually leave the reaction zone unburned as carbon particles. It was observed by the authors that the limiting mist for complete combustion required more excess air the larger the average drop size of the spray.

The explanation for the above follows the same reasoning as was used on the lower limit mists, except that, for richer fuel mists, flame propagation rates increase as the mist becomes richer in fuel vapors with the result that burning of the vaporized portion occurs too rapidly to permit the remaining fuel drops to vaporize, so that both highly fuel-rich and less fuel-rich regions reach the flame front; the latter readily burn to completion, whereas the former regions do not.*

Table 18-2 lists comparisons of propagation rates in mists and in homogeneous vapor mixtures. These rates are propagation rates in a tube and were determined by the time of passage of the flame between two fine strips of tin at known separations. The data indicate that the rate in the mist is lower than the rate in the homogeneous mixture of fuel and air. The explanation is as before, with an application of the LeChatelier principle: since the mist is composed of fuel-rich and fuel-poor areas, the rate will average out accordingly, whereas the richer homogeneous mixture will burn at its uniformly higher rate.

A meager amount of information on droplet combustion exists in the chemical literature from 1923 to 1949. At this time Burgoyne and Richardson⁽¹⁸⁻²⁹⁾, in an investigation on the hazards of fuel-mist explosions in industrial establishments, took up the study. They studied low-volatility cutting oils in the form of condensed and atomized mists. The differences in the two mists were in the method of formation. The former was formed by vaporizing the fuel completely and then having the vapor condense on nuclei in an air stream. Such a mist is of very fine size, small enough that settling in a tube is very slow. The atomized mist was formed by the method of an impinging air stream on a film of liquid. The inflammability limits were measured in the usual manner, described in Chapter 16, by upward propagation in a closed tube. It was found that as the diameter of the tube was decreased from 7 to 1.75 cm, the lower limit for condensed mists was raised, but the upper limit was unaffected. It is probable that there is a limiting diameter of tube, below which all mists would be quenched, just as occurs in homogeneous gas mixtures; likewise, above a certain diameter, the lower limit probably stays fixed. The effects of diluents on the condensed mists were studied also and it was found that 30 per cent nitrogen, or 22 per cent carbon dioxide or 5.3 per cent methyl bromide in the air would completely suppress inflammation. Table 18-3 shows the effect of carbon dioxide in proportions less than required for complete extinction.

In accord with Haber and Wolff it was found that the lower limit of n-hexane, n-heptane, n-octane, isooctane, cyclohexane, and benzene were rather constant at 57 mg per liter of air, in a two-inch-diameter tube, which is close to the limit for the pure vapor state. Also, since the upper limits are lower for mists than for pure vapors, the amount of diluent necessary as a suppressor was found to be less. For example, where 5.2 per cent methyl bromide suppressed an oil mist, 7.2 per cent was required to suppress a flame of n-hexane vapor.

It appears from these two reports that, although little has been reported on static ignition limits of fuel mists, the order of magnitude of effects to be expected can be fairly well approximated. Generally the lower limit will not vary much from the vapor value, but the upper limit will probably vary in proportion to the mean drop size of the mist.

* The reader is referred at this point to Chapter 19 for a discussion of Wohlenberg's reaction interface extension theory. It is in a situation such as this one that this theory may be applied to fuel-mist combustion since, as a result of the presence of the mist, islands of fuel are "floating" in surroundings of air. This is slightly different from Wohlenberg's and Rummel's models of turbulent mixing, but in droplet combustion the picture is somewhat simplified since the interface extension of the fuel is the only consideration, if a rather loose adaptation of the idea is allowed.

TABLE 18-2. COMPARISON OF PROPAGATION RATES IN MISTS AND IN COMPLETELY VAPORIZED MIXTURES. (Haber and Wolff) (18-28)

	Fuel, mg/l	Rate, meters/second	
		Mist	Vapor
Petroleum	52.0	1.1	1.3
	72.0	4.9	5.4
	85.0	5.7	6.6
Tetralin	47.0	0.7	0.8
	94.0	1.1	1.9
Quinolin	72.0	---	0.6

TABLE 18-3. THE EFFECT OF CO₂ IN SUPPRESSING THE INFLAMMABILITY OF OIL MISTS. (Burgoyne and Richardson) (18-29)

Per cent CO ₂ in (air + CO ₂)	mg oil/liter (air + CO ₂)	mg oil/ liter air
0	55	55
13.0	68	78
17.4	91	110
21.9	noninflammable	

Bolt and his associates⁽¹⁸⁻³⁰⁾ have used the spinning disk atomizer (Chapter 2) and photographic analysis to determine the lifetime of sprays whose mean size is in the 50-130 micron range. Their results for sprays agree with those of Godsave's for single droplets in that the burning life of the drop is proportional to the square of the diameter; in other words, the burning rate varies as the first power of the diameter. They observed that the ring formed by the burning drops was of less diameter than the ring formed by the drops when not ignited. They attributed this change in radius to a small droplet size when the flame is present. The decreased size may be a result of radiation to the drops increasing their evaporation rate before they reach the ring, or may be the result of radiation effects on the disk and the fluid on its surface, leading to a change in the fluid viscosity. In any case, a complete explanation appears difficult because of the numerous uncontrolled variables involved.

Anson⁽¹⁸⁻³¹⁾ has studied the combustion stability of kerosene sprays as a function of mean spray size. By injecting kerosene into a small-scale combustion chamber under varying injection pressures, mean spray sizes in the range 50 - 150 microns were obtained. He then related stability limits of mean spray sizes to given air-stream velocities, and observed that the fine sprays extended the range of stable combustion.

Browning and Thorpe⁽¹⁸⁻³²⁾ obtained flame stability diagrams for mixtures of n-heptane, isooctane, and benzene burning with air on Bunsen tubes. They varied stream temperature and burner diameter and found that only at low temperatures and high fuel concentrations did the results differ from those obtained with homogeneous, gaseous combustion. These results seem to indicate that except for these latter conditions the fuel spray is completely vaporized and burned in the flame zone.

Control

Kirtley and Lewis(18-33) have investigated the case where the liquid fuel is completely vaporized, but where the mixing with air is heterogeneous. This situation tends to parallel the nonhomogeneous mixing in fuel spray systems, and their results are comparable too, in that the stability limits of all fuels studied were wider under nonhomogeneous mixing conditions. They used a wide variety of liquid fuels, but conclude that the extinction limits of the various fuels cannot be compared due to the dependence of mixing on fuel density and fuel velocity. They also attempted to relate burning velocity with propagation limits, but could not obtain any correlation.

Garner and Cheetham(18-34) have designed a gas-turbine-type combustion chamber which is capable of atomizing and burning fuel at the rate of 50 cc per hour with air flows of 5 to 40 grams per minute. They investigated the lean extinction limits of several hydrocarbons at pressures between 100 mm Hg and atmospheric. Although the problem of mean drop size is only approached qualitatively by varying the atomizing pressure, they observe, in accord with other investigators, that at high flow rates the extinction limit becomes leaner as the mean drop size is reduced. They also observe a reversal in their stability curves at lower air rates which is controlled by some minimum drop size, below which the stability limit moves toward the rich side. This is consistent with other observations in which it is generally reported that spray flames have a lower lean limit than homogeneous gas flames. The reason for this is that the nonhomogeneous vapor-air concentrations afford the flame region a higher fuel concentration near the limit than exists in the homogeneous gas flame. As a result the spray flame may still be stabilized although its mean fuel-air mixture is outside the limit region for the gas flame. The point of reversal then signifies the mean drop size below which the spray behaves as a homogeneously vaporized mixture.

The authors do not explain the reversal in terms of limit fuel-air concentrations as above, but instead explain the stability problem in terms of the air-velocity flow pattern in which low-pressure regions cause reverse flow of air and combustion products which stabilize the flame. The limits are also related to static inflammability limits and normal burning velocity in the reverse flow region. These studies showed that, at atmospheric pressure, the order of the stability limits for the different fuels varied in the same manner as the static inflammability limits at lower pressures, however, the limits appear to converge.

FLAME STABILITY IN HIGH-VELOCITY SYSTEMS

In practical combustion chambers, air velocities are high and the hot gases necessary to ignite the oncoming mixture must come from the freshly burned recirculated gases. The action of the reverse-flow zone has been mentioned earlier and is of major importance in high-velocity systems. It is quite often possible to set up reverse-flow conditions in a chamber by directing the spray nozzle upstream, although this method is also combined with a baffle system. The stability of such a system may be limited by excessive evaporation due to the quantity of heat brought back into the reverse-flow zone or to the quantity of fuel introduced; in either event the upper limit of inflammability may be reached which would cause instability. The placement of the injection system relative to the flame holder can be very important under such circumstances. The length of path between the fuel nozzle and the flame front represents a competition between rate of vaporization and rate of dilution of the vapors in the total air supply. If the fuel is highly volatile, a smaller mass of spray is required to attain the proper fuel/air ratio in the gas phase and also the flame holder may be placed farther away from the nozzle to provide better mixing. Where the fuel is not readily vaporized, it is necessary to place the flame holder nearer to the injection point so that the fuel vapor reaching the eddy zone may not be diluted below its lower inflammability limit. With less volatile fuels, the flame holder must be designed not to trap too much liquid on its surface, otherwise the flame holder may be cooled excessively and the flame will be blown off. These requirements are all functions of the size of chamber, drop-size distribution, flow velocity, and design of flame holder, but are not too difficult to establish empirically.

Hottell, et al., (18-35, 18-36) have employed the system used by Williams(18-37) (see Chapter 16) to study the stability of flames from air-fuel spray mixtures at high velocities. They introduced the heterogeneous mixture into a combustion chamber three inches square by 17 inches long. The flame holders were stainless steel rods, which were heated at variable rates to control the

rate of evaporation from their surfaces. The fuel used was diesel oil (boiling range 319 to 630 F) for most of their investigations.

Their data may be summarized as follows. Where comparison is made to homogeneous mixtures, reference is usually meant to the data of Reference 18-37 on the same type of apparatus.

- (a) Whereas increased velocity reduced the lean limit air/fuel ratio, at blowout, for the homogeneous mixtures, it increased the limit for the liquid spray.
- (b) Adding heat to the flame holder increased the stability of leaner mixtures for gaseous fuels, but, with liquid fuel sprays, adding heat eventually extinguished the flame.
- (c) The stability limits for burning liquid sprays were much leaner than for gaseous fuel, the air/vaporized-fuel ratio being as lean as 50:1, which is well outside the range for gaseous hydrocarbon-air mixtures. Likewise, the rich limit for the liquid spray was on the lean side of stoichiometric. This point checks the early observation of Haber and Wolff(18-28).

Drop-size effects were studied qualitatively by varying the atomizing velocity. It was observed however that, as the atomizing velocity was increased, thus decreasing the average drop size, the limits shifted to the rich side. This is to be expected since the mixture is then approaching homogeneity. Likewise, variation toward richer limits with smaller drops may be due to a decreased collection efficiency on the flame holder. These effects are illustrated in Figure 18-6, reproduced from Reference 18-35.

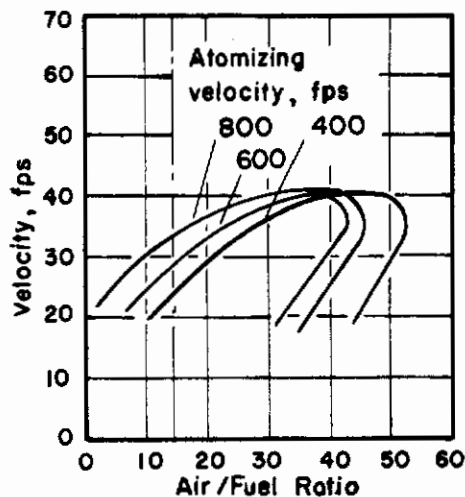


FIGURE 18-6. EFFECT OF ATOMIZING VELOCITY ON STABILITY LIMITS (Hottell, et al.)(18-35)

Another important observation in these studies is that the flame-holding ability of the flame holder is related to its ability to collect liquid drops on its surface. This was shown rather strikingly by the fact that as soon as the last droplet had evaporated from the flame holder the flame was extinguished.

Four possible mechanisms of flame blowout are proposed by the authors. In the lean limit, blowout is said to occur when vapor binding occurs, or when there is insufficient fuel regardless of vapor binding. The effect of vapor binding is to reduce the heat-transfer coefficient and thus the heat available for evaporation. Rich-limit blowout is due to:

- (a) Collecting excess fuel with insufficient vaporization and excessive cooling of the flame holder, the result being that liquid is sloughed off the flame holder.

(b) Accumulating excess fuel vapor in the eddy zone.

Williams and Maddocks⁽¹⁸⁻³⁶⁾ have investigated the effect of the size of the flame holder on flame stability. An interesting part of the results is the fact that, in contrast to the effect in homogeneous gas mixtures, as the diameter of the flame holder is increased from 1/16 to 1/2 in. there is a reduction in the rich stability limit and in the maximum attainable velocity, while below 1/16 in., the effect is the same as occurs with homogeneous mixtures. Below 1/40 in., stable combustion could not be maintained.

This effect cannot be explained by application of the collection-efficiency parameter, because such an explanation would predict the opposite effect, that is, the greater the size of rod, the smaller the collection efficiency. Therefore the stabilizer would be hotter and the shift would be to richer mixtures rather than to the leaner ones that the data show. It is possible that the heat-transfer coefficient, which varies inversely with the square root of the diameter, is the controlling parameter, for increased heat transfer would explain the improved vaporization and the accompanying shift to richer mixtures. The increased heat-transfer coefficient probably explains the ability of small rods to attain temperature equilibrium rapidly with the result that the fuel concentrations can be changed quite rapidly and the flame will retain its stability. If a rod greater than 1/4-in. diameter was used, blowout resulted even though the change occurred within the normal stability limits.

CONCLUDING REMARKS

Stabilization limits in heterogeneous mists are different from those in homogeneous fuel-air systems; however this does not imply that the burning process itself occurs differently. The chemical factors remain the same, but physical properties such as heat transfer to the flame holder, fuel volatility, drop-size distribution, and air velocity exert a controlling effect.

The actions occurring in practical combustion chambers are numerous and complicated; therefore most of the work in this phase of combustion has been of an empirical nature. Knowledge of sprays at present is still too limited to predict what type of spray is needed for the most efficient combustion of liquid drops in a combustion chamber. Probably until there is a marked advance in the technique for determining drop-size distribution and evaluating the physical effects that depend on it, it will not be possible to apply the fundamentals of gas-phase combustion to the combustion of fuel sprays. At present, the application of the knowledge of sprays to combustion-chamber performance remains of a general nature; in particular, only vague relations can be established for such measurements as spray cone angles and combustion performance. Such parameters involve also the geometry of the combustion system.

In the following chapter the theory of diffusion flames will be discussed; this will aid in answering some of the questions on burning fuel droplets since the flame surrounding a droplet is a diffusion flame. However, the theory, at present, is only able to approximate the observed conditions for a single drop in controlled surroundings. A better understanding of this simple phenomenon will be a necessary prerequisite to the full description of the behavior of a cloud of burning drops of varying sizes.

It should be said in conclusion that the problem of single-droplet burning is sufficiently solved for the present, so that it is now necessary to shift the experimental emphasis to the burning of the spray assembly. This is not to imply that the theory of droplet burning is completely understood, but as one reviews the subject one observes that the main difference in the results of these theories is in the assumed model of the burning droplet; depending upon the model chosen, burning and evaporation rates have been predicted within reasonable orders of magnitude.

Comair
REFERENCES

- 18-1. Joyce, J. R., Atomization of Liquid Fuels for Combustion; J. Inst. Fuels, Vol. 22, 1949, p. 150.
- 18-2. Gibbs, R., Computing Combustion Volume for Burning Oil Fuel; Chem. Eng., January, 1949, p. 112.
- 18-3. Houghton, G. H., from Perry's "Chemical Engineer's Handbook", McGraw-Hill, New York, 1941, p. 1991.
- 18-4. Probert, R. P., Influence of Spray Particle Size and Distribution in Combustion of Oil Droplets; Phil. Mag., Vol. 37, 1946, p. 94.
- 18-5. Godsave, G. A. E., Combustion of Fuel Droplets; Nature, Vol. 164, 1949, p. 708; Vol. 166, 1950, p. 1111.
- 18-6. Kumagai, S., and Isoda, H., Combustion of Fuel Droplets; Nature, Vol. 166, 1950, p. 1111.
- 18-7. Lloyd, P., Fuel Problem in Gas Turbines; Proc. Inst. Mech. Eng., Vol. 159, 1948, p. 220.
- 18-8. Gudkov-Belyakov, V. K., Critical Analysis of the Theory of the Combustion of Fuel in Liquid Phase; Dizelstroenie, Vol. 9, 1940, p. 10.
- 18-9. Neuman, K., Investigation of the Spontaneous Ignition of Liquid Fuel; V. D. I., Vol. 70, 1926, p. 1071.
- 18-10. Khudyakov, G. N., Combustion of Drops of Liquid Fuel while in "Flight"; Bull. Acad. Sci. USSR, April, 1949, p. 508.
- 18-11. Lloyd, P. and Probert, R. P., The Problem of Burning Residual Oils in Gas Turbines; Proc. Inst. Mech. Eng., Vol. 163, 1950, p. 206.
- 18-12. Wolfhard, H. G. and Parker, W. G., Evaporation Processes in a Burning Kerosene Spray; J. Inst. Pet., Vol. 35, 1949, p. 118.
- 18-13. Pilcher, J. M., et. al., Battelle Memorial Institute Progress Reports 1950-1951, OAR Contract AF 33(038)-12656.
- 18-14. Lloyd, P., "Development of the British Gas Turbine Jet Unit", ASME Report, January, 1947, p. 462.
- 18-15. Godsave, G. A. E., Burning of Single Droplets of Fuel, Part I. Temperature Distribution and Heat Transfer in the Pre-Flame Region; N.G.T.E. Report No. R-66, March, 1950.
- 18-16. Tanford, C. and Pease, R. N., Theory of Burning Velocity; J. Chem. Phys., Vol. 15, 1947, pp. 431, 433, and 861.
- 18-17. Godsave, G. A. E., Burning of Single Droplets of Fuel, Part II Experimental Results; N. G. T. E. Report No. R-87, April, 1951.
- 18-18. Godsave, G. A. E., Burning of Single Droplets of Fuel, Part III Comparison of Experimental and Theoretical Burning Rates and Discussion of the Mechanism of the Combustion Process; N.G.T.E. Report No. R-88, August, 1952.

- 18-19. Godsave, G. A. E., Studies of the Combustion of Drops in a Fuel Spray - The Burning of Single Drops of Fuel; Fourth Symposium on Combustion, William and Wilkins, Baltimore, 1953, p. 818.
- 18-20. Goldsmith, M. and Penner, S. S., On the Burning of Single Drops of Fuel in An Oxidizing Atmosphere; Jet Propulsion, Vol. 24, 1954, p. 245.
- 18-21. Hall, A. R. and Diederichsen, J., An Experimental Study of the Burning of Single Drops of Fuel in Air at Pressures up to 20 Atmospheres; Fourth Symposium on Combustion, William and Wilkins, Baltimore, 1953, p. 837.
- 18-22. Spalding, D. B., Combustion of Liquid Fuel in a Gas Stream; I. Fuel, Vol. 29, 1950, p. 2; Vol. 30, Combustion of Fuel Particles, 1951, p. 121.
- 18-23. Ackerman, G., V.D.I. Forschungschift, 1937, p. 382.
- 18-24. Spalding, D. B., The Combustion of Liquid Fuels; Fourth Symposium on Combustion, William and Wilkins, Baltimore, 1953, p. 847.
- 18-25. Spalding, D. B., Experiments on the Burning and Extinction of Liquid-Fuel Spheres; Fuel, Vol. 32, 1953, p. 169.
- 18-26. Topps, J. E. C., An Experimental Study of Evaporation and Combustion of Falling Drop-lets; Jour. Inst. Petrol., Vol. 37, 1951, p. 535.
- 18-27. Spalding, D. B., Combustion of Liquid Fuel in a Gas Stream II. Experimental; Fuel, Vol. 29, 1950, p. 25.
- 18-28. Haber, F. and Wolff, H., On Mist Explosions; Z. fur. Angew. Chem., Vol. 33, 1923, p. 373.
- 18-29. Burgoyne, J. H. and Richardson, J. F., Inflammability of Oil Mists; Fuel, Vol. 28, 1949, p. 2.
- 18-30. Bolt, J. A., Boyle, T. A., and Mirsky, W., The Generation and Burning of Uniform - Size Liquid fuel drops, University of Michigan Report, Project M-988 ARDC-USAF, Contract No. AF 33(600)-5057, May, 1953.
- 18-31. Anson, D., Influence of the Quality of Atomization on the Stability of Combustion of Liquid Fuel Sprays; Fuel, Vol. 32, 1953, p. 39.
- 18-32. Browning, J. A. and Thorpe, M. L., Flame Stability of Liquid-Vapor Air Mixtures; Project Squid, Tech. Memos., Dartmouth 1 and 2, 1952.
- 18-33. Kirtley, J. G. and Lewis A., Flame Stability Studies of Different Vaporized Fuels Under Non-Homogeneous Mixing Conditions in a Small-Scale Combustion Tube; Fuel, Vol. 33, 1954, p. 5.
- 18-34. Garner, F. H. and Cheetham, H. A., The Flow Pattern of Gas-Turbine Combustion; Jour. Inst. Petrol., Vol. 37, 1951, p. 554.
- 18-35. Hottel, H. C. and May, W. G., "Flame Stabilization in Air Fuel Spray Mixtures, Part I, Characteristics of a Transverse Red Stabilizer", Fourth Symposium on Combustion, Williams and Wilkins, Baltimore, 1953, p. 715.
- 18-36. Williams, G. C. and Maddocks, F. E., Jr., "Flame Stabilization in Air-Fuel Spray Mixtures, Part II, The Effect of Stabilizer Dimensions", Fourth Symposium on Combustion, William and Wilkins, Baltimore, 1953, p. 727.

Continued
18-37. Williams, G. C. and Hottell, H. C., and Scurlock, A. C., "Flame Stabilization and Propagation in High Velocity Gas Streams", Third Symposium on Combustion, Flame, and Explosion Phenomena, Williams and Wilkins, Baltimore, 1949, p. 21.

Contrails

CHAPTER 19. DIFFUSION FLAMES

ABSTRACT

Although the diffusion flame is more common in application than the premixed flame, and is the end flame condition in many instances when a premixed flame is also involved, it is the subject of less research than the premixed flame; this situation possibly results because the extra complication of mixing fuel and air is an essential part of diffusion flame phenomena. On the other hand, this mixing process is usually the rate-controlling factor in the diffusion flame; thus, the conditions of mixing are often of more importance than chemical kinetic considerations. In this chapter, experimental and theoretical work are analyzed as a unit for each of four types of diffusion flame, the confined laminar flame, the unconfined laminar flame, and the confined and unconfined turbulent flames. In the confined flame, both fuel and oxidant are in limited supply, while in the unconfined flame only the fuel is limited. Also, in the unconfined flame, buoyancy effects may play a large part in the observed phenomena. The review of the literature on this basis of classification indicates many areas where a large amount of fundamental work remains to be done with respect to the diffusion flame.

Contracts

DIFFUSION FLAMES

by

A. Levy and A. A. Putnam

In the ignition and combustion phenomena described thus far, the discussion has been concerned mainly with homogeneous premixed gases. In these, diffusive mixing is not involved, and the burning velocities are functions of the reaction-rate parameters. Due to the complexity of the reactions, most work in combustion has been limited to studies of premixed gases; there are, however, many instances where burning takes place between unmixed gases. Flames produced in such a manner are referred to as diffusion flames and exist as laminar or turbulent diffusion flames. When the temperature of combustion is high enough, the reaction velocity is subordinate to the rate of mixing as a controlling step for both laminar and turbulent diffusion flames. In the case of the laminar diffusion flame, combustion occurs in a thin flame front created by the reaction zone where the fuel and air molecules are interdiffused. Such flames are observed in burning candles, and in the outer flame surrounding the blue Bunsen cone. In most instances, however, such as in the high-velocity combustion applications referred to previously, turbulent mixing is the chief factor in determining combustion rates.

Diffusion flames may not only be classified as laminar or turbulent, but they may also be classified as open or confined. If the supply of oxidant is not much larger than the supply of fuel, as in a combustion chamber that is relatively small, compared to the size of the fuel supply line, the flame is confined and may even be underventilated. If the supply of oxidant is large, the flame is not constricted and, especially in laminar flames, buoyancy forces may have a large effect.

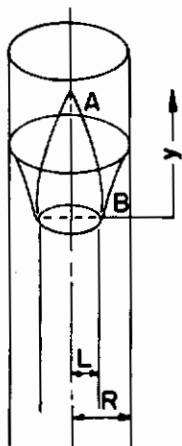
LAMINAR DIFFUSION FLAMES

Confined Flames

Burke and Schumann⁽¹⁹⁻¹⁾ investigated diffusion flames with the fuel and air flows held equal and constant at about 2 ft. per sec. At these low rates of flow, the flames were never more than 10 inches in height, and the influence of burning on the mixing (diffusion) process could be neglected. The flames were produced in an apparatus consisting of two concentric tubes shown in Figure 19-1. Because the rim of the inner tube, through which the fuel was supplied, was well below the rim of the outer tube, the flame assumed a definite shape. Depending upon whether the flame was over-ventilated or underventilated, the laminar diffusion flame appeared as A or B, respectively, as shown in the figure. A flat diffusion flame could have been obtained if parallel plane surfaces, rather than concentric tubes, had separated the air and gas.

Four simplifying assumptions are made by Burke and Schumann in their mathematical treatment:

- (1) The velocities of the gas and of the air in the flame region are equal and constant.
- (2) The coefficient of diffusion is constant.
- (3) Interdiffusion is radial.
- (4) The two gas streams mix only by diffusion.



A Overventilated flame
B Underventilated flame

FIGURE 19-1. LAMINAR DIFFUSION FLAMES (SCHEMATIC)

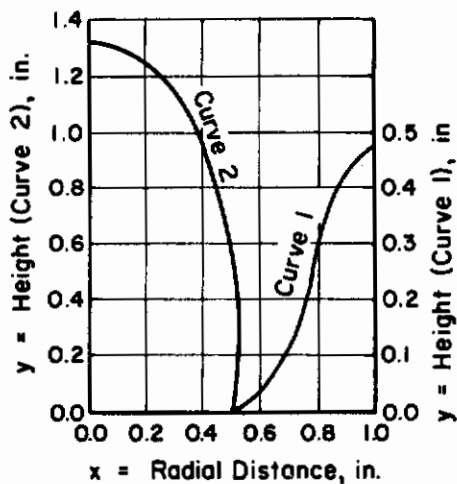


FIGURE 19-2. FLAME SHAPES CALCULATED BY EQUATION 19-3

Burke and Schumann⁽¹⁹⁻¹⁾

Actually, as the temperature increases, the velocities and diffusion coefficient must also increase; but any increases are approximately in the same proportion so that temperature effects can be disregarded. Assumption (3) holds quite well for tall flames and (4) merely implies parallel streamline flow*.

The diffusion equation in cylindrical coordinates is

$$\frac{\partial C_{ry}}{\partial t} = D \left[\frac{\partial^2 C_{ry}}{\partial r^2} + \frac{1}{r} \frac{\partial C_{ry}}{\partial r} \right] \quad (19-1)$$

and, because velocity is constant, the equation in terms of distance along the axis of the tube (y ordinate) is

$$\frac{\partial C_{ry}}{\partial y} = \frac{D}{V} \left[\frac{\partial^2 C_{ry}}{\partial r^2} + \frac{1}{r} \frac{\partial C_{ry}}{\partial r} \right], \quad (19-2)$$

where D is the diffusion coefficient, V is the velocity of the gas, C_{ry} is the concentration of gas, and r is the radial distance from the axis of the tube. The equation is solved in terms of Bessel functions of the first kind. By making the additional assumption that the fuel and oxidant combine in stoichiometric proportions at the front**, the boundary conditions on C_{ry} for the individual solutions on fuel and oxidant side are determined; that is, at the flame front where $r = x$, $C_{ry} = 0$ and the concentration gradients must be related by i , the number of moles of oxygen that combine with one mole of fuel. Hence,

$$\sum \frac{1}{\mu} \frac{J_1(\mu L) J_0(\mu x)}{J_0(\mu R)^2} e^{-\frac{D\mu^2 y}{V}} = \frac{R^2 C_2}{2 LiC} - \frac{L}{2} \quad (19-3)$$

where μR assumes the values of all positive roots of the equation $J_1(\mu R) = 0$. The values of x and y which satisfy the equation define the shape of the flame front. C_1 and C_2 are the initial fuel and oxygen concentrations respectively, and $C = C_1 + C_2 / i$. Figure 19-2 illustrates the two flame shapes that result from these calculations.

Bell and Putnam⁽¹⁹⁻³⁾ have generalized the set of curves presented by Burke and Schumann for $R/L = 2$, and have replotted them in the form of Dy/VL^2 as a function of r/L for various values of \bar{C} , where \bar{C} is given by

$$(1/\bar{C}) - 1 = (i C_1 - C'_2) / C_2, \quad (19-4)$$

where C'_2 is the oxidant concentrate in the jet, if any. It is seen that \bar{C} is constant for any particular fuel-oxidant combination. Bell and Putnam also showed that for $\bar{C} > 0.45$, the theoretical flame shape was influenced little by the ratio of R/L , if $R/L \geq 2$.

The equations for flat flames are handled in the same manner, with use of the corresponding boundary conditions. The diffusion equation now is

$$\frac{\partial C_{ry}}{\partial r} = \frac{D}{V} \frac{\partial^2 C_{ry}}{\partial r^2} \quad (19-5)$$

Solving the equation for the boundary conditions, that is, that the fuel and air are at stoichiometric concentration and $C_{ry} = 0$, the concentration equation for the flame front is

$$\sum_1^{\infty} \frac{1}{n} \sin \frac{n\pi L}{R} \cos \frac{n\pi x}{R} e^{-\frac{Dn^2 \pi^2 y}{VR^2}} = \frac{\pi}{2} \left(\frac{C_2}{iC} - \frac{L}{R} \right), \quad (19-6)$$

where L and R refer to the half widths of the parallel walls here.

* A more extensive discussion of Burke and Schumann's assumption is given by Barr and Mullins⁽¹⁹⁻²⁾.

** This assumption of complete combustion at the flame front is discussed later.

Returning to the axially symmetric flame, it was observed that DY/VL^2 was a function of $(i C_1 - C_2')/C_2$, where Y is the flame height. From Burke and Schumann's curves, DY/VR^2 increases with $(i C_1 - C_2')/C_2$ for overventilated flames, and decreases for underventilated flames. Thus, as Burke and Schumann pointed out:

- (1) Y is independent of volume flow rate,
- (2) Y is proportional to velocity,
- (3) Y varies inversely with diffusivity,
- (4) The introduction of an inert gas decreases the height of an overventilated flame and increases the height of an underventilated flame,
- (5) A change in fuel which increases i shortens an underventilated flame and lengthens an overventilated flame,
- (6) There is no effect of pressure on height at constant mass flow rate (since D varies inversely with pressure), and
- (7) There should be little temperature dependence at constant mass flow rate.

Generally, all the above effects have been borne out by experiment and are illustrated in Tables 19-1 through 19-4, taken from the work of Burke and Schumann. The temperature effect, Table 19-4, indicates some shortening of the flame as the temperature is increased. The data are rather limited, but it would appear that over this wide temperature range, the diffusivity increases to a greater extent than the gas velocity, as is to be expected.

Jost⁽¹⁹⁻⁴⁾ presents a very simple treatment of diffusion flames, which does not define the shape of the flame, but does arrive at most of the other conclusions arrived at by more complicated treatment of Burke and Schumann.

Considering the flow through two concentric tubes of radii L and R , where L refers to the inner tube again, the maximum flame height, Y , is determined by the time required for the fuel and air to diffuse to stoichiometric proportions.

The air must diffuse into the gas a distance L for the overventilated flame (see Figure 19-1), and the gas into air, a distance $R-L$ for the underventilated flame. These depths of penetration, δ , in a time, t , can be expressed as

$$\delta^2 = 2 Dt, \quad (19-7)$$

where D is the diffusion coefficient. If t is the time needed for the gas to flow at a constant velocity from the mouth of the inner tube to the tip of the flame, then

$$t = \frac{Y}{V} \quad (19-8)$$

where V is the gas velocity; combining Equations (19-7) and (19-8) gives

$$Y = \frac{V\delta^2}{2D}. \quad (19-9)$$

Equation (19-9) is capable of explaining all the effects that were explained by Equations (19-3) and (19-6) except the effect of an inert gas (Conclusion Number 4, above).

It is to be noted that the reaction mechanism and reaction rate are of secondary importance since burning is assumed to occur in an infinitesimally thin zone and at stoichiometric conditions; the rate controlling process is just the rate of diffusion of the two gases to the point of reaction at the flame front.

TABLE 19-1. FLAME HEIGHT PROPORTIONAL TO GAS FLOW

Air, cu ft/hr	Methane, cu ft/hr	Flame Height, inch	Col. 3 Col. 2
7.0	0.38	1.23	4.56
18.0	1.00	4.47	4.47
29.5	1.64	7.25	4.42
41.1	2.28	9.90	4.32

TABLE 19-2. EFFECT OF INCREASE IN i

Gas	i	Height, inch	
		Calculated	Experimental
Manufactured gas	1.05	1.66	1.44
Methane	2.00	0.93	0.87
Ethane	3.50	0.67	0.62

TABLE 19-3. EFFECT OF GAS DIFFUSIVITY

Air, cu ft/hr	Hydrogen, cu ft/hr	CO, cu ft/hr	Height, inch
22.2	25		2.75
22.2		25	6.95

TABLE 19-4. EFFECT OF TEMPERATURE ON METHANE FLAME

Temperature, C	Height, inch
20	0.78
370	0.69
510	0.70

Guyomard⁽¹⁹⁻⁵⁾ makes some short comments on modifying Burke and Schumann's work to correct for temperature; he also studies briefly a system with a parabolic fuel velocity profile, such as might be given by fuel from a pipe passing into open air; the specific formula he gives for flame height apparently applies to methane, although it is not so stated.

Barr and Mullins⁽¹⁹⁻²⁾ have studied the diffusion flame as part of a more general program dealing with the combustion of gases in a vitiated atmosphere. "Vitiated" as used by the authors refers to the contamination of the air by the products of combustion (water vapor, carbon dioxide) so that the resulting air is reduced in oxygen content compared with pure air. The vitiation is measured by an index, a , defined as the fractional partial pressure or volume of oxygen in the air, for example, $a \approx C_2 = 0.21$ for pure air.

Combustion in vitiated atmospheres is related to full-scale combustion chamber problems. Since the fuel usually enters the chamber in the form of droplets of various sizes, combustion occurs over a finite length of the chamber. Unless secondary air is introduced in sufficient amount, the larger fuel drops must burn in an atmosphere partially choked with reaction products from the faster burning fractions of the fuel spray. This has a large effect on the efficiency of the over-all combustion process as a result. For the most part, the effects of vitiation are threefold. These are:

- (1) A sharp lowering of the flame temperature, especially in rich mixtures where more oxygen is needed for complete combustion. A corollary to this is the reduced efficiency in the evaporation of the fuel spray.
- (2) Cracking and polymerization is increased. Ordinarily, a certain amount of cracking occurs in the primary zone. This is actually beneficial, since the cracking produces volatile hydrocarbons. But the lack of oxygen reduces the benefit of the cracking and permits more polymerization.
- (3) The limits of inflammability are reduced.

It was found, for example, that a diffusion flame of a Calor gas-air mixture (Calor gas is a mixture of lower saturated hydrocarbons consisting mainly of propane and butane) could not be ignited by a heated Nichrome spiral for $a < 0.17$. Similar effects have been noted, and studied quantitatively, by Lewis and von Elbe⁽¹⁹⁻⁶⁾ in their ignition studies on the methane-oxygen-nitrogen system; the greater the vitiation the more energy was required for spark ignition.

Barr and Mullins made their studies on diffusion flames of Calor gas and air at flow velocities of less than one foot per second. Also, the air and fuel velocities were not equal, whereas Burke and Schumann's velocities were equal. The tests were run in concentric tubes with L equal to 0.46 cm, and R equal to 2.46 cm. The vitiated diffusion flames are described as flimsy, unstable, blue flames. With decreasing oxygen content, the yellow crown in the top of the flame becomes smaller, pointed, and finally disappears. The faint luminous halo around the flame broadens, the gap between the burner and base of the flame increases, and the entire flame surface broadens and lengthens with increased vitiation.

In a series of experiments with $a = 0.21$ (normal air), Barr shows that as the air velocity is increased there is a rapid decrease in the flame height above a fuel velocity of 0.7 cm/sec. However, it appears from the data that as the air velocity is increased to about 13 cm/sec (for these particular tests), the mixing becomes independent of the air velocity again.

The authors present a sequence of photographs of the flames at pressures between one atmosphere and 0.06 atmosphere. There is some tendency toward a changing flame shape, but the flame heights remain remarkably constant over more than a tenfold change in pressure ratio. One cannot quantitatively compare the data of the other workers with these data because of the extremely low flow velocities used by these authors. The comparisons can only be qualitative and in this sense the general agreement is quite good. As the oxygen content is reduced, the flames which were overventilated exhibit increased flame heights. The dependence on flow velocity is no longer a direct proportionality, but now varies in a more complicated way.

The question of what happens to the flame length when the exhaust gases are recirculated is of practical interest. Assuming no change in the diffusion process at increased temperatures, and a constant fuel flow, the authors calculate that the height would not be changed by as much as 10 per cent for a mass flow of recirculated gases equal to twice the mass flow of pure air.

Barr(19-7) extended this study with the concentric tube system to cover a range of both butane and air velocities. Using a 2.2-cm outer tube, a 0.85-cm jet, fuel flows from 0.01 to 100 cc/sec, and air flows from 1 to 3000 cc/sec, Barr observed a wide variety of flame types. Over most of the range of variables, the flames had much the same forms as indicated in Figure 19-2, with modifications caused by smoking tendencies. At higher air velocities, this region of normal forms was bounded by lifted flames, which become tilted and then vortexlike in character as the fuel velocity was decreased. (See also Garside and Jackson)(19-8). At low fuel velocities, before extinction, the flame took on a meniscus shape. Near the extinction limit using low air flow velocities, the meniscus flame was also apparent, but was longer and became unstable as the fuel velocity increased.

In a later paper(19-9), Barr made a more detailed study of enclosed, overventilated, laminar flames. He found that whereas increases in air flow caused only a slight decrease in flame length, increases in the fuel flow caused even larger increases in flame length.

Barr also examined the influence of the jet diameter on flame height. At constant rates of fuel flow and air flow, an increase in the ratio of inner to outer diameter from 0.133 to 0.905 had only a slight tendency to decrease flame height. This later observation seems to indicate that any enclosed, overventilated flame system can be treated theoretically by Burke and Schumann's method by using the volume flow rates to determine the equivalent jet diameter to give a uniform flow velocity.

Although Barr has given no correlating equation for his data, one of the forms

$$\frac{DY}{q_f} = A + B (q_f/q_a) (Y/L), \tag{19-10}$$

appears to be satisfactory, where q_f and q_a are the volume flow rates of fuel and air, respectively, and A and B are constants evaluated from the data. In this equation,

$$A \gg \frac{(B q_f Y)}{(q_a L)}$$

Unconfined Flames

Hottel and Hawthorne(19-10) studied diffusion flames in the cases where (1) the fuel flows into still air, and (2) where fuel and air flow at different velocities. Precautions were taken to minimize rotation and to control turbulence by placing straighteners and screens in the gas stream. In some instances, primary air was mixed with the fuel gas. The gas studied was manufactured gas and the burning took place from nozzle ports of 1/8-, 3/16-, and 1/4-inch diameters. Since the outer chamber diameter was much larger than the nozzle diameter, these flames had the characteristics of the open flame.

Figure 19-3 presents a qualitative picture of the results of an experiment performed in the course of this study to confirm the type of concentration gradients that might be expected in diffusion flames. The authors obtained these curves by sampling across the flame surface at several distances from the burner port. As simple diffusion theory predicts(19-11), the curves resulting from these experiments show that the maximum concentration gradients occur at the flame boundary, where the fuel and air combine in stoichiometric proportions.

Further experimental evidence indicating that oxygen is completely consumed at the flame front separating the fuel and air has been shown recently(19-12). With the aid of spectroscopic

Contrails

evidence, very little, if any, oxygen has been shown to penetrate the diffusion flame interface. This does not preclude the fact that the combustion products dilute the diffusing fuel stream, but nevertheless the fuel-air concentrations are essentially stoichiometric at the flame front.

It may be noted that Zeldovich⁽¹⁹⁻¹³⁾, extending Shvab's work⁽¹⁹⁻¹¹⁾, made a lengthy mathematical study of the diffusion flame process, and shows that the temperature profile is the same as the "products" profile of Figure 19-3, if the thermal and molecular diffusivities are equal. Also, the peak temperature equals the theoretical flame temperature for a stoichiometric mixture. Actually, due to conduction losses to the surroundings, radiation losses, and the rounding off of the temperature peak (since the reaction is not, in reality, infinitely fast), the theoretical flame temperature for a stoichiometric mixture is not obtained.

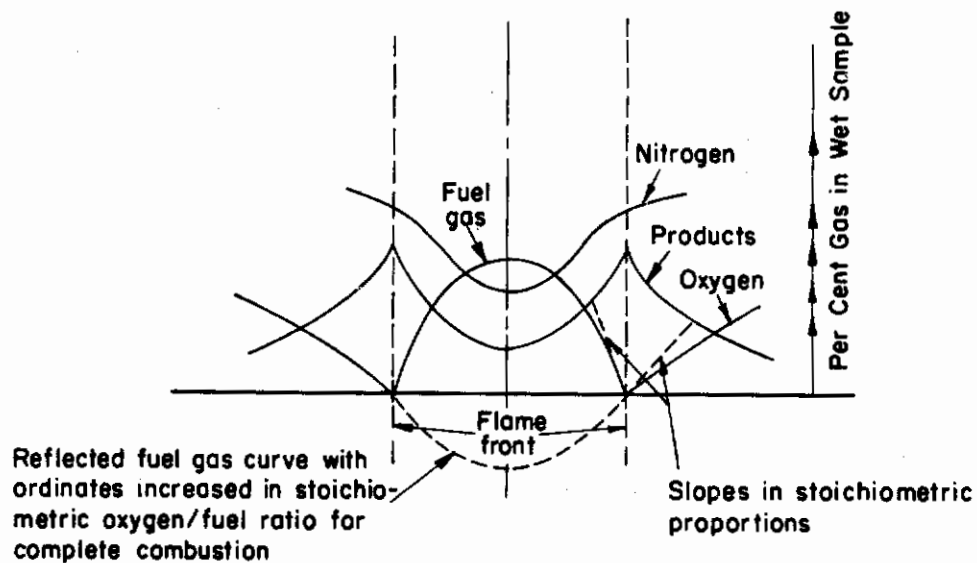


FIGURE 19-3 DISTRIBUTION OF GASES IN A DIFFUSION FLAME

Hottel and Hawthorne⁽¹⁹⁻¹⁰⁾

Figure 19-4 schematically indicates typical temperatures and concentrations at the front as calculated by Zeldovich. The amount of overlap of the concentrations indicates the thickness of the diffusion flame; as the combustion becomes more intense this thickness decreases.

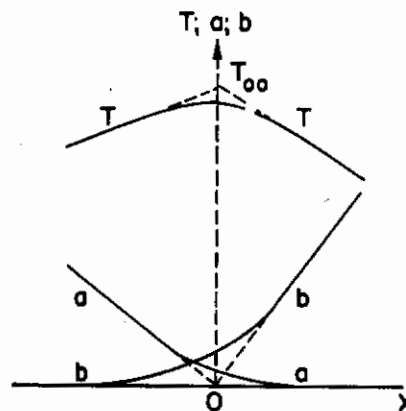


FIGURE 19-4 TEMPERATURE AND CONCENTRATION GRADIENTS AT THE REACTION SURFACE

Zeldovich⁽¹⁹⁻¹³⁾

Hottel and Hawthorne have analyzed the open diffusion flame, using the same assumptions as Burke and Schumann. They obtain the relation

$$\frac{1 + a_0}{1 + a_t} = 1 - e^{-\frac{1}{4\theta}} \quad (19-11)$$

where a_0 is the mole air/mole fuel gas in the nozzle fluid, a_t is the moles air/moles fuel gas for complete combustion, and

$$\theta = \frac{4Dt}{d^2} \quad (19-12)$$

where d is the nozzle diameter. For short flames, the height of the flame, Y , they point out, is given by tV , and thus

$$Y = \frac{q_f \theta}{\pi D} \quad (19-13)$$

This result is in agreement with observation.

Figure 19-5 indicates the actual change in flame height as the flow rate increases. The decreased rate of increase with increasing velocity, in the laminar region, is explained on the basis of a change in flow velocity along the length of the flame. For longer flames (those of Hottel and Hawthorne were more than 5 in. long as were those of Rembert⁽¹⁹⁻¹⁴⁾, whose data they also analyze), the buoyancy effects and the momentum interchange effect became increasingly important in the open flame, and the flow velocity tends to decrease along the flame length. Equation 19-12 no longer holds, and Hottel and Hawthorne advance the empirical relation,

$$Y = A \log (q_f \theta) + B \quad (19-14)$$

to fit their data.

Hottel and Hawthorne carried out a dimensional analysis of the open diffusion flame. They introduced the Grashof number,

$$G = d^3 \rho^2 \beta g(\Delta t) / \mu^2 \quad ,$$

where β is the temperature coefficient of expansion and the other terms have the usual meaning, to provide for the buoyancy effects. The dimensionless groups $q_f \theta / YD$, Y/d , G , and a_0 thus determine the flame height. They also noted that, for their tests, the changes in the diameter, d , did not affect the height; this observation allows the combination of two groups into one, namely, $(Y G^{1/3} / d)$.

It appears logical to extend this result and propose an equation of the form

$$\frac{q_f \theta}{YD} = A + B f \left[\left(\frac{Y G^{1/3}}{d} \right), a_0 \right] \quad (19-15)$$

for expressing flame height data. Then, regarding a_0 as constant, for the tests of Hottel and Hawthorne, $f(\xi) = \xi^2$ appears quite satisfactory, where $\xi \equiv Y G^{1/3} / d$. The similarity of this form to that proposed for Barr's data on closed flames (Equation 19-10) may also be noted.

Wohl, Gazley, and Kapp⁽¹⁹⁻¹⁵⁾ have made an extensive investigation of the flames of manufactured gas and butane in about the same flow range as Hottel and Hawthorne. Their studies start in the laminar range and go into the turbulent range at velocities over 100 fps. Unlike Hottel and Hawthorne, they preferred to burn their flame in open, still air, rather than use secondary air. The experimental data consisted principally of shadow photographs and measurements of flame heights. The photographs show the behavior of the flames at various Reynolds numbers. A photograph of a 100 per cent manufactured-gas flame at $N_R = 1980$ shows a well-defined inner cone of fuel to the tip of the flame. This tip is much below the actual top of the luminous flame.

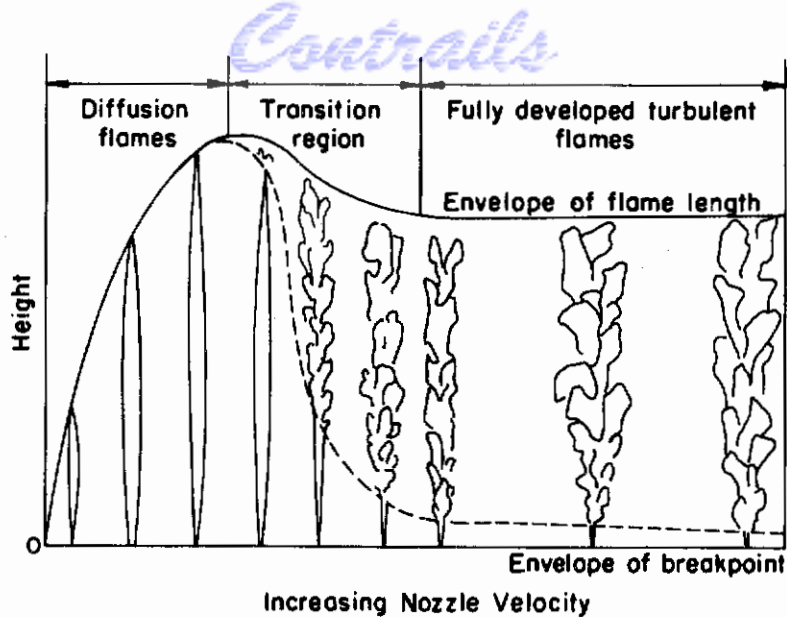


FIGURE 19-5. CHANGE IN FLAME APPEARANCE WITH VARYING NOZZLE VELOCITY

Hottel and Hawthorne⁽¹⁹⁻¹⁰⁾

Wohl, et al., noted that $(1 + a_t)$ was sufficiently greater than $(1 + a_o)$ that the approximate equation,

$$\frac{4 \pi D Y}{q_f} \cong (1 + a_t)/(1 + a_o), \quad (19-16)$$

could be used for the theoretical flame height (compare with Equation 19-11).

Like others, Wohl, et al., found that this equation does not fit the data for longer flames. For their data on 100 per cent city gas flames, they advanced the relation.

$$Y = 1/(0.206/\sqrt{q_f} + 0.354/q_f), \quad (19-17)$$

where Y, q_f are measured in centimeters and cc/sec. They explain this relation, which bears little resemblance to Equation 19-16, as follows. \underline{D} is not constant, and the average value is assumed to vary linearly with height, thus

$$D = D_o + kY. \quad (19-18)$$

If $kY \gg D_o$, then Equation 19-16 becomes

$$Y = \sqrt{\frac{q_f (1 + a_t)}{4\pi k(1 + a_o)}}, \quad (19-19)$$

which accounts for the lead term of Equation 19-17. By including the second term in the approximation of Equation 19-16, and not dropping D_o , a form of equation like that of Equation 19-17 is obtained.

With 50 per cent city gas mixture, the diameter of the jet appeared to be important, and the correlating equation took the form

$$Y = 1/(0.244/\sqrt{q_f} + 3.15 d/q_f). \quad (19-20)$$

This effect of diameter is explained on the basis that this mixture is inflammable at elevated temperatures; thus a premixed flame appears in part of the region and supports the diffusion flame.

In the case of butane, the kinetic viscosity is extremely low compared to air (0.035 cm²/sec compared with 0.155 cm²/sec). Thus, one may have an initially turbulent jet at very low flow rates. However, because of the interdiffusion with the surrounding air and the increase in temperature, the flow rapidly becomes laminar. The laminar-type flame is observed even at initial Reynolds numbers of 11,000. For this reason Wohl, et al., were able to describe their butane data successfully with the equation

$$Y = 9.9 \sqrt{\frac{q_f}{(1 + a_0)}}, \quad (19-21)$$

which is similar in form to Equation (19-19).

Hottel, in a discussion of the paper by Wohl, et al.,⁽¹⁹⁻¹⁵⁾ has shown that marked similarity exists between his approach and that of Wohl. Hottel took some of Wohl's results and transformed them into his terminology, and then plotted flame height against log (q_fθ), as he had done with his own data. It was found that Wohl's equation is not linear as is Hottel's equation, but the data fall close to the curve. Actually, Wohl's equation appears somewhat better at the lower flow rates, and Hottel's equation appears preferable at the higher flow rates.

Barr⁽¹⁹⁻¹⁹⁾ suggests that an equation for the height of an open flame could be obtained as follows. The velocity of the gas, which decreases with height in the open flame, is considered to vary exponentially with height. Thus, t (See Equation 19-12) is given by

$$t = \int_0^Y \frac{dy}{V \exp(-by)}, \quad (19-22)$$

and

$$Y = \frac{1}{b} \ln \left(1 + \frac{q_f \theta b}{\pi D} \right), \quad (19-23)$$

as contrasted with Equations 19-13 through 19-20.

In concluding this section, it might be noted that the study of ethane-nitrogen-air or ethylene-nitrogen-air mixtures as jet fuels would appear more fruitful than some of the past investigations. These gases all have nearly the same molecular weight, and the ratio of moles of reactants to products is near one. Use of diluent nitrogen permits control of the final temperature. Once these systems were understood, then the superimposed effects brought about by use of the much lighter fuels, such as hydrogen, or the much heavier fuels, such as butane, could be determined.

TURBULENT DIFFUSION FLAMES

Turbulent diffusion flames are usually discussed from the viewpoint of turbulent mixing as the rate-controlling factor; the reaction rate is not considered to be controlling, or even important. In all but a few possible exceptions, this has proved to be a satisfactory approach. However, as has been indicated in Chapter 12, turbulence itself is not well understood; when a turbulent system involves the presence of a flame which acts as a volume source, the complications become apparent.

However, laminar and turbulent diffusion flames have at least one common feature: the flame must be held at some point or in some area. In the laminar diffusion flame, the adjacent fuel and air interdiffuse near the edge of the burner. At some distance less than the quenching distance, a combustible mixture of varying composition is reached over a region greater than the

normal flame thickness. In this region, at the quenching distance, a premixed flame occurs, and holds the diffusion flame. In fact, the diffusion flame can be pictured as a stepwise series of premixed flames, each with a hotter but more dilute entering composition.

In the case of the turbulent flame, this seating of the flame near the burner often does not occur. On the contrary, there are only local regions where the maximum flame speed can exceed the oncoming velocity; therefore, the holding points shift as these local, low velocity regions shift about in the turbulent stream. This is clearly shown by the photographs of Yagi and Saji(19-16). Furthermore, all of the leading edges of the flame must move at maximum premixed flame speed through the turbulent mixture, stretching and spreading the flame. When the flame can no longer find large enough local regions where it can "buck" the oncoming stream and not be quenched, the flame will blow off unless held by a pilot flame or spark.

Before covering the experimental work on confined or unconfined turbulent flames, the theoretical considerations of Wohlenberg(19-17), which are based on some investigations of turbulent mixing by Rummel(19-18), should be discussed. These involve both the turbulent and kinetic aspects of the problem. It is observed in the mixing process, induced by turbulence where two streams enter along parallel paths, that, in the inner zone, where chemical reactions occur, the surface is composed of a relatively turbulent mixture of islands or streams of gas and air. These islands, also referred to as concentration zones, are composed of fuel-rich and air-rich zones and between these zones chemical reactions and diffusion processes occur in a thin zone.

Wohlenberg has expanded these observations into what he terms the reaction interface extension. His model consists of an array of islandlike volumes of air and fuel, which originate at the boundary between the fuel and air streams, as in a vortex shedding phenomenon, and continue to break up thereafter and become a random mixture. Due to the high concentrations of the respective air and fuel zones, the reactants tend to diffuse toward each other across the interface separating them. If every collision results in a reaction, the interzone would only be as deep as about five molecular free paths. However, the fraction of collisions which result in chemical reaction is small since besides being a probability function, it also is dependent upon the reaction energy and temperature; consequently, the interface, or interzone as Wohlenberg refers to it, takes on a measurable thickness. (See also Reference 19-12). The scale of the turbulence probably determines the size of the islands; however, and since the actual collision range is so small compared to turbulent scales it is not likely, as Wohlenberg points out, that turbulence would increase the number of collisions.

Wohlenberg has defined this potential flame front in terms of a reaction interface extension, \underline{A} , which is a specific area per unit volume of mixture, and a mean depth, \underline{l} , which is the penetration distance into the reaction zone normal to this surface. The specific volume is then equal to the product $\underline{A}\underline{l}$, a dimensionless quantity. For a uniform mixture then, it is obvious that $\underline{A}\underline{l}$ is unity, and thus for any mixture there exists a maximum extension, $\underline{A} = 1/\underline{l}$.

This model allows for the evaluation of combustion as a function of the molecular diffusion, kinetics of the molecular collision, and the reaction interface area. The primary variables are expressible in turn as functions of pressure, temperature, velocity, and fuel/air ratio.

For stable combustion, the fuel-air supply must be in equilibrium with its consumption by the chemical reaction; therefore, Wohlenberg attacks the problem by setting up equations for the rate of energy release as a result of (a) effective collision and (b) the diffusion processes. The problem becomes one of evaluation of the effect of turbulence on the supply of the reactants to the interzone. Obviously, turbulence increases \underline{A} and decreases \underline{l} . Now if \underline{l} is made so small that the diffusion process is no longer controlling, the collision equation will define the combustion process. In the usual diffusion study the development is based on the reverse situation.

Whatever the situation, it follows that the collision equation and the supply equations are both functions of the reaction interface extension, and by equating these quantities under the proper combustion conditions, one can relate the progress of combustion to the fraction of material consumed.

The actual significance of the reaction interface extension must be verified further before applying it to other combustion studies. If A is a significant quantity, then its role in such a combustion picture can be very useful, and may possibly have an extensive application in the burning of fuel spray-air mixtures, where the island concept is appropriate. The heterogeneous system will, of course, complicate the development in its present form.

Some workers have claimed that the instability of lean hydrogen-oxygen flames is due to the fact that the gas mixture might not be completely homogeneous; but instead, due to the high diffusivity of hydrogen, diffusion may take place as high-concentration filaments, so that only part of the fresh gas is burned(19-17). This concept has been used to offer a possible explanation for the fact that only 10 per cent of the hydrogen burns at its lower limit (3.85 per cent hydrogen). The presence of these high-concentration filaments parallels Wohlenberg and Rummel's concept of fuel-rich and air-rich islands in the midst of an air-rich continuum, and Wohlenberg's treatment might be modified to apply to such a situation. This is a difficult problem, experimentally, since the flame appears uniform throughout.

In two subsequent papers(19-20, 19-21), Wohlenberg considers in detail the specific reaction of dodecane and air. He not only gives specific values for maximum energy release rates which are limited by kinetic considerations, but indicates that "tail-end" diffusion is the rate limiting factor in the actual case; that is, the final diffusion of the fuel and oxygen to each other must take place by the molecular diffusion process and not as a result of turbulent mixing.

Unconfined Flames

The unconfined turbulent diffusion flame is treated ordinarily as a problem in turbulent mixing of a jet. (See Chapter 12). This gives results which can be interpreted in terms of completeness of combustion, but does not indicate the stability of the flame. In fact, a systematic treatment of diffusion flame stability, for either laminar or turbulent flames, is greatly to be desired. Some discussion of the stability problem is given by Scholefield and Garside(19-22), and this will be discussed first.

Figure 19-5 shows that as the nozzle velocity increases, the flame moves into a turbulent region. A turbulent flame first occurs near the tip, and then moves downward to a point near the jet. When this point is reached, the length of the flame ceases to show any variation with velocity. Scholefield and Garside show that a jet alone, without combustion, exhibits this same pattern of breakdown into turbulent flow with increasing velocity. For some jets, this break region first moves down slowly and then takes a sudden jump to rest at the nozzle. It is thus expected that some diffusion flames will show the same characteristics as the flow rate increases.

Figure 19-6 shows some of Scholefield and Garside's results on flame stability. Below a certain jet diameter, the velocity at blow-off is independent of diameters. Above that diameter, the velocity at blow-off becomes dependent on diameter; the larger the diameter the more unstable the flame. It appears that finally blow-off occurs at a constant value of Reynolds number. However, above the same critical diameter, as mentioned before, the flame will not blow off completely, but will persist as a lifted flame. In this case, the final blow-off velocity increases with jet diameter. Observation of the lifted flame indicates that it first appears as an annulus, and gradually closes in on the center. When it closes in completely, even the lifted flame blows off. It might be noted that this phenomenon starts to occur with rich bunsen-type flames (and other pre-mixed open flames) and increases in range with increasingly rich primary mixtures. (See Figure 17 of Reference 19-23, for instance).

Returning to the problem of where transition takes place from the laminar to turbulent-type flame, it must be pointed out that the Reynolds number corresponding to cold flow does not, in itself, determine the transition point. Hottel and Hawthorne(19-10) listed the Reynolds numbers at which transition commenced as 2000 for hydrogen, about 3500 for city gas, 5000 for CO, from 6000 to 9000 for city gas or hydrogen with some primary air, and about 9000 to 10,000 for propane and acetylene. Wohl, et al., (19-15) indicated a value of 11,000 for butane.

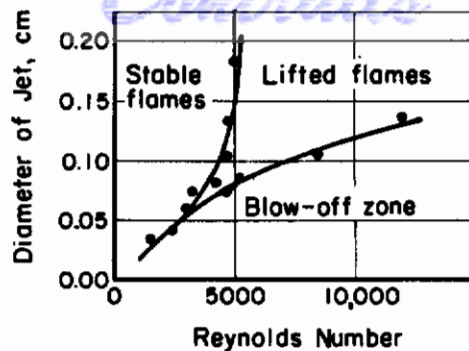


FIGURE 19-6. STABILITY RANGES OF DIFFUSION FLAMES FOR CARBURETOR-TYPE JETS

Scholefield and Garside(19-22)

Once the flame is completely turbulent, the turbulent diffusion rate becomes a primary factor in promoting mixing. From the simplest dimensional considerations of turbulence, the diffusivity is given by

$$D_t = \alpha V d, \quad (19-24)$$

where α is a proportionality constant. Substitution of this result into Equation 19-12 shows that the ratio of flame height to jet diameter is a function of only the properties of the primary mixture.

Hawthorne, et al., (19-24) carried out a much more detailed analysis of the open turbulent jet flame. They incorporated information on jet mixing, and considered buoyancy and momentum forces. In the final equation, however, they neglected buoyancy terms (this assumes a high nozzle velocity and small diameter) and obtained the following relation for flame height:

$$\frac{Y}{d} = \frac{5.3}{C_t} \sqrt{\frac{T_f}{\alpha_t T_n}} \left[C_t + (1 - C_t) \frac{M_s}{M_n} \right], \quad (19-25)$$

where Y is the visible flame height, d is the nozzle diameter, T_f is the adiabatic flame temperature, T_n is the temperature of the nozzle fluid, M_s, n are the molecular weights of the surroundings and nozzle fluid, C_t is the mole fraction of nozzle fluid in the unreacted stoichiometric mixture, and α_t is the ratio of moles of reactant to moles of product, for stoichiometric combustion. The visible height was found to be somewhat greater than the height at which combustion was 99 per cent complete, based on a gas analysis on the axis.

It is interesting to note that the actual calculations yield the ratio of flow width to jet diameter at the level where the concentration reaches C_t . In the cold jet, such a width increases linearly with height above some break point, s , such that

$$w = \alpha (y - s), \quad (19-26)$$

where α again is a proportionality constant. For many cases, $s \ll y$, and may be disregarded. Therefore Hawthorne, et al., found empirically the ratio of visible flame height to computed width by plotting Y/d against w/d for tests on propane, hydrogen-propane, acetylene, city gas, hydrogen, CO_2 - city gas, and CO. This gave the numerical constant of Equation 19-25.

Hawthorne, et al., also obtained axial concentrations as a function of distance along the flame. Whereas the reciprocal of the time-mean concentrations of nozzle fluid in a sample reduced to its unreacted constituents was found to vary linearly with distance in the confined flame, the reciprocal concentration increased more slowly at first and at an increasingly rapid rate for the unconfined stream. On his curves Hawthorne indicates the distances at which combustion is 99 per cent complete; this is at a concentration of air two or three times as much as required for stoichiometric

combustion. This is a result of an "unmixedness" which is discussed extensively. Even though the time average value of the mixture is stoichiometric at a given point, there are numerous islands of fuel and others of oxygen passing the point in time, as Wohlenberg has pointed out. Thus, even at a stoichiometric time-average ratio, only a small amount of fuel and oxygen may have had the opportunity to burn. Before the islands are broken up so that all the fuel has oxygen within the range of molecular diffusion, much more than the necessary amount of oxygen will have been grossly mixed with the fuel. Further discussion of the analysis and interpretation of data obtained under these conditions is given in Reference 19-25.

Hawthorne, et al., in developing their equation for flame height average out radial variations in concentration, velocity, and temperature. Baron(19-26) accounts for the variation by using Reichardt's hypothesis (See Chapter 12), and obtains Equation 19-25, with a negligible change in the value of the numerical constant. Because of the similarity of equations, Baron identified symbols term to term and thus identified C_t of Hawthorne, et al., with his concentration at the tip of the flame; this infers that the tip concentration is that of a stoichiometric mixture. However, as noted previously, the time-average tip concentration is far leaner than stoichiometric. This discrepancy may be the result of the different spread coefficient for the cold and hot jets; this point should be investigated more carefully.

Baron also computes the flame shape as

$$\frac{df}{h} = 0.29 \sqrt{\ln\left(\frac{Y}{h}\right)} \quad (19-27)$$

and shows that this agrees with a photograph of a city gas flame taken by Wohl, et al., (19-15). Finally, Baron indicated the procedure for analysing systems of multiple, parallel jet flames.

Wohl, et al., (19-15) studied turbulent flames for jets of 50 and 100 per cent city gas. They expressed their data in the form

$$\frac{Y}{d} = \frac{1}{\left(\beta + \frac{\gamma}{V}\right)}, \quad (19-28)$$

where β and γ differ for the two mixtures. It may be noted (and was noted by Wohl) that for large $\frac{Y}{d}$, this is the form developed in the first part of this section. Wohl, et al., point out that by adding a small constant velocity to the stream velocity in their equations for turbulent diffusivity, this exact form of equation is obtained. They also show that reasonable values of β can be predicted by using for the value of α in Equation 19-24 the product of 0.00255 (obtained from cold flow jet tests) and an arbitrary constant of about 1.

Yagi and Saji(19-16) obtained some high-speed photographs of turbulent diffusion flames, which show that at any instant, the flame appears to have a diaphanous form extending over only part of the combustion zone. Such photographs probably led to their formulation of the equation for flame height as a function of the critical diffusion across a cylindrical shell with the thickness proportional to the mixing length. The resulting equation for flame height is

$$\frac{(Y - s)}{d} = 10.8 (2 - \log \gamma)(1 + M)^{-1} \left(\frac{\rho_{fg}}{\rho_{nf}}\right)^{1/2} [(1 - \alpha) Q + \alpha] \quad (19-29)$$

where

$$\alpha = \left(1 - \frac{\gamma}{100}\right) [2.3 (2 - \log \gamma)]^{-1}, \quad 100 \gg \gamma > 0,$$

and γ is per cent fuel concentration at the tip relative to the initial fuel concentration, M is the primary air/fuel ratio, Q is the theoretical combustion gas volume without excess air, ρ_{fg} , ρ_{nf} are the

nozzle fluid density and mean flame density. Assuming γ at the flame tip to be 3 per cent*, Yagi and Saji computed flame lengths in good agreement with the visible lengths obtained by Hawthorne, et al., and for some previous data by Yagi.

For use of their equation to predict the length of pulverized coal flames, Yagi and Saji replaced

$$(1 + M)^{-1} [(1 - \alpha) Q + \alpha]$$

$$[1.25 M_w^{-1} (1 - \alpha) Q' + \alpha] ,$$

where M_w is the ratio, by weight, of primary air to the pulverized coal, and Q' is the theoretical combustion gas volume (nm^3) per unit weight of pulverized coal (kg). Again the agreement between calculated and observed flame lengths is reasonable, although a γ value of 1-1/2 per cent seems to be a better assumption than the 3 per cent used for gaseous fuels.

Thring and Newby⁽¹⁹⁻²⁷⁾ make some remarks, based on similarity considerations, about an unconfined jet flame burning oil. They note that for sufficiently large Reynolds numbers and $h > 15 r$,

$$\frac{1}{C_m} = \frac{y}{r'} \sqrt{\frac{\rho_f}{\rho_o}} K , \quad (19-30)$$

where C_m is the mass concentration of the nozzle fluid on the axis, y is the distance along the axis, ρ_f is the density of the flame gases at their actual temperature, ρ_o is the density of the nozzle gases at their temperature, K is a constant evaluated from the relative distribution of velocity and concentration normal to the jet axis, and $r' = r \sqrt{\rho_o / \rho_f}$. Thus, r' is the aperture of a jet through which the same mass flow rate of nozzle fluid will have emerged at the same jet momentum, but with the density ρ_f instead of ρ_o . If the original fuel jet is an oil stream with high pressure air or steam injection, r is not the actual nozzle radius, $d/2$, and

$$r' = \frac{m}{\sqrt{\rho_f \pi G}} \quad (19-31)$$

where m is the mass flow rate of nozzle fluid and G is the momentum flow through the nozzle. Thring and Newby point out that when the effect of temperature change along the axis is taken into account, perfect similarity cannot be preserved. They finally suggest that

$$Y' = \alpha \left[\frac{10.5 r'}{C'_t} \right] , \quad (19-32)$$

where Y' is the distance along the axis to the point where the time mean concentration of nozzle fluid is equal to the stoichiometric mass concentration, C'_t , and $0.9 \leq \alpha \leq 1.1$.

Enclosed Flames

Thring and Newby⁽¹⁹⁻²⁷⁾ point out the following differences between the free jet and a jet enclosed downstream. The walls interfere with the free expansion of the jet; the amount of surrounding fluid is finite, (recirculation must occur beyond the point where all the available air is entrained); and the jet momentum is eventually converted mainly to static pressure. Thus, confined jets, unlike free jets, are not all similar. Moreover, Thring and Newby show that for jets in containers of large diameter, and with large quantities of excess air, the reciprocal concentration on the axis times the ratio of jet diameter, d , to container diameter, D , is proportional to the ratio of axial distance to chamber diameter. However, as the third parameter,

* This is not 97 per cent completion of combustion; such a value would have to come from a gas analysis as per Hawthorne, et al.

increases (where m_a is mass flow rate of air), the curves fall off more and more rapidly toward a finite value of the reciprocal concentration times the diameter ratio. This is a result, of course, of the finite amount of air, and the recirculation.

As with the free jet, when combustion occurs the problem becomes more complicated. Thring and Newby, in comparing the cold and hot enclosed jets, replace r' by $m/\sqrt{G\pi\rho_f}$, as before. They then find that tests on an oil-fired furnace using both air and steam atomization correlate quite well with cold flow tests on a 1/10-scale model.

They also discuss the "mixedness" of Hawthorne, et al., and make some computations on the fraction of fuel unreacted at the stoichiometric mixture position. Finally, they suggest that for a jet in a very large chamber, but with limited air,

$$Y' = 10.5 r' \alpha \left\{ \frac{1}{2.4 C'_t} - \ln 1.7 \left(1 - \frac{C'_\infty}{C'_t} \right) \right\} \quad (19-33)$$

where $C'_\infty = m/(m + m_a)$ and $0.8 \leq \alpha \leq 1.2$.

Berry, et al., (19-28) culminated a series of articles on turbulent transport by a study of a coaxial flame. Shortly after leaving straightening vanes, the air in a 4-in. tube mixes with the natural gas from a central, 1-in. tube. Extensive studies were made of temperature, concentration, and velocity profiles at average cold flow velocities of 10, 25, and 50 fps. There is some asymmetry in the data as a result of both gravitational effects and the off-axis location of the spark found necessary to hold the flame.

At 10 and 25 fps, the upstream flame surface, as defined by the 1600°F temperature profile, remains fixed, but at 50 fps the profile moves downstream. This is taken by Berry, et al., as indicating that the "flame velocity" increases directly with flow velocity (or intensity of turbulence) at first, and then less rapidly, as appears to be the case in some instances with premixed turbulent flames. However, such an explanation leads to no better understanding of the turbulent diffusion flame.

Rummel(19-18)(19-4) reports the concentration and velocity (essentially) curves of flat diffusion flames in which air and fuel are introduced side by side into a confined chamber. The concentration curves are much as would be expected from the previous discussion of axially symmetric flames. Rummel conducted model tests, in which he mixed 1/2 per cent H₂ in air to simulate the fuel, and studied the concentrations in a cold system. Changes in concentration pattern as a result of velocity changes and changes in injection angle are readily apparent. For instance, an increase of impingement angle of the fuel and air jets increases the rate of mixing considerably. This is interpreted as indicating in a combustion system, a considerable decrease in flame length. However, as indicated by Thring and Newby(19-27), it is a long step from a cold flow model to a combustion system, if quantitative results are desired.

Sawai, et al., (19-29) treat mathematically the flat flame system in which gas and air jets are of the same width and are symmetrically spaced in a combustion chamber. They make the same assumptions as Burke and Schumann(19-1), and thus are forced to compute an average velocity and corresponding jet concentration from the actual jet velocities and widths, and size of the combustion chamber. Since they consider the turbulent case, the coefficient of eddy diffusion, D_t , is used and is assumed to be given by $\alpha U a$ where \underline{U} is the average velocity, and \underline{a} is the chamber width. The length of the flame then becomes

$$Y = \frac{a}{\pi^2 \alpha} \ln \frac{P}{\pi} \left[\frac{q_f + q_o/i}{C_1 q - q_f + \frac{q_o}{i}} \right], \quad (19-34)$$

Continuity

where q_f is the fuel flow rate, q_o is the oxidant flow rate, i is the moles of oxidant required to burn one mole of fuel, q is the total flow rate (with air, $q \neq q_f + q_o$), and C_1 is the concentration of fuel at the flame tip. For fuel and air jets each of half the width of the combustion chamber, $p = 2\sqrt{2}$, whereas for jets on opposite sides of the chamber and one-third its width, $p = 9/2$. For very small jets of width, b , separated by the small distance, δ , and centered on the axis $p = \pi^2(\delta + b)/\sqrt{2} a$. This last solution appears unrealistic, since such a system is more like a close pair of free jets, and the diffusivity would not be a function of a and U as assumed. If Barr's⁽¹⁹⁻⁹⁾ observations that the length of the axially symmetric laminar flame is little affected by the ratio of inner to outer tube diameter, as long as the flow ratios are constant, is any indication of what can happen in the turbulent case, then the first two solutions above may be quite reasonable.

One test was made with a burner having small, closely spaced jets, and α was determined as 0.016. Flame height was not found to vary as long as the ratio of fuel to air velocity was preserved. Although this result is in agreement with the prediction of the theoretical equation, the agreement does not confirm the theoretical equation.

Sawai, et al., continued their investigation by using model tests with liquids, in which changes in pH in the mixing zone between the two liquids indicate the position of the flame front*. As noted previously, such tests are more of a qualitative than quantitative value. For the system studied, in which the wall jets are separated by a partitioning, it is shown, among other things, that "flame height" decreases with increasing excess air, increases slightly with increasing Reynolds number, and increases first and then decreases with increasing partition thickness.

Hottel and Person⁽¹⁹⁻³¹⁾ studied a different diffusion flame system from those previously discussed. Air was introduced with a large tangential velocity component at the lower end of a cylindrical combustion chamber about 6 in. in diameter. Fuel was admitted axially from a 2-in. pipe. The completeness of combustion of the vortex combustion system at various heights was measured, by use of a variable length chamber, followed by spray quenching, mixing, and analysis. The completeness of combustion was found to be independent of the tangential velocity or the ratio of radial to tangential velocity. For a given length of chamber, the combustion efficiency increased about linearly with fuel/air ratio to near a maximum, then flattened out and began to drop off as the stoichiometric ratio was approached. The peak efficiency increased with the length of the combustion chamber, and occurred at lower values of fuel/air ratio as the length increased.

The first observations above are explained on the basis that an increase in rate of throughput is balanced by an increase in the local rate of mixing, since the chemical reaction is so fast that it is not the controlling factor.

It is worth noting that, in this system, an increase in pressure drop alone does not correspond to an increase in efficiency.

Corner⁽¹⁹⁻³²⁾ and Goldenberg⁽¹⁹⁻³³⁾⁽¹⁹⁻³⁴⁾ discuss combustion of solids in pipe form. Corner considers the solid-fuel rocket-type unit, in which heat transfer to the surface decomposes the solid, and the vapors burn in the stream. Goldenberg considers the carbon tube where both heat and oxygen at the surface are necessary, and a secondary reaction of the CO follows in the main stream. Since diffusion is a controlling factor in both of these processes, the situation is analyzed on the basis of turbulent pipe flow.

Goldenberg also gives some experimental results of gas composition at the end of the tube, with variables of carbon temperature, flow rate, and tube length. He indicates no disagreement with his mathematical analysis, and draws some conclusions relating to the chemical aspects of carbon combustion. It would seem that there should be some correlation between this work and that of Berry, et al.,⁽¹⁹⁻²⁸⁾ on the coaxial diffusion flame.

*See Reference 19-30 for report of other work of this type.

Continued
CONCLUDING REMARKS

A consideration of the previous discussions of the reported work on diffusion flames indicates there are many large areas which should be investigated. Some of these are as follows:

Considerably more work is required of the type Barr has reported. This consists of surveying the changes in the flame as various parameters are changed. For instance, in all four types of flames (laminar open, laminar enclosed, turbulent open, and turbulent enclosed), what changes take place with changes in (a) the ratio of primary air to fuel, (b) the initial temperature of the fuel, (c) the flame temperature, and (d) the molecular weight of the fuel? Some of these effects are known in a scattered fashion, but in many instances the observations apply only to a small region. In view of recent interest in combustion in ram jets and turbojets, pressure has also become an important variable.

The flame stability of the various types of diffusion flames merits more study. What factors are of basic importance in determining the flame holding ability of laminar and turbulent diffusion flames? In view of Berry's results, it might also be asked how the flame propagates through the turbulent mixture, and if there are quenching effects.

Since turbulence appears to be the limiting factor in the rate of combustion of turbulence diffusion flames, systems with multiple small jets and systems using grids should be studied. Results of such studies should be valuable in the design of practical, high duty combustion chambers.

More attention should be given to the use of dimensional analysis and similarities in analyzing combustion data. Surely, in the many empirical and semiempirical equations there should be some common grouping of factors.

The combustion of droplets, the ballistics of droplets, and dispersions have been covered in previous chapters. However, it should be noted that more basic work is required on heterogeneous combustion where liquid fuels are involved.

The degree of "unmixedness" is an important parameter in turbulent diffusion flames. This factor should be investigated thoroughly, both experimentally and theoretically, since it is through this factor that time mean concentration can be related to completeness of combustion.

Attempts should also be made to break units like can-type combustors, and the high pressure oil flame, into fundamental components which can be studied.

REFERENCES

- 19-1. Burke, S. P., and Schumann, T. E. W., Diffusion Flame; Ind. Eng. Chem., Vol. 20, 1928, p. 998.
- 19-2. Barr, J., and Mullins, B. P., Combustion in Vitiated Atmospheres; Fuel, Vol. 28, 1949, pp. 181, 200, 225, 228, 241.
- 19-3. Bell, J. C., and Putnam, A. A., Molecular Diffusion of a Jet in an Infinite Medium; Battelle Technical Report No. 15035-1, August 1953.
- 19-4. Jost, W., Explosion and Combustion Processes in Gases, McGraw-Hill, New York, 1946, p. 210.
- 19-5. Guyomard, F., Théorie Simplifiée de la hauteur des flammes laminaires de diffusion; Comptes Rendus, Vol. 234, 1952, p. 67.

- 19-6. Lewis, B., and von Elbe, G., Ignition and Flame Stabilization in Gases; Trans. ASME, Vol. 70, 1948, p. 143.
- 19-7. Barr, J., Diffusion Flames, "Fourth Symposium on Combustion", Williams and Wilkins, Baltimore, 1953, p. 765.
- 19-8. Garside, J. E., and Jackson, B., Polyhedral Diffusion Flames, Nature, Vol. 168, No. 4286, December 22, 1951, p. 1085.
- 19-9. Barr, J., Length of Cylindrical Laminar Diffusion Flames, Fuel, Vol. 33, No. 1, January 1954, p. 51.
- 19-10. Hottel, H. C., and Hawthorne, W. R., Diffusion in Laminar Flame Jets, "Third Symposium on Combustion, Flame, and Explosion Phenomena", Williams and Wilkins, Baltimore, Md., 1949, p. 254.
- 19-11. Shvab, V. A., Relation Between the Temperature and Velocity Fields of the Flame of a Gas Burner, Gas Energy. izd. M-L, 1948.
- 19-12. Wolfhard, H. G. and Parker, W. G., Temperature Measurements of Flames Containing Incandescent Particles; Proc. Phys. Soc., Vol. B62, 1949, p. 523.
- 19-13. Zeldovich, Y. B., On the Theory of Combustion of Initially Unmixed Gases; J. Tech. Phys. USSR, Vol. 19, 1949, p. 1199; (Translation, NACA TM-1296, June, 1951).
- 19-14. Rembert, E. W., and Haslam, R. T., Factors Influencing Length of a Gas Flame Burning in Secondary Air; Ind. Eng. Chem., Vol. 17, 1925, p. 1236.
- 19-15. Wohl, K., Gazley, C., and Kapp, N., Diffusion Flames, "Third Symposium on Combustion, Flame, and Explosion Phenomena", Williams and Wilkins, Baltimore, Md., 1949, p. 288.
- 19-16. Yagi, S. and Saji, K., Problems of Turbulent Diffusion and Flame Jets, "Fourth Symposium on Combustion", Williams and Wilkins, Baltimore, Md., 1953, p. 771.
- 19-17. Wohlenberg, W. J., Influence of Reaction Interface Extension in Gaseous Fuel Combustion; Trans. A.S.M.E., Vol. 70, 1948, p. 143.
- 19-18. Rummel, L., "Der Einfluss des Mischvorganges auf die Verbrennung von Gas and Luft in Feuerungen"; Verlag Stahleisen, Dusseldorf, 1937.
- 19-19. Behrens, H., Hydrogen Diffusion and Flame Structure; Die Naturwissen, Vol. 32, 1949, p. 297; Z. Physik. Chem., Vol. 196, 1950, p. 78.
- 19-20. Wohlenberg, W. J., Minimum Depth of the Flame Front for Stable Combustion and Maximum Time Mean Energy Release Rate over an Interval of Combustion Progress for Second-Order Reactions in a Gaseous System at Constant Pressure; "Fourth Symposium on Combustion", Williams and Wilkins, Baltimore, Md., 1953, p. 796.
- 19-21. Wohlenberg, W. J., Interface Extension Versus Upper Limiting Time-Mean Energy Release Rate of the Constant-Pressure Steady-State Combustion Process; Trans. A.S.M.E., Vol. 76, No. 4, p. 679.
- 19-22. Scholefield, D. A., and Garside, J. E., The Structure and Stability of Diffusion Flames, "Third Symposium on Combustion, Flame, and Explosion Phenomena", Williams and Wilkins, Baltimore, Md., 1949, p. 102.
- 19-23. Wohl, K., Quenching, Flash-Back, Blow-Off-Theory and Experiment; "Fourth Symposium on Combustion", Williams and Wilkins, Baltimore, Md., 1953, p. 68.

- 19-24. Hawthorne, W. R., Weddell, D. S., and Hottel, H. C., Mixing and Combustion in Turbulent Gas Jets; "Third Symposium on Combustion, Flame, and Explosion Phenomena", Williams and Wilkins, Baltimore, Md., 1949, p. 266.
- 19-25. Richardson, J. M., Howard, H. C., and Smith, R. W., The Relation Between Sampling-Tube Measurements and Concentration Fluctuations in a Turbulent Gas Jet, "Fourth Symposium on Combustion", Williams and Wilkins, Baltimore, Md., 1953, p. 814.
- 19-26. Baron, T., Reactions in Turbulent Free Jets - The Turbulent Diffusion Flame, Chem. Eng. Progress, Vol. 50, No. 2, p. 73.
- 19-27. Thring, M. W., and Newby, M. P., Combustion Length of Enclosed Turbulent Jet Flame, "Fourth Symposium on Combustion", Williams and Wilkins, Baltimore, Md., 1953, p. 789.
- 19-28. Berry, V. J., Mason, D. M., and Sage, B. H., Material Transfer in Turbulent Gas Streams - A Coaxial Flame; Ind. Eng. Chem., Vol. 45, No. 7, 1953, p. 1596.
- 19-29. Sawai, I., Kunugi, M., and Jinns, H., Turbulent Diffusion Flames; "Fourth Symposium on Combustion", Williams and Wilkins, Baltimore, Md., 1953, p. 805.
- 19-30. Hottel, H. C., Burning in Laminar and Turbulent Fuel Jets, *ibid*, p. 97.
- 19-31. Hottel, H. C., and Person, R. A., Heterogeneous Combustion of Gases in a Vortex System", *ibid*, p. 781.
- 19-32. Corner, I., The Effect of Turbulence on Heterogeneous Reaction Rates; Trans. Faraday Soc., Vol. 43, 1947, p. 635.
- 19-33. Goldenberg, S. A., Turbulent Heterogeneous Combustion; Izvestiia Akademii Nauk SSSR, No. 8, 1950, p. 1154.
- 19-34. Goldenberg, S. A., Investigation of the Process of Turbulent Combustion, With Consideration of Secondary Reactions, Izvestiia Akademii Nauk SSSR, No. 5, 1951, p. 657.

Contrails